

Echocardiography in cardiovascular medicine

Edited by

Sanjeev Bhattacharyya and Francesca Innocenti

Published in

Frontiers in Cardiovascular Medicine

Frontiers in Oncology



FRONTIERS EBOOK COPYRIGHT STATEMENT

The copyright in the text of individual articles in this ebook is the property of their respective authors or their respective institutions or funders. The copyright in graphics and images within each article may be subject to copyright of other parties. In both cases this is subject to a license granted to Frontiers.

The compilation of articles constituting this ebook is the property of Frontiers.

Each article within this ebook, and the ebook itself, are published under the most recent version of the Creative Commons CC-BY licence. The version current at the date of publication of this ebook is CC-BY 4.0. If the CC-BY licence is updated, the licence granted by Frontiers is automatically updated to the new version.

When exercising any right under the CC-BY licence, Frontiers must be attributed as the original publisher of the article or ebook, as applicable.

Authors have the responsibility of ensuring that any graphics or other materials which are the property of others may be included in the CC-BY licence, but this should be checked before relying on the CC-BY licence to reproduce those materials. Any copyright notices relating to those materials must be complied with.

Copyright and source acknowledgement notices may not be removed and must be displayed in any copy, derivative work or partial copy which includes the elements in question.

All copyright, and all rights therein, are protected by national and international copyright laws. The above represents a summary only. For further information please read Frontiers' Conditions for Website Use and Copyright Statement, and the applicable CC-BY licence.

ISSN 1664-8714
ISBN 978-2-8325-4964-3
DOI 10.3389/978-2-8325-4964-3

About Frontiers

Frontiers is more than just an open access publisher of scholarly articles: it is a pioneering approach to the world of academia, radically improving the way scholarly research is managed. The grand vision of Frontiers is a world where all people have an equal opportunity to seek, share and generate knowledge. Frontiers provides immediate and permanent online open access to all its publications, but this alone is not enough to realize our grand goals.

Frontiers journal series

The Frontiers journal series is a multi-tier and interdisciplinary set of open-access, online journals, promising a paradigm shift from the current review, selection and dissemination processes in academic publishing. All Frontiers journals are driven by researchers for researchers; therefore, they constitute a service to the scholarly community. At the same time, the *Frontiers journal series* operates on a revolutionary invention, the tiered publishing system, initially addressing specific communities of scholars, and gradually climbing up to broader public understanding, thus serving the interests of the lay society, too.

Dedication to quality

Each Frontiers article is a landmark of the highest quality, thanks to genuinely collaborative interactions between authors and review editors, who include some of the world's best academicians. Research must be certified by peers before entering a stream of knowledge that may eventually reach the public - and shape society; therefore, Frontiers only applies the most rigorous and unbiased reviews. Frontiers revolutionizes research publishing by freely delivering the most outstanding research, evaluated with no bias from both the academic and social point of view. By applying the most advanced information technologies, Frontiers is catapulting scholarly publishing into a new generation.

What are Frontiers Research Topics?

Frontiers Research Topics are very popular trademarks of the *Frontiers journals series*: they are collections of at least ten articles, all centered on a particular subject. With their unique mix of varied contributions from Original Research to Review Articles, Frontiers Research Topics unify the most influential researchers, the latest key findings and historical advances in a hot research area.

Find out more on how to host your own Frontiers Research Topic or contribute to one as an author by contacting the Frontiers editorial office: frontiersin.org/about/contact

Echocardiography in cardiovascular medicine

Topic editors

Sanjeev Bhattacharyya — Barts Heart Centre, United Kingdom

Francesca Innocenti — Careggi University Hospital, Italy

Citation

Bhattacharyya, S., Innocenti, F., eds. (2024). *Echocardiography in cardiovascular medicine*. Lausanne: Frontiers Media SA. doi: 10.3389/978-2-8325-4964-3

Table of contents

- 07 **Editorial: Echocardiography in cardiovascular medicine**
Sanjeev Bhattacharyya and Francesca Innocenti
- 09 **Necropsy Validation of a Novel Method for Left Ventricular Mass Quantification in Porcine Transthoracic and Transdiaphragmal Echocardiography**
Charlotte Burup Kristensen, Stefan Michael Sattler, Anniel Frederike Lubberding, Jacob Tfelt-Hansen, Thomas Jespersen, Christian Hassager and Rasmus Mogelvang
- 19 **Cardiac and Vascular Remodeling After 6 Months of Therapy With Sacubitril/Valsartan: Mechanistic Insights From Advanced Echocardiographic Analysis**
Sara Monosilio, Domenico Filomena, Federico Luongo, Michele Sannino, Sara Cimino, Matteo Neccia, Marco Valerio Mariani, Lucia Ilaria Birtolo, Giulia Benedetti, Giovanni Tonti, Gianni Pedrizzetti, Carmine Dario Vizza, Viviana Maestrini and Luciano Agati
- 28 **Left Atrial Appendage Mechanical Dispersion Assessed by Speckle-Tracking Echocardiography as a Determinant of Left Atrial Appendage Blood Stasis in Patients With Atrial Fibrillation**
Yankai Mao, Huajie Zhao, Chan Yu, Yuan Yang, Mingming Ma, Yunhe Wang, Ruhong Jiang, Bowen Zhao, Zhelan Zheng and Chenyang Jiang
- 38 **Automated analysis of limited echocardiograms: Feasibility and relationship to outcomes in COVID-19**
Patricia A. Pellikka, Jordan B. Strom, Gabriel M. Pajares-Hurtado, Martin G. Keane, Benjamin Khazan, Salima Qamruddin, Austin Tutor, Fahad Gul, Eric Peterson, Ritu Thamman, Shivani Watson, Deepa Mandale, Christopher G. Scott, Tasneem Naqvi, Gary M. Woodward and William Hawkes
- 50 **Lateral annular systolic excursion ratio: A novel measurement of right ventricular systolic function by two-dimensional echocardiography**
Jonathan D. Stock, Eric S. Rothstein, Scott E. Friedman, Anthony S. Gemignani, Salvatore P. Costa, Andrew J. Milbridge, Rui Zhang, Cynthia C. Taub, Daniel J. O'Rourke and Robert T. Palac
- 60 **Additive effects of type 2 diabetes and metabolic syndrome on left ventricular torsion and linear deformation abnormalities during dobutamine stress echocardiography**
Falah Aboukhouder, Clothilde Philouze, Antoine Grandperrin, Stéphane Nottin and Philippe Obert
- 73 **Automatic view classification of contrast and non-contrast echocardiography**
Ye Zhu, Junqiang Ma, Zisang Zhang, Yiwei Zhang, Shuangshuang Zhu, Manwei Liu, Ziming Zhang, Chun Wu, Xin Yang, Jun Cheng, Dong Ni, Mingxing Xie, Wufeng Xue and Li Zhang

- 83 **The diagnostic accuracy of contrast echocardiography in patients with suspected cardiac masses: A preliminary multicenter, cross-sectional study**
Ying Li, Weidong Ren, Xin Wang, Yangjie Xiao, Yueqin Feng, Pengli Shi, Lijuan Sun, Xiao Wang, Huan Yang and Guang Song
- 95 **Cardiac and vascular effects of low-dose steroids during the early phase of septic shock: An echocardiographic study**
François Bagate, Alexandre Coppens, Paul Masi, Nicolas de Prost, Guillaume Carteaux, Keyvan Razazi and Armand Mekontso Dessap
- 105 **Intracardiac echocardiography Chinese expert consensus**
Zhong Jingquan, Long Deyong, Chu Huimin, Fu Hua, Han Xuebin, Jiang Chenyang, Li Yan, Li Xuebin, Tang Min, Wang Zulu, Xue Yumei, Zhang Jinlin, Zhang Wei, Zhang Xiaochun, Zhou Daxin, Zhang Yun, Ma Changsheng, Paul C. Zei and Luigi Di Biase
- 137 **A prediction model for major adverse cardiovascular events in patients with heart failure based on high-throughput echocardiographic data**
Qinliang Sun, Shuangquan Jiang, Xudong Wang, Jingchun Zhang, Yi Li, Jiawei Tian and Hairu Li
- 157 **The role of stress echocardiography in transcatheter aortic valve implantation and transcatheter edge-to-edge repair era: A systematic review**
Rita Pavasini, Gioele Fabbri, Nicola Bianchi, Maria Angela Deserio, Federico Sanguettoli, Luca Zanarelli, Elisabetta Tonet, Giulia Passarini, Matteo Serenelli and Gianluca Campo
- 168 **Echocardiographic predictors of thrombus in left atrial appendage—The role of novel transthoracic parameters**
Damian Kaufmann, Elżbieta Wabich, Agnieszka Kapton-Cieślicka, Monika Gawatko, Monika Budnik, Beata Uziębło-Życzkowska, Paweł Krzesiński, Katarzyna Starzyk, Beata Wożakowska-Kapton, Maciej Wójcik, Robert Błaszczuk, Jarosław Hiczekiewicz, Jan Budzianowski, Katarzyna Mizia-Stec, Maciej T. Wybraniec, Katarzyna Kosmalska, Marcin Fijałkowski, Anna Szymańska, Mirosław Dłużniewski, Maciej Haberka, Michał Kucio, Błażej Michalski, Karolina Kupczyńska, Anna Tomaszuk-Kazberuk, Katarzyna Wilk-Śledziwska, Renata Wachnicka-Truty, Marek Koziński, Paweł Burchardt and Ludmiła Daniłowicz-Szymanowicz
- 178 **Echocardiography protocol: A tool for infrequently used parameters in mice**
Emily Ann Todd, Monique Williams, Ali Kamiar, Monica Anne Rasmussen and Lina A. Shehadeh
- 194 **Correlation analysis between myocardial work indices and liver function classification in patients with hepatitis B cirrhosis: A study with non-invasive left ventricular pressure-strain loop**
Yang Cao, Huihui Zhang, Shuai Li, Siliang Li, Shuowen Sun, Jinwen Chen, Ting Ye, Xijun Zhang and Jianjun Yuan

- 203 **A comparable efficacy and safety between intracardiac echocardiography and transesophageal echocardiography for percutaneous left atrial appendage occlusion**
Zhi-Yuan Zhang, Feng Li, Jie Zhang, Lei Zhang, Huan-Huan Liu, Ning Zhao, Fan Yang, Qi Kong, Yi-Ting Zhou, Ling-Ling Qian and Ru-Xing Wang
- 216 **Exploring the prospect of intrinsic wave propagation in evaluating myocardial stiffness among patients with type 2 diabetes**
Qiao Cheng, Xiao Huang, Xinying Fan, Jie Sun, Jun Zhang, Qiaoying Tang, Youbin Deng and Xiaojun Bi
- 224 **The potential impact of hereditary hemochromatosis on the heart considering the disease stage and patient age—the role of echocardiography**
Michał Świątczak, Katarzyna Rozwadowska, Katarzyna Sikorska, Krzysztof Młodziński, Agata Świątczak, Grzegorz Raczak and Ludmiła Daniłowicz-Szymanowicz
- 237 **Development and validation of a deep learning pipeline to measure pericardial effusion in echocardiography**
Chi-Yung Cheng, Cheng-Ching Wu, Huang-Chung Chen, Chun-Hui Hung, Tien-Yu Chen, Chun-Hung Richard Lin and I-Min Chiu
- 247 **Evaluation of left atrial and ventricular remodeling in atrial fibrillation subtype by using speckle tracking echocardiography**
Shirui Lu, Hongyun Liu, Jie Sun, Jun Zhang, Li Li, Qiaoying Tang, Yani Liu and Youbin Deng
- 259 **Mitral valve aneurysms: echocardiographic characteristics, formation mechanisms, and patient outcomes**
Yi Wang, Shuang Wang, Dandan Chen, Mengmei Li, Sulin Mi, Li Xiong, Wanwan Song, Wei Wang, Shanye Yin and Bin Wang
- 267 **Tricuspid annular and right atrial volume changes are associated in healthy adults—insights from the three-dimensional speckle-tracking echocardiographic MAGYAR-Healthy Study**
Attila Nemes, Árpád Kormányos, Gergely Rácz, Zoltán Ruzsa, Alexandru Achim, Nóra Ambrus and Csaba Lengyel
- 276 **Right vs. left ventricular longitudinal strain for mortality prediction after transcatheter aortic valve implantation**
Neria E. Winkler, Shehab Anwer, Kelly A. Reeve, Jonathan M. Michel, Albert M. Kasel and Felix C. Tanner
- 286 **Assessment of myocardial function and cardiac performance using left ventricular global longitudinal strain in athletes after COVID-19: a follow-up study**
J. Schellenberg, L. Matits, D. A. Bizjak, J. Kersten, J. Kirsten, S. Vollrath and J. M. Steinacker

- 295 **Cardiac remodeling on echocardiogram is related to contrast-associated acute kidney injury after coronary angiography: a cross-section study**
Qingqing Chen, Duanbin Li, Hangpan Jiang, Tianli Hu, Yecheng Tao, Changqing Du and Wenbin Zhang
- 304 **Short-term echocardiographic follow-up after hospitalization for COVID-19: a focus on early post-acute changes**
Oleksii Honchar and Tetiana Ashcheulova
- 315 **Anomalous papillary muscle insertion into the mitral valve leaflet in hypertrophic obstructive cardiomyopathy: a lip nevus sign in echocardiography**
Jian Liu, Tong Tan, Peijian Wei, Jianrui Ma, Lishan Zhong, Hailong Qiu, Shengwen Wang, Jian Zhuang, Wei Zhu, Huiming Guo and Jimei Chen
- 322 **Prevalence, sex differences, and implications of pulmonary hypertension in patients with apical hypertrophic cardiomyopathy**
Vidhu Anand, Megan K. Covington, Ushasi Saraswati, Christopher G. Scott, Alexander T. Lee, Robert P. Frantz, Nandan S. Anavekar, Jeffrey B. Geske, Adelaide M. Arruda-Olson and Kyle W. Klarich
- 330 **Features of trastuzumab-related cardiac dysfunction: deformation analysis outside left ventricular global longitudinal strain**
Giang M. Nhat, Nguyen H. Hai, Vo T. Duc, Ho H. Q. Tri and Chau N. Hoa
- 338 **Characteristics of patients with newly diagnosed hematological malignancies referred for echocardiography**
Jarosław Kępski, Sebastian Szmit and Ewa Lech-Marańda



OPEN ACCESS

EDITED AND REVIEWED BY
Sebastian Kelle,
German Heart Center Berlin, Germany

*CORRESPONDENCE
Sanjeev Bhattacharyya
✉ sanjeev.bhattacharyya@nhs.net

RECEIVED 02 May 2024
ACCEPTED 13 May 2024
PUBLISHED 21 May 2024

CITATION
Bhattacharyya S and Innocenti F (2024)
Editorial: Echocardiography in cardiovascular
medicine.
Front. Cardiovasc. Med. 11:1427059.
doi: 10.3389/fcvm.2024.1427059

COPYRIGHT
© 2024 Bhattacharyya and Innocenti. This is
an open-access article distributed under the
terms of the [Creative Commons Attribution
License \(CC BY\)](#). The use, distribution or
reproduction in other forums is permitted,
provided the original author(s) and the
copyright owner(s) are credited and that the
original publication in this journal is cited, in
accordance with accepted academic practice.
No use, distribution or reproduction is
permitted which does not comply with
these terms.

Editorial: Echocardiography in cardiovascular medicine

Sanjeev Bhattacharyya^{1,2*} and Francesca Innocenti³

¹Echocardiography Laboratory, St Bartholomew's Hospital, London, United Kingdom,
²Echocardiography Laboratory, Cleveland Clinic London, London, United Kingdom, ³High-Dependency
Unit, Department of Clinical and Experimental Medicine, Careggi University Hospital, Florence, Italy

KEYWORDS

echocardiography, contrast, strain, artificial intelligence, three-dimensional

Editorial on the Research Topic Echocardiography in cardiovascular medicine

Echocardiography is one of the most versatile, non-invasive cardiac imaging modalities that facilitates accurate diagnosis, risk stratification, and guidance of therapy in every cardiovascular disease. The modality has evolved over several decades and encompasses a range of different techniques including deformation, contrast, and three-dimensional imaging as well as stress echocardiography and transoesophageal echocardiography. In this research topic, manuscripts have demonstrated both the breadth and depth of echocardiography in advancing our understanding of cardiovascular disease.

Identification of cardiac masses and distinguishing between non-malignant masses (thrombi, pseudo-tumours) and benign or malignant tumours is important. The diagnosis relies on a combination of clinical history, location of mass, and characteristics including mobility, morphology, whether the mass crossed tissues planes and the presence of pericardial effusion. Other modalities including positron emission tomography and cardiac magnetic resonance often provide complementary information. In certain cases, invasive biopsy is required. [Li et al.](#) show how using contrast enhanced echocardiography assessed using a quantitative approach (the ratio of peak contrast intensity of the mass compared to adjacent myocardium) can help differentiate between avascular thrombus (ratio close to zero) and malignant cardiac tumours (ratio > 1). Although the evidence base for contrast is strong, contrast is underutilised ([1](#)). Incorporation of contrast into routine echocardiographic practice for characterisation of cardiac masses should be encouraged as it can be performed rapidly and may result in less downstream testing if the result is conclusive.

Another area, which is gaining an increasing space in echocardiographic evaluation, is the employment of parameters of myocardial contractility. Conventional echocardiographic parameters, such as left ventricular ejection fraction (LVEF), maintain a definite diagnostic and prognostic value. They provide information on chamber performance, however they are highly dependent on pre- and afterload. Therefore, in the presence of diseases, like sepsis, where the loading conditions are altered, LVEF may be falsely normal, while myocardial contractility is depressed ([Bagate et al.](#), [Nhat et al.](#)). From this point of view, strain echocardiography appears to be a promising tool, as it requires a limited set of images evaluated during a standard echocardiographic assessment. It provides incremental diagnostic and prognostic roles, especially in the presence of a normal LVEF, where a subtle impairment of myocardial function may evolve and influence the outcome. In this situation, an early diagnosis

could help identifying patients at risk of unfavourable evolution (Aboukhouidir et al., Lu et al., Schellenberg et al.). The analysis of the strain rate was applied on LV as well as right ventricle (RV) and left atrium (Mao et al.) by different authors who participated in the Research Topic. The analysis of RV systolic function is limited in conventional echocardiography, but its contribution to the prognostic assessment, in the presence of ischemic or valvular disease, is relevant. Winkler et al. showed that in patients undergoing transcatheter aortic valve implantation, a depressed RV global longitudinal strain was independently associated with an increased mortality. The evaluation of RV by strain echocardiography is actually confined to the research area, but we hope that in a near future, it could become widely available, as already happens for the LV. Nemes et al., showed three-dimensional speckle tracking can be used to map the tricuspid annulus and quantify right atrial function. The insights may help us understand the mechanisms of tricuspid valve disease.

Apical hypertrophic cardiomyopathy (HCM) characterised by hypertrophy localised to the left ventricular apex has a very variable clinical presentation. Anand et al. examined the prevalence and risk markers of pulmonary hypertension (estimated pulmonary artery systolic pressure > 36 mmHg) in a cohort of 542 patients with apical HCM at Mayo Clinic. They identified pulmonary hypertension was present in 34% of the cohort. Risk factors associated with pulmonary hypertension were female sex, atrial fibrillation, congestive heart failure and elevated filling pressure on echocardiography. The presence of pulmonary hypertension was associated with increased mortality. This knowledge may help better risk stratify patients with apical HCM. This will be important if therapeutic agents in apical HCM are identified in the future.

Artificial Intelligence (AI) is increasingly having an impact in all aspects of echocardiography from acquisition, detection of views, auto-measurement and quantification and more recently diagnosis of pathology. View classification is one of the first steps required for analysis of images. Most works showing the ability of convolutional neural networks to classify views has focussed on non-contrast images. Contrast enhanced echocardiography is often used in clinical practice to improve accuracy of left ventricular ejection fraction quantification. Zhu et al. showed a convolutional neural network can accurately classify both contrast-enhanced and non-contrast views. During the first wave of the COVID pandemic, emergency limited echocardiographic protocols were created to reduced exposure to COVID patients. Pellikka et al. examined the feasibility of incorporating automated AI analysis into these studies. In clinical reports, left

ventricular ejection fraction (LVEF) was most commonly visually estimated (39%) and not quoted in 5%. Application of the AI with automated analysis of ejection fraction and longitudinal strain was feasible in 87% patients. In addition to improving the proportion of LVEF quantified, the AI quantified parameters were associated with outcomes. This study highlights how AI automated analysis can be used as a tool to improve quantification in echocardiography. Furthermore, Cheng et al. used a deep learning method to identify and grade the size pericardial effusion. These studies show the incremental progress being made in the field to improve workflow and quantification of pathology.

Echocardiography is the most widely used cardiovascular imaging modality. The topic has shown how echocardiography can be utilised in a range of different ways from a focussed study to a more comprehensive evaluation including strain, three-dimensional echocardiography or the employment of contrast medium. Appropriate training in conjunction with standard protocols for image acquisition and image processing are essential. However, artificial intelligence can be used as a tool to increase reproducibility and accuracy.

Author contributions

SB: Writing – original draft, Writing – review & editing. FI: Writing – original draft, Writing – review & editing.

Conflict of interest

The authors declare that the research was conducted in the absence of any commercial or financial relationships that could be construed as a potential conflict of interest.

The author(s) declared that they were an editorial board member of Frontiers, at the time of submission. This had no impact on the peer review process and the final decision.

Publisher's note

All claims expressed in this article are solely those of the authors and do not necessarily represent those of their affiliated organizations, or those of the publisher, the editors and the reviewers. Any product that may be evaluated in this article, or claim that may be made by its manufacturer, is not guaranteed or endorsed by the publisher.

Reference

1. Bhattacharyya S, Khattar R, Lloyd G, Senior R, Echocardiography BS. Implementation of echocardiographic contrast agents into clinical practice: a United Kingdom National Health Service Survey on behalf of the British Society of Echocardiography. *Eur Heart J-Card Img.* (2013) 14(6):550–4. doi: 10.1093/ehjci/jes212



Necropsy Validation of a Novel Method for Left Ventricular Mass Quantification in Porcine Transthoracic and Transdiaphragmal Echocardiography

Charlotte Burup Kristensen^{1*}, Stefan Michael Sattler^{1,2}, Anni Frederike Lubberding², Jacob Tfelt-Hansen^{1,3}, Thomas Jespersen², Christian Hassager^{1,4} and Rasmus Mogelvang^{1,4,5}

OPEN ACCESS

Edited by:

Leonid Goubergrits,
Charité Universitätsmedizin
Berlin, Germany

Reviewed by:

Christoph Sinning,
University Medical Center
Hamburg-Eppendorf, Germany
Ythan Goldberg,
Albert Einstein College of Medicine,
United States

*Correspondence:

Charlotte Burup Kristensen
charlotte.burup.kristensen@regionh.dk

Specialty section:

This article was submitted to
Cardiovascular Imaging,
a section of the journal
Frontiers in Cardiovascular Medicine

Received: 03 February 2022

Accepted: 31 March 2022

Published: 03 May 2022

Citation:

Kristensen CB, Sattler SM,
Lubberding AF, Tfelt-Hansen J,
Jespersen T, Hassager C and
Mogelvang R (2022) Necropsy
Validation of a Novel Method for Left
Ventricular Mass Quantification in
Porcine Transthoracic and
Transdiaphragmal Echocardiography.
Front. Cardiovasc. Med. 9:868603.
doi: 10.3389/fcvm.2022.868603

¹ Department of Cardiology, The Heart Center Rigshospitalet, Copenhagen, Denmark, ² Department of Biomedical Sciences, Faculty of Health and Medical Sciences, University of Copenhagen, Copenhagen, Denmark, ³ Department of Forensic Genetics, Faculty of Health and Medical Sciences, University of Copenhagen, Copenhagen, Denmark, ⁴ Department of Clinical Medicine, Faculty of Health and Medical Sciences, University of Copenhagen, Copenhagen, Denmark, ⁵ Cardiovascular Research Unit, University of Southern Denmark, Svendborg, Denmark

Introduction: Increased left ventricular mass (LVM) is one of the most powerful predictors of adverse cardiovascular events. Clinical evaluation requires reliable, accurate and reproducible echocardiographic LVM-quantification to manage patients. For this purpose, we have developed a novel two-dimensional (2D) method based on adding the mean wall thickness to the left ventricular volume acquired by the biplane method of disks, which has recently been validated in humans using cardiac magnetic resonance as reference value. We assessed the hypothesis that the novel method has better accuracy than conventional one-dimensional (1D) methods, when compared to necropsy LVM in pigs.

Materials and Methods: Echocardiography was performed during anesthesia in 34 Danish Landrace pigs, weight 47–59 kg. All pigs were euthanized, cardiac necropsy was performed and the left ventricle was trimmed and weighed for necropsy LVM. Trans-thoracic echocardiography was applied for parasternal images. Transdiaphragmal echocardiography was applied for the apical images, which are otherwise difficult to obtain in pigs. We compared the conventional 1D- and 2D-methods and the novel 2D-method to the LVM from cardiac necropsy.

Results: Necropsy LVM was 132 ± 11 g (mean \pm SD). The novel method had better accuracy than other methods (mean difference \pm 95% limits of agreement; coefficients of variation; standard error of the estimate, Pearson's correlation). Novel (-1 ± 20 g; 8%; 11 g; $r = 0.70$), Devereux ($+26 \pm 37$ g; 15%; 33 g; $r = 0.52$), Area-Length ($+27 \pm 34$ g; 13 %; 33 g; $r = 0.63$), Truncated Ellipsoid ($+10 \pm 30$ g; 12%; 19 g; $r = 0.63$),

biplane endo-/epicardial tracing (-3 ± 2 g; 10%; 14 g; $r = 0.57$). No proportional bias in linear regression was detected for any method, when compared to necropsy LVM.

Conclusion: We confirm high accuracy of the novel 2D-based method compared to conventional 1D/2D-methods.

Keywords: left ventricular mass, echocardiography, left ventricular hypertrophy, necropsy, animal model

INTRODUCTION

Increased left ventricular mass (LVM) is a well-known strong and independent predictor of adverse cardiovascular events and sudden death (1–4). The natural adaptive mechanisms of almost every cardiac condition are reflected in the degree of left ventricular (LV) hypertrophy. Increased LVM is associated with LV fibrosis (5) and reduction in LVM by blood pressure management (6) or valvular surgery (7) is associated with better outcome (6). For this reason, LVM has the potential to be used as a prognostic marker to detect clinical deterioration and may facilitate decision making for clinicians. Unfortunately, recommended conventional one-dimensional (1D) linear echocardiographic methods are less accurate and not suited for individual usage (8). Consequently, LVM quantification is often not performed or ignored and not included in the individual clinical decision-making.

We have recently presented a novel two-dimensional (2D) method based on adding the mean wall thickness to the left ventricular volume acquired by the biplane method of disks (9). The method is validated in humans using cardiac magnetic resonance (CMR) as gold standard. Furthermore, it is simpler but still as accurate as three-dimensional (3D) echocardiography and compared to the other 1D/2D/3D-methods it performs better regardless of LV geometry. The novel 2D-based method also demonstrated better reproducibility compared to the other methods, which is necessary for detection of small differences that may indicate early signs of deterioration.

Our aim was to assess whether the novel method has better accuracy than conventional 1D methods, when compared to necropsy LVM in pigs.

MATERIALS AND METHODS

Study Population

We included thirty-four female Danish Landrace pigs, weight range 47–59 kg. All pigs were part of a project investigating arrhythmias during myocardial infarction and echocardiography was performed as part of the protocol (10, 11). The experiments were performed under the animal license number (2015-15-0201-00613) authorized by the Danish Animal Inspectorate in accordance with EU legislations for animal protection and care.

Procedure

The pigs were premedicated, intubated and ventilated and anesthesia was maintained with continuous propofol infusion of 12.5 mg/h/kg (Propolipid 10 mg/ml, Fresenius Kabi AB, Uppsala, Sweden) and fentanyl 5 µg/h/kg (Fentanyl-Hameln 50 µg/ml, Hameln, Germany). Echocardiography was performed

at baseline after placing a pulmonary artery catheter but before any other intervention. As part of the initial protocols, myocardial infarction was induced by balloon occlusion of the left anterior descending (LAD) artery just after the take-off of the first diagonal (D1) branch for 60–120 min and electrophysiological outcomes were studied. Pigs were euthanized at the end of the procedure by inducing ventricular fibrillation (VF) *via* burst pacing (50 Hz, 3 s, 7 V output) and cardiac necropsy was performed minutes after.

Echocardiographic Acquisition and Analysis

Echocardiographic examinations were performed using an iE33 Echocardiography System scanner (Philips Medical Systems Netherlands B.V., Best, The Netherlands) with the pigs in supine position. The protocol for echocardiographic assessment included four views; the parasternal long-axis view (PLAX), the parasternal short-axis view (PSAX), the apical four-chamber view (A4CH) and the apical two-chamber view (A2CH). PLAX and PSAX were acquired by trans-thoracic echocardiography (TTE) using the S5-1-xMATRIX array transducer (1–5 MHz). A4CH and A2CH were acquired by trans-diaphragmal echocardiography (TDE) (**Figure 1**) through a small midline incision distal of the sternal xiphoid (12). The TDE approach was necessary to achieve appropriate images as the heart is aligned differently in the thorax of pigs compared to humans (13). For the apical views we used the Pediatric X7-2-xMATRIX array transducer (2–7 MHz) and because of limited space in the acoustic window we applied electronic rotation function *iRotate*, instead of physical rotation of the probe. All images were transferred as Digital Imaging and Communications in Medicine (DICOM) files to a local workstation and analyzed using the software EchoPAC Version: 203 Revision: 66.0 (GE Healthcare Vingmed Ultrasound, Horten, Norway). End-diastole was defined as the first frame with closure of the mitral valve. End-systole was defined as the frame with the smallest LV volume. End-diastolic volume (EDV), end-systolic volume (ESV) and left ventricular ejection fraction (LVEF) was evaluated by the 1D Teichholtz method (14) and by the 2D biplane methods of disks (8). We evaluated five different methods for LVM quantification, all presented in **Table 1**. All LVM-measurements were made at end-diastole. The electrocardiogram (ECG) was applied as reference in PLAX to find the corresponding frame in PSAX, where the mitral valve is not fully visible. Three of the methods; Devereux (15), Truncated Ellipsoid (TE) (16) and Area-Length (A-L) (17) are well-recognized and described in the current echocardiographic guidelines (8). For the biplane tracing of the endo- and epicardium we traced both the endo-

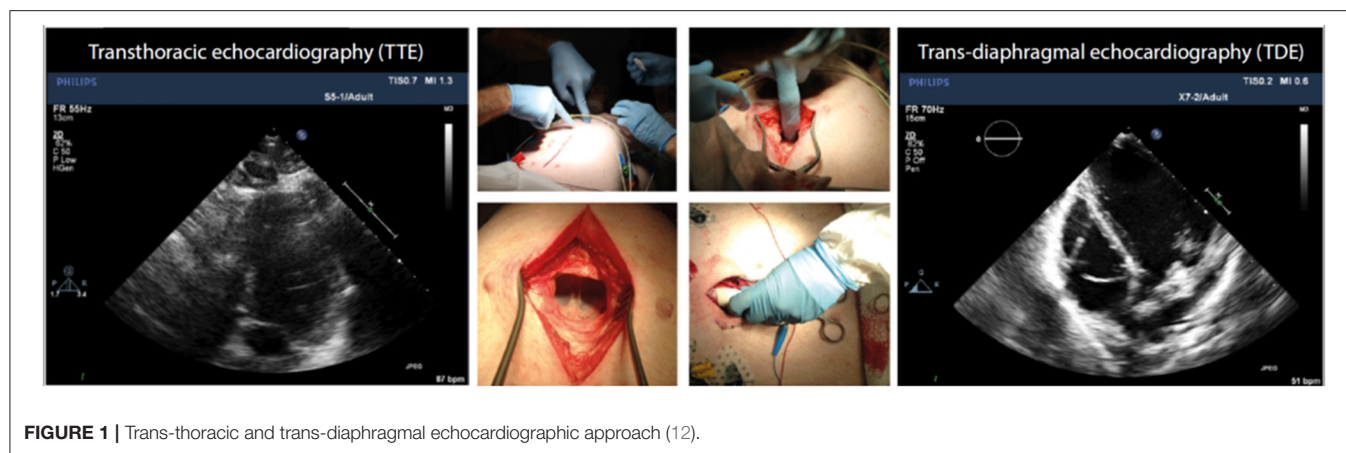


FIGURE 1 | Trans-thoracic and trans-diaphragmal echocardiographic approach (12).

TABLE 1 | Methods for left ventricular mass quantification.

Method type	Method name	TTE	TDE
1D	Devereux	PLAX	–
2D	Truncated Ellipsoid	PSAX	AP4CH
2D	Area-Length	PSAX	AP4CH
2D	Biplane tracing of the endo- and epicardium	–	AP4CH + AP2CH
2D	Novel	PSAX	AP4CH + AP2CH

TTE, trans-thoracic echocardiography; TDE, trans-diaphragmal echocardiography; 1D, one-dimensional; 2D, two-dimensional; PLAX, parasternal long-axis; PSAX, parasternal short-axis; AP4CH, apical four-chamber; AP2CH apical two-chamber.

and the epicardium, subtracted the inner volume (tracing of the endocardium) with the outer volume (tracing of the epicardium) to achieve the myocardial volume. The novel method (Figure 2) recently described (9) is validated in humans using CMR. The method adds the LV wall thickness from PSAX to EDV acquired by tracing of the endocardium in the biplane model, i.e., no tracing of the epicardium is necessary. The myocardial density/gravity of 1.05 g/ml was applied to convert myocardial volume to LVM. All measurements were performed by one reader (CK). Intra-reader analysis was performed by the same reader (CK) on same recordings and compared to the baseline measurements. Inter-reader analysis was performed by another reader (SS) on the same recordings and compared to the baseline measurements. For intra/inter-reader variability we only included pigs who had feasible measurements for all methods.

Necropsy

At the end of the experiment, ~10 min after VF was induced, a midline sternotomy was performed, the pericardium was removed and the heart including both ventricles and atria was explanted. If present, epicardial fat (which in general is scarce in young, lean pigs) and soft tissue was removed, and total heart weight measured. For measuring LVM the free wall of the right ventricle as well as valves, atria, papillary muscles and blood clots were removed. We used a commonly available digital scale

(Wedo Electronic Precision Scale Optimo 1000, Werner Dorsch GmbH, Dieburg, Germany).

Statistics

Statistical data analysis was performed in SPSS v25.0 (IBM Corp. IBM SPSS Statistics for Windows, Version 25.0. Armonk, NY). LVM-quantifications were performed in Windows Excel 2010 (Microsoft Office Professional Plus). Continuous variables expressed as mean and standard deviation (SD) and categorical values expressed as frequencies and percentage. Correlation was evaluated using Pearson's *r*. The accuracy was evaluated by paired *t*-test and presented as mean difference (bias) and 95% limits of agreement (LOA). The variations were expressed as the standard error of the estimate (SEE) and as coefficients of variation (CV) in percent and we adjusted the CV according to the anatomical LVM from necropsy. In the same manner we plotted the differences according to necropsy LVM. We decided to use this approach because we considered the necropsy LVM as the true value and not a method for comparison. Proportional bias was evaluated by linear regression with the necropsy LVM as independent variable and mean difference as dependent variable. Intra- and inter-reader variability was expressed as bias, LOA, SEE and CV compared to the baseline measurements. *P*-values <0.05 were considered statistically significant.

RESULTS

The baseline characteristics for the pigs are presented in Table 2. The total mass of the hearts by necropsy ranged from 200 to 295 g and the necropsy LVM ranged from 110 to 155 g. The hearts were relatively uniform in geometry and no pig had significant valve disease. Induced infarcts affected 15–20% of LV by visual inspection. LVEF by the biplane model of disks was $62 \pm 6\%$ (mean \pm SD) and ranged from 47 to 74%.

Figure 3 demonstrated the mean difference between the quantified LVM and the necropsy LVM (y-axis) according to the necropsy LVM (x-axis) (left panel) and correlation for LVM quantified by echocardiography (y-axis) according to necropsy LVM (x-axis) (right panel) for the various methods for the whole population. The novel model presented the lowest mean

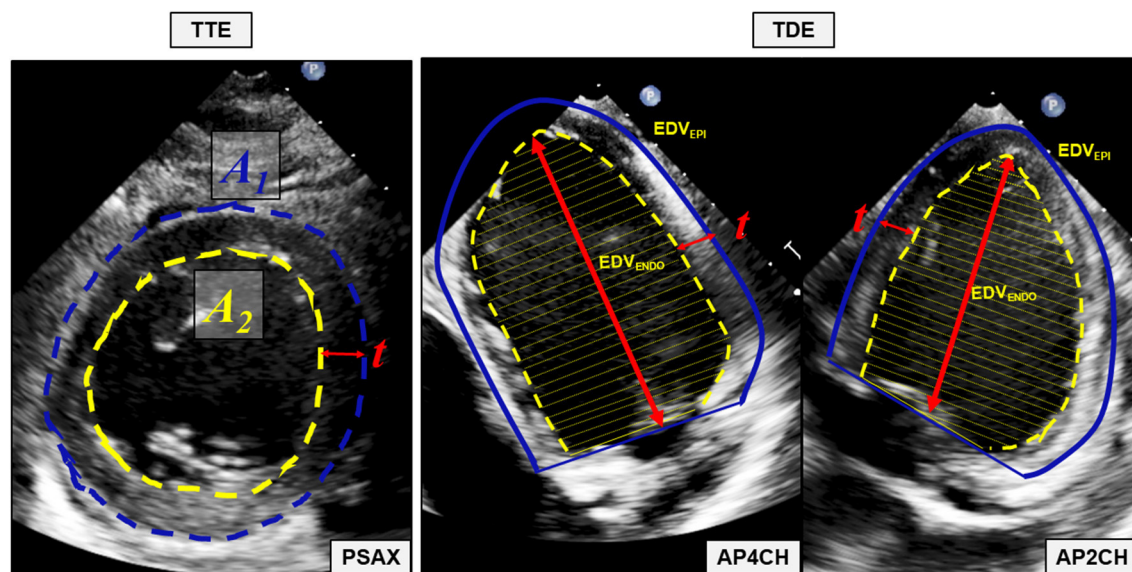


FIGURE 2 | The novel 2D-based echocardiographic method for quantification of left ventricular mass. Mean wall thickness (t) is calculated by tracing of the endocardium (A_2) and the epicardium (A_1) in the parasternal short axis (PSAX) view. The left ventricular volume defined by the endocardium (EDV_{ENDO}) is acquired using the biplane methods of disks with tracings of the endocardium in the apical four chamber (AP4CH) and apical two-chamber (AP2CH) view. Mean wall thickness (t) is added to each unique disk and a new volume, the left ventricular volume defined by the defined by the epicardium (EDV_{EPI}) is quantified. Myocardial volume is calculated by subtracting EDV_{ENDO} from EDV_{EPI} and left ventricular mass is quantified by multiplying the myocardial volume with the myocardial density/gravity of 1.05 g/ml. **TTE** transthoracic echocardiography, **TDE**, transdiaphragmatic echocardiography; **PSAX**, parasternal short axis view; **A₁**, Area defined by the epicardium; **A₂**, Area defined by the endocardium; **t**, mean wall thickness; **AP4CH**, apical four chamber view; **EDV_{ENDO}**, the left ventricular volume defined by the endocardium; **EDV_{EPI}**, the left ventricular volume defined by the epicardium; **AP2CH**, apical two-chamber view.

TABLE 2 | Baseline characteristics.

	Mean \pm SD	Range
Pig weight (kg)	52 \pm 2	47–59
Total heart weight by necropsy (g)	241 \pm 22	200–295
Necropsy LVM (g)	132 \pm 11	110–155
SBP (mmHg)	131 \pm 16	88–169
DBP (mmHg)	82 \pm 15	41–113
Heart rate (bpm)	81 \pm 15	50–113
MWTd PLAX (cm)	0.93 \pm 0.08	0.8–1.2
MWTd PSAX (cm)	0.97 \pm 0.08	0.8–1.2
LVIDd (cm)	4.8 \pm 0.3	4.4–5.4
LVIDs (cm)	3.2 \pm 0.4	2.7–4.0
EDV Teichholtz (ml)	110 \pm 14	89–141
EDV Biplane (ml)	97 \pm 18	71–130
ESV Teichholtz (ml)	42 \pm 12	27–71
ESV Biplane (ml)	37 \pm 9	22–56
LVEF Teichholtz (ml)	61 \pm 10	38–77
LVEF Biplane (ml)	62 \pm 6	47–74

SD, standard deviation; LVM, left ventricular mass; SBP, systolic blood pressure; DBP, diastolic blood pressure; MWTd, mean wall thickness diastole; PLAX, parasternal long-axis; PSAX, parasternal short-axis; LVIDd, left ventricular internal diameter diastole; LVIDs, left ventricular internal diameter systole; EDV, end-diastolic volume; ESV, end-systolic volume; LVEF, left ventricular ejection fraction.

difference and the smallest variation than any of the other methods; CV was 8% compared to 10–13% for the other

2D-methods and 15% for the cube formula by Devereux. No method presented significant proportional bias in linear regression. The novel method had the best correlation to necropsy LVM; Pearson's $r = 0.70$, $p < 0.001$ followed by A-L and TE, both $r = 0.63$, $p < 0.001$. The results for all pigs ($n = 34$) are also presented in Table 3A.

We performed a subgroup analysis of the pigs where it was possible to quantify LVM by all echocardiographic methods ($n = 21$). The results for this subgroup are presented in Table 3B. The percentual difference between echocardiographic LVM and necropsy LVM was plotted in the y-axis for each pig (Figure 4). The novel method was the most accurate method for 11 (52%) of the pigs, followed by TE and biplane tracing of the endo-/epicardium, both 4 (19%) of the pigs, respectively. Devereux was the least accurate method for 10 (48%) pigs followed by A-L for 7 (33%) of the pigs.

Intra- and inter-reader variability is presented in Table 4 and we observe similar reproducibility as compared to the other 1D- and 2D-methods.

DISCUSSION

We demonstrate the accuracy of various echocardiographic methods for LVM-quantification in a porcine model with necropsy LVM as reference for LVM. The novelty of our approach is the study design combining necropsy validation with a novel echocardiographic method and

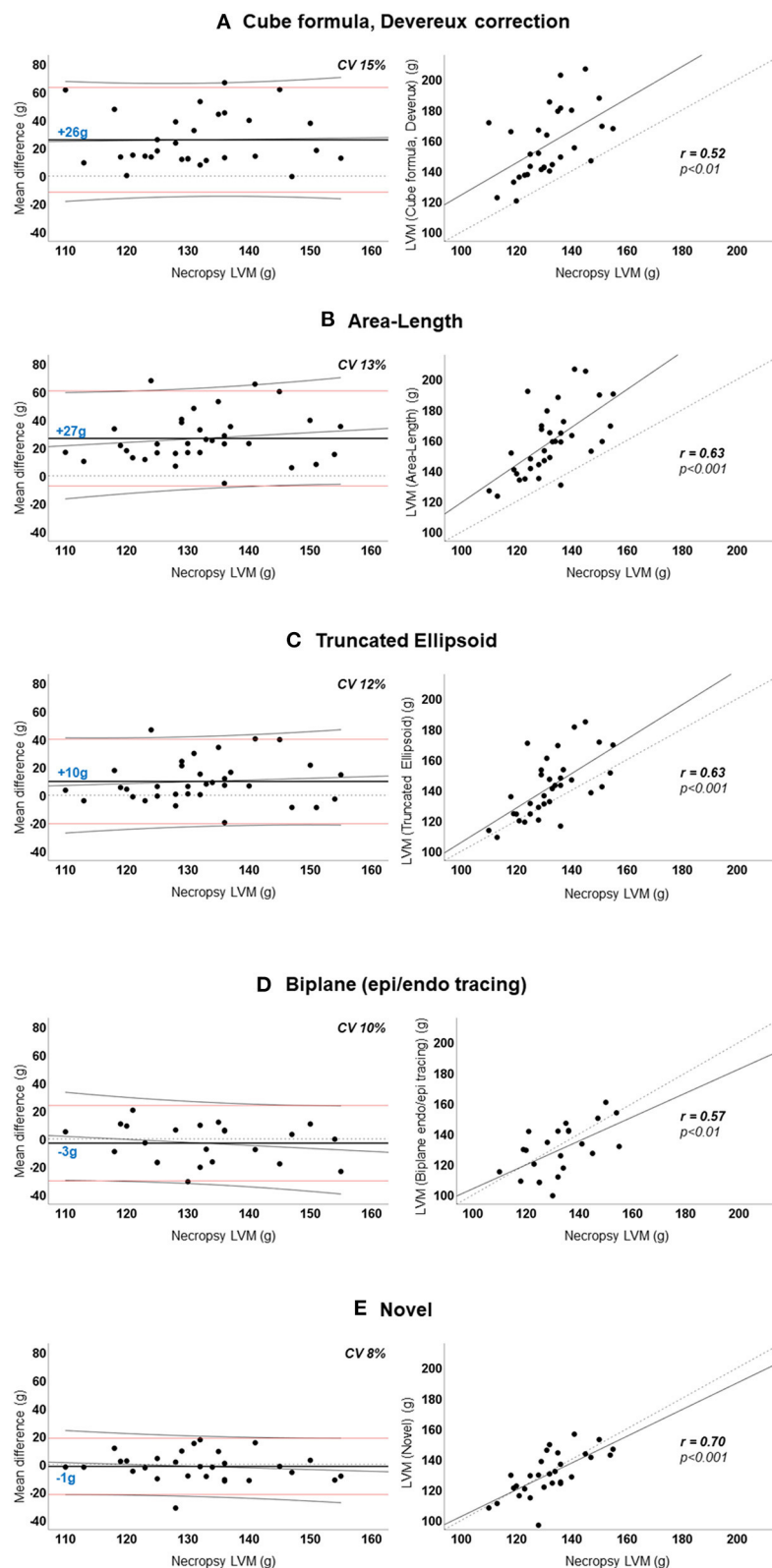


FIGURE 3 | (A–E) Agreement between echocardiographic left ventricular mass and necropsy left ventricular mass. *Left panel:* Agreement between mean difference (echocardiographic-LVM – necropsy-LVM) and necropsy-LVM. Horizontal dotted black line indicates 0 (no difference). Horizontal solid black line and blue number is the mean difference; positive value indicates overestimation by echocardiography. Horizontal red lines are the 95% limits of agreement. Diagonal thin black line is the regression line with 95% confidence interval visualizing the proportional bias. *Right panel:* Linear regression curves of echocardiographic-LVM and necropsy-LVM with Pearson's correlation coefficient (r). Diagonal dotted line is the reference line. **LVM**, left ventricular mass; **CV**, coefficient of variation.

TABLE 3A | Accuracy of various methods for left ventricular mass quantification among all pigs ($n = 34$).

	Mean \pm SD (g)	Bias* \pm 95%LOA (g)	CV (%)	SEE (g)	Pearson's	
					r	p
Necropsy left ventricular mass	132 \pm 11					
Devereux	157 \pm 22	+26 \pm 37	15	33	0.52	<0.01
Area-Length	159 \pm 22	+27 \pm 34	13	33	0.63	<0.001
Truncated Ellipsoid	142 \pm 20	+10 \pm 30	12	19	0.63	<0.001
Biplane tracing of the endo-/epicardium	130 \pm 16	-3 \pm 27	10	14	0.57	<0.01
Novel	131 \pm 14	-1 \pm 20	8	11	0.70	<0.001

Accuracy evaluated with necropsy left ventricular mass as reference value. SD, standard deviation, bias mean difference; LOA, limits of agreement; CV, coefficients of variation; SEE, standard error of the estimate; r, Pearson's correlation coefficient.

*Positive value indicates overestimation of left ventricular mass by echocardiography compared to left ventricular mass by necropsy.

TABLE 3B | Accuracy of various methods for left ventricular mass quantification among the pigs with 100% feasible measurements ($n = 21$).

	Mean \pm SD (g)	Bias* \pm 95%LOA (g)	CV (%)	SEE (g)	Pearson's	
					r	p
Necropsy left ventricular mass	131 \pm 12					
Devereux	159 \pm 24	+28 \pm 42	16	37	0.46	<0.05
Area-Length	159 \pm 24	+27 \pm 32	12	33	0.80	<0.001
Truncated Ellipsoid	142 \pm 22	+10 \pm 28	11	18	0.81	<0.001
Biplane tracing of the endo-/epicardium	129 \pm 16	-3 \pm 28	11	15	0.53	<0.05
Novel	132 \pm 14	0 \pm 16	6	8	0.80	<0.001

Accuracy evaluated with necropsy left ventricular mass as reference value. SD, standard deviation, bias mean difference; LOA, limits of agreement; CV, coefficients of variation; SEE, standard error of the estimate; r, Pearson's correlation coefficient.

*Positive value indicates overestimation of left ventricular mass by echocardiography compared to left ventricular mass by necropsy.

improved imaging tools. The most important findings are the following:

- 1) The novel method for LVM-quantification is characterized by higher accuracy to LVM by necropsy and at least as good reproducibility as for the other 1D- and 2D-methods.
- 2) The conventional linear method by Devereux, which is recommended by current guidelines (8), overestimates LVM and demonstrates lower accuracy compared to the other methods.
- 3) We highlight an alternative way to increase echocardiographic apical image quality in animal models, by applying a trans-diaphragmatic approach and by applying the function *iRotate* since correct physical rotation of the probe may be difficult.

Comparison to Previous Necropsy Validation Studies

Most studies with necropsy comparisons are published several decades ago and are naturally based on M-mode without 2D-guiding, or by less refined 2D echocardiographic technology. In 1979 Wyatt et al. (17) demonstrated better correlation and lower mean errors deploying 2D methods compared to linear methods and Salcedo et al. (18) demonstrated improved accuracy using 2D-methods. In 1986 Schiller et al. (19) confirmed high correlation and low SEE using 2D-methods. Two other studies

by Woythaler et al. (20) in 1983 and Park et al. (21) in 1996 could not illustrate any improvement in 2D-methods compared to linear methods. On the contrary, some studies demonstrate excellent accuracy of linear methods among subjects with normal LV geometry (22, 23) and some studies unsatisfactory accuracy despite normal LV geometry (24). A direct comparison to these studies may be misleading compared to current imaging technology and improved post-processing software. A recent study by Miyashita et al. (25) validating LVM to necropsy values in pigs, demonstrates overestimation of LVM using linear methods as 2D-guided M-mode, in particular among the pigs with ischemic heart disease and LV dilatation. The same study also demonstrates a much narrower LOA using 2D-methods, which is in line with our results. The strength of our study compared to previous necropsy validation studies is that we have examined a variety of different methods on the same population, which makes it easier to compare the methods with each other instead of one-by-one in different populations.

Aspects of Necropsy Validation as Reference for Left Ventricular Mass

What is the true value of LVM and how can it be measured? Previous studies have applied angiography, direct linear measures or echocardiography to validate LVM against cardiac autopsy in human models (15, 16, 20–24, 26–28) or cardiac necropsy in animal models (17–19, 29). Our validation

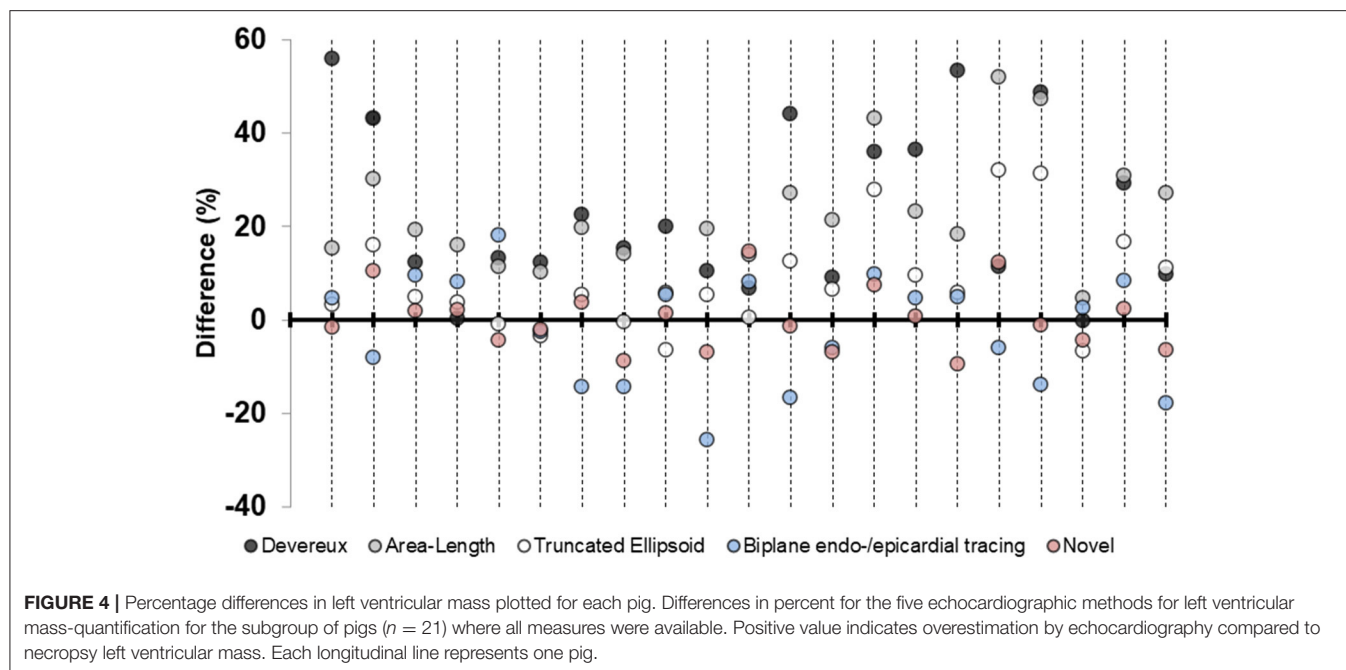


TABLE 4 | Precision (reproducibility) of the various methods for left ventricular mass quantification among the pigs where all measures were available ($n = 21$).

	Intra-reader variation			Inter-reader variation		
	Bias* \pm 95%LOA (g)	CV (%)	SEE (g)	Bias* \pm 95%LOA (g)	CV (%)	SEE (g)
Devereux	9 \pm 37	11.4	21.2	5 \pm 32	10.0	17.4
Area-Length	0 \pm 28	9.1	14.9	-10 \pm 30	9.9	18.9
Truncated Ellipsoid	0 \pm 25	8.9	13.0	-8 \pm 26	9.8	16.3
Biplane tracing of the endo-/epicardium	-5 \pm 23	9.2	13.0	-8 \pm 21	8.8	13.9
Novel	3 \pm 23	8.7	12.2	-9 \pm 22	8.7	14.5

SD, standard deviation, bias mean difference; LOA, limits of agreement; CV, coefficients of variation; SEE, standard error of the estimate; r , Pearson's correlation coefficient.

* Positive value indicates overestimation by intra- or inter-reader measurements.

methodology was to explant the heart of the pig immediately postmortem and to isolate the LV without papillary muscles and without any preservation. There are several aspects to consider when validating to the anatomical LVM by autopsy/necropsy. These are:

- 1) *The time between measurement and actual autopsy/necropsy.* Validation studies to human autopsy are usually limited by increased time duration between measurement and actual autopsy, whereas animal studies are usually validated at the same day, or at least preserved at the same day as the measurement by echocardiography was made. Human studies report durations of up to 454 days (28) between echocardiography and autopsy. As we performed necropsy immediately postmortem and at the same day as echocardiographic assessment, we were less limited by potential changes of the LV that may occur over time.
- 2) *The preservation methodology.* Formaldehyde or the aqueous solution of formaldehyde, also known as formalin, have often been applied as preservation methodology. This approach is reported to reduce LVM and volume without significant impact on myocardial density (30–32), whereas some studies

report increased LVM after preservation (33). To overcome this potential limitation, several studies report adjustment of shrinkage by adding 5% to autopsy/necropsy LVM (23) or adjustment of increase by reducing autopsy/necropsy LVM by 2–3% (33). However, no adjustment at all (16, 24) is also reported. We did not use any preservation methodology and did not apply any adjustment to the weighed necropsy LVM.

- 3) *The autopsy/necropsy methodology.* Most studies report similar autopsy/necropsy methodology with removal of atria, right ventricle, epicardial fat and valves inspired by Geiser and Bove (16). In contrast to previous reports, we removed the papillary muscles from the myocardium. We claim that this approach is most truthful since the papillary muscles are excluded when LVM is measured by both echocardiography and CMR (9). We washed the hearts and removed visual blood clots and although we were very thorough, there may still be small clots left in the trabeculae or inside the vessels of the heart. The significance of this small amount of blood is probably negligible.
- 4) *Inhibition of the cardiac cycle in diastole or systole.* Cardiac arrest and eventually cardiac death was initiated by induced

VF and consequently, most hearts were inhibited contracted, i.e., in systole. Inhibition in systole or diastole has impact on the volumes of the heart but should not affect the LVM significantly (16). This may even have minimized the effect of potential blood left in the vessels of the heart.

- 5) *Edema or fibrosis affecting the density/gravity of the LV.* Edema may be present in the ischemic region of the LV but also to some degree in adjacent and remote areas (34). During myocardial infarction, the density of the myocardium increases during initial edema and remains slightly higher after transition to fibrotic tissue compared to healthy myocardium (32). The pigs in our study were part of a protocol where myocardial infarction was induced by balloon occlusion of the LAD, which may have affected the density of the myocardium. Infarct sizes were determined to be within 15–20% of the LV myocardial mass.

Necropsy Compared to Gold Standard Cardiac Magnetic Resonance

Necropsy validation has gradually been replaced by imaging modalities such as CMR, which is now considered the gold standard or reference method for left ventricular mass (35, 36). Excellent agreement between LVM by necropsy and by CMR-segmentation has been reported (37–40). Studies using CMR as reference method report overestimation of LVM by linear methods (41, 42) and better agreement for the 2D-methods (43). We Kristensen et al. (9) have demonstrated similar overestimation for the 1D-methods and better agreement for 2D-methods, especially the novel method. Also, reproducibility from the whole cohort and accuracy of the patients with normal geometry were very similar to the accuracy for the pigs in this cohort, which all had normal geometry as well.

The Porcine and the Human Heart

The porcine heart is aligned differently in the thoracic cage compared to the human heart (13). In humans, the upright orientation of the body and the location of the heart in the thoracic cage, gives the heart a “trapezoidal shape” with its apex pointing downward to the left with an oblique angle to the long axis of the body. Since pigs walk on four legs and have differences in the shape of the thoracic cage, the heart is “Valentines heart” shaped with its apex pointing forward and perpendicular to the long axis of the body. In supine position, the heart will orientate with its axis pointing more downwards and toward the diaphragm. This facilitates parasternal images acquisition through transthoracic acquisition in pigs. However, correctly aligned apical views become more difficult to acquire. To be able to place the transducer as close to the apex of the heart as possible, we made a small incision below the sternum and placed the probe under the diaphragm for transdiaphragmatic acquisition, which improved the image quality significantly (12). Because of limited space within the incision and consequently difficulties in performing physical rotation of the probe, we also applied the *iRotate* application for optimal 4CH- and 2CH-view. We recommend this echocardiographic approach among research animals who are euthanized at the study day. Other potentially

differences that have been described between the human and porcine hearts are a more conical morphology of the LV and the heart, coarser papillary muscles and thicker LV wall compared to humans (13). The wall thickness range in our cohort was 0.8–1.2 cm, which would be mildly abnormal if translated to human references (8).

Limitations

The pigs in this cohort did not have any structural or congenital heart disease and the geometrical pattern of the LV was considered normal and uniform for all pigs. The results from this study may not be applicable to deviating LV geometries. All pigs were subjected to acute myocardial infarction affecting 15–20% of the LV. Affected myocardium might have had higher weight due to edema. As echocardiography was performed before myocardial infarction, this could have resulted in a systematic error. We were not able to perform 3D echocardiography due to technical limitations such as, difficulties in pausing the respirator, reverberations and artifacts disturbing the images. As the purpose of this study was to validate echocardiographic method on pigs with the intention of usage on humans, geometrical differences between porcine and human hearts must be kept in mind.

CONCLUSIONS

We demonstrate necropsy validation in a porcine model of a recently presented 2D-based echocardiographic method for LVM-quantification. We confirm high accuracy of the novel 2D-based echocardiographic method compared to the other conventional 1D/2D echocardiographic methods.

DATA AVAILABILITY STATEMENT

The raw data supporting the conclusions of this article will be made available by the authors, without undue reservation.

ETHICS STATEMENT

The animal study was reviewed and approved by the Danish Animal Inspectorate in accordance with EU legalisations for animal protection and care (animal license number 2015-15-0201-00613).

AUTHOR CONTRIBUTIONS

CK, SS, JT-H, and RM planned the study. CK, SS, and AL conceived the study. CK performed the echocardiographic examinations, the data analysis, and wrote the manuscript. SS contributed to the inter-observer analysis. TJ and CH provided critical feedback. All authors discussed the results and contributed to the manuscript.

FUNDING

This work was funded by the Novo Nordisk Foundation Tandem Programme (TJ and JT-H), registered under Grant No. 31364.

REFERENCES

- Levy D, Garrison RJ, Savage DD, Kannel WB, Castelli WP. Prognostic implications of echocardiographically determined left ventricular mass in the Framingham heart study. *N Engl J Med.* (1990) 322:1561–6. doi: 10.1056/NEJM199005313222203
- Casale PN, Devereux RB, Milner M, Zullo G, Harshfield GA, Pickering TG, et al. Value of echocardiographic measurement of left ventricular mass in predicting cardiovascular morbid events in hypertensive men. *Ann Intern Med.* (1986) 105:173–8. doi: 10.7326/0003-4819-105-2-173
- Barbieri A, Bursi F, Mantovani F, Valenti C, Quaglia M, Berti E, et al. Prognostic impact of left ventricular mass severity according to the classification proposed by the American Society of Echocardiography/European Association of Echocardiography. *J Am Soc Echocardiogr.* (2011) 24:1383–91. doi: 10.1016/j.echo.2011.08.012
- Narayanan K, Reinier K, Teodorescu C, Uy-Evanado A, Aleong R, Chugh H, et al. Left ventricular diameter and risk stratification for sudden cardiac death. *J Am Heart Assoc.* (2014) 3:e001193. doi: 10.1161/JAHA.114.001193
- Charles CJ, Lee P, Li RR, Yeung T, Ibrahim Mazlan SM, Tay ZW, et al. A porcine model of heart failure with preserved ejection fraction: magnetic resonance imaging and metabolic energetics. *ESC Hear Fail.* (2020) 7:92–102. doi: 10.1002/ehf2.12536
- Koren MJ, Ulin RJ, Koren AT, Laragh JH, Devereux RB. Left ventricular mass change during treatment and outcome in patients with essential hypertension. *Am J Hypertens.* (2002) 15:1021–8. doi: 10.1016/S0895-7061(02)03061-3
- Guenzinger R, Wildhirt SM, Voegele K, Wagner I, Schwaiger M, Bauernschmitt R, et al. Comparison of magnetic resonance imaging and transthoracic echocardiography for the identification of LV mass and volume regression indices 6 months after mitral valve repair. *J Card Surg.* (2008) 23:126–32. doi: 10.1111/j.1540-8191.2007.00558.x
- Lang RM, Badano LP, Mor-Avi V, Afilalo J, Armstrong A, Ernande L, et al. Recommendations for cardiac chamber quantification by echocardiography in adults: an update from the American Society of Echocardiography and the European Association of Cardiovascular Imaging. *J Am Soc Echocardiogr.* (2015) 28:1–39.e14. doi: 10.1016/j.echo.2014.10.003
- Kristensen CB, Myhr KA, Grund FF, Vejstrup N, Hassager C, Mogelvang R. Quantification of left ventricular mass using two-dimensional transthoracic echocardiography - a novel method with high accuracy and reproducibility. *Research Square [Preprint].* (2021). doi: 10.21203/rs.3.rs-1139410/v1
- Sattler SM, Lubberding AF, Kristensen CB, Mogelvang R, Blanche P, Fink-Jensen A, et al. Effect of the antipsychotic drug haloperidol on arrhythmias during acute myocardial infarction in a porcine model. *Int J Cardiol Hear Vasc.* (2019) 26:100455. doi: 10.1016/j.ijcha.2019.100455
- Lubberding AF, Sattler SM, Grunnet M, Sørensen US, Tfelt-Hansen J, Jespersen T. Arrhythmia development during inhibition of small-conductance calcium-activated potassium channels in acute myocardial infarction in a porcine model. *Europace.* (2019) 21:1584–93. doi: 10.1093/europace/euz223
- Citerni C, Kirchhoff J, Olsen LH, Sattler SM, Gentilini F, Forni M, et al. Characterization of atrial and ventricular structural remodeling in a porcine model of atrial fibrillation induced by atrial tachypacing. *Front Vet Sci.* (2020) 7:179. doi: 10.3389/fvets.2020.00179
- Crick SJ, Sheppard MN, Ho SY, Gebstein L, Anderson RH. Anatomy of the pig heart: comparisons with normal human cardiac structure. *J Anat.* (1998) 193:105–19. doi: 10.1046/j.1469-7580.1998.19310105.x
- Teichholz LE, Kreulen T, Herman M V, Gorlin R. Problems in echocardiographic volume determinations: echocardiographic-angiographic correlations in the presence of absence of asynergy. *Am J Cardiol.* (1976) 37:7–11. doi: 10.1016/0002-9149(76)90491-4
- Devereux RB, Reichek N. Echocardiographic determination of left ventricular mass in man. Anatomic validation of the method. *Circulation.* (1977) 55:613–8. doi: 10.1161/01.CIR.55.4.613
- Geiser EA, Bove KE. Calculation of left ventricular mass and relative wall thickness. *Arch Pathol.* (1974) 97:13–21.
- Wyatt HL, Heng MK, Meerbaum S, Hestenes JD, Cobo JM, Davidson RM, et al. Cross-sectional echocardiography. I. Analysis of mathematic models for quantifying mass of the left ventricle in dogs. *Circulation.* (1979) 60:1104–13. doi: 10.1161/01.CIR.60.5.1104
- Salcedo EE, Gockowski K, Tarazi RC. Left ventricular mass and wall thickness in hypertension. Comparison of M mode and two dimensional echocardiography in two experimental models. *Am J Cardiol.* (1979) 44:936–40. doi: 10.1016/0002-9149(79)90225-X
- Schiller NB, Skioldebrand CG, Schiller EJ, Mavroudis CC, Silverman NH, Rahimtoola SH, et al. Canine left ventricular mass estimation by two-dimensional echocardiography. *Circulation.* (1983) 68:210–6. doi: 10.1161/01.CIR.68.1.210
- Woythaler JN, Singer SL, Kwan OL, Meltzer RS, Reubner B, Bommer W, et al. Accuracy of echocardiography versus electrocardiography in detecting left ventricular hypertrophy: comparison with postmortem mass measurements. *J Am Coll Cardiol.* (1983) 2:305–11. doi: 10.1016/S0735-1097(83)80167-3
- Park SH, Shub C, Nobrega TP, Bailey KR, Seward JB. Two-dimensional echocardiographic calculation of left ventricular mass as recommended by the American Society of Echocardiography: correlation with autopsy and M-mode echocardiography. *J Am Soc Echocardiogr.* (1996) 9:119–28. doi: 10.1016/S0894-7317(96)90019-X
- Reichek N, Helak J, Plappert T, Sutton MS, Weber KT. Anatomic validation of left ventricular mass estimates from clinical two-dimensional echocardiography: initial results. *Circulation.* (1983) 67:348–52. doi: 10.1161/01.CIR.67.2.348
- Devereux RB, Alonso DR, Lutas EM, Gottlieb GJ, Campo E, Sachs I, et al. Echocardiographic assessment of left ventricular hypertrophy: comparison to necropsy findings. *Am J Cardiol.* (1986) 57:450–8. doi: 10.1016/0002-9149(86)90771-X
- Bachenberg TC, Shub C, Hauck AJ, Edwards WD. Can anatomical left ventricular mass be estimated reliably by m-mode echocardiography? A clinicopathological study of ninety-three patients. *Echocardiography.* (1991) 8:9–15. doi: 10.1111/j.1540-8175.1991.tb01399.x
- Miyashita S, Hammoudi N, Watanabe S, Bikou O, Yamada K, Agüero J, et al. Echocardiographic left ventricular mass estimation: two-dimensional area-length method is superior to M-mode linear method in swine models of cardiac diseases. *J Cardiovasc Transl Res.* (2020) 13:648–58. doi: 10.1007/s12265-019-09937-7
- Troy BL, Pombo J, Rackley CE. Measurement of left ventricular wall thickness and mass by echocardiography. *Circulation.* (1972) 45:602–11.
- Daniels SR, Meyer RA, Liang Y, Bove KE. Echocardiographically determined left ventricular mass index in normal children, adolescents and young adults. *J Am Coll Cardiol.* (1988) 12:703–8. doi: 10.1016/S0735-1097(88)80060-3
- Gopal AS, Schnellbaeher MJ, Shen Z, Akinboboye OO, Sapin PM, King DL. Freehand three-dimensional echocardiography for measurement of left ventricular mass: *in vivo* anatomic validation using explanted human hearts. *J Am Coll Cardiol.* (1997) 30:802–10. doi: 10.1016/S0735-1097(97)00198-8
- Schmidt MA, Freidlin RZ, Ohazama CJ, Jones M, Laurienzo JM, Brenneman CL, et al. Anatomic validation of a novel method for left ventricular volume and mass measurements with use of real-time 3-dimensional echocardiography. *J Am Soc Echocardiogr.* (2001) 14:1–10. doi: 10.1067/mje.2001.108132
- Fox CH, Johnson FB, Whiting J, Roller PP. Formaldehyde fixation. *J Histochem Cytochem.* (1985) 33:845–53. doi: 10.1177/33.8.3894502
- Leonard KC, Worden N, Boettcher ML, Dickinson E, Hartstone-Rose A. Effects of freezing and short-term fixation on muscle mass, volume, and density. *Anat Rec.* (2021) 305:199–208. doi: 10.1002/ar.24639
- Ford WR, Menon V, Bhambhani A, Liyanage R, Khan MI, Jugdutt BI. Changes in myocardial density during postinfarction healing: effect on estimation of *in vivo* left ventricular mass by echocardiographic imaging. *Can J Physiol Pharmacol.* (1997) 75:1075–82. doi: 10.1139/y97-132
- Kennedy JW, Reichenbach DD, Baxley WA, Dodge HT. Left ventricular mass. A comparison of angiographic measurements with autopsy weight. *Am J Cardiol.* (1967) 19:221–3. doi: 10.1016/0002-9149(67)90536-X
- Pahlm US, Ubachs JFA, Heiberg E, Engblom H, Erlinge D, Göteborg M, et al. Regional wall function before and after acute myocardial infarction; an experimental study in pigs. *BMC Cardiovasc Disord.* (2014) 14:118. doi: 10.1186/1471-2261-14-118
- Myerson SG, Bellenger NG, Pennell DJ. Assessment of left ventricular mass by cardiovascular magnetic resonance. *Hypertension.* (2002) 39:750–5. doi: 10.1161/hy0302.104674

36. Alfakih K, Bloomer T, Bainbridge S, Bainbridge G, Ridgway J, Williams G, et al. A comparison of left ventricular mass between two-dimensional echocardiography, using fundamental and tissue harmonic imaging, and cardiac MRI in patients with hypertension. *Eur J Radiol.* (2004) 52:103–9. doi: 10.1016/j.ejrad.2003.09.015
37. François CJ, Fieno DS, Shors SM, Finn JP. Left ventricular mass: manual and automatic segmentation of true FISP and FLASH cine MR images in dogs and pigs. *Radiology.* (2004) 230:389–95. doi: 10.1148/radiol.2302020761
38. Simprini LA, Goyal P, Codella N, Fieno DS, Afroz A, Mullally J, et al. Geometry-independent inclusion of basalmiocardium yields improved cardiacmagnetic resonance agreement with echocardiography and necropsy quantified left-ventricular mass. *J Hypertens.* (2013) 31:2069–76. doi: 10.1097/HJH.0b013e328362d935
39. Codella NCF, Lee HY, Fieno DS, Chen DW, Hurtado-Rua S, Kochar M, et al. Improved left ventricular mass quantification with partial voxel interpolation *in vivo* and necropsy validation of a novel cardiac MRI segmentation algorithm. *Circ Cardiovasc Imaging.* (2012) 5:137–46. doi: 10.1161/CIRCIMAGING.111.966754
40. Farber NJ, Reddy ST, Doyle M, Rayarao G, Thompson D V., Olson P, et al. *Ex vivo* cardiovascular magnetic resonance measurements of right and left ventricular mass compared with direct mass measurement in excised hearts after transplantation: a first human SSFP comparison. *J Cardiovasc Magn Reson.* (2014) 16:74. doi: 10.1186/s12968-014-0074-0
41. Stewart GA, Foster J, Cowan M, Rooney E, McDonagh T, Dargie HJ, et al. Echocardiography overestimates left ventricular mass in hemodialysis patients relative to magnetic resonance imaging. *Kidney Int.* (1999) 56:2248–53. doi: 10.1046/j.1523-1755.1999.00786.x
42. Bellenger NG, Marcus NJ, Davies C, Yacoub M, Banner NR, Pennell DJ. Left ventricular function and mass after orthotopic heart transplantation: a comparison of cardiovascular magnetic resonance with echocardiography. *J Heart Lung Transplant.* (2000) 19:444–52. doi: 10.1016/S1053-2498(00)00079-6
43. Takeuchi M, Nishikage T, Mor-Avi V, Sugeng L, Weinert L, Nakai H, et al. Measurement of left ventricular mass by real-time three-dimensional echocardiography: validation against magnetic resonance and comparison with two-dimensional and m-mode measurements. *J Am Soc Echocardiogr.* (2008) 21:1001–5. doi: 10.1016/j.echo.2008.07.008

Conflict of Interest: The authors declare that the research was conducted in the absence of any commercial or financial relationships that could be construed as a potential conflict of interest.

Publisher's Note: All claims expressed in this article are solely those of the authors and do not necessarily represent those of their affiliated organizations, or those of the publisher, the editors and the reviewers. Any product that may be evaluated in this article, or claim that may be made by its manufacturer, is not guaranteed or endorsed by the publisher.

Copyright © 2022 Kristensen, Sattler, Lubberding, Tfelt-Hansen, Jespersen, Hassager and Mogelvang. This is an open-access article distributed under the terms of the Creative Commons Attribution License (CC BY). The use, distribution or reproduction in other forums is permitted, provided the original author(s) and the copyright owner(s) are credited and that the original publication in this journal is cited, in accordance with accepted academic practice. No use, distribution or reproduction is permitted which does not comply with these terms.



Cardiac and Vascular Remodeling After 6 Months of Therapy With Sacubitril/Valsartan: Mechanistic Insights From Advanced Echocardiographic Analysis

Sara Monosilio^{1†}, Domenico Filomena^{1†}, Federico Luongo¹, Michele Sannino¹, Sara Cimino¹, Matteo Neccia¹, Marco Valerio Mariani¹, Lucia Ilaria Birtolo¹, Giulia Benedetti¹, Giovanni Tonti², Gianni Pedrizzetti³, Carmine Dario Vizza¹, Viviana Maestrini¹ and Luciano Agati^{1*}

OPEN ACCESS

Edited by:

Riccardo Liga,
Pisana University Hospital, Italy

Reviewed by:

Choon-Sik Jhun,
The Pennsylvania State University,
United States
Attila Oláh,
Semmelweis University, Hungary

*Correspondence:

Luciano Agati
luciano.agati@uniroma1.it

[†]These authors have contributed
equally to this work and share first
authorship

Specialty section:

This article was submitted to
Cardiovascular Imaging,
a section of the journal
Frontiers in Cardiovascular Medicine

Received: 25 February 2022

Accepted: 21 April 2022

Published: 18 May 2022

Citation:

Monosilio S, Filomena D, Luongo F, Sannino M, Cimino S, Neccia M, Mariani MV, Birtolo LI, Benedetti G, Tonti G, Pedrizzetti G, Vizza CD, Maestrini V and Agati L (2022) Cardiac and Vascular Remodeling After 6 Months of Therapy With Sacubitril/Valsartan: Mechanistic Insights From Advanced Echocardiographic Analysis. *Front. Cardiovasc. Med.* 9:883769. doi: 10.3389/fcvm.2022.883769

¹ Department of Clinical, Internal, Anesthesiological and Cardiovascular Sciences, "Sapienza" University of Rome, Policlinico Umberto I, Rome, Italy, ² Cardiology Division, "G. D'Annunzio" University, Chieti, Italy, ³ Department of Engineering and Architecture, University of Trieste, Trieste, Italy

Background: Effects of Sacubitril/Valsartan (S/V) on left ventricular (LV) mechanics and ventricular-arterial coupling in patients with heart failure with reduced ejection fraction (HFrEF) are not completely understood. The aim of this study was to evaluate both cardiac and vascular remodeling in a group of HFrEF patients undergoing S/V therapy.

Methods: Fifty HFrEF patients eligible to start a therapy with S/V were enrolled. Echocardiographic evaluation was performed at baseline and after 6 months of follow-up (FU). Beside standard evaluation, including global longitudinal strain (GLS), estimated hemodynamic forces (HDFs) and non-invasive pressure-volume curves (PV loop) were assessed using dedicated softwares. HDFs were evaluated over the entire cardiac cycle, in systole and diastole, both in apex to base (A-B) and latero-septal (L-S) directions. The distribution of LV HDFs was evaluated by L-S over A-B HDFs ratio (L-S/A-B HDFs ratio). Parameters derived from estimated PV loop curves were left ventricular end-systolic elastance (E_{es}), arterial elastance (E_a), and ventricular-arterial coupling (VAC).

Results: At 6 months of FU indexed left ventricular end-diastolic and end-systolic volumes decreased (EDVi: 101 ± 28 mL vs. 86 ± 30 mL, $p < 0.001$; ESVi: 72 ± 23 mL vs. 55 ± 24 mL, $p < 0.001$), ejection fraction and GLS significantly improved (EF: $29 \pm 6\%$ vs. $37 \pm 7\%$, $p < 0.001$; GLS: $-9 \pm 3\%$ vs. $-13 \pm 4\%$, $p < 0.001$). A reduction of E_a (2.11 ± 0.91 mmHg/mL vs. 1.72 ± 0.44 mmHg/mL, $p = 0.008$) and an improvement of E_{es} (1.01 ± 0.37 mmHg/mL vs. 1.35 ± 0.6 mmHg/mL, $p < 0.001$) and VAC (2.3 ± 1.1 vs. 1.5 ± 0.7 , $p < 0.001$) were observed. Re-alignment of HDFs occurred, with a reduction of diastolic L-S/A-B HDFs ratio [23 ($20-35$)% vs. 20 ($11-28$)%, $p < 0.001$].

Conclusion: S/V therapy leads to a complex phenomenon of reverse remodeling involving increased myocardial contractility, HDFs distribution improvement, and afterload reduction.

Keywords: sacubitril/valsartan, echocardiography, speckle-tracking, hemodynamic forces, pressure-volume loop

INTRODUCTION

Sacubitril/Valsartan (S/V) was proven to significantly modify the clinical course of patients with heart failure with reduced ejection fraction (HFrEF), improving symptoms, outcomes and functional capacity as a consequence of cardiac reverse remodeling (RR) (1–7). Studies on S/V induced RR focused on volumetric changes and improvement of cardiac function in terms of ejection fraction. This approach fails to describe the complex effects of S/V on cardiovascular (CV) physiopathology. Data on intraventricular pressure gradients (IVPGs) distribution are missing and those on vascular properties changes are frequently limited to hypertensive cohorts. The aim of our study was to evaluate both cardiac and vascular remodeling in a group of HFrEF patients after 6 months of therapy with S/V, in terms of volumes, contractility, IVPGs distribution, vascular properties and ventricular-arterial coupling.

METHODS

In this prospective, observational, single-center study, fifty symptomatic patients with HFrEF and an indication to receive S/V according to recommendations (8) were consecutively enrolled from January 2020 to November 2020. Before the introduction of S/V, all patients were receiving optimized medical therapy. All patients started from S/V minimal dose of 24/26 mg b.i.d. Titration up to the maximal tolerate dose was conducted every 2 weeks. Patients with diagnosis of myocarditis or who underwent coronary revascularization, cardiac resynchronization therapy (CRT) device implantation and mitral valve interventions in the last 6 months or during the follow-up period were excluded. Patients with atrial fibrillation and those who experienced death during follow-up period were excluded. All patients were in sinus rhythm and had a good acoustic window. The study was performed in accordance to the Helsinki declaration. All subjects provided written informed consent. All enrolled patients were evaluated at baseline and after 6 months of follow-up.

The study protocol included medical evaluation, blood test, transthoracic echocardiogram at baseline (before starting S/V) and after 6 months. During medical evaluation cardiovascular risk factors, past medical history, medical therapy, New York Heart Association (NYHA) functional class, systolic and diastolic blood pressure were collected. Blood test including blood count, creatinine and plasmatic potassium were collected. Transthoracic Echocardiography (TTE) was performed using standard equipment (*Epiq 7, Philips*). Left and right ventricle (LV and RV) dimensions, wall thickness, global and regional systolic function, indexes of diastolic function, presence and grade of valve stenosis and regurgitation were evaluated according to current guidelines (9). Three dimensional (3D) LV end-diastolic volume (EDV), LV end-systolic volume (ESV) and LV ejection fraction (EF) were calculated using an automated software (*HeartModel, Philips Healthcare*). LV end-diastolic pressure (EDP) was also estimated (10). Comparing baseline and follow-up echocardiography, LV RR was defined as a relative increase in LVEF > 10% with a concomitant relative reduction of LVESV > 15%. Images were analyzed

offline with dedicated software to assess the parameters listed below.

Speckle Tracking Echocardiography (ST-E) Analysis

ST-E analysis was performed using an automated 2D strain analytical software (*AutoStrain, Philips Healthcare*). The software automatically traced the endocardial border of the left ventricle in apical three, two and four chamber views, providing the mean value of endocardial global longitudinal strain (Endo-GLS).

Non-invasive Pressure-Volume Loop Analysis (PV Loop)

PV loops were reconstructed using a dedicated software (QStrain, Medis BV, Leiden, NL). LV volumes, estimated EDP and brachial systolic and diastolic pressures were used as input. The software reconstructs the PV loop by determining the end-systolic pressure-volume relationship (ESPVR) and end-diastolic pressure-volume relationship (EDPVR) using the single-beat algorithms previously described in literature (11–13). Once the EDPVR and ESPVR are identified, the ES and ED LV volumes and systolic and diastolic brachial pressures were used to close the PV loop. Finally, the PV relation is depicted for the entire cardiac cycle where each point of the curve is described as (V_t , P_t). In the PV loop the classic phases of the cardiac cycle are displayed: isovolumetric contraction, ejection, isovolumetric relaxation, and diastolic filling. Based on this integrated PV loop analysis, the following hemodynamic parameters were calculated (14, 15):

- *LV systolic elastance (E_{es})*: reflecting LV contractility and representing the slope of the end-systolic pressure-volume relation (ESPVR);
- *Arterial Elastance (E_a)*: reflecting the effective arterial afterload and representing the slope of the line connecting EDV on the volume axis to the end-systolic PV point on the PV loop;
- *Ventricular-Arterial Coupling (VAC)*: calculated as the ratio between E_a/E_{es} ;
- *Stroke Work (SW)*: the external work performed by the myocardium to eject blood, computed as the area enclosed by the PV loop;
- *Mechanical Potential Energy (PE)*: the energy generated within the contraction that is not converted to external work and calculated as the area enclosed by the ESPVR line, the isovolumic relaxation line and the end-diastolic pressure-volume relation (EDPVR);
- *Pressure-volume area (PVA)*: the total mechanical energy generated by the contraction of the left ventricle, equal to the sum of PE and SW;
- *Work efficiency (WE)*: the efficiency of the mechanical energy transfer from the ventricle to the arterial tree, expressed as the SW/PVA ratio.
- *LV end-diastolic stiffness coefficient (β)*: representing LV end-diastolic passive filling properties and calculated as the curve-fit parameter β of the EDPVR curve.

The mathematical formulas used are reported in **Supplementary Methods**.

Hemodynamic Forces (HDFs)

HDFs represent the flow forces exchanged between the blood and the endocardial boundary. HDFs were assessed using a dedicated prototype software (QStrain, Medis BV, Leiden, NL) based on a previously validated mathematical model (16). Both systolic and diastolic endocardial borders are semi-automatically traced in all the three long-axis views. LV endocardial displacement and the estimated mitral and aortic valve areas are used by the model as input data for HDF calculation. HDFs were normalized for the LV volume and expressed as a percentage of the force of gravity to compare ventricles of different sizes. HDFs were assessed over the entire cardiac cycle, in systole and diastole, and both in longitudinal (apex to base; A-B) and horizontal (latero-septal; L-S) directions. The main orientation of HDFs vector was evaluated calculating the L-S over A-B HDFs ratio (L-S/A-B HDFs ratio, %) providing a comparison between longitudinal and transverse components. HDFs directions were graphically represented using a polar histogram (17).

Based on all parameters derived by standard and advanced echocardiography the following features were described:

- *Cardiac remodeling* in terms of changes in LV volumes and systolic function, GLS, E_{es} , LV diastolic stiffness, HDFs strength and distribution, non-invasive systolic pulmonary pressure, mitral regurgitation grade;
- *Vascular remodeling* in terms of changes in blood pressure measurements and E_a ;
- *Ventricular-arterial coupling and energy conversion efficiency* in terms of changes in VAC, SW, PE, PVA and WE.

Intra- and Intra-Observer and Inter-Observer Variability

Intra-observer and inter-observer variability for HDFs and PV loop measurements were assessed in a sample of 10 patients. Two investigators measured blinded the same exam, and one investigator repeated the analysis 1 week later, blinded to the previous measurements.

Statistical Analysis

Statistical analysis was performed with Statistical Package for Social Sciences, version 23.0 (SPSS, Chicago, IL). Variables have been analyzed to test normal distribution. They were presented as mean \pm standard deviation or median and 25th–75th percentiles, when appropriate. Paired comparisons of continuous variables were performed with two-tailed paired Student's *t*-test or Wilcoxon test, when appropriate. Paired comparisons of categorical variables were conducted with the McNemar test. Interclass correlation coefficients (ICCs) were calculated to assess inter-observer and intra-observer agreement of HDFs and PV loop measurements. Differences were considered statistically significant when $p < 0.05$.

RESULTS

General and clinical characteristics of the whole population are depicted in **Tables 1, 2**. Mean age was 70 ± 12 y.o., male subjects were 41 (87%). Coronary artery disease (CAD) was the cause of

TABLE 1 | General characteristics of the whole population.

Parameters	HFrEF Patients <i>N</i> = 47
Baseline	
Age, y.o.	70 ± 12
BMI, kg/m ²	24 ± 7
BSA, m ²	1.9 ± 0.2
Male Sex, <i>n</i> (%)	41 (87%)
Diabetes, <i>n</i> (%)	39 (82%)
Hypertension, <i>n</i> (%)	7 (15%)
Smoke Habit, <i>n</i> (%)	24 (51%)
Dyslipidaemia, <i>n</i> (%)	28 (59%)
PMK, <i>n</i> (%)	29 (61%)
LBBB, <i>n</i> (%)	15 (31%)
CAD, <i>n</i> (%)	26 (55%)

HFrEF, Heart Failure reduced Ejection Fraction; BMI, body mass index; BSA, body surface area; PMK, pacemaker; CAD, coronary artery disease. LBBB, left bundle branch block.

TABLE 2 | Baseline vs. follow up clinical data.

Parameters	Baseline <i>N</i> = 47	Follow-Up <i>N</i> = 47	<i>p</i>
SBP, mmHg	126 ± 11	119 ± 16	0.002
DBP, mmHg	78 ± 8	71 ± 8	0.001
HR, bpm	71 ± 13	67 ± 9	0.041
NYHA Class \geq II, <i>n</i> (%)	47 (100%)	25 (53%)	<0.001
Creatinine, mg/dL	1.1 ± 0.3	1.2 ± 0.4	0.322
eGFR, mL/min	75 ± 31	73 ± 31	0.331
K+, meq/L	4.3 ± 0.5	4.4 ± 0.4	0.140

DBP, diastolic blood pressure; eGFR, estimated glomerular filtration rate; HR, heart rate; NYHA, New York heart association; SBP, systolic blood pressure.

HFrEF in a half of cases (26 patients, 55%). All patients were in NYHA class \geq II (40% were in NYHA class II, 51% in NYHA class III, 9% in NYHA class IV). Before starting S/V all patients were receiving optimal medical therapy (OMT), including angiotensin converting enzyme inhibitors (ACEi) or angiotensin receptor blockers, beta blockers, diuretics and mineral-corticoid receptor antagonists. None of the patients was taking sodium-glucose cotransporter 2 inhibitors at baseline nor during follow-up period. Due to the death of 3 patients, comparisons between baseline and follow-up clinical and echocardiographic parameters were performed on a total of 47 patients. At 6 months of follow-up all patients discontinued ACEi, 33 patients (70%) were taking beta blockers, 10 (21%) mineral-corticoid receptor antagonists and 23 (49%) diuretics. One patient (2%) was re-hospitalized due to acute decompensated heart failure. The vast majority of the population experienced an improvement in symptoms as documented by a reduction of NYHA class at least of 1 point. The comparison of clinical and biochemical parameters between baseline and follow-up is showed in **Table 2**.

Cardiac Remodeling

Standard and advanced echocardiographic parameters and their comparison between baseline and follow-up are depicted in

TABLE 3 | Baseline vs. follow-up standard echocardiography parameters, global longitudinal strain and hemodynamic parameters estimated by echocardiography.

Parameters	Baseline <i>N</i> = 47	Follow-Up <i>N</i> = 47	<i>p</i>
LVESVi, mL/m ²	72 ± 23	55 ± 24	<0.001
LVEDVi, mL/m ²	101 ± 28	86 ± 30	<0.001
LVEF, %	29 ± 6	37 ± 7	<0.001
LVMass/i, g/m ²	191 (172–228)	172 (142–186)	<0.001
Mitral Regurgitation moderate to severe, <i>n</i> (%)	24 (51%)	11 (23%)	0.001
LAVi mL/m ²	51 (37–61)	45 (37–58)	0.276
Average E/e'	13 (10–17)	10 (8–11)	<0.001
LVEDP, mmHg	20 ± 4	18 ± 2	<0.001
TAPSE, mm	19 ± 4	19 ± 3	0.212
Right ventricle S', cm/s	11 ± 2	11 ± 2	0.412
Tricuspid Regurgitation moderate to severe, <i>n</i> (%)	12 (25%)	7 (15%)	0.125
PASP, mmHg	36 ± 12	30 ± 6	0.006
LV-GLS-endo, %	−9 ± 3	−13 ± 4	<0.001
Ea, mmHg/mL	2.11 ± 0.91	1.72 ± 0.44	0.008
Ees, mmHg/mL	1.01 ± 0.37	1.35 ± 0.6	<0.001
VAC,-	2.3 ± 1.1	1.5 ± 0.7	<0.001
SW, Joule	0.94 ± 0.4	0.95 ± 0.31	0.899
PE, Joule	2.11 ± 0.71	1.51 ± 0.71	<0.001
PVA, Joule	3.05 ± 0.93	2.5 ± 0.87	<0.001
WE,-	0.31 ± 0.09	0.40 ± 0.10	0.001
Diastolic stiffness coefficient β, −	5,94 ± 0,47	6,10 ± 0,17	0.057

E_a, arterial elastance; *E_{es}*, end-systolic ventricular elastance; *EDP*, end-diastolic pressure; *EDVi*, end diastolic volume indexed; *EF*, ejection fraction; *ESVi*, end systolic volume indexed; *GLS-endo*, endocardial global longitudinal strain; *LAVi*, left atrial volume indexed; *LV*, left ventricle; *Mass/i*, mass indexed; *PASP*, pulmonary arterial systolic pressure; *PE*, potential energy; *PVA*, pressure-volume area; *SW*, stroke work; *TAPSE*, tricuspid annular plane systolic excursion; *VAC*, ventricular-arterial coupling; *WE*, work efficiency.

Tables 3, 4. At 6 months follow-up a significant reduction in LV mass ($p < 0.001$), LVEDVi ($p < 0.001$) and LVESVi ($p < 0.001$) and an improvement in LVEF ($p < 0.001$) were observed (**Table 3, Figure 1A**). Twenty-two (47%) patients reached criteria of RR. At ST-E analysis, LV-GLS significantly improved. As assessed by PVloop analysis, left ventricular end-systolic elastance significantly improved ($p < 0.001$) (**Table 3, Figure 1C**). A significant reduction in average E/e' ($p < 0.001$) and, consequently, in EDP ($p < 0.001$) was observed. LV end-diastolic stiffness coefficient β did not change. After S/V treatment patients with moderate-to-severe mitral regurgitation had halved ($p = 0.001$). Left atrial volume also decreased, although its reduction was not statistically significant ($p = 0.276$). Moreover, there was a significant reduction in PASP ($p = 0.006$). At follow-up there was also an improvement in HDFs alignment, with an increase in HDFs A-B values and consequently a significant reduction of HDFs LS/AB ratio in every phase of the cardiac cycle (**Table 4; Figure 2**).

Vascular Remodeling

Systolic and diastolic blood pressure showed a significant reduction after 6 months of therapy with S/V ($p = 0.002$ and $p =$

TABLE 4 | Baseline vs. follow up echocardiographic estimated hemodynamic forces.

	Baseline <i>N</i> = 47	Follow-Up <i>N</i> = 47	<i>p</i>
HDFs: entire cardiac cycle			
A-B, (%)	6.1 (4.8–6.3)	8 (6.6–16)	<0.001
L-S, (%)	1.8 (1.3–2.1)	2 (1.8–2.7)	0.431
L-S/A-B HDFs Ratio, (%)	32 (30–42)	22 (6–25)	<0.001
HDFs: systole			
A-B, (%)	7.3 (6.8–8.2)	10.3 (7.5–24.6)	<0.001
L-S, (%)	1.7 (1.3–2.5)	2.1 (1.7–2.9)	0.013
L-S/A-B HDFs Ratio, (%)	23 (20–35)	20 (11–28)	0.001
HDFs: diastole			
A-B, (%)	3.6 (2.9–4.7)	6.8 (3.4–7.9)	<0.001
L-S, (%)	1.9 (1.4–2.7)	1.9 (1.2–2.7)	0.057
L-S/A-B HDFs Ratio, (%)	53 (48–72)	33 (23–38)	<0.001

HDFs, hemodynamic forces; *A-B* apex to base direction; *L-S*, latero-septal direction; *L-S/A-B HDFs Ratio*, latero-septal direction over apex to base direction ratio.

0.001, respectively) (**Table 2**). As evaluated by PV loop analysis, arterial elastance significantly reduced ($p = 0.008$) (**Table 3; Figure 1B**).

Ventricular-Arterial Coupling and Energy Conversion Efficiency

After 6 months of S/V therapy, VAC significantly improved ($p < 0.001$). While SW did not differ between baseline and follow-up ($p = 0.899$), potential energy (**Figure 1D**) and pressure volume area significantly reduced ($p < 0.001$ and $p < 0.001$, respectively). Thus, WE significantly improved ($p = 0.001$).

Intra- and Inter-Observer Agreement

Both intra- and inter-observer agreement were good to excellent for all the parameters. ICCs are reported in **Supplementary Table 1**.

DISCUSSION

In this study, the occurrence of both cardiac and vascular remodeling in 47 HFrEF patients after 6 months of therapy with S/V was described. The strength of our study is the comprehensive evaluation of CV remodeling after S/V not only in terms of volumetric remodeling but also, for the first time, in terms of deformation, intraventricular pressure gradients, hemodynamics and vascular remodeling using non-invasive methods for PV loop analysis and intraventricular HDFs assessment. Conventionally, cardiovascular remodeling has been identified with reverse LV remodeling in terms of “volumetric” parameters: reduction of LVEDV, LVESV and improvement of LVEF (6, 18, 19). Recently, S/V has been demonstrated to induce improvement in LV function in terms of muscular deformation by ST-E (18). However, the description of changes in the cardiovascular mechanics via ejection fraction and volumes is a crude simplification. This approach fails to describe the complexity of a muscular pump interacting with the intracavitary blood flow and coupled with the arterial tree.

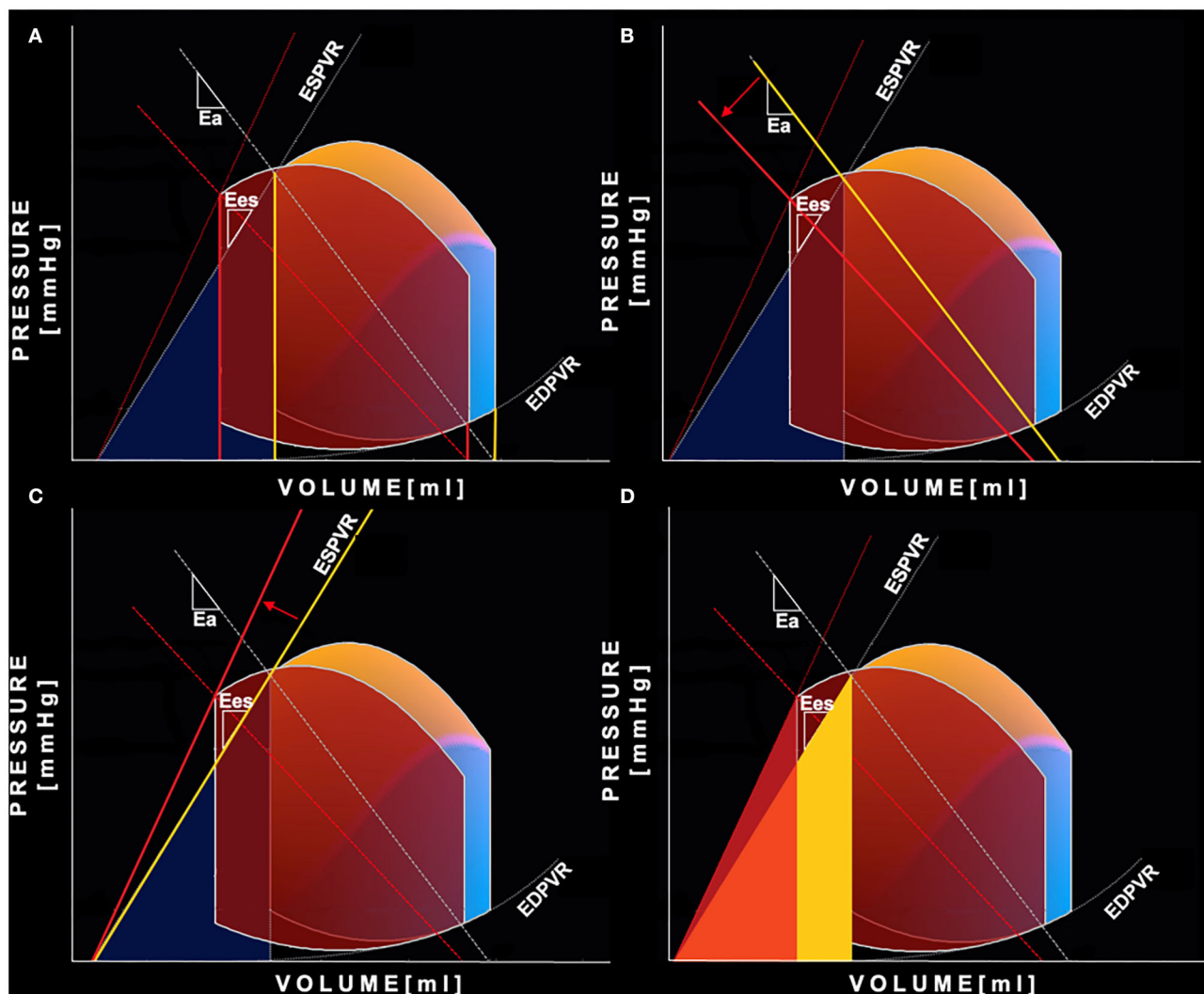
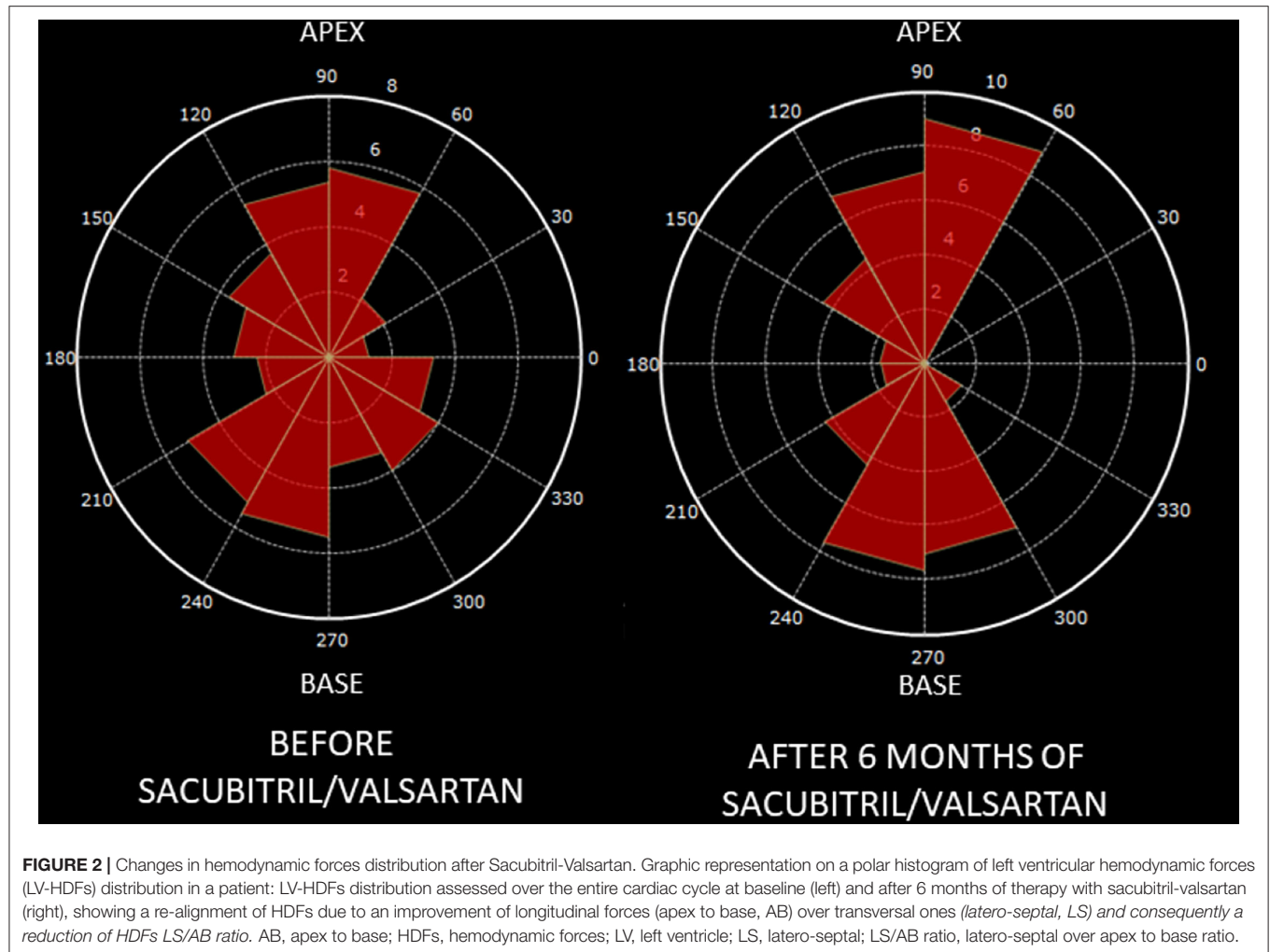


FIGURE 1 | Pressure-Volume curve changes after Sacubitril-Valsartan. Representation of the non-invasive PV loop analysis of a patient before (yellow-blue PV loop) and after 6 months (red PV loop) of therapy with Sacubitril- Valsartan. **(A)** shows the reduction of both left ventricular end-systolic and end-diastolic volumes (yellow is “before,” red is “after”). The greater relative reduction of the end-systolic volume leads to an increase in stroke volume and ejection fraction. **(B)** shows decreased left ventricular afterload reflected by a less steep arterial elastance line (yellow is “before,” red is “after”); **(C)** shows increased end-systolic left ventricular elastance—steeper end-systolic pressure volume relation (yellow is “before,” red is “after”); **(D)** shows reduction of mechanical potential energy: the light yellow area is the PE before the therapy, the red is PE after the therapy. In orange is displayed the area of overlap between the aforementioned areas. PE, potential energy; PV loop, pressure-volume loop.

Cardiac Remodeling

In the overall cohort, we observed a significant improvement in LVEF and an important reduction in LVESVi and LVEDVi. A concomitant end-systolic volumes reduction and EF improvement (LV RR) was observed in 47% of the total cohort. Our results are in line with previous reports in literature. Several studies have shown that the therapy with S/V induces cardiac remodeling (3, 4) with a dose-dependent effect (3). Compared with ACEi, angiotensin receptor neprilysin inhibitors (ARNIs) were found to induce more frequently RR in terms of EF improvement and volumes reduction, clinically reflected by a lower NYHA class and better performances at 6-minutes walking test (6MWT) (5). In our study, the LVEF

improvement is supported by the higher systolic myocardial deformation and increased intrinsic contractility observed after 6 months (significant increase in both GLS and E_{es}). These findings are in line with previous reports investigating the effect of S/V on myocardial strain (18, 20). Preclinical evidences showed that Sacubitril and Valsartan have a synergic effect, attenuating cardiomyocyte cell death, hypertrophy and impaired contractility (21). Moreover, the natriuretic and diuretic effects of S/V could reduce cardiac preload, allowing the heart to work on the most efficient part of the Frank-Starling curve and improving the stroke volume. Changes in cardiac preload, together with LV volume reduction, influence also diastolic properties. Precisely, we documented a reduction



in LV EDP without a significant reduction in LV stiffness coefficient (β). This may be counterintuitive if we do not focus on the diastolic properties of the failing heart. In patients with HFrEF, the LV is characterized by high diastolic capacitance and stiffness. The end diastolic point of the PV loop is determined not only by the curve fit parameters of the EDPVR but it is also extremely influenced by the volume status. Even in the absence of changes in stiffness, a preload reduction causes a volume-dependent decrease in EDP and the end-diastolic point (V_{ED} , P_{ED}) shifts down-left along the EDPVR. Thus, the decrease in filling pressure after S/V are mainly due to a reduction in volume overload. We should acknowledge that the follow-up period in our study is relatively short and possible effects of S/V on LV diastolic stiffness may need a longer time. Another known beneficial effect of S/V is the reduction in severity of functional mitral regurgitation due to lower cardiac preload, reduced LV volumes and increased LV systolic function leading to a rebalancing of closing and tethering forces. All the aforementioned beneficial effects, summed with a possible role of S/V in reducing the pulmonary vascular tone, concur to an improvement of post-capillary pulmonary pressures (22, 23).

In our report, we documented a realignment of HDFs during S/V therapy. HDFs are forces exchanged between the blood and the myocardium during the cardiac cycle. Blood flows into the cardiac chambers because of intra-ventricular pressure gradients (IVPGs), changing throughout the entire cardiac cycle. They are generated by the totality of the cardiac structure (opening and closing valves, contracting and relaxing myocardium, vessels) (24). Recently, non-invasive HDFs analysis, using the application of a mathematical model to echocardiographic or magnetic resonance “cine” images, has been validated (16, 25). HDFs magnitude and alignment have been recently proposed as novel markers of cardiac function. Briefly, in normal hearts HDFs are mainly directed in apex-to-base (or longitudinal) direction, while latero-septal (or transversal) HDFs are significantly weaker. Misalignment of HDFs has been reported in abnormal cardiac conditions and related to dyssynchrony and regional heterogeneity in myocardial contraction and relaxation (26–28). In HFrEF patients HDFs are significantly lower and misaligned, diverging from the normal apex-to-base direction toward the latero-septal one (29). A recent pathophysiological model suggested a link between HDFs misalignment/re-alignment and adverse-remodeling/reverse-remodeling (27, 28). Cardiac

endothelial mechano-receptors can distinguish changes in shear stress vectors (tangential vs. perpendicular direction) and activate ultrastructural adaptive responses, such as turnover of contractile proteins and regulation of myofibril orientation (30).

Vascular Remodeling

After 6 months of therapy with S/V, both SBP and DBP significantly improved. Moreover, P/V loop analysis showed a significant reduction in E_a . Reduction of blood pressure may be explained not only by the diuretic and natriuretic effect but also by vascular remodeling. S/V was proven to improve endothelium-dependent and independent vasorelaxation (31) and to reduce arterial stiffness (32). Thus, S/V could significantly change both the static (total vascular resistance) and pulsatile components (e.g., total wave reflections) of the total arterial load (33). These biological effects are also mediated by an increased availability of natriuretic peptides with vasoactive properties and by modulation of both sympathetic nervous system and renin-angiotensin system (34, 35).

Ventricular-Arterial Coupling and Energy Conversion Efficiency

The ultimate effect of S/V is an amelioration of ventricular-arterial coupling, as demonstrated in our cohort of patients by a significant reduction in E_a/E_{es} ratio. Arterial load and stiffness are closely linked with systolic and diastolic function and LV hypertrophy (14). Improvements in arterial compliance, peripheral resistance, and wave reflections optimize LV afterload. This reduces early and peak systolic myocardial stress and oxygen demand. Complementary improvement in LV systolic function and organ perfusion lead to neuro-humoral and sympathetic modulation, contrasting vascular dysfunction (36). The amelioration of E_a , E_{es} , and VAC is the physiopathological cause of the improvement of LVEF, used as a surrogate of systolic function. Actually, the relationship between VAC and EF can be mathematically described as $LVEF = E_{es}/(E_{es} + E_a)$, showing how EF is affected both by inotropic state and total afterload (37). The optimization of VAC improves the energetic efficiency of the cardiovascular system. In order to maintain adequate stroke volume and peripheral perfusion, the failing heart uses compensation mechanisms, which increase energy consumption. However, a significant part of the energetic expenditure is wasted and do not concur to blood ejection (38). During S/V therapy, we observed a reduction in PE and PVA while SW did not differ. PVA reduction reflects a decrease in the total mechanical energy of contraction and consequently in myocardial oxygen consumption, while PE is the amount of energy not converted to external work (or ejection, equivalently) (39, 40). Consequently, during S/V therapy WE improves, reflecting a more efficient mechanical energy transfer from the ventricle to the arterial system. It has been demonstrated that WE is a monotonic function of VAC and can be formulated as $SW/PVA = 1/[1 + (E_a/E_{es})/2]$ (41). An optimization of contractile state and/or a reduction of arterial afterload improves VAC, reduces energetic demand and increases WE.

Limitations

The most important limit of our study is the small sample size. Therefore, our results, especially those regarding HDFs estimation, should be considered as preliminary observations. Moreover, HDFs computation by echocardiography depends on image quality and it has to be considered as an estimation of real hemodynamic forces. Vascular afterload was assessed only with PV loop derived parameters. Finally, significant clinical outcomes were not evaluated, due to the limited number of major cardiac events observed during follow-up.

CONCLUSIONS

After 6 months of S/V therapy, cardiovascular remodeling was observed in our cohort of HFrEF patients, in terms of volumes reduction, increased myocardial contractility, intraventricular-pressure gradients distribution improvement and optimization of vascular afterload. The ultimate effect is an amelioration of ventricular-arterial coupling and mechanical energy conversion efficiency. Our findings highlight the pleiotropic effect of S/V therapy generating a virtuous circle of both cardiac and vascular remodeling.

DATA AVAILABILITY STATEMENT

The raw data supporting the conclusions of this article will be made available by the authors, without undue reservation.

ETHICS STATEMENT

The studies involving human participants were reviewed and approved by Policlinico Umberto I. The patients/participants provided their written informed consent to participate in this study.

AUTHOR CONTRIBUTIONS

SM, DF, LA, and VM contributed to conception and design of the study. MS and FL organized the database. SM performed the statistical analysis and wrote the first draft of the manuscript. DF, SC, MN, MM, LIB, GB, GT, GP, and CDV wrote sections of the manuscript. All authors contributed to manuscript revision, read, and approved the submitted version.

FUNDING

This study received funding from Novartis. The funder was not involved in the study design, collection, analysis, interpretation of data, the writing of this article or the decision to submit it for publication.

SUPPLEMENTARY MATERIAL

The Supplementary Material for this article can be found online at: <https://www.frontiersin.org/articles/10.3389/fcvm.2022.883769/full#supplementary-material>

REFERENCES

- McMurray JJV, Packer M, Desai AS, Gong J, Lefkowitz MP, Rizkala AR, et al. Angiotensin-neprilysin inhibition versus enalapril in heart failure. (2014) 5:132–3. doi: 10.1161/circ.132.suppl_3.19363
- Velazquez EJ, Morrow DA, DeVore AD, Duffy CI, Ambrosy AP, McCague K, et al. Angiotensin-neprilysin inhibition in acute decompensated heart failure. *N Engl J Med.* (2019) 380:539–48. doi: 10.1056/NEJMoa1812851
- Martens P, Belien H, Dupont M, Vandervoort P, Mullens W. The reverse remodeling response to sacubitril/valsartan therapy in heart failure with reduced ejection fraction. *Cardiovasc Ther.* (2018) 36:e12435. doi: 10.1111/1755-5922.12435
- Almufleh A, Marbach J, Chih S, Stadnick E, Davies R, Liu P, et al. Ejection fraction improvement and reverse remodeling achieved with Sacubitril/Valsartan in heart failure with reduced ejection fraction patients. *Am J Cardiovasc Dis.* (2017) 7:108–13.
- Wang Y, Zhou R, Lu C, Chen Q, Xu T, Li D. Effects of the angiotensin-receptor neprilysin inhibitor on cardiac reverse remodeling: meta-analysis. *J Am Heart Assoc.* (2019) 8:e012272. doi: 10.1161/JAHA.119.012272
- Januzzi JL, Prescott MF, Butler J, Felker GM, Maisel AS, McCague K, et al. Association of change in n-terminal pro-b-type natriuretic peptide following initiation of sacubitril-valsartan treatment with cardiac structure and function in patients with heart failure with reduced ejection fraction. *JAMA J Am Med Assoc.* (2019) 322:1085–95. doi: 10.1001/jama.2019.12821
- Docherty KF, Campbell RT, Brooksbank KJM, Dreisbach JG, Forsyth P, Godeseth RL, et al. Effect of neprilysin inhibition on left ventricular remodeling in patients with asymptomatic left ventricular systolic dysfunction late after myocardial infarction. *Circulation.* (2020) 144:199–209. doi: 10.1161/CIRCULATIONAHA.121.054892
- Ponikowski P, Voors AA, Anker SD, Bueno H, Cleland JGF, Coats AJS, et al. 2016 ESC Guidelines for the diagnosis and treatment of acute and chronic heart failure. *Eur Heart J.* (2016) 37:2129–200. doi: 10.1093/eurheartj/ehw128
- Galderisi M, Cosyns B, Edvardsen T, Cardim N, Delgado V, Di Salvo G, et al. Standardization of adult transthoracic echocardiography reporting in agreement with recent chamber quantification, diastolic function, and heart valve disease recommendations: an expert consensus document of the European Association of Cardiovascular Imag. *Eur Heart J Cardiovasc Imaging.* (2017) 18:1301–10. doi: 10.1093/ehjci/jex244
- Ommen SR, Nishimura RA, Appleton CP, Miller FA, Oh JK, Redfield MM, et al. Clinical utility of Doppler echocardiography and tissue Doppler imaging in the estimation of left ventricular filling pressures: a comparative simultaneous Doppler-catheterization study. *Circulation.* (2000) 102:1788–94. doi: 10.1161/01.CIR.102.15.1788
- Chen CH, Fetis B, Nevo E, Rochitte CE, Chiou KR, Ding PYA, et al. Noninvasive single-beat determination of left ventricular end-systolic elastance in humans. *J Am Coll Cardiol.* (2001) 38:2028–34. doi: 10.1016/S0735-1097(01)01651-5
- Antonini-Canterin F, Poli S, Vriz O, Pavan D, Bello V, Nicolosi G. The ventricular-arterial coupling: from basic pathophysiology to clinical application in the echocardiography laboratory. *J Cardiovasc Echogr.* (2013) 23:91–5. doi: 10.4103/2211-4122.127408
- Klotz S, Hay I, Dickstein ML, Yi GH, Wang J, Maurer MS, et al. Single-beat estimation of end-diastolic pressure-volume relationship: a novel method with potential for noninvasive application. *Am J Physiol Heart Circ Physiol.* (2006) 291:H403–12. doi: 10.1152/ajpheart.01240.2005
- Ikonidis I, Aboyans V, Blacher J, Brodmann M, Brutsaert DL, Chirinos JA, et al. The role of ventricular-arterial coupling in cardiac disease and heart failure: assessment, clinical implications and therapeutic interventions. A consensus document of the European Society of Cardiology Working Group on Aorta & Peripheral Vascular Diseases, European Association of Cardiovascular Imaging, and Heart Failure Association. *Eur J Heart Fail.* (2019) 21:402–24. doi: 10.1002/ehf.1436
- Suga H, Goto Y, Futaki S, Kawaguchi O, Yaku H, Hata K, et al. Systolic pressure-volume area (PVA) as the energy of contraction in Starling's law of the heart. *Heart Vessels.* (1991) 6:65–70. doi: 10.1007/BF02058751
- Pedrizetti G, Arvidsson PM, Töger J, Borgquist R, Domenichini F, Arheden H, et al. On estimating intraventricular hemodynamic forces from endocardial dynamics: a comparative study with 4D flow MRI. *J Biomech.* (2017) 60:203–10. doi: 10.1016/j.jbiomech.2017.06.046
- Pedrizetti G, Martiniello AR, Bianchi V, D'Onofrio A, Caso P, Tonti G. Changes in electrical activation modify the orientation of left ventricular flow momentum: novel observations using echocardiographic particle image velocimetry. *Eur Heart J Cardiovasc Imaging.* (2016) 17:203–9. doi: 10.1093/ehjci/jev137
- Castrichini M, Manca P, Nuzzi V, Barbati G, de Luca A, Korcova R, et al. Sacubitril/valsartan induces global cardiac reverse remodeling in long-lasting heart failure with reduced ejection fraction: standard and advanced echocardiographic evidences. *J Clin Med.* (2020) 9:906. doi: 10.3390/jcm9040906
- Cimino S, Maestrini V, Cantisani D, Petronilli V, Filomena D, Mancone M, et al. 2D/3D echocardiographic determinants of left ventricular reverse remodelling after MitraClip implantation. *Eur Heart J Cardiovasc Imaging.* (2019) 20:558–64. doi: 10.1093/ehjci/jez157
- Mazzetti S, Scifo C, Abete R, Margonato D, Chioffi M, Rossi J, et al. Short-term echocardiographic evaluation by global longitudinal strain in patients with heart failure treated with sacubitril/valsartan. *ESC Heart Fail.* (2020) 7:964–72. doi: 10.1002/ehf2.12656
- Von Lueder TG, Wang BH, Kompa AR, Huang L, Webb R, Jordaan P, et al. Angiotensin receptor neprilysin inhibitor LCZ696 attenuates cardiac remodeling and dysfunction after myocardial infarction by reducing cardiac fibrosis and hypertrophy. *Circulation Heart Fail.* (2015) 8:71–8. doi: 10.1161/CIRCHEARTFAILURE.114.001785
- Tran JS, Havakuk O, McLeod JM, Hwang J, Kwong HY, Shavell D, et al. Acute pulmonary pressure change after transition to sacubitril/valsartan in patients with heart failure reduced ejection fraction. *ESC Heart Fail.* (2021) 8:1706–10. doi: 10.1002/ehf2.13225
- Clements RT, Vang A, Fernandez-Nicolas A, Kue NR, Mancini TJ, Morrison AR, et al. Treatment of pulmonary hypertension with angiotensin ii receptor blocker and neprilysin inhibitor sacubitril/valsartan. *Circulation Heart Fail.* (2019) 12:1–6. doi: 10.1161/CIRCHEARTFAILURE.119.005819
- Vallalonga F, Airale L, Tonti G, Argulian E, Milan A, Narula J, et al. Introduction to hemodynamic forces analysis: moving into the new frontier of cardiac deformation analysis. *J Am Heart Assoc.* (2021) 10:e023417. doi: 10.1161/JAHA.121.023417
- Pedrizetti G. On the computation of hemodynamic forces in the heart chambers. *J Biomech.* (2019) 95:109323. doi: 10.1016/j.jbiomech.2019.109323
- Filomena D, Cimino S, Maestrini V, Cantisani D, Petronilli V, Mancone M, et al. Changes in intraventricular flow patterns after mitralclip implant in patients with functional severe mitral regurgitation. *J Am Soc Echocardiogr.* (2019) 32:1250–53.e1. doi: 10.1016/j.echo.2019.05.022
- Filomena D, Cimino S, Monosilio S, Galea N, Mancuso G, Francone M, et al. Impact of intraventricular haemodynamic forces misalignment on left ventricular remodelling after myocardial infarction. *ESC Heart Fail.* (2022) 9:496–505. doi: 10.1002/ehf2.13719
- Pedrizetti G, la Canna G, Alfieri O, Tonti G. The vortex - an early predictor of cardiovascular outcome? *Nat Rev Cardiol.* (2014) 11:545–53. doi: 10.1038/nrcardio.2014.75
- Dal Ferro M, De Paris V, Colli D-2. pdf, Stolfo D, Caiffa T, Barbati G, et al. Left ventricular response to cardiac resynchronization therapy: insights from hemodynamic forces computed by speckle tracking. *Front Cardiovasc Med.* (2019) 6:59. doi: 10.3389/fcvm.2019.00059
- Gopalan SM, Flaim C, Bhatia SN, Hoshijima M, Knoell R, Chien KR, et al. Anisotropic stretch-induced hypertrophy in neonatal ventricular myocytes micropatterned on deformable elastomers. *Biotechnol Bioeng.* (2003) 81:578–87. doi: 10.1002/bit.10506
- Seki T, Goto K, Kansui Y, Ohtsubo T, Matsumura K, Kitazono T. Angiotensin II receptor-neprilysin inhibitor sacubitril/valsartan improves endothelial dysfunction in spontaneously hypertensive rats. *J Am Heart Assoc.* (2017) 6:1–10. doi: 10.1161/JAHA.117.006617
- Williams B, Cockcroft JR, Kario K, Zappe DH, Brunel PC, Wang Q, et al. Effects of sacubitril/valsartan versus olmesartan on central hemodynamics in the elderly with systolic Hypertension. *Hypertension.* (2017) 69:411–20. doi: 10.1161/HYPERTENSIONAHA.116.08556
- Karagodin I, Kalantari S, Yu DB, Kim G, Sayer G, Addetia K, et al. Echocardiographic evaluation of the effects of sacubitril-valsartan on vascular

- properties in heart failure patients. *Int J Cardiovasc Imaging*. (2020) 36:271–8. doi: 10.1007/s10554-019-01708-4
34. Hughes AD, Nielsen H, Sever PS. The effect of atrial natriuretic peptide on human isolated resistance arteries. *Br J Pharmacol*. (1989) 97:1027–30. doi: 10.1111/j.1476-5381.1989.tb12558.x
 35. Melo LG, Veress AT, Ackermann U, Sonnenberg H. Chronic regulation of arterial blood pressure by ANP: role of endogenous vasoactive endothelial factors. *Am J Physiol*. (1998) 275:H1826–33. doi: 10.1152/ajpheart.1998.275.5.H1826
 36. Hartupee J, Mann DL. Neurohormonal activation in heart failure with reduced ejection fraction. *Nat Rev Cardiol*. (2016) 14:30–8. doi: 10.1038/nrcardio.2016.163
 37. Monge García MI, Santos A. Understanding ventriculo-arterial coupling. *Ann Transl Med*. (2020) 8:795. doi: 10.21037/atm.2020.04.10
 38. Russell K, Eriksen M, Aaberge L, Wilhelmsen N, Skulstad H, Gjesdal O, et al. Assessment of wasted myocardial work: a novel method to quantify energy loss due to uncoordinated left ventricular contractions. *Am J Physiol Heart Circ Physiol*. (2013) 305:996–1003. doi: 10.1152/ajpheart.00191.2013
 39. Suga H. Total mechanical energy of a ventricle model and cardiac oxygen consumption. *Am J Physiol*. (1979) 236:H498–505. doi: 10.1152/ajpheart.1979.236.3.H498
 40. Suga H, Hayashi T, Shirahata M. Regression of cardiac oxygen consumption on ventricular pressure-volume area in dog. *Am J Physiol*. (1981) 240:H320–5. doi: 10.1152/ajpheart.1981.240.3.H320
 41. Asanoi H, Sasayama S, Kameyama T. Ventriculoarterial coupling in normal and failing heart in humans. *Circ Res*. (1989) 65:483–93. doi: 10.1161/01.RES.65.2.483

Conflict of Interest: The authors declare that the research was conducted in the absence of any commercial or financial relationships that could be construed as a potential conflict of interest.

Publisher's Note: All claims expressed in this article are solely those of the authors and do not necessarily represent those of their affiliated organizations, or those of the publisher, the editors and the reviewers. Any product that may be evaluated in this article, or claim that may be made by its manufacturer, is not guaranteed or endorsed by the publisher.

Copyright © 2022 Monosilio, Filomena, Luongo, Sannino, Cimino, Neccia, Mariani, Birtolo, Benedetti, Tonti, Pedrizzetti, Vizza, Maestrini and Agati. This is an open-access article distributed under the terms of the Creative Commons Attribution License (CC BY). The use, distribution or reproduction in other forums is permitted, provided the original author(s) and the copyright owner(s) are credited and that the original publication in this journal is cited, in accordance with accepted academic practice. No use, distribution or reproduction is permitted which does not comply with these terms.



Left Atrial Appendage Mechanical Dispersion Assessed by Speckle-Tracking Echocardiography as a Determinant of Left Atrial Appendage Blood Stasis in Patients With Atrial Fibrillation

OPEN ACCESS

Edited by:

Attila Kovacs,
Semmelweis University, Hungary

Reviewed by:

Balint Szilveszter,
Semmelweis University, Hungary
Szilvia Herczeg,
Semmelweis University, Hungary
Diana Ruxandra Florescu,
University of Medicine and Pharmacy
of Craiova, Romania

*Correspondence:

Zhelan Zheng
1186034@zju.edu.cn
Chenyang Jiang
cyjjiang@zju.edu.cn

[†] These authors have contributed
equally to this work and share last
authorship

Specialty section:

This article was submitted to
Cardiovascular Imaging,
a section of the journal
Frontiers in Cardiovascular Medicine

Received: 26 March 2022

Accepted: 16 May 2022

Published: 06 June 2022

Citation:

Mao Y, Zhao H, Yu C, Yang Y,
Ma M, Wang Y, Jiang R, Zhao B,
Zheng Z and Jiang C (2022) Left Atrial
Appendage Mechanical Dispersion
Assessed by Speckle-Tracking
Echocardiography as a Determinant
of Left Atrial Appendage Blood Stasis
in Patients With Atrial Fibrillation.
Front. Cardiovasc. Med. 9:905293.
doi: 10.3389/fcvm.2022.905293

Yankai Mao¹, Huajie Zhao², Chan Yu¹, Yuan Yang¹, Mingming Ma¹, Yunhe Wang³,
Ruhong Jiang³, Bowen Zhao¹, Zhelan Zheng^{2*†} and Chenyang Jiang^{3*†}

¹ Department of Diagnostic Ultrasound & Echocardiography, Sir Run Run Shaw Hospital, Zhejiang University School of Medicine, Hangzhou, China, ² Department of Echocardiography and Vascular Ultrasound Center, First Affiliated Hospital, Zhejiang University School of Medicine, Hangzhou, China, ³ Department of Cardiology, Key Laboratory of Cardiovascular Intervention and Regenerative Medicine of Zhejiang Province, Sir Run Run Shaw Hospital, School of Medicine, Zhejiang University, Hangzhou, China

Aims: We sought to investigate the relationship of left atrial appendage (LAA) mechanical dispersion (MD) with LAA dense spontaneous echo contrast (SEC) or thrombus, and to compare its usefulness in the identification of thrombogenesis with left atrial (LA) MD or LA/LAA strain parameters in patients with atrial fibrillation (AF).

Methods: We conducted a cross-sectional study of 493 consecutive patients with AF [65(58.5–71.0) years, male 66.9%] who underwent echocardiography prior to catheter ablation. We measured the LAA and LA global longitudinal strain (GLS) using speckle-tracking echocardiography (STE). LAA MD and LA MD was defined as the standard deviation (SD) of time to peak positive strain corrected by the R-R interval.

Results: Patients with LAA dense SEC/thrombus ($n = 70$) had significantly higher LAA MD than controls ($n = 423$) [median 14.2(11.6–16.8)% vs 9.4(6.2–12.1)%, $p < 0.01$]. Multivariable analysis showed that LAA MD was independently associated with LAA dense SEC/thrombus in four different models (Odds ratio, 1.23–1.24; $p < 0.01$), and provided additional diagnostic value over clinical and standard echocardiographic parameters. Whereas, LA MD was not independently associated with LAA dense SEC/thrombus and had no incremental value over other LA/LAA mechanical parameters.

Conclusion: LAA mechanical dispersion was an independent determinant of LAA dense SEC/thrombus in AF patients, incremental to conventional risk factors and superior to LA mechanical dispersion.

Keywords: left atrial appendage, mechanical dispersion, speckle-tracking echocardiography, atrial fibrillation, left atrium

INTRODUCTION

Atrial fibrillation (AF) is the most common clinically relevant cardiac arrhythmia, posing patients at higher risk of ischemic stroke (1). Importantly, AF-related stroke is associated with an increased mortality and worse outcomes than non-AF strokes (2). Preventive strategies are essential and should be delivered based on risk stratification. CHA2DS2-VASc scoring system is the most prevalent scheme for stratifying stroke risk in AF patient (3), but there is a lack of direct mechanistic link with stroke and its predictive power is modest in those with a score of <2 (4).

For the past century, left atrial appendage (LAA) has been regarded to be the major source of AF-related strokes (5, 6), as more than 95% of thrombus formation originated from LAA (7). Hence, it would be of great clinical significance to identify individuals at high risk of LAA thrombus, especially those with low CHA2DS2-VASc score. The structural and functional remodeling of LAA and LA during AF, including cavity dilation, endocardial fibroelastosis and depressed myocardial function are all potential markers of LAA thrombus and spontaneous echo contrast (SEC) (8–12). Besides the well-established predictors like LA enlargement, LAA morphology and LAA peak flow velocities (13–15), subclinical myocardial dysfunction of LAA and LA detected with speckle-tracking echocardiography (STE) (16) has emerged as useful markers. Impaired LA and LAA global longitudinal strain (GLS) are closely correlated with LAA blood stasis (17–21). STE can also measure the timing of myocardial contraction, known as mechanical dispersion (MD), which represents the degree of discoordination of wall motion. Recently, the role of LA MD in thrombogenesis was investigated as a further step to dissect the mechanism when LA function is depressed, and it was proved to have incremental values in identifying LAA thrombi or sludge (22, 23) and previous stroke/transient ischemic attack (TIA) in AF patients (24, 25). Similarly, we found LAA MD is greater in AF patients with a history of thromboembolism than those without in our previous studies (25, 26), supporting the hypothesis that LAA dyssynchrony may play a central role in the mechanism of thrombogenesis. Whereas, the direct mechanistic link between LAA MD and LAA blood stasis has not been fully addressed. The purpose of this study was to quantify the association of LAA mechanical dispersion with LAA dense SEC or thrombus and to compare its value in the risk stratification for thrombogenesis with LA MD or LA/LAA GLS in patients with AF.

MATERIALS AND METHODS

Study Population

We prospectively included 656 consecutive AF patients without significant valvular diseases or prosthetic valves. All patients were referred for catheter ablation to one of two Chinese tertiary hospitals (Sir Run Run Shaw Hospital, Zhejiang University School of Medicine and First affiliated hospital, Zhejiang University School of Medicine) between April 2019 and May 2021. Exclusion criteria: (1) cardiomyopathy, (2) congenital heart disease, (3) history of any cardiac surgery and/or cardiac device

implantation, (4) cardiac mass, (5) inadequate image quality to perform strain analysis, and (6) sinus rhythm at the time of echocardiography. Patients were classified as having either paroxysmal or persistent AF according to the guidelines (3, 27). Clinical information including demographic data, medical history, medication history, and baseline examination data were comprehensively assessed and CHA2DS2-VASc score was computed accordingly (3). Venous blood samples were obtained from the basilic vein after overnight fast. Laboratory data, including homocysteine, lipid levels were collected and analyzed.

The study protocol was approved by the institutional medical ethics committees of the two participating hospitals and was conducted in accordance with the Declaration of Helsinki and its later amendments. All patients provided their written, informed consent.

Standard Echocardiography

All participants routinely underwent transthoracic echocardiography (TTE) and transesophageal echocardiography (TEE) after admission. Echocardiographic examinations were performed using a Vivid E95 scanner (GE Vingmed Ultrasound AS, Horten, Norway) equipped with a M5Sc (1.4–4.6 MHz) and 6VT (3.0–8.0 MHz) probe. The grayscale frame rate was set to 60–90 frames/second. Standard echocardiographic measurements were taken according to current recommendations (28). LA and LAA volumes (LAV and LAAV) were determined by modified Simpson's method from apical four- and two-chamber views on TTE (LAV) and two orthogonal views typically at 45° and 135° on TEE (LAAV), respectively. The LA and LAA emptying fraction (LAEF and LAAEF) were calculated as $[\text{maximum volume (Vmax)} - \text{minimal volume (Vmin)}] / \text{Vmax} \times 100\%$. LAA peak emptying velocity (EV) and filling velocity (FV) was obtained with the sampling placed in the proximal third of the LAA cavity. LAA and the inlet of the pulmonary veins were excluded from LA tracing. All volumetric variables were subsequently indexed by body surface area.

Lidocaine hydrochloride spray was used for local anesthesia before TEE studies. LAA were carefully examined for the presence of dense SEC or thrombus by sweeping from 0° to 180° at the mid-esophageal position. The dense SEC was defined as very slow swirling smoke-like echoes detectable within LAA throughout the cardiac cycle. A thrombus was defined as a fixed or mobile, irregularly shaped, echo-dense mass that was clearly distinct from adjacent endocardium and pectinate muscles. The presence of dense SEC or thrombus was verified by two independent observers.

Speckle-Tracking Echocardiography

All strain analysis was performed with vendor-dependent software (EchoPAC PC version 203, GE Vingmed Ultrasound AS, Horten Norway). The LA and LAA endocardial borders were manually traced in apical four-chamber and two-chamber views (LA) and mid-esophageal views obtained at 0°, 45°, 90°, and 135° (LAA), respectively. Regions of interest were manually adjusted to fit the wall thickness. All tracking was reviewed to ensure it truly represented LA/LAA wall motion, and poorly

tracked segments would be rejected. The strain curves of the global and regional LA /LAA wall were generated, and global peak positive longitudinal strain (GLS) was measured and averaged from two apical views for LA and four mid-esophageal views for LAA. LAA and LA MD was defined as the standard deviation (SD) of the time to peak positive strain of each segment and expressed as a percentage of the R-R' interval. Higher values of MD indicate a greater degree of mechanical dyssynchrony. The reference frame of zero strain was set at left ventricular (LV) end-diastole (R-R gating) (29). To resolve the problem of beat-to-beat variation in STE measurements we used the index-beat method (22, 30). A cardiac cycle was selected for analysis where the preceding and pre-preceding R-R interval are of similar duration. All echocardiographic analysis was performed by one investigator experienced with strain imaging and blinded to the patients' information. Among the 11,832 LAA segments and 5,916 LA segments analyzed, STE analysis was feasible in 16,926 (95.4%) segments.

Statistical Analysis

IBM SPSS package 25.0 (SPSS, Inc., Chicago, IL, United States) and MedCalc version 12.5.0.0 (MedCalc Software, Mariakerke, Belgium), was used to perform the statistical analyses. Statistical significance was defined as $P < 0.05$. Continuous data were presented as mean \pm standard deviation for normally distributed variables and median (interquartile range) for non-Gaussian variables. Categorical variables were summarized as number and percentages. Comparisons of the variables were performed by using independent Student's *t*-test, the Mann-Whitney *U* test, Chi-square test or Fisher's exact test where appropriate. Multivariate binary logistic regression analysis

was performed to determine the independent markers using variables with $p < 0.05$ in the univariate analysis. Receiver operating characteristic (ROC) curves for different variables to test their abilities to discriminate patients with and without LAA dense SEC/thrombus, and the optimal cutoff value was determined as the value closest to the corner of the ROC curve. The incremental value of LAA MD and other mechanical parameters was tested by comparing global χ^2 values in a series of models, areas under the ROC curve (AUCs) and net reclassification improvement.

Inter- and intra-observer variability for LA/LAA GLS and LA/LAA MD were studied in a random sample of 25 patients. Measurements were repeated >4 weeks apart by the same observer and by another experienced reader. The mean absolute differences between repeated measurements were calculated and assessed using Bland-Altman plots.

RESULTS

Demographic and Clinical Characteristics

Out of 656 patients with AF, we excluded 58 patients either with congenital heart disease ($n = 10$), history of cardiac surgery and/or cardiac device implantation ($n = 12$), cardiac mass ($n = 3$), cardiomyopathies ($n = 16$), and inadequate image quality to perform strain analysis ($n = 17$). We also excluded patients who were in sinus rhythm at the time of echocardiography ($n = 105$). A total of 493 patients were included in the final analysis [median age, 65 (58.5, 71.0) years; 33.1% women, 47.5% persistent AF]. A total of 70 (14.2%) patients had dense SEC in

TABLE 1 | Baseline clinical characteristics.

Clinical characteristic	All patients ($n = 493$)	Dense SEC or thrombus ($n = 70$)	Controls ($n = 423$)	<i>P</i> -value
Age, y	65 (58.5–71.0)	69.5 (63.8–74.3)	64 (58–71)	<0.01
Female	163 (33.1)	49 (70)	281 (66.4)	0.56
Body mass index, kg/m ²	24.5 (22.3–26.7)	24.4 (22.3–26.3)	24.5 (22.4–26.7)	0.55
Body surface area, m ²	1.7 (1.6–1.9)	1.7 (1.6–1.8)	1.7 (1.6–1.9)	0.12
CHA2DS2-VASc score	2 (1–3)	3 (1.8–4)	2 (1–3)	<0.01
Persistent AF	234 (47.5)	56 (80.0)	178 (42.1)	<0.01
Prior stroke/TIA	72 (14.6)	19 (27.1)	53 (12.5)	0.01
Anticoagulation	236 (47.9)	37 (52.9)	199 (47.1)	0.37
Warfarin	82 (16.6)	17 (24.3)	65 (15.4)	
Rivaroxaban	125 (25.4)	13 (18.6)	112 (26.5)	
Dabigatran	29 (5.9)	7 (10)	22 (5.2)	
Heart failure	37 (7.5)	12 (17.1)	25 (5.9)	0.001
LV ejection fraction $< 50\%$	24 (4.9)	11 (15.7)	13 (3.1)	
Old myocardial infarction	5 (1)	1 (1.4)	4 (0.9)	0.71
Coronary artery disease	77 (15.6)	16 (22.9)	61 (14.4)	0.07
Hypertension	291 (59.0)	48 (68.6)	243 (57.4)	0.08
Diabetes	82 (16.6)	11 (15.7)	71 (16.8)	0.82
Dyslipidemia	169 (34.3)	19 (27.1)	150 (35.5)	0.17
Homocysteine, $\mu\text{mol/L}$	11.8 (9.7–14.6)	13.3 (10.7–17.0)	11.7 (9.4–14.1)	<0.01

Data are expressed as median (interquartile range), or number (percentage).

AF, atrial fibrillation; LV, left ventricle; SEC, spontaneous echo contrast; TIA, transient ischemic attack.

TABLE 2 | Echocardiographic parameters by groups.

Parameters	All patients (n = 493)	Dense SEC or thrombus (n = 70)	Controls (n = 423)	P-value
LV parameters				
LV end-diastolic volume index, mL/m ²	65.6 ± 14.2	68.5 ± 16.9	65.1 ± 13.7	0.11
LV end-systolic volume index, mL/m ²	22.3 (17.7–27.7)	24.0 (18.1–33.8)	22.0 (17.8–27.3)	0.06
LV mass index, g/m ²	97.5 (84.2–115.8)	103.7 (91.8–123.2)	96.0 (83.4–114.1)	0.03
LV ejection fraction, %	64.9 (59.4–70.3)	61.9 (56.3–69.0)	65.3 (59.9–70.3)	0.01
LA parameters				
LAVI _{max} , mL/m ²	42.0 (32.3–53.8)	58.5 (48.6–69.0)	40.5 (31.2–49.5)	<0.01
LAVI _{min} , mL/m ²	26.1 (16.6–40.0)	47.0 (35.7–58.2)	24.4 (16.0–36.1)	<0.01
LA emptying fraction, %	35.6 (22.5–50.0)	21.8 (15.0–28.5)	38.2 (24.6–51.8)	<0.01
LA GLS, %	14.6 (9.5–25.5)	9.0 (7.1–11.0)	17.5 (10.9–26.8)	<0.01
LA MD, %	8.0 (5.5–10.4)	10.2 (8.1–13.5)	7.7 (5.2–9.9)	<0.01
LAA parameters				
LAAVI _{max} , mL/m ²	3.5 (2.5–4.7)	5.0 (3.7–7.3)	3.3 (2.4–4.2)	<0.01
LAAVI _{min} , mL/m ²	1.4 (0.6–2.5)	3.5 (2.1–4.3)	1.2 (0.6–2.1)	<0.01
LAA emptying fraction, %	55.6 (40.0–71.4)	37.5 (22.6–50.0)	60 (45.5–75.0)	<0.01
LAA emptying velocity, cm/s	46.0 (33.0–63.0)	28.0 (24.0–36.0)	49.0 (36.3–66.0)	<0.01
LAA filling velocity, cm/s	51.0 (38.0–66.0)	32.5 (24.0–44.8)	54.0 (42.0–68.0)	<0.01
LAA GLS, %	11.8 (8.7–16.1)	7.8 (6.0–9.3)	12.4 (9.4–16.8)	<0.01
LAA MD, %	9.9 (6.7–12.7)	14.2 (11.6–16.8)	9.4 (6.2–12.1)	<0.01

Data are expressed as mean ± SD or median (interquartile range).

GLS, global longitudinal strain; LA, left atrium; LAA, left atrial appendage; LAAVI, LAA volume index; LAVI, LA volume index; LV, left ventricle; MD, mechanical dispersion; SEC, spontaneous echo contrast.

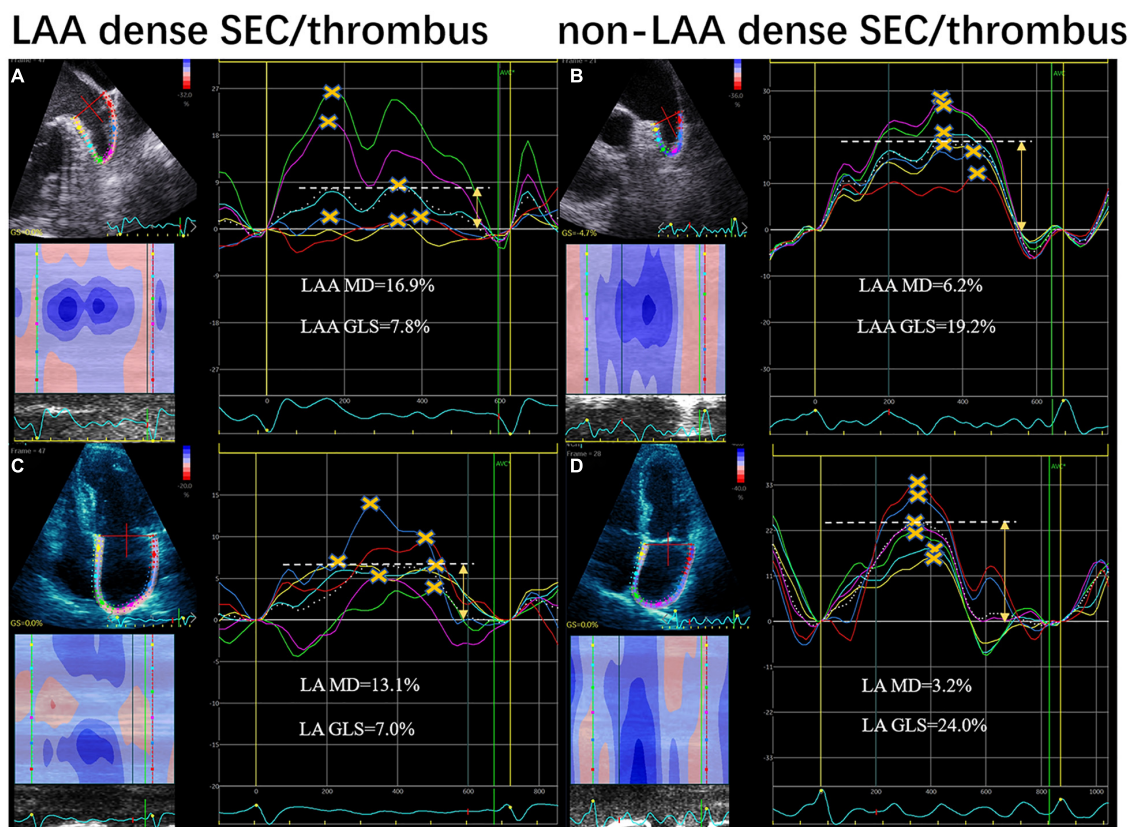


FIGURE 1 | LAA and LA strain curves from speckle-tracking in patients with LAA dense spontaneous echo contrast and thrombus (A,C) and controls (B,D). Yellow crosses indicate the positive peaks of each curve. Yellow arrows indicate the global peak longitudinal strain (GLS). Mechanical dispersion (MD) was defined as the SD of time to peak and expressed as a percentage of the R-R interval. LA, left atrium; LAA, left atrial appendage.

TABLE 3 | Univariable analyses of associations with LAA dense SEC or thrombus.

Variables	OR (95% CI)	P-value
Clinical parameters		
Age, y	1.06 (1.03–1.09)	<0.01
Female	0.85 (0.49–1.47)	0.56
Body mass index, kg/m ²	0.97 (0.89–1.05)	0.39
CHA2DS2-VASc score	1.36 (1.16–1.60)	<0.01
Persistent AF	5.51 (2.97–10.2)	<0.01
Prior stroke/TIA	2.60 (1.43–4.74)	0.002
Anticoagulation	1.26 (0.76–2.10)	0.37
Heart failure	3.29 (1.57–6.91)	0.002
Homocysteine	1.07 (1.03–1.11)	<0.01
Echocardiographic parameters		
LV end-diastolic volume index, mL/m ²	1.02 (0.99–1.04)	0.06
LV end-systolic volume index, mL/m ²	1.05 (1.02–1.07)	<0.01
LV mass index, g/m ²	1.01 (1.00–1.02)	0.04
LV ejection fraction, %	0.95 (0.93–0.98)	0.001
LAVI _{max} , mL/m ²	1.07 (1.05–1.09)	<0.01
LAVI _{min} , mL/m ²	1.08 (1.06–1.10)	<0.01
LA emptying fraction, %	0.94 (0.92–0.96)	<0.01
LA GLS, %	0.83 (0.78–0.88)	<0.01
LA MD, %	1.26 (1.17–1.35)	<0.01
LAAVI _{max} , mL/m ²	1.57 (1.37–1.79)	<0.01
LAAVI _{min} , mL/m ²	2.43 (1.97–2.99)	<0.01
LAA emptying fraction, %	0.94 (0.93–0.96)	<0.01
LAA emptying velocity, cm/s	0.91 (0.88–0.93)	<0.01
LAA filling velocity, cm/s	0.92 (0.90–0.94)	<0.01
LAA GLS, %	0.68 (0.62–0.76)	<0.01
LAA MD, %	1.29 (1.21–1.37)	<0.01

AF, atrial fibrillation; GLS, global longitudinal strain; LA, left atrium; LAA, left atrial appendage; LAAVI, LAA volume index; LAVI, LA volume index; LV, left ventricle; MD, mechanical dispersion; CI, Confidence intervals; OR, odds ratio; SEC, spontaneous echo contrast; TIA, transient ischemic attack.

LAA, while 38 (54.3%) had thrombus in LAA. The remaining patients were designated as the control group ($n = 423$, 85.8%). **Table 1** summarizes clinical characteristics of the study population. Patients with dense SEC/thrombus were older, with higher CHA2DS2-VASc scores, higher incidence of persistent AF, previous TIA or stroke and heart failure. In addition, patients in the SEC/thrombus group had significantly higher plasma homocysteine levels. A total of 236 (47.9%) patients were on anticoagulation prior to ablation, and the usage of anticoagulants didn't differ between two groups ($P = 0.367$). According to the standard of peri-procedural care for catheter ablation of AF, all patients were on anticoagulation at the time of ablation procedure. TEE was normally performed several hours before the ablation and anticoagulants were not discontinued. In patients not receiving anticoagulation ($n = 257$), 125 had a CHADS-VASc score ≥ 2 . The underuse of anticoagulants in these patients were due to poor compliance, high bleeding risk, or other contraindications.

Echocardiographic Parameters

Table 2 shows a comparison of echocardiographic parameters between the patients with and without dense SEC or thrombus.

Although LV volumes were comparable between two groups, the patients with dense SEC or thrombus had significantly lower LV ejection fraction (EF). Patients in this group also had increased LA /LAA volumes index (LAVI, LAAVI), decreased LA/LAA function (presented as emptying fraction and GLS), and reduced LAA flow velocities. Furthermore, LAA MD were more pronounced in SEC/thrombus group than in the controls [median 9.4 (6.2–12.1)% vs. 14.2 (11.6–16.8)%, respectively; $P < 0.01$]. **Figure 1** shows representative LA and LAA strain curves in patients with and without dense SEC or thrombus.

Determinants of Left Atrial Appendage Dense Spontaneous Echo Contrast or Thrombus

In the univariate logistic regression analysis, LAA dense SEC or thrombus was significantly associated with various clinical and echocardiographic parameters (**Table 3**). LAA MD remained to be independent in four different multivariate models (OR 1.23–1.24, $p < 0.01$) (**Table 4**). We also confirmed the independent association of homocysteine (OR 1.05–1.07, $p < 0.05$), LA GLS (OR 0.87–0.89, $p < 0.01$), LAAFI (OR 0.94–0.95, $p < 0.01$), and LAA GLS (OR 0.82–0.89, $P < 0.05$) with dense SEC or thrombus in at least two models. However, LA MD was not an independent contributor in any multivariate models.

ROC curve analysis results are listed in **Supplementary Table 1**. The AUCs for LAA parameters were higher than clinical, LV and LA variables. Importantly, the AUCs for LAA MD (0.82), LAA GLS (0.84), and LA GLS (0.80) were comparable but higher than that of LA MD (0.74, all $p < 0.05$). The optimal cutoff value for LAA MD to identify LAA dense SEC or thrombus was $> 11.2\%$, with a sensitivity of 80.0% and specificity of 67.16%. We also calculated cutoff values for LAA GLS, LA GLS, and LA MD.

Incremental Value of Left Atrial Appendage Mechanical Dispersion for Identifying Dense Spontaneous Echo Contrast or Thrombus and Comparison With Other Left Atrial/Left Atrial Appendage Mechanics

The addition of LA/LAA mechanics (LA GLS, LAA GLS, LA MD, LAA MD) to CHA2DS2-VASc score significantly improved AUCs in ROC curve analyses. Moreover, the AUC of CHA2DS2-VASc score plus LAA MD was significantly higher than adding LA MD (0.83 vs. 0.76, $P = 0.04$), but comparable to adding LAA GLS or LA GLS ($P = 0.61$ and 0.48 , respectively, **Figure 2**). We also assessed the incremental value of LAA MD, LAA GLS, LA GLS or LA MD over one another by comparing the global χ^2 value in modeling steps. The initial model based on CHA2DS2-VASc score, LVEF, LAVI_{max}, and LAAFI ($\chi^2 = 106.6$) was significantly improved by adding LA MD ($\chi^2 = 114.6$, $P < 0.01$) and further improved by adding LA GLS ($\chi^2 = 123.2$, $P < 0.01$), LAA GLS ($\chi^2 = 141.1$, $P < 0.01$)

TABLE 4 | Multivariate analyses of associations with LAA dense SEC or thrombus.

Variable	Model 1		Model 2		Model 3		Model 4	
	OR (95% CI)	P-value	OR (95% CI)	P-value	OR (95% CI)	P-value	OR (95% CI)	P-value
Clinical parameters								
Age	1.02 (0.98, 1.06)	0.45	1.01 (0.97–1.06)	0.57	1.02 (0.98–1.06)	0.26		
CHA2DS2-VASc score	0.99 (0.76–1.29)	0.94	0.99 (0.75–1.31)	0.97	1.02 (0.79–1.32)	0.86	1.01 (0.79–1.28)	0.96
Persistent AF	1.17 (0.50–2.72)	0.72	1.04 (0.41–2.62)	0.94	1.25 (0.54–2.91)	0.60		
Homocysteine	1.05 (1.01–1.10)	0.02	1.07 (1.02–1.12)	0.009	1.06 (1.01–1.10)	0.02	1.07 (1.02–1.13)	0.006
LV parameters								
LV end-systolic volume index, mL/m ²					1.00 (0.94–1.07)	0.93	1.01 (0.97–1.04)	0.71
LV mass index, g/m ²					1.01 (0.99–1.02)	0.35		
LV ejection fraction, %					0.99 (0.95–1.03)	0.61	1.00 (0.93–1.07)	0.94
LA parameters								
LAVI _{max} , mL/m ²	1.02 (1.00–1.05)	0.05					1.01 (0.98–1.04)	0.45
LA emptying fraction, %	0.99 (0.96–1.02)	0.59						
LA GLS, %	0.89 (0.83–0.97)	0.005	0.93 (0.85–1.01)	0.08	0.87 (0.81–0.94)	<0.01	0.92 (0.85–1.00)	0.05
LA MD, %	1.05 (0.95–1.16)	0.37	1.10 (0.99–1.23)	0.09	1.07 (0.96–1.18)	0.23	1.11 (0.99–1.24)	0.07
LAA parameters								
LAAVI _{max} , mL/m ²			1.18 (0.98–1.43)	0.08				
LAA emptying fraction, %			0.99 (0.97–1.02)	0.50				
LAA emptying velocity, cm/s			0.99 (0.95–1.04)	0.77				
LAA filling velocity, cm/s			0.95 (0.92–0.97)	<0.01			0.94 (0.92–0.97)	<0.01
LAA GLS, %	0.84 (0.75–0.94)	0.002	0.90 (0.80–1.00)	0.06	0.82 (0.74–0.91)	<0.01	0.89 (0.79–0.99)	0.04
LAA MD, %	1.24 (1.14–1.35)	<0.01	1.23 (1.13–1.34)	<0.01	1.24 (1.14–1.35)	<0.01	1.24 (1.14–1.35)	<0.01

AF, atrial fibrillation; GLS, global longitudinal strain; LA, left atrium; LAA, left atrial appendage; LAAVI, LAA volume index; LAVI, LA volume index; LV, left ventricle; MD, mechanical dispersion; CI, Confidence intervals; OR, odds ratio; SEC, spontaneous echo contrast.

Model 1 adjusted with clinical and LA echocardiographic parameters.

Model 2 adjusted with clinical and LAA echocardiographic parameters.

Model 3 adjusted with clinical and LV echocardiographic parameters.

Model 4 adjusted with multi mixed parameters.

and finally LAA MD ($\chi^2 = 168.4$, $P < 0.01$). Similarly, the same initial model was significantly improved by adding LA GLS ($P = 0.04$) and LAA GLS ($P = 0.02$) in the last step of sequential models (Figure 3). However, the addition of LA MD provided no incremental value ($P = 0.21$) over other LA/LAA mechanical parameters.

Moreover, we summarized the prevalence of LAA dense SEC or thrombus according to different LA /LAA mechanics and CHA2DS2-VASc score (Figure 4). LAA MD significantly increased the risk of LAA blood stasis in patients with CHA2DS2-VASc score <2 (OR 36.3, 95% CI 4.7–280.4, $P = 0.001$) (Supplementary Table 2). Adding LAA MD, LAA GLS, and LAGLS to CHA2DS2-VASc score led to significant net reclassification improvement (0.30, 0.27 and 0.26, all $P < 0.01$) whereas adding LA MD did not lead to significant improvement (0.17, $P = 0.06$) (Supplementary Tables 3–6).

Reproducibility

Bland-Altman analysis for inter-and intra-observer variability was shown in Supplementary Figure 1. For inter-observer reproducibility, the mean differences in LA GLS, LAA GLS, LA MD, and LAA MD were $1.1 \pm 2.7\%$, $0.7 \pm 3.0\%$, $2.1 \pm 2.3\%$ and $3.0 \pm 3.5\%$, respectively. The mean differences between the repeated measures of the same observer in LA GLS, LAA GLS, LA

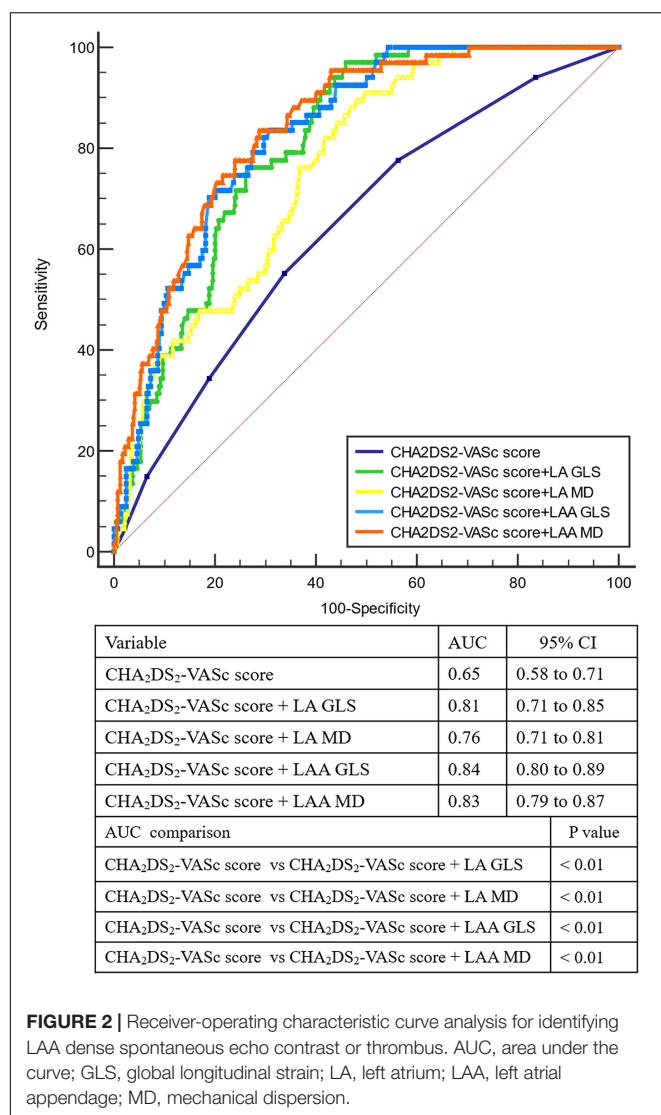
MD and LAA MD were $-0.7 \pm 2.8\%$, $-0.6 \pm 2.5\%$, $0.8 \pm 3.1\%$, and $2.4 \pm 3.8\%$, respectively.

DISCUSSION

In this cross-sectional study, we found that LAA mechanical dispersion assessed by speckle-tracking echocardiography was an independent determinant of LAA dense SEC or thrombus in patients with AF, incremental to clinical and echocardiographic parameters and other strain measurements. This study also identified similarly significant reclassification improvement by adding LAA MD, LAA GLS, and LA GLS to CHA2DS2-VASc score. Moreover, LAA MD was superior to LA MD in identifying LAA dense SEC or thrombus.

Left Atrial Appendage Mechanical Dispersion as a Mechanism of Thrombogenesis

As the most common site for thrombus formation (7), LAA should be given meticulous attention in the setting of AF. In line with previous results (20, 21, 31), our findings confirmed that LAA EF, LAA flow velocities and LAA GLS are significant contributors to LAA stasis, with the latter two remaining



independent in at least two multivariate models. We also found AF patients with dense SEC or thrombus in LAA had higher LAA MD than those without. The LAA MD cutoff of >11.2% help clinicians to sensitively identify patients at higher risk for LAA dense SEC or thrombus, especially in those with CHA₂DS₂-VASc score <2. To the best of our knowledge, this is the first study demonstrating that LAA MD is an independent determinant of LAA stasis in AF patients using speckle-tracking echocardiography. What's more, LAA MD provided incremental values over clinical, conventional TTE and TEE parameters.

The mechanistic link as to how abnormal LAA MD causes thrombosis remains unclear. Previous studies found an association among disturbances in the LAA conduction, LAA fibrosis and LAA thrombus (9, 11, 32). We speculate that LAA fibrotic changes increase LAA discoordination during filling phase, which consequently slow down the regional blood flow and lead to thrombogenesis.

Reflecting this change, LAA MD might contribute to LAA blood stasis.

Comparison of Predictive Values Among Left Atrial/Left Atrial Appendage Mechanics

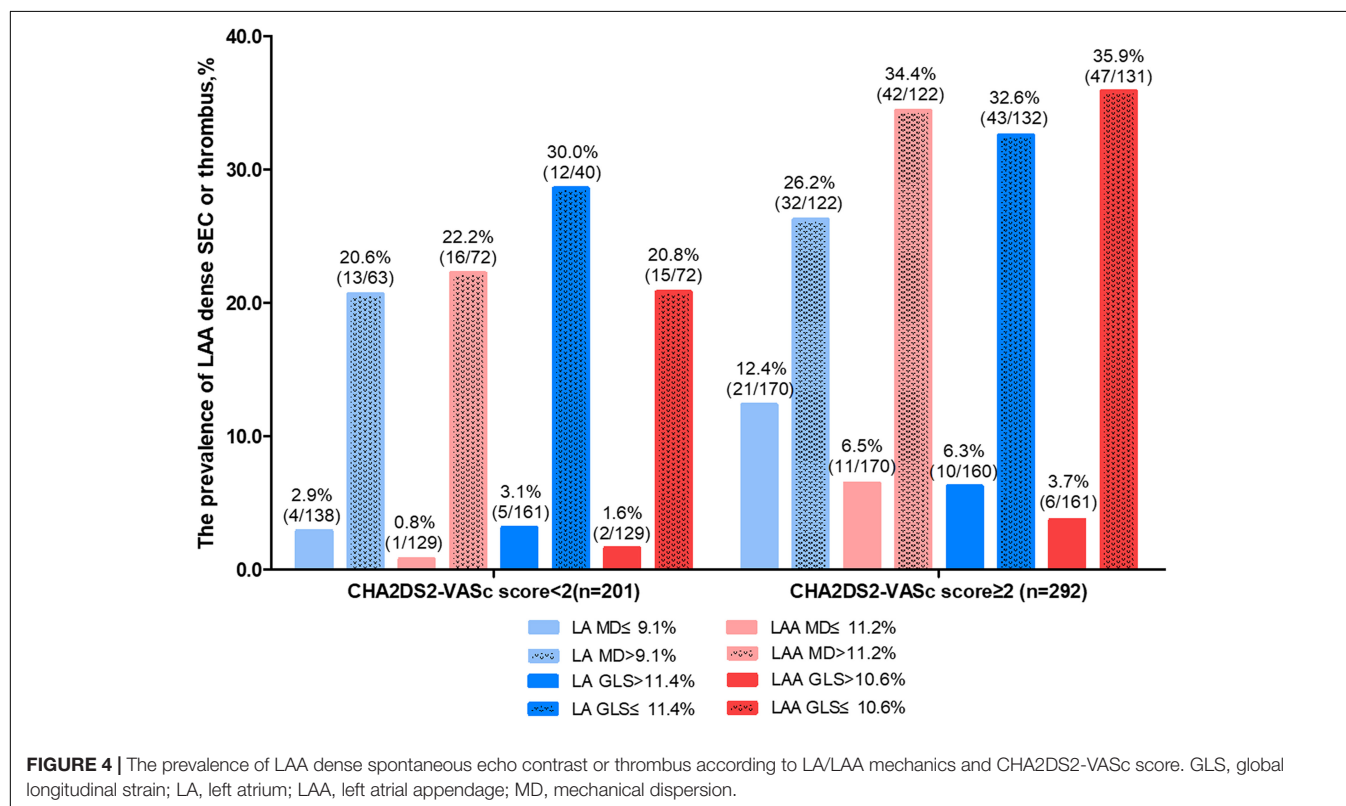
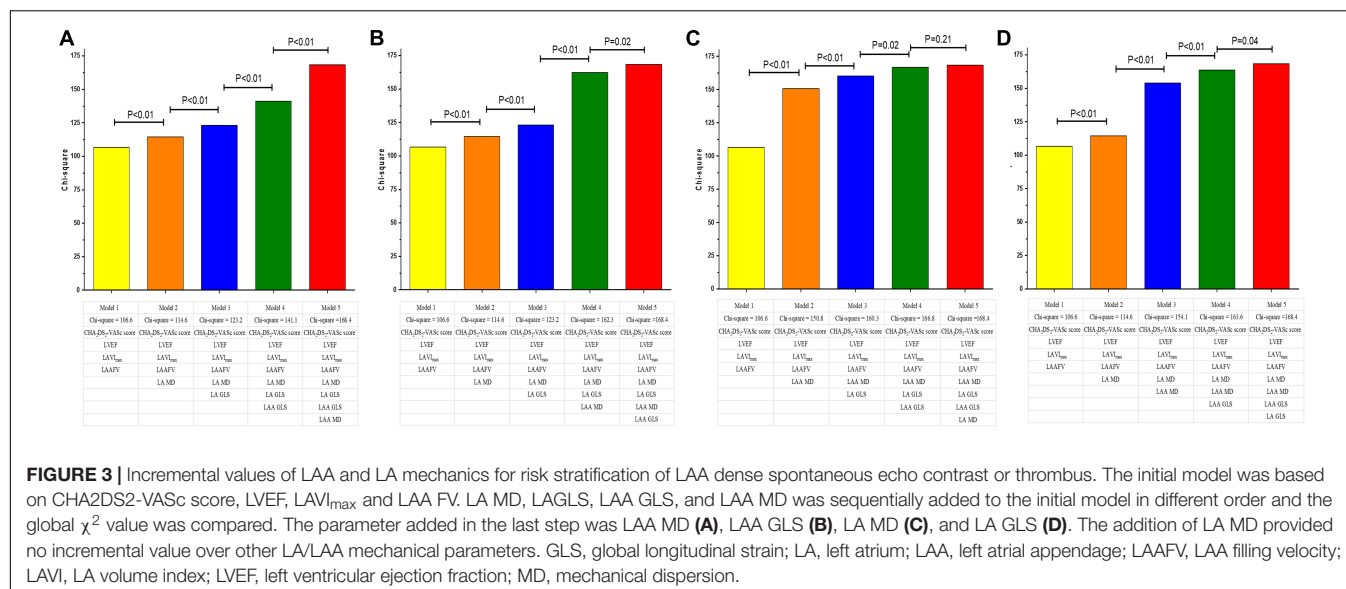
Although the correlation of LA MD with LAA thrombus or sludge has been demonstrated previously (22, 23), our study revealed that LAA MD, rather than LA MD had an independent association with LAA dense SEC or thrombus. LA MD did not maintain its significance when adjusted for LAVI_{max} and LA GLS. As a sensitive marker of LA dysfunction and asynchrony, impairment of LA MD precedes morphological changes (33). In the present study, the majority of patients had LA enlargement (70.9%), indicating that most of them had experienced significant LA remodeling, hence, predictive value of LA MD became less pronounced compared with LA volume or LA GLS. In addition, mechanical discordance between LA and LAA existed in 25% of AF patients (34), suggesting that LA dispersion may not represent LAA wall motion discoordination and a dedicated analysis of LAA dyssynchrony would provide extra information. These findings indicated that LAA myocardial function should be assessed even in the presence of LA enlargement and dysfunction.

Clinical Implications

The findings in this study suggest that LAA MD could potentially reduce underuse of anticoagulants by improving decision making for anticoagulation in patients at a high risk of LAA thrombus despite a low CHA₂DS₂-VASc score. LAA remodeling is partially reversible (35), and therapies aiming at LAA MD might potentially benefit patients by improving LAA mechanics and future studies are needed to validate this hypothesis. Although LAA MD is superior to LA MD in predicting LAA blood stasis, its assessment is more time-consuming and less validated than LA strain measurements. Given the comparable predictive value of LA GLS, it may be an alternative to LAA mechanics in patients who could not tolerate TEE or TEE images were inadequate for strain analysis.

Study Limitations

There are several limitations and technical considerations in the present study. First of all, this is a cross-sectional, observational study consisting of patients referring for catheter ablation of AF. Therefore, selection bias should be taken into account. Second, given the complex and variable morphology of LAA, although we examined the LAA from four different views, it is still difficult to visualize its entirety and small thrombi within a side lobe might be overlooked. Third, vendor specificity of STE and lack of specific strain packages should be considered. Although we analyzed LA and LAA strain using software for evaluating the LV, the 2D strain package allowed manual adjustment of a region of interest to fit the thickness of LA and LAA wall. Fourth, the cutoff value of LAA MD was derived from ROC analysis and reported in the same derivation cohort, rather than in an independent group of patients. This



cutoff should be externally verified by further prospective multicenter studies.

CONCLUSION

Left atrial appendage mechanical dispersion assessed by speckle-tracking echocardiography was an independent determinant of LAA dense SEC or thrombus in AF patients, incremental

to clinical risk factors and conventional echocardiographic parameters, and superior to LA mechanical dispersion.

DATA AVAILABILITY STATEMENT

The datasets used and/or analyzed during the current study are available from the corresponding author upon reasonable request.

ETHICS STATEMENT

The studies involving human participants were reviewed and approved by the Sir Run Run Shaw Hospital, Zhejiang University School of Medicine, Hangzhou, China; First Affiliated Hospital, Zhejiang University School of Medicine, Hangzhou, China. The patients/participants provided their written informed consent to participate in this study.

AUTHOR CONTRIBUTIONS

CJ and ZZ: conceptualization and methodology. YM and HZ: data curation and writing – original draft preparation. YY and CY: investigation, visualization, and formal analysis. MM and BZ: visualization and writing – review and editing. YW:

resources and validation. RJ: resources and funding acquisition. All authors contributed to the article and approved the submitted version.

FUNDING

This research was supported by the National Natural Science Foundation of China under Grant No. 81900289.

SUPPLEMENTARY MATERIAL

The Supplementary Material for this article can be found online at: <https://www.frontiersin.org/articles/10.3389/fcvm.2022.905293/full#supplementary-material>

REFERENCES

- Virani SS, Alonso A, Benjamin EJ, Bittencourt MS, Callaway CW, Carson AP, et al. Heart disease and stroke statistics-2020 update: a report from the American heart association. *Circulation*. (2020) 141:e139–596. doi: 10.1161/CIR.0000000000000757
- Kirchhof P, Auricchio A, Bax J, Crijns H, Camm J, Diener HC, et al. Outcome parameters for trials in atrial fibrillation: recommendations from a consensus conference organized by the German atrial fibrillation competence NETWORK and the European heart rhythm association. *Europace*. (2007) 9:1006–23. doi: 10.1093/europace/eum191
- Kirchhof P, Benussi S, Kotecha D, Ahlsson A, Atar D, Casadei B, et al. 2016 ESC guidelines for the management of atrial fibrillation developed in collaboration with EACTS. *Europace*. (2016) 18:1609–78.
- van den Ham HA, Klungel OH, Singer DE, Leufkens HG, van Staa TP. Comparative performance of ATRIA, CHADS₂, and CHA₂DS₂-VASc risk scores predicting stroke in patients with atrial fibrillation: results from a national primary care database. *J Am Coll Cardiol*. (2015) 66:1851–9. doi: 10.1016/j.jacc.2015.08.033
- Welch W. *A System of Medicine*. 2nd ed. London: MacMillan and Co, Ltd (1909).
- Mahajan R, Brooks AG, Sullivan T, Lim HS, Alasady M, Abed HS, et al. Importance of the underlying substrate in determining thrombus location in atrial fibrillation: implications for left atrial appendage closure. *Heart*. (2012) 98:1120–6. doi: 10.1136/heartjnl-2012-301799
- Cresti A, García-Fernández MA, Sievert H, Mazzone P, Baratta P, Solari M, et al. Prevalence of extra-appendage thrombosis in non-valvular atrial fibrillation and atrial flutter in patients undergoing cardioversion: a large transoesophageal echo study. *EuroIntervention*. (2019) 15:e225–30. doi: 10.4244/EIJ-D-19-00128
- Ayrala S, Kumar S, O'Sullivan DM, Silverman DI. Echocardiographic predictors of left atrial appendage thrombus formation. *J Am Soc Echocardiogr*. (2011) 24:499–505. doi: 10.1016/j.echo.2011.02.010
- Akoun N, Fernandez G, Wilson B, McGann C, Kholmovski E, Marrouche N. Association of atrial fibrosis quantified using LGE-MRI with atrial appendage thrombus and spontaneous contrast on transesophageal echocardiography in patients with atrial fibrillation. *J Cardiovasc Electrophysiol*. (2013) 24:1104–9. doi: 10.1111/jce.12199
- Shirani J, Alaedddini J. Structural remodeling of the left atrial appendage in patients with chronic non-valvular atrial fibrillation: implications for thrombus formation systemic embolism, and assessment by transesophageal echocardiography. *Cardiovasc Pathol*. (2000) 9:95–101. doi: 10.1016/s1054-8807(00)00030-2
- Ma N, Lu R, Zhao D, Jiang Z, Tang M, Bao C, et al. Left atrial appendage fibrosis and 3-year clinical outcomes in atrial fibrillation after endoscopic ablation: a histologic analysis. *Ann Thorac Surg*. (2020) 109:69–76. doi: 10.1016/j.athoracsur.2019.05.055
- Fatkin D, Kelly RP, Feneley MP. Relations between left atrial appendage blood flow velocity, spontaneous echocardiographic contrast and thromboembolic risk in vivo. *J Am Coll Cardiol*. (1994) 23:961–9. doi: 10.1016/0735-1097(94)90644-0
- Di Biase L, Santangeli P, Anselmino M, Mohanty P, Salvetti I, Gili S, et al. Does the left atrial appendage morphology correlate with the risk of stroke in patients with atrial fibrillation? Results from a multicenter study. *J Am Coll Cardiol*. (2012) 60:531–8. doi: 10.1016/j.jacc.2012.04.032
- Wysokinski WE, Ammash N, Sobande F, Kalsi H, Hodge D, McBane RD. Predicting left atrial thrombi in atrial fibrillation. *Am Heart J*. (2010) 159:665–71. doi: 10.1016/j.ahj.2009.12.043
- Handke M, Harloff A, Hetzel A, Olschewski M, Bode C, Geibel A. Left atrial appendage flow velocity as a quantitative surrogate parameter for thromboembolic risk: determinants and relationship to spontaneous echo contrast and thrombus formation—a transesophageal echocardiographic study in 500 patients with cerebral ischemia. *J Am Soc Echocardiogr*. (2005) 18:1366–72. doi: 10.1016/j.echo.2005.05.006
- Moravi V, Lang RM, Badano LP, Belohlavek M, Cardim NM, Derumeaux G, et al. Current and evolving echocardiographic techniques for the quantitative evaluation of cardiac mechanics: ASE/EAE consensus statement on methodology and indications endorsed by the Japanese society of echocardiography. *J Am Soc Echocardiogr*. (2011) 24:277–313.
- Cameli M, Lunghetti S, Mandoli GE, Righini FM, Lisi M, Curci V, et al. Left atrial strain predicts pro-thrombotic state in patients with non-valvular atrial fibrillation. *J Atr Fibrillation*. (2017) 10:1641. doi: 10.4022/jafb.1641
- Karabay CY, Zehir R, Guler A, Oduncu V, Kalayci A, Aung SM, et al. Left atrial deformation parameters predict left atrial appendage function and thrombus in patients in sinus rhythm with suspected cardioembolic stroke: a speckle tracking and transesophageal echocardiography study. *Echocardiography*. (2013) 30:572–8.
- Kurzawski J, Janion-Sadowska A, Sadowski M. Left atrial appendage function assessment and thrombus identification. *Int J Cardiol Heart Vasc*. (2016) 14:33–40. doi: 10.1016/j.ijcha.2016.11.003
- Saraçoğlu E, Ural D, Kılıç S, Vuruşkan E, Şahin T, Ağaçdiken Ağır A. Left atrial appendage 2D-strain assessed by transesophageal echocardiography is associated with thromboembolic risk in patients with atrial fibrillation. *Türk Kardiyol Dern Ars*. (2019) 47:111–21.
- Ono K, Iwama M, Kawasaki M, Tanaka R, Watanabe T, Onishi N. Motion of left atrial appendage as a determinant of thrombus formation in patients with a low CHADS₂ score receiving warfarin for persistent atrial fibrillation. *Cardiovasc Ultrasound*. (2012) 10:50. doi: 10.1186/1476-7120-10-50
- Kupczynska K, Michalski BW, Miskowicz D, Kasprzak JD, Szymczyk E, Wejner Mik P, et al. Incremental value of left atrial mechanical dispersion over CHA₂ DS₂ -VASc score in predicting risk of thrombus formation. *Echocardiography*. (2018) 35:651–60. doi: 10.1111/echo.13899
- Providência R, Faustino A, Ferreira MJ, Gonçalves L, Trigo J, Botelho A, et al. Evaluation of left atrial deformation to predict left atrial stasis in patients with

- non-valvular atrial fibrillation—a pilot-study. *Cardiovasc Ultrasound*. (2013) 11:44. doi: 10.1186/1476-7120-11-44
24. Ciuffo L, Inoue YY, Tao S, Gucuk Ipek E, Balouch M, Lima J, et al. Mechanical dyssynchrony of the left atrium during sinus rhythm is associated with history of stroke in patients with atrial fibrillation. *Eur Heart J Cardiovasc Imaging*. (2018) 19:433–41. doi: 10.1093/ehjci/jex156
 25. Mao Y, Yu C, Yang Y, Ma M, Wang Y, Jiang R, et al. Comparison of left atrial and left atrial appendage mechanics in the risk stratification of stroke in patients with atrial fibrillation. *Cardiovasc Ultrasound*. (2021) 19:7. doi: 10.1186/s12947-020-00232-z
 26. Mao Y, Ma M, Yang Y, Yu C, Wang Y, Jiang R, et al. Left atrial appendage mechanical dispersion provides incremental value for thromboembolic risk stratification over CHA2DS2-VASc Score in atrial fibrillation. *Int J Cardiol*. (2020) 307:41–7. doi: 10.1016/j.ijcard.2020.02.031
 27. January CT, Wann LS, Calkins H, Chen LY, Cigarroa JE, Cleveland JC Jr., et al. 2019 AHA/ACC/HRS Focused update of the 2014 AHA/ACC/HRS guideline for the management of patients with atrial fibrillation: a report of the American college of cardiology/American heart association task force on clinical practice guidelines and the heart rhythm society in collaboration with the society of thoracic surgeons. *Circulation*. (2019) 140:e125–51. doi: 10.1161/CIR.0000000000000665
 28. Lang RM, Badano LP, Mor-Avi V, Afilalo J, Armstrong A, Ernande L, et al. Recommendations for cardiac chamber quantification by echocardiography in adults: an update from the American Society of Echocardiography and the European Association of Cardiovascular Imaging. *Eur Heart J Cardiovasc Imaging*. (2015) 16:233–70.
 29. Badano LP, Koliass TJ, Muraru D, Abraham TP, Aurigemma G, Edvardsen T, et al. Standardization of left atrial, right ventricular, and right atrial deformation imaging using two-dimensional speckle tracking echocardiography: a consensus document of the EACVI/ASE/Industry Task Force to standardize deformation imaging. *Eur Heart J Cardiovasc Imaging*. (2018) 19:591–600. doi: 10.1093/ehjci/jeu042
 30. Bunting KV, Gill SK, Sitch A, Mehta S, O'Connor K, Lip GY, et al. Improving the diagnosis of heart failure in patients with atrial fibrillation. *Heart*. (2021) 107:902–8.
 31. Tamura H, Watanabe T, Hirono O, Nishiyama S, Sasaki S, Shishido T, et al. Low wall velocity of left atrial appendage measured by trans-thoracic echocardiography predicts thrombus formation caused by atrial appendage dysfunction. *J Am Soc Echocardiogr*. (2010) 23:545–52. doi: 10.1016/j.echo.2010.02.006
 32. Krul SP, Berger WR, Smit NW, van Amersfoort SC, Driessen AH, van Boven WJ, et al. Atrial fibrosis and conduction slowing in the left atrial appendage of patients undergoing thoracoscopic surgical pulmonary vein isolation for atrial fibrillation. *Circ Arrhythm Electrophysiol*. (2015) 8:288–95.
 33. Hong J, Gu X, An P, Luo T, Lv Q, Kang J, et al. Left atrial functional remodeling in lone atrial fibrillation: a two-dimensional speckle tracking echocardiographic study. *Echocardiography*. (2013) 30:105. doi: 10.1111/echo.12200
 34. Warraich HJ, Gandhavadi M, Manning WJ. Mechanical discordance of the left atrium and appendage: a novel mechanism of stroke in paroxysmal atrial fibrillation. *Stroke*. (2014) 45:1481–4. doi: 10.1161/STROKEAHA.114.004800
 35. Machino-Ohtsuka T, Seo Y, Ishizu T, Yanaka S, Nakajima H, Atsumi A, et al. Significant improvement of left atrial and left atrial appendage function after catheter ablation for persistent atrial fibrillation. *Circ J*. (2013) 77:1695–704. doi: 10.1253/circj.12-1518

Conflict of Interest: The authors declare that the research was conducted in the absence of any commercial or financial relationships that could be construed as a potential conflict of interest.

Publisher's Note: All claims expressed in this article are solely those of the authors and do not necessarily represent those of their affiliated organizations, or those of the publisher, the editors and the reviewers. Any product that may be evaluated in this article, or claim that may be made by its manufacturer, is not guaranteed or endorsed by the publisher.

Copyright © 2022 Mao, Zhao, Yu, Yang, Ma, Wang, Jiang, Zhao, Zheng and Jiang. This is an open-access article distributed under the terms of the Creative Commons Attribution License (CC BY). The use, distribution or reproduction in other forums is permitted, provided the original author(s) and the copyright owner(s) are credited and that the original publication in this journal is cited, in accordance with accepted academic practice. No use, distribution or reproduction is permitted which does not comply with these terms.



OPEN ACCESS

EDITED BY

Sanjeev Bhattacharyya,
Barts Heart Centre, United Kingdom

REVIEWED BY

Vincenzo Castiglione,
Sant'Anna School of Advanced
Studies, Italy
Filip Zemrak,
Barts Health NHS Trust,
United Kingdom

*CORRESPONDENCE

Patricia A. Pellikka
pellikka.patricia@mayo.edu

SPECIALTY SECTION

This article was submitted to
Cardiovascular Imaging,
a section of the journal
Frontiers in Cardiovascular Medicine

RECEIVED 05 May 2022

ACCEPTED 27 June 2022

PUBLISHED 22 July 2022

CITATION

Pellikka PA, Strom JB,
Pajares-Hurtado GM, Keane MG,
Khazan B, Qamruddin S, Tutor A, Gul F,
Peterson E, Thamman R, Watson S,
Mandale D, Scott CG, Naqvi T,
Woodward GM and Hawkes W (2022)
Automated analysis of limited
echocardiograms: Feasibility and
relationship to outcomes in COVID-19.
Front. Cardiovasc. Med. 9:937068.
doi: 10.3389/fcvm.2022.937068

COPYRIGHT

© 2022 Pellikka, Strom,
Pajares-Hurtado, Keane, Khazan,
Qamruddin, Tutor, Gul, Peterson,
Thamman, Watson, Mandale, Scott,
Naqvi, Woodward and Hawkes. This is
an open-access article distributed
under the terms of the [Creative
Commons Attribution License \(CC BY\)](#).
The use, distribution or reproduction
in other forums is permitted, provided
the original author(s) and the copyright
owner(s) are credited and that the
original publication in this journal is
cited, in accordance with accepted
academic practice. No use, distribution
or reproduction is permitted which
does not comply with these terms.

Automated analysis of limited echocardiograms: Feasibility and relationship to outcomes in COVID-19

Patricia A. Pellikka^{1*}, Jordan B. Strom²,
Gabriel M. Pajares-Hurtado², Martin G. Keane³,
Benjamin Khazan³, Salima Qamruddin⁴, Austin Tutor⁴,
Fahad Gul⁵, Eric Peterson⁵, Ritu Thamman⁶, Shivani Watson⁶,
Deepa Mandale⁷, Christopher G. Scott⁸, Tasneem Naqvi⁷,
Gary M. Woodward⁹ and William Hawkes⁹

¹Department of Cardiovascular Medicine, Mayo Clinic, Rochester, MN, United States, ²Richard A. and Susan F. Smith Center for Outcomes Research in Cardiology, Beth Israel Deaconess Medical Center, Boston, MA, United States, ³Temple Heart and Vascular Center, Philadelphia, PA, United States, ⁴Ochsner Health System, New Orleans, LA, United States, ⁵Einstein Medical Center, Philadelphia, PA, United States, ⁶Department of Medicine, University of Pittsburgh, Pittsburgh, PA, United States, ⁷Department of Cardiovascular Medicine, Mayo Clinic, Scottsdale, AZ, United States, ⁸Department of Health Sciences Research, Mayo Clinic, Rochester, MN, United States, ⁹Ultrasonics Ltd., Oxford, United Kingdom

Background: As automated echocardiographic analysis is increasingly utilized, continued evaluation within hospital settings is important to further understand its potential value. The importance of cardiac involvement in patients hospitalized with COVID-19 provides an opportunity to evaluate the feasibility and clinical relevance of automated analysis applied to limited echocardiograms.

Methods: In this multisite US cohort, the feasibility of automated AI analysis was evaluated on 558 limited echocardiograms in patients hospitalized with COVID-19. Reliability of automated assessment of left ventricular (LV) volumes, ejection fraction (EF), and LV longitudinal strain (LS) was assessed against clinically obtained measures and echocardiographic findings. Automated measures were evaluated against patient outcomes using ROC analysis, survival modeling, and logistic regression for the outcomes of 30-day mortality and in-hospital sequelae.

Results: Feasibility of automated analysis for both LVEF and LS was 87.5% (488/558 patients). AI analysis was performed with biplane method in 300 (61.5%) and single plane apical 4- or 2-chamber analysis in 136 (27.9%) and 52 (10.7%) studies, respectively. Clinical LVEF was assessed using visual estimation in 192 (39.3%), biplane in 163 (33.4%), and single plane or linear methods in 104 (21.2%) of the 488 studies; 29 (5.9%) studies did not have clinically reported LVEF. LV LS was clinically reported in 80 (16.4%). Consistency between automated and clinical values demonstrated Pearson's R, root mean square error (RMSE) and intraclass correlation coefficient (ICC) of 0.61, 11.3% and 0.72, respectively, for LVEF; 0.73, 3.9% and 0.74, respectively for LS; 0.76,

24.4ml and 0.87, respectively, for end-diastolic volume; and 0.82, 12.8 ml, and 0.91, respectively, for end-systolic volume. Abnormal automated measures of LVEF and LS were associated with LV wall motion abnormalities, left atrial enlargement, and right ventricular dysfunction. Automated analysis was associated with outcomes, including survival.

Conclusion: Automated analysis was highly feasible on limited echocardiograms using abbreviated protocols, consistent with equivalent clinically obtained metrics, and associated with echocardiographic abnormalities and patient outcomes.

KEYWORDS

echocardiography, artificial intelligence, deformation imaging, strain rate imaging, machine learning, COVID-19

Introduction

The use of artificial intelligence (AI) as a method for automating medical image analysis has the potential to transform patient care (1). In echocardiography, AI applications have demonstrated significant value at numerous stages of the analysis pipeline, including automatic view classification (2–4), quantitative assessment of image quality (5, 6), automated contouring (7–9), assessment of regional wall motion (10), and disease classification (11–13). Notwithstanding the advantages of automated, high-throughput analysis, the benefits of AI driven analysis include savings of time (9, 14), improved prognostication (11, 15), reduced variability (16), and greater precision (6, 13). While the value of automated analysis is increasingly reported, validation of commercially available software with automated capabilities alongside clinical assessment remains limited (9, 17, 18). As a result, understanding of the capabilities and limitations of automated echocardiographic analysis remains incomplete.

Continued assessment of automated analysis using real-world data is essential to evaluate potential feasibility and relevance to clinical practice. In cases of severe infection, coronavirus disease 2019 (COVID-19) patients frequently present with prognostically significant cardiac involvement (19–21). Echocardiographic indices of both left- (LV) and right-ventricular (RV) function have been reported to effectively identify COVID-19 patients requiring urgent treatment or intervention (22), predict prognosis (18, 23) and allow longitudinal assessment (24). However, the use of limited echocardiographic acquisition protocols during the early stages of the pandemic (18, 21, 25, 26) often omitted some of the pre-requisites for advanced strain analysis [e.g., electrocardiogram monitoring and sufficient image quality from the three apical views (27)], limiting the information available to clinicians for patient risk stratification. Automated AI algorithms are capable of disease prediction (12, 13, 28) and functional

quantification (6, 29), using limited or single-view images, without the requirement for additional work or expertise. However, the efficacy of automated analysis in patient assessment and risk stratification, including the potential impact of implementing automated analysis alongside routine practice, remains incompletely understood.

In this multi-site, retrospective study, we sought to evaluate (1) the feasibility of automated quantification of LV systolic function using limited echocardiograms from COVID-19 patients; (2) the agreement between automated quantification and clinical findings; (3) the association of automated assessment of the LV with in-hospital patient outcomes.

Methods

Patient population

This study was approved by the Institutional Review Boards and conducted among consecutive inpatient adults diagnosed with COVID-19 (positive antigen or polymerase chain reaction test) who underwent clinically indicated transthoracic echocardiography at six institutions: Beth Israel Deaconess Medical Center, Harvard Medical School (Boston); Temple University Hospital (Philadelphia); Einstein Medical Center (Philadelphia); Ochsner Medical Center (New Orleans); The University of Pittsburgh Medical Center; and Mayo Clinic Health System sites across Minnesota, Wisconsin, Florida, and Arizona, between February and December 2020. Only the first transthoracic echocardiogram performed during the hospital admission for COVID-19 was considered. Echocardiographic studies were included in the analysis if either an apical 4-chamber or apical 2-chamber image clip was available for analysis. Those with insufficient image quality to assess LV ejection fraction (EF) clinically and to evaluate the AI derived contours of the LV were excluded.

Data collection

Patient baseline characteristics, medical history, and in-hospital outcomes were obtained at each site from review of electronic health records. These included patient demographics, presenting signs/symptoms, comorbidities at the time of initial hospital presentation, in-hospital sequelae, and echocardiographic findings. Outcomes included 30-day all-cause mortality, incident acute coronary syndrome (ACS), congestive heart failure (CHF), acute kidney injury, and major adverse cardiovascular and cerebrovascular events (MACCE), defined as the composite of ACS, CHF, stroke, coagulation disorder (disseminated intravascular coagulation or other acquired bleeding disorder), myocarditis, or pericarditis. Coronary artery disease (CAD) was defined as prior myocardial infarction (MI), coronary revascularization, or angiography showing stenosis >50% diameter. Echocardiographic variables were obtained from echocardiography reports and included (where available) qualitative assessment of cardiac function (regional wall motion abnormalities, LV size, LV wall thickness, left atrial size, RV size, LVEF, end-diastolic and end-systolic volumes, and LV longitudinal strain (LS).

Echocardiographic analysis

As echocardiographic data was collected predominantly during the first wave of the pandemic, abbreviated and focused protocols were frequently utilized to minimize scan times and staff exposure risk (30), sometimes without placement of electrocardiographic leads (31, 32). Only studies that included at least one cardiac cycle from any of the apical views were considered. Echocardiographic examinations were performed using GE (Vivid E95 = 49.1%, Vivid S70 = 27.9%, Vivid E9 = 2.5%, Vivid IQ = 1.6%) and Philips (CX50 = 11.3%, EPIQ 7C = 3.9%, EPIQ CVx = 3.0%, iE33 = 0.7%) systems. Quantification of echocardiographic measures was obtained from two sources:

Clinically derived echocardiographic assessment

Quantitative assessment of LV function was obtained from clinical echocardiographic reports. The method of LVEF quantification (e.g., Simpson's biplane method of disks, single plane, linear, or visual estimation) was recorded. Protocols for echocardiographic acquisition and quantification were conducted according to local procedures and clinical standards in place at the time of data collection.

AI derived assessment

Quantitative assessment of LV function was obtained from automated AI driven echocardiography analysis algorithms

(EchoGo Core v1.3.2, Ultrasonics Ltd, Oxford). LV LS was calculated as the average of the end-systolic longitudinal strain from apical 4- and 2-chamber views. Where one view was unavailable, single view longitudinal strain values were calculated. LV volumes and LVEF were determined using the Simpson's biplane method of disks. Where biplane LVEF was not feasible with both apical 4- and 2-chamber views, a single plane LVEF was calculated when feasible. The AI algorithms process apical 4- and 2-chamber images to automatically select cardiac cycles, contour the endocardial border, and calculate volumes, ejection fraction and longitudinal strain (18). Data for algorithm training were collected from an international dataset of clinically indicated echocardiograms, containing a range of patient pathologies (including coronary artery disease, heart failure, COVID-19, myocardial infarction, and prior cardiovascular disease) and were strictly independent of the participants of the current study.

Feasibility of assessment

The endocardial border of apical 4- and 2-chamber images were automatically contoured by EchoGo Core and were presented to operators for approval. All operators held professional qualifications in echocardiography (e.g., British Society of Echocardiography or American Society of Echocardiography). All studies were processed through EchoGo Core, irrespective of image quality. A study was considered feasible for AI analysis if operators approved either apical 4- or 2-chamber views. Studies where AI analysis was not feasible (e.g., no contours approved for analysis) were included in the feasibility evaluation but not in the final analysis.

Statistical analysis

Continuous variables were expressed as means \pm standard deviations (\pm SD) or medians and interquartile ranges (IQR). Continuous data were compared between groups based on automated LS and EF using the Student's *t*-test or the Wilcoxon rank sum test, as appropriate. Categorical data was presented as counts and percentages and compared using the χ^2 test. Pairwise comparisons of continuous and categorical data were conducted using paired *t*-tests and McNemar's test, respectively. Agreement analysis was conducted using Bland Altman statistics, linear Deming regression root mean square errors (RMSE), Pearson's correlation coefficients, and intraclass correlation coefficients (ICC). For agreement of LVEF between AI and clinical values, the analysis was conducted using comparable methods (e.g., biplane vs. biplane). Discordance between automated and clinically assessed LVEF was defined by an inter-method difference of >10%, which has been reported as the minimum detectable difference between observers (33, 34).

TABLE 1 Baseline patient characteristics.

Patient baseline characteristics	Value
Age (Years)	62.24 ± 15.52
Male, <i>n</i> (%)	279 (57.4%)
BSA (m ²)	2.11 ± 0.27
BMI (Kg/m ²)	30.6 ± 6.68
Obesity, <i>n</i> (%)	136 (27.9%)
Systolic Blood Pressure (mm Hg)	124 ± 21
Diastolic Blood Pressure (mm Hg)	71 ± 14
Non-Hispanic White, <i>n</i> (%)	238 (50.0%)
Black or African American, <i>n</i> (%)	136 (28.6%)
Native American or Alaska Native, <i>n</i> (%)	29 (6.1%)
Hispanic, <i>n</i> (%)	96 (19.9%)
Diabetes Mellitus, <i>n</i> (%)	197 (40.4%)
Hypertension, <i>n</i> (%)	283 (58.0%)
Coronary Artery Disease, <i>n</i> (%)	77 (15.8%)
Cancer, <i>n</i> (%)	48 (9.8%)
Mechanical Ventilation During TTE, <i>n</i> (%)	126 (25.8%)
Vasopressor or Inotrope Use During TTE, <i>n</i> (%)	112 (23.0%)

BMI, body mass index; BSA, body surface area; TTE, transthoracic echocardiography.

For LVEF and LS, univariate logistic regression was performed to evaluate the association of AI and clinical echocardiographic measures with in-hospital outcomes and 30-day mortality. Patient origin was included in logistic regression equations to adjust for site related differences. Results from logistic regression models are reported as odds ratios (OR) and 95% confidence intervals. To account for the time to mortality, Cox proportional hazards regression was implemented. Kaplan-Meier estimates were used to provide a description of 30-day patient survival, with censoring after death, discharge or 30 days. Differences between survival curves were tested using the log-rank test. For LVEF, patients were classified into hyperdynamic (>70%, normal (55 to 70%), borderline (45 to 55%) and abnormal (<45%) (27, 35, 36). For LS, patients were classified as supranormal (<−20%), normal (−18 to −20%), borderline (−16 to −18%) and abnormal (>−16%) (27, 35, 36). Hyperdynamic and supranormal categories were included due to reports of being moderately prevalent in COVID-19 (24) with potential clinical significance (37, 38). All analysis was conducted using Python v3.9.7 in Spyder v5.1.5 using a two-tailed *p*-value < 0.05 to define significance.

Results

Feasibility of AI analysis

Of 558 patient echocardiograms with at least one apical cardiac cycle, automated analysis of both LVEF and LS was

feasible in 488 (87.5%). AI feasibility was 93.7% for the Mayo Clinic, 80.8% for Beth Israel Deaconess Medical Center, 100% for the University of Pittsburgh, 91.5% for Ochsner Medical Center, 72% for Temple University Medical Center and 89.7% for Einstein Medical Center (Supplementary Table 1). Reasons for rejection in the 70 studies included inability to fully assess endocardial border delineation in 66 (94.3%), incorrect frame selection in 2 (2.9%) and software errors in 2 (2.9%). There were 14 studies with clinically reported LVEF (1 assessed using biplane methods and 13 using linear methods) where automated analysis was not feasible.

Of the 488 accepted studies, AI analysis was performed with biplane method in 300 (61.5%) and single plane apical 4- or 2-chamber analysis in 136 (27.9%) and 52 (10.7%) studies, respectively. Clinical assessment of LVEF was recorded in 459 (94.1%) of the 488 studies at the time of the echocardiogram. Clinical LVEF was assessed using visual estimation in 192 (39.3%), biplane methods in 163 (33.4%), and single plane or linear methods in 104 (21.2%). LV LS was clinically reported in 80 (16.4%) patients.

Patient characteristics

Baseline patient characteristics, demographics, and clinically derived echocardiographic parameters are reported in Table 1. The mean age was 62.2 ± 15.5 years and 279 (57.2%) were male. Indications for echocardiography included assessment of LV function in 223 (45.7%), hypoxemia in 88 (18.0%), arrhythmia in 46 (9.4%), suspected acute coronary syndrome in 26 (5.3%), assessment of RV function in 23 (4.7%), hypotension in 19 (3.9%), chest pain in 13 (2.7%), and others in 50 (10.2%).

Comparison of AI and clinically derived assessment

Comparison of the AI derived assessment to the values obtained from clinical echocardiography reports is reported in Table 2 and displayed in Figure 1. Agreement between automated and clinical LVEF using all available data had a mean difference of 0.91%, correlation coefficient 0.61, RMSE 11.3%, and an ICC 0.73. Inter-method agreement was highest when comparing like-for-like methods, with a correlation of 0.80 and an ICC of 0.85 for LVEF obtained using the biplane method. Agreement between automated and clinical LS using all available data (biplane or single plane for automated assessment) had a mean difference of −0.42%, correlation coefficient 0.73, RMSE 3.9% and an ICC 0.78. When restricting the comparison to cases where automated assessment was feasible on both apical 4- and 2-chamber views, agreement of LS demonstrated a mean difference −0.62%, correlation 0.73, RMSE 3.9%, and an ICC of 0.78.

TABLE 2 Agreement between automated metrics of LV function and values derived at the time of limited transthoracic echocardiogram.

	<i>n</i>	Mean diff	LoA	Pearson's <i>r</i>	ICC	RMSE
LS all	80	−0.417	7.945	0.725	0.782	3.876
Biplane LS	56	−0.62	7.738	0.739	0.791	3.877
LS Apical 4-chamber	75	−0.259	7.621	0.799	0.85	3.852
LVEF all	459	0.913	24.011	0.606	0.728	11.292
LVEF (biplane only)	112	2.606	14.792	0.796	0.848	7.024
LV EDV	168	−0.939	47.605	0.761	0.865	24.438
LV ESV	168	−2.85	26.068	0.82	0.897	12.78

N comparisons indicates the number of datapoints available for extraction from clinical reports for comparison against the AI. LVEF all and LS all indicate data used from all comers, including all available methods of single view, biplane and triplane calculations. ICC, Intra-class correlation coefficient; LoA, Bland Altman limits of agreement; LS, longitudinal strain; LVEF, left ventricular ejection fraction; LV EDV, left ventricular end-diastolic volume; LV ESV, left ventricular end-systolic volume; RMSE, root mean square error.

Relationship of AI derived abnormalities with clinical echocardiographic abnormalities

The relationship of AI derived assessment and reported echocardiographic abnormalities was examined (Table 3). AI derived assessment identified 120 (24.6%) patients as having an LVEF <50% and 245 (50.2%) patients with LS >−16%. Patients with abnormal LVEF or LS determined by the AI method exhibited a significantly greater proportion of echocardiographic abnormalities in both the LV and RV, and more often had left atrial enlargement. The relationship of clinically assessed abnormality of LVEF and LS using the same cut points (<50% and >−16%, respectively) was similarly related to other reported echocardiographic abnormalities (Supplementary Table 2).

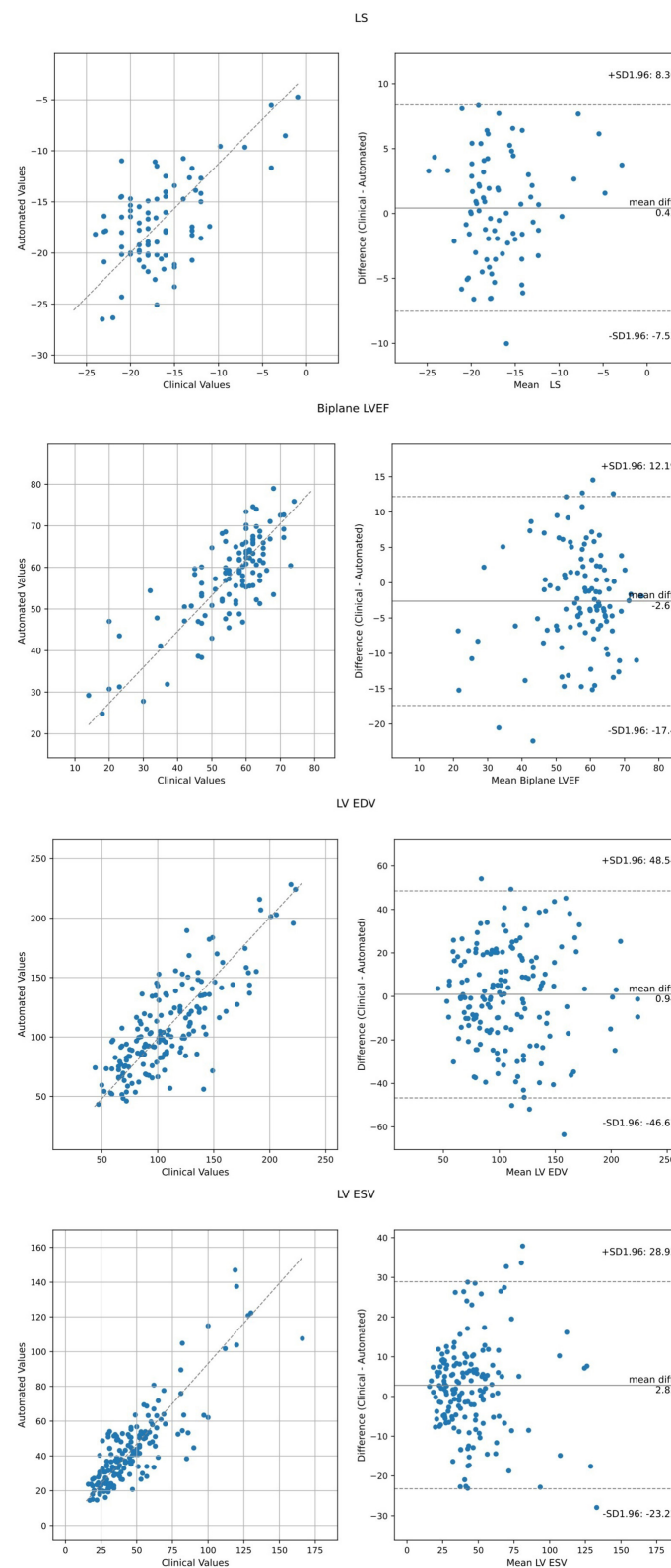
ROC analysis of the ability of AI LVEF and LS to identify clinical systolic dysfunction (defined as a clinical LVEF < 50%) achieved an area under the curve of 0.894 and 0.863, a sensitivity of 85.7% and 81.3%, and a specificity of 78.6% and 83.1%, respectively (Figure 2). Pairwise comparison between automated and clinical methods did not demonstrate any significant differences for LVEF (57 ± 12 vs. 56 ± 14%, *p* = 0.11) or LS (−17.0 ± 4.3 vs. −16.6 ± 4.7%, *p* = 0.36). Automated and clinical assessment of LS and LVEF demonstrated inter-method agreement in 70.0 and 79.6% of cases, respectively, when identifying LVEF <50% or LS >−16%, respectively. For LVEF, there were 61 (13.3%) cases where the automated assessment was <50% but the clinical values were >50% and 33 (7.2%) cases where the automated assessment was >50% and the clinical assessment was <50%. AI reported LVEF was different by a margin of more than 10% in 164 patients (36%) with 73% of these occurring in patients where the clinical assessment was performed using linear or manual methods. For LS, there were 11 (13.8%) of 80 cases where the automated assessment was >−16% and the clinical assessment was <−16% and 13 (16.3%) cases where the automated assessment was <−16% but the clinical assessment was >−16%. When comparing patients identified by clinically derived LVEF and LS, automated

assessment characterized a significantly smaller proportion as abnormal [AI vs. clinical: LVEF: 56 (12.2%) patients vs. 89 (19.3%) patients, *p* < 0.001, LS: 18 (22.5%) patients vs. 31 (38.8%) patients, *p* < 0.001, Table 3].

AI derived LVEF and LS and outcomes

During the first 30 days of hospitalization, death occurred in 103 (21.3%), acute coronary syndrome in 39 (8%), congestive heart failure in 49 (10%), and MACCE in 117 (24.0%). Using logistic regression adjusted by site (Table 4), automated LVEF and LS were associated with in-hospital death (LVEF *p* = 0.025, LS *p* = 0.03), ACS (LVEF *p* < 0.001, LS *p* < 0.001), CHF (LVEF *p* < 0.001, LS *p* < 0.001), acute kidney injury (LVEF *p* = 0.012, LS *p* = 0.03), and MACCE during hospital admission (LVEF *p* < 0.001, LS *p* < 0.001). Automated LVEF and LS were associated with mortality using Cox regression to account for increased risk over longer durations of hospitalization (LVEF *p* = 0.017, LS *p* = 0.033, Supplementary Table 3). Clinically derived LVEF and LS were associated with risk of CHF (LVEF *p* < 0.001, LS *p* = 0.001) and MACCE, (LVEF *p* < 0.001, LS *p* = 0.001) but not in-hospital death (LVEF *p* = 0.286, LS *p* = 0.158) or acute kidney injury (LVEF *p* < 0.43, LS *p* = 0.694). Clinical LVEF (*p* < 0.001) but not LS (*p* = 0.118) was associated with ACS. Cox regression of clinical LVEF and LS was associated with mortality for LVEF (*p* = 0.019) but not for LS (*p* = 0.181, Supplementary Table 3).

When categorized into hyperdynamic, normal, borderline, and abnormal classes based on LVEF, survival rates were 77.6, 83.3, 85.1, and 71.1%, respectively, for clinical LVEF and 81.7, 84.8, 80.0, and 71.6%, respectively, for automated LVEF (Figure 3). When categorized into supranormal, normal, borderline, and abnormal classes based on LS, survival rates were 90.0, 100, 88.2, and 79.2%, respectively, for clinical LVEF and 82.5, 88.7, 77.1, and 80.1%, respectively, for automated LS. There were no significant differences in the overall survival between clinical and automated assessment at any level (supranormal/hyperdynamic, normal, borderline, and abnormal *p* > 0.05).

**FIGURE 1**

Agreement analysis between automated metrics of LV function relative to clinically derived values using Bland Altman analysis and Deming Regression. LVEF and LS values represent all available data, including biplane and single plane (either apical 4- or 2-chamber).

TABLE 3 Echocardiographic analysis of cardiac structure and function according to automated indices of LS ($> -16\%$) and LVEF ($< 50\%$).

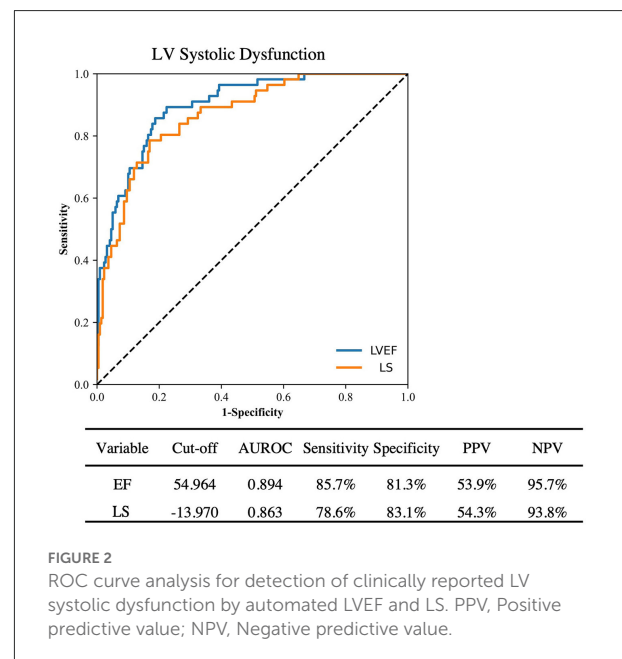
Variable	N	All	LS $\leq -16\%$	LS $> -16\%$	p-value	LVEF $\geq 50\%$	LVEF $< 50\%$	p-value
Clinical LVEF (%)	459	56.35 \pm 13.97	61.27 \pm 8.92	51.52 \pm 16.2	<0.001	60.12 \pm 9.96	45.3 \pm 17.75	<0.001
Clinical LVEF $< 50\%$	459	89 (19.3%)	14 (6.0%)	75 (32.0%)	<0.001	33 (10.0%)	56 (48.0%)	<0.001
Clinical LS (%)	80	-16.60 \pm 4.66	-18.09 \pm 3.09	-13.98 \pm 5.75	<0.001	-17.71 \pm 3.14	-11.38 \pm 6.85	<0.001
Clinical LS $> -16\%$	80	31 (38.8%)	13 (25.0%)	18 (62.0%)	<0.001	21 (32.0%)	10 (71.0%)	0.01
RWMSI	441	1.19 \pm 0.43	1.06 \pm 0.21	1.32 \pm 0.54	<0.001	1.08 \pm 0.23	1.54 \pm 0.66	<0.001
RWMA	433	93 (21.5%)	24 (11.0%)	69 (33.0%)	<0.001	44 (13.0%)	49 (47.0%)	<0.001
Septal thickness (mm)	384	9.06 \pm 4.62	8.97 \pm 3.87	9.16 \pm 5.31	0.69	9.1 \pm 4.65	8.94 \pm 4.54	0.78
Posterior wall thickness (mm)	382	8.94 \pm 7.85	8.53 \pm 3.62	9.37 \pm 10.67	0.29	8.64 \pm 3.96	9.92 \pm 14.77	0.18
LV size	458							
Normal		409 (89.3%)	219 (96.0%)	190 (83.0%)	<0.001	327 (95.0%)	82 (73.0%)	<0.001
Enlarged		49 (10.7%)	10 (4.0%)	39 (17.0%)	<0.001	19 (5.0%)	30 (27.0%)	<0.001
LV hypertrophy	465	100 (21.5%)	32 (14.0%)	68 (29.0%)	<0.001	60 (17.0%)	40 (34.0%)	<0.001
Left atrial size	350							
Normal		268 (76.6%)	141 (81.0%)	127 (72.0%)	0.07	211 (81.0%)	57 (65.0%)	<0.001
Enlarged		82 (23.4%)	33 (19.0%)	49 (28.0%)	0.07	51 (19.0%)	31 (35.0%)	<0.001
Right ventricular function	448							
Normal		369 (82.4%)	204 (91.0%)	165 (74.0%)	<0.001	297 (88.0%)	72 (65.0%)	<0.001
Reduced		79 (17.6%)	21 (9.0%)	58 (26.0%)	<0.001	41 (12.0%)	38 (35.0%)	<0.001

LS, longitudinal strain; LVEF, left ventricular ejection fraction; RWMSI, regional wall motion score index; RWMA, regional wall motion abnormality; LV, left ventricular.

Kaplan Meier analysis demonstrated increased risk of death for those with abnormal LVEF, relative to normal LVEF, for both clinical (log-rank $p = 0.004$) and automated (log-rank $p = 0.01$) assessment. Relative to borderline LVEF, patients with abnormal LVEF demonstrated increased likelihood of death for clinical assessment (log-rank $p = 0.01$) but not for automated assessment (log-rank $p = 0.19$).

Discussion

This study has evaluated the feasibility and clinical relevance of automated echocardiographic analysis software on a multi-site COVID-19 cohort, with an ethnically diverse population (50% non-Hispanic white), using limited echocardiographic studies. The main findings are: (1) Automated analysis of limited echocardiograms was feasible in 87.5% of patients in which at least one apical cardiac cycle was obtained, even under abbreviated protocols, with biplane analysis of LVEF and LS possible in 61.5% of patients; (2) Automated LVEF, LS, and volumes had good to excellent agreement with clinically derived values; (3) Automated LVEF and LS were able to stratify individuals with cardiac dysfunction, including clinically reported echocardiographic abnormalities; (4) Automated LVEF and LS were associated with adverse in-hospital and 30-day outcomes and were comparable to clinically derived assessment. These findings suggest that automated assessment of LV function is highly feasible under abbreviated protocols and



provides prognostically relevant information while increasing the data available for risk stratification.

During the COVID-19 pandemic, it was quickly reported that cardiac complications were common in cases of serious infection and were associated with poor patient outcomes (19, 38–41). While the implementation of abbreviated protocols

TABLE 4 Site adjusted univariate logistic regression of automated and clinical LVEF and LS and clinical outcomes.

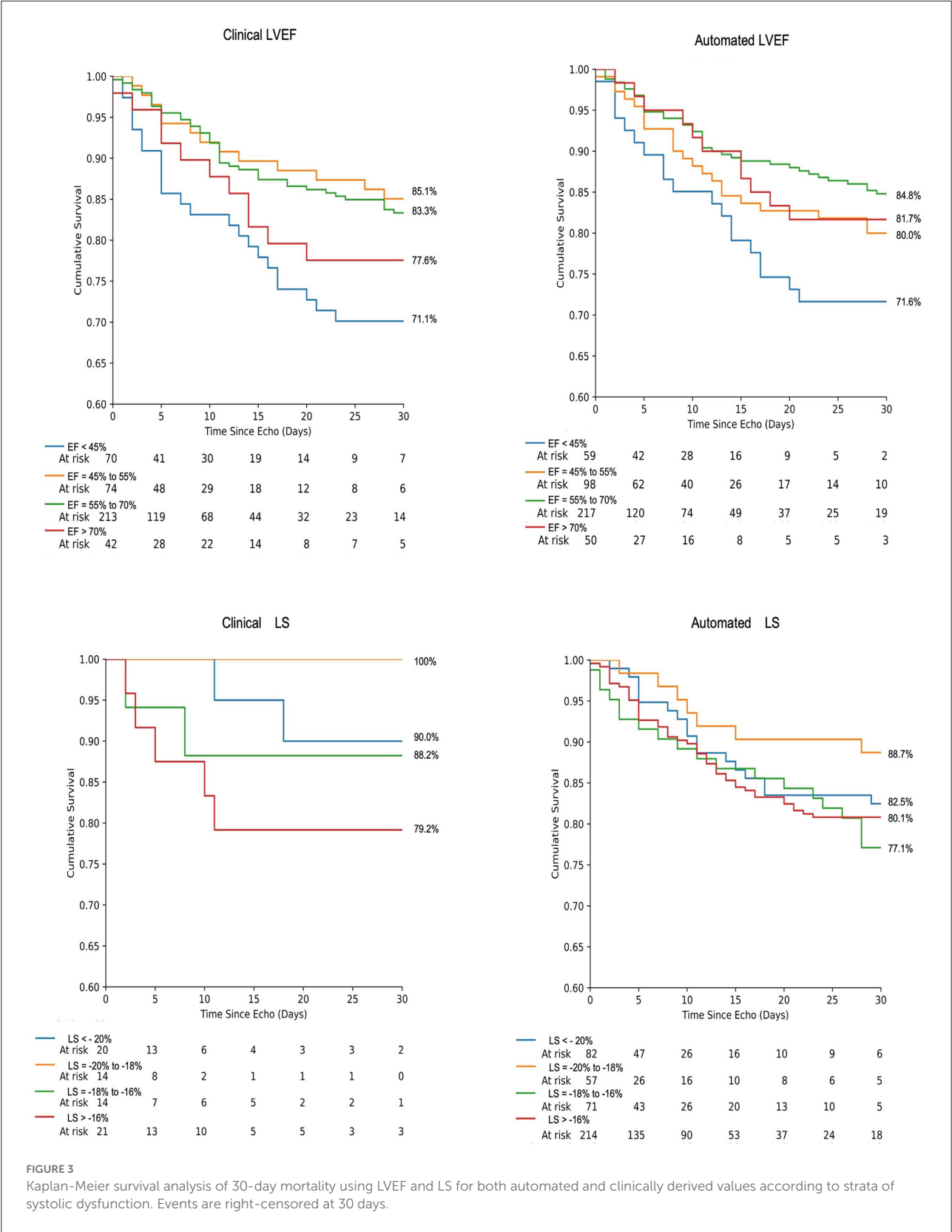
Variable + Site	Odds Ratio	95% CI LL	95% CI UL	p-value
Death				
Clinical LVEF	0.989	0.974	1.005	0.179
Automated LVEF	0.98	0.963	0.998	0.026
Clinical LS	1.094	0.965	1.241	0.161
Automated LS	1.051	1.003	1.1	0.035
ACS				
Clinical LVEF	0.954	0.935	0.973	<0.001
Automated LVEF	0.943	0.92	0.967	<0.001
Clinical LS	1.249	0.951	1.639	0.109
Automated LS	1.19	1.103	1.283	<0.001
Congestive heart failure				
Clinical LVEF	0.949	0.931	0.966	<0.001
Automated LVEF	0.94	0.919	0.962	<0.001
Clinical LS	1.625	1.153	2.289	0.005
Automated LS	1.16	1.085	1.24	<0.001
MACCE				
Clinical LVEF	0.956	0.941	0.97	<0.001
Automated LVEF	0.949	0.932	0.966	<0.001
Clinical LS	1.289	1.112	1.493	0.001
Automated LS	1.18	1.122	1.24	<0.001
Acute kidney injury				
Clinical LVEF	0.992	0.978	1.006	0.24
Automated LVEF	0.98	0.965	0.995	0.011
Clinical LS	1.02	0.921	1.13	0.704
Automated LS	1.044	1.003	1.087	0.034

Clinical LVEF was assessed in 459, automated LVEF in 488, clinical LS in 80, and automated LS in 488. ACS: acute coronary syndrome, CI LL: 95% confidence interval lower limit, CI UL: 95% confidence interval upper limit, MACCE, major adverse cardiovascular and cerebrovascular events. LVEF, left ventricular ejection fraction; LS, longitudinal strain.

(31, 32, 42) enabled the identification of serious cardiac abnormalities relevant to patient care, the focus on brevity and minimized contact may have led to omission of important information relevant for risk stratification or quantitative assessment of cardiac function. In the present study, clinical assessment of LV function using biplane LVEF methods was performed in 33.4% and strain analysis was performed in 16.4% patients. By contrast, for AI assessment, biplane methods were used for both LVEF and LS in 61.5% of patients with single planar measures in all others. These findings do not necessarily reflect differences in the feasibility of biplane methods, but rather reflect the increased availability of information under the same circumstance, using the automated approach. Thus, automated analysis can facilitate streamlined image acquisitions (9, 17, 43) while increasing the reporting of strain analysis to compliment clinical decision making, without requiring additional bedside expertise or time for analysis. Additionally, the strength of the agreement between automated and clinical assessment increased when consistent quantitative methods were used. The consistency of quantification afforded by automated analysis could help to reduce the inherent variability

associated with more manual approaches. With feasibility of 85% and good to excellent agreement between automated values and those obtained clinically, results from the present study provide additional evidence of the potential complementary nature of automated analysis, even in the setting of limited imaging protocols.

In addition to high feasibility, the ability to provide clinically relevant information to assist in patient risk stratification is a core requirement for medical devices. In the present study, patients with an automated LS of >−16% or LVEF of <50% were more likely to present with clinically identified cardiac abnormalities such as LV hypertrophy, regional wall motion abnormalities, and left atrial enlargement. Furthermore, both LS and LVEF were significantly associated with poor patient outcomes, with LS identifying patients with a 29% increased risk of MACCE (ACS, coagulation disorder, myocarditis, congestive heart failure, pericarditis, or stroke) per 1% increase (less negative) in LS. The risk of adverse in-hospital outcomes when stratified by LVEF or LS was largely consistent between clinical and automated assessments, providing further evidence of the validity of automated analysis. These findings are in line with



recent work reporting that abnormal systolic LV function, as defined by AI derived LVEF and/or LS, are associated with adverse cardiac events and death (9, 17, 18). Importantly, automated and clinically derived assessment were comparable in their association with patient outcomes, suggesting that the prognostic value of this information is preserved despite automation (9). Together, these results indicate that automated analysis of LVEF and LS provides clinically relevant estimations and may provide additional information relevant to patient care.

Technological advances in both computing and instrumentation have steadily increased the availability of quantitative echocardiographic assessment in routine practice. Such assessment, including LS, have consistently demonstrated value for patient risk stratification and prognostication in a range of conditions (44–47). However, inter- and intra-operator variability present a challenge to clinical interpretation of quantitative data (34, 48). With the potential for substantial reductions of variability in analysis, AI provides a potential solution, but evidence of its feasibility remains limited. The feasibility of automated contours in comprehensive transthoracic echocardiographic datasets is reported to range from 60.6% (9) to 95% (17) which may, in part, be dependent upon image quality (6). Feasibility in the present study, which required at least one apical cardiac cycle, demonstrates the potential of automated algorithms even under challenging conditions with abbreviated protocols. However, further work, including prospective studies, is required to understand the feasibility and utility of automated analysis in different patient conditions undergoing limited echocardiograms, where image quality and availability are variable.

An important finding of this study was the discordance between automated and clinical characterization of abnormal systolic function by LVEF and LS. Automated and clinical assessment were discordant in 20 and 30% of cases for LVEF and LS, respectively. When comparing those deemed to have abnormal LVEF and LS using clinical assessment as the reference, classifications using automated assessment identified a significantly smaller population as abnormal (AI vs. clinical: LVEF: 12.2 vs. 19.3%, LS: 22.5 vs. 38.8%). However, this investigation did not demonstrate significant differences in relationship to overall mortality when stratified using clinical or automated assessment; thus, the clinical implications of such discrepancies are unclear. Such differences may reflect a bias from clinical interpretation of echocardiograms, where additional information can support differential diagnosis while the use of only apical views for automated assessment may underestimate patient risk. Indeed, the use of limited methods in the clinical estimation of LVEF (linear and visual estimation) contributed to 73% of the observed differences of more than 10% between AI and the clinical interpretation. Although no differences were observed in patient outcomes between AI and clinical methods, limited sample size and a relatively low event rate precluded further investigation of the clinical implications of discordance between the AI and the clinical interpretation.

Further work is required to understand the relationship between automated assessment and clinical interpretation for risk stratification.

This study has several limitations. The retrospective nature of the investigation limits the generalizability of the findings to routine practice and further work is required to understand the real-time implications of the AI technology in varied populations. In addition, the clinical assessment of LVEF or LS was limited and as such, a comparison of AI feasibility to clinical feasibility was not possible. The limited sample of clinical LS values is a significant limitation when evaluating the association with patient outcomes. Automated assessment of RV function was not conducted and may have provided further prognostic information (18, 37). Secondly, the data consist of limited echocardiographic examinations conducted during the early COVID-19 pandemic; abbreviated examinations may have been of poorer quality due to risks of exposure. Echocardiographic protocols and clinical management of patients were conducted according to the local procedures in place at the time of data collection and regional and/or institutional bias may exist within the dataset. However, the resulting dataset is reflective of inter-site differences in practice and is a robust test of the AI algorithms. Finally, the cut-offs used for establishing the boundaries of normal, borderline and abnormal LVEF and GLS have varied between reports within the literature (27, 35, 36) and as such, the cut-offs utilized within the current study may not accurately distinguish normality from abnormality. Nevertheless, the implemented LVEF and GLS cut-offs provide further understanding of the findings from logistic regression models, whereby variables were modeled in a continuous manner.

Conclusions

In a multi-center study conducted during a pandemic, automated analysis of ultrasound images was highly feasible, correlated with clinical observation, and associated with outcome.

Data availability statement

The anonymized and aggregate raw data supporting the conclusions of this article will be made available by the authors, without undue reservation.

Ethics statement

The studies involving human participants were reviewed and approved by Mayo Clinic Institutional Review Board. Written informed consent for participation was not required for this study in accordance with the national legislation and the institutional requirements.

Author contributions

PP, WH, and GW designed the study. PP and WH drafted the manuscript. CS and WH organized the database and performed statistical analysis. JS and GP-H obtained local approval and data collection for Beth Israel Deaconess Medical Center. MK and BK obtained local approval and data collection for Temple Heart and Vascular Center. SQ and AT obtained local approval and data collection for Ochsner Health System. FG and EP obtained local approval and data collection for Einstein Medical Center. RT and SW obtained local approval and data collection for University of Pittsburgh. DM and TN obtained local approval and data collection for Mayo Clinic Scottsdale Arizona. PP oversaw local approval and data collection for Mayo Clinic Rochester Minnesota. All authors contributed to manuscript revision and read and approved the submitted version.

Acknowledgments

The authors appreciate the dedicated assistance of Katherine Tilkes, Halley Davison, William Hansen, MSc, Hania Piotrowska, BSc, Rizwan Sarwar, MD, Ashley Akerman, Ph.D., and cardiac sonographers at all sites. PP is supported as the Betty Knight Scripps Professor of Cardiovascular Disease Clinical Research at Mayo Clinic.

References

- Oren O, Gersh BJ, Bhatt DL. Artificial intelligence in medical imaging: switching from radiographic pathological data to clinically meaningful endpoints. *Lancet Digit Health*. (2020) 2:e486–8. doi: 10.1016/S2589-7500(20)30160-6
- Madani A, Arnaut R, Mofrad M, Arnaut R. Fast and accurate view classification of echocardiograms using deep learning. *NPJ Digi Med*. (2018) 1:6. doi: 10.1038/s41746-017-0013-1
- Shahin AI, Almotairi S. An accurate and fast cardio-views classification system based on fused deep features and LSTM. *IEEE Access*. (2020) 8:135184–94. doi: 10.1109/ACCESS.2020.3010326
- Van Woudenberg N, Liao Z, Abdi AH, Girgis H, Luong C, Vaseli H, et al. Quantitative echocardiography: Real-time quality estimation and view classification implemented on a mobile android device. In: *Simulation, Image Processing, and Ultrasound Systems for Assisted Diagnosis and Navigation*. 2018. *Lecture Notes in Computer Science*. Cham: Springer (2018) 11042, p. 74–81. doi: 10.1007/978-3-030-01045-4_9
- Abdi AH, Luong C, Tsang T, Allan G, Nouranian S, Jue J, et al. Automatic quality assessment of echocardiograms using convolutional neural networks: feasibility on the apical four-chamber view. *IEEE Trans Med Imaging*. (2017) 36:1221–30. doi: 10.1109/TMI.2017.2690836
- Huang KC, Huang CS, Su MY, Hung CL, Ethan Tu YC, Lin LC, et al. Artificial intelligence aids cardiac image quality assessment for improving precision in strain measurements. *JACC: Cardiovasc Imaging*. (2021) 14:335–45. doi: 10.1016/j.jcmg.2020.08.034
- Leclerc S, Smistad E, Ostvik A, Cervenansky F, Espinosa F, Espeland T, et al. LU-net: a multistage attention network to improve the robustness of segmentation of left ventricular structures in 2-D echocardiography. *IEEE Trans Ultrason Ferroelectr Freq Control*. (2020) 67:2519–30. doi: 10.1109/TUFFC.2020.3003403
- Azarmehr N, Ye X, Sacchi S, Howard JP, Francis DP, Zolgharni M. Segmentation of left ventricle in 2D echocardiography using deep learning. In: Zheng Y, Williams B, Chen K, editors. *Medical Image Understanding and Analysis. MIUA 2019. Communications in Computer and Information Science*. Cham: Springer (2020) 1065, 497–504. doi: 10.1007/978-3-030-39343-4_43
- Kawakami H, Wright L, Nolan M, Potter EL, Yang H, Marwick TH. Feasibility, reproducibility, and clinical implications of the novel fully automated assessment for global longitudinal strain. *J Am Soc Echocardiograph*. (2021) 34:136–45.e2. doi: 10.1016/j.echo.2020.09.011
- Kusunose K, Abe T, Haga A, Fukuda D, Yamada H, Harada M, et al. Deep Learning approach for assessment of regional wall motion abnormality from echocardiographic images. *JACC Cardiovasc Imaging*. (2020) 13:374–81. doi: 10.1016/j.jcmg.2019.02.024
- Zhang J, Gajjala S, Agrawal P, Tison GH, Hallock LA, Beussink-Nelson L, et al. Fully automated echocardiogram interpretation in clinical practice: feasibility and diagnostic accuracy. *Circulation*. (2018) 138:1623–35. doi: 10.1161/CIRCULATIONAHA.118.034338
- Ghorbani A, Ouyang D, Abid A, He B, Chen JH, Harrington RA, et al. Deep learning interpretation of echocardiograms. *NPJ Digit Med*. (2020) 3:10–10. doi: 10.1038/s41746-019-0216-8
- Ouyang D, He B, Ghorbani A, Yuan N, Ebinger J, Langlotz CP, et al. Video-based AI for beat-to-beat assessment of cardiac function. *Nature*. (2020) 580:252–6. doi: 10.1038/s41586-020-2145-8
- Alsharqi M, Woodward J, Mumith A, Markham C, Upton R, Leeson P. Artificial intelligence and echocardiography. *Echo Res Pract*. (2018) 5:R115–25. doi: 10.1530/ERP-18-0056

Conflict of interest

GW and WH are employed by Ultromics Ltd.

The remaining authors declare that the research was conducted in the absence of any commercial or financial relationships that could be construed as a potential conflict of interest.

This study received funding from Ultromics Ltd. The funder had the following involvement with the study: The AI measurements in this study were performed by Ultromics Ltd.

Publisher's note

All claims expressed in this article are solely those of the authors and do not necessarily represent those of their affiliated organizations, or those of the publisher, the editors and the reviewers. Any product that may be evaluated in this article, or claim that may be made by its manufacturer, is not guaranteed or endorsed by the publisher.

Supplementary material

The Supplementary Material for this article can be found online at: <https://www.frontiersin.org/articles/10.3389/fcvm.2022.937068/full#supplementary-material>

15. Cerna AEU, Jing L, Good CW, vanMaanen DP, Raghunath S, Suever JD, et al. Deep-learning-assisted analysis of echocardiographic videos improves predictions of all-cause mortality. *Nat Biomed Eng.* (2021) 5:546–54. doi: 10.1038/s41551-020-00667-9
16. Salte IM, Østvik A, Smistad E, Melichova D, Nguyen TM, Karlsen S, et al. Artificial intelligence for automatic measurement of left ventricular strain in echocardiography. *JACC Cardiovasc Imaging.* (2021) 14:1918–28. doi: 10.1016/j.jcmg.2021.04.018
17. Kitano T, Nabeshima Y, Negishi K, Takeuchi M. Prognostic value of automated longitudinal strain measurements in asymptomatic aortic stenosis. *Heart.* (2020) 2020: 318256. doi: 10.1136/heartjnl-2020-318256
18. Karagodin I, Carvalho Singulane C, Woodward GM, Xie M, Tucay ES, Tude Rodrigues AC, et al. Echocardiographic correlates of in-hospital death in patients with acute COVID-19 infection: the world alliance societies of echocardiography (WASE-COVID) study. *J Am Soc Echocardiogr.* (2021) 34:819–30. doi: 10.1016/j.echo.2021.05.010
19. Lala A, Johnson KW, Januzzi JL, Russak AJ, Paranjpe I, Richter F, et al. Prevalence and impact of myocardial injury in patients hospitalized with COVID-19 infection. *J Am Coll Cardiol.* (2020) 76:533–46. doi: 10.1016/j.jacc.2020.06.007
20. Ghio S, Baldi E, Vicentini A, Lenti MV, Di Sabatino A, Di Matteo A, et al. Cardiac involvement at presentation in patients hospitalized with COVID-19 and their outcome in a tertiary referral hospital in Northern Italy. *Intern Emerg Med.* (2020) 15:1457–65. doi: 10.1007/s11739-020-02604-9
21. Giustino G, Croft LB, Stefanini GG, Bragato R, Silbiger JJ, Vicenzi M, et al. Characterization of myocardial injury in patients with COVID-19. *J Am Coll Cardiol.* (2020) 76:2043–55. doi: 10.1016/j.jacc.2020.08.069
22. Yuan N, Wu S, Rader F, Siegel RJ. Determining which hospitalized coronavirus disease 2019 patients require urgent echocardiography. *J Am Soc Echocardiogr.* (2021) 34:831–8. doi: 10.1016/j.echo.2021.03.010
23. Krishna H, Ryu AJ, Scott CG, Mandale DR, Naqvi TZ, Pellikka PA. Cardiac abnormalities in COVID-19 and relationship to outcome. *Mayo Clin Proc.* (2021) 96:932–42. doi: 10.1016/j.mayocp.2021.01.006
24. Karagodin I, Singulane CC, Descamps T, Woodward GM, Xie M, Tucay ES, et al. Ventricular changes in patients with acute COVID-19 infection: follow-up of the world alliance societies of echocardiography (WASE-COVID) study. *J Am Soc Echocardiogr.* (2022) 35:295–304. doi: 10.1016/j.echo.2021.10.015
25. Baycan OF, Barman HA, Atici A, Tatlisu A, Bolen F, Ergen P, et al. Evaluation of biventricular speckle-tracking echocardiography in COVID-19 using speckle tracking echocardiography. *Int J Cardiovasc Imaging.* (2020) 37:135–44. doi: 10.1007/s10554-020-01968-5
26. Ehud R, Guy B, Yishay S, Yael L, Alon K, Philippe T, et al. The predictive role of left and right ventricular speckle-tracking echocardiography in COVID-19. *JACC Cardiovasc Imaging.* (2020) 13:2471–4. doi: 10.1016/j.jcmg.2020.07.026
27. Lang RM, Badano LP, Mor-Avi V, Afilalo J, Armstrong A, Ernande L, et al. Recommendations for cardiac chamber quantification by echocardiography in adults: an update from the American society of echocardiography and the European association of cardiovascular imaging. *J Am Soc Echocardiogr.* (2015) 28:1–39.e14. doi: 10.1016/j.echo.2014.10.003
28. Duffy G, Cheng PP, Yuan N, He B, Kwan AC, Shun-Shin MJ, et al. High-throughput precision phenotyping of left ventricular hypertrophy with cardiovascular deep learning. *JAMA Cardiol.* (2022) 7:386–95. doi: 10.1001/jamacardio.2021.6059
29. Asch FM, Poilvert N, Abraham T, Jankowski M, Cleve J, Adams M, et al. Automated echocardiographic quantification of left ventricular ejection fraction without volume measurements using a machine learning algorithm mimicking a human expert. *Circ Cardiovasc imaging.* (2019) 12:e009303. doi: 10.1161/CIRCIMAGING.119.009303
30. Kirkpatrick JN, Grimm R, Johri AM, Kimura BJ, Kort S, Labovitz AJ, et al. Recommendations for echocardiography laboratories participating in cardiac point of care cardiac ultrasound (POCUS) and critical care echocardiography training: report from the american society of echocardiography. *J Am Soc Echocardiogr.* (2020) 33:409–22.e4. doi: 10.1016/j.echo.2020.01.008
31. Skulstad H, Cosyns B, Popescu BA, Galderisi M, Salvo GD, Donal E, et al. COVID-19 pandemic and cardiac imaging: EACVI recommendations on precautions, indications, prioritization, and protection for patients and healthcare personnel. *Eur Heart J Cardiovasc Imaging.* (2020) 21:592–8. doi: 10.1093/ehjci/jeaa072
32. Anand V, Thaden JJ, Pellikka PA, Kane GC. Safe operation of an echocardiography practice during the COVID-19 pandemic: single-center experience. *Mayo Clin Proc.* (2021) 96:531–6. doi: 10.1016/j.mayocp.2020.12.015
33. Thavendiranathan P, Grant AD, Negishi T, Plana JC, Popović ZB, Marwick TH. Reproducibility of echocardiographic techniques for sequential assessment of left ventricular ejection fraction and volumes: application to patients undergoing cancer chemotherapy. *J Am Coll Cardiol.* (2013) 61:77–84. doi: 10.1016/j.jacc.2012.09.035
34. Lambert J, Lamacie M, Thampinathan B, Altaha MA, Esmailzadeh M, Nolan M, et al. Variability in echocardiography and MRI for detection of cancer therapy cardiotoxicity. *Heart.* (2020) 106:817–23. doi: 10.1136/heartjnl-2019-316297
35. Potter E, Marwick TH. Assessment of left ventricular function by echocardiography: the case for routinely adding global longitudinal strain to ejection fraction. *JACC Cardiovasc Imaging.* (2018) 11:260–74. doi: 10.1016/j.jcmg.2017.11.017
36. Asch FM, Miyoshi T, Addetia K, Citro R, Daimon M, Desale S, et al. Similarities and differences in left ventricular size and function among races and nationalities: results of the world alliance societies of echocardiography normal values study. *J Am Soc Echocardiogr.* (2019) 32:1396–406.e2. doi: 10.1016/j.echo.2019.08.012
37. Ruge M, Gomez JMD, de Lavallaz JDF, Simmons JA, Canzolino J, Volgman AS, et al. COVID-19 infection. *J Am Coll Cardiol.* (2021) 77:3150. doi: 10.1016/S0735-1097(21)04505-8
38. Kim J, Volodarskiy A, Sultana R, Pollie MP, Yum B, Nambiar L, et al. Prognostic Utility of right ventricular remodeling over conventional risk stratification in patients with COVID-19. *J Am Coll Cardiol.* (2020) 76:1965–77. doi: 10.1016/j.jacc.2020.08.066
39. Li Y, Li H, Zhu S, Xie Y, Wang B, He L, et al. Prognostic value of right ventricular longitudinal strain in patients with COVID-19. *JACC Cardiovasc Imaging.* (2020) 13:2287–99. doi: 10.1016/j.jcmg.2020.04.014
40. Lombardi CM, Carubelli V, Iorio A, Inciardi RM, Bellasi A, Canale C, et al. Association of troponin levels with mortality in Italian patients hospitalized with coronavirus disease 2019: results of a multicenter study. *JAMA Cardiol.* (2020) 5:1274–80. doi: 10.1001/jamacardio.2020.3538
41. Petrilli CM, Jones SA, Yang J, Rajagopalan H, O'Donnell L, Chernyak Y, et al. Factors associated with hospital admission and critical illness among 5279 people with coronavirus disease 2019 in New York City: prospective cohort study. *BMJ.* (2020) 369:m1966. doi: 10.1136/bmj.m1966
42. Johri AM, Galen B, Kirkpatrick JN, Lanspa M, Mulvagh S, Thamman R, et al. Statement on point-of-care ultrasound during the 2019 novel coronavirus pandemic. *J Am Soc Echocardiogr.* (2020) 33:670–3. doi: 10.1016/j.echo.2020.04.017
43. Knackstedt C, Bekkers SCAM, Schummers G, Schreckenber M, Muraru D, Badano LP, et al. Fully automated versus standard tracking of left ventricular ejection fraction and longitudinal strain the FAST-EFs multicenter study. *J Am Coll Cardiol.* (2015) 66:1456–66. doi: 10.1016/j.jacc.2015.07.052
44. Liou K, Negishi K, Ho S, Russell EA, Cranney G, Ooi S-Y. Detection of obstructive coronary artery disease using peak systolic global longitudinal strain derived by two-dimensional speckle-tracking: a systematic review and meta-analysis. *J Am Soc Echocardiogr.* (2016) 29:724–35.e4. doi: 10.1016/j.echo.2016.03.002
45. Shetye A, Nazir SA, Squire IB, McCann GP. Global myocardial strain assessment by different imaging modalities to predict outcomes after ST-elevation myocardial infarction: a systematic review. *World J Cardiol.* (2015) 7:948–60. doi: 10.4330/wjc.v7.i12.948
46. Oikonomou EK, Kokkinidis DG, Kampatsis PN, Amir EA, Marwick TH, Gupta D, et al. Assessment of prognostic value of left ventricular global longitudinal strain for early prediction of chemotherapy-induced cardiotoxicity: a systematic review and meta-analysis. *JAMA Cardiol.* (2019) 4:1007–18. doi: 10.1001/jamacardio.2019.2952
47. Al Saikhan L, Park C, Hardy R, Hughes A. Prognostic implications of left ventricular strain by speckle-tracking echocardiography in the general population: a meta-analysis. *Vasc Health Risk Manag.* (2019) 15:229–51. doi: 10.2147/VHRM.S206747
48. Negishi T, Negishi K, Thavendiranathan P, Cho G-Y, Popescu BA, Vinereanu D, et al. SUCCOUR investigators. effect of experience and training on the concordance and precision of strain measurements. *JACC Cardiovasc Imaging.* (2017) 10:518–22. doi: 10.1016/j.jcmg.2016.06.012



OPEN ACCESS

EDITED BY

Francesco Bandera,
University of Milan, Italy

REVIEWED BY

Yosuke Nabeshima,
University of Occupational and
Environmental Health Japan, Japan
Lilia Oretto,
Mediterranean Pediatric Cardiology
Center, Italy

*CORRESPONDENCE

Eric S. Rothstein
Eric.S.Rothstein@Hitchcock.Org

†These authors share first authorship

SPECIALTY SECTION

This article was submitted to
Cardiovascular Imaging,
a section of the journal
Frontiers in Cardiovascular Medicine

RECEIVED 16 June 2022

ACCEPTED 12 August 2022

PUBLISHED 02 September 2022

CITATION

Stock JD, Rothstein ES, Friedman SE,
Gemignani AS, Costa SP, Milbridge AJ,
Zhang R, Taub CC, O'Rourke DJ and
Palac RT (2022) Lateral annular systolic
excursion ratio: A novel measurement
of right ventricular systolic function by
two-dimensional echocardiography.
Front. Cardiovasc. Med. 9:971302.
doi: 10.3389/fcvm.2022.971302

COPYRIGHT

© 2022 Stock, Rothstein, Friedman,
Gemignani, Costa, Milbridge, Zhang,
Taub, O'Rourke and Palac. This is an
open-access article distributed under
the terms of the [Creative Commons
Attribution License \(CC BY\)](#). The use,
distribution or reproduction in other
forums is permitted, provided the
original author(s) and the copyright
owner(s) are credited and that the
original publication in this journal is
cited, in accordance with accepted
academic practice. No use, distribution
or reproduction is permitted which
does not comply with these terms.

Lateral annular systolic excursion ratio: A novel measurement of right ventricular systolic function by two-dimensional echocardiography

Jonathan D. Stock^{1,2†}, Eric S. Rothstein^{1*†}, Scott E. Friedman²,
Anthony S. Gemignani², Salvatore P. Costa¹,
Andrew J. Milbridge^{1,2}, Rui Zhang^{1,2}, Cynthia C. Taub^{1,2},
Daniel J. O'Rourke² and Robert T. Palac²

¹Heart and Vascular Center, Dartmouth-Hitchcock Medical Center, Lebanon, NH, United States,

²Division of Cardiology, White River Junction VA Medical Center, White River Junction, VT, United States

Introduction: Accurate assessment of right ventricular (RV) systolic function has prognostic and therapeutic implications in many disease states. Echocardiography remains the most frequently deployed imaging modality for this purpose, but estimation of RV systolic function remains challenging. The purpose of this study was to evaluate the diagnostic performance of a novel measurement of RV systolic function called lateral annular systolic excursion ratio (LASER), which is the fractional shortening of the lateral tricuspid annulus to apex distance, compared to right ventricular ejection fraction (RVEF) derived by cardiac magnetic resonance imaging (CMR).

Methods: A retrospective cohort of 78 consecutive patients who underwent clinically indicated CMR and transthoracic echocardiography within 30 days were identified from a database. Parameters of RV function measured included: tricuspid annular plane systolic excursion (TAPSE) by M-mode, tissue Doppler S', fractional area change (FAC) and LASER. These measurements were compared to RVEF derived by CMR using Pearson's correlation coefficients and receiver operating characteristic curves.

Results: LASER was measurable in 75 (96%) of patients within the cohort. Right ventricular systolic dysfunction, by CMR measurement, was present in 37% ($n = 29$) of the population. LASER has moderate positive correlation with RVEF ($r = 0.54$) which was similar to FAC ($r = 0.56$), S' ($r = 0.49$) and TAPSE ($r = 0.37$). Receiver operating characteristic curves demonstrated that LASER (AUC = 0.865) outperformed fractional area change (AUC = 0.767), tissue Doppler S' (AUC = 0.744) and TAPSE (AUC = 0.645). A cohort derived dichotomous cutoff of 0.2 for LASER was shown to provide optimal diagnostic characteristics (sensitivity of 75%, specificity of 87% and accuracy of 83%) for identifying abnormal RV function. LASER had the highest sensitivity, accuracy, positive and negative predictive values among the parameters studied in the cohort.

Conclusions: Within the study cohort, LASER was shown to have moderate positive correlation with RVEF derived by CMR and more favorable diagnostic performance for detecting RV systolic dysfunction compared to conventional echocardiographic parameters while being simple to obtain and less dependent on image quality than FAC and emerging techniques.

KEYWORDS

right ventricle (RV), right ventricular systolic function, RV function, cardiac magnetic resonance imaging, two-dimensional echocardiography, TAPSE, fractional area change

Introduction

Accurate characterization of right ventricular (RV) systolic function has diagnostic and prognostic value in a variety of disease states including heart failure, pulmonary hypertension, chronic pulmonary disease, atrial fibrillation, valvular heart disease, congenital heart disease, pulmonary embolism and acute coronary syndrome (1–14). The imaging gold standard for assessing RV systolic function is volumetric analysis by cardiac magnetic resonance imaging (CMR) owing to its reproducibility and lack of reliance on geometric assumptions (15–19). However, transthoracic echocardiography (TTE) remains the most widely deployed imaging modality for this purpose due to its wide availability, portability and ease of use. The American Society of Echocardiography (ASE) has published guidelines for the assessment of RV function relying on qualitative and quantitative parameters using two-dimensional echocardiography, M-mode and tissue Doppler imaging with emerging roles of three-dimensional echocardiography and free wall longitudinal strain (20). Unfortunately, accurate assessment of RV function by TTE remains challenging owing to the RV's complex geometry, trabecular muscle structure and the difficulty in acquiring standardized imaging planes (21, 22).

Traditionally, the most commonly adopted parameters for measuring RV function have been M-mode derived tricuspid annular plane systolic excursion (TAPSE) and peak systolic annular velocity (S'). These measures are simple to obtain, reproducible and familiar to imagers due to decades of clinical use (20, 23–26). Despite these advantages, these one-dimensional parameters are highly angle dependent, may

neglect radial contractile function, do not account for cardiac translational motion and correlate weakly with CMR derived right ventricular ejection fraction (RVEF) (15, 16, 20, 27, 28).

Two-dimensional fractional area change (FAC) offers a more comprehensive assessment of right ventricular systolic function by incorporating both longitudinal and radial contractile elements leading to improved diagnostic accuracy and correlation with CMR derived RVEF (27–29). However, FAC may suffer from foreshortening and interference from trabeculations. Accurate FAC measurement is highly dependent on the acquisition of a single imaging plane that visualized the base, free wall and apex of the RV.

Right ventricular free wall strain by speckle-tracking and RVEF by three-dimensional echocardiography are emerging techniques for the measurement of RV function. These techniques, though promising, rely on excellent image quality and have variable feasibility rates in inpatient and critical care settings (20, 30–38).

In clinical practice, there remains a need for a single parameter combining the simplicity and practicality of the one-dimensional parameters with the diagnostic accuracy of the more image quality dependent two and three-dimensional parameters. Lateral annular systolic excursion ratio (LASER) is a novel linear parameter which measures the fractional shortening of the linear distance between the lateral tricuspid annulus and the right ventricular apex (Figure 1). LASER is similar to TAPSE in that it incorporates the excursion of the lateral tricuspid annulus during systole, however, it improves upon the measurement by introducing an anchoring point at the RV apex which eliminates the angle dependence of the measurement and error associated with cardiac translation. Being a linear parameter with two anchoring points, LASER is less dependent on the acquisition of an optimal imaging plane and requires only the visualization of the lateral tricuspid annulus and the RV apex. Thus, LASER has the potential to be applicable across a diversity of patients and care settings.

The purpose of this study was to determine the correlation of LASER with RVEF derived by CMR and to determine the

Abbreviations: RV, Right Ventricle; CMR, Cardiac Magnetic Resonance Imaging; TTE, Transthoracic Echocardiogram; ASE, American Society of Echocardiography; TAPSE, Tricuspid Annular Plane Systolic Excursion; RVEF, Right Ventricular Ejection Fraction; FAC, Fractional Area Change; LASER, Lateral Annular Systolic Excursion Ratio; RVEDV, Right Ventricular End-Diastolic Volume; RVESV, Right Ventricular End-Systolic Volume.

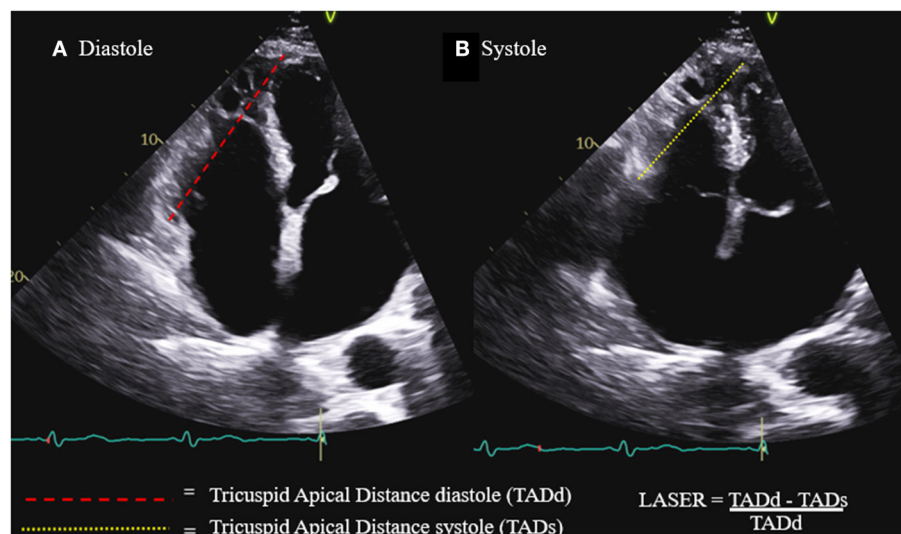


FIGURE 1

Lateral annular systolic excursion ratio (LASER) is the ratio of the systolic shortening of the tricuspid annulus to apex distance (B) compared to the length of the tricuspid annulus to apex distance in diastole (A).

diagnostic ability of LASER for detecting abnormal RV function in comparison to TAPSE, S' and FAC.

Materials and methods

Study population

The study sample began with 163 consecutive adult patients who underwent CMR for any clinical indication between January 1, 2015 and December 31, 2018 at the White River Junction Veterans Affairs Medical Center in White River Junction, Vermont and at Dartmouth-Hitchcock Medical Center in Lebanon, New Hampshire. From this population, 82 patients were identified as having a TTE acquired within 30 days of CMR. Exclusion criteria were limited to patients who had a clinical event requiring hospitalization or urgent visit between the dates of the TTE and CMR or had a significant clinical change between studies one review of the health record, patients with irregular heart rhythms such as atrial fibrillation and patients who had otherwise uninterpretable short axis cine images on CMR making them unsuitable for volumetric analysis. Focused and technically limited echocardiograms including those with sub-optimal imaging windows were included in the study.

There were 78 patients who met the above inclusion criteria. Patient demographics, number of days between the CMR and TTE, and the indication for the CMR were collected by chart review. This study was approved by the local institutional review boards at both sites.

Cardiac magnetic resonance imaging

CMR images were acquired using Siemens 1.5 Tesla whole body scanners (Siemens Healthineers, Erlangen, Germany) at both sites using a dedicated cardiac coil and electrocardiographic gating. Steady-state free precession cine images were acquired in short and long axis imaging planes. Right ventricular end-diastolic volumes (RVEDV) and right ventricular end-systolic volumes (RVESV) were quantitated in short-axis cine images (slice thickness 8 mm) with basal and apical image positions defined by the pulmonic valve annulus and the distal most myocardium respectively. The quantitation was accomplished according to a pre-specified analytic approach using commercially available software. Endocardial borders were measured by planimetry inclusive of trabeculae consistent with established standards. End-diastole and end-systole were defined by the largest and smallest cavity sizes, respectively.

Echocardiography

Transthoracic echocardiograms were acquired by experienced sonographers using Philips Epiq, Philips iE33 (Philips Professional Healthcare, Amsterdam, Netherlands) and GE Vivid e95 ultrasound machines (GE Healthcare, Chicago, Illinois). Each examination included two-dimensional, M-mode, spectral Doppler and tissue Doppler imaging in the parasternal long axis (PLAX), parasternal short axis (PSAX), apical four chamber (A4C) and RV focused imaging planes as

TABLE 1 Patient characteristics and cardiac magnetic resonance imaging data of the sample population.

Characteristics	Sample population (<i>n</i> = 78)
Age (years)	58 ± 16 (18–83)
Male	58 (74%)
Body mass index (kg/m ²)	29 ± 6.4 (14–49)
Time interval between imaging tests (days)	8.7 ± 9.2 (0–28)
Right ventricular end-diastolic volume index (mL/m ²)	78.3 ± 24.7 (30–154)
Right ventricular ejection fraction (%)	49.7 ± 13.3 (15–75)
Normal right ventricular function	49 (63%)
Abnormal right ventricular function	29 (37%)
Left ventricular ejection fraction (%)	46 ± 18 (12–80)

Continuous variables are expressed as mean ± standard deviation (range) and proportions are expressed as number (percent).

TABLE 2 Diversity of clinical indications for cardiac magnetic resonance imaging by category.

Indications	Quantity
Valvular heart disease	8
Cardiac mass or thrombus	5
Congenital heart disease	3
Pericardial disease	5
Infiltrative cardiomyopathy	7
Hypertrophic cardiomyopathy	8
Non-ischemic cardiomyopathy	18
Myocarditis and sarcoidosis	9
Arrhythmia	5
Ischemic cardiomyopathy and viability	10

specified in the ASE guidelines (15). Some TTE examinations were clinical question focused and did not include M-mode and/or tissue Doppler imaging of the right ventricle.

Parameters of RV function were measured and calculated by two experienced readers (ER and RP) according to the ASE guidelines and included: TAPSE by M-mode, tissue Doppler S' and RV fractional area change (FAC). The measurement of LASER, as demonstrated in Figure 1, involves the identification of the lateral tricuspid annulus and drawing a line from this point to the endocardial tip of the RV apex. This line represents tricuspid annulus to apex distance (TAD). This distance is measured both in diastole and in systole. LASER is then calculated as the fractional shortening of this distance from diastole to systole: $\text{LASER} = (\text{TADd} - \text{TADs}) / \text{TADd}$.

TABLE 3 Pearson's correlation coefficients (*r*) for each echocardiographic parameter of right ventricular systolic function when compared to right ventricular ejection fraction (RVEF) by cardiac magnetic resonance imaging.

Correlation of measurements with RVEF

Measurement	<i>n</i>	<i>r</i>	<i>p</i>
LASER	75	0.54	<0.001
Fractional area change	72	0.56	<0.001
Tissue Doppler S'	53	0.49	<0.001
TAPSE by M-mode	58	0.37	0.004

LASER, Lateral tricuspid annular systolic excursion ration; TAPSE, Tricuspid annular plane systolic excursion.

Reproducibility

Inter-observer and intra-observer reproducibility for each parameter of RV function including LASER were examined in a random sample of 17 patients. Intra-observer reproducibility was tested by a single reader (JS) and inter-observer reproducibility was tested between two readers (ER and JS). Readers were blinded to clinical history, CMR data and all previous measurements. All reproducibility measurements were acquired >30 days after initial measurements were made to reduce recall bias.

Statistical analysis

Statistical analysis was performed using MedCalc statistical software version 18.6 (MedCalc Software, Ostend, Belgium). Each echocardiographic parameter of RV function including LASER was compared with CMR derived RVEF using correlation analysis to obtain Pearson's correlation coefficients. The cohort-derived diagnostic performance of each parameter for detecting abnormal RVEF, defined as < 50%, was determined by constructing receiver operating characteristic (ROC) curves (39). Area under the curve (AUC) was then used to rank the relative discriminatory strength of each parameter within the cohort using the Delong approach (40). An optimal cutoff to dichotomize abnormal and normal values for LASER was determined using Youden's index. The ASE recommended dichotomous cutoffs for abnormal TAPSE, S' and FAC were used for these parameters. The overall diagnostic accuracy for each parameter was compared using Fisher's exact test. Stepwise logistic regression analysis was performed to determine which parameters add the most predictive information in identifying abnormal RVEF. Inter-observer and intra-observer reproducibility was tested using Bland-Altman analysis as well as calculation of the mean relative difference between repetitive measurements (41).

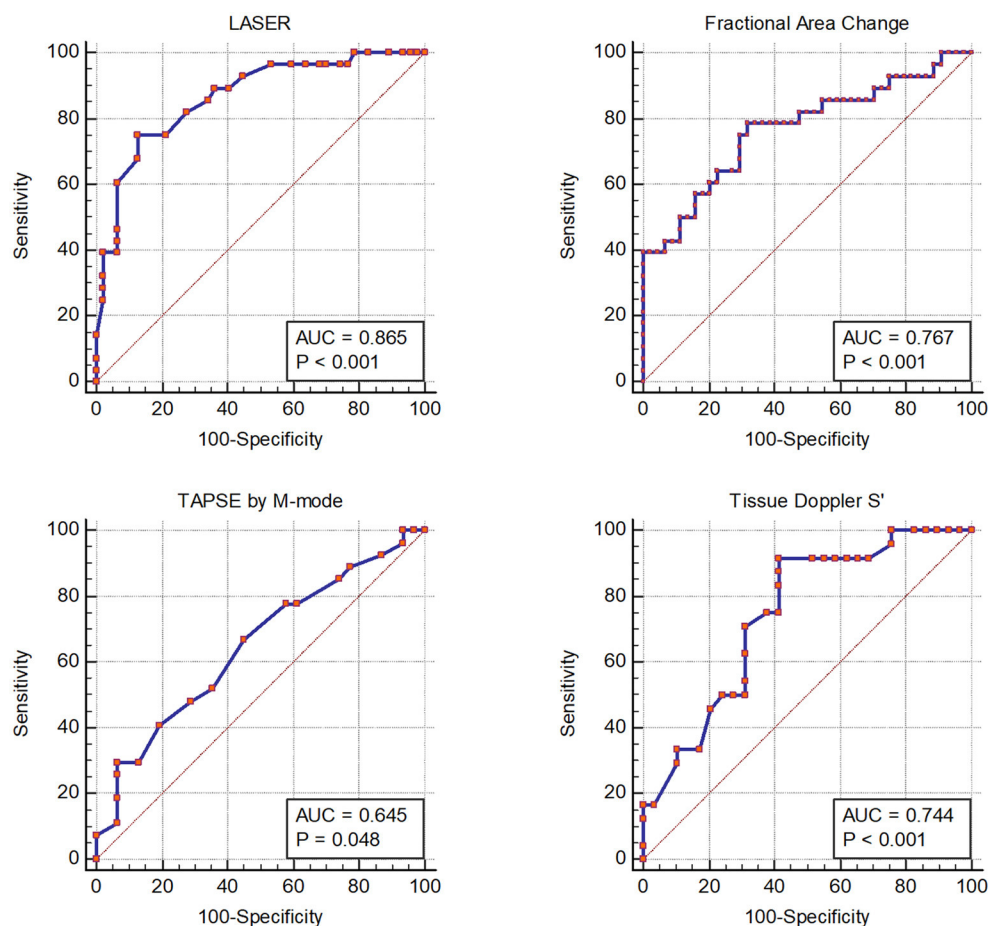


FIGURE 2

Receiver operator characteristic curves showing the diagnostic performance of each echocardiographic parameter of right ventricular systolic function compared to right ventricular ejection fraction by cardiac magnetic resonance imaging.

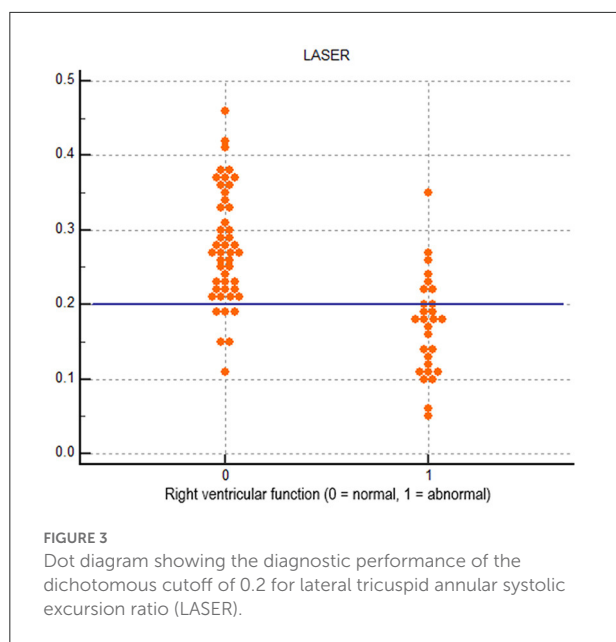
Results

Sample characteristics

Baseline characteristics and CMR derived volumetric data for the cohort is displayed in [Table 1](#). The cohort was predominantly male with a broad range of body mass indices represented. The mean time interval between the TTE and CMR was 8.7 days with a standard deviation of 9.2 days. RV function was variable with a mean ejection fraction of 49.7% with a standard deviation of 13.3% and range of 15–75%. The proportion of patients with abnormal RV function was 37%. [Table 2](#) shows the diversity of clinical indications for CMR represented in the study cohort across 10 categories of indications.

Echocardiographic parameters compared to cardiac magnetic resonance imaging

LASER, FAC, tissue Doppler S' and TAPSE by M-mode were able to be measured in 75 (96%), 72 (92%), 53 (68%) and 58 (74%) patients within the cohort respectively. LASER was attainable in 96% of studies and FAC was attainable in 92% of the studies. Measurement of TAPSE and tissue Doppler S' were dependent upon requisite M-mode and tissue Doppler image acquisition which were not available in all patients. There were 44 (56%) patients within the cohort in whom all four parameters could be measured. The Pearson's correlation coefficient (r) for each parameter of RV function compared to CMR derived RVEF is shown in [Table 3](#). FAC ($r = 0.56$) had the highest correlation followed by LASER ($r = 0.54$), tissue Doppler S' ($r = 0.49$) and TAPSE ($r = 0.37$).



Receiver operating characteristic curves for each echocardiographic parameter of RV function compared to CMR derived RVEF are displayed in [Figure 2](#). LASER (AUC = 0.865) had the highest diagnostic ability for detecting abnormal RVEF followed by FAC (AUC = 0.767), tissue Doppler S' (AUC = 0.744) and TAPSE (AUC = 0.645). The optimal dichotomous cutoff value between normal and abnormal LASER was determined to be 0.2 with a Youden's Index of 0.62 and an associated sensitivity and specificity of 75% and 87% respectively ([Figure 3](#)).

[Table 4](#) displays the cohort derived diagnostic performance of each parameter for detecting abnormal RVEF using the cohort derived cutoff value for LASER (0.2) and cutoff values recommended by the American Society of Echocardiography for FAC (35%), tissue Doppler S' (9.5 cm/s) and TAPSE (17 mm). LASER had the highest sensitivity (75%), accuracy (83%), positive predictive value (78%) and negative predictive value (85%). LASER's diagnostic accuracy was statistically comparable to that of FAC ($p = 0.231$) by Fisher's exact test. The diagnostic accuracy of LASER was significantly higher than tissue Doppler S' ($p = 0.008$) and TAPSE ($p = 0.006$).

Stepwise logistic regression analysis was performed using the patients in which all parameters were measure ($n = 44$). The model showed most predictive parameters for abnormal RVEF in our cohort were LASER ($p = 0.004$) and S' (0.030) with LASER being the most important component of the model. FAC and TAPSE did not add additional value beyond LASER or S' in the model.

Reproducibility

[Table 5](#) shows the inter-observer and intra-observer reproducibility for the measurement of each parameter of RV function. The traditional 1-dimensional parameters of S' and TAPSE proved to be most reproducible with mean relative differences between observers of 1.3 and 3.4% respectively. LASER and FAC were slightly less reproducible with mean relative differences of 4.2 and 5.4% respectively.

Discussion

This is the first study evaluating the correlation and diagnostic performance of the novel measurement of RV function LASER in a broad cohort of patients with a high prevalence of abnormal RV function. Measurement of LASER was achievable in 96% of patients despite many of the echocardiograms being technically limited or problem focused. These data suggest LASER is attainable across a variety clinical care settings such as the emergency department, critical care unit or cardiac catheterization laboratory where optimal image quality may be difficult to obtain or when the scanner is not a registered diagnostic cardiac sonographer.

The LASER technique has moderate positive correlation ($r = 0.54$) with CMR derived RVEF, comparable to that of FAC ($r = 0.56$) while the one-dimensional parameters of tissue Doppler S' ($r = 0.49$) and TAPSE ($r = 0.37$) had fair correlation. The correlation of FAC with RVEF in this study was similar to that in larger cohorts with Kim et al. reporting a correlation coefficient of 0.55 in 272 patients with coronary artery disease and Pavlicek et al. reporting 0.472 in 223 patients ([15, 16](#)). The correlation of TAPSE and S' with RVEF has been variable and weak in large cohorts. Kim et al. reported correlation coefficients for TAPSE and S' of 0.48 and 0.36 respectively, whereas Pavlicek et al. reported 0.336 and 0.476 ([15, 16](#)). The correlations of TAPSE and S' with RVEF in this cohort were similar to the prior values reported by the aforementioned authors.

The diagnostic ability of LASER to detect abnormal RV function was favorable using receiver operating characteristic curves with an AUC of 0.865 which was larger than that of FAC (0.767), TAPSE (0.645) and S' (0.744). Using the cohort derived cutoff of 0.2, LASER had the highest sensitivity, accuracy, positive predictive value and negative predictive value among the studied parameters of RV function using ASE recommended cutoffs. The diagnostic accuracy of LASER was 83% which was statistically similar to FAC (74%) with a p value of 0.231 and better than TAPSE (60%) and S' (61%) with p values of 0.008 and 0.006 respectively. The diagnostic performance of FAC, TAPSE and S' in this cohort was similar to the diagnostic performance reported by Pavlicek et al. with AUCs of 0.728, 0.716 and 0.779 for each parameter respectively ([16](#)). Agasthi et al. in a large cohort of 500 patients reported a lower diagnostic performance

TABLE 4 Cohort derived test characteristics for each echocardiographic parameter of right ventricular systolic function.

Diagnostic performance of right ventricular measurements

Measurement	n	Prevalence	Sensitivity	Specificity	Accuracy	PPV	NPV
LASER	75	37%	75%	87%	83%	78%	85%
Fractional area change	72	39%	50%	89%	74%*	74%	74%
Tissue Doppler S'	53	45%	33%	83%	61%†	62%	60%
TAPSE by M-mode	58	47%	48%	71%	60%‡	59%	61%

Prevalence represents the prevalence of abnormal right ventricular ejection fractions within each parameter's sample.

LASER, Lateral annular systolic excursion ratio; TAPSE, Tricuspid annular plane systolic excursion; PPV, Positive predictive value; NPV, Negative predictive value.

*Statistically insignificant difference compared to LASER $p = 0.231$ (Fisher's Exact).

†Statistically significant difference compared to LASER $p = 0.008$ (Fisher's Exact).

‡Statistically significant difference compared to LASER $p = 0.006$ (Fisher's Exact).

TABLE 5 Inter-observer and intra-observer reproducibility of measurements.

Methodologic reproducibility

Measurement	Inter-observer reproducibility			Intra-observer reproducibility		
	Mean difference \pm standard deviation	Mean relative difference (%)	95% limits of agreement	Mean difference \pm standard deviation	Mean relative difference (%)	95% limits of agreement
LASER	0.02 \pm 0.04	4.2	−0.06 to 0.09	0.02 \pm 0.03	4.2	−0.04 to 0.09
FAC	4.7 \pm 6.7	5.4	−8.5 to 18.0	−0.15 \pm 7.8	4.4	−1.5 to 1.5
S' (cm/s)	0.00 \pm 0.87	1.3	−1.7 to 1.7	0.00 \pm 0.61	0.4	−1.2 to 1.2
TAPSE (mm)	−0.05 \pm 3.2	3.4	−0.68 to 0.57	−0.06 \pm 0.17	2.1	−0.39 to 0.28

LASER, lateral annular systolic excursion ratio; TAPSE, tricuspid annular plane systolic excursion; FAC, fractional area change.

of FAC, TAPSE and S' with AUCs of 0.6658, 0.5819 and 0.5909 respectively, though a different dichotomous cutoff for abnormal RVEF was used (28). The stepwise logistic regression model suggests that FAC and TAPSE do not add additional diagnostic value over LASER and S' which further suggests that LASER as a simple measure may be a robust parameter for discriminating abnormal RV function.

Overall, this study shows LASER is a simple to acquire, robust and reproducible measurement of RV function with similar diagnostic performance to FAC and better diagnostic performance than the traditional one-dimensional parameters of TAPSE and S'. The main advantage of LASER over FAC is that it can be performed in most patients even when image quality is poor as it requires only the visualization of the lateral tricuspid annulus and RV apex. Although not evaluated in this study, theoretically this also translates to RV free wall strain and RVEF by 3DE as these measurements also require good image quality with perfect imaging windows for visualization of the entire RV free wall throughout the cardiac cycle. A possible niche use for LASER may indeed be in the emergency department, critical care unit or cardiac catheterization laboratory where a rapid assessment of RV function is often necessary for clinical decision making and perfect imaging planes may be difficult to acquire.

Study limitations and future directions

Though the study cohort included a broad diversity of pathology and a high prevalence of abnormal RV function, the size of the cohort was relatively small at 78 patients and included mostly men. The echocardiograms included were not acquired for the purpose of studying RV function nor was a single standardized protocol used for each echocardiogram. Rather, images were acquired following different acquisition protocols depending on the indication for the study with focused echocardiograms and stress echocardiograms being included in the cohort. One could argue that this may better represent “real-world” images in a busy clinical practice, but it also limits the yield of useful data as many of the included patients lacked the requisite tissue Doppler or M-mode image acquisitions for the measurement of S' and TAPSE reducing the sample size for these measurements. This limited sample size may reduce the certainty of the comparisons and explain some of the variability in the diagnostic performance of these parameters compared to larger cohorts with images acquired using a standardized research protocol. However, the calculated AUC for S' and TAPSE were similar to those reported in larger studies (15, 16).

Another limitation related to the retrospective nature of the dataset is the time interval range between the acquisition of CMR images and TTE images. Acquiring the CMR and TTE images on different days introduces the possibility of different preload and afterload conditions which may influence RVEF and introduce unaccounted for variation between the TTE derived functional parameters and CMR derived RVEF (42), although the study team did its best to exclude any patients where clear clinical changes occurred.

It is important to note that this cutoff of 0.2 was derived from our cohort and not from a healthy volunteer population and further studies in either healthy volunteer populations or with larger proportions of normally functioning right ventricles will be necessary to fully understand cutoff values.

LASER is the sum of both the radial and longitudinal vectors of right ventricular motion, and in this study we were unable to determine the precise contribution of each vector. If the longitudinal vector contributes significantly more than the radial vector, it is certainly possible that the sensitivity of LASER may be impaired in conditions that primarily induce radial dysfunction, such as some cases of pulmonary hypertension. Furthermore, we were also unable to use our data set to evaluate the performance of LASER with different RV shapes. An understanding of the strengths and limitations of LASER as a measurement of RV function would ideally be addressed in a future CMR based study that would be able to evaluate LASER with optimal visualization of the free wall and without interference from trabeculations.

Additionally, RV Free wall strain and 3D RV functional assessment were not performed, as these software packages were not available in the echocardiography laboratories during the study period.

Lastly, the chosen dichotomous cutoff value for abnormal RVEF was $<50\%$ in this study as it was similar to two other large cohorts used to assess parameters of RV structure and function (15, 16). Other studies have used an RVEF $<45\%$ to dichotomize normal from abnormal (27–29). The optimal cutoff value for defining abnormal RVEF is not known with some authors advocating for age, sex and BMI adjusted cutoffs (17).

Given the above limitations, further studies are required to verify the diagnostic performance of LASER in larger, more diverse cohorts prior to deployment of the measure in clinical practice. Disease specific outcome data and correlation with right ventricular systolic pressure will also establish the usefulness of this simple linear measure acquired by two-dimensional echocardiography.

Conclusion

This study demonstrates that LASER, a novel, easy to measure parameter of RV systolic function, has moderate correlation with RVEF derived by CMR and diagnostic accuracy

comparable to FAC and superior to TAPSE and S'. The advantage of LASER is that it is less reliant on image quality and optimal imaging planes compared to other parameters such as FAC, free wall strain and RVEF by 3DE making it potentially suitable for deployment in a wide range of clinical care settings.

Data availability statement

The raw data supporting the conclusions of this article will be made available by the authors, without undue reservation.

Ethics statement

The study was approved by the internal review boards at the White River Junction VA Medical Center and Dartmouth-Hitchcock Medical Center. Ethical review and approval/written informed consent was not required as per local legislation and institutional requirements.

Author contributions

ER, JS, SF, and RP conceived the study, formulated hypotheses, and collected and analyzed the data. JS, ER, and RP performed the statistical analysis. JS and ER prepared the manuscript. AM, AG, DO'R, RZ, and RP critically evaluated the data and edited the manuscript. All authors read and approved the final manuscript and agreed to be accountable for all aspects of the work.

Acknowledgments

The authors would like to thank the research support personnel at both the White River Junction VA Medical Center and the Heart and Vascular Center at Dartmouth-Hitchcock Medical Center. This work was presented as an abstract at the American Society of Echocardiography scientific sessions June 18–21, 2021.

Conflict of interest

The authors declare that the research was conducted in the absence of any commercial or financial relationships that could be construed as a potential conflict of interest.

Publisher's note

All claims expressed in this article are solely those of the authors and do not necessarily represent those of their affiliated

organizations, or those of the publisher, the editors and the reviewers. Any product that may be evaluated in this article, or

claim that may be made by its manufacturer, is not guaranteed or endorsed by the publisher.

References

1. Surkova E, Muraru D, Genovese D, Aruta P, Palermo C, Badano LP. Relative prognostic importance of left and right ventricular ejection fraction in patients with cardiac diseases. *J Am Soc Echocardiogr.* (2019) 32:1407–1415.e3. doi: 10.1016/j.echo.2019.06.009
2. Ghio S, Gavazzi A, Campana C, Inserra C, Klersy C, Sebastiani R, et al. Independent and additive prognostic value of right ventricular systolic function and pulmonary artery pressure in patients with chronic heart failure. *J Am Coll Cardiol.* (2001) 37:183–8. doi: 10.1016/S0735-1097(00)01102-5
3. Gavazzi A, Berzuini C, Campana C, Inserra C, Ponzetta M, Recusani F, et al. Value of right ventricular ejection fraction in predicting short-term prognosis of patients with severe chronic heart failure. *J Heart Lung Transplant.* (1997) 16:774–85.
4. Gulati A, Ismail TF, Jabbour A, Alpendurada F, Guha K, Ismail NA, et al. The prevalence and prognostic significance of right ventricular systolic dysfunction in nonischemic dilated cardiomyopathy. *Circulation.* (2013) 128:1623–33. doi: 10.1161/CIRCULATIONAHA.113.002518
5. Cohen S, Gaddam S, Gemignani A, Wu WC, Sharma S, Choudhary G. Right ventricular function relates to functional capacity in men with atrial fibrillation and preserved left ventricular ejection fraction. *Echocardiography.* (2013) 30:542–50. doi: 10.1111/echo.12099
6. D'Alonzo GE. Survival in patients with primary pulmonary hypertension: Results from a national prospective registry. *Ann Intern Med.* (1991) 115:343. doi: 10.7326/0003-4819-115-5-343
7. Burgess MI, Mogulkoc N, Bright-Thomas RJ, Bishop P, Egan JJ, Ray SG. Comparison of echocardiographic markers of right ventricular function in determining prognosis in chronic pulmonary disease. *J Am Soc Echocardiogr.* (2002) 15:633–9. doi: 10.1067/mje.2002.118526
8. Poliacikova P, Cockburn J, Pareek N, James R, Lee L, Trivedi U, et al. Prognostic impact of pre-existing right ventricular dysfunction on the outcome of transcatheter aortic valve implantation. *J Invasive Cardiol.* (2013) 25:142–5.
9. Schwartz LA, Rozenbaum Z, Ghantous E, Kramarz J, Biner S, Topilsky Y, et al. Impact of right ventricular dysfunction and tricuspid regurgitation on outcomes in patients undergoing transcatheter aortic valve replacement. *J Am Soc Echocardiogr.* (2017) 30:36–46. doi: 10.1016/j.echo.2016.08.016
10. Graham TP, Bernard YD, Mellen BG, Celermajer D, Baumgartner H, Sanders SP, et al. Long-term outcome in congenitally corrected transposition of the great arteries: a multi-institutional study. *J Am Coll Cardiol.* (2000) 36:255–61.
11. Dursunoglu N, Dursunoglu D, Yildiz AI, Rota S. Evaluation of cardiac biomarkers and right ventricular dysfunction in patients with acute pulmonary embolism. *Anatol J Cardiol.* (2016) 16:276–82.
12. Mehta SR, Eikelboom JW, Natarajan MK, Diaz R, Yi C, Yusuf S, et al. Impact of right ventricular involvement on mortality and morbidity in patients with inferior myocardial infarction. *J Am Coll Cardiol.* (2001) 37:37–43. doi: 10.1016/S0735-1097(00)01089-5
13. Antoni ML, Scherptong RWC, Atary JZ, Boersma E, Holman ER, Bax JJ, et al. Prognostic value of right ventricular function in patients after acute myocardial infarction treated with primary percutaneous coronary intervention. *Circ Cardiovasc Imaging.* (2010) 3:264–71. doi: 10.1161/CIRCIMAGING.109.914366
14. Anavekar NS, Skali H, Bourgoun M, Ghali JK, Kober L, Solomon SD, et al. Usefulness of right ventricular fractional area change to predict death, heart failure, and stroke following myocardial infarction (from the VALIANT ECHO Study). *Am J Cardiol.* (2008) 101:607–12. doi: 10.1016/j.amjcard.2007.09.115
15. Kim J, Srinivasan A, Seoane T, Di Franco A, Peskin CS, McQueen DM, et al. Echocardiographic linear dimensions for assessment of right ventricular chamber volume as demonstrated by cardiac magnetic resonance. *J Am Soc Echocardiogr.* (2016) 29:861–70. doi: 10.1016/j.echo.2016.05.002
16. Pavlicek M, Wahl A, Rutz T, de Marchi SF, Hille R, Wustmann K, et al. Right ventricular systolic function assessment: rank of echocardiographic methods vs. cardiac magnetic resonance imaging. *Eur J Echocardiogr.* (2011) 12:871–80. doi: 10.1093/ejehocardi/jer138
17. Maceira AM, Prasad SK, Khan M, Pennell DJ. Reference right ventricular systolic and diastolic function normalized to age, gender and body surface area from steady-state free precession cardiovascular magnetic resonance. *Eur Heart J.* (2006) 27:2879–88. doi: 10.1093/eurheartj/ehl336
18. Grothues F, Moon JC, Bellenger NG, Smith GS, Klein HU, Pennell DJ. Interstudy reproducibility of right ventricular volumes, function and mass with cardiac magnetic resonance. *Am Heart J.* (2004) 147:218–23. doi: 10.1016/j.ahj.2003.10.005
19. Geva T. Is MRI the preferred method for evaluating right ventricular size and function in patients with congenital heart disease? MRI is the preferred method for evaluating right ventricular size and function in patients with congenital heart disease. *Circulation Cardiovasc Imaging.* (2014) 7:190–7. doi: 10.1161/CIRCIMAGING.113.000553
20. Lang RM, Badano LP, Mor-Avi V, Afzal J, Armstrong A, Voigt JU, et al. Recommendations for cardiac chamber quantification by echocardiography in adults: an update from the American Society of Echocardiography and the European Association of Cardiovascular Imaging. *Eur Heart J Cardiovasc Imaging.* (2015) 16:233–70. doi: 10.1093/ehjci/jev014
21. Sheehan F, Redington A. The right ventricle: anatomy, physiology and clinical imaging. *Heart.* (2008) 94:1510–5. doi: 10.1136/hrt.2007.132779
22. Helbing WA. Right ventricular function: the comeback of echocardiography? *Eur J Echocardiogr.* (2004) 5:99–101. doi: 10.1016/j.euje.2003.12.001
23. Garcia Giorro R, Renes Carreño E, Mayordomo S, Marín H, Perez Vela JL, Corres Peiretti MA, et al. Evaluation of right ventricular function after cardiac surgery: the importance of tricuspid annular plane systolic excursion and right ventricular ejection fraction. *J Thorac Cardiovasc Surg.* (2016) 152:613–20. doi: 10.1016/j.jtcvs.2016.04.041
24. Kaul S, Tei C, Hopkins JM, Shah PM. Assessment of right ventricular function using two-dimensional echocardiography. *Am Heart J.* (1984) 107:526–31. doi: 10.1016/0002-8703(84)90095-4
25. Lytrivi ID, Lai WW, Ko HH, Nielsen JC, Parness IA, Srivastava S. Color Doppler tissue imaging for evaluation of right ventricular systolic function in patients with congenital heart disease. *J Am Soc Echocardiogr.* (2005) 18:1099–104. doi: 10.1016/j.echo.2005.03.029
26. Dokainish H, Abbey H, Gin K, Ramanathan K, Lee P, Pui J. Usefulness of tissue Doppler imaging in the diagnosis and prognosis of acute right ventricular infarction with inferior wall acute left ventricular infarction. *Am J Cardiol.* (2005) 95:1039–42. doi: 10.1016/j.amjcard.2004.12.056
27. Focardi M, Cameli M, Carbone SF, Massoni A, De Vito R, Lisi M, et al. Traditional and innovative echocardiographic parameters for the analysis of right ventricular performance in comparison with cardiac magnetic resonance. *Eur Heart J.* (2014) 16:47–52. doi: 10.1093/ehjci/jeu156
28. Agasthi P, Chao CJ, Siegel RJ, Pujari SH, Mookadam F, Venepally NR, et al. Comparison of echocardiographic parameters with cardiac magnetic resonance imaging in the assessment of right ventricular function. *Echocardiography.* (2020) 37:1792–802. doi: 10.22541/au.159183046.66745518
29. Hamilton-Craig CR, Stedman K, Maxwell R, Anderson B, Stanton T, Chan J, et al. Accuracy of quantitative echocardiographic measures of right ventricular function as compared to cardiovascular magnetic resonance. *Int J Cardiol Heart Vasc.* (2016) 12:38–44. doi: 10.1016/j.ijcha.2016.05.007
30. Haack ML, Scherptong RW, Antoni ML, Marsan NA, Vliegen HW, Delgado V, et al. Prognostic value of right ventricular longitudinal peak systolic strain in patients with pulmonary hypertension. *Circulation Cardiovasc Imaging.* (2012) 5:628–36. doi: 10.1161/CIRCIMAGING.111.971465
31. Ternacle J, Berry M, Cognet T, Kloeckner M, Damy T, Lim P, et al. Prognostic value of right ventricular two-dimensional global strain in patients referred for cardiac surgery. *J Am Soc Echocardiogr.* (2013) 26:721–6. doi: 10.1016/j.echo.2013.03.021
32. Motoki H, Borowski AG, Shrestha K, Hu B, Kusunose K, Klein A. Right ventricular global longitudinal strain provides prognostic value incremental to the left ventricular ejection fraction in patients with heart failure. *J Am Soc Echocardiogr.* (2014) 27:726–32. doi: 10.1016/j.echo.2014.02.007
33. Greiner S, André F, Heimisch M, Aurich M, Steen H, Katus HA, et al. A closer look at right ventricular 3D volume quantification by

transthoracic echocardiography and cardiac MRI. *Clin Radiol.* (2019) 74:490.e7–e14. doi: 10.1016/j.crad.2019.03.005

34. Genovese D, Rashedi N, Weinert L, Narang A, Addetia K, Patel AR, et al. Machine learning-based three-dimensional echocardiographic quantification of right ventricular size and function: validation against cardiac magnetic resonance. *J Am Soc Echocardiogr.* (2019) 32:969–77. doi: 10.1016/j.echo.2019.04.001

35. Medvedofsky D, Addetia K, Patel AR, Sedlmeier A, Baumann R, Mor-Avi V, et al. Novel approach to three-dimensional echocardiographic quantification of right ventricular volumes and function from focused views. *J Am Soc Echocardiogr.* (2015) 28:1222–31. doi: 10.1016/j.echo.2015.06.013

36. Ostenfeld E, Shahgaldi K, Winter R, Willenheimer R, Holm J. Comparison of different views with three-dimensional echocardiography: apical views offer superior visualization compared with parasternal and subcostal views. *Clin Physiol Funct Imaging.* (2008) 28:409–16. doi: 10.1111/j.1475-097X.2008.00823.x

37. Fernández-Golfín C, Zamorano JL. Three-dimensional echocardiography and right ventricular function: the beauty and the beast? *Circ Cardiovasc Imaging.* (2017) 10:e006099. doi: 10.1161/CIRCIMAGING.117.006099

38. Shimada YJ, Shiota M, Siegel RJ, Shiota T. Accuracy of right ventricular volumes and function determined by three-dimensional echocardiography in comparison with magnetic resonance imaging: a meta-analysis study. *J Am Soc Echocardiogr.* (2010) 23:943–53. doi: 10.1016/j.echo.2010.06.029

39. Tandri H, Daya SK, Nasir K, Bomma C, Lima JA, Calkins H, et al. Normal reference values for the adult right ventricle by magnetic resonance imaging. *Am J Cardiol.* (2006) 98:1660–4. doi: 10.1016/j.amjcard.2006.07.049

40. DeLong ER, DeLong DM, Clarke-Pearson DL. Comparing the areas under two or more correlated receiver operating characteristic curves: a nonparametric approach. *Biometrics.* (1988) 44:837–45. doi: 10.2307/2531595

41. Bland JM, Altman DG. Statistical methods for assessing agreement between two methods of clinical measurement. *Lancet.* (1986) 327:307–10. doi: 10.1016/S0140-6736(86)90837-8

42. Burger W, Jockwig B, Rücker G, Kober G. Influence of right ventricular pre- and afterload on right ventricular ejection fraction and preload recruitable stroke work relation. *Clin Physiol.* (2000) 21:85–92. doi: 10.1046/j.1365-2281.2001.00300.x



OPEN ACCESS

EDITED BY

Sanjeev Bhattacharyya,
Barts Heart Centre, United Kingdom

REVIEWED BY

Mani Vannan,
Piedmont Heart Institute, United States
Haotian Gu,
King's College London,
United Kingdom

*CORRESPONDENCE

Philippe Obert
philippe.obert@univ-avignon.fr

SPECIALTY SECTION

This article was submitted to
Cardiovascular Imaging,
a section of the journal
Frontiers in Cardiovascular Medicine

RECEIVED 11 July 2022

ACCEPTED 22 August 2022

PUBLISHED 08 September 2022

CITATION

Aboukhoudir F, Philouze C,
Grandperrin A, Nottin S and Obert P
(2022) Additive effects of type 2
diabetes and metabolic syndrome on
left ventricular torsion and linear
deformation abnormalities during
dobutamine stress echocardiography.
Front. Cardiovasc. Med. 9:991415.
doi: 10.3389/fcvm.2022.991415

COPYRIGHT

© 2022 Aboukhoudir, Philouze,
Grandperrin, Nottin and Obert. This is
an open-access article distributed
under the terms of the [Creative
Commons Attribution License \(CC BY\)](#).
The use, distribution or reproduction in
other forums is permitted, provided
the original author(s) and the copyright
owner(s) are credited and that the
original publication in this journal is
cited, in accordance with accepted
academic practice. No use, distribution
or reproduction is permitted which
does not comply with these terms.

Additive effects of type 2 diabetes and metabolic syndrome on left ventricular torsion and linear deformation abnormalities during dobutamine stress echocardiography

Falah Aboukhoudir^{1,2}, Clothilde Philouze¹,
Antoine Grandperrin¹, Stéphane Nottin¹ and Philippe Obert^{1*}

¹UPR4278 LaPEC, Laboratory of Experimental Cardiovascular Physiology, Avignon University, Avignon, France, ²Cardiology Department, Duffaut Hospital Center, Avignon, France

Objective: The interplay between metabolic syndrome (MS) and type 2 diabetes (T2D) on regional myocardial mechanics and the potential additional effects of their combination remain poorly understood. In this context, we evaluated left ventricular (LV) torsion and linear deformation at rest and under dobutamine (DB) stress in patients with T2D, MS or both.

Methods: Thirty-nine T2D patients without MS (T2D), 37 MS patients free from T2D (MS), 44 patients with both T2D and MS (T2D-MS group) and 38 healthy patients (control group) were prospectively recruited. Speckle-tracking echocardiography (STE) was conducted at rest and low dose DB to evaluate LV myocardial longitudinal (LS) as well as circumferential (CS) strain and early diastolic strain rate (LSrd, CSrd) and twist-untwist mechanics.

Results: At rest, MS, T2D and controls presented with similar resting LS and LSrd while significant lower values were obtained in T2D-MS compared to controls. DB revealed reduced LS, LSrd, CS and CSrd in MS and T2D groups compared to controls. In T2D-MS, the decline in LS and LSrd established at rest was exacerbated under DB. Stress echocardiography revealed also lower basal rotation and subsequently lower twist in MS and T2D patients compared to controls. T2D-MS showed major impairments of apical rotation and twist under DB stress, with values significantly lower compared to the 3 other groups. From stepwise multiple linear regression analysis, epicardial adipose tissue for Δ (rest to DB) LS, numbers of MS factors for Δ CS and Δ Twist emerged as major independent predictors.

Conclusion: These results demonstrate synergic and additive effects of T2D and MS on LV torsion and linear deformation abnormalities in asymptomatic

patients with metabolic diseases. They also highlight the usefulness of speckle tracking echocardiography under DB stress in detecting multidirectional myocardial mechanics impairments that can remain barely detectable at rest, such as in isolated T2D or MS patients.

KEYWORDS

uncomplicated type 2 diabetes, metabolic syndrome, asymptomatic patients, dobutamine stress echocardiography, speckle-tracking imaging, twist-untwist mechanics

Introduction

Type 2 diabetes mellitus (T2D) is a major risk factor for cardiovascular diseases and is associated with the development of a specific cardiopathy, the diabetic cardiomyopathy (1). Diabetic cardiomyopathy is the leading cause of morbidity and mortality in T2D patients and is thought to develop rapidly after the onset of diabetes (2). Early diagnosis and cardiac follow-up of patients are therefore of paramount importance. In a previous study, we reported the usefulness of speckle-tracking echocardiography under dobutamine (DB) stress in unmasking multidirectional early left ventricle (LV) dysfunction in asymptomatic T2D patients (3). Indeed, in this population, deformation indexes were similar to those of aged and sex-matched healthy subjects at rest. The latter finding is, however, not unanimously reported in the literature, some authors observing an altered regional myocardial function at rest (4–10), while others reported results consistent with ours (11, 12). Such inconsistencies may originate from variability in the clinical characteristics of the studied populations. Indeed, factors such as glycemic control or the presence of extracardiac complications and comorbidities can influence the extent of the cardiac alterations (13–20). Of note, the presence of concomitant metabolic syndrome (MS) could worsen the impairment of regional myocardial function. MS is frequent in T2D patients and is a well-recognized risk factor for cardiovascular diseases and heart failure (21, 22). Previous studies from our laboratory already highlighted major impairments of longitudinal strain (LS) in asymptomatic MS patients (23, 24), a finding in line with other investigations led in similar populations (25–27). Moreover, the components of MS (dyslipidemia and elevated abdominal adiposity, blood pressure and fasting glycemia) are individually associated with LV dysfunction, the cardiovascular risk increasing with each additional MS factor (23, 27). However, to our knowledge, no study has yet depicted the interplay between MS and T2D on regional myocardial function and the potential additional deleterious effect of their combination.

Most of the aforementioned studies focused on longitudinal deformations solely, while a knowledge of the multidirectional deformations is crucial for a better understanding of the extent

of myocardial damages at a subclinical stage. Indeed, LS are mainly driven by the LV subendocardial layer, while the median and subepicardial layers mostly govern the circumferential strains (CS) and torsional mechanics. LS are therefore often impacted early, being sensitive to microvascular dysfunction, while CS and torsional mechanics are affected in more advanced stages (28). Yet, data regarding the multidirectional impact of MS on regional myocardial function are sparse and conflicting (23, 26, 27). Although the variability in the characteristics of the populations enrolled is likely to be a contributing factor, it must be underlined that these previous evaluations were carried out at rest. Similarly to what we previously reported in T2D patients, resting deformation imaging might not be sensitive enough to detect subtle dysfunctions, and the early alterations of myocardial regional mechanics may require the use of stress echocardiography to be unmasked (3). DB challenge could notably uncover a blunted response of myocardial torsional mechanics, the latter playing a central role in heart response to increased workload (29).

The aims of the present study were then to perform a comprehensive, multidirectional characterization of LV regional myocardial function at rest and under DB stress in asymptomatic T2D, MS and T2D-MS patients and to evaluate the potential synergic and additive effects of the MS and T2D combination compared to T2D and MS alone.

Materials and methods

Study population

According to the aims of this study, patients with T2D and/or MS (30) were prospectively recruited from our cardiology department from January 2015 to July 2020. The exclusion criteria were poor echogenicity, severe obesity, insulin therapy, LV ejection fraction < 55%, known cardiovascular diseases, and T2D-related complications, including moderate to severe autonomic neuropathy, proliferative retinopathy, and nephropathy. All the subjects were free from epicardial coronary disease, attested by negative findings on a high-dose

of DB stress echocardiography ($40 \mu\text{g.kg}^{-1}.\text{min}^{-1}$) or coronary angiography when appropriate. Patients with hypertension but well-controlled blood pressure were included, those with superior to grade 1 hypertension were excluded. A total of 39 T2D patients without MS (T2D group), 37 MS patients free from T2D (MS group) and 44 patients with both T2D and MS (T2D-MS group) were enrolled. Thirty-eight healthy patients matched for sex, with similar age and normal echocardiographic findings, were also enrolled during routine checkups as a control group. As previously described (3), a medical survey was performed to check for exclusion/inclusion criteria and clinical data. Then, blood samples were collected in a fasting state for measurement of biological data such as glycemia, glycated hemoglobin, total cholesterol, high- and low-density lipoproteins (HDL, LDL), triglycerides, ultra-sensitive C-reactive protein or pro-brain natriuretic peptide. The study protocol was approved by the local human ethics committee (IRB-15/05.01) and all subjects provided written informed consents. The **Figure 1** represents the flowchart of our study population.

Echocardiography recordings

All patients underwent both resting and stress echocardiography, with the subject in left lateral decubitus position, using commercially available ultrasound equipment (Vivid E95; GE Healthcare, Milwaukee, WI, United States). At rest and each step of stress echocardiography protocol, bidimensional cine loops of the LV were recorded in parasternal short axis (base, papillary muscles and apex), parasternal long axis and apical 4- and 2-chamber views and saved for blinded offline analysis. Grayscale images were saved at a frame rate of 80–90 fps. Stress echocardiography was performed using the same protocol that was previously described by our group (3). Briefly, DB was infused intravenously in incremental doses of 10, 20, 30 and $40 \mu\text{g.kg}^{-1}.\text{min}^{-1}$ in 3-min stages. The test was stopped when age-adjusted heart rate limit was reached, when severe hypertension (systolic BP > 250 mmHg or diastolic BP > 120 mmHg) or symptomatic reduction in systolic BP > 40 mmHg from baseline developed, or when ventricular arrhythmia occurred. β -blocker intake was interrupted at least 72 h prior to DB stress echocardiography.

Echocardiography analysis

A blinded data analysis was performed post-processing by one experienced reader (EchoPAC 201; GE Healthcare) and all measurements were average from 3 cardiac cycles. Intra and inter-observer reliability at rest and during low-dose DB of deformation imaging indexes has been reported in detail elsewhere (3), with good concordance correlation coefficients ($r > 0.82$ in each case). All standard echocardiographic and

Doppler parameters of LV systolic and diastolic function were measured according to recent guidelines (31). Speckle tracking echocardiography analysis was performed in accordance with guidelines of American Society of Echocardiography and European Association of Cardiovascular Imaging (31).

Left ventricular morphology and global function at rest

Left ventricular end-diastolic (LVEDV) and end-systolic (LVESV) volumes and ejection fraction were measured using the Simpson biplane method. LV mass was calculated using the Devereux formula and indexed to height (Cornell adjustment). LV end-diastolic volumes were used as preload index. LV diastolic function was assessed from peak early (E wave) and atrial (A wave) transmitral flow velocities. Peak e' average from septum and lateral walls and E/ e' ratio were evaluated using Tissue Doppler and used as indices of LV relaxation and filling pressures, respectively (32). Epicardial adipose tissue was identified and measured as previously described (33). To estimate cardiac afterload, the meridional wall stress was calculated according to the formula proposed by Jamal et al. (34).

Left atrial morphology

According to current recommendations (35), left atrial volume (LAV) was calculated using the biplane method in apical 4- and 2-chamber views and indexed to body surface area.

Left ventricular strain and twist mechanics

The 2D-strain analysis was conducted at rest and at a DB stage corresponding to a target heart rate between 110 and 120 bpm, in order to ensure sufficient temporal resolution for robust speckle tracking. For each view, the 3 cardiac cycles displaying the best image quality were selected. LS and CS and their corresponding early diastolic strain rate (LSrd and CSrd, respectively) as well as twist mechanics (apical and basal rotations, twist and twisting/untwisting rates) were obtained as previously detailed by our group (36). Briefly, EchoPAC data were exported as “.txt files” in order to be processed with a specific toolbox (Scilab version 4.1; Consortium Scilab, INRIA-ENPC, Paris, France). To adjust all strain parameters for inter-subject differences in heart and frame rates, the time sequence was also normalized to the percentage of systolic duration (i.e., time was 100% at end systole). Spreadsheet calculation allowed the detection of peak LSrd and CSrd, peak of LV twist and untwist rates, and the time to these peaks. A quality control

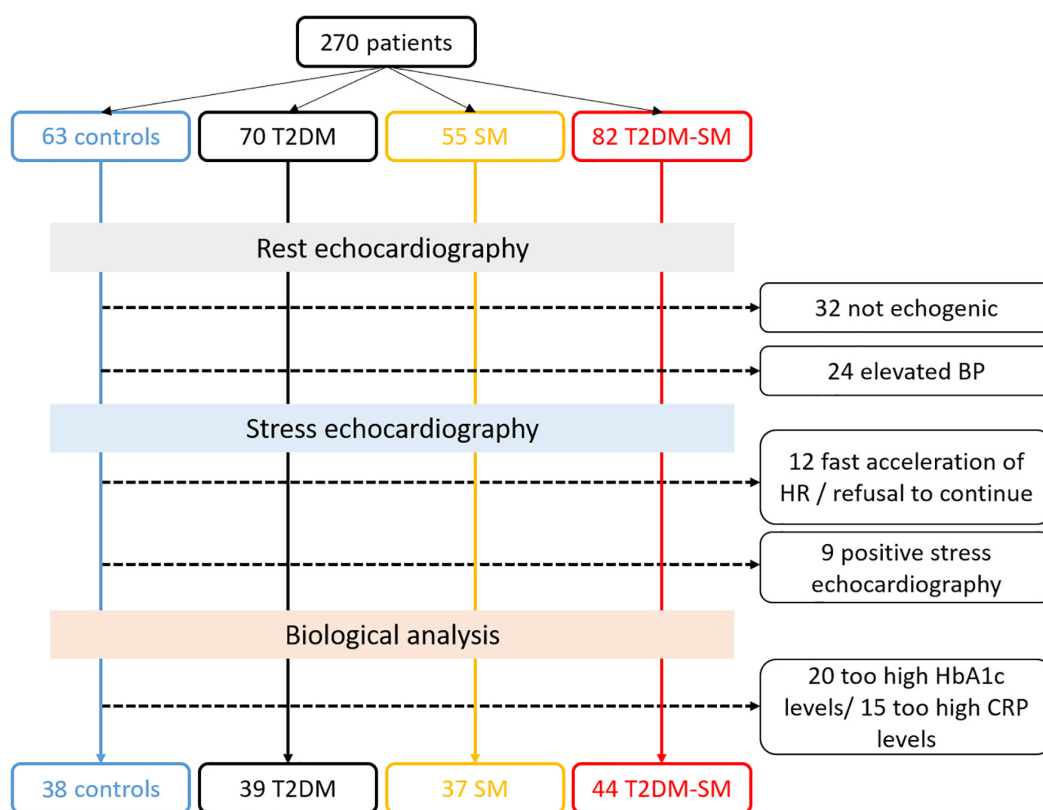


FIGURE 1

Flow chart of patient recruitment with exclusion criteria consideration.

was finally performed by an experienced investigator in order to replace or delete abnormal data. For each parameter, delta values (Δ) calculated as the difference between data at low dose DB minus data at rest were obtained.

Statistical analysis

Statistical analysis was performed using IBM SPSS statistics 20.0™ software (IBM Corp., United States). Values are expressed as mean \pm SD, otherwise specified. Statistical significance was defined as p value < 0.05 . Normality was assessed using Shapiro–Wilk test and non-Gaussian biological variables were log-transformed. Biological, demographic variables and resting standard echocardiographic data were analyzed using a generalized linear model (GLM). Chi-square test was used for categorical data. Deformation imaging indexes were analyzed using a linear mixed-effect model with random intercept and group and conditions as well as age (when applicable, see **Table 4**) as fixed effects. In case of significant interaction between groups and conditions, a GLM was used for group's comparison at rest and low-dose DB while a t -test for paired samples assessed DB response within each group. Covariates such as loading indexes, hypertension, medical

treatment, inflammation, body mass index (BMI) or waist circumference were included in the different models, when appropriate. Inter-group comparison for delta (Δ) values was assessed using a GLM. Pearson correlations were used to investigate the association between LS, CS, apical rotation or Twist measured under DB stress condition as well as their Δ changes from rest to low dose DB with clinical, biological and echocardiographic parameters. A multiple stepwise linear regression analysis was used to determine the independent predictors of Δ values for each STE variable, with $p < 0.15$ in bivariate testing used as a requirement to enter the model.

Results

Baseline clinical and echocardiographic characteristics

The clinical data are presented in **Table 1**. Populations were matched on sex, but T2D-MS were slightly older than the 3 other groups. Body mass index and waist circumference were significantly higher in the 3 groups of patients when compared to controls, with values being also significantly greater

in MS and T2D-MS than T2D. Similar results were obtained regarding the number of MS factors. Additionally, among the 5 MS components, no inter-group differences were noticed for the prevalence of low HDL while significant differences were obtained in each case in the patients compared to controls for the prevalence of the 4 other variables. The 2 groups with MS presented with also a greater prevalence of increased BP and hypertriglyceridemia compared to T2D and, as expected, the 2 groups with T2D had a higher prevalence of increased plasma glucose compared to MS. Concerning the lipid profile, no differences were noticed between controls and T2D patients. The 2 groups with MS had reduced HDL and increased triglycerides compared to controls. Triglycerides were especially elevated in MS, values being also greater than in the 2 other diabetic groups. As expected, fasting glycemia and glycated hemoglobin were greater in T2D and T2D-MS than in MS and controls, while no differences were obtained between the 2 diabetic groups. Fasting glycemia was also slightly increased in MS compared to controls. Noteworthy, ultra-sensitive C-reactive protein levels were also substantially increased in the 3 groups of patients compared to controls, with values being also higher in T2D-MS compared to MS.

Results of conventional echocardiography are summarized in **Table 2**. LAV indexed was significantly increased in T2D-MS patients compared to MS and controls. While no inter-group differences were noticed for LVEDV and LVESV indexed, values of LV wall thicknesses as well as relative wall thickness and LV mass indexed were significantly higher in the T2D-MS patients compared to the 3 other groups. Similar values of LV ejection fraction, E and E/A ratio were noticed between the 4 groups. No inter-group differences were obtained for longitudinal systolic velocities by TDI while early diastolic velocities and E/e' ratio were significantly decreased and increased, respectively, in the 3 groups of patients compared to controls. Of note, differences were also significant in T2D-MS compared to MS. Epicardial adipose tissue was markedly increased in T2D-MS patients compared to the 3 other groups, with values being also higher in MS and T2D patients than in controls.

Speckle-tracking echocardiography at rest and under dobutamine infusion

Speckle tracking echocardiography data are presented in **Table 3** and **Figure 2**. At rest, no inter-group differences were noticed for twist mechanics (e.g., twist as well as twist and untwist rates), basal rotation and Cs. The 3 groups of patients presented with, however, greater apical rotations than controls. While no differences were obtained between MS, T2D and controls for LS and LSrd, values in T2D-MS patients were significantly reduced compared to controls.

Low-dose DB revealed major inter-group differences for most speckle tracking echocardiography indexes. Indeed, LS, LSrd, CS and CSrd were now significantly decreased in MS and T2D compared to controls. Additionally, the reductions of LS and LSrd observed at rest in T2D-MS were further exacerbated under DB, differences being significant not only compared to controls but also to MS and T2D. As for MS and T2D, Cs and CSrd were also significantly reduced in T2D-MS compared to controls. While no differences were obtained under DB between MS, T2D and controls for apical rotation, lower basal rotation and subsequently twist were demonstrated in these 2 groups of patients compared to controls. Apical rotation and twist were, however, dramatically impaired in T2D-MS patients, with values reduced significantly compared to controls, but also to T2D and MS for apical rotation and in T2D only for twist. Overall, twist mechanics was predominantly depressed in the 2 groups presented with MS. All speckle tracking echocardiography indexes were significantly increased in the 4 groups in response to DB infusion, except for apical rotations that did not change in T2D-MS patients.

Results of the univariate analysis of speckle tracking echocardiography indexes under low dose DB conditions as well as in response to low dose DB (e.g., Δ changes from rest to low dose DB) are depicted in **Table 4**. For most of the indexes, good correlations were obtained with age, number of MS factors, hypertension, metabolic markers of T2D, abdominal obesity, inflammation and epicardial adipose tissue. From stepwise multiple linear regression analyses, epicardial adipose tissue ($\beta = 0.34$, $p < 0.001$; $r^2 = 0.12$, $p < 0.001$) for Δ SL, numbers of MS factors for Δ CS and Δ Twist ($\beta = 0.27$, $p = 0.003$; $r^2 = 0.08$, $p = 0.003$ and $\beta = -0.30$, $p < 0.001$; $r^2 = 0.09$, $p < 0.001$) and number of MS factors and presence of T2D ($\beta = -0.27$, $p = 0.002$; $\beta = -0.18$, $p = 0.03$, $r^2 = 0.13$, $p < 0.001$) for Δ apical rotation emerged as major independent predictors. The inter-group differences under DB stress previously mentioned for LS, apical and basal rotations as well as twist were still evident after accounting for, in addition to age and sex, others potential confounding factors such as hypertension, abdominal obesity and systemic inflammation. For CS, differences between controls and the 3 other groups under DB disappeared when waist circumference and ultra-sensitive C-reactive protein were introduced as covariates. For twist, differences between patients and controls under DB were still evident when hypertension and abdominal obesity were used as covariates, but disappeared between T2D and T2D-MS. All speckle tracking echocardiography variables were, however, not influenced by medical treatments. Indexes of loading conditions did not differ between the 4 groups at rest. They were, however, significantly impacted by DB. However, no correlations were demonstrated between loading conditions and speckle tracking echocardiography indexes under stress conditions.

TABLE 1 Clinical characteristics.

	Controls	T2D	MS	T2D-MS	P value
Demographic characteristics					
Gender M/F	19/19	25/14	20/17	29/15	0.40
Age (years)	51 ± 7	54 ± 9	52 ± 8	58 ± 6***,†††,‡	< 0.001
Body mass index (kg/m ²)	24.1 ± 3.6	26.1 ± 3.8***	29.2 ± 3.9***,###	28.7 ± 3.6***,###	< 0.001
Waist circumference (cm)	80 ± 15	95 ± 13***	104 ± 9***,###	104 ± 11***,###	< 0.001
Number of SM factors	0.9 ± 0.8	1.8 ± 0.4***	3.6 ± 0.7***,###	3.7 ± 0.7***,###	< 0.001
Increased BP (%)	8 (21)	15 (40)***	29 (78)***,###	38 (86)***,###	< 0.001
Increased plasma glucose (%)	2 (5)	39 (100)***	28 (75)***,##	44 (100)***,††	< 0.001
Increased abdominal obesity (%)	19 (50)	35 (89)***	35 (95)***	43 (98)***	< 0.001
Hypertriglyceridemia (%)	5 (13)	8 (20)	28 (75)***,###	25 (57)***,##	< 0.001
Decreased HDL (%)	25 (65)	29 (74)	28 (75)	38 (86)	0.18
Smoking <i>n</i> (%)	12 (31)	11 (28)	12 (32)	17 (38)	0.78
Biological parameters					
HDL cholesterol (g/L)	0.54 ± 0.11	0.50 ± 0.14	0.45 ± 0.11**	0.42 ± 0.10***,##	< 0.001
LDL cholesterol (g/L)	1.26 ± 0.28	1.17 ± 0.37	1.40 ± 0.36#	1.16 ± 0.45††	0.01
Triglycerides (g/L) [§]	1.10 ± 0.50	1.15 ± 0.34	2.07 ± 1.40***,###	1.62 ± 0.67***,##	< 0.001
Fasting glycemia g/L	0.89 ± 0.07	1.38 ± 0.57***	1.05 ± 0.11*,###	1.39 ± 0.32***,†††	< 0.001
HbA1c%	5.4 ± 0.3	7.5 ± 1.9***	5.6 ± 0.3***	7.4 ± 1.3***,†††	< 0.001
CRPus (g/L) [§]	1.2 ± 0.7	2.3 ± 2.0**	2.1 ± 1.8**	3.6 ± 3.7***,†	< 0.001
Pro-BNP (pg/mL) [§]	6.7 ± 2.5	9.1 ± 11.6	7.2 ± 6.6	7.2 ± 5.5	0.47
Medications					
Antihypertensive drugs <i>n</i> (%)	-	3 (8)	15 (40)**	24 (54)***	< 0.001
Antidyslipidemic drugs <i>n</i> (%)	-	10 (25)	12 (32)	19 (44)**	0.88

M/F, males or females; BP, blood pressure; HDL and LDL, high- and low-density lipoproteins; HbA1c, glycated hemoglobin; CRPus, ultra-sensitive c-reactive protein; *Pro-BNP*, pro-brain natriuretic peptide.

p* < 0.05, *p* < 0.01, ****p* < 0.001 vs. controls; #textitp < 0.05, ##*p* < 0.01, ###*p* < 0.001 vs. T2D; †*p* < 0.05, ††*p* < 0.01, †††*p* < 0.001 vs. MS; §data were log transformed before statistical analysis.

Discussion

To our knowledge, the present study is the first one to comprehensively assess regional myocardial mechanics under DB stress in asymptomatic T2D, MS and T2D-MS patients and to evaluate the potential synergic and additive effect of the T2D-MS combination compared to T2D and MS alone. The major findings were, firstly, that patients with combined T2D and MS exhibited globally a more important impairment of regional myocardial function compared to patients with only T2D or MS and, secondly, that only DB stress allowed unmasking alterations that were otherwise undetectable at rest in these last 2 groups of patients.

The present findings further illustrate the challenges in the characterization of cardiac impairments in patients with metabolic diseases and the pitfalls of comparing studies with different patient inclusion criteria and clinical characteristics in this area. Indeed, most studies focusing on cardiac regional function in metabolic disease did not discriminate between patients with T2D or MS only and patients with combined T2D-MS, while factors associated with T2D, such as glycemic

control or MS components may influence the extent of cardiac dysfunction (13, 18–20, 23, 25). As a matter of fact, in our study, only patients with combined T2D-MS exhibited at rest an altered longitudinal function, with significantly reduced LS and LSrd, while patients with isolated T2D or MS presented with a preserved longitudinal function. This observation could help explaining, at least in part, the discrepancies found in the literature regarding the presence or not of a decreased LS in patients with T2D (4–12).

While literature is extensive on longitudinal function in metabolic disorders, comparative data are scarcer regarding circumferential and rotational parameters, despite their key role in cardiac performance. Indeed, the LV twist motion induced by apical counterclockwise and basal clockwise rotations in systole aids ventricular ejection, while early diastolic untwist generates suction and facilitates diastolic filling (37). Systolic twist acts to limit myocardial energy expenditure by creating high intraventricular systolic pressures with minimal muscle shortening, resulting in efficient LV contraction (37). Moreover, the resultant elastic recoil of the LV has important implications for diastolic filling. In fact, the elastic recoil occurring during

TABLE 2 Echocardiographic characteristics.

	Controls	T2D	MS	T2D-MS	P value
2D/TM					
LAV (ml/m ²)	22.6 ± 7.1	23.2 ± 6.3	22.5 ± 9.1	26.4 ± 8.6*,†	0.04
LVEDV (ml/m ²) (ml/m ²)	40.1 ± 6.5	38.9 ± 10.1	38.5 ± 8.9	39.9 ± 8.4	0.82
LVESV (ml/m ²) (ml/m ²)	14.5 ± 3.9	13.3 ± 4.4	13.2 ± 3.9	14.2 ± 4.4	0.45
IVSd (mm)	8.0 ± 1.5	7.9 ± 1.3	8.3 ± 1.6	9.7 ± 1.7***,###,†††	< 0.001
PWd (mm)	7.8 ± 1.3	7.6 ± 1.5	8.2 ± 1.7	9.2 ± 1.9***,###,†	< 0.001
RWT	0.32 ± 0.06	0.32 ± 0.05	0.33 ± 0.07	0.40 ± 0.10***,###,†	< 0.001
LVmass/height ^{2.7} (g/m ^{2.7})	32.1 ± 9.8	32.7 ± 8.2	34.7 ± 8.4	38.4 ± 9.2***,###,†	0.007
LVEF Simpson (%)	63.7 ± 7.7	65.2 ± 5.7	65.1 ± 7.7	63.4 ± 7.3	0.52
EAT (mm)	3.2 ± 1.1	5.2 ± 1.7***	5.2 ± 1.6***	6.8 ± 1.9***,###,†††	< 0.001
Pulsed Doppler					
E (cm/s)	77.1 ± 16.4	74.2 ± 14.8	77.6 ± 15.4	79.0 ± 15.8	0.56
E/A	1.04 ± 0.33	0.99 ± 0.24	1.05 ± 0.29	0.94 ± 0.22	0.20
TDI parameters					
s' (cm/s)	9.2 ± 2.0	8.5 ± 2.2	8.2 ± 1.4	8.2 ± 1.9	0.12
e' (cm/s)	10.3 ± 2.7	8.5 ± 1.8***	9.2 ± 1.9**	8.3 ± 1.9***,†	< 0.001
E/e' ratio	7.8 ± 1.9	8.8 ± 1.7*	8.7 ± 1.8*	10.0 ± 2.9***,###,††	< 0.001

LAV, left atrial volume indexed; LV-ED/-ESV, end-systolic/end-diastolic left ventricle volume indexed to body surface area; IVSd, end-diastolic interventricular septum thickness; PWd, end-diastolic posterior wall thickness; RWT, relative wall thickness; LVEF, left ventricle ejection fraction; EAT, epicardial adipose tissue; E, mitral flux early diastolic wave; A, mitral flux late diastolic wave; s', systolic mitral annulus tissue velocity; e', early diastolic mitral annulus tissue velocity.

* $p < 0.05$, ** $p < 0.01$, *** $p < 0.001$ vs. controls; #textitp < 0.05, ## $p < 0.01$, ### $p < 0.001$ vs. T2D; † $p < 0.05$, †† $p < 0.01$, ††† $p < 0.001$ vs. MS.

early diastole is thought to be a result of the vigorous contraction and compression of cardiac proteins such as titin (38). The potential energy stored in the spring like titin is unleashed during diastole, promoting myocardial relaxation and diastolic filling (38). In our study, basal rotations, twist and untwisting rate were preserved at rest, whereas apical rotations were significantly enhanced in patients (e.g., T2D, MS or both) compared to controls. These salient findings differed from those previously reported. Indeed, Tadic et al. (27) showed an increase in both twist and untwisting rate at rest in MS patients. Interestingly, in this paper, authors described a progressive increment of twist-untwist parameters with each additional MS factor (from 1 to 5). Another study reported preserved rotations and twist in patients with MS, and an increase of untwisting rate (23). Tadic et al. (8) and Crendal et al. (23) also reported an increase of twist and untwisting rate in T2D patients compared to controls. However, in these studies, the authors did not distinguish between isolated MS and T2D, which may have probably impacted their results. In our study, the increase in apical rotation probably acts as a compensatory mechanism to preserve twist, and so ejection, in patients with T2D and/or MS.

Although our results indicate an overall preservation of cardiac function in patients with isolated T2D or MS, the absence of myocardial dysfunction cannot be ascertained, as an evaluation at rest may not be sensitive enough in these populations. Indeed, as we previously demonstrated in T2D patients, an adrenergic stress may reveal functional impairments that remained otherwise subtle at rest (3). However, in this

previous work, we did not discriminate between T2D and T2D-MS patients. The present results further specify the myocardial regional function impairments that DB stress echocardiography allows unmasking in these different groups of patients with metabolic diseases. To our knowledge, we are the first to carry out such an investigation. Our results revealed interesting specificities between groups. Indeed, patients with T2D showed an alteration of basal rotation and twist, while patients with MS presented an additional alteration of untwisting rate, and patients with both T2D-MS exhibited severe alterations in all these components of myocardial mechanics, with an additional drop of apical rotations. These salient findings revealed a continuum from T2D or MS alone to combination of both T2D and MS and strengthen the importance of stress echocardiography, especially in asymptomatic T2D and MS patients for whom impairments remain discreet at rest. The lack of functional reserve in rotational mechanics we unveiled in T2D-MS is of paramount importance because it plays a major role in myocardial performance under stress. Indeed, in such conditions (e.g., physical exercise or dobutamine infusion), the elevated heart rate results in reduced diastolic filling time, requiring the diastolic function to be subsequently drastically improved to attain the same end-diastolic volume in a shorter amount of time (38). In athletes, previous studies have shown the importance of untwisting rate in facilitating LV filling (29, 39, 40). These results might thus help understanding, at least in part, the development of severe exercise intolerance previously reported in diabetic

TABLE 3 Hemodynamic and speckle tracking echocardiography data.

	Rest				GLM	DB				GLM	MM
	Controls	T2D	MS	T2D-MS	<i>p</i>	Controls	T2D	MS	T2D-MS	<i>p</i>	<i>p</i>
STE Deformation imaging											
LS (%)	−21.3 ± 1.7	−20.4 ± 2.6	−20.6 ± 3.5	−19.5 ± 2.7**	0.03	−24.3 ± 2.5	−22.3 ± 2.4**	−22.1 ± 3.1***	−20.6 ± 2.3***,##,††	< 0.001	T: < 0.001 G: < 0.001 T*G: 0.13
LSrd (s ^{−1})	1.4 ± 0.4	1.3 ± 0.4	1.4 ± 0.5	1.1 ± 0.3**,†	0.04	1.9 ± 0.4	1.6 ± 0.4**	1.7 ± 0.4*	1.4 ± 0.4***,##,†	< 0.001	T: < 0.001 G: < 0.001 T*G: 0.31
CS (%)	−21.6 ± 3.1	−20.0 ± 3.3	−20.6 ± 3.4	−21.2 ± 3.7	0.26	−27.0 ± 4.0	−23.7 ± 4.1**	−24.9 ± 4.8*	−23.7 ± 4.5**	0.008	T: < 0.001 G: 0.006 T*G: 0.16
CSrd (s ^{−1})	1.8 ± 0.6	1.4 ± 0.4**	1.5 ± 0.5*	1.5 ± 0.4**	0.02	2.5 ± 0.8	2.0 ± 0.6**	2.1 ± 0.7*	1.8 ± 0.5***,†	< 0.001	T: < 0.001 G: < 0.001 T*G: 0.13
Basal Rotation (°)	−7.6 ± 2.7†††	−6.9 ± 3.5†††	−7.1 ± 3.6†††	−7.7 ± 3.0†††	0.63	−14.0 ± 4.6	−11.5 ± 4.5**	−10.1 ± 3.0***	−11.5 ± 3.5**	0.001	T: < 0.001 G: 0.007 T*G: 0.04
Apical rotation (°)	9.5 ± 4.3†††	12.4 ± 4.2**,††	12.6 ± 5.5**,†	11.6 ± 5.3*	0.03	16.3 ± 7.4	15.2 ± 5.9	14.6 ± 8.0	10.8 ± 4.0***,##,††	0.01	T: < 0.001 G: 0.02 T*G: < 0.001
Twist (°)	16.0 ± 6.2†††	18.0 ± 4.9†††	18.4 ± 6.4††	18.2 ± 7.5†	0.66	29.2 ± 8.4	25.3 ± 8.1*	22.5 ± 9.8***	20.6 ± 6.0***,##	< 0.001	T: < 0.001 G: 0.04 T*G: 0.01
Twisting rate (°/s)	102 ± 39†††	109 ± 32†††	116 ± 38†††	112 ± 49†††	0.56	255 ± 68	232 ± 57	209 ± 61**,‡	200 ± 51***,‡	< 0.001	T: < 0.001 G: 0.03 T*G: < 0.001
Untwisting rate (°/s)	−122 ± 56	−117 ± 48	−121 ± 45	−102 ± 45	0.32	−250 ± 82	−239 ± 82	−208 ± 63**	−190 ± 55***,##	0.003	T: < 0.001 G: 0.001 T*G: 0.09
Hemodynamics											
HR (bpm)	74 ± 8	75 ± 9	73 ± 9	74 ± 10	—	112 ± 7	110 ± 6	111 ± 7	110 ± 4	—	T: < 0.001 G: 0.75 T*G: 0.49
SBP (mmHg)	124 ± 12	124 ± 13	132 ± 13***,##	130 ± 11*	0.04	138 ± 11	137 ± 13	136 ± 12	141 ± 17	0.40	T: < 0.001 G: 0.04 T*G: 0.11
DBP (mmHg)	70 ± 10	71 ± 10	76 ± 18	−75 ± 11	—	72 ± 10	75 ± 9	73 ± 13	72 ± 11	—	T: < 0.98 G: 0.18 T*G: 0.12
σ _{es} (g/cm ²)	81.2 ± 31.1	72.6 ± 22.2	82.3 ± 22.1	75.6 ± 20.9	0.37	51.2 ± 25.7	45.3 ± 15.8	58.6 ± 19.3**	43.5 ± 14.8†††	0.02	T: < 0.001 G: < 0.009 T*G: 0.73
EDV (ml)	71.7 ± 15.4	78.0 ± 21.8	75.4 ± 18.9	78.0 ± 18.6	—	66.6 ± 17.2	74.4 ± 18.2	72.6 ± 21.2	73.4 ± 19.2	—	T: < 0.01 G: 0.15 T*G: 0.12

HR, heart rate; SBP/DBP, systolic/diastolic blood pressure; LS, longitudinal strain; LSrd, early diastolic longitudinal strain rate; CS, circumferential strain; CSrd, early diastolic circumferential strain rate; σ_{es}, end-systolic meridional wall stress; EDV, end-diastolic volume.

p* < 0.05, *p* < 0.01, ****p* < 0.001 vs. controls; ‡*p* < 0.05, ##*p* < 0.01, ###*p* < 0.001 vs. T2D; †*p* < 0.05, ††*p* < 0.01, †††*p* < 0.001 vs. MS; ‡*p* < 0.05, ††*p* < 0.01, †††*p* < 0.001 vs. DB in the same group.

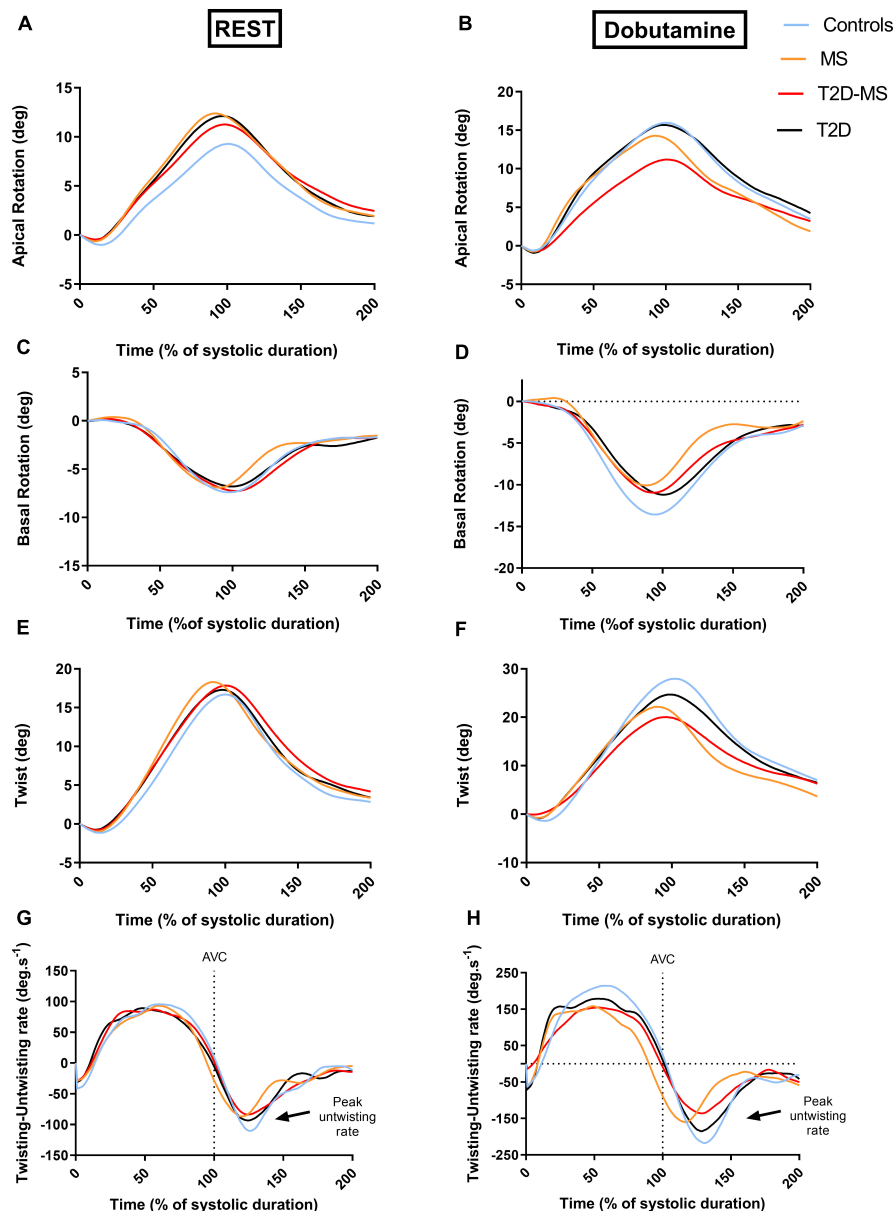


FIGURE 2

Patterns of apical (A,B) and basal rotations (C,D) as well as twist and twisting/untwisting rates (E,F) all over the cardiac cycle at rest (A,C,E,G) and low dose of dobutamine (B,D,F,H). The curve for each group was obtained from averaging data of all the subjects. For each group, data of the curves were averaged at every percent of systolic duration from data of all subjects.

populations (41, 42). Furthermore, the drop in torsional deformations may profoundly affect LV function by altering the distribution of LV wall stresses and therefore myocardial strains. Previous studies have indeed suggested that torsion may serve to equalize transmural sarcomere shortening, and so reduce transmural gradients of oxygen utilization, wall stress, and contractile work during ejection (43). A reduction in torsional deformations could thus increase the gradient of sarcomere work and oxygen utilization across the myocardium, accelerating the development of subendocardial fibrosis (44).

In line with this hypothesis, Zhang et al. (45) reported an association between LV twist and myocardial fibrosis in patients with hypertrophic cardiomyopathy. These alterations could lead to a lower cardiomyocyte ability to store elastic energy and may explain, consequently, the drop of untwisting rate. Taken together, our results underline the importance of characterizing LV twist-untwist adaptations in patients with T2D, MS or both, for a better understanding of exercise intolerance mechanisms in each population and the implementation of relevant interventions.

TABLE 4 Univariate and multivariate correlation analysis of delta changes in STE indexes with clinical, biological and echocardiographic indexes.

	Dobutamine								Univariate							
	LS		CS		Apical rot.		Twist		Δ LS		Δ CS		Δ Apical rot.		Δ Twist	
	r	p	r	p	r	p	r	p	r	p	r	p	r	p	r	p
Gender	−0.15	0.06	−0.02	0.86	0.17	0.03	0.14	0.09	−0.05	0.52	0.10	0.26	0.16	0.04	0.07	0.39
Age	0.28	0.001	0.09	0.27	−0.12	0.13	−0.06	0.45	0.22	0.007	0.21	0.01	−0.19	0.02	−0.15	0.09
Hypertension	0.26	0.001	0.07	0.37	−0.19	0.02	−0.24	0.005	0.17	0.03	0.18	0.03	−0.19	0.02	−0.20	0.01
Smoking	−0.01	0.85	−0.07	0.36	−0.17	0.03	−0.20	0.01	0.02	0.74	−0.05	0.57	−0.07	0.37	−0.08	0.31
MS number	0.41	< 0.001	0.21	0.01	−0.19	0.01	−0.29	0.001	0.22	0.007	0.26	0.003	−0.31	< 0.001	−0.34	< 0.001
BMI	0.17	0.03	0.18	0.03	0.13	0.11	−0.23	0.007	0.16	0.04	0.18	0.04	−0.25	0.003	−0.29	0.001
WC	0.27	0.001	0.27	0.001	−0.07	0.33	−0.19	0.02	0.16	0.04	0.18	0.03	−0.23	0.008	−0.27	0.01
HDL	−0.13	0.10	−0.18	0.04	0.12	0.16	0.18	0.03	0.001	0.98	−0.003	0.98	0.19	0.02	0.19	0.02
TG [§]	0.15	0.07	0.18	0.04	0.06	0.43	−0.01	0.84	0.07	0.34	0.04	0.63	−0.03	0.66	0.05	0.54
CRP _{us} [§]	0.17	0.03	0.22	0.01	−0.05	0.53	−0.06	0.42	0.08	0.33	0.19	0.03	−0.19	0.03	−0.19	0.03
HbA1c	0.26	0.001	0.18	0.04	0.17	0.04	−0.10	0.21	0.06	0.42	0.08	0.50	−0.23	0.008	−0.15	0.04
Glycemia	0.25	0.007	0.19	0.02	0.16	0.04	−0.11	0.18	0.06	0.41	0.10	0.23	−0.18	0.02	−0.08	0.36
T2DM dur.	0.03	0.77	−0.03	0.79	−0.18	0.10	−0.02	0.84	−0.14	0.21	−0.02	0.86	−0.18	0.13	−0.08	0.46
RWT	0.28	0.001	−0.02	0.77	−0.25	0.002	−0.26	0.002	0.05	0.54	−0.01	0.89	−0.10	0.22	−0.05	0.52
LVMi	0.19	0.01	−0.04	0.64	−0.16	0.04	−0.21	0.01	−0.01	0.90	−0.03	0.68	−0.11	0.19	−0.12	0.16
EDV	0.006	0.43	0.16	0.06	−0.02	0.79	−0.13	0.12	0.05	0.49	−0.07	0.42	0.13	0.23	−0.05	0.57
σ_{es}	−0.07	0.38	0.02	0.81	0.08	0.32	−0.008	0.92	−0.05	0.54	−0.03	0.67	0.09	0.29	0.09	0.30
EAT	0.60	< 0.0001	0.18	0.04	−0.28	0.001	−0.33	< 0.001	0.36	< 0.0001	0.19	0.04	−0.28	0.001	−0.26	0.004

Δ , delta value; *LS*, longitudinal strain; *CS*, circumferential strain; *rot.*, rotation; *BMI*, body mass index; *WC*, waist circumference; *HDL*, high-density lipoproteins; *TG*, triglycerides; *CRP_{us}*, ultra-sensitive c-reactive protein; *HOMA-IR*, homeostasis model assessment of insulin resistance; *dur.*, duration; Δ SI-DI, strain imaging diastolic index obtained from apical views for Δ LS, and from short-axis views at apex for Δ apical CS and rot, at papillary muscles for Δ mid CS and at base for Δ basal rot; LVMi, left ventricular mass indexed to height; EAT, epicardial adipose tissue thickness; §, data were log transformed before statistical analysis. Bold values indicate significant results.

Even if this study was not intended to investigate the mechanisms underlying cardiac function impairments in our patients, our regression analyses offered some interesting leads. As could have been expected, MS factors and T2D parameters were global contributors to the blunted response to DB stress. However, these purely metabolic variables were statistically overwhelmed by epicardial adipose tissue thickness, that showed strong correlations with all deformation indexes. In previous studies from our laboratory, we already observed close relationships between epicardial adipose tissue thickness and regional myocardial function impairments in T2D or MS populations (3, 24). This fat pad has gained growing attention over the last years as its expansion has been associated with cardiovascular damages, such as arterial stiffness and inflammation, hemodynamic impairments and myocardial injury-related biomarkers, in metabolic diseases or heart failure (46–50). Indeed, while being cardioprotective in a physiological context, this adipose tissue switches to a deleterious, pro-inflammatory secretory profile in a pathological environment (51, 52). As a matter of fact, *in vitro* studies have reported that exposing cardiomyocytes to the epicardial adipose tissue secretome from T2D patients induces an alteration of calcium fluxes, insulin resistance and contractile dysfunction (53). Epicardial adipose tissue is thus now being recognized as a valuable target in cardiometabolic diseases (50) and our results tend to support that epicardial adipose tissue implication should be considered and investigated at the earliest stages of myocardial dysfunction.

Clinical implications

The detection of early signs of myocardial alteration is of paramount importance to improve patient care by preventing the development of irreversible damages and the progression to heart failure. The present study emphasizes that rest echocardiography is not sufficient enough to ascertain the absence of nascent cardiac dysfunction in asymptomatic patients with metabolic diseases and underlines the usefulness of performing a stress echocardiography in unmasking early myocardial function impairments, especially in case of isolated MS or TD2. Our results also emphasize that asymptomatic patients with T2D or MS only or a combination of T2D-MS do not present with the same alterations of LV myocardial mechanics.

Study limitations

The main limitation of this study is the choice to perform the analyses under low dose DB, at submaximal heart rate. This decision was taken to minimize the impact of DB on loading conditions, but also to ensure a sufficient image quality

for speckle-tracking analysis (54). In future studies, it would, however, be of interest to conduct the assessments at maximal heart rate, under physiological stress conditions such as physical exercise, provided that the inherent image quality limitations can be overcome. This would have the additional advantage of allowing a better understanding of the myocardial mechanisms of exercise intolerance in these different populations.

The second limitation to this study is that echocardiographic epicardial adipose tissue thickness measurement does not take into account the 3D shape and volume of this fat pad and is therefore no gold standard for its evaluation. However, Iacobellis et al. (33) found a good correlation with MRI volume measurements, and the reproducibility of epicardial adipose tissue measurements is good in our laboratory (24).

Conclusion

Collectively, our results clearly demonstrate the usefulness of speckle tracking echocardiography under DB stress in detecting multidirectional myocardial mechanics impairments that can remain barely detectable at rest in asymptomatic patients with metabolic diseases. These results also highlight the different levels of impairment according to the patient's clinical profile. This should be kept in mind when setting up a preventive cardiac check-up for patients with metabolic disorders.

Data availability statement

The raw data supporting the conclusions of this article will be made available by the authors, without undue reservation.

Ethics statement

The studies involving human participants were reviewed and approved by the local human ethics committee (IRB-15/05.01). The patients/participants provided their written informed consent to participate in this study.

Author contributions

FA contributed to conception of the project, submission to the ethics committee, participants recruitment, echocardiographic recordings, writing of the manuscript, and final approval of the manuscript. PO and CP contributed to conception of the project, submission to the ethics committee, echocardiographic data analysis, statistical analysis, writing of the manuscript, and final approval of the manuscript. AG contributed to echocardiographic data analysis, statistical analysis, writing of the final manuscript, and final approval of

the manuscript. SN contributed to conception of the project, echocardiographic data analysis, writing of the manuscript, and final approval of the manuscript. All authors are in agreement for the order of presentation of the authors and have read and approved the final version of the manuscript.

Funding

This study was funded by a grant from the French Society of Cardiology. It was also supported by the Avignon hospital center and by the Platform 3A, funded by the European Regional Development Fund, the French Ministry of Research, Higher Education and Innovation, the Provence-Alpes-Côte-d'Azur region, the Departmental Council of Vaucluse, and the Urban Community of Avignon.

References

- Seferović PM, Petrie MC, Filippatos GS, Anker SD, Rosano G, Bauersachs J, et al. Type 2 diabetes mellitus and heart failure: A position statement from the Heart Failure Association of the European Society of Cardiology. *Eur J Heart Fail.* (2018) 20:853–72. doi: 10.1002/ehf.1170
- Waddingham MT, Edgley AJ, Tsuchimochi H, Kelly DJ, Shirai M, Pearson JT. Contractile apparatus dysfunction early in the pathophysiology of diabetic cardiomyopathy. *World J Diabetes.* (2015) 6:943–60.
- Philouze C, Obert P, Nottin S, Benamor A, Barthez O, Aboukhouidir F. Dobutamine stress echocardiography unmasks early left ventricular dysfunction in asymptomatic patients with uncomplicated Type 2 diabetes: A comprehensive two-dimensional speckle-tracking imaging study. *J Am Soc Echocardiogr.* (2018) 31:587–97. doi: 10.1016/j.echo.2017.12.006
- Ernande L, Rietzschel ER, Bergerot C, De Buyzere ML, Schnell F, Groisne L, et al. Impaired myocardial radial function in asymptomatic patients with Type 2 diabetes mellitus: A speckle-tracking imaging study. *J Am Soc Echocardiogr.* (2010) 23:1266–72.
- Karagöz A, Bezgin T, Kutlutürk I, Külahcıoğlu S, Tanboğa IH, Güler A, et al. Subclinical left ventricular systolic dysfunction in diabetic patients and its association with retinopathy. *Herz.* (2014) 40:240–6.
- Nakai H, Takeuchi M, Nishikage T, Lang RM, Otsuji Y. Subclinical left ventricular dysfunction in asymptomatic diabetic patients assessed by two-dimensional speckle tracking echocardiography: Correlation with diabetic duration. *Eur Heart J Cardiovasc Imaging.* (2009) 10:926–32. doi: 10.1093/ehjcard/jep097
- Ng ACT, Delgado V, Bertini M, van der Meer RW, Rijzewijk LJ, Shanks M, et al. Findings from left ventricular strain and strain rate imaging in asymptomatic patients with Type 2 diabetes mellitus. *Am J Cardiol.* (2009) 104:1398–401.
- Tadic M, Ilic S, Cuspidi C, Stojceviski B, Ivanovic B, Bukarica L, et al. Left ventricular mechanics in untreated normotensive patients with Type 2 diabetes mellitus: A two- and three-dimensional speckle tracking study. *Echocardiography.* (2015) 32:947–55.
- Wang J, Fang F, Wai-Kwok Yip G, Sanderson JE, Lee P-W, Feng W, et al. Changes of ventricular and peripheral performance in patients with heart failure and normal ejection fraction: Insights from ergometry stress echocardiography. *Eur J Heart Fail.* (2014) 16:888–97. doi: 10.1002/ehf.124
- Zoroufian A, Razmi T, Taghavi-Shavazi M, Lotfi-Tokaldany M, Jalali A. Evaluation of subclinical left ventricular dysfunction in diabetic patients: Longitudinal strain velocities and left ventricular dyssynchrony by two-dimensional speckle tracking echocardiography study. *Echocardiography.* (2014) 31:456–63. doi: 10.1111/echo.12389
- Cognet T, Vervueren P-L, Derclé L, Bastié D, Richaud R, Berry M, et al. New concept of myocardial longitudinal strain reserve assessed by a dipyridamole infusion using 2D-strain echocardiography: The impact of diabetes and age, and the prognostic value. *Cardiovasc Diabetol.* (2013) 12:84. doi: 10.1186/1475-2840-12-84
- Wierzbowska-Drabik K, Hamala P, Kasprzak JD. Delayed longitudinal myocardial function recovery after dobutamine challenge as a novel presentation of myocardial dysfunction in type 2 diabetic patients without angiographic coronary artery disease. *Eur Heart J Cardiovasc Imaging.* (2015) 16:676–83. doi: 10.1093/ehjci/jev004
- Chen X, Guo H, Yang Q, Fang J, Kang X. Quantitative evaluation of subclinical left ventricular dysfunction in patients with type 2 diabetes mellitus by three-dimensional echocardiography. *Int J Cardiovasc Imaging.* (2020) 36:1311–9.
- Enomoto M, Ishizu T, Seo Y, Kameda Y, Suzuki H, Shimano H, et al. Myocardial dysfunction identified by three-dimensional speckle tracking echocardiography in type 2 diabetes patients relates to complications of microangiopathy. *J Cardiol.* (2016) 68:282–7. doi: 10.1016/j.jjcc.2016.03.007
- Roy S, Kant R, Kumar B, Khapre M, Bairwa M. Systolic dysfunction in asymptomatic type 2 diabetic patients, a harbinger of microvascular complications: A cross-sectional study from North India. *Diab Vasc Dis Res.* (2020) 17:1479164120944134. doi: 10.1177/1479164120944134
- Zhang X, Wei X, Liang Y, Liu M, Li C, Tang H. Differential changes of left ventricular myocardial deformation in diabetic patients with controlled and uncontrolled blood glucose: A three-dimensional speckle-tracking echocardiography-based study. *J Am Soc Echocardiogr.* (2013) 26:499–506. doi: 10.1016/j.echo.2013.02.016
- Zhen Z, Chen Y, Shih K, Liu J-H, Yuen M, Wong DS-H, et al. Altered myocardial response in patients with diabetic retinopathy: An exercise echocardiography study. *Cardiovasc Diabetol.* (2015) 14:123. doi: 10.1186/s12933-015-0281-5
- Hatani Y, Tanaka H, Mochizuki Y, Suto M, Yokota S, Mukai J, et al. Association of body fat mass with left ventricular longitudinal myocardial systolic function in type 2 diabetes mellitus. *J Cardiol.* (2020) 75:189–95.
- Antakly-Hanon Y, Ben Hamou A, Garçon P, Moëuf Y, Banu I, Fumery M, et al. Asymptomatic left ventricular dysfunction in patients with type 2 diabetes free of cardiovascular disease and its relationship with clinical characteristics: The DIACAR cohort study. *Diabetes Obes Metab.* (2021) 23:434–43. doi: 10.1111/dom.14236
- Song X-T, Fan L, Yan Z-N, Rui Y-F. Echocardiographic evaluation of the effect of poor blood glucose control on left ventricular function and ascending aorta elasticity. *J Diabetes Complications.* (2021) 35:107943. doi: 10.1016/j.jdiacomp.2021.107943
- Ferreira JP, Verma S, Fitchett D, Ofstad AP, Lauer S, Zwiener I, et al. Metabolic syndrome in patients with type 2 diabetes and atherosclerotic cardiovascular disease: A post hoc analyses of the EMPA-REG OUTCOME trial. *Cardiovasc Diabetol.* (2020) 19:200. doi: 10.1186/s12933-020-01174-6
- Savji N, Meijers WC, Bartz TM, Bhambhani V, Cushman M, Nayor M, et al. The association of obesity and cardiometabolic traits with incident HFpEF and HFrEF. *JACC Heart Fail.* (2018) 6:701–9. doi: 10.1016/j.jchf.2018.05.018

Conflict of interest

The authors declare that the research was conducted in the absence of any commercial or financial relationships that could be construed as a potential conflict of interest.

Publisher's note

All claims expressed in this article are solely those of the authors and do not necessarily represent those of their affiliated organizations, or those of the publisher, the editors and the reviewers. Any product that may be evaluated in this article, or claim that may be made by its manufacturer, is not guaranteed or endorsed by the publisher.

23. Crendal E, Walther G, Vinet A, Dutheil F, Naughton G, Lesourd B, et al. Myocardial deformation and twist mechanics in adults with metabolic syndrome: Impact of cumulative metabolic burden. *Obesity*. (2013) 21:E679–86. doi: 10.1002/oby.20537
24. Serrano-Ferrer J, Crendal E, Walther G, Vinet A, Dutheil F, Naughton G, et al. Effects of lifestyle intervention on left ventricular regional myocardial function in metabolic syndrome patients from the RESOLVE randomized trial. *Metabolism*. (2016) 65:1350–60. doi: 10.1016/j.metabol.2016.05.006
25. Cañon-Montañez W, Santos ABS, Nunes LA, Pires JCG, Freire CMV, Ribeiro ALP, et al. Central obesity is the key component in the association of metabolic syndrome with left ventricular global longitudinal strain impairment. *Rev Esp Cardiol Engl Ed*. (2018) 71:524–30. doi: 10.1016/j.rec.2017.10.008
26. Samiei N, Bayat M, Firouzi A, Dehghani F, Parsaee M, Rahimi S, et al. Subclinical systolic and diastolic dysfunctions in patients with metabolic syndrome and angiographically normal coronary arteries: An echocardiographic study. *J Clin Ultrasound*. (2018) 46:195–201. doi: 10.1002/jcu.22568
27. Tadic M, Cuspidi C, Majstorovic A, Pencic B, Backovic S, Ivanovic B, et al. Does the metabolic syndrome impact left-ventricular mechanics? A two-dimensional speckle tracking study. *J Hypertens*. (2014) 32:1870–8. doi: 10.1097/HJH.0000000000000257
28. Mor-Avi V, Lang RM, Badano LP, Belohlavek M, Cardim NM, Derumeaux G, et al. Current and evolving echocardiographic techniques for the quantitative evaluation of cardiac mechanics: ASE/EAE consensus statement on methodology and indications endorsed by the Japanese Society of Echocardiography. *J Am Soc Echocardiogr*. (2011) 24:277–313.
29. Doucende G, Schuster I, Rupp T, Startun A, Dauzat M, Obert P, et al. Kinetics of Left Ventricular Strains and Torsion During Incremental Exercise in Healthy Subjects: The key role of torsional mechanics for systolic-diastolic coupling. *Circ Cardiovasc Imaging*. (2010) 3:586–94. doi: 10.1161/CIRCIMAGING.110.943522
30. Alberti KGMM, Eckel RH, Grundy SM, Zimmet PZ, Cleeman JI, Donato KA, et al. Harmonizing the metabolic syndrome: A joint Interim statement of the International Diabetes Federation Task Force on Epidemiology and Prevention; National Heart, Lung, and Blood Institute; American Heart Association; World Heart Federation; International Atherosclerosis Society; and International Association for the study of obesity. *Circulation*. (2009) 120:1640–5. doi: 10.1161/CIRCULATIONAHA.109.192644
31. Lang RM, Badano LP, Mor-Avi V, Afilalo J, Armstrong A, Ernande L, et al. Recommendations for cardiac chamber quantification by echocardiography in adults: An update from the American Society of Echocardiography and the European Association of Cardiovascular Imaging. *J Am Soc Echocardiogr*. (2015) 28:1–39.e14.
32. Nagueh SF, Smiseth OA, Appleton CP, Byrd BF, Dokainish H, Edvardsen T, et al. Recommendations for the evaluation of left ventricular diastolic function by echocardiography: An update from the American Society of Echocardiography and the European Association of Cardiovascular Imaging. *J Am Soc Echocardiogr*. (2016) 29:277–314.
33. Iacobellis G, Ribaudo MC, Assael F, Vecchi E, Tiberti C, Zappaterreno A, et al. Echocardiographic epicardial adipose tissue is related to anthropometric and clinical parameters of metabolic syndrome: A new indicator of cardiovascular risk. *J Clin Endocrinol Metab*. (2003) 88:5163–8. doi: 10.1210/jc.2003-030698
34. Jamal F, Strotmann J, Weidemann F, Kukulski T, D'hooge J, Bijnens B, et al. Noninvasive quantification of the contractile reserve of stunned myocardium by ultrasonic strain rate and strain. *Circulation*. (2001) 104:1059–65. doi: 10.1161/hc3501.093818
35. Badano LP, Kolias TJ, Muraru D, Abraham TP, Aurigemma G, Edvardsen T, et al. Standardization of left atrial, right ventricular, and right atrial deformation imaging using two-dimensional speckle tracking echocardiography: A consensus document of the EACVI/ASE/Industry Task Force to standardize deformation imaging. *Eur Heart J Cardiovasc Imaging*. (2018) 19:591–600. doi: 10.1093/ehjci/jej042
36. Maufrais C, Schuster I, Doucende G, Vitiello D, Rupp T, Dauzat M, et al. Endurance training minimizes age-related changes of left ventricular twist-untwist mechanics. *J Am Soc Echocardiogr*. (2014) 27:1208–15. doi: 10.1016/j.echo.2014.07.007
37. Sengupta PP, Tajik AJ, Chandrasekaran K, Khandheria BK. Twist mechanics of the left ventricle: Principles and application. *JACC Cardiovasc Imaging*. (2008) 1:366–76.
38. Esch BT, Warburton DER. Left ventricular torsion and recoil: Implications for exercise performance and cardiovascular disease. *J Appl Physiol*. (2009) 106:362–9. doi: 10.1152/japplphysiol.00144.2008
39. Kovács A, Apor A, Nagy A, Vágó H, Tóth A, Nagy A, et al. Left ventricular untwisting in Athlete's heart: Key role in early diastolic filling? *Int J Sports Med*. (2013) 35:259–64. doi: 10.1055/s-0033-1349076
40. Izem O, Mourot L, Tordi N, Grandperrin A, Obert P, Rupp T, et al. Key role of left ventricular untwisting in endurance cyclists at onset of exercise. *J Appl Physiol*. (2021) 131:1565–74. doi: 10.1152/japplphysiol.00907.2020
41. Poitras VJ, Hudson RW, Tschakovsky ME. Exercise intolerance in Type 2 diabetes: Is there a cardiovascular contribution? *J Appl Physiol*. (2018) 124:1117–39. doi: 10.1152/japplphysiol.00070.2017
42. Sacre JW, Jellis CL, Haluska BA, Jenkins C, Coombes JS, Marwick TH, et al. Association of exercise intolerance in Type 2 diabetes with skeletal muscle blood flow reserve. *JACC Cardiovasc Imaging*. (2015) 8:913–21. doi: 10.1016/j.jcmg.2014.12.033
43. Ingels NB, Hansen DE, Daughters GT, Stinson EB, Alderman EL, Miller DC. Relation between longitudinal, circumferential, and oblique shortening and torsional deformation in the left ventricle of the transplanted human heart. *Circ Res*. (1989) 64:915–27. doi: 10.1161/01.res.64.5.915
44. Beyar R, Sideman S. Left ventricular mechanics related to the local distribution of oxygen demand throughout the wall. *Circ Res*. (1986) 58:664–77. doi: 10.1161/01.res.58.5.664
45. Zhang H-J, Wang H, Sun T, Lu M-J, Xu N, Wu W-C, et al. Assessment of left ventricular twist mechanics by speckle tracking echocardiography reveals association between LV twist and myocardial fibrosis in patients with hypertrophic cardiomyopathy. *Int J Cardiovasc Imaging*. (2014) 30:1539–48. doi: 10.1007/s10554-014-0509-6
46. Wang C-P, Hsu H-L, Hung W-C, Yu T-H, Chen Y-H, Chiu C-A, et al. Increased epicardial adipose tissue (EAT) volume in type 2 diabetes mellitus and association with metabolic syndrome and severity of coronary atherosclerosis. *Clin Endocrinol (Oxf)*. (2009) 70:876–82. doi: 10.1111/j.1365-2265.2008.03411.x
47. Al-Talabany S, Mordi I, Graeme Houston J, Colhoun HM, Weir-McCall JR, Matthew SZ, et al. Epicardial adipose tissue is related to arterial stiffness and inflammation in patients with cardiovascular disease and type 2 diabetes. *BMC Cardiovasc Disord*. (2018) 18:31. doi: 10.1186/s12872-018-0770-z
48. Koepp KE, Obokata M, Reddy YNV, Olson TP, Borlaug BA. Hemodynamic and functional impact of epicardial adipose tissue in heart failure with preserved ejection fraction. *JACC Heart Fail*. (2020) 8:657–66.
49. van Woerden G, Gorter TM, Westenbrink BD, Willems TP, van Veldhuisen DJ, Rienstra M. Epicardial fat in heart failure patients with mid-range and preserved ejection fraction. *Eur J Heart Fail*. (2018) 20:1559–66. doi: 10.1002/ehf.1283
50. Packer M. Epicardial adipose tissue may mediate deleterious effects of obesity and inflammation on the myocardium. *J Am Coll Cardiol*. (2018) 71:2360–72.
51. Baker AR, Silva NF, Quinn DW, Harte AL, Pagano D, Bonser RS, et al. Human epicardial adipose tissue expresses a pathogenic profile of adipocytokines in patients with cardiovascular disease. *Cardiovasc Diabetol*. (2006) 5:1. doi: 10.1186/1475-2840-5-1
52. Camarena V, Sant D, Mohseni M, Salerno T, Zaleski ML, Wang G, et al. Novel atherogenic pathways from the differential transcriptome analysis of diabetic epicardial adipose tissue. *Nutr Metab Cardiovasc Dis NMCD*. (2017) 27:739–50. doi: 10.1016/j.numecd.2017.05.010
53. Greulich S, Maxhera B, Vandenplas G, Wiza DH, Smiris K, Mueller H, et al. Secretory products from epicardial adipose tissue of patients with Type 2 diabetes mellitus induce cardiomyocyte dysfunction. *Circulation*. (2012) 126:2324–34.
54. Burns AT, La Gerche A, MacIsaac AI, Prior DL. Augmentation of left ventricular torsion with exercise is attenuated with age. *J Am Soc Echocardiogr*. (2008) 21:315–20. doi: 10.1016/j.echo.2007.08.013



OPEN ACCESS

EDITED BY

Xiang Li,
Harvard Medical School, United States

REVIEWED BY

Shen Zhao,
Sun Yat-sen University, China
Gongning Luo,
Harbin Institute of Technology, China

*CORRESPONDENCE

Mingxing Xie
xiemx@hust.edu.cn
Wufeng Xue
xuewf@szu.edu.cn
Li Zhang
zli429@hust.edu.cn

†These authors have contributed
equally to this work

SPECIALTY SECTION

This article was submitted to
Cardiovascular Imaging,
a section of the journal
Frontiers in Cardiovascular Medicine

RECEIVED 08 July 2022

ACCEPTED 22 August 2022

PUBLISHED 14 September 2022

CITATION

Zhu Y, Ma J, Zhang Z, Zhang Y, Zhu S,
Liu M, Zhang Z, Wu C, Yang X,
Cheng J, Ni D, Xie M, Xue W and
Zhang L (2022) Automatic view
classification of contrast
and non-contrast echocardiography.
Front. Cardiovasc. Med. 9:989091.
doi: 10.3389/fcvm.2022.989091

COPYRIGHT

© 2022 Zhu, Ma, Zhang, Zhang, Zhu,
Liu, Zhang, Wu, Yang, Cheng, Ni, Xie,
Xue and Zhang. This is an open-access
article distributed under the terms of
the [Creative Commons Attribution
License \(CC BY\)](#). The use, distribution
or reproduction in other forums is
permitted, provided the original
author(s) and the copyright owner(s)
are credited and that the original
publication in this journal is cited, in
accordance with accepted academic
practice. No use, distribution or
reproduction is permitted which does
not comply with these terms.

Automatic view classification of contrast and non-contrast echocardiography

Ye Zhu^{1,2,3†}, Junqiang Ma^{4,5†}, Zisang Zhang^{1,2,3},
Yiwei Zhang^{1,2,3}, Shuangshuang Zhu^{1,2,3}, Manwei Liu^{1,2,3},
Ziming Zhang^{1,2,3}, Chun Wu^{1,2,3}, Xin Yang⁶, Jun Cheng^{4,5},
Dong Ni^{4,5}, Mingxing Xie^{1,2,3*}, Wufeng Xue^{4,5*} and
Li Zhang^{1,2,3*}

¹Department of Ultrasound, Union Hospital, Tongji Medical College, Huazhong University of Science and Technology, Wuhan, China, ²Clinical Research Center for Medical Imaging in Hubei Province, Wuhan, China, ³Hubei Province Key Laboratory of Molecular Imaging, Wuhan, China, ⁴National-Regional Key Technology Engineering Laboratory for Medical Ultrasound, Guangdong Key Laboratory for Biomedical Measurements and Ultrasound Imaging, Shenzhen, China, ⁵School of Biomedical Engineering, Health Science Center, Shenzhen University and Medical Ultrasound Image Computing (MUSIC) Lab, Shenzhen, China, ⁶Media and Communication Lab (MC Lab), Electronics and Information Engineering Department, Huazhong University of Science and Technology, Wuhan, China

Background: Contrast and non-contrast echocardiography are crucial for cardiovascular diagnoses and treatments. Correct view classification is a foundational step for the analysis of cardiac structure and function. View classification from all sequences of a patient is laborious and depends heavily on the sonographer's experience. In addition, the intra-view variability and the inter-view similarity increase the difficulty in identifying critical views in contrast and non-contrast echocardiography. This study aims to develop a deep residual convolutional neural network (CNN) to automatically identify multiple views of contrast and non-contrast echocardiography, including parasternal left ventricular short axis, apical two, three, and four-chamber views.

Methods: The study retrospectively analyzed a cohort of 855 patients who had undergone left ventricular opacification at the Department of Ultrasound Medicine, Wuhan Union Medical College Hospital from 2013 to 2021, including 70.3% men and 29.7% women aged from 41 to 62 (median age, 53). All datasets were preprocessed to remove sensitive information and 10 frames with equivalent intervals were sampled from each of the original videos. The number of frames in the training, validation, and test datasets were, respectively, 19,370, 2,370, and 2,620 from 9 views, corresponding to 688, 84, and 83 patients. We presented the CNN model to classify echocardiographic views with an initial learning rate of 0.001, and a batch size of 4 for 30 epochs. The learning rate was decayed by a factor of 0.9 per epoch.

Results: On the test dataset, the overall classification accuracy is 99.1 and 99.5% for contrast and non-contrast echocardiographic views. The average

precision, recall, specificity, and F1 score are 96.9, 96.9, 100, and 96.9% for the 9 echocardiographic views.

Conclusions: This study highlights the potential of CNN in the view classification of echocardiograms with and without contrast. It shows promise in improving the workflow of clinical analysis of echocardiography.

KEYWORDS

echocardiography, contrast, view classification, convolutional neural network, artificial intelligence (AI)

Introduction

Transthoracic echocardiography is one of the most important non-invasive imaging techniques, with the advantages of non-radiation, easy bedside operation, and real-time evaluation (1). With changes in relative position between the transducer and the patient, sonographers obtain multiple views from different perspectives. In particular, the apical views and short axis views are most commonly used in routine clinical workflows (1, 2). Currently, view classification is the prerequisite for the post-processing and analysis of cardiac structure and function. However, it generally depends on the sonographer's experience and is time-consuming especially for large datasets. It is a challenging task due to the inter-view similarity, intra-view variability and noise.

Earlier research adopted classical machine learning algorithms to classify echocardiograms with multiple views. They generally extracted features using the Histogram of Oriented Gradients (HOG) (3), Bag of Word (BoW) (4, 5), and classified echocardiography view using the Support Vector Machine (SVM) (3–7). Current studies have mainly focused on Convolutional neural networks (CNNs), which have brought about a series of breakthroughs for medical image analysis (8, 9). CNNs tend to recognize visual patterns from raw image pixels in an end-to-end learning process. The initial layers are used to observe local geometric structures (such as edges, blobs, etc.), whereas the neurons in the higher layers focus more on the global distribution of human organs. A large number of studies have confirmed the feasibility and accuracy of CNNs with various depth in echocardiographic view classification (10–13). For a closer look of the echocardiographic images, Madani et al. has used U-Net to extract the regions of interest, improving the signal-to-noise ratio. The precision and efficiency of the network were further promoted (14). Echocardiography has rich temporal domain information, while single CNNs only focuses on spatial location information. A study indicated that the dense optical flow technique represented temporal motion information, building two strands of CNNs with temporal-spatial information fusion and improving classification accuracy from 89.5% of single CNN to 92.1% of the fusion network (12). In addition, several studies optimized the algorithm based on

CNNs, ensuring the classification accuracy and significantly improving efficiency. CNNs can be used to facilitate automatic multiplanar reformation and orientation guidance (15) and deploy on mobile devices for downstream analysis (16). CNNs simplify the image processing process, assist novices in identifying standard images, reduce observer variability, and improve analyzing efficiency.

Existing studies have mainly focused on two-dimensional grayscale or Doppler echocardiograms (3–7, 10–16). Most of them dealt with common cardiac views: apical two-chamber (A2C), apical three-chamber (A3C) and apical four-chamber (A4C), as well as the parasternal short-axis (PSAX). Although extensive studies have been carried out on conventional echocardiography, no single study focuses on the view classification of contrast echocardiography. Contrast echocardiography significantly enhances the boundaries of the left ventricular endocardium, which has great clinical significance in the quantification of cardiac function (2). In addition, contrast echocardiography effectively reduces missed diagnoses of apical hypertrophic cardiomyopathy (17), intracardiac thrombi, and non-compaction cardiomyopathy (18). However, the contrast agent fills the heart cavity, making the mitral valve ring obscure, which increases the difficulty of identifying the primary views. Therefore, this study sets out to evaluate the discriminative capability of CNNs in identifying the PSAX, A2C, A3C, A4C views from non-contrast or contrast echocardiographic videos.

Materials and methods

Study design

All datasets were collected from 855 patients who underwent left ventricular opacification at the Department of Ultrasound Medicine, Wuhan Union Medical College Hospital from 2013 to 2021. This study was approved by the Ethics Committee of Tongji Medical College, Huazhong University of Science and Technology, Wuhan, China. In the study population, 70.3% are male and 29.7% are female, aging from 41 to 62 with a median age of 53. Indications of

TABLE 1 Baseline characteristics.

Variable	All (N = 855)	Training (N = 688)	Validation (N = 84)	Testing (N = 83)
Demographics				
Age (years)	53 (41, 62)	53 (40, 62)	53 (42, 62)	51 (43, 63)
Sex (male)	601 (70.3%)	476 (69.2%)	65 (77.4%)	59 (71.1%)
Indication				
Myocardial hypertrophy	360 (42.0%)	285 (41.4%)	37 (44.0%)	38 (45.8%)
NCM	85 (9.9%)	61 (8.9%)	11 (13.1%)	13 (15.7%)
DCM	17 (2.0%)	12 (1.7%)	3 (3.6%)	2 (2.4%)
NCM & DCM	32 (4.0%)	29 (4.0%)	2 (2.4%)	1 (1.2%)
RWMA	118 (13.8%)	98 (14.2%)	13 (11.9%)	7 (8.4%)
Others	243 (28.4%)	203 (29.5%)	18 (21.4%)	22 (26.5%)

Data are expressed as median (interquartile range) or number (%). NCM, non-compaction of ventricular myocardium; DCM, dilated cardiomyopathy; RWMA, regional wall motion abnormality; Others, other conditions that required contrast echocardiography.

TABLE 2 Distribution of the clip number in the dataset.

Class	Training	Validation	Testing	Total
2DE.A2C	222 (2,220)	28 (280)	28 (280)	278 (2,780)
2DE.A3C	233 (2,330)	31 (310)	30 (300)	294 (2,940)
2DE.A4C	219 (2,190)	25 (250)	30 (300)	274 (2,740)
2DE.PSAX	226 (2,260)	29 (290)	31 (310)	286 (2,860)
C2DE.A2C	224 (2,240)	29 (290)	30 (300)	283 (2,830)
C2DE.A3C	182 (1,820)	20 (200)	26 (260)	228 (2,280)
C2DE.A4C	221 (2,210)	25 (250)	30 (300)	276 (2,760)
C2DE.PSAX	223 (2,230)	24 (240)	29 (290)	276 (2,760)
Other	187 (1,870)	26 (260)	28 (280)	241 (2,410)
Total	1,937 (19,370)	237 (2,370)	262 (2,620)	2,436 (24,360)

For training, validation and testing datasets, clips are from separate echocardiographic videos. The numbers in parentheses indicate the number of images. 2DE, two-dimensional echocardiography; C2DE, contrast two-dimensional echocardiography; A2C, apical 2-chamber; A3C, apical 3-chamber; A4C, apical 4-chamber; PSAX, parasternal left ventricular short axis; Other, including parasternal left ventricular long axis, pulmonary artery long axis, and major artery short axis.

left ventricular opacification in routine clinical practice are shown in **Table 1**. Each sample consisted of data from the echocardiographic examination of a patient, including M-mode, two-dimensional, three-dimensional, Doppler and other still images or videos. The echocardiograms were mainly acquired with GE Vivid E9, Philips iE33, IE Elite, EPIQ 7C, and EPIQ 5.

Data preprocessing

The echocardiograms were stored in DICOM format. This study mainly analyzed two-dimensional grayscale videos (contrast and non-contrast echocardiography). All videos are anonymized.

The PSAX and apical views play an essential role in the diagnosis and treatment of cardiovascular diseases. The PSAX view focuses on mitral valve and left ventricular wall motion. The A2C, A3C, and A4C views are mainly used to assess cardiac structure and function comprehensively. Moreover, it is of

incremental value for detecting apical abnormalities in contrast echocardiography. Thus, the dataset was divided into nine categories, including the above-mentioned views of contrast and non-contrast echocardiograms, and an additional class including all the rest views (parasternal left ventricular long axis, pulmonary artery long axis, and major artery short axis views, etc.). All views included diverse image quality and were reviewed independently by two experts. Low-quality and inefficient videos were excluded (contrast echocardiography with underfilling or echocardiography with the incompleteness of heart chambers).

The dataset consisted of video clips from the 10 temporally sampled frames with equivalent intervals from each of the original sequences. Considering the different types of equipment for image acquisition, all clips were downsampled to 256×256 pixels by linear interpolation and the intensity is normalized into $[0, 1]$. Quality control is carried out by random sampling the preprocessed clips, to ensure that the dataset did not contain sensitive information. To maintain sample independence, all samples were randomly split into training, validation and test datasets in an approximate 8:1:1 ratio. The training dataset was

used for model development. The validation dataset was used for tuning model parameters, and the testing dataset was used for evaluating the performance of the final model. The training, validation, and test datasets included 688, 84, and 83 studies, respectively (corresponding to 1,937, 237, and 262 clips from 9 views). The datasets are derived from real world data. The distribution of each dataset is shown in **Table 2**.

View classification model architecture and training process

View classification tasks were mainly performed by CNNs. This study chose the deep residual network with 34 layers (called EchoV-Net) to classify 9 classes of echocardiographic views. Numerous studies have demonstrated that the residual network (ResNet) can improve accuracy from considerably increased depth (19). EchoV-Net was developed based on ResNet, as shown in **Table 3**. We conducted comparative experiments to validate the performance. The detailed results are listed in Table 2 and Figure 1 of **Supplementary materials**. The overview diagram of view classification task is shown in **Figure 1**. For echocardiographic view classification, the model was trained to minimize the cross-entropy loss between the true label and prediction using an Adam optimizer with an initial learning rate of 0.001, and a batch size of 4 for 30 epochs. The learning rate was decayed by a factor of 0.9 each epoch. The 10 frames of each video were used as the model input. The final model was selected with the lowest loss of the validation dataset. The model was implemented on the software Python (version 3.7.10) and PyTorch (version 1.7.1), and on the server with one NVIDIA GeForce RTX3090 GPU and 24GB of memory.

Model evaluation and visualization

In the process of video classification, we evaluated 10 sampled images of each video, averaged the results, and assigned the video to the class with the maximum probability. The four metrics, namely accuracy, precision (also called “positive predictive value”), recall (also called “sensitivity”), specificity, and F1-score were used to evaluate the classification performance of EchoV-Net. All metrics were calculated separately in a single category (cardiac view), with the current category defined as a positive class, and the other 8 categories as negative classes. The overall accuracy is defined as the ratio of the number of correctly classified videos to the number of all samples. The top-1 accuracy is defined as the accuracy of the first prediction category that matched the true label. The top-2 accuracy is defined as the accuracy of the first two prediction categories that matched the true label. The precision is defined as the number of correctly classified positive samples divided by the number of true positive samples. The recall is

TABLE 3 The architecture of EchoV-Net.

Layer name	Output size	Feature map
Conv1	128 × 128	5 × 5, 64, stride 2
Conv2	64 × 64	3 × 3 max pool, stride 2
		$\begin{bmatrix} 3 \times 3, 64 \\ 3 \times 3, 64 \end{bmatrix} \times 3$
Conv3	32 × 32	$\begin{bmatrix} 3 \times 3, 128 \\ 3 \times 3, 128 \end{bmatrix} \times 4$
Conv4	16 × 16	$\begin{bmatrix} 3 \times 3, 256 \\ 3 \times 3, 256 \end{bmatrix} \times 6$
Conv5	8 × 8	$\begin{bmatrix} 3 \times 3, 512 \\ 3 \times 3, 512 \end{bmatrix} \times 3$
	1 × 1	Average pool, 9-d fc, softmax

defined as the number of correctly classified positive samples divided by the number of all positive samples. The specificity is defined as the correctly classified negative samples divided by all the negative samples. The F1-score is the harmonic average of precision and recall. Additionally, confusion matrices are calculated and plotted as heatmaps to visualize the results of multi-view classification.

$$Accuracy = \frac{TP + TN}{TP + FP + TN + FN}$$

$$Precision = \frac{TP}{TP + FP}$$

$$Recall = \frac{TP}{TP + FN}$$

$$Specificity = \frac{TN}{TN + FP}$$

$$F1 - score = 2 \times \frac{Precision \times Recall}{Precision + Recall}$$

The following strategies enhanced the interpretability of the classification model. The feature obtained by EchoV-Net was visualized using t-distributed stochastic neighbor embedding (t-SNE). t-SNE is a non-parametric dimensionality reduction technique that visualizes high-dimensional data by giving each sample a location in a two or three-dimensional map (20). In addition, gradient-weighted class activation mapping (Grad-CAM) was created to explain which critical anatomical structures (regions of the pixel) that affect image classification results (21).

Re-evaluation by another expert

Due to fatigue and the similarity of views, there is inherent variation when observers explain echocardiograms,

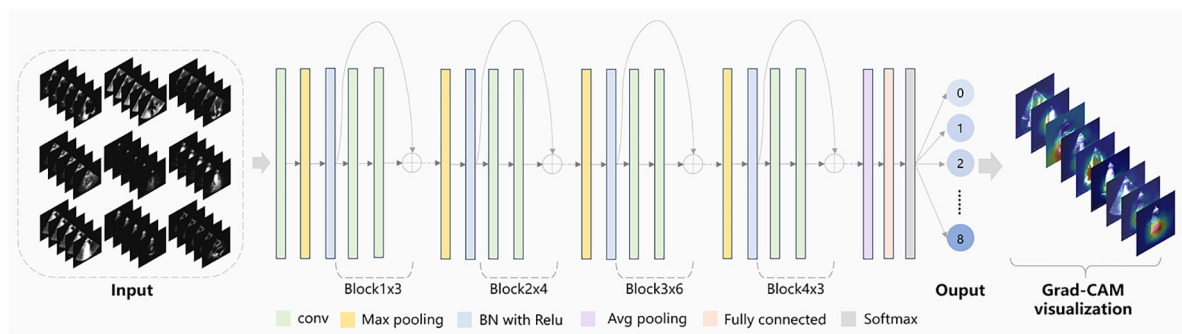


FIGURE 1
Schematic diagram of echocardiographic view classification.

especially the apical views. Another expert specializing in cardiovascular imaging performed a blinded review of the samples, when there was disagreement between the initial label and the prediction by EchoV-Net. The expert received the paired echocardiograms and a set of labels including the initial human label and the prediction by EchoV-Net, and then tried to decide which label corresponded more closely to his or her evaluation of echocardiographic views. When reviewing the prediction results, experts recorded the reasons for misclassification of samples, such as poor image quality or contrast agent underfilling.

Statistical analysis

All analyses were performed with R (version 4.1.2) or Python (version 3.7). The Kolmogorov-Smirnov test was used to assess the normality of patients' age. Continuous variables were presented as the median (1st and 3rd interquartile range) and categorical variables were shown as frequency (%). The accuracy, precision, recall, specificity and F1-score were described as percentages. A value of $P < 0.05$ was considered statistically significant. The classification model was developed using the PyTorch package (22). DICOM images were processed by Pydicom and OpenCV 3.0.

Results

Our model successfully distinguished non-contrast and contrast echocardiographic views (as shown in the confusion matrix in Figure 2). The numbers on the diagonal are the number of correctly classified videos. On the test dataset, 96.9% (254 out of 262) of the videos are correctly classified. The top-1 accuracy of the model for the 2DE view is 99.5%, and it is 99.1% for the C2DE views (Figure 3).

The evaluation of the view classification is shown in Table 4. The A2C and A3C for 2DE and A4C and PSAX for C2DE are

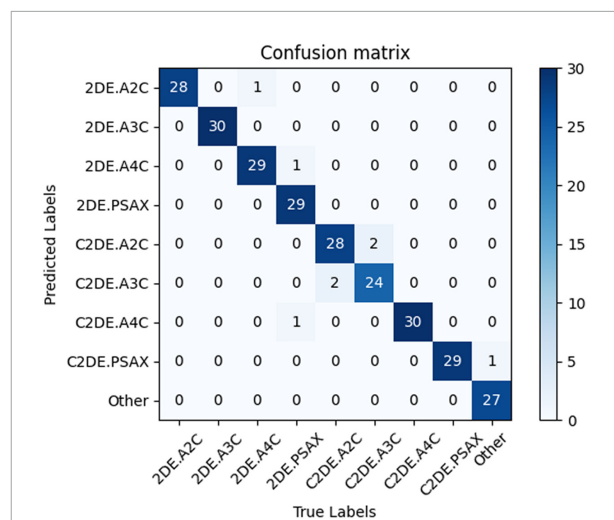


FIGURE 2
The confusion matrix demonstrated the results of view classifications within the test dataset. Numbers along the diagonal line represented successful classifications, while non-diagonal entries were misclassified. 2DE, two-dimensional echocardiography; C2DE, contrast two-dimensional echocardiography; A2C, apical 2-chamber; A3C, apical 3-chamber; A4C, apical 4-chamber; PSAX, parasternal left ventricular short axis; Other, including parasternal left ventricular long axis, pulmonary artery long axis, and major artery short axis.

fully correctly classified. However, the recall of PSAX in 2DE and A2C and A3C in C2DE are reduced to 93.55, 93.33, and 92.31%, respectively.

All metrics of the model are above 95% at the single video level. For the nine target views (i.e., A2C, A3C, A4C, PSAX and Other), the averages overall accuracy, top-2 accuracy, recall, precision, specificity, and F1 score are 97.0, 98.9, 96.9, 96.9, 100.0, and 96.9%, respectively.

The output of the fully connected layer in EchoV-Net is further interpreted by t-SNE (Figure 4) and Grad-CAM (Figure 5), showing obvious cluster results, and the classification criterion is consistent with the anatomical

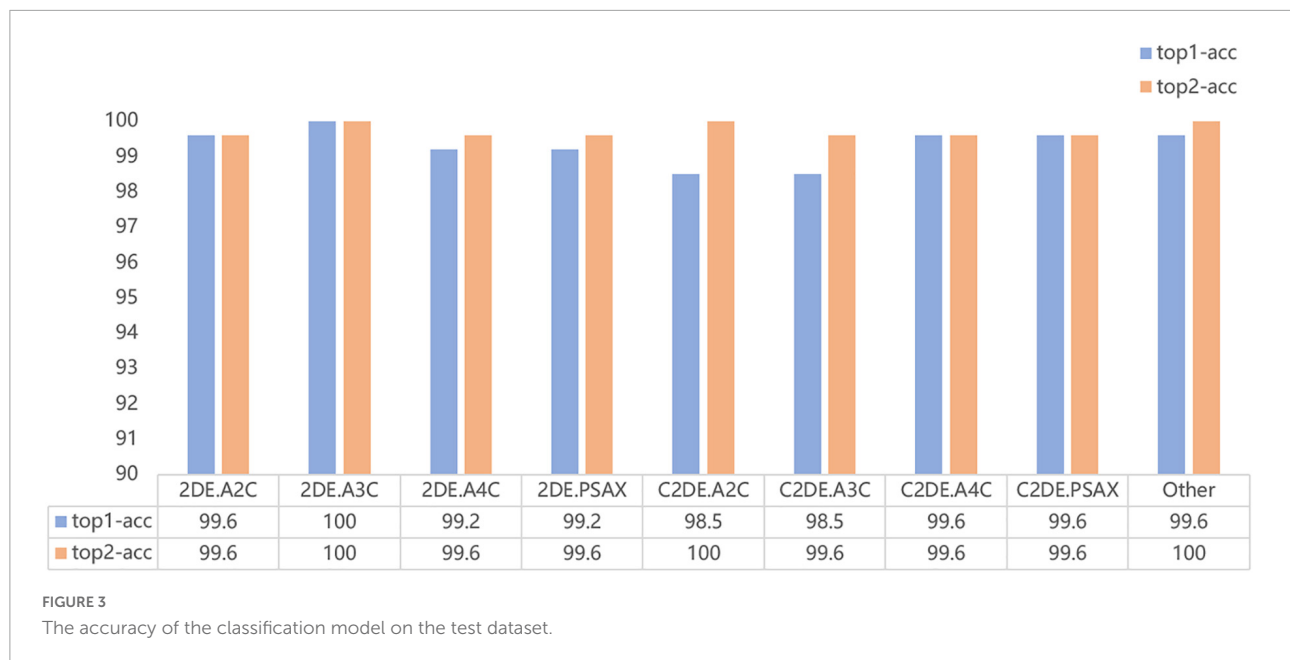


TABLE 4 The results of view classification on the test dataset.

Cardiac view	Precision	Recall	Specificity	F1 score
2DE.A2C	96.55	100.00	99.60	98.25
2DE.A3C	100.00	100.00	100.00	100.00
2DE.A4C	96.67	96.67	99.60	96.67
2DE.PSAX	100.00	93.55	100.00	96.67
C2DE.A2C	93.33	93.33	99.10	93.33
C2DE.A3C	92.31	92.31	99.20	92.31
C2DE.A4C	96.77	100.00	99.60	98.36
C2DE.PSAX	96.67	100.00	99.60	98.31
Other	100.00	96.43	100.00	98.18

2DE, two-dimensional echocardiography; C2DE, contrast two-dimensional echocardiography; A2C, apical 2-chamber; A3C, apical 3-chamber; A4C, apical 4-chamber; PSAX, parasternal left ventricular short axis; Other, including parasternal left ventricular long axis, pulmonary artery long axis, and major artery short axis.

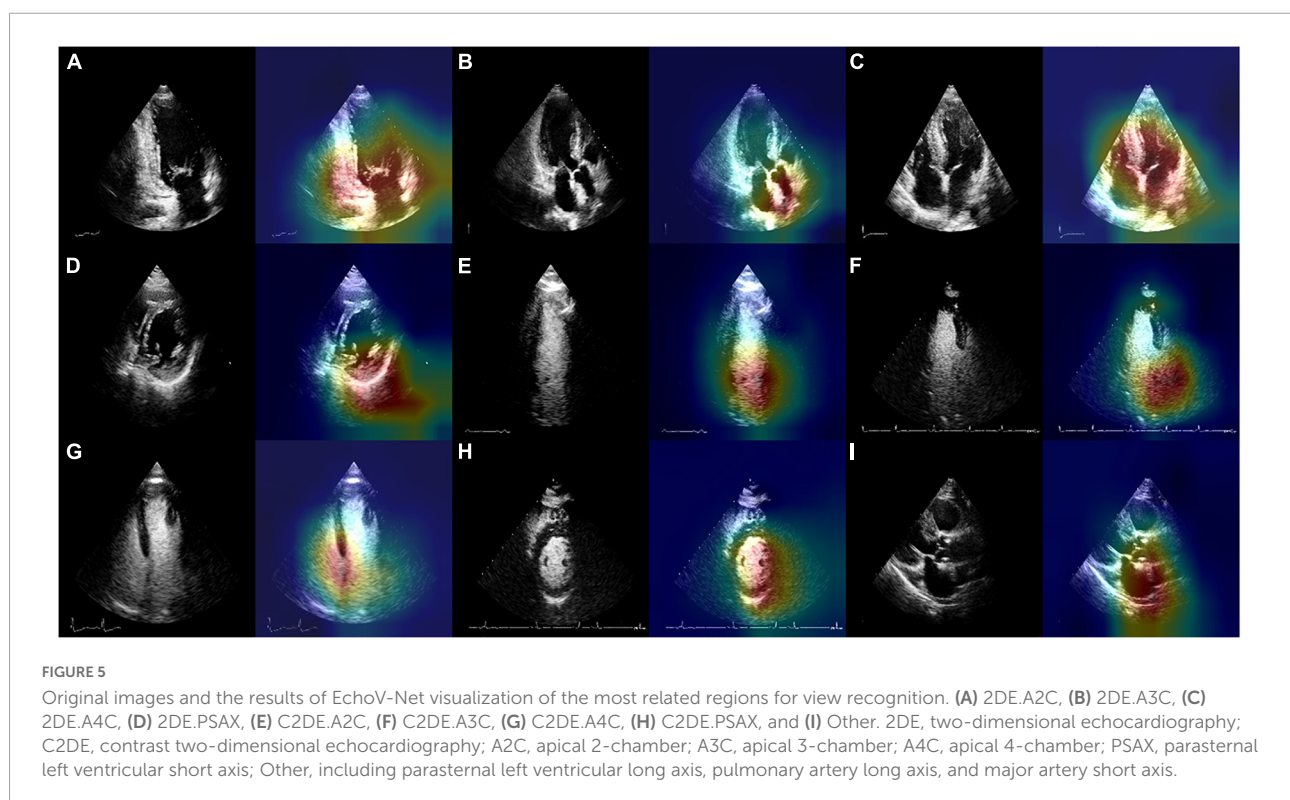
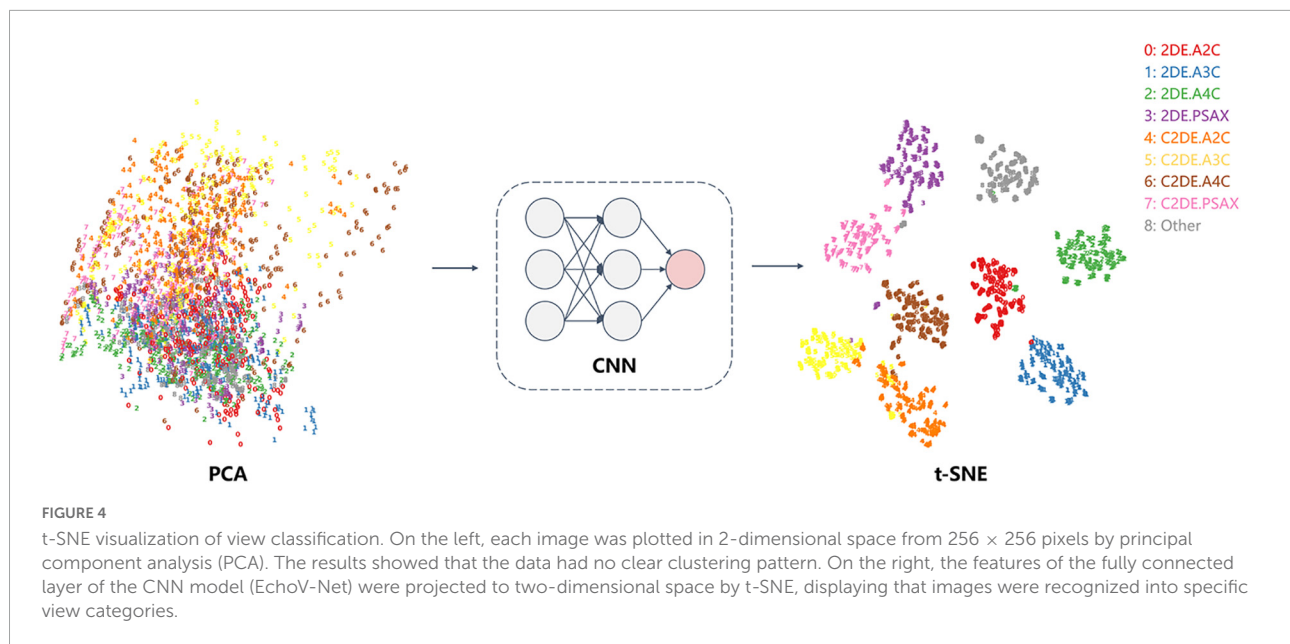
structure discerned by the cardiac sonographer. The Grad-CAM visual experiments indicate that the CNNs focus more on the mitral valve structure, the left ventricular outflow tract, and the cross of ventricle and atrium in A2C, A3C, and A4C, respectively. In addition, compared with non-contrast echocardiography, contrast echocardiography has a clearer cardiac contour, thus the regions of interest for CNNs focus more on the cardiac chamber cross junction (Supplementary materials and Figure 4). The F1 score of A4C in C2DE is 98.4%, and only 96.7% in 2DE (shown in Table 4).

Blinded reviews are performed for inconsistent results (shown in Table 5 and Figure 6). One expert with more than 5 years of clinical experience notes that 50% (4 out of 8) of the videos have considerable flaws and 37.5% (3 out of 8) of videos have incomplete cardiac structure, making it hard for the expert to identify the view. However, one video is misclassified

by EchoV-Net despite good image quality. The expert prefers the initial human label in 87.5% (7 out of 8) cases based on the most likely outcomes (top-1 prediction). For one video, the expert prefers the prediction of EchoV-Net to the human label.

Discussion

Echocardiographic view classification is the basis of the analysis and interpretation of echocardiography. The above target views are the standard views recommended by the guidelines for clinical diagnosis. In this study, we proposed a CNN-based automatic echocardiographic view classification system, which classified the PSAX and A2C, A3C, and A4C views of contrast and non-contrast echocardiography. The system was developed by a training set of 688 cases



containing 19,370 echocardiographic images. In the independent testing set of 83 cases with 2,620 images, the experimental results show that EchoV-Net accurately classified target views in contrast and non-contrast echocardiography, laying a foundation for subsequent AI-based cardiac function assessment and cardiovascular disease diagnoses.

Several factors lead to unsatisfactory view classification results. The intra-view variability of echocardiograms of the same cardiac view exists due to individual variations among subjects, different acquisition parameters (angle, depth, transducer performance, etc.), and the sonographer's experience. The inter-view similarity of echocardiograms of different cardiac views exists due to similar information

TABLE 5 Videos with the discordance between model prediction and human label.

Video	Human label	Top-1 prediction	Top-2 prediction	Expert results
565-14.dcm	2DE.A4C	2DE.A2C	2DE.PSAX	2DE.A4C
509-39.dcm	2DE.PSAX	2DE.A4C	C2DE.PSAX	2DE.PSAX
554-9.dcm	C2DE.A3C	C2DE.A2C	C2DE.A4C	C2DE.A3C
504-29.dcm	Other	C2DE.PSAX	Other	Other
558-47.dcm	C2DE.A2C	C2DE.A3C	C2DE.A2C	C2DE.A2C
306-29.dcm	C2DE.A3C	C2DE.A2C	C2DE.A3C	C2DE.A3C
172-53.dcm	C2DE.A2C	C2DE.A3C	C2DE.A2C	C2DE.A3C
314-62.dcm	2DE.PSAX	C2DE.A4C	2DE.PSAX	2DE.PSAX

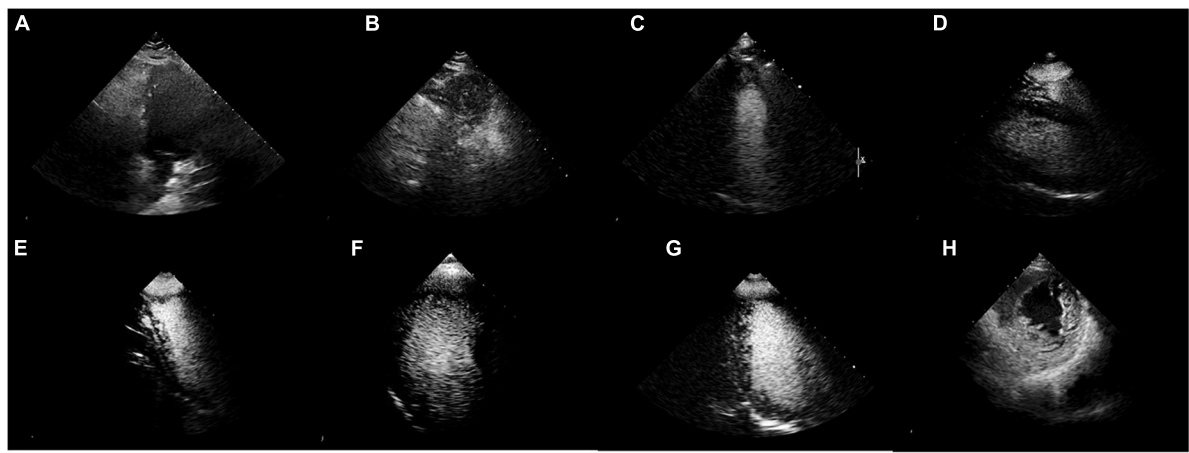


FIGURE 6 Misclassified samples. (A–D) Were of poor image quality. (E–G) Showed incomplete cardiac structures. (H) Was actually 2DE.PSAX, the top-1 prediction was C2DE.A4C, but the top-2 prediction was 2DE.PSAX.

(e.g., valve and ventricular wall movement, left ventricle, etc.). The contrast agent fills the cavity of the left ventricle, enhancing visualization of endocardium boundaries, but it obscures the mitral valve, aortic valve and other structures, making it hard to which may the classifiers to distinguish A2C from A3C in C2DE. Besides, echocardiograms are mainly derived from positive cases, the abnormalities in cardiac anatomy increase the heterogeneity of the data. The speckle noise and clutter noise lower the clarity of the images, limiting the accuracy of view classification. For the PASX views in 2DE, the patient's poor acoustic window makes it hard to identify the myocardium of the left ventricle. For the poor quality and low-level contrast images, it is necessary for experts to play an active role in quality control. What's more, in the retrospectively collected data, view distribution is imbalanced. All the above-mentioned issues increase the difficulty in classifying the key echocardiographic views in contrast and non-contrast echocardiography.

The size and image quality of echocardiograms are essential for the development and validation of a model.

In this study, we used a large dataset with a wide range of image quality that ensured data diversity and independence, making our model more robust to noise and poor image quality. However, in terms of computational efficiency, there is no comprehensive solution. A study carried out by Vaseli et al. attempted to overcome this problem. They adopted an knowledge distillation approach to compress the model and improve the efficiency of echocardiographic view classification (23). AI is often considered as a “black box,” which is challenging to understand, and thus we improved the interpretability of this model through several visualization methods, which showed that the model automatically classified echocardiograms depending on interpretable clinical features. The results indicate that the AI tasks have the potential to improve the work efficiency of sonographers and provide support for high-throughput analysis of echocardiography.

In future work, more echocardiographic views (e.g., parasternal long-axis views of the left ventricle, apical five-chamber view, etc.) need to be incorporated into our model,

in addition to the frequently used ones. More high-quality and multimodal echocardiograms are expected to be used to improve the echocardiographic view classification system. In addition, we will continue exploring the causes of non-standard echocardiography to develop man-machine interactive quality control AI system and improve the performance of view classification.

Conclusion

The main goal of the current study is to determine the feasibility and effectiveness of CNNs in view classification for contrast and non-contrast echocardiography. The results show that the EchoV-Net achieves expert-level view classification and accurately identifies the main categories in contrast-enhanced and non-contrast echocardiography. This study is expected to accelerate the automatic interpretation of contrast echocardiography and expand the clinical application of contrast echocardiography. In the future, the model also is expanded to classify other modalities of echocardiographic views (e.g., to distinguish colors, continuous-waves, pulsed-waves Doppler echocardiography), which has foundational significance for research, clinical practice, and sonographers' training.

Data availability statement

The original contributions presented in this study are included in the article/**Supplementary material**, further inquiries can be directed to the corresponding authors.

Ethics statement

This study was approved by the Ethics Committee of Tongji Medical College, Huazhong University of Science and Technology, Wuhan, China. Written informed consent was not required for this study in accordance with the local legislation and institutional requirements.

References

1. Lang RM, Badano LP, Mor-Avi V, Afilalo J, Armstrong A, Ernande L, et al. Recommendations for cardiac chamber quantification by echocardiography in adults: an update from the American Society of Echocardiography and the European Association of Cardiovascular Imaging. *Eur Heart J Cardiovasc Imaging*. (2015) 16:1–39.e14. doi: 10.1093/ehjci/jev014
2. Senior R, Becher H, Monaghan M, Agati L, Zamorano J, Vanoverschelde JL, et al. Clinical practice of contrast echocardiography: recommendation by the European Association of Cardiovascular Imaging (EACVI) 2017. *Eur Heart J Cardiovasc Imaging*. (2017) 18:1205–1205af. doi: 10.1093/ehjci/jex182
3. Agarwal D, Shriram KS, Subramanian N. Automatic view classification of echocardiograms using histogram of oriented gradients. *Proceedings of the IEEE 10th International Symposium on Biomedical Imaging*. San Francisco, CA: IEEE (2013). p. 1368–71. doi: 10.1109/ISBI.2013.6556787
4. Penatti OAB, Werneck RD, de Almeida WR, Stein BV, Pazinato DV, Mendes PR, et al. Mid-level image representations for real-time heart view plane classification of echocardiograms. *Comput Biol Med*. (2015) 66:66–81. doi: 10.1016/j.compbiomed.2015.08.004

Author contributions

YEZ, JM, DN, MX, WX, and LZ conceived of the study. YIZ, SZ, and ML labeled the data. YEZ, JM, and ZSZ created and ran the data processing pipeline and wrote the manuscript. YEZ and JM designed and evaluated the deep learning models. CW, ZMZ, JC, XY, and LZ provided language help and proofed the manuscript. All authors contributed to the article and approved the submitted version.

Funding

This work was supported by the National Natural Science Foundation of China (grant numbers: 82151316, 82171964, and 81922033).

Conflict of interest

The authors declare that the research was conducted in the absence of any commercial or financial relationships that could be construed as a potential conflict of interest.

Publisher's note

All claims expressed in this article are solely those of the authors and do not necessarily represent those of their affiliated organizations, or those of the publisher, the editors and the reviewers. Any product that may be evaluated in this article, or claim that may be made by its manufacturer, is not guaranteed or endorsed by the publisher.

Supplementary material

The Supplementary Material for this article can be found online at: <https://www.frontiersin.org/articles/10.3389/fcvm.2022.989091/full#supplementary-material>

5. Qian Y, Wang L, Wang C, Gao X. The synergy of 3D SIFT and sparse codes for classification of viewpoints from echocardiogram videos. *Proceedings of the MICCAI International Workshop on Medical Content-Based Retrieval for Clinical Decision Support*. Toronto: (2012). p. 68–79. doi: 10.1007/978-3-642-36678-9_7
6. Wu H, Bowers DM, Huynh TT, Souvenir R. Echocardiogram view classification using low-level features. *Proceedings of the 2013 IEEE 10th International Symposium on Biomedical Imaging*. San Francisco, CA: IEEE (2013). p. 752–5. doi: 10.1109/ISBI.2013.6556584
7. Khamis H, Zurakhov G, Azar V, Raz A, Friedman Z, Adam D. Automatic apical view classification of echocardiograms using a discriminative learning dictionary. *Med Image Anal.* (2017) 36:15–21. doi: 10.1016/j.media.2016.10.007
8. Anwar SM, Majid M, Qayyum A, Awais M, Alnowami M, Khan MK. Medical image analysis using convolutional neural networks: a review. *J Med Syst.* (2018) 42:226. doi: 10.1007/s10916-018-1088-1
9. Litjens G, Kooi T, Bejnordi BE, Setio AAA, Ciompi F, Ghafoorian M, et al. A survey on deep learning in medical image analysis. *Med Image Anal.* (2017) 42:60–88. doi: 10.1016/j.media.2017.07.005
10. Kusunose K, Haga A, Inoue M, Fukuda D, Yamada H, Sata M. Clinically feasible and accurate view classification of echocardiographic images using deep learning. *Biomolecules.* (2020) 10:665. doi: 10.3390/biom10050665
11. Zhang J, Gajjala S, Agrawal P, Tison GH, Hallock LA, Beussink-Nelson L, et al. Fully automated echocardiogram interpretation in clinical practice. *Circulation.* (2018) 138:1623–35. doi: 10.1161/CIRCULATIONAHA.118.034338
12. Gao X, Li W, Loomes M, Wang L. A fused deep learning architecture for viewpoint classification of echocardiography. *Informat Fusion.* (2017) 36:103–13. doi: 10.1016/j.inffus.2016.11.007
13. Madani A, Arnaout R, Mofrad M, Arnaout R. Fast and accurate view classification of echocardiograms using deep learning. *NPJ Digit Med.* (2018) 1:6. doi: 10.1038/s41746-017-0013-1
14. Madani A, Ong JR, Tibrewal A, Mofrad MRK. Deep echocardiography: data-efficient supervised and semi-supervised deep learning towards automated diagnosis of cardiac disease. *NPJ Digit Med.* (2018) 1:59. doi: 10.1038/s41746-018-0065-x
15. Ostvik A, Smistad E, Aase SA, Haugen BO, Lovstakken L. Real-time standard view classification in transthoracic echocardiography using convolutional neural networks. *Ultrasound Med Biol.* (2019) 45:374–84. doi: 10.1016/j.ultrasmedbio.2018.07.024
16. Smistad E, Ostvik A, Salte IM, Melichova D, Nguyen TM, Haugaa K, et al. Real-time automatic ejection fraction and foreshortening detection using deep learning. *IEEE Trans Ultrason Ferroelectr Freq Control.* (2020) 67:2595–604. doi: 10.1109/TUFFC.2020.2981037
17. Cardim N, Galderisi M, Edvardsen T, Plein S, Popescu BA, D'Andrea A, et al. Role of multimodality cardiac imaging in the management of patients with hypertrophic cardiomyopathy: an expert consensus of the European Association of Cardiovascular Imaging Endorsed by the Saudi Heart Association. *Eur Heart J Cardiovasc Imaging.* (2015) 16:280. doi: 10.1093/ehjci/jeu291
18. Porter TR, Mulvagh SL, Abdelmoneim SS, Becher H, Belcik JT, Bierig M, et al. Clinical applications of ultrasonic enhancing agents in echocardiography: 2018 American society of echocardiography guidelines update. *J Am Soc Echocardiogr.* (2018) 31:241–74. doi: 10.1016/j.echo.2017.11.013
19. He K, Zhang X, Ren S, Sun J. Deep residual learning for image recognition. *Proceedings of the 2016 IEEE Conference on Computer Vision and Pattern Recognition (CVPR)*. Las Vegas, NV: IEEE (2016). p. 770–8. doi: 10.1109/CVPR.2016.90
20. Laurens VDM, Hinton G. Visualizing data using t-SNE. *J Mach Learn Res.* (2008) 9:2579–605.
21. Selvaraju RR, Cogswell M, Das A, Vedantam R, Parikh D, Vision DB. Grad-CAM: visual explanations from deep networks via gradient-based localization. *Proceedings of the 2017 IEEE International Conference on Computer Vision (ICCV)*. (Vol. 128), Venice: IEEE (2020). p. 336–59. doi: 10.1007/s11263-019-01228-7
22. Paszke A, Gross S, Massa F, Lerer A, Chintala S. PyTorch: an imperative style, high-performance deep learning library. *Proceedings of the 33rd International Conference on Neural Information Processing Systems*. Vancouver: (2019).
23. Vaseli H, Liao Z, Abdi AH, Girgis H, Tsang T. Designing lightweight deep learning models for echocardiography view classification. *Proceedings of the Image-Guided Procedures, Robotic Interventions, and Modeling*. San Diego, CA: (2019). doi: 10.1117/12.2512913



OPEN ACCESS

EDITED BY

Sanjeev Bhattacharyya,
Barts Heart Centre, United Kingdom

REVIEWED BY

Valeria Pergola,
University Hospital of Padua, Italy
Satish Ramkumar,
Barts Health NHS Trust,
United Kingdom

*CORRESPONDENCE

Guang Song
songg84@163.com

SPECIALTY SECTION

This article was submitted to
Cardiovascular Imaging,
a section of the journal
Frontiers in Cardiovascular Medicine

RECEIVED 04 August 2022

ACCEPTED 29 August 2022

PUBLISHED 16 September 2022

CITATION

Li Y, Ren W, Wang X, Xiao Y, Feng Y,
Shi P, Sun L, Wang X, Yang H and
Song G (2022) The diagnostic accuracy
of contrast echocardiography in
patients with suspected cardiac
masses: A preliminary multicenter,
cross-sectional study.
Front. Cardiovasc. Med. 9:1011560.
doi: 10.3389/fcvm.2022.1011560

COPYRIGHT

© 2022 Li, Ren, Wang, Xiao, Feng, Shi,
Sun, Wang, Yang and Song. This is an
open-access article distributed under
the terms of the [Creative Commons
Attribution License \(CC BY\)](#). The use,
distribution or reproduction in other
forums is permitted, provided the
original author(s) and the copyright
owner(s) are credited and that the
original publication in this journal is
cited, in accordance with accepted
academic practice. No use, distribution
or reproduction is permitted which
does not comply with these terms.

The diagnostic accuracy of contrast echocardiography in patients with suspected cardiac masses: A preliminary multicenter, cross-sectional study

Ying Li¹, Weidong Ren¹, Xin Wang¹, Yangjie Xiao¹,
Yueqin Feng², Pengli Shi³, Lijuan Sun⁴, Xiao Wang⁵, Huan Yang⁶
and Guang Song^{1*}

¹Department of Ultrasound, Shengjing Hospital of China Medical University, Shenyang, China,

²Department of Ultrasound, The First Hospital of China Medical University, Shenyang, China,

³Department of Ultrasound, The Fourth Affiliated Hospital of China Medical University, Shenyang,

China, ⁴Department of Ultrasound, The First Hospital of Qinhuangdao, Qinhuangdao, China,

⁵Department of Ultrasound, Anshan Central Hospital, Anshan, China, ⁶Department of Ultrasound, Yingkou Central Hospital, Yingkou, China

Background: To evaluate the diagnostic accuracy of contrast echocardiography (CE) in patients with suspected cardiac masses.

Methods: A multicenter, prospective study involving 108 consecutive patients with suspected cardiac masses based on transthoracic echocardiography performed between November 2019 and December 2020 was carried out. CE examinations were performed in all patients. The echocardiographic diagnosis was established according to the qualitative (echogenicity, boundary, morphology of the base, mass perfusion, pericardial effusion, and motility) and quantitative (area of the masses and peak intensity ratio of the masses and adjacent myocardium A1/A2) evaluations.

Results: Final confirmed diagnoses were as follows: no cardiac mass ($n = 3$), pseudomass ($n = 3$), thrombus ($n = 36$), benign tumor ($n = 30$), and malignant tumor ($n = 36$). ROC analysis revealed the optimal A1/A2 with cutoff value of 0.295 for a cardiac tumor from a thrombus, with AUC, sensitivity, specificity, PPV, and NPV of 0.958 (95% confidence interval (CI): 0.899–0.988), 100, 91.7, 95.7, and 100%, respectively. CE was able to distinguish malignant from benign tumors with an AUC of 0.953 (95% CI: 0.870–0.990). Multivariate logistic regression analysis revealed that tumor area, base, and A1/A2 were associated with the risk of malignant tumor (OR = 1.003, 95% CI: 1.00003–1.005; OR = 22.64, 95% CI: 1.30–395.21; OR = 165.39, 95% CI: 4.68–5,850.94, respectively). When using A1/A2 > 1.28 as the only diagnostic criterion to identify the malignant tumor, AUC, sensitivity, specificity, PPV, and NPV were 0.886 (95% CI: 0.784–0.951), 80.6, 96.7, 96.7, and 80.7%, respectively.

Conclusion: CE has the potential to accurately differentiate cardiac masses by combining qualitative and quantitative analyses. However, more studies with a

large sample size should be conducted to further confirm these findings.

Clinical trial registration: <http://www.chictr.org.cn/>, identifier: ChiCTR1900026809.

KEYWORDS

cardiac mass, heart neoplasms, echocardiography, ultrasound enhancing agents, sensitivity, specificity

Introduction

Cardiac masses have captured researchers' attention since the beginning of the field of echocardiography. Cardiac masses can be classified into non-neoplastic masses (thrombi, vegetations, calcifications, or other rare conditions), benign tumors, or malignant tumors (1, 2). Non-neoplastic masses account for 75% of all cases (3). Cardiac tumors are among the least prevalent of all tumors. The estimated prevalence of primary cardiac tumors is 0.001–0.03% (4), whereas metastatic cardiac tumors have been reported to occur 10–1,000 times as often (2.3–18.3%) (5). Primary cardiac tumors are divided into benign and malignant based on their histological characteristics (6). A previous study has demonstrated that the proportions of cardiac tumors in the left atrium, right atrium, left ventricle, right ventricle, and other sites were 34, 26, 6, 7, and 27%, respectively (7).

Cardiac masses may occur in any cardiac chamber adjacent to large blood vessels or pericardium. The treatments for cardiac tumors include surgical removal and chemoradiotherapy. The choice of treatment depends on the histopathological type, the extent of cancer invasion, and patient risk stratification (8). Early detection and accurate differentiation of cardiac masses might prolong survival and improve quality of life in affected patients. Several imaging modalities, including transthoracic echocardiography (TTE), transesophageal echocardiography (TEE), cardiac magnetic resonance (CMR), and positron emission tomography, have a crucial role in the assessment of cardiac masses (2). Given the diversity of cardiac masses, there are no guidelines or consensus regarding the best diagnostic approach. A recently published paper has comprehensively summarized the utility of these imaging modalities (9), stating that TTE is usually the first choice for cardiac mass examination. Once a cardiac mass is suspected based on TTE results, patients may be scanned using CMR for further evaluation due to the high resolution of cardiac mass boundary it provides. Positron emission tomography is helpful for staging malignancies and optimizing biopsy location.

TTE can help to determine the presence, size, shape, echogenicity, mobility, attachment point, and hemodynamic effects of the cardiac masses (10). The sensitivity of TTE to diagnose cardiac masses is 93% (11). However, it is not sufficient for some patients when image quality is suboptimal

and echo are complex. With an accuracy of less than 70%, it is very challenging to differentiate between benign and malignant tumors using TTE (12). Contrast echocardiography (CE) is a rapidly developing technology in recent years. The published guidelines for CE state that it can improve the image quality and help to distinguish between benign and malignant lesions (class of recommendation: benefits are greater than risks, and the procedure can be useful if performed) (13). However, most studies on CE diagnosis of cardiac masses are case reports (14–16), while the rest are retrospective (12) or small sample-sized prospective studies (17). The evidence for differential diagnosis of cardiac masses using CE is insufficient. Therefore, the present study aimed to evaluate the diagnostic accuracy of CE in patients with suspected cardiac masses.

Materials and methods

A group of six tertiary hospitals in North China, including the second largest hospital in China, conducted this prospective study. All the data collected were sent to Shengjing Hospital of China Medical University, as in our previous multicenter study (18). The study followed the STARD guidelines.

Study participants

Consecutive patients with suspected cardiac masses based on TTE performed between November 2019 and December 2020 were eligible for inclusion. All patients were adults. Exclusion criteria included allergies to albumin, blood products, and ultrasound enhancing agents; severe heart failure (New York Heart Association Class IV) and severe arrhythmia patients; respiratory failure; severe liver or kidney dysfunction; and mental illness or epilepsy (19).

Echocardiographic image acquisition

Echocardiographic examinations were performed with the patient in the left lateral position by a radiologist with more than 10 years of TTE experience using a Philips iE33 ultrasound system (Philips Medical Systems, Bothell, WA,

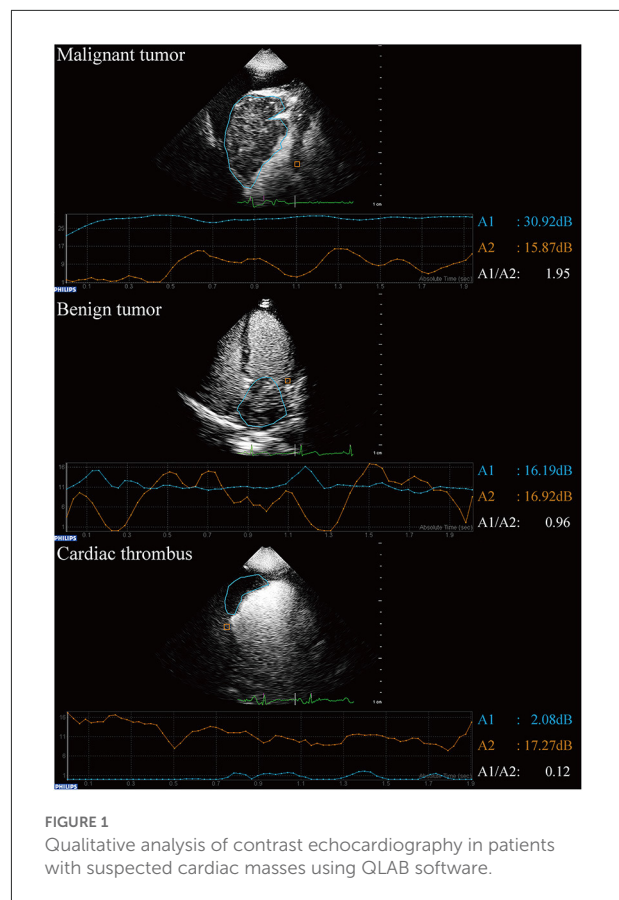
USA) and a TTE probe (S5-1, 1–5 MHz) at each center. All images and measurements were obtained according to the echocardiography guideline (20). Subsequently, all patients were examined using CE according to the latest published guidelines (13, 21).

Contrast echocardiography protocol

This protocol was written according to the recently published guideline for CE (13). Commercial ultrasound enhancing agents were used in the CE process (SonoVue; Bracco, Plan-Les-Ouates, Switzerland). First, the left ventricular opacification (LVO) mode was initiated with a low mechanical index of 0.2 and 30-Hz frame rates. Then, 0.8 mL of prepared ultrasound enhancing agents were quickly injected *via* the peripheral vein, with a slow (10–20 s) 3–5 mL saline flush. This was repeated as needed for optimal delineation of the left ventricular cavity and cardiac masses. The above-mentioned morphological and hemodynamic features of cardiac lesions were observed and saved digitally in this mode. Second, the myocardial contrast echocardiography (MCE) mode was turned on with a very low mechanical index of 0.08 and 30-Hz frame rates. After filling in the left ventricle and the myocardium, the ultrasound enhancing agents were continuously infused with a dedicated Vueject® syringe pump (Bracco, Milano, Italy) at a rate of 1 mL/min. The intermittent-flash (high mechanical index of 1.0) technique was used to destroy the microbubbles. Notably, the high mechanical index ultrasound impulse was transmitted between 5–10 frames to destroy the microbubbles. Perfusion was confirmed post contrast replenishment after the impulse to prevent a false positive reading due to saturation artifact. Finally, imaging results for the enhancement of the masses and adjacent normal myocardium before and after the flash were stored.

Echocardiographic image analysis

The qualitative analysis included echogenicity (uniform/non-uniform), boundary (well-demarcated/not well-demarcated), morphology of the base under CE (narrow with peduncle/narrow with notch/broad) (22), mass perfusion (no perfusion/mild perfusion/intense perfusion) (23), motility (absent/present) (24), and pericardial effusion (absent/present). Quantitative analysis was performed using QLAB software (version 13.0; Philips Medical Systems, Andover, MA, USA). The area of the masses was measured when the long maximum diameter was apparent. The region of interest was depicted along the boundary of each lesion and within the adjacent myocardium section (23). The peak intensity of the masses and of the adjacent myocardium were measured as A1 and A2, respectively (Figure 1) (25). The ratio of A1 to A2 was then calculated (26). $A1/A2 > 1$ was considered to indicate a high possibility of malignant tumor, while a mass with a



ratio between 0 and 1 was considered to be a benign tumor or thrombus (26, 27). The mass with A1 close to zero was considered a thrombus.

All analyses were performed independently by two investigators (Y.L. and X.W.) with more than 6 years of experience with CE and more than 10 years of experience with TTE. To improve the specificity of CE differentiation of malignant tumor from benign tumor based on the pilot study, the final diagnosis was made based on the combination of qualitative and quantitative results (26). Disagreements were discussed and resolved by involving a senior CE expert (W.R.) for adjudication.

Follow-up and validation

All patients were followed up to determine all-cause mortality by checking their medical records, performing telephone interviews, and *via* outpatient exams every 6 months until March 1, 2022. (I) Pseudomass was defined as a variant or prominent normal structure, including Eustachian valve or Chiari network, Crista terminalis, and Coumadin ridge (28). Diagnosis was confirmed by CMR. No morphological changes were identified by follow-up imaging. (II) Thrombus was defined as a distinct mass of echoes that can be seen

throughout systole and diastole (29). Either of the following two criteria had to be met: i) a significantly diminishing size or full resolution after anticoagulation therapy and confirmation of thrombus upon follow-up TEE or computed tomography (CT); or ii) pathological confirmation (24). (III) All tumors had to be confirmed by surgery or biopsy. Tumors were classified as benign or malignant based on histology (pathologic analysis) results in accordance with the 2015 World Health Organization classification of tumors of the heart and pericardium (6).

Measurement variability

To determine the intra-observer variability for all qualitative and quantitative indexes, measurements of 50 randomly selected cases were reassessed 2 weeks later by an investigator (Y.X.) who was blinded to the previous measurement results. To determine the inter-observer variability, measurements were repeated by a second observer (Y.F.) who was blinded to the results obtained by the first investigator. The two investigators were equally experienced.

Sample size calculation

The appropriate sample size was estimated with a 5% level of type I error and a minimal statistical power of 80% using PASS software (PASS 21.0.3. NCSS, LLC, Kaysville, UT, USA). The average sensitivity was 92.9% and the average specificity was 78.3% when using CE to differentiate malignant tumors from benign tumors based on Xia et al. (12) and our previous study (26) findings. When the prevalence/ratio was 35.0% (number of patients with malignant tumor/number of total cardiac tumor patients), the test required a minimum sample size of 46 (16 participants with malignant tumors and 30 participants with benign tumors).

The sensitivity was greater than 88.9% and specificity was greater than 80% when using CE to differentiate cardiac tumors from non-neoplastic cardiac masses in our previous study (26). When the prevalence/ratio was 57.1% (number of patients with thrombus/total number of patients with cardiac mass) (26), a sample size of 65 participants (37 participants with tumors and 28 participants with non-neoplastic cardiac masses) were sufficient to differentiate cardiac tumors from non-neoplastic cardiac masses. Therefore, 81 (16 malignant tumors, 30 benign tumors, and 35 non-neoplastic cardiac masses) was the minimum sample size for this study.

Statistical analysis

Continuous parameters were expressed as the mean \pm standard deviation, and differences between groups

were analyzed using independent-samples *t*-tests. Non-normally distributed parameters were expressed as the median (interquartile range, IQR), and differences between groups were analyzed using the Mann-Whitney *U* test. Comparison of categorical parameters between groups was analyzed using Pearson's chi-squared test or Fisher's exact test. Univariate logistic regression analysis was performed to evaluate the association between different echocardiographic parameters of cardiac tumors. Additionally, multivariate analysis was performed with the identified significant variables ($P < 0.05$). Odds ratio (OR) and 95% confidence intervals (CIs) were also calculated. Receiver operating characteristic (ROC) analysis was conducted to assess the differentiating capacity of variables for cardiac masses. Youden's *J* statistic was used to determine the optimal cutoff value. Finally, the area under the receiver operating characteristic curve (AUC), accuracy, sensitivity, specificity, positive predictive value (PPV), and negative predictive value (NPV) were calculated. Interclass correlation coefficient was used for continuous variables, and weighted kappa (κ_w) was used for categorical measurements. A *P* value of < 0.05 was used to define statistical significance. Statistical analyses were performed using Stata (version 16.0; StataCorp, College Station, TX, USA).

Results

Population characteristics

A total of 46,111 TTEs were performed at six departments between November 1, 2019 and December 31, 2020. During this period, 110 (0.24%) examinations were carried out in patients with suspected cardiac masses. Two patients with allergic constitution refused CE (Figure 2). As a result, 108 patients with a median age of 61.5 years (IQR: 52.0–67.5 years) were enrolled in the study, of which 68 (63.0%) were men. The baseline demographic and clinical characteristics of all patients are summarized in Table 1. In these 108 patients: three patients did not have any cardiac masses, three patients had a cardiac pseudomass, 36 patients had a cardiac thrombus, 30 patients had a benign tumor, and 36 patients had a malignant tumor. These results revealed that the history of previous cardiovascular disease and malignancy were significantly different among the four groups.

Two cases of cardiac pseudomass were hypertrophy of the interatrial septum, and one case of cardiac pseudomass was hypertrophy of papillary muscle. All patients with a cardiac thrombus received anticoagulation therapy, and none underwent a pathological analysis. Thrombi were all solitary. A total of 75% (27/36) of the thrombi were dissolved, and in 25% of cases (9/36) the thrombus volume was significantly reduced. Benign tumors were confirmed by surgery (28/30) and biopsy (2/30). Malignant tumors were confirmed by surgery

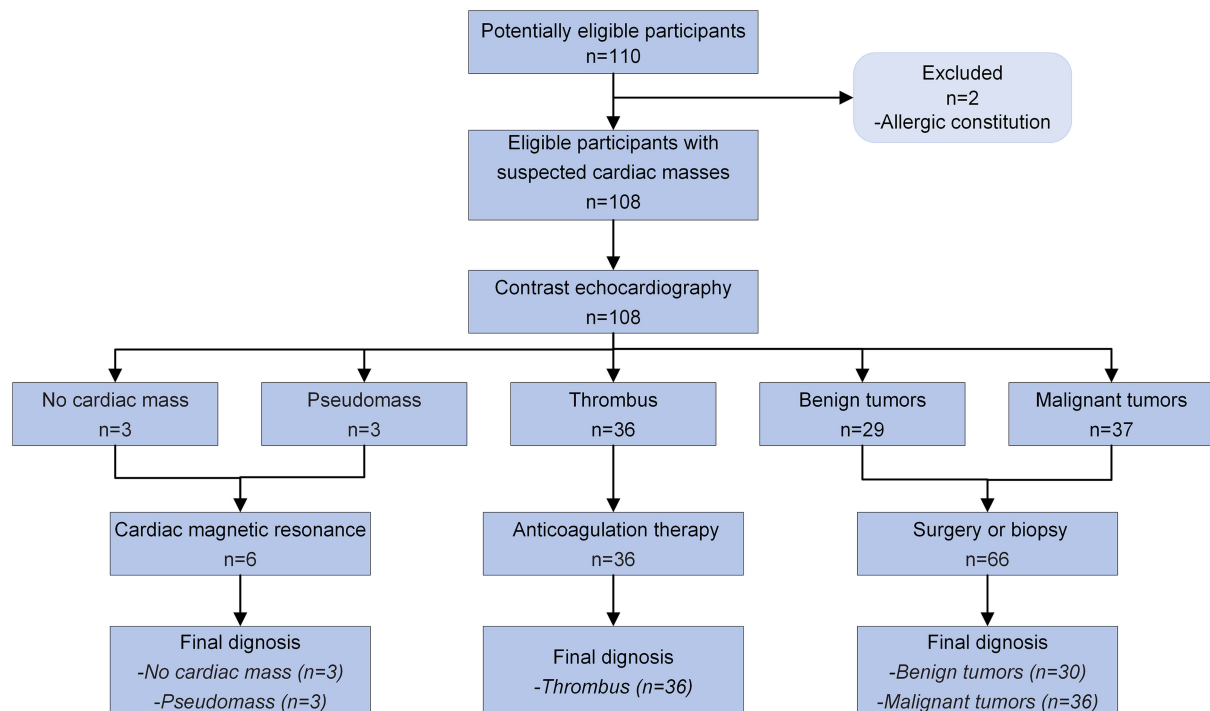


FIGURE 2

Diagnostic flow diagram for patients with suspected cardiac masses using contrast echocardiography according to STARD 2015.

(all three were primary malignant tumors) and biopsy (27/30). The diagnoses made by two investigators (YL and XW) were consistent in 104 cases. Four controversial cases were discussed and diagnosed with the help of a senior CE expert (W.R.): one case in the thrombus group with A1/A2 of 2.12 (correct diagnosis before treatment); two cases in the benign group with A1/A2 of 1.21 and 1.16 (erroneous diagnoses before treatment); and one case in the malignant group with A1/A2 of 0.54 (erroneous diagnosis before treatment). More details on the location and histopathology of cardiac tumors are shown in [Supplementary Tables S1, S2](#). No adverse drug reactions were observed in any of the 108 patients.

Comparison and differentiation of cardiac tumors from thrombi

Compared to the thrombus group, a larger area, higher rate of non-uniform echogenicity, wider base, higher perfusion intensity, and higher A1/A2 were identified in the tumor group ($P < 0.05$; [Table 2](#)). Multivariate regression analysis revealed that the base and enhancement A1/A2 were associated with the presence of cardiac tumor compared to the thrombus (OR = 7.53, 95% CI: 1.10–51.56; OR = 20.09, 95% CI: 4.17–96.72,

respectively; [Table 2](#)). The AUC for A1/A2 was 0.958 (95% CI: 0.899–0.988) when the cutoff value for A1/A2 was set to 0.295. The accuracy, sensitivity, specificity, PPV, and NPV are shown in [Table 3](#).

Comparison and differentiation of malignant tumors from benign tumors

Compared to the benign group, a larger area, higher rate of non-uniform echogenicity, not well-demarcated boundary, wider base, presence of motility, and higher A1/A2 were identified in the tumor group ($P < 0.05$; [Table 4](#)). Multivariate regression analysis revealed that the area, base, and A1/A2 were associated with the presence of malignant tumor compared to the benign tumor (OR = 1.003, 95% CI: 1.00003–1.005; OR = 22.64, 95% CI: 1.30–395.21; OR = 165.39, 95% CI: 4.68–5,850.94, respectively; [Table 4](#)). When the cutoff value for A1/A2 was set to 1.28, the AUC for A1/A2 was 0.886 (95% CI: 0.784–0.951). When the cutoff value for the tumor area was set to 1,302.2 mm², the AUC for the tumor area was 0.725 (95% CI: 0.601–0.828). The accuracy, sensitivity, specificity, PPV, and NPV are shown in [Table 5](#).

TABLE 1 Characteristics of the population.

	No cardiac mass (<i>n</i> = 3) and pseudomass (<i>n</i> = 3)	Thrombus (<i>n</i> = 36)	Benign tumor (<i>n</i> = 30)	Malignant tumor (<i>n</i> = 36)	<i>P</i> value
Age, mean (SD), years	58.7 (10.7)	57.1 (14.7)	55.1 (13.3)	65.1 (9.8)	0.117
Sex (Male/Female)					0.810
Male	4	21	21	22	
Female	2	15	9	14	
BMI, mean (SD), kg/m ²	24.5 (0.8)	24.6 (2.1)	23.6 (2.1)	24.0 (2.0)	0.153
Symptom					0.069
Asymptomatic	4	8	5	2	
Dyspnea	0	13	11	21	
Chest pain	0	7	6	5	
Palpitations	1	4	2	3	
Others	1	4	6	5	
History of cardiovascular disease	6	33	18	19	<0.001
History of malignant disease	0	2	3	33	<0.001
Localization					0.084
Left ventricle	3	4	0	1	
Left atrium	0	5	8	1	
Right ventricle	0	8	5	9	
Right atrium	1	12	13	19	
Others*	2	7	4	6	

SD, standard deviation; * details are shown in the [Supplementary Table S3](#).

Follow-up

The median follow-up duration was 570 days (IQR: 447–691 days). The 1-year survival rates for no mass/pseudomass, thrombus, benign tumor, and malignant tumor groups were 100, 88.9, 100, and 80.6%, respectively. Patients in the malignant group had a lower survival rate compared to patients in the benign group ($P = 0.014$, [Figure 3](#)).

Reproducibility

The inter- and intra-observer reproducibility values were excellent for all qualitative and quantitative indexes ([Supplementary Table S3](#)).

Discussion

CE is a useful tool for patients with suspected cardiac masses. In the present study, the diagnostic sensitivity and specificity of CE were high when differentiating cardiac tumors from non-neoplastic cardiac masses. At the same time, CE was superior

to conventional TTE and comparable to pathologic analysis for differentiating malignant tumors from benign tumors. To the best of our knowledge, this is the first multicenter diagnostic study of CE in patients with suspected cardiac masses.

Cardiac masses are often encountered during clinical practice. They can be serious or even life-threatening. Improving the diagnostic efficiency of cardiac mass is an urgent goal of radiologists. TTE, transesophageal echocardiography, and CMR are commonly used in diagnostic procedures. Currently, CMR is the hottest topic in cardiac mass research. Several retrospective studies have shown that the CMR features demonstrate excellent accuracy for the differentiation of cardiac thrombi from tumors and can be helpful for the distinction of benign and malignant neoplasms ([24](#), [30–34](#)). A prospective CMR study has demonstrated that tumor size (>3.25 cm), invasion, and first-pass perfusion are useful imaging characteristics in differentiating benign from malignant tumors ([35](#)). Another prospective CMR study has revealed that invasiveness, irregular border, and late heterogeneous gadolinium enhancement are better variables for differentiating benign and malignant tumors ([36](#)). However, all of the above studies were limited to qualitative or semi-quantitative analysis. Therefore, a diagnostic imaging technique with quantitative parameters is urgently

TABLE 2 Comparison of echocardiographic parameters between thrombus and tumor.

	Thrombus (<i>n</i> = 36)	Tumor (<i>n</i> = 66)	<i>P</i> value	Univariate regression		Multivariate regression*	
				OR (95%CI)	<i>P</i> value	OR (95%CI)	<i>P</i> value
Area, mean (SD), mm ²	966.5 (378.4)	1,484.5 (783.4)	<0.001	1.001 (1.000–1.002)	0.001	1.00 (0.99–1.01)	0.188
Echogenicity			0.008	3.08 (1.31–7.21)	0.010	2.31 (0.51–10.43)	0.278
Uniform	24	26					
Non-uniform	12	40					
Boundary			0.143	1.95 (0.79–4.80)	0.147		
Well-demarcated	27	40					
Not well-demarcated	9	26					
Base			<0.001	21.69 (4.81–97.86)	<0.001	7.53 (1.10–51.56)	0.040
Narrow with peduncle	0	17					
Narrow with notch	34	12					
Broad	2	37					
Mass perfusion			<0.001	0.24 (0.06–0.93)	0.040	1.44 (0.18–11.38)	0.731
No perfusion	23	0					
Mild perfusion	10	29					
Intense Perfusion	3	37					
Motility			0.097	2.33 (0.84–6.46)	0.103		
Absent	30	45					
Present	6	21					
Pericardial effusion			0.275	1.71 (0.69–4.24)	0.244		
Absent	27	42					
Present	9	24					
Enhancement A1/A2, median (IQR)	0.05 (0.04–0.17)	1.16 (0.71–1.88)	<0.001	38.82 (8.33–180.93)	<0.001	20.09 (4.17–96.72)	<0.001

CI, confidence interval; IQR, interquartile range; OR, odds ratio; SD, standard deviation. * variables entered into the multivariate regression included area, echogenicity, base, mass perfusion, and enhancement A1/A2.

TABLE 3 Comparison of diagnostic performance in differentiating thrombus from cardiac tumor.

	Sensitivity	Specificity	AUC	Accuracy	PPV	NPV
Combined qualitative and quantitative analysis	100% (94.6%–100%)	100% (90.3%–100%)	1.000 (0.964–1.000)	100% (96.5%–100%)	100%	100%
Using A1/A2 alone (Cutoff value = 0.295)	100% (94.6%–100%)	91.7% (77.5%–98.3%)	0.958 (0.899–0.988)	97.1% (91.6%–99.4%)	95.7% (88.2%–98.5%)	100%

AUC, the area under the receiver operating characteristic curve; NPV, negative predictive value; PPV, positive predictive value.

needed to share the burden of CMR and to reduce pathology specialist workload.

At present, TTE is still the first diagnostic procedure used to evaluate cardiac masses. Conventional TTE usually assesses the following characteristics of cardiac masses: site, base, mortality, and echogenicity. However, cardiac tumors, especially differentiating benign and malignant tumors, are very challenging to analyze using conventional TTE. An accurate diagnosis based on qualitative information depends more on the experience of the radiologist. To address this issue, CE

has become an indispensable part of echocardiography with rapid development in the recent decade (37). The application of ultrasound enhancing agents based on conventional TTE can clearly display the endocardial boundary of the left ventricle and improve the accuracy of the left ventricular ejection fraction measurement (13). CE data can also be quantitatively analyzed. Kirkpatrick et al. have published the first study that demonstrated the diagnostic utility of A1 and A2 values using CE in cardiac masses in 2004 (38). Since then, several radiologists have shared their diagnosis experiences

TABLE 4 Comparison of echocardiographic parameters between malignant tumor and benign tumor.

	Benign tumor (<i>n</i> = 30)	Malignant tumor (<i>n</i> = 36)	<i>P</i> value	Univariate regression		Multivariate regression*	
				OR (95%CI)	<i>P</i> value	OR (95%CI)	<i>P</i> value
Area, mean (SD), mm ²	1,153.98 (721.68)	1,759.86 (732.47)	<0.001	1.001 (1.0004–1.002)	0.003	1.003 (1.00003–1.005)	0.023
Echogenicity			0.034	2.97 (1.07–8.26)	0.037	2.30 (1.00003–1.005)	0.487
Uniform	16	10					
Non-uniform	14	26					
Boundary			0.015	3.67 (1.26–10.70)	0.017	24.46 (0.94–636.52)	0.055
Well-demarcated	23	17					
Not well-demarcated	7	19					
Base			<0.001	16.43 (4.86–55.55)	<0.001	22.64 (1.30–395.21)	0.033
Narrow with peduncle	15	2					
Narrow with notch	8	4					
Broad	7	30					
Mass perfusion			0.057	2.62 (0.96–7.12)	0.060		
Mild perfusion	17	12					
Intense Perfusion	13	24					
Motility			0.018	0.28 (0.09–0.82)	0.021	2.05 (0.15–28.56)	0.592
Absent	16	29					
Present	14	7					
Pericardial effusion			0.071	2.94 (0.94–8.57)	0.077		
Absent	23	19					
Present	7	17					
Enhancement A1/A2, median (IQR)	0.73 (0.25)	1.76 (0.61)	<0.001	84.07 (10.18–694.37)	<0.001	165.39 (4.68–5850.94)	0.005

CI, confidence interval; IQR, interquartile range; OR, odds ratio; SD, standard deviation. * variables entered into the multivariate regression included area, echogenicity, boundary, base, motility, and enhancement A1/A2.

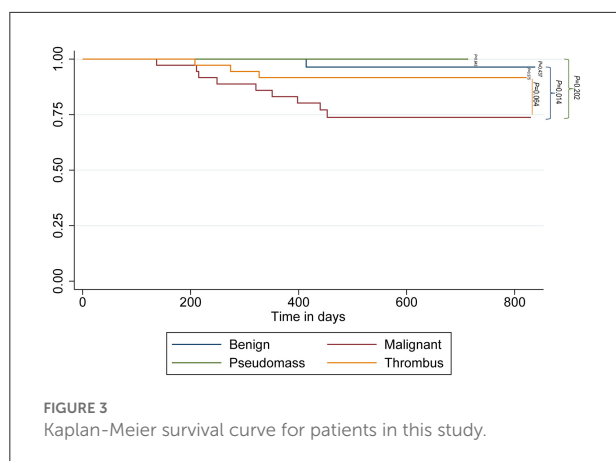
TABLE 5 Comparison of diagnostic performance in differentiating malignant tumor from benign tumor.

	Sensitivity	Specificity	AUC	Accuracy	PPV	NPV
Combined qualitative and quantitative analysis	97.2% (85.5–99.9%)	93.3% (77.9–99.2%)	0.953 (0.870–0.990)	95.5% (87.3–99.1%)	94.6% (82.1–98.5%)	96.6% (80.2–99.5%)
Area alone (Cutoff value = 1,302.2)	75.0% (57.8–87.9%)	70.0% (50.6–85.3%)	0.725 (0.601–0.828)	72.7% (60.4–83.0%)	75.0% (62.7–84.2%)	70.0% (55.8–81.1%)
Using A1/A2 alone (Cutoff value = 1.00)	83.3% (67.2–93.6%)	83.3% (65.3–94.4%)	0.833 (0.721–0.914)	83.3% (72.1–91.4%)	85.7% (72.7–93.1%)	80.6% (66.4–89.8%)
Using A1/A2 alone (Cutoff value = 1.28)	80.6% (64.0–91.8%)	96.7% (82.8–99.9%)	0.886 (0.784–0.951)	87.9% (77.5–94.6%)	96.7% (80.7–99.5%)	80.7% (68.0–89.0%)

AUC, the area under the receiver operating characteristic curve; NPV, negative predictive value; PPV, positive predictive value.

using CE to identify cardiac masses (12, 17, 23, 26, 27, 39–41). Five of these studies have provided the evidence for the indispensable differential diagnostic value of A1/A2 (12, 26, 27, 38, 40). Xia et al. have found a significant difference in A1/A2 between malignant and benign tumors ($1.34 \pm$

0.43 vs. 0.65 ± 0.17 , $P < 0.01$) (12). Mao et al. have revealed that $A1/A2 > 1$ had a high diagnostic accuracy in differentiation of a benign mass from a malignant metastatic tumor in a cohort study (27). Furthermore, $A1/A2 > 1$ was a significant and independent predictor of future death in patients



with cardiac masses and a history of extracardiac malignant tumors (27).

Differentiation between cardiac tumors and thrombi

The present study found that CE had an excellent accuracy in the diagnosis of intracardiac thrombi. Setting A1/A2 with a cutoff value of 1 had a 91.7% specificity and nearly 100% sensitivity when diagnosing a thrombus. Interestingly, the A1/A2 value for most thrombi was around zero. However, three cases had a much higher A1/A2 (1.91, 2.12, and 1.85, respectively), likely because these three cases were fresh thrombi. The loose texture of a fresh thrombus and the ability of the ultrasound-enhancing agents to enter from the periphery at the beginning of CE result in a higher A1/A2, which is consistent with a previous study (19). Conversely, the texture of an old thrombus is dense, and the microbubbles of the ultrasound-enhancing agents cannot enter, resulting in A1/A2 values close to zero. Differentiation of a fresh thrombus from an old thrombus has important clinical value: a fresh thrombus is easier to remove than an old one (42). A fresh thrombus is also less fixed to the left ventricular wall and more fragile because of its collagen-poor organization (43). The risk of fresh thrombus shedding should be evaluated with great care.

Another perfusion phenomenon was demonstrated by Uenishi et al. (23). They found that ultrasound-enhancing agents often do not enter the interior of the thrombus (81.8%, 27/33) or only stay at its periphery (12.1%, 4/33). The ultrasound enhancing agents usually perfuse the periphery of the cardiac tumor (44.7%, 21/47) or even the entire tumor (48.9%, 23/47). The perfusion patterns identified in the present study and the findings by Uenishi et al. require more samples to confirm in the future (23).

Differentiation between cardiac tumors and thrombi

The present study combined CE quantitative parameters with qualitative echocardiographic assessment to improve the diagnostic accuracy of cardiac tumors compared to our previous study (26). The resulting accuracy was comparable to that of CMR (accuracy = 98.4%) (34).

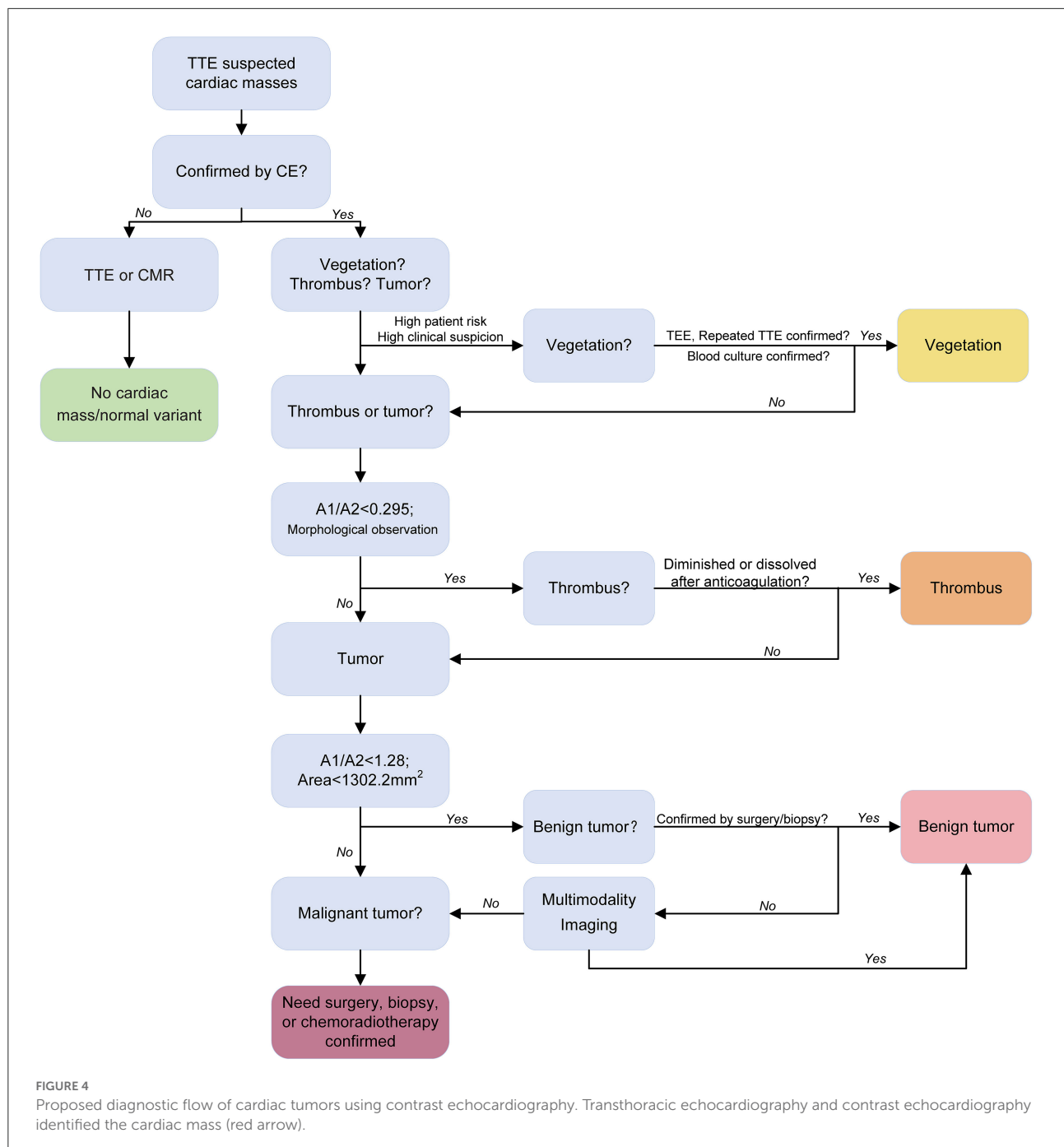
CE can improve the image quality and assess the blood supply inside the tumor. Benign tumors often have sparse blood supply, while malignant tumors have rich blood supply (44, 45). Previous studies have usually used 1.0 as the cutoff value for A1/A2 to differentiate malignant tumors from benign tumors (26, 38, 40). However, benign tumors may have an A1/A2 which is close to or slightly more than 1 [1.32 in a hemangioma (38), 1.08 in a rhabdomyoma, 0.84 in a fibroma, 0.92 in a hemangioma (40), and 1.06–1.15 in myxomas (26)]. Some malignant tumors containing necrotic tissue result in an A1/A2 of <1 [3.6%, 2/55 in Mao et al. (27)]. The present results revealed that 1.28 is better than 1 as the cutoff value for A1/A2 to differentiate malignant tumors from benign tumors. For less experienced radiologists, only using A1/A2 with a cutoff value of 1.28 would achieve a good diagnostic result. The tumor area/size is also helpful during differentiation, which is consistent with a previous study (35).

The strengths of the present study include the novelty of the diagnostic approach to differentiate cardiac masses, prospective study design, and relatively large sample size. Simple, quick, highly repeatable quantitative parameter (A1/A2) is of great help for clinical diagnosis, especially for radiologists who do not have much experience in diagnosing cardiac masses using TTE. The proposed diagnostic flow for cardiac tumors using CE is shown in Figure 4.

Other modalities

TEE can also be useful in the diagnosis of cardiac masses. Several previous studies have shown that the use of ultrasound-enhancing agents can increase the diagnostic accuracy of cardiac thrombi in a TEE exam for atrial fibrillation patients (46–48). Xia et al. have found that the combination of TEE and CE was feasible for the detection of suspected cardiac masses with an accuracy of 97.8–100%, especially in diagnosing and differentiating between benign and malignant lesions (12).

Cardiac CT may offer an alternative to CMR, especially when other imaging modalities are non-diagnostic or contraindicated (9, 49). Compared to other cardiac imaging modalities, cardiac CT is optimal for the evaluation of calcified masses (9, 49). Disadvantages of cardiac CT include radiation exposure, low risk of contrast-induced nephropathy, and limited soft tissue and temporal resolutions compared to magnetic resonance imaging (9). Several studies have revealed



that cardiac CT can differentiate between cardiac tumors and thrombi (50–53). A prospective study with a large sample is needed to confirm this finding.

Limitations

The present study had several limitations. First, the study only included 36 patients with a thrombus and 66 patients with

a cardiac tumor. The incidence of primary malignant cardiac tumor is extremely low. Only three cases were included in the study. Therefore, the limited spectrum of the cardiac tumor represents a limitation. Second, the participating hospitals in this study were tertiary. Intracardiac thrombus with a well-demarcated boundary, broad base, and low echocardiographic suspicion is usually treated at secondary hospitals instead of transferring to our hospitals. Therefore, most thrombi in the present study were atypical and without a broad base. Third, due

to the low number of pseudomass cases in the study, more cases need to be included in future analyses. Finally, the recruitment period for patients was short. Long-term follow-up may be needed to determine whether A1/A2 can predict the prognosis for patients with cardiac tumors. Fourth, the study analysis did not explore the diagnostic performance of CE performed by less experienced radiologists (54). The experience with CE may be an underlying confounder in this study.

Conclusion

In summary, CE has the potential to accurately differentiate cardiac masses by combining qualitative and quantitative analyses. However, more studies with a large sample size should be conducted to further confirm the present study findings.

Data availability statement

The original contributions presented in the study are included in the article/**Supplementary material**, further inquiries can be directed to the corresponding author/s.

Ethics statement

The studies involving human participants were reviewed and approved by the Ethics Committee of Shengjing Hospital of China Medical University. Written informed consent to participate in this study was provided by the participants' legal guardian/next of kin. Written informed consent was obtained from the individual(s), and minor(s)' legal guardian/next of kin, for the publication of any potentially identifiable images or data included in this article.

References

1. Basso C, Rizzo S, Valente M, Thiene G. Cardiac masses and tumours. *Heart*. (2016) 102:1230–45. doi: 10.1136/heartjnl-2014-306364
2. Aggelis C, Dimitroglou Y, Raftopoulos L, Sarri G, Mavrogeni S, Wong J, et al. Cardiac masses: the role of cardiovascular imaging in the differential diagnosis. *Diagnostics*. (2020) 10:1088. doi: 10.3390/diagnostics10121088
3. Melo MD, Paiva MG, Santos MV, Rochitte CE, Moreira VD, Saleh MH, et al. Brazilian position statement on the use of multimodality imaging in cardio-oncology - 2021. *Arq Bras Cardiol*. (2021) 117:845–909.
4. Basso C, Rizzo S, Valente M, Thiene G. Prevalence and pathology of primary cardiac tumours. *TIC*. (2012) 6:8.
5. Maleszewski JJ, Anavekar NS, Moynihan TJ, Klarich KW. Pathology, imaging, and treatment of cardiac tumours. *Nat Rev Cardiol*. (2017) 14:536–49. doi: 10.1038/nrcardio.2017.47
6. Burke A, Tavora F. The 2015 WHO classification of tumors of the heart and pericardium. *J Thorac Oncol*. (2016) 11:441–52. doi: 10.1016/j.jtho.2015.11.009
7. Nomoto N, Tani T, Konda T, Kim K, Kitai T, Ota M, et al. Primary and metastatic cardiac tumors: echocardiographic diagnosis, treatment and prognosis in a 15-years single center study. *J Cardiothorac Surg*. (2017) 12:103. doi: 10.1186/s13019-017-0672-7
8. Joshi M, Kumar S, Noshirwani A, Harky A. The current management of cardiac tumours: a comprehensive literature review. *Braz J Cardiovasc Surg*. (2020) 35:770–80. doi: 10.21470/1678-9741-2019-0199
9. Tyebally S, Chen D, Bhattacharyya S, Mughrabi A, Hussain Z, Manisty C, et al. Cardiac tumors: JACC cardiooncology state-of-the-art review. *JACC CardioOncol*. (2020) 2:293–311. doi: 10.1016/j.jacc.2020.05.009
10. Patel R, Lim RP, Saric M, Nayar A, Babb J, Ettel M, et al. Diagnostic performance of cardiac magnetic resonance imaging and echocardiography in evaluation of cardiac and paracardiac masses. *Am J Cardiol*. (2016) 117:135–40. doi: 10.1016/j.amjcard.2015.10.014
11. Meng Q, Lai H, Lima J, Tong W, Qian Y, Lai S. Echocardiographic and pathologic characteristics of primary cardiac tumors: a study of 149 cases. *Int J Cardiol*. (2002) 84:69–75. doi: 10.1016/S0167-5273(02)00136-5
12. Xia H, Gan L, Jiang Y, Tang Q, Zhang P, Tang X, et al. Use of transesophageal echocardiography and contrast echocardiography in the evaluation of cardiac masses. *Int J Cardiol*. (2017) 236:466–72. doi: 10.1016/j.ijcard.2017.01.073
13. Porter TR, Mulvagh SL, Abdelmoneim SS, Becher H, Belcik JT, Bierig M, et al. Clinical applications of ultrasonic enhancing agents in echocardiography: 2018 american society of echocardiography guidelines update. *J Am Soc Echocardiogr*. (2018) 31:241–74. doi: 10.1016/j.echo.2017.11.013

Author contributions

All authors listed have made a substantial, direct, and intellectual contribution to the work and approved it for publication.

Funding

This study has received funding by the New Medical Technology Project of Shengjing Hospital (2017–029).

Conflict of interest

The authors declare that the research was conducted in the absence of any commercial or financial relationships that could be construed as a potential conflict of interest.

Publisher's note

All claims expressed in this article are solely those of the authors and do not necessarily represent those of their affiliated organizations, or those of the publisher, the editors and the reviewers. Any product that may be evaluated in this article, or claim that may be made by its manufacturer, is not guaranteed or endorsed by the publisher.

Supplementary material

The Supplementary Material for this article can be found online at: <https://www.frontiersin.org/articles/10.3389/fcvm.2022.1011560/full#supplementary-material>

14. Gaibazzi N, Giumelli C, Martella EM, Passeri G. Contrast-echocardiography for the differential diagnosis of atrial masses. *Eur Heart J*. (2013) 34:1957. doi: 10.1093/eurheartj/ehd091
15. Bhattacharyya S, Khattar R, Senior R. Characterisation of intra-cardiac masses by myocardial contrast echocardiography. *Int J Cardiol*. (2013) 163:e11–3. doi: 10.1016/j.ijcard.2012.06.098
16. Abdelmoneim SS, Pellikka PA, Mulvagh SL. Contrast echocardiography for assessment of left ventricular thrombi. *J Ultrasound Med*. (2014) 33:1337–44. doi: 10.7863/ultra.33.8.1337
17. Barchitta A, Basso C, Piovesana PG, Antonini-Canterin F, Ruzza L, Bianchi A, et al. Opacification patterns of cardiac masses using low-mechanical index contrast echocardiography: comparison with histopathological findings. *Cardiovasc Pathol*. (2017) 30:72–7. doi: 10.1016/j.carpath.2017.06.006
18. Yin LX, Ma CY, Wang S, Wang YH, Meng PB, Pan XF, et al. Reference values of carotid ultrafast pulse-wave velocity: a prospective, multicenter, population-based study. *J Am Soc Echocardiogr*. (2021) 34:629–41. doi: 10.1016/j.echo.2021.01.003
19. Li Y, Wang X, Ren W, Xiao Y, Yu X, Tan X. Cardiac thrombotic stability determined by contrast-enhanced echocardiography: investigative protocol and preliminary results. *BMC Cardiovasc Disord*. (2021) 21:267. doi: 10.1186/s12872-021-02085-4
20. Lang RM, Bierig M, Devereux RB, Flachskampf FA, Foster E, Pellikka PA, et al. Recommendations for chamber quantification. *Eur J Echocardiogr*. (2006) 7:79–108. doi: 10.1016/j.euje.2005.12.014
21. Senior R, Becher H, Monaghan M, Agati L, Zamorano J, Vanoverschelde JL, et al. Clinical practice of contrast echocardiography: recommendation by the European Association of Cardiovascular Imaging (EACVI) 2017. *Eur Heart J Cardiovasc Imaging*. (2017) 18:1205–1205af. doi: 10.1093/ehjci/jex182
22. Park SB, Kang DH, Choi CW, Kim HW, Kim SJ. Clinical outcomes of ligation-assisted endoscopic resection for duodenal neuroendocrine tumors. *Medicine*. (2018) 97:e0533. doi: 10.1097/MD.00000000000010533
23. Uenishi EK, Caldas MA, Tsutsui JM, Abduch MC, Sbrano JC, Kalil Filho R, et al. Evaluation of cardiac masses by real-time perfusion imaging echocardiography. *Cardiovasc Ultrasound*. (2015) 13:23. doi: 10.1186/s12947-015-0018-3
24. Pazos-Lopez P, Pozo E, Siqueira ME, Garcia-Lunar I, Cham M, Jacobi A, et al. Value of CMR for the differential diagnosis of cardiac masses. *JACC Cardiovasc Imaging*. (2014) 7:896–905. doi: 10.1016/j.jcmg.2014.05.009
25. Wienczek JG, Feinstein SB, Walker R, Aronson S. Pitfalls in quantitative contrast echocardiography: the steps to quantitation of perfusion. *J Am Soc Echocardiogr*. (1993) 6:395–416. doi: 10.1016/S0894-7317(14)80239-3
26. Wang X, Li Y, Ren W, Yu X, Tan X. Clinical diagnostic value of contrast-enhanced ultrasonography in the diagnosis of cardiac masses: A pilot study. *Echocardiography*. (2020) 37:231–8. doi: 10.1111/echo.14597
27. Mao YH, Deng YB, Liu YN, Wei X, Bi XJ, Tang QY, et al. Contrast echocardiographic perfusion imaging in clinical decision-making for cardiac masses in patients with a history of extracardiac malignant tumor. *JACC Cardiovasc Imaging*. (2019) 12:754–6. doi: 10.1016/j.jcmg.2018.08.033
28. Poterucha TJ, Kochav J, O'Connor DS, Rosner GF. Cardiac tumors: clinical presentation, diagnosis, and management. *Curr Treat Options Oncol*. (2019) 20:66. doi: 10.1007/s11864-019-0662-1
29. Stratton JR, Lighty GW, Pearlman AS, Ritchie JL. Detection of left ventricular thrombus by two-dimensional echocardiography: sensitivity, specificity, and causes of uncertainty. *Circulation*. (1982) 66:156–66. doi: 10.1161/01.CIR.66.1.156
30. Giusca S, Meres D, Ochs A, Buss S, Andre F, Seitz S, et al. Incremental value of cardiac magnetic resonance for the evaluation of cardiac tumors in adults: experience of a high volume tertiary cardiology centre. *Int J Cardiovasc Imaging*. (2017) 33:879–88. doi: 10.1007/s10554-017-1065-7
31. Caspar T, El Ghannudi S, Ohana M, Labani A, Lawson A, Ohlmann P, et al. Magnetic resonance evaluation of cardiac thrombi and masses by T1 and T2 mapping: an observational study. *Int J Cardiovasc Imaging*. (2017) 33:551–9. doi: 10.1007/s10554-016-1034-6
32. Mousavi N, Cheezum MK, Aghayev A, Padera R, Vita T, Steigner M, et al. Assessment of cardiac masses by cardiac magnetic resonance imaging: histological correlation and clinical outcomes. *J Am Heart Assoc*. (2019) 8:e007829. doi: 10.1161/JAHA.117.007829
33. Beroukhi RS, Ghelani S, Ashwath R, Balasubramanian S, Biko DM, Buddhe S, et al. Accuracy of cardiac magnetic resonance imaging diagnosis of pediatric cardiac masses: a multicenter study. *JACC Cardiovasc Imaging*. (2021) 15:1391–405. doi: 10.1016/j.jcmg.2021.07.010
34. Shenoy C, Grizzard JD, Shah DJ, Kassi M, Reardon MJ, Zagurovskaya M, et al. Cardiovascular magnetic resonance imaging in suspected cardiac tumour: a multicentre outcomes study. *Eur Heart J*. (2021) 43:71–80. doi: 10.1093/eurheartj/ehab635
35. Kassi M, Polsani V, Schutt RC, Wong S, Nabi F, Reardon MJ, et al. Differentiating benign from malignant cardiac tumors with cardiac magnetic resonance imaging. *J Thorac Cardiovasc Surg*. (2019) 157:1912–22.e2. doi: 10.1016/j.jtcvs.2018.09.057
36. Yue P, Xu Z, Wan K, Xie X, Ji S, Sun J, et al. Differential and prognostic value of cardiovascular magnetic resonance derived scoring algorithm in cardiac tumors. *Int J Cardiol*. (2021) 331:281–8. doi: 10.1016/j.ijcard.2021.01.068
37. J.R. Lindner. Contrast echocardiography: current status and future directions. *Heart*. (2021) 107:18–24. doi: 10.1136/heartjnl-2020-316662
38. Kirkpatrick JN, Wong T, Bednarz JE, Spencer KT, Sugeng L, Ward RP, et al. Differential diagnosis of cardiac masses using contrast echocardiographic perfusion imaging. *J Am Coll Cardiol*. (2004) 43:1412–9. doi: 10.1016/j.jacc.2003.09.065
39. Mansencal N, Revault-d'Alphonse L, Pelage JP, Farcot JC, Lacombe P, Dubourg O. Usefulness of contrast echocardiography for assessment of intracardiac masses. *Arch Cardiovasc Dis*. (2009) 102:177–83. doi: 10.1016/j.acvd.2008.12.007
40. Tang QY, Guo LD, Wang WX, Zhou W, Liu YN, Liu HY, et al. Usefulness of contrast perfusion echocardiography for differential diagnosis of cardiac masses. *Ultrasound Med Biol*. (2015) 41:2382–90. doi: 10.1016/j.ultrasmedbio.2015.05.010
41. Ren M, Huang L, Ye X, Xv Z, Ouyang C, Han Z. Evaluation of Cardiac Space-Occupying Lesions by Myocardial Contrast Echocardiography and Transesophageal Echocardiography. *J Healthc Eng*. (2022) 2022:2066033. doi: 10.1155/2022/2066033
42. Niemann M, Gaudron PD, Bijns B, Stork S, Beer M, Hillenbrand H, et al. Differentiation between fresh and old left ventricular thrombi by deformation imaging. *Circ Cardiovasc Imaging*. (2012) 5:667–75. doi: 10.1161/CIRCIMAGING.112.974964
43. Brass LF, Newman DK, Wannemacher KM, Zhu L, Stalker TJ. Signal transduction during platelet plug formation. *Platelets*. (2013) 23:19–46. doi: 10.1016/B978-012369367-9/50778-3
44. Taqui S, Ferencik M, Davidson BP, Belcik JT, Moccetti F, Layoun M, et al. Coronary microvascular dysfunction by myocardial contrast echocardiography in nonelderly patients referred for computed tomographic coronary angiography. *J Am Soc Echocardiogr*. (2019) 32:817–25. doi: 10.1016/j.echo.2019.03.001
45. Lee DZJ, Chan RH, Montazeri M, Hoss S, Adler A, Nguyen ET, et al. Left ventricular apical aneurysms in hypertrophic cardiomyopathy: equivalent detection by magnetic resonance imaging and contrast echocardiography. *J Am Soc Echocardiogr*. (2021) 34:1262–72. doi: 10.1016/j.echo.2021.07.015
46. von der Recke G, Schmidt H, Illien S, Lüderitz B, Omran H. Use of transesophageal contrast echocardiography for excluding left atrial appendage thrombi in patients with atrial fibrillation before cardioversion. *J Am Soc Echocardiogr*. (2002) 15:1256–61. doi: 10.1067/mje.2002.123961
47. Jung PH, Mueller M, Schuhmann C, Eickhoff M, Schneider P, Seemueller G, et al. Contrast enhanced transesophageal echocardiography in patients with atrial fibrillation referred to electrical cardioversion improves atrial thrombus detection and may reduce associated thromboembolic events. *Cardiovasc Ultrasound*. (2013) 11:1. doi: 10.1186/1476-7120-11-1
48. Ebelt H, Offhaus A, Wiora M, Roehl P, Schwenzky A, Weida A, et al. Impact of ultrasound contrast agent on the detection of thrombi during transesophageal echocardiography. *Open Heart*. (2019) 6:e001024. doi: 10.1136/openhrt-2019-001024
49. Kassop D, Donovan MS, Cheezum MK, Nguyen BT, Gambill NB, Blankstein R, et al. Cardiac masses on cardiac CT: a review. *Curr Cardiovasc Imaging Rep*. (2014) 7:9281. doi: 10.1007/s12410-014-9281-1
50. Hong YJ, Hur J, Kim YJ, Lee HJ, Hong SR, Suh YJ, et al. Dual-energy cardiac computed tomography for differentiating cardiac myxoma from thrombus. *Int J Cardiovasc Imaging*. (2014) 30:121–8. doi: 10.1007/s10554-014-0490-0
51. Hong YJ, Hur J, Han K, Im DJ, Suh YJ, Lee HJ, et al. Quantitative analysis of a whole cardiac mass using dual-energy computed tomography: comparison with conventional computed tomography and magnetic resonance imaging. *Sci Rep*. (2018) 8:15334. doi: 10.1038/s41598-018-33635-0
52. Qian WL, Jiang Y, Liu X, Guo YK, Li Y, Tang X, et al. Distinguishing cardiac myxomas from cardiac thrombi by a radiomics signature based on cardiovascular contrast-enhanced computed tomography images. *BMC Cardiovasc Disord*. (2021) 21:152. doi: 10.1186/s12872-021-01961-3
53. Lee JW, Park CH, Im DJ, Lee KH, Kim TH, Han K, et al. CT-based radiomics signature for differentiation between cardiac tumors and a thrombus: a retrospective, multicenter study. *Sci Rep*. (2022) 12:8173. doi: 10.1038/s41598-022-12229-x
54. Wei Q, Yan YJ, Wu GG, Ye XR, Jiang F, Liu J, et al. The diagnostic performance of ultrasound computer-aided diagnosis system for distinguishing breast masses: a prospective multicenter study. *Eur Radiol*. (2022) 32:4046–55. doi: 10.1007/s00330-021-08452-1



OPEN ACCESS

EDITED BY

Francesca Innocenti,
Careggi University Hospital, Italy

REVIEWED BY

Robert Naeije,
Université libre de Bruxelles, Belgium
Jan Edvin Engvall,
Linköping University Hospital, Sweden

*CORRESPONDENCE

François Bagate
francois.bagate@aphp.fr

SPECIALTY SECTION

This article was submitted to
Cardiovascular Imaging,
a section of the journal
Frontiers in Cardiovascular Medicine

RECEIVED 19 May 2022

ACCEPTED 06 September 2022

PUBLISHED 26 September 2022

CITATION

Bagate F, Coppens A, Masi P,
de Prost N, Carteaux G, Razzi K and
Mekontso Dessap A (2022) Cardiac
and vascular effects of low-dose
steroids during the early phase
of septic shock: An echocardiographic
study.
Front. Cardiovasc. Med. 9:948231.
doi: 10.3389/fcvm.2022.948231

COPYRIGHT

© 2022 Bagate, Coppens, Masi, de
Prost, Carteaux, Razzi and Mekontso
Dessap. This is an open-access article
distributed under the terms of the
[Creative Commons Attribution License
\(CC BY\)](#). The use, distribution or
reproduction in other forums is
permitted, provided the original
author(s) and the copyright owner(s)
are credited and that the original
publication in this journal is cited, in
accordance with accepted academic
practice. No use, distribution or
reproduction is permitted which does
not comply with these terms.

Cardiac and vascular effects of low-dose steroids during the early phase of septic shock: An echocardiographic study

François Bagate^{1,2*}, Alexandre Coppens¹, Paul Masi^{1,2},
Nicolas de Prost^{1,2,3}, Guillaume Carteaux^{1,2,3}, Keyvan Razzi^{1,2}
and Armand Mekontso Dessap^{1,2,3}

¹AP-HP, CHU Henri Mondor, DHU A-TVH, Service de Médecine Intensive Réanimation, Créteil, France, ²Université Paris Est Créteil, Faculté de Médecine, Groupe de Recherche Clinique CARMAS, Créteil, France, ³INSERM U955, Institut Mondor de Recherche Biomédicale, Créteil, France

Background: Low-dose steroids are known to increase arterial pressure during septic shock through restoration of vasopressor response to norepinephrine. However, their effects on cardiac performance and ventriculo-arterial coupling (VAC) have never been scrutinized during human septic shock. The aim of this study was to perform a comprehensive description of the cardiovascular effects of low-dose steroids using modern echocardiographic tools (including speckle tracking imaging).

Methods: This prospective study was conducted in the intensive care unit (ICU) of a university hospital in France. Consecutive adult patients admitted for septic shock and requiring low-dose steroid therapy were prospectively enrolled within 24 h of septic shock onset. We recorded hemodynamic and echocardiographic data to explore left ventricle (LV) contractility, loading conditions and VAC just before the initiation of low-dose steroids (50 mg intravenous hydrocortisone plus 50 µg enteral fludrocortisone) and 2–4 h after.

Results: Fifty patients [65 (55–73) years; 33 men] were enrolled. Arterial pressure, heart rate, almost all LV afterload parameters, and most cardiac contractility parameters significantly improved after steroids. VAC improved with steroid therapy and less patients had uncoupled VAC (> 1.36) after (24%) than before (44%) treatment.

Conclusion: In this comprehensive echocardiographic study, we confirmed an improvement of LV afterload after initiation of low-dose steroids. We also observed an increase in LV contractility with improved cardiovascular efficiency (less uncoupling with decreased VAC).

KEYWORDS

low-dose steroid therapy, hydrocortisone, fludrocortisone, septic shock, echocardiography, global longitudinal strain, ventriculo-arterial coupling

Introduction

Relative adrenal insufficiency, also appraised as critical illness-related corticosteroid insufficiency is common during septic shock. It is the main pathophysiological rationale for the use of low-dose corticosteroid therapy in septic shock (1). The anti-inflammatory (2) and vasoactive (3) properties of corticosteroids have been well known for several decades. Several studies have demonstrated the peripheral vascular effects of low-dose steroids in septic shock, including an increase in mean arterial pressure (MAP) through restoration of systemic vascular resistance and enhanced vasopressor response to norepinephrine (4–8).

In addition to vasoplegia, septic shock is also characterized by myocardial dysfunction, with a major interaction between contractility and loading conditions (9). Animal models of sepsis suggest a protective role for low-dose hydrocortisone in myocardial injury (10). However, the effect of low-dose steroids on cardiac performance has never been scrutinized during human septic shock. We hypothesized that low-dose steroid therapy may enhance cardiac contractility in addition to its vasopressive effects during human septic shock. Given the strong interaction between left ventricle (LV) contractility and loading conditions during human septic shock (9, 11), it is crucial to assess all components of cardiac performance in this setting. The aim of the present study was to perform a comprehensive description of the effect of low-dose steroid therapy on cardiac and vascular function (contractility, preload, and afterload, with their interactions) during human septic shock, using modern echocardiographic tools.

Abbreviations: MAP, mean arterial pressure; LV, left ventricle; ICU, intensive care unit; ACCP, American College of Chest Physicians; SCCM, Society of Critical Care Medicine; LVEF, left ventricular ejection fraction; IRB, institutional review board; TTE, left transthoracic echocardiography; PRICES, Preferred Reporting Items for Critical care Echocardiography Studies; E, early wave of transmitral diastolic blood flow; A, late wave of transmitral diastolic blood flow; e', tissue Doppler diastolic wave velocity at mitral valve annulus; VTI, velocity time integral; LVOT, left ventricle outflow tract; DAP, diastolic arterial pressure; E_a , end-systolic arterial elastance; DSI, diastolic shock index; s', tissue Doppler imaging, with peak systolic wave; LV-GLS, left ventricle global longitudinal peak systolic strain; E_{es} , left ventricle end-systolic maximal elastance; $E_{es(sb)}$, E_{es} estimated by the modified single-beat method; E_d , left ventricular end-diastolic elastance; P_d , diastolic arterial pressure; V_d , left ventricular volume at the onset of ejection; V_0 , volume axis intercept of the end-systolic pressure volume relation; V_{es} , left ventricular end-systolic volume; SV, stroke volume; $[E_{nd(est)}]$, non-invasive estimated normalized left ventricular elastance at the onset of ejection; $[E_{nd(avg)}]$, group-average normalized left ventricular elastance at the onset of ejection; VAC, ventricular-arterial coupling; CPI, cardiac power index; $LVEF_{EA}$, LVEF adjusted by E_a ; SOFA, Sequential Organ Failure Assessment; SAPS, Simplified Acute Physiologic Score; ARDS, of acute respiratory distress syndrome; SD, standard deviation.

Materials and methods

Patients

We conducted a prospective observational monocenter study in the medical intensive care unit (ICU) of Henri Mondor University Hospital, Créteil, France, between August 8, 2018 and May 29, 2021. All consecutive patients admitted during this period for septic shock (as defined according to the American College of Chest Physicians (ACCP)/Society of Critical Care Medicine (SCCM) Consensus Conference (12) and requiring low-dose steroid therapy, according to guidelines (13, 14), were prospectively enrolled within 24 h of septic shock onset. Non-inclusion criteria were age less than 18 years, pregnancy, patients under protection (guardianship, curators or safeguard of justice), chronic heart failure with reduced left ventricular ejection fraction (LVEF < 45%) documented in patient's history, severe valvular disease and prior corticosteroid therapy.

The study was approved on July 12, 2018 by the institutional ethics committee, Institutional Review Board (IRB) Mondor (reference number: 2201948) as a component of standard care, and patient consent was waived, as per French law. Written and oral information about the study was given to the families.

Treatment protocol

Norepinephrine was the first-choice vasopressor therapy (used to target a MAP of 65 mmHg or more); dobutamine was added, based on physician decision, in the presence of decreased LVEF (<45%) with ongoing signs of hypoperfusion despite adequate MAP and correction of hypovolemia with absence of fluid responsiveness. Catecholamine dose and fluid management were kept constant between the two ultrasound assessments, unless significant hemodynamic instability; patients who required a change in norepinephrine dose and/or fluid loading during the study protocol were secondarily excluded. The steroid replacement therapy consisted of hydrocortisone 50 mg intravenously every 6 h plus enteral fludrocortisone (50 µg/day). The patients were followed up until ICU discharge.

Echocardiography

Transthoracic echocardiography (TTE) was performed in early phase of septic shock after hemodynamic stabilization by trained operators (competent in advanced critical care echocardiography) (15). The TTE studies were performed on a GE Vivid S7 or E9 ultrasound system (GEMS, Buc, France), with a 1.5–4.5 MHz (M5S-D) transducer. The first TTE was performed at the initiation of steroid replacement therapy (just

before first intravenous bolus of hydrocortisone 50 mg plus enteral fludrocortisone 50 µg). The second TTE was performed 2–4 h after the initiation of low-dose steroid therapy. The echocardiographic results were reported based on the Preferred Reporting Items for Critical care Echocardiography Studies (PRICES) statement of the European Society of Intensive Care Medicine (16). All individual measurements were averaged over a minimum of three cardiac cycles (five to ten in case of non-sinus rhythm) and collected at end-expiration.

Assessment of contractility and loading conditions

Preload

Preload was assessed using estimates of LV filling pressures [E/A and E/e' ratios from pulsed-wave Doppler early (E) and late (A) and tissue Doppler early (e') diastolic wave velocity at the lateral and septal mitral valve annulus] (17) and respiratory variations of velocity time integral (VTI) of the left ventricle outflow tract (LVOT) as a surrogate of fluid responsiveness (18, 19).

Afterload

Afterload was assessed using the following indices: (i) diastolic arterial pressure (DAP) which is often used as a surrogate of LV afterload in clinical practice (20); (ii) systemic vascular resistance (the most commonly used measure of vascular tone) (21) = $\frac{80 \times \text{mean arterial pressure (mmHg)}}{\text{cardiac output (L.min}^{-1})}$; (iii) end-systolic arterial elastance (E_a), to reflect the pulsatile component of peripheral load (22) = $\frac{0.9 \times \text{systolic arterial pressure (mmHg)}}{\text{stroke volume (mL)}}$; (iv) diastolic shock index (DSI), that could reflect the severity of circulatory dysfunction during vasodilatory conditions = $\frac{\text{heart rate (bpm)}}{\text{diastolic arterial pressure (mmHg)}}$ (23); and (v) LV end-systolic wall stress (to reflect the combined effects of peripheral loading conditions and factors internal to the heart according to Laplace's principle) = $\frac{\text{Systolic arterial pressure (mmHg)} \times \text{left ventricle end-systolic volume (mL)}}{1000}$ (21).

Systolic function and left ventricular contractility

LV systolic function was assessed using indices obtained from the following techniques: (i) two-dimensional echocardiography, with LVEF (computed from LV volume using bi-plane Simpson method (24) when image quality was good, or visually estimated when poor image quality did not allow sufficient identification of the endocardium) (25); (ii) tissue Doppler imaging, with peak systolic wave (s') at the lateral and septal mitral valve annulus (26); (iii) speckle tracking imaging, with LV global longitudinal peak systolic strain (LV-GLS), derived from apical long-axis (three-, four- and two-chamber) clips obtained with a frame rate ≥ 50 Hz whenever possible with on-line analyses conducted by two trained

operators on the semi-automated EchoPAC package (GEMS, Buc, France); (iv) the LV end-systolic maximal elastance estimated by the modified single-beat method [$E_{es(sb)}$], as proposed by Chen et al. (27).

Description of left ventricle end-systolic maximal elastance using single-beat method

The LV end-systolic maximal elastance (E_{es}) is a major determinant of the LV systolic performance and the interaction between heart and vascular system. E_{es} corresponds to the slope of the end-systolic pressure-volume relation, which is classically invasively determined by catheter with LV pressures and volumes recorded under different cardiac loading conditions. Several alternatives have been proposed for estimating E_{es} without loading interventions, and these are generally referred to as single-beat methods [$E_{es(sb)}$]. The algorithm for $E_{es(sb)}$ proposed by Chen et al. (27) is based on the following steps and principles:

(a) If we consider LV elastances during isovolumic contraction [$E_d = P_d/(V_d - V_0)$] and at end systole [$E_{es(sb)} = P_{es}/(V_{es} - V_0)$], their ratio [$E_{Nd} = E_d/E_{es(sb)}$], called the time and amplitude normalized time varying elastance, has been shown to be conserved during the isovolumic contraction period in humans (28).

(b) If we consider the onset of ejection (end of isovolumic contraction) for E_d , then $E_{es(sb)}$ can be computed from (a) using E_{Nd} , stroke volume (which equals $V_d - V_{es}$), diastolic arterial pressure (which equals P_d) and systolic arterial pressure (which equals $P_{es}/0.9$), as follows: $E_{es(sb)} = [P_d - (E_{Nd} \times P_s \times 0.9)]/[SV \times E_{Nd}]$ (27).

(c) To estimate E_{Nd} , a regression model has been developed using systolic function (LVEF) and arterial load (ratio of arterial diastolic to systolic pressure), along with pre-ejection and ejection times, as follows: non-invasive estimated normalized left ventricular elastance at the onset of ejection [$E_{Nd(est)} = 0.0275 - 0.165 \times \text{LVEF} + 0.3656 \times (P_d/P_s) + 0.515 \times E_{Nd(avg)}$]; where $E_{Nd(avg)}$ (group-average normalized left ventricular elastance at the onset of ejection) = $\sum a_i \times t_{Nd}^i$; a_i values are 0.35695, -7.2266, 74.249, -307.39, 684.54, -856.92, 571.95, and -159.1 for $i = 0$ to $i = 7$, respectively; the t_{Nd} value is determined by the ratio of pre-ejection time (R-wave to flow onset) to total ejection time (R-wave to end-flow), with the time at onset defined by the aortic Doppler waveform (29).

Global function

We also assessed the heart-arterial interaction with the ventricular-arterial coupling (VAC) = $\frac{E_a}{E_{es(sb)}}$ (30), as suggested by recent guidelines (31); a VAC > 1.36 was considered as reflecting uncoupling with an alteration of LV ejection efficiency (32, 33). LV stroke volume, cardiac output and cardiac index were derived from LVOT diameter and VTI. We also assessed cardiac power index (CPI), a parameter of global cardiac function representing the cardiac pumping ability which is an important determinant of outcome in cardiogenic

shock = $\frac{\text{mean arterial pressure (mmHg)} \times \text{cardiac index (L.min}^{-1}.m^{-2})}{145}$ (34, 35). Last, an afterload-adjusted LV ejection fraction (LVEF_{EA}) was assessed using a simple non-linear approach as recently proposed = $LVejectionfraction \times \sqrt{\text{arterial elastance}}$ (36).

Other variables collected

The following data were collected at inclusion: age, sex, body mass index, past medical history, standard treatments, Sequential Organ Failure Assessment (SOFA) score (37), Simplified Acute Physiologic Score (SAPS) II (38). In addition, we collected septic shock characteristics, hemodynamic parameters (blood pressure and heart rate before and after steroid administration, fluid balance, dose of norepinephrine, inotrope need, arterial blood lactate, cardiac rhythm, ventilatory support with respiratory mechanics (mode of ventilation, tidal volume, respiratory rate, positive end expiratory pressure, plateau pressure, driving pressure, respiratory system compliance) for patients under invasive ventilation at the time of the echo examinations. Moreover, the following outcomes were recorded: renal replacement therapy, presence of acute respiratory distress syndrome (ARDS) as per the Berlin definition and vital status at ICU discharge.

Definitions

We defined septic cardiomyopathy as the appearance at echocardiography of hypokinesia (LVEF < 45% or when inotrope infusion was needed to achieve a value \geq 45%) during the first day of septic shock with the absence of acute coronary syndrome or history of chronic heart failure in the medical charts. We assessed the change in MAP between baseline and 2–4 h after steroid administration. We defined steroid MAP responders (non-responders) as patients with a relative increase in MAP above (below) the median value of the cohort.

Statistical analysis

Statistical analyses were performed with the JMP software (version 14; SAS Institute Inc., Cary, NC) and Graph-Pad Prism software (version 8; GraphPad Software Inc., La Jolla, CA, USA). The primary endpoint of this study was the change in LV contractility after the first administration of low-dose steroid therapy. For the analysis of the primary endpoint, the LV-GLS was chosen for its robustness, reproducibility and sensitivity. We calculated that a sample size of at least 43 patients would have a 90% power to detect a 20% improvement in LV-GLS after low-dose steroid therapy initiation, considering a baseline LV-GLS of −14% with a standard deviation (SD) of 4%, based on previous echocardiographic studies in septic

shock patients (39–41). Taking into account the feasibility of LV-GLS in our ICU (42), we therefore planned to include a total of 50 patients. In addition, we performed subgroup analyses. We compared the evolution of echocardiographic and hemodynamic parameters in response to low-dose steroids according to the presence on septic cardiomyopathy and according to MAP response. Descriptive statistics are presented as mean (+/−SD), median (interquartile range), or proportion, based on data type and distribution. Normality of continuous variables was assessed with the Shapiro–Wilk test. Comparisons of categorical variables were made using the Chi-2 test or Fisher exact test, as appropriate. Continuous variables were compared using a *T*-test or Mann–Withney test for independent variables, and a paired *T*-test or paired Wilcoxon test for paired variables, with Benjamini–Hochberg correction for multiple comparisons. The reproducibility of some echocardiographic variables in our laboratory was assessed using the British Standards Institution coefficient (twice the standard deviation of the differences in repeated measurements) (43). A *p*-value < 0.05 in bilateral configuration was considered for statistical significance.

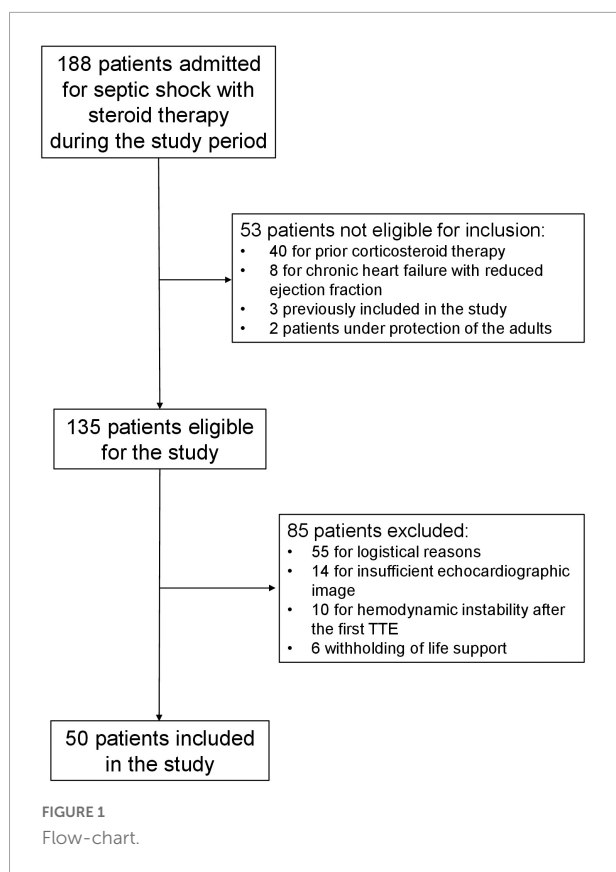
Results

Patient characteristics

During the study period, 188 patients admitted for septic shock and receiving steroid therapy were screened for enrolment. Among these patients, 135 were eligible for the study and 85 were excluded for logistical reasons, poor echogenicity, hemodynamic instability, or withdrawing of life support; finally, 50 patients were included in the study (Figure 1). The logistical reasons for excluding eligible patients from this study were lack of echocardiography-trained operators and urgent examination or procedure. Clinical characteristics, comorbidities and organ failures at inclusion are presented in Table 1. Patients were included a median of 12 [6–20] h after septic shock onset. In this cohort, fludrocortisone was administrated in 41 (82%) patients because the enteral access was not available in all patients (contraindication or waiting for the radiographic control of the gastric tube placement). Echocardiographic and hemodynamic data before and after initiation of low-dose steroids are shown in Table 2. The reproducibility of some echocardiographic variables is reported in Supplementary Table 1. The median delay between the two assessments was 172 (135–218) min. Respiratory settings were comparable between the two hemodynamic assessments.

Hemodynamics

At inclusion, all patients were receiving norepinephrine, at a median dose of 3.8 (2.3–5.5) mg/h, after a significant fluid



resuscitation [median fluid balance of 3 (2–4) L since admission] (Table 1). As compared to baseline values, there was a significant increase in systolic, mean and diastolic arterial pressure after low-dose steroids, along with a significant decrease in heart rate (Table 2).

Loading conditions

To the exception of LV end-systolic wall stress, all afterload parameters significantly improved after low-dose steroid therapy (with an increase in end-systolic arterial elastance, systemic vascular resistance, diastolic arterial pressure, and a decrease in diastolic shock index) (Table 2). Among preload parameters, only E/e' significantly decreased after low-dose steroid therapy. However, this variation might not be considered as clinically relevant. We did not find a significant change in global function (stroke volume, cardiac index, and CPI).

Contractility and ventriculo-arterial coupling

To the exception of LVEF, all contractility parameters (LV global longitudinal strain, tissue Doppler peak systolic wave

TABLE 1 Clinical characteristics of study patients and organ failures.

Variables	Patients, <i>n</i> = 50
Age (years)	65 (55–73)
Male sex	33 (66%)
Body mass index (kg/m ²)	25.9 (22.2–29.4)
SAPS II at ICU admission	54 (46–84)
Comorbidities	
Diabetes mellitus	17 (34%)
Arterial hypertension	22 (44%)
Atrial fibrillation	6 (12%)
Pacemaker implant present	2 (4%)
Ischaemic heart disease	9 (18%)
HFpEF	12 (24%)
Chronic renal replacement therapy	1 (2%)
COPD	3 (6%)
Immunodeficiency	10 (20%)
Cirrhosis	6 (12%)
Infection source	
Pulmonary	26 (52%)
Abdominal	5 (10%)
Urinary	6 (12%)
Other origin	13 (26%)
Nosocomial infection	16 (32%)
Low-dose steroid therapy	
Hydrocortisone	50 (100%)
Fludrocortisone	41 (82%)
Organ failures at inclusion	
Delay between norepinephrine introduction and inclusion (h)	12 (6–20)
SOFA score at inclusion	10 (10–12)
GCS before intubation	15 (9–15)
Sinus rhythm	47 (94%)
Fluid balance since admission (L)	3 (2–4)
Norepinephrine dose (mg/h)	3.8 (2.3–5.5)
Dobutamine use	3 (6%)
Arterial blood lactate (mmol/L)	1.9 (1.3–3.6)
Mechanical ventilation	46 (92%)
Neuromuscular-blocking agent use	22 (44%)
PaO ₂ /FiO ₂	198 (153–272)
Tidal Volume (mL)	400 (375–450)
Plateau pressure (cm H ₂ O)	21 (18–24)
Positive end expiratory pressure (cm H ₂ O)	8 [6–10]
Outcomes	
Acute respiratory distress syndrome	23 (46%)
ECMO	4 (8%)
Renal replacement therapy	16 (32%)
Duration of catecholamine (d)	4 (2–6)
Duration mechanical ventilation (d)	9 (6–20)
ICU length of stay (d)	12 (7–22)
Death in ICU	19 (38%)

Values are expressed as number (%) or median (interquartile range). SAPS II, Simplified Acute Physiology Score II; ICU, intensive care unit; HFpEF, heart failure with preserved ejection fraction; COPD, chronic obstructive pulmonary disease; TTE, transthoracic echocardiography; SOFA score, Sequential Organ Failure Assessment; GCS, Glasgow coma scale; PaO₂, partial pressure of oxygen in arterial blood; FiO₂, fraction of inspired oxygen; PEEP, positive end-expiratory pressure; ECMO, extracorporeal membrane oxygenation.

at mitral annulus, and-systolic maximal elastance by single-beat method) significantly improved after low-dose steroid therapy (Table 2, Figure 2, and Supplementary Figure 1). VAC significantly decreased after low-dose steroid therapy;

uncoupled VAC was present in 18/41 (44%) before low-dose steroid therapy and 10/41 (24%) after ($p < 0.01$).

Subgroups analyses

Overall, the hemodynamic and echocardiographic changes induced by low-dose steroids were similar in patients with or without septic myocardial dysfunction (**Supplementary Figure 2**). MAP responders significantly improved their macrocirculation and afterload parameters, contrary to non-responders (**Supplementary Figure 3**).

Discussion

The main findings of this echocardiographic study in septic shock patients were that in addition to their role in peripheral vascular tone (increased afterload), low-dose steroids increased the LV contractility and improved the cardiovascular efficiency.

In this cohort of septic shock patients, the hemodynamic effects of low-dose steroids therapy were coherent with the literature. Indeed, all arterial pressures (systolic, diastolic, and mean) increased in accordance with previous reports on this topic (7). Moreover, all LV afterload parameters assessed (except one) improved after low-doses steroid therapy, also in

TABLE 2 Evolution of hemodynamic and echocardiographic parameters in septic shock patients before and after initiation of low-dose steroid therapy.

		Before steroid (n = 50)	After steroid(n = 50)	P-value
Macrocirculation				
SAP (mmHg)	n = 50	118 (+/-21)	127 (+/-27)	<0.01*
Pulse pressure (mmHg)	n = 50	64 (+/-22)	68 (+/-25)	0.049
MAP (mmHg)	n = 50	73 (70–78)	79 (71–87)	<0.01*
Heart rate (rpm)	n = 50	104 (90–123)	100 (85–112)	0.023*
Preload and diastolic function				
LV end-diastolic volume (mL)	n = 49	112 (78–139)	107 (83–130)	0.63
E/A ratio at mitral valve	n = 44	0.92 (0.77–1.09)	0.84 (0.74–1.14)	0.34
E/e' ratio at mitral mean valve	n = 41	9 (7–14)	9 (7–11)	0.02*
e' mean (cm. s ⁻¹)	n = 41	9 (6–11)	9 (7–10)	0.16
Respiratory change in VTI LVOT (%) [#]	n = 48	5 (0–10)	4 (0–6)	0.08
LV afterload				
Ea (mmHg.mL ⁻¹)	n = 50	1.71 (1.37–2.19)	1.90 (1.45–2.27)	0.02*
SVR (mmHg.L ⁻¹ .min)	n = 50	893 (740–1,288)	1,065 (746–1,464)	<0.01*
LV end-systolic wall stress (mmHg L)	n = 49	5.70 (3.80–7.58)	6.37 (3.93–8.28)	0.46
DAP (mmHg)	n = 50	54 (51–57)	58 (53–66)	<0.01*
Diastolic shock index	n = 50	1.95 (+/-0.45)	1.75 (+/-0.51)	<0.01*
LV contractility				
LVEF (%)	n = 49	59 (40–64)	55 (46–63)	0.42
LVEF _{EA} (%)	n = 49	58 (+/-17)	60 (+/-15)	0.17
LV-GLS (%)	n = 47	-13.0 (+/-5.2)	-14.2 (+/-5.1)	0.001*
s' mean of lateral and septal annulus (cm. s ⁻¹)	n = 42	10.4 (+/-3.8)	11.2 (+/-3.5)	0.02*
s' at mitral lateral annulus (cm. s ⁻¹)	N = 47	11.3 (+/-4.5)	12.4 (+/-4.5)	0.01*
Ees(sb) (mmHg.mL ⁻¹)	n = 41	1.41 (+/-0.65)	1.64 (+/-0.63)	0.004*
Global function				
Stroke volume (mL)	n = 50	62 (51–79)	61 (46–81)	0.57
Cardiac Index (L.min ⁻¹ .m ⁻²)	n = 50	3.5 (2.5–4.3)	3.2 (2.5–4.5)	0.22
Cardiac power index (W.m ⁻²)	n = 50	0.57 (0.41–0.71)	0.53 (0.39–0.73)	0.34
VAC	n = 41	1.30 (0.91–1.79)	1.18 (0.92–1.35)	0.007*

Values are expressed as number (%) or median (interquartile range) or mean (+/-SD), as appropriate. SAP, systolic arterial pressure; MAP, mean arterial pressure; LV, left ventricle; E, early wave of transmitral diastolic blood flow; A, late wave of transmitral diastolic blood flow; E/A, ratio of early to late pulsed-wave Doppler of diastolic transmitral flow velocity; e', early tissue Doppler diastolic wave velocity at the lateral/septal mitral valve annulus; E/e', ratio of early pulsed-wave Doppler to early tissue Doppler diastolic wave velocity at the mitral valve annulus; VTI LVOT, velocity-time integral of left ventricular outflow tract; Ea, end-systolic arterial elastance; SVR, systemic vascular resistance; DAP, diastolic arterial pressure; LVEF, left ventricular ejection fraction; LVEF_{EA}, afterload-adjusted LVEF (LVEF × √Ea); LV-GLS, left ventricular global longitudinal strain; S', tissue Doppler peak systolic wave at mitral annulus; Ees(sb), LV end-systolic maximal elastance by single-beat method; VAC, ventricular-arterial coupling. Paired *t*-test or Wilcoxon paired test were used for Gaussian and non-Gaussian variables, respectively. [#] Absolute variation index VTI LVOT (%), absolute variation/pre low-dose steroid therapy. *Denote an adjusted *p*-value < 0.05 with Benjamini-Hochberg correction as compared to before with after low-dose steroids therapy.

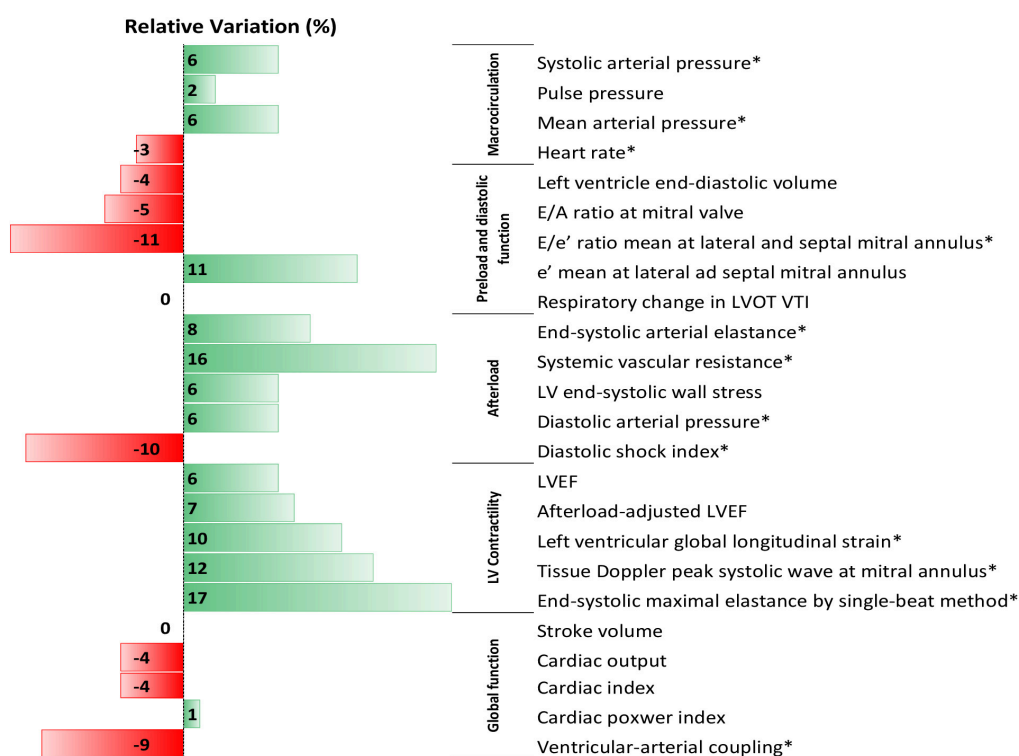


FIGURE 2

Data bars of median values of percent relative variation in hemodynamic and echocardiographic parameters after initiation of low-dose steroid therapy in septic shock patients. *Denote an adjusted p -value < 0.05 with Benjamini-Hochberg correction as compared to before with after low-dose steroids therapy.

accordance with previous reports (5, 44). These hemodynamic effects were not homogeneous in the entire cohort as reflected by a greater increase in afterload in MAP responders as compared to non-responders. Although septic myocardial dysfunction was previously shown to be associated with relative adrenal insufficiency (45), we found no difference in the cardiovascular effects of low-dose steroids between patients with and without septic myocardial dysfunction.

In previous studies evaluating hemodynamic effects of hydrocortisone in human septic shock, hydrocortisone increased MAP and systemic vascular resistances, with either decreased cardiac index and heart rate (5, 44) or no obvious effects on cardiac performance (4). The decrease in heart rate may be ascribable to fever control (46). However, these studies did not assess cardiac contractility *per se*. Our finding of increased cardiac contractility with low-dose steroids is in accordance with previous reports suggesting inotropic properties (47) and a possible protective effect on myocardium in the early phase of septic shock (10). Adrenal insufficiency is a cause of cardiac failure (48) and hydrocortisone increased cardiac output in healthy volunteers with hypoaldosteronism (49). The increase in LV contractility induced by low-dose steroids in septic shock was not necessarily expected. Indeed, some LV contractility indices are inversely correlated with

afterload during septic shock (9). New echocardiographic tools (tissue Doppler and strain) seem to be more suitable than traditional parameters of systolic function (LVEF) to detect subtle myocardial dysfunction, and to be less influenced by afterload than other LV contractility parameters during sepsis (50). LV strain and especially tissue Doppler s' were less prone to changes in LV loading conditions (9). Our data showed a significant increase of these parameters of systolic function without any change of LVEF.

End-systolic elastance is a theoretical load independent variable of LV contractile function deduced from the pressure-volume loops, obtained by invasive ventricular catheterization. Herein, we assessed LV end-systolic elastance by the bedside single beat method proposed by Chen et al. (27), which is considered the most accurate non-invasive method and is recommended by guidelines (31). Despite the improvement in afterload with increased end-systolic arterial elastance after initiation of corticosteroid replacement therapy, we detected a significant increase in LV end-systolic elastance by the single-beat method. The reported increase in this variable may be credible since tissue Doppler s' and strain were also increased. However, Chen's methods presents the following limitations: (i) it is based on complex assumptions, equations, and regression models; (ii) echo-derived LVEF is incorporated in $E_{es(sb)}$

estimate; (ii) the formula of $E_{es(sb)}$ uses the ratio of pre-ejection to total systolic time raised to multiple powers, such that small variations in the measurements of time intervals may lead to relatively large changes in the estimated $E_{es(sb)}$ value.

VAC reflects the complex interaction between LV performance and arterial load and represents cardiovascular efficiency. When this ratio between arterial elastance and LV elastance at systole is close to 1.0, it indicates an optimal coupling between LV and arterial system resulting in efficient LV stroke work (51). In septic shock, both arterial elastance and LV elastance can profoundly be altered with various degrees of vasoplegia and/or LV myocardial depression. Evaluation of VAC was recently proposed, not only to understand the hemodynamic pathophysiology in septic shock, but also to predict the response to cardiovascular therapies (52). VAC is mathematically related to LVEF. However, this theoretical relationship is correct only if V_o (an extrapolated value representing the left ventricular volume intercept of the volume axis at a theoretical end-systolic pressure of 0 mmHg) is assumed to be null, like in the normal heart, but this is not the case in heart failure or during hemodynamic instability (53). We herein demonstrate a significant improvement in VAC (tending toward 1.0) after initiation of low-dose steroids with decrease of uncoupled VAC. This result suggest a holistic effect of low-dose steroids on the hemodynamic system, not restricted to the vascular system, but also involving the cardiac contractility with an improved interaction between the heart and the vasculature. However, we cannot exclude a homeometric adaption of the heart. Indeed, according to the Anrep's effect (54), the heart may adapt to increased loading through an increased contractility to preserve ventricular-arterial coupling.

The main strength of our study is the comprehensive hemodynamic assessment involving modern echocardiographic tools. Steroid replacement therapy improves global outcomes in septic shock patients in some studies but not all. Depicting the effect of steroids on cardiac contractility could be interesting to personalize this therapy. Moreover, cardiac and vascular effect of low-dose steroid therapy may justify extending this therapy to patients in cardiogenic shock (55). Our study also has some limitations. First, the design was monocentric and unblinded, with a relatively limited sample size. Second, the delay between the two echocardiographic evaluations was not constant (time window between 2 and 4 h), due to logistical issues and the pragmatic design. Although this time window is debatable, it was chosen in reference to the previous physiological studies on hemodynamic impact of hydrocortisone and fludrocortisone (49, 56). Third, we did not to assess the hemodynamic effect of low-dose steroids based on adrenal function, and future studies are needed to scrutinize this point. Fourth, excluded patients with unstable hemodynamics may have different cardiac contractile properties and vascular system responses to corticosteroids. Fifth, we could not perform a multivariable because of the limited sample size and the collinearity between

some hemodynamic parameters. Sixth, although catecholamine dose and fluid management were kept constant between the two-ultrasound assessments, we cannot exclude their influence on observed hemodynamic modifications. For example, fluids and vasopressors both have inotropic effects *via* Starling and Anrep effect, respectively, among other mechanisms.

Finally, the interpretation of the hemodynamic variations could be limited by the absence of a control group and the open label design, inasmuch as the hemodynamic profile of septic shock may vary with time. Indeed, while the delay between the two-ultrasound assessments was relatively short, the relationship between low-dose steroid therapy and modification of hemodynamics could be influence by the natural course of septic shock.

Conclusion

We herein report a comprehensive assessment by bedside echocardiography of the hemodynamic impact of low-dose steroids in the early phase of septic shock. We confirmed an increase of arterial pressure, a decrease of heart rate and an improvement of LV afterload after initiation of low-dose steroids. Moreover, we suggested for the first time an increase of LV contractility with improvement of the cardiovascular efficiency as assessed by VAC. However, this possible positive inotropic effect needs to be confirmed in future studies.

Data availability statement

The raw data supporting the conclusions of this article will be made available by the authors, without undue reservation.

Ethics statement

The study was approved on July 12, 2018 by the Institutional Ethics Committee, Institutional Review Board (IRB) Mondor (reference number: 2201948) as a component of standard care, and patient consent was waived. Written and oral information about the study was given to the families.

Author contributions

FB had full access to all of the data in the study and took responsibility for the integrity of the data, and the accuracy of the data analysis. FB and AM designed the study and wrote the manuscript. FB, AC, PM, and KR performed echocardiographies. FB, AC, and PM collected the data. FB,

AC, PM, NP, GC, KR, and AM contributed to interpretation of data, drafting of the submitted article, and critical revisions for intellectual content. All authors read and approved the final manuscript.

Acknowledgments

We are very indebted to all physicians and nurses of the Henri Mondor Medical Intensive Care Unit for their help for the care of patients.

Conflict of interest

The authors declare that the research was conducted in the absence of any commercial or financial relationships that could be construed as a potential conflict of interest.

Publisher's note

All claims expressed in this article are solely those of the authors and do not necessarily represent those of their affiliated organizations, or those of the publisher, the editors and the reviewers. Any product that may be evaluated in this article, or claim that may be made by its manufacturer, is not guaranteed or endorsed by the publisher.

References

1. Annane D, Pastores SM, Arlt W, Balk RA, Beishuizen A, Briegel J, et al. Critical illness-related corticosteroid insufficiency (CIRCI): a narrative review from a multispecialty task force of the society of critical care medicine (SCCM) and the European society of intensive care medicine (ESICM). *Intensive Care Med.* (2017) 43:1781–92. doi: 10.1007/s00134-017-4914-x
2. Rhen T, Cidlowski JA. Antiinflammatory action of glucocorticoids—new mechanisms for old drugs. *N Engl J Med.* (2005) 353:1711–23.
3. Yard AC, Kadowitz PJ. Studies on the mechanism of hydrocortisone potentiation of vasoconstrictor responses to epinephrine in the anesthetized animal. *Eur J Pharmacol.* (1972) 20:1–9. doi: 10.1016/0014-2999(72)90209-9
4. Bollaert PE, Charpentier C, Levy B, Debouverie M, Audibert G, Larcan A. Reversal of late septic shock with supraphysiologic doses of hydrocortisone. *Crit Care Med.* (1998) 26:645–50. doi: 10.1097/00003246-199804000-00010
5. Briegel J, Forst H, Haller M, Schelling G, Kilger E, Kuprat G, et al. Stress doses of hydrocortisone reverse hyperdynamic septic shock: a prospective, randomized, double-blind, single-center study. *Crit Care Med.* (1999) 27:723–32.
6. Oppert M, Reinicke A, Graf KJ, Barckow D, Frei U, Eckardt KU. Plasma cortisol levels before and during “low-dose” hydrocortisone therapy and their relationship to hemodynamic improvement in patients with septic shock. *Intensive Care Med.* (2000) 26:1747–55.
7. Bellissant E, Annane D. Effect of hydrocortisone on phenylephrine—mean arterial pressure dose-response relationship in septic shock. *Clin Pharmacol Ther.* (2000) 68:293–303. doi: 10.1067/mcp.2000.109354
8. Annane D, Sebille V, Charpentier C, Bollaert PE, Francois B, Korach JM, et al. Effect of treatment with low doses of hydrocortisone and fludrocortisone on mortality in patients with septic shock. *JAMA.* (2002) 288:862–71.
9. Boissier F, Razazi K, Seemann A, Bedet A, Thille AW, de Prost N, et al. Left ventricular systolic dysfunction during septic shock: the role of loading conditions. *Intensive Care Med.* (2017) 43:633–42. doi: 10.1007/s00134-017-4698-z
10. Liao R, Zhang J, Zhao H, Zhang Z, Yang K. [Protective effect of low-dose hydrocortisone on myocardium in early septic shock]. *Zhonghua Wei Zhong Bing Ji Jiu Yi Xue.* (2020) 32:210–4. doi: 10.3760/cma.j.cn121430-20191024-00039
11. Chauvet J-L, El-Dash S, Delastre O, Bouffandeau B, Jussierand D, Michot J-B, et al. Early dynamic left intraventricular obstruction is associated with hypovolemia and high mortality in septic shock patients. *Crit Care.* (2015) 19:262. doi: 10.1186/s13054-015-0980-z
12. Dellinger RP, Levy MM, Rhodes A, Annane D, Gerlach H, Opal SM, et al. Surviving Sepsis Campaign: international guidelines for management of severe sepsis and septic shock, 2012. *Intensive Care Med.* (2013) 39:165–228.
13. Annane D, Pastores SM, Rochwerf B, Arlt W, Balk RA, Beishuizen A, et al. Guidelines for the diagnosis and management of critical illness-related corticosteroid insufficiency (CIRCI) in critically ill patients (Part I): society of critical care medicine (SCCM) and European society of intensive care medicine (ESICM) 2017. *Intensive Care Med.* (2017) 43:1751–63. doi: 10.1007/s00134-017-4919-5
14. Rhodes A, Evans LE, Alhazzani W, Levy MM, Antonelli M, Ferrer R, et al. Surviving Sepsis Campaign: international guidelines for management of sepsis and septic shock: 2016. *Intensive Care Med.* (2017) 43:304–77. doi: 10.1007/s00134-017-4683-6
15. Expert Round Table on Echocardiography in ICU. International consensus statement on training standards for advanced critical care echocardiography. *Intensive Care Med.* (2014) 40:654–66. doi: 10.1007/s00134-014-3228-5

Supplementary material

The Supplementary Material for this article can be found online at: <https://www.frontiersin.org/articles/10.3389/fcvm.2022.948231/full#supplementary-material>

SUPPLEMENTARY FIGURE 1

Box and whiskers plot of percent relative variation in hemodynamic and echocardiographic parameters after initiation of low-dose steroid therapy in septic shock patients. SAP, systolic arterial pressure; PP, pulse pressure; MAP, mean arterial pressure; HR, heart rate; LVEDV, left ventricle end-diastolic volume; E/A, ratio of early to late pulsed-wave Doppler of diastolic transmitral flow velocity; E/e', ratio of early pulsed-wave Doppler to early tissue Doppler diastolic wave velocity at the mitral valve annulus; e', early tissue Doppler diastolic wave velocity at the mitral valve annulus; VTI LVOT, velocity-time integral of left ventricular outflow tract; Ea, end-systolic arterial elastance; SVR, systemic vascular resistance; LV-ESWS, left ventricular end-systolic wall stress; DAP, diastolic arterial pressure; DSI, diastolic shock index; LVEF, left ventricular ejection fraction; LVEF_{Ea}, afterload-adjusted LVEF (LVEF x \sqrt{Ea}); LV-GLS, left ventricular global longitudinal strain; S', tissue Doppler peak systolic wave at mitral annulus; Ees(sb), left ventricular end-systolic maximal elastance by single-beat method; CO, cardiac output; CI, cardiac index; CPI, cardiac power index; VAC, ventricular arterial coupling.

SUPPLEMENTARY FIGURE 2

Data bars of median values of percent relative variation in hemodynamic and echocardiographic parameters after initiation of low-dose steroid therapy in septic shock patients, according to septic cardiomyopathy.

*Denote an adjusted p -value < 0.05 with Benjamini-Hochberg correction as compared to septic cardiomyopathy and non-septic cardiomyopathy.

SUPPLEMENTARY FIGURE 3

Data bars of median values of percent relative variation in hemodynamic and echocardiographic parameters after initiation of low-dose steroid therapy in septic shock patients, according to steroid responders.

*Denote an adjusted p -value < 0.05 with Benjamini-Hochberg correction as compared to responders and non-responders.

16. Sanfilippo F, Huang S, Herpain A, Balik M, Chew MS, Clau-Terré F, et al. The PRICES statement: an ESICM expert consensus on methodology for conducting and reporting critical care echocardiography research studies. *Intensive Care Med.* (2021) 47:1–13. doi: 10.1007/s00134-020-06262-5
17. Nagueh SF, Smiseth OA, Appleton CP, Byrd BF, Dokainish H, Edvardsen T, et al. Recommendations for the evaluation of left ventricular diastolic function by echocardiography: an update from the American society of echocardiography and the European association of cardiovascular imaging. *J Am Soc Echocardiogr.* (2016) 29:277–314. doi: 10.1016/j.echo.2016.01.011
18. Slama M, Masson H, Teboul J-L, Arnout M-L, Susic D, Frohlich E, et al. Respiratory variations of aortic VTI: a new index of hypovolemia and fluid responsiveness. *Am J Physiol Heart Circ Physiol.* (2002) 283:H1729–33.
19. Vignon P, Repessé X, Bégot E, Léger J, Jacob C, Bouferrache K, et al. Comparison of echocardiographic indices used to predict fluid responsiveness in ventilated patients. *Am J Respir Crit Care Med.* (2017) 195:1022–32. doi: 10.1164/rccm.201604-0844OC
20. Chirinos JA, Segers P. Noninvasive evaluation of left ventricular afterload: part 2: arterial pressure-flow and pressure-volume relations in humans. *Hypertension.* (2010) 56:563–70. doi: 10.1161/HYPERTENSIONAHA.110.157339
21. Greim CA, Roewer N, Schulte am Esch J. Assessment of changes in left ventricular wall stress from the end-systolic pressure-area product. *Br J Anaesth.* (1995) 75:583–7. doi: 10.1093/bja/75.5.583
22. Kelly RP, Ting CT, Yang TM, Liu CP, Maughan WL, Chang MS, et al. Effective arterial elastance as index of arterial vascular load in humans. *Circulation.* (1992) 86:513–21. doi: 10.1161/01.CIR.86.2.513
23. Ospina-Tascón GA, Teboul J-L, Hernandez G, Alvarez I, Sánchez-Ortiz AI, Calderón-Tapia LE, et al. Diastolic shock index and clinical outcomes in patients with septic shock. *Ann Intensive Care.* (2020) 10:41.
24. Lang RM, Bierig M, Devereux RB, Flachskampf FA, Foster E, Pellikka PA, et al. Recommendations for chamber quantification. *Eur J Echocardiogr.* (2006) 7:79–108. doi: 10.1016/j.euje.2005.12.014
25. Gudmundsson P, Rydberg E, Winter R, Willenheimer R. Visually estimated left ventricular ejection fraction by echocardiography is closely correlated with formal quantitative methods. *Int J Cardiol.* (2005) 101:209–12. doi: 10.1016/j.ijcard.2004.03.027
26. Seo JS, Kim DH, Kim WJ, Song JM, Kang DH, Song JK. Peak systolic velocity of mitral annular longitudinal movement measured by pulsed tissue Doppler imaging as an index of global left ventricular contractility. *Am J Physiol Heart Circ Physiol.* (2010) 298:H1608–15. doi: 10.1152/ajpheart.01231.2009
27. Chen C-H, Fetis B, Nevo E, Rochitte CE, Chiou K-R, Ding P-A, et al. Noninvasive single-beat determination of left ventricular end-systolic elastance in humans. *J Am Coll Cardiol.* (2001) 38:2028–34. doi: 10.1016/S0735-1097(01)01651-5
28. Senzaki H, Chen C-H, Kass DA. Single-beat estimation of end-systolic pressure-volume relation in humans. *Circulation.* (1996) 94:2497–506. doi: 10.1161/01.CIR.94.10.2497
29. Shishido T, Hayashi K, Shigemitsu K, Sato T, Sugimachi M, Sunagawa K. Single-beat estimation of end-systolic elastance using bilinearly approximated time-varying elastance curve. *Circulation.* (2000) 102:1983–9. doi: 10.1161/01.cir.102.16.1983
30. Sunagawa K, Maughan WL, Burkoff D, Sagawa K. Left ventricular interaction with arterial load studied in isolated canine ventricle. *Am J Physiol.* (1983) 245:H773–80.
31. Ikonomidis I, Aboyans V, Blacher J, Brodmann M, Brutsaert DL, Chirinos JA, et al. The role of ventricular–arterial coupling in cardiac disease and heart failure: assessment, clinical implications and therapeutic interventions. A consensus document of the European society of cardiology working group on aorta & peripheral vascular diseases, European association of cardiovascular imaging, and heart failure association. *Eur J Heart Fail.* (2019) 21:402–24. doi: 10.1002/ehf.1436
32. Chen C-H, Nakayama M, Nevo E, Fetis BJ, Maughan WL, Kass DA. Coupled systolic-ventricular and vascular stiffening with age. *J Am Coll Cardiol.* (1998) 32:1221–7. doi: 10.1016/S0735-1097(98)00374-X
33. Guarracino F, Ferro B, Morelli A, Bertini P, Baldassarri R, Pinsky MR. Ventriculoarterial decoupling in human septic shock. *Crit Care Lond Engl.* (2014) 18:R80. doi: 10.1186/cc13842
34. Yildiz O, Aslan G, Demirozu ZT, Yenigun CD, Yazicioglu N. Evaluation of resting cardiac power output as a prognostic factor in patients with advanced heart failure. *Am J Cardiol.* (2017) 120:973–9. doi: 10.1016/j.amjcard.2017.06.028
35. Fincke R, Hochman JS, Lowe AM, Menon V, Slater JN, Webb JG, et al. Cardiac power is the strongest hemodynamic correlate of mortality in cardiogenic shock: a report from the SHOCK trial registry. *J Am Coll Cardiol.* (2004) 44:340–8.
36. Monge García MI, Jian Z, Settels JJ, Hunley C, Cecconi M, Hatib F, et al. Determinants of left ventricular ejection fraction and a novel method to improve its assessment of myocardial contractility. *Ann Intensive Care.* (2019) 9:48. doi: 10.1186/s13613-019-0526-7
37. Vincent JL, Moreno R, Takala J, Willatts S, De Mendonça A, Bruining H, et al. The SOFA (Sepsis-related Organ Failure Assessment) score to describe organ dysfunction/failure. On behalf of the working group on sepsis-related problems of the European society of intensive care medicine. *Intensive Care Med.* (1996) 22:707–10. doi: 10.1007/BF01709751
38. Le Gall JR, Lemeshow S, Saulnier F. A new simplified acute physiology score (SAPS II) based on a European/North American multicenter study. *JAMA.* (1993) 270:2957–63.
39. Orde SR, Pulido JN, Masaki M, Gillespie S, Spoon JN, Kane GC, et al. Outcome prediction in sepsis: speckle tracking echocardiography based assessment of myocardial function. *Crit Care.* (2014) 18:R149. doi: 10.1186/cc13987
40. Shahul S, Gulati G, Hacker MR, Mahmood F, Canelli R, Nizamuddin J, et al. Detection of myocardial dysfunction in septic shock: a speckle-tracking echocardiography study. *Anesth Analg.* (2015) 121:1547–54. doi: 10.1213/ANE.0000000000000943
41. Ng PY, Sin WC, Ng AK-Y, Chan WM. Speckle tracking echocardiography in patients with septic shock: a case control study (SPECKSS). *Crit Care Lond Engl.* (2016) 20:145. doi: 10.1186/s13054-016-1327-0
42. Bagate F, Masi P, d'Humières T, Al-Assaad L, Chakra LA, Razazi K, et al. Advanced echocardiographic phenotyping of critically ill patients with coronavirus-19 sepsis: a prospective cohort study. *J Intensive Care.* (2021) 9:12. doi: 10.1186/s40560-020-00516-6
43. Bland JM, Altman DG. Statistical methods for assessing agreement between two methods of clinical measurement. *Lancet Lond Engl.* (1986) 1:307–10.
44. Keh D, Boehnke T, Weber-Cartens S, Schulz C, Ahlers O, Bercker S, et al. Immunologic and hemodynamic effects of “low-dose” hydrocortisone in septic shock: a double-blind, randomized, placebo-controlled, crossover study. *Am J Respir Crit Care Med.* (2003) 167:512–20. doi: 10.1164/rccm.200205-446OC
45. Bagate F, Razazi K, Boissier F, Seemann A, de Prost N, Carreaux G, et al. Association between relative adrenal insufficiency and septic cardiomyopathy: a preliminary report. *Intensive Care Med.* (2017) 43:1924–6. doi: 10.1007/s00134-017-4901-2
46. Schortgen F, Charles-Nelson A, Bouadma L, Bizouard G, Brochard L, Katsahian S. Respective impact of lowering body temperature and heart rate on mortality in septic shock: mediation analysis of a randomized trial. *Intensive Care Med.* (2015) 41:1800–8. doi: 10.1007/s00134-015-3987-7
47. Tanz RD, Kerby CF. The inotropic action of certain steroids upon isolated cardiac tissue; with comments on steroidal cardiotonic structure-activity relationships. *J Pharmacol Exp Ther.* (1961) 131:56–64.
48. Mekontso-Dessap A, Marrache D, Vieillard-Baron A. Images in cardiology: acute adrenal insufficiency complicated by cardiogenic shock. *Heart.* (2005) 91:e31. doi: 10.1136/hrt.2004.055095
49. Laviolle B, Le Maguet P, Verdier MC, Massart C, Donal E, Laine F, et al. Biological and hemodynamic effects of low doses of fludrocortisone and hydrocortisone, alone or in combination, in healthy volunteers with hypoadosteronism. *Clin Pharmacol Ther.* (2010) 88:183–90. doi: 10.1038/clpt.2010.83
50. Hestenes SM, Halvorsen PS, Skulstad H, Remme EW, Espinoza A, Hyler S, et al. Advantages of strain echocardiography in assessment of myocardial function in severe sepsis: an experimental study*. *Crit Care Med.* (2014) 42:e432–40. doi: 10.1097/CCM.0000000000000310
51. De Tombe PP, Jones S, Burkoff D, Hunter WC, Kass DA. Ventricular stroke work and efficiency both remain nearly optimal despite altered vascular loading. *Am J Physiol Heart Circ Physiol.* (1993) 264:H1817–24. doi: 10.1152/ajpheart.1993.264.6.H1817
52. Pinsky MR, Guarracino F. How to assess ventriculoarterial coupling in sepsis. *Curr Opin Crit Care.* (2020) 26:313–8. doi: 10.1097/MCC.0000000000000721
53. Mihaileanu S, Antohi E. Revisiting the relationship between left ventricular ejection fraction and ventricular–arterial coupling. *ESC Heart Fail.* (2020) 7:2214–22. doi: 10.1002/ehf2.12880
54. von Anrep G. On the part played by the suprarenals in the normal vascular reactions of the body. *J Physiol.* (1912) 45:307–17. doi: 10.1113/jphysiol.1912.sp001553
55. Mekontso Dessap A, Bagate F, Delmas C, Morichau-Beauchant T, Cholley B, Cariou A, et al. Low-dose corticosteroid therapy for cardiogenic shock in adults (COCCA): study protocol for a randomized controlled trial. *Trials.* (2022) 23:4. doi: 10.1186/s13063-021-05947-6
56. Laviolle B, Donal E, Le Maguet P, Laine F, Bellissant E. Low doses of fludrocortisone and hydrocortisone, alone or in combination, on vascular responsiveness to phenylephrine in healthy volunteers. *Br J Clin Pharmacol.* (2013) 75:423–30. doi: 10.1111/j.1365-2125.2012.04359.x



OPEN ACCESS

EDITED BY

Shaojie Chen,
Cardioangiological Center Bethanien
(CCB), Germany

REVIEWED BY

Zhiyu Ling,
Chongqing Medical University, China
Kyoung-Min Park,
Sungkyunkwan University, South Korea

*CORRESPONDENCE

Zhong Jingquan
18560086597@163.com
Long Deyong
dragon2008@vip.sina.com

SPECIALTY SECTION

This article was submitted to
Cardiovascular Imaging,
a section of the journal
Frontiers in Cardiovascular Medicine

RECEIVED 05 August 2022

ACCEPTED 13 September 2022

PUBLISHED 06 October 2022

CITATION

Jingquan Z, Deyong L, Huimin C,
Hua F, Xuebin H, Chenyang J, Yan L,
Xuebin L, Min T, Zulu W, Yumei X,
Jinlin Z, Wei Z, Xiaochun Z, Daxin Z,
Yun Z, Changsheng M, Zei PC and
Di Biase L (2022) Intracardiac
echocardiography Chinese expert
consensus.
Front. Cardiovasc. Med. 9:1012731.
doi: 10.3389/fcvm.2022.1012731

COPYRIGHT

© 2022 Jingquan, Deyong, Huimin,
Hua, Xuebin, Chenyang, Yan, Xuebin,
Min, Zulu, Yumei, Jinlin, Wei, Xiaochun,
Daxin, Yun, Changsheng, Zei and
Di Biase. This is an open-access article
distributed under the terms of the
[Creative Commons Attribution License
\(CC BY\)](#). The use, distribution or
reproduction in other forums is
permitted, provided the original
author(s) and the copyright owner(s)
are credited and that the original
publication in this journal is cited, in
accordance with accepted academic
practice. No use, distribution or
reproduction is permitted which does
not comply with these terms.

Intracardiac echocardiography Chinese expert consensus

Zhong Jingquan^{1,2*}, Long Deyong^{3*}, Chu Huimin⁴, Fu Hua⁵,
Han Xuebin⁶, Jiang Chenyang⁷, Li Yan⁸, Li Xuebin⁹,
Tang Min¹⁰, Wang Zulu¹¹, Xue Yumei¹², Zhang Jinlin¹³,
Zhang Wei⁸, Zhang Xiaochun¹⁴, Zhou Daxin¹⁴, Zhang Yun¹,
Ma Changsheng³, Paul C. Zei¹⁵ and Luigi Di Biase¹⁶

¹Key Laboratory of Cardiovascular Remodeling and Function Research, Chinese Ministry of Education, Chinese National Health Commission and Chinese Academy of Medical Sciences, State and Shandong Province Joint Key Laboratory of Translational Cardiovascular Medicine, Department of Cardiology, Qilu Hospital, Cheeloo College of Medicine, Shandong University, Jinan, China, ²Department of Cardiology, Qilu Hospital (Qingdao), Cheeloo College of Medicine, Shandong University, Qingdao, China, ³Beijing Anzhen Hospital, Capital Medical University, Beijing, China, ⁴Ningbo First Hospital, Zhejiang University, Ningbo, China, ⁵West China Hospital, Sichuan University, Chengdu, China, ⁶The Affiliated Cardiovascular Hospital, Shanxi Medical University, Taiyuan, China, ⁷Sir Run Run Shaw Hospital of Zhejiang University, Hangzhou, China, ⁸Tangdu Hospital, The Fourth Military Medical University, Xi'an, China, ⁹Peking University People's Hospital, Beijing, China, ¹⁰Fuwai Hospital of Chinese Academy of Medical Sciences and Peking Union Medical College, Beijing, China, ¹¹General Hospital of Northern Theater Command, Shenyang, China, ¹²Guangdong Provincial People's Hospital, Guangzhou, China, ¹³Wuhan Asian Heart Hospital, Wuhan, China, ¹⁴Zhongshan Hospital, Fudan University, Shanghai, China, ¹⁵Brigham and Women's Hospital, Boston, MA, United States, ¹⁶Albert Einstein College of Medicine, Montefiore Medical Center, Bronx, NY, United States

In recent years, percutaneous catheter interventions have continuously evolved, becoming an essential strategy for interventional diagnosis and treatment of many structural heart diseases and arrhythmias. Along with the increasing complexity of cardiac interventions comes ever more complex demands for intraoperative imaging. Intracardiac echocardiography (ICE) is well-suited for these requirements with real-time imaging, real-time monitoring for intraoperative complications, and a well-tolerated procedure. As a result, ICE is increasingly used many types of cardiac interventions. Given the lack of relevant guidelines at home and abroad and to promote and standardize the clinical applications of ICE, the members of this panel extensively evaluated relevant research findings, and they developed this consensus document after discussions and correlation with front-line clinical work experience, aiming to provide guidance for clinicians and to further improve interventional cardiovascular diagnosis and treatment procedures.

KEYWORDS

intracardiac echocardiography, arrhythmia, transseptal puncture, congenital heart disease, structural heart disease, left atrial appendage closure, device implantation and lead extraction, cardiomyopathy and pulmonary arterial hypertension

Process of forming this consensus

The consensus was written by the “Chinese ICE Expert Group,” which includes experts in echocardiography, cardiac electrophysiology, congenital heart disease, valvular heart disease and so on. The consensus was initiated by Professor Zhang Yun and Ma Changsheng, and Professor Zhong Jingquan and Long Deyong were mainly responsible for the completion of the manuscript. We held three relevant meetings (2022.1.15, 2022.4.2, and 2022.4.23) regarding the consensus. Details of meetings are provided in the **Table 1**.

Overview of intracardiac echocardiography

Definition and background of intracardiac echocardiography

Intracardiac echocardiography (ICE) is an ultrasound imaging technique able to perform real-time high-quality imaging and/or hemodynamic measurement of the heart and its adjacent tissues with an ultrasound probe placed at the tip of a catheter delivered into the cardiac chambers via peripheral vessels (1–3). In view of its ability to directly visualize the cardiac structures and reveal the anatomical relationship between various parts of the heart, ICE has been increasingly used to guide cardiac interventions and monitor intraoperative complications. It is an important adjunct in various cardiac interventions.

A catheter with an ultrasound transducer was first delivered into the cardiac chambers of a dog via the jugular vein to obtain endocardial echo images of the left and right ventricles as early as 1960 (4). Since then, scientists and engineers further developed early ultrasound probes to image intracardiac structures (5, 6). With the invention of the phased array ultrasound transducer and other devices in succession (7, 8), ICE has been increasingly applied to guide clinical practice such as transseptal puncture (9–11). In recent years, percutaneous catheter interventions have continuously evolved, becoming an essential strategy for interventional diagnosis and treatment of many structural heart diseases and arrhythmias. Along with the increasing complexity of cardiac interventions comes ever more complex demands for intraoperative imaging. ICE is well-suited for these requirements with real-time imaging, real-time monitoring for intraoperative complications, and a well-tolerated procedure (3, 12, 13). As a result, ICE is increasingly used many types of cardiac interventions. Given the lack of relevant guidelines at home and abroad and to promote and standardize the clinical applications of ICE, the members of this panel extensively evaluated relevant research findings at home and abroad, and they developed this consensus document after discussions and correlation with front-line clinical work

experience, aiming to provide guidance for clinicians and to further improve interventional cardiovascular diagnosis and treatment procedures.

Types of intracardiac echocardiography catheters

Intracardiac echocardiography catheters currently in use can be classified into the following two types by their technologic principles: the mechanical rotary ultrasound catheter and the phased array ultrasound catheter (14). The former, with a mechanical 360° rotary ultrasound transducer placed at its tip, provides circular sectional images perpendicular to its long axis. With a single ultrasound frequency, the catheter is only suitable for short-range imaging within 6–8 cm around the probe, instead of Doppler imaging. It is poorly maneuverable as it needs to be placed in the right atrium under the guidance of a long sheath. As a result, the catheter is now mainly used for electrophysiological studies, if at all (12, 15). The latter, composed of a handle and a catheter, is the most commonly used type of ICE catheter in clinical practice. The handle has three rows of knobs to manipulate the catheter to flex and fix in four directions: anterior (A), posterior (P), left (L), and right (R) (1–3, 12, 16). With a 64-element phased array ultrasound transducer placed at the tip, the catheter provides a 90° fan-shaped visual field by longitudinal scanning. With a variable ultrasound frequency (5–10 MHz) and a maximum penetration depth of 15–16 cm, the catheter is able to scan the cardiac chambers in all directions, along with Doppler imaging, via the manipulation of the handle. One currently utilized phased array ICE catheter integrates the 2D intracardiac US image with the 3D electroanatomical mapping system by embedding a position sensor at its tip. In this way, the ultrasound sector can be represented on the three-dimensional map to correlate the anatomical structures imaged with real-time catheter position (13), further improving the clinician’s understanding of intraprocedural cardiac anatomy in the context of planned interventions.

Clinical applications of intracardiac echocardiography

Initially, ICE was mainly used to guide the interventional closure of atrial septal defect (ASD) and patent foramen ovale (PFO), with comparable image quality to that of transesophageal echocardiography (TEE). Nowadays, ICE is more common imaging modality used during these procedures, as it requires neither general anesthesia nor sonographer assistance (2, 13). In addition, ICE can image the interatrial septum, identify the location and anatomy of the fossa ovalis and assist proceduralists in selecting an ideal transseptal puncture site, and improve the

TABLE 1 Details of meetings.

Minutes of ICE Chinese expert consensus conference	
Time:	2022.1.15 Startup meeting
Location:	Jinan
Person:	14
Experts:	Zhang Yun, Zhong Jingquan, Zhang Jinlin, Chu Huimin, Li Yan, Tang Min, Ma Changsheng, Long Deyong, Jiang Chenyang, Zhang Wei, Fu Hua, Xue Yumei, Zhou Daxin, Zhang Xiaochun
Meeting Minutes:	<p>This launch was the first symposium of the ICE expert consensus, which invited leading experts in electrophysiology and structural heart disease to discuss the direction and structure of the expert consensus. Different sections are also assigned to each participating expert to claim different sections for content writing.</p> <p>There was particularly intense discussion based on the setting of different sections, the wording and selection principles of the questions, the grade of recommendation, and the addition of quantitative tables. In particular, the popularity and practicability of consensus will be increased in the presentation of expression, selection of the source of illustrations, different standardized operations, highlighting clinical pathways, technical points, technical operations, image recognition and other modes.</p> <p>To make ICE ultrasound application technology more standardized, standardized, and prospective. It also combines overseas application experience with local use methods to develop field norms and standards that are more in line with the use of Chinese clinicians.</p>
Meeting Summary:	<p>(1) Add English version based on Chinese version consensus</p> <p>(2) Establishment of a writing expert group and members of the group of reviewing experts (voting and making recommendations)</p> <p>(3) Experts from the writing group lead different sections.</p>
Minutes of ICE Chinese expert consensus conference	
Time:	2022.4.2 Reading Conference
Location:	Meeting online
Person:	9
Experts:	Zhong Jingquan, Zhang Jinlin, Chu Huimin, Ma Changsheng, Jiang Chenyang, Zhang Wei, Fu Hua, Xue Yumei, Zhang Xiaochun
Meeting Minutes:	<p>Based on the division of labor of the kick-off meeting, this meeting will read and optimize the overall content focusing on the previously given division of labor, and inspect the integrity and integrity of the content in stages.</p> <p>Due to the large number of ICE application scenarios, the content presented in order to increase the overall and comprehensive nature of the consensus needs to be subdivided, so 8 contributing experts were raised to 15 to supplement the plate content:</p> <p>Wang Zulu – Application of ICE in Cryoablation;</p> <p>Li Xuebin – Application of ICE in Lead Extraction;</p> <p>Han Xuebin – Application of ICE in Pulmonary Arterial Hypertension;</p> <p>Xue Yumei – Application of ICE in Reduction of Catheter Ablation-associated Complications;</p> <p>Zhang Wei – Application of ICE in Congenital Heart Disease;</p> <p>Fu Hua – ICE Guided Catheter Ablation for Atrial Fibrillation</p> <p>Chu Huimin – Application of ICE in Left Atrial Appendage Closure.</p>
Meeting Summary:	<p>(1) Content writing of newly added plates</p> <p>(2) Refinement of recommendation grades and text refinement</p> <p>(3) Recommendation of the list of review experts after the completion of the manuscript</p>
Minutes of ICE Chinese expert consensus conference	
Time:	2022.4.23 Review Meeting
Location:	Meeting online
Person:	42
Experts:	Zhang Yun, Zhong Jingquan, Zhang Jinlin, Chu Huimin, Li Yan, Tang Min, Ma Changsheng, Long Deyong, Jiang Chenyang, Zhang Wei, Fu Hua, Xue Yumei, Zhang Xiaochun, Xie Ruiqin, Xu Jian, Han Xuebin, Li Shufeng, He Jiangui, Zheng Liangrong, Wang Zulu, Shu Maoqin, Yuan Zuyi, Xu Yawei, Liu Yan, Liu Liwen, Zhang Xiaochun, Chen Minglong, Fan Jie, Liu Qiming, Liu Xu, Xia Yunlong, Jiang Tingbo, Li Xuebin, Zhu Wenqing, Dong Jianzeng, Li Shuyan, Wang Jianan, Kong Xiangqing, Tang Baopeng, Liu Xingpeng, Sang Caihua, Chen Mao

(Continued)

TABLE 1 (Continued)

Minutes of ICE China expert consensus conference

Meeting Minutes:	<p>All sections have completed the writing of the content based on the recommendations of the launch meeting and the manuscript reading meeting. Invited 15 writing experts and nearly 30 reviewers to participate in this review, hoping to collect most of the special suggestions and endorsements in the field of electrophysiology and be more authoritative. In particular, extensive suggestions were listened to one by one in the recommendation section of recommendation grade and content:</p> <ol style="list-style-type: none"> (1) The grade of recommendation was adjusted in order to be rigorous and in line with current evidence support. (2) The pictures selected in the text were selected from the cases in the expert clinic, optimized and streamlined. (3) The full text was optimized and uniformly worded. (4) Two overseas experts were invited to write and review the manuscript.
Meeting Summary:	<ol style="list-style-type: none"> (1) Invite two overseas experts as invited reviewers. (2) Picture pixel improvement, evidence level readjustment as recommended. (3) Translation of English manuscripts. (4) The revised version of this opinion shall be sent to all writing and reading experts to uniformly collect the suggestions on the final version and complete the revision.

overall success rate and safety of transseptal puncture (12). ICE is now used in a variety of interventional procedures requiring transseptal puncture, such as radiofrequency catheter ablation for atrial fibrillation (AF) or left ventricular arrhythmias, mitral valve intervention, and left atrial appendage closure (LAAC) (12). Surgeons are sometimes unable to precisely determine the relationship between the ablation target and a specific anatomical site because of the low resolution of 3D navigation and the 2D image overlay of fluoroscopy/radiography. However, ICE, as mentioned above, can clearly and accurately visualize the detailed and precise anatomical relationship between each cardiac chamber of interest in real time throughout the procedure, and assess the contact between the catheter and tissue, thereby improving the accuracy and efficacy of ablation. It plays an important role in the interventions of complicated arrhythmias such as atrial fibrillation, atrial flutter and ventricular arrhythmia (3, 12). In addition, with its ability to visualize the structures of the esophagus, arteries, atrial appendages, etc., ICE is expected to avoid or reduce the occurrence of complications, increase operators' confidence, shorten the learning curve and increase success rates (17). Moreover, ICE is used to guide a variety of interventions and monitor related complications, such as transcatheter aortic valve replacement (TAVR), closure of patent ductus arteriosus (PDA), closure of para-valvular leak (PVL), closure of ventricular septal defect (VSD), balloon pulmonary valvuloplasty, radiofrequency ablation of the interventricular septum for hypertrophic obstructive cardiomyopathy, left ventricular pacing, interatrial septal pacing, interventricular septal pacing, pericardiocentesis, myocardial tissue biopsy, screening of intracardiac thrombus, and implantation and removal of cardiac implantable electronic devices (2, 3, 12, 15).

Early use of ICE was associated with a complication incidence of approximately 4%, mainly atrial tachycardia induced by the catheter manipulation in the right atrium (18). Despite its significant clinical application value, one factor restricting the wide clinical application of ICE is its high cost.

However, data from a study in the United States indicated that the overall cost of intraoperative ICE is comparable to that of TEE (19). The overall cost-effectiveness and/or value added for ICE remains to be evaluated.

In conclusion, with the ability to image intracardiac structures and the adjacent anatomical relationship in real-time, ICE has gradually increased in use to guide interventional procedures for multiple structural heart diseases and arrhythmias and monitor intraoperative complications. Recommendations for the clinical application of ICE are shown in Table 2. Compared with X-ray and TEE, ICE has advantages of no radiation exposure, better tolerance, and no need for general anesthesia and sonographer assistance. Nowadays, 4D (real-time three-dimensional) ICE which can obtain high-quality 2D and 3D images in real time, has been gradually applied. In the future, ICE with higher image resolution and definition, reduced catheter diameter, and lower price, will very likely be even more widely used in a variety of clinical settings.

Application of intracardiac echocardiography in interventional diagnosis and treatment of arrhythmias

Intracardiac echocardiography helps the operator understand the key anatomy associated with arrhythmias, determine the spatial relationship between mapping and ablation catheters and their corresponding cardiac structures, and directly observe and guide the adjustment of degree of contact between the tip of the ablation catheter and the tissue. ICE can be used to monitor the formation, site, extent, and degree of ablation lesions to help determine the efficacy of ablation. Moreover, ICE can be used to monitor for complications in real-time to help determine their sites and severity. With the real-time monitoring function of ICE,

TABLE 2 Summary of recommended ICE applications.

Surgery/Procedure	Recommendation description	Recommended category
Transseptal puncture	The application of ICE guidance is recommended in the process of transseptal puncture. Particularly in patients with oversized or undersized atria or abnormal atrial septal anatomy or structures, thoracocyllosis, pectus excavatum, congenital cardiac anomalies etc. ICE-guided transseptal puncture is recommended, with expected increased procedural (TSP) success rates and decreased complications.	Recommended
Screening for atrial thrombus	ICE may replace TEE for screening patients for LAA thrombus who are reluctant to receive or not able to tolerate TEE, and whose atrial thrombus cannot be diagnosed or ruled out by CTA	Recommended
Catheter ablation of atrial fibrillation	ICE can be utilized to assist in guiding catheter ablation of atrial fibrillation to reduce the radiation exposure of patients and operators.	Recommended
Cryoballoon ablation for atrial fibrillation	ICE may be applied to guide balloon positioning and assesses PV occlusion occlusion, etc., to reduce the x-ray exposure time and the use of contrast medium when the non-balloon obstructive ablation is used.	Can be useful
Other atrial tachyarrhythmia	ICE may be used for imaging guidance during radiofrequency catheter ablation for premature atrial contractions, atrial tachycardia, atrial flutter, inappropriate sinus tachycardia, etc.	Can be useful
Catheter ablation for fascicular ventricular tachycardia	Assist in the identification of the origin of the ventricular tachycardia and judgment of catheter contact.	May be useful
Catheter ablation for ventricular arrhythmia originating from the outflow tract	ICE may be attempted to assist catheter ablation.	May be useful
Catheter ablation for ventricular arrhythmia originating from papillary muscles and regulatory tracts	ICE-assisted catheter ablation is recommended.	Recommended
Catheter ablation for ventricular arrhythmia originating from the left ventricular roof and other special heart chambers	ICE-assisted catheter ablation may be useful in guiding catheter-tissue contact, catheter manipulation.	May be useful
Catheter ablation for organic ventricular tachycardia	ICE may be used to assist in the identification of the myocardial matrix and scarred region with organic ventricular tachycardia and in the judgment of catheter contact and monitor ablation-related complications.	Can be useful
Monitoring of the complications during ablation	Help to monitor such complications as pericardial tamponade, acute thrombosis, as well as ablation injuries, to improve the overall surgical safety	Recommended
Occlusion of atrial septal defect and patent foramen ovale	ICE may be applied to guide the occlusion of secundum atrial septal defect and patent foramen ovale	Can be useful
Interventional procedure for ventricular septal defect	ICE may be used to guide interventional VSD closure in patients with complex anatomy.	Can be useful
Patent ductus arteriosus, etc.	ICE is recommended for interventional occlusion of PDA in patients with a large PDA, with renal insufficiency and allergies to contrast agents	Can be useful
Transcatheter aortic valve intervention	ICE may replace TEE in elderly aortic valve stenosis patients with esophageal lesions or not suitable for general anesthesia.	Can be useful
Transcatheter mitral valve intervention	ICE can be used to guide transseptal puncture and assess mitral regurgitation	May be useful
Transcatheter pulmonary valve intervention	ICE can be used in transcatheter pulmonary valve intervention to image the outflow tract of the right ventricle and pulmonary valve	Can be useful
Tricuspid valve invention	The ICE-guided procedure is recommended in patients with throat or esophageal lesions and those in whom anesthesia is contraindicated	Recommended
PVL intervention	3D/4D ICE-guided tricuspid valve invention	Can be useful
	ICE is applied to localize Perivalvular leak (PVL), help to select devices and determine the residual leak during the procedure and identify perioperative complications	Can be useful
	ICE-guided 3D/4D interventional procedure for PVL	Can be useful
Left atrial appendage occlusion	ICE may be used to evaluate structure and morphology of the left atrial appendage for guiding occlusion, selection of the best device type and size, assessing residual shunt, and related complications, etc.	Recommended
Radiofrequency catheter ablation in the ventricular septum for hypertrophic obstructive cardiomyopathy	ICE may be used to provide detailed anatomical information of the interventricular septum.	Recommended

(Continued)

TABLE 2 (Continued)

Surgery/Procedure	Recommendation description	Recommended category
Myocardial biopsy	ICE may be used for guiding the endomyocardial biopsy to reduce the risks associated with biopsy.	Can be useful
Left ventricular assist device implantation	ICE may be considered to guide the assist device implantation in the left ventricle when other imaging modalities are not appropriate	May be useful
Use in pregnant patients	ICE may be recommended preferentially to guide the conventional catheter ablation for tachyarrhythmia during pregnancy, pacemaker implantation, and interventional zero-ray therapy for some structural heart diseases.	Recommended
Preoperative examination or postoperative follow-up	ICE is performed in preoperative examination or postoperative follow-up	Not recommended
Removal of pacemaker electrode in high-risk cases	ICE is used for guiding lead extraction, reducing radiation exposure, and monitoring for operational complications	Can be useful

Is recommended: With definite clinical benefits, ICE can be preferentially applied.

Can be useful: With most clinical benefits and better efficacy, ICE can be applied in most cases.

May be useful: With insufficient evidence of clinical benefit, ICE may be applied based on the clinical realities.

Is not recommended: Without clinical benefit or with clinical damage, ICE is not recommended.

complications can often be detected and managed before a hemodynamic change occurs. ICE can visualize the entire cardiac structure and accurately locate the aortic root and pulmonary sinus even when manipulated in the right heart. ICE is moreover instructive during ablation of arrhythmias originating from the outflow tracts, and it is critical for mapping and ablation of arrhythmias originating from protruding intracardiac structures, such as papillary muscle, false tendon, and moderator band. Furthermore, ICE allows observation of myocardial contraction, ventricular arrhythmia substrates such as scar/fibrosis, all the while enabling reduction of exposure to X-ray radiation and contrast agents.

Application of intracardiac echocardiography in atrial arrhythmia

During interventional procedures for atrial arrhythmias, ICE can aid in the assessment of anatomical characteristics of the pulmonary veins (number, diameter, anatomical variation), the guidance of transseptal puncture, the screening for atrial/atrial appendage thrombus, and the monitoring of ablation lesion formation (3, 20). ICE can also monitor for and avoid possible complications in real-time, including esophageal thermal injury, inadvertent aortic puncture during TSP, and early detection of cardiac tamponade/thrombosis, so as to improve surgical safety (3). In addition, ICE is performed via an endovascular (venous) approach under local anesthesia, avoiding the risks of general anesthesia and discomfort from esophageal instrumentation (21). ICE is performed independently by the operator, thereby reducing labor costs (22). ICE-guided low X-ray or zero X-ray catheter ablation and LAAC have become increasingly mature and prevalent (23–25).

Application of intracardiac echocardiography in screening of left atrial appendage thrombus

Intracardiac echocardiography and TEE have distinct advantages and limitations. TEE has traditionally been the gold standard for the exclusion of left atrial and left atrial appendage thrombi and for anatomic delineation during catheter ablation for atrial fibrillation and LAAC. It is however, associated with increased patient discomfort and risk. Patients need to fast prior to the examination, and they need to be highly cooperative during the examination, and there is risk of esophageal injury during the examination. Left atrial CTA may also be used for the exclusion of left atrial appendage thrombi, but limitations include relatively high false-positive rates and the need for institutional experience for high quality images and accurate interpretation. IV contrast agent injection is required, with associated risks of anaphylaxis and kidney injury. Compared with TEE, ICE is expensive, as it uses a disposable catheter, but it is associated with less discomfort, greater compliance, lower incidence of complications, and less overall procedural radiation exposure. Many clinical studies evaluation ICE for left atrial and left atrial appendage thrombi have shown that (26–29). ICE is equivalent to TEE in clinical application. During ICE examinations, the left atrium and left atrial appendage can be scanned with the ICE catheter placed in the right atrium, coronary sinus ostium, right ventricular outflow tract, and pulmonary artery via a femoral venous approach (26). When the ICE probe is placed in the right ventricular outflow tract and pulmonary artery, the quality of left atrial appendage (LAA) imaging is significantly better, allowing effective identification of left atrial appendage thrombus. In contrast, when the ICE probe is placed in the right atrium, the quality of LAA imaging can be relatively poor (29). Since the coronary sinus ostium is close to the left atrial appendage, ICE placed in the coronary sinus can clearly show a cross-sectional view of the parallel left atrial

appendage. The disadvantages of ICE include the following: The operation of the catheter tip is restricted in the coronary sinus, and the ICE catheter tip is relatively stiff and may be associated with the risk of dissection or venous perforation if not performed properly (3).

Intracardiac echocardiography is a good option for the screening of left atrial and left atrial appendage thrombi in patients unable or unwilling to undergo TEE due to esophageal pathology, comorbidities rendering repeated sedation events riskier, or if left atrial CTA cannot confirm or rule out left atrial appendage thrombus. Further, ICE in patients who have undergone TEE or CTA, especially for when TEE suggests of “significant clouding,” “suspected thrombus,” and other unclear findings ICE may add additional diagnostic value (30, 31).

Application of intracardiac echocardiography in transseptal puncture

Transseptal puncture was first used for left atrial manometry by Ross et al. (32) in 1959 and rapidly popularized in the 1980s with the development of percutaneous balloon mitral valvuloplasty (PBMV) (33). Today, transseptal puncture has become essential in the process of cardiac interventional procedures such as catheter ablation of the left heart, intervention for congenital heart disease, LAAC and Left Ventricular Assist Device (LVAD) implantation. Transseptal puncture is traditionally performed under the primary guidance of conventional 2D fluoroscopy. Despite a high success rate (34), this approach has significant limitations. First, the specific procedure may dictate the optimal puncture site to facilitate catheter manipulation within the area of interest. Second, for patients with normal cardiac anatomy, a conventional fluoroscopy-guided transseptal puncture is safe and effective, but for patients with anatomical variations, which may not be known prior to the procedure the risk of puncture failure and complications may be significant. These risks include cardiac tamponade, puncture of the aortic root, arterial embolism, and pulmonary vein perforation.

Using ICE as the primary tool to guide transseptal puncture can make the puncture process easier, safer, and more specifically directed within the interatrial septum. Unlike TEE, ICE can be used in combination with the mapping system for 3D reconstruction by a single operator, with a wider field of view and no need for general anesthesia. One particular ICE system (Cartosound, Biosense Webster) enables contouring the cardiac structures visualized on ICE onto the EA map, as a magnet-enabled ICE catheter tip allows orientation of the catheter and hence ICE images within the 3D map. Before the transseptal puncture is performed, the operator can reconstruct key structures including the left atrium, fossa ovalis and aorta using ICE, and then select and mark the appropriate puncture site by adjusting the image sector as needed for subsequent steps. For the actual puncture procedure, ICE can visualize the entire TSP process. As a key step, when the puncture needle sheath is

delivered into the fossa ovalis, a “tenting sign” will be observed at the fossa ovalis by ICE. Microbubbles seen using saline injection after the needle is inserted can help to further confirm the needle tip location in relation to the fossa ovalis. Proper entry of the needle tip into the left atrium can be confirmed by microbubble shadowing in the left atrium during saline injection through the needle (Flow chart 1 shown in **Supplementary materials**). Excessive needle insertion should be avoided (3, 25, 35, 36).

Intracardiac echocardiography is even more valuable for transseptal puncture in patients with abnormal anatomical structures, such as interatrial septal thickening and interatrial septal aneurysm, and it is quite valuable for transseptal puncture after cardiac surgery, and after interatrial septal closure. ICE can accurately determine the positional relationship between the needle sheath and fossa ovalis, select an appropriate puncture site, improve the success rates of puncture, and avoid serious complications (37, 38). Therefore, ICE guidance can be routinely considered in these patients. In addition, an entirely zero X-ray transseptal puncture can be achieved under real-time ICE guidance, which is of great significance for pregnant and pediatric patients with arrhythmias (**Figure 1**). However, the zero X-ray approach is only suitable for experienced operators; normally, the transseptal puncture should be done in conjunction with conventional radiography and ICE.

Intracardiac echocardiography-guided catheter ablation for atrial fibrillation

Intracardiac echocardiography plays an important role during the entire course of catheter ablation for atrial fibrillation, improving the comfort, safety and efficiency of the procedure. Even for pulmonary vein antrum isolation, ICE real-time image monitoring also helps to improve the safety and accuracy of the procedure.

As for point-by-point ablation solely based on the contours of the left atrium and pulmonary veins in fast anatomy mapping (FAM), there is often a spatial deviation between the planned ablation point and the real point. This may be caused by shifts in patient respiratory movement during the procedure, mapping inaccuracies, or anatomic-spatial changes resulting from changes in rhythm. However, with ICE two-dimensional imaging in combination with the Carto-Sound module to construct three-dimensional models of the left atrium and pulmonary veins in a 3D electroanatomical mapping system, the accuracy of FAM can be improved. In most clinical studies, the ultrasound catheter was placed in the right atrium. To further improve the model accuracy, the ICE catheter was then placed in the left atrium in some studies. In this way, the modeling was not only feasible but also more accurate (compared with modeling in the right atrium) (39). On this basis, some study sites performed zero X-ray radiofrequency ablation for atrial fibrillation with the integration of ICE and 3D electroanatomical mapping. As a result, 19 of 21 patients with atrial fibrillation received zero X-ray radiofrequency

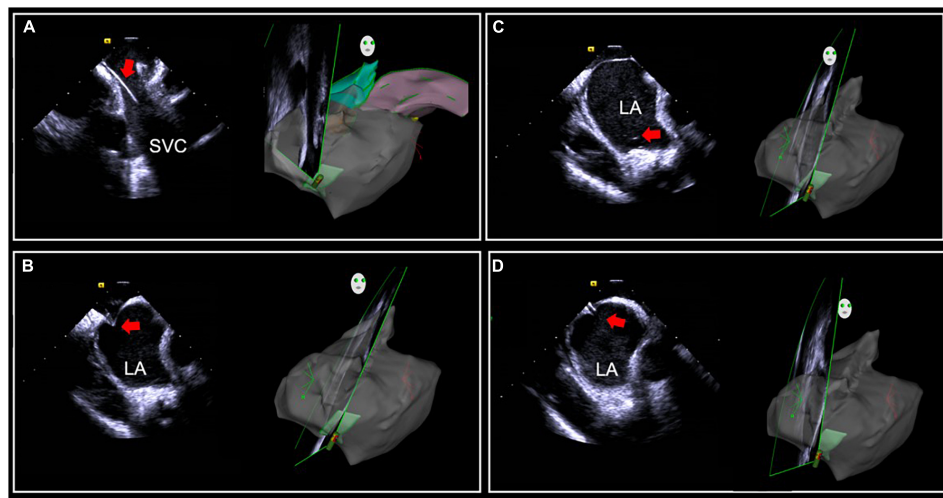


FIGURE 1

Intracardiac (ICE)-guided zero X-ray transseptal puncture. (A) Guidewire and sheath seen in SVC. (B) "Tenting sign" in the fossa ovalis by puncture needle sheath. (C) Saline injection microbubbles into the left atrium after the needle is inserted. (D) Needle tip into the left atrium. SVC, superior vena cava; LA, left atrium.

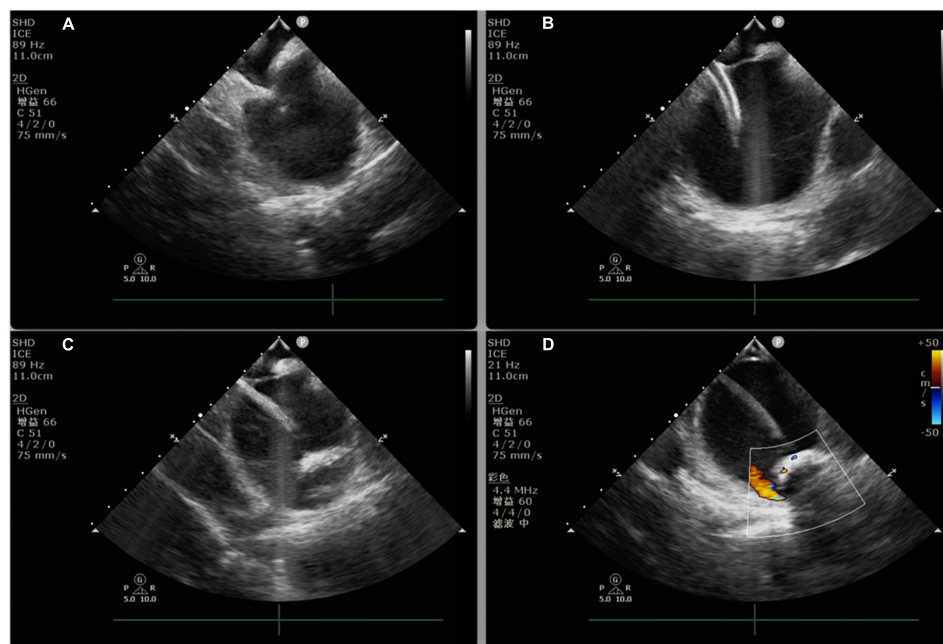


FIGURE 2

Intracardiac echocardiography-guided cryoablation. (A) ICE-guided low transseptal puncture; (B) cryoablation sheath delivered through the low transseptum; (C) cryoballoon delivered into the left superior pulmonary vein under ICE guidance; (D) ICE color Doppler ultrasound applied to assess cryoballoon closure.

ablation throughout the entire course of the procedure (25). In addition, the procedure was safe and effective (40), without any procedure-related complications. In cryoablation for atrial fibrillation, PV occlusion assessment by ICE-guided balloon positioning can reduce the duration of X-ray exposure and

the dose of a contrast agent, thereby improving the efficiency of the procedure.

Real-time three-dimensional ICE, or four-dimensional ICE, is a new technique emerging in recent years. Few studies have been reported on ICE-guided catheter ablation for atrial

fibrillation. However, with the conduct of relevant research, we expect it to be useful in the whole process of catheter ablation for atrial fibrillation with improved efficiency and safety (Flow chart 2 shown in **Supplementary materials**).

Application of intracardiac echocardiography in other atrial arrhythmias

Intracardiac echocardiography is also useful during the ablation of other atrial arrhythmias similar to that in atrial fibrillation ablation, primarily including the screening of LA thrombus, delineation of anatomical structures, direct observation of the contact and movement of catheter relative to the endocardium and the change of focus on ablation during radiofrequency ablation, monitoring for thrombus during ablation, and possible prevention of steam pops. In addition, the examination process of ICE-guided ablation for left atrial-related atrial arrhythmias is similar to that of ICE-guided ablation for atrial fibrillation. For right atrial-related atrial arrhythmias, the ICE catheter can be placed in the right atrium to visualize important anatomical structures such as the tricuspid isthmus, tricuspid annulus, right atrial appendage, coronary sinus ostium, and superior vena cava by rotating and flexing the catheter clockwise or counterclockwise from the “home-view.” Several articles have suggested that ICE can visualize such anatomical structures as trabecula, depression, and Eustachian valve above the tricuspid isthmus line for the ablation of typical atrial flutter, reducing the surgical time and fluoroscopy time, and improve the success rate and safety of the procedure (41–44). For atrial tachycardia originating from the non-coronary cusp, the ICE catheter can be placed in the right atrium or right ventricular outflow tract to monitor the ablation process.

Application of intracardiac echocardiography in cryoablation

Pulmonary vein isolation (PVI) is the standard approach for treating atrial fibrillation, restoring and maintaining sinus rhythm (45). Cryoballoon ablation (CBA) has emerged as an established modality to perform PVI in patients with atrial fibrillation (45, 46). CBA is as effective as radiofrequency ablation in maintaining sinus rhythm, but CBA tends to be associated with more radiation exposure and higher contrast agent dose (45). In CBA for atrial fibrillation, the use of ICE to guide balloon positioning and assess closure can reduce the duration of X-ray exposure and the dose of contrast agent, without affecting the success rate and safety of the procedure (47). However, there is still a lack of data that ICE-guided CBA is clearly more efficient and safer than two-dimensional X-ray imaging-guided CBA in performing PVI. In addition, ICE-based color Doppler flow imaging (CDFI) requires less exposure to contrast agents. In PVI, the presence of flow around the balloon observed with CDFI indicates incomplete obstruction, in which case the operator should adjust the balloon position, without

the need for venography (48). Therefore, ICE is an emerging option for those who cannot undergo fluoroscopy due to renal insufficiency or contrast media allergy.

Pulmonary vein isolation alone demonstrates a low success rate in patients with persistent atrial fibrillation. Given this, some studies reported the application of CBA for PVI with additional substrate ablation in the treatment of persistent atrial fibrillation in recent years: (1) left atrial roof linear ablation (49); (2) left atrial posterior wall isolation (PWI) (50); (3) segmental pulmonary vein isolation or extended pulmonary vein antrum ablation (51); (4) left atrial appendage isolation; (5) ablation of non-pulmonary vein triggers (52). The above studies suggest that the application of CBA for PVI with additional substrate ablation may improve the ablation success rate of persistent atrial fibrillation, but this finding remains to be confirmed by multicenter randomized controlled studies. PVI with additional substrate ablation mostly requires the application of non-balloon obstructive ablation techniques. In this case, imaging or blood flow monitoring by ICE may help to guide cryoballoon positioning and improve the efficiency and efficacy of ablation (53) (**Figure 2**). However, ICE-guided CBA should be performed by experienced and technically trained operators (Flow chart 3 shown in **Supplementary materials**).

Application of intracardiac echocardiography in reduction of catheter ablation-associated complications

Rapid diagnosis and prevention of potential complications during ablation is one of the most important functions of ICE (54). A recent study showed (55) an early mortality of 0.46% in patients undergoing catheter ablation for atrial fibrillation. Prompt management of postoperative complications and congestive heart failure may be crucial to reducing mortality. Although the experience of operators and their knowledge of indications are essential, immediate prevention, diagnosis, and management of surgical complications are particularly critical to reducing the mortality of atrial fibrillation ablation. Major complications associated with the leading causes of death include cardiac perforation during ablation, left atrial thrombus, esophageal injury, and pulmonary vein stenosis (55).

The application of ICE in catheter ablation can reduce the incidence of perioperative complications, especially the incidence of serious complications such as thromboembolism and cardiac tamponade (3, 55–64), and shorten the average length of stay of patients (60). Studies have demonstrated that ICE-guided circumferential pulmonary vein ablation with the Carto-Sound system is safe and feasible in patients with atrial fibrillation compared with conventional X-ray radiography (65), and there was no significant difference in the incidence of complications such as puncture site hematoma and cardiac tamponade between the two groups (65–67). The integration of ICE and electroanatomical mapping allows zero X-ray transseptal puncture and safe and effective ablation of left-sided

tachycardia (including atrial fibrillation, atypical atrial flutter, left-sided accessory pathway, ventricular tachycardia, and focal atrial tachycardia) (68). In this way, the incidence of complications (stroke/transient ischemic attack, pericardial effusion, cardiac tamponade, pseudoaneurysm requiring surgery or intervention, esophageal injury, transient phrenic nerve palsy, and displacement of cardiac implantable device) within 30 days after surgery is 1.9%, and the incidence of transseptal puncture-related cardiac tamponade is 0.2%.

Acute cardiac tamponade is one of the most common serious complications associated with catheter manipulation during ablation. ICE can detect early pericardial effusion along the lower ventricular border and posterior left atrium, which can be managed by reversing anticoagulant therapy to prevent cardiac tamponade (54, 57, 59, 62, 63). Meanwhile, pericardiocentesis can be performed as early as possible, with a drainage tube placed if necessary. ICE also allows continuous monitoring of the dynamic changes of pericardial fluid during drainage (54, 57). The ICE catheter is advanced from the right atrium with the tip pointing anteriorly, and then deflected across the tricuspid valve and into the right ventricle where the inferoposterior border of the heart can be seen (54). Clockwise rotation at the interventricular septum reveals images of the left ventricular cavity, mitral valve, and posteroinferior space of the pericardium (54).

Thromboembolism is another serious complication associated with left cardiac ablation. ICE-guided catheter ablation allows real-time observation of the factors associated with increased stroke risk, such as thrombosis at the catheter, sheath, and endocardial lesion sites and clot formation on the ablation electrodes (54). Once a soft thrombus is detected by ICE, the clot can be aspirated into the sheath, and a higher dose of anticoagulant can be administered to prevent serious thromboembolic complications (54). If the thrombus is firmly attached to the catheter, ICE can guide to remove the thrombus into the right atrium (55).

Esophageal injury and atrio-esophageal fistula are important issues in atrial fibrillation ablation. The incidence of the atrio-esophageal fistula is 0.05–2%, while the esophageal injury is still common (54). The ability of ICE to identify the position of the esophagus in relation to the left atrium is comparable to that of magnetic resonance imaging. In addition, with the real-time imaging function of ICE, operators can monitor the position of the ablation catheter and the esophagus in real-time during catheter ablation, and reduce RF energy to reduce the risk of esophageal injury when the catheter ablates the area close to the posterior wall of the left atrium (54). However, there is still a lack of data from clinical studies on the effectiveness of ICE in monitoring the position of the esophagus during catheter ablation for atrial fibrillation (69).

Pulmonary vein stenosis is associated with ablation sites at the pulmonary vein antrum, likely when lesions are delivered in a more ostial location. This complication can be mitigated

or avoided by accurately localizing the optimal ablation site with ICE (54, 61). ICE can also monitor development of tissue edema, a marker for energy delivery, at the ablation site. With ablation site real-time monitoring on ICE, energy delivery can be stopped immediately once manifestations of local overheating such as tissue blanching or microbubble generation are found at the ablation site, so as to prevent further damage, including risks of steam pop, and potential excessive ablation that may increase risks of PV stenosis (61, 70). Moreover, ICE can measure pulmonary vein flow velocity. In patients undergoing repeat ablation procedures, the application of ICE to measure pulmonary vein flow velocity in addition to assessing PV anatomy and vein caliber are important steps prior to re-ablation (54).

Complications associated with ICE application itself are rare. However, as the ICE catheter is relatively stiff and may result in vascular injury and/or perforation during its advancement, it should be advanced with care (57).

Short learning curve and low learning difficulty for intracardiac echocardiography-guided catheter ablation

The ability to accurately and clearly delineate cardiac anatomy is directly related to procedural efficiency, efficacy, and safety. False lumens and other anatomic inaccuracies are inevitable with conventional contact-type three-dimensional reconstruction, affecting the operators' judgment of ablation targets or special structures. ICE, as a non-contact three-dimensional reconstruction technique, is not limited by catheter position. With ICE, the atrial body, pulmonary veins, atrial appendages and other structures can be entirely reconstructed in an objective and accurate manner through simple sector adjustments. Furthermore, based on the integration of ICE and contact-type reconstruction of key structures, a more realistic and accurate anatomical model can be obtained after image fusion, creating an anatomic framework for subsequent ablation (Figure 3).

During ablation, ICE can not only track the ablation catheter in real time and identify the catheter position in complex structures such as the left atrial appendage-pulmonary vein ridge, but it can also help avoid esophageal injury and excessive ablation at thinner parts of the myocardium.

Intracardiac echocardiography-guided standardized approach to ablation procedures may improve several procedural outcomes. Beginners can obtain satisfactory ablation results with ICE-guided low X-ray catheter ablation for atrial fibrillation, with an average fluoroscopy time of 2.3 ± 3.0 min. The learning curve is short, with the fluoroscopy time dropping rapidly to 9 s from 3.8 min during a study evaluating learning curve (71).

Experts' recommendation: (1) If possible, ICE-guided transseptal puncture is recommended, especially for patients with abnormal interatrial septal anatomy. (2) Routine TEE

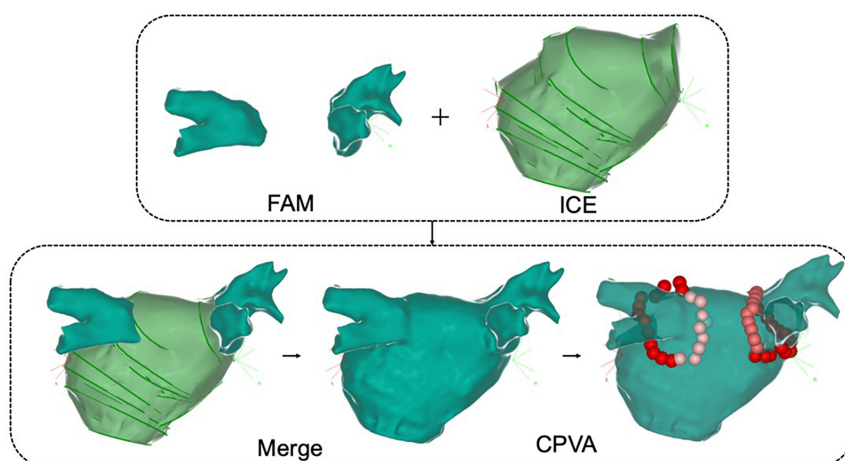


FIGURE 3

Intracardiac echocardiography combined with fast anatomical reconstruction for left atrial model reconstruction. FAM, fast anatomical mapping; Merge, ICE combined with three-dimensional reconstruction; CPVA, circumferential pulmonary vein ablation.

or left atrial and pulmonary vein CT examination should be performed before catheter ablation in patients with atrial fibrillation to rule out left atrial appendage thrombus and preliminarily assess the shape and size of the left atrial appendage; for patients with suspected thrombus that is difficult to distinguish preoperatively or unable to tolerate and unable to undergo left atrial and pulmonary vein CT or TEE examination, ICE can be applied intraoperatively to provide additional assessment for left atrial appendage thrombus and re-assess the shape and size of the left atrial appendage; meanwhile, ICE can also be used as an alternative monitoring and assessment technique in patients intolerable to TEE. (3) If possible, ICE-guided catheter ablation requiring low X-ray or zero X-ray is recommended for atrial fibrillation in medical centers to reduce the radiation exposure of patients and surgeons. (4) Imaging and blood flow monitoring by ICE may help to guide cryoballoon positioning and improve the efficiency and efficacy of ablation. (5) Catheter ablation for patients who are not suitable for radiation including pregnant women should be performed under ICE guidance. (6) During the training of new electrophysiologists, instruction in ICE is recommended.

Application of intracardiac echocardiography in interventional diagnosis and treatment of ventricular arrhythmia

Intracardiac echocardiography plays an important role in the catheter ablation for ventricular arrhythmias, just as in interventions for atrial arrhythmias. It is mainly used to monitor cardiac structures in real-time, reduce the duration of surgery

and radiation exposure (72), delineate dyskinetic areas in detail (73), and rapidly identify intraoperative complications (74).

Application of intracardiac echocardiography in fascicular ventricular tachycardia

Left posterior fascicular ventricular tachycardia (VT) is the most common type of idiopathic ventricular tachycardia, and its electrophysiological mechanism remains controversial. It is traditionally considered to be a macro-reentrant arrhythmia originating from the left posterior fascicle, which needs to be differentiated from the ventricular tachycardia originating from papillary muscles in clinical practice. However, definitive differentiation between the two based on ECG and EP is sometimes difficult. In fact, it has been proved that the mechanism of a part of fascicular ventricular tachycardia is closely related to such structures as Purkinje fibers and false tendons around the papillary muscles (75). For this part of left posterior fascicular ventricular tachycardia, the target for successful ablation may not be conventionally in the left mid-posterior septum, but around such anatomical structures as the left posterior papillary muscle and/or the false tendon attached to it. Since these structures and septa are very close to each other, especially during episodes of ventricular tachycardia when cardiac chambers shrink, and these structures are anatomically complex in three dimensions, they may be difficult to distinguish in an ordinary three-dimensional mapping system. By visualizing the position of the ablation catheter relative to the left interventricular septum, papillary muscles and false tendon intraoperatively, ICE can identify the true anatomical position of the optimal target, as well as the degree of contact between the catheter and the target, which is of great significance in further exploring the mechanism of left posterior fascicular ventricular tachycardia and improving

the success rate of ablation. Therefore, in recent years, ICE has been gradually recognized for its advantages in the mapping and ablation of left posterior fascicular ventricular tachycardia.

Application of intracardiac echocardiography in ventricular arrhythmia originating from outflow tracts

Idiopathic outflow tract ventricular arrhythmias mainly include monomorphic ventricular premature beats, non-sustained ventricular tachycardia, and sustained monomorphic ventricular tachycardia. Right ventricular outflow tract ventricular arrhythmia is the most common type of ventricular arrhythmias in clinical practice, mostly idiopathic, accounting for about 80% of outflow tract ventricular arrhythmias (76). In recent years, with the further understanding of right ventricular outflow tract ablation, reversed U-curve ablation above the pulmonary valve has become a common approach to deliver the ablation catheter to the target site with adequate contact force and stability (77). However, without ICE-guided precise anatomical orientation of ablation targets, it remains difficult to determine the exact ideal ablation position: Whether the catheter tip is placed above the pulmonary valve? Is the catheter in place? The anatomical position is difficult to determine by angiography alone. However, ICE can clearly demonstrate the adjacent relationship between the ablation catheter and the pulmonary valve, pulmonary artery and right ventricular outflow tract, and observe the contact between the catheter and the corresponding anatomical position of the ablation target in real time. Moreover, ICE along with its three-dimensional model can help operators understand the anatomical sites of mapping and ablation in a more intuitive way, thus likely improving the success rate. A close adjacent relationship between the left coronary artery and the anteroseptal site of the right ventricular outflow tract can be confirmed by ICE combined with electroanatomical mapping. Continuous ICE images can be obtained by rotating the imaging catheter in the right ventricle to mark the anatomical images of the left coronary artery. To delineate the structure of the ventricular outflow tract, the ICE catheter is usually placed in the right atrium and rotated clockwise from the tricuspid valve, with the aortic valve on the long axis and the pulmonary valve on the short axis. In addition, placement of the ICE catheter directly within the RVOT can help to visualize that region.

The right ventricular outflow tract myocardial tissue anatomically extends to the pulmonary valve and pulmonary artery, making the positioning of ablation targets more complex. Some cases failing with subvalvular ablation may be successfully treated by supra-ventricular ablation. However, for supra-ventricular ablation, a transvalvular approach may lead to valve injury and other complications. In this case, the application of ICE not only helps to avoid such complications, but also enables sound reconstruction and real-time monitoring of the pulmonary artery, aortic valve, left anterior descending artery and right

ventricular outflow tract during the surgery, and avoids the use of fluoroscopy and contrast agent and the occurrence of such complications as valvular insufficiency. With ICE placed in the right atrial appendage to obtain real-time cross-section images of pulmonary valves (78), it is easier to locate each pulmonary valve and determine the ablation target, thus performing a successful ablation.

Given the complex anatomy (coronary arteries, etc.) adjacent to the right ventricular outflow tract, RF energy transmitted close to the coronary arteries may cause obstruction of major epicardial vessels (e.g., left anterior descending artery) and possibly myocardial infarction. It is therefore essential to identify the anatomic location of these structures, traditionally using coronary angiography. ICE enables accurate reconstruction and real-time dynamic observation of proximal arterial anatomy during ablation, avoiding the use of contrast agents and further reducing risk to patients. Right ventricular outflow tract ventricular arrhythmias usually originate from the root of the pulmonary artery. Without ICE, operators may be unable to determine the relationship between the ablation target and a specific anatomical structure at that site due to trabecular muscles and fibrous tissues arranged in a crisscross pattern at this site, the low resolution of 3D navigation and the 2D image overlay of fluoroscopy/radiography. However, ICE can visualize fine anatomical landmarks of the heart in real time and guide the catheter operation (17) throughout the procedure, thereby increasing operators' confidence and shortening their learning curve. Therefore, ICE is expected to improve the success rates and reduce complications for these procedures.

With improved understanding and experience, the recognized incidence of ventricular arrhythmia originating from the left ventricular outflow tract is increasing year by year, especially ventricular premature beat/ventricular tachycardia originating from the aortic sinus and its adjacent areas. As the aortic sinus is located in the central part of the heart and with adjacent tissues are critical and anatomically complex, patients whose ventricular arrhythmias originate from these anatomically complex regions (coronary artery, etc. **Figure 4**), may be at risk for serious complications such as valve injury, cardiac perforation, even acute myocardial infarction and complete atrioventricular block. As the aortic root is the continuation of the left ventricular outflow tract, where the blood flow is fast and under high pressure, the ablation catheter may not fit easily and stably, and sometimes ablation energy can be difficult to deliver effectively. Therefore, anatomic reconstruction of the area around this ablation target is particularly important. ICE can construct a three-dimensional model of the left ventricular outflow tract, assess the distance between the artery and the catheter, eliminate the potential risks of ablation within this area, and clarify the feasibility of ablation. With the ICE probe placed in the right atrium to image anteriorly, the mapping position and the position of the ablation catheter in relation to the aorta, aortic valve,

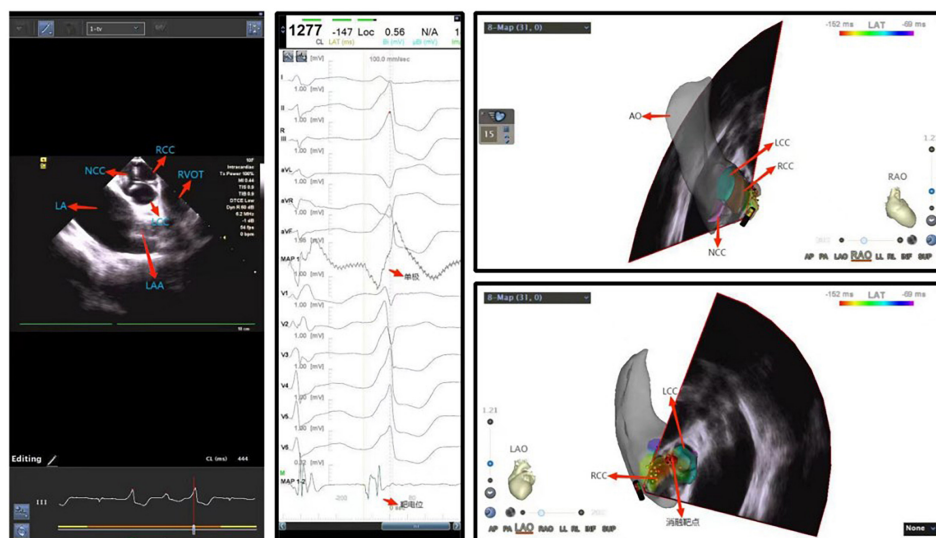


FIGURE 4

Ventricular premature beat between left and right coronary cusps. NCC, non-coronary cusp; RCC, right coronary cusp; LCC, left coronary cusp; LA, left atrium; LAA, left atrial appendage.

coronary ostium and other structures can be monitored in real time, which helps to reduce the potential damage to the aortic valve or coronary artery, increase surgical safety and improve the success rate of ablation. In particular, ICE also plays an increasingly important role in the ablation of pediatric outflow tract ventricular arrhythmias (79).

Application of intracardiac echocardiography in ventricular arrhythmia originating from papillary muscles

Ventricular arrhythmias originating from the left and right ventricular papillary muscles and moderator bands are relatively common in clinical practice. As these anatomical structures are located on the inner surface of the cardiac chamber, neither conventional X-ray radiography nor three-dimensional imaging systems can visualize their locations. In addition, these structures are not always in a fixed position due to the catheter advancement as they have smooth surfaces and move independently during the cardiac cycle. In this case, in the mapping and ablation for such arrhythmias with conventional approaches, the catheter may be difficult to direct toward the ablation target or remain stable during ablation (Figure 5). In particular, the contact of the catheter to the left ventricular anterior papillary muscle is challenging when the electrophysiologist only applies X-ray for imaging guidance, while ICE shows great advantages (Figure 6). As a result, ablation for such arrhythmias may have lower success rates and a higher recurrence rate, compared with that for ventricular arrhythmias originating from other sites (80). In recent years, ICE has become an indispensable adjunct to

such arrhythmias in the following ways: (1) to visualize the anatomical location of papillary muscles and quickly guide the preliminary placement of mapping catheter; (2) help the surgeon clarify the segments (tip, middle, and root) and sides of the papillary muscle where the catheter is located through real-time ultrasonic sector and three-dimensional tracking, so as to determine the exact position of the optimal target; (3) ensure good contact between the catheter and the papillary muscle under real-time monitoring and through subtle adjustment of the catheter, contributing to accurate mapping (pacing and activation mapping) and effective ablation; (4) help to observe the ablation effect and degree of injury (tissue edema or blanching) during surgery, monitor the occurrence of pop and complications, reduce radiation exposure and improve safety (Flow chart 4 shown in **Supplementary materials**).

Application of intracardiac echocardiography in ventricular arrhythmias originating from the top of left ventricle (aka left ventricle summit) and other special sites in cardiac chambers

Ventricular arrhythmias may originate at the top of the left ventricle, or LV summit, often the mid-myocardium or epicardium, located at the junction between the aorta and the left ventricular inflow tract. In this junction also lies a layer of tough fibrous tissue on the intimal surface that connects the aorta and mitral valve, often termed the aorto-mitral continuity, with the epicardial surface is close to the coronary artery and covered with a thick layer of epicardial adipose (81). Catheter ablation for arrhythmias arising from this region comes with a low success rate in this area

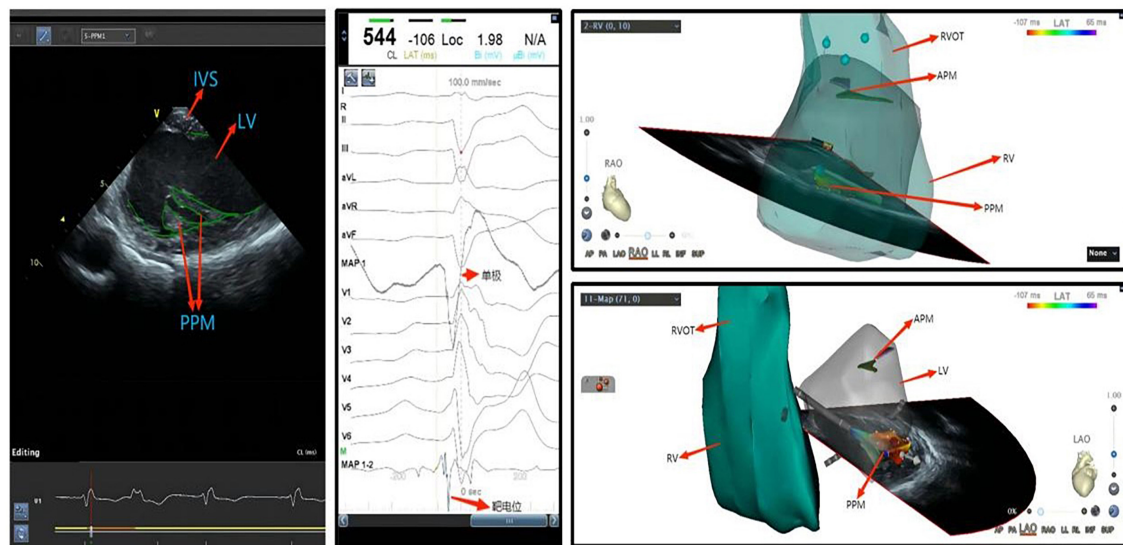


FIGURE 5

Ventricular premature beat of left ventricular posterior papillary muscle. IVS, interventricular septum; LV, left ventricle; APM, anterior papillary muscle; PVOT, right ventricular outflow tract; PPM, posterior papillary muscle; RV, right ventricle; LV, left ventricle.

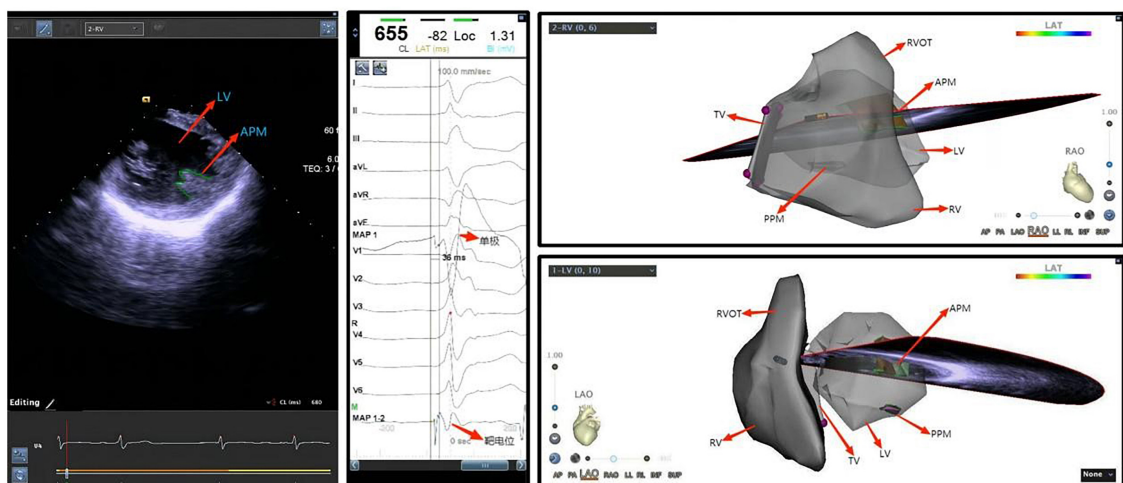


FIGURE 6

Ventricular premature beat of left ventricular anterior papillary muscle. LV, left ventricle; APM, anterior papillary muscle; TV, tricuspid valve; PVOT, right ventricular outflow tract; PPM, posterior papillary muscle; RV, right ventricle; LV, left ventricle.

because the proximal coronary artery is covered with a thick layer of epicardial adipose, and catheter ablation in this area may pose a potential risk of injury to these vessels (82). Coronary sinus or large cardiac vena cava venography is usually used to guide positioning in clinical practice, and often endocardial ablation as well as epicardial ablation are adopted for treatment. The application of ICE assisted catheter ablation has demonstrated that: Although ICE has resolution that is too low to delineate distal small vessels, when the catheter is placed in the right ventricular outflow tract, it still can delineate

the left anterior descending coronary artery, the left ventricle, the aorta and other anatomical structures, presenting the 3D space position and adjacent relationship to guide the ablation catheter accurately in this challenging anatomy. The operator can then perform ablation successfully in this area in the absence of venography or angiography (83). ICE also plays a unique role in cardiac chambers that are difficult to be visualized by X-ray imaging guidance and in special types of ventricular premature beats that are difficult to be located by surface ECG (Figure 7).

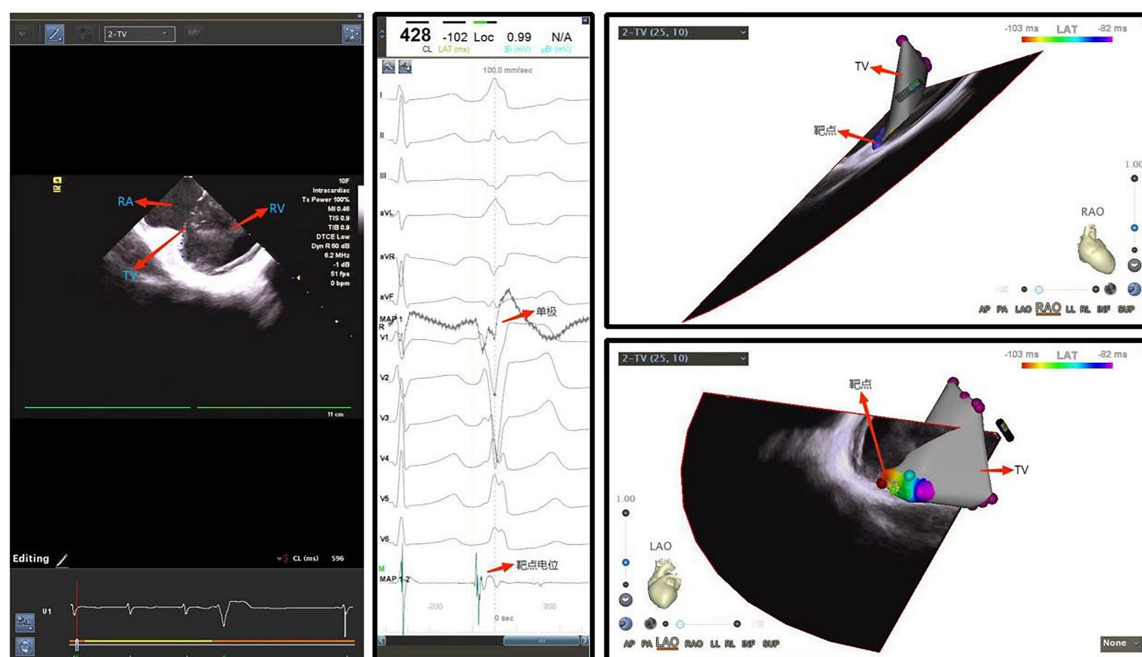


FIGURE 7

Ventricular premature beat originating from the tricuspid annulus. RA, right atrium; TV, tricuspid valve; RV, right ventricle.

Application of intracardiac echocardiography in ventricular tachycardia with ischemic cardiomyopathy

In ischemic cardiomyopathy, ventricular scar may mediate macroreentrant ventricular tachycardia. Some patients after infarct may eventually develop ventricular aneurysm, further complicating the anatomic considerations for catheter ablation. The ablation strategy for these patients is most commonly guided by either activation mapping and/or substrate mapping in the scar area. Ablation in ventricular tachycardia patients with ischemic cardiomyopathy is challenging in part because cardiomegaly and often thinned ventricular walls may increase the challenge and risks to mapping and ablation. Preoperatively, scar regions can be approximately localized by transthoracic echocardiography (TTE) and cardiac CT/MRI. Contours of the left (or right) ventricle and associated structures can be reconstructed with ICE via the right ventricle or sometimes the right atrium or CS. ICE can localize the catheter in relationship with the ventricular tissues, resulting in likely lowered risk of cardiac perforation due to excessive contact force. Especially in ischemic cardiomyopathy patients with ventricular aneurysm, left ventricular anatomy is often distorted, so that ICE reconstruction of a ventricular aneurysm and the aneurysmal neck can be helpful to define the anatomy and hence potential ablation target (84) (Figure 8).

Another important advantage of ICE for such patients is the delineation and quantification of the scar area. The

scar area appears as a hyperechoic area on the ultrasound sector, and the marginal area appears as a mixture of medium to high echo densities, which is significantly different from that of normal ventricular myocardium (85). A study of 18 patients with organic ventricular tachycardia (83% with ischemic cardiomyopathy) showed that the ICE-defined scar area was 86% concordant with the scar area measured by substrate mapping (86). This approach is not limited to ischemic cardiomyopathy (87). A propensity score study that ultimately included 1324 patients with organic ventricular tachycardia showed a lower readmission rate and reoperation rate for ventricular tachycardia in the ICE group than those in the non-ICE group (88).

Experts' recommendation: (1) As a safe, effective, efficient, and comprehensive approach with unique advantages in identifying and locating ablation targets and specific cardiac anatomy, and with superiority to other techniques in identifying small abnormal foci, ICE is recommended as an imaging modality in radiofrequency ablation of left and right ventricular outflow tract arrhythmias, post-TAVR ventricular tachycardia and VSD-induced ventricular tachycardia in adults. Radiofrequency ablation of ventricular tachycardia augmented by ICE may also reduce readmission rates, the possibility of repeated ablation, and the incidence of complications. (2) ICE can be actively applied in ventricular arrhythmia patients with ventricular wall dysfunction who require ablation.

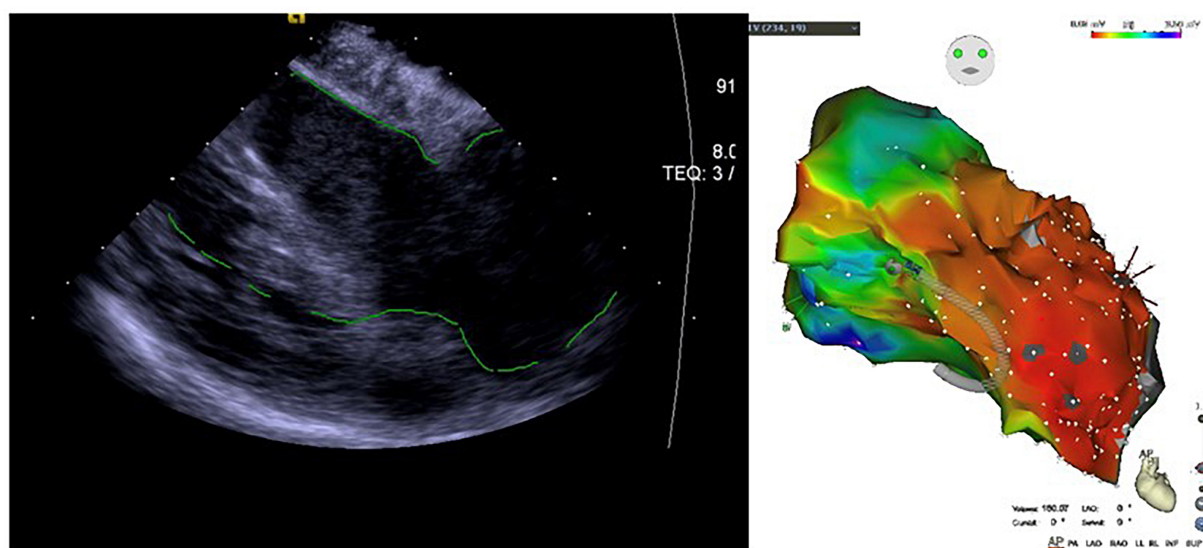


FIGURE 8

Application of ICE in ischemic cardiomyopathy with ventricular aneurysm-induced ventricular tachycardia.

Application of intracardiac echocardiography in congenital heart disease

Application of intracardiac echocardiography in atrial septal defect and patent foramen ovale

Intracardiac echocardiography is now the most widely used technique in ASD and PFO closure among the interventional closure treatments for various congenital heart diseases. Statistical results in the United States indicate that the use of ICE in ASD closure has increased from an initial 9.7% to more than 50% today (89). In the past, TEE was considered the gold standard to guide interventional closures of ASD and PFO (90, 91), but now several studies have confirmed that use of ICE has better safety and clinical outcomes than TEE and is a more suitable ultrasonographic approach to guide the closure of secondary ASD and PFO (92, 93).

Intracardiac echocardiography has a higher image resolution than TEE. Despite the lack of multiplanar imaging capabilities, it can still image the interatrial septum from multiple views with its flexible probe, thereby obtaining images similar to or better than those obtained by TEE (94). ICE can accurately assess the dimensions of the fossa ovalis, the diameter of interatrial septum, the width or length of tunnel, and the diameter of tunnel inlet and outlet; it can also display any shunt at the atrial level in patients with PFO and determine whether there is a long valvula venae cavae inferioris or Chiari's

network, interatrial septum aneurysm, double-layer septum and other abnormalities and special complex structures (95). In ASD closure, ICE can accurately measure the diameter of the ASD on multiple views before and after closure device release, assess the length and thickness of ASD edges, such as superior and inferior vena cava edges, anterosuperior edge and superior edge of interatrial septum, and posterior part of diaphragm, and display the relationship between ASD and surrounding structures (right pulmonary vein, coronary sinus, mitral valve, tricuspid valve, etc.), which is helpful in selecting an appropriate size of closure device and to rule out the possibility of other defects or rare conditions such as venous sinus ASD (96). Moreover, real-time color Doppler flow monitoring by ICE can be performed intraoperatively to further exclude other potential defects. ICE can better display the posterior and inferior edges of interatrial septum (97), as well as the relationship between closure device and superior vena cava (especially in young children) than TEE (98). It can be used in the closure of complex ASDs such as ASD with diameter of more than 38 mm and/or ASD with edge damage except anterosuperior edge damage, porous ASD and ASD with impaired systolic function (99–101). In addition, ICE has been shown to be more accurate than TEE in performing anatomical measurements and guiding implantation (particularly for patients with smaller left atria) (98). Intraoperatively, ICE can monitor and guide the operation process in real time in an effective and safe manner, assist the surgeon in accurately locating the PFO slit, and make the guidewire pass through the slit quickly, thereby shortening the operation time; guide the surgeon to release the closure device under direct vision throughout the procedure, determine

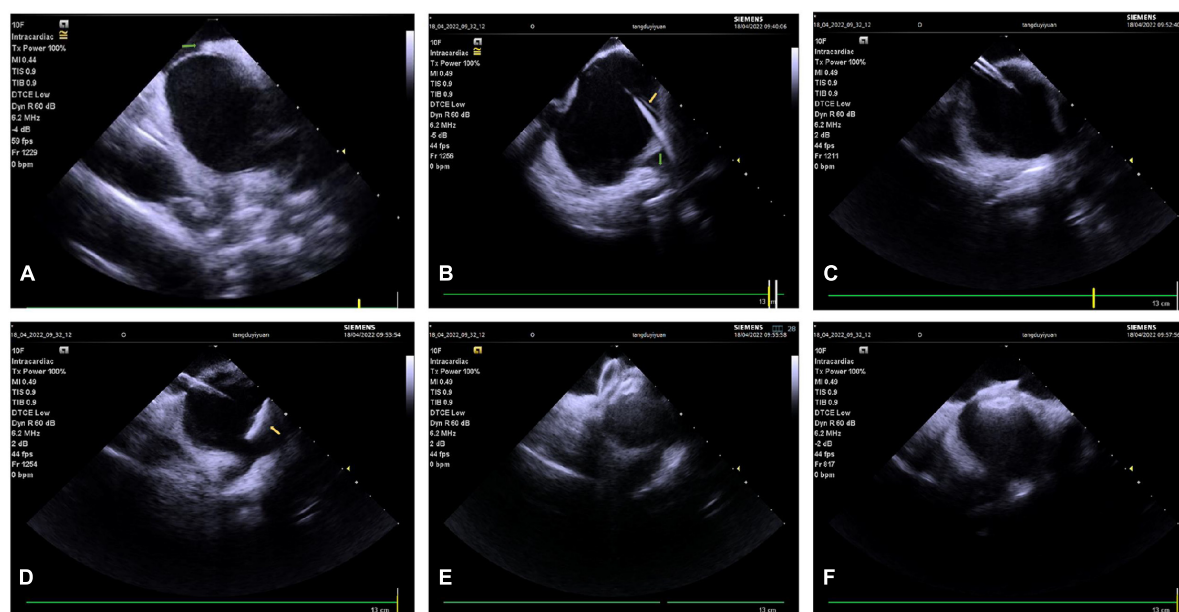


FIGURE 9

Patent foramen ovale closure procedure guided by ICE. (A) PFO slit (green arrow). (B) The guidewire passes through the PFO slit (yellow arrow points to the highlighted echo which represents the guidewire, and green arrow points to the left superior pulmonary vein). (C) Send the delivery sheath to the ostium of the left superior pulmonary vein. (D) Release the left plate of the closure device (the yellow arrow points to the left plate). (E) Perform a pull test after the closure device is fully expanded. (F) The closure device is released. PFO, patent foramen ovale.

whether the closure device is tilted or in a wrong position, and observe whether the closure device is stable, avoiding the X-ray artifacts caused by TEE transesophageal probe. In addition, the surgeon can confirm whether there is residual shunt by injecting normal saline and/or by color Doppler examination under the guidance of ICE. In PFO closure, in case of a particularly long tunnel, the closure may be performed by transseptal puncture, otherwise, there may be a large amount of residual shunt (102). ICE is considered an important tool to guide the transseptal puncture (103) (Figure 9).

Another significant advantage of ICE is that it can significantly shorten intraoperative X-ray exposure time (104), effectively reducing the radiation hazard to patients (especially children, pregnant women, obese patients) and surgeons. It also does not have major drawbacks that are associated with TEE, such as esophageal perforation, the need for general anesthesia/deep sedation, and possible associated complications from endotracheal intubation (Flow chart 5 shown in **Supplementary materials**).

Cost is one of the major factors restricting the wide application of ICE in clinical practice. ICE itself is more expensive than TEE, but if ICE is used, general anesthesia may be exempted and the average hospital stay can be shortened (89, 105), thus reducing other costs during the hospital stay.

Application of intracardiac echocardiography in other common congenital heart diseases

Currently, there is relatively little experience with ICE for PDA and VSD procedures. Percutaneous interventional PDA closure is currently the standard of care for PDA, and conventional therapy is aortography-guided interventional closure. However, for most patients with PDA, a large amount of contrast agent is required in aortography, and in some cases, images obtained are not clear enough to assess PDA anatomy (106, 107), so the size of PDA may be underestimated, thus affecting the surgeon's choice of device, and leading to risk of embolization (108). In addition, patients with contrast agent allergy or renal insufficiency (108–110) are at risk with aortography. The results of available studies suggest that ICE is comparable to aortography or cardiac CTA in terms of the accuracy of measuring PDA diameter on the pulmonary artery side, but the amount of contrast agent required for ICE-guided PDA assessment is significantly lower than that for aortography. Therefore, ICE is now considered a reasonable substitute for aortography as a routine test for assessing the relevant structures of PDA, especially in patients with large PDA, renal insufficiency, or contrast agent allergy (111).

In the percutaneous closure of membranous VSD, TEE plays an important role in the anatomical assessment of the

defect and the surgeon's intraoperative decision. However, due to the long duration of VSD closure, TEE related examinations should be performed under general anesthesia. ICE provides clear images of the membrane of VSD, and its measurement results are similar to those obtained by TEE; in addition, ICE and TEE are comparable in judging the relationship between the defect and the aortic valve and tricuspid valve, measuring the size of the defect and giving guidance at different stages.

Experts' recommendation: (1) ICE performs well in anatomical measurements of relevant structures, real-time guidance of closure device implantation, assessment of post-closure residual shunt, etc. If possible, medical centers should apply ICE to guide the interventional procedure of secondary ASD and PFO; (2) ICE is recommended to guide the interventional closure in patients with complex or special ASD and PFO, especially the closure in patients with complex ASD, intolerant to TEE, with impaired left ventricular systolic function and unable to receive fluoroscopy, especially children, pregnant women, obese patients; (3) ICE is recommended to guide the interventional closure of PDA in patients with large PDA, renal insufficiency, and contrast agent allergy; (4) ICE is recommended to guide the closure in VSD patients with complex anatomy.

Application of intracardiac echocardiography in interventional procedure of valvular heart diseases

Transcatheter aortic valve replacement interventional procedure

Severe symptomatic aortic valve stenosis is a life-threatening disease with a 2-year mortality rate as high as 50% (112), and TAVR has become an effective treatment for this disease (113, 114). However, there are many risks associated with TAVR, including annular rupture, ventricular perforation, aortic dissection, coronary occlusion, and valve prosthesis displacement, as well as prosthetic valve PVL due to improper valve placement. Most complications cannot be detected in the early stages without guidance from echocardiography (115). Preoperative and perioperative imaging is essential for accurate determination of valve size, and assessment of postoperative aortic and paravalvular regurgitation, and other complications (116). TEE is currently commonly used for intraoperative guidance to TAVR in China and elsewhere. As an alternative to TEE, ICE dispenses with general anesthesia and endotracheal intubation during TAVR, especially in patients with esophageal disease.

Kadakia reported a TAVR case (117) that was successfully treated under the guidance of 3D ICE imaging. We found that the ICE was comparable to conventional TEE imaging in evaluating the valve position and aortic incompetence during TAVR and demonstrated comparable diagnostic imaging quality to multidetector computed tomography (MDCT) (118). Given this case report, ICE-guided TAVR may become an important alternative to TEE imaging and may allow for low-intensity sedation or anesthesia, potentially improving procedural safety and logistics (117). The aortic annulus and aortic sinus diameters measured by ICE were found to be comparable to those obtained by MDCT (116). Additional studies have assessed the intraoperative guidance of ICE and TEE during TAVR (119), where 50 patients with severe aortic valve stenosis scheduled for TAVR were randomized into two groups for ICE monitoring and TEE monitoring, respectively. The results showed that ICE was indeed capable of continuous monitoring. The ICE group had a much lower need for probe repositioning during the procedure. The ICE view displayed a higher coaxiality with the ascending aorta, indicated by the length of the ascending aorta depicted. In ICE group, both coronary ostia were visualized more frequently. The annulus measurements by ICE correlated closely with the readings by conventional TEE.

Intraoperative pressure gradients were underestimated by TEE compared with conventional measurements, but not by ICE. Both ICE and TEE detected new intracardiac thrombi. In this study, the authors concluded that ICE was compatible with sedation and local anesthesia and could be used for guidance in place of TEE. Also, it appeared to better match the operational flow during TAVR than TEE. In a study of 21 patients scheduled for TAVR, the major intraoperative imaging modality was 3D ICE (118). These patients were selected unanimously by the multidisciplinary TAVR team. This study is the first to prospectively evaluate the safety and feasibility of ICE-guided TAVR in the absence of endotracheal intubation. It is concluded that ICE is safe and feasible in selected patients in the absence of major complications, and intraoperative ICE can detect perivalvular leak and help guide necessary treatment. With the continued emphasis on the use of conscious sedation in TAVR procedures, it is very important to consider ICE as the major intraoperative imaging tool. 3D ICE probes are currently available for volumetric imaging; however, measurement of cross-sectional size of annular valves is difficult in its present form (105, 120). In addition, ICE makes it easier to measure tricuspid regurgitation (TR) and aortic valve flow velocity and to assess perioperative pulmonary arterial pressure and other hemodynamics (121). ICE can measure the aortic valve complex and provide more precise aortic pressure gradients (119, 121). In addition to providing imaging guidance, ICE dispenses with endotracheal intubation, shortens the operation time, and avoids the complications induced by general anesthesia and TEE (122). Therefore,

ICE-guided TF TAVR in the absence of endotracheal intubation is a viable option in patients deemed appropriate by the multidisciplinary team.

Para-valvular leak is one of the most common complications of TAVR. A case of PVL on postoperative echocardiography and cardiovascular imaging was described (114). Eccentric aortic regurgitation after TAVR monitored by TEE is easily misdiagnosed as PVL, while ICE can accurately evaluate the main complications during the procedure, provide more accurate images, and further evaluate the cause and severity of regurgitation (114, 121). In this patient, the diagnosis of PVL was confirmed by ICE, and the eccentric aortic regurgitation was caused by the frozen tip of bioprosthetic valve of TAVR. Therefore, this study concluded that ICE is a reasonable alternative to or at least a complement to standard imaging modalities for assessment after TAVR implantation.

As for the operation of the ICE catheter during the TAVR procedure, one should advance the 8-Fr AcuNavTM catheter to the superior vena cava from the right internal jugular vein and rotate the catheter counterclockwise to obtain images of the ascending aorta and assess its anatomy preoperatively. Images of the interatrial septum can be obtained when the catheter is advanced a few centimeters further to judge whether there is ASD or PFO. Counterclockwise rotation is continued to obtain long-axis views of the right atrium, tricuspid valve, and right ventricle, where the preoperative TR and estimated right ventricular systolic pressure can be measured. When the catheter is advanced counterclockwise with forward flexion in the right ventricle, the long-axis view of the left ventricle displays left ventricular contraction and pericardial effusion, and this position can be maintained during much of the operation. When the catheter is returned clockwise and pulled to the right atrium, the long-axis view of the aortic valve is obtained, where the preoperative aortic valve velocity and the diameter of the aortic valve complex can be measured. After TAVR, evaluation for complications such as PVL from the margin of the non-coronary valve leaflet can be performed (121).

There are limitations associated with ICE, including the need for additional venous access, the learning curve related to new devices, and the possible increased cost (115). Special care is required in the operation of the ICE probe to avoid arrhythmias and perforation of the right heart and vena cava (123).

Experts' recommendations: (1) ICE is a recommended alternative to TEE for TAVR in elderly patients with aortic valve stenosis who have esophageal lesions or are not suitable for general anesthesia; (2) ICE is equivalent to CT 3D reconstruction in the measurement of aortic valve and supra- and subvalvular structures and detection of possible complications during and after operation, and even superior to TEE in some cases; (3) It is suitable for surgeons

experienced in both TAVR and ICE (Flow chart 6 shown in **Supplementary materials**).

Transcatheter mitral valve intervention

Intracardiac echocardiography-guided mitral intervention includes Balloon Mitral Valvuloplasty, Transcatheter Edge-to-Edge Repair (TEER), and Transcatheter Mitral Valve Replacement (TMVR). ICE-guided transseptal puncture, ICE catheter access to the left atrium, and imaging and functional assessment of the mitral valve are fundamental operations of these therapeutic approaches, and we will uniformly describe them in detail. Additional procedures with different approaches are described in the corresponding sections.

Transseptal puncture

Transseptal puncture is a key step in mitral valve intervention, and it directly affects the success rate of mitral valve intervention. Under fluoroscopic guidance, deliver the ICE probe to the inferior position of the right atrium via the femoral vein, i.e., at the level of the tricuspid annulus, and appropriately rotate the catheter, until the right atrium, tricuspid valve, right ventricle, and right ventricular outflow tract can be visualized (home view). At this point, the posterior leaflet of the tricuspid valve is usually in the direction of 9 o'clock, while the anterior leaflet (or septal leaflet) is in the direction of 3 o'clock. This is the most fundamental view of ICE. Under fluoroscopy, deliver the ICE probe to the middle of the right atrium, rotate the catheter in the clockwise direction with a slight P curve to obtain the long-axis view of the interatrial septum, and along with the interatrial septum, its junction with the superior and inferior vena cava can be visualized. Further rotate the catheter in the clockwise direction with P curve to obtain the short-axis view of the atrial septum. At this point, the anterior (aortic) and posterior borders of the interatrial septum can now be visualized. Once the sheath/needle drag procedure is started, the "Tenting sign" of the puncture needle can be identified in the long-axis view of the interatrial septum. Then, rotate the ICE catheter in the counterclockwise direction until both the needle tent and the mitral annulus can be visualized to determine the optimal level of the puncture site.

Intracardiac echocardiography catheter access to the left atrium

After successful puncture, fix the puncture needle, push the dilator sheath into the left atrium, withdraw the sheath core, and the "tram track sign" can be observed in the ultrasound image. Deliver the stiffened guidewire to the left superior pulmonary vein or place in the left atrium, preferably looped for stability and ability to track the sheath. At this point, it should be determined that the activated clotting time (ACT) is within the therapeutic range before subsequent operations. The peripheral

arterial balloon dilates the interatrial septum so that the sheath can smoothly pass through the interatrial septum. Adjust the A/P knob of the ICE catheter under fluoroscopy to align the catheter with the track of the stiffened guidewire, and gently push the catheter into the left atrium. In case of resistance during the procedure, slightly adjust the R/L knob or rotate the catheter in the clockwise/counterclockwise direction and push the catheter again, or adjust the ICE catheter under left or right anterior oblique fluoroscopy.

Imaging of the left heart system

After entering the left atrium, the ICE ultrasound probe can display images of the left atrial appendage, pulmonary veins, and mitral valve. Preoperative TEE for mitral valve intervention can identify most intra-atrial appendage thrombi, but when it is difficult to differentiate intra-atrial thrombi from normal pectinate muscle tissues by TEE, intraoperative application of ICE may be considered to re-identify the presence of intra-atrial appendage thrombi (31, 124). Release the tension knob, restore A/P and L/R curve to the middle position, rotate the ICE catheter until it faces the right shoulder, adjust the A/P curve to display the pulmonary veins, and obtain the pulmonary vein blood flow spectrum. In the middle position, rotate the ICE catheter until the mitral valve structure is visualized, slightly adjust the R/L curve to obtain the best bijunctional view, and assess the structure and function of mitral valve by color Doppler and multiplanar imaging.

Intervention for mitral incompetence

Henning et al. first reported the application of ICE in TEER (125). However, due to the lack of multiplanar 3D imaging technique and lack of experience in the application of ICE at that time, ICE was only used as an auxiliary imaging technique for TEE in TEER. Then, the team reported an additional case of TEER guided by ICE alone, in which they placed an ICE probe in the left and right atria of the patient, respectively, so as to simulate orthogonal 2D images (126). 4D ICE can perform real-time volumetric imaging and multiplanar reconstruction and may be an effective alternative to TEE for TEER intraoperative imaging in patients who cannot tolerate or have contraindications to TEE (127, 128). The steerable guide catheter (SGC) crosses the interatrial septum to the left atrium via a stiffened guidewire. A single transseptal puncture is recommended, with the SGC and ICE catheter entering the left atrium through the same puncture site. The location and extent of mitral regurgitation can be identified through the combination of ICE orthogonal 2D and 3D imaging and color Doppler. As 4D ICE can acquire 4D images and achieve multiplanar imaging, the ICE catheter can be fixed after the ICE probe acquires a mitral valve image in the left atrium, with only modest adjustments. The catheter delivery system (CDS) should be manipulated under continuous monitoring by ICE to avoid penetration of the CDS tip into the atrial sidewall. Rotate the

ICE catheter in the counterclockwise direction after the CDS moves in the M direction and rotate the ICE catheter in the clockwise direction after the CDS moves in the P direction. Slowly and repeatedly adjust until the CDS is manipulated from the top of the left atrium to the central position of the mitral valve after completion of M-direction movement, with the tip of the clip in the annular plane above the center of the mitral valve. Under the guidance of multiplanar reconstruction and color Doppler, place the clip in the area with the most severe regurgitation. Under the guidance of orthogonal 2D and real-time 3D atrial images, make the clip arm perpendicular to the binding plane of the mitral valve, open the clip arm and place it into the left ventricle below the mitral leaflet. Clamp and release under continuous monitoring. Measure the position and extent of mitral regurgitation, transvalvular pressure gradient of mitral valve and pulmonary vein blood flow spectrum again after the operation, and compare with those before the operation. Perform supplementary clamping if necessary.

Intervention for mitral stenosis

Salem et al. first reported ICE-guided PBMV (129), and there are also more subsequent series of case reports on ICE-guided PBMV (130, 131). ICE guides intraoperative transseptal puncture, balloon positioning, evaluation of therapeutic effect, and monitoring of complications. The hemodynamic data measured by ICE are comparable to those measured by TTE and cardiac catheter. However, PBMV can be performed under local anesthesia combined with TTE monitoring in most patients, so ICE does not show significant advantages in terms of application in PBMV.

Transcatheter mitral valve replacement

Transcatheter mitral valve replacement guided by CS combined with ICE can be used to treat severe mitral incompetence caused by biological valve deterioration or prosthetic valve ring dysfunction and severe mitral annular calcification (MAC) (132, 133). ICE can guide intraoperative transseptal puncture, mitral valve crossing, valve positioning release, and functional assessment after valve release.

Due to the distance limitation of ICE imaging, the guidewire in the left atrium should be retained after mitral valve intervention, so that ICE probe can enter the left atrium for evaluation of therapeutic effect. Although ICE has shown many advantages in mitral valve intervention, it is not recommended to completely replace TEE at present due to the lack experience in relevant application, the lack of uniform operating specifications, the lack of popularity of 3D ICE and other reasons.

Experts' recommendation: (1) ICE imaging from within the left atrium can be helpful if not critical in guiding transseptal puncture and evaluating the mitral regurgitation in the mitral valve intervention; (2) However, mitral valve intervention requires a large sheath to operate across the interatrial septum,

which will affect the entry of the ICE catheter into the left atrium, and the treatment of mitral valve disorders mostly requires the guidance of 3D images, so it is currently not the main recommended method.

Pulmonary valve intervention

Intracardiac echocardiography can clearly show the right ventricular outflow tract, pulmonary valve, and proximal pulmonary artery. Therefore, ICE comes with a good application prospect in the transcatheter intervention of pulmonary valve. At present, there is still little experience in the application of ICE in pulmonary valve intervention, limited to guiding transcatheter pulmonary valve replacement (TPVR) (134, 135). In the middle view of the right atrium, ICE can be used to evaluate tricuspid valve function and estimate right ventricular pressure (if TR is present). In the view of the right ventricular outflow tract, in addition to displaying the anatomical structure of the outflow tract, color Doppler and continuous Doppler can also be used to evaluate the valve regurgitation and transvalvular pressure gradient before and after the operation. ICE can also be used to monitor complications (such as pericardial effusion or thrombosis) during the operation.

Post-TPVR infective endocarditis (IE) is a potentially fatal complication. Previous studies showed that the incidence of post-TPVR IE and transcatheter pulmonary valve-related IE was 5.1 and 1.9%, respectively (136). TEE is the most commonly used imaging method to detect valvular vegetations and diagnose IE. However, due to the long distance of the pulmonary valve from the esophageal ultrasound probe, some lesions still cannot be detected by TEE. For cases in which post-TPVR IE is suspected but the test result by TEE is negative, ICE can assist in the definitive diagnosis (136, 137).

Experts' recommendation: (1) ICE plays a good role in the assessment of pulmonary valve intervention and complications, and is not inferior to TEE; (2) Pulmonary valve intervention and ICE share the same approach and may interfere with each other; (3) It can be recommended as an effective alternative to TTE and TEE (Flow chart 7 shown in [Supplementary materials](#)).

Tricuspid valve intervention

The incidence of TR is high in the elderly population (138). The one-year survival rate for patients with severe TR is 64% only (139). The effectiveness of drug therapy for TR is limited, and the mortality rate of surgical procedures is high (140). Therefore, various transcatheter treatment techniques have emerged in recent years, including transcatheter edge-to-edge repair, annuloplasty, and valve replacement. TEE is the standard imaging technique for tricuspid valve intervention,

but there are also some technical problems, for example, the tricuspid annulus is far away from the esophageal ultrasound probe; the calcification of left heart valve prosthesis and tissues will interfere with the imaging; the delivery system and other devices will form acoustic shadows under ultrasound. Studies have found that the tricuspid valve structure is not adequately visualized in 50% of cases using TEE imaging alone in tricuspid valve intervention, and clips can be implanted under the guidance of ICE in 2/3 of these cases (141). Therefore, ICE is an important complementary technique to TEE in the intraoperative imaging of tricuspid valve intervention.

Due to the complexity and variability of the anatomical structure of tricuspid valve, there is no uniform standard for ICE imaging planes for tricuspid valve intervention. Hagemeyer et al. summarized the basic imaging planes of ICE in tricuspid valve intervention (142). In the home view, bend the ultrasound probe forward toward the right atrial free wall (left/right knob), and slightly rotate the catheter in a clockwise or counterclockwise direction. This view is often perpendicular to the long axis of the right ventricle, and the position of the clip arm can be determined based on the relationship with the valve leaflet. It is the ideal view for capturing the valve. To clearly visualize the antero-septal junction, advance the catheter to a high level in the right atrium; to clearly visualize the postero-septal junction, withdraw the catheter. Maintaining a stable field of view for intracardiac operation during intervention is essential and requires a second surgeon to assist in fixation or fine-tuning during operation to obtain an optimal imaging plane. 4D volumetric imaging ICE can bring great changes in tricuspid valve intervention. 4D volumetric imaging ICE is superior to TEE for visualization of the tricuspid annulus, especially the lateral annulus, and can be used for transcatheter annuloplasty, valve repair, and valve replacement for tricuspid in competence (140, 143). It should be noted that intravenous anesthetic drugs reduce systemic pressure while mechanical ventilation increases intrathoracic pressure. These will affect the accurate assessment of TR during operation. The application of the ICE system in conscious TR patients under local anesthesia can avoid these effects, making the assessment of TR more accurate and reliable.

Experts' recommendation: (1) The image of ICE in transcatheter tricuspid valvuloplasty is non-inferior to, or potentially superior to that of TEE; (2) It is recommended that patients with throat or esophageal lesions and anesthesia contraindications should receive the guidance of ICE; (3) The guidance of 3D/4D ICE will have a great role in promoting the tricuspid valve intervention (Flow chart 8 shown in [Supplementary materials](#)).

Paravalvular leak intervention

Long-term follow-up after surgical heart valve replacement has found that PVL occurs in 5–17% of patients (144, 145), and

the incidence of PVL is three times higher with TMVR than with TAVR (146). PVL is also an important complication of TAVR, and it is mostly seen in early self-expanding valves (147, 148). Intervention is required when patients with moderate to severe PVL present with congestive heart failure and/or hemolysis. Surgical repair or valve replacement is the main intervention with high mortality. As interventional techniques and closure devices continuously develop, a growing number of centers use percutaneous PVL closure. 2020ACC/AHA guidelines state that percutaneous closure is recommended for PVL patients with high risk or contraindications for surgery, NYHA grade III/IV or refractory hemolysis, and appropriate anatomical structure (class IIa, level of evidence B-NR) (149). Percutaneous PVL closure often requires general anesthesia and the guidance of TEE, which undoubtedly brings more risks. Therefore, the application of ICE in PVL closure is of great significance. Ruparelia et al. conducted a retrospective study on the efficacy and safety of ICE-guided PVL closure (150). The results of this study showed that the success rate of ICE-guided PVL closure was 77.8%, which was similar to that of TEE, and there were no ICE-related complications. In postoperative follow-up, 78.6% of patients had improvement in heart failure symptoms without persistent hemolysis. There was no death within 30 days after surgery, and the 1-year survival rate after surgery was 71.4%. The results of this study suggest that ICE-guided PVL closure is safe and effective.

Intracardiac echocardiography imaging can locate the PVL intraoperatively, guide transseptal puncture, assist in device selection, determine residual leakage, and identify perioperative complications. For aortic PVL, the proposed transfemoral approach should be used for closure. For mitral PVL, if the PVL is close to the lateral side (6–10 o'clock direction of the atrial view of the mitral valve), use the antegrade approach of transseptal puncture for closure, and if the PVL is close to the septal side (2–4 o'clock direction of the atrial view of the mitral valve), use the retrograde approach for closure. For most patients, the placement of the ICE catheter in the right atrium can meet the imaging requirements of the operation, and very few patients require placement of the ICE catheter in the right ventricle or even the left atrium. For patients with failed PVL closure under ICE guidance, a repeated closure or other treatments can be considered. Although disposable catheters increase surgical costs, ICE-guided PVL closure avoids the need for anesthesiologists and reduces the time of surgery. There are currently no reports on PVL closure after ICE-guided TAVR. As most ICEs on the market can only assess regurgitation bundles by 2D and color Doppler, and due to the safety concerns associated with catheter placement, their clinical application is still greatly limited. The recent advent of real-time 3D/volumetric imaging can contribute to the further display of anatomical structures by ICE, thus improving the success rate of the operation, with good application prospects.

Experts' recommendation: (1) The application of ICE in aortic and mitral PVL is worth recommending, especially in patients intolerant to TEE examination; (2) 3D/4D ICE is more helpful in PVL intervention.

Others

Application of intracardiac echocardiography in left atrial appendage closure

In LAAC, ICE is increasingly favored by surgeons and patients for its more flexible and convenient operation, richer and more comprehensive viewing angles, improved tolerance and safety, less X-ray exposure and contrast agent dosage compared with TEE. Almost all patients can tolerate ICE-guided LAAC under local anesthesia. The specific process is as follows (**Supplementary material**). It focuses on the multi-angle scanning and evaluation of the LAA. Combining the flexible operation of ICE catheter with the systematic evaluation of LAA, the 3D electroanatomical mapping system can even achieve zero X-ray and zero-contrast agent LAAC (24).

As ICE avoids the adverse effects and esophageal injury due to TEE probe entering the esophagus, and is well tolerated by patients, LAAC can be completed under local anesthesia. After the ICE catheter reaches the right atrium, three conventional sites, namely the right atrial body, right ventricular outflow tract and proximal segment of the coronary sinus, are usually recommended for layer-by-layer scanning of the LA/LAA to rule out the possible presence of atrial and atrial appendage thrombi, of which the right ventricular outflow tract is the best scanning site to rule out thrombi. In LAAC, if ICE is used to guide the transseptal puncture, the method for judging the level of puncture point is as follows: Select the site where the membrane at the lower end of the interatrial septum is close to the muscle; the method for judging the anteroposterior position of puncture point: The ICE sector is in the same plane as the puncture needle tip and the left superior pulmonary vein (LSPV) ridge site. After successful puncture of the interatrial septum, under the guidance of X-ray, adjust the direction of the ICE catheter tip, and deliver the ICE catheter into the LA along the direction of the guidewire; or deliver along the location of the septal marker point in a 3D electroanatomical system.

The LAA is a 3D structure in the cardiac cavity, so its dimensions should be evaluated in three dimensions. The ICE catheter delivered into the LA allows close and multi-angle scanning of the LAA, avoiding the limitations of TEE application in patients with cardiac transposition and atrial appendage variations. Multi-angle assessment is the key point for ICE-guided LAAC. Routinely long-axis layer-by-layer scanning can be performed through three anatomical positions that are orthogonal, namely X axis (left pulmonary vein), Y axis

(ostium of right pulmonary vein) and Z axis (mitral annulus) (as shown in **Figure 10**). The diameter of LAA opening and landing zone and effective working depth can be measured to better adapt to different anatomical structures and axial directions of different atrial appendages. The position, closure effect, compression and stability of the closure device can be evaluated in three dimensions after the closure device is expanded (**151**).

Place the ICE catheter in the LSPV and with a P curve, with the sector pointing to the LAA. Send the pigtail catheter into LAA, and an obvious catheter marker can be seen in the ultrasonic view, based on which the landing zone and left circumflex artery (LCX) are located. Send the delivery sheath into the ostium of LAA under the guidance of the pigtail catheter (as shown in **Figure 11A**). After the tip of the sheath entering the LAA reaches the required depth for closure, withdraw the pigtail catheter, and send the closure device (or fixation disk) to the LAA landing zone. Expand the closure device (Watchman closure device) or fixation disk (ACP or LAmbré closure device), and note that the site bearing the maximum force should be medial to the LCX (as shown in **Figure 11B**). Continue to expand the closure disk (ACP or LAmbré closure device, as shown in **Figure 11C**). If necessary, slightly or partially withdraw the closure device to adjust the position of the closure

device (as shown in **Figure 11D**). After the closure device is at the desired position, perform a pull test under the guidance of ICE (as shown in **Figure 11E**). Finally perform color Doppler to examine whether there is residual shunt at the edge of the closure device (as shown in **Figure 11F**).

After the closure device (disk) is expanded, ICE is applied to evaluate the closure effect (including the position of closure device, closure tightness and stability) layer by layer from multiple angles. After the release criteria of each closure device (e.g., Watchman closure device should meet PASS principle) are met, completely release the closure device, and then perform ICE examination again from multiple angles to evaluate the release effect of the closure device, avoid the displacement of the closure device and the effect of closure device on adjacent structures (such as pulmonary vein and mitral valve), and observe whether there is pericardial effusion. If the release criteria are not met, withdraw (fully withdraw/partially withdraw/slightly withdraw) the closure device, adjust the position and expand again, and re-evaluate the expanding effect.

It should be noted that: (1) For AF patients who meet the indications for LAAC, after successful puncture of the interatrial septum under the guidance of ICE, it is recommended that the ICE catheter be delivered into the LA or LSPV through the transseptal puncture point and the layer-by-layer scanning

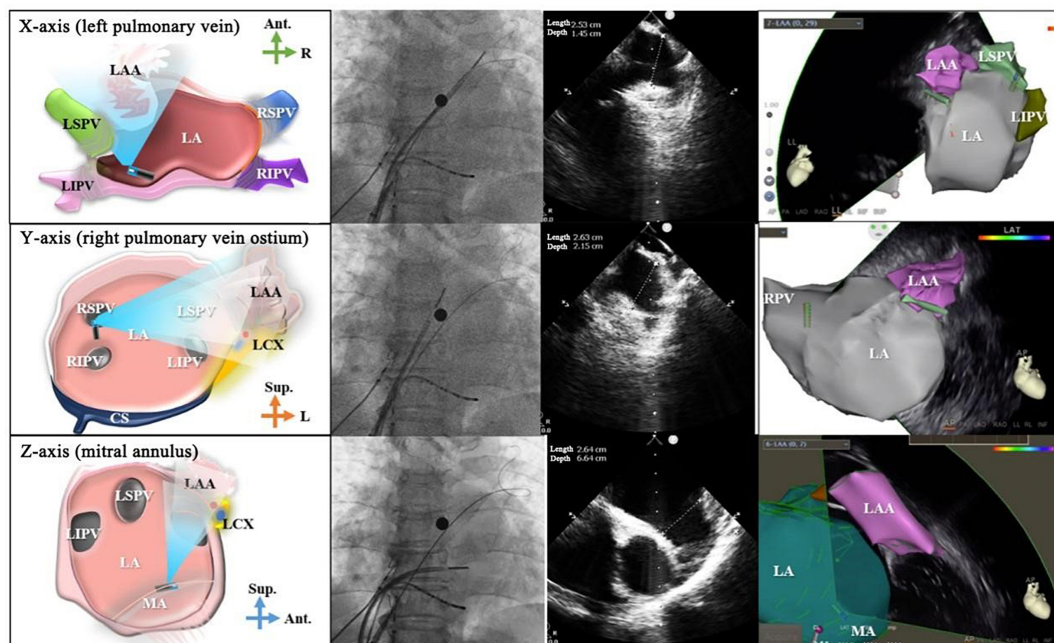


FIGURE 10

Multi-angle left atrial appendage measurement. From the top to bottom: schematic diagrams for atrial appendage assessment, X-ray images, ultrasound images and 3D electroanatomical diagrams from X axis, Y axis, and Z axis. The projection position of the X-ray is AP. The first column shows the schematic diagrams, the second column shows the effect of X-ray, the third column shows the images of ICE, and the fourth column shows the images of 3D mapping system. LAA, left atrial appendage; LSPV, left superior pulmonary vein; LIPV, left inferior pulmonary vein; LA, left atrium; RSPV, right superior pulmonary vein; RIPV, right inferior pulmonary vein; LCX, left circumflex artery; Ant., anterior; Sup., superior; R, right; L, left; MA, mitral annulus; RPV, right pulmonary vein.

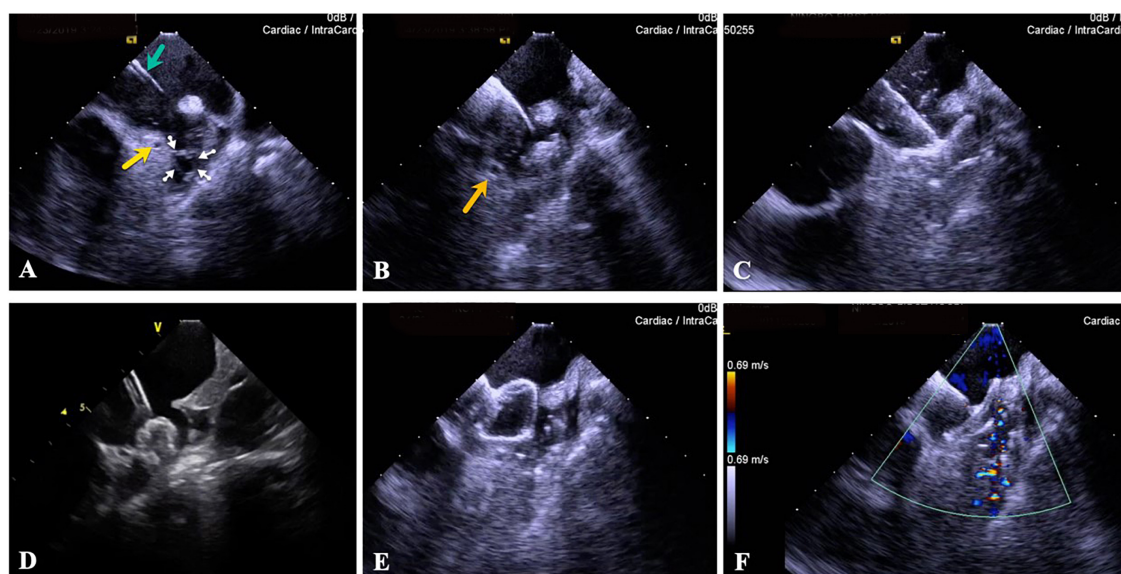


FIGURE 11

Process of ICE-guided LAAC. (A) Send the delivery sheath to the ostium of LAA (green arrow), and the pigtail catheter to the inside of LAA (small white arrow), and note the position of the LCX (yellow arrow). (B) Expand the closure device fixation disk, and note that it should be medial to the LCX (orange arrow). (C) Expand the closure disk. (D) Slightly withdraw the closure device (disk). (E) Pull test. (F) There is no residual shunt at the edge of the closure device as assessed by color Doppler flow monitoring at the end of closure. ICE, intracardiac echocardiography; LAA, left atrial appendage; LCX, left circumflex artery.

through “three axes and six directions” that are orthogonal from three anatomical marks be performed to assess the shape, size, and anatomical structure of the LAA. (2) A closure device of appropriate size should be selected according to the width and available depth of the LAA opening measured by angiography and ICE. After implantation of the closure device, angiography and ICE can be carried out to confirm that there is no large amount of residual shunt around the closure device, and the final pull test can be performed to examine the anchorage of the closure device.

Application of intracardiac echocardiography in pregnant patients

Management of arrhythmias during pregnancy is an important challenge, and arrhythmias during pregnancy will lead to many adverse effects on the mother and fetus. There are many drawbacks associated with antiarrhythmic drugs, e.g., limited drug options, significant adverse reactions, and ineffective treatment. Despite a small radiation exposure, the conventional catheter ablation still brings risks to pregnant women and fetuses, which limits its use in special populations (152).

In recent years, as 3D electroanatomical mapping systems and ICE technique developed, completely zero X-ray catheter ablation has become feasible and in many institutions routine, which makes catheter ablation possible for the treatment

of arrhythmias during pregnancy, including conventional supraventricular tachycardia and ventricular premature beats, as well as complex arrhythmias such as atrial fibrillation and ventricular tachycardia. ICE technique combined with 3D electroanatomical mapping system allows visualization of the multi-electrode catheter, facilitates electrode placement, and makes subsequent ablation of the left heart system viable after the ICE-guided transseptal puncture is completed (153–155). In addition to catheter ablation during pregnancy, ICE can also be used during pacemaker implantation and zero X-ray therapy for some congenital heart diseases. However, the indications for zero X-ray interventional operations during pregnancy should be strictly specified, and the success rates of these operations, complications, radiation exposure and other risks require continued evaluation and experience. For the sake of safety, zero X-ray operation may not always be viable, so surgeons should collaborate with the Gynecology and Obstetrics team and the anesthesiology team in planning procedures in this patient population.

Application of intracardiac echocardiography in left ventricular assist device implantation

Intracardiac echocardiography is a viable option to guide LVAD implantation, especially when other imaging modes are not appropriate. However, to avoid serious iatrogenic

complications, clinicians must understand the limitations of experience, the limitations of imaging, and the risks associated with this technique. In some special cases, X-ray, TTE, and TEE are clinically not indicated for LVAD implantation, while ICE can guide the LVAD implantation in such cases. Moreover, compared with TTE and TEE, ICE can be used in patients requiring positive pressure ventilation and intubation. However, for ICE in the chambers of the heart, soft guidewire wrapping is possible during transaortic implantation of LVAD, in which case excessive tension of the guidewire may lead to a potential complication (vascular perforation). Moreover, ICE is sometimes challenging to image the descending aorta due to its limited spatial resolution, which may bring additional risks (156).

Intracardiac echocardiography can be used as an alternative or supplement to TEE for perioperative and postoperative management of LVADs. There are case reports where the device structure, hemodynamics and related complications after ICE-guided LVAD implantation are evaluated (157–159). Compared with TTE, TEE, or 3D computed tomography, ICE features high success rate of treatment, no need for general anesthesia, no need for radiation exposure, and shortened recovery time (5, 159) (Flow chart 10 shown in [Supplementary materials](#)).

Application of intracardiac echocardiography in myocardial biopsy

Intracardiac echocardiography-guided endomyocardial biopsy (EMB) is an interesting application of ICE. ICE enables precise localization for biopsy, reduces the risks associated with operations, and reduces the need for diagnostic thoracotomy, and is more maneuverable in selected cases (160). With this emerging technique, the diagnostic yield of biopsy is significantly improved, with fewer complications (161).

A series of patients with right ventricular mass undergoing ICE-guided EMB demonstrated safety and efficacy (60). The diagnosis of both cardiac metastatic tumors and primary cardiac tumors is based on histopathology. According to this series of cases, EMB is a valuable tool for preoperative diagnosis and surgical planning of intracardiac masses suspected of tumors, while ICE is worthy of further attention for its ability to accurately locate cardiac structures and guide biopsy sampling in the target area. ICE can be used to guide EMB of cardiac masses. Allowing a correct positioning of the biptome, ICE reduces the procedure-related risks and the need for a diagnostic open-chest procedure, reserving the more invasive approach to selected cases (160).

Electroanatomical mapping combined with ICE-guided EMB is feasible in patients with suspected arrhythmic

cardiomyopathy and ventricular arrhythmia of unknown origin. This method can significantly improve the positive rate of biopsy and reduce complications (161) (Flow chart 11 shown in [Supplementary materials](#)).

Application of intracardiac echocardiography in hypertrophic obstructive cardiomyopathy

Radiofrequency ablation of the interventricular septum is currently a novel surgical technique for hypertrophic obstructive cardiomyopathy, and its feasibility has been demonstrated in some studies (162, 163). Accurate localization of the anterior mitral leaflet and the ventricular septal flapping area is the key to radiofrequency ablation of the interventricular septum. Previously, the localization of the target area during the interventricular septal ablation for hypertrophic cardiomyopathy was mainly achieved by TEE combined with CARTO system (164). Intraoperative continuous TEE monitoring is limited due to limited patient tolerance, and general anesthesia and esophageal intubation also bring additional risks such as gastroesophageal injury and aspiration (165). In addition, ICE is non-inferior to TTE in imaging the overall cardiac structure (166). Previous studies have demonstrated that ICE can provide detailed information on the anatomical structure of the interventricular septum (166). As an organic combination of ICE image and 3D positioning system image, CARTO-Sound clearly displays the mitral valve and interventricular septal flapping area, and can be used to guide the selective precise ablation of the tip. 3D models of left ventricle, left ventricle outflow tract, anterior mitral leaflet and aortic root are constructed by ICE, which can accurately trace the site of interventricular septum obstruction (anterior leaflet and interventricular septal flapping area), and intraoperatively monitor the contact of the ablation catheter and the ablation injury in real-time. Patients can benefit from ICE-guided interventricular septal ablation. A small-scale study showed that 20 patients with significantly symptomatic hypertrophic obstructive cardiomyopathy had aortic transvalvular pressure gradient of greater than 50 mmHg by preoperative resting TTE and were followed up for 6 months after interventricular septal ablation. In patients with interventricular septal hypertrophy and obstruction, short anterior mitral leaflet and normally positioned papillary muscles, the NYHA cardiac function classification was significantly improved, and left ventricle outflow tract pressure and pressure gradient were significantly reduced (100). In addition, the feasibility of ICE-guided interventricular septal ablation in hypertrophic cardiomyopathy has also been confirmed in some small-scale studies (162, 167), and it is worthy of further study.

Application of intracardiac echocardiography in pulmonary arterial hypertension

In patients with aortic valve stenosis and pulmonary arterial pressure undergoing TAVR, the use of ICE instead of right heart catheterization for pulmonary arterial pressure monitoring is safe and feasible (168). The pulmonary arterial hypertension is mainly treated with drugs, while balloon atrial septostomy (BAS) can be performed as a bridging therapy or palliative therapy for poorly controlled patients awaiting lung transplantation (169, 170). Under the guidance of ICE, the surgeon can accurately locate the fossa ovalis and the surrounding anatomical structures, reducing the need for radiation. The feasibility of ICE-guided balloon or implantable device atrial septostomy has been demonstrated in studies (171–174). ICE-guided BAS combined with radiofrequency ablation has been shown in animal experiments to be effective in reducing spontaneous closure after atrial septostomy (175). ICE-guided AS is promising. Potts shunt has some advantages over AS in patients with severe pulmonary arterial hypertension who fail to respond to drug treatment: (1) It has a more reliable patency; (2) It does not lead to persistent hypoxemia in the upper part of the body, so the coronary artery and cerebral circulation are not affected. However, this procedure comes with high risks during the establishment of descending aorta and main pulmonary artery channels. In the future, 4D ICE real-time volumetric imaging and multiplanar reconstruction techniques can be used to guide the puncture, which may improve the operation safety, so that this operation can be further popularized and applied for the benefit of more patients. In addition, ICE can clearly show the right ventricular outflow tract, pulmonary valve, and proximal pulmonary artery. Therefore, ICE is also promising in percutaneous pulmonary artery sympathetic denervation ablation for pulmonary arterial hypertension. However, the use of ICE in pulmonary arterial hypertension needs to be further explored and validated in relevant clinical studies.

Application of intracardiac echocardiography in lead extraction

With the increasing use of cardiac electronic implantable devices such as pacemakers, device-related complications, such as infection, thrombosis and device/lead failure, occur frequently. Transvenous lead extraction (TLE) is an important technique for managing cardiac electronic implantable device-related infections (176). In TLE, conventional fluoroscopy, TEE and preoperative CT imaging have their own limitations: The wear and residue of non-visualized components such as lead insulation layer cannot be identified under fluoroscopy, and the

adhesion of leads to tissues cannot be assessed; CT imaging is incapable of real-time guidance and assessment; TEE is performed close to the back of the heart, so the images for other regions are of poor quality and reproducibility.

As a unique imaging technique, ICE can guide TLE or be combined with new techniques intraoperatively, and it is safe and feasible (177–180). ICE can evaluate the lead condition, thrombus, neoplasm, lead “ghost” and adhesion of leads to tissues under direct vision, and can also timely detect the hyperechogenicity around the lead (181) (LAEs, which are usually classified as thrombus or neoplasm, prevalent in three-quarters of patients undergoing lead implantation, and are found in the right atrium, tricuspid valve, right ventricle and superior vena cava) to prevent such complications as embolism; it is currently being explored to remove LAEs under the guidance of ICE. Preoperative evaluation of the adhesion of leads to vessels, valves, right atrial free walls, and right atrial appendages by ICE is of great significance, contributing to the identification of high-risk valves, risk assessment of lead extraction, tool selection, and early judgment of the need for surgical extraction or delayed extraction; ICE enables dynamic risk assessment intraoperatively, real-time monitoring of complications, accurate identification of false cardiac tamponade due to traction under TEE during lead extraction, and dynamic assessment of tricuspid valve function. It is of great significance to reduce postoperative complications and improve operation safety (Flow chart 12 shown in [Supplementary materials](#)).

Intracardiac echocardiography has been widely used in cardiac interventions such as radiofrequency ablation, and it is also suitable for TLE based on the said advantages. With the advancement of technique and the application of 3D ultrasound imaging, the imaging quality of ICE will be further improved in the future. Therefore, the application prospect of ICE-guided TLE is promising.

Conclusion

Nowadays, ICE has been applied in a variety of cardiovascular interventional operations. In addition to the applications introduced above, ICE can also be used to guide the implantation of leadless pacemaker (182), left bundle branch pacing (183), etc. At the same time, for patients who have implanted pacemaker, zero-fluoroscopy ablation can also be completed with the assistance of ICE (184). However, more clinical evidence is needed to prove the feasibility of these operations.

Currently, catheter with a diameter of 8F has emerged, which will expand the application of ICE, such as cardiovascular interventional procedures in children and so on. With the application of 4D ICE, the improvement of image quality and the decrease of cost, ICE will be more widely used in the future.

Limitations

Because there are few authoritative clinical studies related to ICE in the world, some of viewpoints in our consensus are lack of considerable clinical studies to support them, and they were based on the clinical experience of the experts or case reports, we don't use "I-III" and "a-c" to express evidence level but use "Recommend," "Can be useful," "Maybe useful," "Not recommended," (Table 2) which is also one of the reasons why our manuscript is consensus rather than a guideline.

As there are few expert consensus related to ICE in the world, the flowcharts (in **Supplementary material**) in our manuscript are developed based on the experience of Chinese experts. It may not be applicable to medical centers in different countries and regions, but it can be used as a reference.

Some emerging technologies (such as 4D ICE and 8F catheter) related to ICE are only mentioned in this manuscript, and their clinical applications are not elaborated too much, because they are rarely used in China. We hope that we will have the opportunity to improve the expert consensus with the application of these technologies in the future.

Author contributions

All authors listed have made a substantial, direct, and intellectual contribution to the work, and approved it for publication.

Acknowledgments

Thank the following experts for their contributions to reviewing and proofreading the articles: Chen Mao (West China Hospital, Sichuan University, China), Chen Minglong (The First Affiliated Hospital with Nanjing Medical University, China), Dong Jianzeng (The First Affiliated Hospital of Zhengzhou University, China), Fan Jie (The First People's Hospital of Yunnan Province, China), He Jiangui (The First Affiliated Hospital of Sun Yat-sen University, China), Jiang Tingbo (The First Affiliated Hospital of Soochow University, China), Kong Xiangqing (The First Affiliated Hospital with Nanjing Medical University, China), Li Shufeng (The Second Affiliated Hospital of Harbin Medical University, China), Li Shuyan (The First Hospital of Jilin University, China), Liu

Liwen (Xi Jing Hospital, The First Affiliated Hospital of Fourth Military Medical University, China), Liu Qiming (The Second Xiangya Hospital of Central South University, China), Liu Xingpeng (Beijing Chaoyang Hospital, Capital Medical University, China), Liu Xu (Shanghai Chest Hospital Shanghai Jiao Tong University, China), Liu Yan (Qilu Hospital, Cheeloo College of Medicine, Shandong University, China), Sang Caihua (Beijing Anzhen Hospital of Capital Medical University, China), Shu Maoqin (The Southwest Hospital of Amu), Tang Baopeng (The First Affiliated Hospital of Xinjiang Medical University, China), Wang Jian'an (The Second Affiliated Hospital Zhejiang University School of Medicine, China), Xia Yunlong (The First Affiliated Hospital of Dalian Medical University, China), Xie Ruiqin (The Second Hospital of Hebei Medical University, China), Xu Jian (The First Affiliated Hospital of USTC, Anhui Provincial Hospital, China), Xu Yawei (Tenth People's Hospital of Tongji University, China), Yuan Zuyi (The First Affiliated Hospital of Xi'an Jiaotong University, China), Zheng Liangrong (The First Affiliated Hospital, Zhejiang University School of Medicine, China), and Zhu Wenqing (Zhongshan Hospital of Fudan University, China).

Conflict of interest

The authors declare that the research was conducted in the absence of any commercial or financial relationships that could be construed as a potential conflict of interest.

Publisher's note

All claims expressed in this article are solely those of the authors and do not necessarily represent those of their affiliated organizations, or those of the publisher, the editors and the reviewers. Any product that may be evaluated in this article, or claim that may be made by its manufacturer, is not guaranteed or endorsed by the publisher.

Supplementary material

The Supplementary Material for this article can be found online at: <https://www.frontiersin.org/articles/10.3389/fcvm.2022.1012731/full#supplementary-material>

References

1. Saad EB, Costa IP, Camanho LE. Use of intracardiac echocardiography in the electrophysiology laboratory. *Arquivos Brasileiros Cardiol.* (2011) 96:e11–7.
2. George JC, Varghese V, Mogtader A. Intracardiac echocardiography: evolving use in interventional cardiology. *J Ultrasound Med Off J Am Institute Ultrasound Med.* (2014) 33:387–95.

3. Enriquez A, Saenz LC, Rosso R, Silvestry FE, Callans D, Marchlinski FE, et al. Use of intracardiac echocardiography in interventional cardiology: working with the anatomy rather than fighting it. *Circulation*. (2018) 137:2278–94. doi: 10.1161/CIRCULATIONAHA.117.031343
4. Cieszyński T. [Intracardiac method for the investigation of structure of the heart with the aid of ultrasonics]. *Arch Immunol Therapiae Exp*. (1960) 8:551–7.
5. Kimoto S, Omoto R, Tsunemoto M, Muroi T, Atsumi K, Uchida RJU. Ultrasonic tomography of the liver and detection of heart atrial septal defect with the aid of ultrasonic intravenous probes. *Ultrasonics*. (1964) 2:82–6.
6. Kossoff G. Diagnostic applications of ultrasound in cardiology. *Australasian Radiol*. (1966) 10:101–6.
7. Eggleton RC, Townsend C, Kossoff G, Herrick J, Hunt R, Templeton G, et al. *Computerized Ultrasonic Visualization of Dynamic Ventricular Configuration*. Vol. 111. Chicago IL: Palmer House (1969). p. 10–3.
8. Bom N, Lancee C, Van Egmond FJU. An ultrasonic intracardiac scanner. *Ultrasonics*. (1972) 10:72–6.
9. Glassman E, Kronzon I. Transvenous intracardiac echocardiography. *Am J Cardiol*. (1981) 47:1255–9.
10. Pandian NG, Kreis A, Weintraub A, Motarjeme A, Desnoyers M, Isner JM, et al. Real-time intravascular ultrasound imaging in humans. *Am J Cardiol*. (1990) 65:1392–6.
11. Bruce CJ, Packer DL, Seward JB. Intracardiac Doppler hemodynamics and flow: new vector, phased-array ultrasound-tipped catheter. *Am J Cardiol*. (1999) 83:1509–12. A9. doi: 10.1016/s0002-9149(99)00136-8
12. Vitulano N, Pazzano V, Pelargonio G, Narducci ML. Technology update: intracardiac echocardiography - a review of the literature. *Med Devices (Auckland, NZ)*. (2015) 8:231–9. doi: 10.2147/MDER.S49567
13. Liu CF. The evolving utility of intracardiac echocardiography in cardiac procedures. *J Atrial Fibrillat*. (2014) 6:1055.
14. Banchs JE, Patel P, Naccarelli GV, Gonzalez MD. Intracardiac echocardiography in complex cardiac catheter ablation procedures. *J Interv Cardiac Electrophysiol Int J Arrhythmias Pacing*. (2010) 28:167–84.
15. Basman C, Parmar YJ, Kronzon I. Intracardiac echocardiography for structural heart and electrophysiological interventions. *Curr Cardiol Rep*. (2017) 19:102.
16. Packer DL, Stevens CL, Curley MG, Bruce CJ, Miller FA, Khandheria BK, et al. Intracardiac phased-array imaging: methods and initial clinical experience with high resolution, under blood visualization: initial experience with intracardiac phased-array ultrasound. *J Am Coll Cardiol*. (2002) 39:509–16.
17. Weng S, Tang M, Zhou B, Ding L, Yu F, Qi Y, et al. Spatial distribution of idiopathic ventricular arrhythmias originating around the pulmonary root: lessons from intracardiac echocardiography. *JACC Clin Electrophysiol*. (2022) 8:665–76. doi: 10.1016/j.jacep.2022.01.020
18. Mullen MJ, Dias BF, Walker F, Siu SC, Benson LN, McLaughlin PR. Intracardiac echocardiography guided device closure of atrial septal defects. *J Am Coll Cardiol*. (2003) 41:285–92.
19. Alboliras ET, Hijazi ZM. Comparison of costs of intracardiac echocardiography and transesophageal echocardiography in monitoring percutaneous device closure of atrial septal defect in children and adults. *Am J Cardiol*. (2004) 94:690–2. doi: 10.1016/j.amjcard.2004.05.048
20. Huiyu L, Jingquan Z. Application of intracardiac echocardiography in interventional procedure of atrial fibrillation. *Biomed Eng Res*. (2021) 40:5.
21. Freitas-Ferraz AB, Bernier M, Vaillancourt R, Ugalde PA, Nicodème F, Paradis JM, et al. Safety of transesophageal echocardiography to guide structural cardiac interventions. *J Am Coll Cardiol*. (2020) 75:3164–73.
22. Hemam ME, Kuroki K, Schurmann PA, Dave AS, Rodríguez DA, Sáenz LC, et al. Left atrial appendage closure with the Watchman device using intracardiac vs transesophageal echocardiography: procedural and cost considerations. *Heart Rhythm*. (2019) 16:334–42. doi: 10.1016/j.hrthm.2018.12.013
23. Ribeiro JM, Teixeira R, Puga L, Costa M, Gonçalves L. Comparison of intracardiac and transesophageal echocardiography for guidance of percutaneous left atrial appendage occlusion: a meta-analysis. *Echocardiography (Mount Kisco, NY)*. (2019) 36:1330–7. doi: 10.1111/echo.14415
24. Chu H, Du X, Shen C, He B, Feng M, Liu J, et al. Left atrial appendage closure with zero fluoroscopic exposure via intracardiac echocardiographic guidance. *J Formosan Med Assoc Taiwan Yi Zhi*. (2020) 119:1586–92. doi: 10.1016/j.jfma.2020.07.021
25. Ferguson JD, Helms A, Mangrum JM, Mahapatra S, Mason P, Bilchick K, et al. Catheter ablation of atrial fibrillation without fluoroscopy using intracardiac echocardiography and electroanatomic mapping. *Circ Arrhythm Electrophysiol*. (2009) 2:611–9.
26. Baran J, Stec S, Pilichowska-Paszkiel E, Zaborska B, Sikora-Frąć M, Kryński T, et al. Intracardiac echocardiography for detection of thrombus in the left atrial appendage: comparison with transesophageal echocardiography in patients undergoing ablation for atrial fibrillation: the Action-Ice I study. *Circ Arrhythm Electrophysiol*. (2013) 6:1074–81. doi: 10.1161/CIRCEP.113.000504
27. Ikegami Y, Tanimoto K, Inagawa K, Shiraishi Y, Fuse J, Sakamoto M, et al. Identification of left atrial appendage thrombi in patients with persistent and long-standing persistent atrial fibrillation using intra-cardiac echocardiography and cardiac computed tomography. *Circ J Off J Japanese Circ Soc*. (2017) 82:46–52. doi: 10.1253/circj.CJ-17-0077
28. Ren JF, Marchlinski FE, Supple GE, Hutchinson MD, Garcia FC, Riley MP, et al. Intracardiac echocardiographic diagnosis of thrombus formation in the left atrial appendage: a complementary role to transesophageal echocardiography. *Echocardiography (Mount Kisco, NY)*. (2013) 30:72–80. doi: 10.1111/j.1540-8175.2012.01819.x
29. Anter E, Silverstein J, Tschabrunn CM, Shvilkin A, Haffajee CI, Zimetbaum PJ, et al. Comparison of intracardiac echocardiography and transesophageal echocardiography for imaging of the right and left atrial appendages. *Heart Rhythm*. (2014) 11:1890–7.
30. Sriram CS, Banchs JE, Moukabay T, Moradkhan R, Gonzalez MD. Detection of left atrial thrombus by intracardiac echocardiography in patients undergoing ablation of atrial fibrillation. *J Interv Cardiac Electrophysiol Int J Arrhythm Pacing*. (2015) 43:227–36.
31. Baran J, Zaborska B, Piotrowski R, Sikora-Frąć M, Pilichowska-Paszkiel E, Kulakowski P. Intracardiac echocardiography for verification for left atrial appendage thrombus presence detected by transesophageal echocardiography: the ActionICE II study. *Clin Cardiol*. (2017) 40:450–4. doi: 10.1002/clc.22675
32. Ross J Jr., Braunwald E, Morrow AG. Transseptal left atrial puncture; new technique for the measurement of left atrial pressure in man. *Am J Cardiol*. (1959) 3:653–5. doi: 10.1016/0002-9149(59)90347-9
33. De Ponti R, Cappato R, Curnis A, Della Bella P, Padeletti L, Raviele A, et al. Trans-septal catheterization in the electrophysiology laboratory: data from a multicenter survey spanning 12 years. *J Am Coll Cardiol*. (2006) 47:1037–42. doi: 10.1016/j.jacc.2005.10.046
34. Alkhouli M, Rihal CS, Holmes DR Jr. Transseptal techniques for emerging structural heart interventions. *JACC Cardiovasc Interv*. (2016) 9:2465–80.
35. Reddy VY, Morales G, Ahmed H, Neuzil P, Dukkupati S, Kim S, et al. Catheter ablation of atrial fibrillation without the use of fluoroscopy. *Heart Rhythm*. (2010) 7:1644–53.
36. Baykaner T, Quadros KK, Thosani A, Yasmeh B, Mitra R, Liu E, et al. Safety and efficacy of zero fluoroscopy transseptal puncture with different approaches. *Pacing Clin Electrophysiol*. (2020) 43:12–8.
37. Santangeli P, Di Biase L, Burkhardt JD, Horton R, Sanchez J, Bailey S, et al. Transseptal access and atrial fibrillation ablation guided by intracardiac echocardiography in patients with atrial septal closure devices. *Heart Rhythm*. (2011) 8:1669–75.
38. Guo Q, Sang C, Bai R, Lai Y, Long D, Li S, et al. Transseptal puncture in patients with septal occluder devices during catheter ablation of atrial fibrillation. *EuroIntervention*. (2022) 17:1112–9.
39. Singh SM, Heist EK, Donaldson DM, Collins RM, Chevalier J, Mela T, et al. Image integration using intracardiac ultrasound to guide catheter ablation of atrial fibrillation. *Heart Rhythm*. (2008) 5:1548–55.
40. Feng Z, Xu Z, Dandan Y, Cuizhen Y, Xuebin L, Ding L. Fluorless or low-fluoroscopy atrial fibrillation ablation with intracardiac echocardiography technologies: a single center experience. *Chin J Cardiac Pacing Electrophysiol*. (2020) 34:7.
41. Bencsik G, Pap R, Sághy L. Intracardiac echocardiography for visualization of the Eustachian valve during radiofrequency ablation of typical atrial flutter. *Europace Eur Pacing Arrhythmias Cardiac Electrophysiol J Work Groups Cardiac Pacing Arrhythm Cardiac Cell Electrophysiol Eur Soc Cardiol*. (2009) 11:901. doi: 10.1093/europace/eup123
42. Herman D, Osmancik P, Zdarska J, Prochazkova R. Routine use of intracardiac echocardiography for atrial flutter ablation is associated with reduced fluoroscopy time, but not with a reduction of radiofrequency energy delivery time. *J Atrial Fibrillat*. (2017) 10:1553. doi: 10.4022/jafib.1553
43. Bencsik G, Pap R, Makai A, Klausz G, Chadaide S, Traykov V, et al. Randomized trial of intracardiac echocardiography during cavotricuspid isthmus ablation. *J Cardiovasc Electrophysiol*. (2012) 23:996–1000. doi: 10.1111/j.1540-8167.2012.02331.x

44. Bencsik G. Novel strategies in the ablation of typical atrial flutter: role of intracardiac echocardiography. *Curr Cardiol Rev.* (2015) 11:127–33. doi: 10.2174/1573403x10666141013121843
45. Kuck KH, Brugada J, Fournkranz A, Metzner A, Ouyang F, Chun KR, et al. Cryoballoon or radiofrequency ablation for paroxysmal atrial fibrillation. *N Engl J Med.* (2016) 374:2235–45.
46. Chinese Society of Pacing and Electrophysiology, Professional Committee of Heart Rhythm of Chinese Medical Doctor Association, Expert Working Committee on Atrial Fibrillation Prevention and Treatment of Atrial Fibrillation Center Union of China. Atrial fibrillation: current understanding and treatment recommendations (2021). *Chin J Cardiac Arrhythm.* (2022) 26:15–88.
47. Rubesch-Kütemeyer V, Molatta S, Vogt J, Gutleben KJ, Horstkotte D, Nölker G. Reduction of radiation exposure in cryoballoon ablation procedures: a single-center study applying intracardiac echocardiography and other radioprotective measures. *Europace Eur Pacing Arrhythm Cardiac Electrophysiol J Work Groups Cardiac Pacing Arrhythm Cardiac Cell Electrophysiol Eur Soc Cardiol.* (2017) 19:947–53. doi: 10.1093/europace/euw139
48. Maalouf J, Whiteside HL, Pillai A, Omar A, Berman A, Saba S, et al. Reduction of radiation and contrast agent exposure in a cryoballoon ablation procedure with integration of electromagnetic mapping and intracardiac echocardiography: a single center experience. *J Interv Cardiac Electrophysiol Int J Arrhythm Pacing.* (2020) 59:545–50. doi: 10.1007/s10840-019-00667-z
49. Akkaya E, Berkowitsch A, Zaltsberg S, Greiss H, Hamm CW, Sperzel J, et al. Second-generation cryoballoon ablation for treatment of persistent atrial fibrillation: three-year outcome and predictors of recurrence after a single procedure. *J Cardiovasc Electrophysiol.* (2018) 29:38–45. doi: 10.1111/jce.13372
50. Aryana A, Allen SL, Pujara DK, Bowers MR, O'Neill PG, Yamauchi Y, et al. Concomitant pulmonary vein and posterior wall isolation using cryoballoon with adjunct radiofrequency in persistent atrial fibrillation. *JACC Clin Electrophysiol.* (2021) 7:187–96.
51. Saleh M, Coleman KM, Vaishnav AS, Shein J, Makker P, Skipitaris N, et al. Intracardiac echocardiography guided nonocclusive balloon cryothermal applications to achieve antral isolation during pulmonary vein isolation. *J Interv Cardiac Electrophysiol Int J Arrhythm Pacing.* (2021) 62:329–36. doi: 10.1007/s10840-020-00905-9
52. Wei HQ, Guo XG, Sun Q, Yang JD, Xie HY, Cao ZJ, et al. Electrical isolation of the superior vena cava using second-generation cryoballoon in patients with atrial fibrillation. *J Cardiovasc Electrophysiol.* (2020) 31:1307–14.
53. Aryana A, Su W, Kuniss M, Okishige K, de Asmundis C, Tondo C, et al. Segmental nonocclusive cryoballoon ablation of pulmonary veins and extrapulmonary vein structures: best practices III. *Heart Rhythm.* (2021) 18:1435–44. doi: 10.1016/j.hrthm.2021.04.020
54. Ruisi CP, Brysiewicz N, Asnes JD, Sugeng L, Marieb M, Clancy J, et al. Use of intracardiac echocardiography during atrial fibrillation ablation. *Pacing Clin Electrophysiol.* (2013) 36:781–8.
55. Ren JF, Chen S, Callans DJ, Jiang C, Marchlinski FE. Role of intracardiac echocardiography for catheter ablation of atrial fibrillation: reduction of complications and mortality. *J Am Coll Cardiol.* (2020) 75:1244–5. doi: 10.1016/j.jacc.2019.11.067
56. Ren JF, Marchlinski FE, Callans DJ. Left atrial thrombus associated with ablation for atrial fibrillation: identification with intracardiac echocardiography. *J Am Coll Cardiol.* (2004) 43:1861–7.
57. Saliba W, Thomas J. Intracardiac echocardiography during catheter ablation of atrial fibrillation. *Europace.* (2008) 10(Suppl. 3):III42–7.
58. La Greca C, Cirasa A, Di Modica D, Sorgato A, Simoncelli U, Pecora D. Advantages of the integration of ICE and 3D electroanatomical mapping and ultrasound-guided femoral venipuncture in catheter ablation of atrial fibrillation. *J Interv Card Electrophysiol.* (2021) 61:559–66. doi: 10.1007/s10840-020-00835-6
59. Kitamura T, Nakajima M, Kawamura I, Kaszynski RH, Ohbe H, Sasabuchi Y, et al. Safety and effectiveness of intracardiac echocardiography in ventricular tachycardia ablation: a nationwide observational study. *Heart Vessels.* (2021) 36:1009–15. doi: 10.1007/s00380-020-01766-y
60. Isath A, Padmanabhan D, Haider SW, Siroky G, Perimbeti S, Correa A, et al. Does the use of intracardiac echocardiography during atrial fibrillation catheter ablation improve outcomes and cost? A nationwide 14-year analysis from 2001 to 2014. *J Interv Card Electrophysiol.* (2021) 61:461–8. doi: 10.1007/s10840-020-00844-5
61. Marrouche NE, Martin DO, Wazni O, Gillinov AM, Klein A, Bhargava M, et al. Phased-array intracardiac echocardiography monitoring during pulmonary vein isolation in patients with atrial fibrillation: impact on outcome and complications. *Circulation.* (2003) 107:2710–6. doi: 10.1161/01.CIR.0000070541.83326.15
62. Friedman DJ, Pokorney SD, Ghanem A, Marcello S, Kalsekar I, Yadalam S, et al. Predictors of cardiac perforation with catheter ablation of atrial fibrillation. *JACC Clin Electrophysiol.* (2020) 6:636–45.
63. Balakrishnan M, Hutchinson MD. Prevention and early recognition of complications during catheter ablation by intracardiac echocardiography. *Card Electrophysiol Clin.* (2021) 13:357–64. doi: 10.1016/j.jccp.2021.03.002
64. Aldhoon B, Wichterle D, Peichl P, Cihak R, Kautzner J. Complications of catheter ablation for atrial fibrillation in a high-volume centre with the use of intracardiac echocardiography. *Europace.* (2013) 15:24–32. doi: 10.1093/europace/eus304
65. Lerman BB, Markowitz SM, Liu CF, Thomas G, Ip JE, Cheung JW. Fluorless catheter ablation of atrial fibrillation. *Heart Rhythm.* (2017) 14:928–34. doi: 10.1016/j.hrthm.2017.02.016
66. Lurie A, Amit G, Divakaramenon S, Acosta JG, Healey JS, Wong JA. Outcomes and safety of fluorless catheter ablation for atrial fibrillation. *CJC Open.* (2021) 3:303–10.
67. Iwasaki YK, Fujimoto Y, Ito-Hagiwara K, Oka E, Hayashi H, Yamamoto T, et al. Metal interference alert guided septal approach with 3 catheter positions on intracardiac echocardiography for a near-zero fluoroscopy catheter ablation of atrial fibrillation. *Int J Cardiol Heart Vasc.* (2021) 37:100896. doi: 10.1016/j.ijcha.2021.100896
68. Zizek D, Antolic B, Prolic Kalinsek T, Stublar J, Kajdic N, Jelenc M, et al. Intracardiac echocardiography-guided transseptal puncture for fluorless catheter ablation of left-sided tachycardias. *J Interv Card Electrophysiol.* (2021) 61:595–602. doi: 10.1007/s10840-020-00858-z
69. Santoro A, Baiocchi C, Lumia G, Zacà V, Romano A, Spera L, et al. Detection of oesophageal course during left atrial catheter ablation. *Indian Pacing Electrophysiol J.* (2020) 20:221–6.
70. Ren JF, Marchlinski FE. Utility of intracardiac echocardiography in left heart ablation for tachyarrhythmias. *Echocardiography (Mount Kisco, NY).* (2007) 24:533–40.
71. Zei PC, Hunter TD, Gache LM, O'Riordan G, Baykaner T, Brodt CR. Low-fluoroscopy atrial fibrillation ablation with contact force and ultrasound technologies: a learning curve. *Pragmatic Observational Res.* (2019) 10:1–7. doi: 10.2147/POR.S181220
72. Jongbloed MR, Bax JJ, van der Burg AE, Van der Wall EE, Schalij MJ. Radiofrequency catheter ablation of ventricular tachycardia guided by intracardiac echocardiography. *Eur J Echocardiogr J Working Group Echocardiogr Eur Soc Cardiol.* (2004) 5:34–40.
73. Bala R, Ren JF, Hutchinson MD, Desjardins B, Tschabrunn C, Gerstenfeld EP, et al. Assessing epicardial substrate using intracardiac echocardiography during VT ablation. *Circ Arrhythmia Electrophysiol.* (2011) 4:667–73.
74. Ren JF, Marchlinski FE. Early detection of iatrogenic pericardial effusion: importance of intracardiac echocardiography. *JACC Cardiovasc Interv.* (2010) 3:127; author reply 127–8. doi: 10.1016/j.jcin.2009.11.004
75. Zhang J, Liang M, Wang Z, Zhang X, Fan J, Jia Y, et al. Catheter ablation of premature ventricular complexes associated with left ventricular false tendons. *Heart Rhythm.* (2021) 18:1968–75.
76. Yamada T. Idiopathic ventricular arrhythmias: relevance to the anatomy, diagnosis and treatment. *J Cardiol.* (2016) 68:463–71. doi: 10.1016/j.jjcc.2016.06.001
77. Zhang J, Tang C, Zhang Y, Su X. Pulmonary sinus cusp mapping and ablation: a new concept and approach for idiopathic right ventricular outflow tract arrhythmias. *Heart Rhythm.* (2018) 15:38–45. doi: 10.1016/j.hrthm.2017.08.007
78. Ho RT. Cross-sectional imaging of the trileaflet pulmonary valve from the right atrial appendage by intracardiac echocardiography. *J Cardiovasc Electrophysiol.* (2019) 30:1378–9. doi: 10.1111/jce.14021
79. Lee BK, McCanta AC, Batra AS. Pulmonary Cusp positioning of a right ventricular outflow tract ventricular tachycardia in a pediatric patient identified using intracardiac echocardiography. *J Innovat Cardiac Rhythm Manag.* (2020) 11:4118–21. doi: 10.19102/icrm.2020.110605
80. Latchamsetty R, Yokokawa M, Morady F, Kim HM, Mathew S, Tilz R, et al. Multicenter outcomes for catheter ablation of idiopathic premature ventricular complexes. *JACC Clin Electrophysiol.* (2015) 1:116–23.
81. Yamada T, Doppalapudi H, Litovsky SH, McDerrery HT, Kay GN. Challenging radiofrequency catheter ablation of idiopathic ventricular arrhythmias originating from the left ventricular summit near the left main coronary artery. *Circ Arrhythm Electrophysiol.* (2016) 9:e004202. doi: 10.1161/CIRCEP.116.004202
82. Jauregui Abularach ME, Campos B, Park KM, Tschabrunn CM, Frankel DS, Park RE, et al. Ablation of ventricular arrhythmias arising near the anterior epicardial veins from the left sinus of Valsalva region: ECG features, anatomic

- distance, and outcome. *Heart Rhythm*. (2012) 9:865–73. doi: 10.1016/j.hrthm.2012.01.022
83. Rivera S, Vecchio N, Ricapito P, Ayala-Paredes F. Non-fluoroscopic catheter ablation of arrhythmias with origin at the summit of the left ventricle. *J Int Cardiac Electrophysiol Int J Arrhythm Pacing*. (2019) 56:279–90. doi: 10.1007/s10840-019-00522-1
84. Briceno DF, Enriquez A, Romero J, Tapias C, Santangeli P, Schaller R, et al. How to use intracardiac echocardiography to identify ventricular tachycardia substrate in ischemic cardiomyopathy. *HeartRhythm Case Rep*. (2020) 6:663–70.
85. Hussein A, Jimenez A, Ahmad G, Mesubi O, Klein T, Gurm G, et al. Assessment of ventricular tachycardia scar substrate by intracardiac echocardiography. *Pacing Clin Electrophysiol*. (2014) 37:412–21.
86. Bunch TJ, Weiss JP, Crandall BG, Day JD, DiMarco JP, Ferguson JD, et al. Image integration using intracardiac ultrasound and 3D reconstruction for scar mapping and ablation of ventricular tachycardia. *J Cardiovasc Electrophysiol*. (2010) 21:678–84.
87. Barrett C, Tzou WS. Utility of intracardiac echocardiography for guiding ablation of ventricular tachycardia in nonischemic cardiomyopathy. *Card Electrophysiol Clin*. (2021) 13:337–43. doi: 10.1016/j.ccep.2021.03.008
88. Field ME, Gold MR, Reynolds MR, Goldstein L, Lee SHY, Kalsekar I, et al. Real-world outcomes of ventricular tachycardia catheter ablation with versus without intracardiac echocardiography. *J Cardiovasc Electrophysiol*. (2020) 31:417–22. doi: 10.1111/jce.14324
89. Alqahtani F, Bhirud A, Aljohani S, Mills J, Kawsara A, Runkana A, et al. Intracardiac versus transesophageal echocardiography to guide transcatheter closure of interatrial communications: nationwide trend and comparative analysis. *J Interv Cardiol*. (2017) 30:234–41. doi: 10.1111/joic.12382
90. Hellenbrand WE, Fahey JT, McGowan FX, Weltin GG, Kleinman CS. Transesophageal echocardiographic guidance of transcatheter closure of atrial septal defect. *Am J Cardiol*. (1990) 66:207–13.
91. Van Der Velde ME, Perry SB. Transesophageal echocardiography during interventional catheterization in congenital heart disease. *Echocardiography (Mount Kisco, NY)*. (1997) 14:513–28.
92. Bartel T, Konorza T, Neudorf U, Ebralize T, Eggebrecht H, Gutersohn A, et al. Intracardiac echocardiography: an ideal guiding tool for device closure of interatrial communications. *Eur J Echocardiogr J Work Group Echocardiogr Eur Soc Cardiol*. (2005) 6:92–6. doi: 10.1016/j.euje.2004.07.007
93. Kavvouras C, Vavuranakis M, Vaina S, Lampropoulos K, Bazoukis G, Tse G, et al. Intracardiac echocardiography for percutaneous patent foramen ovale and atrial septal defect occlusion. *Herz*. (2019) 44:445–9.
94. Koenig P, Cao QL. Echocardiographic guidance of transcatheter closure of atrial septal defects: is intracardiac echocardiography better than transesophageal echocardiography? *Pediatric Cardiol*. (2005) 26:135–9. doi: 10.1007/s00246-004-0952-6
95. Ali S, George LK, Das P, Koshy SK. Intracardiac echocardiography: clinical utility and application. *Echocardiography (Mount Kisco, NY)*. (2011) 28:582–90.
96. Barker PC. Intracardiac echocardiography in congenital heart disease. *J Cardiovasc Transl Res*. (2009) 2:19–23.
97. Bartel T, Konorza T, Arjmand J, Ebralidze T, Eggebrecht H, Caspari G, et al. Intracardiac echocardiography is superior to conventional monitoring for guiding device closure of interatrial communications. *Circulation*. (2003) 107:795–7. doi: 10.1161/01.cir.0000057547.00909.1c
98. Hijazi Z, Wang Z, Cao Q, Koenig P, Waight D, Lang R. Transcatheter closure of atrial septal defects and patent foramen ovale under intracardiac echocardiographic guidance: feasibility and comparison with transesophageal echocardiography. *Catheter Cardiovasc Interv Off J Soc Cardiac Angiogr Interv*. (2001) 52:194–9. doi: 10.1002/1522-726x(200102)52:2<194::aid-ccd1046>3.0.co;2-4
99. Assaidi A, Sumian M, Mauri L, Mancini J, Ovaert C, Salaun E, et al. Transcatheter closure of complex atrial septal defects is efficient under intracardiac echocardiographic guidance. *Arch Cardiovasc Dis*. (2014) 107:646–53. doi: 10.1016/j.acvd.2014.06.010
100. Bartel T, Müller S. To close or not to close an atrial septal defect in ischemic cardiomyopathy. *Catheter Cardiovasc Interv Off J Soc Cardiac Angiogr Interv*. (2013) 81:651–3.
101. Awad SM, Garay FF, Cao QL, Hijazi ZM. Multiple Amplatzer septal occluder devices for multiple atrial communications: immediate and long-term follow-up results. *Catheter Cardiovasc Interv Off J Soc Cardiac Angiogr Interv*. (2007) 70:265–73. doi: 10.1002/ccd.21145
102. Tande AJ, Knickelbine T, Chavez I, Mooney MR, Poulouse A, Harris KM. Transseptal technique of percutaneous PFO closure results in persistent interatrial shunting. *Catheter Cardiovasc Interv Off J Soc Cardiac Angiogr Interv*. (2005) 65:295–300. doi: 10.1002/ccd.20377
103. Ren JF, Marchlinski FE, Callans DJ, Herrmann HC. Clinical use of AcuNav diagnostic ultrasound catheter imaging during left heart radiofrequency ablation and transcatheter closure procedures. *J Am Soc Echocardiogr Off Publ Am Soc Echocardiogr*. (2002) 15:1301–8. doi: 10.1067/mje.2002.124646
104. Rigatelli G, Cardaioli P, Roncon L, Giordan M, Bedendo E, Oliva L, et al. Impact of intracardiac echocardiography on radiation exposure during adult congenital heart disease catheter-based interventions. *Int J Cardiovasc Imaging*. (2007) 23:139–42. doi: 10.1007/s10554-006-9125-4
105. Alkhouli M, Hijazi ZM, Holmes DR Jr., Rihal CS, Wieggers SE. Intracardiac echocardiography in structural heart disease interventions. *JACC Cardiovasc Interv*. (2018) 11:2133–47.
106. Shafi NA, Singh GD, Smith TW, Rogers JH. Sizing of patent ductus arteriosus in adults for transcatheter closure using the balloon pull-through technique. *Catheter Cardiovasc Interv Off J Soc Cardiac Angiogr Interv*. (2018) 91:1159–63. doi: 10.1002/ccd.27303
107. Goleczka M, Szkutnik M, Bialkowski J, Smerdzinski S, Knop M, Sukiennik A, et al. Transcatheter closure of patent ductus arteriosus in elderly patients: initial and one-year follow-up results-do we have the proper device? *J Interv Cardiol*. (2020) 2020:4585124. doi: 10.1155/2020/4585124
108. Feltes TF, Bacha E, Beekman RH III, Cheatham JP, Feinstein JA, Gomes AS, et al. Indications for cardiac catheterization and intervention in pediatric cardiac disease: a scientific statement from the American Heart Association. *Circulation*. (2011) 123:2607–52. doi: 10.1161/CIR.0b013e31821b1f10
109. Goss JE, Chambers CE, Heupler FA Jr. Systemic anaphylactoid reactions to iodinated contrast media during cardiac catheterization procedures: guidelines for prevention, diagnosis, and treatment. Laboratory performance standards committee of the society for cardiac angiography and interventions. *Catheter Cardiovasc Diagnosis*. (1995) 34:99–104; discussion 105. doi: 10.1002/ccd.1810340403
110. Sardinha DM, Simor A, de Oliveira Moura LD, Silva A, Batista Lima KV, Dias Garcez JC, et al. Risk factors for acute renal failure after cardiac catheterization most cited in the literature: an integrative review. *Int J Environ Res Public Health*. (2020) 17:3392. doi: 10.3390/ijerph17103392
111. Yoshimoto, H, Yasuto M, Inoue T, Kagiya Y, Teramachi Y, Takase R, et al. Intracardiac echocardiography as a guide for transcatheter closure of patent ductus arteriosus. *J Interv Cardiol*. (2020) 2020:5147193.
112. Arora S, Misenheimer JA, Ramaraj R. Transcatheter aortic valve replacement: comprehensive review and present status. *Texas Heart Institute J*. (2017) 44:29–38.
113. Mack MJ, Brennan JM, Brindis R, Carroll J, Edwards F, Grover F, et al. Outcomes following transcatheter aortic valve replacement in the United States. *JAMA*. (2013) 310:2069–77.
114. Bykhovsky MR, Atianzar K, Agarwal S, Shivaram P, Amin Z. Use of intracardiac echocardiography to differentiate post-transcatheter aortic valve replacement valve insufficiency masquerading as paravalvular leak. *CASE (Philadelphia, PA)*. (2020) 4:111–4. doi: 10.1016/j.case.2019.11.004
115. Bartel T, Edris A, Velik-Salchner C, Müller S. Intracardiac echocardiography for guidance of transcatheter aortic valve implantation under monitored sedation: a solution to a dilemma? *Eur Heart J Cardiovasc Imaging*. (2016) 17:1–8. doi: 10.1093/ehjci/jev280
116. Rendon A, Hamid T, Kanaganayagam G, Karunaratne D, Mahadevan VS. Annular sizing using real-time three-dimensional intracardiac echocardiography-guided trans-catheter aortic valve replacement. *Open Heart*. (2016) 3:e000316. doi: 10.1136/openhrt-2015-000316
117. Kadakia MB, Silvestry FE, Herrmann HC. Intracardiac echocardiography-guided transcatheter aortic valve replacement. *Catheter Cardiovasc Interv Off J Soc Cardiac Angiogr Interv*. (2015) 85:497–501.
118. Dhoble A, Nakamura M, Makar M, Castellanos J, Jilaihawi H, Cheng W, et al. 3D intracardiac echocardiography during TAVR without endotracheal intubation. *JACC Cardiovasc Imaging*. (2016) 9:1014–5. doi: 10.1016/j.jcmg.2015.08.009
119. Bartel T, Bonaros N, Müller L, Friedrich G, Grimm M, Velik-Salchner C, et al. Intracardiac echocardiography: a new guiding tool for transcatheter aortic valve replacement. *J Am Soc Echocardiogr Off Publ Am Soc Echocardiogr*. (2011) 24:966–75. doi: 10.1016/j.echo.2011.04.009
120. Hahn RT, Little SH, Monaghan MJ, Kodali SK, Williams M, Leon MB, et al. Recommendations for comprehensive intraprocedural echocardiographic

- imaging during TAVR. *JACC Cardiovasc Imaging*. (2015) 8:261–87. doi: 10.1016/j.jcmg.2014.12.014
121. Yagasaki H, Goto Y, Mori Y, Noda T. Transcatheter aortic valve replacement with intracardiac echocardiography from the right internal jugular vein. *Cardiovasc Diagn Ther*. (2018) 8:525–9. doi: 10.21037/cdt.2018.07.06
122. Dehédin B, Guinot PG, Ibrahim H, Allou N, Provenchère S, Dilly MP, et al. Anesthesia and perioperative management of patients who undergo transfemoral transcatheter aortic valve implantation: an observational study of general versus local/regional anesthesia in 125 consecutive patients. *J Cardiothoracic Vasc Anesthesia*. (2011) 25:1036–43. doi: 10.1053/j.jvca.2011.05.008
123. Kanda H, Maruyama S, Toyama Y, Kamiya H, Kunisawa T. Intracardiac echocardiography instead of transesophageal echocardiography in surgical aortic valve replacement. *J Cardiothoracic Vasc Anesthesia*. (2020) 34:853–5. doi: 10.1053/j.jvca.2019.10.056
124. He G, Liu H, Huang X, Deng X, Yang G, Luo D, et al. Intracardiac versus transesophageal echocardiography for diagnosis of left atrial appendage thrombosis in atrial fibrillation: a meta-analysis. *Clin Cardiol*. (2021) 44:1416–21. doi: 10.1002/clc.23698
125. Henning A, Mueller II, Mueller K, Zuern C, Walker T, Gawaz M, et al. Percutaneous edge-to-edge mitral valve repair escorted by left atrial intracardiac echocardiography (ICE). *Circulation*. (2014) 130:e173–4. doi: 10.1161/CIRCULATIONAHA.114.012504
126. Patzelt J, Seizer P, Zhang YY, Walker T, Schreieck J, Gawaz M, et al. Percutaneous mitral valve edge-to-edge repair with simultaneous batrial intracardiac echocardiography: first-in-human experience. *Circulation*. (2016) 133:1517–9. doi: 10.1161/CIRCULATIONAHA.115.020923
127. Patzelt J, Schreieck J, Camus E, Gawaz M, Seizer P, Langer HF. Percutaneous mitral valve edge-to-edge repair using volume intracardiac echocardiography-first in human experience. *CASE (Philadelphia, PA)*. (2017) 1:41–3. doi: 10.1016/j.case.2017.01.006
128. Sanchez CE, Yakubov SJ, Singh G, Rogers JH, Kander NH, Tang GHL. 4-Dimensional intracardiac echocardiography in transcatheter mitral valve repair with the mitraclip system. *JACC Cardiovasc Imaging*. (2021) 14:2033–40.
129. Salem MI, Makaryus AN, Kort S, Chung E, Marchant D, Ong L, et al. Intracardiac echocardiography using the AcuNav ultrasound catheter during percutaneous balloon mitral valvuloplasty. *J Am Soc Echocardiogr Off Publ Am Soc Echocardiogr*. (2002) 15:1533–7.
130. Green NE, Hansgen AR, Carroll JD. Initial clinical experience with intracardiac echocardiography in guiding balloon mitral valvuloplasty: technique, safety, utility, and limitations. *Catheter Cardiovasc Interv Off J Soc Cardiac Angiogr Interv*. (2004) 63:385–94. doi: 10.1002/ccd.20177
131. Saji M, Ragosta M, Dent J, Lim DS. Use of intracardiac echocardiography to guide percutaneous transluminal mitral commissurotomy: a 20-patient case series. *Catheter Cardiovasc Interv Off J Soc Cardiac Angiogr Interv*. (2016) 87:E69–74. doi: 10.1002/ccd.25943
132. Pommier T, Guenancia C, Sagnard A, Ferrand B, Didier R, Fichot M, et al. Safety and efficacy of transcatheter mitral valve replacement guided by intracardiac echocardiography. *JACC Cardiovasc Interv*. (2021) 14:1620–2.
133. Cubeddu RJ, Sarkar A, Navas V, Navia JL. 'Minimalist approach' for transcatheter mitral valve replacement using intracardiac echocardiography and conscious sedation: a case series. *Eur Heart J Case Rep*. (2020) 4:1–5. doi: 10.1093/ehjcr/ytta058
134. Awad SM, Masood SA, Gonzalez I, Cao QL, Abdulla RI, Heitschmidt MG, et al. The use of intracardiac echocardiography during percutaneous pulmonary valve replacement. *Pediatric Cardiol*. (2015) 36:76–83.
135. Whiteside W, Pasquali SK, Yu S, Bocks ML, Zampi JD, Armstrong AK. The utility of intracardiac echocardiography following Melody™ transcatheter pulmonary valve implantation. *Pediatric Cardiol*. (2015) 36:1754–60. doi: 10.1007/s00246-015-1230-5
136. McElhinney DB, Benson LN, Eicken A, Kreutzer J, Padera RF, Zahn EM. Infective endocarditis after transcatheter pulmonary valve replacement using the Melody valve: combined results of 3 prospective North American and European studies. *Circ Cardiovasc Interv*. (2013) 6:292–300. doi: 10.1161/CIRCINTERVENTIONS.112.000087
137. Bouajila S, Chalard A, Dauphin C. Usefulness of intracardiac echocardiography for the diagnosis of infective endocarditis following percutaneous pulmonary valve replacement. *Cardiol Young*. (2017) 27:1406–9. doi: 10.1017/S104795117000403
138. Singh JP, Evans JC, Levy D, Larson MG, Freed LA, Fuller DL, et al. Prevalence and clinical determinants of mitral, tricuspid, and aortic regurgitation (the Framingham Heart Study). *Am J Cardiol*. (1999) 83:897–902.
139. Nath J, Foster E, Heidenreich PA. Impact of tricuspid regurgitation on long-term survival. *J Am Coll Cardiol*. (2004) 43:405–9.
140. Topilsky Y, Khanna AD, Oh JK, Nishimura RA, Enriquez-Sarano M, Jeon YB, et al. Preoperative factors associated with adverse outcome after tricuspid valve replacement. *Circulation*. (2011) 123:1929–39.
141. Curio J, Abulgasim K, Kasner M, Rroku A, Lauten A, Lendlein A, et al. Intracardiac echocardiography to enable successful edge-to-edge transcatheter tricuspid valve repair in patients with insufficient TEE quality. *Clin Hemorheol Microcirculat*. (2020) 76:199–210. doi: 10.3233/CH-209211
142. Hagemeyer D, Ali FM, Ong G, Fam NP. The role of intracardiac echocardiography in percutaneous tricuspid intervention: a new ICE Age. *Interv Cardiol Clin*. (2022) 11:103–12. doi: 10.1016/j.iccl.2021.09.006
143. Davidson CJ, Abramson S, Smith RL, Kodali SK, Kipperman RM, Eleid MF, et al. Transcatheter tricuspid repair with the use of 4-dimensional intracardiac echocardiography. *JACC Cardiovasc Imaging*. (2022) 15:533–8.
144. Hammermeister K, Sethi GK, Henderson WG, Grover FL, Oprian C, Rahimtoola SH. Outcomes 15 years after valve replacement with a mechanical versus a bioprosthetic valve: final report of the Veterans Affairs randomized trial. *J Am Coll Cardiol*. (2000) 36:1152–8. doi: 10.1016/s0735-1097(00)00834-2
145. Ionescu A, Fraser AG, Butchart EG. Prevalence and clinical significance of incidental paraprosthetic valvar regurgitation: a prospective study using transoesophageal echocardiography. *Heart (British Cardiac Society)*. (2003) 89:1316–21. doi: 10.1136/heart.89.11.1316
146. García E, Sandoval J, Unzué L, Hernandez-Antolin R, Almería C, Macaya C. Paravalvular leaks: mechanisms, diagnosis and management. *Eurointervention J Europcr Collaborat Working Group Interv Cardiol Eur Soc Cardiol*. (2012) 8(Suppl. Q):Q41–52.
147. Van Belle E, Juthier F, Susen S, Vincentelli A, Iung B, Dallongeville J, et al. Postprocedural aortic regurgitation in balloon-expandable and self-expandable transcatheter aortic valve replacement procedures: analysis of predictors and impact on long-term mortality: insights from the FRANCE2 Registry. *Circulation*. (2014) 129:1415–27.
148. Athappan G, Patvardhan E, Tuzcu EM, Svensson LG, Lemos PA, Fraccaro C, et al. Incidence, predictors, and outcomes of aortic regurgitation after transcatheter aortic valve replacement: meta-analysis and systematic review of literature. *J Am Coll Cardiol*. (2013) 61:1585–95.
149. Otto CM, Nishimura RA, Bonow RO, Carabello BA, Erwin JP III, Gentile F, et al. 2020 ACC/AHA guideline for the management of patients with valvular heart disease: executive summary: a report of the American College of Cardiology/American Heart Association Joint Committee on Clinical Practice Guidelines. *Circulation*. (2021) 143:e35–71.
150. Ruparel N, Cao J, Newton JD, Wilson N, Daniels MJ, Ormerod OJ. Paravalvular leak closure under intracardiac echocardiographic guidance. *Catheter Cardiovasc Interv Off J Soc Cardiac Angiogr Interv*. (2018) 91:958–65. doi: 10.1002/ccd.27318
151. Xianfeng D, Bing L, Weidong Z, Yingbo Q, Bin H, Mingjun F, et al. The feasibility, efficacy and safety of one-stop treatment of atrial fibrillation guided by intracardiac echocardiography. *Chin J Cardiac Arrhythm*. (2021) 25:484–90.
152. Tamirisa KP, Elkayam U, Briller JE, Mason PK, Pillarisetti J, Merchant FM, et al. Arrhythmias in pregnancy. *JACC Clin Electrophysiol*. (2022) 8:120–35.
153. Chen G, Sun G, Xu R, Chen X, Yang L, Bai Y, et al. Zero-fluoroscopy catheter ablation of severe drug-resistant arrhythmia guided by Ensite NavX system during pregnancy: two case reports and literature review. *Medicine (Baltimore)*. (2016) 95:e4487. doi: 10.1097/MD.0000000000004487
154. Driver K, Chisholm CA, Darby AE, Malhotra R, Dimarco JP, Ferguson JD. Catheter ablation of arrhythmia during pregnancy. *J Cardiovasc Electrophysiol*. (2015) 26:698–702.
155. Li MM, Sang CH, Jiang CX, Guo XY, Li SN, Wang W, et al. Maternal arrhythmia in structurally normal heart: prevalence and feasibility of catheter ablation without fluoroscopy. *Pacing Clin Electrophysiol*. (2019) 42:1566–72. doi: 10.1111/pace.13819
156. Yastrebov K, Brunel L, Paterson HS, Williams ZA, Wise IK, Burrows CS, et al. Implantation of Impella CP left ventricular assist device under the guidance of three-dimensional intracardiac echocardiography. *Sci Rep*. (2020) 10:17485.
157. Kassi M, Rosenbaum AN, Wiley BM, Behfar A. Novel use for intracardiac echocardiography: evaluation of patients with continuous flow left ventricular assist devices. *JACC Cardiovasc Imaging*. (2019) 12:363–6. doi: 10.1016/j.jcmg.2018.06.022
158. Rohm CL, Howard B, Lakhani B, Wilim M, Holden RW, Snipelisky D. Use of intracardiac echocardiography to evaluate continuous-flow left ventricular assist device function in a man with obesity. *Texas Heart Institute J*. (2021) 48:e207303. doi: 10.14503/THIJ-20-7303

159. El Banayosy A, Koerner MM, Brehm C, Stevenson ER, Pae WE Jr., Clemson B, et al. Intracardiac echocardiography for diagnosis and management of left ventricular assist device inlet obstruction. *ASAIO J (Am Soc Artificial Int Organs)* 1992. (2014) 60:e1–2. doi: 10.1097/MAT.0000000000000142
160. Zanobini M, Dello Russo A, Saccocci M, Conti S, De Camilli E, Vettor G, et al. Endomyocardial biopsy guided by intracardiac echocardiography as a key step in intracardiac mass diagnosis. *BMC Cardiovasc Disord.* (2018) 18:15. doi: 10.1186/s12872-018-0749-9
161. Casella M, Dello Russo A, Vettor G, Lumia G, Catto V, Sommariva E, et al. Electroanatomical mapping systems and intracardiac echo integration for guided endomyocardial biopsy. *Exp Rev Med Devices.* (2017) 14:609–19. doi: 10.1080/17434440.2017.1351875
162. Cooper RM, Shahzad A, Hasleton J, Digiovanni J, Hall MC, Todd DM, et al. Radiofrequency ablation of the interventricular septum to treat outflow tract gradients in hypertrophic obstructive cardiomyopathy: a novel use of CARTOSound technology to guide ablation. *Europace.* (2016) 18:113–20. doi: 10.1093/europace/euv302
163. Yang H, Yang Y, Xue Y, Luo S. Efficacy and safety of radiofrequency ablation for hypertrophic obstructive cardiomyopathy: a systematic review and meta-analysis. *Clin Cardiol.* (2020) 43:450–8.
164. Valdigem BP, Correia EB, Ribeiro Moreira DA, Costa de Souza Le Bihan D, Pinto Filho IM, Paladino Filho AT, et al. Focused endocardial septal ablation: a new technique to treat post myectomy recurrent gradient. *Ann Thorac Surg.* (2021) 112:e279–81. doi: 10.1016/j.athoracsur.2021.01.029
165. Mathur SK, Singh P. Transoesophageal echocardiography related complications. *Indian J Anaesthesia.* (2009) 53:567–74.
166. Cooper RM, Shahzad A, Newton J, Vejstrup N, Axelsson A, Sharma V, et al. Intra-cardiac echocardiography in alcohol septal ablation: a prospective comparative study against trans-thoracic echocardiography. *Echo Res Pract.* (2015) 2:9–17. doi: 10.1530/ERP-15-0002
167. Shelke AB, Menon R, Kapadiya A, Yalagudri S, Saggu D, Nair S, et al. A novel approach in the use of radiofrequency catheter ablation of septal hypertrophy in hypertrophic obstructive cardiomyopathy. *Indian Heart J.* (2016) 68:618–23. doi: 10.1016/j.ihj.2016.02.007
168. Müller S, Velik-Salchner C, Edlinger M, Bonaros N, Heinz A, Feuchtnr G, et al. Intracardiac doppler echocardiography for monitoring of pulmonary artery pressures in high-risk patients undergoing transcatheter aortic valve replacement. *J Am Soc Echocardiogr Off Publ Am Soc Echocardiogr.* (2016) 29:83–91. doi: 10.1016/j.echo.2015.09.003
169. Pulmonary Embolism and Pulmonary Vascular Disease Group of Chinese Thoracic Society, Pulmonary Embolism and Pulmonary Vascular Disease Working Committee of China Respiratory Association, National Collaborative Group on Prevention and Treatment of Pulmonary Embolism and Pulmonary Vascular Disease. Guidelines for the diagnosis and treatment of pulmonary hypertension (2021 Edition). *Natl Med J China.* (2021) 101:11–51.
170. Pokala SK, Zhang C, Chen Z, Gamboa AM, Cristofaro SL, Keilin SA, et al. Lymph node metastasis in early gastric adenocarcinoma in the United States of America. *Endoscopy.* (2018) 50:479–86.
171. Chen YW, Pan HC, Wang KY, Liang KW. Consecutive sessions of rescue balloon atrial septostomy for an idiopathic pulmonary arterial hypertension patient with refractory right heart failure - usefulness of intracardiac echocardiography guidance. *Acta Cardiol Sin.* (2017) 33:310–4. doi: 10.6515/acs20160425a
172. Baglini R. Atrial septostomy in patients with end-stage pulmonary hypertension. No more needles but wires, energy and close anatomical definition. *J Interv Cardiol.* (2013) 26:62–8. doi: 10.1111/j.1540-8183.2012.00759.x
173. Kuhn BT, Javed U, Armstrong EJ, Singh GD, Smith TW, Whitcomb CJ, et al. Balloon dilation atrial septostomy for advanced pulmonary hypertension in patients on prostanoid therapy. *Catheter Cardiovasc Interv.* (2015) 85:1066–72. doi: 10.1002/ccd.25751
174. Roy AK, Gaine SP, Walsh KP. Percutaneous atrial septostomy with modified butterfly stent and intracardiac echocardiographic guidance in a patient with syncope and refractory pulmonary arterial hypertension. *Heart Lung Circ.* (2013) 22:668–71. doi: 10.1016/j.hlc.2013.01.005
175. Yan C, Niu G, Niu H, Li L, Wan L, Li H. Stable interatrial communication combining balloon atrial septostomy and radiofrequency catheter ablation. *J Am Coll Cardiol.* (2018) 72:1873–5. doi: 10.1016/j.jacc.2018.07.058
176. Heart Rhythm Branch of the Chinese Society of Biomedical Engineering. Chinese expert consensus on infection and management of cardiac implantable devices 2013. *J Clin Electrocardiol.* (2013) 22:241–53.
177. Schaller RD, Sadek MM, Cooper JM. Simultaneous lead traction from above and below: a novel technique to reduce the risk of superior vena cava injury during transvenous lead extraction. *Heart Rhythm.* (2018) 15:1655–63. doi: 10.1016/j.hrthm.2018.05.022
178. Maheshwari A, Desai ND, Giri J, Kobayashi T, Kolansky DM, Schaller RD. Use of intracardiac echocardiography during transvenous lead extraction to avoid a catastrophic injury. *JACC Clin Electrophysiol.* (2019) 5:744–5. doi: 10.1016/j.jacep.2019.01.013
179. Narducci ML, Pelargonio G, Russo E, Marinaccio L, Di Monaco A, Perna F, et al. Usefulness of intracardiac echocardiography for the diagnosis of cardiovascular implantable electronic device-related endocarditis. *J Am Coll Cardiol.* (2013) 61:1398–405. doi: 10.1016/j.jacc.2012.12.041
180. Narducci ML, Di Monaco A, Pelargonio G, Leoncini E, Boccia S, Mollo R, et al. Presence of 'ghosts' and mortality after transvenous lead extraction. *Europace Eur Pacing Arrhythmias Cardiac Electrophysiol J Working Groups Cardiac Pacing Arrhythmias Cardiac Cell Electrophysiol Eur Soc Cardiol.* (2017) 19:432–40.
181. Sadek MM, Cooper JM, Frankel DS, Santangeli P, Epstein AE, Marchlinski FE, et al. Utility of intracardiac echocardiography during transvenous lead extraction. *Heart Rhythm.* (2017) 14:1779–85.
182. Kautzner J, Wunschova H, Haskova J. Leadless pacemaker implant guided by intracardiac echocardiography in a patient after Mustard repair. *Pacing Clin Electrophysiol.* (2022) 45:571–3. doi: 10.1111/pace.14417
183. Zhang J, Sun Y, Zhang Z, Jiang C, Fu G. Intracardiac ultrasound-guided left bundle branch pacing in a bradycardia patient. *Clin Case Rep.* (2020) 8:1030–3. doi: 10.1002/ccr3.2798
184. Shimamoto K, Yamagata K, Wakamiya A, Ueda N, Kamakura T, Wada M, et al. Zero-fluoroscopy ablation in patients with cardiac electronic implantable devices. *J Cardiovasc Electrophysiol.* (2022) 33:423–9.



OPEN ACCESS

EDITED BY

Masaki Izumo,
St. Marianna University School
of Medicine, Japan

REVIEWED BY

Kimi Sato,
University of Tsukuba, Japan
Toshinari Onishi,
Sakai City Medical Center, Japan
Norio Suzuki,
St. Marianna University School
of Medicine, Japan

*CORRESPONDENCE

Jiawei Tian
jwttian2004@163.com
Hairu Li
lihairu0419@126.com

SPECIALTY SECTION

This article was submitted to
Cardiovascular Imaging,
a section of the journal
Frontiers in Cardiovascular Medicine

RECEIVED 19 August 2022

ACCEPTED 10 October 2022

PUBLISHED 28 October 2022

CITATION

Sun Q-L, Jiang S-Q, Wang X-D,
Zhang J-C, Li Y, Tian J-W and Li H-R
(2022) A prediction model for major
adverse cardiovascular events
in patients with heart failure based on
high-throughput echocardiographic
data.
Front. Cardiovasc. Med. 9:1022658.
doi: 10.3389/fcvm.2022.1022658

COPYRIGHT

© 2022 Sun, Jiang, Wang, Zhang, Li,
Tian and Li. This is an open-access
article distributed under the terms of
the [Creative Commons Attribution
License \(CC BY\)](#). The use, distribution
or reproduction in other forums is
permitted, provided the original
author(s) and the copyright owner(s)
are credited and that the original
publication in this journal is cited, in
accordance with accepted academic
practice. No use, distribution or
reproduction is permitted which does
not comply with these terms.

A prediction model for major adverse cardiovascular events in patients with heart failure based on high-throughput echocardiographic data

Qinliang Sun¹, Shuangquan Jiang¹, Xudong Wang¹,
Jingchun Zhang², Yi Li¹, Jiawei Tian^{1*} and Hairu Li^{1*}

¹Department of Ultrasound Imaging, The Second Affiliated Hospital of Harbin Medical University, Harbin, China, ²Department of Gastroenterology, Digestive Disease Hospital, Heilongjiang Provincial Hospital Affiliated to Harbin Institute of Technology, Harbin, China

Background: Heart failure (HF) is a serious end-stage condition of various heart diseases with increasing frequency. Few studies have combined clinical features with high-throughput echocardiographic data to assess the risk of major cardiovascular events (MACE) in patients with heart failure. In this study, we assessed the relationship between these factors and heart failure to develop a practical and accurate prognostic dynamic nomogram model to identify high-risk groups of heart failure and ultimately provide tailored treatment options.

Materials and methods: We conducted a prospective study of 468 patients with heart failure and established a clinical predictive model. Modeling to predict risk of MACE in heart failure patients within 6 months after discharge obtained 320 features including general clinical data, laboratory examination, 2-dimensional and Doppler measurements, left ventricular (LV) and left atrial (LA) speckle tracking echocardiography (STE), and left ventricular vector flow mapping (VFM) data, were obtained by building a model to predict the risk of MACE within 6 months of discharge for patients with heart failure. In addition, the addition of machine learning models also confirmed the necessity of increasing the STE and VFM parameters.

Results: Through regular follow-up 6 months after discharge, MACE occurred in 156 patients (33.3%). The prediction model showed good discrimination C-statistic value, 0.876 ($p < 0.05$), which indicated good identical calibration and clinical efficacy. In multiple datasets, through machine learning multi-model comparison, we found that the area under curve (AUC) of the model with VFM and STE parameters was higher, which was more significant with the XGboost model.

Conclusion: In this study, we developed a prediction model and nomogram to estimate the risk of MACE within 6 months of discharge among patients with heart failure. The results of this study can provide a reference for

clinical physicians for detection of the risk of MACE in terms of clinical characteristics, cardiac structure and function, hemodynamics, and enable its prompt management, which is a convenient, practical and effective clinical decision-making tool for providing accurate prognosis.

KEYWORDS

speckle tracking, vector flow mapping, heart failure, prediction model, nomogram

Introduction

Urbanization and the widespread use of cars have shifted many people from active to sedentary lifestyles, increasing the incidence of chronic diseases such as obesity, hypertension, diabetes, and coronary artery disease. Heart failure is a serious manifestation of the late stage of various heart diseases, and its risk factors include coronary diseases, hypertension, and diabetes, lifestyle factors such as smoking and alcohol consumption. Heart failure remains a serious clinical and public health problem as the total number of patients living with heart failure increases, reflecting the chronic course of the disease as well as population growth and aging (1). With high readmission and mortality rate, heart failure places a huge financial burden on the healthcare system (2–4).

All efforts must be underway to examine clinical, laboratory, and imaging data to better characterize heart failure phenotypes (5, 6) and to develop cost-effective strategies to reliably identify at-risk populations at an early stage. Therefore, early identification of individuals with high-risk factors will provide an opportunity for the early intervention and prevention of MACE in these individuals. Stratifying patients according to risk of future outcomes and optimizing treatment strategies can help reduce their follow-up costs and mortality (7–9).

The 2019 American College of Cardiology expert consensus on heart failure suggests that assessing risk-increasing factors can help inform decisions about preventive interventions (10). Many risk prediction models have been published internationally (11–16). Predictors of hospitalization rates were age, history of hospitalization for heart failure, edema, systolic blood pressure, and estimated glomerular filtration rate (11). In 2019, the Korean Acute Heart Failure Registry establishes a risk score that predicts the risk of HF specific readmission or death at 30 days after discharge by using 12 predictors (12). In this study, Wang Lei developed a prediction model and nomogram to estimate the risk of irreversible worsening of cardiac function among acute decompensated HF patients, which provided a reference for clinicians to detect and treat cardiac deterioration in a timely manner (13). Compared with traditional HF risk and non-race-specific machine learning models, Race-specific and ML-based HF risk models that combine clinical, laboratory, and biomarker data demonstrated superior performance which can identify distinct race-specific contributors of HF (14). A multivariate

Abbreviations: A, late diastolic transmitral flow velocity; a', late diastolic relaxation velocity at septal mitral annular position; ac, atrium contraction; ANOVA, analysis of variance; ALT, alanine transaminase; ApoA, apolipoproteinA; ACEI, Angiotensin-converting enzyme inhibitors; ApoB, apolipoproteinB; AR, aortic regurgitation; ARBS, angiotensin receptor blockers; AST, aspartate transaminase; AUC, area under curve; BSA, body surface area; C2, 2-chamber; C3, 3-chamber; C4, 4-chamber; CI, cardiac index; CV, cardiovascular; CW, clockwise; CCW, counter-clockwise; DBP, diastolic blood pressure; DCM, dilated cardiomyopathy; ed, early diastole; e', early diastolic relaxation velocity at septal mitral annular position; E, early diastolic transmitral flow velocity; EL, energy loss; ELC3P3, energy loss from 3-chamber images during isovolumic relaxation period; GDMT, Guideline Determined Medication Therapy; GHb, glycated hemoglobin; GLS, global longitudinal strain; GLS_{ac}C2LV, left ventricular global longitudinal strain from 2-chamber images during atrial systolic period; GLS_{ed}C3LV, left ventricular global longitudinal strain from 3-chamber images during early diastolic period; GLS_{ac}LV, average of left ventricular global longitudinal strain during atrial systolic period; GLSR, global systolic strain rate; GLSR_{conduit}C4LA, left atrial global longitudinal strain rate during conduit period; HF, heart failure; HCM, hypertrophic cardiomyopathy; HFpEF, heart failure with preserved ejection fraction; HFmrEF, heart failure with mildly reduced ejection fraction; HFrEF, heart failure with reduced ejection fraction; HFimpEF, heart failure with improved ejection fraction; HR, heart rate; HPLS, hyperlipidemia stability; ICM, ischemic cardiomyopathy; INR, international normalized ratio; IQRs, interquartile ranges; IVPD, intraventricular pressure difference; IVPDC2P4, intraventricular pressure differences from 2-chamber images during LV early filling period; IVPG, intraventricular pressure gradient; KNN, k-nearest neighbor classifier; L, lateral side; LA, left atrial; LAD, left atrium diameter; LASSO, Least Absolute Shrinkage and Selection Operator; LV, left ventricular; LVEDd, left ventricular end diastolic diameter; LVEDs, left ventricular end systolic diameter; LVEF, left ventricular ejection fraction; LAVI, left atrial volume index; LVMI, left ventricular mass

index; MACE, major cardiovascular events; MEL, mean energy loss; MI, myocardial infarction; MLP, Multi-Layer Perceptron; NA, not available; NT-pro BNP, N-terminal pro-brain natriuretic peptide; NYHA, New York Heart Association; P, inorganic phosphorus; P1, isovolumic contraction period; P2, ejection period; P3, isovolumetric relaxation period; P4, diastolic filling period; P5, atrial contraction period; PALS, peak atrial longitudinal strain; PALS_{conduit}LA, Peak LA longitudinal peak strain during conduit period; s, systolic; S, septal side; SBP, systolic blood pressure; SGLT-2, sodium-dependent glucose transporters 2; STE, speckle tracking echocardiography; SVM, support vector machine; TRV, tricuspid regurgitant flow velocity; TRPD, tricuspid regurgitation pressure difference; VFM, vector flow mapping; VIF, the variance inflation factor; VorAreaC4S, LV vortex area from 4-chamber images during systolic period; XGBoost, extreme gradient boosting classifier.

Cox regression model has been developed and validated to predict long-term mortality and readmission risk of Chinese patients with chronic heart failure (15). A convenient and accurate prognostic dynamic nomogram model for the risk of all-cause death in acute heart failure patients was developed by Yin T, et al., which included N-terminal pro-brain natriuretic peptide (NT-pro BNP) and growth stimulation expresses gene 2 proteins (16).

However, most of these models are insufficient to reflect the overall situation of the patient. The aim of this study was to develop a predictive model and a predictive nomogram model to estimate the risk of MACE within 6 months of discharge among patients with HF taking into account clinical characteristics, laboratory parameters of blood tests, speckle-tracking echocardiographic analysis, hemodynamic analysis, which can better represent the structure and function of the heart.

Materials and methods

Study cohort and study protocol

This was a single center study. Between July 2021 and February 2022, 505 consecutive patients who were previously diagnosed with chronic heart failure referred to our institution for routine evaluation were screened for eligibility for this study. Criteria and definitions used in the diagnosis of heart failure followed the 2021 heart failure guidelines (17). Inclusion criteria were: (1) consecutive patients who were previously diagnosed with chronic heart failure; (2) pharmacologic therapy followed Guideline Determined Medication Therapy (GDMT) criteria before enrollment in the study. Exclusion criteria were: (1) patients younger than 18 years; (2) history of heart valve replacement, congenital heart disease, severe heart Valve disease, malignant tumors. (3) poor echocardiography windows, or suboptimal cardiac imaging. According to the criteria, 468 patients with HF were finally included (Figure 1). Heart failure patients were classified into the following four categories according to LVEF, including heart failure with preserved ejection fraction (HFpEF), heart failure with mildly reduced ejection fraction (HFmrEF), heart failure with reduced ejection fraction (HFrEF), heart failure with improved ejection fraction (HFimpEF).

All scans were performed by a VFM imaging specialist, and all images were post-processing and analyzed by two professional VFM researchers. Eligible patients were prospectively followed up at 28 days, 3 months, and 6 months after discharge. The study protocol followed the Declaration of Helsinki and was approved by the Research Ethics Committee. All subjects gave written informed consent for additional research tests and for the use of their data for research purposes.

Standard echocardiography

All echocardiographic examinations follow the guidelines of the American Society of Echocardiography and use commercially available ultrasound equipment (LISENDO 880, Hitachi Healthcare America, Twinsburg, Ohio, USA) (18, 19).

Speckle-tracking echocardiography

Left atrial (LA) and LV endocardial boundaries were manually determined using QRS early end-diastolic frames as a reference for image analysis (19). The trace can be adjusted manually if necessary. The LV global longitudinal strain (GLS), the LV global systolic strain rate (GLSR) were calculated by the software from 4-, 3-, and 2-chamber images, and averaged for GLS and GLSR. We defined the following components of LA strain: LA reservoir strain = peak (maximal) longitudinal LA strain; LA pump strain = longitudinal LA strain measured between onset of the P wave and onset of the QRS complex; and LA conduit strain = LA reservoir strain–LA pump strain (20). Peak atrial longitudinal strain (PALS) represented LA reservoir function, and peak atrial contraction strain represented LA pump function, which were measured from the average of the strain curves of all segments at the end of ventricular systole. Strain rate analysis was used to measure the peak LA strain rate during the same time-phase divisions described above. Oana Mirea assess the level of agreement between non-dedicated (left ventricular tracking software) and novel dedicated tracking software for RV and LA strain, and found left atrial mean values showed no statistical difference when obtained with the two tracking tools (21; Figure 2).

Vector flow mapping

Images were analyzed using commercially available off-line software (DASRS1, Hitachi Aloka Medical Ltd., Tokyo, Japan). Using the initial point of the QRS complex as a reference point for image analysis, the LV endocardial border was tracked manually in end-diastolic frames and automatically by the software. Previous studies have limited validation studies (22–26), but the published data may contain useful clinical features. They included: (1) indexes of vortex from the flow-velocity curve, such as vortex area, circulation, maximum vorticity, and the vortex was automatically tracked and analyzed throughout the cardiac cycle (27, 28); (2) energy loss (EL) and mean energy loss (MEL), which were calculated as peak values (23, 24); (3) the intraventricular pressure difference (IVPD) and the intraventricular pressure gradient (IVPG), which were measured on a line that went through the center of the LV from the base to the apex (28, 29). The STE and VFM analysis were post-processed and analyzed by two professional VFM researchers (QL. SUN, Y. LI) (Figure 2).

Patients(n=505) who were Inpatient in the cardiology department from June 1, 2021 to February 28, 2022

Exclusions(n=37)

- 2 Heart valve replacement;
- 7 Congenital heart disease;
- 3 Malignant tumors
- 8 Poor echocardiography windows, or suboptimal cardiac imaging
- 17 Severe Heart Valve Disease

Analytic cohort (n=468)

FIGURE 1

Flowchart demonstrating the process of selection from a total of 504 patients.

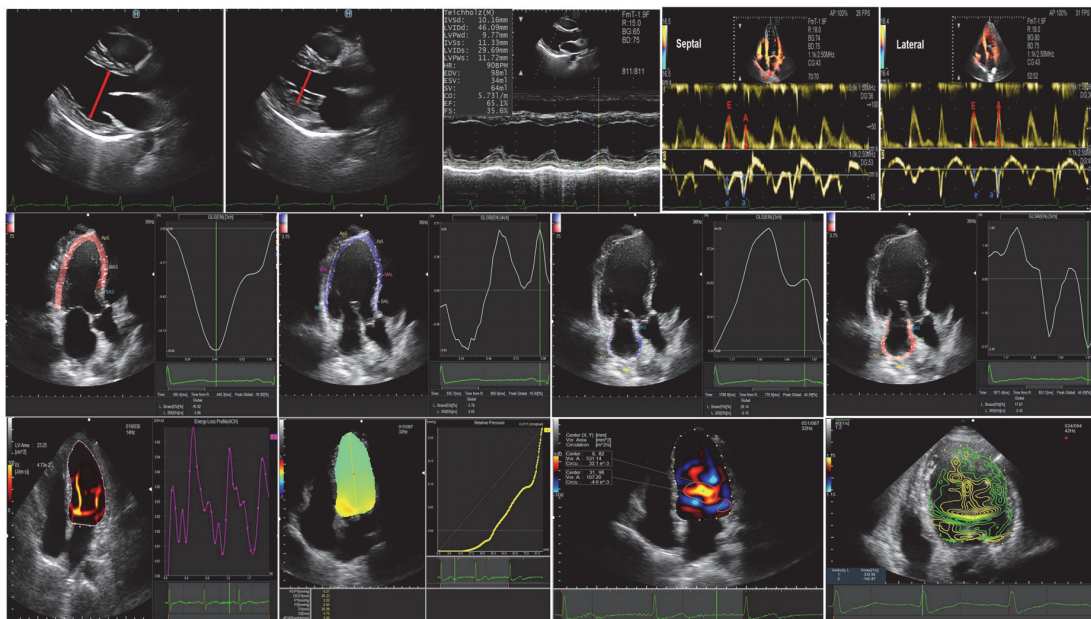


FIGURE 2

Conventional echocardiography, speckle-tracking echocardiography, and vortex flow mapping echocardiography.

Follow-up and clinical outcome data

Follow-up information was obtained during clinical consultations and patients who did not attend scheduled consultations were contacted through telephone interviews with family members. The primary endpoint of the study was the incidence of major adverse cardiac events (MACE). MACE was defined as a complex of congestive HF hospitalization, non-fatal myocardial infarction (MI), non-fatal stroke, and

cardiovascular (CV) death. If there are multiple events, the first event is timed for analysis. Eligible patients were prospectively followed up at 28 days, 3 months, and 6 months after discharge. Clinical and echocardiographic parameters were tested for prediction of MACE in the study population. Clinical data, including clinical symptoms and signs, comorbidities, laboratory test results, treatment during hospitalization, and clinical outcomes were obtained by reviewing each patient's medical records.

Statistical analysis

We used R (R Foundation, Vienna, Austria) and Python (Python Software Foundation, Beaverton, Oregon, USA) for statistical analysis. Continuous variables are expressed as mean \pm SD, frequencies (percentages) for categorical variables and medians (interquartile ranges, IQRs) for skewed variables.

The *t*-test was used to compare the means of continuous variables when the data were normally distributed, else, the Mann-Whitney *U* test was used. One-way analysis of variance (ANOVA) was used for comparisons among multiple groups. Categorical data comparisons between groups were performed using the χ^2 test. The statistical significance level for each test was set at $\alpha = 0.05$; $P < 0.05$ (two-tailed) was considered statistically significant. The Least Absolute Shrinkage and Selection Operator (LASSO) regression algorithm and 10-fold cross-validation were used to filter out the best variables most associated with 6-month MACE incidence. The importance of variables is sorted by machine learning, a logistic regression model is constructed after screening through Venn diagrams, and generates nomograms. We used the Kaplan-Meier method to compare survival between groups. The concordance index (C-index) was used to measure the discriminative abilities of the nomograms [Harrell et al. (30)]. Calibration was performed by examining the survival probability plot predicted by the nomogram.

Results

Study population

A total of 468 patients were included, with an average age of 62 years, including 321 males (47.30%). There were 156 cases of MACE, the incidence rate was 33.3%. Patients are divided into four categories based on LVEF: including HFpEF (147 patients, 31.4%), HFmrEF (95 patients, 20.29%), HFrEF (136 patients, 29.06%), HFimpEF (90 patients, 19.23%). Demographic and baseline criteria are detailed by MACE (Table 1) and by LVEF classification (Table 2). Echocardiographic characteristics of STE parameters and VFM parameters are detailed by MACE (Table 3) and by LVEF classification (Table 4).

Select optimal prognostic variables and model development

Feature selection was performed using the LASSO regression algorithm *via* the R package glmnet and 10-fold cross-validation. This is consistent with the glmnet package recommendation for choosing λ , as either λ min (minimum mean square error) or this value plus one standard error. When lambda equaled 0.035, twenty-six optimal

prognostic variables were identified, including New York Heart Association (NYHA), hyperlipidemia stability (HPLS), ischemic cardiomyopathy (ICM), age, diastolic blood pressure (DBP), left ventricular end diastolic diameter (LVEDd), left ventricular end systolic diameter (LVESd), peak mitral valve blood flow during atrial contraction (A), LV ejection fraction (LVEF), aortic regurgitation (AR), inorganicphosphorus (P), glycatedhemoglobin (GHB), apolipoproteinB (ApoB), sodium ion (Na), N-terminal brain natriuretic peptide (NTproBNP), international normalized ratio (INR), fibrinogen, cardiac index (CI), LV vortex area from 4-chamber images during systolic period (VorAreaC4S), LV energy loss from 3-chamber images during isovolumic relaxation period (ELC3P3), intraventricular pressure differences from 2-chamber images during LV early filling period (IVPDC2P4), LA global longitudinal strain rate during conduit period (GLSRconduitC4LA), LV global longitudinal strain from 3-chamber images during early diastolic period (GLSedC3LV), LV global longitudinal strain from 2-chamber images during atrial systolic period (GLSacC2LV), average of LV global longitudinal strain during atrial systolic period (GLSacLV), peakLA longitudinal peak strain during conduit period (PALSconduitLA) (Figures 3A,B).

Correlation heatmap showing associations between clinical features and ultrasound parameters after lasso dimension reduction analysis (Figure 4A). Here, we used three different popular machine-learning methods including extreme gradient boosting classifier (XGBoost), random forest classifier, k-nearest neighbor classifier (KNN), which were widely applied in bioinformatics in order to calculate the importance of each influencing factor to the classification model and rank it, the top 20 parameters were selected (Figures 4B–D). R (Venn Diagram package) was employed to generate the Venn diagram, then 13 variables were recognized through the Venn diagram (Figure 4E), including NTproBNP, NYHA, GLSLV, LVEDd, LVESd, A, Na, PALSconduitLA, VorAreaC4S, ApoB, IVPDC2P4, GLSacC2LV, DBP. In this study, LVEF with high clinical acceptance was included, and the variance inflation factor (VIF) was calculated by collinearity analysis. LVESd was excluded because of the higher VIF, and A was excluded because of the higher missing. Finally, 12 candidate predictors were selected to build the prediction model, including NYHA, DBP, NTproBNP, Na, ApoB, LVEF, LVEDd, GLSLV, PALSconduitLA, GLSacC2LV, VorAreaC4S, IVPDC2P4, and built a nomogram based on the logistic regression model (Table 5).

Nomogram interpretation and model validation

Nomogram for predicting MACE risk, and the point was the selected scoring standard or scale. For each independent variable, by drawing a line (through the ruler) perpendicular to the point axis, the intersection points represent the values of the

TABLE 1 Baseline characteristics for heart failure (HF) patients during follow-up divided by major cardiovascular events (MACE).

Variables	Overall (<i>n</i> = 468)	No event at follow-up (<i>n</i> = 312)	Event at follow-up (<i>n</i> = 156)	Statistics	<i>P</i> value
Patient characteristics					
Sex, male, <i>n</i> (%)	321 (68.59)	212 (67.95)	109 (69.87)	0.18	0.673
Age (years), median [IQR]	62.00 [53.00, 69.00]	62.00 [53.00, 69.00]	62.00 [53.00, 68.00]	−0.02	0.982
BSA (m ²), median [IQR]	1.79 [1.68, 1.93]	1.79 [1.68, 1.93]	1.78 [1.66, 1.95]	0.28	0.783
DBP (mmHg), median [IQR]	90.00 [80.00, 100.00]	90.00 [80.00, 101.00]	90.00 [80.00, 100.00]	1.85	0.063
SBP (mmHg), median [IQR]	150.00 [120.00, 170.00]	150.00 [126.00, 170.00]	140.00 [120.00, 170.00]	2.65	0.008
Smoke, <i>n</i> (%)	213 (45.51)	136 (43.59)	77 (49.36)	1.4	0.237
Alcohol, <i>n</i> (%)	134 (28.63)	85 (27.24)	49 (31.41)	0.88	0.347
HR (bpm), median [IQR]	79.00 [70.00, 90.00]	78.00 [69.00, 88.00]	81.00 [71.00, 92.00]	−1.88	0.059
NYHA class, <i>n</i> (%)				63.19	< 0.001
I	145 (30.98)	127 (40.71)	18 (11.54)		
II	96 (20.51)	70 (22.44)	26 (16.67)		
III	114 (24.36)	67 (21.47)	47 (30.13)		
IV	113 (24.15)	48 (15.38)	65 (41.67)		
LVEF classification, <i>n</i> (%)				129.42	< 0.001
HFpEF, <i>n</i> (%)	147 (31.41)	127 (40.71)	20 (12.82)		
HFmrEF, <i>n</i> (%)	95 (20.29)	63 (20.19)	32 (20.51)		
HFrEF, <i>n</i> (%)	136 (29.06)	41 (13.14)	95 (60.90)		
HFimpEF, <i>n</i> (%)	90 (19.23)	81 (25.96)	9 (5.77)		
Medical history					
Hypertension, <i>n</i> (%)	332 (70.94)	231 (74.04)	101 (64.74)	4.36	0.037
Hyperlipidemia, <i>n</i> (%)	233 (49.79)	171 (54.81)	62 (39.74)	9.44	0.002
Diabetes mellitus, <i>n</i> (%)	161 (34.40)	114 (36.54)	47 (30.13)	1.89	0.169
HCM, <i>n</i> (%)	16 (3.42)	15 (4.81)	1 (0.64)	5.47	0.019
DCM, <i>n</i> (%)	68 (14.53)	32 (10.26)	36 (23.08)	13.76	< 0.001
Ischemic cardiomyopathy, <i>n</i> (%)	200 (42.74)	123 (39.42)	77 (49.36)	4.2	0.041
Atrial fibrillation, <i>n</i> (%)	105 (22.44)	60 (19.23)	45 (28.85)	5.53	0.019
Medications					
ACEI/ARBS, <i>n</i> (%)	249 (53.21)	167 (53.53)	82 (52.56)	0.04	0.844
ARNI, <i>n</i> (%)	230 (49.15)	154 (49.36)	76 (48.72)	0.02	0.896
β-blockers, <i>n</i> (%)	440 (94.02)	292 (93.59)	148 (94.87)	0.3	0.581
Aldosterone antagonists, <i>n</i> (%)	431 (92.09)	289 (92.63)	142 (91.03)	0.37	0.545
SGLT-2 inhibitors, <i>n</i> (%)	204 (43.59)	128 (41.03)	76 (48.72)	2.5	0.114
diuretics, <i>n</i> (%)	270 (57.69)	148 (47.44)	122 (78.21)	40.34	< 0.001
Antiplatelets, <i>n</i> (%)	305 (65.17)	190 (60.90)	115 (73.72)	7.53	0.006
Anticoagulants, <i>n</i> (%)	268 (57.26)	173 (55.45)	95 (60.90)	1.26	0.261
Statins, <i>n</i> (%)	144 (30.77)	102 (32.69)	42 (26.92)	1.63	0.202
Laboratory examinations					
Glycatedhemoglobin (%), median [IQR]	6.00 [5.60, 7.20]	6.10 [5.50, 7.10]	6.00 [5.60, 7.50]	0.54	0.587
ApolipoproteinA (g/L), median [IQR]	1.15 [1.00, 1.32]	1.18 [1.05, 1.35]	1.07 [0.92, 1.23]	4.39	< 0.001
ApolipoproteinB (g/L), median [IQR]	0.92 [0.72, 1.10]	0.90 [0.72, 1.10]	0.96 [0.73, 1.11]	−0.7	0.483
Inorganicphosphorus (mmol/L), median [IQR]	1.07 [0.93, 1.19]	1.04 [0.90, 1.17]	1.11 [0.98, 1.22]	−3.29	< 0.001
Na (mmol/L), median [IQR]	139.00 [137.00, 141.40]	139.00 [137.00, 141.20]	138.60 [136.00, 141.90]	1.68	0.092
INR, median [IQR]	1.03 [0.97, 1.12]	1.02 [0.96, 1.09]	1.06 [1.00, 1.20]	−4.51	< 0.001
AST (U/L), median [IQR]	22.00 [17.00, 31.00]	21.00 [16.00, 29.00]	25.00 [19.00, 35.00]	−3.48	< 0.001
ALT (U/L), median [IQR]	24.00 [16.00, 35.00]	24.00 [17.00, 35.00]	23.00 [15.00, 36.00]	0.71	0.478
Creatin (umol/L), median [IQR]	84.00 [69.00, 102.00]	82.00 [69.00, 98.00]	87.00 [72.00, 116.00]	−2.58	0.01

(Continued)

TABLE 1 (Continued)

Variables	Overall (<i>n</i> = 468)	No event at follow-up (<i>n</i> = 312)	Event at follow-up (<i>n</i> = 156)	Statistics	<i>P</i> value
Urea/Crea, median [IQR]	83.96 [71.56, 100.66]	83.14 [70.79, 100.66]	86.91 [73.03, 100.61]	−0.73	0.468
Plasma D-dimer (ng/mL), median [IQR]	125.00 [67.00, 263.00]	119.00 [61.00, 235.00]	155.00 [84.00, 323.00]	−3.08	0.002
Fibrinogenr (g/L), median [IQR]	3.01 [2.59, 3.49]	2.98 [2.59, 3.41]	3.11 [2.62, 3.63]	−1.67	0.095
SerumcalciumproteinI (ug/L), median [IQR]	0.11 [0.08, 0.14]	0.11 [0.08, 0.14]	0.11 [0.08, 0.13]	−0.33	0.74
NTproBNP (pg/mL), median [IQR]	971.00 [303.0, 2383.00]	626.00 [223.0, 1565.00]	2372.00 [902.0, 6245.0]	−8.77	<0.001
General echocardiographic data					
LVEDd (mm), median [IQR]	44.40 [31.30, 53.30]	39.70 [29.10, 50.00]	51.20 [42.10, 59.20]	−7.59	<0.001
LVEDd (mm), median [IQR]	55.80 [48.30, 64.20]	53.10 [47.30, 60.80]	61.80 [54.40, 69.40]	−7.05	<0.001
LAD (mm), median [IQR]	40.50 [37.00, 44.30]	39.80 [36.30, 42.80]	42.70 [39.00, 46.60]	−5.18	<0.001
LAVI (ml/m ²), median [IQR]	35.68 [27.89, 47.82]	33.36 [26.22, 44.71]	40.42 [33.39, 51.36]	−4.62	<0.001
LVMI (g/m ²), median [IQR]	134.25 [107.54, 164.68]	129.41 [99.62, 159.00]	142.01 [122.18, 174.90]	−4.45	<0.001
E (m/s), median [IQR]	0.80 [0.62, 1.01]	0.78 [0.60, 1.00]	0.88 [0.67, 1.11]	−3.09	0.002
A (m/s), median [IQR]	0.78 [0.33, 0.98]	0.81 [0.51, 1.00]	0.55 [0.00, 0.90]	3.83	<0.001
E/A, mean (± SD)	1.13 ± 0.81	1.00 ± 0.63	1.42 ± 1.05	−3.89	<0.001
e'-S (m/s), median [IQR]	4.90 [3.70, 6.20]	5.10 [4.00, 6.40]	4.30 [3.20, 5.70]	4.42	<0.001
a'-S (m/s), mean (± SD)	7.48 ± 2.54	7.90 ± 2.42	6.53 ± 2.56	4.92	<0.001
e'-L (m/s), median [IQR]	6.80 [4.90, 9.20]	7.30 [5.20, 9.40]	6.20 [4.20, 8.60]	3.39	<0.001
a'-L (m/s), mean (± SD)	9.53 ± 3.29	9.88 ± 3.08	8.73 ± 3.58	2.96	0.003
e'/a'-S, mean (± SD)	0.70 ± 0.29	0.69 ± 0.28	0.73 ± 0.32	−1.31	0.191
e'/a'-L, mean (± SD)	0.80 ± 0.44	0.79 ± 0.42	0.84 ± 0.50	−1.02	0.31
TRV (m/s), mean (± SD)	2.90 ± 0.60	2.85 ± 0.59	2.96 ± 0.61	−1.41	0.159
TRPD (mmHg), mean (± SD)	34.96 ± 14.64	33.73 ± 14.50	36.43 ± 14.66	−1.34	0.181
tei-RV, median [IQR]	0.37 [0.29, 0.45]	0.35 [0.27, 0.44]	0.40 [0.33, 0.47]	−4.25	<0.001
tei-LV, median [IQR]	0.38 [0.31, 0.44]	0.36 [0.29, 0.43]	0.41 [0.37, 0.47]	−5.96	<0.001
E/e'-RVav, median [IQR]	6.84 [5.39, 8.40]	6.55 [5.16, 8.09]	7.38 [5.85, 9.22]	−4.28	<0.001
E/e'-LVav, median [IQR]	14.16 [10.50, 18.29]	13.16 [9.66, 16.49]	16.13 [13.20, 21.76]	−6.29	<0.001
LVEF, median [IQR]	41.80 [32.40, 61.00]	50.20 [36.00, 62.00]	34.70 [27.50, 43.70]	8.34	<0.001

p < 0.05 indicates statistical significance. BSA, body surface area; DBP, diastolic blood pressure; SBP, systolic blood pressure; HR, heart rate; NYHA, New York Heart Association; DCM, Dilated cardiomyopathy; HCM, hypertrophic cardiomyopathy; ACEI, Angiotensin-converting enzyme inhibitors; ARBS, angiotensin receptor blockers; SGLT-2, sodium-dependent glucose transporters 2; INR, international normalized ratio; ALT, alanine transaminase; AST, aspartate transaminase; LVEDd, left ventricular end diastolic diameter; LVESd, left ventricular end systolic diameter; LAD, left atrium diameter; LAVI, left atrial volume index; LVMI, left ventricular mass index; A, late diastolic transmitral flow velocity; E, early diastolic transmitral flow velocity; e', early diastolic relaxation velocity at septal mitral annular position; L, lateral side; S, septal side; TRV, tricuspid regurgitant flow velocity; TRPD, tricuspid regurgitation pressure difference; LVEF, left ventricular ejection fraction; NA, not available.

independent variables. The value of each variable is scored on a scale of 0 to 100, and the scores for each variable are summed to estimate the position perpendicular to the axis. That sum enables us to predict the probability of MACE risk in patient with HF (Figure 5A). Estimated odds ratios determined in a logistic regression model as shown in the forest plot (Figure 5B). Receiver operating characteristic curve for the nomogram generated using bootstrap resampling, which showed a good discriminative ability for the prediction model (C-statistics: 0.876 [95% CI, 0.844–0.907]) (Figure 5C). The Nomogram calibration plots of the model based on the bootstrap method showed good performance (Figure 5D). When the solid line (performance nomogram) was closer to the dotted line (ideal model), the prediction accuracy of the nomogram was better. Decision curve analysis for predictive models (Figure 5E). Solid red line is predictive models, solid blue line is patients with

MACE, and solid horizontal line is patients without MACE. The graph shows the expected net benefit per patient in relation to the nomogram MACE risk prediction. Decision curve analysis indicated that the clinical validity of the model was moderate.

Survival curves based on nomogram scores and predictive risk

Patients were divided into four groups according to the quartile total nomogram scores (nomgroup = 0, 1, 2, 3), and each group had 117 patients. A prediction model with a prediction probability of less than 0.5 is considered a low risk group, and patients were divided into high-risk and low-risk groups (low-risk group = 1, high-risk group = 2). Of these, 342 patients (73.08%) belonged to the low-risk group.

TABLE 2 Baseline characteristics for heart failure (HF) patients divided by left ventricular end fraction (LVEF) classification.

Variables	Overall (n = 468)	HFpEF (n = 147)	HFmrEF (n = 95)	HFrEF (n = 136)	HFimpEF (n = 90)	Statistics	P value
Patient characteristics							
Sex, male, n (%)	321 (68.59)	96 (65.31)	57 (60.00)	102 (75.00)	66 (73.33)	7.52	0.057
Age (years), median [IQR]	62.00 [53.00, 69.00]	61.00 [53.00, 68.00]	64.00 [55.00, 71.00]	63.00 [53.00, 69.00]	58.00 [52.00, 67.00]	5.59	0.133
BSA (m ²), median [IQR]	1.79 [1.68, 1.93]	1.80 [1.68, 1.95]	1.79 [1.69, 1.92]	1.78 [1.66, 1.92]	1.80 [1.66, 1.93]	0.94	0.816
DBP (mmHg), median [IQR]	90.00 [80.00, 100.00]	98.00 [90.00, 110.00]	88.00 [78.00, 100.00]	85.00 [75.00, 93.00]	90.00 [80.00, 100.00]	34.84	< 0.001
SBP (mmHg), median [IQR]	150.00 [120.00, 170.00]	160.00 [140.00, 180.00]	146.00 [121.00, 166.00]	130.00 [115.00, 150.00]	150.00 [120.00, 170.00]	54.36	< 0.001
Smoke, n (%)	213 (45.51)	63 (42.86)	46 (48.42)	65 (47.79)	39 (43.33)	1.2	0.753
Alcohol, n (%)	134 (28.63)	36 (24.49)	25 (26.32)	49 (36.03)	24 (26.67)	5.30	0.151
HR (bpm), median [IQR]	79.00 [70.00, 90.00]	77.00 [67.00, 85.00]	77.00 [70.00, 86.00]	85.00 [75.00, 96.00]	78.00 [69.00, 89.00]	26.40	< 0.001
NYHA class, n (%)						NA	NA
I	145 (30.98)	109 (74.15)	10 (10.52)	0 (0.00)	26 (28.89)		
II	96 (20.51)	25 (17.01)	51 (53.68)	10 (7.35)	10 (11.11)		
III	114 (24.36)	12 (8.16)	22 (23.15)	49 (36.03)	31 (34.44)		
IV	113 (24.15)	1 (0.68)	12 (12.63)	77 (56.62)	23 (25.56)		
Medical history							
Hypertension, n (%)	332 (70.94)	125 (85.03)	67 (70.53)	77 (56.62)	63 (70.00)	27.74	< 0.001
Hyperlipidemia, n (%)	233 (49.79)	95 (64.63)	47 (49.47)	47 (34.56)	44 (48.89)	25.60	< 0.001
Diabetes mellitus, n (%)	161 (34.40)	52 (35.37)	37 (38.95)	36 (26.47)	36 (40.00)	5.97	0.113
HCM, n (%)	16 (3.42)	16 (10.88)	0 (0.00)	0 (0.00)	0 (0.00)	NA	NA
DCM, n (%)	68 (14.53)	0 (0.00)	5 (5.26)	51 (37.50)	12 (13.33)	NA	NA
Ischemic cardiomyopathy, n (%)	200 (42.74)	25 (17.01)	60 (63.16)	63 (46.32)	52 (57.78)	64.99	< 0.001
Atrial fibrillation, n (%)	105 (22.44)	23 (15.65)	14 (14.74)	48 (35.29)	20 (22.22)	20.05	< 0.001
Medications							
ACEI/ARBs, n (%)	249 (53.21)	127 (86.40)	36 (37.90)	52 (38.24)	34 (37.78)	94.83	< 0.001
ARNI, n (%)	230 (49.15)	26 (17.69)	61 (64.21)	81 (59.56)	62 (68.89)	86.77	< 0.001
β-blockers, n (%)	440 (94.02)	130 (88.44)	92 (96.84)	133 (97.79)	85 (94.44)	12.97	0.005
Aldosterone antagonists, n (%)	431 (92.09)	136 (92.51)	85 (89.47)	126 (92.64)	84 (93.33)	1.18	0.76
SGLT-2 inhibitors, n (%)	204 (43.59)	47 (31.97)	36 (37.90)	78 (57.35)	43 (47.78)	20.44	< 0.001
diuretics, n (%)	270 (57.69)	30 (20.41)	72 (75.79)	116 (85.29)	52 (57.78)	138.92	< 0.001
Antiplatelets, n (%)	305 (65.17)	77 (52.38)	72 (75.79)	92 (67.65)	64 (71.11)	17.08	< 0.001
Anticoagulants, n (%)	268 (57.27)	72 (48.98)	59 (62.11)	85 (62.50)	52 (57.78)	6.57	0.087
Statins, n (%)	144 (30.77)	59 (40.14)	29 (30.53)	30 (22.06)	26 (28.89)	11.05	0.011
Laboratory examinations							
Glycatedhemoglobin (%), median [IQR]	6.00 [5.60, 7.20]	6.00 [5.50, 6.80]	6.10 [5.60, 8.00]	5.90 [5.60, 7.00]	6.00 [5.80, 7.80]	12.61	0.006
ApolipoproteinA (g/L), median [IQR]	1.15 [1.00, 1.32]	1.20 [1.09, 1.38]	1.12 [0.99, 1.35]	1.07 [0.92, 1.21]	1.17 [1.03, 1.31]	27.39	< 0.001
ApolipoproteinB (g/L), median [IQR]	0.92 [0.72, 1.10]	0.94 [0.72, 1.15]	0.90 [0.71, 1.12]	0.93 [0.73, 1.09]	0.87 [0.69, 1.02]	4.71	0.195
Inorganicphosphorus (mmol/L), median [IQR]	1.07 [0.93, 1.19]	1.02 [0.89, 1.15]	1.08 [0.98, 1.18]	1.13 [0.98, 1.22]	1.04 [0.89, 1.19]	16.50	< 0.001
Na (mmol/L), median [IQR]	139.00 [137.00, 141.40]	139.00 [137.00, 142.00]	138.60 [137.00, 141.40]	138.50 [136.30, 141.40]	139.00 [137.30, 141.00]	4.23	0.238
INR, median [IQR]	1.03 [0.97, 1.12]	1.00 [0.96, 1.06]	1.02 [0.97, 1.09]	1.09 [1.02, 1.22]	1.02 [0.96, 1.08]	46.31	< 0.001
AST (U/L), median [IQR]	22.00 [17.00, 31.00]	19.00 [16.00, 26.00]	23.00 [16.00, 34.00]	27.00 [20.00, 36.00]	21.00 [17.00, 29.00]	26.04	< 0.001
ALT (U/L), median [IQR]	24.00 [16.00, 35.00]	21.00 [15.00, 30.00]	26.00 [17.00, 38.00]	24.00 [15.00, 35.00]	25.00 [19.00, 37.00]	6.14	0.11
Creatin (umol/L), median [IQR]	84.00 [69.00, 102.00]	79.00 [66.00, 93.00]	84.00 [68.00, 105.00]	91.00 [75.00, 116.00]	81.00 [71.00, 95.00]	17.69	< 0.001

(Continued)

TABLE 2 (Continued)

Variables	Overall (<i>n</i> = 468)	HFpEF (<i>n</i> = 147)	HFmrEF (<i>n</i> = 95)	HFrEF (<i>n</i> = 136)	HFimpEF (<i>n</i> = 90)	Statistics	<i>P</i> value
Urea/Crea, median [IQR]	83.96 [71.56, 100.66]	83.26 [71.45, 105.80]	85.19 [72.39, 99.56]	84.17 [73.03, 99.12]	83.13 [69.46, 102.71]	0.6	0.89
Plasma D-dimer (ng/mL), median [IQR]	125.00 [67.00, 263.00]	87.00 [56.00, 158.00]	142.00 [82.00, 263.00]	186.00 [93.00, 344.00]	110.00 [58.00, 242.00]	33.00	< 0.001
Fibrinogenr (g/L), median [IQR]	3.01 [2.59, 3.49]	2.99 [2.59, 3.38]	3.03 [2.57, 3.58]	3.02 [2.50, 3.63]	2.99 [2.67, 3.49]	0.49	0.92
SerumcalciumproteinI (ug/L), median [IQR]	0.11 [0.08, 0.14]	0.11 [0.08, 0.14]	0.10 [0.08, 0.14]	0.11 [0.08, 0.14]	0.10 [0.07, 0.14]	3.36	0.339
NTproBNP (pg/mL), median [IQR]	971.00 [303.00, 2383.00]	283.00 [52.00, 799.00]	833.00 [452.00, 1980.00]	2959.00 [1551.00, 7144.00]	1030.00 [304.00, 1788.00]	180.37	< 0.001
General echocardiographic data							
LVEsd (mm), median [IQR]	44.40 [31.30, 53.30]	28.60 [24.70, 32.30]	43.10 [40.00, 46.30]	56.20 [51.90, 61.10]	47.90 [33.70, 55.00]	303.31	< 0.001
LVEDd (mm), median [IQR]	55.80 [48.30, 64.20]	47.30 [44.20, 49.70]	55.80 [52.800, 6.10]	65.80 [60.60, 71.70]	58.70 [50.50, 65.20]	245.00	< 0.001
LAD (mm), median [IQR]	40.50 [37.00, 44.30]	37.70 [35.00, 41.30]	40.00 [37.30, 42.00]	44.20 [40.30, 48.70]	41.00 [36.50, 44.00]	75.81	< 0.001
LAVI (g/m ²), median [IQR]	35.69 [27.89, 47.82]	30.65 [25.11, 41.12]	34.20 [26.88, 44.32]	42.07 [34.80, 56.68]	35.15 [27.32, 49.87]	50.32	< 0.001
LVMI (g/m ²), median [IQR]	134.25 [107.54, 164.68]	108.33 [92.91, 136.72]	127.38 [108.26, 153.64]	158.73 [134.46, 187.16]	138.60 [118.58, 166.09]	96.57	< 0.001
E (m/s), median [IQR]	0.80 [0.62, 1.01]	0.75 [0.60, 0.90]	0.70 [0.60, 0.83]	1.00 [0.80, 1.24]	0.80 [0.61, 1.00]	48.36	< 0.001
A (m/s), median [IQR]	0.78 [0.33, 0.98]	0.84 [0.64, 1.00]	0.84 [0.62, 1.00]	0.42 [0.00, 0.80]	0.78 [0.30, 1.00]	47.41	< 0.001
E/A ratio, mean (± SD)	0.79 [0.64, 1.32]	0.77 [0.64, 0.90]	0.75 [0.60, 0.90]	1.44 [0.73, 2.52]	0.80 [0.65, 1.29]	25.67	< 0.001
e'-S (m/s), median [IQR]	4.90 [3.70, 6.20]	5.60 [4.50, 6.70]	4.50 [3.60, 5.90]	4.50 [3.10, 5.50]	4.80 [3.50, 6.00]	40.54	< 0.001
a'-S (m/s), mean (± SD)	7.50 [5.70, 9.10]	8.7 [7.40, 10.20]	7.00 [5.90, 8.50]	5.50 [4.10, 7.60]	7.40 [5.30, 9.00]	70.43	< 0.001
e'-L (m/s), median [IQR]	6.80 [4.90, 9.20]	8.7 [6.10, 10.30]	6.20 [4.30, 8.40]	6.30 [4.50, 8.70]	6.50 [4.60, 8.80]	35.78	< 0.001
a'-L (m/s), mean (± SD)	9.4 [7.50, 11.60]	10.2 [9.00, 12.10]	9.0 [7.60, 11.40]	8.0 [5.50, 11.10]	8.7 [7.20, 11.10]	28.40	< 0.001
e'/a'-S, mean (± SD)	0.66 [0.52, 0.81]	0.62 [0.52, 0.73]	0.65 [0.46, 0.83]	0.71 [0.59, 0.88]	0.66 [0.46, 0.83]	11.60	0.009
e'/a'-L, mean (± SD)	0.73 [0.52, 0.90]	0.76 [0.59, 0.93]	0.65 [0.47, 0.85]	0.77 [0.54, 0.95]	0.66 [0.49, 0.86]	9.49	0.023
TRV (m/s), mean (± SD)	2.80 [2.40, 3.22]	2.82 [2.42, 3.10]	2.70 [2.400, 2.90]	2.81 [2.52, 3.31]	2.85 [2.40, 3.40]	2.96	0.397
TRP (mmHg), mean (± SD)	31.00 [24.00, 42.00]	31.00 [24.00, 38.00]	29.00 [23.00, 33.00]	32.00 [25.00, 44.00]	32.00 [24.00, 46.00]	4.02	0.26
tei-RV, median [IQR]	0.37 [0.29, 0.45]	0.30 [0.25, 0.38]	0.37 [0.31, 0.43]	0.42 [0.37, 0.49]	0.38 [0.29, 0.44]	77.33	< 0.001
tei-LV, median [IQR]	0.38 [0.31, 0.44]	0.31 [0.26, 0.38]	0.38 [0.34, 0.43]	0.44 [0.39, 0.50]	0.37 [0.32, 0.47]	114.76	< 0.001
E/e'-RVav, median [IQR]	6.84 [5.39, 8.40]	6.19 [5.12, 7.57]	6.71 [5.16, 7.73]	7.43 [5.82, 9.45]	6.98 [5.59, 8.37]	21.51	< 0.001
E/e'-LVav, median [IQR]	14.16 [10.51, 18.29]	10.08 [8.30, 13.62]	14.82 [12.25, 17.09]	17.61 [13.46, 23.88]	15.31 [11.57, 20.62]	113.05	< 0.001
LVEF, median [IQR]	41.80 [32.40, 61.00]	62.00 [61.00, 64.00]	43.40 [41.30, 46.60]	29.30 [26.60, 33.50]	35.50 [30.80, 57.90]	350.79	< 0.001

p < 0.05 indicates statistical significance. BSA, body surface area; DBP, diastolic blood pressure; SBP, systolic blood pressure; HR, heart rate; NYHA, New York Heart Association; DCM, Dilated cardiomyopathy; HCM, hypertrophic cardiomyopathy; ACEI, angiotensin-converting enzyme inhibitors; ARBS, angiotensin receptor blockers; SGLT-2, sodium-dependent glucose transporters 2; INR, international normalized ratio; ALT, alanine transaminase; AST, aspartate transaminase; LVEDd, left ventricular end diastolic diameter; LVESd, left ventricular end systolic diameter; LAD, left atrium diameter; LAVI, left atrial volume index; LVMI, left ventricular mass index; A, late diastolic transmitral flow velocity; E, early diastolic transmitral flow velocity; e', early diastolic relaxation velocity at septal mitral annular position; L, lateral side; S, septal side; TRV, tricuspid regurgitant flow velocity; TRPD, tricuspid regurgitation pressure difference; LVEF, left ventricular ejection fraction; NA, not available.

The KM survival curves and cumulative survival curves were used to compare survival times among different groups was made by log-rank test. The median survival time (LT50) for different groups. The horizontal axis of the KM survival curve represents time, and the vertical axis represents probability (Figure 6).

Performance of machine learning algorithms among the groups

We divided patients into training and validation sets using MACE as the categorical outcome variable. Parameters include general parameters, STE-related parameters and VFM-related

TABLE 3 Echocardiographic characteristics of speckle tracking echocardiography (STE) parameters and vector flow mapping (VFM) parameters divided by major cardiovascular events (MACE).

Variables	Overall (<i>n</i> = 468)	No event at follow-up (<i>n</i> = 312)	Event at follow-up (<i>n</i> = 156)	Statistics	<i>P</i> value
STE parameters					
GLS-LV (%), median [IQR]	−10.81 [−14.90, −8.22]	−12.04 [−16.30, −9.47]	−8.64 [−11.28, −6.47]	−8.05	< 0.001
GLSR-sLV (s ^{−1}), median [IQR]	−0.60 [−0.76, −0.46]	−0.64 [−0.83, −0.49]	−0.50 [−0.62, −0.36]	−6.76	< 0.001
GLSR-edLV (s ^{−1}), median [IQR]	0.56 [0.40, 0.76]	0.61 [0.44, 0.81]	0.49 [0.35, 0.64]	4.54	< 0.001
GLSR-aclV (s ^{−1}), median [IQR]	0.49 [0.32, 0.68]	0.51 [0.38, 0.71]	0.42 [0.27, 0.58]	4.13	< 0.001
PALS-reservoir LA (%), median [IQR]	21.14 [12.96, 30.29]	24.08 [15.69, 32.48]	17.11 [10.36, 23.34]	6.16	< 0.001
PALS-conduit LA (%), median [IQR]	9.53 [6.58, 13.45]	10.66 [7.47, 14.37]	7.60 [5.50, 10.30]	6.5	< 0.001
PALS-pump LA (%), median [IQR]	11.42 [4.98, 17.06]	13.39 [5.89, 18.02]	8.81 [4.00, 14.04]	4.65	< 0.001
GLSR-reservoir LA (s ^{−1}), median [IQR]	0.95 [0.66, 1.37]	1.09 [0.73, 1.46]	0.83 [0.62, 1.08]	5.44	< 0.001
GLSR-conduit LA (s ^{−1}), median [IQR]	−0.93 [−1.30, −0.69]	−0.99 [−1.38, −0.73]	−0.81 [−1.06, −0.63]	−4.6	< 0.001
GLSR-pump LA (s ^{−1}), median [IQR]	−1.21 [−1.83, −0.68]	−1.33 [−1.96, −0.78]	−0.99 [−1.61, −0.58]	−4.01	< 0.001
VFM parameters					
MeanELP1 [J/(m ³ s)], median [IQR]	3.05 [1.84, 4.89]	3.16 [2.01, 4.94]	2.90 [1.40, 4.84]	1.91	0.057
MeanELP2 [J/(m ³ s)], median [IQR]	2.35 [1.47, 3.63]	2.49 [1.59, 3.78]	1.97 [1.20, 3.29]	3.22	0.001
MeanELP3 [J/(m ³ s)], median [IQR]	2.46 [1.42, 4.08]	2.54 [1.40, 4.31]	2.41 [1.44, 3.90]	0.86	0.391
MeanELP4 [J/(m ³ s)], median [IQR]	4.36 [2.54, 7.49]	4.45 [2.61, 7.61]	4.18 [2.40, 7.17]	1.48	0.138
MeanELP5 [J/(m ³ s)], median [IQR]	4.40 [2.56, 7.50]	4.79 [2.79, 7.92]	4.04 [2.04, 6.61]	2.69	0.007
EnergyLossP1 [J/(m s e ³)], median [IQR]	20.44 [13.13, 33.81]	20.31 [13.13, 32.68]	20.54 [13.19, 37.08]	0.16	0.872
EnergyLossP2 [J/(m s e ³)], median [IQR]	14.75 [10.38, 23.13]	14.99 [10.38, 23.80]	14.37 [10.69, 22.32]	1.06	0.289
EnergyLossP3 [J/(m s e ³)], median [IQR]	14.69 [8.76, 24.14]	14.15 [7.67, 23.70]	16.15 [9.87, 25.07]	−1.82	0.068
EnergyLossP4 [J/(m s e ³)], median [IQR]	27.11 [16.70, 46.62]	26.46 [16.03, 45.89]	28.40 [18.08, 48.99]	−0.66	0.509
EnergyLossP5 [J/(m s e ³)], median [IQR]	30.26 [18.18, 50.42]	30.98 [19.60, 52.08]	30.01 [16.48, 46.00]	1.01	0.315
IVPDP1 (mmHg), median [IQR]	0.78 [0.47, 1.22]	0.86 [0.52, 1.26]	0.67 [0.40, 1.00]	3.72	< 0.001
IVPDP2 (mmHg), median [IQR]	1.02 [0.71, 1.41]	1.07 [0.71, 1.45]	0.91 [0.71, 1.29]	2.09	0.036
IVPDP3 (mmHg), median [IQR]	−0.36 [−0.60, −0.25]	−0.38 [−0.63, −0.28]	−0.32 [−0.52, −0.20]	−3.28	0.001
IVPDP4 (mmHg), median [IQR]	−0.97 [−1.39, −0.65]	−1.03 [−1.42, −0.70]	−0.86 [−1.17, −0.56]	−3.23	0.001
IVPDP5 (mmHg), median [IQR]	0.52 [0.29, 0.89]	0.53 [0.27, 0.91]	0.51 [0.30, 0.78]	0.46	0.649
IVPGP1 (mmHg/mme ³), median [IQR]	−8.96 [−15.22, −5.53]	−9.91 [−15.97, −6.02]	−7.74 [−12.11, −4.37]	−4.07	< 0.001
IVPGP2 (mmHg/mme ³), median [IQR]	−12.12 [−16.90, −8.30]	−12.84 [−17.95, −8.57]	−10.42 [−15.23, −8.15]	−2.59	0.01
IVPGP3 (mmHg/mme ³), median [IQR]	4.45 [3.00, 7.30]	4.89 [3.37, 7.69]	3.76 [2.47, 6.32]	3.89	< 0.001
IVPGP4 (mmHg/mme ³), median [IQR]	11.98 [7.98, 17.47]	13.25 [8.80, 18.25]	10.15 [6.57, 14.56]	3.97	< 0.001
IVPGP5 (mmHg/mme ³), median [IQR]	−6.46 [−10.95, −3.31]	−6.62 [−11.55, −3.34]	−6.06 [−9.53, −3.30]	−1.02	0.309
VorArea-s (mm ²), median [IQR]	454.22 [354.72, 574.46]	456.49 [344.67, 568.96]	452.18 [367.50, 577.34]	−0.14	0.888
Circulation-s (m ² /s e ³), median [IQR]	16.90 [11.77, 22.03]	17.42 [12.43, 22.27]	16.10 [10.37, 21.37]	1.95	0.051
VorArea-ed (mm ²), median [IQR]	359.00 [257.14, 476.48]	356.72 [248.46, 468.67]	362.95 [291.99, 493.80]	−1.96	0.05
Circulation-ed (m ² /s e ³), median [IQR]	13.13 [7.57, 21.80]	13.03 [7.40, 21.90]	13.90 [7.60, 21.77]	−0.35	0.727
VorArea-ac (mm ²), median [IQR]	428.02 [323.87, 531.24]	425.12 [324.89, 523.87]	441.81 [319.24, 552.93]	−0.41	0.682
Circulation-ac (m ² /s e ³), median [IQR]	18.03 [12.10, 25.53]	18.97 [12.77, 26.57]	15.77 [10.93, 23.57]	2.73	0.006
vorticity-ac-CCW (1/s), median [IQR]	−105.8 [−142.94, −80.24]	−107.2 [−144.99, −84.58]	−103.6 [−140.37, −75.86]	−1.2	0.231
vorticity-ac-CW (1/s), median [IQR]	114.97 [85.83, 149.68]	119.39 [89.86, 153.89]	108.21 [78.40, 145.27]	2	0.045
vorticity-ed-CCW (1/s), median [IQR]	−99.07 [−135.19, −76.44]	−97.37 [−134.90, −74.64]	−101.4 [−136.47, −80.00]	0.58	0.564
vorticity-ed-CW (1/s), median [IQR]	101.54 [72.03, 140.46]	99.37 [71.15, 140.68]	107.40 [76.73, 139.43]	−1.05	0.292
vorticity-s-CCW (1/s), median [IQR]	−100.7 [−130.23, −75.93]	−102.9 [−132.92, −78.65]	−97.6 [−124.15, −68.81]	−1.97	0.049
vorticity-s-CW (1/s), median [IQR]	110.59 [82.79, 149.78]	115.23 [86.19, 152.53]	103.63 [74.75, 144.74]	2.31	0.021

p < 0.05 indicates statistical significance. STE, speckle tracking echocardiography; GLS, global longitudinal strain; GLSR, global systolic strain rate; PALS, peak atrial longitudinal strain; VFM, vector flow mapping; MeanEL, mean energy loss; IVPD, intraventricular pressure difference; IVPG, intraventricular pressure gradient; s, systolic; ed, early diastolic; ac, atrium contraction; P1-P5, isovolumic contraction period, ejection period, isovolumetric relaxation period, diastolic filling period, atrium contraction period; CW, clockwise; CCW, counter-clockwise.

TABLE 4 Echocardiographic characteristics of speckle tracking echocardiography (STE) parameters and vector flow mapping (VFM) parameters divided by left ventricular end fraction (LVEF) classification.

Variables	Overall (<i>n</i> = 468)	HFpEF (<i>n</i> = 147)	HFmrEF (<i>n</i> = 95)	HFrEF (<i>n</i> = 136)	HFimpEF (<i>n</i> = 90)	Statistics	<i>P</i> value
STE parameters							
GLS-LV (%), median [IQR]	−10.81 [−14.90, −8.22]	−16.25 [−18.74, −13.16]	−11.06 [−12.81, −9.30]	−7.29 [−9.11, −5.99]	−10.07 [−12.64, −8.05]	246.93	< 0.001
GLSR-sLV (s ^{−1}), median [IQR]	−0.60 [−0.76, −0.46]	−0.83 [−0.96, −0.66]	−0.60 [−0.68, −0.49]	−0.43 [−0.53, −0.35]	−0.55 [−0.70, −0.46]	189.24	< 0.001
GLSR-edLV (s ^{−1}), median [IQR]	0.56 [0.40, 0.76]	0.76 [0.54, 0.98]	0.55 [0.41, 0.70]	0.46 [0.32, 0.59]	0.49 [0.38, 0.66]	99.02	< 0.001
GLSR-acLV (s ^{−1}), median [IQR]	0.49 [0.32, 0.68]	0.56 [0.44, 0.76]	0.57 [0.46, 0.72]	0.34 [0.25, 0.49]	0.45 [0.33, 0.61]	77.00	< 0.001
PALS-reservoir LA (%), median [IQR]	21.14 [12.96, 30.29]	30.86 [21.19, 37.80]	23.32 [18.88, 29.11]	12.70 [9.11, 19.07]	18.72 [11.47, 26.94]	151.51	< 0.001
PALS-conduit LA (%), median [IQR]	9.53 [6.58, 13.45]	13.78 [10.92, 18.03]	9.53 [7.25, 12.35]	6.87 [5.01, 9.56]	8.49 [6.48, 10.66]	137.72	< 0.001
PALS-pump LA (%), median [IQR]	11.42 [4.98, 17.06]	16.64 [11.14, 21.79]	13.17 [9.05, 17.06]	5.07 [3.49, 10.55]	9.72 [4.52, 15.41]	103.30	< 0.001
GLSR-reservoir LA (s ^{−1}), median [IQR]	0.95 [0.66, 1.37]	1.42 [0.96, 1.83]	1.08 [0.82, 1.35]	0.69 [0.55, 0.91]	0.89 [0.62, 1.25]	133.14	< 0.001
GLSR-conduit LA (s ^{−1}), median [IQR]	−0.93 [−1.30, −0.69]	−1.24 [−1.66, −0.88]	−0.95 [−1.24, −0.73]	−0.72 [−0.96, −0.58]	−0.83 [−1.13, −0.65]	77.08	< 0.001
GLSR-pump LA (s ^{−1}), median [IQR]	−1.21 [−1.83, −0.68]	−1.60 [−2.28, −1.14]	−1.36 [−1.89, −1.04]	−0.68 [−1.28, −0.48]	−1.00 [−1.61, −0.60]	89.56	< 0.001
VFM parameters							
MeanELP1 [J/(m ³ s)], median [IQR]	3.05 [1.84, 4.89]	3.56 [2.27, 5.68]	3.10 [2.09, 4.24]	2.51 [1.30, 4.30]	2.88 [1.73, 5.22]	18.06	< 0.001
MeanELP2 [J/(m ³ s)], median [IQR]	2.35 [1.47, 3.63]	3.16 [2.14, 4.78]	2.10 [1.52, 2.99]	1.66 [1.08, 3.15]	2.09 [1.32, 3.54]	55.33	< 0.001
MeanELP3 [J/(m ³ s)], median [IQR]	2.46 [1.42, 4.08]	3.16 [1.99, 5.2]	2.13 [1.33, 3.37]	2.29 [1.30, 3.47]	2.15 [1.28, 4.08]	26.55	< 0.001
MeanELP4 [J/(m ³ s)], median [IQR]	4.36 [2.54, 7.49]	4.90 [3.20, 8.04]	4.19 [2.32, 7.10]	3.95 [2.16, 7.28]	4.18 [2.39, 7.47]	10.93	0.012
MeanELP5 [J/(m ³ s)], median [IQR]	4.41 [2.56, 7.50]	5.78 [3.42, 9.42]	4.27 [2.82, 7.01]	3.64 [1.88, 5.77]	3.77 [2.35, 7.23]	34.34	< 0.001
EnergyLossP1 [J/(m s e ³)], median [IQR]	20.45 [13.13, 33.81]	20.20 [13.29, 30.70]	20.86 [14.55, 32.68]	21.61 [12.68, 36.57]	18.96 [12.61, 36.64]	0.40	0.941
EnergyLossP2 [J/(m s e ³)], median [IQR]	14.75 [10.38, 23.13]	16.12 [11.69, 25.93]	14.07 [10.32, 20.20]	15.13 [9.17, 23.80]	13.68 [9.78, 21.71]	6.22	0.102
EnergyLossP3 [J/(m s e ³)], median [IQR]	14.69 [8.76, 24.14]	14.75 [9.58, 24.97]	12.10 [7.88, 19.17]	16.53 [9.54, 25.71]	14.15 [7.52, 23.54]	6.25	0.1
EnergyLossP4 [J/(m s e ³)], median [IQR]	27.11 [16.70, 46.62]	26.06 [15.96, 42.05]	25.75 [15.93, 44.21]	30.35 [20.08, 50.68]	25.60 [17.25, 46.62]	3.67	0.3
EnergyLossP5 [J/(m s e ³)], median [IQR]	30.26 [18.19, 50.42]	31.57 [20.18, 53.73]	29.88 [19.78, 50.33]	28.34 [16.17, 44.75]	26.64 [17.43, 46.89]	3.39	0.336
IVPDP1 (mmHg), median [IQR]	0.78 [0.47, 1.22]	1.13 [0.71, 1.46]	0.71 [0.43, 1.15]	0.62 [0.378, 0.96]	0.71 [0.43, 1.00]	49.71	< 0.001
IVPDP2 (mmHg), median [IQR]	1.02 [0.71, 1.41]	1.12 [0.74, 1.56]	1.05 [0.72, 1.39]	0.90 [0.70, 1.28]	1.020 [0.657, 1.33]	8.35	0.039
IVPDP3 (mmHg), median [IQR]	−0.36 [−0.60, −0.25]	−0.51 [−0.74, −0.33]	−0.31 [−0.43, −0.24]	−0.34 [−0.57, −0.16]	−0.34 [−0.52, −0.24]	37.65	< 0.001
IVPDP4 (mmHg), median [IQR]	−0.97 [−1.39, −0.65]	−1.22 [−1.71, −0.88]	−0.88 [−1.22, −0.63]	−0.81 [−1.16, −0.52]	−0.97 [−1.32, −0.61]	45.79	< 0.001
IVPDP5 (mmHg), median [IQR]	0.52 [0.29, 0.89]	0.67 [0.33, 1.13]	0.61 [0.32, 0.91]	0.45 [0.27, 0.70]	0.45 [0.21, 0.78]	13.80	0.003
IVPGP1 (mmHg/mme ³), median [IQR]	−8.96 [−15.22, −5.53]	−14.52 [−19.48, −8.47]	−8.45 [−13.37, −5.40]	−6.96 [−10.34, −3.93]	−8.35 [−12.47, −5.18]	67.63	< 0.001
IVPGP2 (mmHg/mme ³), median [IQR]	−12.12 [−16.90, −8.30]	−14.45 [−20.48, −9.29]	−12.58 [−16.63, −8.44]	−10.15 [−14.84, −7.49]	−12.21 [−16.32, −8.01]	22.76	< 0.001
IVPGP3 (mmHg/mme ³), median [IQR]	4.45 [3.00, 7.30]	6.56 [4.38, 10.20]	3.78 [2.96, 5.18]	3.73 [1.99, 6.74]	4.06 [2.95, 6.51]	58.77	< 0.001

(Continued)

TABLE 4 Continued

Variables	Overall (<i>n</i> = 468)	HFpEF (<i>n</i> = 147)	HFmrEF (<i>n</i> = 95)	HFrEF (<i>n</i> = 136)	HFimpEF (<i>n</i> = 90)	Statistics	<i>P</i> value
IVPGP4 (mmHg/mme ³), median [IQR]	11.98 [7.98, 17.47]	15.80 [11.76, 23.72]	11.01 [7.73, 15.08]	9.23 [5.65, 13.70]	11.46 [7.26, 16.12]	75.75	< 0.001
IVPGP5 (mmHg/mme ³), median [IQR]	−6.46 [−10.95, −3.31]	−9.11 [−14.72, −4.37]	−7.71 [−10.88, −4.05]	−5.04 [−7.80, −2.87]	−5.76 [−9.65, −2.50]	24.53	< 0.001
VorArea-s (m ² /s e ³), median [IQR]	454.22 [354.72, 574.46]	423.08 [337.60, 551.43]	460.09 [384.78, 576.38]	461.12 [360.21, 579.91]	465.20 [350.05, 587.72]	3.07	0.381
Circulation-s (m ² /s e ³), median [IQR]	16.90 [11.77, 22.03]	18.57 [14.27, 23.33]	17.13 [12.63, 23.23]	15.03 [8.50, 19.30]	16.10 [10.80, 21.07]	19.85	< 0.001
VorArea-ed (mm ²), median [IQR]	359.00 [257.14, 476.48]	337.17 [225.00, 471.63]	345.53 [263.20, 448.11]	386.44 [284.88, 509.13]	359.00 [289.74, 470.27]	7.96	0.047
Circulation-ed (m ² /s e ³), median [IQR]	13.13 [7.57, 21.80]	14.63 [9.03, 22.30]	12.57 [7.33, 20.87]	12.87 [7.07, 21.17]	13.10 [7.13, 21.73]	2.85	0.416
VorArea-ac (mm ²), median [IQR]	428.02 [323.87, 531.24]	404.47 [312.14, 504.52]	447.10 [338.74, 556.72]	457.42 [346.38, 561.19]	417.28 [324.89, 517.32]	7.85	0.049
Circulation-ac (m ² /s e ³), median [IQR]	18.03 [12.10, 25.53]	19.70 [13.30, 27.10]	19.00 [13.40, 27.13]	15.47 [10.83, 21.93]	17.90 [11.73, 24.73]	10.65	0.014
vorticity-ac-CCW (1/s), median [IQR]	−105.79 [−142.94, −80.24]	−113.56 [−152.41, −89.29]	−103.55 [−148.56, −76.79]	−94.59 [−131.58, −73.93]	−106.5 [−135.9, −86.7]	10.76	0.013
vorticity-ac-CW (1/s), median [IQR]	114.97 [85.83, 149.68]	128.97 [95.50, 165.98]	117.48 [91.04, 151.08]	107.01 [73.69, 133.29]	105.04 [88.66, 137.78]	22.55	< 0.001
vorticity-ed-CCW (1/s), median [IQR]	−99.07 [−135.19, −76.44]	−96.51 [−127.33, −78.97]	−92.34 [−124.11, −69.19]	−107.40 [−151.76, −81.92]	−99.77 [−131.18, −74.86]	7.01	0.072
vorticity-ed-CW (1/s), median [IQR]	101.54 [72.03, 140.46]	98.34 [71.22, 140.46]	98.33 [71.15, 143.29]	115.89 [74.59, 140.68]	95.48 [72.29, 140.17]	2.94	0.401
vorticity-s-CCW (1/s), median [IQR]	−100.69 [−130.23, −75.93]	−112.44 [−145.15, −83.37]	−97.57 [−124.52, −77.99]	−90.01 [−122.77, −67.34]	−104.3 [−134.5, −85.9]	17.34	< 0.001
vorticity-s-CW (1/s), median [IQR]	110.59 [82.79, 149.78]	132.47 [99.22, 173.11]	105.17 [80.06, 147.14]	97.38 [69.16, 131.18]	105.57 [75.87, 144.28]	37.41	< 0.001

p < 0.05 indicates statistical significance. STE, speckle tracking echocardiography; GLS, global longitudinal strain; GLSR, global systolic strain rate; PALS, peak atrial longitudinal strain; VFM, vector flow mapping; MeanEL, mean energy loss; IVPD, intraventricular pressure difference; IVPG, intraventricular pressure gradient; s, systolic; ed, early diastolic; ac, atrium contraction; P1-P5, isovolumic contraction period, ejection period, isovolumetric relaxation period, diastolic filling period, atrium contraction period; CW, clockwise; CCW, counter-clockwise.

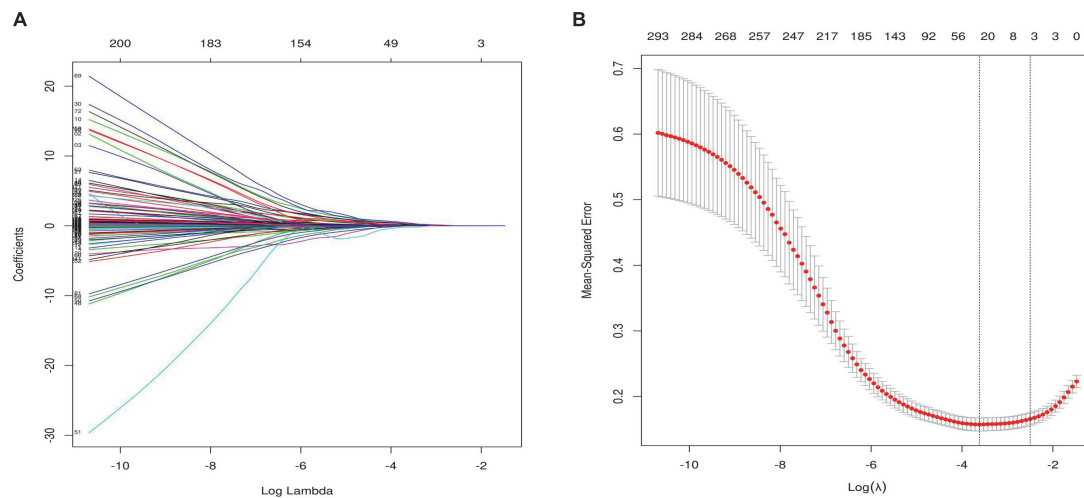


FIGURE 3

Feature selection using the least absolute shrinkage and selection operator (LASSO) binary logistic regression model. **(A)** LASSO coefficient profiles of the 320 features. Vertical line was drawn at the value selected using 10-fold cross-validation, where optimal resulted in 26 non-zero coefficients. **(B)** Tuning parameter (λ) selection in the LASSO model used 10-fold cross-validation via minimum criteria. A coefficient profile plot was produced against the log (λ) sequence. The area under the receiver operating characteristic (AUC) curve was plotted versus log(λ). This is consistent with the glmnet package recommendation for choosing λ , as either λ min (minimum mean square error) or this value plus one standard error.

parameters. General parameters include basic characterization parameters, clinical parameters, blood laboratory test results, and conventional ultrasound parameters. Four machine learning models were used to complete the data sample classification task, including: XGBoost Classifier, Random Forest Classifier, Multi-Layer Perceptron (MLP) Classifier, support vector machine (SVM) Classifier. By repeated sampling 10 times and each resampling training validation set of 20.0% of the total sample, training set of 80.0%, the model classification was successively performed and drew the ROC curve. General Parameters group (AUC: 0.79, accuracy: 0.75, AUC: 0.76, accuracy: 0.74, AUC: 0.68, accuracy: 0.69, AUC: 0.70, accuracy: 0.72, respectively), General Parameters and STE group (AUC: 0.81, accuracy: 0.75; AUC: 0.80, accuracy: 0.76, AUC: 0.67, accuracy: 0.73, AUC: 0.70, accuracy: 0.74, respectively), General Parameter, STE and VFM group (AUC: 0.84, accuracy: 0.77, AUC: 0.82, accuracy: 0.79, AUC: 0.71, accuracy: 0.72, AUC: 0.74, accuracy: 0.76, respectively) were classified in the test set performance (**Figures 7A–C**).

Comparing AUC and accuracy, the XGBoost classifier performed the best among all four learning algorithms. In each group, we found that AUC and accuracy of four learning algorithms were higher when the parameters included general parameters, STE-related parameters and VFM-related parameters, and were more pronounced when using the XGBoost classifier. The inclusion of STE and VFM parameters in the XGBoost classifier model improved its ability to correctly classify MACE patients compared to other learning algorithms (AUC: 0.84, accuracy: 0.77). The inclusion of the

STE and VFM parameters in the XGBoost classifiers model showed an improved ability to classify patients with MACE correctly compared with the other learning algorithms, which is more beneficial to predicting the occurrence of MACE. The performances (AUC and accuracy) of the model in classifying patients correctly in each group using learning algorithms are shown (**Figures 7D,E**). Calibration plot of four learning algorithms (**Figure 7F**). When the solid line was closer to the dotted line (perfectly calibrated), the prediction accuracy was better. Among the comparison of Brier scores for the above four learning algorithms, XGBoost is the lowest, and his prediction calibration is the best (Brier scores = 0.07).

Discussion

The primary objective of this study was to develop a scoring system to predict MACE risk in patients with chronic heart failure. This study used clinical trial data from patients with CHF, and age was not included in the risk assessment model due to the short follow-up time. In previous models, the most common parameters used to predict major adverse cardiovascular events were general clinical data, blood test parameters, and conventional ultrasound parameters (11–16). There are also articles that use LA and LV strain parameters to create models. LA function assessed by speckle tracking echocardiography is an independent prognostic marker in heart failure patients with reduced ejection fraction (31). These results suggest that STE variable information corresponding to two-dimensional and doppler analysis can provide independent

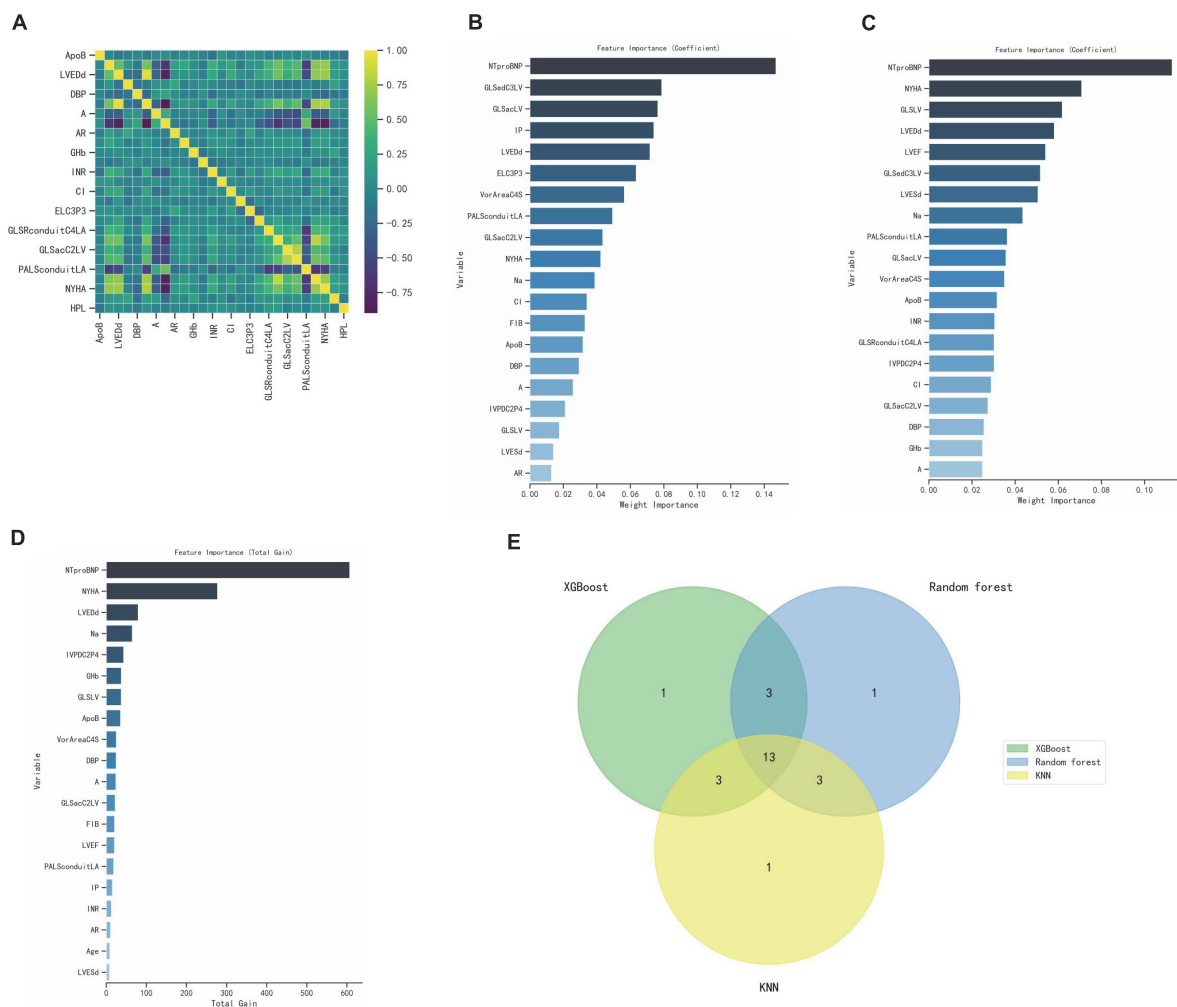


FIGURE 4

Select optimal prognostic variables. (A) Correlation heatmap showing associations between clinical features and ultrasound parameters. (B–D) XGBoost, Random forest, KNN calculate the importance of each influencing factor to the classification model and rank it, the top 20 parameters were selected. (E) Venn diagram, 13 variables were recognized.

assessments of diastolic function and LV filling pressures, which are increasingly moving toward precision medicine (32).

Left atrial (LA) function is closely related to LV function and plays a key role in maintaining optimal cardiac functional performance. The left atrium, through its reservoir, conduit, and booster pump stages, regulates filling of the left ventricle, while the LV influences LA function throughout the cardiac cycle. Long-term exposure to high LV filling pressures leads to an increase in LA volume, presumably reduced LA function is only a marker of LV deterioration (33, 34). In patients with HFrEF, LA function index measured at first admission was associated with cardiovascular outcomes during the first 6 months of follow-up (35), and LA systolic function measured by LA strain rate was shown to provide prognostic stratification for outpatients with new-onset HF (36). The prognostic value of LA function has also been

explored using other imaging techniques. Decreased LA ejection fraction measured by cardiac magnetic resonance imaging was associated with a higher incidence of AF and poorer prognosis in patients with HF (37). Previous studies have shown that LV diastolic dysfunction is related to LA volume (38, 39). Moreover, LV diastolic function is closely related to atrial function; Thus, the transmitral flow parameters of LV must be interpreted in terms of LV relaxation, LA function, and loading parameters, each of which affects LV filling pressure. Due to the high dimensionality and complexity of variables affecting LV diastolic function and filling pressures, echocardiographic assessment requires a multiparametric approach (19, 40). Heart failure patients are divided into four categories based on LVEF: HFpEF, HFmrEF, HFrEF HFimpEF (17). Different subtypes have different clinical features and disease courses, and different conditions can lead to misjudgment of heart

TABLE 5 Prognostic model for major cardiovascular events (MACE) based on logistic regression model.

Predictor	Estimate	SE	Z	p	Odds ratio	Lower (95% CI)	Upper (95% CI)
IVPDC2P4 (mmHg)	0.345	0.163	2.116	0.034	1.411	1.039	1.978
VorAreaC4S (mm ²)	0.001	0.001	1.664	0.046	1.001	1	1.002
GLSacC2LV (%)	0.155	0.079	1.967	0.049	1.168	1.003	1.367
PALSconduitLA (%)	−0.06	0.039	−1.539	0.024	0.942	0.87	1.014
GLSLV (%)	−0.041	0.056	−0.726	0.048	0.96	0.86	1.072
LVEDd (mm)	0.05	0.021	2.379	0.017	1.051	1.009	1.096
LVEF (%)	0.033	0.022	1.495	0.035	1.033	0.99	1.079
ApoB (g/L)	1.145	0.458	2.501	0.012	3.143	1.288	7.821
Na (mmol/L)	−0.056	0.034	−1.674	0.044	0.945	0.885	1.009
NTproBNP (mmol/L)	0.001	0.001	4.745	0.001	1	1	1.001
DBP (mmHg)	−0.014	0.007	−1.972	0.049	0.986	0.971	1
NYHA II	2.263	0.797	2.841	0.005	9.611	2.439	64.577
NYHA III	2.918	0.857	3.406	0.001	18.503	4.052	134.706
NYHA IV	3.367	0.896	3.758	0.001	28.979	5.799	222.979

$p < 0.05$ indicates statistical significance. IVPDC2P4, intraventricular pressure differences from 2-chamber images during LV early filling period; VorAreaC4S, LV vortex area from 4-chamber images during systolic period; GLSacC2LV, left ventricular global longitudinal strain from 2-chamber images during atrial systolic period; PALSconduitLA, peakLA longitudinal peak strain during conduit period; GLSLV, left ventricular global longitudinal strain; LVEDd, left ventricular end diastolic diameter; LVEF, left ventricular ejection fraction; ApoB, apolipoproteinB; NT-pro BNP, N-terminal pro-brain natriuretic peptide; DBP, diastolic blood pressure; NYHA, New York Heart Association.

failure and bring difficulties to the diagnosis of heart failure. It is well-known that HFpEF differs in clinical features and disease course (including treatment strategies), but all-cause readmission rates remained the highest in HFpEF vs. HFrEF and HFmrEF (41). This study hopes to establish a predictive model suitable for different heart failure populations, and only LVEF analysis variables are included, not LVEF classification. We will continue to expand the sample size and construct respective prediction models for different types of heart failure patients, so as to improve the prediction effect of the model.

Currently, left chamber fluid mechanics is lacking to participate in model construction. There is a growing interest in the imaging and visualization of intracardiac blood flow (42). VFM is a two-dimensional cross-sectional image acquired based on b-type color Doppler echocardiography, which can enable visualize the cross-sectional image with blood flow as a velocity vector (43). As mentioned earlier, calculate the flow vector using the continuity equation and decompose the vector into vertical and parallel velocity components, determined from wall motion spot tracking and color doppler images (25). The advantages of VFM are that it is relatively inexpensive, less time-consuming, easy to use at the bedside, and does not require the use of contrast agents. This model adds the VFM parameters compared with the previous models, which makes the significance of the model more explanatory and the evaluation more comprehensive. The potential application of VFM to quantify aortic regurgitation has been reported. Compared with other conventional measures, energy loss can more clearly quantify patients, subjective symptoms and help to assess disease severity based on cardiac

stress (24, 44, 45). Automated phenotype calculation is an efficient strategy to fuse multidimensional parameters of LV structure and function to collect STE- and CFM-related parameters (46).

In this study, the left ventricular high-throughput parameters were constructed by collecting mechanics and hydrodynamic parameters, including STE parameters of LV and LA, VFM parameters of LV flow. For the first time, we integrate multiple echocardiographic parameters to meaningfully reflect changes in left ventricular structure and function. Through screening, key indicators are incorporated into the construction of the model. Based on selecting optimal prognostic variables, a logistic regression model and nomogram is constructed, which can well-predict the possibility of MACE within 6 months. Here, we evaluated the relationship between these factors and HF to create a practical and accurate prognostic dynamic nomogram model to identify high-risk groups of heart failure and ultimately develop targeted treatment options. From Figure 5C, we can find the performance effect of constructing the new model is good [C-statistics: 0.876 (95% CI, 0.844– 0.907)]. From Figure 6, survival curves were generated using the Kaplan–Meier method, and log-rank tests were used to compare survival curves, which based on nomogram scores and predictive risk. For survival analysis, significant differences among the groups were seen according to Kaplan–Meier survival curves. We can find patients with high nomogram scores and predictive risk had the shortest survival time. Although the number of high-risk group was significantly fewer than low risk group, the number of patients with MACE was significantly more than the low risk group,

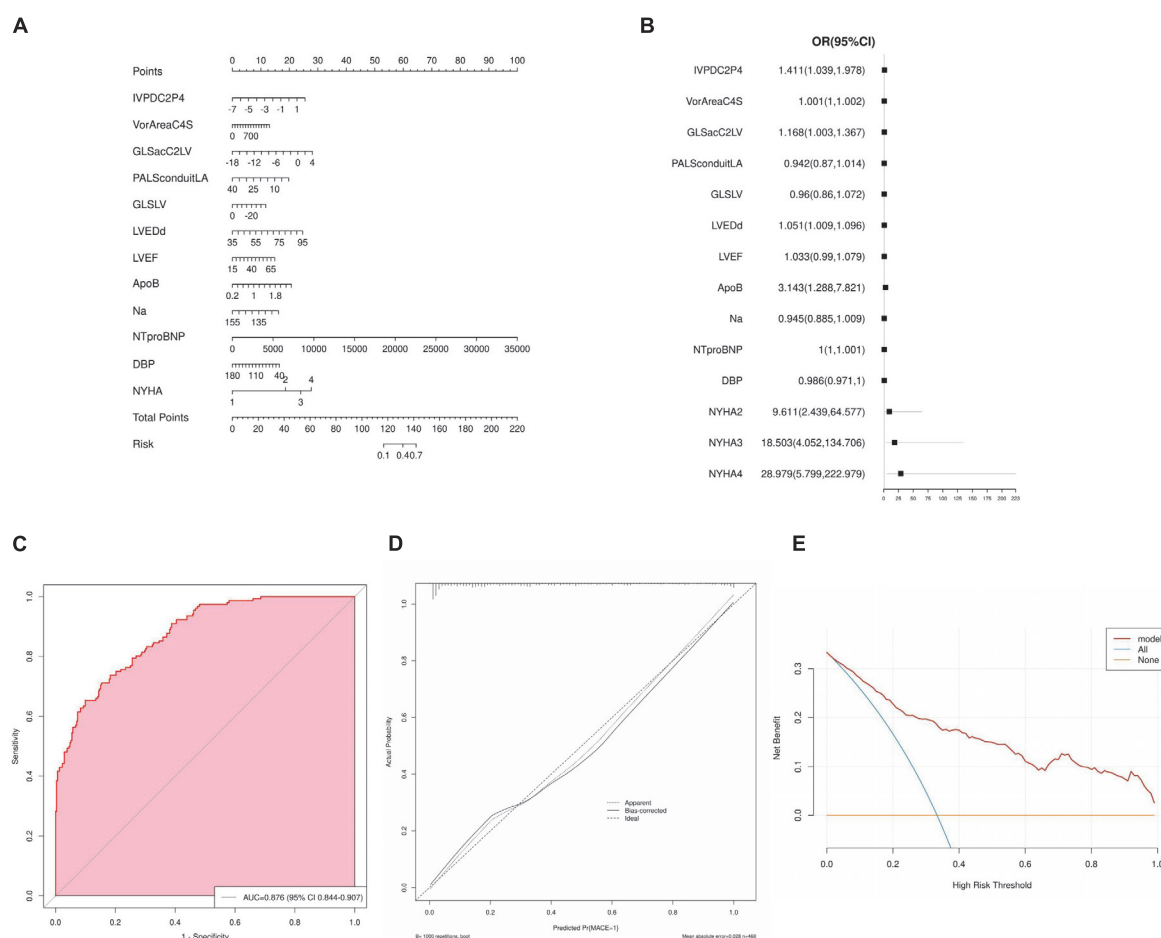


FIGURE 5

Nomogram interpretation and model validation. **(A)** Nomogram for predicting major cardiovascular events (MACE) risk, and the point was the selected scoring standard or scale. **(B)** Odds ratios determined in a logistic regression model as shown in the forest plot. **(C)** Receiver operating characteristic curve for the nomogram. **(D)** The Nomogram calibration plots of the model. **(E)** Decision curve analysis for predictive models.

better demonstrating the clinical significance of the model. In each group, we found that AUC and accuracy of four learning algorithms were higher when the parameters included general parameters, STE-related parameters and VFM-related parameters, and were more pronounced when using the XGBoost classifier. The inclusion of general parameters and STE-related parameters and VFM-related parameters in the XGBoost classifiers model showed an improved ability to classify patients with MACE correctly compared with the other learning algorithms (AUC: 0.84, accuracy: 0.77), which is more beneficial to predicting the occurrence of MACE. Calibration plot of four learning algorithms, we can find among the comparison of Brier scores, XGBoost is the lowest, and his prediction calibration is the best (Brier scores = 0.07). By machine learning, we found that the AUC of the models generated by general parameters, STE-related parameters and VFM-related parameters was higher than that of the other models, but the increase in AUC was not significant.

Furthermore, analyzing and extracting data from STE and VFM techniques requires a certain amount of time and effort, which is often difficult to perform in routine clinical practice. However, with continuous attempts to explore and screen more valuable parameters, the most valuable indicators can be easily extracted from data, which is beneficial for disease assessment and clinical decision-making in patients with heart failure.

Study limitations

There were several limitations to this study that require comment. First, this was a single-center study with a limited sample size. A larger study sample from various centers may be helpful to further confirm these observations. The findings of the present study, although showing statistical significance, were based on a relatively small number of

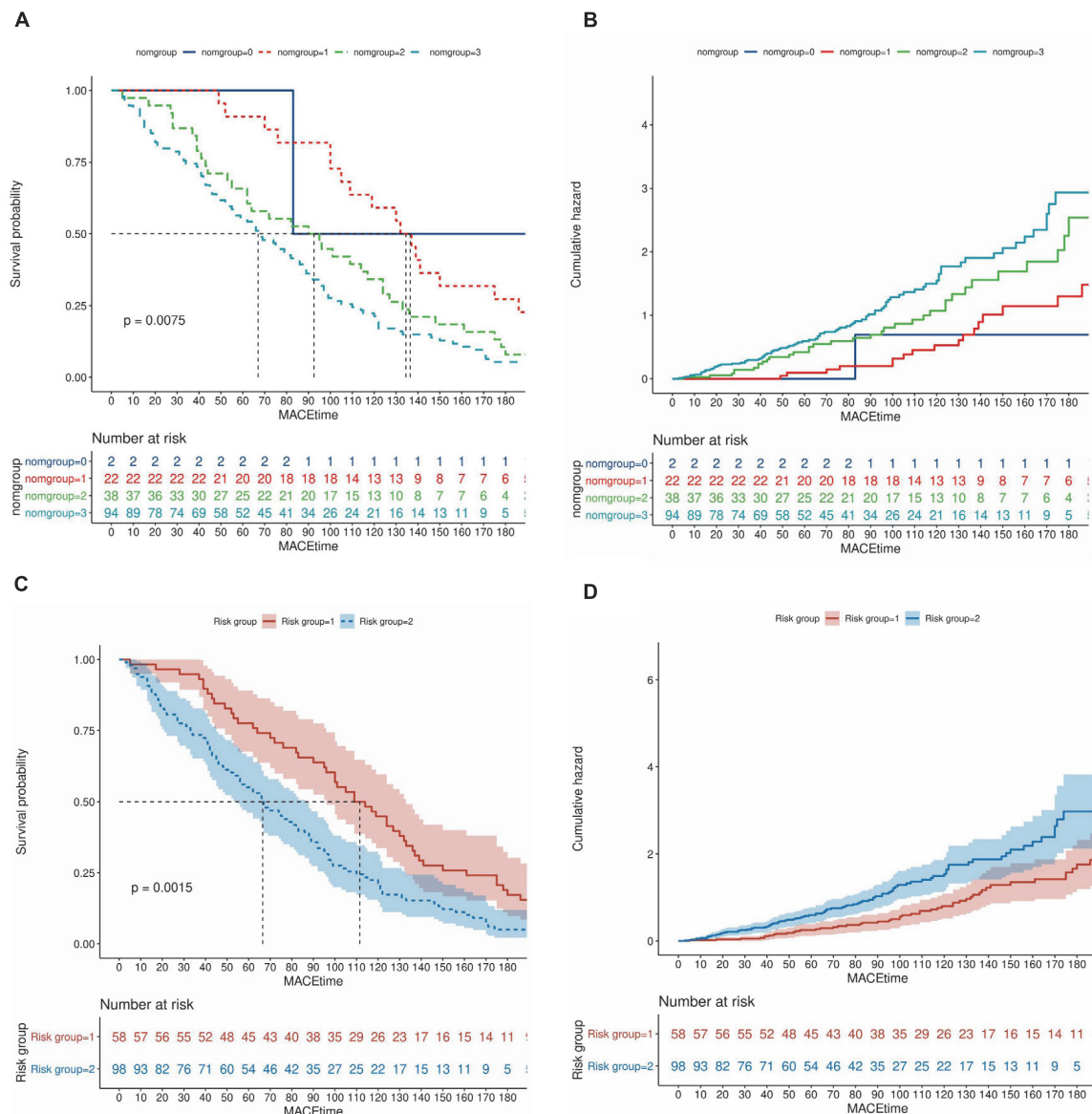


FIGURE 6

Survival curves based on nomogram scores and predictive risk. (A,B) Patients were divided into four groups according to the quartile total nomogram scores (nomgroup = 0, 1, 2, 3), the KM survival curves and cumulative survival curves were used to compare survival times among different groups was made by log-rank test. (C,D) Patients were divided into high- and low-risk groups (low-risk group = 1, high-risk group = 2) according to the predicted probabilities of the prediction model. The median survival time (LT50) for different groups. The horizontal axis of the KM survival curve represents time, and the vertical axis represents probability.

patients and are indeed not suitable for data from countries that respond to an aging population. The results should therefore be regarded as preliminary, and further enlarge studies adequately powered for clinical outcomes are warranted to confirm our results. Second, a relatively short follow-up duration was used to detect cardiac events in this study, the effective time follow-up within 6 months is relatively short, the specific time of MACE cannot be clearly defined by patients, therefore logist regression is used to draw nomograph

this time, only to predict the possibility of MACE within 6 months after discharge. In future studies, the continuous follow-up will be summarized to establish an effective cox prediction model. Third, VFM technology relies on strict contour condition provided by the endocardial-blood interface and is limited by the frame rate applied and the Nyquist limit. Aliasing may result in errors in the VFM calculated blood flow data, mild aliasing was manually corrected on the selected frames. However, severe aliasing could not be

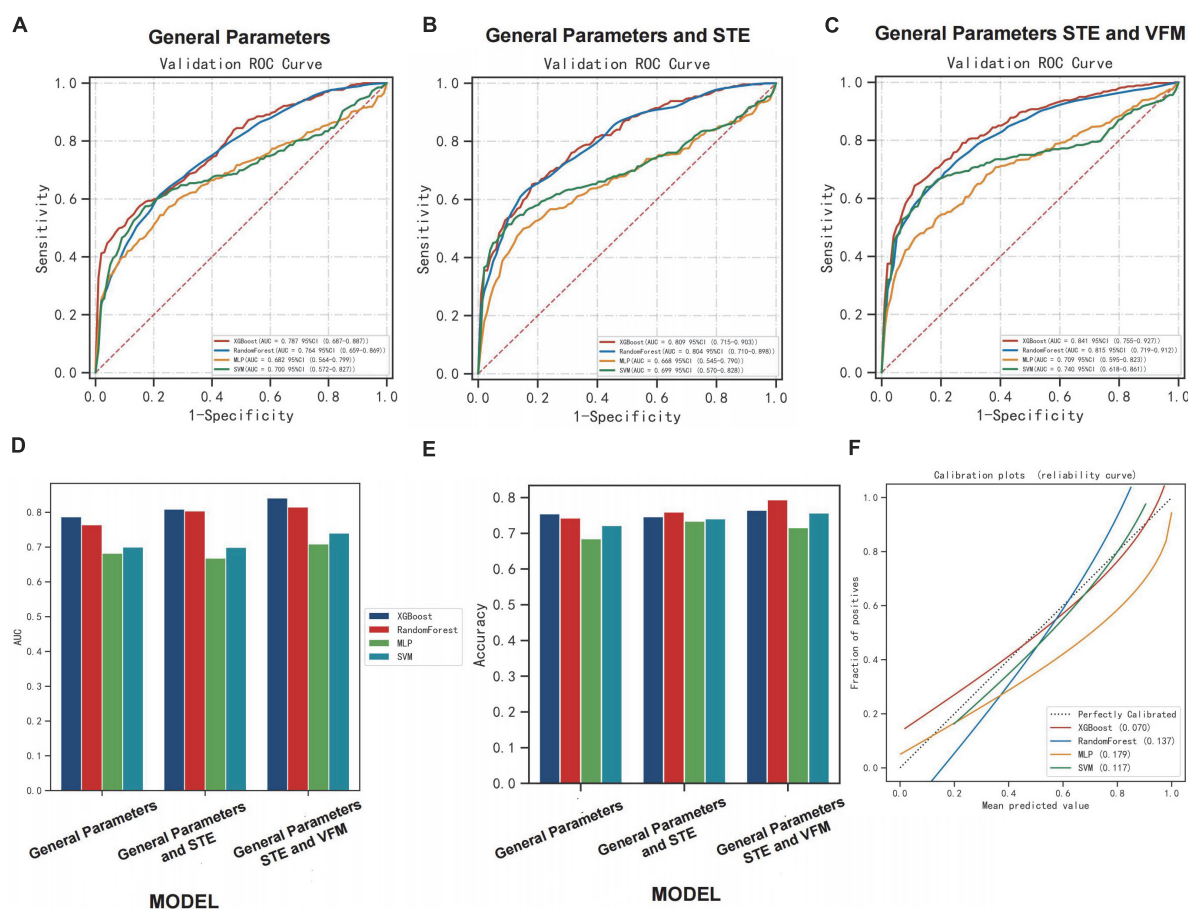


FIGURE 7

Performance of machine learning algorithms among the groups. (A–C) The ROC curve of the model performance in classifying patients correctly in each group using learning algorithms. (D,E) The performances [area under curve (AUC) and accuracy] of the model in classifying patients correctly in each group using learning algorithms. (F) The calibration plots of learning algorithms in group [General Parameters, speckle tracking echocardiography (STE) and vector flow mapping (VFM) group].

corrected can underestimate the true velocity, we should minimize this phenomenon by optimizing the Nyquist limit and ensuring appropriate patient selection. Patients with valvular heart diseases were not included in the analysis due to severe aliasing produced by the fast valve flow. Fourth, we did not include additional measurements for right ventricular function, which would need to be addressed in future investigations.

Conclusion

In this study, we developed a prediction model and nomogram to estimate the risk of MACE within 6 months of discharge among patients with heart failure. The findings may provide a reference for clinical physicians for detection of the risk of MACE in terms of clinical characteristics, cardiac structure and function, hemodynamics, and enable

its prompt management, which is a convenient, practical and effective clinical decision making tool for providing accurate prognosis.

Data availability statement

The original contributions presented in the study are included in the article/supplementary material, further inquiries can be directed to the corresponding authors.

Ethics statement

Written informed consent was obtained from the individual(s) for the publication of any potentially identifiable images or data included in this article.

Author contributions

QL-S proposed the hypothesis, designed the experiments, and drafted the manuscript. QL-S, SQ-J, XD-W, and YL made contributions to data collection. QL-S and JC-Z made contributions to the analysis and interpretation of the data. JW-T and HR-L conceived the study, participated in its design, and helped edit the manuscript. All authors contributed to the article and approved the submitted version.

Funding

This study was funded by China Postdoctoral Science Foundation (2021MD703828) and Heilongjiang Postdoctoral Fund (LBH-Z20172).

References

- Groenewegen A, Rutten FH, Mosterd A, Hoes AW. Epidemiology of heart failure. *Eur J Heart Fail.* (2020) 22:1342–56. doi: 10.1002/ehf.1858
- Ambrosy AP, Parikh RV, Sung SH, Tan TC, Narayanan A, Masson R, et al. Analysis of worsening heart failure events in an integrated health care system. *J Am Coll Cardiol.* (2022) 80:111–22. doi: 10.1016/j.jacc.2022.04.045
- Lesyuk W, Kriza C, Kolominsky-Rabas P. Cost-of-illness studies in heart failure: a systematic review 2004–2016. *BMC Cardiovasc Disord.* (2018) 18:74. doi: 10.1186/s12872-018-0815-3
- Urbich M, Globe G, Pantiri K, Heisen M, Bennison C, Wirtz HS, et al. A systematic review of medical costs associated with Heart Failure in the USA (2014–2020). *Pharmacoeconomics.* (2020) 38:1219–36. doi: 10.1007/s40273-020-00952-0
- Thenappan T, Prins KW, Cogswell R, Shah SJ. Pulmonary hypertension secondary to heart failure with preserved ejection fraction. *Can J Cardiol.* (2015) 31:430–9. doi: 10.1016/j.cjca.2014.12.028
- Francis GS, Cogswell R, Thenappan T. The heterogeneity of heart failure: will enhanced phenotyping be necessary for future clinical trial success? *J Am Coll Cardiol.* (2014) 64:1775–6. doi: 10.1016/j.jacc.2014.07.978
- Hsu B, Korda RJ, Lindley RJ, Douglas KA, Naganathan V, Jorm LR. Use of health and aged care services in Australia following hospital admission for myocardial infarction, stroke or heart failure. *BMC Geriatr.* (2021) 21:538. doi: 10.1186/s12877-021-02519-w
- Valley TS, Sjoding MW, Ryan AM, Iwashyna TJ, Cooke CR. Intensive care unit admission and survival among older patients with chronic obstructive pulmonary disease, Heart Failure, or Myocardial Infarction. *Ann Am Thorac Soc.* (2017) 14:943–51. doi: 10.1513/AnnalsATS.201611-847OC
- Hsu B, Korda R, Naganathan V, Lewis P, Ooi SY, Brieger D, et al. Burden of cardiovascular diseases in Australia following aged care services. *Age Ageing.* (2021) 50:1845–9. doi: 10.1093/ageing/afab083
- Arnett DK, Blumenthal RS, Albert MA, Buroker AB, Goldberger ZD, Hahn EJ, et al. 2019 ACC/AHA guideline on the primary prevention of cardiovascular disease: a report of the American College of Cardiology/American Heart Association task force on clinical practice guidelines. *J Am Coll Cardiol.* (2019) 74:e177–232.
- Voors AA, Ouwerkerk W, Zannad F, van Veldhuisen DJ, Samani NJ, Ponikowski P, et al. Development and validation of multivariable models to predict mortality and hospitalization in patients with heart failure. *Eur J Heart Fail.* (2017) 19:627–34. doi: 10.1002/ehf.785
- Lim NK, Lee SE, Lee HY, Cho HJ, Choe WS, Kim H, et al. Risk prediction for 30-day heart failure-specific readmission or death after discharge: data from the Korean Acute Heart Failure (KorAHF) registry. *J Cardiol.* (2019) 73:108–13.
- Wang L, Zhao YT. Development and validation of a prediction model for irreversible worsened cardiac function in patients with acute decompensated heart failure. *Front Cardiovasc Med.* (2021) 8:785587. doi: 10.3389/fcvm.2021.785587
- Segar MW, Jaeger BC, Patel KV, Nambi V, Ndumele CE, Correa A, et al. Development and validation of machine learning-based race-specific models to predict 10-year risk of heart failure: a multicohort analysis. *Circulation.* (2021) 143:2370–83. doi: 10.1161/CIRCULATIONAHA.120.053134
- Zhuang B, Shen T, Li D, Jiang Y, Li G, Luo Q, et al. A model for the prediction of mortality and hospitalization in chinese heart failure patients. *Front Cardiovasc Med.* (2021) 8:761605. doi: 10.3389/fcvm.2021.761605
- Yin T, Shi S, Zhu X, Cheang I, Lu X, Gao R, et al. A survival prediction for acute heart failure patients via web-based dynamic nomogram with internal validation: a prospective cohort study. *J Inflamm Res.* (2022) 15:1953–67. doi: 10.2147/JIR.S348139
- Bozkurt B, Coats Andrew JS, Tsutsui H, Abdelhamid Ca M, Adamopoulos S, Albert N, et al. Universal definition and classification of heart failure: a report of the Heart Failure Society of America, Heart Failure Association of the European Society of Cardiology, Japanese Heart Failure Society and Writing Committee of the Universal Definition of Heart Failure: Endorsed by the Canadian Heart Failure Society, Heart Failure Association of India, Cardiac Society of Australia and New Zealand, and Chinese Heart Failure Association. *Eur J Heart Fail.* (2021) 23:352–80. doi: 10.1002/ehf.2115
- Lang RM, Badano LP, Mor-Avi V, Afkalo J, Armstrong A, Ernande L, et al. Recommendations for cardiac chamber quantification by echocardiography in adults: an update from the American Society of Echocardiography and the European Association of Cardiovascular Imaging. *J Am Soc Echocardiogr.* (2015) 28:1–39.e14. doi: 10.1016/j.echo.2014.10.003
- Nagueh SF, Smiseth OA, Appleton CP, Byrd BF, Dokainish H, Edvardsen T, et al. Recommendations for the evaluation of left ventricular diastolic function by echocardiography: an update from the american society of echocardiography and the european association of cardiovascular imaging. *Eur Heart J Cardiovasc Imaging.* (2016) 17:1321–60. doi: 10.1093/ehjci/jew082
- Unger ED, Dubin RF, Deo R, Daruwalla V, Friedman JL, Medina C, et al. Association of chronic kidney disease with abnormal cardiac mechanics and adverse outcomes in patients with heart failure and preserved ejection fraction. *Eur J Heart Fail.* (2016) 18:103–12. doi: 10.1002/ehf.445
- Mirea O, Duchenne J, Voigt JU. Comparison between nondedicated and novel dedicated tracking tool for right ventricular and left atrial strain. *J Am Soc Echocardiogr.* (2022) 35:419–25. doi: 10.1016/j.echo.2021.11.011
- Asami R, Tanaka T, Shimizu M, Seki Y, Nishiyama T, Sakashita H, et al. Ultrasonic vascular vector flow mapping for 2-D flow estimation. *Ultrasound Med Biol.* (2019) 45:1663–74. doi: 10.1016/j.ultrasmedbio.2019.02.014

Conflict of interest

The authors declare that the research was conducted in the absence of any commercial or financial relationships that could be construed as a potential conflict of interest.

Publisher's note

All claims expressed in this article are solely those of the authors and do not necessarily represent those of their affiliated organizations, or those of the publisher, the editors and the reviewers. Any product that may be evaluated in this article, or claim that may be made by its manufacturer, is not guaranteed or endorsed by the publisher.

23. Garcia D, Del Alamo JC, Tanne D, Yotti R, Cortina C, Bertrand E, et al. Two-dimensional intraventricular flow mapping by digital processing conventional color-Doppler echocardiography images. *IEEE Trans Med Imaging*. (2010) 29:1701–13. doi: 10.1109/TMI.2010.2049656
24. Stugaard M, Koriyama H, Katsuki K, Masuda K, Asanuma T, Takeda Y, et al. Energy loss in the left ventricle obtained by vector flow mapping as a new quantitative measure of severity of aortic regurgitation: a combined experimental and clinical study. *Eur Heart J Cardiovasc Imaging*. (2015) 16:723–30. doi: 10.1093/ehjci/jev035
25. Asami R, Tanaka T, Kawabata KI, Hashiba K, Okada T, Nishiyama T. Accuracy and limitations of vector flow mapping: left ventricular phantom validation using stereo particle image velocimetry. *J Echocardiogr*. (2017) 15:57–66. doi: 10.1007/s12574-016-0321-5
26. Du Y, Goddi A, Bortolotto C, Shen Y, Dell'Era A, Calliada F, et al. Wall shear stress measurements based on ultrasound vector flow imaging: theoretical studies and clinical examples. *J Ultrasound Med*. (2020) 39:1649–64. doi: 10.1002/jum.15253
27. Rodríguez Muñoz D, Moya Mur JL, Fernández-Golfín C, Becker Filho DC, González Gómez A, Fernández Santos S, et al. Left ventricular vortices as observed by vector flow mapping: main determinants and their relation to left ventricular filling. *Echocardiography*. (2015) 32:96–105. doi: 10.1111/echo.12584
28. Ji L, Hu W, Yong Y, Wu H, Zhou L, Xu D. Left ventricular energy loss and wall shear stress assessed by vector flow mapping in patients with hypertrophic cardiomyopathy. *Int J Cardiovasc Imaging*. (2018) 34:1383–91. doi: 10.1007/s10554-018-1348-7
29. Chen M, Jin JM, Zhang Y, Gao Y, Liu SL. Assessment of left ventricular diastolic dysfunction based on the intraventricular velocity difference by vector flow mapping. *J Ultrasound Med*. (2013) 32:2063–71. doi: 10.7863/ultra.32.12.2063
30. Harrell FE, Lee KL, Mark DB. Multivariable prognostic models: issues in developing models, evaluating assumptions and adequacy, and measuring and reducing errors. *Stat Med*. (1996) 15:361–87. doi: 10.1002/(SICI)1097-0258(19960229)15:4<361::AID-SIM168>3.0.CO;2-4
31. Malagoli A, Rossi L, Bursi F, Zanni A, Sticozzi C, Piepoli MF, et al. Left atrial function predicts cardiovascular events in patients with chronic heart failure with reduced ejection fraction. *J Am Soc Echocardiogr*. (2019) 32:248–56. doi: 10.1016/j.echo.2018.08.012
32. Collins FS, Varmus H. A new initiative on precision medicine. *N Engl J Med*. (2015) 372:793–5. doi: 10.1056/NEJMp1500523
33. Matsuda Y, Toma Y, Ogawa H, Matsuzaki M, Katayama K, Fujii T, et al. Importance of left atrial function in patients with myocardial infarction. *Circulation*. (1983) 67:566–71. doi: 10.1161/01.cir.67.3.566
34. Rosca M, Lancellotti P, Popescu BA, Piérard LA. Left atrial function: pathophysiology, echocardiographic assessment, and clinical applications. *Heart*. (2011) 97:1982–9. doi: 10.1136/heartjnl-2011-300069
35. Chrysohoou C, Kotrogiannis I, Antoniou CC, Brili S, Vaina S, Latsios G, et al. Left atrial function predicts heart failure events in patients with newly diagnosed left ventricular systolic heart failure during short-term follow-up. *Angiology*. (2014) 65:817–23. doi: 10.1177/0003319713506109
36. Sanchis L, Andrea R, Falces C, Lopez-Sobrinho T, Montserrat S, Perez-Villa F, et al. Prognostic value of left atrial strain in outpatients with de novo heart failure. *J Am Soc Echocardiogr*. (2016) 29:1035–42.e1. doi: 10.1016/j.echo.2016.07.012
37. Pellicori P, Zhang J, Lukaschuk E, Joseph AC, Bourantas CV, Loh H, et al. Left atrial function measured by cardiac magnetic resonance imaging in patients with heart failure: clinical associations and prognostic value. *Eur Heart J*. (2015) 36:733–42. doi: 10.1093/eurheartj/ehu405
38. Tsang TS, Barnes ME, Gersh BJ, Bailey KR, Seward JB. Left atrial volume as a morphophysiological expression of left ventricular diastolic dysfunction and relation to cardiovascular risk burden. *Am J Cardiol*. (2002) 90:1284–9. doi: 10.1016/s0002-9149(02)02864-3
39. Hung MJ, Cherg WJ. Analysis of left atrial volume change rate for evaluation of left ventricular diastolic function. *Echocardiography*. (2004) 21:593–601. doi: 10.1111/j.0742-2822.2004.03154.x
40. Mottram PM, Marwick TH. Assessment of diastolic function: what the general cardiologist needs to know. *Heart*. (2005) 91:681–95. doi: 10.1136/hrt.2003.029413
41. Cui X, Thunström E, Dahlström U, Zhou J, Ge J, Fu M. Trends in cause-specific readmissions in heart failure with preserved vs. reduced and mid-range ejection fraction. *ESC Heart Fail*. (2020) 7:2894–903. doi: 10.1002/ehf2.12899
42. Rodríguez Muñoz D, Markl M, Moya Mur JL, Barker A, Fernández-Golfín C, Lancellotti P, et al. Intracardiac flow visualization: current status and future directions. *Eur Heart J Cardiovasc Imaging*. (2013) 14:1029–38. doi: 10.1093/ehjci/jet086
43. Uejima T, Koike A, Sawada H, Aizawa T, Ohtsuki S, Tanaka M, et al. A new echocardiographic method for identifying vortex flow in the left ventricle: numerical validation. *Ultrasound Med Biol*. (2010) 36:772–88. doi: 10.1016/j.ultrasmedbio.2010.02.017
44. Li C, Zhang J, Li X, Zhou C, Li H, Tang H, et al. Quantification of chronic aortic regurgitation by vector flow mapping: a novel echocardiographic method. *Eur J Echocardiogr*. (2010) 11:119–24. doi: 10.1093/ejechoard/jep175
45. Kainuma A, Itatani K, Akiyama K, Naito Y, Ishii M, Shimizu M, et al. Preoperative left ventricular energy loss in the operating theater reflects subjective symptoms in chronic aortic regurgitation. *Front Surg*. (2022) 9:739743. doi: 10.3389/fsurg.2022.739743
46. Cho JS, Shrestha S, Kagiya N, Hu L, Ghaffar YA, Casaclang-Verzosa G, et al. A network-based “Phenomics” approach for discovering patient subtypes from high-throughput cardiac imaging data. *JACC Cardiovasc Imaging*. (2020) 13:1655–70. doi: 10.1016/j.jcmg.2020.02.008



OPEN ACCESS

EDITED BY

Masaki Izumo,
St. Marianna University School
of Medicine, Japan

REVIEWED BY

Alberto Guido Pozzoli,
Ospedale Regionale di Lugano,
Switzerland
Maria Concetta Pastore,
Università del Piemonte Orientale, Italy

*CORRESPONDENCE

Rita Pavasini
pvsrti@unife.it

SPECIALTY SECTION

This article was submitted to
Cardiovascular Imaging,
a section of the journal
Frontiers in Cardiovascular Medicine

RECEIVED 08 June 2022

ACCEPTED 03 November 2022

PUBLISHED 16 November 2022

CITATION

Pavasini R, Fabbri G, Bianchi N,
Deserio MA, Sanguettoli F, Zanarelli L,
Tonet E, Passarini G, Serenelli M and
Campo G (2022) The role of stress
echocardiography in transcatheter
aortic valve implantation
and transcatheter edge-to-edge
repair era: A systematic review.
Front. Cardiovasc. Med. 9:964669.
doi: 10.3389/fcvm.2022.964669

COPYRIGHT

© 2022 Pavasini, Fabbri, Bianchi,
Deserio, Sanguettoli, Zanarelli, Tonet,
Passarini, Serenelli and Campo. This is
an open-access article distributed
under the terms of the [Creative
Commons Attribution License \(CC BY\)](#).
The use, distribution or reproduction in
other forums is permitted, provided
the original author(s) and the copyright
owner(s) are credited and that the
original publication in this journal is
cited, in accordance with accepted
academic practice. No use, distribution
or reproduction is permitted which
does not comply with these terms.

The role of stress echocardiography in transcatheter aortic valve implantation and transcatheter edge-to-edge repair era: A systematic review

Rita Pavasini*, Gioele Fabbri, Nicola Bianchi,
Maria Angela Deserio, Federico Sanguettoli, Luca Zanarelli,
Elisabetta Tonet, Giulia Passarini, Matteo Serenelli and
Gianluca Campo

Cardiology Unit, Azienda Ospedaliero-Universitaria di Ferrara, Ferrara, Italy

Objectives: In the last decade, percutaneous treatment of valve disease has changed the approach toward the treatment of aortic stenosis (AS) and mitral regurgitation (MR). The clinical usefulness of stress echocardiography (SE) in the candidates for transcatheter aortic valve implantation (TAVI) and transcatheter edge-to-edge repair (TEER) of MR remains to be established. Therefore, the key aim of this review is to assess the main applications of SE in patients undergoing TAVI or TEER.

Methods: We searched for relevant studies to be included in the systematic review on PubMed (Medline), Cochrane library, Google Scholar, and Biomed Central databases. The literature search was conducted in February 2022. The inclusion criteria of the studies were: observational and clinical trials or meta-analysis involving patients with AS or MR evaluated with SE (excluding those in which SE was used only for screening of pseudo-severe stenosis) and treated with percutaneous procedures.

Results: Thirteen studies published between 2013 and 2021 were included in the review: five regarding candidates for TEER and eight for TAVI. In TEER candidates, seeing an increase in MR grade, and stroke volume of >40% during SE performed before treatment was, respectively, related to clinical benefits ($p = 0.008$) and an increased quality of life. Moreover, overall, 25% of patients with moderate secondary MR at rest before TEER had the worsening of MR during SE. At the same time, in SE performed after TEER, an increase in mean transvalvular diastolic gradient and in systolic pulmonary pressure is expected, but without sign and symptoms of heart failure. Regarding TAVI, several studies showed that contractile reserve (CR) is not predictive of post-TAVI ejection fraction recovery and mortality in low-flow low-gradient AS either at 30 days or at long-term.

Conclusion: This systematic review shows in TEER candidates, SE has proved useful in the optimization of patient selection and treatment response, while its role in TAVI candidates is less defined. Therefore, larger trials are needed to test and confirm the utility of SE in candidates for percutaneous procedures of valve diseases.

KEYWORDS

stress echocardiography, Mitraclip, TAVI, aortic stenosis, mitral regurgitation, TEER

Introduction

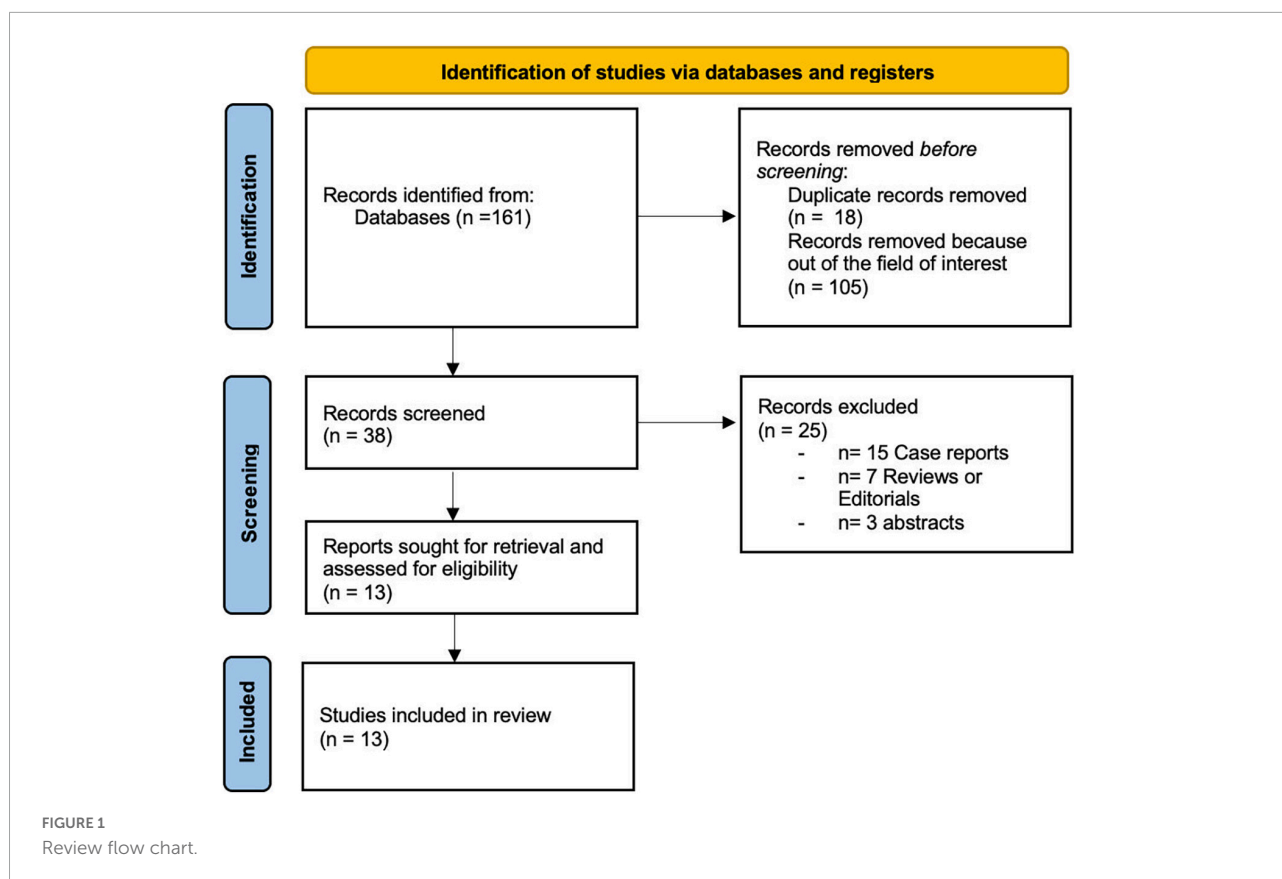
Mitral regurgitation (MR) and aortic stenosis (AS) are the most prevalent valve diseases in Europe (1, 2). The clinical approach toward both valve diseases has changed due to being able to treat them percutaneously in patients with high surgical risk. Transcatheter edge-to-edge repair (TEER) is used for the treatment of either primary or secondary MR treatment (3), while transcatheter aortic valve implantation (TAVI) is used for AS (4). Stress echocardiography (SE) is a valuable tool in the assessment of asymptomatic severe valvular disease used to determine the severity of the disease (5). However, due to lack of robust evidence, its use is not recommended in the guidelines for the management of most valvular diseases (1). In the context of AS, dobutamine SE serves as the cornerstone in confirming a low-flow, low-gradient (LFLG) phenotype (in the case of an ejection fraction below 50%), but it also helps distinguish severe from pseudo-severe AS and evaluate the presence of contractile reserve (CR), defined as an increase of at least 20% in stroke volume (SV) during the examination (1–8). Whereas, in patients with MR, SE is useful to evaluate symptom onset (also in relation to hemodynamical changes and exercise), confirm the severity of MR, assess pulmonary pressure, and evaluate CR. However, historically, SE has been underused in Europe, as shown in the Euro Valve Survey in heart disease (2). In fact, only 3.1% of patients with AS and 2.2–4.6% of patients with MR receive SE in the diagnostic work-up for valve disease diagnosis (2). However, considering the prevalence of frail and severely compromised patients with both MR and AS undergoing transcatheter procedures (6, 7), the use of SE before TAVI or TEER implantation could potentially represent an additional tool leading to a better patient selection. In this context, however, it is important to mention that the presence of concomitant significant MR in patients with LFLG AS worsens the low-flow state, resulting in a reduced forward stroke volume (9). Nonetheless, given its potential positive impact, we performed a systematic review of the literature on the applications of SE in candidates for percutaneous procedures for the treatment of MR and AS. The aim was to highlight the most relevant applications of this diagnostic tool in the

contemporary population of patients with heart valve disease who are candidates for TAVI or TEER.

Methods

Search strategy and selection criteria

We performed a systematic review of literature following the Preferred Reporting Items for Systematic reviews and Meta-Analyses (PRISMA) statement, updated to 2021 version (10). We included studies regarding the use of SE in (i) candidates for percutaneous procedures for AS (TAVI) or (ii) of MR (TEER). Accordingly, the following terms using Medical subject heading (MeSH) strategy were searched: “(stress echo or contractile reserve or dobutamine) and (TAVI OR TAVR),” “(stress echocardiography or dobutamine echocardiography or exercise echocardiography) and (Mitraclip or (transcatheter mitral valve repair) or (transcatheter edge-to-edge repair) or (TEER) OR (TMVR).” The databases analyzed were PubMed, Biomed Central, Web of Science, Cochrane Library. The literature search was carried out in February 2022. Only full-text article published in English and in peer-reviewed journals were selected. The inclusion criteria of the studies were: observational, clinical trials or meta-analysis involving patients with AS or MR evaluated with SE (excluding those in which SE was used only for screening of pseudo-severe stenosis) and treated with percutaneous procedures. Exclusion criteria: (i) abstract or posters; (ii) reviews or editorials; (iii) rationale and study protocols. The main aim of the systematic review is to summarize relevant studies exploring the role of SE in candidates for TAVI or TEER in defining diagnosis of valvular disease severity and prognosis before or after percutaneous valvular treatment. No limitation in the number of patients included was applied. Literature search, screening of the literature and quality appraisal of selected items was performed by two independent reviewers (GF and NB). Divergences have been solved by discussion and consensus. In case of discordance a third reviewer (RP) was asked to solve the disagreement and reach consensus. The quality of the included studies has been assessed using pre-specified electronic forms



of MINORS criteria (11). The minimum score obtained was 16 and the maximum was 20. No studies were excluded based on quality assessment.

Results

Search strategy

Overall, 161 studies were selected (Figure 1).

After a first evaluation, 38 records were screened and of these, 25 were excluded for varied reasons (Figure 1). Finally, 13 studies published between 2013 and 2021 were included in the review (Table 1). In particular five concerned candidates for TEER (349 patients), while eight included candidates for TAVI (895 patients). We presented the results of the systematic review, answering questions related to the use of SE in TAVI and TEER candidates (Tables 1, 2).

Stress echocardiography in candidates for transcatheter edge-to-edge repair

Velu et al. (12) showed that patients undergoing SE before TEER ($n = 36$) might have a dual response: in case of MR

reduction during SE patients remained in NYHA III–IV or died within 6 months, while 62% (18 out of 29) of the patients with stable or increased MR during SE had clinical benefit ($p = 0.008$), above all in terms of quality of life if an increase in stroke volume during SE in seen (12). Curio et al. (13) instead compared the outcome of 55 patients with moderate MR that become severe during SE with patients with severe MR at rest ($n = 166$), showing that the combined end-point of all-cause death and hospitalization was significantly worst in patients with severe MR at rest. Izumo et al. (14) showed that patients with moderate MR that become severe during SE ($n = 46$) reported a higher event-free survival rate if treated with TEER rather than if medically managed after a 13-month follow-up period (log-rank $p = 0.017$). However, the Cox proportional-hazard analysis suggested that in case of TEER treatment the composite endpoint of all-cause mortality and hospitalization for HF occurred more frequently (hazard ratio: 0.419, $p = 0.044$) (14). Finally, regarding the effect of TEER on mitral valve function, Paranskaya et al. (15), performed dobutamine SE after TEER in 20 patients showing that both mean *trans*-mitral pressure gradient (TPG) (3.3 ± 0.8 mmHg vs. 4.0 ± 0.6 mmHg; $p < 0.001$) and mitral valve orifice area (2.9 ± 0.3 cm² vs. 3.9 ± 0.4 cm²; $p < 0.001$) were significantly increased during SE, as well as LVEF ($41 \pm 18\%$ vs. $46 \pm 21\%$; $p < 0.001$) and systolic pulmonary artery pressure (sPAP) (42 ± 11 mmHg vs.

TABLE 1 Studies on SE in candidates for TEER.

References	Study type	N	Role of SE	Type of MR	Stress used	Outcome
Velu et al. (12)	Prospective	39	Assessment of MR grade and LV function during stress before TEER	50% secondary MR	Handgrip or low dose dobutamine	SV increase >40% was associated with better quality of life [improvement on 4/8 subscales of RAND Short Form-36 on Quality of Life was observed: Physical Functioning ($p < 0.001$), Social Functioning ($p < 0.001$), Mental Health ($p = 0.022$) and Vitality ($p = 0.026$)]. Decreased MR grade during SE was associated with worse outcome after TEER ($p = 0.008$).
Curio et al. (13)	Retrospective	221	Verify presence of severe exercise-induced MR	77% secondary MR (75% of severe MR and 84% of moderate MR)	Handgrip	Patients with severe exercise-induced MR may be a group with earlier stage of disease that can benefit from TEER (mortality rate after 2 years of severe exercise-induced MR and severe resting MR were similar with log rank $p = 0.16$). The combined end-point of all-cause death and hospitalization was significantly worst in patients with severe MR at rest (log rank $p = 0.01$). Previous HF hospitalization (log rank $p < 0.01$) and large LVEDd >53.5 mm (AUC 0.696 $p < 0.001$; sensitivity 86% specificity 54%; log rank $p < 0.001$ for cut-off) are prognostic factors.
Izumo et al. (14)	Case-control	46	Verify presence of severe exercise-induced MR	100% secondary MR	Bicycle ergometer	Patients treated with TEER had better event-free survival rate than the ones treated with medical therapy (log rank $p = 0.017$). LVEF during stress (HR 0.919; $p = 0.028$) and TEER procedure (HR 0.419; $p = 0.044$) were independently associated with the composite endpoint of all-cause mortality and hospitalization for HF.
Paranskaya et al. (15)	Prospective	20	Evaluation IMS after multiple TEER	60% secondary 40% primary/mixed	Full-dose dobutamine	During SE, the mean transvalvular gradient increases (3.3 ± 0.8 mmHg vs. 4.0 ± 0.6 mmHg; $p < 0.001$), along with MVOA (2.9 ± 0.3 cm ² vs. 3.9 ± 0.4 cm ² ; $p < 0.001$). These results confirm the preserved pliability and elasticity of the valve even after multiple clips implantation.
Boerlage-van Dijk et al. (16)	Retrospective	23	Evaluation presence of IMS after successful TEER	26% degenerative; 74% secondary	Bicycle ergometer	PHT is the only intraprocedural parameter associated with mean transvalvular gradient after TEER with a cut-off of 91 ms (AUC 0.8 $p < 0.001$). During SE, MTDG (from 3.6 ± 1.7 to 6.3 ± 2.7 mmHg, $n = 23$, $p < 0.001$) and sPAP (from 35 ± 12 mmHg to 47 ± 7 mmHg, $n = 23$, $p = 0.035$) increased significantly, but without signs or symptoms of HF or increased BNP levels.

BNP, none natriuretic peptide; HF, heart failure; IMS, iatrogenic mitral stenosis; LV, left ventricular; LVEDd, left ventricular end diastolic diameter; MR, mitral regurgitation; MTDG, mean transvalvular diastolic gradient; MVOA, mitral valve orifice area; PHT, pressure half time; SE, stress echocardiography; sPAP, systolic pulmonary artery pressure; SV, stroke volume; N, number of patients; TEER, transcatheter edge to edge repair.

44 ± 12 mmHg; $p = 0.014$). The degree of MR was stable during stress ($p = 0.68$) (15). Boerlage-van Dijk et al. (16) obtained similar results in terms of increased TPG during SE (from 3.6 ± 1.7 to 6.3 ± 2.7 mmHg, $n = 23$, $P < 0.001$), but also demonstrated that higher TPG and sPAP did not lead to more symptoms of heart failure (16) (Table 1).

Stress echocardiography in transcatheter aortic valve implantation patients

Hayek et al. (8) showed that in 49 patients with LFLG AS, more than a half (55%) did not have CR and that these patients had worse short- and intermediate-term survival compared with

those with CR (log rank $p = 0.029$). Thirty-day mortality was 21 vs. 5%, 1-year mortality 30 vs. 9%, and 2-year mortality 46 vs. 26% compared with those with CR ($p < 0.001$). As opposite, Ribeiro et al. (17) showed that the 45% of 234 patients enrolled in the True or Pseudo-Severe Aortic Stenosis-TAVI registry (TOPAS-TAVI) Registry with LFLG AS had CR, however, the absence of CR at baseline dobutamine SE was not associated with any negative effect on clinical outcomes (30 days, 1 and 2 years mortality) or LVEF changes at follow-up (17). The same results were found by Buchanan et al. (18) (all-cause mortality at 30 days: 13% with CR vs. 10% without CR, $p = 1.00$ and 1 year mortality: 29% with CR vs. 33% without CR, HR 1.20, 95% CI 0.49–2.96, $p = 0.69$) (18) and Sato et al. (19). Maes et al. (20) confirmed that the absence of CR had no effect on clinical outcomes or changes in LVEF over time also in a subgroup of

TOPAS-TAVI registry of 92 patients with LVEF < 30% (20). Barbash et al. (21) in 61 patients with LFLG AS undergoing TAVI showed that CR assessed with dobutamine SE did not predict LVEF recovery but did predict lower mortality (21). Saevik et al. (22) demonstrated safety and feasibility of low-dose dobutamine SE in 50 patients with high gradient AS, showing reduced CR in 40% of them (22). Finally D'Andrea et al. (23) showed that a cutoff value for left ventricle global longitudinal strain (LV GLS) of $> -12\%$ well distinguished patients without significant CR and with lack of positive remodeling after TAVI at follow-up (23) (Table 2).

Discussion

Stress echocardiography in candidates for transcatheter edge-to-edge repair

How can stress echocardiography help the clinician select transcatheter edge-to-edge repair candidates?

To understand the potential usefulness of SE in patients undergoing TEER, it is necessary to consider the lessons learned from the Cardiovascular Outcomes Assessment of the Mitraclip Percutaneous Therapy for Heart Failure Patients with Functional Mitral Regurgitation (COAPT) trial (24), and the Percutaneous Repair with the Mitraclip Device for Severe Functional/Secondary Mitral Regurgitation (MITRA-FR) trial (25), both contributing to the elaboration of the concept of proportionate and disproportionate MR (26). This concept helped clinicians distinguish to what extent symptoms are caused by the amount of MR or by left ventricular dysfunction (26). In this context, SE might be useful to evaluate (i) the changes of the left ventricle functional reserve during stress; (ii) the variation of MR grade during exercise; (iii) the changes in pulmonary pressures; (iv) the onset of symptoms in relation to hemodynamical changes. These measurements can change the decisional process that leads to an indication for TEER (Figure 2).

In a small prospective study ($n = 36$), Velu et al. (12) enrolled patients who underwent SE with handgrip and/or dobutamine before successful TEER with Mitraclip (50% secondary MR). The aim of the study was to evaluate which parameters were associated with mortality or NYHA class $>II$ in a 6-month follow-up. The endpoint occurred in 18 patients (50%). The seven patients with decreased MR grade during SE remained in NYHA III-IV or died within 6 months, while 62% of patients with stable or increased MR grade during SE reported clinical benefits ($p = 0.008$) (12). A left ventricular stroke volume increase of $>40\%$ during stress was associated with an increased quality of life after the procedure, and patients who did not achieve this goal had a higher heart rate during stress and rest (12). The study shows that if MR is maintained during SE, the

patient's outcome is better. In fact, the absence of an increase in stroke volume during SE is related to a critical dysfunction of the left ventricle, which cannot adapt stroke volume to stress, resulting in an increase in heart rate to compensate for the lack of positive inotropism (12). At the same time, a decreased grade of MR during SE is indicative of the fact that MR is a minor determinant of the patient symptoms during exercise compared to the abnormal left ventricle function (12). The study of Velu et al. (12) also showed that the endpoint occurred in a high number of patients (50%), reflecting the severity of the underlying disease.

Curio et al. (13) tried to understand if SE might be useful in selecting patients at an early stage of the disease, thus truly benefiting from TEER (77% of patients with secondary MR). This retrospective study (13) ($n = 221$) explored the effect of TEER treatment in patients with handgrip-induced severe MR and patients with severe MR at rest. Patients with handgrip-induced severe MR were considered as having an earlier stage of the disease. The primary endpoint was all-cause mortality and HF hospitalization in a follow-up of 2 years (13). Patients with severe MR at rest had a significantly lower left ventricular ejection fraction (LVEF), larger left ventricle end-diastolic diameter (LVEDd) and larger left atrial volumes compared to patients with severe handgrip-induced MR (13). However, MR improvement after TEER was greater in patients with severe resting MR, even if it was significant in both groups, resulting in a reduction of systolic pulmonary artery pressure (sPAP) after procedure (13). The 2-year mortality rate was 4% in patients with handgrip-induced severe MR and 8% in patients with severe resting MR (13). Patients with severe resting MR suffered more frequently from the combined endpoint ($p = 0.01$), and the difference was driven by HF hospitalization ($p = 0.02$). However, in both groups, a significant reduction of HF hospitalizations in the 2 years after the procedure compared with the 2 years before the procedure was achieved (13). Independent predictors of worse outcomes were preprocedural hospitalization for HF ($p < 0.01$) and larger LVEDd with a cutoff of 53 mm (AUC 0.696, sensitivity 86%, specificity 54%) (13). Patients with residual MR greater than mild showed a worse 2-year outcome (13). These results suggest that in patients at an early stage of MR disease, the outcome after the TEER procedure is better (13). However, it does not explain whether MR severity itself or LV remodeling caused by MR are responsible for the prognostic divergence between groups.

In another study, Izumo et al. (14) enrolled patients ($n = 46$) with exercise-induced MR (defined as an increase in effective regurgitant orifice area (EROA) $\geq 0.13 \text{ cm}^2$ during semi-supine bicycle ergometer), which have been then treated with TEER or with conservative management (14). All patients enrolled had secondary MR. At baseline, patients had an EROA of $0.26 \pm 0.10 \text{ cm}^2$ and $0.20 \pm 0.08 \text{ cm}^2$, and a regurgitant volume of $42 \pm 13 \text{ ml}$ and $33.6 \pm 13.6 \text{ ml}$ in the TEER group compared to those treated with conservative management, respectively.

TABLE 2 Studies on SE in candidates for TAVI.

References	Study type	N	Role of SE	Stress used	Outcome
Hayek et al. (8)	Retrospective	49	Assessment of contractile reserve	Low-dose dobutamine	30-day mortality is lower in LFLGAS patients with CR prior to TAVI Long term mortality is lower in LFLGAS patients with CR prior to TAVI (HR: 4.47; $p = 0.037$)
Ribeiro et al. (17)	Prospective	234	Assessment of contractile reserve	Low-dose dobutamine	There are no differences in 30-day mortality in LFLGAS patients with or without CR prior to TAVI, although in those with CR mortality tends to be lower (1.2 vs. 5.6% in patients with and without contractile reserve, respectively; $p = 0.13$) There are no differences in long term mortality in LFLGAS patients with or without CR prior to TAVI (28.7 vs. 35.3% in patients with and without contractile reserve, respectively, Log Rank: $p = 0.704$) CR failed to predict LVEF recovery in LFLGAS patients after TAVI Mortality after TAVI in LFLGAS patients is lower than reported in SAVR studies
Buchanan et al. (18)	Retrospective	61	Assessment of contractile reserve	Full dose dobutamine	There are no differences in 30-day mortality in LFLGAS patients with or without CR prior to TAVI (13% in patients with CR vs. 10% in patients without CR; $p = 1.00$) There are no differences in long term mortality in LFLGAS patients with or without CR prior to TAVI (29% in patients with CR vs. 33% in patients without CR; $p = 0.72$) SVi increased significantly after TAVI only in LFLGAS patients with CR prior to TAVI (35% in the group with CR vs. 29% in the group without CR; $p = 0.04$) CR failed to predict LVEF recovery in LFLGAS patients after TAVI (10 vs. 10% in the group with CR and group without CR, respectively, $p = 0.76$)
Sato et al. (19)	Prospective	235	Assessment of contractile reserve	Low-dose dobutamine	LFLGAS with reduced EF, CR or AS severity stratification performed by dobutamine stress echocardiography is not associated with survival nor in patients treated with SAVR nor in those treated with TAVI (HR: 1.09; 95% CI 0.78–1.53; $p = 0.62$)
Maes et al. (20)	Prospective	92	Assessment of contractile reserve	Low-dose dobutamine	There are no differences in 30-days mortality in LFLGAS patients with very low LVEF with or without CR prior to TAVI, although in those with CR mortality tends to be lower (HR 0.47 95% CI 0.04–5.34; $p = 0.54$) There are no differences in long term mortality in LFLGAS patients with very low LVEF with or without CR prior to TAVI (HR 1.37 95% CI 0.58–3.26; $p = 0.47$) CR failed to predict LVEF recovery in LFLGAS patients with very low LVEF after TAVI (mean [SD] relative increase of 27% [35%] vs. 26% [42%]; $p = 0.95$)
Barbash et al. (21)	Prospective	99	Assessment of contractile reserve	Full dose dobutamine	There are no differences in 30-day mortality in LFLGAS patients with or without CR prior to TAVI, although in those with CR mortality tends to be lower (6.25% in patients with CR vs. 30% in patients without CR; $p = 0.26$) There are no differences in long term mortality in LFLGAS patients with or without CR prior to TAVI (25% in patients with CR vs. 40% in patients without CR; $p = 0.41$) CR failed to predict LVEF recovery in LFLGAS patients after TAVI (30% in patients with CR vs. 57% in patients without CR; $p = 0.35$)
Saevik et al. (22)	Prospective	50	Assessment of contractile reserve Safety and feasibility of the exam	Low-dose dobutamine	CR was found in a lower proportion of high-gradient AS patients than in LFLGAS patients' studies DSE is safe and feasible in high gradient AS patients
D'Andrea et al. (23)	Prospective	75	Assessment of contractile reserve	Low-dose dobutamine	LVGLS values $> -12\%$ prior to TAVI are a strong predictor of pre-procedural CR absence (multiple partial correlation coefficient = 0.6, $p < 0.00001$) and lack of post-procedural remodeling in LFLGAS patients (correlation coefficient = 0.44, $p < 0.0001$) Pre-procedural CR predicts a greater increase in LVGLS in LFLGAS patients after TAVI

AS, aortic stenosis; DSE, dobutamine stress echocardiography; CR, contractile reserve; LVEF, left ventricular ejection fraction; LVGLS, left ventricular global longitudinal strain; LFLGAS, low flow-low-gradient aortic stenosis; TAVI, transcatheter aortic valve implantation; SAVR, surgical aortic valve replacement; SVi, indexed stroke volume; SD, standard deviation.

The authors specified that the decision to treat with TEER or conservatively was left to the clinician and related to routine clinical practice. The primary endpoint was the occurrence of death and hospitalization (14). The mean follow-up was

13 months. Patients treated with TEER were older, with a higher prevalence of NYHA \geq II, smaller left ventricle and higher LVEF compared to those in the optimal medical therapy (control) group (14). However, there were no differences in

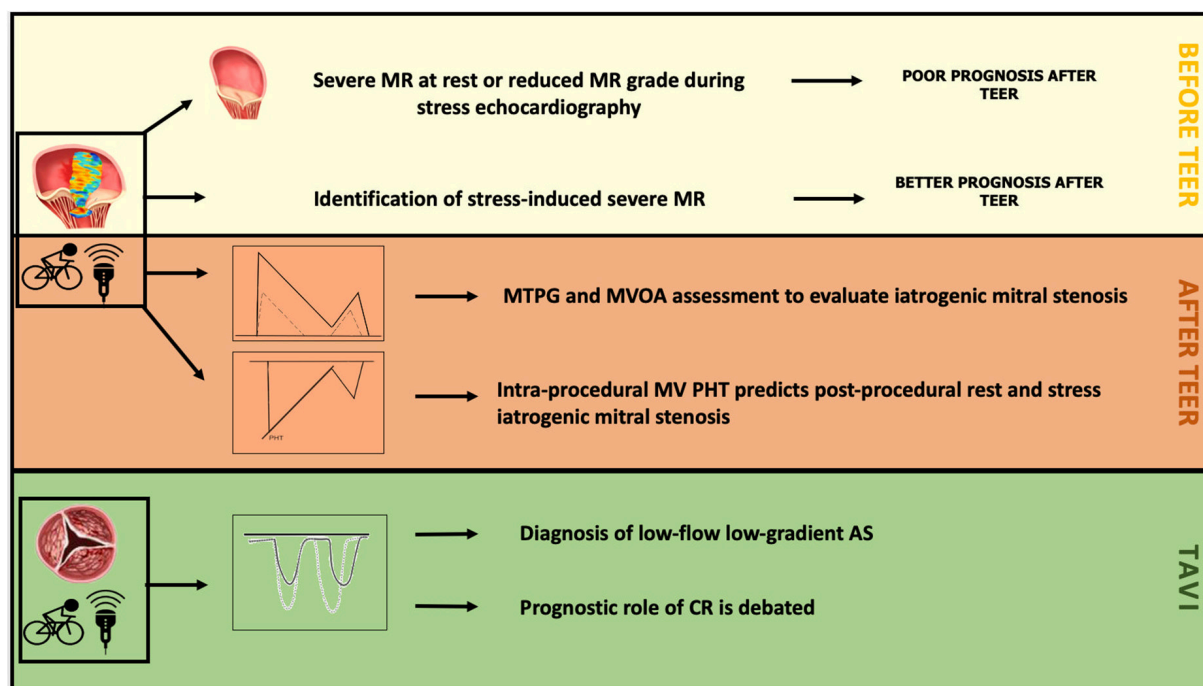


FIGURE 2

Role of stress echocardiography (SE) in TEER and TAVI. MR, mitral regurgitation; TEER, transcatheter edge-to-edge repair; TAVI, transcatheter aortic valve implantation; MVOA, mitral valve opening area; MTPG, mean *trans*-valvular pressure gradient; MV, mitral valve; PHT, pressure half-time; AS, aortic stenosis; CR, contractile reserve.

stroke volume and cardiac output between the groups. Event-free survival was higher in the TEER group (Log Rank $p = 0.017$), reaching 82% at 12 months and 56% at 24 months (14). LVEF during exercise (HR 0.919, $p = 0.028$) and TEER (HR 0.419, $p = 0.044$) were independently associated with clinical outcomes. Moreover, 25% of patients with moderate secondary MR at rest showed worsening of MR during exercise. The event-free survival of these patients was similar to those with severe MR at rest (14). These patients, who might benefit from TEER, are underestimated in clinical practice due to the underuse of SE.

In conclusion, the benefits of using SE are twofold. First, SE may help predict the outcome of patients after TEER treatment. Second, it helps identify patients with an earlier stage of the disease who may undergo TEER with a greater benefit.

How can stress echocardiography evaluate anatomical response to transcatheter edge-to-edge repair?

Transcatheter edge-to-edge repair procedure is guided by transesophageal echocardiography (TOE). TOE is necessary to choose the correct position during clip releasing and check for the presence of residual MR or excessive increase in *trans*-valvular diastolic gradient in order to avoid iatrogenic mitral stenosis (IMS) (defined by a post-TEER diastolic gradient

≥ 5 mmHg) (Figure 2) (16). The reliability of the measures of MR or IMS done during the TEER is debatable because influenced by the general anesthesia and loading conditions. Doppler measurements are operator dependent and strongly influenced by left ventricle function, left atrial compliance, and loading conditions, and real-time monitoring evaluation of left atrial pressure during TEER is proven to be able to predict the outcome independently from echocardiographic findings (27). Therefore, considering this, although SE in clinical practice is not often used in patient evaluation after TEER some authors considered it to better explain echocardiographic findings after the procedure. Boerlage-van Dijk et al. (16), in a retrospective study ($n = 51$, but only 23 underwent SE, of whom 74% with secondary MR), investigated which echocardiographic parameters were associated with iatrogenic mitral stenosis (IMS) during TEER implantation with TOE and after with SE in 13-month follow-up. During intra-procedural assessment mean *trans*valvular diastolic gradient (MTDG) was higher after the procedure than during the procedure ($p < 0.001$), while pressure half-time (PHT) did not change significantly (16). PHT was the only intraprocedural parameter that predicted post-procedural IMS with good accuracy (AUC 0.9) using a cut-off of 91 ms (16). However, during SE performed after TEER with bicycle echocardiography, MTDG and sPAP increased significantly, but

without signs or symptoms of HF or any significant difference in brain natriuretic peptide (BNP) plasma level (16). The change of these parameters after TEER was comparable to that described after surgical edge-to-edge mitral valve repair technique (16).

Finally, Paranskaya et al. (15) performed a small prospective study to evaluate the impact of multiple clips on mitral valve function and *trans*-mitral gradients. They included in the study 20 patients (60% with secondary mitral regurgitation) with residual less than moderate MR, but with increased MTDG [from 2.3 ± 0.1 (range 1.0–4.5) to 3.3 ± 0.8 (range 1.8–5.0) mmHg; $p = 0.002$] and reduced mitral valve orifice area (MVOA) [from 5.8 ± 0.9 (range 4.0–7.6) to 2.9 ± 0.3 (range 2.5–3.6) cm²; $p < 0.001$] after TEER. Under SE, both MTDG and MVOA significantly increased, supporting the hypothesis of a preserved pliability and elasticity of the valve after multiple clip implantation (15).

Stress echocardiography in transcatheter aortic valve implantation patients

How can stress echocardiography help the clinician select patients with low-flow, low-gradient aortic stenosis who are candidates for transcatheter aortic valve implantation?

As stated before, SE is the gold standard for CR assessment in patients with LFLG-AS with EF < 50% (1–8). However, the prognostic role of CR for patients who are candidates for TAVI or SAVR has been questioned due to recent data. In LFLG-AS patients undergoing SAVR, the peri-procedural risk was considered greater if CR was absent (17). Data from the Transcatheter Aortic Valve Replacement in Patients With Low-Flow, Low-Gradient Aortic Stenosis (TOPAS-TAVI) registry published by Ribeiro et al. (17) as well as the findings from the sub-analysis of Maes et al. (20) and other smaller studies (18, 21) do not confirm these results for patients undergoing TAVI, although in patients with CR there was a trend toward lower 30-day mortality (1.2 vs. 5.6% in patients with and without CR, respectively; $p = 0.13$). Reasons for that might be related to the less invasive nature of the procedure, requiring less postoperative care, and being the percutaneous procedure altogether better tolerated by the patient (18, 20). Contrastingly, Hayek et al. (8) showed that 30-day mortality was significantly lower in patients with CR treated with TAVI compared to patients without CR (5 vs. 21%, $p < 0.001$). It should also be remembered that the population of Hayek et al. (8) consisted of a small and very heterogeneous sample, also including patients with preserved left ventricular ejection fraction LVEF (23% of the sample population), while the other studies enrolled only patients with reduced LVEF (17, 18, 20, 21). Finally, Sato et al. (19) showed that in LF-LG AS with reduced ejection fraction,

CR or AS severity stratification performed by dobutamine stress echocardiography was not associated with survival, neither in patients treated with SAVR nor in those treated with TAVI (19).

In conclusion, data reveal a discordancy about the efficacy of CR in predicting the outcome in LFLG AS for both TAVI and SAVR candidates. As seen above, mortality in patients undergoing TAVI is not related to CR presence, either at 30 days (although there is a tendency for a better peri-procedural outcome in patients with CR) or at long term (17, 18, 20, 21). However, the total mortality remains lower for TAVI patients without CR compared to that reported in SAVR studies (17). Furthermore, since CR is not predictive of the outcome of TAVI patients, TAVI should not be discouraged by an absence of pre-procedural CR (17) (Figure 2). Finally, no studies specifically address how to use SE in the evaluation of patients undergoing TAVI with LFLG AS and concomitant severe MR, or specifically with LFLG AS with LVEF higher than 50% [besides the few patients enrolled in Hayek et al. (8) study].

How can stress echocardiography help the clinician select patients with high-gradient aortic stenosis who are candidates for transcatheter aortic valve implantation?

In classic high-gradient AS, SE is not usually performed and there is little data about it. Saevik et al. (22) published an initial analysis of a cohort of patients with symptomatic high-gradient AS and LVEF > 40% in which pre-procedural CR was evaluated with a low-dose DSE pre-TAVI. The aim was to evaluate the safety and feasibility of the DSE in this subset of patients and look for the presence of CR (22). Of the 50 patients enrolled, 45 (90%) completed the protocol. Only 10% of them reported minor events that caused test interruption (22). Symptoms rapidly regressed with dobutamine suspension (22).

Ten (20%) patients showed low indexed stroke volume (SV_i) before the exam (22). CR was found in 20 (40%), with an average increase in SV_i of 32%. Interestingly, no difference in the prevalence of CR between patients with low-flow and normal-flow at baseline was found nor was a relationship with NT-proBNP or diastolic parameters or mass (22). The proportion of patients with CR was lower in high-gradient AS patients than in LFLG patients, but this could be explained by a higher SV_i (43 ± 10 ml/m²) at baseline and by the presence of preserved LVEF (baseline LVEF 66%) (22).

Can contractile reserve predict long-term outcome in low-flow, low-gradient patients undergoing transcatheter aortic valve implantation?

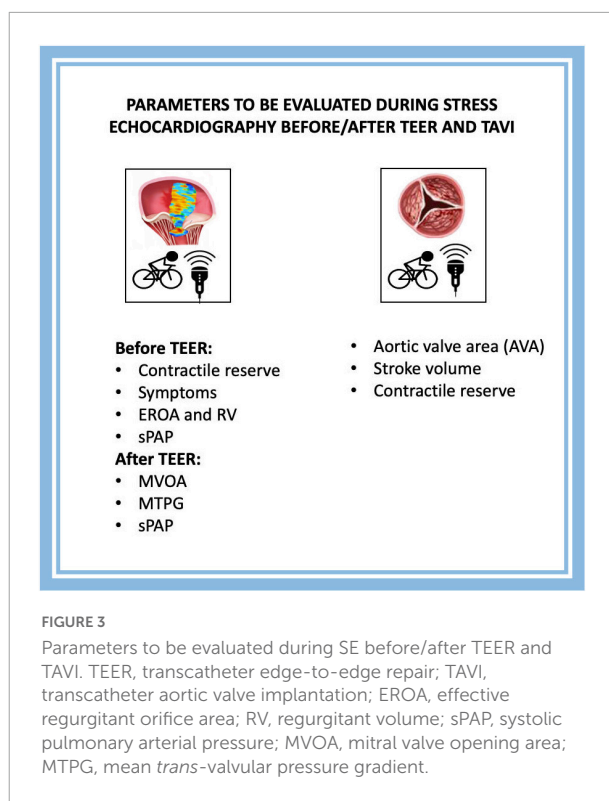
Several studies tried to correlate the long-term outcome of LFLG patients undergoing TAVI with the presence of CR at pre-procedure dobutamine SE (DSE), but the results are conflicting (17, 18, 20, 21).

Barbash et al. (21) showed how the advantage in terms of reduced mortality changes over time in patients with CR, progressively decreasing until reaching an overlap of the two mortality curves in patients with and without CR. Similarly, both in the TOPAS-TAVI registry (with a mean follow-up of 21 months), and in the Buchanan et al. study (follow-up = 12 months), patients with LVEF < 30% showed the absence of a significative correlation between the presence of pre-procedural CR and long-term mortality (17, 18, 20, 21).

Discordant results come from the Hayek et al. (8) study, where 81% of the dead patients did not show CR at the pre-procedure DSE (1-year mortality 30 vs. 9% and 2-year mortality 46 vs. 26% of the CR group vs. no-CR group, respectively, $p < 0.001$) (8). As pointed out by Ribeiro et al. (17), however, a large part of long-term deaths in patients undergoing TAVI are non-cardiac, and mainly due to comorbidities, such as chronic obstructive pulmonary disease (COPD), or pre-operative anemia (mainly driven by iron deficiency). Considering this, it is important to note that in the Hayek et al. (8) study the only significant difference between the two groups stratified by the presence of CR at the baseline was precisely the higher prevalence of COPD in patients without CR (63 vs. 32%; $p = 0.030$). This may be enough to explain the higher mortality, despite the multivariate analysis showing both COPD and CR as independent predictors of mortality (8, 17). After TAVI, Anjan et al. (28) demonstrated that an increase in SVi is related to an improvement in 1-year survival. Buchanan et al. (18) showed that SVi significantly increases after TAVI only in patients with CR. In this setting, DSE demonstrated low ($\leq 65\%$) specificity and sensitivity in predicting it (28). Finally, left ventricular global longitudinal strain (LVGLS) was analyzed as a parameter useful to predict the presence of CR and the post-TAVI reverse remodeling (23), showing that a pre-procedural LVGLS > -12% was a strong predictor of pre-procedural CR absence (sensitivity 84%; specificity 93%; AUC 0.92 [95% CI, 0.86–0.99], $p < 0.00001$) and lack of post-procedural remodeling ($p < 0.0001$) (23). A greater increase in the absolute value of LVGLS after TAVI has been highlighted in patients with pre-procedure CR (+3.9%, $p < 0.0001$ vs. + 2.3%, $p = 0.01$) (23).

Clinical perspectives and limitations of systematic review

The main limitations of studies about the use of SE in candidates for TAVI or TEER are related to the small size of the samples, the absence of randomized design, and not standardized SE protocols. Considering all of this, a formal meta-analysis of data was not possible. When using SE in candidates for TEER we expect (Figure 3)



the confirmation of indication through the evaluation of symptoms during stress, and the quantification of worsening of MR or elevated sPAP. We also expect to test the possible positive effect of TEER mainly with CR assessment. After TEER in case of IMS, SE is of paramount importance to understand if the increased MTPG is or not related to HF.

Regarding candidates for TAVI, the only clear indication to SE is in the context of LFLG AS to confirm a diagnosis of stenosis (Figure 3). The role of CR is still uncertain and not necessary for an indication to TAVI. New trials are needed to understand if SE might be relevant also for patients with paradoxical low-flow, low-gradient AS or with combined valvular disease (e.g., MR and AS).

Conclusion

This systematic review shows that there are few studies analyzing the role of SE in candidates for TAVI and TEER. In a TEER context, SE is useful before TEER and in patients with secondary mitral regurgitation for two reasons. First, to identify patients developing severe MR during SE who are in an early phase of the disease and might benefit from an earlier intervention. Second, to identify patients with reduced CR and

MR who have more advanced disease and poor prognosis. Conversely, in TAVI candidates, the role of SE is limited to confirming the severity of the diagnosis in the case of LFLG AS and reduced LVEF (as established by recommendations). New studies are needed to better explore the role of SE after TEER and verify if SE might be relevant also for patients with paradoxical low-flow, low-gradient AS, or with combined valvular disease.

Data availability statement

The original contributions presented in this study are included in the article/supplementary material, further inquiries can be directed to the corresponding author.

Author contributions

RP, ET, GP, and GC: conception, design, analysis, and interpretation of data. GF, NB, FS, MD, LZ, RP, GC, and MS: drafting of the manuscript and revising it critically for important

intellectual content. MS, GC, and RP: drafting of the manuscript and revising it critically for important intellectual content, data collection, and verification of data. All authors contributed to the final approval of the manuscript submitted.

Conflict of interest

The authors declare that the research was conducted in the absence of any commercial or financial relationships that could be construed as a potential conflict of interest.

Publisher's note

All claims expressed in this article are solely those of the authors and do not necessarily represent those of their affiliated organizations, or those of the publisher, the editors and the reviewers. Any product that may be evaluated in this article, or claim that may be made by its manufacturer, is not guaranteed or endorsed by the publisher.

References

- Vahanian A, Beyersdorf F, Praz F, Milojevic M, Baldus S, Bauersachs J, et al. ESC/EACTS scientific document group; ESC scientific document group. 2021 ESC/EACTS guidelines for the management of valvular heart disease. *Eur Heart J*. (2021) 43:ehab395. doi: 10.1093/eurheartj/ehab395
- Iung B, Delgado V, Rosenhek R, Price S, Prendergast B, Wendler O, et al. Contemporary presentation and management of valvular heart disease: the EURObservational research programme valvular heart disease II survey. *Circulation*. (2019) 140:1156–69. doi: 10.1161/CIRCULATIONAHA.119.041080
- Flint N, Price MJ, Little SH, Mackensen GB, Wunderlich NC, Makar M, et al. State of the art: transcatheter edge-to-edge repair for complex mitral regurgitation. *J Am Soc Echocardiogr*. (2021) 34:1025–37. doi: 10.1016/j.echo.2021.03.240
- Masson JB, Kovac J, Schuler G, Ye J, Cheung A, Kapadia S, et al. Transcatheter aortic valve implantation: review of the nature, management, and avoidance of procedural complications. *JACC Cardiovasc Interv*. (2009) 2:811–20.
- Lancellotti P, Pellikka P, Budts W, Chaudhry FA, Donal E, Dulgheru R, et al. The clinical use of stress echocardiography in non-ischaemic heart disease: recommendations from the European Association of Cardiovascular Imaging and the American Society of Echocardiography. *Eur Heart J Cardiovasc Imaging*. (2016) 17:1191–229.
- Solla-Suárez P, Avanzas P, Pascual I, Bermúdez-Menéndez De La Granda M, Almendarez M, Arche-Coto JM, et al. Frailty assessment in a cohort of elderly patients with severe symptomatic aortic stenosis: insights from the frailty evaluation in severe aortic stenosis (FRESAS) registry. *J Clin Med*. (2021) 10:2345. doi: 10.3390/jcm10112345
- Metze C, Matzik AS, Scherner M, Körber MI, Michels G, Baldus S, et al. Impact of frailty on outcomes in patients undergoing percutaneous mitral valve repair. *JACC Cardiovasc Interv*. (2017) 10:1920–9. doi: 10.1016/j.jcin.2017.07.042
- Hayek S, Pibarot P, Harzand A, Cheng JW, Gay H, Chrysoshoou C, et al. Dobutamine stress echocardiography for risk stratification of patients with low-gradient severe aortic stenosis undergoing TAVR. *JACC Cardiovasc Imaging*. (2015) 8:380–2. doi: 10.1016/j.jcmg.2014.09.012
- Katte F, Franz M, Jung C, Figulla HR, Leistner D, Jakob P, et al. Impact of concomitant mitral regurgitation on transvalvular gradient and flow in severe aortic stenosis: a systematic ex vivo analysis of a subentity of low-flow low-gradient aortic stenosis. *EuroIntervention*. (2018) 13:1635–44. doi: 10.4244/EIJ-D-17-00476
- Page MJ, McKenzie JE, Bossuyt PM, Boutron I, Hoffmann TC, Mulrow CD, et al. The PRISMA 2020 statement: an updated guideline for reporting systematic reviews. *BMJ*. (2021) 372:n71.
- Slim K, Nini E, Forestier D, Kwiatkowski F, Panis Y, Chipponi J. Methodological index for non-randomized studies (minors): development and validation of a new instrument. *ANZ J Surg*. (2003) 73:712–6. doi: 10.1046/j.1445-2197.2003.02748.x
- Velu JF, Baan J, de Bruin-Bon H, van Mourik MS, Nassif M, Koch KT, et al. Can stress echocardiography identify patients who will benefit from percutaneous mitral valve repair? *Int J Cardiovasc Imaging*. (2019) 35:645–51. doi: 10.1007/s10554-018-1507-x
- Curio J, Tarar W, Al-Hindwan HSA, Neumann R, Berger C, Hoting M-O, et al. The mitralclip procedure in patients with moderate resting but severe exercise-induced mitral regurgitation. *J Invasive Cardiol*. (2020) 32:E1–8.
- Izumo M, Kuwata S, Ishibashi Y, Suzuki T, Ohara H, Watanabe M, et al. Prognostic impact of transcatheter mitral valve repair in patients with exercise-induced secondary mitral regurgitation. *Eur Heart J Cardiovasc Imaging*. (2021) 22:530–8. doi: 10.1093/ehjci/jeaa200
- Paranskaya L, D'Ancona G, Bozdog-Turan I, Kische S, Akin I, Turan GR, et al. Mitral valve repair using multiple Mitraclips®: a dobutamine stress echocardiography evaluation. *EuroIntervention*. (2013) 8:1372–8.
- Boerlage-van Dijk K, van Riel A, de Bruin-Bon R, Wiegerinck EMA, Koch KT, Vis MM, et al. Mitral inflow patterns after mitralclip implantation at rest and during exercise. *J Am Soc Echocardiogr*. (2014) 27:24–31.e1. doi: 10.1016/j.echo.2013.09.007
- Ribeiro HB, Lerakis S, Gilard M, Cavalcante JL, Makkar R, Herrmann HC, et al. Transcatheter aortic valve replacement in patients with low-flow, low-gradient aortic stenosis: the TOPAS-TAVI registry. *J Am Coll Cardiol*. (2018) 71:1297–308.
- Buchanan KD, Rogers T, Steinvil A, Koifman E, Xu L, Torguson R, et al. Role of contractile reserve as a predictor of mortality in low-flow, low-gradient severe aortic stenosis following transcatheter aortic valve replacement. *Catheter Cardiovasc Interv*. (2019) 93:707–12. doi: 10.1002/ccd.27914
- Sato K, Sankaramangalam K, Kandregula K, Bullen JA, Kapadia SR, Krishnaswamy A, et al. Contemporary outcomes in low-gradient aortic stenosis patients who underwent dobutamine stress echocardiography. *J Am Heart Assoc*. (2019) 8:e011168. doi: 10.1161/JAHA.118.011168
- Maes F, Lerakis S, Barbosa Ribeiro H, Gilard M, Cavalcante JL, Makkar R, et al. Outcomes from transcatheter aortic valve replacement in patients with low-flow, low-gradient aortic stenosis and left ventricular ejection fraction less than 30%: a substudy from the TOPAS-TAVI registry. *JAMA Cardiol*. (2019) 4:64–70. doi: 10.1001/jamacardio.2018.4320

21. Barbash IM, Minha S, Ben-Dor I, Dvir D, Magalhaes MA, Torguson R, et al. Relation of preprocedural assessment of myocardial contractility reserve on outcomes of aortic stenosis patients with impaired left ventricular function undergoing transcatheter aortic valve implantation. *Am J Cardiol.* (2014) 113:1536–42. doi: 10.1016/j.amjcard.2014.01.433
22. Sævik M, Beitnes JO, Aaberge L, Halvorsen PS. Safety and feasibility of dobutamine stress echocardiography in symptomatic high-gradient aortic stenosis patients scheduled for transcatheter aortic valve implantation. *J Clin Ultrasound.* (2021) 49:38–48. doi: 10.1002/jcu.22915
23. D'Andrea A, Carbone A, Agricola E, Riegler L, Sperlongano S, Tocci G, et al. Predictive value of left ventricular myocardial deformation for left ventricular remodeling in patients with classical low-flow, low-gradient aortic stenosis undergoing transcatheter aortic valve replacement. *J Am Soc Echocardiogr.* (2019) 32:730–6. doi: 10.1016/j.echo.2019.03.002
24. Stone GW, Lindenfeld J, Abraham WT, Kar S, Lim DS, Mishell JM, et al. Transcatheter mitral-valve repair in patients with heart failure. *N Engl J Med.* (2018) 379:2307–18.
25. Obadia J-F, Messika-Zeitoun D, Leurent G, Iung B, Bonnet G, Piriou N, et al. Percutaneous repair or medical treatment for secondary mitral regurgitation. *N Engl J Med.* (2018) 379:2297–306.
26. Grayburn PA, Sannino A, Packer M. Proportionate and disproportionate functional mitral regurgitation: a new conceptual framework that reconciles the results of the MITRA-FR and COAPT trials. *JACC Cardiovasc Imaging.* (2019) 12:353–62. doi: 10.1016/j.jcmg.2018.11.006
27. Kuwata S, Taramasso M, Czopak A, Luciani M, Pozzoli A, Ho E, et al. Continuous direct left atrial pressure: intraprocedural measurement predicts clinical response following MitraClip therapy. *JACC Cardiovasc Interv.* (2019) 12:127–36. doi: 10.1016/j.jcin.2018.07.051
28. Anjan VY, Herrmann HC, Pibarot P, Stewart WJ, Kapadia S, Tuzcu EM, et al. Evaluation of flow after transcatheter aortic valve replacement in patients with low-flow aortic stenosis: a secondary analysis of the PARTNER randomized clinical trial. *JAMA Cardiol.* (2016) 1:584. doi: 10.1001/jamacardio.2016.0759



OPEN ACCESS

EDITED BY

Masaki Izumo,
St. Marianna University School
of Medicine, Japan

REVIEWED BY

Eiji Yamashita,
Gunma Prefectural Cardiovascular
Center, Japan
Jun Tanaka,
Mitsui Memorial Hospital, Japan

*CORRESPONDENCE

Ludmiła Daniłowicz-Szymanowicz
ludmila.danilowicz-szymanowicz@
gumed.edu.pl

SPECIALTY SECTION

This article was submitted to
Cardiovascular Imaging,
a section of the journal
Frontiers in Cardiovascular Medicine

RECEIVED 30 September 2022

ACCEPTED 31 October 2022

PUBLISHED 30 November 2022

CITATION

Kaufmann D, Wabich E,
Kapton-Cieślicka A, Gawatko M,
Budnik M, Uziębło-Życzkowska B,
Krzesiński P, Starzyk K,
Wożakowska-Kapton B, Wójcik M,
Błaszczak R, Hiczekiewicz J,
Budzianowski J, Mizia-Stec K,
Wybraniec MT, Kosmala K,
Fijałkowski M, Szymańska A,
Dłużniewski M, Haberk M, Kucio M,
Michalski B, Kupczyńska K,
Tomasz-Kazberuk A,
Wilk-Sledziowska K,
Wachnicka-Truty R, Kozłowski M,
Burchardt P and
Daniłowicz-Szymanowicz L (2022)
Echocardiographic predictors
of thrombus in left atrial
appendage—The role of novel
transthoracic parameters.
Front. Cardiovasc. Med. 9:1059111.
doi: 10.3389/fcvm.2022.1059111

Echocardiographic predictors of thrombus in left atrial appendage—The role of novel transthoracic parameters

Damian Kaufmann¹, Elżbieta Wabich¹,
Agnieszka Kapton-Cieślicka^{2,3}, Monika Gawatko^{2,3,4,5},
Monika Budnik^{2,3}, Beata Uziębło-Życzkowska⁶,
Paweł Krzesiński^{2,6}, Katarzyna Starzyk⁷,
Beata Wożakowska-Kapton⁷, Maciej Wójcik⁸,
Robert Błaszczak⁸, Jarosław Hiczekiewicz^{9,10},
Jan Budzianowski^{9,10}, Katarzyna Mizia-Stec^{2,11},
Maciej T. Wybraniec^{2,11}, Katarzyna Kosmala¹²,
Marcin Fijałkowski^{2,13}, Anna Szymańska^{2,14},
Mirosław Dłużniewski¹⁴, Maciej Haberk^{2,15}, Michał Kucio¹⁵,
Błażej Michalski^{2,16}, Karolina Kupczyńska^{2,16},
Anna Tomasz-Kazberuk^{2,17}, Katarzyna Wilk-Sledziowska^{2,17},
Renata Wachnicka-Truty¹⁸, Marek Kozłowski^{2,18},
Paweł Burchardt^{2,19} and Ludmiła Daniłowicz-Szymanowicz^{1*}

¹Department of Cardiology and Electrotherapy, Medical University of Gdańsk, Gdańsk, Poland,

²“Club 30,” Polish Cardiac Society, Warsaw, Poland, ³1st Chair and Department of Cardiology, Medical University of Warsaw, Warsaw, Poland, ⁴West German Heart and Vascular Centre, Institute of Pharmacology, University of Duisburg-Essen, Essen, Germany, ⁵Department of Cardiology, Maastricht University Medical Centre, Cardiovascular Research Institute Maastricht, Maastricht, Netherlands, ⁶Department of Cardiology and Internal Diseases, Military Institute of Medicine, Warsaw, Poland, ⁷1st Clinic of Cardiology and Electrotherapy, Świętokrzyskie Cardiology Centre, Collegium Medicum Jan Kochanowski University, Kielce, Poland, ⁸Department of Cardiology, Medical University of Lublin, Lublin, Poland, ⁹Clinical Department of Cardiology, Nowa Sól Multidisciplinary Hospital, Nowa Sól, Poland, ¹⁰Collegium Medicum, Department of Interventional Cardiology and Cardiac Surgery, University of Zielona Góra, Zielona Góra, Poland, ¹¹1st Department of Cardiology, School of Medicine in Katowice, Medical University of Silesia, Katowice, Poland, ¹²Department of Cardiology, St. Vincent Hospital, Gdynia, Poland, ¹³1st Department of Cardiology, Medical University of Gdańsk, Gdańsk, Poland, ¹⁴Department of Heart Diseases, Postgraduate Medical School, Katowice, Poland, ¹⁵Department of Cardiology, School of Health Sciences, Medical University of Silesia, Katowice, Poland, ¹⁶Department of Cardiology, Medical University of Łódź, Łódź, Poland, ¹⁷Department of Cardiology, Medical University of Białystok, Białystok, Poland, ¹⁸Department of Cardiology and Internal Medicine, Medical University of Gdańsk, Gdańsk, Poland, ¹⁹Department of Hypertension, Angiology, and Internal Medicine, Poznań University of Medical Sciences, Poznań, Poland

Introduction: The left atrium appendage thrombus (LAAT) formation is a complex process. A CHA₂DS₂-VASc scale is an established tool for determining the thromboembolic risk and initiation of anticoagulation treatment in patients with atrial fibrillation or flutter (AF/AFL). We aimed to identify whether any transthoracic echocardiography (TTE) parameters could have an additional impact on LAAT detection.

Methods: That is a sub-study of multicenter, prospective, observational study LATTEE (NCT03591627), which enrolled 3,109 consecutive patients with AF/AFL referred for transesophageal echocardiography (TEE) before cardioversion or ablation.

Results: LAAT was diagnosed in 8.0% of patients. The univariate logistic regression analysis [based on pre-specified in the receiver operating characteristic (ROC) analysis cut-off values with $AUC \geq 0.7$] identified left ventricular ejection fraction (LVEF) $\leq 48\%$ and novel TTE parameters i.e., the ratios of LVEF and left atrial diameter (LAD) ≤ 1.1 (AUC 0.75; OR 5.64; 95% CI 4.03–7.9; $p < 0.001$), LVEF to left atrial area (LAA) ≤ 1.7 (AUC 0.75; OR 5.64; 95% CI 4.02–7.9; $p < 0.001$), and LVEF to indexed left atrial volume (LAVI) ≤ 1.1 (AUC 0.75, OR 6.77; 95% CI 4.25–10.8; $p < 0.001$) as significant predictors of LAAT. In a multivariate logistic regression analysis, LVEF/LAVI and LVEF/LAA maintained statistical significance. Calculating the accuracy of the abovementioned ratios according to the CHA₂DS₂-VASc scale values revealed their highest predictive power for LAAT in a setting with low thromboembolic risk.

Conclusion: Novel TTE indices could help identify patients with increased probability of the LAAT, with particular applicability for patients at low thromboembolic risk.

KEYWORDS

transthoracic echocardiography, left atrial appendage thrombus, NOAC, echocardiographic indices, thromboembolic risk, predictors of left atrial thrombus

Introduction

Atrial fibrillation and flutter (AF/AFL) are the most common sustained cardiac arrhythmias in adults (1, 2), with thromboembolic complications as the main reason for morbidity and mortality (3). The CHA₂DS₂-VASc scale is an established clinical tool which is recommended for determining the thromboembolic risk and anticoagulation treatment indications in AF/AFL patients (4). However, thrombus formation is a complex process, which involves many hemorheological, tissue and humoral factors; hence the mere assessment of the thrombus mass formation based only on the abovementioned scale could be insufficient (5). Therefore, it could be reasonable to relate the CHA₂DS₂-VASc scale to some morphological parameters, which could have a possible impact on thrombus development, and echocardiography could be a valuable tool in this issue. Transesophageal echocardiography (TEE) is regarded as the gold standard in detecting the left atrial (LA) appendage thrombus (LAAT) before cardioversion or ablation procedure (6, 7). However, in certain situations, its performance is hampered or even not possible, for instance, due to logistical difficulties related to restricting access to the TEE in small district hospitals, as well as in certain situations, such as the COVID-19 pandemic, in which the implementation of the study was limited. Therefore, it seems reasonable to verify whether any routinely assessed

transthoracic echocardiography (TTE) parameters could help identify patients with a high probability of LAAT, which could allow clinicians to avoid unnecessary diagnostics and influence the appropriate management of a patient.

Many studies have focused so far on the search for echocardiographic parameters that predict the risk of LAAT (8–11), revealing LA enlargement [both diameter (LAD), surface area (LAA), indexed volume (LAVI)], and decreased left ventricular ejection fraction (LVEF) as the most associated with thrombus formation. However, the predictive power of these conventional variables is insufficient (8, 9). Therefore, we hypothesized that perhaps parameters determining the size, area, and volume of the atrium, in combination with other echocardiographic parameters such as LVEF, may prove valuable as a marker of increased risk of LAAT formation in real-world AF/AFL patients referred for TEE before electrical cardioversion or catheter ablation in the era of modern anticoagulation.

Materials and methods

Study population

The study is a sub-analysis of the real-world Left Atrial Thrombus on Transesophageal Echocardiography (LATTEE)

registry (NCT03591627), which evaluated the determinants of LAAT depending on echocardiographic and clinical parameters in patients with AF/AFL referred for electrical cardioversion or catheter ablation. Exact details on the study rationale and design have been published previously (12), while the primary data concerning the prevalence of a thrombus depending on anticoagulation strategy were further precisely delineated (13). In sum, the LATTEE was a prospective, observational study enrolling consecutive patients with AF/AFL admitted to 13 cardiology departments between November 2018 and May 2020 in whom TEE was performed before direct current cardioversion or catheter ablation. Diagnosis

of AF/AFL was based on previous European Society of Cardiology Guidelines on managing AF by attending physicians (14). Regarding non-emergency electrical cardioversion for AF/AFL, four centers performed TEE routinely in all patients, and nine centers performed TEE only in those patients who were suspected of ineffective antithrombotic therapy within the last 3 weeks. The study was conducted according to clinical practice guidelines and the Declaration of Helsinki. The Ethics Committee approved the study of the Medical University of Warsaw (AKBE/113/2018), which waived the requirement of obtaining informed consent from the patients.

TABLE 1 Comparison of the clinical characteristics between patients with (LAAT+) and without LAAT (LAAT-).

Variable	LAAT- (<i>n</i> = 2,859)	LAAT+ (<i>n</i> = 250)	<i>p</i> ^a
Demographics			
Age (years)	67 [59–73]	72 [64–78]	<0.001
AF/AFL type			
AF/AFL paroxysmal	1,247 (44%)	33 (13%)	<0.001
AF/AFL persistent	1,365 (48%)	183 (73%)	<0.001
AF/AFL long-standing persistent	237 (8%)	34 (14%)	0.007
AF chronic	109 (4%)	20 (8%)	0.004
Comorbidities			
Heart failure	1,165 (41%)	171 (69%)	<0.001
Heart failure with reduced LVEF	380 (13%)	96 (39%)	<0.001
Hypertension	2,171 (76%)	195 (79%)	0.393
Diabetes mellitus	683 (24%)	91 (37%)	<0.001
Previous stroke	206 (7.2%)	29 (12%)	0.017
TIA	75 (3%)	15 (6%)	0.005
Previous ischemic stroke/TIA/systemic embolism	278 (9.7%)	35 (14%)	0.040
Previous hemorrhagic stroke	14 (0.5%)	3 (1.2%)	0.148
Vascular disease	949 (33%)	118 (47%)	<0.001
Myocardial infarction	372 (13%)	59 (28%)	<0.001
Coronary artery disease	811 (29%)	94 (38%)	0.002
Peripheral artery disease	149 (5%)	26 (10%)	<0.001
Moderate to severe mitral stenosis	12 (0.4%)	5 (2%)	0.009
Moderate to severe mitral regurgitation	442 (15%)	81 (32%)	<0.001
Moderate to severe aortic stenosis	47 (1.6%)	15 (6%)	<0.001
CIED	341 (12%)	57 (23%)	<0.001
eGFR < 50 (mL/min)	82 [64–103]	74 [51–93]	<0.001
Previous bleeding	114 (4.0%)	17 (6.9%)	0.05
Anemia	431 (16%)	53 (23%)	<0.01
Labile INR	50 (2%)	23 (9%)	<0.001
Smoking	902 (33%)	109 (46%)	<0.001
Alcohol	106 (4%)	23 (9%)	<0.001
Thromboembolic risk and indications to chronic OAC			
CHA ₂ DS ₂ -VASc score	3 [2–4]	4 [3–5]	0.010
Antithrombotic therapy			
Chronic OAC therapy	2,553 (89%)	200 (80%)	<0.001

^a*p*-value refers for the differences between LAAT (+) and LAAT (-) groups.

AF, atrial fibrillation; AFL, atrial fibrillation; CIED, cardiac implanted electrical device; eGFR, estimated glomerular filtration rate; INR, international normalized ratio; LAAT, left atrial appendage thrombus; MS, mitral stenosis; OAC, an oral anticoagulant. TIA, transient ischemic attack.

Data collection and study endpoint

Data were gathered prospectively and included precise demographics, medical history, comorbidities, CHA₂DS₂-VASc score calculation, pharmacotherapy, and results of routine laboratory blood tests. Chronic oral anticoagulation (OAC) was defined as OAC treatment for at least 3 weeks before the procedure. In all patients' obligatory transoesophageal echocardiography (TOE) parameters such as presence and location of LAAT, presence of spontaneous echocardiographic contrast, as well as LAA outflow velocity (LAAV) were obtained. TTE study was conducted in the vast majority of participants and involved gathering data regarding: LVEF, LAD, LAA, left atrial volume (LAV) and LAVI (calculated as a ratio of left atrial volume to body surface area). Trained echocardiographers performed all examinations as it was defined in the primary protocol (12). Additionally, the novel parameters (ratios of LVEF and LA parameters: LVEF/LAD, LVEF/LAA, and LVEF/LAVI) were investigated. Both TTE and TOE parameters were analyzed and interpreted locally. The primary endpoint of the study was the presence of LAAT.

Statistical analysis

Continuous data were presented as the median (25th–75th percentiles), categorical as a number (n) and percentage (%). Differences between LAAT+ and LAAT- groups were calculated with the Mann-Whitney *U*-test and the qualitative data with the χ^2 or Yates χ^2 test. The accuracy of pre-specified cut-off values for analyzed parameters and their association as potential predictors of the study endpoint was determined by area (AUC) under the receiver operating characteristic (ROC) curve. Only AUC values ≥ 0.7 were considered for further analysis (15). For comparison of unpaired ROC curves Venkatraman's test was utilized. The association between the analyzed parameters (differed between LAAT+ and LAAT-

groups) and the endpoint was assessed using univariable logistic regression analysis with cut-off values pre-specified in ROC analysis. Multivariable analysis was applied to continuous data (dichotomized according to the cut-off values identified in ROC analyses) and categorical data associated with the endpoint in the univariable regression analysis ($p \leq 0.05$). The set of variables accepted for the model was determined by the backward elimination method from the set of all statistically significant predictors. The statistical analysis was conducted with an R 4.0.5 environment (R Core Team, Vienna, Austria).

Results

Study population

A total of 3,109 patients who met the inclusion criteria were enrolled in the LATTEE registry. Altogether, nearly 9 out of 10 were on OACs. Prevalence of LAAT was 8.0% (7.3% on chronic OAC vs. 15% without OAC; $p < 0.001$) and it was doubled in patients on vitamin K antagonist (VKA) compared to patients on non-VKA-OACs (NOACs) (13 vs. 6.0%; $p < 0.01$). Patients with LAAT were older and more often had chronic AF and comorbidities, resulting in a higher CHA₂DS₂-VASc score, as shown in **Table 1**. All clinical parameters of the study population were presented in previous work (13).

Echocardiographic parameters

TTE data were obtained for 2,599 (84%) study participants, and **Table 2** presents the results. LAAT+ patients had lower LVEF and greater LAD, LAA, LAV, and LAVI values. The compared groups differed significantly in terms of the echocardiographic indices, i.e., LAAT+ in comparison to LAAT- patients had a lower ratio of LVEF to LA indices: LVEF/LAD 0.9 vs. 1.2 ($p < 0.001$), LVEF/LAA 1.4 vs. 2.1 ($p < 0.001$), and LVEF/LAVI 0.7 vs. 1.2 respectively ($p < 0.001$), as shown in **Table 2**.

TABLE 2 Comparison of LVEF, LA parameters and ratios in LAAT+ and LAAT- patients.

Variable	LAAT- (<i>n</i> = 2,859)	LAAT+ (<i>n</i> = 250)	<i>p</i> ^a
LVEF (%)	55 [45–60]	40 [30–51]	<0.001
LAD (mm)	45 [41–49]	47 [45–51]	<0.001
LAA (cm ²)	26 [22–30]	28 [24.8–33]	<0.001
LAV (ml)	85 [69–109]	97 [76–123]	<0.001
LAVI (mL/m ²)	44 [35–55]	52 [42.9–63]	<0.001
LVEF/LAD ratio	1.2 [0.98–1.4]	0.9 [0.62–1.09]	<0.001
LVEF/LAA ratio	2.1 [1.6–2.51]	1.4 [0.97–1.83]	<0.001
LVEF/LAVI ratio	1.2 [0.88–1.57]	0.7 [0.52–1.05]	<0.001

^a*p*-values refer for the differences between LAAT+ and LAAT- groups.

LAA, left atrial area; LAD, left atrial diameter; LAAT, left atrial appendage thrombus; LAV, left atrial volume; LAVI, left atrial volume index; LVEF, left ventricular ejection fraction.

Significant predictors of left atrial thrombus

Table 3 presents the results of ROC analysis with pre-specified cut-off values for LAAT prediction. The LA parameters alone did not have adequate predictive power (AUC lower than < 0.7), whereas ratios of LVEF with LA parameters significantly improved the level of LAAT prediction with high specificity and positive predictive value.

The univariate logistic regression analysis (based on pre-specified in the ROC analysis cut-off values with AUC ≥ 0.7) revealed a considerable number of clinical parameters, as well

as LVEF, LVEF/LAD, LVEF/LAA and LVEF/LAVI ratios as the significant predictors for LAAT. These data are presented in **Figure 1**. C-Statistics analyses showed that the accuracy power of new echocardiographic indices (LVEF/LAD, LVEF/LAA, LVEF/LAVI ratios) differed significantly from conventional parameters (LAD, LAA, LAVI—in all combinations $p < 0.05$) but not for LVEF ($p > 0.05$). In a multivariate logistic regression analysis, which included all parameters which proved to be statistically significant in the univariate test (with AUC ≥ 0.7 for continuous variables from **Table 3**), only a few clinical parameters, as well as LVEF/LAVI and LVEF/LAA ratio maintained its statistical significance, as shown in **Figure 1**.

Significant predictors of left atrial appendage thrombus in subpopulation of patients with heart failure

Among the entire study population, 43% of the patients, i.e., 1,336, were diagnosed with heart failure (HF). Of the HF types, the most common was HF with preserved ejection fraction (HFpEF), then reduced ejection fraction (HFrEF) and mid-range ejection fraction (HFmEF), 38, 35, and 27%, respectively. Most HF patients had symptoms consistent with NYHA I-II (72%).

The results of logistic regression analysis and ROC with specific cut-off values for LAAT prediction in patients with HF subtypes are presented in **Table 4**. In each of the HF subtypes tested, AUC and OR values were lower than those obtained for the entire study population. The new echocardiographic indices differed in statistical power depending on the HF subtype, and more precisely, they had highest prediction for LAAT formation in patients with HFpEF, where they obtained acceptable values for LVEF/LAA ≤ 1.8 [AUC 0.7, OR 4.1, 95% CI (1.9–9), $p = 0.001$] and LVEF/LAVI ≤ 1.1 [0.71, OR 4.4, 95% CI (1.7–11.6), $p = 0.003$].

Accuracy of transthoracic echocardiographic indices for left atrium appendage thrombus detection according to CHA₂DS₂-VASc score values

Based on the statistical significance of novel echocardiographic ratios, we determined their odds ratio for LAAT prediction in different CHA₂DS₂-VASc groups. For this purpose, we divided patients into three subgroups accordingly to (A) 0–1, (B) 2–3, and (C) 4 and more points on the CHA₂DS₂-VASc score. In ROC analysis, the appropriate cut-off values for LAAT prediction were determined, as shown in **Table 5**. The obtained data show that the discussed indices were characterized by better accuracy and predictive power than conventional parameters, and that the LVEF/LAA index predicts the formation of LAAT with the highest statistical power.

Discussion

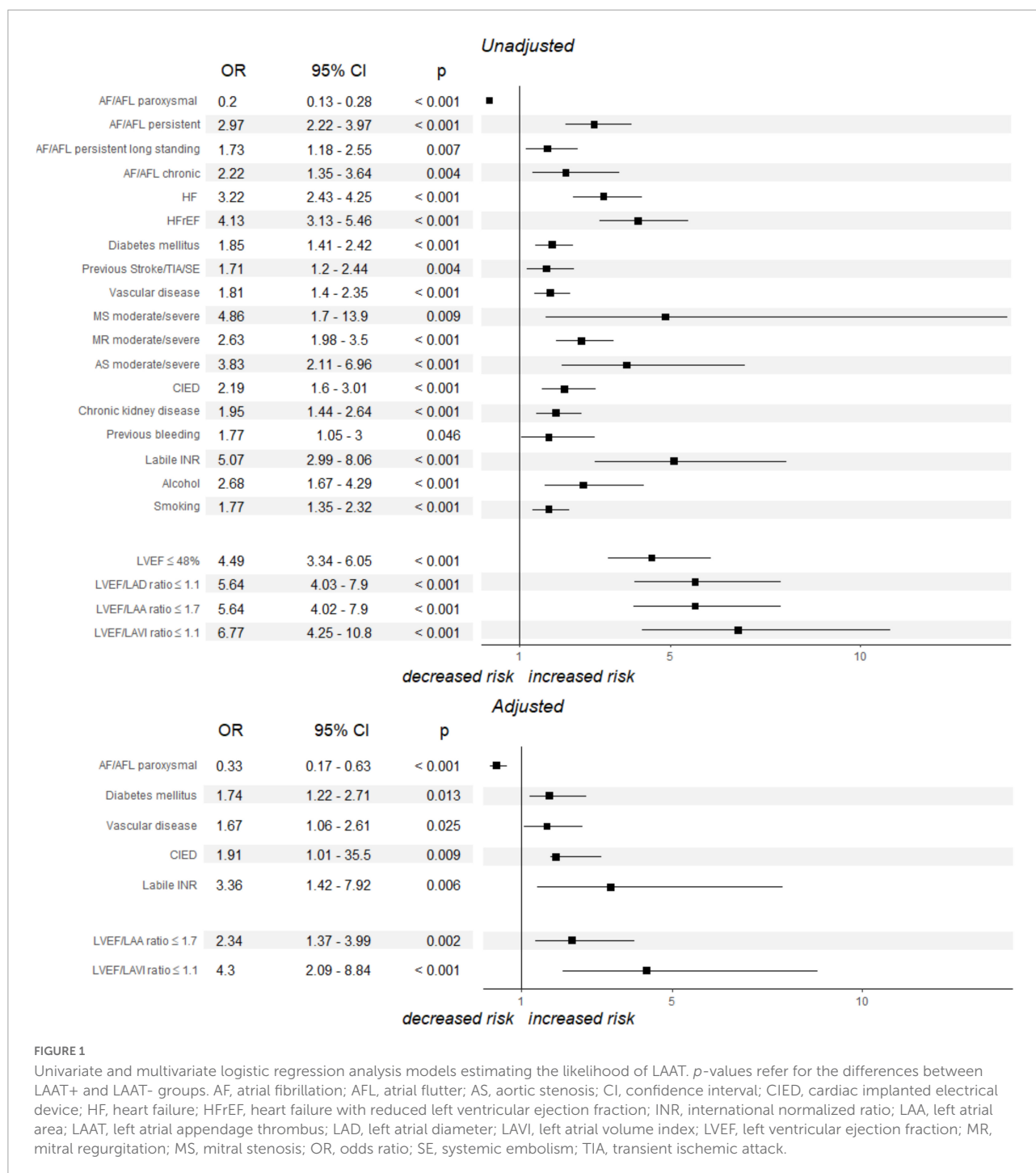
The major finding in this prospective, observational study is that LAAT formation was strongly associated with echocardiographic parameters, additionally to well-known clinical variables. We determined that simple, routinely examined echocardiographic parameters presented as the novel indices, including LVEF and LA parameters seem to be accurate predictors of LAAT presence, mainly according to different CHA₂DS₂-VASc score groups with peculiar applicability for patients with relatively lower thromboembolic risk.

To date, several risk stratification methods utilizing clinical parameters have been developed to help pinpoint patients with AF/AFL who are at high risk for thromboembolic

TABLE 3 Accuracy of the pre-specified cut-off values for analyzed parameters as the predictors of LAAT.

Parameter	AUC	Characteristics (%)		Predictive value (%)	
		Sensitivity	Specificity	Positive	Negative
Age ≥ 72 years	0.61	74	46	94	13
LVEF $\leq 48\%$	0.74	71	65	96	17
LAD ≥ 45 mm	0.63	53	67	95	12
LAA ≥ 26 cm ²	0.62	53	66	94	12
LAV ≥ 89 mL	0.59	55	59	93	11
LAVI ≥ 51 mL/m ²	0.64	68	54	94	14
LVEF/LAD ratio ≤ 1.1	0.75	62	79	97	16
LVEF/LAA ratio ≤ 1.7	0.75	71	70	96	18
LVEF/LAVI ratio ≤ 1.1	0.75	56	84	97	15

AUC, an area under the curve; CI, confidence interval; LAA, left atrial area; LAD, left atrial diameter; LAAT, left atrial appendage thrombus; LAV, left atrial volume; LAVI, left atrial volume index; LVEF, left ventricular ejection fraction.



complications, among which the most recognized is the CHA₂DS₂-VASc score (16). Nonetheless, some other investigators had a differing viewpoint on this issue (17, 18). The role of data derived from the TTE study as a marker of LAAT formation has been studied extensively over the last decades (10, 19–22). For example, in the study of Scherr et al., which enrolled 585 patients referred for catheter ablation of AF, LAD ≥ 45 mm and a CHADS₂ score ≥ 2 proved

to be significant predictors of LA thrombus in multivariate regression analysis (10). Our data are in line with those observations. Moreover, the capacity for predicting LAAT by combining LA area and volume parameters and LVEF seems stronger than using any single echocardiographic parameter. In our study, we proposed some novel echocardiographic indices, easy to obtain from the routinely checked parameters, which could have an additional impact on LAAT detection.

TABLE 4 Univariate regression analysis and ROC study results of novel echocardiographic parameters in subpopulation of patients with HF.

Parameter	AUC	OR 95%	<i>p</i> ^a
HF with reduced EF			
LVEF/LAA \leq 1.0	0.59	2 [1.2–3.4]	0.01
LVEF/LAVI \leq 0.6	0.56	2.1 [1.1–4.1]	0.023
HF with mid-range EF			
LVEF/LAA \leq 1.5	0.68	2.2 [1.1–4.6]	0.033
LVEF/LAVI \leq 0.9	0.60	3.8 [3.6–9.2]	0.002
HF with preserved EF			
LVEF/LAA \leq 1.8	0.70	4.1 [1.9–9]	0.001
LVEF/LAVI \leq 1.1	0.71	4.4 [1.7–11.6]	0.003
HF with mid-range EF and HF with reduced EF			
LVEF/LAA \leq 2	0.67	4.3 [2.1–8.9]	0.001
LVEF/LAVI \leq 1	0.72	4.5 [2.3–8.5]	0.001

^a*p*-values refer for the differences between LAAT (+) and LAAT (-) groups.
AUC, an area under the curve; EF, ejection fraction; HF, heart failure; LAA, left atrial area;
LAVI, left atrial volume index; LVEF, left ventricular ejection fraction; OR, odds ratio.

Of the TTE indices, the LVEF/LAD with a cut-off value of \leq 1.1, LVEF/LAA ratio \leq 1.7 and LVEF/LAVI \leq 1.1 had the highest predictive accuracy (AUC \geq 0.7) predictive power and statistical significance in the univariate logistic regression analysis. Importantly, in the multivariate logistic regression analysis, LVEF/LAVI and LVEF/LAA maintained statistical significance.

For better prediction of LAAT, models combining clinical and echocardiographic parameters have been proposed (17, 19–24). For example, Van Chien et al., in their study of 144 anticoagulant-naïve patients, proposed models that combined CHA₂DS₂-VASc score with LA volume index and LA longitudinal strain (17). In another study conducted by Ayrala et al. on 334 patients who received VKA or VKA and heparin, the authors showed that patients with CHADS₂ score of \leq 1 a normal LAVI in combination with normal LVEF are a robust negative predictor of LAA thrombus formation (19). Our results are under data from the literature; indeed, the calculation of LVEF/LAVI and LVEF/LAA ratio in different CHA₂DS₂-VASc score groups had a significant association with LAAT. Notably, the highest OR for LAAT prediction of presented echocardiographic indexes is for patients with low thromboembolic risk (Table 5). For example, LVEF/LAA index \leq 1.5 in low-risk patients (with 0 or 1 points in CHA₂DS₂-VASc score) was characterized by an OR 29, CI 5.87–145.52 with an excellent AUC equal to 0.92. Similarly, the positive predictive value of the pre-specified cut-offs was higher for patients with a lower CHA₂DS₂-VASc score. That could be of great clinical value, helping clinicians identify patients with a high likelihood of LAAT, regardless of a low CHA₂DS₂-VASc score.

HF patients constitute a special population within atrial fibrillation patients, and their increasing coexistence is associated with significantly elevated in-hospital mortality (25). The occurrence of AF in patients with HF may lead to clinical

TABLE 5 Accuracy of echocardiographic indices in LAAT prediction according to CHA₂DS₂-VASc score values.

Parameters	AUC	Characteristics (%)		Predictive value (%)		OR 95%	<i>p</i> ^a
		Sensitivity	Specificity	Positive	Negative		
Subgroup A (CHA ₂ DS ₂ -VASc 0–1 point)							
LVEF/LAA ≤ 1.5	0.92	89	89	100	17	29 [5.9–145]	<0.001
LVEF/LAVI ≤ 0.7	0.78	92	60	98	21	18 [4.7–68]	<0.001
LVEF ≤ 48%	0.72	85	62	99	9	9 [2.8–25]	<0.001
LAD ≥ 41 mm	0.74	37	100	100	4	15 [0.9–264]	0.003
LAA ≥ 26 cm ²	0.79	62	100	100	6	29 [1.7–511]	<0.001
Subgroup B (CHA ₂ DS ₂ -VASc 2–3 points)							
LVEF/LAA ≤ 1.5	0.77	78	72	97	22	9 [5–16.2]	<0.001
LVEF/LAVI ≤ 0.9	0.75	77	67	96	21	6.6 [3.5–12.2]	<0.001
LVEF ≤ 47%	0.76	74	68	96	19	5.9 [3.7–10]	<0.001
LAD ≥ 45 mm	0.67	53	74	96	12	3.2 [1.87–5.2]	<0.001
LAA ≥ 29 cm ²	0.67	69	58	95	14	3.1 [1.8–5.1]	<0.001
Subgroup C (CHA ₂ DS ₂ -VASc 4 and more points)							
LVEF/LAA ≤ 2.0	0.70	43	87	96	17	4.3 [2.5–7.4]	<0.001
LVEF/LAVI ≤ 0.9	0.69	70	64	94	20	3.7 [2.3–6.1]	<0.001
LVEF ≤ 55%	0.70	38	92	98	15	7.7 [3.7–14.3]	0.001
LAD ≥ 44 mm	0.55	39	72	92	13	1.7 [1.1–2.5]	0.019
LAA ≥ 29 cm ²	0.55	29	82	92	13	1.8 [1.1–3.1]	0.02

^a*p*-values refer for the differences between LAAT (+) and LAAT (-) groups.
AUC, an area under the curve; LAA, left atrial area; LAD, left atrial diameter; LAAT, left atrial thrombus; LVEF, left ventricular ejection fraction; OR, odds ratio.

disease progression and increases mortality, on the other hand, presence of HF in AF patients interfere with preservation of sinus rhythm through atrial remodeling, increases the number of strokes and mortality (26, 27). Despite the fact that congestive HF is a part of CHA₂DS₂-VASc score whether every HF subtype generates the same risk of LAAT formation is still in question (28, 29). In a recently published work, also based on data from the LATTEE registry Wybraniec et al. examined a population of 1,336 patients with HF and showed that the diagnosis of HFrEF, but neither HFmrEF nor HFpEF, confers a considerable risk of LAT formation (30). In our study we evaluated the usefulness of the new echocardiographic parameters i.e., LVEF/LAA and LVEF/LAVI in all HF subtypes, however, the results are unsatisfactory and indicate the need to look for other LAT predictors in this group of patients.

Based on our results, it could be suggested that clinical risk scores should be combined with echocardiographic parameters to receive the most accurate data regarding LAAT formation. A significant advantage of our results boosts the fact that our research was based on a large, modernly anticoagulated group of patients, 82% of whom were on chronic NOAC. To the best of our knowledge, this is the first study that shows the usefulness of novel echocardiographic parameters in clinical presentation in identifying high-risk individuals of LAAT occurrence in the era of contemporary anticoagulation.

Limitations of the study

Our study has some limitations. Firstly, the study was a registry and therefore has a limitation of its design. Secondly, despite the fact that we included a relatively large group of patients with AF/AFL, by inclusion criteria these were patients admitted for ablation or cardioversion procedures and therefore, the results cannot be extrapolated to the whole population of patients with AF/AFL. Thirdly, it is worth noting that echocardiographic study was performed at the discretion of attending physicians, and thus, data including TTE are missing for some patients. Moreover, a few promising parameters, such as LV stroke volume, LV end-systolic and end-diastolic volume as well as parameters of left ventricular diastolic dysfunction and peak atrial longitudinal strain that could identify patients at increased risk of LAAT, were not included in the methodology of that registry (31, 32). Additionally, the study did not investigate into the rate of ischemic stroke on follow-up, but only the presence of LAAT. Furthermore, TOE was performed routinely in most centers prior to direct current cardioversion and catheter ablation, however, some participating centers performed TOE only in subjects with suboptimal anticoagulation before the procedure or in those with doubts regarding adherence to NOAC and its effectiveness which might have led to some selection bias. Finally, study aimed to check which echocardiographic parameters can predict

LAAT formation based on regular patients qualified to TEE in the everyday clinical practice hence we did not exclude a peculiar group of patients with “valvular AF” from the analysis.

Conclusion

Simple, routinely examined echocardiographic parameters presented as the novel indices, including LVEF and LA parameters, seem to be accurate predictors of LAAT presence. Further use of those parameters could help predict LAAT in different CHA₂DS₂-VASc score groups with particular applicability for patients with low thromboembolic risk.

Data availability statement

The raw data supporting the conclusions of this article will be made available by the authors, without undue reservation.

Ethics statement

The studies involving human participants were reviewed and approved by the Ethics Committee of the Medical University of Warsaw. Written informed consent for participation was not required for this study in accordance with the national legislation and the institutional requirements.

Author contributions

DK and LD-S: formal analysis, resources, writing—original draft preparation, visualization, data curation, and agreed to the published version of the manuscript. AK-C, MG, and MB: conceptualization, methodology, validation, investigation, data curation, writing—review and editing, project administration, and agreed to the published version of the manuscript. EW, BU-Ż, PK, KS, MCW, RB, JH, JB, KM-S, MTW, KTK, MF, AS, MD, MH, MCK, BM, KRK, AT-K, KW-Ś, RW-T, MRK, and PB: investigation, data curation, writing—review and editing, and agreed to the published version of the manuscript. LD-S: conceptualization, methodology, resources, writing—original draft preparation, visualization, supervision, data curation, and agreed to the published version of the manuscript. All authors contributed to the article and approved the submitted version.

Acknowledgments

The LATTEE Registry was initiated on the Scientific Platform of the “Club 30” of the Polish Cardiac Society. We thank IG-G for helping with data collection.

Conflict of interest

Authors AK-C, BW-K, and MRK received honoraria for lectures from Bayer, Boehringer Ingelheim, and Pfizer, outside the submitted work. Author LD-S received speaker fees from Bayer, Boehringer Ingelheim, and Pfizer—outside the submitted work. Author KM-S received speaker fees from Bayer, Pfizer, Boehringer Ingelheim, AstraZeneca, Novartis, and Servier—outside the submitted work. Author AT-K received speaker fees from Boehringer-Ingelheim—outside the submitted work.

The remaining authors declare that the research was conducted in the absence of any commercial or financial

relationships that could be construed as a potential conflict of interest.

Publisher's note

All claims expressed in this article are solely those of the authors and do not necessarily represent those of their affiliated organizations, or those of the publisher, the editors and the reviewers. Any product that may be evaluated in this article, or claim that may be made by its manufacturer, is not guaranteed or endorsed by the publisher.

References

- Haim M, Hoshen M, Reges O, Rabi Y, Balicer R, Leibowitz M. Prospective national study of the prevalence, incidence, management and outcome of a large contemporary cohort of patients with incident non-valvular atrial fibrillation. *J Am Heart Assoc.* (2015) 4:e001486. doi: 10.1161/JAHA.114.001486
- Sheikh A, Patel NJ, Nalluri N, Agnihotri K, Spagnola J, Patel A, et al. Trends in hospitalization for atrial fibrillation: epidemiology, cost, and implications for the future. *Prog Cardiovasc Dis.* (2015) 58:105–16. doi: 10.1016/j.pcad.2015.07.002
- Heeringa J, van der Kuip DAM, Hofman A, Kors JA, van Herpen G, Stricker BHC, et al. Prevalence, incidence and lifetime risk of atrial fibrillation: the rotterdam study. *Eur Heart J.* (2006) 27:949–53. doi: 10.1093/eurheartj/ehi825
- Olesen JB, Torp-Pedersen C, Hansen ML, Lip GYH. The value of the CHA2DS2-VASc score for refining stroke risk stratification in patients with atrial fibrillation with a CHADS2 score 0–1: a nationwide cohort study. *Thromb Haemost.* (2012) 107:1172–9. doi: 10.1160/TH12-03-0175
- Wasmer K, Köbe J, Decherding D, Milberg P, Pott C, Vogler J, et al. CHADS and CHADS2-VASc score of patients with atrial fibrillation or flutter and newly detected left atrial thrombus. *Clin Res Cardiol.* (2013) 102:139–44. doi: 10.1007/s00392-012-0507-4
- Koca V, Bozat T, Akkaya V, Sarikamis C, Turk T, Vural H, et al. Left atrial thrombus detection with multiplane transesophageal echocardiography: an echocardiographic study with surgical verification. *J Heart Valve Dis.* (1999) 8:63–6.
- Fuster V, Rydén LE, Cannom DS, Crijns HJ, Curtis AB, Ellenbogen KA, et al. ACC/AHA/ESC 2006 guidelines for the management of patients with atrial fibrillation: a report of the American college of cardiology/American heart association task force on practice guidelines and the European society of cardiology committee for practice guidelines (writing committee to revise the 2001 guidelines for the management of patients with atrial fibrillation): developed in collaboration with the European heart rhythm association and the heart rhythm society. *Circulation.* (2006) 114:e257–354. doi: 10.1161/circulationaha.106.177292
- Ellis K, Ziada KM, Vivekananthan D, Latif AA, Shaarouqi M, Martin D, et al. Transthoracic echocardiographic predictors of left atrial appendage thrombus. *Am J Cardiol.* (2006) 97:421–5. doi: 10.1016/j.amjcard.2005.08.065
- Manning WJ, Silverman DI, Keighley CS, Oettgen P, Douglas PS. Transesophageal echocardiographically facilitated early cardioversion from atrial fibrillation using short-term anticoagulation: final results of a prospective 4.5-year study. *J Am Coll Cardiol.* (1995) 25:1354–61. doi: 10.1016/0735-1097(94)00560-D
- Scherr D, Dalal D, Chilukuri K, Dong J, Spragg D, Henrikson CA, et al. Incidence and predictors of left atrial thrombus prior to catheter ablation of atrial fibrillation. *J Cardiovasc Electrophysiol.* (2009) 20:379–84. doi: 10.1111/j.1540-8167.2008.01336.x
- Wallace TW, Atwater BD, Daubert JP, Voora D, Crowley AL, Bahnson TD, et al. Prevalence and clinical characteristics associated with left atrial appendage thrombus in fully anticoagulated patients undergoing catheter-directed atrial fibrillation ablation. *J Cardiovasc Electrophysiol.* (2010) 21:849–52. doi: 10.1111/j.1540-8167.2010.01729.x
- Kapłon-Cieślicka A, Budnik M, Gawalko M, Wójcik M, Błaszczak R, Uziębło-Życzkowska B, et al. The rationale and design of the LATTEE registry - the first multicenter project on the scientific platform of the “Club 30” of the Polish cardiac society. *Kardiol Pol.* (2019) 77:1078–80. doi: 10.33963/KP.1501
- Kapłon-Cieślicka A, Gawalko M, Budnik M, Uziębło-Życzkowska B, Krzesiński P, Starzyk K, et al. Left atrial thrombus in atrial fibrillation/flutter patients in relation to anticoagulation strategy: LATTEE registry. *J Clin Med.* (2022) 11:2705. doi: 10.3390/jcm11102705
- Hindricks G, Potpara T, Dagres N, Arbelo E, Bax JJ, Blomström-Lundqvist C, et al. 2020 ESC Guidelines for the diagnosis and management of atrial fibrillation developed in collaboration with the European association for cardio-thoracic surgery (EACTS): the task force for the diagnosis and management of atrial fibrillation of the European society of cardiology (ESC) developed with the special contribution of the European heart rhythm association (EHRA) of the ESC. *Eur Heart J.* (2021) 42:373–498. doi: 10.1093/eurheartj/ehaa612
- Safari S, Baratloo A, Elfil M, Negida A. Evidence based emergency medicine; Part 5 receiver operating curve and area under the curve. *Emerg.* (2016) 4:111–3.
- Bertaglia E, Anselmino M, Zorzi A, Russo V, Toso E, Peruzzo F, et al. NOACs and atrial fibrillation: incidence and predictors of left atrial thrombus in the real world. *Int J Cardiol.* (2017) 249:179–83. doi: 10.1016/j.ijcard.2017.07.048
- Van Chien D, Thai Giang P, Son PT, Van Truong L, Nguyen Son P. Novel models for the prediction of left atrial appendage thrombus in patients with chronic nonvalvular atrial fibrillation. *Cardiol Res Pract.* (2019) 2019:1496535. doi: 10.1155/2019/1496535
- Sugiura S, Fujii E, Senga M, Sugiura E, Nakamura M, Ito M. Clinical features of patients with left atrial thrombus undergoing anticoagulant therapy. *J Interv Card Electrophysiol.* (2012) 34:59–63. doi: 10.1007/s10840-011-9633-6
- Ayrala S, Kumar S, O'Sullivan DM, Silverman DI. Echocardiographic predictors of left atrial appendage thrombus formation. *J Am Soc Echocardiogr.* (2011) 24:499–505. doi: 10.1016/j.echo.2011.02.010
- Agmon Y, Khandheria BK, Gentile F, Seward JB. Clinical and echocardiographic characteristics of patients with left atrial thrombus and sinus rhythm: experience in 20 643 consecutive transesophageal echocardiographic examinations: experience in 20 643 consecutive transesophageal echocardiographic examinations. *Circulation.* (2002) 105:27–31. doi: 10.1161/hc0102.101776
- Chen L, Zinda A, Rossi N, Han X-J, Sprankle S, Bullock-Palmer R, et al. A new risk model of assessing left atrial appendage thrombus in patients with atrial fibrillation - Using multiple clinical and transesophageal echocardiography parameters. *Int J Cardiol.* (2020) 314:60–3. doi: 10.1016/j.ijcard.2020.04.039
- Uziębło-Życzkowska B, Krzesiński P, Jurek A, Kapłon-Cieślicka A, Gorczyca I, Budnik M, et al. Left ventricular ejection fraction is associated with the risk of thrombus in the left atrial appendage in patients with atrial fibrillation. *Cardiovasc Ther.* (2020) 2020:3501749. doi: 10.1155/2020/3501749
- Kapłon-Cieślicka A, Budnik M, Gawalko M, Peller M, Gorczyca I, Michalska A, et al. Atrial fibrillation type and renal dysfunction as important predictors of left atrial thrombus. *Heart.* (2019) 105:1310–5. doi: 10.1136/heartjnl-2018-314492
- Lip GYH, Rumley A, Dunn FG, Lowe GDO. Thrombogenesis in mitral regurgitation and aortic stenosis. *Angiology.* (1996) 47:1117–25. doi: 10.1177/000331979604701201

25. Reinhardt SW, Chouairi F, Miller PE, Clark KAA, Kay B, Fuery M, et al. National trends in the burden of atrial fibrillation during hospital admissions for Heart failure. *J Am Heart Assoc.* (2021) 10:e019412. doi: 10.1161/JAHA.120.019412
26. Liao Y-C, Liao J-N, Lo L-W, Lin Y-J, Chang S-L, Hu Y-F, et al. Left atrial size and left ventricular end-systolic dimension predict the progression of paroxysmal atrial fibrillation after catheter ablation: predictors of AF progression after ablation. *J Cardiovasc Electrophysiol.* (2017) 28:23–30. doi: 10.1111/jce.13115
27. Wang TJ, Larson MG, Levy D, Vasan RS, Leip EP, Wolf PA, et al. Temporal relations of atrial fibrillation and congestive heart failure and their joint influence on mortality: the Framingham heart study. *Circulation.* (2003) 107:2920–5. doi: 10.1161/01.cir.0000072767.89944.6e
28. Sartipy U, Dahlström U, Fu M, Lund LH. Atrial fibrillation in heart failure with preserved, mid-range, and reduced ejection fraction. *JACC Heart Fail.* (2017) 5:565–74. doi: 10.1016/j.jchf.2017.05.001
29. Mulder BA, van Veldhuisen DJ, Rienstra M. What should the C ('congestive heart failure') represent in the CHA₂DS₂-VASc score? *Eur J Heart Fail.* (2020) 22:1294–7. doi: 10.1002/ehf.1946
30. Wybraniec MT, Mizia-Szubryt M, Cichoń M, Wrona-Kolasa K, Kapłon-Cieślicka A, Gawalko M, et al. Heart failure and the risk of left atrial thrombus formation in patients with atrial fibrillation or atrial flutter. *ESC Heart Fail.* (2022). [Epub ahead of print]. doi: 10.1002/ehf2.14105
31. Cameli M, Lunghetti S, Mandoli GE, Righini FM, Lisi M, Curci V, et al. Left atrial strain predicts pro-thrombotic state in patients with non-valvular atrial fibrillation. *J Atr Fibrillation.* (2017) 10:1641. doi: 10.4022/jafib.1641
32. Doukky R, Garcia-Sayan E, Gage H, Nagarajan V, Demopoulos A, Cena M, et al. The value of diastolic function parameters in the prediction of left atrial appendage thrombus in patients with nonvalvular atrial fibrillation. *Cardiovasc Ultrasound.* (2014) 12:10. doi: 10.1186/1476-7120-12-10

COPYRIGHT

© 2022 Kaufmann, Wabich, Kapton-Cieślicka, Gawalko, Budnik, Uziębło-Życzkowska, Krzesiński, Starzyk, Woźakowska-Kapton, Wójcik, Błaszczak, Hiczkiewicz, Budzianowski, Mizia-Stec, Wybraniec, Kosmala, Fijałkowski, Szymańska, Dłużniewski, Haberka, Kucio, Michalski, Kupczyńska, Tomaszuk-Kazberuk, Wilk-Siedzińska, Wachnicka-Truty, Kosiński, Burchardt and Daniłowicz-Szymanowicz. This is an open-access article distributed under the terms of the [Creative Commons Attribution License \(CC BY\)](https://creativecommons.org/licenses/by/4.0/). The use, distribution or reproduction in other forums is permitted, provided the original author(s) and the copyright owner(s) are credited and that the original publication in this journal is cited, in accordance with accepted academic practice. No use, distribution or reproduction is permitted which does not comply with these terms.



OPEN ACCESS

EDITED BY

Ryo Torii,
University College London,
United Kingdom

REVIEWED BY

Alexis Théron,
Assistance Publique - Hôpitaux
de Marseille, France
Marius Keller,
Tübingen University Hospital,
Germany

*CORRESPONDENCE

Lina A. Shehadeh
lshehadeh@med.miami.edu

†These authors have contributed
equally to this work

SPECIALTY SECTION

This article was submitted to
Cardiovascular Imaging,
a section of the journal
Frontiers in Cardiovascular Medicine

RECEIVED 07 September 2022

ACCEPTED 29 November 2022

PUBLISHED 21 December 2022

CITATION

Todd EA, Williams M, Kamiar A,
Rasmussen MA and Shehadeh LA
(2022) Echocardiography protocol:
A tool for infrequently used
parameters in mice.
Front. Cardiovasc. Med. 9:1038385.
doi: 10.3389/fcvm.2022.1038385

COPYRIGHT

© 2022 Todd, Williams, Kamiar,
Rasmussen and Shehadeh. This is an
open-access article distributed under
the terms of the [Creative Commons
Attribution License \(CC BY\)](#). The use,
distribution or reproduction in other
forums is permitted, provided the
original author(s) and the copyright
owner(s) are credited and that the
original publication in this journal is
cited, in accordance with accepted
academic practice. No use, distribution
or reproduction is permitted which
does not comply with these terms.

Echocardiography protocol: A tool for infrequently used parameters in mice

Emily Ann Todd^{1†}, Monique Williams^{2,3†}, Ali Kamiar^{2,3},
Monica Anne Rasmussen¹ and Lina A. Shehadeh^{2,3*}

¹Department of Medical Education, University of Miami Leonard M. Miller School of Medicine, Miami, FL, United States, ²Department of Medicine, University of Miami Leonard M. Miller School of Medicine, Miami, FL, United States, ³Interdisciplinary Stem Cell Institute, University of Miami Leonard M. Miller School of Medicine, Miami, FL, United States

Echocardiography is frequently used to evaluate cardiac function in rodent models of cardiovascular disease. Whereas methods to acquire the commonly used echocardiography parameters are well-described in published protocols or manuals, many important parameters are ill-defined and often open to subjective interpretation. Such lack of uniformity has engendered conflicting interpretations of the same parameters in published literature. In particular, parameters such as mitral regurgitation, mitral stenosis, pulmonary regurgitation, and aortic regurgitation that are required to define more esoteric etiologies in rarer mouse models often remain equivocal. The aim of this methods paper is to provide a practical guide to the acquisition and interpretation of infrequently used echocardiography parameters and set a framework for comprehensive analyses of right ventricle (RV), pulmonary artery (PA) pulmonary valve (PV), left atrium (LA), mitral valve (MV), and aortic valve (AoV) structure and function.

KEYWORDS

echocardiography, mitral regurgitation, mitral stenosis, pulmonary regurgitation, aortic regurgitation, cardiovascular disease, left ventricular outflow tract, right ventricular outflow tract

1 Introduction

Echocardiography is a non-invasive imaging modality and a pillar of preclinical cardiovascular research. Rodent models for human disease are routinely analyzed *via* a common set of parameters that are limited to <30% of those possible from modern echocardiographic instrumentation. The remaining ~70% of parameters that are often essential for comprehensive and accurate characterization of murine cardiovascular pathology have not to our knowledge been formally standardized and the relevant procedures are absent from current protocols and manuals of rodent echocardiographic imaging technology. While there are examples of uncommon parameters being acquired to expand on a pathology, details of the acquisition procedures used for such parameter is often lacking. Here we provide an easily accessible protocol of infrequently used views

and parameters that will allow for more complete analyses of the right ventricle (RV), pulmonary artery (PA), pulmonary valve (PV), left atrium (LA), mitral valve (MV), and aortic valve (AoV).

2 Materials and equipment

The images acquired in this paper were captured using Vevo 2100 and 3100 imaging systems and analysis with Vevo Lab, however, the methods described may be applicable to other multi-modal imaging systems.

2.1 Methods

Cardiac function and morphology were assessed using either Vevo 2100 or 3100 imaging systems with a high frequency transducer probe MS400 (VisualSonics, Toronto, ON, Canada). The anterior chest and abdomen of mice were depilated using Nair depilatory cream (Church and Dwight Co., Ewing, NJ, USA) 1 day before experiments (1). On the day of image acquisition, mice were anesthetized with 2.5–3.0% isoflurane at 0.8 L/min flow rate and maintained with 1–1.5% isoflurane (1). After anesthesia, mice were restrained in a supine position on a pad with heater, temperature sensor and ECG electrodes (1). Temperature and heart rate were maintained at 37°C and maximum of 500 beats per minute, respectively (1, 2).

2.1.1 Parasternal long axis view

To obtain parasternal long axis (PLAX) views, the mouse is placed in a supine position with the right side of the platform inclined at 45° counterclockwise (Figure 1A), and the transducer probe placed in the rail system oriented diagonally 30–40° clockwise from the right upper extremity to the left abdomen.

2.1.2 Parasternal short axis view

The parasternal short axis view (PSAX) is derived from the PLAX view by rotating the transducer probe in the rail system to approximately 90° clockwise (Figure 1B).

2.1.3 Apical view

To obtain apical views, the platform is placed slightly lateral with the head of the mouse pointing to the left, and the right upper side of the platform positioned 30° counterclockwise. The transducer probe is placed diagonally oriented toward the head (Figure 1C).

2.1.4 Aorta

With the anterior portion of the platform tilted 45° superiorly and slightly to the left, the transducer probe is shifted from the PSAX view cranially to the level of the aortic valve (Figure 1D).

2.2 Right-sided parameters

2.2.1 Right ventricle

Right-sided heart assessment is important for evaluating right heart failure (RHF) and pulmonary hypertension in rodent models, but the possible methodologies are underused in mice despite the availability of clinical guidelines for such imaging (2). Higher frequency, higher resolution, and smaller transducers have permitted advancement of RV imaging in mice despite difficulties related to the morphology and retrosternal position of the RV (2, 3). Given the difficulty in obtaining an apical four chamber view in mice and due to the frequent visual obstruction of the RV by the ribs and sternum in the parasternal short axis (PSAX), the parasternal long axis (PLAX) is the preferred echocardiographic window.

2.2.1.1 Right ventricular internal diameter

Right ventricular internal diameter (RVID) provides metric dimensions of the right ventricle during systole and diastole. To obtain this parameter, a PSAX or PLAX M-mode image should be captured with the M-mode line positioned over the RV. Obtaining the correct view may require repositioning the platform 45° to the right. Furthermore, skin reverberation artifacts can easily be confused with the RV, therefore flow on Doppler or movement in a B-mode image should be used to confirm that the RV is correctly identified. In PSAX or PLAX M-mode, RVID;s and RVID;d should be selected [instead of the intraventricular septum (IVS) IVS;s and IVS;d] to measure the diameter of the right ventricle (Figure 2). This parameter will also measure IVS, left ventricular internal diameter (LVID), and left ventricular pulmonary wall (LVPW). Increased RVID would be indicative of right ventricular dilation or volume overload and thus useful to evaluate RHF.

2.2.1.2 Right ventricular outflow tract length

Right ventricular outflow tract (RVOT) length is the measurement of the right ventricular outflow tract at end diastole. It can be measured by selecting “RVOT” in a PLAX B-mode image containing the RV (Figure 3A). The RVOT is located just proximal to the PV. RVOT is another indicator of RV size (2); a dilated RVOT suggests right ventricular volume overload.

2.2.1.3 Right ventricular outflow tract velocity time integral

Right ventricular outflow tract velocity time integral (RVOT VTI) is a measurement of blood flow through the RVOT. It can be measured as the area under the curve in a pulsed wave (PW) Doppler image of PLAX with the yellow marker on the flow of the RVOT (Figure 3B). Mean velocity, mean gradient, peak velocity, and peak gradient are automatically

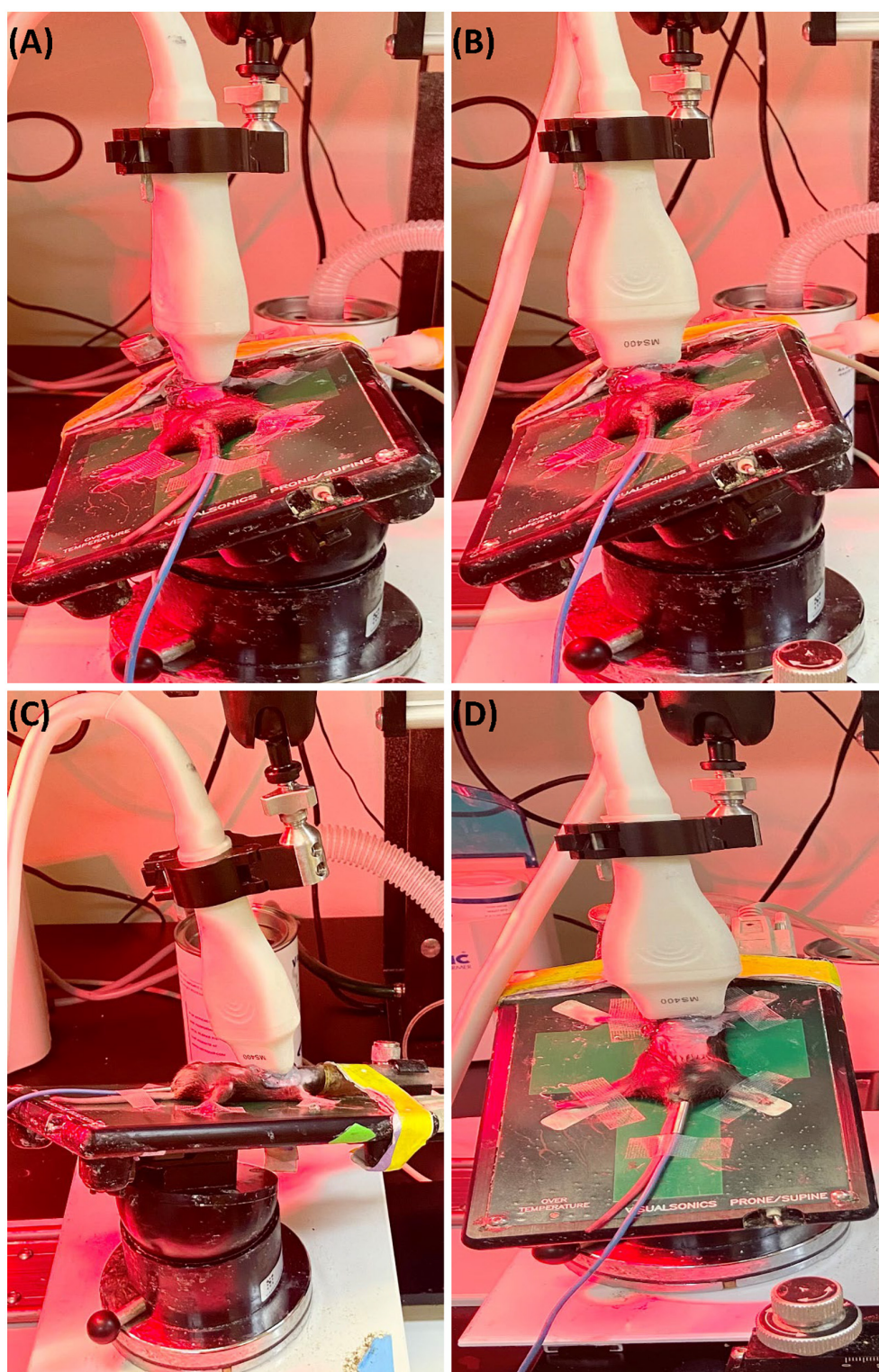


FIGURE 1

(A) Representative image showing probe positioning to obtain parasternal long axis (PLAX) views. (B) Parasternal short axis (PSAX) views are derived from the PLAX view by rotating the transducer probe in the rail system to approximately 90° clockwise. (C) To obtain apical views, the transducer probe is placed diagonally toward the head. (D) Views of the aorta can be acquired by shifting the transducer probe from the PSAX view cranially to the level of the aortic valve.

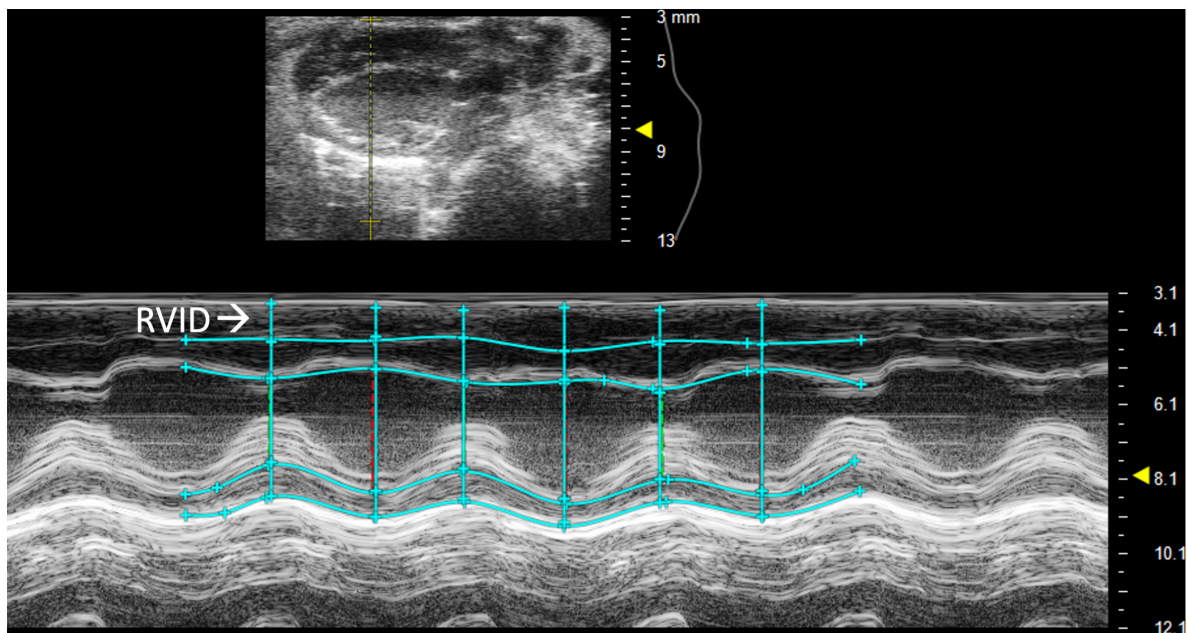


FIGURE 2

Right ventricular internal diameter (RVID), a measurement of the right ventricle during systole and diastole, is obtained by analyzing parasternal long axis (PLAX) view images in M-mode.

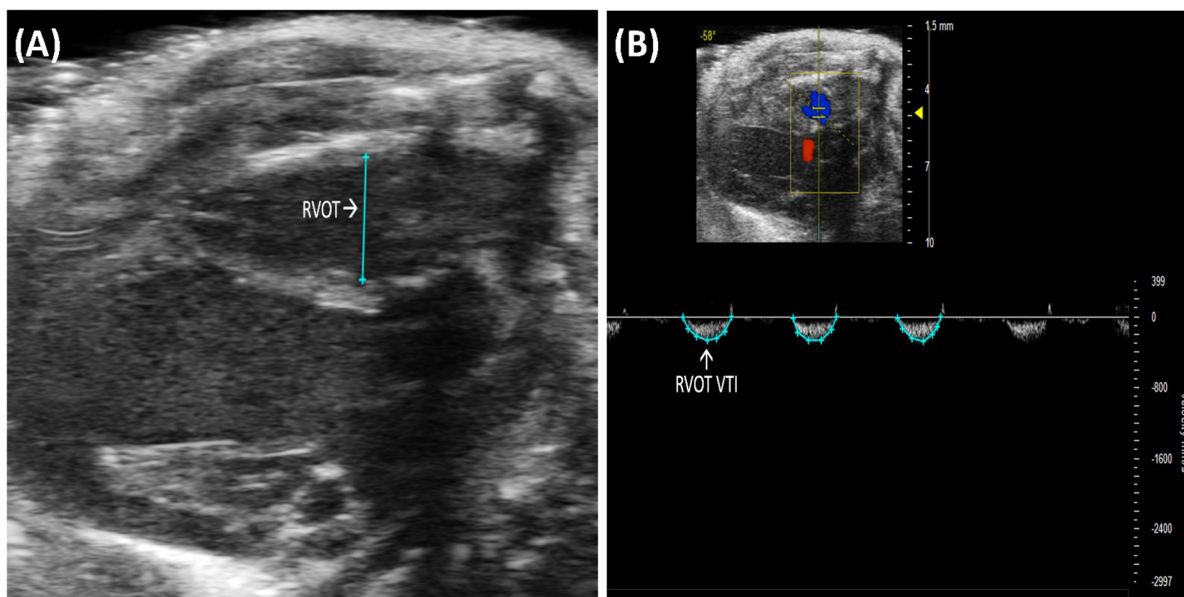


FIGURE 3

(A) Right ventricular outflow tract (RVOT) measures the size of the right ventricular outflow tract at the end of diastole and is acquired and analyzed in B-mode of the parasternal long axis (PLAX) view. (B) Right ventricular outflow tract velocity time integral (RVOT VTI) measures blood flow through the right ventricular outflow tract (RVOT) and is acquired by pulsed wave (PW) Doppler imaging of the RVOT in B-mode of the parasternal long axis (PLAX) view.

calculated. RVOT VTI is a surrogate for RV stroke volume (SV), hence, the ratio of RVOT VTI to pulmonary artery systolic pressure represents pulmonary arterial compliance, an

important measure for pulmonary arterial hypertension (PAH) (4). Right ventricular systolic pressure is equal to pulmonary artery systolic pressure (5) and can be measured by right heart

catheterization in mice. RVOT and RVOT VTI can be used to calculate right ventricular SV and cardiac output (CO).

$$RVOT\ SV = 0.785 \times RVOT^2 \times RVOT\ VTI$$

$$RVOT\ CO = \frac{RVOT\ SV \times HR\ from\ RVOT}{1000}$$

2.2.2 Pulmonary artery and valve

Pulmonary and right ventricular parameters are more informative when applied concurrently. RV dysfunction in the absence of elevated PA pressures indicates isolated RHF, while RV dysfunction concurrent with elevated PA pressures could indicate pulmonary hypertension leading to RHF or LHF leading to RHF. PA and PV measures may be incorrectly assumed to be interchangeable; however, the PA is anatomically distal to the PV in mice, and images should be captured accordingly. Measurements are made of PW Doppler mode images with the marker overlying either the PA or PV (Figures 4, 5).

2.2.2.1 Pulmonary artery velocity time integral

Pulmonary artery velocity time integral (PA VTI) is a direct measure of blood flow through the pulmonary artery. It is

calculated as the area under the curve in a PW Doppler image of the PA (Figure 4). Mean velocity, mean gradient, peak velocity, and peak gradient are automatically generated. This measure can be used to evaluate PAH because increased PA flow accompanies PAH (6).

2.2.2.2 Pulmonary regurgitation peak velocity

Pulmonary regurgitation peak velocity (PR Peak Vel) relates to degrees of pulmonic regurgitation in mouse models. PR Peak Vel is the maximum velocity of the regurgitant stream. Like most other pulmonary measures it is performed with a PW Doppler mode image of pulmonary artery flow (Figure 6). This measure allows for classification of the severity of the regurgitation.

2.2.2.3 Pulmonic valve diameter

Pulmonic valve diameter (PV diameter) measures, in millimeters, the length of the pulmonic valve. This measurement can be performed using a PLAX or PSAX view of the pulmonic valve; however, visualization is typically easier in PLAX (Figure 7). PV diameter can be used to assess whether

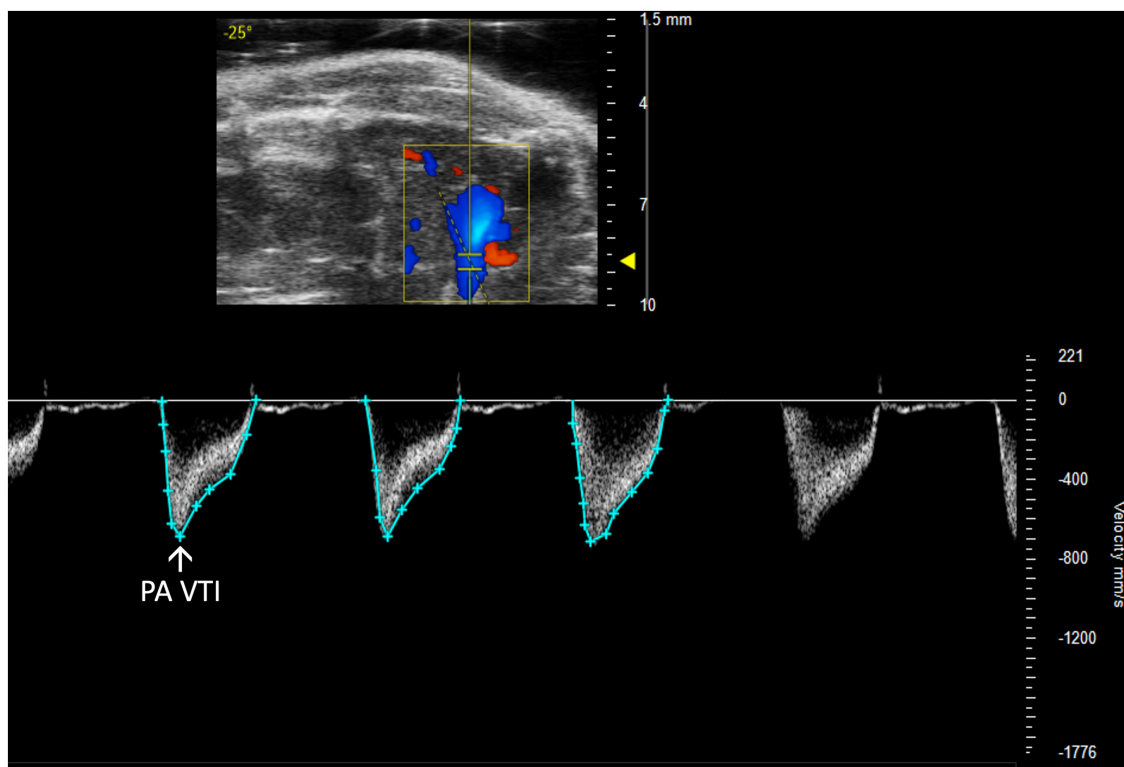


FIGURE 4

Pulmonary artery velocity time integral (PA VTI) directly measures blood flow through the pulmonary artery and is acquired as the area under the curve in pulsed wave (PW) Doppler mode of the parasternal long axis (PLAX) view.

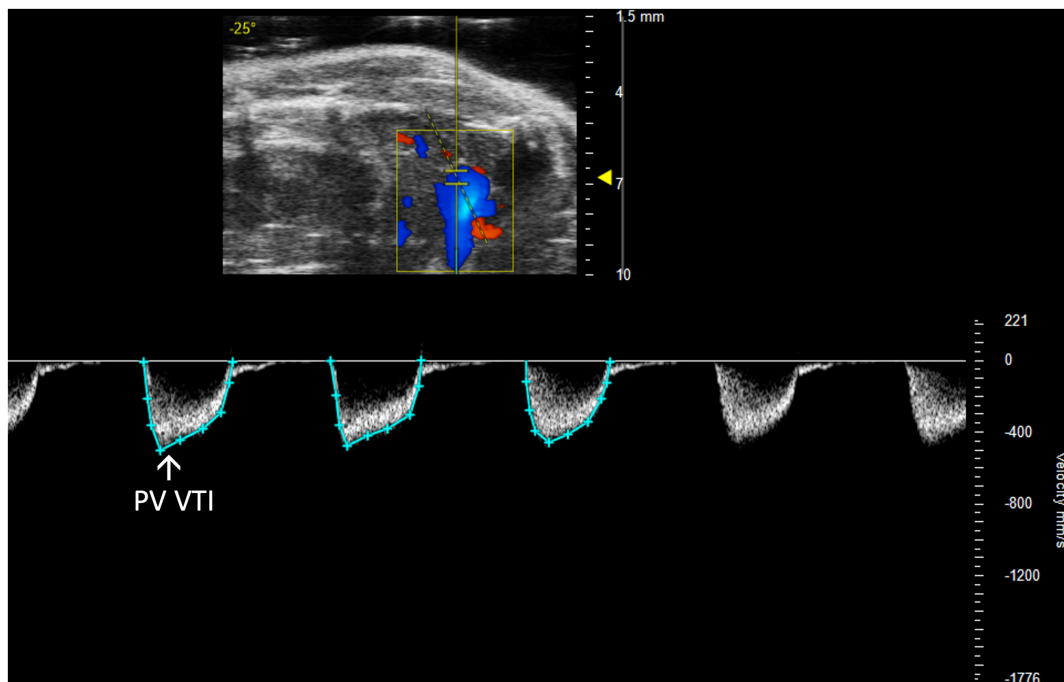


FIGURE 5

The pulmonary valve velocity time integral (PV VTI), a measure of blood flow through the pulmonary valve, is calculated by measuring the area under the curve in pulsed wave (PW) Doppler mode of the parasternal long axis view (PLAX).

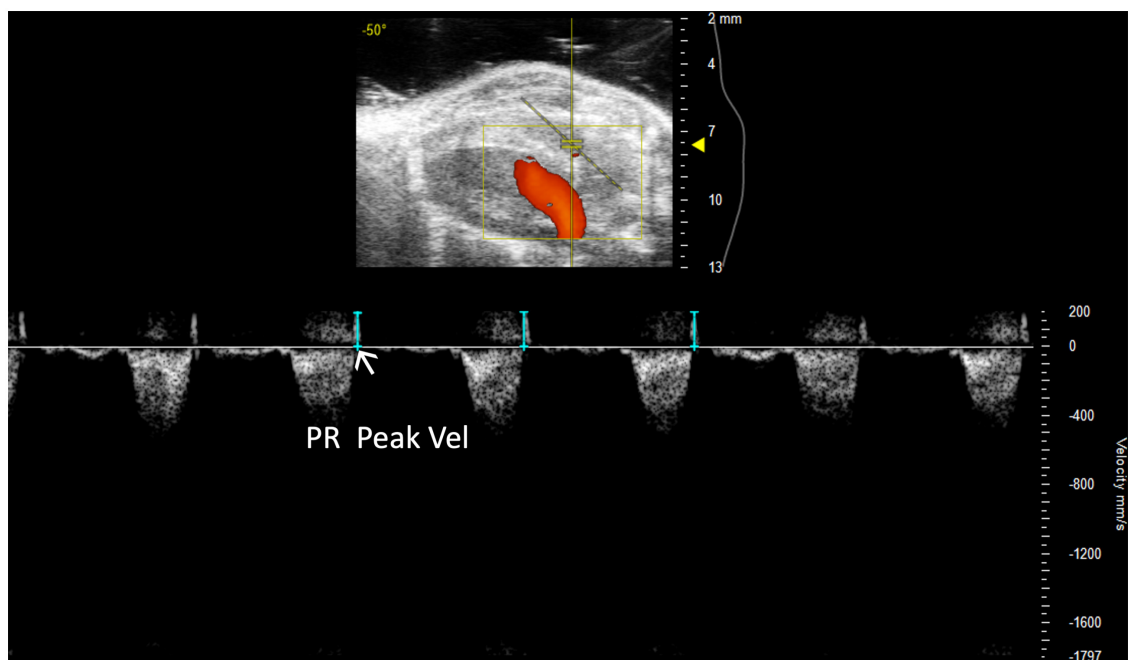


FIGURE 6

Representative image displaying pulmonary regurgitation peak velocity (PR Peak Vel), a parameter used in mouse models of pulmonic regurgitation which is acquired in pulsed wave Doppler mode of the parasternal long axis (PLAX) view.

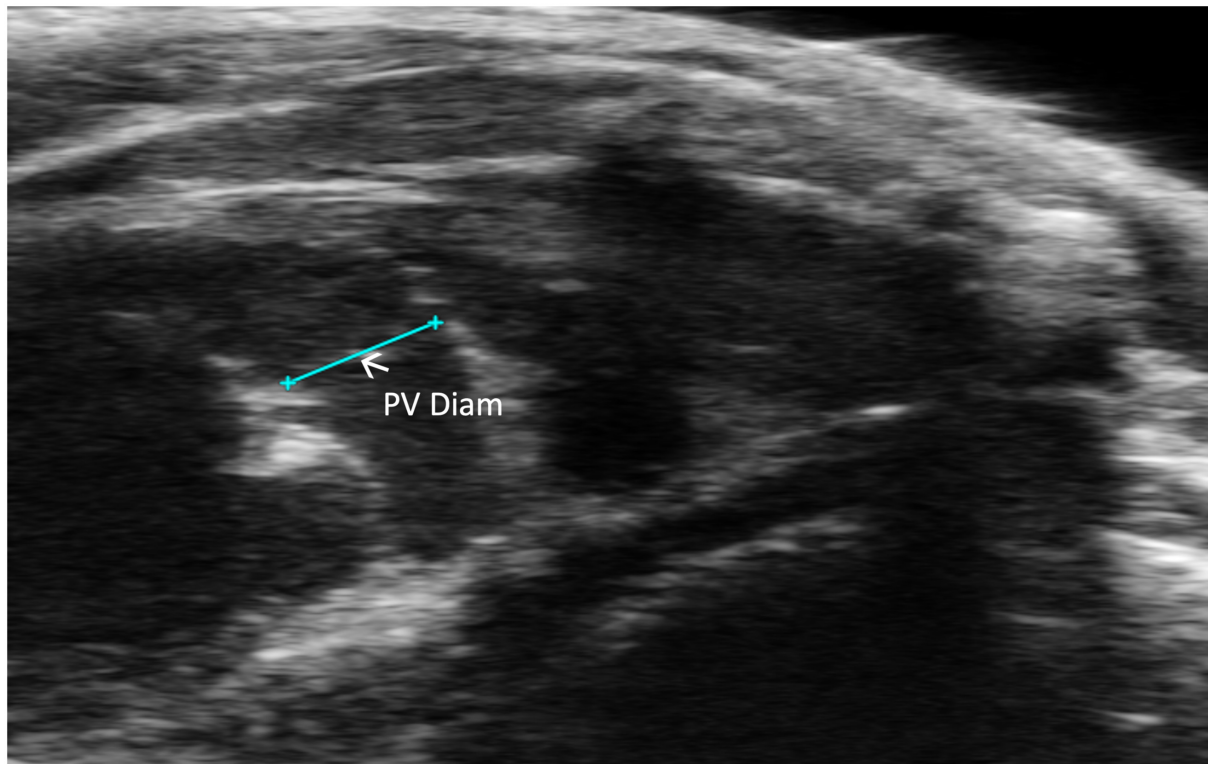


FIGURE 7

Pulmonic valve (PV) diameter is acquired and analyzed in B-mode of the parasternal long axis (PLAX) view.

pulmonic valve stenosis or dilation is present. The PV diameter can also be used with PV VTI to calculate PV SV and CO.

$$PV\ SV = 0.785 \times PV\ diam^2 \times PV\ VTI$$

$$PV\ CO = \frac{PV\ SV \times HR\ from\ PV\ diam}{1000}$$

2.3 Left-sided parameters

2.3.1 Left atrium

Left atrial size is rarely evaluated in small animal echocardiography despite the reciprocity between LA reservoir function and LV systolic function and thus cardiac output (7). In other words, LA pathology, leading to decreased preload affects CO and LV systolic function. Furthermore, the LA can be used as a marker of chronic LV dysfunction (8) as is influenced by elevated left ventricular end diastolic pressure (LVEDP) propagating backwards (9).

2.3.1.1 Left atrial depth

Left atrial depth can be measured vertically at end diastole. To perform this parameter, a PLAX M-mode image should be

captured with the yellow line positioned over the LA, which is located inferior to the aorta (Figure 8).

2.3.2 Left ventricle

Although extensively characterized because of the accessibility of imaging the LV, many parameters are inadequately described in literature.

2.3.2.1 Left ventricular outflow length

Left ventricular outflow tract length (LVOT) measures, in millimeters, the left ventricular outflow tract, just proximal to the aortic valve, at end diastole. It is measured by selecting “LVOT” under “AoV Flow” in a PLAX B-mode image containing the left ventricular outflow tract (Figure 9). LVOT would be a valuable measure for mouse models of aortic stenosis because it can be used to calculate aortic valve area (AVA) (see below).

2.3.2.2 Left ventricular outflow tract velocity time integral

Left ventricular outflow tract velocity time integral (LVOT VTI) is defined as a measurement of blood flow out of the ascending aorta. It can be measured as the area under the curve in a PLAX PW Doppler mode image with the cursor over the flow of the ascending aorta (Figure 10). LVOT VTI has

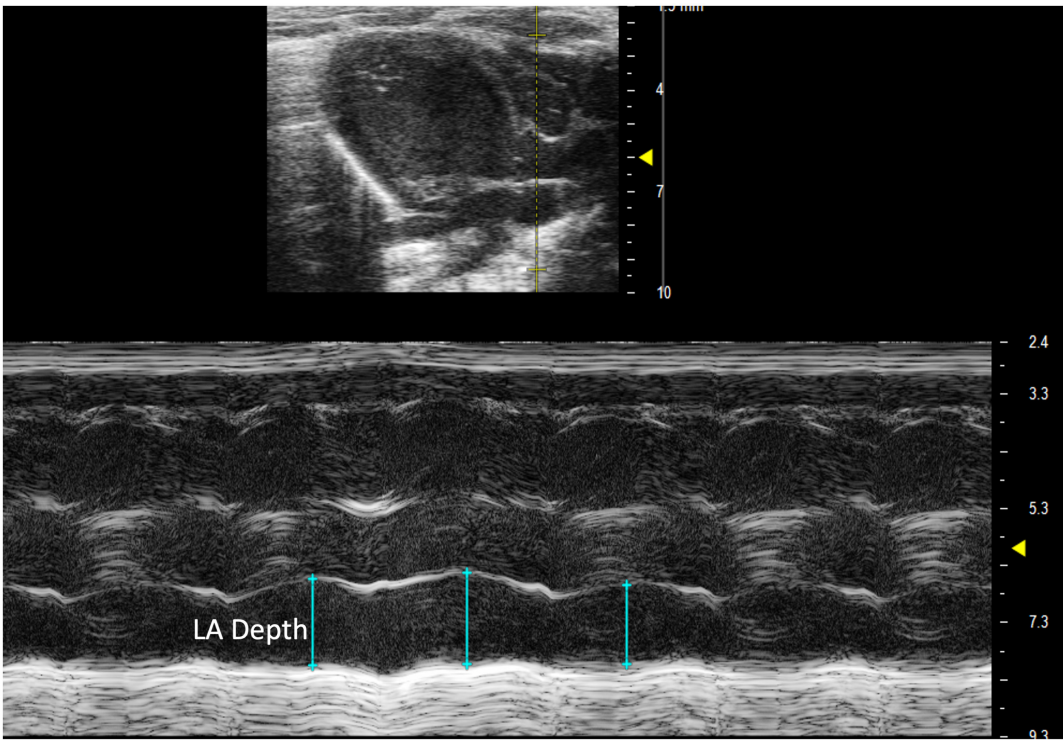


FIGURE 8
Parasternal long axis (PLAX) M-mode view displaying left atrial depth measurement just inferior to the aorta.

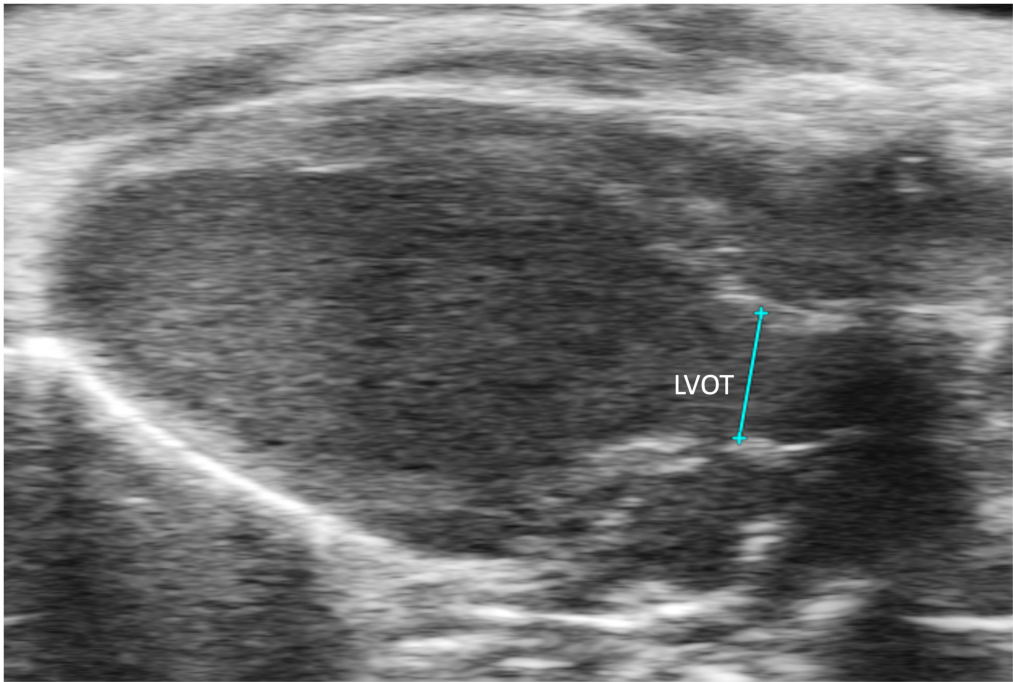


FIGURE 9
The left ventricular outflow tract (LVOT) length is acquired in the B-mode of the parasternal long axis view (PLAX).

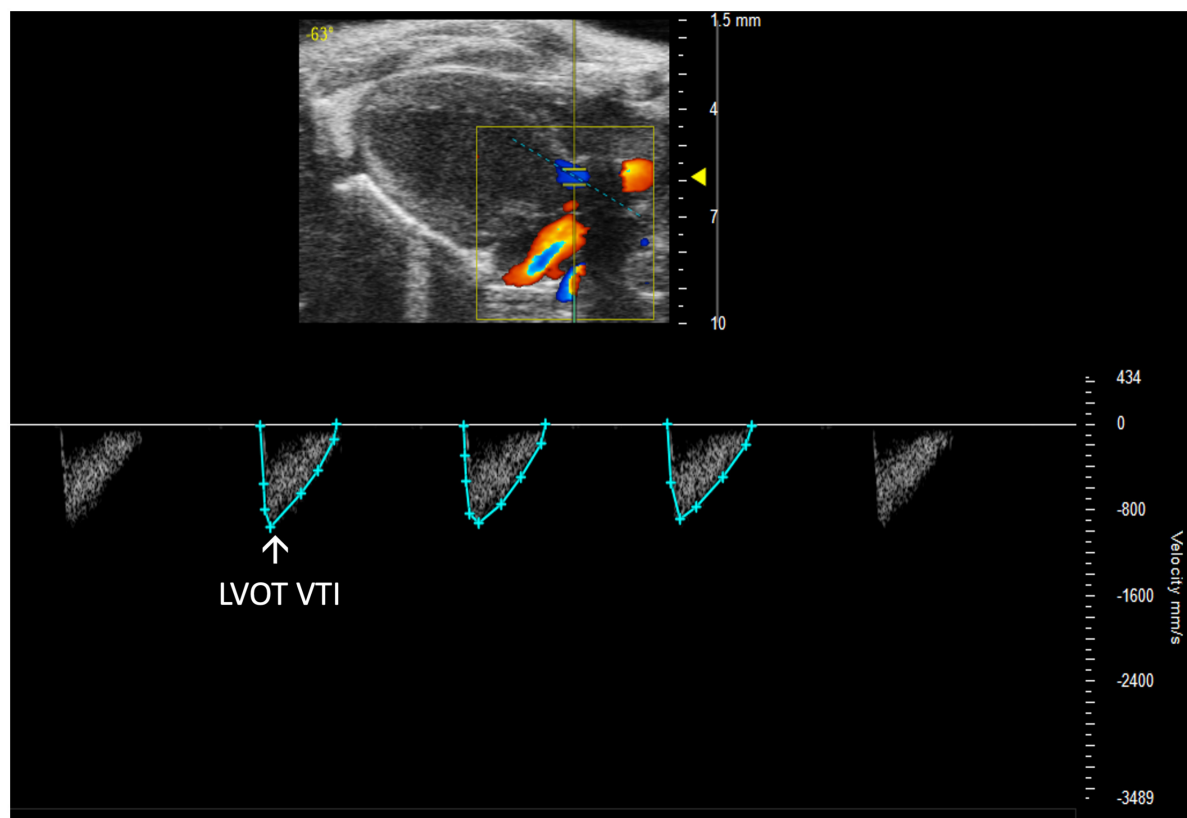


FIGURE 10

Representative image displaying left ventricular outflow tract velocity time integral (LVOT VTI), a measure of blood flow out of the ascending aorta which is obtained by calculating the area under the curve in the PW Doppler mode of the parasternal long axis view.

been shown to be representative of CO in humans and more predictive than EF or Doppler derived CO in patients with heart failure (10). Thus, we hypothesize that LVOT VTI is an accurate measure of systolic function and CO in mice as well, but this remains an interesting area of study for future directions. LVOT and LVOT VTI can be used to calculate SV, CO, and AVA:

$$LVOT\ SV = 0.785 \times LVOT^2 \times LVOT\ VTI$$

$$LVOT\ CO = \frac{LVOT\ SV \times HR\ from\ LVOT}{1000}$$

$$AVA = \frac{\left(\frac{LVOT}{2}\right)^2 \times \pi \times LVOT\ VTI\ Peak\ Vel}{AV\ Peak\ Vel}$$

2.3.3 Mitral valve

2.3.3.1 Mitral regurgitation

Mitral regurgitation (MR) has not been well-described in mice because of their resistance to developing mitral valve prolapse (11). However, Li et al. recently reported the first mouse model of severe MR (Figure 11, 12). To continue development

of mouse models of MR, it is important to be able to recognize the presence of mitral regurgitation, which appears as a mixed color pattern of systolic backflow from the LV to the LA on PSAX Color Doppler.

2.3.3.2 Mitral valve pressure half time

Mitral stenosis is another disease that is not well-replicated in mice. However, mitral valve pressure half time (MV PHT) is a potentially useful parameter in the setting of mitral stenosis (10). MV PHT is the time interval, in milliseconds, for the maximum mitral gradient to reduce to half the maximum initial value. It is most accurately measured in a PW Doppler image of the mitral valve by measuring maximum velocity, calculating half of the maximum velocity, and dropping another velocity measurement on the mitral valve curve equal to half of the maximum velocity. Finally, the peaks of the velocity measurements are measured as MV PHT, and the velocity measurements can be deleted (Figure 12).

2.3.3.3 Mitral valve ejection time

Mitral valve ejection time (MV ET) is equal to the duration of diastolic filling of the LV; therefore, can be used to further

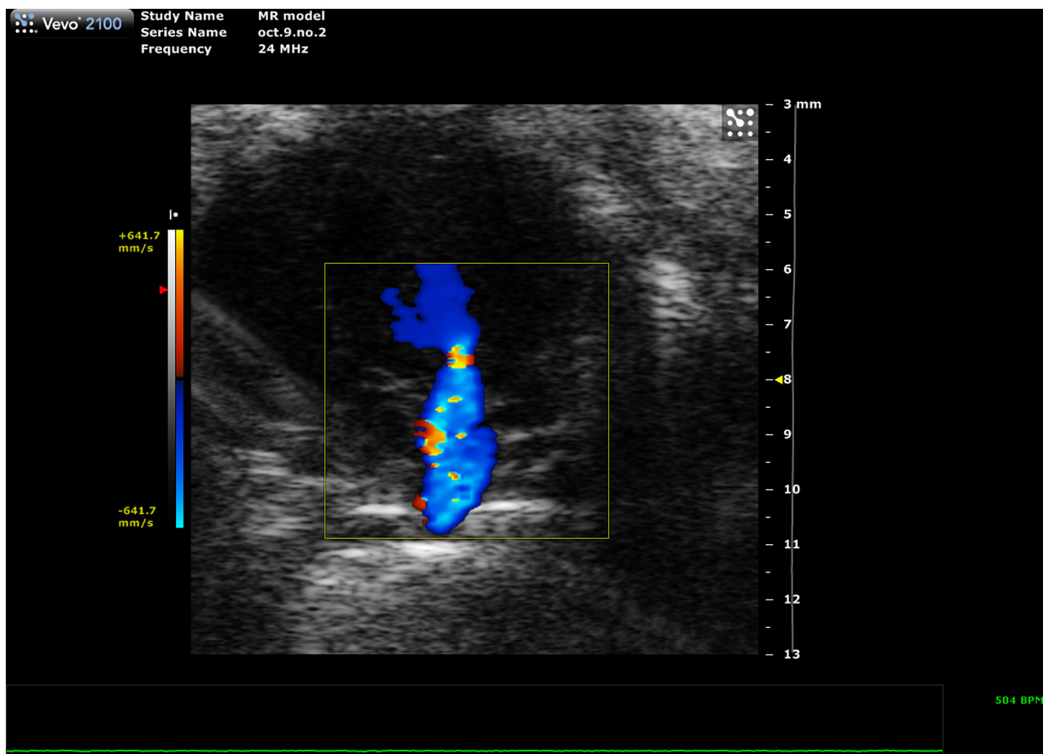


FIGURE 11
Representative image showing a mixed color pattern of systolic backflow from the left ventricle to the left atrium in severe mitral regurgitation.

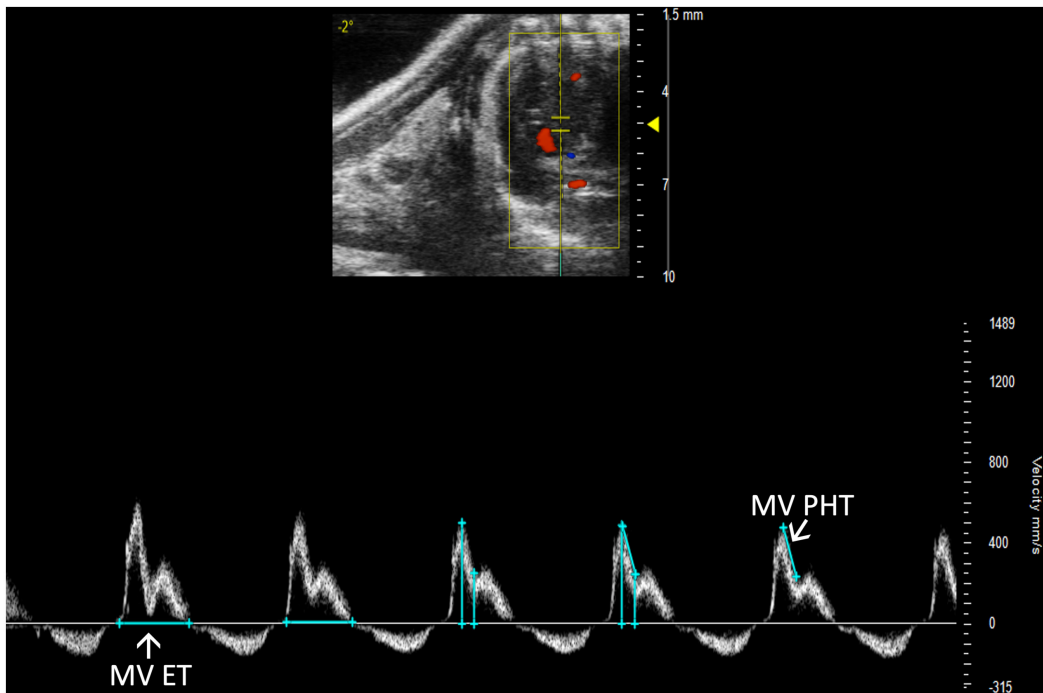


FIGURE 12
Pulsed wave (PW) Doppler mode image showing mitral valve pressure half time (MV PHT), a measure of mitral stenosis and mitral valve ejection time (MV ET), the duration of diastolic filling in the left ventricle.

characterize diastolic dysfunction. MV ET is measured at the end of IVRT to the beginning of IVCT on a PW Doppler of the mitral valve (**Figure 12**).

2.3.4 Aortic valve

Aortic regurgitation has been seen in existing mouse models; however, methods for analysis beyond visual recognition have not been well-established.

2.3.4.1 Aortic insufficiency deceleration

Aortic insufficiency pressure half time (AI PHT) is the rate of deceleration of Doppler signal, indicating the degree of regurgitation and LVEDP (**13**). The same method to measure MV PHT is used to measure AI PHT in PW Doppler mode of the aortic valve (**Figure 13**). Aortic insufficiency half time is automatically calculated.

2.3.4.2 Aortic acceleration time

Aortic acceleration time (AAT) has been validated by Perez et al. to assess LV contractility in mice. It is measured in PW Doppler mode as the time to peak aortic velocity (**Figure 14**). Studies in humans suggest that the ratio of AAT to aortic ejection time (AET) predicts aortic stenosis severity (**14**), although it has not yet been evaluated in mice.

3 Anticipated results

Normalizing the acquisition and analysis of infrequently used parameters coupled with commonly used values will provide further insight into both left and right-sided cardiac function. In recent years, the importance of the right heart has become more evident but a complete understanding remains elusive. Implementing the additional parameters described here will generate a more comprehensive picture of cardiovascular disease in mouse models that can be applied to parallel human conditions.

3.1 Limitations

All analyses are limited by human error in image acquisition. The RV must be captured in PLAX M-mode in order to measure RV parameters, however, as noted by Brittain et al., sometimes the RV is only visible when dilated. If the transducer is misaligned with blood flow for Doppler modes, blood velocity will be decreased for LVOT VTI and RVOT VTI measurements and SV and CO will be falsely low (**3**). To obtain the most accurate readings, blood flow direction should be as vertical as possible (up or down) and the dotted line aligned with blood flow in all PW Doppler images. Another limitation

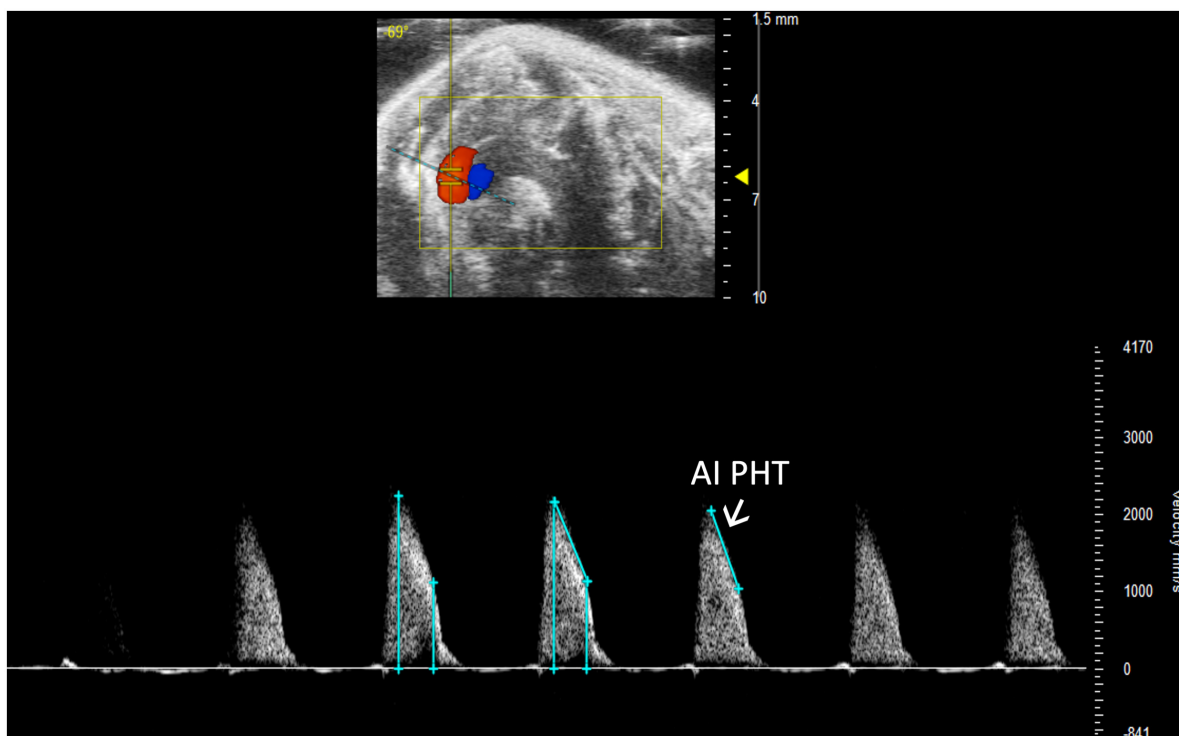


FIGURE 13

Aortic insufficiency pressure half time (AI PHT) represents the degree of regurgitation and reflects the left ventricular end diastolic pressure and is measured in pulsed wave (PW) Doppler mode of the aortic valve.

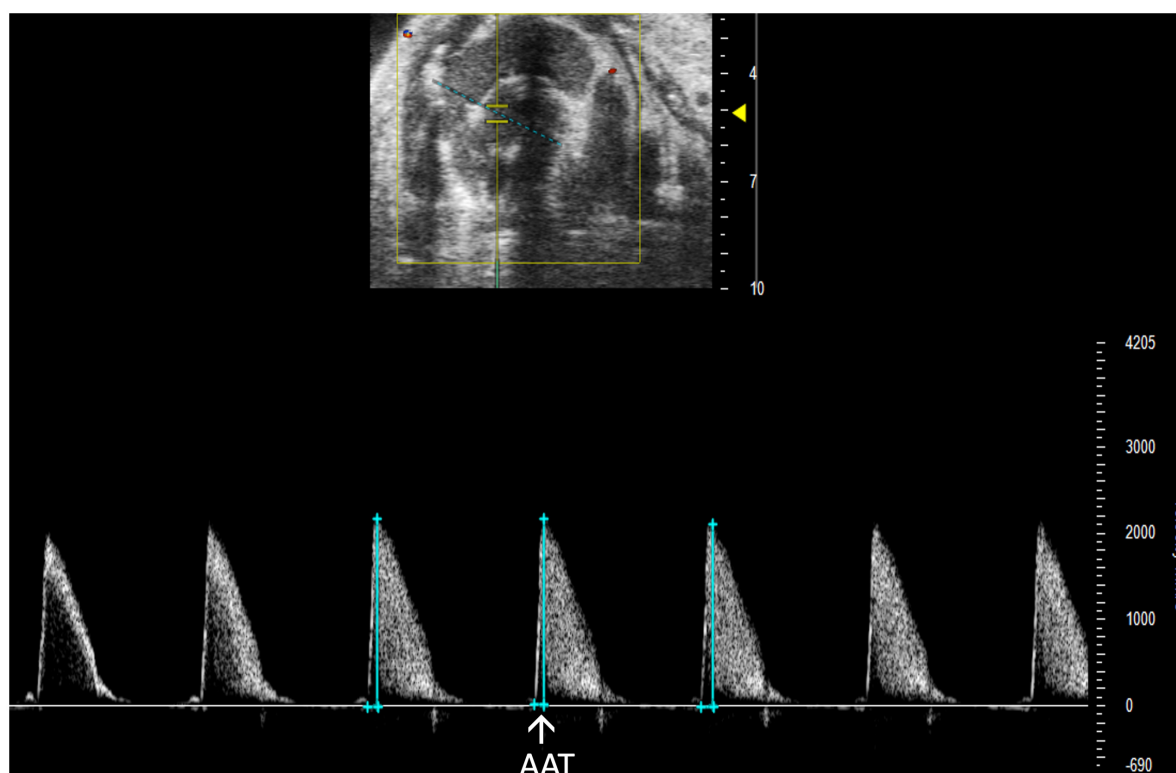


FIGURE 14

Pulsed wave (PW) Doppler mode image showing analysis of the aortic acceleration time (AAT), a measurement of left ventricular contractility in mice.

is the increased training and effort required to accurately and reproducibly perform a significant number of additional parameters as well as the increased time required to capture the extra views.

4 Discussion

In our quest to improve resources, expand and optimize echocardiography parameters in rodent models, we realized a need for protocols and information to define and facilitate infrequently used parameters. Here, we present multiple parameters that are rarely used and provide a thorough description of echocardiography acquisition and analysis of these parameters. Although VisualSonics Vevo imaging systems were used to obtain these images and derive parameters, the same approaches should be applicable to other comparable imaging systems such as S-Sharp (15, 16). In a study that measured the grey scale imaging performance of 17 preclinical transducers over 10 years, all except one S-sharp transducer were Vevo transducers (17), thus, our protocol likely covers the instruments commonly available for use. A summary of these infrequently used parameters combined with common echocardiography parameters as well as data values from 10 to

12-week-old male and female mice from C57BL/6, BalbC, and 129Sv mouse strains can be found in **Table 1**.

Previously, the importance of the right heart was underestimated (18). Within the last decade, significant progress has been made in our understanding of the mechanisms involved in acute and chronic right heart failure as well as the role of the pulmonary system (19). However, complete understanding of right heart and pulmonary circuit function remains elusive (18). Exploring right heart and pulmonary function by echocardiography acquisition and analysis of infrequently used parameters such as RVID, RVOT, RVOT VTI, PA VTI, PV Diameter, and PR Peak Velocity in various mouse models may provide more insight into right heart and pulmonary valve dysfunction.

In contrast, left-sided parameters are frequently characterized due to ease of accessibility to the left ventricle during echocardiography acquisition. Despite accessibility, some left-sided parameters including, LA size and depth, LVOT, LVOT VTI, visual assessment of MR and AR, MV PHT, MV ET, AI PHT, and AAT are rarely acquired and analyzed. These values, coupled with frequently used left and right heart parameters, may provide further insight into cardiac function.

This manuscript serves as a guide to understanding the acquisition and analysis of infrequently used echocardiography

TABLE 1 Anatomic structures, modes, definitions, and reference values of both common and infrequently used parameters for the C57BL/6, BalbC, and 129Sv mouse strains.

Anatomic structure	Mode	Parameter	Definition	C57BL/6 (<i>n</i> = 11)	BalbC (<i>n</i> = 10)	129Sv (<i>n</i> = 9)
Mitral valve (MV)	PW Doppler	MV E (mm/s)	Mitral valve early peak	754.47 ± 412.82	939.27 ± 167.53	374.77 ± 126.08
		MV A (mm/s)	Mitral valve atrial peak	556.38 ± 265.92	525.27 ± 244.75	258.80 ± 91.50
		IVRT (ms)	Isovolumetric relaxation time	15.23 ± 4.81	13.31 ± 2.89	20.76 ± 8.83
		IVCT (ms)	Isovolumetric contraction time	10.58 ± 4.37	9.69 ± 2.73	19.24 ± 9.34
		MV VTI (mm)	Velocity time interval of mitral valve inflow	23.10 ± 13.19	32.63 ± 5.69	11.95 ± 4.74
		NFT (ms)	No flow time	71.82 ± 12.79	83.28 ± 9.07	90.61 ± 11.63
		AET (ms)	Aortic ejection time	45.15 ± 7.23	62.64 ± 4.17	49.41 ± 10.39
		MV PHT (ms)	Mitral valve pressure half time	4.31 ± 2.30	7.24 ± 2.32	4.12 ± 0.70
		MV ET (ms)	Mitral valve ejection time	55.74 ± 14.25	72.28 ± 13.02	56.25 ± 9.26
	PW tissue Doppler	E' (mm/s)	Mitral valve early peak	−18.72 ± 7.47	−22.51 ± 3.95	−18.64 ± 3.47
Aortic valve (AoV)	PW Doppler	A' (mm/s)	Mitral valve atrial peak	−23.11 ± 12.05	−19.62 ± 5.69	−20.11 ± 3.48
		AV peak (mm/s)	Peak velocity of blood flow through the aortic valve	2537.54 ± 870.16	1024.86 ± 134.84	2265.77 ± 1453.38
		AET (ms)	Aortic ejection time	56.16 ± 13.11	62.64 ± 4.17	49.41 ± 6.46
		AI PHT (ms)	Aortic insufficiency pressure half time	22.65 ± 3.35	30.31 ± 4.84	20.70 ± 4.42
		AAT (ms)	Aortic acceleration time	11.76 ± 2.70	15.24 ± 2.63	10.80 ± 3.17
Pulmonary artery (PA) and valve (PV)	PW Doppler	PV peak (mm/s)	Peak velocity of blood flow through the pulmonic valve	−640.94 ± 164.23	−682.15 ± 141.19	−632.16 ± 240.09
		PAT (ms)	Pulmonic valve acceleration time	18.69 ± 4.25	24.83 ± 4.96	25.46 ± 4.07
		PET (ms)	Pulmonic valve ejection time	58.45 ± 6.95	63.89 ± 4.50	62.64 ± 6.01
		PV VTI (mm)	Velocity time interval of blood through the pulmonic valve	26.20 ± 5.36	32.29 ± 7.04	27.29 ± 12.43
		PR Peak Vel (mm/s)	Maximum velocity of regurgitant stream through the pulmonic valve	149.18 ± 40.46	206.17 ± 135.15	117.32 ± 42.55
		PA VTI (mm)	Velocity time interval of blood flow through the pulmonary artery	29.95 ± 6.65	32.29 ± 7.04	28.24 ± 6.10
	PSLAX B-mode	PV diameter (mm)	Length of the pulmonic valve	1.38 ± 0.18	1.16 ± 0.25	1.42 ± 0.09
Left atrium (LA)	PSLAX M-mode	LA (mm)	Depth of the left atrium	2.04 ± 0.44	1.29 ± 0.34	2.98 ± 0.69

(Continued)

TABLE 1 (Continued)

Anatomic structure	Mode	Parameter	Definition	C57BL/6 (<i>n</i> = 11)	BalbC (<i>n</i> = 10)	129Sv (<i>n</i> = 9)
Left ventricle (LV)	PSLAX B-mode	ENDOmajr;s/d (mm)	Length of the LV endocardium during systole and diastole	6.35 ± 0.81/7.28 ± 0.90	6.58 ± 0.68/7.26 ± 0.72	5.88 ± 0.52/6.81 ± 0.53
		EPImajr;s/d (mm)	Length of the LV epicardium during systole and diastole	7.24 ± 0.73/7.94 ± 0.84	7.02 ± 0.71/7.76 ± 0.74	6.68 ± 0.48/7.45 ± 0.58
		LVOT (mm)	Left ventricular outflow tract length	1.58 ± 0.26	1.51 ± 0.10	1.77 ± 0.18
	PSAX B-mode	ENDOarea;s/d (mm)	Area of the LV endocardium during systole and diastole	5.48 ± 3.46/12.40 ± 4.15	7.24 ± 1.72/13.03 ± 2.02	3.94 ± 1.62/9.12 ± 1.56
		EPIarea;s/d (mm)	Area of the LV epicardium during systole and diastole	18.98 ± 5.14/24.76 ± 6.57	17.66 ± 2.64/23.02 ± 3.09	19.06 ± 2.40/22.68 ± 3.31
		IVS;s/d (mm)	Intraventricular septum during systole and diastole	1.27 ± 0.25/0.81 ± 0.14	0.96 ± 0.16/0.61 ± 0.10	1.19 ± 0.13/0.90 ± 0.16
	PSLAX M-mode	LVID;s/d (mm)	Left ventricular internal diameter during systole and diastole	2.35 ± 0.43/3.67 ± 0.31	2.98 ± 0.51/3.91 ± 0.46	1.58 ± 0.22/2.36 ± 0.42
		LVPW;s/d (mm)	Left ventricular posterior wall during systole and diastole	1.21 ± 0.36/0.89 ± 0.32	0.76 ± 0.16/0.65 ± 0.10	1.00 ± 0.14/0.72 ± 0.08
		LVAW;s/d (mm)	Left ventricular anterior wall during systole and diastole	1.52 ± 0.27/0.97 ± 0.18	1.08 ± 0.15/0.69 ± 0.09	1.52 ± 0.40/1.03 ± 0.32
	PSAX M-mode	LVID;s/d (mm)	Left ventricular internal diameter during systole and diastole	2.45 ± 0.70/3.85 ± 0.47	2.99 ± 0.48/3.95 ± 0.39	2.12 ± 0.55/3.37 ± 0.38
		LVPW;s/d (mm)	Left ventricular posterior wall during systole and diastole	1.13 ± 0.22/0.77 ± 0.13	0.75 ± 0.13/0.65 ± 0.11	1.11 ± 0.22/0.80 ± 0.18
		PSLAX PW Doppler	LVOT VTI (mm)	22.27 ± 9.66	16.19 ± 3.08	37.10 ± 18.93
Right ventricle (RV)	PSLAX M-mode	RVID;s/d (mm)	Right ventricular internal diameter during systole and diastole	0.79 ± 0.15 /1.16 ± 0.11	0.99 ± 0.31/1.23 ± 0.31	0.86 ± 0.30 /1.20 ± 0.45
	PSLAX B-mode	RVOT (mm)	Right ventricular outflow tract length	1.46 ± 0.23	1.47 ± 0.20	1.60 ± 0.14
	PSLAX PW Doppler	RVOT VTI (mm)	Right ventricular outflow tract length velocity time integral	18.05 ± 9.83	16.10 ± 7.54	15.38 ± 6.55

Infrequently used parameters are highlighted in gray. Male and female mice at the age of 10–12 weeks of age were used. Data are Mean ± SD.

parameters. With the continued development of mouse models that mimic human cardiac disease it is imperative to define and integrate a complete repertoire of echocardiography parameters to maximize data yields and avoid overlooking elements of unique pathologies.

Data availability statement

The raw data supporting the conclusions of this article will be made available by the authors, without undue reservation.

Ethics statement

The animal study was reviewed and approved by IACUC.

Author contributions

ET, MW, and LS perceived the project. MW and AK acquired the images. ET, MW, AK, and MR analyzed the images. ET and MW drafted the manuscript. All authors revised the manuscript, approved the final version of the manuscript, and agreed to be accountable for all aspects of the work.

Funding

This work was supported by the following grants to LS: National Institute of Health (1R01HL140468) and the Miami Heart Research Institute and the American Heart Association

References

1. Irion CI, Williams M, Capcha JC, Eisenberg T, Lambert G, Takeuchi LM, et al. Col4a3(−/−) Mice on Balb/C background have less severe cardiorespiratory phenotype and SGLT2 over-expression compared to 129x1/Svj and C57Bl/6 backgrounds. *Int J Mol Sci.* (2022) 23:6674. doi: 10.3390/ijms23126674
2. Kohut A, Patel N, Singh H. Comprehensive echocardiographic assessment of the right ventricle in murine models. *J Cardiovasc Ultrasound.* (2016) 24:229–38. doi: 10.4250/jcu.2016.24.3.229
3. Brittain E, Penner NL, West J, Hemnes A. Echocardiographic assessment of the right heart in mice. *J Vis Exp.* (2013) 81:50912. doi: 10.3791/50912
4. Bhattacharya PT, Troutman GS, Mao F, Fox AL, Tanna MS, Zamani P, et al. Right ventricular outflow tract velocity time integral-to-pulmonary artery systolic pressure ratio: a non-invasive metric of pulmonary arterial compliance differs across the spectrum of pulmonary hypertension. *Pulm Circ.* (2019) 9:2045894019841978. doi: 10.1177/2045894019841978
5. Thibault HB, Kurtz B, Raheer MJ, Shaik RS, Waxman A, Derumeaux G, et al. Noninvasive assessment of murine pulmonary arterial pressure: validation and application to models of pulmonary hypertension. *Circ Cardiovasc Imaging.* (2010) 3:157–63. doi: 10.1161/CIRCIMAGING.109.887109
6. Shah M, Phillips MR, Quintana M, Stupp G, McLean SE. Echocardiography allows for analysis of pulmonary arterial flow in mice with congenital diaphragmatic hernia. *J Surg Res.* (2018) 221:35–42. doi: 10.1016/j.jss.2017.06.080
7. Barbier P, Solomon SB, Schiller NB, Glantz SA. Left atrial relaxation and left ventricular systolic function determine left atrial reservoir function. *Circulation.* (1999) 100:427–36. doi: 10.1161/01.CIR.100.4.427
8. Colazzo F, Castiglioni L, Sironi L, Fontana L, Nobili E, Franzosi M, et al. Murine left atrium and left atrial appendage structure and function: echocardiographic and morphologic evaluation. *PLoS One.* (2015) 10:e0125541. doi: 10.1371/journal.pone.0125541
9. Medrano G, Hermosillo-Rodriguez J, Pham T, Granillo A, Hartley CJ, Reddy A, et al. Left atrial volume and pulmonary artery diameter are noninvasive measures of age-related diastolic dysfunction in mice. *J Gerontol A Biol Sci Med Sci.* (2016) 71:1141–50. doi: 10.1093/gerona/glv143
10. Tan C, Rubenson D, Srivastava A, Mohan R, Smith MR, Billick K, et al. Left ventricular outflow tract velocity time integral outperforms ejection fraction and Doppler-derived cardiac output for predicting outcomes in a select advanced heart failure cohort. *Cardiovasc Ultrasound.* (2017) 15:18. doi: 10.1186/s12947-017-0109-4
11. Perez JET, Ortiz-Urbina J, Heredia CP, Pham TT, Madala S, Hartley CJ, et al. Aortic acceleration as a noninvasive index of left ventricular

(965480). MW was a recipient of NIH Diversity Supplement Award.

Acknowledgments

We would like to thank Laurie Rich from VisualSonics for confirming the accuracy of our description about the technical details of image acquisition using their system. We would also like to thank Hesham Sadek from University of Texas Southwestern Medical Center for providing the MR image, and Keith Webster from Baylor College of Medicine for reading the manuscript and providing feedback.

Conflict of interest

The authors declare that the research was conducted in the absence of any commercial or financial relationships that could be construed as a potential conflict of interest.

Publisher's note

All claims expressed in this article are solely those of the authors and do not necessarily represent those of their affiliated organizations, or those of the publisher, the editors and the reviewers. Any product that may be evaluated in this article, or claim that may be made by its manufacturer, is not guaranteed or endorsed by the publisher.

contractility in the mouse. *Sci Rep.* (2021) 11:536. doi: 10.1038/s41598-020-79866-y

12. Li S, Nguyen NUN, Xiao F, Menendez-Montes I, Nakada Y, Tan WLW, et al. Mechanism of eccentric cardiomyocyte hypertrophy secondary to severe mitral regurgitation. *Circulation.* (2020) 141:1787–99. doi: 10.1161/CIRCULATIONAHA.119.043939

13. Sallach S, Reimold S. Echocardiographic Evaluation of Aortic Regurgitation. In: Solomon SD, Bulwer B editors. *Essential Echocardiography: Contemporary Cardiology.* Totowa, NJ: Humana Press (2007).

14. Gamaza-Chulian S, Diaz-Retamino E, Camacho-Freire S, Ruiz-Fernandez D, Gutierrez-Barrios A, Oneto-Otero J. Acceleration time and ratio of acceleration time to ejection time in aortic stenosis: new echocardiographic diagnostic parameters. *J Am Soc Echocardiogr.* (2017) 30:947–55. doi: 10.1016/j.echo.2017.06.001

15. Yamashita S, Suzuki T, Iguchi K, Sakamoto T, Tomita K, Yokoo H, et al. Cardioprotective and functional effects of levosimendan and milrinone in mice

with cecal ligation and puncture-induced sepsis. *Naunyn Schmiedebergs Arch Pharmacol.* (2018) 391:1021–32. doi: 10.1007/s00210-018-1527-z

16. Hsu WT, Tseng YH, Jui HY, Kuo CC, Wu KK, Lee CM. 5-Methoxytryptophan attenuates postinfarct cardiac injury by controlling oxidative stress and immune activation. *J Mol Cell Cardiol.* (2021) 158:101–14. doi: 10.1016/j.yjmcc.2021.05.014

17. Moran CM, Inglis S, McBride K, McLeod C, Pye SD. The imaging performance of diagnostic ultrasound scanners using the edinburgh pipe phantom to measure the resolution integral – 15 years of experience. *Ultraschall Med.* (2022) 43:393–402. doi: 10.1055/a-1194-3818

18. El Hajj MC, Viray MC, Tedford RJ. Right heart failure: a hemodynamic review. *Cardiol Clin.* (2020) 38:161–73. doi: 10.1016/j.ccl.2020.01.001

19. Thandavarayan RA, Chitturi KR, Guha A. Pathophysiology of acute and chronic right heart failure. *Cardiol Clin.* (2020) 38:149–60. doi: 10.1016/j.ccl.2020.01.009



OPEN ACCESS

EDITED BY

Sanjeev Bhattacharyya,
Barts Heart Centre, United Kingdom

REVIEWED BY

Søren Møller,
University of Copenhagen, Denmark
Alik Tsagkridi,
Barts Heart Centre, United Kingdom

*CORRESPONDENCE

Xijun Zhang
✉ sophia3936@163.com
Jianjun Yuan
✉ yuan2373@163.com

[†]These authors have contributed equally to this work.

SPECIALTY SECTION

This article was submitted to Cardiovascular Imaging, a section of the journal Frontiers in Cardiovascular Medicine

RECEIVED 18 December 2022

ACCEPTED 21 February 2023

PUBLISHED 08 March 2023

CITATION

Cao Y, Zhang H, Li S, Li S, Sun S, Chen J, Ye T, Zhang X and Yuan J (2023) Correlation analysis between myocardial work indices and liver function classification in patients with hepatitis B cirrhosis: A study with non-invasive left ventricular pressure-strain loop.
Front. Cardiovasc. Med. 10:1126590.
doi: 10.3389/fcvm.2023.1126590

COPYRIGHT

© 2023 Cao, Zhang, Li, Li, Sun, Chen, Ye, Zhang and Yuan. This is an open-access article distributed under the terms of the [Creative Commons Attribution License \(CC BY\)](#). The use, distribution or reproduction in other forums is permitted, provided the original author(s) and the copyright owner(s) are credited and that the original publication in this journal is cited, in accordance with accepted academic practice. No use, distribution or reproduction is permitted which does not comply with these terms.

Correlation analysis between myocardial work indices and liver function classification in patients with hepatitis B cirrhosis: A study with non-invasive left ventricular pressure-strain loop

Yang Cao^{1†}, Huihui Zhang^{2†}, Shuai Li², Siliang Li², Shuowen Sun², Jinwen Chen³, Ting Ye³, Xijun Zhang^{2*} and Jianjun Yuan^{2*}

¹Department of Ultrasound, People's Hospital of Zhengzhou University, Henan Provincial People's Hospital, Zhengzhou, China, ²Department of Ultrasound, Henan Provincial People's Hospital, Zhengzhou, China, ³Department of Ultrasound, People's Hospital of Henan University, Henan Provincial People's Hospital, Zhengzhou, China

Background: Liver cirrhosis is closely associated with cardiac dysfunction. The aims of this study were to evaluate left ventricular systolic function in patients with hepatitis B cirrhosis by non-invasive left ventricular pressure-strain loop (LVPSL) technique, and to explore the correlation between myocardial work indices and liver function classification.

Methods: According to the Child-Pugh classification, 90 patients with hepatitis B cirrhosis were further divided into three groups: Child-Pugh A group ($n = 32$), Child-Pugh B group ($n = 31$), and Child-Pugh C group ($n = 27$). During the same period, 30 healthy volunteers were recruited as the control (CON) group. Myocardial work parameters, which included global work index (GWI), global constructive work (GCW), global wasted work (GWW), and global work efficiency (GWE), were derived from the LVPSL and compared among the four groups. The correlation between myocardial work parameters and Child-Pugh liver function classification was evaluated, and the independent risk factors affecting left ventricular myocardial work in patients with cirrhosis were investigated by univariable and multivariable linear regression analysis.

Results: GWI, GCW and GWE of Child-Pugh B and C groups were lower than those of CON group, while GWW was higher than that of CON group, and the changes were more obvious in Child-Pugh C group ($P < 0.05$). Correlation analysis revealed that GWI, GCW, and GWE were negatively correlated with liver function classification to various degrees ($r = -0.54$, -0.57 , and -0.83 , respectively, all $P < 0.001$), while GWW was positively correlated with liver function classification ($r = 0.76$, $P < 0.001$). Multivariable linear regression analysis showed that GWE was positively correlated with ALB ($\beta = 0.17$, $P < 0.001$), and negatively correlated with GLS ($\beta = -0.24$, $P < 0.001$).

Conclusions: The changes in the left ventricular systolic function in patients with hepatitis B cirrhosis were identified using non-invasive LVPSL technology, and myocardial work parameters are significantly correlated with liver function classification. This technique may provide a new method for the evaluation of cardiac function in patients with cirrhosis.

KEYWORDS

liver cirrhosis, myocardial work, pressure-strain loop, echocardiography, left ventricular

1. Introduction

Liver cirrhosis is a common chronic progressive liver disease with a high mortality rate, which may cause multiple system dysfunction in the advanced stage. In Asian populations, chronic viral hepatitis B is the primary cause of liver cirrhosis (1). Cirrhotic cardiomyopathy (CCM) is one of the significant complications of cirrhosis and is closely related to the poor prognosis of patients with liver cirrhosis (2). It comprises a triad of impaired myocardial contractile responses to stress (systolic dysfunction), inadequate ventricular relaxation (diastolic dysfunction), and electrophysiological abnormalities in the absence of any known cardiac disease (3). Patients with cirrhosis may have various cardiovascular complications and even induce heart failure under stress conditions such as load or clinical invasive operation (4, 5). Heart failure due to CCM is claimed to be the third cause of mortality in liver transplant patients following infection and rejection (6). Therefore, the evaluation of left ventricular systolic function in patients with cirrhosis in the early stage is extremely important for treatment and prognosis.

Left ventricular systolic function and myocardial oxygen consumption can be accurately assessed with the use of pressure-volume loop measured by cardiac catheterization, but this method is an invasive examination with limited use in clinical practice (7). The left ventricular global longitudinal strain (GLS) measured by two-dimensional speckle tracking echocardiography (2D-STE) can be used to quantitatively evaluate left ventricular systolic function, but its load-dependent limitations affect the objective evaluation of myocardial systolic function (8). The left ventricular pressure-strain loop (LVPSL) is a new technique developed on the basis of 2D-STE, which allows for a more accurate assessment of left ventricular myocardial work by considering the effect of afterload on strain (9, 10). The results of non-invasive LVPSL in assessing myocardial work were significantly correlated with the invasive cardiac catheterization results (11). This method is simple, non-invasive, and reproducible, allowing for a more objective and accurate assessment of left ventricular function.

LVPSL technology has been widely used in the diagnosis of many cardiovascular diseases, but no studies have yet applied it to patients with cirrhosis. We hypothesized that LVPSL might provide incremental value for the assessment of left ventricular systolic function in patients with cirrhosis. The aim of this study was (1) to evaluate the left ventricular myocardial work of patients with different degrees of hepatitis B cirrhosis by using LVPSL technology; (2) to explore the correlation between myocardial work indices and liver function classification; (3) to find the clinical factors impairing the left ventricular myocardial work.

2. Materials and methods

2.1. Study population

From July 2020 to May 2021, a total of 90 patients with hepatitis B cirrhosis were recruited in this study, including 50

males and 40 females. The diagnosis of liver cirrhosis is based on clinical symptoms, laboratory data, imaging and pathological examination (12). According to the Child-Pugh classification, the patients with liver cirrhosis were divided into three groups: Child-Pugh A group ($n = 32$, 56% men, age 42.9 ± 9.4 years), Child-Pugh B group ($n = 31$, 55% men, age 41.8 ± 7.6 years), and Child-Pugh C group ($n = 27$, 56% men, age 41.5 ± 10.6 years). Thirty healthy volunteers were allocated to the control (CON) group (57% men, age 41.9 ± 10.9 years). The exclusion criteria were as follows: (i) coronary atherosclerotic heart disease, hypertension, congenital heart disease and other cardiovascular diseases; (ii) patients with chronic kidney disease, chronic respiratory disease, thyroid dysfunction and other diseases that may lead to secondary heart damage; (iii) patients with gastrointestinal bleeding in the last month; (iv) diabetes, hyperlipidemia and obesity; (v) poor-quality of ultrasound images. The participant selection process is illustrated in the flowchart in **Figure 1**. This study was approved by the ethics committee of Henan Provincial People's Hospital and informed consent was obtained from all subjects before image acquisitions.

2.2. Clinical features

Clinical data of all subjects were collected, such as age, BMI, BSA, heart rate (HR), systolic blood pressure (SBP), diastolic blood pressure (DBP) and pulse pressure (PP). Albumin (ALB), total bilirubin (TBil), alanine aminotransferase (ALT), aspartate aminotransferase (AST), and brain natriuretic peptide (BNP) level in patients with cirrhosis were obtained by standard laboratory techniques.

2.3. Conventional ultrasonic parameters

All subjects were underwent conventional echocardiography examination according to the American Society of Echocardiography guidelines (13), using a GE Vivid E95 colour Doppler ultrasound system (GE Vingmed Ultrasound AS, Horten, Norway) equipped with M5Sc-D transducer (1.4–4.6 MHz) and C1-6 transducer (3.5–5.0 MHz). Before examination, the brachial artery blood pressure was measured three times with an electronic manometer, and then the average was taken for analysis (assuming left ventricular systolic pressure equal to the brachial artery pressure). All subjects were instructed to take a supine position and breathe calmly. Using the C1-6 probe, the portal vein inner diameter (Dpv) and its flow velocity (Vpv) were obtained in the first longitudinal section of the hepatic portal under the right costal margin. Then the subjects were instructed to assume the left-lateral position and the electrocardiogram was attached. By adjusting the frequency, gain and image size, the endocardial surface was clearly displayed. Conventional parameters were measured in the parasternal long-axis view of the left ventricle, such as

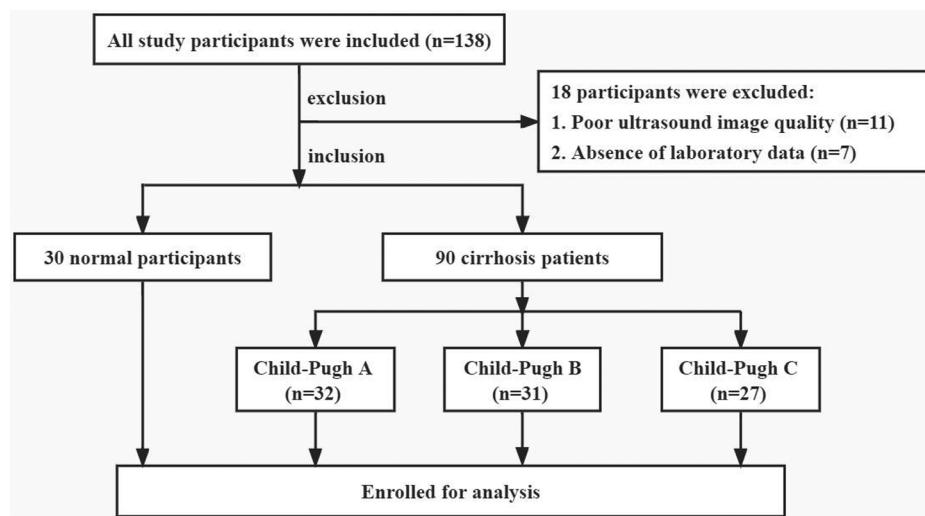


FIGURE 1
Flowchart of study populations.

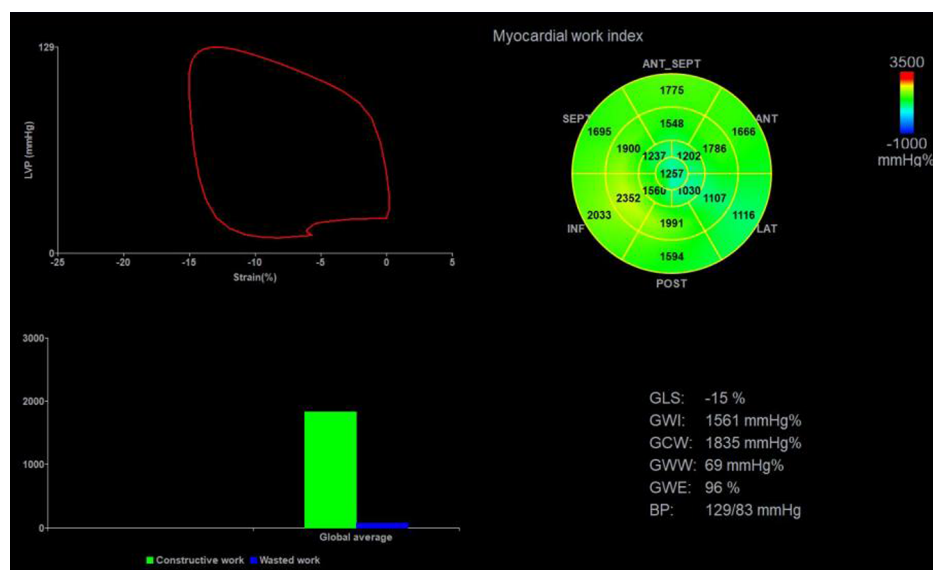


FIGURE 2
Left ventricular myocardial work parameters were obtained by non-invasive PSL technique. Top left: PSL curve; Top right: the 17-segment myocardial work index bull's eye diagram; Bottom left: comparison diagram of GCW (green column) and GWW (blue column); Bottom right: the parameters regarding myocardial work. PSL, pressure-strain loop; GLS, global longitudinal strain; GWI, global work index; GWE, global work efficiency; GCW, global constructive work; GWW, global wasted work.

the left atrial diameter (LAD), left ventricular end-diastolic diameter (LVDd), left ventricular end-systolic diameter (LVDs), interventricular septum thickness (IVST) and left ventricular posterior wall thickness (LVPWT). Left ventricular ejection fraction (LVEF) was calculated by Simpson's biplane method. The mitral and aortic valve Doppler spectral images were obtained. Dynamic images consisting of five consecutive cardiac cycles from the apical four-, three-, and two-chamber views were collected at frame rate of 50–70 frames/s, and the images were stored and copied to a mobile hard disk for analysis.

2.4. Quantitative analysis of GLS and myocardial work parameters

The stored dynamic images were imported into the Echopac version 203 workstation (GE Vingmed ultrasound, Horten, Norway) in original format for offline analysis. The aortic valve closure time was marked by the anterior flow spectrogram of the aortic valve to define the duration of isovolumic contraction, ejection, and isovolumic diastolic. The software can automatically identify and track the left ventricular myocardial motion trajectory and the region of interest was adjusted by correcting

the endocardial border or width until a satisfactory image was obtained. Finally, after entering the mean brachial artery blood pressure value, the software automatically obtained GLS, the LVPSL curve, and myocardial work parameters, as shown in **Figure 2**. The myocardial work parameters are as follows:

- (1) Global work index (GWI): the total work within the area of the LVPSL curve calculated from mitral valve closure to mitral valve opening.
- (2) Global constructive work (GCW): work performed by shortening in systole and lengthening during the isovolumic diastole phase.
- (3) Global wasted work (GWW): the negative work performed by lengthening in systole and shortening during the isovolumic diastole phase.
- (4) Global work efficiency (GWE): the percentage of GCW in the sum of GCW and GWW.

2.5. Statistical analysis

All statistical analyses were performed using SPSS version 26.0 software (IBM, Armonk, NY, USA). Continuous variables with normal distribution were presented as mean \pm standard deviation, and those with non-normal distribution were presented as median (interquartile range). One-way analysis of variance was used for comparison among multiple groups when the variances were homogeneous, and the least significant difference t-test was used for further pairwise comparison. The rank sum test was used to compare non-normally distributed data. Categorical variables were expressed as frequencies and percentages and compared by the χ^2 -test between the groups. Correlations between myocardial work parameters and Child-Pugh liver function classification were examined by Spearman correlation coefficients. The factors with P -value <0.05 in univariable linear regression results were incorporated into the multivariable linear regression analysis models by means of stepwise selection to detect the independent predictors of abnormal myocardial function in patients with liver cirrhosis. In the

multivariable linear regression model, there was no multicollinearity between variables. Intra-observer and inter-observer variability of myocardial work parameters were assessed in 15 cirrhosis patients and 15 healthy volunteers selected randomly and tested using the intraclass correlation coefficients (ICCs). All tests were two-sided, and $P < 0.05$ was considered statistically significant.

3. Results

3.1. Clinical and laboratory parameters

A total of 90 patients with liver cirrhosis were enrolled in this study, with an average age of 42.1 ± 9.1 years. The clinical and laboratory characteristics of the study subjects are illustrated in **Table 1**. Compared with the CON group, TBil, ALT, AST and BNP were significantly increased, and ALB was decreased in the liver cirrhosis groups, especially in the Child-Pugh C group ($P < 0.05$). There were no significant differences in sex, age, BMI, BSA, HR, SBP, DBP, and PP among the four groups ($P > 0.05$).

3.2. Conventional ultrasound parameters

The conventional ultrasound parameters of each group are summarized in **Table 2**. LAD, IVST and LVPWT in the cirrhosis groups were increased compared to the CON group ($P < 0.05$). Compared with the CON group and the Child-Pugh A group, Child-Pugh B and C groups had higher Dpv and lower Vpv ($P < 0.05$). No significant differences were identified among the four groups in terms of LVDd, LVDs and LVEF ($P > 0.05$).

3.3. GLS and myocardial work parameters

The absolute value of GLS in the cirrhosis groups was significantly decreased compared to the CON group, especially in

TABLE 1 Clinical and laboratory parameters.

	CON ($n = 30$)	Child-Pugh A ($n = 32$)	Child-Pugh B ($n = 31$)	Child-Pugh C ($n = 27$)	P -value
Male gender, n (%)	17 (57%)	18 (56%)	17 (55%)	15 (56%)	0.99
Age (years)	42.0 ± 10.9	42.9 ± 9.4	41.8 ± 7.6	41.5 ± 10.6	0.95
BMI (kg/m^2)	23.4 ± 2.7	23.2 ± 2.9	23.2 ± 2.3	23.3 ± 3.0	0.99
BSA (m^2)	1.7 ± 0.3	1.7 ± 0.4	1.7 ± 0.4	1.7 ± 0.4	0.99
HR (bpm)	68.8 ± 9.6	70.4 ± 9.6	71.7 ± 10.4	71.5 ± 6.6	0.62
SBP (mm Hg)	124.6 ± 9.2	121.8 ± 11.8	119.4 ± 9.4	119.9 ± 11.3	0.21
DBP (mm Hg)	77.0 ± 8.8	76.8 ± 8.8	75.2 ± 5.5	75.3 ± 7.1	0.71
PP (mm Hg)	47.6 ± 9.0	45.0 ± 10.7	44.2 ± 8.7	44.6 ± 9.9	0.52
ALB (g/L)	43.7 ± 6.7	$39.4 \pm 5.3^*$	$32.0 \pm 8.4^{***}$	$22.9 \pm 6.1^{*****}$	<0.001
TBil ($\mu\text{mol}/\text{L}$)	12.1 ± 3.1	$26.0 \pm 6.8^*$	$49.7 \pm 10.9^{***}$	$66.6 \pm 14.2^{*****}$	<0.001
ALT (U/L)	24.6 ± 6.4	$36.4 \pm 4.6^*$	$52.1 \pm 9.9^{***}$	$69.0 \pm 12.4^{*****}$	<0.001
AST (U/L)	23.9 ± 6.1	$33.8 \pm 7.7^*$	$52.9 \pm 14.3^{***}$	$81.4 \pm 11.9^{*****}$	<0.001
BNP (pg/ml)	34.5 ± 9.0	$68.7 \pm 10.3^*$	$128.5 \pm 14.5^{***}$	$186.8 \pm 42.3^{*****}$	<0.001

Data are expressed as mean \pm SD or as number (percentage).

BMI, body mass index; BSA, body surface area; HR, heart rate; SBP, systolic blood pressure; DBP, diastolic blood pressure; PP, pulse pressure; ALB, Albumin; TBil, total bilirubin; ALT, alanine aminotransferase; AST, aspartate aminotransferase; BNP, brain natriuretic peptide.

* $P < 0.05$ vs. CON; ** $P < 0.05$ vs. Child-Pugh A; *** $P < 0.05$ vs. Child-Pugh B.

TABLE 2 Conventional ultrasound parameters.

	CON (n = 30)	Child-Pugh A (n = 32)	Child-Pugh B (n = 31)	Child-Pugh C (n = 27)	P-value
Dpv (mm)	9.9 ± 1.4	10.6 ± 1.6	12.7 ± 1.6***	14.3 ± 1.2*****	<0.001
Vpv (m/s)	19.9 ± 4.1	18.1 ± 3.0	15.8 ± 2.4***	13.8 ± 2.0***	<0.001
LAD (mm)	30.7 ± 2.9	33.9 ± 2.6*	35.1 ± 4.7*	39.0 ± 4.0*****	<0.001
LVDd (mm)	47.1 ± 3.4	48.2 ± 4.3	47.8 ± 3.4	48.5 ± 3.4	0.52
LVDs (mm)	27.8 ± 3.9	28.8 ± 3.8	28.3 ± 4.0	29.1 ± 3.8	0.63
IVST (mm)	8.4 ± 1.2	9.9 ± 1.2*	10.1 ± 1.5*	10.3 ± 1.5*	<0.001
LVPWT (mm)	8.6 ± 0.9	9.6 ± 1.2*	10.0 ± 1.4*	10.2 ± 1.4*	<0.001
LVEF (%)	67.5 ± 5.2	68.1 ± 5.0	69.6 ± 6.8	68.6 ± 5.9	0.56

Data are expressed as mean ± SD. Dpv, portal vein inner diameter; Vpv, portal vein flow velocity; LAD, left atrial diameter; LVDd, left ventricular end-diastolic diameter; LVDs, left ventricular end-systolic diameter; IVST, interventricular septum thickness; LVPWT, left ventricular posterior wall thickness; LVEF, left ventricular ejection fraction. * $P < 0.05$ vs. CON; ** $P < 0.05$ vs. Child-Pugh A; *** $P < 0.05$ vs. Child-Pugh B.

TABLE 3 GLS and myocardial work parameters.

	CON (n = 30)	Child-Pugh A (n = 32)	Child-Pugh B (n = 31)	Child-Pugh C (n = 27)	P-value
GLS (%)	-21.2 ± 2.3	-19.4 ± 2.3*	-17.4 ± 3.3***	-15.0 ± 2.5*****	<0.001
GWl (mm Hg%)	2,030.2 ± 358.4	1,914.1 ± 337.3	1,719.7 ± 324.3*	1,518.0 ± 198.0*****	<0.001
GCW (mm Hg%)	2,331.8 ± 384.1	2,140.0 ± 381.6	1,935.6 ± 218.5*	1,728.6 ± 242.2*****	<0.001
GWw (mm Hg%)	47.5 (16.5)	58.0 (19.3)*	71.0 (35.0)***	120.0 (25.0)*****	<0.001
GWE (%)	98.0 (0.3)	97.0 (1.0)*	96.0 (3.0)***	93.0 (2.0)*****	<0.001

Data are expressed as mean ± SD or as median (quartile range). GLS, global longitudinal strain; GWl, global work index; GCW, global constructive work; GWw, global wasted work; GWE, global work efficiency.

* $P < 0.05$ vs. CON; ** $P < 0.05$ vs. Child-Pugh A; *** $P < 0.05$ vs. Child-Pugh B.

the Child-Pugh C group ($P < 0.05$). Compared with the CON group, GWl, GCW and GWE in Child-Pugh B and C groups were significantly decreased, while GWw was increased ($P < 0.05$). Compared with Child-Pugh A and B groups, GWl, GCW and GWE in Child-Pugh C group were further decreased, while GWw was further increased ($P < 0.05$). (Table 3 and Figures 3, 4).

3.4. Correlation between myocardial work parameters and Child-Pugh classification

Spearman correlation analysis results showed that GWl, GCW, GWE were negatively correlated with Child-Pugh classification (GWl: $r = -0.54$, $P < 0.001$; GCW: $r = -0.57$, $P < 0.001$; GWE: $r = -0.83$, $P < 0.001$) and GWw was positively correlated with Child-Pugh classification (GWw: $r = 0.76$, $P < 0.001$). GWE showed more significant correlation than other myocardial work parameters, as exhibited in Figure 5.

3.5. Potential associated factors for GWE in cirrhosis patients

HR, ALB, TBil, Dpv, IVST, LVPWT and GLS were incorporated into the multivariable linear regression analysis model of GWE by means of stepwise selection based on the univariable linear regression analysis results. The results showed that GWE was positively correlated with ALB ($\beta = 0.17$, $P < 0.001$), and negatively correlated with GLS ($\beta = -0.24$, $P < 0.001$). The detailed data are listed in Table 4.

3.6. Reproducibility test

Intra-observer and inter-observer variability for myocardial work parameters are summarized in Table 5. The results showed good repeatability and reproducibility in global myocardial work parameters.

4. Discussion

This study mainly illustrates the myocardial function of patients with different degrees of hepatitis B cirrhosis by non-invasive PSL technique. The main findings are as follows: (1) Compared with the CON group, there was no significant change in LVEF in the cirrhosis groups, but the myocardial work parameters had changed. GWl, GCW and GWE in Child-Pugh B and C groups were significantly lower than those in control group, while GWw was significantly higher than that in control group, and the change was more obvious in Child-Pugh C group. (2) GWl, GCW and GWE were negatively correlated with Child-Pugh classification, while GWw was positively correlated with Child-Pugh classification. (3) GWE was independently correlated with ALB and GLS respectively.

Liver cirrhosis is the terminal stage of various chronic liver diseases with high mortality rate, which can damage the function of other organs to varying degrees, and it has become a serious public health problem (14). As one of the important complications of cirrhosis, CCM is closely related to the prognosis and survival rate of patients, and has gradually received clinical attention in recent years. The onset of CCM is

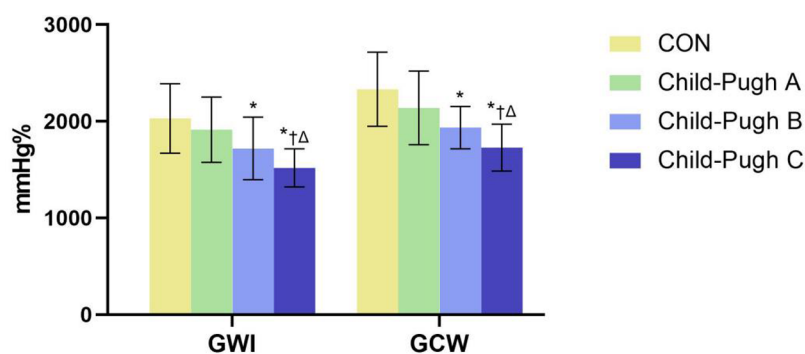


FIGURE 3

The bar chart showed differential changes of GWI and GCW among the four groups. GWI, global work index; GCW, global constructive work. * $P < 0.05$ vs. CON. † $P < 0.05$ vs. Child-Pugh A. Δ $P < 0.05$ vs. Child-Pugh B.

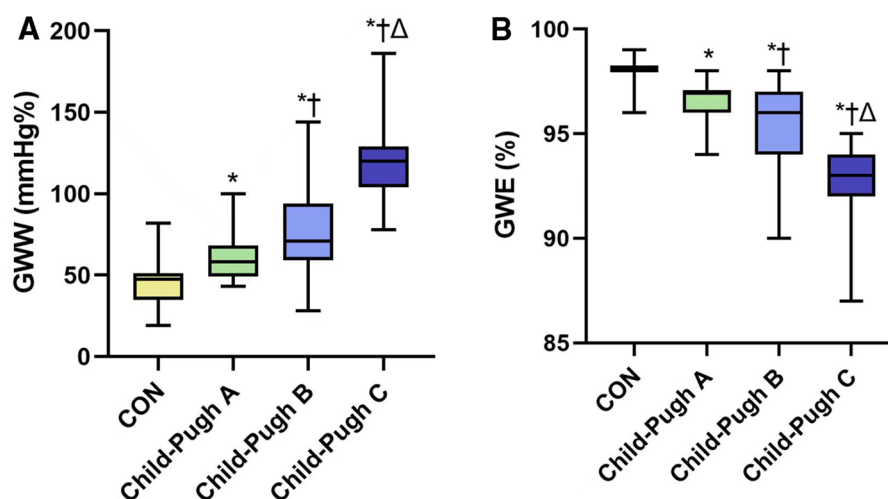


FIGURE 4

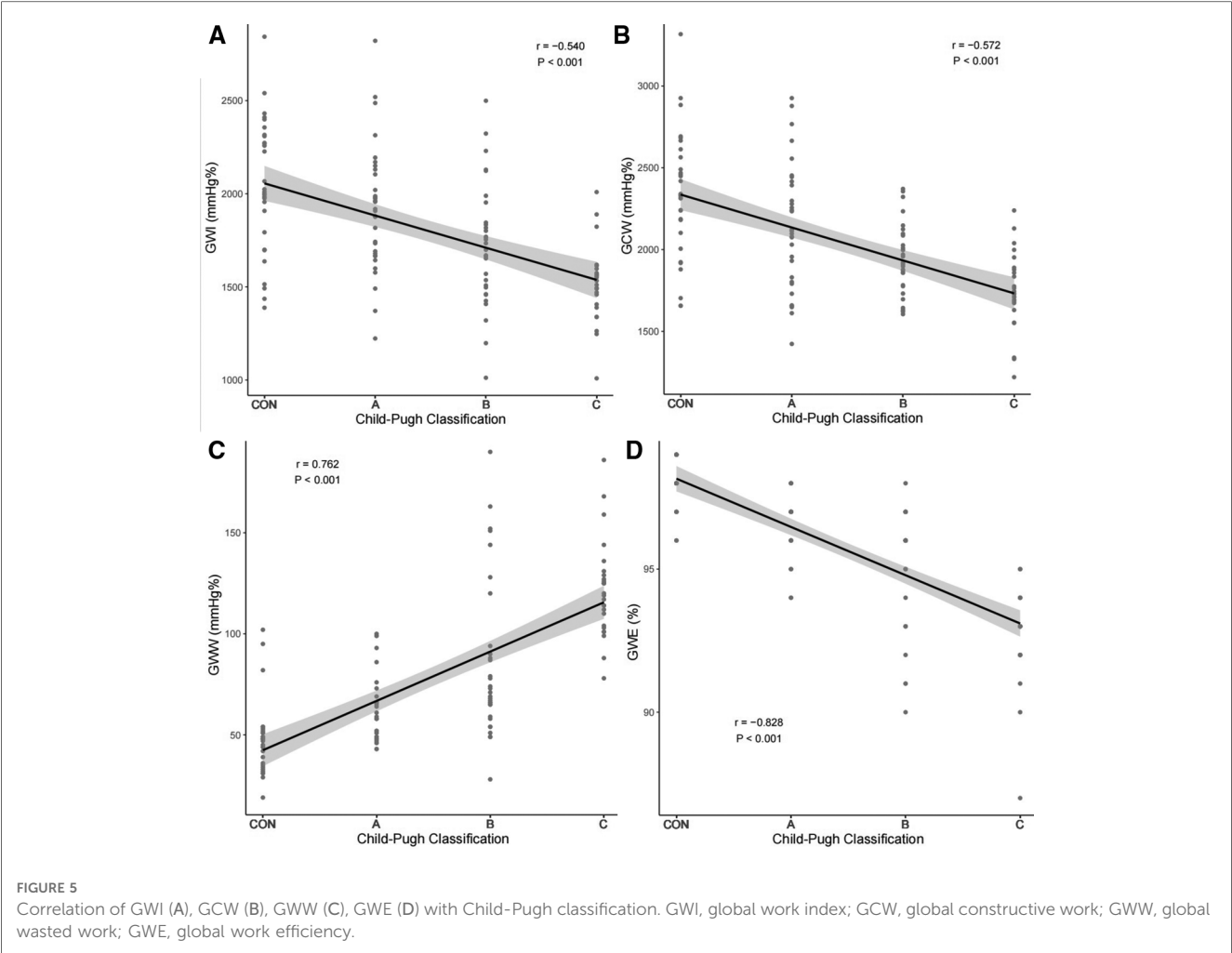
The boxplots showed differential changes of GWW (A) and GWE (B) among the four groups. GWW, global wasted work; GWE, global work efficiency. * $P < 0.05$ vs. CON. † $P < 0.05$ vs. Child-Pugh A. Δ $P < 0.05$ vs. Child-Pugh B.

usually insidious and the myocardial damage is not obvious in the resting state, but it may cause serious adverse consequences during some clinical procedures that affect hemodynamics (15). Therefore, early detection of cardiac function impairment in patients with cirrhosis and evaluation of its relationship with the progression of cirrhosis may be crucial for clinical diagnosis and treatment, prognosis assessment and prevention of cardiovascular adverse events.

Previous studies have shown that GLS can reflect left ventricular systolic function sensitively (16, 17). In this study, the absolute value of GLS in cirrhosis patients was lower than that in the control group. With the deterioration of liver function, the absolute value of GLS further decreased, which was consistent with the results of Sampaio et al. (18). However, GLS was load-dependent, and the increase of afterload will underestimate the true value of myocardial strain, which might affect the accuracy of its evaluation of cardiac function. Compared with GLS, non-invasive PSL technology can evaluate cardiac systolic function

more objectively and accurately and reflect myocardial oxygen consumption by comprehensively considering myocardial deformation and afterload (19). At present, this technique has made significant progress in the diagnosis of cardiovascular diseases, such as hypertension, dilated cardiomyopathy, myocardial amyloidosis, and coronary artery diseases with preserved ejection fraction, and its feasibility and application value have been confirmed (20–22).

The results of this study showed that GWI, GCW, GWE and GWW in Child-Pugh B and C groups were significantly different from controls, but there was no significant difference in LVEF among all groups. This indicates that myocardial work parameters may reflect subclinical myocardial function damage. Impaired liver function and portal hypertension in patients with cirrhosis can lead to increase vasodilator substances in the body, which may result in peripheral vascular dilatation and reduced afterload (23). In addition, the blood volume was redistributed and the circulation was in a hyperdynamic state in patients with



cirrhosis, which masked the performance of reduced left ventricular systolic function, resulting in no significant change in LVEF (24, 25). In addition, compared with Child-Pugh A and B groups, the GWI, GCW and GWE in Child-Pugh C group were

further decreased, while the GWW was further increased, indicating that the left ventricular systolic function of patients with cirrhosis decreased gradually with the deterioration of liver function. This may be related to impaired function of β -receptors on the surface of myocardial membrane, altered transmembrane currents and overproduction of cardiodepressant factors such as nitric oxide, endocannabinoid and cytokines, which can inhibit the contraction of myocardial cells (26). These reasons may lead to the decrease of the myocardial work index and effective work, manifesting as the decrease of GWI, GCW and GWE. Meanwhile, the electrical signal conduction of myocardium in

TABLE 4 Potential associated factors of GWE in cirrhosis patients.

Variables	Univariable analysis		Multivariable analysis	
	β	P-value	β	P-value
Age	-0.01	0.57	-	-
BSA	-0.46	0.42	-	-
BMI	0.03	0.76	-	-
HR	-0.05	0.04	-	-
ALB	0.21	<0.001	0.17	<0.001
TBil	-0.05	<0.001	-	-
Dpv	-0.65	<0.001	-	-
IVST	-0.45	<0.001	-	-
LVPWT	-0.44	0.004	-	-
LVEF	-0.05	0.19	-	-
GLS	-0.48	<0.001	-0.24	<0.001

GWE, global work efficiency; BSA, body surface area; BMI, body mass index; HR, heart rate; ALB, albumin; TBil, total bilirubin; Dpv, portal vein inner diameter; IVST, interventricular septum thickness; LVPWT, left ventricular posterior wall thickness; LVEF, left ventricular ejection fraction; GLS, global longitudinal strain.

TABLE 5 Reproducibility test.

	Intra-observer variability			Inter-observer variability		
	ICC	95% CI	P-value	ICC	95% CI	P-value
GWI	0.98	0.96–0.99	<0.001	0.98	0.95–0.99	<0.001
GCW	0.97	0.94–0.99	<0.001	0.96	0.89–0.98	<0.001
GWW	0.97	0.93–0.99	<0.001	0.96	0.93–0.98	<0.001
GWE	0.97	0.94–0.99	<0.001	0.98	0.95–0.99	<0.001

ICC, intraclass correlation coefficient; CI, confidence interval; GWI, global work index; GCW, global constructive work; GWW, global wasted work; GWE, global work efficiency.

patients with cirrhosis is interrupted or delayed due to myocardial fibrosis, which may lead to asynchronous myocardial contraction, as shown by the elongation of myocardial cells during systole phase, resulting in reduced GCW and increased GWW (27). In addition, the correlation analysis results showed that GWI, GCW and GWE were negatively correlated with Child-Pugh classification, while GWW was positively correlated with Child-Pugh classification. This also indicates that with the aggravation of cirrhosis, the left ventricular systolic function decreased gradually. GWW is on the rise, and GWI, GCW and GWE are on the decline.

Furthermore, this study showed that ALB and GLS were independent predictors for GWE in patients with cirrhosis. The decrease of plasma colloid osmotic pressure and insufficient effective blood volume in patients with cirrhosis can activate the sympathetic nervous system and the renin-angiotensin-aldosterone system, resulting in a compensatory state of hyperkinetic circulation with high cardiac output and low peripheral resistance (28). Patients with lower ALB levels may be in a state of greater cardiac volume overload. GLS mainly reflects the longitudinal strain of myocardium in the subendocardial region, which is prone to ischemia and fibrosis (29). The higher cardiac capacity load and greater stress on the subendocardial myocardium in patients with cirrhosis may be prone to microvascular dysfunction, fibrosis and other changes resulting in systolic dysfunction. CCM consortium recommended that absolute values of GLS can be used to detect left ventricular systolic dysfunction in cirrhotic patients with preserved LVEF (30). Recent studies have shown that GLS is also of great significance in predicting poor prognosis and risk stratification in patients with heart failure (31, 32).

5. Limitations

Several limitations of the present study should be acknowledged. Firstly, this is a retrospective, single-center study with a small sample size and needs to be expanded for further study to confirm our results. Secondly, most patients with hepatitis B cirrhosis included in this study had taken drugs to control disease progression, and the effects of drugs on left ventricular function cannot be ruled out. Thirdly, we only evaluated the global myocardial function of left ventricle, and the regional myocardial work of 17 segments was not assessed. Finally, we only included patients with cirrhosis caused by hepatitis B virus, and excluded patients with alcoholic cirrhosis or other causes, which may limit the generalizability of our findings in clinical applications.

6. Conclusions

The non-invasive LVPSL technology can quantitatively analyze the changes of left ventricular myocardial function in patients with hepatitis B cirrhosis under different disease states. The myocardial work parameters of left ventricular were significantly correlated

with liver function classification. GWE was independently correlated with ALB and GLS respectively. This technique can sensitively detect abnormal cardiac function in cirrhosis patients with preserved LVEF, which has a broad prospect of clinical application.

Data availability statement

The original contributions presented in the study are included in the article/Supplementary Material, further inquiries can be directed to the corresponding author/s.

Ethics statement

The studies involving human participants were reviewed and approved by Medical Ethics Committee of Henan Provincial People's Hospital. The patients/participants provided their written informed consent to participate in this study.

Author contributions

YC and HZ analyzed images, collected data, and wrote the manuscript. SL, SL, SS, JC, TY assisted in recruitment and data analysis. XZ, JY contributed to the study design and manuscript revision. All authors contributed to the article and approved the submitted version.

Funding

This study was supported by Medical Scientific and Technological Research Project of Henan Provincial Science and Technology Department (212102310652) and the key project of Medical Science and Technology in Henan Province (SBGJ202102013).

Acknowledgments

The authors acknowledge Songyan Liu (GE Company, Zhengzhou, China) for his technical support. We would also like to acknowledge the editors of this manuscript.

Conflict of interest

The authors declare that the research was conducted in the absence of any commercial or financial relationships that could be construed as a potential conflict of interest.

Publisher's note

All claims expressed in this article are solely those of the authors and do not necessarily represent those of their affiliated

organizations, or those of the publisher, the editors and the reviewers. Any product that may be evaluated in this article, or claim that may be made by its manufacturer, is not guaranteed or endorsed by the publisher.

References

- Asrani SK, Devarbhavi H, Eaton J, Kamath PS. Burden of liver diseases in the world. *J Hepatol.* (2019) 70:151–71. doi: 10.1016/j.jhep.2018.09.014
- Liu H, Lee SS. Diagnostic criteria of cirrhotic cardiomyopathy: out with the old, in with the new? *Hepatology.* (2021) 74:3523–5. doi: 10.1002/hep.32021
- Shahvaran SA, Menyhart O, Csedik L, Patai AV. Diagnosis and prevalence of cirrhotic cardiomyopathy: a systematic review and meta-analysis. *Curr Probl Cardiol.* (2021) 46:100821. doi: 10.1016/j.cpcardiol.2021.100821
- Wiese S, Hove JD, Bendtsen F, Møller S. Cirrhotic cardiomyopathy: pathogenesis and clinical relevance. *Nat Rev Gastroenterol Hepatol.* (2014) 11:177–86. doi: 10.1038/nrgastro.2013.210
- Liu H, Yoon KT, Zhang J, Lee SS. Advances in cirrhotic cardiomyopathy. *Curr Opin Gastroenterol.* (2021) 37:187–93. doi: 10.1097/MOG.0000000000000733
- Lee RF, Glenn TK, Lee SS. Cardiac dysfunction in cirrhosis. *Best Pract Res Clin Gastro Enterol.* (2007) 21:125–40. doi: 10.1016/j.bpg.2006.06.003
- Tulner SAF, Klautz RJM, van Rijk-Zwikker GL, Engbers FHM, Bax JJ, Baan J, et al. Perioperative assessment of left ventricular function by pressure-volume loops using the conductance catheter method. *Anesth Analg.* (2003) 97:950–7. doi: 10.1213/01.ANE.0000078814.81889.B3
- Manganaro R, Marchetta S, Dulgheru R, Ilardi F, Sugimoto T, Robinet S, et al. Echocardiographic reference ranges for normal non-invasive myocardial work indices: results from the EACVI NORRE study. *Eur Heart J Cardiovasc Imaging.* (2019) 20:582–90. doi: 10.1093/ehjci/jez188
- Boe E, Skulstad H, Smiseth OA. Myocardial work by echocardiography: a novel method ready for clinical testing. *Eur Heart J Cardiovasc Imaging.* (2019) 20:18–20. doi: 10.1093/ehjci/jez156
- Russell K, Eriksen M, Aaberge L, Wilhelmssen N, Skulstad H, Remme EW, et al. A novel clinical method for quantification of regional left ventricular pressure-strain loop area: a non-invasive index of myocardial work. *Eur Heart J.* (2012) 33:724–33. doi: 10.1093/eurheartj/ehs016
- Hubert A, Rolle VL, Leclercq C, Galli E, Samset E, Cassot C, et al. Estimation of myocardial work from pressure-strain loops analysis: an experimental evaluation. *Eur Heart J Cardiovasc Imaging.* (2018) 19:1372–9. doi: 10.1093/ehjci/jez024
- Ruiz-del-Arbo L, Achécar L, Serradilla R, Rodríguez-Gandía MA, Rivero M, Garrido E, et al. Diastolic dysfunction is a predictor of poor outcomes in patients with cirrhosis, portal hypertension, and a normal creatinine. *Hepatology.* (2013) 58:1732–41. doi: 10.1002/hep.26509
- Lang RM, Badano LP, Mor-Avi V, Afkalo J, Armstrong A, Ernande L, et al. Recommendations for cardiac chamber quantification by echocardiography in adults: an update from the American society of echocardiography and the European association of cardiovascular imaging. *Eur Heart J Cardiovasc Imaging.* (2015) 16:233–70. doi: 10.1093/ehjci/jev014
- Xiao J, Wang F, Wong NK, He J, Zhang R, Sun R, et al. Global liver disease burdens and research trends: analysis from a Chinese perspective. *J Hepatol.* (2019) 71:212–21. doi: 10.1016/j.jhep.2019.03.004
- Møller S, Bernardi M. Interactions of the heart and the liver. *Eur Heart J.* (2013) 34:2804–11. doi: 10.1093/eurheartj/ehz246
- Alashi A, Mentias A, Abdallah A, Feng K, Gillinov M, Rodriguez L, et al. Incremental prognostic utility of left ventricular global longitudinal strain in asymptomatic patients with significant chronic aortic regurgitation and preserved left ventricular ejection fraction. *JACC Cardiovasc Imaging.* (2018) 11:673–82. doi: 10.1016/j.jcmg.2017.02.016
- Sun JP, Xu TY, Ni XD, Yang XS, Hu JL, Wang SC, et al. Echocardiographic strain in hypertrophic cardiomyopathy and hypertensive left ventricular hypertrophy. *Echocardiography.* (2019) 36:257–65. doi: 10.1111/echo.14222
- Sampaio F, Pimenta J, Bettencourt N, Fontes-Carvalho R, Silva AP, Valente J, et al. Systolic and diastolic dysfunction in cirrhosis: a tissue-Doppler and speckle tracking echocardiography study. *Liver Int.* (2013) 33:1158–65. doi: 10.1111/liv.12187
- Zhu H, Guo Y, Wang X, Yang C, Li Y, Meng X, et al. Myocardial work by speckle tracking echocardiography accurately assesses left ventricular function of coronary artery disease patients. *Front Cardiovasc Med.* (2021) 8:727389. doi: 10.3389/fcvm.2021.727389
- Chan J, Edwards NFA, Khandheria BK, Shiino K, Sabapathy S, Anderson B, et al. A new approach to assess myocardial work by non-invasive left ventricular pressure-strain relations in hypertension and dilated cardiomyopathy. *Eur Heart J Cardiovasc Imaging.* (2019) 20:31–9. doi: 10.1093/ehjci/jez131
- Clemmensen TS, Eiskjær H, Ladefoged B, Mikkelsen F, Sørensen J, Grantham SO, et al. Prognostic implications of left ventricular myocardial work indices in cardiac amyloidosis. *Eur Heart J Cardiovasc Imaging.* (2021) 22:695–704. doi: 10.1093/ehjci/jeaa097
- Edwards NFA, Scalia GM, Shiino K, Sabapathy S, Anderson B, Chamberlain R, et al. Global myocardial work is superior to global longitudinal strain to predict significant coronary artery disease in patients with normal left ventricular function and wall motion. *J Am Soc Echocardiogr.* (2019) 32:947–57. doi: 10.1016/j.echo.2019.02.014
- Goldberg DS, Fallon MB. The art and science of diagnosing and treating lung and heart disease secondary to liver disease. *Clin Gastroenterol Hepatol.* (2015) 13:2118–27. doi: 10.1016/j.cgh.2015.04.024
- Møller S, Bendtsen F. The pathophysiology of arterial vasodilatation and hyperdynamic circulation in cirrhosis. *Liver Int.* (2018) 38:570–80. doi: 10.1111/liv.13589
- Møller S, Lee SS. Cirrhotic cardiomyopathy. *J Hepatol.* (2018) 69:958–60. doi: 10.1016/j.jhep.2018.01.006
- Carvalho MVH, Kroll PC, Kroll RTM, Carvalho VN. Cirrhotic cardiomyopathy: the liver affects the heart. *Braz J Med Biol Res.* (2019) 52:e7809. doi: 10.1590/1414-431X20187809
- Kim SA, Kim MN, Shim WJ, Park SM. Layer-specific dyssynchrony and its relationship to the change of left ventricular function in hypertensive patients. *Heart Vessels.* (2016) 31:528–34. doi: 10.1007/s00380-014-0626-0
- Bernardi M, Moreau R, Angeli P, Schnabl B, Arroyo V. Mechanisms of decompensation and organ failure in cirrhosis: from peripheral arterial vasodilation to systemic inflammation hypothesis. *J Hepatol.* (2015) 63:1272–84. doi: 10.1016/j.jhep.2015.07.004
- Langeland S, D Hooge J, Wouters PF, Leather A, Claus P, Bijns B, et al. Experimental validation of a new ultrasound method for the simultaneous assessment of radial and longitudinal myocardial deformation independent of insonation angle. *Circulation.* (2005) 112:2157–62. doi: 10.1161/CIRCULATIONAHA.105.554006
- Izzy M, VanWagner LB, Lin G, Altieri M, Findlay JY, Oh JK, et al. Redefining cirrhotic cardiomyopathy for the modern era. *Hepatology.* (2020) 71:334–45. doi: 10.1002/hep.30875
- Bax JJ, Delgado V, Sogaard P, Singh JP, Abraham WT, Borer JS, et al. Prognostic implications of left ventricular global longitudinal strain in heart failure patients with narrow QRS complex treated with cardiac resynchronization therapy: a subanalysis of the randomized EchoCRT trial. *Eur Heart J.* (2017) 38:720–6. doi: 10.1093/eurheartj/ehw506
- Halliday BP, Senior R, Pennell DJ. Assessing left ventricular systolic function: from ejection fraction to strain analysis. *Eur Heart J.* (2021) 42:789–97. doi: 10.1093/eurheartj/ehaa587



OPEN ACCESS

EDITED BY

Francesca Innocenti,
Careggi University Hospital, Italy

REVIEWED BY

Eustaquio Maria Onorato,
U.O. Cardiologia Universitaria, Ospedale
Galeazzi—Sant'Ambrogio, Istituto di Ricovero
e Cura a Carattere Scientifico (IRCCS), Italy
Tobias Zeus,
University Hospital of Düsseldorf, Germany

*CORRESPONDENCE

Ru-Xing Wang
✉ ruxingw@aliyun.com

[†]These authors have contributed equally to this work

RECEIVED 27 March 2023

ACCEPTED 09 May 2023

PUBLISHED 24 May 2023

CITATION

Zhang Z-Y, Li F, Zhang J, Zhang L, Liu H-H,
Zhao N, Yang F, Kong Q, Zhou Y-T, Qian L-L
and Wang R-X (2023) A comparable efficacy
and safety between intracardiac
echocardiography and transesophageal
echocardiography for percutaneous left atrial
appendage occlusion.
Front. Cardiovasc. Med. 10:1194771.
doi: 10.3389/fcvm.2023.1194771

COPYRIGHT

© 2023 Zhang, Li, Zhang, Zhang, Liu, Zhao,
Yang, Kong, Zhou, Qian and Wang. This is an
open-access article distributed under the terms
of the [Creative Commons Attribution License](#)
(CC BY). The use, distribution or reproduction in
other forums is permitted, provided the original
author(s) and the copyright owner(s) are
credited and that the original publication in this
journal is cited, in accordance with accepted
academic practice. No use, distribution or
reproduction is permitted which does not
comply with these terms.

A comparable efficacy and safety between intracardiac echocardiography and transesophageal echocardiography for percutaneous left atrial appendage occlusion

Zhi-Yuan Zhang[†], Feng Li[†], Jie Zhang[†], Lei Zhang, Huan-Huan Liu,
Ning Zhao, Fan Yang, Qi Kong, Yi-Ting Zhou, Ling-Ling Qian
and Ru-Xing Wang^{*}

Department of Cardiology, Wuxi People's Hospital Affiliated to Nanjing Medical University, Wuxi, China

Background: Accumulated clinical studies utilized intracardiac echocardiography (ICE) to guide percutaneous left atrial appendage occlusion (LAAO). However, its procedural success and safety compared to traditional transesophageal echocardiography (TEE) remained elusive. Therefore, we performed a meta-analysis to compare efficacy and safety of ICE and TEE for LAAO.

Methods: We screened studies from four online databases (including the Cochrane Library, Embase, PubMed, and Web of Science) from their inception to 1 December 2022. We used a random or fixed-effect model to synthesize the clinical outcomes and conducted a subgroup analysis to identify the potential confounding factors.

Results: A total of twenty eligible studies with 3,610 atrial fibrillation (AF) patients (1,564 patients for ICE and 2,046 patients for TEE) were enrolled. Compared with TEE group, there was no significant difference in procedural success rate [risk ratio (RR) = 1.01; $P = 0.171$], total procedural time [weighted mean difference (WMD) = -5.58 ; $P = 0.292$], contrast volume (WMD = -2.61 ; $P = 0.595$), fluoroscopic time (WMD = -0.34 ; $P = 0.705$; $I^2 = 82.80\%$), procedural complications (RR = 0.82; $P = 0.261$), and long-term adverse events (RR = 0.86; $P = 0.329$) in the ICE group. Subgroup analysis revealed that ICE group might be associated with the reduction of contrast use and fluoroscopic time in the hypertension proportion <90 subgroup, with lower total procedure time, contrast volume, and the fluoroscopic time in device type subgroup with multi-seal mechanism, and with the lower contrast use in paroxysmal AF (PAF) proportion ≤ 50 subgroup. Whereas, ICE group might increase the total procedure time in PAF proportion >50 subgroup and contrast use in multi-center subgroup, respectively.

Conclusion: Our study suggests that ICE may have comparable efficacy and safety compared to TEE for LAAO.

KEYWORDS

atrial fibrillation, intracardiac echocardiography, transesophageal echocardiography, left atrial appendage closure, implantable devices, cardiac mapping

1. Introduction

Atrial fibrillation (AF) is the most common persistent atrial arrhythmia worldwide, with a prevalence estimated to be between 2% and 4% in adults. An expected 2.3-fold increase in prevalence is anticipated due to extended life expectancy in the general population and increased detection of undiagnosed AF (1). Cardioembolic stroke is the most concerning complication of AF, as abnormal blood flow in the left atrium increases the likelihood of thrombus rupture from the left atrial appendage (LAA), subsequently leading to thromboembolisms in the peripheral and cerebral arteries (2).

The primary prevention strategy of thromboembolism for AF is the use of oral anticoagulants (OACs). However, challenge remains due to the limitation of adherence and bleeding risk for safety and efficacy of OACs. Since most thrombus in nonvalvular AF originates from the LAA, left atrial appendage occlusion (LAAO) is an emerging alternative for OACs. Transesophageal echocardiography (TEE) is the standard imaging modality to guide LAAO and is the most widely used imaging modality. However, it has some significant limitations, including increased pain with local or conscious anesthesia, prolonged procedure time and hospitalization burden with general anesthesia, aggravated risk of possible esophageal injury under “one-stop” ablation, and high dependence on a dedicated echocardiography operator.

Recently, an expert consensus suggested that intracardiac echocardiography (ICE) might be considered as an alternative imaging modality to guide LAAO, especially with the progress of the “one-stop” ablation therapy for AF (3). However, studies comparing TEE with ICE for LAAO were limited, leading to the related outcomes (e.g., efficacy and safety outcomes) remaining elusive. Therefore, we evaluated the clinical outcomes of TEE and ICE guidance for LAAO to further assess the safety and efficacy outcomes between two imaging modalities.

2. Methods

2.1. Study design

This systematic review was carried on according to the PRISMA guidelines. The registered protocol is displayed in the PROSPERO database (CRD42022368692).

2.2. Search strategy

Two independent reviewers (ZYZ and FL) conducted comprehensive searches of four online databases (Cochrane Library, Embase, PubMed and Web of Science) from inception to 1 December 2022. Search keywords were “ICE”, “Intracardiac echocardiography”, “TEE”, “transesophageal echocardiography”, “atrial fibrillation”, “left atrial appendage closure”, “LAAC”, “left atrial appendage occlusion”, and “LAAO”. Clinical studies related

to the outcomes of ICE or outcomes comparing TEE vs. ICE for LAAO were included. Reference lists of review articles were hand searched, and eligible articles were searched for potential publications not previously identified.

2.3. Search design

Two reviewers (ZYZ and JZ) independently searched the literature and screen the titles, abstracts, and full texts to select all relevant studies that met the inclusion criteria. A study would be included if the following criteria were met: (1) randomized controlled trials and cohort, observational studies, and single-arm studies; (2) studies comparing clinical outcomes comparing TEE vs. ICE for endocardial LAAO, including efficacy outcome (e.g., procedural success) and safety outcomes (e.g., short-term complications and long-term complications); (3) studies with full text published in peer-reviewed journals; and studies containing the most data for multiple publications of the same study. Case reports, editorial, review articles, studies without original data letters and studies reporting clinical outcomes with hybrid LAAO procedures were excluded. Meanwhile, a third reviewer (R.X.W) resolved any disagreements about eligibility.

2.4. Data extraction and quality assessment

Data from eligible studies included in the analysis were extracted by two independent researchers (ZYZ and FL), and any potential disagreements were resolved by a third researcher (RXW). The extracted data mainly included: title, first author, publication year, study design, sample size, follow-up time, LAAO device, pre-procedure imaging and ICE location. Meanwhile, we also extracted relevant clinical outcomes, including: acute procedural success, total procedural time, fluoroscopic time, contrast volume, short-term complications, and long-term complications.

Two independent researchers (ZYZ and JZ) evaluated study quality by two appraisal tools. The Newcastle-Ottawa Quality Assessment Scale (NOS) was used to evaluate the two-arm observation (4). The Institute of Health Economics checklist was used for the single-arm study (5). Any disagreements were discussed and resolved by consulting a third researcher (RXW).

2.5. Statistical analysis

Stata version 16.0 was used for statistical analyses. Continuous variables were displayed as means \pm SD, and categorical variables were presented as frequencies and percentages. For observational studies with two arms, we calculated the relative risk (RR) and corresponding 95% confidence intervals (CI) for each outcome. For single-arm analysis, we calculated the incidence of events (number of events divided by number of patients) and 95% confidence intervals. $P < 0.05$ was considered statistically significant.

Meanwhile, chi-square tests and I^2 were used to quantify and assess statistical heterogeneity among studies. If the I^2 value was more than 50% and/or $P < 0.05$ for the chi-squared test, we considered the between-study heterogeneity to be significant, and we would adopt a random-effect model. Otherwise, we would adopt fixed-effect model. Sensitivity analysis was performed by sequentially omitting one study at a time to assess the effect of a single study on the overall risk, and potential publication bias was also evaluated *via* Egger's test.

In addition, subgroup analysis was conducted to screen potential determinants of LAAO outcomes between ICE and TEE groups. According to the characteristics of eligible studies, a total of eight subgroup factors were identified, including study design, age cutoff, ICE group sample size, AF type, male proportion, hypertension proportion, device types, and duration of follow up. If the study design included more than one center, it was defined as a multicenter subgroup; otherwise, it was defined as a single-center subgroup. According to age cutoff values of 75, two subgroups were divided, including ≥ 75 years subgroup and < 75 years subgroups. If over 50% of patients had paroxysmal AF (PAF), they were classified as $\geq 50\%$ PAF subgroup, otherwise they were classified as $< 50\%$ PAF subgroup. According to the proportion of the male, they were divided into $\geq 70\%$ subgroups

and $< 70\%$ subgroups. Similarly, the proportion of hypertension with $\geq 90\%$ subgroup and $< 90\%$ subgroup, respectively, also was defined. According to the sealing position, the existing sealers could be roughly divided into plug type and disc type. Plug type sealers, also known as single sealers, included Watchman, Plauto, and Lefort. Disc sealer was also called dual sealer, including ACP, Lambre, Laches, and Leftear. If the LAAO devices included only dual-seal mechanism devices, it was assigned to dual-seal mechanism subgroup, and if the LAAO devices included only single-seal mechanism devices, it was assigned to the single-seal mechanism subgroup. In addition, studies using both dual-seal mechanism devices and single-seal mechanism devices were divided into multi-seal mechanism subgroup. Follow-up time was divided into two subgroups (≥ 12 months and < 12 months).

3. Results

3.1. Study selection and quality assessment

This meta-analysis included 20 studies with a total of 3,610 AF patients (1,564 patients for ICE and 2,046 patients for TEE) consisting of 10 observational two-arm studies (965 ICE patients

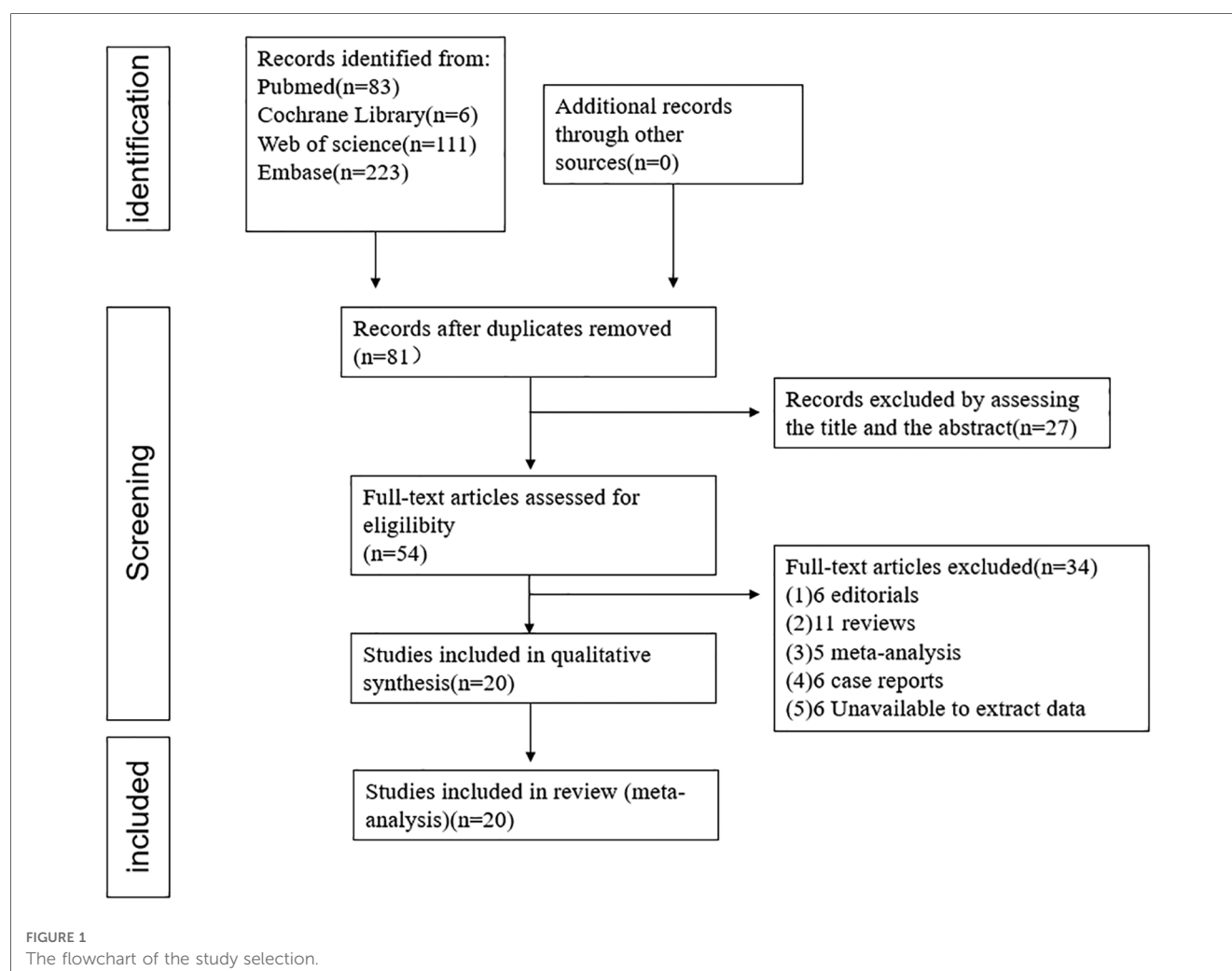


TABLE 1 Baseline characteristics and procedure-related indices of eligible studies.

First author	Year	Study design	Follow-up (Months)	ICE sample size		Gender (male%)		Age		Hypertension (%)		PAF (%)		LAAO device	
				ICE Group	TEE Group	ICE Group	TEE Group	ICE Group	TEE Group	ICE Group	TEE Group	ICE Group	TEE Group	ICE Group	TEE Group
Gianni	2021	Single-center	2	122	68	66	60	72 ± 8	75 ± 9	NA	NA	NA	NA	Watchman FLX	
Pommier	2021	Single-center	1	175	49	70	73	76 ± 8	75 ± 7	91	96	29	23	Watchman/ACP	
Alkhouli	2020	Single-center	1.5	90	196	62.2	55.6	75.7 ± 8.0	75.2 ± 7.8	92.2	87.2	NA	NA	Watchman	
Hemam	2019	Multi-center	4	53	51	62.3	60.8	77 ± 10	76 ± 7	81	90	NA	NA	Watchman	
Nielsen-Kudsk	2019	Multi-center	12	130	955	60	65	75 ± 8	75 ± 9	NA	NA	NA	NA	Amulet	
Berti	2018	Multi-center	15	187	417	66	65	76 ± 8	74 ± 7	NA	NA	32	36	ACP/Amulet	
Kim	2018	Multi-center	25.6	41	103	58.5	49.5	71.4 ± 9.3	72.3 ± 9.2	90.2	83.5	34.1	27.2	Watchman/ACP/Amulet	
Frangieh	2017	Single-center	0	32	44	81	57	74.6 ± 9.3	80.3 ± 7.7	84	86	69	54	Watchman	
Korsholm2	2017	Single-center	1.7	109	107	62	74	73.0 ± 7.8	73.0 ± 9.7	83	80	48	42	ACP/Amulet	
Reis	2018	Single-center	23	26	56		53	74 ± 8		86.6		30.5		Watchman/ACP/Amulet	
Dallan	2022	Single-center	1.5	136		55.1		76 ± 8.4		85.3		53.7		Watchman FLX	
Turagam1	2022	Single-center	12	15		33		71.3 ± 10.8						Watchman	
Chen	2022	Single-center	12	56		57.1		69.4 ± 7.5		69.6		41.1		LAmbre	
Turagam2	2021	Single-center	1.5	30		53		75.4 ± 8.4		90		NA		Watchman	
Filby	2021	Single-center	1.5	71		54.9		76 ± 8.8		81.7		59.2		Watchman/Watchman FLX	
Korsholm1	2020	Single-center	1.7	92		25		73.3 ± 8.5		76		51		Watchman FLX	
Khalili	2019	Single-center	0	15		73		75.6 ± 10		NA		13.3		Watchman	
Matsuo	2016	Single-center	1.5	27		40.7		77.0 ± 8.5		88.9		14.8		Watchman	
Masson	2015	Single-center	2	37		67.6		74.7 ± 8.2		94.6		51.3		ACP	
Berti	2014	Multi-center	0	121		57		77 ± 7.6		89.3		20.7		ACP/Amulet	

First author	Pre-procedure imaging			CHA ₂ DS ₂ -VASC			HAS-BLED			Prior stroke (%)			Congestive heart failure (%)			History of CAD (%)			Diabetes mellitus (%)			ICE location		
	ICE Group	TEE Group		ICE Group	TEE Group		ICE Group	TEE Group		ICE Group	TEE Group		ICE Group	TEE Group		ICE Group	TEE Group		ICE Group	TEE Group		ICE Group	TEE Group	
Gianni	CT/TEE			4.1 ± 1.4	4.3 ± 1.3		2.7 ± 1.3	2.7 ± 1.2		NA	NA		NA	NA		NA	NA		NA	NA		100%LA		
Pommier	CT			4.2 ± 1.38	4.5 ± 1.49		4.07 ± 0.99	3.93 ± 1.02		70	64		17	17		29	28		34	21		100%LA		
Alkhouli	CT/TEE			4.7 ± 1.4	4.8 ± 1.6		2.8 ± 1.2	2.9 ± 1.1		36.5	42.9		56.7	48.5		52.2	51		33.3	43.9		100%LA		
Henam	NA			4.5 ± 1.8	4.5 ± 1.6		NA	NA		42	33		19	25		NA	NA		34	29		100%LA		
Nielsen-Kudsk	CT and TEE			4.1 ± 1.6	4.2 ± 1.6		3.3 ± 1.1	3.2 ± 0.9		42	25		NA	NA		NA	NA		NA	NA		100%LA		
Berti	TEE	TEE		4.27 ± 1.40	4.25 ± 1.40		3.25 ± 1.00	3.15 ± 1.10		NA	NA		NA	NA		NA	NA		NA	NA		100%LA		
Kim	TEE	TEE		4.3 ± 1.4	4.3 ± 1.4		3.0 ± 1.5	3.1 ± 1.4		48.8	42.7		43.9	39.8					26.8	25.2		100%LSPV		
Frangieh	NA	NA		4.3 ± 5.2	4 ± 1.5		3.6 ± 1.4	3.4 ± 0.8		28	21		NA	NA		63	61		36	44		100%LA		
Korsholm2	CT	CT		4.1 ± 1.6	4.4 ± 1.6		4.1 ± 0.9	4.1 ± 1.1		46	55		15	20		NA	NA		21	22		100%LA		
Reis	TEE	TEE		4.7 ± 1.4			3.3 ± 1.0			41.5			NA			22			86.6			100%LA		
Dallan	CT			4.4 ± 1.3			NA			NA			22.1			33.1			31.6			100%LA		
Turagam1	TEE			4.1 ± 1.7			3.4 ± 1.4			NA			NA			NA			NA			100%LA		
Chen	NA			4.0 ± 1.5			2.6 ± 0.8			46.4			41.1			19.6			28.6			100%LA		
Turagam2	NA			4.6 ± 1.6			3.4 ± 1.1			43.3			30						13.3			100%LA		
Filby	CT			4.2 ± 1.4			3.6 ± 1.0			21.1			22.5			49.3			28.2			100%LA		
Korsholm1	CT			3.9 ± 1.7			2.4 ± 1.0			42			16						26			100%LA		
Khalili	TEE			4.6 ± 1						NA			NA						NA			100%RA		
Matsuo	TEE			5.3 ± 1.6			4.4 ± 1.1			37			55.6						44.4			100%LA		
Mason	NA			4.5 ± 1.3			4.2 ± 0.7			40.5			NA						45.9			100%LA		
Berti	TEE			4.4 ± 1.3			3.3 ± 1.0			31.4			13.2						24			38%LA,62%RA		

Note: AF, atrial fibrillation; PAF, paroxysmal atrial fibrillation; LAAO, left atrial appendage closure; CAD, coronary artery disease; ICE, intracardiac echocardiography; TEE, transesophageal echocardiography; LA, left atria; RA, right atria.

and 2,046 TEE patients) (6–15) and 10 single-arm studies (599 ICE patients) (16–25). The selection flowchart was displayed in **Figure 1**. The average age of the patients included in the studies ranged from 71.3 to 80.3 years. Among the included clinical studies, the mean CHA₂DS₂-VASc score and HAS-BLED score ranged from 3.9 to 5.3 and 2.4 to 4.4. Eleven studies included Watchman or Watchman FLX (6, 8, 9, 13, 16, 17, 19–23), six included the ACP or Amulet device (10, 11, 14, 18, 24, 25) and three studies included both (7, 12, 14). The baseline characteristics and procedure-related indexes of the eligible studies were presented in **Table 1**. In this meta-analysis, all two-arm studies had a moderate-to-high quality (**Supplementary Table S1**). Ten single-arm studies all had a score higher than fifteen (**Supplementary Table S1**).

3.2. Primary outcome

3.2.1. Procedural success rate

All eligible two-arms studies reported the acute procedural success data and there was no significant difference in procedural success rate (RR = 1.01; 95% CI: 1.00, 1.02; $P = 0.171$; $I^2 = 0.00\%$) between two groups (**Figure 2**) (6–15). Our result was consistent with those of several other meta-analyses (26–28). Subgroup analysis was performed with a total of eight subgroup factors for the acute procedural success of LAAO, and the results are displayed in **Figure 3**. There was no significant difference between TEE group and ICE group in the study design subgroup, follow-up subgroup, ICE sample size subgroup, male

proportion subgroup, age cutoff subgroup, hypertension proportion subgroup, PAF proportion subgroup, and device types subgroup, suggesting that all subgroup results were consistent with the pooled result.

We also performed a sensitivity analysis and the results showed no significant change, ranging from 1.00 (95% CI: 0.99, 1.02) to 1.01 (95% CI: 1.00, 1.03), in the overall combined proportion, suggesting that there was no single study in the domination of the combined proportion and heterogeneity. Moreover, no publication bias was presented in Egger's test ($P = 0.208$).

3.2.2. Pooled rate of procedural success in ICE group

A total of 20 eligible studies (1,564 patients undergoing LAAO with ICE procedural guidance) reported the rate of procedural success in ICE Group (6–15). The pooled rate of procedural success was 0.99 (95% CI: 0.98, 1.00; $P = 0.02$; $I^2 = 43.69\%$) with the random-effect model (**Figure 4**). Meanwhile we performed a subgroup analysis with eight subgroup factors for procedural success in ICE group, and the results are shown in **Table 2**. Overall, the pooled rate of procedural success in ICE Group does not differ significantly between subgroups.

Also, sensitivity analysis showed that no significant change was detected in the overall combined proportion, ranging from 0.98 (95% CI: 0.97, 0.99) to 0.99 (95% CI: 0.98, 1.00), indicating that no single study dominated the combined proportion and heterogeneity. Moreover, Egger's test was performed and result

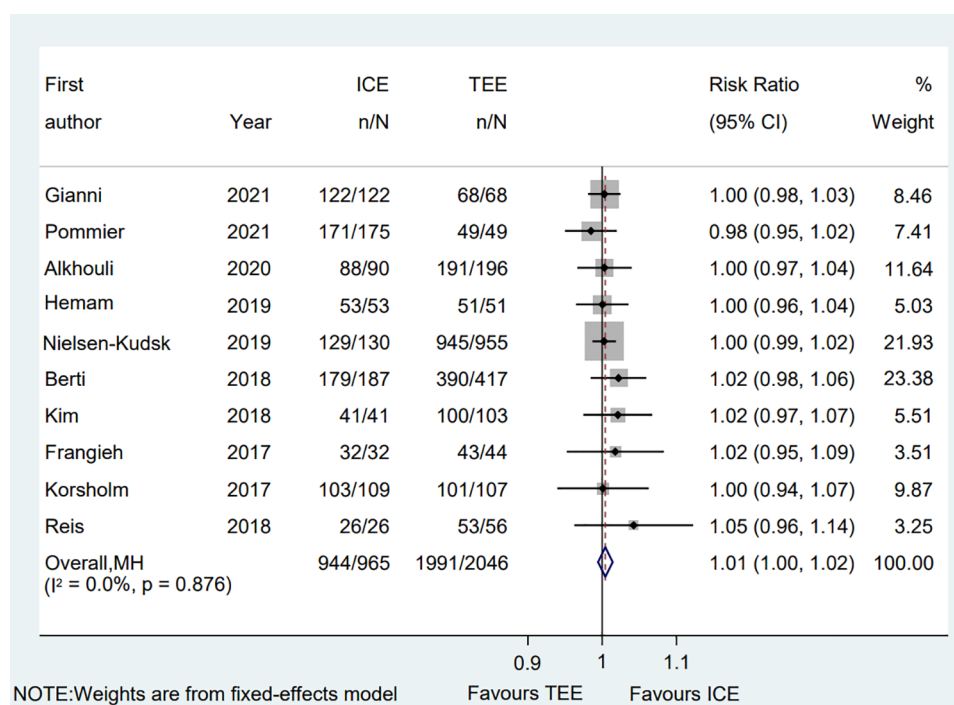


FIGURE 2

Forest plot of the procedural success between ICE and TEE groups. Comparison of the rates of the procedural success between ICE and TEE groups. ICE, intracardiac echocardiography; TEE, transesophageal echocardiography; RR, risk ratio; CI, confidence interval.

showed no publication bias ($P = 0.068$), which indicated that the results were robust.

3.3. Secondary outcome

3.3.1. Total procedure time

A total of ten clinical studies provided the total procedural time, and the data on the total procedural time was similar between groups (WMD = -5.58 ; 95% CI: $-15.97, 4.81$; $P = 0.29$) (6–15). Significant heterogeneity was observed ($I^2 = 96.4\%$) (Figure 5). Subgroup analysis was performed with a total of seven subgroup factors for total procedure time, and the results are displayed in **Supplementary Table S2**. Interestingly, in the PAF proportion $\geq 50\%$ subgroup, the procedural time in the TEE group was shorter than in the ICE group (WMD = 14.20 ; 95% CI: $7.6, 20.8$; $P = 0.000$). Meanwhile, compared with the TEE group, the ICE group was associated with shorter procedural time in the multi-seal mechanism devices subgroup (WMD =

-31.56 ; 95% CI: $-55.57, -7.5$; $P = 0.010$; $I^2 = 95.8\%$). Sensitivity analysis showed that no significant change, ranging from -7.80 (95% CI: $-18.72, 3.11$) to -1.35 (95% CI: $-10.13, 7.44$), was detected in the overall combined proportion. Moreover, no publication bias was shown in Egger's test ($P = 0.535$).

3.3.2. Contrast volume

A total of six eligible studies reported the contrast volume (6–8, 10, 13, 14). The pooled results indicated that compared with the TEE procedure, the ICE procedure showed no significant difference (WMD = -2.61 ; 95% CI: $-12.25, 7.02$; $P = 0.595$; $I^2 = 84.80\%$) (Figure 6). The subgroup analysis showed that in the PAF proportion $< 50\%$ subgroup, the ICE group's contrast volume was significantly decreased compared with the TEE group (WMD = -15.02 ; 95% CI: $-27.08, -2.97$; $P = 0.015$; $I^2 = 78.60\%$). Moreover, in the hypertension proportion $< 90\%$ subgroup, the contrast volume in the ICE group was much lower than that in the TEE group (WMD = -12.95 ; 95% CI: $-22.83,$

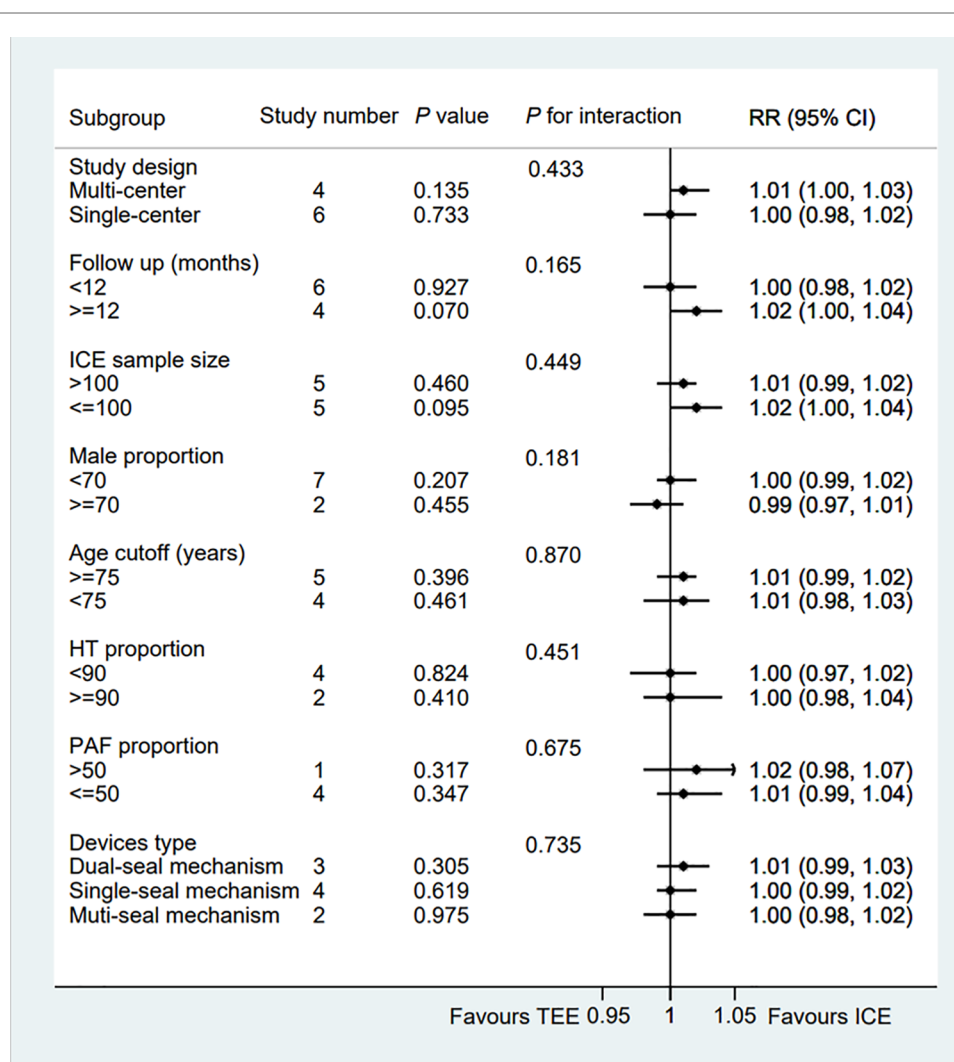


FIGURE 3

Forest plot of subgroup analysis of the procedural success between ICE and TEE groups. Subgroup analysis of the rates of the procedural success between ICE and TEE groups. ICE, intracardiac echocardiography; TEE, transesophageal echocardiography; RR, risk ratio; CI, confidence interval.

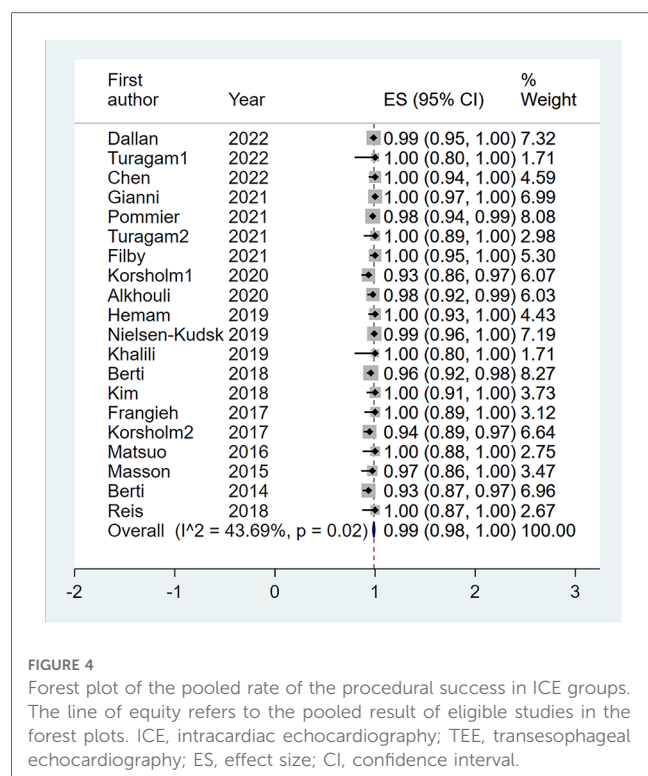


FIGURE 4

Forest plot of the pooled rate of the procedural success in ICE groups. The line of equity refers to the pooled result of eligible studies in the forest plots. ICE, intracardiac echocardiography; TEE, transesophageal echocardiography; ES, effect size; CI, confidence interval.

−3.07; $P = 0.010$; $I^2 = 62.90\%$). Meanwhile, the ICE group was associated with less contrast volume than the TEE group in the muti-seal mechanism devices subgroup (WMD = −22.00; 95% CI: −32.01, −11.99; $P = 0.000$). Interestingly, in the muti-centered subgroup, ICE-guided LAAO required a greater amount of contrast volume than TEE-guided LAAO (WMD = 47.00; 95% CI: 19.59, 74.42; $P = 0.001$) (**Supplementary Table S3**).

Meanwhile, sensitivity analysis showed that no single study dominated the combined proportion and heterogeneity, ranging from −4.81 (95% CI: −15.29, 5.66) to 1.26 (95% CI: −8.55, 11.06). Moreover, Egger's test was performed and result showed no publication bias ($P = 0.371$), which suggested that the results were robust.

3.3.3. Fluoroscopic time

A total of ten eligible studies reported the fluoroscopic time and the pooled result showed that the fluoroscopic time guided by ICE was significantly equivalent to that guided by TEE (WMD = −0.34; 95% CI: −2.09, 1.41; $P = 0.705$; $I^2 = 82.80\%$) (**Figure 7**) (6–15). Subgroup analysis was performed with a total of seven subgroup factors for the fluoroscopic time, and the results were displayed in **Supplementary Table S4**. Compared with the TEE group, the fluoroscopic time in the ICE group was much shorter in the hypertension proportion <90% subgroup (WMD = −1.49; 95% CI: −2.87, −0.10; $P = 0.035$; $I^2 = 33.50\%$) as well as the muti-seal mechanism devices subgroup (WMD = −3.49; 95% CI: −5.53, −1.45; $P = 0.001$; $I^2 = 0.00\%$). No significant change was detected in the overall combined proportion by sensitivity analysis, ranging from −0.72 (95% CI: −2.48, 1.03) to 0.07 (95% CI: −1.74, 1.87). Moreover, no publication bias was shown in Egger's test ($P = 0.941$).

TABLE 2 Subgroup analysis of the rate of procedural success in ICE group.

Subgroup factors	Numbers of study	Pooled incidence	95% CI	I^2 (%)	P for interaction
Study design					0.670
Multi-centered	5	0.99	(0.98, 1.0)	31.86	
Single-centered	15	0.98	(0.95, 1.0)	66.08	
ICE Sample size					0.280
>100	7	0.98	(0.95, 0.99)	68.51	
≤100	13	0.99	(0.98, 1.0)	4.01	
Male proportion					0.990
<70	16	0.99	(0.97, 1.0)	54.17	
≥70	3	0.99	(0.97, 1.0)	–	
Age cutoff					0.890
≥75	11	0.99	(0.97, 1.0)	35.33	
<75	8	0.99	(0.96, 1.0)	60.83	
HT proportion					0.720
<90	10	0.98	(0.96, 1.0)	57.21	
≥90	4	0.99	(0.97, 1.0)	0	
PAF proportion					0.580
>50	5	0.98	(0.96, 1.0)	52.71	
≤50	8	0.98	(0.96, 0.99)	42.03	
Devices type					0.230
Dual-seal mechanism	6	0.94	(0.94, 0.99)	57.64	
Single-seal mechanism	11	0.98	(0.98, 1.0)	26.89	
Muti-seal mechanism	2	0.96	(0.96, 1.0)	–	

ICE, intracardiac echocardiography; TEE, transesophageal echocardiography; CI, confidence interval.

3.3.4. Pooled safety outcomes

Common perioperative complications include cardiac effusion, cardiac tamponade, device migration, device thrombus, stroke/TIA, bleeding, hematoma, renal complications, cardiac arrest, and death. The data on procedural complications was available in nine clinical studies (6–8, 10–15). Complications from each eligible study were listed independently in **Supplementary Tables S5, S6**. The rate of procedural complications in ICE group was similar with that of TEE group (RR = 0.82; 95% CI: 0.58, 1.16; $P = 0.261$; $I^2 = 23.50\%$) (**Figure 8**). Sensitivity analysis was performed and the results showed no significant change in the overall combined proportion, ranging from 0.70 (95% CI: 0.45, 1.10) to 0.87 (95% CI: 0.61, 1.25). Egger's test also showed no publication bias ($P = 0.696$). Meanwhile, seven clinical studies were followed up and reported long-term adverse events (6–11, 14). In terms of long-term adverse events, the ICE group showed a similar result to TEE group (RR = 0.86; 95% CI: 0.64, 1.16; $P = 0.329$; $I^2 = 41.10\%$) (**Figure 9**).

4. Discussion

Among twenty enrolled published original articles, a total of 3,610 patients (including 1,564 patients for ICE and 2,046 patients for TEE) were evaluated. Compared with previous meta-

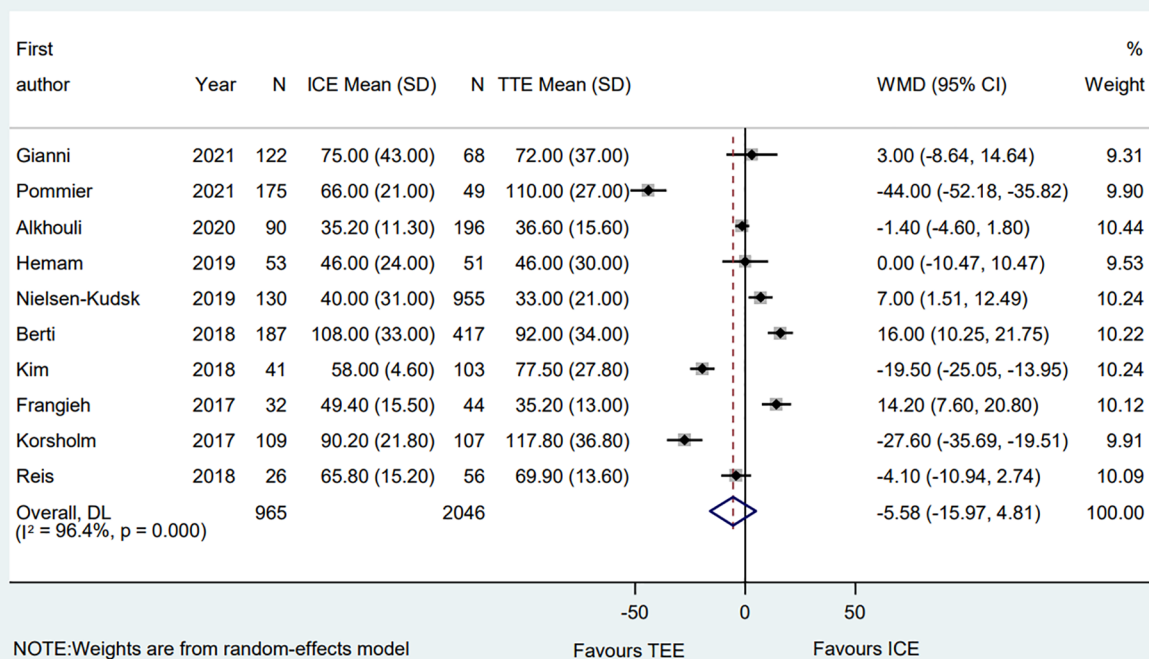


FIGURE 5

Forest plot of the total procedural time between ICE and TEE groups. Comparison of the rates of the total procedural time between ICE and TEE groups. ICE, intracardiac echocardiography; TEE, transesophageal echocardiography; WMD, weighted mean difference; CI, confidence interval.

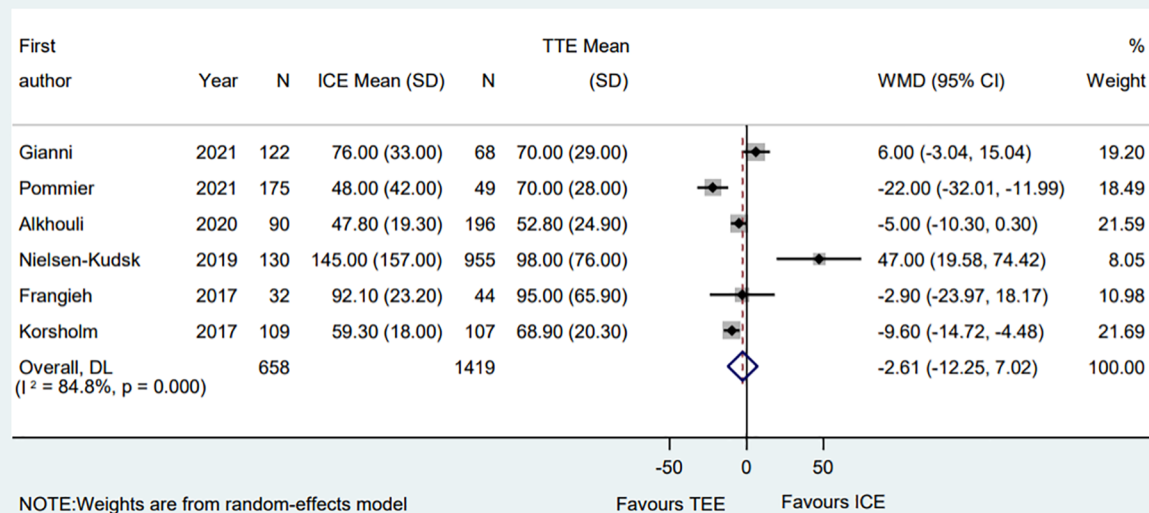


FIGURE 6

Forest plot of the contrast volume between ICE and TEE groups. Comparison of the rates of the contrast volume between ICE and TEE groups. ICE, intracardiac echocardiography; TEE, transesophageal echocardiography; WMD, weighted mean difference; CI, confidence interval.

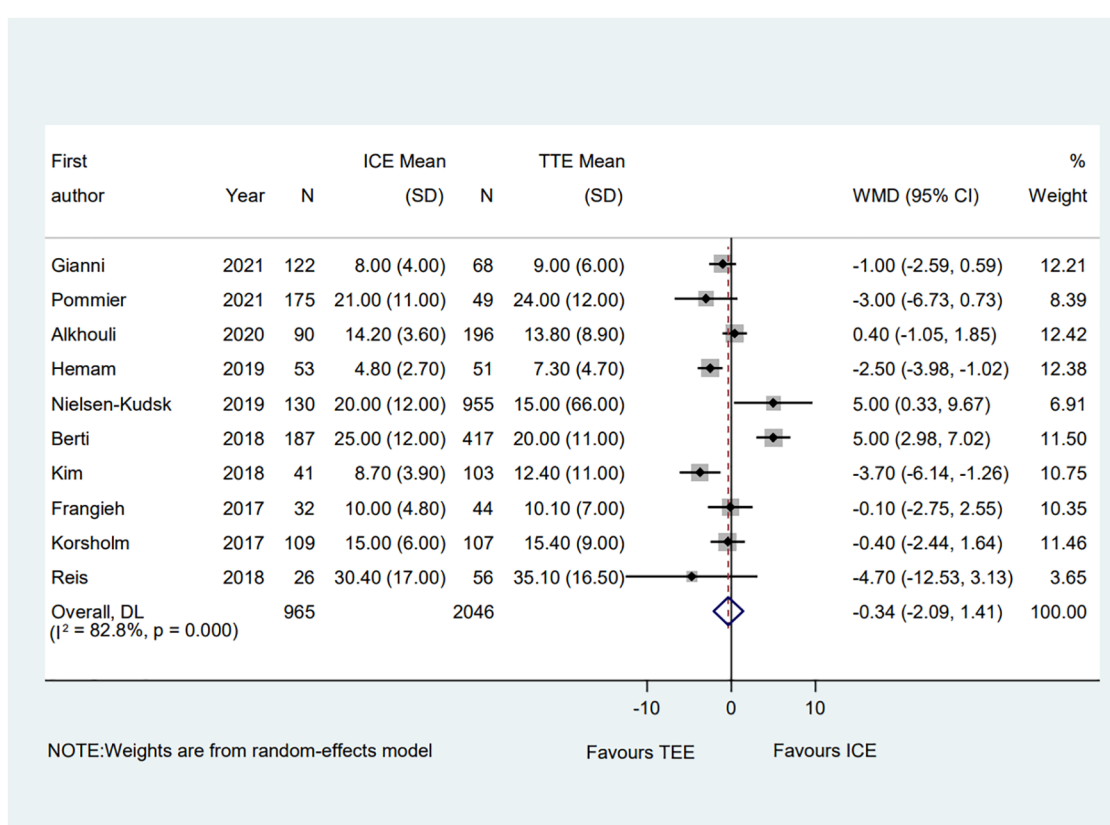


FIGURE 7

Forest plot of the fluoroscopic time between ICE and TEE groups. Comparison of the rates of the fluoroscopic time between ICE and TEE groups. ICE, intracardiac echocardiography; TEE, transesophageal echocardiography; WMD, weighted mean difference; CI, confidence interval.

analysis, we included recent publications and single-arm studies. Meanwhile we performed subgroup analysis for each endpoint event. Our main findings were as follows. Compared with TEE group, (1) ICE group showed comparable efficacy and safety outcomes for LAAO, including the acute procedural success rate, total procedure time, contrast volume, the fluoroscopic time, and safety outcomes; (2) ICE group might reduce the use of contrast agent and fluoroscopic time in the hypertension proportion <90 subgroup; (3) ICE group might be associated with lower total procedure time, contrast volume, and the fluoroscopic time in device type subgroup with multi-seal mechanism; (4) The total procedure time might be longer in PAF proportion >50 subgroup while the contrast use might be less in PAF proportion ≤50 subgroup for ICE group; (5) ICE group might be related in an increased use of contrast in multi-center subgroup.

AF is an important pathogenesis of ischemic stroke, with approximately 5% of stroke patients being associated with AF each year, ultimately resulting in high rates of mortality and morbidity (3). LAAO has been demonstrated to be an alternative to prevent stroke in AF patients, particularly for individuals who are intolerant to oral anticoagulants. Intraoperative imaging is a crucial factor for LAAO. While TEE is currently the mainstream method, ICE is increasingly being used as an alternative to TEE.

In this meta-analysis, we compared the acute procedural success between the TEE and ICE groups. Similar with previous

studies (26–28), we found no significant difference between the two groups. We then conducted a subgroup analysis to further compare the advantages and disadvantages of the two groups. The result showed that, regardless of the subgroup, there was no significant difference in acute procedural success rate. TEE is the gold standard imaging method for LAAO, providing clear images of the right atrium, left atrium, atrial septum, and left atrial appendage anatomy for LAAO. However, TEE-guided LAAO has some disadvantages, such as increased pain with local or conscious anesthesia, prolonged procedure time and hospitalization burden with general anesthesia, aggravated risk of possible esophageal injury under “one-stop” ablation, and high dependence on a dedicated echocardiography operator. To explore the safety of ICE and TEE, we recorded both the preprocedural complications and the long-term complications. For the short-term adverse events, the results showed that ICE was not inferior to TEE in guiding LAA occlusion procedures in terms of peri-procedural complications. Additionally, the long-term adverse events were comparable between groups, indicating that ICE had a reliable performance on safety.

Hypertension is one of the common comorbidities and modifiable risk factors in cardiovascular diseases, which could lead to the enlargement of left atria diameter, promotion of atrial fibrosis, and impairment of the endothelial function, ultimately causing the initiation and progression of AF and related stroke

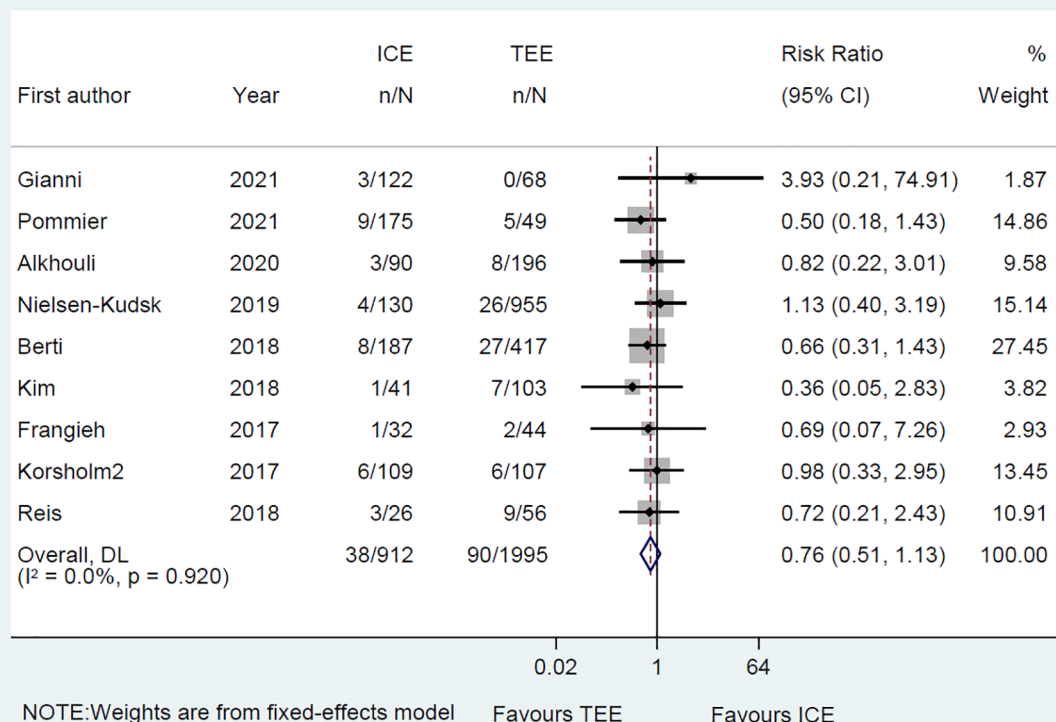


FIGURE 8

Forest plot of the preprocedural complications between ICE and TEE groups. Comparison of the rates of the preprocedural complications between ICE and TEE groups. ICE, intracardiac echocardiography; TEE, transesophageal echocardiography; RR, risk ratio; CI, confidence interval.

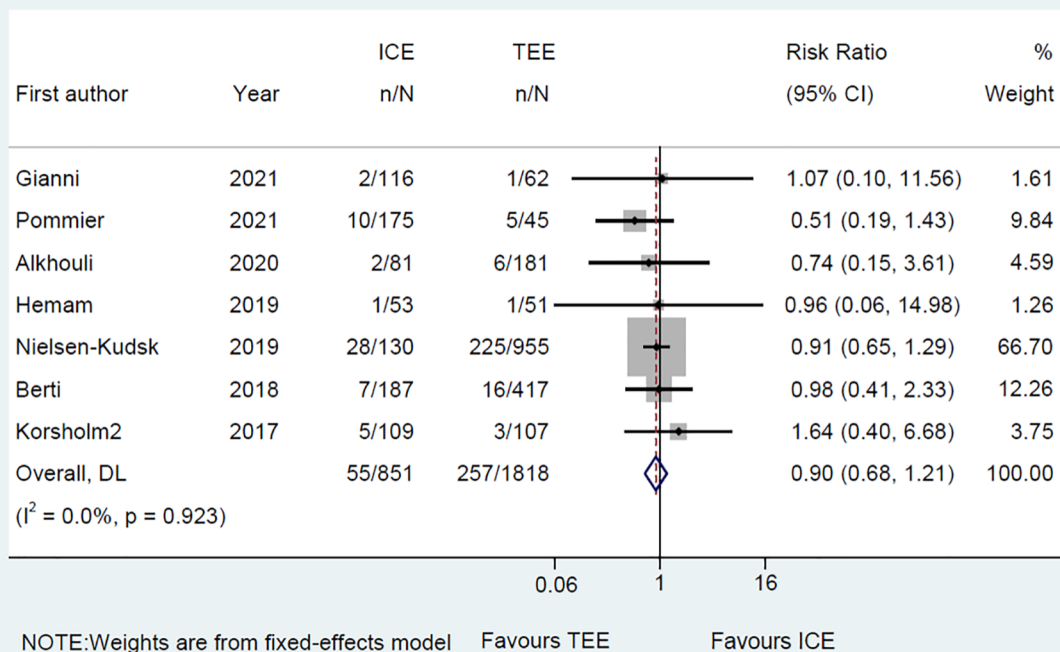


FIGURE 9

Forest plot of the long-term adverse events between ICE and TEE groups. Comparison of the rates of the long-term adverse events between ICE and TEE groups. ICE, intracardiac echocardiography; TEE, transesophageal echocardiography; RR, risk ratio; CI, confidence interval.

(29). However, few studies reported the role of hypertension on the procedure of LAAO for AF. Our subgroup results showed that ICE group might reduce the use of contrast agent and fluoroscopic time in the hypertension proportion <90 subgroup in comparison with the TEE group, suggesting that the lower proportion of hypertension may be associated with the more benefit for AF patients with LAAO procedure. This result might provide a basis for a randomized control trial to further evaluate the role of hypertension on the use of contrast agent and the fluoroscopic time between ICE-guided and TEE-guided LAAO.

At present, multiple types of devices for LAAO were applied in clinical procedure, mainly including single-seal mechanism device, dual-seal mechanism devices, and both mechanism device (30). Accumulated studies had revealed that selective application of the device type for LAAO might showed a similarly clinical outcomes based on the specific morphologies of LAA (31). Interestingly, ICE-guided LAAO might be associated with lower total procedure time, contrast volume, and the fluoroscopic time in device type subgroup with multi-seal mechanism. We could make a reasonable speculation that the application of multi-seal mechanism devices is associated with the mastery of the ICE-guided LAAO procedure by operators. Whereas, more studies should be performed to demonstrate this result.

Studies on the impact of AF type during LAAO procedure are emerging. A recent lesson from the prospective Left Atrial Appendage Occluder Registry Germany (LAARGE) had suggested that the procedure time and fluoroscopy time were longer for LAAO procedure in PAF patients than non-PAF patients, which might be significantly related in the challenge of LAA movement due to the higher rate of sinus rhythm in PAF patients during LAAO procedure (32). Similarly, our subgroup also indicated that the total procedure time in ICE-guided LAAO might be longer in PAF proportion >50 subgroup. In addition, the contrast use might be less in PAF proportion ≤ 50 subgroup for ICE-guided LAAO group, potentially suggesting that ICE-guided LAAO might reduce the contrast use for non-PAF patients.

Additionally, our subgroup results suggested that ICE-guided LAAO might be associated with an increased use of contrast in multi-center subgroup, which indicated that ICE-guided LAAO showed unsatisfied performance on the contrast use in multi-center subgroup in comparison with single-center subgroup. This might be explained by the multiple possibilities, including center heterogeneity, team quality heterogeneity, and relatively rigid procedure protocol rarely with decision-making strategy in multi-center study. Moreover, only one multi-center study (10) reported the contrast use for subgroup analysis, which might cause potential bias due to the limited sample size. Therefore, more prospective studies are needed to further demonstrate our results.

Also, a total of two studies compared the cost of hospitalization between ICE group and TEE group (8, 9), which showed that the global charges were similar between the ICE-guided LAAO and TEE-guided LAAO in American centers. Whereas, in other medical centers, the hospital charges of ICE-guided LAAO might be higher in comparison with TEE-guided LAAO due to the higher cost of ICE catheter (33). Also, local medical team experience and environment would play an important role on the determination of

the appropriate imaging modality to be implemented. Therefore, more prospective, randomized studies will probably clarify the comparison of ICE and TEE for guiding the LAAO procedure, especially in terms of efficacy, safety, and hospital charges.

5. Limitations

Our study has several limitations. First, the studies included in this meta-analysis were nonrandomized and observational in design, which might lead to potential selection bias. Second, the sample size included in the study is small which may affect the stability of the result indicators, reduce the efficiency of the test, and introduce potential research bias. Third, different studies were followed with different tests, which may have affected the follow-up results. In addition, clinical studies lacked a uniform definition of procedural success and procedure-related complications. Therefore, a prospective, randomized study is needed to clarify the clinical outcomes of LAAO with the comparison of ICE vs. TEE monitoring.

6. Conclusions

Our results demonstrate that ICE may have comparable efficacy and safety compared to TEE for LAAO.

Data availability statement

The data that support the findings of this study are available from the corresponding author upon reasonable request.

Author contributions

R-XW developed the concept of the study; Z-YZ, FL and JZ designed this study and carried out the data analysis; FL, and Z-YZ conducted meta-analysis registration in the PROSPERO platform with help from R-XW; Z-YZ wrote the manuscript with help from FL, JZ, LZ, H-HL, NZ, FY, QK; Y-TZ, L-LQ and R-XW provided critical reviews of the paper. All authors contributed to the article and approved the submitted version.

Conflict of interest

The authors declare that the research was conducted in the absence of any commercial or financial relationships that could be construed as a potential conflict of interest.

Publisher's note

All claims expressed in this article are solely those of the authors and do not necessarily represent those of their

affiliated organizations, or those of the publisher, the editors and the reviewers. Any product that may be evaluated in this article, or claim that may be made by its manufacturer, is not guaranteed or endorsed by the publisher.

References

- Hindricks G, Potpara T, Dagres N, Arbelo E, Bax JJ, Blomström-Lundqvist C, et al. 2020 ESC guidelines for the diagnosis and management of atrial fibrillation developed in collaboration with the European association for cardio-thoracic surgery (EACTS): the task force for the diagnosis and management of atrial fibrillation of the European society of cardiology (ESC) developed with the special contribution of the European heart rhythm association (EHRA) of the ESC. *Eur Heart J*. (2021) 42(5):373–498. doi: 10.1093/eurheartj/ehaa612
- Jame S, Barnes G. Stroke and thromboembolism prevention in atrial fibrillation. *Heart*. (2020) 106(1):10–7. doi: 10.1136/heartjnl-2019-314898
- Berti S, Pastormerlo L E, Korsholm K, Saw J, Alkhouli M, Costa MP, et al. Intracardiac echocardiography for guidance of transcatheter left atrial appendage occlusion: an expert consensus document. *Catheter Cardiovasc Interv*. (2021) 98(4):815–25. doi: 10.1002/ccd.29791
- Furlan A D, Pennick V, Bombardier C, van Tulder M. 2009 Updated method guidelines for systematic reviews in the cochrane back review group. *Spine*. (2009) 34(18):1929–41. doi: 10.1097/BRS.0b013e3181b1c99f
- Guo B, Moga C, Harstall C, Schopflocher D. A principal component analysis is conducted for a case series quality appraisal checklist. *J Clin Epidemiol*. (2016) 69:199–207.e2. doi: 10.1016/j.jclinepi. 2015.07.010
- Gianni C, Horton RP, Della Rocca DG, Mohanty S, Al-Ahmad A, Bassiouny MA, et al. Intracardiac echocardiography- versus transesophageal echocardiography-guided left atrial appendage occlusion with watchman FLX. *J Cardiovasc Electrophysiol*. (2021) 32(10):2781–4. doi: 10.1111/jce.15220
- Pommier T, Guenancia C, Richard C, Sagnard A, Fichot M, Salignon-Vernay C, et al. Safety and efficacy of left atrial appendage occlusion with the ACP or watchman device guided by intracardiac echocardiography from the left atrium. *Clin Cardiol*. (2021) 44(10):1402–8. doi: 10.1002/clc.23696
- Alkhouli M, Chaker Z, Alqahtani F, Raslan S, Raybuck B. Outcomes of routine intracardiac echocardiography to guide left atrial appendage occlusion. *JACC Clin Electrophysiol*. (2020) 6(4):393–400. doi: 10.1016/j.jacep.2019.11.014
- Hemam ME, Kuroki K, Schurmann PA, Dave AS, Rodríguez DA, Sáenz LC, et al. Left atrial appendage closure with the watchman device using intracardiac vs transesophageal echocardiography: procedural and cost considerations. *Heart Rhythm*. (2019) 16(3):334–42. doi: 10.1016/j.hrthm.2018.12.013
- Nielsen-kudsk JE, Berti S, De backer O, Aguirre D, Fassini G, Cruz-Gonzalez I, et al. Use of intracardiac compared with transesophageal echocardiography for left atrial appendage occlusion in the amulet observational study. *JACC Cardiovasc Interv*. (2019) 12(11):1030–9. doi: 10.1016/j.jcin.2019.04.035
- Berti S, Pastormerlo LE, Santoro G, Brscic E, Montorfano M, Vignali L, et al. Intracardiac versus transesophageal echocardiographic guidance for left atrial appendage occlusion: the LAAO Italian multicenter registry. *JACC Cardiovasc Interv*. (2018) 11(11):1086–92. doi: 10.1016/j.jcin.2018.05.008
- Kim DY, Shin SY, Kim J-S, Kim SH, Kim YH, Lim HE. Feasibility of intracardiac echocardiography imaging from the left superior pulmonary vein for left atrial appendage occlusion. *Int J Cardiovasc Imaging*. (2018) 34(10):1571–9. doi: 10.1007/s10554-018-1374-5
- Frangieh AH, Alibegovic J, Templin C, Gaemperli O, Obeid S, Manka R, et al. Intracardiac versus transesophageal echocardiography for left atrial appendage occlusion with watchman. *Catheter Cardiovasc Interv*. (2017) 90(2):331–8. doi: 10.1002/ccd.26805
- Korsholm K, Jensen JM, Nielsen-kudsk JE. Intracardiac echocardiography from the left atrium for procedural guidance of transcatheter left atrial appendage occlusion. *JACC Cardiovasc Interv*. (2017) 10(21):2198–206. doi: 10.1016/j.jcin.2017.06.057
- Reis L, Paiva L, Costa M, Silva J, Teixeira R, Botelho A, et al. Registry of left atrial appendage closure and initial experience with intracardiac echocardiography. *Rev Port Cardiol (Engl Ed)*. (2018) 37(9):763–72. doi: 10.1016/j.repc.2018.03.009
- Dallan LAP, Arruda M, Yoon S-H, Rana MA, Mogalappalli A, Carneiro HA, et al. Novel computed tomography angiography-based sizing methodology for WATCHMAN FLX device in left atrial appendage closure. *J Cardiovasc Electrophysiol*. (2022) 33(8):1781–7. doi: 10.1111/jce.15548
- Turagam MK, Neuzil P, Hala P, Hala P, Mraz T, Dukupati SR, Reddy VY. Intracardiac echocardiography-guided left atrial appendage closure with a novel foam-based conformable device: safety and 1-year outcomes. *JACC Clin Electrophysiol*. (2022) 8(2):197–207. doi: 10.1016/j.jacep.2021.10.001
- Chen Y-H, Wang L-G, Zhou X-D, Fang Y, Su L, Wu SJ, et al. Outcome and safety of intracardiac echocardiography guided left atrial appendage closure within zero-fluoroscopy atrial fibrillation ablation procedures. *J Cardiovasc Electrophysiol*. (2022) 33(4):667–76. doi: 10.1111/jce.15370
- Turagam MK, Neuzil P, Petru J, Hala P, Mraz T, Baroch J, et al. Intracardiac echocardiography-guided implantation of the watchman FLX left atrial appendage closure device. *J Cardiovasc Electrophysiol*. (2021) 32(3):717–25. doi: 10.1111/jce.14927
- Filby SJ, Dallan LAP, Cochet A, Kobayashi A, Attizzani GF, Rashid I, et al. Left atrial appendage occlusion using cardiac CT angiography and intracardiac echocardiography: a prospective, single-center study. *J Invasive Cardiol*. (2021) 33(11):E851–E6.
- Korsholm K, Samaras A, Andersen A, Jensen JM, Nielsen-Kudsk JE. The watchman FLX device: first European experience and feasibility of intracardiac echocardiography to guide implantation. *JACC Clin Electrophysiol*. (2020) 6(13):1633–42. doi: 10.1016/j.jacep.2020.06.028
- Khalili H, Patton M, Taii HA, Bansal P, Brady M, Taylor J, et al. 4D Volume intracardiac echocardiography for intraprocedural guidance of transcatheter left atrial appendage closure. *J Atr Fibrillation*. (2019) 12(4):2200. doi: 10.4022/jafib.2200
- Matsuo Y, Neuzil P, Petru J, Chovanec M, Janotka M, Choudry S, et al. Left atrial appendage closure under intracardiac echocardiographic guidance: feasibility and comparison with transesophageal echocardiography. *J Am Heart Assoc*. (2016) 5(10):e003695. doi: 10.1161/JAHA.116.003695
- Masson J-B, Kouz R, Riahi M, Nguyen Thanh HK, Potvin J, Naim C, et al. Transcatheter left atrial appendage closure using intracardiac echocardiographic guidance from the left atrium. *Can J Cardiol*. (2015) 31(12):1497.e7–1497.e14. doi: 10.1016/j.cjca.2015.04.031
- Berti S, Paradossi U, Meucci F, Trianni G, Tzikas A, Rezzaghi M, et al. Periprocedural intracardiac echocardiography for left atrial appendage closure: a dual-center experience. *JACC Cardiovasc Interv*. (2014) 7(9):1036–44. doi: 10.1016/j.jcin.2014.04.014
- Ribeiro JM, Teixeira R, Puga L, Costa M, Gonçalves L. Comparison of intracardiac and transesophageal echocardiography for guidance of percutaneous left atrial appendage occlusion: a meta-analysis. *Echocardiography*. (2019) 36(7):1330–7. doi: 10.1111/echo.14415
- Liang G, Xu B, Wang S, Li C, Zhong G. Imaging with intracardiac echocardiography compared to transesophageal echocardiography during left atrial appendage occlusion. *Rev Cardiovasc Med*. (2020) 21(1):93–101. doi: 10.31083/j.rcm.2020.01.569
- Akella K, Murtaza G, Turagam M, Sharma S, Madoukh B, Amin A, et al. Evaluating the role of transesophageal echocardiography (TEE) or intracardiac echocardiography (ICE) in left atrial appendage occlusion: a meta-analysis. *J Interv Card Electrophysiol*. (2021) 60(1):41–8. doi: 10.1007/s10840-019-00677-x
- Brundel B, Ai X, Hills MT, Kuipers MF, Lip GYH, de Groot NMS. Atrial fibrillation. *Nat Rev Dis Prim*. (2022) 8(1):21. doi: 10.1038/s41572-022-00347-9
- Saw J, Holmes DR, Cavalcante JL, Freeman JV, Goldsweig AM, Kavinsky CJ, et al. SCAI/HRS expert consensus statement on transcatheter left atrial appendage closure. *Heart Rhythm*. (2023) 20(5):e1–e16. doi: 10.1016/j.hrthm.2023.01.007
- Holmes DR Jr, Korsholm K, Rodés-Cabau J, Saw J, Berti S, Alkhouli MA. Left atrial appendage occlusion. *EuroIntervention*. (2023) 18(13):e1038–65. doi: 10.4244/EIJ-D-22-00627
- Kany S, Brachmann J, Lewalter T, Akin I, Sievert H, Zeymer U, et al. Impact of atrial fibrillation pattern on outcomes after left atrial appendage closure: lessons from the prospective LAARGE registry. *Clin Res Cardiol*. (2022) 111(5):511–21. doi: 10.1007/s00392-021-01874-3
- Bartel T, Müller S, Biviano A, Hahn RT. Why is intracardiac echocardiography helpful? Benefits, costs, and how to learn. *Eur Heart J*. (2014) 35(2):69–76. doi: 10.1093/eurheartj/eh411

Supplementary material

The Supplementary Material for this article can be found online at: <https://www.frontiersin.org/articles/10.3389/fcvm.2023.1194771/full#supplementary-material>



OPEN ACCESS

EDITED BY

Francesca Innocenti,
Careggi University Hospital, Italy

REVIEWED BY

Ricardo Jorge Gelpi,
University of Buenos Aires, Argentina
Mihai Strachinaru,
Erasmus Medical Center, Netherlands

*CORRESPONDENCE

Xiaojun Bi
✉ bixiaojun185@aliyun.com

RECEIVED 09 February 2023

ACCEPTED 16 May 2023

PUBLISHED 12 June 2023

CITATION

Cheng Q, Huang X, Fan X, Sun J, Zhang J,
Tang Q, Deng Y and Bi X (2023) Exploring the
prospect of intrinsic wave propagation in
evaluating myocardial stiffness among patients
with type 2 diabetes.
Front. Cardiovasc. Med. 10:1162500.
doi: 10.3389/fcvm.2023.1162500

COPYRIGHT

© 2023 Cheng, Huang, Fan, Sun, Zhang, Tang,
Deng and Bi. This is an open-access article
distributed under the terms of the [Creative
Commons Attribution License \(CC BY\)](#). The use,
distribution or reproduction in other forums is
permitted, provided the original author(s) and
the copyright owner(s) are credited and that the
original publication in this journal is cited, in
accordance with accepted academic practice.
No use, distribution or reproduction is
permitted which does not comply with these
terms.

Exploring the prospect of intrinsic wave propagation in evaluating myocardial stiffness among patients with type 2 diabetes

Qiao Cheng, Xiao Huang, Xinying Fan, Jie Sun, Jun Zhang,
Qiaoying Tang, Youbin Deng and Xiaojun Bi*

Department of Medical Ultrasound, Tongji Hospital, Tongji Medical College, Huazhong University of Science and Technology, Wuhan, China

Background: Diabetes predisposes affected individuals to impaired myocardial perfusion and ischemia, leading to cardiac dysfunction. Increased myocardial stiffness is an independent and significant risk factor in diastolic dysfunction. This study sought to estimate myocardial stiffness in Type 2 diabetes (T2DM) patients using the intrinsic wave velocity propagation (IVP) along the longitudinal wall motion during late diastole and evaluate the value of IVP in assessing cardiac function and structure.

Methods: 87 and 53 participants with and without T2DM (control group) were enrolled. Of the 87 T2DM patients (DM group), 43 were complicated with hypertension (DM+H group), and 44 were not (DM-H group). Ultrasound parameters were measured and analyzed, including color M-mode flow propagation velocity, global longitudinal systolic strain (GLS), and IVP.

Results: IVP was higher in the DM group than in the control group (1.62 ± 0.25 m/s and 1.40 ± 0.19 m/s, $P < 0.001$). After stratification for hypertension, IVP in both DM+H (1.71 ± 0.25 m/s) and DM-H (1.53 ± 0.20 m/s) groups were found to be significantly higher than that in the control group (1.40 ± 0.19 m/s); also, the difference of IVP between DM+H and DM-H group reached statistical significance. Moreover, IVP was significantly correlated with flow propagation velocity during early diastole (Pve) ($r = -0.580$, $P < 0.001$), flow propagation velocity during late diastole (Pva) ($r = 0.271$, $P < 0.001$), GLS ($r = 0.330$, $P < 0.001$), interventricular septal thickness at end-diastole (IVSd) ($r = 0.321$, $P < 0.001$), blood glucose ($r = 0.246$, $P < 0.003$), systolic blood pressure ($r = 0.370$, $P < 0.001$) and diastolic blood pressure ($r = 0.389$, $P < 0.001$).

Conclusions: The results indicated the application potential of IVP in assessing the early detection of cardiac function changes noninvasively and sensitively. The correlation with myocardial stiffness warrants further studies to substantiate its potential clinical utility.

KEYWORDS

type 2 diabetes mellitus, myocardial stiffness, intrinsic wave velocity propagation, diastolic function, two-dimensional speck tracking

Introduction

Diabetes is a severe global health problem associated with the increased risk of heart failure (1). Diabetes predisposes affected individuals to impaired myocardial perfusion and ischemia, exerting deleterious effects on the myocardium (2). Hyperglycemia facilitates the formation of advanced glycation end products (AGEs), which cross-links with

extracellular matrix proteins, leading to increased fibrosis, elevated myocardial stiffness (MS), impaired myocardial relaxation and diastolic dysfunction, and eventually heart failure (3–5). Increased myocardial stiffness is an independent and significant risk factor in diastolic dysfunction (6–8). Thus, early detection of MS is strategic; however, methods assessing MS in diabetes remain poorly studied. Though the gold standard in assessing MS, cardiac catheterization is an invasive method unfit for routine screening (9). The quality of cardiac magnetic resonance imaging with late gadolinium enhancement, on the other hand, is limited by a long scanning time, patient movement, or in those with irregular depth and rate of breathing, as well as arrhythmias despite its application to non-invasive quantification of myocardial fibrosis (10).

Now, the possibility of imaging the heart at very high frame rates allows minute tracking of many wave-like phenomena, such as shear wave elastography technique using acoustic radiation force to mechanically stimulate tissue and monitor the response (11, 12), naturally occurring shear waves generated by aortic and mitral valves closure (13–15).

It was hypothesized that during left ventricular (LV) filling after atrial contraction, the fast traction on the mitral annulus by the atrial contraction generates a wave into the LV, which travels from base to apex with a speed proportional to myocardial elasticity. The propagating wave velocity along longitudinal tissue motion direction is referred to as the Intrinsic Velocity Propagation (IVP) (16, 17). It is generated through the dynamic nature of the heart and allows quantification in all LV segments. It is possible that this wave is related to tissue stiffness and has a radial component. Previous studies (18–20) have demonstrated the feasibility of IVP measurement in normal volunteers and confirmed that IVP was strongly influenced by passive tissue properties. The wave speed was consistent with the pressure-dependent increase in myocardial stiffness, indicating the potential of IVP in evaluating MS.

This work aimed to explore whether there is a relationship between IVP and diastolic dysfunction and discuss the potential of IVP in assessing MS in T2DM patients.

Materials and methods

Study population

This pilot study was conducted between April 2019 and March 2021 in Tongji Hospital, the most widely circulating hospital in its region. One hundred forty participants were enrolled, with 87 patients diagnosed as T2DM (DM group) and 53 healthy controls (control group). Among the T2DM patients, 43 were complicated with hypertension (DM + H group), and 44 were exempt from other complications (DM-H group). The diagnosis criteria of T2DM were promulgated by WHO: fasting blood glucose (FPG) ≥ 7.0 mmol/L or 2-hour postprandial blood glucose (2hPG) ≥ 11.1 mmol/L. Patients were excluded from the study if they were complicated with valvular heart disease, congenital heart disease, coronary heart disease, cardiomyopathy,

and history of cardiac surgery in case of possible confounding; those with poor echocardiographic image quality were also excluded. The control group was chosen from healthy people undergoing a physical examination, including biochemical routines, electrocardiogram, and echocardiography. They had no history of diabetes, hypertension, cardiovascular disease, or cardiac surgery. All experiments were carried out in accordance with the ethical standards put forward by the Declaration of Helsinki and approved by a local institutional review board. Each participant signed written informed consent.

Echocardiography examination

Echocardiography was acquired using Vivid E9 commercial scanners (GE Healthcare, Horten, Norway) equipped with an M5S transducer at a frequency of 1.7–3.4 MHz. The rate of conventional two-dimensional ultrasound images is ≥ 70 frames/s. Three consecutive cardiac cycles are stored in each section. Several conventional echocardiographic parameters were measured, including interventricular septal thickness at end-diastole (IVSd), left ventricular posterior wall thickness at end-diastole (LVPWd), left ventricular internal diameter at end-diastole (LVIDd), left ventricular ejection fraction (LVEF), Mitral E velocity, Mitral A velocity, and Mitral annular septal e' velocity. E/A and E/e' ratios were later calculated.

Flow propagation velocity examination

The speed scale and scanning speed (100 mm/s) were adjusted to obtain the first-color M-mode aliasing on the apical four-chamber view. Early and late diastolic filling waves on the M-mode map, including flow propagation velocity during early diastole (Vpe) and flow propagation velocity during late diastole (Vpa), were then recorded.

Global Longitudinal Systolic Strain (GLS)

EchoPac (GE Healthcare) analysis software was applied to calculate GLS offline. The movement trajectory of each point in the cardiac tissue during the cardiac cycle was automatically tracked by two-dimensional speckle tracing in apical long-axis, two-chamber, and four-chamber standard view, respectively. The myocardial deformation of each ventricular wall segment in the region of interest was recorded.

IVP measurement

The tissue Doppler frame rate was adjusted to 350–450 frames/s. To minimize the bias caused by the Doppler Angle, the imaging field of view was adjusted carefully to align each left ventricular wall with the incident ultrasound beam. The ultrasound images of each LV wall were stored in apical long-axis, two-chamber,

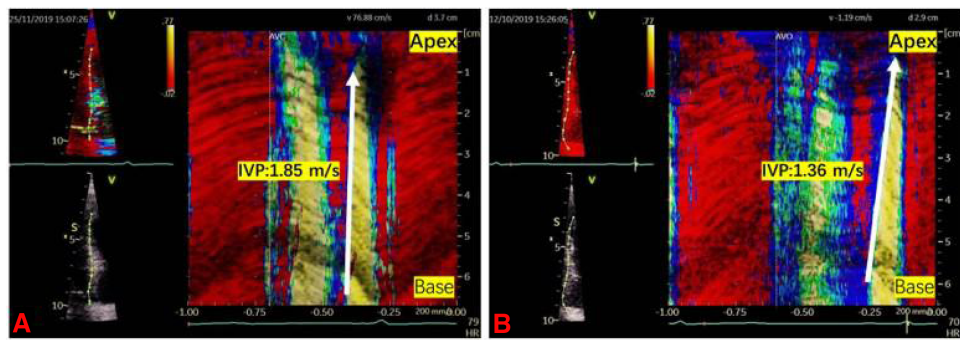


FIGURE 1
Two examples illustrating the intrinsic wave velocity propagation. IVP was the slope of isovelocity wavefront propagating in time and space during late diastole (the white arrow). (A) IVP in a DM-H group patient was 1.85 m/s. (B) IVP in a control group participant was 1.36 m/s.

and four-chamber standard views, respectively. Data were recorded and analyzed using the EchoPac workstation (GE Healthcare). Q analysis was first entered, then the left ventricular myocardium was traced using the curved anatomy M type (CMM) to reconstruct the axial tissue velocity map. The ratio of the tissue velocity map was adjusted to create velocity aliasing; the scanning speed was adjusted to the maximum. The velocity aliasing was used to identify the onset of motion. The wave speed, IVP, was the slope of isovelocity wavefront propagating in time and space during late diastole (Figure 1). The mean IVP measurement was obtained by averaging the wave velocity of six LV walls using the apical four-chamber, two-chamber, and long-axis views.

Reproducibility analysis

Bland-Altman analysis was applied to test Intra- and inter-observer variability of IVP in 20 randomly selected data sets. Two observers were blind to both results made by each other and the medical history and examination data of each subject.

Statistical analyses

All statistical parameters were performed using IBM SPSS (Version 24.0. Armonk, NY: IBM Corp). Continuous data were expressed as mean ± SD; categorical data were expressed as percentages. The normality of data was tested using the Shapiro-Wilk test. Between-group comparison of the mean was made by student's t-test; Among-groups comparisons of normally distributed continuous variables was achieved by One-way ANOVA; comparisons of skewedly distributed variables was done by Kruskal Wallis test. When significant at the 0.05 level, pairwise comparisons were performed, and *Post hoc* analysis was achieved through the Bonferroni test. The correlation between IVP and echocardiographic parameters was tested by Pearson correlation analysis. Bland-Altman analysis was used on 20 randomly selected data sets to analyze inter and intra-observer

variability and consistency. *P* < 0.05 was considered statistically significant.

Results

Primary findings

As was shown in Table 1, patients of the DM + H group were significantly older than those of the DM-H group. There was no difference in T2DM disease duration between DM + H and DM-H groups. However, a significant difference regarding diabetic retinopathy and diabetic nephropathy was observed between the two groups.

Overall, the IVP of the DM group was higher than that of the control group (1.62 ± 0.25 m/s and 1.40 ± 0.19 m/s, *P* < 0.001). Such phenomenon was also observed in IVSd (9.85 ± 1.14 mm

TABLE 1 Comparisons of baseline clinical characteristics between the T2DM group and control group.

Variable	Diabetes mellitus (<i>n</i> = 87)		Controls (<i>n</i> = 53)
	DM + H (<i>n</i> = 43)	DM-H (<i>n</i> = 44)	
Age (y)	56 ± 1 ^b	50 ± 12	54 ± 11
Male (%)	67	61	53
Duration of T2DM (y)	8 ± 7 ^a	8 ± 7 ^a	—
Blood glucose (mmol/l)	12.57 ± 4.80 ^a	14.73 ± 6.08 ^a	5.18 ± 0.45
HbA1c (mmol/l)	9.25 ± 1.93 ^a	11.48 ± 11.94 ^a	5.32 ± 0.43
Systolic blood pressure (mmHg)	149 ± 16 ^{a,b}	114 ± 11 ^a	121 ± 12
Diastolic blood pressure (mmHg)	94 ± 14 ^{a,b}	77 ± 9	75 ± 9
Diabetic complications			
Diabetic retinopathy (%)	44 ^b	34	—
Diabetic nephropathy (%)	44 ^b	7	—
Diabetic foot (%)	7	7	—

^aSignificant between DM + H or DM-H group and control group.
^bSignificant between DM + H and DM-H group.

and 9.23 ± 0.91 mm, $P = 0.001$), Mitral A velocity (84 ± 19 cm/s and 72 ± 21 cm/s, $P = 0.001$), E/A ratio (0.97 ± 0.34 and 1.11 ± 0.35 , $P = 0.016$), Mitral annular septal e' velocity (8.45 ± 2.66 cm/s and 9.53 ± 2.28 , $P = 0.015$), E/e' ratio (9.68 ± 2.90 and 8.21 ± 2.23 , $P = 0.002$), Vpe (54.14 ± 11.20 cm/s and 63.45 ± 10.12 cm/s, $P < 0.001$) and GLS(%) (-17.61 ± 2.20 and -18.60 ± 2.47 , $P = 0.015$). After stratification for hypertension (Table 2), The IVP of DM + H group was higher than that of DM-H group and control group (1.71 ± 0.25 m/s, 1.53 ± 0.20 m/s and 1.40 ± 0.19 m/s, $P < 0.001$). Compared with the control group, IVSd (10.21 ± 0.91 mm and 9.23 ± 0.91 mm, $P < 0.001$), Mitral A velocity (90 ± 17 cm/s and 72 ± 21 cm/s, $P < 0.001$), E/e' ratio (10.01 ± 2.92 and 8.21 ± 2.23 , $P = 0.004$), Vpa (75.67 ± 17.79 cm/s and 66.94 ± 14.43 cm/s, $P = 0.027$), and GLS(%) (-17.28 ± 2.32 and -18.60 ± 2.47 , $P = 0.018$) were significantly higher, while E/A ratio (0.83 ± 0.23 and 1.11 ± 0.35 , $P < 0.001$), mitral annular septal e' velocity (7.60 ± 1.90 cm/s and 9.53 ± 2.28 cm/s, $P = 0.001$), and Vpe (51.77 ± 11.94 cm/s and 63.45 ± 10.12 cm/s, $P < 0.001$) were significantly lower in DM + H group patients. Only Vpe in the DM-H group was significantly lower than in the control group (56.45 ± 10.02 cm/s and 63.45 ± 10.12 cm/s, $P = 0.005$). The differences in IVSd, LVIDd, Mitral E velocity, E/A ratio, E/e' ratio, Vpa, and GLS were observed between the DM-H group and control group. However, they did not reach statistically significant.

The results of correlation analyses were as follows (Figure 2): Pve ($r = -0.580$, $P < 0.001$), Pva ($r = 0.271$, $P < 0.001$), IVSd ($r = 0.321$, $P < 0.001$), LVIDd ($r = 0.170$, $P = 0.045$), systolic blood pressure ($r = 0.370$, $P < 0.001$), diastolic blood pressure ($r = 0.389$, $P < 0.001$), and GLS ($r = 0.330$, $P < 0.001$). No significant correlation was found between IVP and HbA1c, blood glucose, LVPWd, LVEF, Mitral E velocity, Mitral A velocity, E/A ratio, e' velocity, and E/e' ratio.

Reproducibility and repeatability

The results of the Bland-Altman analysis are illustrated in Figure 3. The intra- and inter-observer reproducibility of IVP was acceptable, with mean signed difference = 0.0165 ± 0.082 m/s and -0.0465 ± 0.1812 m/s, respectively. The intraclass correlation coefficients measured of IVP were 0.924 [95% confidence interval (CI): 0.818–0.969] and 0.941 (95% CI: 0.858–0.976), respectively.

Discussion

In this work, IVP, the wave propagation of longitudinal myocardial stretch during late diastole, was proposed to evaluate MS in T2DM patients. The main findings from the investigation are as follows: (1) The IVP of the DM + H group was higher than that of the DM-H group and control group; (2) Mitral A velocity, E/e' ratio, and Vpa were higher in the T2DM patients, while E/A ratio, Mitral annular septal e' velocity, and Vpe were higher in the control group; (3) The association between IVP and part of the above-mentioned conventional ultrasound parameters showcased weak to moderate correlation.

Myocardial relaxation is critical to the diastolic function that allows adequate filling of the ventricles prior to the next cardiac cycle. The early stages of diabetic cardiomyopathy have subtle changes in cardiac function, one of which is left ventricular (LV) diastolic dysfunction that includes impaired early diastolic filling, increased atrial filling, prolonged isovolumic relaxation, and cardiomyocyte disarray and interstitial myocardial fibrosis through histologic examination, the embodiment of altered myocardial stiffness (4, 7).

The generation of IVP is considered at the beginning of ventricular filling after atrial contraction when the base of the LV

TABLE 2 Comparisons of echocardiographic parameters between DM + H group, DM-H group and control group.

Variable	Controls	Diabetes mellitus		DM-H		DM + H		P
	(n = 53)	(n = 87)	P vs. Controls	(n = 44)	P vs. Controls	(n = 43)	P vs. Controls	DM + H vs. DM-H
IVP (m/s)	1.40 ± 0.19	1.62 ± 0.25	<0.001	1.53 ± 0.20	0.013*	1.71 ± 0.25	<0.001*	<0.001*
IVSd (mm)	9.23 ± 0.91	9.85 ± 1.14	0.001	9.50 ± 1.23	0.576	10.21 ± 0.91	<0.001*	0.005*
LVPWd (mm)	9.09 ± 0.88	9.30 ± 1.06	0.240	9.05 ± 1.12	1.000	9.56 ± 0.93	0.067	0.047*
LVIDd (mm)	45.57 ± 3.55	45.10 ± 4.40	0.496	44.86 ± 4.35	1.000	45.35 ± 4.48	1.000	1.000
LVEF (%)	65.17 ± 3.98	65.98 ± 3.65	0.476	65.98 ± 3.50	0.895	65.98 ± 3.85	0.905	1.000
Mitral E velocity (cm/s)	76 ± 20	77 ± 19	0.222	82 ± 21	0.443	73 ± 17	1.000	0.105
Mitral A velocity (cm/s)	72 ± 21	84 ± 19	0.001	78 ± 19	0.397	90 ± 17	<0.001*	0.017*
E / A ratio	1.11 ± 0.35	0.97 ± 0.34	0.016	1.09 ± 0.37	1.000	0.83 ± 0.23	<0.001*	0.001*
Mitral annular septal e' velocity (cm/s)	9.53 ± 2.28	8.45 ± 2.66	0.015	9.27 ± 3.03	1.000	7.60 ± 1.90	0.001*	0.005*
E / e' ratio	8.21 ± 2.23	9.68 ± 2.90	0.002	9.37 ± 2.87	0.106	10.01 ± 2.92	0.004*	0.793
Vpe (cm/s)	63.45 ± 10.12	54.14 ± 11.20	<0.001	56.45 ± 10.02	0.005*	51.77 ± 11.94	<0.001*	0.128
Vpa (cm/s)	66.94 ± 14.43	70.76 ± 17.51	0.185	65.95 ± 16.01	1.000	75.67 ± 17.79	0.027*	0.016*
GLS (%)	-18.60 ± 2.47	-17.61 ± 2.20	0.015	-17.94 ± 2.04	0.477	-17.28 ± 2.32	0.018*	0.555

GLS, global longitudinal systolic strain; IVP, intrinsic wave velocity propagation of myocardial stretch; IVSd, interventricular septal thickness at end-diastole; LVEF, left ventricular ejection fraction; LVIDd, left ventricular internal diameter at end-diastole; LVPWd, left ventricular posterior wall thickness at end-diastole; Vpa, color M-mode flow propagation velocity during late diastole; Vpe, color M-mode flow propagation velocity during early diastole.

Data are expressed as mean \pm SD (median) or as number (percentage).

* $P < 0.05$.

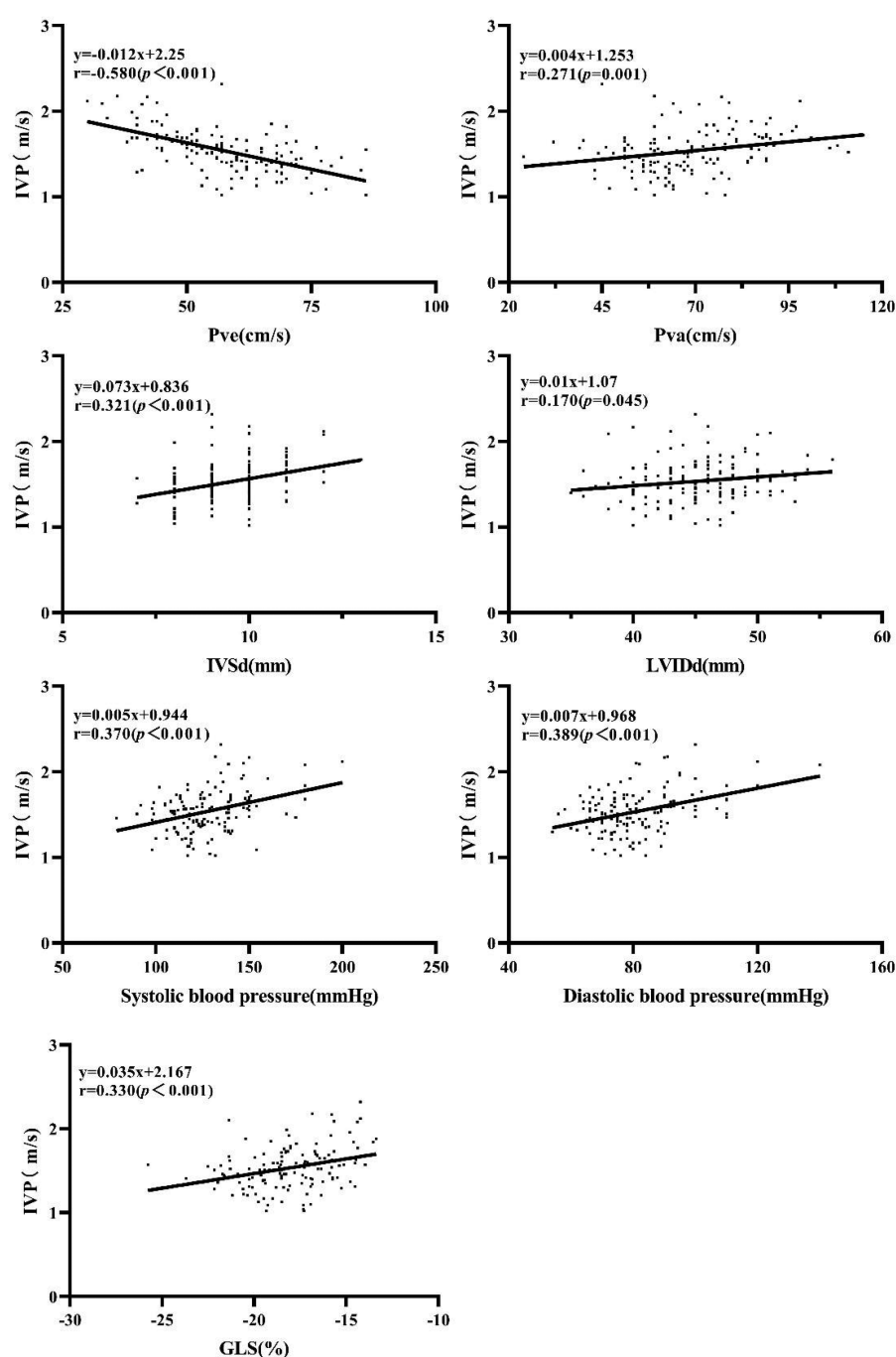


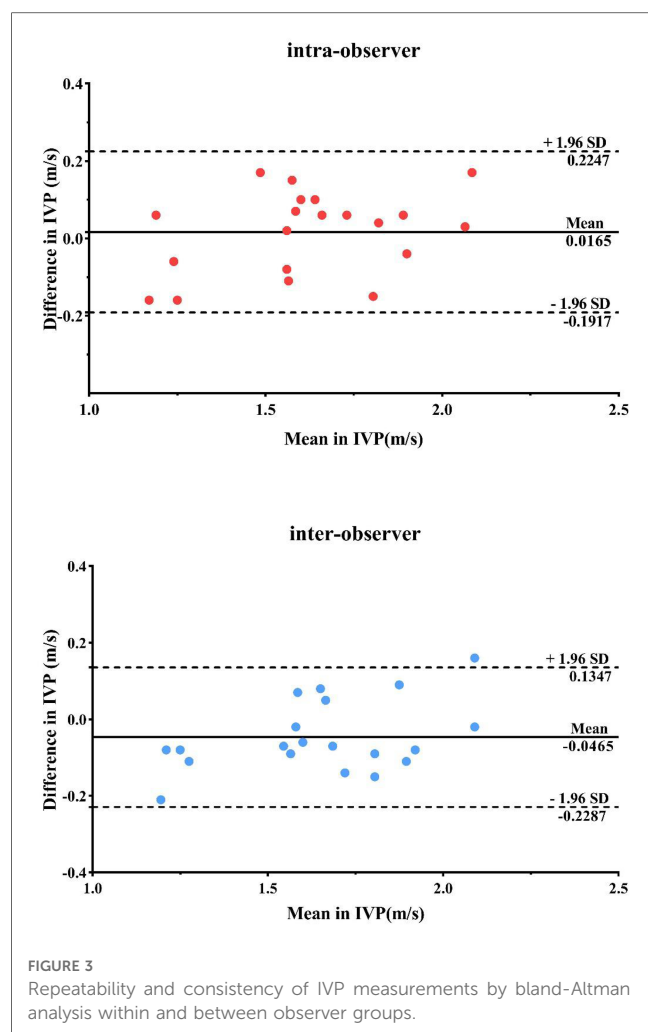
FIGURE 2

Correlation of IVP with Pve Pva, IVSd, LVIDd, systolic blood pressure, diastolic blood pressure, and GLS.

is stretched, and a pulse-like wave is generated that propagates to the apex along the longitudinal wall motion during late diastole (21, 22). Previous studies in Pislariu et al. series (16, 18, 23) have confirmed that the speed of IVP was strongly influenced by passive tissue properties. The higher the ventricular wall tension, the faster the wave speed. IVP was significantly higher in patients with myocardial amyloidosis characterized by myocardial stiffness than in healthy controls (19). An increase in IVP is associated with incremental diastolic dysfunction, which implies

the possibility of a correlation between IVP and myocardial stiffness.

More than two-thirds of T2DM patients are complicated by hypertension (24). Hypertension increases the risk of microvascular and macrovascular complications in diabetic patients (Holman et al. 2008; Kengne et al. 2009). The coexistence of hypertension and diabetes exerts a synergistic adverse effect on impaired subendocardial perfusion that aggravates myocardial oxygen consumption, with resultant



abnormal collagen synthesis, altered tissue elasticity, and elevated myocardial stiffness (25, 26). After stratification for hypertension, the statistical difference of several morphologic and hemodynamic indicators between DM + H, DM-H, and the control group was likely associated with the combined effects of elevated filling pressures, wall stress, and LV afterload, which indicate increased diastolic dysfunction and myocardial stiffness in the case group. Despite the values of IVP being similar between controls and cases and the moderate correlation with indicators, the increasing trend should not be overlooked; besides, cardiac function cannot be embodied by a single parameter. In this study, the IVP value tends to be higher as myocardial condition deteriorates. IVP exhibited a positive association with systolic blood pressure, diastolic blood pressure, IVSd, and LVIDd. It is in line with our previous results (20), which disclosed that IVP was higher in hypertensive patients than in controls and was closely related to LVIDd and LVPWd.

The blood flow from the LA to the LV through the mitral valve can be embodied as the wave; the speed produced under the pressure gradient in the ventricle is referred to as the flow propagation velocity (FPV). FPV is a recognized indicator of changes in myocardial mechanical properties. Reduced flow propagation during early diastole is commonly seen in patients

with impaired LV relaxation (27, 28). When LA filling is impaired, the isovolumic relaxation time is prolonged, accompanied by decreased Vpe. As it develops, the atrial contractions increased compensatively to overcome the early diastolic filling impairment caused by myocardial stiffness; simultaneously, Vpa increases. In the current study, there was a negative correlation between IVP and Vpe and a positive correlation between Vpa, which theoretically supported the potential utility of this new measurement in predicting myocardial stiffness. Nevertheless, flow propagation measurements are also angle-dependent, the volume of blood in early flow propagation (Vpe) influences late flow propagation, and the Vpa slope is uncertain (29), which may partly explain the insignificant association between the DM-H group and the control group in our study. Future research with a larger sample size and a broader spectrum of the population is warranted to address this issue.

E/e' ratio is one of the well-recognized parameters in evaluating LV filling pressure diastolic function (30). In this study, the E/e' ratio was 9.68 ± 2.90 in the DM group, between 9 and 14, which indicated intermediate LV filling pressures; also, there was an insignificant correlation between IVP and E/e' ratio. Diastolic function is a complex process and cannot be evaluated by a single parameter. Despite the negative results, diastolic dysfunction cannot be ruled out due to its low sensitivity (or specificity). GLS is highly sensitive and specific in detecting LV dysfunction (31, 32). Weakened myocardial elasticity and increased myocardial stiffness are associated with decreased GLS, which is consistent with the alteration tendency of IVP in myocardial dysfunction disclosed in this study. It might serve as a complementary method in analyzing myocardial dysfunction.

Here, this work explored the application prospect of IVP in assessing LV diastolic dysfunction in T2DM patients. The results implied that IVP might be potential to evaluate diastolic dysfunction and reflect the change in myocardial stiffness. Different from the generation of acoustic radiation force pulse in shear wave elastography, this novel ultrasound technique detects the wave velocity generated by myocardial stretch from the base to the apex level through high frame rate Doppler ultrasound imaging, which means the external stimulation is not required (33, 34). The convenience of IVP measurement makes it available for research. This novel index might be a potentially highly sensitive and harmless indicator in evaluating early cardiac function variations in some cardiovascular conditions, such as T2DM patients. With technological advancement, such as higher frame rates and velocity range, more accurate measurements are available, which may be helpful in clinical applications.

Study limitations

Several limitations deserve to be addressed: The data quality of IVP is affected by time resolution and low frame frequency. The application of this technique is currently unsuitable for patients with arrhythmias or tachycardia. Limited by experimental

conditions, in this pilot study, the association of IVP with myocardial stiffness was relatively subjective, for there is currently no direct reference standard. Limited by the small sample size, one possibility is that the group variability may be due to inter/intra-observer variability. However, the trend of IVP value changes could not be ignored and was worthy of further exploration. Myocardial stiffness also can be acutely modulated by proteins such as titin, including post-translational modifications (PTMs, such as acetylation, oxidation, and phosphorylation) and isoform switch (35). The atrial contraction in end-diastole leads to a rapid increase in LV strain, which might result in a rapid increase in momentary stiffness in T2DM. More clinical studies with larger sample sizes and combined indicators are warranted further investigation to prove the clinical value of IVP.

Conclusions

The study showed that IVP was higher in T2DM patients when compared to the control group. This novel index might be a promising echocardiographic parameter in assessing early change in cardiac function and structure, implying the possibility of evaluating myocardial stiffness directly and noninvasively. Further clinical studies with larger sample sizes are warranted to explore the clinically relevant.

Data availability statement

The raw data supporting the conclusions of this article will be made available by the authors, without undue reservation.

Ethics statement

The studies involving human participants were reviewed and approved by Medical Ethics Committee of Tongji Hospital,

Tongji Medical College, Huazhong University of Science and Technology. The patients/participants provided their written informed consent to participate in this study.

Author contributions

All authors contributed to the study's conception and design. Material preparation, data collection, and analysis were performed by XH, XF, JS, JZ, QT, and YD. The first draft of the manuscript was written by QC and XB, and all authors commented on previous versions of the manuscript. XB contributed to supervision and is the guarantor of this work. All authors contributed to the article and approved the submitted version.

Acknowledgments

The authors thank all participants and all investigators in Tongji Hospital.

Conflict of interest

The authors declare that the research was conducted in the absence of any commercial or financial relationships that could be construed as a potential conflict of interest.

Publisher's note

All claims expressed in this article are solely those of the authors and do not necessarily represent those of their affiliated organizations, or those of the publisher, the editors and the reviewers. Any product that may be evaluated in this article, or claim that may be made by its manufacturer, is not guaranteed or endorsed by the publisher.

References

- Guariguata L, Whiting DR, Hambleton I, Beagley J, Linnenkamp U, Shaw JE. Global estimates of diabetes prevalence for 2013 and projections for 2035. *Diabetes Res Clin Pract.* (2014) 103:137–49. doi: 10.1016/j.diabres.2013.11.002
- Park JJ. Epidemiology, pathophysiology, diagnosis and treatment of heart failure in diabetes. *Diabetes Metab J.* (2021) 45:146–57. doi: 10.4093/dmj.2020.0282
- Stewart Coats AJ. Common co-morbidities in heart failure—diabetes, functional mitral regurgitation and sleep apnoea. *Int J Heart Fail.* (2019) 1:25–41. doi: 10.36628/ijhf.2019.0004
- Adeghate E, Singh J. Structural changes in the myocardium during diabetes-induced cardiomyopathy. *Heart Fail Rev.* (2014) 19:15–23. doi: 10.1007/s10741-013-9388-5
- Sorrentino R, Esposito R, Santoro C, Vaccaro A, Cocozza S, Scalapogna M, et al. Practical impact of new diastolic recommendations on noninvasive estimation of left ventricular diastolic function and filling pressures. *J Am Soc Echocardiogr.* (2020) 33(2):171–81. doi: 10.1016/j.echo.2019.08.013
- Farjo PD, Barghouthi N, Chima N, Desai A, Fang W, Giordano J, et al. Use of the burden of diabetes Mellitus score for cardiovascular disease risk assessment. *Am J Cardiol.* (2020) 125(12):1829–35. doi: 10.1016/j.amjcard.2020.03.027
- Jia G, Hill MA, Sowers JR. Diabetic cardiomyopathy: an update of mechanisms contributing to this clinical entity. *Circ Res.* (2018) 122:624–38. doi: 10.1161/CIRCRESAHA.117.311586
- Sorop O, Heinonen I, van Kranenburg M, van de Wouw J, de Beer VJ, Nguyen I, et al. Multiple common comorbidities produce left ventricular diastolic dysfunction associated with coronary microvascular dysfunction, oxidative stress, and myocardial stiffening. *Cardiovasc Res.* (2018) 114(7):954–64. doi: 10.1093/cvr/cvy038
- Bermejo J, Yotti R, Pérez del Villar C, del Álamo JC, Rodríguez-Pérez D, Martínez-Legazpi P, et al. Diastolic chamber properties of the left ventricle assessed by global fitting of pressure-volume data: improving the gold standard of diastolic function. *J Appl Physiol.* (2013) 115(4):556–68. doi: 10.1152/jappphysiol.00363.2013
- Kwong RY, Farzaneh-Far A. Value of late gadolinium enhancement imaging in diagnosis of myocardial infarction and unobstructed coronary arteries. *JACC Cardiovasc Imaging.* (2020) 13:1149–51. doi: 10.1016/j.jcmg.2019.12.016
- Song P, Bi X, Mellema DC, Manduca A, Urban MW, Greenleaf JF, et al. Quantitative assessment of left ventricular diastolic stiffness using cardiac shear wave elastography: a pilot study. *J Ultrasound Med.* (2016) 35:1419–27. doi: 10.7863/ultra.15.08053

12. Song P, Bi X, Mellema DC, Manduca A, Urban MW, Pellikka PA, et al. Pediatric cardiac shear wave elastography for quantitative assessment of myocardial stiffness: a pilot study in healthy controls. *Ultrasound Med Biol.* (2016) 42:1719–29. doi: 10.1016/j.ultrasmedbio.2016.03.009
13. Petrescu A, Santos P, Orlowska M, Pedrosa J, Bézy S, Chakraborty B, et al. Velocities of naturally occurring myocardial shear waves increase with age and in cardiac amyloidosis. *JACC Cardiovasc Imaging.* (2019) 12:2389–98. doi: 10.1016/j.jcmg.2018.11.029
14. Strachinaru M, Bosch JG, van Gils L, van Dalen BM, Schinkel A, van der Steen A, et al. Naturally occurring shear waves in healthy volunteers and hypertrophic cardiomyopathy patients. *Ultrasound Med Biol.* (2019) 45:1977–86. doi: 10.1016/j.ultrasmedbio.2019.04.004
15. Strachinaru M, Bosch JG, Schinkel A, Michels M, Feyz L, de Jong N, et al. Local myocardial stiffness variations identified by high frame rate shear wave echocardiography. *Cardiovasc Ultrasound.* (2020) 18:40. doi: 10.1186/s12947-020-00222-1
16. Pislaru C, Pellikka PA, Pislaru SV. Wave propagation of myocardial stretch: correlation with myocardial stiffness. *Basic Res Cardiol.* (2014) 109(6):438. doi: 10.1007/s00395-014-0438-5
17. Voigt JU, Lindenmeier G, Werner D, Flachskampf FA, Nixdorff U, Hatle L, et al. Strain rate imaging for the assessment of preload-dependent changes in regional left ventricular diastolic longitudinal function. *J Am Soc Echocardiogr.* (2002) 15(1):13–9. doi: 10.1067/mje.2002.116536
18. Pislaru C, Alashry MM, Thaden JJ, Pellikka PA, Enriquez-Sarano M, Pislaru SV. Intrinsic wave propagation of myocardial stretch, a new tool to evaluate myocardial stiffness: a pilot study in patients with aortic stenosis and mitral regurgitation. *J Am Soc Echocardiogr.* (2017) 30(11):1070–80. doi: 10.1016/j.echo.2017.06.023
19. Pislaru C, Alashry MM, Ionescu F, Petrescu I, Pellikka PA, Grogan M, et al. Increased myocardial stiffness detected by intrinsic cardiac elastography in patients with amyloidosis: impact on outcomes. *JACC Cardiovasc Imaging.* (2019) 12:375–7. doi: 10.1016/j.jcmg.2018.08.014
20. Zhang J, Deng Y, Tang Q, Sun J, Huang L, Song P, et al. Evaluation of myocardial stiffness in hypertensive patients by intrinsic wave propagation of the myocardial stretch. *Ultrasound Med Biol.* (2020) 46(10):2683–91. doi: 10.1016/j.ultrasmedbio.2020.06.016
21. Laurent S, Cockcroft J, Van Bortel L, Boutouyrie P, Giannattasio C, Hayoz D, et al. Expert consensus document on arterial stiffness: methodological issues and clinical applications. *Eur Heart J.* (2006) 27(21):2588–605. doi: 10.1093/eurheartj/ehl254
22. Mitchell GF, Hwang SJ, Vasan RS, Larson MG, Pencina MJ, Hamburg NM, et al. Arterial stiffness and cardiovascular events: the framingham heart study. *Circulation.* (2010) 121(4):505–11. doi: 10.1161/CIRCULATIONAHA.109.886655
23. De Jesus T, Alashry MM, Padang R, Pislaru SV, Nkomo VT, Pellikka PA, et al. Intrinsic cardiac elastography in patients with primary mitral regurgitation: predictive role after mitral valve repair. *Eur Heart J Cardiovasc Imaging.* (2021) 22:912–21. doi: 10.1093/ehjci/jeaa117
24. Ferrannini E, Cushman WC. Diabetes and hypertension: the bad companions. *Lancet.* (2012) 380:601–10. doi: 10.1016/S0140-6736(12)60987-8
25. Jiang L, Ren Y, Yu H, Guo YK, Liu X, Deng MY, et al. Additive effect of hypertension on left ventricular structure and function in patients with asymptomatic type 2 diabetes mellitus. *J Hypertens.* (2021) 39:538–47. doi: 10.1097/HJH.0000000000002643
26. Smulyan H, Lieber A, Safar ME. Hypertension, diabetes type II, and their association: role of arterial stiffness. *Am J Hypertens.* (2016) 29:5–13. doi: 10.1093/ajh/hpv107
27. Stewart KC, Kumar R, Charonko JJ, Ohara T, Vlachos PP, Little WC. Evaluation of LV diastolic function from color M-mode echocardiography. *JACC Cardiovasc Imaging.* (2011) 4(1):37–46. doi: 10.1016/j.jcmg.2010.09.020
28. Sugimoto K, Kawase N, Aoki T. Assessment of diastolic function using mitral flow propagation velocity in cats. *Can J Vet Res.* (2020) 84(2):124–30.
29. Vanhercke D, Claessens T, Pardaens S, Van Ransbeeck P, Vandekerckhove H, Verdonck P, et al. Assessment of variables affecting late left ventricular flow propagation velocity. *Acta Cardiol.* (2012) 67(4):391–7. doi: 10.1080/AC.67.4.2170679
30. Nagueh SF, Smiseth OA, Appleton CP, Byrd BF 3rd, Dokainish H, Edvardsen T, et al. Recommendations for the evaluation of left ventricular diastolic function by echocardiography: an update from the American society of echocardiography and the European association of cardiovascular imaging. *J Am Soc Echocardiogr.* (2016) 29(4):277–314. doi: 10.1016/j.echo.2016.01.011
31. Kalam K, Otahal P, Marwick TH. Prognostic implications of global LV dysfunction: a systematic review and meta-analysis of global longitudinal strain and ejection fraction. *Heart.* (2014) 100(21):1673–80. doi: 10.1136/heartjnl-2014-305538
32. Lang RM, Badano LP, Mor-Avi V, Afilalo J, Armstrong A, Ernande L, et al. Recommendations for cardiac chamber quantification by echocardiography in adults: an update from the American society of echocardiography and the European association of cardiovascular imaging. *J Am Soc Echocardiogr.* (2015) 28:1–39. e14. doi: 10.1016/j.echo.2014.10.003
33. Bamber J, Cosgrove D, Dietrich CF, Fromageau J, Bojunga J, Calliada F, et al. EFSUMB Guidelines and recommendations on the clinical use of ultrasound elastography. Part 1: basic principles and technology. *Ultraschall Med.* (2013) 34:169–84. doi: 10.1055/s-0033-1335205
34. Cosgrove D, Piscaglia F, Bamber J, Bojunga J, Correia JM, Gilja OH, et al. EFSUMB Guidelines and recommendations on the clinical use of ultrasound elastography. Part 2: clinical applications. *Ultraschall Med.* (2013) 34:238–53. doi: 10.1055/s-0033-1335375
35. Loescher CM, Hobbach AJ, Linke WA. Titin (TTN): from molecule to modifications, mechanics, and medical significance. *Cardiovasc Res.* (2022) 118:2903–18. doi: 10.1093/cvr/cvab328



OPEN ACCESS

EDITED BY

Sanjeev Bhattacharyya,
Barts Heart Centre, United Kingdom

REVIEWED BY

Pavel Zhabeyev,
University of Alberta, Canada
Guido Carlomagno,
Clinica Mediterranea, Italy

*CORRESPONDENCE

Ludmiła Daniłowicz-Szymanowicz
✉ ludwik@gumed.edu.pl

RECEIVED 09 April 2023

ACCEPTED 26 June 2023

PUBLISHED 11 July 2023

CITATION

Świątczak M, Rozwadowska K, Sikorska K,
Młodziński K, Świątczak A, Raczak G and
Daniłowicz-Szymanowicz L (2023) The
potential impact of hereditary
hemochromatosis on the heart considering the
disease stage and patient age—the role of
echocardiography.
Front. Cardiovasc. Med. 10:1202961.
doi: 10.3389/fcvm.2023.1202961

COPYRIGHT

© 2023 Świątczak, Rozwadowska, Sikorska,
Młodziński, Świątczak, Raczak and Daniłowicz-
Szymanowicz. This is an open-access article
distributed under the terms of the [Creative
Commons Attribution License \(CC BY\)](#). The use,
distribution or reproduction in other forums is
permitted, provided the original author(s) and
the copyright owner(s) are credited and that the
original publication in this journal is cited, in
accordance with accepted academic practice.
No use, distribution or reproduction is
permitted which does not comply with these
terms.

The potential impact of hereditary hemochromatosis on the heart considering the disease stage and patient age—the role of echocardiography

Michał Świątczak¹, Katarzyna Rozwadowska¹, Katarzyna Sikorska²,
Krzysztof Młodziński¹, Agata Świątczak³, Grzegorz Raczak¹
and Ludmiła Daniłowicz-Szymanowicz^{1*}

¹Department of Cardiology and Electrotherapy, Faculty of Medicine, Medical University of Gdańsk, Gdańsk, Poland, ²Department of Tropical Medicine and Epidemiology, Faculty of Health Sciences, Medical University of Gdańsk, Gdańsk, Poland, ³Department of Pediatrics, Hematology and Oncology, Faculty of Medicine, Medical University of Gdańsk, Gdańsk, Poland

Background: Hereditary hemochromatosis (HH) is a genetic disease that leads to increased iron accumulation in several organs. Cardiomyocytes are highly susceptible to this damage owing to their high iron uptake, and cardiovascular complications account for 1/3 of the deaths in the natural course of HH. Additionally, excess iron intake and associated oxidative stress may accelerate the aging of the cardiovascular system, regardless of the age of patients with HH. We aimed to investigate the role of standard and speckle-tracking echocardiography (STE) in revealing heart differences in patients with HH considering the disease stage and the patient age.

Methodology: Consecutive patients with HH ($n = 58$) without heart pathologies (except hypertension) and 29 age- and sex-matched healthy individuals underwent echocardiography. Patients were compared according to the time since HH diagnosis (the recently diagnosed HH group [31 patients] with diagnosed HH for less than 6 months and had no more than one venesection; the medium group [11 patients] with diagnosed HH between 6 and 24 months; and the long-lasting group [16 patients] with diagnosed HH for more than 2 years) and the quartile contribution of their age.

Results: Standard echocardiography revealed differences in diastolic parameters between patients with HH and controls, which were the most prominent between healthy and long-lasting HH patients. Regarding systolic function, left ventricular ejection fraction was lower in HH patients, with the most evident differences between the healthy and recently diagnosed HH patients. STE revealed additional differences in systolic parameters, with LV rotation the worst in recently diagnosed patients and its increase in patients with medium and long-lasting HH. Significantly worse peak systolic longitudinal strain values were observed in all patients with HH. Analyses of the results according to the age quartiles of patients with HH revealed that some changes occurred earlier than expected according to age.

Conclusions: Echocardiography can reveal possible heart damage in HH patients at different stages of the disease and highlight potential features of accelerated myocardial aging in these patients.

KEYWORDS

hereditary hemochromatosis, speckle-tracking echocardiography, echocardiography, cardiovascular ageing, iron overload (IO)

1. Introduction

Hereditary hemochromatosis (HH) has a genetic etiology in 80% of cases based on HFE-gene mutations, which leads to increased accumulation of iron in bodily tissues resulting in damage to many organs, including the heart (1). Left ventricular (LV) cardiomyopathy was previously responsible for approximately 30% of the deaths among patients with HH (2). The introduction of genetic tests into routine clinical practice for patients with abnormal iron metabolism has enabled the early diagnosis of HH, before an irreversible injury to organs in many cases, decreasing the probability of death.

The mechanisms underlying HH-induced heart damage are not fully understood. Oxidative stress induced by bioactive iron ions, which destroys the tissues of the involved organs, may contribute to this damage (3). Mitochondria are highly sensitive to oxidative stress-related damage, and cardiomyocytes are characterized by a large number of mitochondria, causing the heart to be a particularly vulnerable organ (1). Additionally, iron overload and oxidative stress causes the impaired vascular endothelium vasodilatory function and has a pro-inflammatory effect, which may eventually lead to accelerated aging of the cardiovascular system, with possible effects on the heart, regardless of the actual patients age (4–6). This manifests as an increased ventricular mass attributed to the increased thickness of the myocardium, eventually leading to impaired LV diastolic function (7) and increased left atrial (LA) size (7, 8). These changes can be easily detected using echocardiography (7–9). However, these features are not typical of recently diagnosed patients with HH, who usually have normal parameters on standard echocardiography (10, 11).

However, speckle-tracking echocardiography (STE), a more accurate technique, may reveal changes that indicate deterioration in systolic parameters (such as rotation indices and peak global longitudinal strain) at the early stages of the disease, despite the absence of symptoms and changes in standard echocardiography, presumably due to hereditary character of the disease and heart damage initiated many years before the diagnosis (10, 11). Moreover, as HH leads to changes similar to cardiovascular aging, it remains unknown whether it accelerates cardiovascular aging. Therefore, we aimed to investigate the role of echocardiography in revealing heart differences, considering the disease stage and the patient age.

2. Materials and method

2.1. Study population

Consecutive patients at different stages of HH [diagnosed based on clinical characteristics, abnormal iron turnover parameters, and the presence of HFE gene mutations (9)] were prospectively enrolled in the study from October 2015 to November 2018. The exclusion criteria were age < 18 years, history of any cardiac diagnosis (apart from hypertension), features of heart damage,

and left ventricular ejection fraction (LVEF) < 50%. The control group comprised healthy age- and sex-matched volunteers. All participants underwent echocardiography, and detailed medical histories including duration of HH and administered treatments with laboratory parameters were obtained. The study protocol was approved by the Local Ethics Committee at the Medical University of Gdańsk (NBBN/452/2016), and written informed consent was obtained from all the participants.

The patients were divided into three groups according to the time of diagnosis and initiation of treatment to investigate the influence of HH duration on the heart. The “recently diagnosed” HH group consisted of patients diagnosed with HH for less than 6 months and had no more than one venesection. The “medium” group consisted of patients who had HH diagnosed between 6 and 24 months (2 years). Finally, the “long-lasting” group consisted of patients diagnosed with HH for more than 2 years. All the parameters in these groups were analyzed and compared according to the age distribution obtained during the statistical analyses to investigate the impact of age.

2.2. Echocardiography examination

All patients underwent echocardiography at the time of enrollment. Patients were examined in the left lateral decubitus position using a GE VIVID E95 ultrasound system (GE Ultrasound, Horten, Norway) equipped with a phased-array transducer (M5S). Standard echocardiographic parameters were obtained according to the guidelines of the American Society of Echocardiography (ASE) and the European Association of Cardiovascular Imaging (EACVI) recommendations (12, 13). Data acquisition was obtained from the parasternal long- and short-axis views and the three standard apical views. Three consecutive cardiac cycles were recorded during quiet respiration for each view. Grayscale recordings were optimized for LV evaluation at a rate of 50–80 frames/s, and only patients with these parameters were included in the subsequent analyses. All echocardiograms were digitally stored, and further offline analysis was performed using a commercial EchoPAC workstation (v204, GE Healthcare, Horten, Norway).

2.2.1. Two-dimensional speckle-tracking analysis (2D STE)

Three endocardial markers were placed in an end-diastolic frame in the apical four-, two- and three-chamber views to perform a two-dimensional (2D) longitudinal speckle-tracking analysis. The contour of the endocardium was automatically tracked using a software to cover the myocardial thickness of the entire LV wall. Adequate tracking can be verified in real-time and corrected by adjusting the region of interest or manually correcting the contour to ensure optimal tracking. The two-dimensional peak systolic longitudinal strain was analyzed from the apical views and calculated with respect to the strain magnitude at aortic valve closure. The LV apical and basal rotation was quantified by scanning the parasternal basal and apical short-axis planes at the end of the expiratory breath hold.

The basal plane was defined as showing the tips of the mitral leaflets, and the apical plane was defined as the level just above the end-systolic LV luminal obliteration. The LV endocardial and epicardial borders of the LV were manually traced. The tracking reliability was visually checked, confirmed, and readjusted when necessary. Counterclockwise rotations viewed from the LV apex were expressed as positive values and clockwise rotations were expressed as negative values. LV twist was defined as the highest net difference in degrees between the apical and basal rotations. LV torsion was defined as the LV twist indexed by the LV diastolic longitudinal length (the distance between the mitral annulus and the apex in end-diastole averaged from the four-, two- and three-chamber apical views). The peak systolic (peak rotation) velocity and early diastolic apical and basal rotation (untwisting) velocities were derived from the rotation rate curves. The untwisting velocity curve was the first negative peak in early diastole, beginning after the peak LV twist and reaching its highest value after mitral valve opening.

2.3. Statistics

Continuous data were presented as the medians (25th–75th percentiles), whereas categorical data were expressed as proportions. We performed the Shapiro-Wilk test to determine the normal distribution of our data. Most of the analyzed parameters did not have normal data distributions, even after logarithmic data transformation; therefore, we selected appropriate statistical analysis methods based on non-parametric tests. The significance of differences between the patients with HH and the control group was assessed using the Wilcoxon test (between patients with HH and controls and between groups of patients divided by disease duration and age distribution based on the obtained quartiles). Comparisons between all groups were performed using the Kruskal–Wallis test for continuous variables (with Dunn's post-hoc test for the multiple comparisons with Bonferroni adjustment to determine the significantly different pairs of groups and control for the overall error rate when conducting multiple comparisons) or by the chi-squared test or Fisher's test for categorical variables. Statistical significance was set at p -values <0.05 were considered significant. Statistical analyses were performed using R version 4.2.1. (R Core Team, Vienna, Austria).

3. Results

3.1. Comparisons between the whole HH group and healthy participants

Fifty-eight consecutive patients diagnosed with HH between 1 month to 20 years were enrolled in the study. Forty-one patients had the C282Y/C282Y mutation, 12 had the C282Y/H63D mutation, four had the H63D/H63D mutation, and one had the C282Y/WT mutation. The median patient age was 45 years (range: 31–57 years). **Table 1** shows the demographic

TABLE 1 The HH patients' characteristics at the time of the first contact.

	HH All <i>n</i> = 58
Age	47 (31–57)
Male sex	66%
Hypertension	38%
DM/IGGT	36%
Months from the time of diagnosis	24 (3–94)
Number of venesections	1 (0–22)
Iron [ug/dl]	205 (169–229)
Ferritin [ng/ml]	581 (274–1,037)
Haemoglobin [mg/dl]	15.1 (14.5–16.1)
TSAT [%]	81 (63–93)
Glucose [mg%]	96 (87–101)
ASPART [U/L]	28 (21–43)
ALAT [U/L]	40 (26–76)

Data are presented as the medians (25th–75th percentile); TSAT, transferrin saturation; DM, diabetes mellitus; IGGT, impaired gestational glucose tolerance; ALAT, alanine aminotransferase; ASPAT, aspartate aminotransferase.

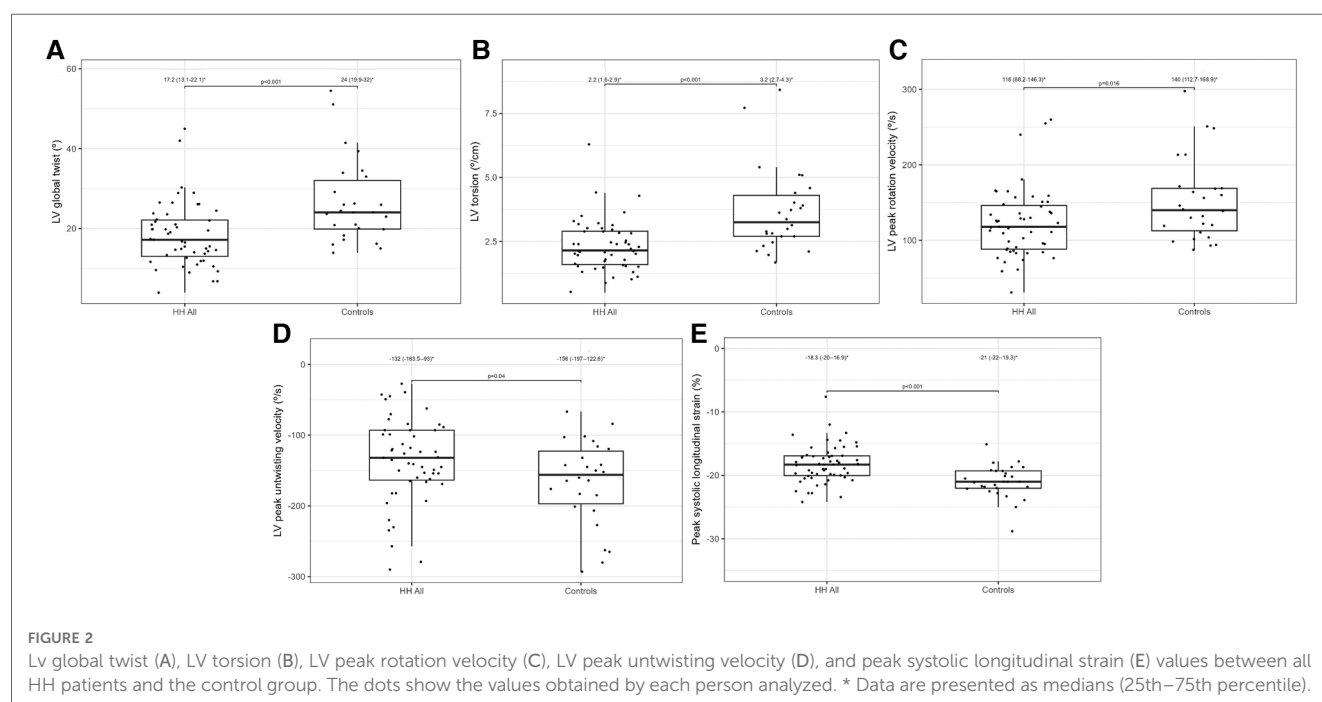
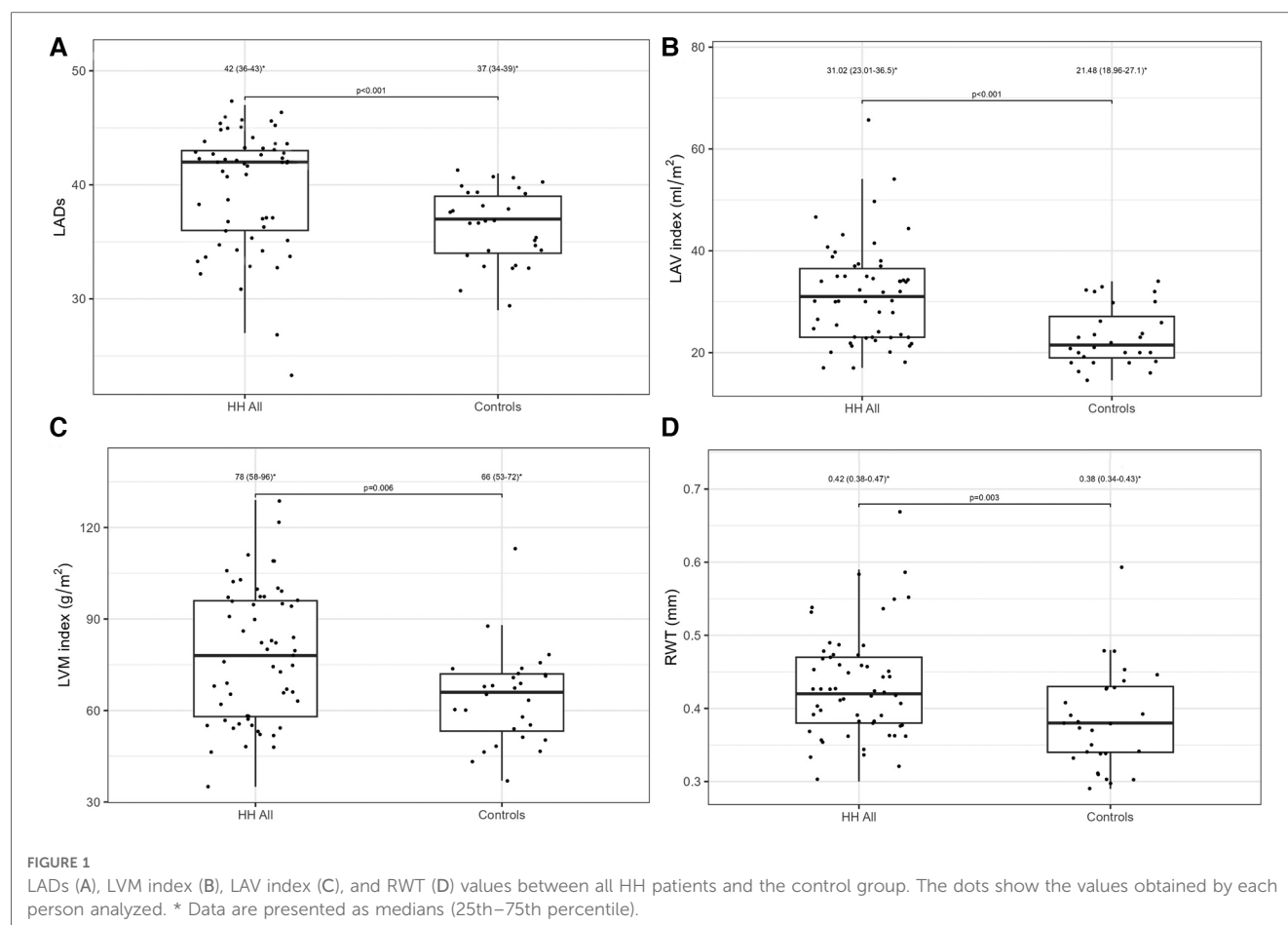
data, medical history, and laboratory results of all the patients with HH. Twenty-nine age- and sex-matched healthy volunteers comprised the control group.

Table 2 presents a comparison of the echocardiographic examination between patients with HH and healthy individuals. Some parameters related to diastolic function [LA size (LADs, LAV index), IVS, PW, RWT, and LVM index] were significantly worse in patients with HH than in healthy individuals (**Figure 1**). The LVEF was within the normal range; however, it was significantly lower in patients with HH. There were no

TABLE 2 Echocardiographic comparison between HH and healthy persons.

	HH All <i>n</i> = 58	Controls <i>n</i> = 29	<i>p</i>
IVS (mm)	10 (10–12)	9 (7–10)	<0.001
PW (mm)	9 (8–11)	8 (7–9)	0.007
Em (cm/s)	0.10 (0.09–0.13)	0.12 (0.09–0.14)	0.059
E/Em	7.0 (5.6–8.3)	6.7 (5.0–7.5)	0.071
LVEDD (mm)	46 (43–48)	44 (42–47)	0.052
LVESD (mm)	28 (25–30)	28 (26–30)	0.442
LVEF (%)	60 (54–62)	63 (61–65)	0.006
RVID (ms)	27 (24–29)	26 (22–29)	0.169
LV basal rotation (°)	−5.5 (−7.1–−2.8)	−7.1 (−8.4–−4.1)	0.063
LV basal rotation velocity (°/s)	−53.6 (−73.3–−22.9)	−51.5 (−60.3–−25.0)	0.406
LV basal untwisting velocity (°/s)	51.1 (31.5–77.9)	48.5 (40.0–62.3)	0.422
LV apical rotation (°)	11.5 (7.9–17.0)	16.9 (13.8–24.5)	0.011
LV apical rotation velocity (°/s)	82.0 (54.5–105.6)	100.0 (56.0–114.0)	0.095
LV apical untwisting velocity (°/s)	−90.0 (−118.0–−59.5)	−130.5 (−167.7–−107.5)	<0.001

Data are presented as medians (25th–75th percentile). IVS, intraventricular septum (mm); PW, posterior wall; E, early mitral velocity; Em, peak mitral annulus velocity; E/Em, early mitral inflow velocity to peak mitral annulus velocity ratio; LVEDD, left ventricle end-diastolic diameter; LVESD, left ventricle end-systolic diameter; LVEF, left ventricular ejection fraction; RVID, right ventricle internal diameter; LV, left ventricle.



significant differences in the LV and the right ventricle sizes. We found differences in many 2D STE parameters, including those related to diastolic function (LV untwisting rate and velocity),

and in many related to systolic function (LV apex rotation, global twist and torsion, and peak systolic longitudinal strain; **Figure 2**).

3.2. Comparisons between HH patients at the different stages of the disease

Table 3 shows the demographic data, medical histories, and laboratory results of patients with HH at the different stages of the disease. There was an increasing trend in the age and frequency of hypertension in the analyzed HH groups, and the rate of glucose disturbances increased noticeably in the long-lasting HH group. Iron levels were stable between the groups with reduced ferritin concentrations in medium and long-lasting HH patients. TSAT and transaminases levels were similar between groups.

Table 4 presents the comparisons of the standard and 2D STE echocardiographic parameters between HH patients in terms of

disease stage. Significant differences in LA size were observed between the controls and each HH group but not between the patients with HH from each group (**Figure 3**). Differences in LV wall thickness, RWT, and LVM index were the most prominent between healthy volunteers and patients with long-lasting HH (**Figure 3**). Differences in LVEF were the most evident between the healthy volunteers, the recently diagnosed group, and the medium HH group (**Table 4**). Regarding the 2D STE parameters, the medium group had significantly better rotation indices than the recently diagnosed patients, with no significant differences compared to the long-lasting HH group. Regarding peak systolic longitudinal strain, significantly worse values were noticed in all the HH groups compared to the controls, with no significant changes between the HH groups: -19.3% $[-20.5--17.3]$ in the recently diagnosed group, -17.5% $[-18.2--15.9]$ in the medium group, and -18.0% $[-19.6--15.6]$ in the long-lasting HH group, contrary to -21.0% $[-22.0--19.3]$ in the control group (**Figure 4**).

Figures 5, 6 present three HH patients from each group with graphical demonstration of twist and peak systolic longitudinal strains.

3.3. Comparisons between HH patients stratified by age

We divided patients with HH into four groups according to age quartiles based on age distribution to investigate the influence of the age on heart changes: the quartile from minimum to Q25 included patients from 18 to 31 years; Q25–Q50 included patients from 32 to 47 years; Q50–Q75 included patients from 48 to 56 years old; and the fourth quartile (Q75 to maximum) included patients from 57 to 77 years. **Table 5** shows the demographic data, medical history, and laboratory results of the patients with HH stratified by age. Among the patients with HH, the incidence of hypertension and diabetes increased with age. The rate of glucose disturbances increased in patients aged 32–47 years. Iron levels were stable between the groups, with

TABLE 3 The HH patient group's characteristics at the time of first contact.

	Recently diagnosed HH <i>n</i> = 31	Medium HH <i>n</i> = 11	Long-lasting HH <i>n</i> = 16
Age	36 (31–54)	44 (30–55)	55 (51–62)
Male sex	20 (65%)	8 (73%)	10 (63%)
Hypertension	7 (23%)	5 (45%)	10 (62%)
DM/IGGT	8 (26%)	3 (27%)	9 (56%)
Months from the time of diagnosis	6 (1–14)	37 (30–52)	152 (121–183)
Number of venesections	0 (0–1)	4 (3–6)	53 (31–76)
Iron [ug/dl]	176 (148–223)	164 (125–178)	165 (134–222)
Ferritin [ng/ml]	422 (272–1,050)	280 (212–430)	190 (66–234)
Haemoglobin [mg/dl]	15.1 (14.3–16.1)	14.2 (13.9–15.4)	15.3 (14–16.1)
TSAT [%]	82 (62–93)	65 (55–83)	72 (68–81)
Glucose [mg%]	94 (87–99)	98 (94–104)	103 (97–105)
ASPART [U/L]	25 (19–38)	23 (17–35)	24 (21–39)
ALAT [U/L]	33 (23–60)	35 (29–70)	26 (23–44)

Data are presented as the medians (25th–75th percentile); TSAT, transferrin saturation; DM, diabetes mellitus; IGGT, impaired gestational glucose tolerance; ALAT, alanine aminotransferase; ASPAT, aspartate aminotransferase.

TABLE 4 Comparison of standard and 2D STE echocardiographic parameters between the controls and HH groups.

	Controls <i>n</i> = 29	Recently diagnosed HH <i>n</i> = 31	Medium HH <i>n</i> = 11	Long-lasting HH <i>n</i> = 16	<i>p</i>
IVS (mm)	9 (7–10) ^{§,¶}	10 (8–11) [¶]	11 (10–11.5) [^]	12 (10.5–13) ^{*,^}	<0.001
PW (mm)	8 (7–9) [¶]	9 (7–10) [¶]	9 (9–10.5)	11 (9.5–12) ^{*,^}	<0.001
Em (cm/s)	0.12 (0.09–0.14) [¶]	0.11 (0.09–0.15) [¶]	0.13 (0.09–0.13)	0.09 (0.09–0.10) ^{*,^}	0.030
E/Em	6.7 (5.0–7.5)	6.56 (5.48–7.90)	7.33 (5.90–8.42)	7.70 (6.57–9.30)	0.161
LVEDD (mm)	44 (42–47)	45 (43–48)	48 (44–50)	46 (45–47)	0.235
LVESD (mm)	28 (26–30)	28 (26–29)	30 (27–31)	28 (25–32)	0.538
LVEF (%)	63 (61–65) ^{*,§}	60 (56–62) [^]	57 (53–61) [^]	62 (58–66)	0.009
RVID (ms)	26 (22–29)	25 (24–29)	27 (26–28)	29 (22–29)	0.182
LV basal rotation (°)	−7.1* (−8.38–−4.13)	−3.5 (−5.8–−1.7) ^{¶,^}	−5.8 (−6.6–−3.0)	−6.8 (−9.4–−6.1) [*]	0.020
LV basal rotation velocity (°/s)	−51.5* (−60.3–−25)	−38.0 (−68.8–−1.0) ^{¶,^}	−53.0 (−67.3–−40.2)	−68.0 (−78–−54.2) [*]	0.070
LV basal untwisting velocity (°/s)	48.5 (40.0–62.3)	43.8 (25.5–63.1) [¶]	49.0 (25.6–79.4)	75.9 (59.3–79.8) [*]	0.024
LV apical rotation (°)	16.9 (13.8–24.5) [*]	10.9 (6.28–14.3) ^{§,^}	17.7 (13–22) [*]	12.0 (9.28–16.9)	<0.001
LV apical rotation velocity (°/s)	100 (56–114)	69.8 (42.4–99.3)	98.0 (83.7–113)	76.3 (60–126.8)	0.159
LV apical untwisting velocity (°/s)	−130.5 (−167.7–−107.5) [*]	−76 (−103.6–−56.5) [^]	−102.7 (−122.7–−73.3)	−111.5 (−130.8–−65.9)	0.003

Data are presented as medians (25th–75th percentile). IVS, intraventricular septum (mm); PW, posterior wall; E, early mitral velocity; Em, peak mitral annulus velocity; E/Em, early mitral inflow velocity to peak mitral annulus velocity ratio; LVEDD, left ventricle end-diastolic diameter; LVESD, left ventricle end-systolic diameter; LVEF, left ventricular ejection fraction; RVID, right ventricle internal diameter; LV, left ventricle. *p*-value: for differences among all groups with Kruskal–Wallis test for continuous variables or with chi-square test for categorical variables, *p* < 0.05 in posthoc tests for differences with group recently diagnosed (*), medium (¶), long-lasting (^) or controls (^).

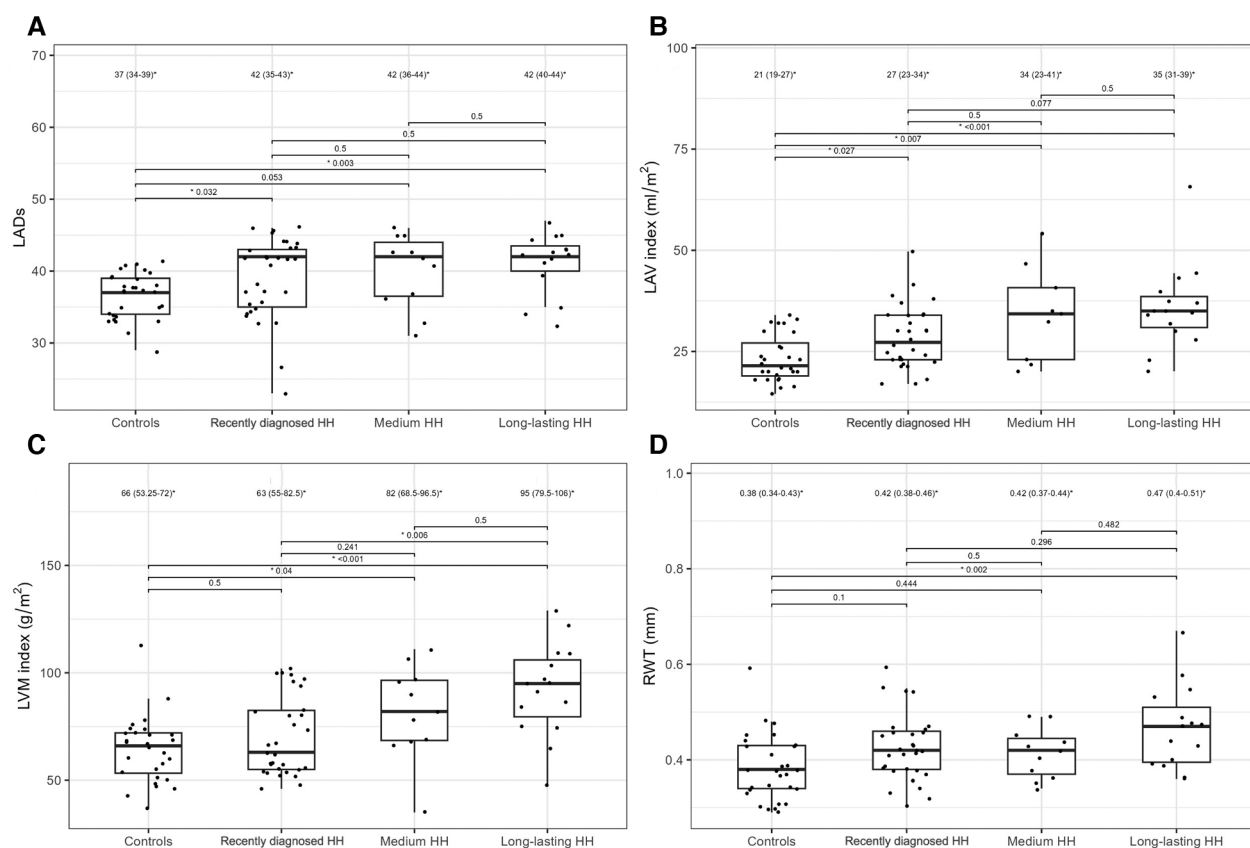


FIGURE 3 LADs (A), LAV index (B), LVM index (C), and RWT (D) values of the controls and HH groups divided according to the stage of the disease. The dots show the values obtained by each person analyzed. The values above the brackets correspond to the *p*-value. * Data are presented as medians (25th–75th percentile).

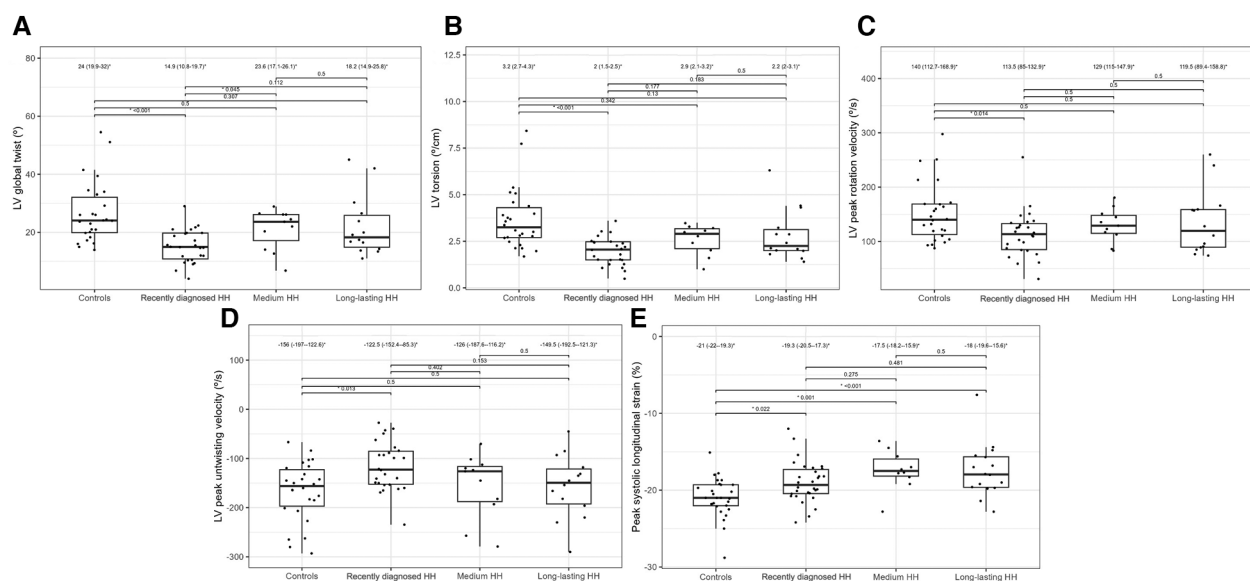


FIGURE 4 LV global twist (A), LV torsion (B), LV peak rotation velocity (C), LV peak untwisting velocity (D), and peak systolic longitudinal strain (E) values of the controls and HH groups divided according to the stage of the disease. The dots show the values obtained by each person analyzed. The values above the brackets correspond to the *p*-value. * Data are presented as medians (25th–75th percentile).

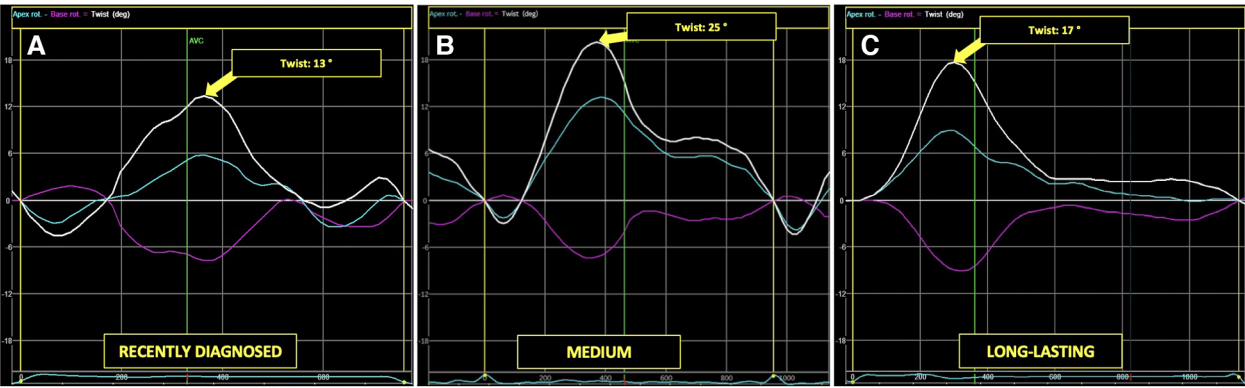


FIGURE 5 The example of LV apical (blue line), basal (pink line), and peak LV rotation twisting (arrow) curves in HH patients at different stages of the disease: the recently diagnosed (A), the medium (B), and the long-lasting (C).

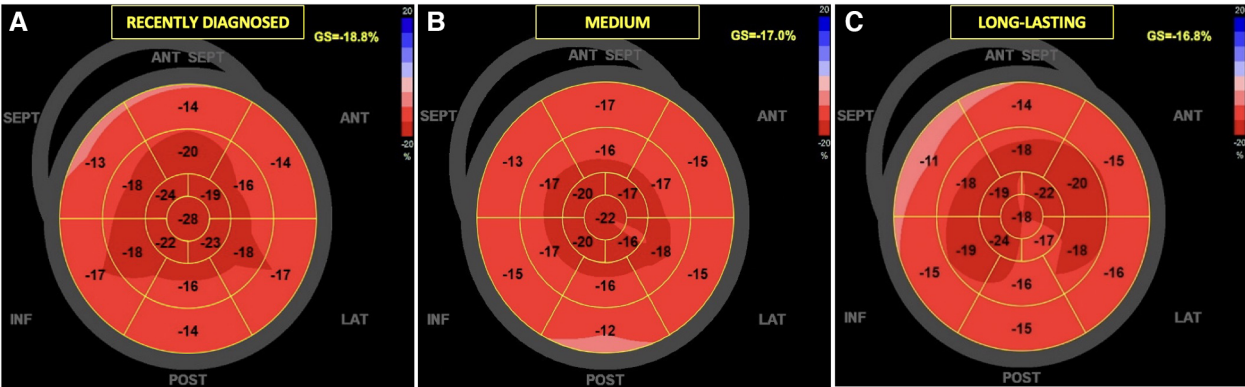


FIGURE 6 The examples of global longitudinal strain in HH patients at different stages of the disease: the recently diagnosed (A), the medium (B), and the long-lasting (C). In the "bull's-eye" map, all myocardial regional deformations, from basal to middle and apical segments are displayed in a single image.

TABLE 5 The HH patient group's characteristics at the time of first contact.

	Age 18–31 year <i>n</i> = 17	Age 32–47 year <i>n</i> = 14	Age 48–56 year <i>n</i> = 13	Age 57–77 year <i>n</i> = 14
Male sex	77%	79%	69%	36%
Hypertension	12%	14%	62%	71%
DM/IGGT	12%	36%	39%	57%
Months from the time of diagnosis	6 (3–25)	19 (3–36)	85 (24–160)	49 (3–145)
Number of venesections	1 (0–1)	1 (0–6)	27 (1–62)	4 (0–49)
Iron [ug/dl]	170 (155–200)	161 (129.75–199)	171 (151–211)	178 (135–219)
Ferritin [ng/ml]	331 (180–640)	334 (224–784)	279 (217–430)	227 (191–457)
Haemoglobin [mg/dl]	15.8 (14.2–16)	15.7 (14.9–16.6)	14.5 (13.7–15.4)	14.8 (13.8–15.1)
TSAT [%]	71 (56–82)	80 (60–91)	68 (65–77)	85 (69–90)
Glucose [mg%]	87 (85–94)	98 (93–114)	98 (96–103)	98 (97–104)
ASPAT [U/L]	23 (17–33)	38 (20–42)	24 (20–38)	24 (22–26)
ALAT [U/L]	40 (23–66)	45 (29–83)	27 (24–37)	31 (24–39)

Data are presented as the medians (25th–75th percentile); TSAT, transferrin saturation; DM, diabetes mellitus; IGGT, impaired gestational glucose tolerance; ALAT, alanine aminotransferase; ASPAT, aspartate aminotransferase.

reduced ferritin concentrations among patients aged 32–47 years and 57–77 years. The levels of TSAT and transaminases were comparable in both.

Table 6 compares the standard and 2D STE echocardiographic parameters of patients with HH stratified by age. Some standard parameters related to diastolic function (LA size, IVS, RWT,

TABLE 6 Comparison of standard and 2D STE echocardiographic parameters between the HH patients stratified by their age.

	Minimum to Q25 Age 18–31 year <i>n</i> = 17	Q25–Q50 Age 32–47 year <i>n</i> = 14	Q50–Q75 Age 48–56 year <i>n</i> = 13	Q75 to maximum Age 57–77 year <i>n</i> = 14	<i>p</i>
IVS (mm)	9 (8–10) ^{§,^}	11.0 (10.0–12.8)*	11 (10–12)*	11 (10–12)*	0.008
PW (mm)	8 (7–9) ^{§,^}	10 (9–11)	10 (9–11)*	10 (9–11)*	0.012
Em (cm/s)	0.14 (0.13–0.16) ^{§,^}	0.11 (0.09–0.13) [^]	0.09 (0.08–0.1)*	0.08 (0.07–0.09)* [§]	<0.001
E/Em	5.6 (4.8–6.7) ^{§,^}	6.4 (5.6–7.8) [^]	7.8 (7.5–9.2)*	9 (7–10)* [§]	<0.001
LVEDD (mm)	47 (43–48)	47 (45–48)	47 (45–51)	43 (42–45)	0.14
LVESD (mm)	28 (26–31)	28 (27–31)	29 (25–30)	25 (24–28)	0.398
LVEF (%)	57 (53–62)	58 (54–61)	60 (59–63)	61 (60–66)	0.111
RVID (ms)	26 (23–28)	28.5 (25–30)	27 (26–30)	27 (25–28)	0.129
LV basal rotation (°)	−4.2 (−5.7–−1.7)	−3.9 (−6.3–−2.6)	−7.6 (−11.0–−4.0)	−6.0 (−7.0–−4.2)	0.089
LV basal rotation velocity (°/s)	−50.5 (−63.6–−0.0)	−55.1 (−75.2–−17.3)	−49.7 (−75.0–−32.3)	−63.1 (−80.9–−42.8)	0.762
LV basal untwisting velocity (°/s)	44.7 (15.2–67.8)	45.0 (34.1–51.0)	77.81 (40.0–80.1)	66.0 (39.0–78.2)	0.188
LV apical rotation (°)	7.8 (5.3–15.1)	12.6 (10.2–16.7)	13.0 (9.0–18.0)	13.2 (11.0–22.9)	0.098
LV apical rotation velocity (°/s)	67.0 (37.2–101.3)	98.1 (63.4–119.6)	82.0 (51.9–87.0)	89.8 (66.0–129.5)	0.227
LV apical untwisting velocity (°/s)	−82.8 (−105.4–−64.2)	−75.7 (−116.1–−60.2)	−76.0 (−119.6–−55.1)	−107.8 (−156.3–−93.9)	0.335

Data are presented as medians (25th–75th percentile). IVS, intraventricular septum (mm); PW, posterior wall; E, early mitral velocity; Em, peak mitral annulus velocity; E/Em, early mitral inflow velocity to peak mitral annulus velocity ratio; LVEDD, left ventricle end-diastolic diameter; LVESD, left ventricle end-systolic diameter; LVEF, left ventricular ejection fraction; RVID, right ventricle internal diameter; LV, left ventricle. *p*-value: for differences among all groups with Kruskal–Wallis test for continuous variables or with chi-square test for categorical variables, *p* < 0.05 in posthoc tests for differences with group age 18–31 year (*), age 32–47 year (°), age 48–56 year (°) or age 57–77 year (°).

LVM index, Em, and E/Em) changed above the normal range most prominently in the third decade of life (Figure 7). In contrast, some STE parameters related to systolic function (LV global twist and torsion) increased significantly from the fourth decade of life (Figure 8).

3.4. The correlations between iron turnover parameters and echocardiographic parameters

Table 7 presents the correlations between iron turnover parameters and measured echocardiographic parameters. Some correlations were observed between the time from diagnosis and the number of venesections with echocardiographic parameters. The correlations were significant; however, they were relatively weak (the *r*-values were lower than 0.7).

4. Discussion

Our results support the role of echocardiography in revealing the differences between patients with HH in terms of the time from the initial diagnosis and the patient age. To the best of our knowledge, this is the first study to address this issue in patients with HH.

4.1. The potential impact of HH on the heart considering the stage of the disease

Standard echocardiography revealed differences in diastolic parameters in the enrolled patients with HH compared with healthy controls. Several authors have documented diastolic

dysfunction in patients with HH (14–16). The cited studies' techniques were based on the standard two-dimensional echocardiography, including M-mode (16) and TDI techniques (14, 15). For example, Candell-Riera et al., showed that patients with idiopathic hemochromatosis presented significantly higher LADs index (22.2 ± 3.7 mm/m²) and LVM index (150 ± 56.2 g/m²) compared to the control group (respectively 19.2 ± 1.7 mm/m² and 91.7 ± 14.6 g/m², respectively) (16). Similarly, Palka et al. revealed deviations in the LADs and the LVM index in their analysis of patients with HH, with 83% being C282Y homozygotes (15). The authors also observed significantly higher values of LVM index (101 ± 26 g/m²) and LADs in patients with HH (3.81 ± 0.74 cm) compared to healthy controls (77 ± 12 g/m² for LVM index and 3.27 ± 0.39 cm for LADs, respectively) (15). Our results are in line with this study: we found significantly higher LADs [42.0 (36.0–43.0) mm/m²] and LAV index values [31.0 (23.0–36.5) ml/m²], and LVM index values [78.0 (58.0–96.0) g/m²] in patients with HH compared to healthy volunteers (37.0 [34.0–39.0] mm/m² for LADs, 21.5 [19.0–27.1] ml/m² for LAV index, and 66.0 [53.0–72.0] g/m² for LVM index, respectively) (Figure 1). Interestingly, Davidsen et al. did not show such differences in the LADs and LVM index values between patients with HH and healthy controls, possibly because all of their patients were regularly treated with venesections (14).

Furthermore, we compared patients with HH at the different stages of the disease. To the best of our knowledge, this is the first such analysis of patients with HH. We revealed worse diastolic parameters measured by standard echocardiography in patients with HH compared to controls, with the most noticeable differences (in morphological and functional parameters) detected between the healthy and long-lasting HH group. The latter had worse LV wall thickness, RWT, LVM index, and Em indices, probably due to the disease's length and the patient's age

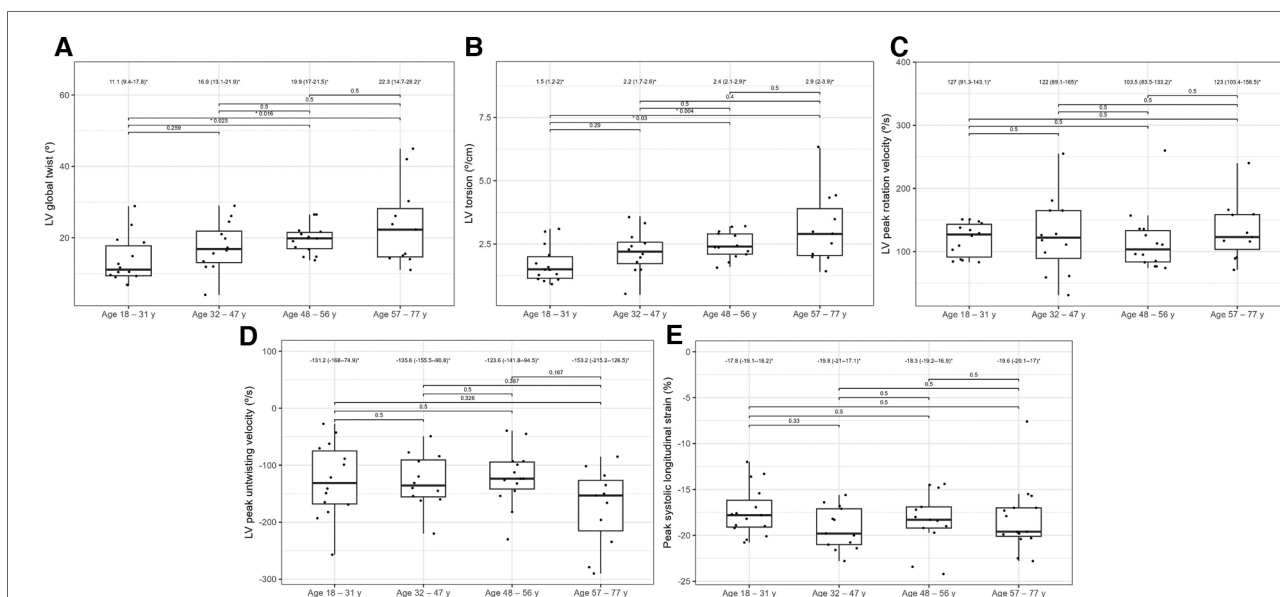
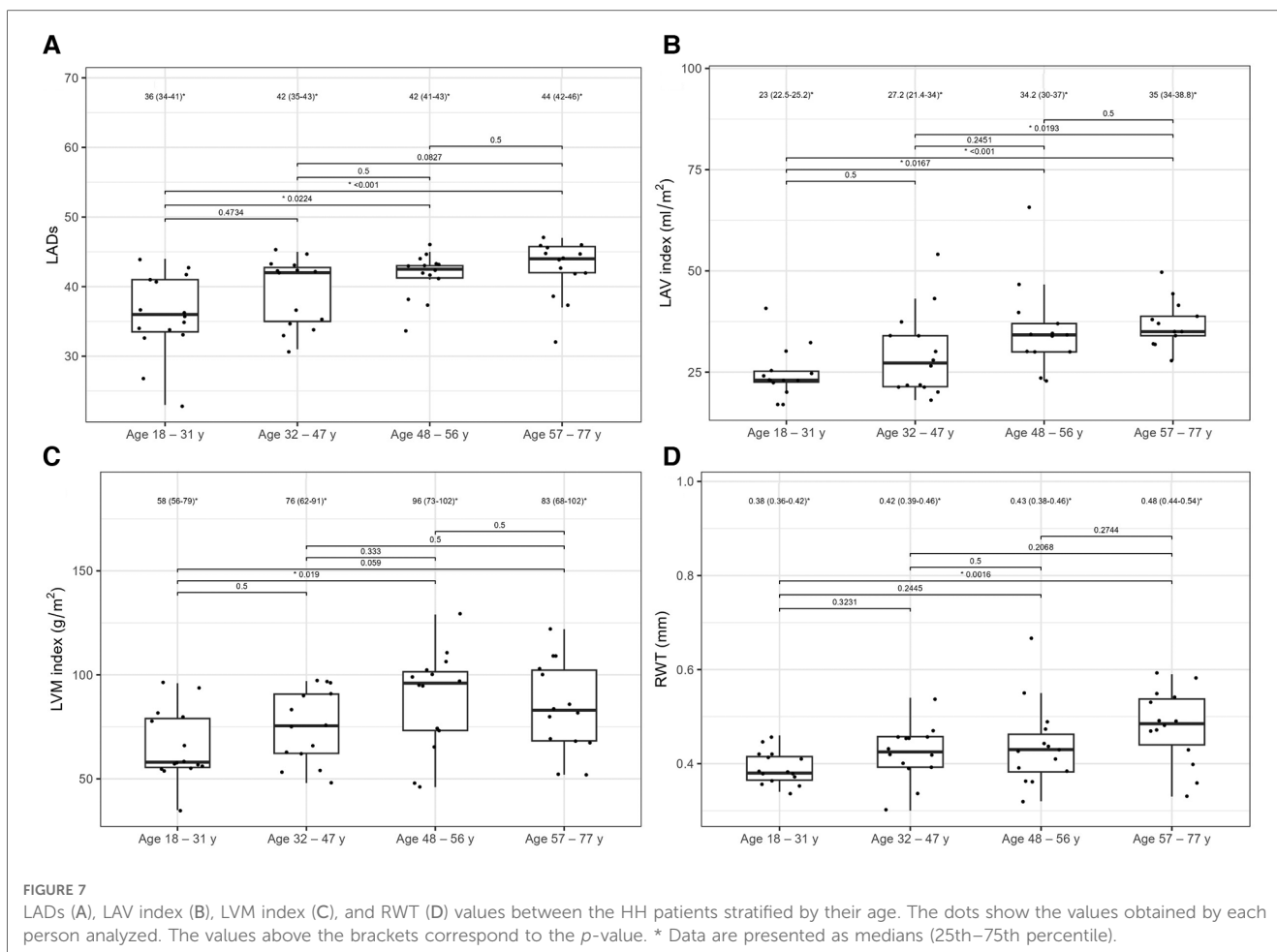


TABLE 7 Correlations between iron turnover, time from diagnosis, number of venesections and 2D STE parameters in HH patients.

Echocardiographic parameter	Iron		Ferritin		TSAT		Time from diagnosis		Numbers of venesections	
	<i>r</i>	<i>p</i>	<i>r</i>	<i>p</i>	<i>r</i>	<i>p</i>	<i>r</i>	<i>p</i>	<i>r</i>	<i>p</i>
LADs	0.11	0.414	0.058	0.669	0.161	0.239	0.189	0.16	0.164	0.224
LAA index (cm ² /m ²)	−0.001	0.996	0.032	0.820	−0.025	0.863	0.295	0.032	0.336	0.014
LAV index (ml/m ²)	0.119	0.39	0.074	0.594	0.050	0.720	0.395	0.003	0.408	0.002
IVS (mm)	0.035	0.797	0.278	0.036	−0.009	0.949	0.522	0.001	0.342	0.009
PW (mm)	0.212	0.114	0.282	0.033	0.007	0.96	0.496	0.001	0.419	0.001
RWT	0.200	0.136	0.244	0.067	0.004	0.975	0.259	0.051	0.247	0.064
LVM index (g/m ²)	0.117	0.385	0.303	0.022	0.087	0.522	0.530	0.001	0.433	0.001
Em	−0.005	0.971	−0.101	0.459	−0.147	0.284	−0.414	0.001	−0.399	0.002
E/Em	0.082	0.548	0.082	0.548	0.141	0.303	0.340	0.01	0.394	0.002
LVEDD (mm)	0.095	0.504	0.172	0.200	0.112	0.409	0.195	0.145	0.156	0.247
LVESD (mm)	0.090	0.481	−0.051	0.706	−0.004	0.977	0.211	0.115	0.084	0.535
LVEF (%)	0.110	0.451	0.112	0.442	0.002	0.987	0.219	0.130	0.107	0.463
RVID (ms)	−0.002	0.987	0.346	0.008	0.098	0.472	0.262	0.049	0.254	0.056
LV basal rotation (°)	0.226	0.107	0.035	0.81	0.129	0.365	−0.302	0.03	−0.21	0.135
LV basal rotation velocity (°/s)	0.14	0.324	−0.057	0.689	0.094	0.514	−0.279	0.045	−0.2	0.156
LV basal untwisting velocity (°/s)	−0.229	0.102	−0.183	0.200	−0.173	0.225	0.343	0.013	0.256	0.067
LV apical rotation (°)	−0.055	0.704	0.104	0.473	−0.095	0.512	0.238	0.092	0.266	0.059
LV apical rotation velocity (°/s)	−0.007	0.962	−0.077	0.595	−0.037	0.800	0.211	0.137	0.161	0.26
LV apical untwisting velocity (°/s)	0.071	0.621	0.098	0.500	0.122	0.4	−0.144	0.315	−0.29	0.84
LV global twist (°)	−0.145	0.310	0.083	0.569	−0.125	0.387	0.342	0.014	0.337	0.015
LV torsion (°/cm)	−0.13	0.366	0.096	0.514	−0.053	0.717	0.316	0.025	0.35	0.013
LV peak rotation velocity (°/s)	−0.186	0.192	−0.061	0.675	−0.089	0.539	0.131	0.361	0.018	0.899
LV peak untwisting velocity (°/s)	0.113	0.429	0.236	0.099	0.156	0.28	−0.238	0.093	−0.055	0.704
Peak systolic longitudinal strain (%)	−0.026	0.848	−0.016	0.907	0.061	0.659	0.261	0.052	0.154	0.256

LADs, left atrial diameter; LAA index, left atrium area/m²; LAV index, left atrium volume/m²; IVS, intraventricular septum (mm); PW, posterior wall; RWT, relative wall thickness; LVM index, left ventricle mass/m²; E, early mitral velocity; Em, peak mitral annulus velocity; E/Em, early mitral inflow velocity to peak mitral annulus velocity ratio; LVEDD, left ventricle end-diastolic diameter; LVESD, left ventricle end-systolic diameter; LVEF, left ventricular ejection fraction; RVID, right ventricle internal diameter; LV, left ventricle.

(Table 4, Figure 3). Hypertension and glucose disturbances, which occur earlier in patients with HH than in the overall population, could have an additional impact on the left ventricular diastolic function (17).

The application of 2D STE in our study allowed for a more precise description of systolic dysfunction. In one of our previous studies, the patients with recently diagnosed HH had worse rotation and strain parameters measured by 2D STE than healthy controls, despite the lack of differences in standard echocardiographic parameters (Figure 4) (10). We confirmed this observation in the presented study of patients with HH at the different stages of the disease.

2D STE may allow for the complex analysis of heart mechanics. A decrease in the untwisting velocity represents a predominance of diastolic dysfunction, and significant decreases in rotation, rotation rate, twist, torsion, and peak systolic longitudinal strain are critical predictors of systolic dysfunction (18–20). Only a few studies (10, 11, 21–23) have used speckle-tracking analysis in the context of iron-overload symptoms. However, these studies involved patients with beta-thalassemia major, an extreme model of systemic iron overload (24). In our study, the recently diagnosed HH group was characterized by the worst parameters of the LV rotation, the twisting and untwisting indices, whereas the percentages of hypertension and glucose disturbances were the lowest in that group compared to the other HH groups (Table 4;

Figure 4), which may exclude the possible influence of these comorbidities on 2D STE parameters. The aforementioned rotation indices improved significantly in the medium and long-lasting groups of patients, possibly due to HH treatment (Table 4; Figure 4). This postulation aligns with previous data in the literature (11, 25). For example, Byrne et al. showed that intensification of venesection therapy may significantly improve radial strains following a 1-year course of phlebotomies (11). In one of our clinical case presentations, we observed similar changes in the rotation, twist, and torsion LV parameters after 6-month therapy with venesections in our patient with recently diagnosed HH (25). However, we did not investigate the direct influence of treatment but compared the patients at the different HH stages. Our results make it unclear why the Long-lasting HH patients did not present further improvement in rotation parameters. That could be explained in two ways: the initial treatment by venesections could only normalize rotation parameters in HH patients without further improvement, and the aging of the enrolled patients could implicate our results (26). However, these explanations must be verified in a further prospective study with the appropriate follow-up observations.

The peak systolic longitudinal strain values in this study were significantly lower in patients with HH at all stages of the disease (Figure 4). This parameter did not improve with treatment initiation and continuation, which suggests early irreversible

changes in the hearts of patients with HH starting at the early stages of the disease. We obtained similar results in our previously published case report, where peak systolic longitudinal strain did not improve within the treatment (25). This finding may have a substantial clinical impact since an impaired peak longitudinal strain value is a well-established prognostic factor for cardiac complications (27–29). However, further research is necessary to verify whether the differences in the peak systolic longitudinal strain between the healthy volunteers and patients with HH at different disease stages are clinically relevant. The LVEF was within the normal range in our patients, despite statistically significant differences between the patients with HH and controls. This finding is consistent with previously documented data (16), indicating that LVEF may not be the best parameter for assessing systolic damages in the patients with HH.

4.2. The potential impact of HH on the heart considering the patient's age

Iron overload may accelerate the aging of the cardiovascular system, including the heart, through oxidative stress, which results in appropriate changes in diastolic and systolic parameters. These changes can be detected by standard echocardiography (increase in the LV width and LVM index, LA enlargement, or changes in mitral flow parameters) or by STE (decrease in rotation, twist, and torsion values of the LV) (10, 15–17).

In the presented study, the echocardiographic features of myocardial walls' thickening in patients with HH appeared more rapidly than in healthy individuals. For instance, Ganau et al. evaluated the effect of age on concentric remodeling in healthy participants and showed that RWT values increased with age and constituted 0.32 ± 0.044 among patients younger than <41 years, 0.34 ± 0.05 for those aged 41–64 years, and 0.37 ± 0.050 for those >64 years (30). Our patients with HH achieved similar RWT values faster than healthy individuals in the cited study (Figure 7). In our study, the LVM index was 76 (62–91) g/m² in the fourth decade, whereas Kaku et al. reported a lower maximum value of the LVM index in the older (the eighth decade of life) healthy volunteers (31). Another important parameter that increases with age is the LA size. Nikitin et al. showed that the LAD was 3.51 ± 0.51 cm in patients aged 20–39 years, 3.99 ± 0.54 cm in those aged 40–59 years, 4.12 ± 0.43 cm in those aged 60–79 years, and 4.19 ± 0.51 in those aged >80 years (32). In our analysis, the LADs increased slightly faster (Figure 7). Similarly, the LAV index increased faster in our patients (Figure 7) than in healthy individuals, as reported by Nikitin et al. (32). Furthermore, we showed increased E/Em values in the older patients compared to the younger patients; however, we did not find any significant differences from the general population (31).

Regarding LVEF, as an index of systolic function, Kaku et al. showed that it does not significantly change with age (31). Similarly, we did not observe any changes in LVEF in our patients with HH with age; however, LVEF was slightly lower than that of the general population (31). STE may allow for a

better understanding of age-related systolic function changes than a standard echocardiography with LVEF measurements. According to Kuznetsova et al., the absolute values of the peak systolic longitudinal strain significantly decreased in a healthy population with age: $24.2 \pm 3.4\%$, in individuals aged <40 years, $23.5 \pm 3.19\%$ in those aged 40–59, and $22.3 \pm 3.62\%$ in those aged >60 years (33). Among our patients with HH, peak systolic longitudinal strain was at a lower level: -17.8 (-19.1 – -16.2) % in patients with HH aged 18–31 years, and was without significant changes in the older patients (among patients aged 32–47: -19.8 [-21.0 – -17.1] %, aged 48–56: 18.3 [-19.2 – -16.9] %, aged 57–77: 19.6 [-20.1 – -17.0] %; Figure 8). Kaku et al. reported that the LV global twist and torsion values increased with age (34). According to that study, the maximum LV twist and torsion values were reached in the seventh decade of life ($12.7 \pm 4.8^\circ$ for LV twist and $1.75 \pm 0.66^\circ/\text{cm}$ for torsion). In our analysis, similar LV twist values were present in patients with HH at a younger age (18–31 years old) and constituted 11.1 (9.4 – 17.8)° for twist and 1.5 (1.2 – 2.0)°/cm for torsion (Figure 8). Increasing the rotation parameters within the age range may result in a decrease in the longitudinal strain of the LV.

Our results showed that thickening of the myocardium and dilatation of the LA occurred faster in patients with HH than in the general population. Similarly, the deterioration in systolic function detected using STE was more prominent in patients with HH than in the general population. This could suggest a harmful effect of the disease on the heart in addition to the aging of the patients; however, this hypothesis needs to be verified.

4.3. Correlation of the obtained results with the parameters of iron metabolism

The presented analysis showed that the correlations between the iron turnover parameters and echocardiographic indices were relatively weak. These findings align with data from the literature (23, 35, 36) and our previous results, including cardiac magnetic resonance assessments (10, 37). There is probably no “direct” relationship between the levels of iron turnover parameters and myocardial function, and myocardial iron overload is not the only mechanism involved in the development of HH cardiomyopathy (1). The precise mechanism of heart involvement in HH is yet to be entirely understood. The excessive capacity of serum transferrin to bind iron, which is typical in patients with HH, results in uncontrolled iron entry into cardiomyocytes, which may increase their susceptibility to oxidative cell stress (3). Cardiomyocytes contain many mitochondria, causing the myocardium to be more vulnerable to oxidative stress damage. Free iron ions that damage the mitochondrial and nuclear DNA may activate fibroblast proliferation and differentiation into myofibroblasts, which are responsible for heart fibrosis (38). Oxidative stress results in the peroxidation of cell membranes, particularly those in the mitochondria, which reduces the amount of adenosine triphosphate generated during oxidative phosphorylation. Oxidative stress impairs heart muscle relaxation and delays

contraction by inhibiting SERCA2 enzyme activity and increasing the cytoplasmic concentration of calcium ions in cardiomyocytes. Therefore, amlodipine, a Ca channel blocker, may be promising as an agent to potentially reduce oxidative stress during iron overload (39).

Magnetic resonance imaging is the gold standard for measuring iron overload (2). Previous studies presented changes in the heart documented on cardiac magnetic resonance (CMR) in patients with beta-thalassemia, most of whom met the current criteria for iron overload in terms of myocardial $T2^* < 20$ ms (40–42). HH is not the same iron overload model as beta-thalassemia, which has been documented in our previous study (37). In all the studied patients with HH, myocardial $T2^*$, $T1$, and $T2^*$ did not fulfill the clinically severe iron overload (20 ms) threshold, which confirms the hypothesis that in modern patients with HH not simple iron storage in the heart could play an essential role in the heart damage process. Therefore, in the present study, we assessed the role of echocardiography, particularly STE, in identifying differences in patients with HH at various disease stages and ages, rather than calculating iron overload.

5. Clinical implications

HH involves a chronic process of complicated iron dysregulation cycles with unavoidable cardiac involvement, leading to changes in the diastolic and systolic functions of the heart. In addition to genetic testing and iron parameter measurement, detecting cardiac involvement early, even in asymptomatic individuals, and utilizing contemporary imaging techniques may have tremendous clinical utility, particularly for monitoring the course of the disease and possible aging of the heart from the oxidative stress generated by free iron ions in patients with HH. Differences in the diastolic parameters can be easily detected using standard echocardiography. In contrast, advanced echocardiography using 2D STE is necessary to better reveal systolic changes that appear notably attenuated and irreversible in patients with HH at different stages of the disease.

6. Study limitations

Our study had some critical limitations. The first was the relatively small sample size, which resulted from the highly selective enrollment process (patients without any cardiovascular symptoms), the demand to achieve the best image quality (frame rate of 50–80 frames/s), and the inclusion of only patients with genetically confirmed HH and without cardiological comorbidities (apart from hypertension). We presented the data of different patients, rather than evaluating the same patients over the years of venesections. We did not present a CMR assessment and could not address the iron overload status. This was a pilot study, and further studies with more homogeneous patients are required.

7. Conclusions

Echocardiography can reveal possible heart damage in patients with HH at different disease stages and highlight features of accelerated myocardial aging in these patients. Further studies with follow-up observations are required to provide a better understanding of these issues.

Data availability statement

The raw data supporting the conclusions of this article will be made available by the authors, without undue reservation.

Ethics statement

The studies involving human participants were reviewed and approved by Independent Bioethics Committee for Scientific Research at Medical University of Gdańsk. The patients/participants provided their written informed consent to participate in this study.

Author contributions

Conceptualization: LD, MŚ, KS; methodology: LD, KS; software: MŚ, KR, LD; validation: MŚ, KR, LD; formal analysis: MŚ, KR, LD; investigation: LD, MŚ, KR, KS; resources: KS, LD; data curation: KR, LD, MŚ, AŚ, KM; writing—original draft preparation: MŚ, LD, KR, AŚ, KM; writing—review and editing: LD, KS; visualization: MŚ, LD; supervision: GR; project administration: LD, KS; funding acquisition: LD. All authors contributed to the article and approved the submitted version.

Funding

Experienced Researchers Grant of the Medical University of Gdansk (71-01415/0004608/61/183/183/2022).

Conflict of interest

The authors declare that the research was conducted in the absence of any commercial or financial relationships that could be construed as a potential conflict of interest.

Publisher's note

All claims expressed in this article are solely those of the authors and do not necessarily represent those of their affiliated organizations, or those of the publisher, the editors and the reviewers. Any product that may be evaluated in this article, or claim that may be made by its manufacturer, is not guaranteed or endorsed by the publisher.

References

- Daniłowicz-Szymanowicz L, Świątczak M, Sikorska K, Starzyński RR, Raczak A, Lipiński P. Pathogenesis, diagnosis, and clinical implications of hereditary hemochromatosis-the cardiologist's point of view. *Diagnostics*. (2021) 11(7):1279. doi: 10.3390/diagnostics11071279
- Gulati V, Hari Krishnan P, Palaniswamy C, Aronow WS, Jain D, Frishman WH. Cardiac involvement in hemochromatosis. *Cardiol Rev*. (2014) 22(2):56–68. doi: 10.1097/CRD.0b013e3182a67805
- Brissot P, Ropert M, Le Lan C, Loréal O. Non-transferrin bound iron: a key role in iron overload and iron toxicity. *Biochim Biophys Acta*. (2012) 1820(3):403–10. doi: 10.1016/j.bbagen.2011.07.014
- Laina A, Stellos K, Stamatiopoulos K. Vascular ageing: underlying mechanisms and clinical implications. *Exp Gerontol*. (2018) 109:16–30. doi: 10.1016/j.exger.2017.06.007
- Brandes RP, Fleming I, Busse R. Endothelial aging. *Cardiovasc Res*. (2005) 66(2):286–94. doi: 10.1016/j.cardiores.2004.12.027
- Seals DR, Jablonski KL, Donato AJ. Aging and vascular endothelial function in humans. *Clin Sci*. (2011) 120(9):357–75. doi: 10.1042/CS20100476
- Agrawal T, Nagueh SF. Changes in cardiac structure and function with aging. *J Cardiovasc Aging*. (2022) 2(1):13. doi: 10.20517/jca.2021.40
- Singh A, Carvalho Singulane C, Miyoshi T, Prado AD, Addetia K, Bellino M, et al. Normal values of left atrial size and function and the impact of age: results of the world alliance societies of echocardiography study. *J Am Soc Echocardiogr*. (2022) 35(2):154–164.e3. doi: 10.1016/j.echo.2021.08.008
- Tadic M, Cuspidi C, Calicchio F, Grassi G, Mancina G. Diagnostic algorithm for HFpEF: how much is the recent consensus applicable in clinical practice? *Heart Fail Rev*. (2021) 26(6):1485–93. doi: 10.1007/s10741-020-09966-4
- Rozwadowska K, Daniłowicz-Szymanowicz L, Fijałkowski M, Sikorska K, Gałaska R, Kozłowski D, et al. Can two-dimensional speckle tracking echocardiography be useful for left ventricular assessment in the early stages of hereditary haemochromatosis? *Echocardiography*. (2018) 35(11):1772–81. doi: 10.1111/echo.14141
- Byrne D, Walsh JP, Daly C, McKiernan S, Norris S, Murphy RT, et al. Improvements in cardiac function detected using echocardiography in patients with hereditary haemochromatosis. *Ir J Med Sci*. (2020) 189(1):109–17. doi: 10.1007/s11845-019-02032-5
- Lang RM, Badano LP, Mor-Avi V, Afilalo J, Armstrong A, Ernande L, et al. Recommendations for cardiac chamber quantification by echocardiography in adults: an update from the American society of echocardiography and the European association of cardiovascular imaging. *J Am Soc Echocardiogr*. (2015) 28(1):1–39.e14. doi: 10.1016/j.echo.2014.10.003
- Nagueh SF, Smiseth OA, Appleton CP, Byrd BF 3rd, Dokainish H, Edvardsen T, et al. Recommendations for the evaluation of left ventricular diastolic function by echocardiography: an update from the American society of echocardiography and the European association of cardiovascular imaging. *Eur Heart J Cardiovasc Imaging*. (2016) 17(12):1321–60. doi: 10.1093/ehjci/jew082
- Davidson ES, Omvik P, Hervig T, Gerds E. Left ventricular diastolic function in patients with treated haemochromatosis. *Scand Cardiovasc J*. (2009) 43(1):32–8. doi: 10.1080/14017430802203811, Erratum in: *Scand Cardiovasc J*. (2009 Feb) 43(1):38.
- Palka P, Macdonald G, Lange A, Burstow DJ. The role of Doppler left ventricular filling indexes and Doppler tissue echocardiography in the assessment of cardiac involvement in hereditary hemochromatosis. *J Am Soc Echocardiogr*. (2002) 15(9):884–90. doi: 10.1067/mje.2002.118032
- Candell-Riera J, Lu L, Serés L, González JB, Batlle J, Permanyer-Miralda G, et al. Cardiac hemochromatosis: beneficial effects of iron removal therapy. An echocardiographic study. *Am J Cardiol*. (1983) 52(7):824–9. doi: 10.1016/0002-9149(83)90422-8
- Rozwadowska K, Daniłowicz-Szymanowicz L, Fijałkowski M, Sikorska K, Szymanowicz W, Lewicka E, et al. Does the age of patients with hereditary hemochromatosis at the moment of their first diagnosis have an additional effect on the standard echocardiographic parameters? *Eur J Transl Clin Med*. (2018) 1(1):18–23. doi: 10.31373/ejtc/95222
- Sun JP, Lee AP, Wu C, Lam YY, Hung MJ, Chen L, et al. Quantification of left ventricular regional myocardial function using two-dimensional speckle tracking echocardiography in healthy volunteers—a multi-center study. *Int J Cardiol*. (2013) 167(2):495–501. doi: 10.1016/j.ijcard.2012.01.071
- Takahashi K, Al Naami G, Thompson R, Inage A, Mackie AS, Smallhorn JF. Normal rotational, torsion and untwisting data in children, adolescents and young adults. *J Am Soc Echocardiogr*. (2010) 23(3):286–93. doi: 10.1016/j.echo.2009.11.018
- Burns AT, La Gerche A, Prior DL, Macisaac AI. Left ventricular untwisting is an important determinant of early diastolic function. *JACC Cardiovasc Imaging*. (2009) 2(6):709–16. doi: 10.1016/j.jcmg.2009.01.015
- Monte I, Buccheri S, Bottari V, Blundo A, Licciardi S, Romeo MA. Left ventricular rotational dynamics in Beta thalassemia major: a speckle-tracking echocardiographic study. *J Am Soc Echocardiogr*. (2012) 25(10):1083–90. doi: 10.1016/j.echo.2012.07.007
- Cheung YF, Liang XC, Chan GC, Wong SJ, Ha SY. Myocardial deformation in patients with Beta-thalassemia major: a speckle tracking echocardiographic study. *Echocardiography*. (2010) 27(3):253–9. doi: 10.1111/j.1540-8175.2009.01005.x
- Di Odoardo LAF, Giuditta M, Cassinerio E, Roghi A, Pedrotti P, Vicenzi M, et al. Myocardial deformation in iron overload cardiomyopathy: speckle tracking imaging in a beta-thalassemia major population. *Intern Emerg Med*. (2017) 12(6):799–809. doi: 10.1007/s11739-017-1670-4
- Anderson LJ. Assessment of iron overload with T2* magnetic resonance imaging. *Prog Cardiovasc Dis*. (2011) 54(3):287–94. doi: 10.1016/j.pcad.2011.07.004
- Świątczak M, Sikorska K, Raczak G, Daniłowicz-Szymanowicz L. Nonroutine use of 2-dimensional speckle tracking echocardiography and fatigue assessment to monitor the effects of therapeutic venesections in a patient with newly diagnosed hereditary hemochromatosis. *Kardiol Pol*. (2020) 78(7-8):786–7. doi: 10.33963/KP.15357
- Młodziński K, Świątczak M, Rohun J, Wolf J, Narkiewicz K, Hellmann M, et al. Vascular aging and damage in patients with iron metabolism disorders. *Diagnostics*. (2022) 12(11):2817. doi: 10.3390/diagnostics12112817
- Kaufmann D, Szwoch M, Kwiatkowska J, Raczak G, Daniłowicz-Szymanowicz L. Global longitudinal strain can predict heart failure exacerbation in stable outpatients with ischemic left ventricular systolic dysfunction. *PLoS One*. (2019) 14(12):e0225829. doi: 10.1371/journal.pone.0225829
- Wabich E, Dorniak K, Ziencuk-Krajka A, Nowak R, Raczak G, Daniłowicz-Szymanowicz L. Segmental longitudinal strain as the most accurate predictor of the patchy pattern late gadolinium enhancement in hypertrophic cardiomyopathy. *J Cardiol*. (2021) 77(5):475–81. doi: 10.1016/j.jjcc.2020.11.004
- Chen MR, Ko HS, Chao TF, Liu HC, Kuo JY, Bulwer BE, et al. Relation of myocardial systolic mechanics to serum ferritin level as a prognosticator in thalassemia patients undergoing repeated transfusion. *Echocardiography*. (2015) 32(1):79–88. doi: 10.1111/echo.12590
- Ganau A, Saba PS, Roman MJ, de Simone G, Realdi G, Devereux RB. Ageing induces left ventricular concentric remodelling in normotensive subjects. *J Hypertens*. (1995) 13(12 Pt 2):1818–22. PMID: 8903659.
- Kaku K, Takeuchi M, Otani K, Sugeng L, Nakai H, Haruki N, et al. Age- and gender-dependency of left ventricular geometry assessed with real-time three-dimensional transthoracic echocardiography. *J Am Soc Echocardiogr*. (2011) 24(5):541–7. doi: 10.1016/j.echo.2011.01.011
- Nikitin NP, Witte KK, Thackray SD, Goodge LJ, Clark AL, Cleland JG. Effect of age and sex on left atrial morphology and function. *Eur J Echocardiogr*. (2003) 4(1):36–42. doi: 10.1053/euje.2002.0611
- Kuznetsova T, Herbots L, Richart T, D'hooge J, Thijs L, Fagard RH, et al. Left ventricular strain and strain rate in a general population. *Eur Heart J*. (2008) 29(16):2014–23. doi: 10.1093/eurheartj/ehn280
- Kaku K, Takeuchi M, Tsang W, Takigiku K, Yasukochi S, Patel AR, et al. Age-related normal range of left ventricular strain and torsion using three-dimensional speckle-tracking echocardiography. *J Am Soc Echocardiogr*. (2014) 27(1):55–64. doi: 10.1016/j.echo.2013.10.002
- Garceau P, Nguyen E.T, Carasso S, Ross H, Pendergrast J, Moravsky G, et al. Quantification of myocardial iron deposition by two-dimensional speckle tracking in patients with β -thalassaemia major and black-fan-diamond anaemia. *Heart*. (2011) 97(5):388–93. doi: 10.1136/hrt.2010.192641
- Ari ME, Ekici F, Çetin İİ, Tavit EB, Yarıllı N, Işık P, et al. Assessment of left ventricular functions and myocardial iron load with tissue Doppler and speckle tracking echocardiography and T2* MRI in patients with β -thalassaemia major. *Echocardiography*. (2017) 34:383–9. doi: 10.1111/echo.13463
- Dorniak K, Daniłowicz-Szymanowicz L, Sikorska K, Rozwadowska K, Fijałkowski J, Glińska A, et al. Left ventricular function and iron loading status in a tertiary center hemochromatosis cohort—a cardiac magnetic resonance study. *Diagnostics*. (2022) 12(11):2620. doi: 10.3390/diagnostics12112620
- Sukumanan A, Chang J, Han M, Mintri S, Khaw BA, Kim J. Iron overload exacerbates age-associated cardiac hypertrophy in a mouse model of hemochromatosis. *Sci Rep*. (2017) 7(1):5756. doi: 10.1038/s41598-017-05810-2
- Zhabiyev P, Sadasivan C, Shah S, Wang F, Oudit GY. Amlodipine rescues advanced iron overload cardiomyopathy in hemojuvelin knockout murine model: clinical implications. *Front Cardiovasc Med*. (2023) 10:1129349. doi: 10.3389/fcvm.2023.1129349
- Carpenter JP, Roughton M, Pennell DJ. Myocardial iron in thalassemia (MINT) investigators. International survey of T2* cardiovascular magnetic resonance in β -thalassaemia major. *Haematologica*. (2013) 98(9):1368–74. doi: 10.3324/haematol.2013.083634
- Pistoia L, Meloni A, Salvadori S, Spasiano A, Lisi R, Rosso R, et al. Cardiac involvement by CMR in different genotypic groups of thalassemia major patients. *Blood Cells Mol Dis*. (2019) 77:1–7. doi: 10.1016/j.bcmd.2019.01.008
- Rezaeian N, Mohtasham MA, Khaleel AJ, Parnianfar N, Kasani K, Golshan R. Comparison of global strain values of myocardium in beta-thalassemia major patients with iron load using specific feature tracking in cardiac magnetic resonance imaging. *Int J Cardiovasc Imaging*. (2020) 36(7):1343–9. doi: 10.1007/s10554-020-01835-3



OPEN ACCESS

EDITED BY

Francesca Innocenti,
Careggi University Hospital, Italy

REVIEWED BY

Chun Ka Wong,
The University of Hong Kong, Hong Kong SAR,
China
Jennifer Mancio,
Guy's and St Thomas' NHS Foundation Trust,
United Kingdom

*CORRESPONDENCE

I-Min Chiu
✉ ray1985@cgmh.org.tw;
✉ outofray@hotmail.com

[†]These authors have contributed equally
to this work

RECEIVED 28 March 2023

ACCEPTED 13 July 2023

PUBLISHED 04 August 2023

CITATION

Cheng C-Y, Wu C-C, Chen H-C, Hung C-H,
Chen T-Y, Lin C-HR and Chiu I-M (2023)
Development and validation of a deep learning
pipeline to measure pericardial effusion in
echocardiography.
Front. Cardiovasc. Med. 10:1195235.
doi: 10.3389/fcvm.2023.1195235

COPYRIGHT

© 2023 Cheng, Wu, Chen, Hung, Chen, Lin and
Chiu. This is an open-access article distributed
under the terms of the [Creative Commons
Attribution License \(CC BY\)](#). The use,
distribution or reproduction in other forums is
permitted, provided the original author(s) and
the copyright owner(s) are credited and that the
original publication in this journal is cited, in
accordance with accepted academic practice.
No use, distribution or reproduction is
permitted which does not comply with these
terms.

Development and validation of a deep learning pipeline to measure pericardial effusion in echocardiography

Chi-Yung Cheng^{1,2†}, Cheng-Ching Wu^{3,4,5†}, Huang-Chung Chen⁶,
Chun-Hui Hung⁷, Tien-Yu Chen⁶, Chun-Hung Richard Lin¹ and
I-Min Chiu^{1,2*}

¹Department of Computer Science and Engineering, National Sun Yat-sen University, Kaohsiung, Taiwan,

²Department of Emergency Medicine, Kaohsiung Chang Gung Memorial Hospital, Kaohsiung, Taiwan,

³School of Medicine, College of Medicine, I-Shou University, Kaohsiung, Taiwan, ⁴Division of Cardiology,
Department of Internal Medicine, E-Da Hospital, I-Shou University, Kaohsiung, Taiwan, ⁵Division of
Cardiology, Department of Internal Medicine, E-Da Cancer Hospital, I-Shou University, Kaohsiung,
Taiwan, ⁶Division of Cardiology, Department of Internal Medicine, Kaohsiung Chang Gung Memorial
Hospital, Kaohsiung, Taiwan, ⁷Skysource Technologies Co., Ltd., Taipei, Taiwan

Objectives: The aim of this study was to develop a deep-learning pipeline for the measurement of pericardial effusion (PE) based on raw echocardiography clips, as current methods for PE measurement can be operator-dependent and present challenges in certain situations.

Methods: The proposed pipeline consisted of three distinct steps: moving window view selection (MWVS), automated segmentation, and width calculation from a segmented mask. The MWVS model utilized the ResNet architecture to classify each frame of the extracted raw echocardiography files into selected view types. The automated segmentation step then generated a mask for the PE area from the extracted echocardiography clip, and a computer vision technique was used to calculate the largest width of the PE from the segmented mask. The pipeline was applied to a total of 995 echocardiographic examinations.

Results: The proposed deep-learning pipeline exhibited high performance, as evidenced by intraclass correlation coefficient (ICC) values of 0.867 for internal validation and 0.801 for external validation. The pipeline demonstrated a high level of accuracy in detecting PE, with an area under the receiving operating characteristic curve (AUC) of 0.926 (95% CI: 0.902–0.951) for internal validation and 0.842 (95% CI: 0.794–0.889) for external validation.

Conclusion: The machine-learning pipeline developed in this study can automatically calculate the width of PE from raw ultrasound clips. The novel concepts of moving window view selection for image quality control and computer vision techniques for maximal PE width calculation seem useful in the field of ultrasound. This pipeline could potentially provide a standardized and objective approach to the measurement of PE, reducing operator-dependency and improving accuracy.

KEYWORDS

echocardiography, deep learning—artificial intelligence, pericardial effusion (PE), width measurements, automated segmentation, moving window (MW)

Abbreviations

A4C, apical four-chamber; AI, artificial intelligence; AUC, area under the receiver operating characteristics curve; CGMH, Chang Gung Memorial Hospital; CNN, convolutional neural network; DICOM, Digital Imaging and Communications in Medicine; EDH, E-Da Hospital; GPU, graphics processing unit; ICC, intraclass correlation coefficient; MWVS, moving window view selection; PE, pericardial effusion; PLAX, parasternal long-axis; PSAX, parasternal short-axis; SC, subcostal.

Introduction

Pericardial effusion (PE) is a condition characterized by the accumulation of fluid within the pericardial space, which is typically diagnosed using transthoracic echocardiography. The buildup of fluid increases pressure within the pericardial sac, potentially leading to cardiac tamponade and decreased cardiac output. PE is a serious condition that requires timely intervention, making early detection and accurate measurement of the width of the effusion critical (1).

Echocardiography is considered the gold standard for the detection of PE due to its accessibility, portability, and ability to provide a comprehensive assessment of both anatomy and function (2–5). However, the presence and severity of PE can be uncertain, with mild effusion sometimes indicating pericardial fat rather than true effusion (6). Additionally, image quality can be compromised by factors such as breast tissue or obscuration from bone or lung. These challenges highlight the need for an accurate and reliable method for measuring PE that is not dependent on operator experience.

Artificial intelligence (AI) has been applied in various clinical settings to aid in the diagnosis of conditions based on echocardiograms, with considerable effort devoted to areas such as left ventricular function assessment, regional wall motion abnormality, right ventricular function, valvular heart disease, cardiomyopathy, and intracardiac mass (7–10). In particular, a study conducted in 2020 employed a deep learning model to detect PE in echocardiography and achieved an accuracy of 0.87–0.9 (11). In clinical practice, information on PE width and severity is crucial for initiating appropriate interventions. To the best of our knowledge, no study has yet analyzed the grading of PE using machine learning. Therefore, our study aimed to develop a deep learning model using echocardiography for PE detection and PE width measurement. Additionally, to facilitate the deployment of the deep learning model, we proposed an end-to-end guideline that can output detection results from raw ultrasound files.

Method

The data collection and protocols utilized in this study were authorized by the Institutional Review Board of E-Da Hospital (EDH; no: EMRP24110N) and the Institutional Review Board of Kaohsiung Chang Gung Memorial Hospital (CGMH; no: 20211889B0 and 202101662B0).

Data collection

In this study, images from routine echocardiography were generated at two medical centers, EDH and CGMH, in southern Taiwan. The deep learning model was trained and internally validated in EDH and externally validated in CGMH.

During the data collection process, we utilized the keyword “pericardial effusion” to search the Hybrid Picture Report System

in EDH in order to gather a list of examination records. We obtained raw data from transthoracic echocardiography examinations with a diagnosis of pericardial effusion, which were performed at EDH between January 1, 2010, and June 30, 2020. These data were divided into training and validation datasets based on the respective examination dates. Examinations with dates prior to December 31, 2018, were used for the development of the model, and examinations with dates after January 1, 2019, were used for internal validation. To evaluate the generalizability of the model, we also retrieved echocardiography data from CGMH between January 1, 2019, and June 30, 2020, for external validation. The study flowchart and data summary are presented in **Figure 1**.

Echocardiography

Images were gathered in a normal manner, with patients lying in the left lateral decubitus position. The ultrasound system (IE33, Philips Healthcare; S70, GE Healthcare; or SC2000, Siemens Healthineers) was used to perform echocardiographic examinations in EDH. Data from CGMH for external validation were acquired using EPIC7 (Philips Healthcare), Vivid E9 (GE Healthcare), or SC2000 (Siemens Healthineers). All examinations were saved in picture archiving and communication systems in the Digital Imaging and Communications in Medicine (DICOM) format.

After extracting the raw DICOM files, we processed the image from each patient to select the proper echocardiography views for developing a deep learning pipeline. The selected views were the parasternal long-axis (PLAX), parasternal short-axis (PSAX), apical four-chamber (A4C), and subcostal (SC) views. Two cardiologists manually measured the thickest point of pericardial effusion during each cardiac cycle as ground truth for width of PE. We employed ImageJ, an open-source software platform specifically designed for the scientific analysis and processing of images, to label and annotate the segmented masks corresponding to the echocardiography images. Upon completing the labeling process, the data was subsequently stored as CSV files on a secure, encrypted hard drive to ensure data integrity and confidentiality.

Deep learning model development

In this study, we developed an end-to-end pipeline for the automated measurement of PE based on the steps outlined below (**Figure 2**). The training subset of videos from EDH was used for the three main tasks of our pipeline:

Step one: moving window view selection (MWVS)

We proposed a pipeline for managing echocardiography files directly from the workstation, similar to the work done by Zhang

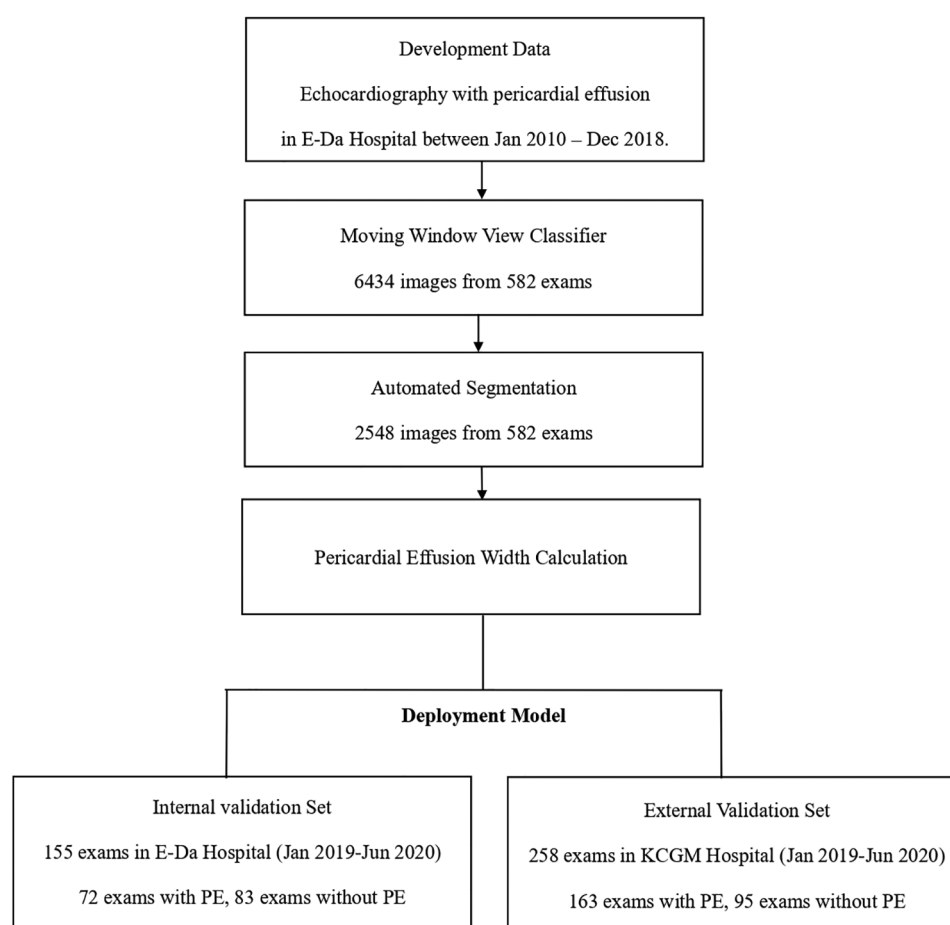


FIGURE 1
Flow chart illustrating the study design and data summary.

et al. and Huang et al., with some adjustments (Figure 2A) (10, 12). To distinguish the four primary views (PLAX, PSAX, A4C, and SC) from other views during each examination, we developed the first deep neural network model. This model was a ResNet-50-based two-dimensional model that aimed to classify each frame from the extracted DICOM files of echocardiography into the selected view types (13). To train this model, we randomly selected 6,434 images from the training dataset of EDH and labeled them according to the four primary views or other views, including low-quality views. We trained the model with a data split of 80% for the training set and 20% for the validation set. The model weight with the best detection performance in the validation set during the training process was preserved. The detection accuracy was assessed for each view class and weighted average result.

In order to effectively manage the input video from patients during data collection, a 48-frame moving window was utilized to filter all videos. For each video, the best 48 frames with regard to specific view type and image quality were selected using a majority voting method (Figure 3). This process, known as MWVS concept, served not only as a view classifier but also as a quality control measure. Videos that did not contain at least 48 consecutive frames that met the image quality criteria of 50% or

higher from one of the four primary views were excluded from further analysis. Additionally, the average view-classifying confidence levels for all images obtained from the selected 48-frame clip were used to evaluate the overall image quality and its correlation with performance. Videos with an average confidence level of less than 0.8 were also excluded from automated segmentation.

Step two: automated segmentation

From the dataset, we randomly selected and annotated 2,548 frames in the EDH training dataset, ensuring an even distribution across the four primary views. We manually labeled the segmented area for pericardial effusion (PE) at three different phases in the cardiac cycle: end-systolic, end-diastolic, and the middle phase between the two aforementioned phases. The differentiation between epicardial adipose tissue and pericardial fluid was established. During this labeling phase, experienced clinicians manually segmented the area of PE based on its characteristic appearances in ultrasound images, while explicitly excluding epicardial adipose tissue. Additionally, we labeled the segmented areas for the four cardiac chambers to

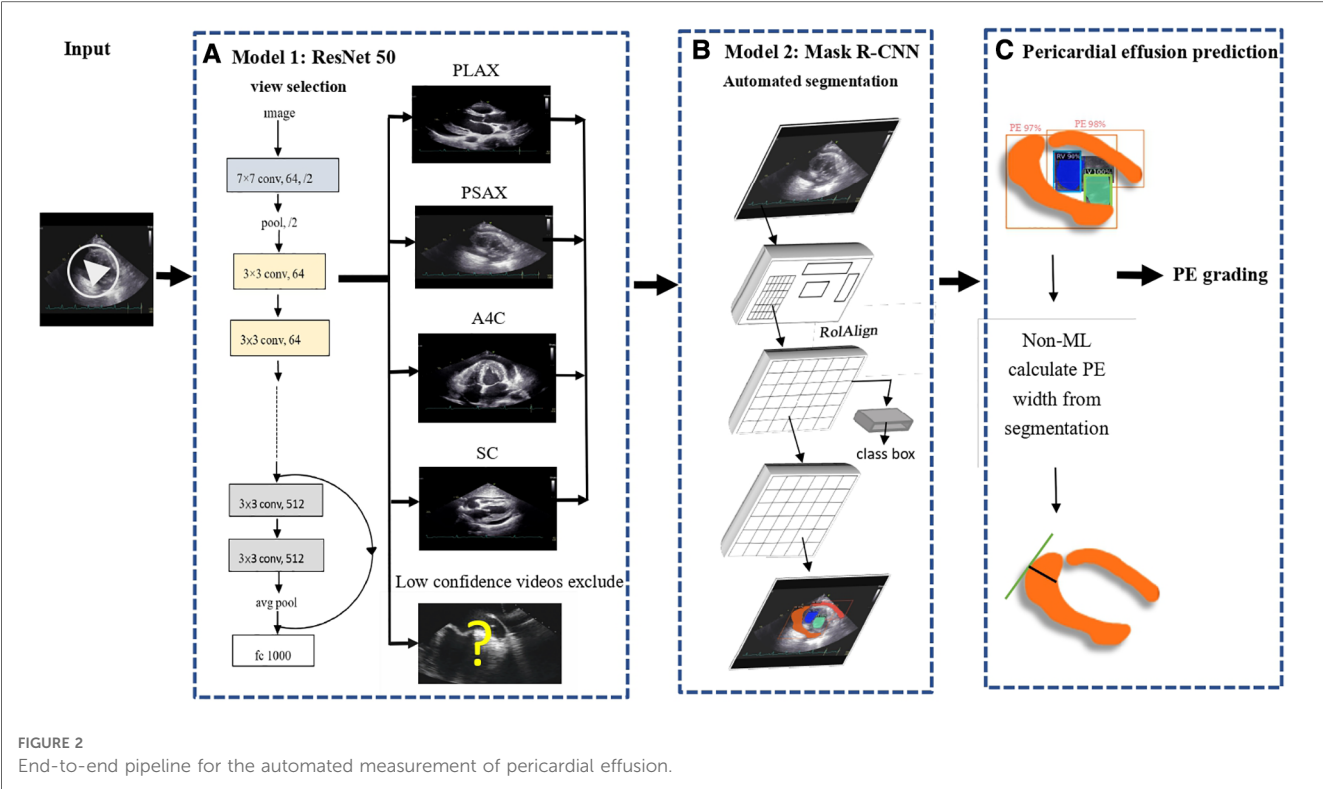


FIGURE 2
End-to-end pipeline for the automated measurement of pericardial effusion.

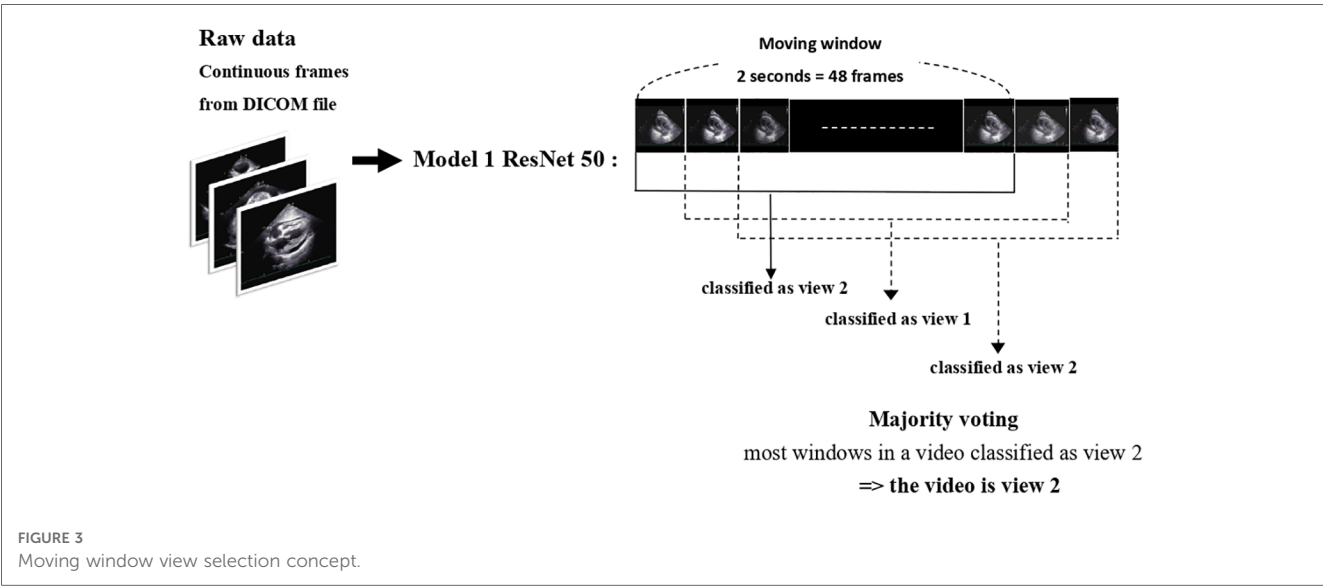


FIGURE 3
Moving window view selection concept.

enhance the model's performance in separating these fluid-containing areas.

To train object instance segmentation based on the labeled ground truth, we utilized a Mask Region-Convolutional Neural Network (R-CNN) framework (Figure 2B). The model was trained with a data split of 80% for the training set and 20% for the validation set. Mask R-CNN is commonly used in medical applications for instance segmentation tasks as it can simultaneously perform pixel-level segmentation and classification of multiple target lesions (14). The implemented model generates bounding boxes and targeting masks for each instance of an object

in an image. The input comprised consecutive ultrasound frames, and the output was a segmented mask indicating the corresponding four cardiac chambers and PE. The accuracy of the segmentation model was assessed using the Dice coefficient metric.

Step three: measurement of pericardial effusion

After generating a segmented mask for pericardial effusion (PE), we proposed a computer vision technique, known as the

maximal width calculator, to calculate the largest width of the PE in each ultrasound frame (**Figure 2C**). To accomplish this, we iterated through the vertical axis in each frame and hypothetically drew a horizontal line to determine if there was an intersection between the segmented mask and the horizontal line. If an intersection existed, we obtained a normal line from the edge of the mask over the intersection point. The length of the normal line that passed through the segmented mask was counted as the width of the PE at that intersection point. The largest width of the PE obtained through the iteration over the vertical axis was regarded as the width of the PE of the frame. This technique was applied to all 48 frames in the ultrasound video to provide the optimal PE width. Detailed explanation of this process was demonstrated in **Supplementary Appendix 1**.

Statistical analysis

In this study, continuous variables are presented as either the mean and standard deviation if they are normally distributed or as the median and interquartile range if they are not. Dichotomous data are presented as numbers and percentages. The chi-squared test was used to analyze categorical variables, while continuous variables were analyzed using either the independent-sample *t*-test if they were normally distributed or the Mann-Whitney *U* test if they were not.

The performance of the proposed pipeline for PE width measurement was evaluated using metrics such as the mean absolute error, intraclass correlation coefficient, and R-square value when comparing the ground truth and detection. Additionally, the detection of the existence of PE and moderate PE was evaluated using sensitivity, specificity, and the area under the receiver operating characteristic curve. The deep learning models in the pipeline were developed using the TensorFlow Python package, image manipulation was performed using OpenCV 3.0 and scikit-image, and all analyses were conducted using SPSS for MAC version 26.

Results

In this study, a total of 995 echocardiographic examinations were analyzed. Of these, 737 examinations were from the EDH dataset, with 582 being utilized for training and 155 for internal validation. Additionally, 258 examinations from the CGMH dataset were included for external validation. However, due to the limited number of SC views present in the CGMH dataset, this view was not included in the external validation analysis.

The demographic and clinical characteristics of the patients who underwent echocardiography are presented in **Table 1**. The mean age of patients in the training, internal validation, and external validation sets were 67.4 ± 15.4 , 59.8 ± 19.2 , and 66.4 ± 16.1 years, respectively. Additionally, 46.5% and 63.2% of patients in the internal and external validation groups, respectively, had PE. The average ejection fraction was $64.3 \pm$

TABLE 1 Demographics, basic characteristics, and clinical findings of the patients.

Variables	Training set	Internal Validation set	External Validation set
Number of patients	582	155	258
Age(y)	67.4 ± 15.4	59.8 ± 19.2	66.4 ± 16.1
Gender	Male 49.5%	Male 53.2%	Male 58.1%
Height, cm	157.9 ± 9.2	162.1 ± 8.4	161.6 ± 8.4
Weight, kg	53.7 ± 35.6	65.9 ± 16.8	61.8 ± 13.3
BMI, kg/m ²	23.3 ± 5.2	24.4 ± 1.5	23.6 ± 4.5
Mode EF %	61.1 ± 13.8	64.3 ± 7.1	61 ± 13.9
Mode EF < 50 (%)	12.8%	8.4%	19.3%
Patients with PE	582 (100%)	72 (46.5%)	163 (63.2)

7.1% in the internal validation group and $61 \pm 13.9\%$ in external validation group.

The performance of the view classifier was evaluated with an average accuracy of 0.91 and 0.87 in predicting image classes in the training and validation sets, respectively. The independent accuracy in the validation set for each class was 0.90, 0.87, 0.93, 0.76, and 0.88 for PLAX, PSAX, A4C, SC, and others, respectively.

The MWVS was used to select the right views from all DICOM files in one examination and to improve video quality. The results of MWVS showed that 80%–100% of the four selected ultrasound views in EDH were successfully passed through for the segmentation model. In the external validation (CGMH dataset), 686 ultrasound videos from the four selected views were obtained. Our MWVS scanned through all DICOM files and 365 (53.2%) ultrasound videos were preserved for segmentation inference. The videos selected by our pipeline were further checked by a cardiologist, and none of them were misclassified as other cardiac views.

We employed a mask R-CNN-based model for image segmentation to effectively localize the cardiac chambers and PE area within four different views (**Figure 4**). The validation set, consisting of 510 images, showed an average Dice coefficient ranging from 0.67 to 0.82 among the four views, with the short-axis view (SC) achieving the lowest result. The best Dice coefficient was observed in the parasternal long-axis view (PLAX) at 0.72, while the SC view had the poorest result of 0.56 (**Table 2**). Using the segmented PE area, we calculated the maximal PE width from each frame.

Figure 5 illustrates the scatter plot of the PE width measurement between the ground truth and model detection, which was determined by finding the largest normal line passing through the segmented mask in each frame. We compared the automated and manual measurements of PE width in both the internal (EDH) and external (CGMH) validation datasets, reporting the mean absolute error and correlation between the two. The mean absolute error was 0.33 cm and 0.35 cm in the internal and external datasets, respectively. Additionally, the interobserver variability was found to be highly correlated for the measurement of PE width between our model and human expert (ICC = 0.867, $p < 0.001$, EDH; ICC = 0.801, $p < 0.001$, CGMH). The R-square value was 0.594 for the EDH dataset and 0.488 for the CGMH validation dataset.

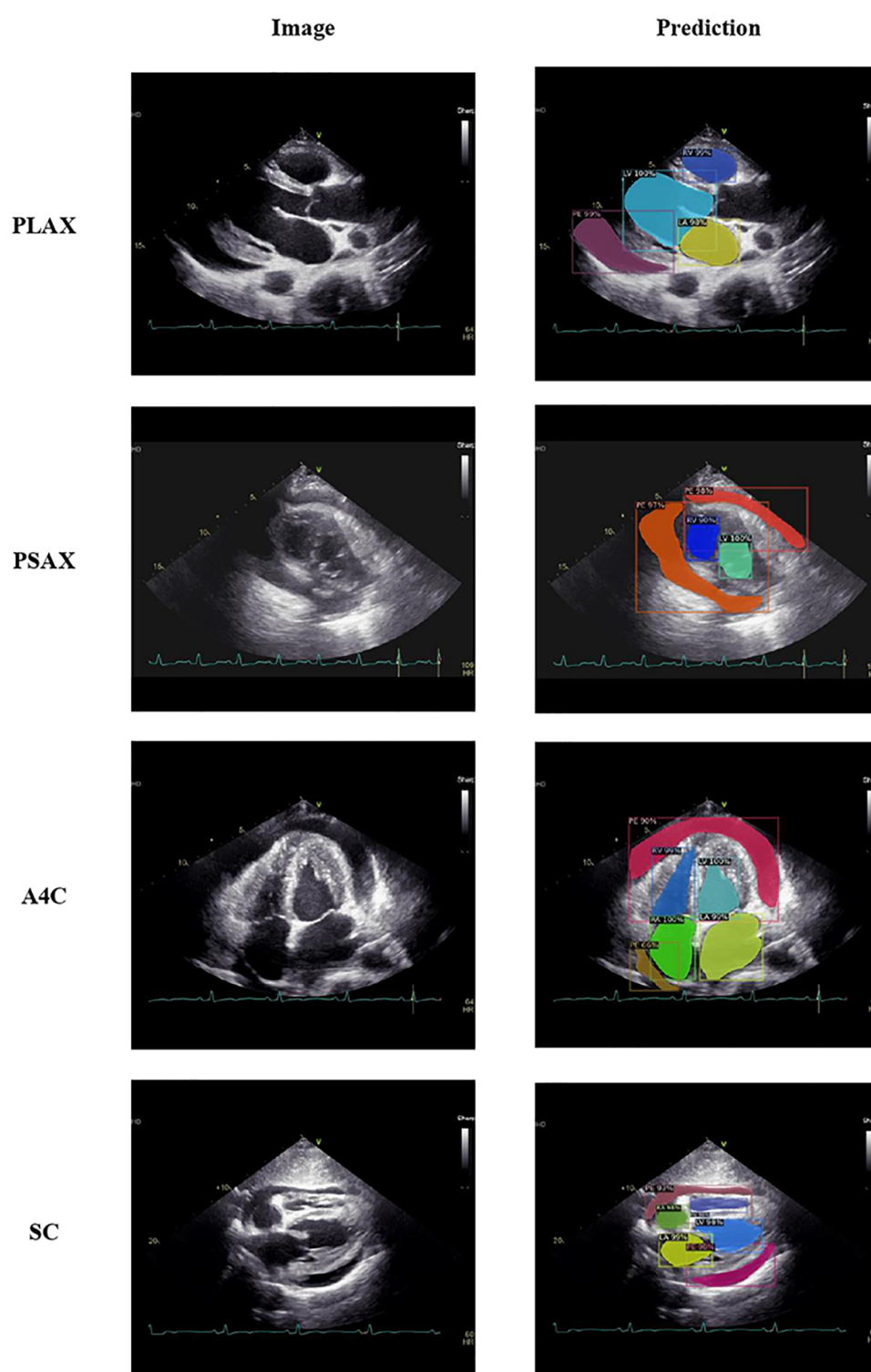


FIGURE 4
Image segmentation over cardiac chambers and pericardial effusion.

Our model accurately detected the existence of PE in the internal validation [AUC = 0.926 (0.902–0.951)] and external validation [AUC = 0.842 (0.794–0.889)]. With regard to recognizing moderate PE or worse, the AUC values improved to

0.941 (0.923–0.960) and 0.907 (0.876–0.943) in the internal and external validation groups, respectively.

We further performed a stratified analysis of the model detection in the different echocardiography views. In the internal

TABLE 2 Dice coefficient of image segmentation.

	Dice coefficient					
	PE	RV	LV	RA	LA	Average
PLAX	0.72	0.86	0.85		0.84	0.82
PSAX	0.69	0.59	0.85			0.71
A4C	0.58	0.81	0.86	0.82	0.83	0.78
SC	0.56	0.66	0.71	0.70	0.72	0.67

validation, the model detection of PE width was highly correlated with the ground truth in the four different views, with ICC ranging from 0.802–0.910. The PLAX and A4C views appeared to have the best detection results with ICCs of 0.910 (0.876–0.935) and 0.907 (0.871–0.932), respectively. In the external validation, similar to internal validation, the model performed better in the PLAX and A4C views, with ICCs of 0.807 (0.726–0.864) and 0.897 (0.846–0.931), respectively. The other performances are listed in **Table 3**.

Discussion

In recent years, computer vision and deep learning techniques have been utilized to aid in the interpretation of echocardiography, estimate cardiac function, and identify local cardiac structures. Deep learning algorithms have also been applied to facilitate the diagnosis of PE (15). Nayak et al. developed a CNN that detected PE in the apical four-chamber (A4C) and short-axis (SC) views with accuracies of 91% and 87%, respectively (11). In this study, we propose a deep learning pipeline that can process raw DICOM files from ultrasound and predict the PE width in a clinical setting. This pipeline combines two deep learning models and one technical calculation algorithm to accurately predict PE width. There have been few efforts to predict PE existence, with some studies being based on computed tomography scans (16, 17). To the best of our knowledge, this is the first video-based machine learning model to measure PE width using

echocardiography. The correlation between the measurement of our model and human experts was high in both the internal and external validation datasets, with the best performance observed in the parasternal long-axis (PLAX) view. The inference speed of our model, using one graphics processing unit (NVIDIA RTX 3090), was approximately 30–40 s for one examination, which is usually faster than human assessment.

The present study introduces two novel concepts for echocardiography analysis: the MWVS and the maximal width calculator of the segmented mask. These methods are particularly important for real-world applications, particularly when working with relatively smaller datasets. Previous studies often rely on datasets manually selected by human experts during dataset cleaning, and use only “textbook-quality” images for training (18–21). In contrast, the present study proposes an analytical pipeline that can automatically analyze echocardiograms and be easily applied to personal devices or web applications, thus eliminating the need for expert sonographers or cardiologists. Madani et al. developed a CNN that simultaneously classified 15 standard echocardiogram views acquired under a range of real-world clinical variations, and the model demonstrated high accuracy for view classification (21). Similarly, this study used echocardiogram video clips obtained from the real world, taken for a variety of clinical purposes, including ejection fraction calculation, and detecting PE, valve disease, regional wall abnormality, cardiomyopathy, and pulmonary arterial hypertension. An initial screening model for view classification and quality control was developed. All raw images from the medical image database were input into the screening model, leaving a specific view of sufficient quality for diagnosis. Additionally, the “moving window” concept was used to retrieve only clips with 48 consecutive frames that fulfilled the image quality criteria. By avoiding limited or idealized training datasets, it is believed that this model is broadly applicable to clinical practice.

The method of MWVS is a novel concept that has not yet been proposed in the field of echocardiography assisted by machine

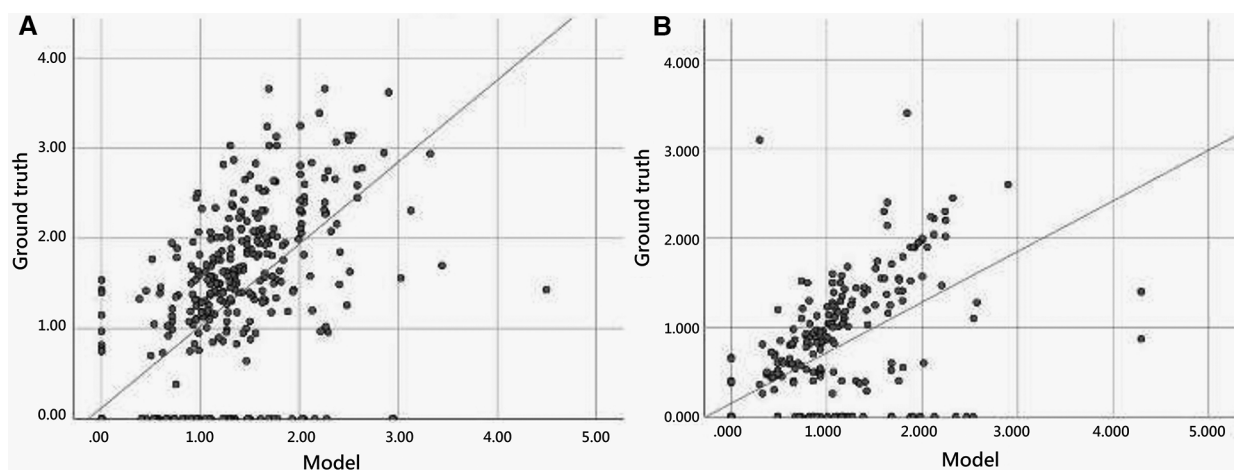


FIGURE 5
Scatter plot of pericardial effusion width measurement between model and manual annotation.

TABLE 3 Stratified analysis of the model detection in the different echocardiography views.

	Number before view selection	Number after moving window selection	Mean Absolute Error (cm)	ICC	R2
Internal validation					
PLAX	<i>n</i> = 155	<i>n</i> = 146	0.28	0.910 (0.876–0.935)	0.700
PSAX	<i>n</i> = 155	<i>n</i> = 155	0.46	0.802 (0.728–0.856)	0.469
A4C	<i>n</i> = 155	<i>n</i> = 155	0.32	0.907 (0.871–0.932)	0.754
SC	<i>n</i> = 155	<i>n</i> = 124	0.40	0.865 (0.808–0.905)	0.590
External validation					
PLAX	222	<i>n</i> = 127	0.32	0.807 (0.726–0.864)	0.457
PSAX	252	<i>n</i> = 138	0.44	0.714 (0.600–0.796)	0.337
A4C	212	<i>n</i> = 100	0.11	0.897 (0.846–0.931)	0.662

learning. MWVS serves as an image quality filter and plays a crucial role in ensuring that the images are of sufficient quality for the next step in the pipeline. In the EDH dataset, echocardiography is performed by well-trained technicians who adhere to a protocol established by the echocardiologist consensus committee. As such, the original images from EDH were of relatively homogeneous quality, and MWVS filtered out fewer patients. Conversely, at CGMH, echocardiography is performed by individual echocardiologists who may have varying techniques. As a result, the original images from CGMH were less homogeneous, and MWVS filtered out more patients. This finding highlights the significance of MWVS in maintaining image quality and highlights the importance of image homogeneity in the applicability of machine learning models.

After segmenting the PE area, we developed a novel computer vision-based technique to calculate the largest PE width in ultrasound video. The current categorization of PE size relies on linear measurements of the largest width of the effusion at end-diastole, and is graded as small (<1 cm), moderate (1–2 cm), or large (>2 cm) (22). This semiquantitative classification method is prone to errors due to asymmetric, loculated effusions and shifts in fluid location during the cardiac cycle (23). Therefore, an automated calculation system could help identify the largest width of the PE in every ultrasound frame without any errors. In comparison to AI-based models, the computer vision technique is more similar to the method used by human experts. AI-based models not only consume more computing resources, but also require a large number of datasets for training and validation. To the best of our knowledge, our study is the first to not only detect but also classify the grade of PE.

Our model's ability to automate the process of classifying PE severity, traditionally categorized as mild, moderate, or severe, signifies a meaningful advancement in this field. Although this may appear straightforward for experienced clinicians, automated segmentation and measurement can be invaluable, especially in contexts where echocardiography expertise may be limited or entirely absent. Importantly, even though our model does not currently provide prediction on hemodynamic instability such as cardiac tamponade, its ability to differentiate moderate to severe PE from none or mild is crucial. This feature allows for early risk stratification in patients, prompting clinicians to initiate appropriate assessments and interventions as early as possible.

Moreover, our work lays the groundwork for the future development of models designed to predict complex clinical scenarios, such as early hemodynamic instability. The integration of our model's segmentation and classification capabilities with other clinically relevant parameters may, in time, lead to major advancements in the prediction and management of such conditions.

This study had certain limitations that should be considered when interpreting the results. Firstly, the study was conducted retrospectively and the model was trained using data from only one hospital. This resulted in a limited sample size and a lack of ethnic diversity, which may impact the generalizability of the findings to other populations. To address this, future studies should utilize a multicenter design with greater heterogeneity in the dataset. However, it is important to note that the images used in this study were obtained using different ultrasonography machines and were interpreted by multiple echocardiographers, and the model achieved similar results during external validation. Secondly, while the proposed pipeline did grade the amount of PE, there was no information on whether there were signs of cardiac tamponade, as PE volume does not necessarily correlate with clinical symptoms (24). Additionally, due to the small sample size, we were unable to conduct subgroup analysis to distinguish the algorithm's performance on transudative vs. exudative effusions. To increase the clinical applicability of the findings, larger studies and validation cohorts are needed to reproduce the results of this study. Further research should also evaluate the collapsibility of the cardiac chambers and the presence of tamponade signs.

Conclusion

In this study, we developed a deep-learning pipeline that automatically calculates the width of the PE from raw ultrasound clips. The model demonstrated high accuracy in detecting PE and classifying the PE width in both internal and external validation. The use of a novel concept, known as MWVS, for image quality filtering and computer vision techniques for calculating the maximal PE width is a novel application in the field of echocardiography.

Data availability statement

The raw data supporting the conclusions of this article will be made available by the authors, without undue reservation.

Ethics statement

This study was authorized by the Institutional Review Board of E-Da Hospital (EDH; no: EMRP24110N) and the Institutional Review Board of Kaohsiung Chang Gung Memorial Hospital (CGMH; no: 20211889B0 and 202101662B0). Written informed consent for participation was not required for this study in accordance with the national legislation and the institutional requirements.

Author contributions

C-YC and C-CW drafted the manuscript and the figures. H-CC and T-YC collected and labeled the data. C-HH built and validated the model. I-MC designed the study flowchart and supervised the study. C-HRL revised the manuscript. All authors contributed to the article and approved the submitted version.

Funding

The study was supported by grants EDCHM109001 and EDCHP110001 from E-Da Cancer Hospital and grant CMRPG8M0181 from the Chang Gung Medical Foundation.

References

- Jung HO. Pericardial effusion and pericardiocentesis: role of echocardiography. *Korean Circ J*. (2012) 42:725–34. doi: 10.4070/kcj.2012.42.11.725
- Ceriani E, Cogliati C. Update on bedside ultrasound diagnosis of pericardial effusion. *Intern Emerg Med*. (2016) 11:477–80. doi: 10.1007/s11739-015-1372-8
- Vakamudi S, Ho N, Cremer PC. Pericardial effusions: causes, diagnosis, and management. *Prog Cardiovasc Dis*. (2017) 59:380–8. doi: 10.1016/j.pcad.2016.12.009
- Malik SB, Chen N, Parker RA III, Hsu JY. Transthoracic echocardiography: pitfalls and limitations as delineated at cardiac CT and MR imaging. *Radiographics*. (2017);37:383–406. doi: 10.1148/rg.2017160105
- Sampaio F, Ribeiros R, Galrinho A, Teixeira R, João I, Trabulo M, et al. Consensus document on transthoracic echocardiography in Portugal. *Rev Port Cardiol (Engl Ed)*. (2018) 37:637–44. doi: 10.1016/j.repc.2018.05.009
- Sagrà-Sauleda J, Mercé AS, Soler-Soler J. Diagnosis and management of pericardial effusion. *World J Cardiol*. (2011) 3(5):135. doi: 10.4330/wjc.v3.i5.135
- de Siqueira VS, Borges MM, Furtado RG, Dourado CN, da Costa RM. Artificial intelligence applied to support medical decisions for the automatic analysis of echocardiogram images: a systematic review. *Artif Intell Med*. (2021) 120:102165. doi: 10.1016/j.artmed.2021.102165
- Zhou J, Du M, Chang S, Chen Z. Artificial intelligence in echocardiography: detection, functional evaluation, and disease diagnosis. *Cardiovasc Ultrasound*. (2021) 19:1–11. doi: 10.1136/heartjnl-2021-319725
- Ouyang D, He B, Ghorbani A, Yuan N, Ebinger J, Langlotz CP, et al. Video-based AI for beat-to-beat assessment of cardiac function. *Nature*. (2020) 580:252–6. doi: 10.1038/s41586-020-2145-8
- Huang M-S, Wang C-S, Chiang J-H, Liu P-Y, Tsai W-C. Automated recognition of regional wall motion abnormalities through deep neural network interpretation of transthoracic echocardiography. *Circulation*. (2020) 142:1510–20. doi: 10.1161/CIRCULATIONAHA.120.047530
- Nayak A, Ouyang D, Ashley EA. A deep learning algorithm accurately detects pericardial effusion on echocardiography. *J Am Coll Cardiol*. (2020) 75 (11_Supplement_1):1563–1563. doi: 10.1016/S0735-1097(20)32190-2
- Zhang J, Gajjala S, Agrawal P, Tison GH, Hallock LA, Beussink-Nelson L, et al. Fully automated echocardiogram interpretation in clinical practice: feasibility and diagnostic accuracy. *Circulation*. (2018) 138:1623–35. doi: 10.1161/CIRCULATIONAHA.118.034338
- He K, Zhang X, Ren S, Sun J. *Deep residual learning for image recognition. Paper presented at: proceedings of the IEEE conference on computer vision and pattern recognition* (2016). doi: 10.48550/arXiv.1512.03385
- He K, Gkioxari G, Dollár P, Mask r-cnn GR. *Paper presented at: proceedings of the IEEE international conference on computer vision* (2017).
- Ghorbani A, Ouyang D, Abid A, He B, Chen JH, Harrington RA, et al. Deep learning interpretation of echocardiograms. *NPJ digital Medicine*. (2020) 3:1–10. doi: 10.1038/s41746-019-0216-8
- Ebert LC, Heimer J, Schweitzer W, Sieberth T, Leipner A, Thali M, et al. Automatic detection of hemorrhagic pericardial effusion on PMCT using deep learning—a feasibility study. *Forensic Sc Med Pathol*. (2017) 13:426–31. doi: 10.1007/s12024-017-9906-1
- Draeos RL, Dov D, Mazurowski MA, Lo JY, Henao R, Rubin GD, et al. Machine-learning-based multiple abnormality prediction with large-scale chest

Acknowledgments

We thank the Biostatistics Center, Kaohsiung Chang Gung Memorial Hospital for statistics work.

Conflict of interest

C-HH was employed by Skysource Technologies Co., Ltd.

The remaining authors declare that the research was conducted in the absence of any commercial or financial relationships that could be construed as a potential conflict of interest.

Publisher's note

All claims expressed in this article are solely those of the authors and do not necessarily represent those of their affiliated organizations, or those of the publisher, the editors and the reviewers. Any product that may be evaluated in this article, or claim that may be made by its manufacturer, is not guaranteed or endorsed by the publisher.

Supplementary material

The Supplementary Material for this article can be found online at <https://www.frontiersin.org/articles/10.3389/fcvm.2023.1195235/full#supplementary-material>

computed tomography volumes. *Med Image Anal.* (2021) 67:101857. doi: 10.1016/j.media.2020.101857

18. Khamis H, Zurakhov G, Azar V, Raz A, Friedman Z, Adam D. Automatic apical view classification of echocardiograms using a discriminative learning dictionary. *Med Image Anal.* (2017) 36:15–21. doi: 10.1016/j.media.2016.10.007

19. Sengupta PP, Huang YM, Bansal M, Ashrafi A, Fisher M, Shameer K, et al. Cognitive machine-learning algorithm for cardiac imaging: a pilot study for differentiating constrictive pericarditis from restrictive cardiomyopathy. *Circulation.* (2016) 9:e004330. doi: 10.1161/CIRCIMAGING.115.004330

20. Gao X, Li W, Loomes M, Wang L. A fused deep learning architecture for viewpoint classification of echocardiography. *Info Fusion.* (2017) 36:103–13. doi: 10.1016/j.inffus.2016.11.007

21. Madani A, Arnaout R, Mofrad M, Arnaout R. Fast and accurate view classification of echocardiograms using deep learning. *NPJ Digit Med.* (2018) 1:1–8. doi: 10.1038/s41746-017-0013-1

22. Karia DH, Xing Y-Q, Kuvin JT, Nesser HJ, Pandian NG. Recent role of imaging in the diagnosis of pericardial disease. *Curr Cardiol Rep.* (2002) 4:33–40. doi: 10.1007/s11886-002-0124-3. PMID: 11743920

23. Prakash AM, Sun Y, Chiaramida SA, Wu J, Lucariello RJ. Quantitative assessment of pericardial effusion volume by two-dimensional echocardiography. *J Am Soc Echocardiogr.* (2003) 16:147–53. doi: 10.1067/mje.2003.35

24. Pérez-Casares A, Cesar S, Brunet-Garcia L, Sanchez-de-Toledo J. Echocardiographic evaluation of pericardial effusion and cardiac tamponade. *Front Pediatr.* (2017) 5:79. doi: 10.3389/fped.2017.00079



OPEN ACCESS

EDITED BY

Sanjeev Bhattacharyya,
Barts Heart Centre, United Kingdom

REVIEWED BY

Jennifer Mancio,
Guy's and St Thomas' NHS Foundation Trust,
United Kingdom
Diana Ruxandra Florescu,
Spitalul Clinic Judetean de Urgenta Craiova,
Romania

*CORRESPONDENCE

Yubin Deng
✉ ybdeng2007@hotmail.com

RECEIVED 19 April 2023

ACCEPTED 21 July 2023

PUBLISHED 10 August 2023

CITATION

Lu S, Liu H, Sun J, Zhang J, Li L, Tang Q, Liu Y
and Deng Y (2023) Evaluation of left atrial and
ventricular remodeling in atrial fibrillation
subtype by using speckle tracking
echocardiography.
Front. Cardiovasc. Med. 10:1208577.
doi: 10.3389/fcvm.2023.1208577

COPYRIGHT

© 2023 Lu, Liu, Sun, Zhang, Li, Tang, Liu and
Deng. This is an open-access article distributed
under the terms of the [Creative Commons
Attribution License \(CC BY\)](#). The use,
distribution or reproduction in other forums is
permitted, provided the original author(s) and
the copyright owner(s) are credited and that the
original publication in this journal is cited, in
accordance with accepted academic practice.
No use, distribution or reproduction is
permitted which does not comply with these
terms.

Evaluation of left atrial and ventricular remodeling in atrial fibrillation subtype by using speckle tracking echocardiography

Shirui Lu, Hongyun Liu, Jie Sun, Jun Zhang, Li Li, Qiaoying Tang,
Yani Liu and Youbin Deng*

Department of Medical Ultrasound, Tongji Hospital, Tongji Medical College, Huazhong University of
Science and Technology, Wuhan, China

Background: Atrial fibrillation (AF) is associated with cardiac structural and functional remodeling. We investigated the left atrial (LA) and left ventricular (LV) changes in AF subtypes by using two-dimensional echocardiography strain techniques.

Methods: The study population consisted of 102 subjects with sinus rhythm (control group) and 463 patients with AF, among which 284 patients had paroxysmal AF (PAF) and 179 patients had persistent AF (PerAF). A speckle tracking automatic functional imaging software was used to perform the strain analysis.

Results: Patients with AF had dilated LA maximum and minimum volume, decreased LA reservoir strain, lower LV ejection fraction (LVEF), and impaired global longitudinal strain (GLS) compared to those of the sinus rhythm control group. In patients with PerAF, the LA maximum and minimum volumes were larger, and the LA reservoir strain [PAF vs. PerAF, 28% (21,33) vs. 19% (14, 28), $P < 0.05$], LVEF, and absolute GLS value [PAF vs. PerAF, -16.9 ± 3.3 vs. $-14.1 \pm 3.5\%$] were lower than those in patients with PAF. Patients with AF regardless of LA enlargement had decreased LA reservoir strain and lower LVEF and absolute GLS value than those in the sinus rhythm control group.

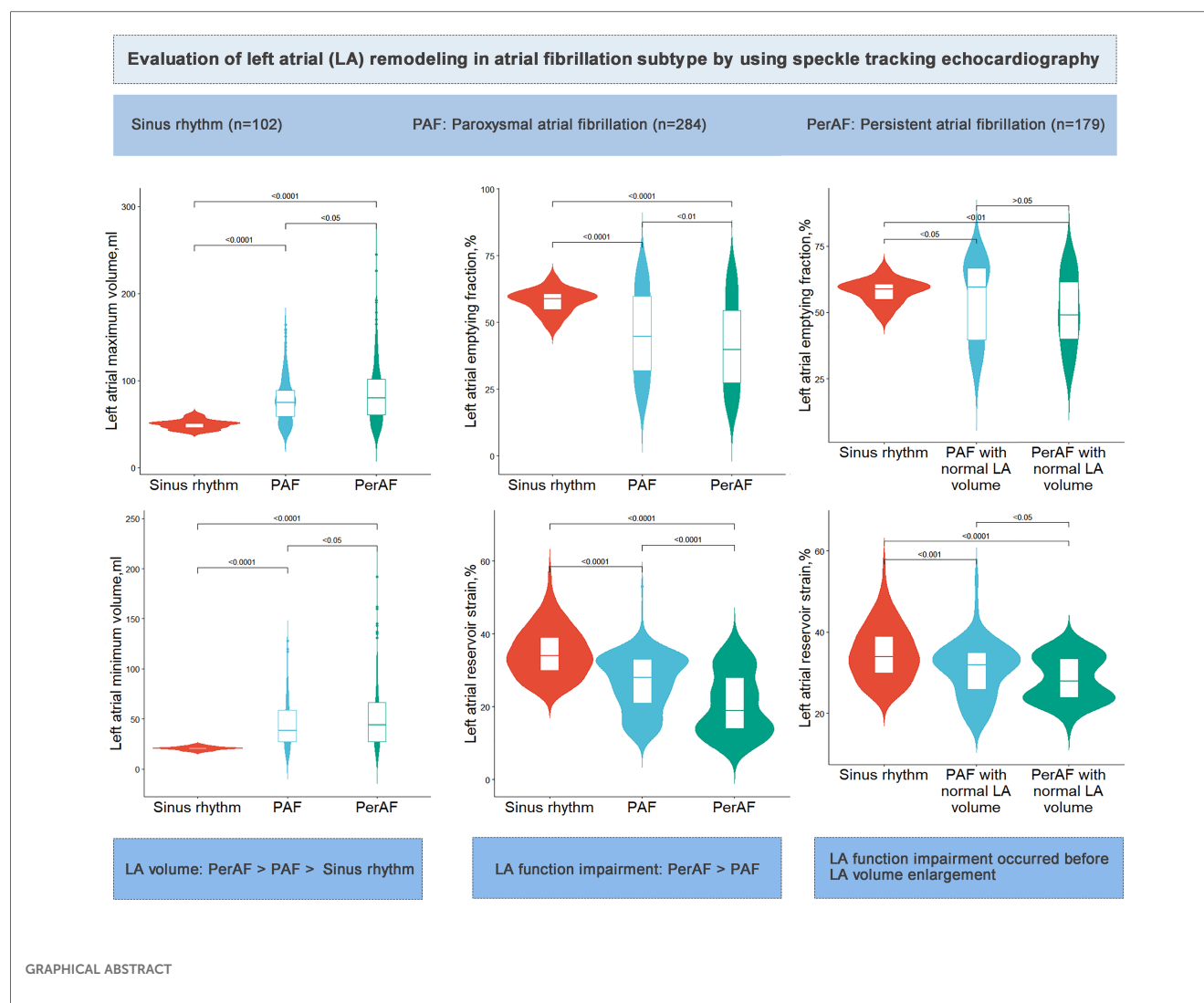
Conclusion: Compared with those with normal sinus rhythm, patients with AF had dilated LA volume and impaired LA function, which were further worsened in patients with PerAF than those in patients with PAF. LA functional impairment occurred before LA enlargement. Left atrioventricular remodeling happened across different stages of AF development.

KEYWORDS

atrial fibrillation, speckle tracking echocardiography, left atrial, left ventricular, strain, volume

Abbreviations

AF, atrial fibrillation; PAF, paroxysmal atrial fibrillation; PerAF, persistent atrial fibrillation; EHRA, European Heart Rhythm Association; LA, left atrial; LV, left ventricular; LAEF, left atrial emptying fraction; LVEF, left ventricular ejection fraction; GLS, global longitudinal strain; E/e', mitral inflow peak early diastolic velocity/mitral annular peak early diastolic velocity; LVEDV, left ventricular end-diastolic volume; LVESV, left ventricular end-systolic volume.



1. Introduction

Atrial fibrillation (AF) is a common cardiac arrhythmia that is becoming increasingly prevalent due to the aging population (1, 2). Despite efforts to understand its pathophysiology and improve treatments, identifying the underlying causes of AF in individual patients remains challenging (3, 4).

Atrial remodeling is a critical feature of AF, and speckle tracking echocardiography has emerged as an excellent approach for evaluating this process (5, 6). This imaging modality provides a non-invasive assessment of left atrial (LA) strain, which is inversely related to LA wall fibrosis and AF burden (6, 7). LA mechanics differ between AF subtypes of paroxysmal AF (PAF) and persistent AF (PerAF), and these characteristics influence the clinical interpretation of these measures (8). According to Kuppahally's report (9), PerAF had more fibrosis and lower midseptal and midlateral LA strains than PAF. However, only minimal differences in LA remodeling were found between PAF and PerAF in another study (7). Therefore, the differences in LA remodeling between AF subtypes remain debatable. In addition, LA size and function may vary at different stages of AF

development. Kojima et al. (10) found that LA functional impairment was observed before LA enlargement in patients with PAF. However, this finding was based on traditional velocity vector imaging and in a relatively small number of subjects, particularly in patients with PAF. There is still a lack of enough evidence on the relationship between LA structural and functional remodeling.

In addition to irregular atrial electrical activity, AF is also characterized by generating irregular activations of the ventricle (11). Mechanical LA remodeling can further damage the active contribution to ventricular filling, resulting in reduced LV function (12). It has been reported that immediate hemodynamic changes caused by AF may contribute to decreased cardiac output and acute heart failure (13). A recent study found that patients with PerAF had significantly reduced LV ejection fraction (LVEF) than that in patients with PAF (8). Although global longitudinal strain (GLS) is a widely used LV strain parameter that provides prognostic information (14), a few studies have externally validated GLS in AF patients.

Thus, this study aimed to evaluate the AF-induced changes in LA mechanics, clarify the association of LA structural and

functional remodeling in AF subtypes, and explore the left atrioventricular functional coupling across different stages of AF progression by using speckle tracking echocardiography.

2. Methods

2.1. Study population

From October 2021 to September 2022, we conducted a prospective study, which enrolled 527 patients diagnosed with AF and 102 healthy subjects with sinus rhythm. The determination of AF subtype and sinus rhythm was based on the 2020 European Society of Cardiology (ESC) guidelines. A standard 12-lead ECG recording or a single-lead ECG tracing of ≥ 30 s, showing heart rhythm with no discernible repeating P waves and irregular RR intervals (when atrioventricular conduction is not impaired), is diagnostic of clinical AF. PAF was defined as terminated spontaneously or with intervention within 7 days of onset. PerAF was defined as continuously sustained beyond 7 days, with episodes terminated by cardioversion (drugs or electrical cardioversion) after ≥ 7 days (1). The exclusion criteria comprised coronary artery disease ($n = 26$), organic valvular disease ($n = 5$), LVEF $< 40\%$ ($n = 9$), previous cardiac surgery ($n = 6$), other heart diseases or other serious non-cardiac diseases ($n = 11$), and suboptimal echocardiographic image quality ($n = 7$). After the application of the exclusion criteria, a total of 463 patients with AF were included in the analysis, among which 284 patients had PAF and 179 patients had PerAF. The Tongji Hospital Ethics Committee approved the study with approval number TJ-IRB20220621, and all participants provided their informed consent before participating in the study.

2.2. Clinical data

At the initiation of the study, we obtained baseline characteristics and clinical data for all participants. Heart rate was determined based on the findings of the standard 12-lead electrocardiogram. Symptoms were scored by European Heart Rhythm Association (EHRA) class (1). We calculated the CHA2DS2-VASc score based on clinical data (1).

2.3. Conventional transthoracic echocardiography

Transthoracic echocardiography was performed using GE Vivid E95 ultrasound equipment (GE Vingmed Ultrasound, Horten, Norway) with an M5Sc transducer (1.7–3.3 MHz) and a frame rate of 70–80 frame/s. According to the prevailing recommendations, M-mode, two-dimensional, color, pulsed, and continuous-wave Doppler data were acquired on standard views adjusting depth, sector width, and gain settings, as required. For participants with sinus rhythm, three cardiac

cycles were stored for each image, while for those with AF, at least 10 were saved. All echocardiographic parameters were analyzed with an index beat (preceding RR/pre-preceding RR close to 1) in AF cases, as recommended (15). The internal diameters were measured in accordance with the quantitative method suggested by the American Society of Echocardiography (16). LV relative wall thickness (RWT) was calculated as $RWT = 2 \times \text{LV posterior wall thickness} / \text{LV end-diastolic dimension}$. LV volumes, LVEF, and LA volumes were measured using the biplane Simpson method. All images were digitally stored for offline analysis.

2.4. Speckle tracking automatic functional imaging

Strain analysis was conducted using a commercial speckle tracking automatic functional imaging (AFI) software (EchoPAC version 2.4, GE Vingmed Ultrasound) (17). This software automatically tracked frame-to-frame speckle changes in two-dimensional images to assess LA and LV strain.

LA function consists of three components, namely, reservoir, conduit, and active pump. The total function of the LA is best reflected by reservoir strain corresponding to LA early diastole with maximum relaxation of its wall, algebraically positive. LA strain was evaluated using AFI-LA methods by the R-wave gating from the apical two- and four-chamber views. During the processing, the LA endocardium surface is manually traced by a point-and-click approach. The epicardial surface tracing is automatically generated by the system in order to obtain a region of interest (ROI). The ROI definition usually starts with delineating the endocardial contour, which should be drawn from the mitral annulus on one side, extrapolates across the pulmonary vein and/or LA appendage orifices, and ends at the mitral annulus on the opposite side. The ROI can be manually adjusted in width and shape, and then the software automatically tracks the quality for each segment and gives the peak LA reservoir strain and strain curves (18) (Figure 1).

LV strain was measured using the AFI method from the apical two-, three-, and four-chamber views (19). The software analyzed the myocardial motion by tracking frame-to-frame speckle changes. When necessary, automatic endocardial recognition was manually adjusted to ensure correct “anchorage” of the algorithm to the mitral annulus, exclude papillary muscles and chordae from tracking, and correctly include the LV apex. The ROI was eventually adjusted to ensure tracking of the whole myocardial thickness. LV outflow pulsed Doppler was used to time end systole. The segmental strain curves in apical view and 18-segment bull’s-eye diagrams related to strain parameters were automatically displayed. GLS was calculated as the average value of the peak systolic strain in 18 LV myocardial segments. All strain measurements were

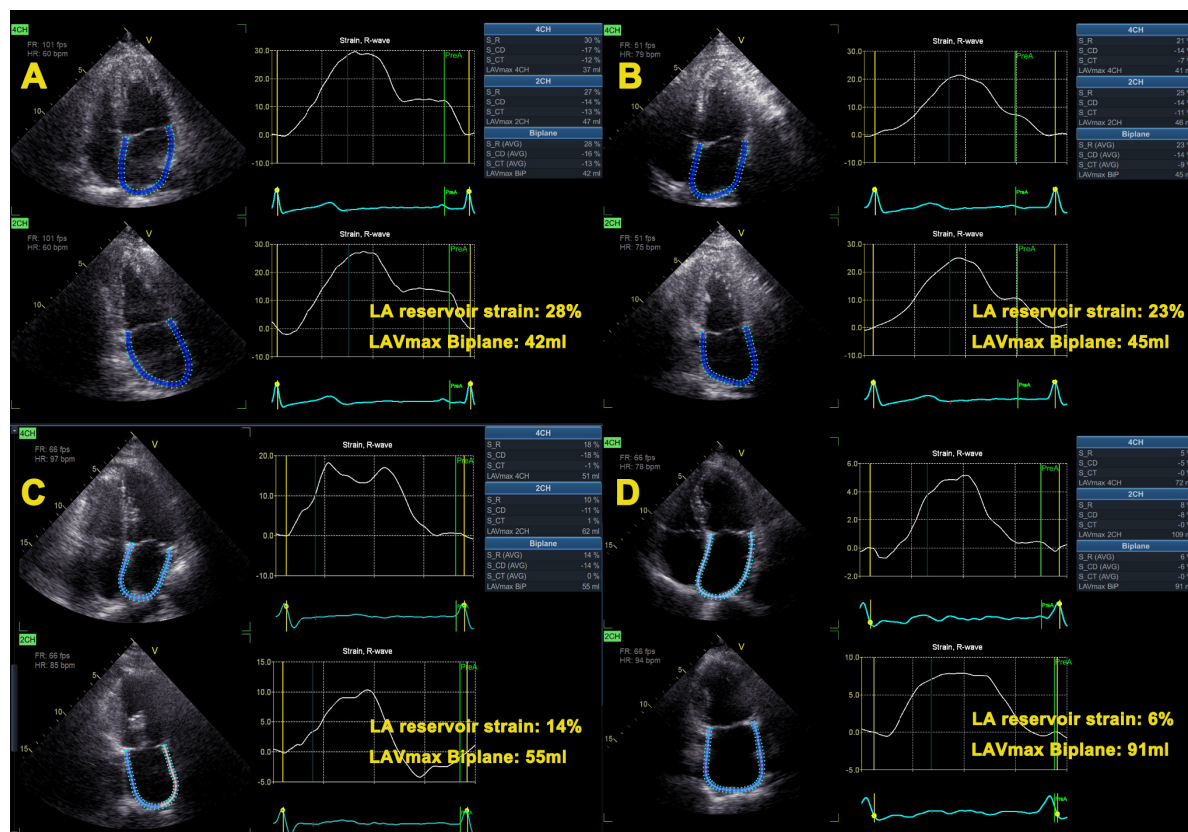


FIGURE 1

Representative cases. Left atrial strain curves of subjects with sinus rhythm (A), paroxysmal atrial fibrillation without left atrial enlargement (B), and persistent atrial fibrillation without (C) and with (D) left atrial volume enlargement. From A to D, the LA reservoir strain gradually decreased. LA, left atrial; LAVmax, left atrial maximal volume.

conducted in accordance with the EACVI/ASE/Industry Task Force guidelines (17, 18).

2.5. Statistical analysis

All statistical analyses were conducted using R version 4.1.1 (R Foundation for Statistical Computing, Vienna, Austria). Normally distributed continuous data were expressed as mean \pm standard deviation, while non-normally distributed data were expressed as median and interquartile range (IQR). Normality distribution was checked using the Shapiro–Wilk test and Q–Q plots. The differences among groups were analyzed using the one-way analysis of variation (ANOVA) for normally distributed data with the Bonferroni correction for pairwise comparisons between the two groups. The Kruskal–Wallis rank sum test was used for non-normally distributed data, and the all-pairwise method was used for further pairwise comparisons between the two groups. Categorical data were presented as percentages and analyzed using the χ^2 -test or Fisher's exact test as appropriate. A receiver operator characteristic (ROC) was performed to obtain the areas under the curve (AUC) and 95% confidence intervals (CIs). A two-tailed P -value < 0.05 was considered a statistically significant difference.

3. Results

3.1. Clinical and echocardiographic characteristics stratified by controls and AF subtype

Patient characteristics stratified by controls and AF subtype are summarized in **Table 1** and **Figure 2**. Compared with the sinus rhythm group, both AF groups showed higher CHA₂DS₂-VASc score, blood pressure, and heart rate, with a higher proportion of hypertension and EHRA classes 3–4. Moreover, both AF groups had greater LA dimensions, dilated LA maximum and minimum volumes, and volume indexes than those in the sinus rhythm group. In addition to LA structure, LA function was impaired in both AF groups, showing decreased LA emptying fraction (LAEF) and impaired LA reservoir strain than sinus rhythm (Graphical Abstract).

In terms of LV, both AF groups showed greater LV end-diastolic volume (LVEDV) and LV end-systolic volume (LVESV), higher mitral inflow peak early diastolic velocity/mitral annular peak early diastolic velocity (E/e'), and impaired LV systolic function compared to those in the sinus rhythm group.

The PerAF group showed dilated LA maximum and minimum volume, decreased LAEF, and impaired LA reservoir strain than those in the PAF group. A higher LVESV, LVESV index, and E/e'

TABLE 1 Clinical and echocardiographic characteristics in controls (sinus rhythm) and atrial fibrillation subtype.

Variables	Sinus rhythm (<i>n</i> = 102)	PAF (<i>n</i> = 284)	PerAF (<i>n</i> = 179)	<i>P</i> -value
Clinical characteristics				
Age, years	64 ± 10	63 ± 12	64 ± 11	0.84
Male, <i>n</i> (%)	65 (64)	187 (66)	113 (63)	0.82
Body mass index, kg/m ²	23.4 ± 2.5	24.1 ± 3.6	24.1 ± 3.3	0.14
Systolic blood pressure, mm Hg	121 ± 8	131 ± 20 ^a	130 ± 19 ^a	<0.001
Diastolic blood pressure, mm Hg	74 ± 9	81 ± 13 ^a	80 ± 12 ^a	<0.001
Heart rate, bpm	72 ± 9	81 ± 17 ^a	78 ± 15 ^a	<0.001
CHA ₂ DS ₂ -VAsC score	0.4 ± 0.8	0.9 ± 0.4 ^a	0.9 ± 0.5 ^a	<0.001
EHRA classes 3–4, <i>n</i> (%)	0 (0.0)	61 (22) ^a	44 (25) ^a	<0.001
Current smoking, <i>n</i> (%)	10 (10)	44 (16)	31 (17)	0.23
Hypertension, <i>n</i> (%)	10 (10)	120 (42) ^a	76 (43) ^a	<0.001
Diabetes, <i>n</i> (%)	8 (8)	30 (11)	21 (12)	0.59
Dyslipidemia, <i>n</i> (%)	3 (3)	24 (9)	12 (7)	0.17
Medication				
Antiarrhythmic medication, <i>n</i> (%)		134 (47)	84 (47)	0.84
Beta-blockers, <i>n</i> (%)		98 (35)	61 (34)	0.97
Calcium blocker, <i>n</i> (%)		33 (12)	21 (12)	0.92
Anticoagulation, <i>n</i> (%)		185 (65)	114 (64)	0.83
Echocardiographic parameters				
LA dimension, mm	32 ± 2	42 ± 7 ^a	43 ± 7 ^a	<0.001
LA volume—min, ml	21 (20, 22)	39 (27, 59) ^a	44 (28, 67) ^{a,b}	<0.001
LA volume—max, ml	50 ± 5	77 ± 25 ^a	86 ± 36 ^{a,b}	<0.001
LA volume index—min, ml/m ²	13 (12, 13)	20 (13, 31) ^a	23 (14, 38) ^{a,b}	<0.001
LA volume index—max, ml/m ²	30 ± 3	45 ± 15 ^a	51 ± 22 ^{a,b}	<0.001
LAEF, %	58 ± 4	46 ± 16 ^a	41 ± 16 ^{a,b}	<0.001
LA reservoir strain, %	34 (30, 39)	28 (21, 33) ^a	19 (14, 28) ^{a,b}	<0.001
E/e'	9.9 ± 1.9	11.1 ± 4.6 ^a	12.1 ± 4.4 ^{a,b}	<0.001
LV end-diastolic dimension, mm	47 ± 8	46 ± 9	48 ± 3	0.134
LVEDV, ml	86 ± 15	92 ± 24 ^a	98 ± 37 ^a	0.001
LVESV, ml	31 (29, 35)	37 (32, 48) ^a	42 (33, 54) ^{a,b}	<0.001
LVEDV index, ml/m ²	52 ± 9	54 ± 16 ^a	59 ± 23 ^{a,b}	0.008
LVESV index, ml/m ²	19 (17, 22)	22 (18, 28) ^a	25 (19, 32) ^{a,b}	<0.001
RWT	0.45 ± 0.08	0.47 ± 0.13	0.49 ± 0.12	0.092
LV mass index, g/m ²	88 (72, 92)	92 (80, 103)	90 (74, 108)	0.069
LVEF, %	62 ± 3	55 ± 9 ^a	53 ± 8 ^{a,b}	<0.001
GLS, -%	18.3 ± 2.1	16.9 ± 3.3 ^a	14.1 ± 3.5 ^{a,b}	<0.001

Data are presented as mean ± SD or median (interquartile range) for continuous variables and count (%) for categorical variables. PAF, paroxysmal atrial fibrillation; PerAF, persistent atrial fibrillation; CHA₂DS₂VAsC, history of congestive heart failure, hypertension, diabetes mellitus, stroke/transient ischemic attack/prior thromboembolism, vascular disease, age, and sex; EHRA, European Heart Rhythm Association; LA, left atrial; min: minimum; max: maximum; LAEF, left atrial emptying fraction; E/e', mitral inflow peak early diastolic velocity/mitral annular peak early diastolic velocity; LV, left ventricular; RWT, relative wall thickness; LVEDV, left ventricular end-diastolic volume; LVESV, left ventricular end-systolic volume; LVEF, left ventricular ejection fraction; GLS, global longitudinal strain.

^a*P* < 0.05 vs. the sinus rhythm group.

^b*P* < 0.05 vs. the paroxysmal atrial fibrillation group.

and lower LVEF and absolute GLS value were also shown in the PerAF group than those in the PAF group.

3.2. Cardiac structure and function remodeling in AF patients

To gain insight into the association between LA size and function, both AF groups were dichotomized into groups according to the recommended LA maximum volume index (≤ 34 ml/m²) (20). There were 70 patients with PAF and normal LA maximum volume index [PAF EL (−) group], 214 patients with PAF and dilated LA maximum volume index [PAF EL (+) group], 39 patients with PerAF and normal LA maximum

volume index [PerAF EL (−) group], and 140 patients with PerAF and dilated LA maximum volume index [PerAF EL (+) group]. Compared with the sinus rhythm group, patients with AF regardless of LA enlargement had significantly lower LAEF, LA reservoir strain, LVEF, and GLS, indicating that impairment of LA and LV function occurred before LA enlargement (Graphical Abstract, Table 2 and Figure 3).

In patients with PAF, LAEF and LA reservoir strain were lower in patients with LA enlargement than those in patients without LA enlargement. Similarly, in patients with PerAF, LAEF and LA reservoir strain were lower in patients with LA enlargement than those in patients without LA enlargement. These results demonstrated that LA function was further impaired as LA volume expands (Table 2 and Figure 3).

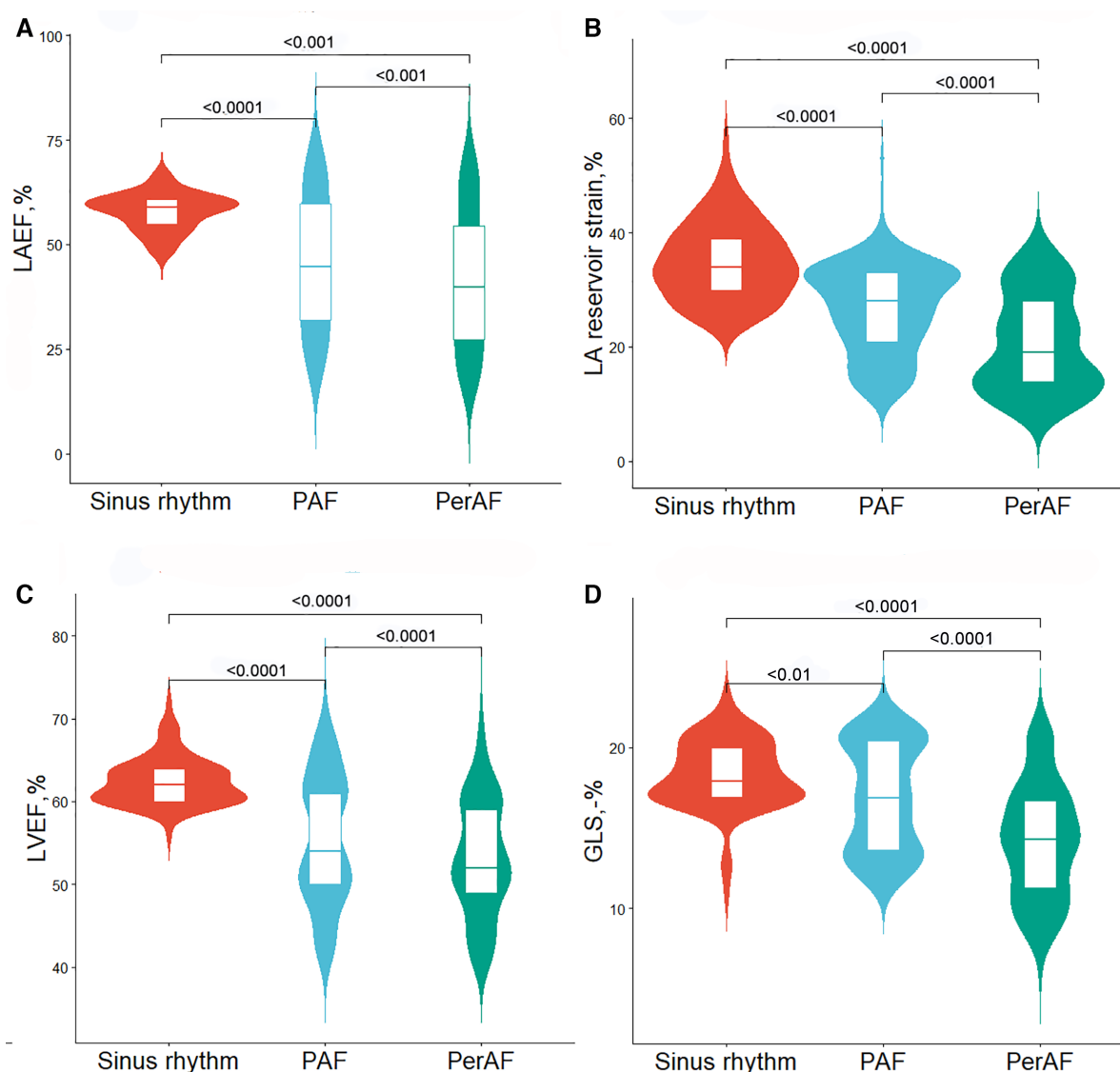


FIGURE 2

Violin plots for comparisons of echocardiographic characteristics between controls and atrial fibrillation subtype. (A) LAEF, (B) LA reservoir strain, (C) LVEF, and (D) GLS. PAF, paroxysmal atrial fibrillation; PerAF, persistent atrial fibrillation; LAEF, left atrial emptying fraction; LA, left atrial; LVEF, left ventricular ejection fraction; GLS, global longitudinal strain. Wider sections of the violin plot represent a higher distribution probability, the thin line in the center white box represents the median, and the white box in the center of the violin represents the interquartile range.

Compared with the PAF EL (+) group, LAEF and LA reservoir strain were lower in the PerAF EL (+) group while higher in the PerAF EL (-) group. Patients with PerAF regardless of LA dilation had higher LVESV index and impaired GLS than those in the PAF EL (+) group. These results demonstrated that as AF progressed, LV systolic function significantly decreased while LA function was also related to the presence of LA enlargement (Table 2 and Figure 3).

To further explore the association between LA structure and function, according to the cutoff of LA reservoir strain obtained from ROC, the LA myocardium was divided into compliant (LA reservoir strain $\geq 24\%$) and stiff (LA reservoir strain $< 24\%$). Table 3 and Figure 4 list the prevalence of LA anatomical remodeling and functional impairment according to AF subtype. The PAF group most frequently had large yet compliant LA,

whereas the PerAF group most frequently had large and stiff LA ($P < 0.001$). Notably, there were 32 (18.4%) PerAF patients with large but compliant LA and 14 (4.9%) PAF patients and 15 (8.4%) PerAF patients with small but stiff LA, which demonstrated that LA function might be normal even if the size was enlarged, whereas the size might be normal even if the function was impaired.

3.3. Evaluation of echocardiographic parameters in the detection of AF

ROC curve analyses showed that LA reservoir strain had a relatively higher diagnostic value than LAEF not only in distinguishing between AF and sinus rhythm (AUC: LA reservoir strain vs. LAEF 0.82 vs. 0.75) but also in distinguishing between

TABLE 2 Echocardiographic characteristics stratified according to atrial fibrillation subgroups with or without left atrial enlargement.

Variables	Sinus rhythm (<i>n</i> = 102)	PAF EL (–) (<i>n</i> = 70)	PAF EL (+) (<i>n</i> = 214)	PerAF EL (–) (<i>n</i> = 39)	PerAF EL (+) (<i>n</i> = 140)	<i>P</i> -value
LAEF, %	58 ± 4	55 ± 15 ^a	43 ± 16 ^{a,b}	51 ± 13 ^{a,c}	39 ± 16 ^{a,b,c,d}	<0.001
LA reservoir strain, %	34 (30, 39)	32 (26, 35) ^a	27 (19, 32) ^{a,b}	28 (24, 34) ^{a,b,c}	16 (12, 24) ^{a,b,c,d}	<0.001
LVEDV, ml	86 ± 15	87 ± 15	94 ± 26 ^{a,b}	89 ± 22 ^c	101 ± 39 ^{a,b,c,d}	<0.001
LVESV, ml	31 (29, 35)	36 (33, 43) ^a	38 (32, 50) ^a	38 (33, 46) ^a	44 (33, 56) ^{a,b}	<0.001
LVEDV index, ml/m ²	52 ± 9	52 ± 12	55 ± 17 ^{a,b}	55 ± 15 ^{a,b}	60 ± 24 ^{a,b,c,d}	0.008
LVESV index, ml/m ²	19 (17, 22)	21 (18, 26) ^a	22 (18, 29) ^a	24 (20, 29) ^{a,b,c}	26 (19, 33) ^{a,b,c,d}	<0.001
E/e'	9.9 ± 1.9	8.7 ± 2.8 ^a	11.9 ± 4.8 ^{a,b}	11.4 ± 4.4 ^b	12.4 ± 4.4 ^{a,b}	<0.001
LVEF, %	62 ± 3	56 ± 7 ^a	55 ± 10 ^a	56 ± 8 ^a	53 ± 7 ^{a,b,c,d}	<0.001
GLS, -%	18.3 ± 2.1	17.3 ± 3.2 ^a	16.8 ± 3.3 ^a	15.6 ± 3.2 ^{a,b,c}	13.7 ± 3.5 ^{a,b,c,d}	<0.001

Data are presented as mean ± SD or median (interquartile range) for continuous variables. PAF, paroxysmal atrial fibrillation; PerAF, persistent atrial fibrillation; EL, enlargement; LAEF, left atrial emptying fraction; LA, left atrial; LVEDV, left ventricular end-diastolic volume; LVESV, left ventricular end-systolic volume; E/e', mitral inflow peak early velocity/mitral annular peak early velocity; LVEF, left ventricular ejection fraction; GLS, global longitudinal strain.

^a*P* < 0.05 vs. the sinus rhythm group.

^b*P* < 0.05 vs. PAF EL (–) group.

^c*P* < 0.05 vs. PAF EL (+) group.

^d*P* < 0.05 vs. PerAF EL (–) group.

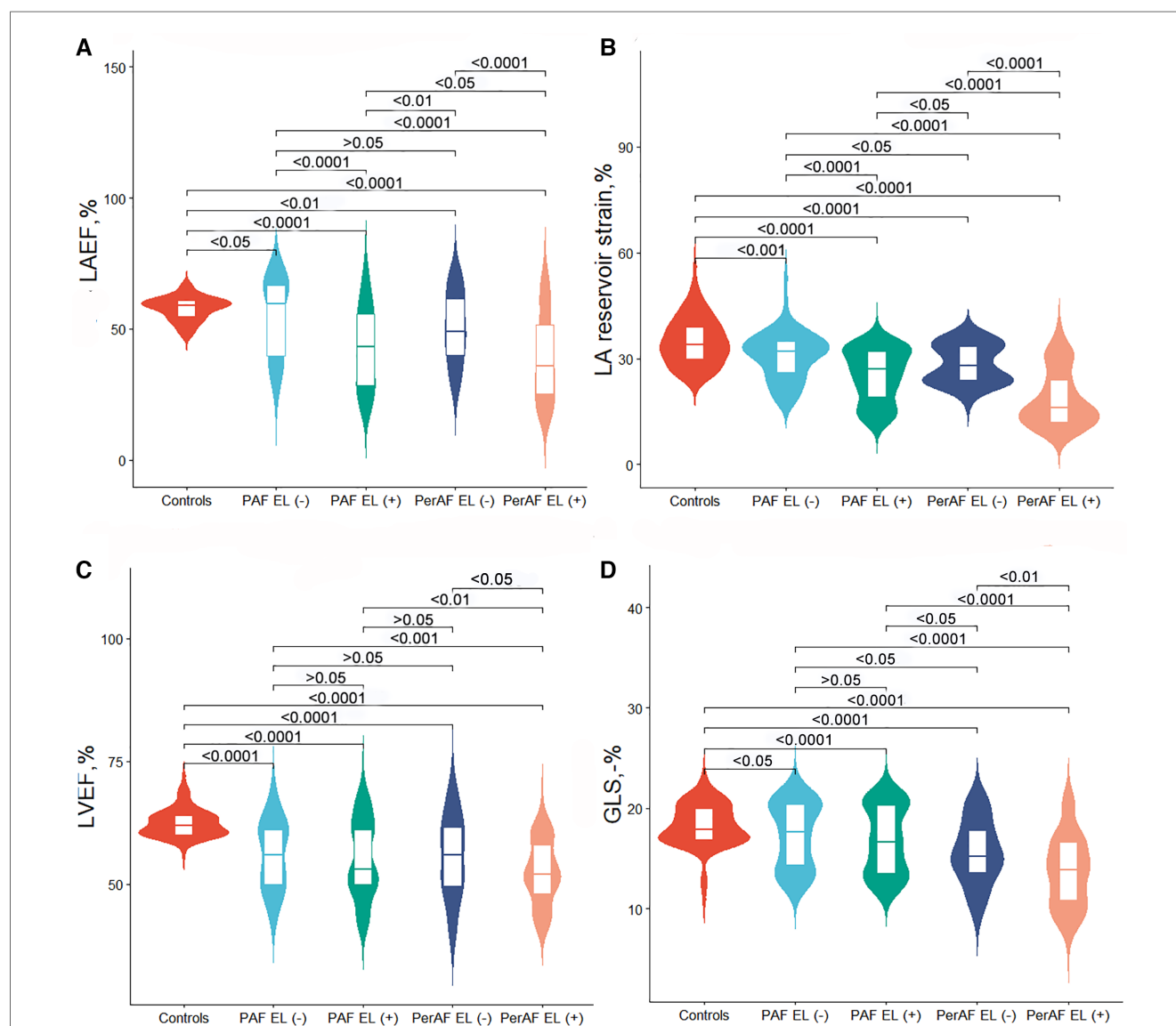


FIGURE 3

Violin plots for comparison of echocardiographic characteristics between controls and atrial fibrillation subgroup with or without left atrial volume enlargement. (A) LAEF, (B) LA reservoir strain, (C) LVEF, and (D) GLS. PAF, paroxysmal atrial fibrillation; PerAF, persistent atrial fibrillation; EL, enlargement; LAEF, left atrial emptying fraction; LA, left atrial; LVEF, left ventricular ejection fraction; GLS, global longitudinal strain.

TABLE 3 Left atrial anatomic remodeling and functional impairment according to the type of atrial fibrillation.

	PAF (<i>n</i> = 284)	PerAF (<i>n</i> = 179)	<i>P</i> -value
Small and compliant LA	56 (19.7)	24 (13.4)	<0.001
Small but stiff LA	14 (4.9)	15 (8.4)	<0.001
Large but compliant LA	123 (43.3)	32 (18.4)	<0.001
Large and stiff LA	91 (32.0)	107 (59.8)	<0.001

PAF, paroxysmal atrial fibrillation; PerAF, persistent atrial fibrillation; LA, left atrial.

PAF and PerAF (AUC: LA reservoir strain vs. LAEF 0.70 vs. 0.57) (Figure 5).

4. Discussion

The present study, which was conducted on 463 patients with AF and 102 subjects with sinus rhythm, identified several

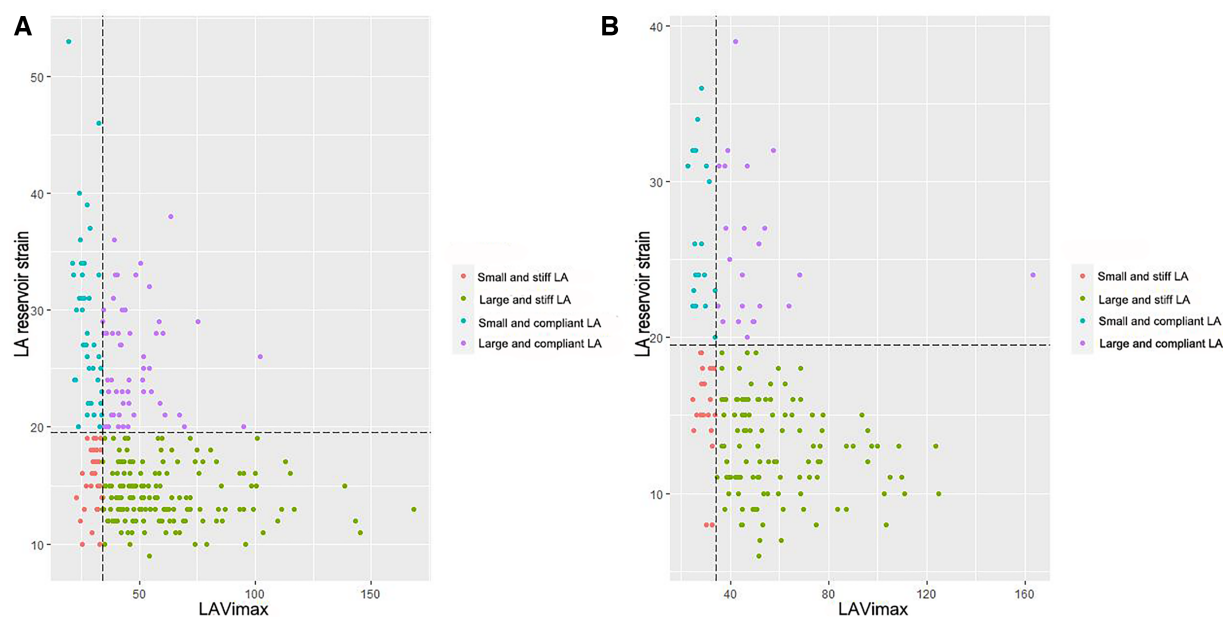


FIGURE 4

The distribution prevalence of left atrial anatomical remodeling and functional impairment according to atrial fibrillation subtype. (A) paroxysmal atrial fibrillation and (B) persistent atrial fibrillation. LA, left atrium; LAVimax, left atrial maximal volume index.

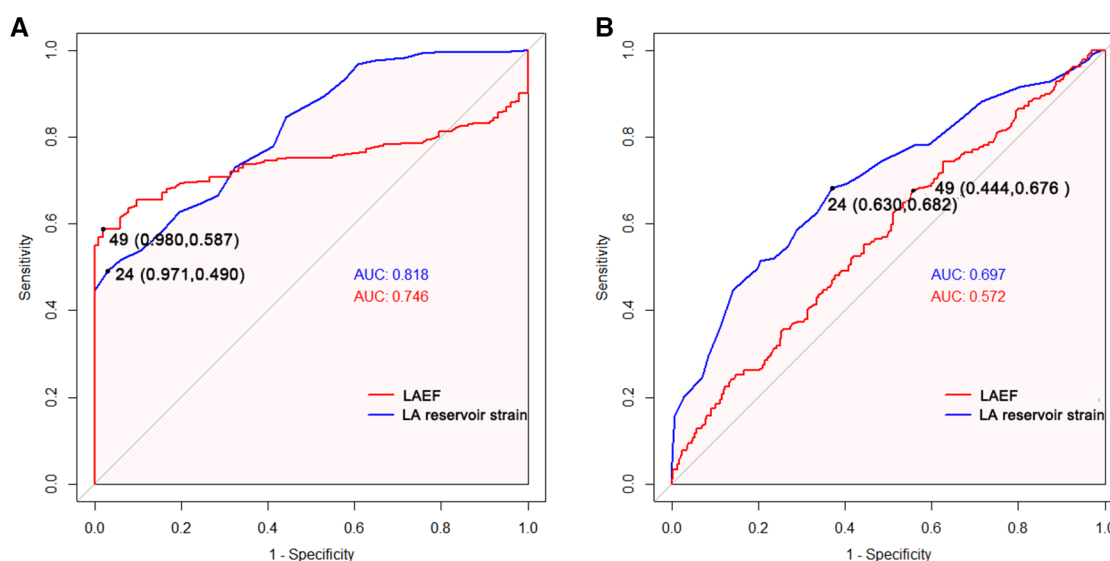


FIGURE 5

Receiver operating characteristic curves of LA function parameters to identify atrial fibrillation in all patients (A) and persistent atrial fibrillation in all atrial fibrillation patients. (B) AUC, area under the curve; LAEF, left atrial emptying fraction; LA, left atrial.

important findings. (1) Compared with sinus rhythm, both PAF and PerAF were associated with larger LA and LV volumes, as well as impaired LA and LV function. (2) PerAF had larger LA maximum and minimum volume and more impaired LA and LV function than PAF (3) The impairment of LA and LV function occurred before LA enlargement in AF. (4) The impairment of LA function was significantly aggravated when LA volume was enlarged in AF. (5) As AF progressed, LV systolic function significantly decreased while LA function varied depending on the presence of LA enlargement.

4.1. AF-induced changes in LA detected by echocardiography

Consistent with previous studies (21, 22), our study confirmed that AF was significantly associated with LA anatomical and functional remodeling. Additionally, our findings confirmed on a larger scale that AF transition from paroxysmal to persistent was often characterized by advancing atrial structural and functional remodeling, which are in accordance with the findings of Olsen et al. (8).

Among the LA function parameters, our report showed that LA reservoir strain had a higher value than LAEF in distinguishing not only between AF and sinus rhythm but also between PAF and PerAF. Raman et al. (23) had similar results with the magnetic resonance feature-tracking strain, which illustrated that LA reservoir strain was a major predictor of the onset of AF in patients with hypertrophic cardiomyopathy. It might be because the LA reservoir function was the most important feature of AF since it respectively reflected the compliance and loading conditions of LA. The development of AF evolves from sole rhythm disturbance to complex cardiomyopathy (24). Experimental studies have shown that the atrial remodeling of AF is characterized by the presence of predominantly interstitial fibrosis, which impacts atrial compliance (25, 26). Additionally, interstitial fibrosis promotes replacement fibrosis, resulting in impaired contractile function of LA cardiomyocytes. Therefore, a comprehensive assessment of LA volume and reservoir strain may provide additional insight into LA remodeling caused by AF.

4.2. LA volume and function remodeling were not always concordant in AF

In line with the study previously mentioned (10), the present report showed that LA volume and function were not always concordant in AF. LA function remodeling has been already impaired before LA volume enlargement, whereas even with enlarged LA volume, LA function impairment may not be apparent. The study also highlighted that large yet compliant atria were more prevalent in PAF, which may indicate a more advanced stage of disease with atrial enlargement yet without impaired strain. It is reported that

this condition could have a greater likelihood of successful AF ablation (27).

The study also indicated that LA function was severely impaired when LA volume was enlarged in AF. This could be because the increased LA volume can increase wall stress, triggering myocyte hypertrophy and fibrosis (28). In addition, LA reservoir strain was higher in PerAF without dilated LA volume than that in PAF with dilated LA, suggesting that LA reservoir strain was not only associated with the AF subtype but also related to the LA volume enlargement.

Although there are several papers demonstrating the impact of AF on LA remodeling as well as the utility of LA size and function on AF recurrence prediction (29–31), our study shows that patients with PerAF had a higher degree of LA anatomical remodeling and functional impairment than that in patients with PAF, reflecting different stages of the disease. Moreover, LA reservoir strain could be a useful indicator in estimating cardiac function remodeling induced by AF even before LA volume dilation and showed better discriminative value than LAEF to separate AF from sinus rhythm patients. This is important to facilitate appropriate clinical management decisions, because both anatomical remodeling and functional impairment could have implications for the success of AF ablation. Therefore, the added value of LA strain detected by speckle tracking echocardiography allows effective triaging of the AF patient, suggesting that it should be implemented in the systematic evaluation of AF patients before ablation. The ability to identify mild disease before morphological changes provides a basis for risk stratification before surgery, particularly in patients with non-dilated LA, and allows more selective prophylactic therapy for postoperative complications. According to Ma et al. (32), LA strain could be of great use in identifying patients with a high risk of AF recurrence after catheter ablation. It is reported that LA strain predicted the incidence of post-operative AF independently of LA dilation in severe aortic stenosis (33). It has also been proven to provide a diagnostic role of thrombotic risk assessment for non-valvular AF patients planned for electrical cardioversion (34). Additionally, patients who have suffered from specific cardiomyopathies and valve diseases such as myocardial infarction are at risk of developing AF, which may lead to a prognostic value of LA strain as a significant predictor of incident AF (35). Nevertheless, there are several limitations of LA strain including the lack of a “universal” definition of normal ranges and the impact of vendors/segmentation on data reproducibility. Although LA strain consists of three phases, i.e., reservoir, conduit, and pump, in the case of normal diastolic function, the relative contribution of the particular LA phases into the LV filling is as follows: reservoir, 40%; conduit, 35%; and pump 25% (36). The impaired phasic function of the LA was described in many cardiovascular diseases. However, in patients with PerAF at the time of the echocardiographic exam, it is impossible to measure the LA pump strain. Further studies are needed to focus on LA strain analysis, especially the reservoir strain, with a large sample to analyze its value in clinical practice.

4.3. Left atrioventricular functional coupling across different stages of AF progression

In our study, LV systolic and diastolic function was significantly impaired in AF than sinus rhythm, which was consistent with the study by Ross Agner et al. (37), who reported that GLS was significantly impaired in AF compared to sinus rhythm controls independent of age, sex, heart rate, LVEF, and LV mass. Our study also suggested that subclinical alterations in LV function may have preceded the deterioration of LV volume dilation.

We found that patients with AF had significantly higher heart rates compared to those in patients with sinus rhythm. However, the fact that myocardial oxygen consumption increases and myocardial efficiency decreases with increased heartbeat is well known. Literature on the relationship between heart rate and strain measurements showed that GLS in normal subjects with high and low heart rates was similar (38). All strain and strain rate variables in the longitudinal, circumferential, and radial directions were not significantly different between pacing rates (39).

Previous studies have shown that atrioventricular coupling is a dynamic and time-variant process in AF (40). On the one hand, AF can lead to progressive ventricular remodeling through tachycardia and irregular ventricular rhythm (41). On the other hand, LV fibrosis in patients with AF may reflect the same process in the LV that leads to atrial fibrosis, which may be associated with a pathologic myocardial process that triggers AF recurrence (40). It is reported that LA reservoir function is closely associated with heart failure (42). AF-associated ventricular remodeling results in myocardial fibrosis, chamber dilation, and mitral and tricuspid regurgitation, all of which contribute to damaging LV diastolic as well as systolic function (43).

5. Limitations

There were several limitations in the present study. First, software available on the market used different algorithms of strain analysis with possible consequent biases in comparison between studies. Second, the number of samples, especially sinus rhythm controls ($n = 102$) and PerAF patients without LA dilation ($n = 39$), was small, and more patients would be required to provide a robust conclusion in this aspect. Third, there was a lack of comparison with other imaging techniques such as three-dimensional echocardiography and cardiac magnetic resonance imaging. Forth, this is a transversal study, and we cannot conclude that LA strain detects an early disease but, rather, that LA strain diagnoses a mild disease. Additionally, there are various factors affecting LA strain. These factors change simultaneously in most cases, making it difficult to assess the net influence of each factor. Through the transversal study, we cannot determine whether the causes of the decrease of LA function and increase of LA volume in the population of patients with AF are the morpho-pathological changes at the level of the LA caused by the presence of AF or if they are the cause of AF.

These confounding factors might also have biased the results. A prospective study in a larger patient population is required to clarify the influence of these confounding factors on LA strain in patients with AF and validate the predictive value of LA strain on long-term outcomes.

6. Conclusions

Compared with the normal sinus rhythm group, patients with AF had dilated LA volume and impaired LA function, which were further worsened in patients with PerAF than those in patients with PAF. LA volume and function remodeling were not always concordant in AF, and LA function impairment could occur before LA volume enlargement. Left atrioventricular remodeling happened across different stages of AF development, and patients with AF had significantly more impaired GLS than the normal sinus rhythm group.

Data availability statement

The raw data supporting the conclusions of this article will be made available by the authors, without undue reservation.

Ethics statement

The studies involving human participants were reviewed and approved by the Tongji Hospital Ethics Committee, with approval number TJ-IRB20220621. The patients/participants provided their written informed consent to participate in this study.

Author contributions

YD, YL, and HL conceived and designed the study. All authors collected the clinical and echocardiographic data. SL, YD, YL, and HL performed the statistical analysis and interpretation of data. SL, YD, YL, and HL wrote the manuscript. All authors contributed to the article and approved the submitted version.

Acknowledgments

We thank the study participants and referring technicians for their participation in this study.

Conflict of interest

The authors declare that the research was conducted in the absence of any commercial or financial relationships that could be construed as a potential conflict of interest.

Publisher's note

All claims expressed in this article are solely those of the authors and do not necessarily represent those of their affiliated

organizations, or those of the publisher, the editors, and the reviewers. Any product that may be evaluated in this article, or claim that may be made by its manufacturer, is not guaranteed or endorsed by the publisher.

References

- Hindricks G, Potpara T, Dagres N, Arbelo E, Bax JJ, Blomstrom-Lundqvist C, et al. 2020 ESC guidelines for the diagnosis and management of atrial fibrillation developed in collaboration with the European Association for Cardio-Thoracic Surgery (EACTS): the task force for the diagnosis and management of atrial fibrillation of the European Society of Cardiology (ESC) developed with the special contribution of the European Heart Rhythm Association (EHRA) of the ESC. *Eur Heart J*. (2021) 42(5):373–498. doi: 10.1093/eurheartj/ehaa612
- Kornej J, Borschel CS, Benjamin EJ, Schnabel RB. Epidemiology of atrial fibrillation in the 21st century: novel methods and new insights. *Circ Res*. (2020) 127(1):4–20. doi: 10.1161/CIRCRESAHA.120.316340
- Brundel B, Ai X, Hills MT, Kuipers MF, Lip GYH, de Groot NMS. Atrial fibrillation. *Nat Rev Dis Primers*. (2022) 8(1):21. doi: 10.1038/s41572-022-00347-9
- Wijesurendra RS, Casadei B. Mechanisms of atrial fibrillation. *Heart*. (2019) 105(24):1860–7. doi: 10.1136/heartjnl-2018-314267
- Voigt JU, Malaescu GG, Haugaa K, Badano L. How to do LA strain. *Eur Heart J Cardiovasc Imaging*. (2020) 21(7):715–7. doi: 10.1093/ehjci/jeaa091
- Cameli M, Mandoli GE, Loiacono F, Sparla S, Iardino E, Mondillo S. Left atrial strain: a useful index in atrial fibrillation. *Int J Cardiol*. (2016) 220:208–13. doi: 10.1016/j.ijcard.2016.06.197
- Hopman L, Mulder MJ, van der Laan AM, Demirkiran A, Bhagirath P, van Rossum AC, et al. Impaired left atrial reservoir and conduit strain in patients with atrial fibrillation and extensive left atrial fibrosis. *J Cardiovasc Magn Reson*. (2021) 23(1):131. doi: 10.1186/s12968-021-00820-6
- Olsen FJ, Darkner S, Chen X, Pehrson S, Johannessen A, Hansen J, et al. Left atrial structure and function among different subtypes of atrial fibrillation: an echocardiographic substudy of the AMIO-CAT trial. *Eur Heart J Cardiovasc Imaging*. (2020) 21(12):1386–94. doi: 10.1093/ehjci/jeaa222
- Kuppahally SS, Akoum N, Burgon NS, Badger TJ, Kholmovski EG, Vijayakumar S, et al. Left atrial strain and strain rate in patients with paroxysmal and persistent atrial fibrillation: relationship to left atrial structural remodeling detected by delayed-enhancement MRI. *Circ Cardiovasc Imaging*. (2010) 3(3):231–9. doi: 10.1161/CIRCIMAGING.109.865683
- Kojima T, Kawasaki M, Tanaka R, Ono K, Hirose T, Iwama M, et al. Left atrial global and regional function in patients with paroxysmal atrial fibrillation has already been impaired before enlargement of left atrium: velocity vector imaging echocardiography study. *Eur Heart J Cardiovasc Imaging*. (2012) 13(3):227–34. doi: 10.1093/ehjcard/erj281
- Allessie M, Ausma J, Schotten U. Electrical, contractile and structural remodeling during atrial fibrillation. *Cardiovasc Res*. (2002) 54(2):230–46. doi: 10.1016/S0008-6363(02)00258-4
- Lyon A, van Mourik M, Cruts L, Heijman J, Bekkers S, Schotten U, et al. Both beat-to-beat changes in RR-interval and left ventricular filling time determine ventricular function during atrial fibrillation. *Europace*. (2021) 23(23 Suppl 1):i21–18. doi: 10.1093/europace/eaab387
- Verhaert DVM, Brunner-La Rocca HP, van Veldhuisen DJ, Vernooy K. The bidirectional interaction between atrial fibrillation and heart failure: consequences for the management of both diseases. *Europace*. (2021) 23(23 Suppl 2):ii40–ii5. doi: 10.1093/europace/eaab368
- Bunting KV, O'Connor K, Steeds RP, Kotecha D. Cardiac imaging to assess left ventricular systolic function in atrial fibrillation. *Am J Cardiol*. (2021) 139:40–9. doi: 10.1016/j.amjcard.2020.10.012
- Kong LY, Sun LL, Chen LL, Lv X, Liu F. Value of index beat in evaluating left ventricular systolic and diastolic function in patients with atrial fibrillation: a dual pulsed-wave Doppler study. *Ultrasound Med Biol*. (2020) 46(2):255–62. doi: 10.1016/j.ultrasmedbio.2019.10.028
- Lang RM, Badano LP, Mor-Avi V, Afilalo J, Armstrong A, Ernande L, et al. Recommendations for cardiac chamber quantification by echocardiography in adults: an update from the American Society of Echocardiography and the European Association of Cardiovascular Imaging. *J Am Soc Echocardiogr*. (2015) 28(1):1–39.e14. doi: 10.1016/j.echo.2014.10.003
- Voigt JU, Pedrizzetti G, Lysansky P, Marwick TH, Houle H, Baumann R, et al. Definitions for a common standard for 2D speckle tracking echocardiography: consensus document of the EACVI/ASE/industry task force to standardize deformation imaging. *Eur Heart J Cardiovasc Imaging*. (2015) 16(1):1–11. doi: 10.1093/ehjci/jeu184
- Badano LP, Kolias TJ, Muraru D, Abraham TP, Aurigemma G, Edvardsen T, et al. Standardization of left atrial, right ventricular, and right atrial deformation imaging using two-dimensional speckle tracking echocardiography: a consensus document of the EACVI/ASE/industry task force to standardize deformation imaging. *Eur Heart J Cardiovasc Imaging*. (2018) 19(6):591–600. doi: 10.1093/ehjci/jeu042
- Negishi K, Negishi T, Kurosawa K, Hristova K, Popescu BA, Vinereanu D, et al. Practical guidance in echocardiographic assessment of global longitudinal strain. *JACC Cardiovasc Imaging*. (2015) 8(4):489–92. doi: 10.1016/j.jcmg.2014.06.013
- Thomas L, Marwick TH, Popescu BA, Donal E, Badano LP. Left atrial structure and function, and left ventricular diastolic dysfunction: JACC state-of-the-art review. *J Am Coll Cardiol*. (2019) 73(15):1961–77. doi: 10.1016/j.jacc.2019.01.059
- Gupta DK, Shah AM, Giugliano RP, Ruff CT, Antman EM, Grip LT, et al. Left atrial structure and function in atrial fibrillation: ENGAGE AF-TIMI 48. *Eur Heart J*. (2014) 35(22):1457–65. doi: 10.1093/eurheartj/ehu500
- Schaaf M, Andre P, Altman M, Maucourt-Boulch D, Placide J, Chevalier P, et al. Left atrial remodeling assessed by 2D and 3D echocardiography identifies paroxysmal atrial fibrillation. *Eur Heart J Cardiovasc Imaging*. (2017) 18(1):46–53. doi: 10.1093/ehjci/jeu028
- Raman B, Smillie RW, Mahmod M, Chan K, Ariga R, Nikolaidou C, et al. Incremental value of left atrial booster and reservoir strain in predicting atrial fibrillation in patients with hypertrophic cardiomyopathy: a cardiovascular magnetic resonance study. *J Cardiovasc Magn Reson*. (2021) 23(1):109. doi: 10.1186/s12968-021-00793-6
- Sohns C, Marrouche NF. Atrial fibrillation and cardiac fibrosis. *Eur Heart J*. (2020) 41(10):1123–31. doi: 10.1093/eurheartj/ehz786
- Dzeshka Mikhail S, Lip Gregory YH, Snezhitskiy V, Shantsila E. Cardiac fibrosis in patients with atrial fibrillation. *J Am Coll Cardiol*. (2015) 66(8):943–59. doi: 10.1016/j.jacc.2015.06.1313
- Everett TH, Olgin JE. Atrial fibrosis and the mechanisms of atrial fibrillation. *Heart Rhythm*. (2007) 4(3, Supplement):S24–S7. doi: 10.1016/j.hrthm.2006.12.040
- Bax M, Ajmone Marsan N, Delgado V, Bax JJ, van der Bijl P. Effect of bi-atrial size and function in patients with paroxysmal or permanent atrial fibrillation. *Am J Cardiol*. (2022) 183:33–9. doi: 10.1016/j.amjcard.2022.07.024
- Kornej J, Seewoster T. Left atrial size and function as markers of AF progression and outcomes. *Int J Cardiol*. (2019) 294:41. doi: 10.1016/j.ijcard.2019.06.047
- Jasic-Szpak E, Marwick TH, Donal E, Przewlocka-Kosmala M, Huynh Q, Gozdzik A, et al. Prediction of AF in heart failure with preserved ejection fraction: incremental value of left atrial strain. *JACC Cardiovasc Imaging*. (2021) 14(1):131–44. doi: 10.1016/j.jcmg.2020.07.040
- Smiseth OA, Baron T, Marino PN, Marwick TH, Flachskampf FA. Imaging of the left atrium: pathophysiology insights and clinical utility. *Eur Heart J Cardiovasc Imaging*. (2022) 23(1):2–13. doi: 10.1093/ehjci/jeab191
- Motoc A, Scheirlynck E, Roosens B, Luchian M-L, Chameleva H, Gevers M, et al. Additional value of left atrium remodeling assessed by three-dimensional echocardiography for the prediction of atrial fibrillation recurrence after cryoballoon ablation. *Int J Cardiovasc Imaging*. (2022) 38(5):1103–11. doi: 10.1007/s10554-021-02493-9
- Ma X-X, Boldt L-H, Zhang Y-L, Zhu M-R, Hu B, Parwani A, et al. Clinical relevance of left atrial strain to predict recurrence of atrial fibrillation after catheter ablation: a meta-analysis. *Echocardiography*. (2016) 33(5):724–33. doi: 10.1111/echo.13184
- Pessoa-Amorim G, Mancio J, Vouga L, Ribeiro J, Gama V, Bettencourt N, et al. Impaired left atrial strain as a predictor of new-onset atrial fibrillation after aortic valve replacement independently of left atrial size. *Rev Esp Cardiol Engl Ed*. (2018) 71(6):466–76. doi: 10.1016/j.rec.2017.10.005
- Sonaglioni A, Lombardo M, Nicolosi GL, Rigamonti E, Anzà C. Incremental diagnostic role of left atrial strain analysis in thrombotic risk assessment of nonvalvular atrial fibrillation patients planned for electrical cardioversion. *Int J Cardiovasc Imaging*. (2021) 37(5):1539–50. doi: 10.1007/s10554-020-02127-6
- Svartstein A-SW, Lassen MH, Skaarup KG, Grove GL, Vyff F, Ravnkilde K, et al. Predictive value of left atrial strain in relation to atrial fibrillation following acute myocardial infarction. *Int J Cardiol*. (2022) 364:52–9. doi: 10.1016/j.ijcard.2022.05.026

36. Kupczynska K, Mandoli GE, Cameli M, Kasprzak JD. Left atrial strain—a current clinical perspective. *Kardiol Pol.* (2021) 79(9):955–64. doi: 10.33963/KP.a2021.0105
37. Ross Agner BF, Katz MG, Williams ZR, Dixen U, Jensen GB, Schwarz KQ. Left ventricular systolic function assessed by global longitudinal strain is impaired in atrial fibrillation compared to sinus rhythm. *J Atr Fibrillation.* (2017) 10(4):1437. doi: 10.4022/jafib.1437 eCollection.
38. Yamauchi Y, Tanaka H, Yokota S, Mochizuki Y, Yoshigai Y, Shiraki H, et al. Effect of heart rate on left ventricular longitudinal myocardial function in type 2 diabetes mellitus. *Cardiovasc Diabetol.* (2021) 20(1):87. doi: 10.1186/s12933-021-01278-7
39. Suzuki R, Matsumoto H, Teshima T, Koyama H. Influence of heart rate on myocardial function using two-dimensional speckle-tracking echocardiography in healthy dogs. *J Vet Cardiol.* (2013) 15(2):139–46. doi: 10.1016/j.jvc.2012.12.004
40. Sengupta Partho P, Narula J. À la mode atrioventricular mechanical coupling. *JACC Cardiovasc Imaging.* (2014) 7(1):109–11. doi: 10.1016/j.jcmg.2013.12.001
41. Gopinathannair R, Etheridge Susan P, Marchlinski Francis E, Spinale Francis G, Lakkireddy D, Olshansky B. Arrhythmia-induced cardiomyopathies. *J Am Coll Cardiol.* (2015) 66(15):1714–28. doi: 10.1016/j.jacc.2015.08.038
42. Reddy YNV, Obokata M, Verbrugge FH, Lin G, Borlaug BA. Atrial dysfunction in patients with heart failure with preserved ejection fraction and atrial fibrillation. *J Am Coll Cardiol.* (2020) 76(9):1051–64. doi: 10.1016/j.jacc.2020.07.009
43. Shantsila E, Shantsila A, Blann AD, Lip GYH. Left ventricular fibrosis in atrial fibrillation. *Am J Cardiol.* (2013) 111(7):996–1001. doi: 10.1016/j.amjcard.2012.12.005



OPEN ACCESS

EDITED BY

Francesca Innocenti,
Careggi University Hospital, Italy

REVIEWED BY

Praveen Varma,
Amrita Vishwa Vidyapeetham University, India
Kwan Chan,
University of Ottawa, Canada

*CORRESPONDENCE

Bin Wang
✉ wangbin87098429@126.com
Shanye Yin
✉ shanye.yin@einsteinmed.edu

[†]These authors have contributed equally to this work

RECEIVED 22 June 2023

ACCEPTED 02 August 2023

PUBLISHED 25 August 2023

CITATION

Wang Y, Wang S, Chen D, Li M, Mi S, Xiong L, Song W, Wang W, Yin S and Wang B (2023) Mitral valve aneurysms: echocardiographic characteristics, formation mechanisms, and patient outcomes. *Front. Cardiovasc. Med.* 10:1233926. doi: 10.3389/fcvm.2023.1233926

COPYRIGHT

© 2023 Wang, Wang, Chen, Li, Mi, Xiong, Song, Wang, Yin and Wang. This is an open-access article distributed under the terms of the [Creative Commons Attribution License \(CC BY\)](https://creativecommons.org/licenses/by/4.0/). The use, distribution or reproduction in other forums is permitted, provided the original author(s) and the copyright owner(s) are credited and that the original publication in this journal is cited, in accordance with accepted academic practice. No use, distribution or reproduction is permitted which does not comply with these terms.

Mitral valve aneurysms: echocardiographic characteristics, formation mechanisms, and patient outcomes

Yi Wang[†], Shuang Wang[†], Dandan Chen[†], Mengmei Li¹, Sulin Mi¹, Li Xiong¹, Wanwan Song¹, Wei Wang¹, Shanye Yin^{2*} and Bin Wang^{1*}

¹Department of Cardiovascular Ultrasound, Zhongnan Hospital of Wuhan University, Wuhan University, Wuhan, China, ²Department of Pathology, Albert Einstein College of Medicine, Bronx, NY, United States

Background: The accurate etiology of mitral valve aneurysm (MVA) formation is not completely understood, and the most effective management approach for this condition remains controversial.

Methods: We retrospectively analyzed 20 MVA patients who underwent either surgical interventions or conservative follow-ups at the Zhongnan Hospital of Wuhan University between 2017 and 2021. We examined their clinical, echocardiographic, and surgical records and tracked their long-term outcomes.

Results: Of the 20 patients, 12 were diagnosed with MVA using transthoracic echocardiography, seven required additional transesophageal echocardiography for a more definitive diagnosis, and one child was diagnosed during surgery. In all these patients, the MVAs were detected in the anterior mitral leaflet. We found that 15 patients (75%) were associated with infective endocarditis (IE), whereas the remaining patients were associated with bicuspid aortic valve and moderate aortic regurgitation (AR) and mild aortic stenosis (5%), congenital heart disease (5%), elderly calcified valvular disease (5%), mitral valve prolapse (5%), and unknown reasons (5%). Of the 17 patients who underwent hospital surgical interventions, two died due to severe cardiac events. The remaining 15 patients had successful surgeries and were followed up for an average of 13.0 ± 1.8 months. We observed an improvement in their New York Heart Association functional class and mitral regurgitation and AR degrees (P -value < 0.001). During follow-up, only one infant had an increased left ventricular end-diastolic diameter and left ventricular end-systolic diameter, whereas the remaining 14 patients had decreased values ($P < 0.001$). In addition, none of the three conservatively managed patients experienced disease progression during the 7–24 months of follow-up.

Conclusions: We recommend using echocardiography as a highly sensitive method for MVA diagnosis. Although most cases are associated with IE or AR, certain cases still require further study to determine their causes. A prompt diagnosis of MVA in patients using echocardiography can aid in its timely management.

KEYWORDS

mitral valve aneurysm, echocardiography, cardiac imaging, infective endocarditis, mitral regurgitation

1. Introduction

Mitral valve aneurysm (MVA) is a relatively uncommon condition characterized by a localized bulging structure of the mitral leaflet toward the left atrium, exhibiting systolic expansion and diastolic collapse (1, 2), as demonstrated in **Figures 1, 2**. Despite the rarity of this condition, several case reports and a few series on MVA have been documented. The exact MVA formation mechanisms remain incompletely understood, with infective endocarditis (IE) and aortic regurgitation (AR) being reported as major contributing factors (3–7). Other factors, such as connective tissue defects and valve degenerative changes, have also been implicated (1–3, 5–13). Moreover, cases of congenital mitral valve aneurysms have been rarely reported (14).

MVA management remains a matter of debate due to its potential for significant clinical issues and adverse outcomes. The most common complication observed is aneurysm perforation induced by concurrent mitral regurgitation (MR) (1–8). In addition, MVA has been associated with thromboembolic events (1, 12), increased mitral valve (MV) mean pressure gradient (15), and symptomatic exertional left ventricular (LV) outflow tract obstruction (14). Consequently, selecting an appropriate management approach, whether a surgical intervention involving

mitral valve repair or replacement or a conservative follow-up strategy, depends on the presence of ruptured or large aneurysms, severe hemodynamic disturbances, uncontrolled infections, or peripheral embolisms. In patients with uncomplicated conditions, a conservative approach with a close follow-up is often adopted. Echocardiography plays a pivotal role in the accurate MVA diagnosis and treatment decision-making for valvular heart diseases.

In this paper, we present a retrospective analysis of 20 MVA patients, focusing on echocardiographic findings, formation mechanisms, patient management, and outcomes. By integrating anatomical assessments, cardiac function, and hemodynamics, echocardiography offers critical insights into MVA diagnosis and management. We aim to contribute to the understanding of this rare condition and provide valuable insights for clinical practice.

2. Methods

2.1. Patients

In this retrospective study, we enrolled 20 patients who were diagnosed with MVA in the Zhongnan Hospital of Wuhan

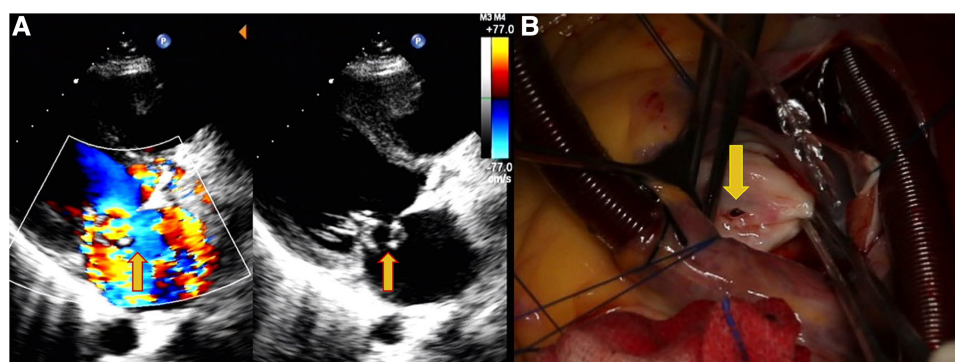


FIGURE 1

Echocardiography data of a 31-year-old female patient with shortness of breath, palpitations, and fever for 7 days. (A) Perforation of the MVA and regurgitation (yellow arrows). (B) Site of the MVA perforation during surgery (yellow arrows).

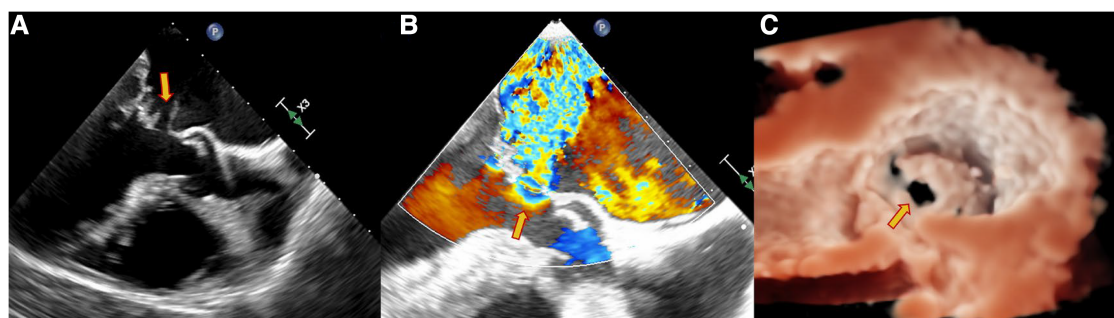


FIGURE 2

Echocardiography data of a 63-year-old male patient with dyspnea for 4 days. TEE showed the perforation of the MVA as pointed out by the yellow arrow. (A) Continuous interruption of the MVA wall. (B) Regurgitation from the MVA. (C) Continuous breaks on the MVA from a 3D view.

University between April 2017 and January 2021. Among these patients, 17 received surgical treatments and three received conservative follow-ups. This study was approved by the Medical Ethics Committee of the Zhongnan Hospital of Wuhan University.

2.2. Echocardiography

Transthoracic echocardiography (TTE) examination is commonly performed for the first-line detection and evaluation of MVA. Additional transesophageal echocardiography (TEE) examination was required when TTE could not clearly evaluate the MVA. All diagnostic TTE or TEE examinations were performed using Philips IE 33 (Philips Healthcare, Bothell, WA, USA) with S5-1, X5-1, S8-3, and X8-2t transducers. TTE and TEE examinations were reviewed by the same senior doctor (BW, with 15 years of experience in echocardiography). The diagnostic marker of MVA was a localized bulging structure of the mitral leaflet toward the left atrium with systolic expansion and diastolic collapse.

The diagnostic echocardiographic findings were recorded, namely, MVA location and size, presence of perforation and vegetation, MR and AR degrees, left ventricular end-diastolic diameter (LVEDD), left ventricular end-systolic diameter (LVESD), left ventricular ejection fraction (LVEF), and other abnormalities, such as bicuspid aortic valve (BAV), endocardial cushion defect (ECD), ventricular septal defect (VSD), and patent foramen ovale (PFO). Other clinical information such as clinical manifestations, clinical diagnosis of infective endocarditis, and New York Heart Association (NYHA) functional class was also recorded.

2.3. Patient management

The indications for surgical interventions were as follows: (1) patients with acute severe primary MR (16); (2) symptomatic patients with severe chronic primary MR irrespective of the LV systolic function (16); (3) asymptomatic patients with severe chronic primary MR and LV systolic insufficiency ($LVEF \leq 60\%$, $LVESD \geq 40$ mm) (16); and (4) IE patients with heart failure, severe valve dysfunction, and large mobile neoplasms (17). The indications for follow-ups were asymptomatic, $LVEF \geq 60\%$, $LVESD \leq 40$ mm, and none/mild MR and none/mild AR (16). Regular clinical and echocardiography reviews and follow-ups were given to the patients after surgical interventions or those with a conservative follow-up strategy. In addition, the clinical manifestations, follow-up time, NYHA functional class, MR and AR degrees, LVEDD, LVESD, and LVEF for the latest follow-up were collected.

2.4. Statistics

Continuous variables were described as average and standard deviation, and categorical variables were described as counts.

Two two-sided tests were performed. First, the Wilcoxon signed-rank test was applied to determine the significant differences in the MR and AR degrees between the first diagnosis and the latest follow-up. Second, a paired *t*-test was applied to determine the significant differences in the cardiac systolic function and left ventricular measures between the first diagnosis and the latest follow-up. The significant difference threshold was $P < 0.05$, and the statistical analysis was performed using SPSS 25.0 software.

3. Results

3.1. Baseline clinical and echocardiographic characteristics of study subjects

Table 1 lists the baseline clinical and echocardiographic characteristics of the 20 patients enrolled in this study, comprising 8 females and 12 males, with a median age of 34 years (range: 7 months–63 years). Among the adult patients, 12 were evaluated using TTE, and seven required additional TEEs for the MVA assessment. Remarkably, the MVA in a 7-month-old child was initially misdiagnosed by TTE, but it was later detected during the surgical intervention for an ECD and a PFO.

Of the 19 adult patients, 16 underwent surgical interventions following diagnosis due to clinical symptoms, such as fever, shortness of breath, fatigue, weight loss, dyspnea, dizziness, chest pain, chest tightness, palpitations, and cerebrovascular accidents. These patients presented with enlarged left ventricles, decreased LVEF, and impaired heart function (all NYHA functional class \geq II). Among them, four had BAVs, three had VSDs, and one had a ruptured right coronary sinus aneurysm in the right ventricle. In contrast, three adult patients received conservative follow-ups for being asymptomatic, and they exhibited normal left ventricles, LVEF, and heart function.

In this cohort of 20 MVA patients, 19 had a single MVA located in the anterior mitral leaflet, involving one or two sub-leaflets of A1–A3. Only one patient had multiple MVAs involving A1, A2, and A3. The size of the MVAs ranged from 0.5 cm \times 0.5 cm to 2.9 cm \times 2.5 cm. Among the 14 patients with ruptured MVAs in the left atrium, the break size ranged from 0.2 to 1.0 cm, with 11 of them experiencing severe MR, one with moderate-to-severe MR, one with moderate MR, and one with mild-to-moderate MR. The remaining six patients had non-ruptured MVAs, including two with severe MR, one with moderate-to-severe MR, one with moderate MR, one with mild MR, and one with no MR.

Clinically diagnosed IE was present in 15 of the 20 patients (75%). Among these 15 patients, 12 had moderate or greater AR, nine had severe AR, and three had moderate AR. Among the five patients without IE, one had an ECD, one had a bicuspid aortic valve with calcification, one had a bicuspid aortic valve with mild aortic regurgitation and calcification, one had a mitral valve prolapse, and one had gallstones. Further details for each patient are listed in **Supplementary Table S1**.

TABLE 1 Baseline characteristics and echocardiographic data of the study subjects.

	All patients (n = 20)	Surgical interventions (n = 17)	Conservative follow-ups (n = 3)
Baseline characteristics			
Age, years	36.2 ± 12.4	35.4 ± 11.7	40.0 ± 18.3
Male	12 (60.0)	12 (71.6)	0 (0)
Symptoms ^a	17 (85.0)	17 (100.0)	0 (0)
NYHA functional class			
I	3 (15.0)	0 (0)	3 (100)
II	5 (25.0)	5 (29.4)	0 (0)
III	9 (45.0)	9 (52.9)	0 (0)
IV	3 (15.0)	3 (17.6)	0 (0)
Echocardiographic measurements			
LVEF, %	61.5 ± 5.8	60.1 ± 5.7	67.0 ± 2.0
Infective endocarditis	15 (75.0)	15 (88.2)	0 (0)
With vegetation	12 (60.0)	12 (71.6)	0 (0)
AVE	3 (15.0)	3 (17.6)	0 (0)
MVE	2 (10.0)	2 (11.8)	0 (0)
AVE and MVE	7 (35.0)	7 (41.2)	0 (0)
Without vegetation	3 (15.0)	3 (17.6)	0 (0)
Enlarged LV	16 (80.0)	16 (94.1)	0 (0)
LVEDD, cm	5.82 ± 1.21	6.09 ± 1.10	4.30 ± 0.20
LVESD, cm	3.99 ± 0.98	4.21 ± 0.88	2.72 ± 0.17
Number of MVAs >1	1 (5.0)	1 (5.9)	0 (0)
Diameter range of MVAs, cm	0.5–2.9 × 0.5–2.5	0.5–2.9 × 0.5–2.5	0.5–0.9 × 0.5–0.7
Location of MVA			
A1	1	0	1 (33.3)
A2	5	4	1 (33.3)
A3	2	1	1 (33.3)
A1–A2	5	5	0 (0)
A2–A3	4	4	0 (0)
A1–A3	1	1	0 (0)
Perforation detected	14 (70.0)	13 (76.4)	1 (33.3)
Average maximal diameter, mm	5.35 ± 2.44	5.62 ± 2.33	2
Mitral regurgitation			
None or mild	3 (15.0)	1 (5.9)	2 (67.7)
Moderate or severe	17 (85.0)	16 (94.1)	1 (33.3)
Aortic regurgitation			
None or mild	8 (40.0)	5 (29.4)	3 (100.0)
Moderate or severe	12 (60.0)	12 (70.6)	0 (0)
Other defects beyond valves	6 (30.0)	5 (29.4)	1 (33.3)
In-hospital death after surgeries	2 (10.0)	2 (11.8)	NA

A1/A2/A3, echocardiographic portions of the aortic leaflet; MVE, mitral valve endocarditis.

Values are mean ± SD or n (%) unless otherwise stated.

^aSymptoms include fever, shortness of breath, fatigue, weight loss, dyspnea, lightheadedness, chest pain, chest oppressive sensation, palpitation, cerebrovascular accident, and a heart murmur.

3.2. Patient outcomes

Among the 17 patients who underwent hospital surgical interventions, two died after surgery due to low cardiac output syndrome or multiorgan failure. However, encouragingly, 15 patients survived and were followed up for 11–18 months (mean follow-up of 13.0 ± 1.8 months). **Table 2** lists the postsurgical follow-up data, revealing a significant improvement in the NYHA functional class compared to baseline ($P < 0.001$). Specifically, two patients (13%) had an improvement from NYHA functional class IV to II, eight patients (53%) had an improvement from class III to I, and five patients (34%) had an improvement from class II to I. In addition, there was a

remarkable enhancement in the MR and AR degrees, as shown in **Tables 3** and **4** ($P < 0.001$).

Analyzing the 14 adults from the cohort (**Figures 3A,B**), the last follow-up measurements revealed a significant reduction in the LVEDD (6.257 ± 0.580 vs. 4.721 ± 0.304 , $P < 0.001$) and LVESD (4.286 ± 0.597 vs. 3.157 ± 0.279 , $P < 0.001$) compared to the preoperative values. However, in 6-month-old infants, increased LVEDD (2.4 vs. 2.7) and LVESD (1.7 vs. 1.9) were observed (**Figures 3A,B**). In assessing the LVEF (%) (**Figure 3C**), comparable values were noted (61.667 ± 5.038 vs. 62.667 ± 3.697 , $P = 0.293$).

In three patients who were managed with a conservative follow-up strategy, the latest follow-up results were available for

TABLE 2 Improvements in cardiac function of patients with surgical interventions (*n* = 15).

Pre-NYHA functional class	Post-NYHA functional class				P-value
	I	II	III	IV	
I	—	—	—	—	<0.001
II	5 (33.3%)	—	—	—	
III	8 (53.3%)	—	—	—	
IV	—	2 (13.3%)	—	—	

TABLE 3 Improvements in the MR degree of patients with surgical interventions (*n* = 15).

Pre-MR degree	Post-MR degree		P-value
	None or mild	Moderate or severe	
None or mild	1 (6.7%)	—	<0.001
Moderate or severe	14 (93.3%)	—	

TABLE 4 Improvements in the AR degree of patients with surgical interventions (*n* = 15).

Pre-AR degree	Post-AR degree		P-value
	None or mild	Moderate or severe	
None or mild	—	—	<0.001
Moderate or severe	10 (100%)	—	

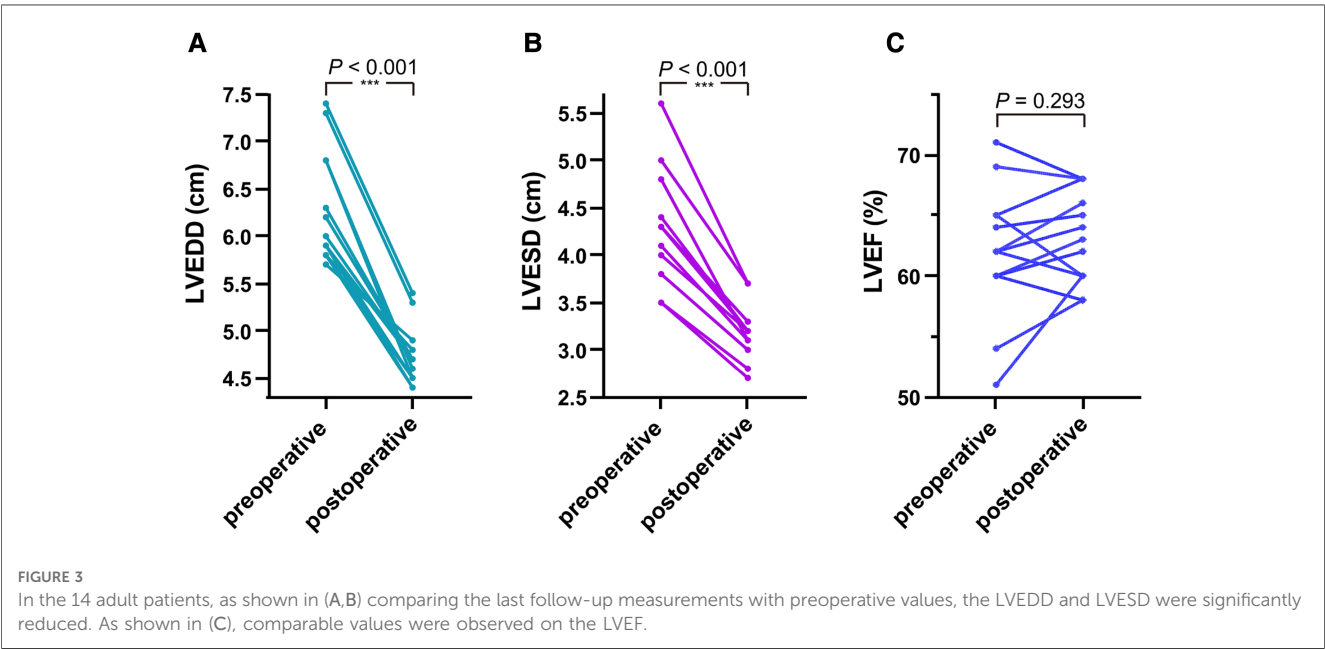
7, 8, and 24 months, respectively. Encouragingly, no progression in NYHA functional class or MR and/or AR degrees was observed compared to baseline, and left ventricular measures remained within the normal range throughout the follow-up period.

These results suggest that surgical interventions resulted in significant improvements in NYHA functional class, MR and AR degrees, and favorable alterations in the left ventricular dimensions for the majority of patients. Those managed

conservatively also exhibited stable clinical and echocardiographic outcomes during the follow-up period.

4. Discussion

Despite significant advancements in antibiotics, critical care, and surgical techniques, MVA remains life-threatening. Early detection and prompt intervention are crucial to prevent complications like rupture and embolism. Echocardiography is the primary screening method for heart vascular diseases and hemodynamic assessment. MVA presents a unique ultrasonic feature of a saccular echo-free space protruding in the left atrium, exhibiting systolic expansion and diastolic collapse. The aneurysm forms on the mitral valve, causing a small disruption in valve continuity known as an orifice that communicates with the left ventricle. Color Doppler flow imaging (CDFI) occasionally reveals blood flow excursions into and out of the MVA during systole and diastole, respectively (3, 18). In our study, we observed this CDFI manifestation in only one patient. The major echocardiographic finding for diagnosing MVA was the visualization of a localized saccular bulge of the mitral leaflet protruding in the left atrium, exhibiting systolic expansion and diastolic collapse, communicating with the left ventricle. Among the patients in our study, 12 were diagnosed with MVAs using TTEs, seven required additional TEEs for further diagnosis, and one infant patient was diagnosed with MVA during surgical intervention for an ECD and a PFO. TEE proved to be a more sensitive tool than TTE in detecting MVA, which is consistent with the previous studies (19, 20). However, misdiagnosis might occur, especially in small hearts, where TTE images may not be clear enough to detect the MVA. Furthermore, MVA has not been previously reported in infants without IE, suggesting a possible association with congenital heart disease.



The MVA formation mechanisms play a crucial role in patient management. The normal mitral valves consist of four layers, and damage to this valvular structure can lead to various lesions, such as prolapse, perforation, and MVA (11). The reported MVA formation mechanisms include direct extension of infection from the aortic valve to the anterior mitral leaflet, impingement of aortic valve regurgitation on the anterior mitral valve leaflet, contact of aortic valve vegetation with the anterior mitral leaflet (kissing lesions), and mitral valve infections (3, 5, 8, 9, 12, 21–27). Aortic valve endocarditis (AVE) is considered the most common cause of MVA (3, 4, 6, 7, 9, 24, 25, 28). In our study, 15 out of 20 patients were clinically diagnosed with infective endocarditis, and among them, 10 had AVE and 12 had moderate or severe aortic regurgitation, consistent with the previous findings. Moreover, MVAs in five patients were not related to endocarditis. In one patient, MVA was associated with BAV and moderate aortic regurgitation. MVA formation in this case might be attributed to the long-term impact of high aortic regurgitation pressure on the anterior mitral valve, leading to structural damage and mitral valve weakness (3, 29). Another case involved a 6-month-old infant with an endocardial cushion defect and a patent foramen ovale. As MVA has not been reported in infants without IE, the MVA, in this case, might be associated with congenital heart disease. The remaining three adult patients had no infective endocarditis or moderate or severe aortic regurgitation. One patient had mild aortic regurgitation with mild aortic valve calcification, another had mitral valve prolapse, and the third had gallstones. These cases suggest that MVA formation can be attributed to various factors, such as elderly calcified vascular disease, mitral valve prolapse, or other isolated vulvitis. All the MVAs in our study were detected on the anterior mitral leaflet, consistent with most previous reports (2, 4, 9, 10, 12, 13, 22, 25, 29, 30). However, some case studies have reported MVAs on the posterior mitral leaflet (31–37), possibly induced by inflammation.

MVA may lead to mitral regurgitation, LV enlargement, and ventricular function deterioration. Among the adult patients in this study, 80% showed varying degrees of LV enlargement and heart failure symptoms (NYHA functional classes II–IV). Surgical treatment was the only effective option for these patients, and most underwent MVR. However, two patients with severe left ventricular enlargement and heart failure symptoms died at the hospital after surgery. The severity of left ventricular enlargement and heart failure might contribute to early postoperative mortality, as observed in previous studies (38). MVR was the preferred approach in most cases due to the association of MVA with other malformations, making valve repair technically challenging. While MV repair had been shown to have better outcomes than MV replacement, as reported in previous studies (4, 39), only a few patients in our study underwent MV repair. Nevertheless, significant improvements in cardiac function and valve hemodynamics were observed during follow-ups for both MV replacement and repair patients. The majority of adult patients exhibited decreased LV size, but in one infant, LV size increased as the heart grew.

5. Conclusions

MVA is a rare disease with no distinct clinical manifestations. The majority of MVAs are associated with IE. Echocardiography, particularly TEE, has demonstrated high sensitivity in MVA diagnosis and assessment. In addition, echocardiography enables the evaluation of chamber changes and cardiac function, providing valuable guidance in determining the optimal timing for surgical interventions in MVA patients.

Data availability statement

The original contributions presented in the study are included in the article/**Supplementary Material**; further inquiries can be directed to the corresponding authors.

Ethics statement

The studies involving humans were approved by the Medical Ethics Committee of the Zhongnan Hospital of Wuhan University. The studies were conducted in accordance with local legislation and institutional requirements. The participants provided their written informed consent to participate in this study. Written informed consent was obtained from the individuals for the publication of any potentially identifiable images or data included in this article.

Author contributions

YW conceived and designed the study, conducted the data analysis, and drafted the manuscript. SW contributed to the study design and collected and interpreted the clinical data. DC and ML participated in the data collection, performed the statistical analysis, and helped in drafting and revising the manuscript. SM, LX, WS, and WW contributed to the study design, collected and interpreted the clinical data, and provided important intellectual content during manuscript preparation. SY contributed to the study design, collected and analyzed the data, and provided important intellectual input during manuscript preparation. BW oversaw the entire study, provided guidance on the study design and data analysis, and critically revised the manuscript for important intellectual content. All authors contributed to the article and approved the submitted version.

Funding

This work was supported by the Hubei Provincial Natural Science Foundation (Grant No. 2021CFB424).

Conflict of interest

The authors declare that the research was conducted in the absence of any commercial or financial relationships that could be construed as a potential conflict of interest.

Publisher's note

All claims expressed in this article are solely those of the authors and do not necessarily represent those of their affiliated organizations, or those of the publisher, the editors and the

reviewers. Any product that may be evaluated in this article, or claim that may be made by its manufacturer, is not guaranteed or endorsed by the publisher.

Supplementary material

The Supplementary Material for this article can be found online at: <https://www.frontiersin.org/articles/10.3389/fcvm.2023.1233926/full#supplementary-material>

SUPPLEMENTAL TABLE S1

Clinical parameters of the patients.

References

- Ruckel A, Erbel R, Henkel B, Kramer G, Meyer J. Mitral valve aneurysm revealed by cross-sectional echocardiography in a patient with mitral valve prolapse. *Int J Cardiol.* (1984) 6:633–7. doi: 10.1016/0167-5273(84)90010-X
- Tariq M, Zahid I, Sami S. Rare aneurysm of anterior mitral valve leaflet—a case report. *J Cardiothorac Surg.* (2019) 14:204. doi: 10.1186/s13019-019-1032-6
- Vilacosta I, San Roman JA, Sarria C, Graupner C, Batlle E, Peral V, et al. Clinical, anatomic, and echocardiographic characteristics of aneurysms of the mitral valve. *Am J Cardiol.* (1999) 84:110–3; A9. doi: 10.1016/S0002-9149(99)00206-4
- Uematsu S, Ashihara K, Tomioka H, Takagi A. Large mitral valve aneurysm with infective endocarditis. *BMJ Case Rep.* (2015) 2015. doi: 10.1136/bcr-2014-209092
- Nagai T, Hamabe A, Arakawa J, Konishi T, Hisadome H, Yoshida M, et al. Mitral valve aneurysm. *Ultraschall Med.* (2013) 34:69–70. doi: 10.1055/s-0032-1330324
- Kawai S, Oigawa T, Sunayama S, Yamaguchi H, Okada R, Hosoda Y, et al. Mitral valve aneurysm as a sequela of infective endocarditis: review of pathologic findings in Japanese cases. *J Cardiol.* (1998) 31(Suppl 1):19–33; discussion 34–6.
- Reid CL, Chandraratna AN, Harrison E, Kawanishi DT, Chandrasoma P, Nimalasuriya A, et al. Mitral valve aneurysm: clinical features, echocardiographic-pathologic correlations. *J Am Coll Cardiol.* (1983) 2:460–4. doi: 10.1016/S0735-1097(83)80272-1
- Halkos ME, Symbas JD, Felner JM, Symbas PN. Aneurysm of the mitral valve: a rare complication of aortic valve endocarditis. *Ann Thorac Surg.* (2004) 78:e65–6. doi: 10.1016/j.athoracsurg.2003.12.073
- Moretti M, Buscaglia A, Senes J, Tini G, Brunelli C, Bezante GP. Anterior mitral valve aneurysm is an uncommon complication of aortic valve infective endocarditis: a case report. *Am J Case Rep.* (2018) 19:1146. doi: 10.12659/AJCR.909922
- Janardhanan R, Kamal MU, Riaz IB, Smith MC. Anterior mitral valve aneurysm: a rare sequelae of aortic valve endocarditis. *Echo Res Pract.* (2016) 3:K7–K13. doi: 10.1530/ERP-16-0003
- Davis RH, Schuster B, Knoebel SB, Fisch C. Myxomatous degeneration of the mitral valve. *Am J Cardiol.* (1971) 28:449–55. doi: 10.1016/0002-9149(71)90009-9
- Werner ME, Riezebos RK, Kuipers RS. A perforated mitral valve aneurysm: a rare but serious complication of aortic valve endocarditis resulting from a regurgitant jet lesion. *Cureus.* (2020) 12:e11644. doi: 10.7759/cureus.11644
- Kolluru A, Behera S, Damarla V, Rajasurya V. Perforation of anterior mitral valve leaflet aneurysm: complication of *Enterococcus faecalis* infective endocarditis. *Cureus.* (2020) 12:e10249. doi: 10.7759/cureus.10249
- Kathir K, Dunn RF. Congenital obstructive mitral-valve aneurysm. *Intern Med J.* (2003) 33:541–2. doi: 10.1046/j.1445-5994.2003.00477.x
- Kim DJ, Cho KI, Jun HJ, Kim YJ, Song YJ, Jhi JH, et al. Perforated mitral valve aneurysm in the posterior leaflet without infective endocarditis. *J Cardiovasc Ultrasound.* (2012) 20:100–2. doi: 10.4250/jcu.2012.20.2.100
- Otto CM, Nishimura RA, Bonow RO, Carabello BA, Erwin JP 3rd, Gentile F, et al. 2020 ACC/AHA guideline for the management of patients with valvular heart disease: executive summary: a report of the American College of Cardiology/American Heart Association Joint Committee on Clinical Practice Guidelines. *Circulation.* (2021) 143:e35–71. doi: 10.1161/CIR.0000000000000932
- Chairs ASToIECGWC, Pettersson GB, Coselli JS Writing Committee; Pettersson GB, Coselli JS, et al. 2016 The American Association for Thoracic Surgery (AATS) consensus guidelines: surgical treatment of infective endocarditis: executive summary. *J Thorac Cardiovasc Surg.* (2017) 153:1241–1258.e29. doi: 10.1016/j.jtcvs.2016.09.093
- Alhuarrat MAD, Pargaonkar S, Kharawala A, Thachil R, Tiwari N. A rare case of concurrent mitral and aortic valve aneurysms in the setting of infective endocarditis. *Clin Case Rep.* (2023) 11(6):e7571. doi: 10.1002/ccr3.7571
- Isik T, Kurt M, Ayhan E, Tanboga IH. Incidental diagnosis of an aneurysm of the mitral valve posterior leaflet. *Anadolu Kardiyol Derg.* (2012) 12:E40–1. doi: 10.5152/akd.2012.235
- Mulholland MDL, Gotlieb MD, Frnc AI. Cardiac valve interstitial cells: regulator of valve structure and function. *Cardiovasc Pathol.* (1997) 6:167–74. doi: 10.1016/S1054-8807(96)00115-9
- Marcos-Alberca P, Rey M, Serrano JM, Fernández-Rozas I, Navarro F, Contreras A, et al. Aneurysm of the anterior leaflet of the mitral valve secondary to aortic valve endocarditis. *J Am Soc Echocardiogr.* (2000) 13:1050–2. doi: 10.1067/mje.2000.105892
- Piazza N, Marra S, Webb J, D'Amico M, Rinaldi M, Boffini M, et al. Two cases of aneurysm of the anterior mitral valve leaflet associated with transcatheter aortic valve endocarditis: a mere coincidence? *J Thorac Cardiovasc Surg.* (2010) 140:e36–8. doi: 10.1016/j.jtcvs.2009.11.012
- Raval AN, Menkis AH, Boughner DR. Mitral valve aneurysm associated with aortic valve endocarditis and regurgitation. *Heart Surg Forum.* (2002) 5:298–9.
- Ruparelia N, Lawrence D, Elkington A. Bicuspid aortic valve endocarditis complicated by mitral valve aneurysm. *J Card Surg.* (2011) 26:284–6. doi: 10.1111/j.1540-8191.2011.01243.x
- Tomsic A, Li WW, van Paridon M, Bindraban NR, de Mol BA. Infective endocarditis of the aortic valve with anterior mitral valve leaflet aneurysm. *Tex Heart Inst J.* (2016) 43:345–9. doi: 10.14503/THIJ-15-5322
- Cai TH, Moody JM Jr., Sako EY. Mitral valve aneurysm due to severe aortic valve regurgitation. *Circulation.* (1999) 100:e53–6. doi: 10.1161/01.CIR.100.12.e53
- Silbiger JJ. Mitral valve aneurysms in infective endocarditis: mechanisms, clinical recognition, and treatment. *J Heart Valve Dis.* (2009) 18:476–80.
- Guler A, Karabay CY, Gursay OM, Guler Y, Candan O, Akgun T, et al. Clinical and echocardiographic evaluation of mitral valve aneurysms: a retrospective, single center study. *Int J Cardiovasc Imaging.* (2014) 30:535–41. doi: 10.1007/s10554-014-0365-4
- Citro R, Silverio A, Ascoli R, Longobardi A, Bossone E, Benedetto G, et al. Anterior mitral valve aneurysm perforation in a patient with preexisting aortic regurgitation. *Monaldi Arch Chest Dis.* (2012) 78:210–1. doi: 10.4081/monaldi.2012.114
- Guler A, Hatipoglu S, Karabay CY, Kirma C. A rare cause of severe mitral regurgitation: mitral valve aneurysm. *Turk Kardiyol Dern Ars.* (2011) 39:690–2. doi: 10.5543/tkda.2011.01671
- Konishi T, Funayama N, Yamamoto T, Hotta D, Kikuchi K, Ohori K, et al. Severe mitral regurgitation due to mitral leaflet aneurysm diagnosed by three-dimensional transesophageal echocardiography: a case report. *BMC Cardiovasc Disord.* (2016) 16:1–5. doi: 10.1186/s12872-015-0179-x
- Jaffe AS, Geltman E, Rodey G, Uitto J. Mitral valve prolapse: a consistent manifestation of type IV Ehlers-Danlos syndrome. The pathogenetic role of the abnormal production of type III collagen. *Circulation.* (1981) 64:121–5. doi: 10.1161/01.CIR.64.1.121

33. Lebowitz MG, Distefano D, Prioleau PG, Uram M, Yannuzzi LA, Fleischmajer R. Pseudoxanthoma elasticum and mitral-valve prolapse. *N Engl J Med.* (1982) 307:228–31. doi: 10.1056/NEJM198207223070406
34. Hong SN, Perk G, Skolnick A, Kronzon I. Evaluation of a posterior mitral valve leaflet aneurysm by real time three-dimensional transesophageal echocardiography. *Echocardiography.* (2009) 26:1089–91. doi: 10.1111/j.1540-8175.2009.00966.x
35. Unger P, Antoine M, Hastir D, Dedobbeleer C, Leeman M. Infective endocarditis presenting as an isolated aneurysm of the posterior mitral leaflet. *Can J Cardiol.* (2013) 29:751.e11–3. doi: 10.1016/j.cjca.2012.09.010
36. de Castro S, Adorisio R, Pelliccia A, Papetti F, Fedele F, Pandian NG. Perforated aneurysms of left side valves during active infective endocarditis complicating hypertrophic obstructive cardiomyopathy. *Eur J Echocardiogr.* (2002) 3:100–2. doi: 10.1053/euje.2001.0123
37. Li YH, Lin JM, Lei MH, Wang TL, Ma HM, Hwang JJ, et al. Mitral valve aneurysm and infective endocarditis: report of four cases. *J Formos Med Assoc.* (1995) 94:499–502.
38. Ho HQ, Nguyen VP, Phan KP, Pham NV. Mitral valve repair with aortic valve replacement in rheumatic heart disease. *Asian Cardiovasc Thorac Ann.* (2004) 12:341–5. doi: 10.1177/021849230401200413
39. Shuhaiber J, Anderson RJ. Meta-analysis of clinical outcomes following surgical mitral valve repair or replacement. *Eur J Cardiothorac Surg.* (2007) 31:267–75. doi: 10.1016/j.ejcts.2006.11.014



OPEN ACCESS

EDITED BY

Francesca Innocenti,
Careggi University Hospital, Italy

REVIEWED BY

Constantina Aggeli,
National and Kapodistrian University of Athens,
Greece
Antoine AbdelMassih,
Cairo University, Egypt

*CORRESPONDENCE

Attila Nemes
✉ nemes.attila@med.u-szeged.hu

RECEIVED 09 January 2023

ACCEPTED 07 August 2023

PUBLISHED 04 September 2023

CITATION

Nemes A, Kormányos Á, Rácz G, Ruzsa Z,
Achim A, Ambrus N and Lengyel C (2023)
Tricuspid annular and right atrial volume
changes are associated in healthy adults—
insights from the three-dimensional speckle-
tracking echocardiographic MAGYAR-Healthy
Study.
Front. Cardiovasc. Med. 10:1140599.
doi: 10.3389/fcvm.2023.1140599

COPYRIGHT

© 2023 Nemes, Kormányos, Rácz, Ruzsa,
Achim, Ambrus and Lengyel. This is an open-
access article distributed under the terms of the
Creative Commons Attribution License (CC BY).
The use, distribution or reproduction in other
forums is permitted, provided the original
author(s) and the copyright owner(s) are
credited and that the original publication in this
journal is cited, in accordance with accepted
academic practice. No use, distribution or
reproduction is permitted which does not
comply with these terms.

Tricuspid annular and right atrial volume changes are associated in healthy adults—insights from the three-dimensional speckle-tracking echocardiographic MAGYAR-Healthy Study

Attila Nemes*, Árpád Kormányos, Gergely Rácz, Zoltán Ruzsa,
Alexandru Achim, Nóra Ambrus and Csaba Lengyel

Department of Medicine, Albert Szent-Györgyi Medical School, University of Szeged, Szeged, Hungary

Introduction: The tricuspid valve and its annulus (TA) and the right atrium (RA) play a significant role in regulating blood flow in the right heart. However, their effect on each other is not fully understood even in normal circumstances. Three-dimensional (3D) speckle-tracking echocardiography (3DSTE) is able to simultaneously assess TA and RA at the same time in a non-invasive way. The present study aimed to examine associations between tricuspid annular (TA) dimensions and right atrial (RA) volumes in healthy adults by 3DSTE.

Methods: The present study comprised 144 healthy subjects (mean age: 34.4 ± 12.6 years, 72 males), who participated in this study on a voluntary basis for screening between 2011 and 2015. In all subjects, electrocardiography, two-dimensional Doppler echocardiography and 3DSTE have been performed.

Results: With increasing end-systolic maximum RA volume, all end-systolic and end-diastolic TA dimensions showed simultaneous increase, but in various degrees resulting in (non-significant) reduction of TA functional properties. Similarly, with increasing diastolic pre-atrial contraction and minimum RA volumes, TA dimensions increased simultaneously (except end-diastolic TA diameter), but in various degrees resulting in reduced TA fractional shortening and fractional area change. With increasing RA dimensions, end-systolic and end-diastolic TA dimensions showed simultaneous increase, but in different, sometimes not significant degrees. While RA stroke volumes showed increasing pattern with TA dilation, RA emptying fractions have not changed substantially.

Conclusions: 3DSTE is suitable for non-invasive assessment of TA dimensions and RA volumes at the same time using the same 3D echocardiographic dataset. Significant associations between TA size and RA volumes exist in healthy circumstances. Strong associations in case of dilation of TA in the presence of higher RA volumes could partly explain functional tricuspid regurgitation later developing in subjects in sinus rhythm.

KEYWORDS

healthy, tricuspid annulus, right atrial, volume, three-dimensional, speckle-tracking, echocardiography

Introduction

In recent years, there has been an increasing interest in the evaluation of the right heart due to newer therapeutic options and advanced imaging techniques (1–4). New findings help to better understand the right heart, its components, their characteristics and interactions, even with the aorta, left heart and venous system, and their dependence on each other (1–4). The tricuspid valve (TV) and its annulus (TA) and the right atrium (RA) play a significant role in regulating blood flow in the right heart. Their effect on each other was examined in subjects with functional tricuspid regurgitation (FTR) (5–7) and even in healthy normal circumstances (8, 9). Three-dimensional speckle-tracking echocardiography (3DSTE) is able to simultaneously assess TA and RA in detail at the same time in a non-invasive way (10–12). The present study aimed to examine associations between tricuspid annular (TA) dimensions and right atrial (RA) volumes respecting the cardiac cycle in healthy adults by 3DSTE.

Patients and methods

Study population

The present study comprised 144 healthy subjects (mean age: 34.4 ± 12.6 years, 72 males), who participated in this study on a voluntary basis for screening between 2011 and 2015. In all subjects, electrocardiography (ECG), two-dimensional Doppler echocardiography (2DE) and 3DSTE have been performed by the same observer (ÁK). A participant was considered to be healthy if they had no acute or chronic illness in their medical history, ECG showed no abnormality, and findings of complete 2DE were in normal ranges. None of the subjects were obese, smoker or had a history of regular drug use. The present study is part of the Motion Analysis of the heart and Great vessels bY three-dimensional speckle-tRacking echocardiography in Healthy subjects (MAGYAR-Healthy) Study. This study aimed to evaluate the physiological associations among 3DSTE-derived and other parameters in healthy adults (“Magyar” means “Hungarian” in Hungarian language). The study was conducted in accordance with the Declaration of Helsinki (as revised in 2013). The study was approved by the Institutional and Regional Human Biomedical Research Committee of University of Szeged, Hungary (No.: 71/2011 and updated versions) and informed consent was given by all subjects.

Two-dimensional Doppler echocardiography

In all cases, the same Toshiba Artida™ echocardiography equipment (Toshiba Medical Systems, Tokyo, Japan) was used

attached to a 1–5 MHz PST-30BT phased-array transducer. During chamber quantifications the rules prescribed in recent guidelines were followed (1). For visual quantification of valvular regurgitations and to exclude significant valvular stenosis, Doppler echocardiography was used. Early and late mitral inflow E and A were also determined to assess LV diastolic function (1, 13).

Three-dimensional speckle-tracking echocardiography

The same Toshiba Artida™ echocardiographic equipment (Toshiba Medical Systems, Tokyo, Japan) was used for 3DSTE as well, but transducer was changed to a PST-25SX matrix-array transducer with 3DSTE capability (10–12, 14, 15). The protocol of the 3DSTE examination followed our routines: firstly, 3D echocardiographic datasets were acquired from the apical window following optimisation of image quality on the right atrium (RA). If RR intervals were constant on ECG (sinus rhythm) and subjects were on breath-hold, pyramid-shaped 3D echocardiographic datasets were digitally stored on hard drive for future analysis.

RA-quantification by 3DSTE

Later, offline analysis was performed with the vendor-provided 3D Wall Motion Tracking software version 2.7 (Ultra Extend, Toshiba Medical Systems, Tokyo, Japan). Data were displayed in selected apical two- (AP2CH) and four-chamber (AP4CH) views and 3 short-axis views at basal, midatrial and superior levels. To create a 3D cast of the RA, definition of reference points on RA endocardium were required in AP2CH and AP4CH views on the edges of the TA ring and the RA apex at end-diastole, then automatic sequential analysis (reconstruction) was performed for the complete endocardial RA surface. Taking into account the cardiac cycle, the following RA volumes were obtained (Figure 1) (14):

- Maximum RA volume, measured at end-systole, just before tricuspid valve opening (Vmax).
- RA volume before atrial contraction, measured at early-diastole at the time of the P wave on the ECG (VpreA).
- Minimum RA volume measured at end-diastole, just before tricuspid valve closure (Vmin).

Using RA volumes, several stroke volumes (SV) and emptying fractions (EF) could be determined featuring different phases of RA function:

Reservoir function:

- Total Atrial Stroke Volume (TASV): $V_{\max} - V_{\min}$.
- Total Atrial Emptying Fraction (TAEF): $TASV / V_{\max} \times 100$.

Conduit function:

- Passive Atrial Stroke Volume (PASV): $V_{\max} - V_{\text{preA}}$.
- Passive Atrial Emptying Fraction (PAEF): $PASV / V_{\max} \times 100$.

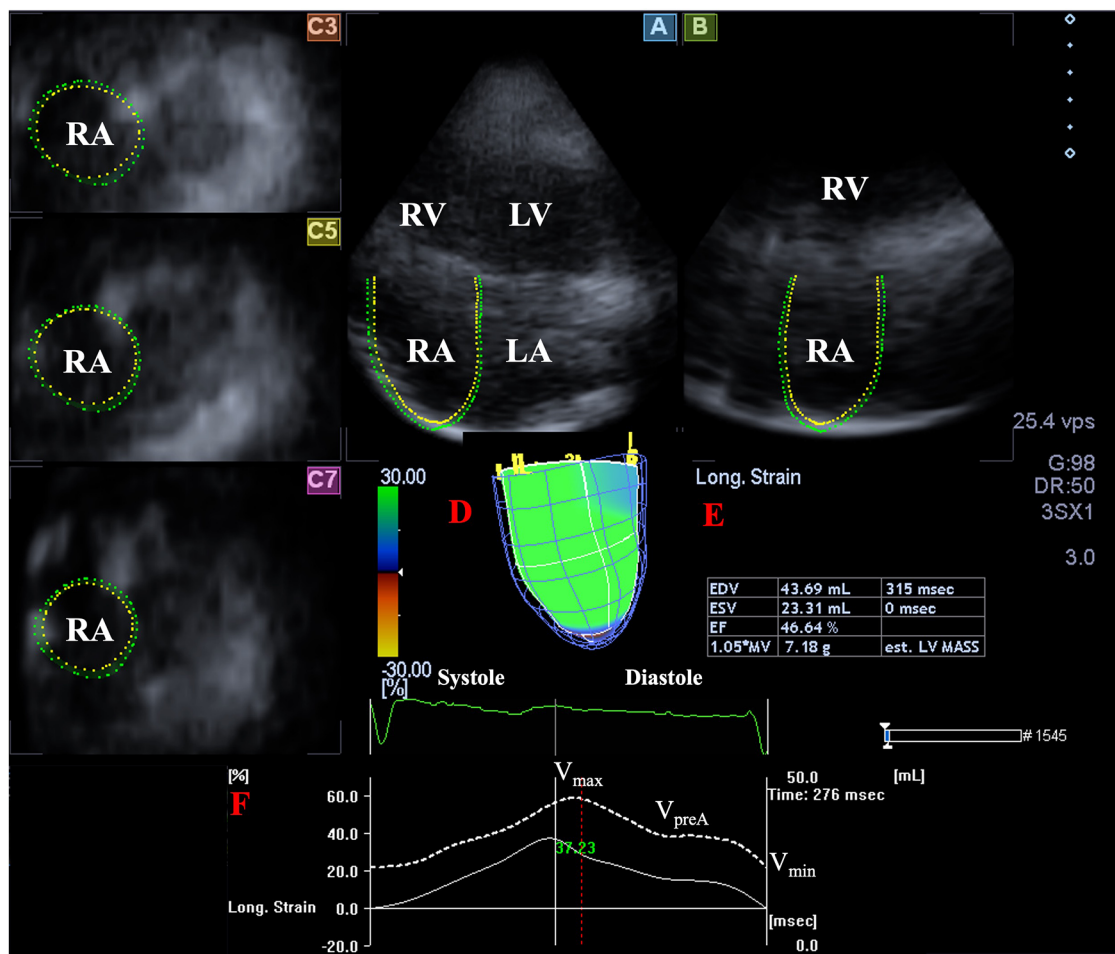


FIGURE 1

Three-dimensional (3D) speckle-tracking echocardiographic analysis of the right atrium in a healthy subject: apical longitudinal four-chamber (A) and two-chamber views (B) and 3 short-axis views at basal (C3), midatrial (C5) and superior (C7) RA levels. 3D virtual RA model (D), RA volumetric data (E) and time—global RA volume change curve (dashed white curve) and time—global RA longitudinal strain curve (white curve) respecting the cardiac cycle are demonstrated (F). LA, left atrium; LV, left ventricle; RA, right atrium; RV, right ventricle; EDV, end-diastolic volume; ESV, end-systolic volume; EF, ejection fraction; est., estimated; MV, myocardial volume; V_{max} , maximum right atrial volume; V_{preA} , volume at the onset of atrial systole; V_{min} , minimum right atrial volume.

Active contraction:

- Active Atrial Stroke Volume (AASV): $V_{preA} - V_{min}$.
- Active Atrial Emptying Fraction (AAEF): $AASV / V_{preA} \times 100$.

TA-quantification by 3DSTE

During assessments, AP2CH and AP4CH views helped to find optimal lateral and septal TA endpoints on C7 short-axis view (Figure 2) (15):

Morphological parameters were measured at end-diastole (just before tricuspid valve closure) and at end-systole (just before tricuspid valve opening):

- TA diameter (TAD), measured by drawing a perpendicular line from the peak of TA curvature to the middle of the straight TA border,
- TA area (TAA), measured by planimetry,
- TA perimeter (TAP), measured by planimetry,

Functional parameters were calculated from morphologic end-diastolic and end-systolic parameters:

- TA fractional shortening (TAFS), defined as $[(\text{end-diastolic TAD} - \text{end-systolic TAD}) / \text{end-diastolic TAD}] \times 100$,
- TA fractional area change (TAFAC), defined as $[(\text{end-diastolic TAA} - \text{end-systolic TAA}) / \text{end-diastolic TAA}] \times 100$.

Statistical analysis

Data were presented in mean \pm standard deviation (SD) format or frequency/percentage format, as appropriate. $p < 0.05$ was considered to be statistically significant. Student t test with Welch correction and one-way analysis of variance (ANOVA) test with Bonferroni correction were used, where appropriated. Fischer's exact test was used for all categorical variables. Pearson's correlation coefficient was calculated for correlations. The Bland–Altman method was used to determine intraobserver

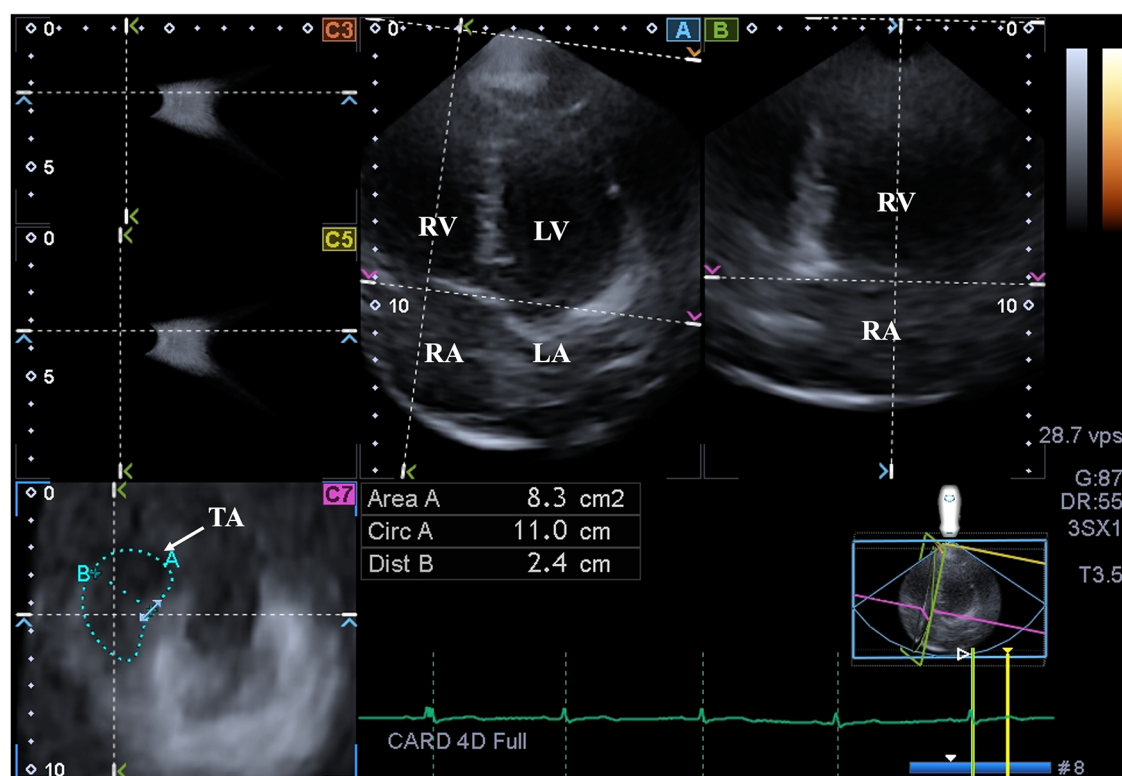


FIGURE 2

Three-dimensional (3D) speckle-tracking echocardiographic assessment of the tricuspid annulus in a healthy subject: apical longitudinal four-chamber (A) and two-chamber views and cross-sectional view (C7) of the tricuspid annulus optimised on (A) and (B) images. White arrow indicate plane of the tricuspid annulus. LA, left atrium; LV, left ventricle; RA, right atrium; RV, right ventricle; Area, tricuspid annular area; Circ, tricuspid annular perimeter; Dist, tricuspid annular diameter.

and interobserver agreements. For intraobserver and interobserver correlations, intraclass correlation coefficients (ICCs) were calculated. Multivariable regression analysis was used for assessment of independent predictors of V_{\max} and TAA-D. GPower 3.1.9 Software (Heinrich-Heine Universität, Düsseldorf, Germany) was applied for power calculation: in the presence of effect size: 0.9, alpha: 0.05, power: 0.8 the minimum group size is $n = 120$. Statistical calculations were performed using SPSS software (SPSS Inc, Chicago, IL, USA).

Results

Clinical and two-dimensional Doppler echocardiographic data

Clinical and routine echocardiographic parameters of healthy adults are presented in **Table 1**. None of the subjects involved had larger than or equal to grade 1 valvular regurgitation or showed significant valvular stenosis on any valves.

Classification of subjects

Mean \pm SD of 3DSTE-derived RA and TA parameters of healthy subjects are presented in **Table 2**. Healthy subjects were

classified into 3 groups according to the normal maximum (V_{\max}), pre-atrial contraction (V_{preA}) and minimum (V_{\min}) RA volumes and end-systolic and end-diastolic TA diameter (TAD-S and TAD-D, respectively), area (TAA-S and TAA-D, respectively) and perimeter (TAP-S and TAP-D, respectively): estimated mean \pm SD served as the lower (33.8 ml, 24.8 ml, 18.1 ml, 1.5 cm, 2.1 cm, 4.0 cm², 5.7 cm², 7.9 cm, 9.3 cm, respectively) and upper (64.0 ml, 46.8 ml, 37.5 ml, 2.1 cm, 2.7 cm, 6.8 cm², 8.9 cm², 10.1 cm, 11.7 cm, respectively) values.

Increase of RA volumes and TA

With increasing end-systolic V_{\max} , all end-systolic and end-diastolic TA dimensions showed simultaneous increase, but in various degrees resulting in (non-significant) reduction of TA functional properties. Similarly, with increasing diastolic V_{preA} and V_{\min} , TA dimensions increased simultaneously (except TAD-D), but in various degrees resulting in reduced TAFS and TAFAC (**Table 3**).

Increase of RA volumes and RA volume-based functional properties

With increasing end-systolic V_{\max} , all SVs and EFs showed simultaneous increase, except AAEF, which remained unchanged.

TABLE 1 Clinical and two-dimensional echocardiographic data.

Data	Measures
Clinical data	
<i>n</i>	144
Mean age (years)	34.4 ± 12.6
Males (%)	72 (50%)
Systolic blood pressure (mmHg)	121.4 ± 4.1
Diastolic blood pressure (mmHg)	78.9 ± 3.4
Heart rate (1/s)	71.3 ± 2.1
Height (cm)	170.8 ± 10.3
Weight (kg)	72.9 ± 15.5
Body surface area (kg/m ²)	1.87 ± 0.36
Two-dimensional echocardiographic data	
LA diameter (mm)	37.8 ± 3.1
LV end-diastolic diameter (mm)	48.4 ± 3.1
LV end-systolic diameter (mm)	32.5 ± 2.6
LV end-diastolic volume (ml)	106.3 ± 23.3
LV end-systolic volume (ml)	38.2 ± 8.9
Interventricular septum (mm)	9.3 ± 1.1
LV posterior wall (mm)	9.4 ± 1.2
LV ejection fraction (%)	65.1 ± 3.5
Early diastolic mitral inflow velocity—E (cm/s)	79.4 ± 16.5
Late diastolic mitral inflow velocity—A (cm/s)	60.0 ± 15.0

LA, left atrial; LV, left ventricular.

TABLE 2 Three-dimensional speckle-tracking echocardiography-derived right atrial volumetric and tricuspid annular parameters.

Parameters	Measures
Maximum right atrial volume (V_{\max} , ml)	48.9 ± 15.1
Pre-atrial contraction left atrial volume (V_{preA} , ml)	35.8 ± 11.0
Minimum left atrial volume (V_{\min} , ml)	27.8 ± 9.7
Total atrial stroke volume (TASV, ml)	21.1 ± 10.0
Total atrial emptying fraction (TAEF, %)	42.5 ± 12.6
Passive atrial stroke volume (PASV, ml)	13.1 ± 8.3
Passive atrial emptying fraction (PAEF, %)	25.8 ± 11.7
Active atrial stroke volume (AASV, ml)	8.0 ± 4.8
Active atrial emptying fraction (AAEF, %)	22.5 ± 11.6
End-systolic tricuspid annular diameter (TAD-S, mm)	1.8 ± 0.3
End-systolic tricuspid annular area (TAA-S, mm ²)	5.4 ± 1.4
End-systolic tricuspid annular perimeter (TAP-S, mm)	9.0 ± 1.1
End-diastolic tricuspid annular diameter (TAD-D, mm)	2.4 ± 0.3
End-diastolic tricuspid annular area (TAA-D, mm ²)	7.3 ± 1.6
End-diastolic tricuspid annular perimeter (TAP-D, mm)	10.5 ± 1.2
Tricuspid annular fractional shortening (TAFS, %)	21.4 ± 8.8
Tricuspid annular fractional area change (TAFAC, %)	26.4 ± 10.6

With increasing diastolic V_{preA} , while SVs showed increasing pattern, EFs had decreasing pattern. With increasing diastolic V_{\min} , while SVs remained unchanged, EFs showed decreasing pattern (Table 3).

Dilation of TA and RA volumes

With increasing TA dimensions, end-systolic and end-diastolic RA dimensions showed simultaneous increase, but in different degrees. While SVs showed increasing pattern with TA dilation, EFs have not changed substantially (Tables 4, 5).

Dilation of TA and TA functional properties

With increasing end-systolic TA dimensions, TA functional properties showed simultaneous decrease, but in different degrees. With increasing end-diastolic TAD-D, TAFS increased, TAFAC remained unchanged. With increasing end-diastolic TAA-D and TAP-D, TA functional properties did not show significant changes (Tables 4, 5).

Correlations and regression analysis

V_{\max} correlated with TAD-D ($r = 0.30$, $p < 0.01$), TAA-D ($r = 0.54$, $p < 0.01$), TAA-P ($r = 0.50$, $p < 0.01$), TAD-S ($r = 0.39$, $p < 0.01$), TAA-S ($r = 0.55$, $p < 0.01$) and TAA-P ($r = 0.49$, $p < 0.01$). Similarly, V_{preA} showed correlations with TAD-D ($r = 0.25$, $p < 0.01$), TAA-D ($r = 0.49$, $p < 0.01$), TAA-P ($r = 0.45$, $p < 0.01$), TAD-S ($r = 0.40$, $p < 0.01$), TAA-S ($r = 0.58$, $p < 0.01$) and TAA-P ($r = 0.49$, $p < 0.01$). V_{\min} correlated with TAD-D ($r = 0.54$, $p < 0.01$), TAA-D ($r = 0.48$, $p < 0.01$), TAA-P ($r = 0.41$, $p < 0.01$), TAD-S ($r = 0.37$, $p < 0.01$), TAA-S ($r = 0.54$, $p < 0.01$) and TAA-P ($r = 0.46$, $p < 0.01$), as well.

The logistic regression analysis identified presence of increased V_{\max} as an independent predictor of TAA-D [hazard ratio (HR) 1.75, 95% CI of HR: 1.18 to 3.33, $p < 0.05$]. Similarly, dilated TAA-D had an independent predictive value for V_{\max} [hazard ratio (HR) 1.80, 95% CI of HR: 1.15 to 3.27, $p < 0.05$].

Feasibility of 3DSTE-derived RA and TA measurements

During evaluations, 94 subjects were excluded due to inferior image quality from the total of 238 subjects, therefore the overall feasibility of simultaneous 3DSTE-derived RA and TA quantifications was 144 out of 238 (61% overall feasibility).

Reproducibility of 3DSTE-derived RA and TA assessments

3DSTE-derived end-diastolic and end-systolic TA dimensions and RA volumes respecting cardiac cycle were measured twice by the same observer (intraobserver agreement) and by two independent observers (interobserver agreement). The values were expressed as mean ± SD together with corresponding ICCs, the results are presented in Table 6.

Discussion

Components of the TV or right atrioventricular valve include fibrous TA, anterior, posterior and septal leaflets, papillary muscles and tendinous cords, which interact with RA and RV during the cardiac cycle. When TV opens in diastole, it helps correct one-way blood flow from the RA to the RV, while in

TABLE 3 Right atrial volumes and tricuspid annular parameters in different right atrial volume groups.

	$V_{\max} \leq 33.8 \text{ ml}$ ($n = 26$)	$33.8 \text{ ml} < V_{\max} < 64.0 \text{ ml}$ ($n = 92$)	$64.0 \text{ ml} \leq V_{\max}$ ($n = 26$)	$V_{\text{preA}} \leq 24.8 \text{ ml}$ ($n = 23$)	$24.8 \text{ ml} < V_{\text{preA}} < 46.8 \text{ ml}$ ($n = 100$)	$46.8 \text{ ml} \leq V_{\text{preA}}$ ($n = 21$)	$V_{\min} \leq 18.1 \text{ ml}$ ($n = 22$)	$18.1 \text{ ml} < V_{\min} < 37.5 \text{ ml}$ ($n = 93$)	$37.5 \text{ ml} \leq V_{\min}$ ($n = 29$)
V_{\max} (ml)	29.6 ± 3.4	47.5 ± 7.5*	73.7 ± 9.1***	31.7 ± 7.9	48.6 ± 10.7 [†]	70.9 ± 13.3 ^{†,††}	34.4 ± 9.7	47.1 ± 11.3 [‡]	65.6 ± 14.6 ^{‡,‡‡}
V_{preA} (ml)	23.1 ± 4.1	35.1 ± 6.5*	50.5 ± 10.8***	21.4 ± 3.3	35.3 ± 5.5 [†]	55.4 ± 8.4 ^{†,††}	23.4 ± 6.2	33.9 ± 5.9 [‡]	51.2 ± 9.7 ^{‡,‡‡}
V_{\min} (ml)	18.1 ± 3.7	27.0 ± 7.4*	39.8 ± 8.1***	16.0 ± 2.9	27.1 ± 6.2 [†]	44.8 ± 4.5 ^{†,††}	15.3 ± 2.3	25.9 ± 4.7 [‡]	43.3 ± 4.5 ^{‡,‡‡}
TASV (ml)	11.5 ± 3.1	20.4 ± 7.7*	33.9 ± 8.9***	15.7 ± 8.0	21.4 ± 9.3 [†]	26.1 ± 12.3 [†]	19.1 ± 9.3	21.2 ± 9.2	22.3 ± 12.7
TAEF (%)	38.9 ± 9.4	42.8 ± 13.6	45.9 ± 10.1*	47.4 ± 12.4	42.9 ± 12.5	35.1 ± 10.7 ^{†,††}	52.9 ± 12.1	43.4 ± 10.3 [‡]	31.7 ± 12.0 ^{‡,‡‡}
PASV (ml)	6.6 ± 3.4	12.3 ± 6.3*	23.2 ± 9.6***	10.4 ± 7.2	13.3 ± 7.9	15.5 ± 11.0	11.0 ± 7.7	13.2 ± 7.8	14.4 ± 10.3
PAEF (%)	22.1 ± 11.0	25.5 ± 11.2	31.4 ± 12.3***	30.4 ± 13.9	25.8 ± 10.9	20.4 ± 11.8 ^{†,††}	30.0 ± 15.3	26.4 ± 10.4	20.5 ± 11.4 ^{‡,‡‡}
AASV (ml)	4.9 ± 2.2	8.1 ± 4.6*	10.8 ± 5.6***	5.3 ± 2.5	8.1 ± 4.5 [†]	10.6 ± 6.2 ^{†,††}	8.1 ± 5.0	8.0 ± 3.9	8.0 ± 6.8
AAEF (%)	21.2 ± 8.8	23.4 ± 13.0	20.9 ± 8.4	24.6 ± 10.2	23.0 ± 12.3	18.2 ± 8.5 [†]	32.2 ± 12.9	23.0 ± 9.4 [‡]	13.9 ± 10.9 ^{‡,‡‡}
TAD-S (mm)	1.7 ± 0.3	1.8 ± 0.2*	2.0 ± 0.4***	1.7 ± 0.3	1.8 ± 0.2 [†]	2.0 ± 0.4 ^{†,††}	1.7 ± 0.2	1.8 ± 0.2 [‡]	1.9 ± 0.4 [‡]
TAA-S (mm)	4.2 ± 1.2	5.4 ± 1.1*	6.6 ± 1.8***	4.4 ± 1.3	5.4 ± 1.2 [†]	6.6 ± 1.9 ^{†,††}	4.3 ± 1.3	5.4 ± 1.2 [‡]	6.2 ± 1.8 ^{‡,‡‡}
TAP-S (mm)	8.3 ± 1.2	9.0 ± 0.9*	9.9 ± 1.1***	8.5 ± 1.2	9.0 ± 1.0 [†]	9.9 ± 1.2 ^{†,††}	8.3 ± 1.2	9.0 ± 0.9 [‡]	9.6 ± 1.2 ^{‡,‡‡}
TAD-D (mm)	2.2 ± 0.3	2.3 ± 0.3*	2.5 ± 0.4***	2.3 ± 0.3	2.3 ± 0.3	2.5 ± 0.4	2.2 ± 0.4	2.4 ± 0.3	2.4 ± 0.4
TAA-D (mm)	6.0 ± 1.4	7.3 ± 1.3*	8.6 ± 1.7***	6.6 ± 1.7	7.3 ± 1.4 [†]	8.6 ± 1.9 ^{†,††}	6.3 ± 1.6	7.3 ± 1.4 [‡]	8.2 ± 1.8 ^{‡,‡‡}
TAP-D (mm)	9.5 ± 1.2	10.5 ± 1.0*	11.2 ± 1.0***	10.0 ± 1.5	10.4 ± 1.0	11.2 ± 1.1 ^{†,††}	9.9 ± 1.3	10.4 ± 1.1 [‡]	10.9 ± 1.1 ^{‡,‡‡}
TAFS (%)	24.3 ± 10.1	21.1 ± 8.7	19.8 ± 7.0	26.1 ± 9.6	20.6 ± 8.5 [†]	19.4 ± 8.0 [†]	24.3 ± 10.8	21.4 ± 8.6	19.1 ± 7.4 [‡]
TAFAC (%)	29.4 ± 12.3	26.5 ± 9.9	23.2 ± 10.5	32.5 ± 11.9	25.6 ± 10.1 [†]	22.3 ± 9.0 [†]	31.2 ± 11.8	25.9 ± 10.2 [‡]	24.1 ± 10.0 [‡]

V_{\max} , maximum end-systolic right atrial volume; V_{preA} , early diastolic pre-atrial contraction right atrial volume; V_{\min} , minimum end-diastolic right atrial volume; TASV, total atrial stroke volume; TAEF, total (right) atrial emptying fraction; PASV, passive (right) atrial stroke volume; PAEF, passive (right) atrial emptying fraction; AASV, active (right) atrial stroke volume; AAEF, active (right) atrial emptying fraction; TAD, tricuspid annular diameter; TAA, tricuspid annular area; TAP, tricuspid annular perimeter; TAFS, tricuspid annular fractional shortening; TAFAC, tricuspid annular fractional area change; S, end-systolic; D, end-diastolic.

* $p < 0.05$ vs. $V_{\max} \leq 33.8 \text{ ml}$.

** $p < 0.05$ vs. $33.8 \text{ ml} < V_{\max} < 64.0 \text{ ml}$.

[†] $p < 0.05$ vs. $V_{\text{preA}} \leq 24.8 \text{ ml}$.

^{††} $p < 0.05$ vs. $24.8 \text{ ml} < V_{\text{preA}} < 46.8 \text{ ml}$.

[‡] $p < 0.05$ vs. $V_{\min} \leq 18.1 \text{ ml}$.

^{‡‡} $p < 0.05$ vs. $18.1 \text{ ml} < V_{\min} < 37.5 \text{ ml}$.

TABLE 4 Right atrial volumes and tricuspid annular parameters in different end-systolic tricuspid annular groups.

	$\text{TAD-S} \leq 1.5 \text{ cm}$ ($n = 16$)	$1.5 \text{ cm} < \text{TAD-S} < 2.1 \text{ cm}$ ($n = 102$)	$2.1 \text{ cm} \leq \text{TAD-S}$ ($n = 26$)	$\text{TAA-S} \leq 4.0 \text{ cm}^2$ ($n = 24$)	$4.0 \text{ cm} < \text{TAA-S} < 6.8 \text{ cm}^2$ ($n = 103$)	$6.8 \text{ cm}^2 \leq \text{TAA-S}$ ($n = 17$)	$\text{TAP-S} \leq 7.9 \text{ cm}$ ($n = 24$)	$7.9 \text{ cm} < \text{TAP-S} < 10.1 \text{ cm}$ ($n = 102$)	$10.1 \text{ cm} \leq \text{TAP-S}$ ($n = 18$)
V_{\max} (ml)	35.6 ± 10.4	49.5 ± 14.4*	54.9 ± 15.6*	35.3 ± 9.8	50.0 ± 13.3 [†]	61.3 ± 18.4 ^{†,††}	36.7 ± 10.5	50.0 ± 13.7 [‡]	58.6 ± 18.6 ^{‡,‡‡}
V_{preA} (ml)	27.0 ± 9.6	35.8 ± 10.1*	41.2 ± 11.9***	25.1 ± 6.9	36.5 ± 8.7 [†]	46.2 ± 15.4 ^{†,††}	27.6 ± 8.1	36.3 ± 9.4 [‡]	43.4 ± 15.5 ^{‡,‡‡}
V_{\min} (ml)	21.3 ± 9.6	27.5 ± 9.0*	32.8 ± 9.8***	19.1 ± 6.6	28.5 ± 8.4 [†]	36.0 ± 11.7 ^{†,††}	20.7 ± 7.5	28.4 ± 8.9 [‡]	34.0 ± 11.4 ^{‡,‡‡}
TASV (ml)	14.3 ± 6.4	22.0 ± 9.9*	22.1 ± 10.6*	16.2 ± 9.1	21.5 ± 9.5 [†]	25.3 ± 11.7 [†]	16.0 ± 8.9	21.7 ± 9.7 [‡]	24.6 ± 10.9 [‡]
TAEF (%)	40.9 ± 15.2	48.7 ± 11.9	39.0 ± 13.1	44.7 ± 15.1	42.3 ± 11.9	40.4 ± 13.1	42.7 ± 14.7	42.7 ± 12.4	41.2 ± 11.4
PASV (ml)	8.6 ± 6.1	13.7 ± 8.2*	13.7 ± 9.1*	10.2 ± 8.2	13.5 ± 7.9	15.1 ± 10.4	9.0 ± 7.4	13.7 ± 8.1 [‡]	15.1 ± 9.5 [‡]
PAEF (%)	23.9 ± 15.5	26.6 ± 10.9	23.8 ± 12.3	27.1 ± 15.9	25.7 ± 10.2	24.2 ± 14.0	23.5 ± 15.2	26.4 ± 10.6	25.6 ± 12.9
AASV (ml)	5.7 ± 2.3	8.3 ± 4.7*	8.3 ± 5.8	6.0 ± 3.4	8.1 ± 4.6 [†]	10.2 ± 6.2 [†]	6.9 ± 3.7	8.0 ± 4.6	9.4 ± 6.4
AAEF (%)	22.7 ± 10.6	23.3 ± 11.6	19.8 ± 11.9	24.3 ± 11.2	22.3 ± 12.0	21.5 ± 9.4	25.5 ± 10.3	22.2 ± 12.1	20.8 ± 10.1
TAD-S (mm)	1.4 ± 0.1	1.8 ± 0.1*	2.3 ± 0.2***	1.6 ± 0.2	1.8 ± 0.2 [†]	2.2 ± 0.3 ^{†,††}	1.7 ± 0.2	1.8 ± 0.2 [‡]	2.2 ± 0.4 ^{‡,‡‡}
TAA-S (mm)	4.0 ± 0.9	5.2 ± 1.2*	6.8 ± 1.6***	3.5 ± 0.4	5.4 ± 0.8 [†]	8.1 ± 1.3 ^{†,††}	3.7 ± 0.5	5.3 ± 0.9 [‡]	7.8 ± 1.4 ^{‡,‡‡}
TAP-S (mm)	8.2 ± 0.9	9.0 ± 1.0*	9.8 ± 1.1***	7.6 ± 0.6	9.1 ± 0.7 [†]	10.8 ± 0.9 ^{†,††}	7.4 ± 0.4	9.1 ± 0.6 [‡]	11.0 ± 0.7 ^{‡,‡‡}
TAD-D (mm)	2.1 ± 0.3	2.3 ± 0.2*	2.7 ± 0.3***	2.1 ± 0.2	2.4 ± 0.2 [†]	2.7 ± 0.4 ^{†,††}	2.1 ± 0.3	2.4 ± 0.3 [‡]	2.6 ± 0.4 ^{‡,‡‡}
TAA-D (mm)	5.7 ± 1.1	7.1 ± 1.3*	9.0 ± 1.6***	5.5 ± 1.0	7.3 ± 1.2 [†]	9.7 ± 1.4 ^{†,††}	5.7 ± 1.1	7.3 ± 1.2 [‡]	9.6 ± 1.4 ^{‡,‡‡}
TAP-D (mm)	9.4 ± 0.9	10.4 ± 1.1*	11.3 ± 1.0***	9.1 ± 0.8	10.5 ± 0.9 [†]	12.0 ± 0.8 ^{†,††}	9.2 ± 0.9	10.5 ± 0.9 [‡]	12.0 ± 0.7 ^{‡,‡‡}
TAFS (%)	31.3 ± 10.5	21.1 ± 8.2*	17.2 ± 5.1***	23.3 ± 9.4	21.6 ± 8.7	17.8 ± 7.8	21.8 ± 8.8	21.9 ± 8.9	18.3 ± 3.5
TAFAC (%)	30.2 ± 12.3	27.1 ± 12.6	24.4 ± 10.4	34.4 ± 10.3	26.1 ± 9.9 [†]	17.1 ± 6.3 ^{†,††}	33.4 ± 10.4	26.1 ± 10.3 [‡]	18.8 ± 5.6 ^{‡,‡‡}

V_{\max} , maximum end-systolic right atrial volume; V_{preA} , early diastolic pre-atrial contraction right atrial volume; V_{\min} , minimum end-diastolic right atrial volume; TASV, total atrial stroke volume; TAEF, total (right) atrial emptying fraction; PASV, passive (right) atrial stroke volume; PAEF, passive (right) atrial emptying fraction; AASV, active (right) atrial stroke volume; AAEF, active (right) atrial emptying fraction; TAD, tricuspid annular diameter; TAA, tricuspid annular area; TAP, tricuspid annular perimeter; TAFS, tricuspid annular fractional shortening; TAFAC, tricuspid annular fractional area change; S, end-systolic; D, end-diastolic.

* $p < 0.05$ vs. $\text{TAD-S} \leq 1.5 \text{ cm}$.

** $p < 0.05$ vs. $1.5 \text{ cm} < \text{TAD-S} < 2.1 \text{ cm}$.

[†] $p < 0.05$ vs. $\text{TAA-S} \leq 4.0 \text{ cm}^2$.

^{††} $p < 0.05$ vs. $4.0 \text{ cm} < \text{TAA-S} < 6.8 \text{ cm}^2$.

[‡] $p < 0.05$ vs. $\text{TAP-S} \leq 7.9 \text{ cm}$.

^{‡‡} $p < 0.05$ vs. $7.9 \text{ cm} < \text{TAP-S} < 10.1 \text{ cm}$.

TABLE 5 Right atrial volumes and tricuspid annular parameters in different end-diastolic tricuspid annular groups.

	TAD-D ≤ 2.1 cm (n = 41)	2.1 cm < TAD-D < 2.7 cm (n = 80)	2.7 cm ≤ TAD-D (n = 23)	TAA-D ≤ 5.7 cm ² (n = 22)	5.7 cm < TAA-D < 8.9 cm ² (n = 97)	8.9 cm ² ≤ TAA-D (n = 25)	TAP-D ≤ 9.3 cm (n = 25)	9.3 cm < TAP-D < 11.7 cm (n = 95)	11.7 cm ≤ TAP-D (n = 24)
V _{max} (ml)	43.4 ± 12.6	49.7 ± 15.6*	55.8 ± 14.7*	36.4 ± 9.5	48.8 ± 13.7 [†]	59.8 ± 16.5 ^{†,††}	36.3 ± 9.2	49.9 ± 13.6 [‡]	57.7 ± 17.5 ^{‡,‡‡}
V _{preA} (ml)	31.9 ± 9.2	36.4 ± 10.6*	40.6 ± 13.1*	27.2 ± 7.8	35.9 ± 9.5 [†]	42.9 ± 13.5 ^{†,††}	27.8 ± 7.0	36.5 ± 10.0 [‡]	41.5 ± 13.4 ^{‡,‡‡}
V _{min} (ml)	24.4 ± 9.0	28.3 ± 9.4*	31.9 ± 10.5*	20.5 ± 6.7	27.9 ± 9.0 [†]	33.7 ± 10.6 ^{†,††}	21.5 ± 6.8	28.1 ± 8.9 [‡]	32.8 ± 11.7 ^{‡,‡‡}
TASV (ml)	19.0 ± 9.8	21.4 ± 10.0	23.8 ± 9.9	15.9 ± 8.2	21.0 ± 9.7 [†]	26.2 ± 10.2 ^{†,††}	14.8 ± 7.8	21.8 ± 9.4 [‡]	24.9 ± 11.2 [‡]
TAEF (%)	43.1 ± 15.1	42.2 ± 11.0	42.3 ± 13.4	42.6 ± 14.2	42.3 ± 12.7	42.2 ± 11.0	40.0 ± 13.3	43.1 ± 12.4	42.6 ± 12.5
PASV (ml)	11.5 ± 7.2	13.3 ± 8.6	15.2 ± 8.9	9.2 ± 7.2	13.0 ± 8.0 [†]	16.9 ± 9.0 ^{†,††}	8.6 ± 6.4	13.4 ± 7.8 [‡]	16.2 ± 10.1 [‡]
PAEF (%)	25.6 ± 12.3	25.5 ± 11.2	27.1 ± 13.0	24.2 ± 14.8	25.5 ± 11.2	28.1 ± 11.0	22.6 ± 12.5	26.2 ± 11.2	27.2 ± 12.6
AASV (ml)	7.5 ± 4.9	8.0 ± 4.5	8.6 ± 5.6	6.7 ± 4.2	8.0 ± 4.5	9.2 ± 5.9	6.2 ± 4.8	8.3 ± 4.6 [‡]	8.7 ± 5.0
AAEF (%)	24.0 ± 13.9	22.2 ± 10.6	21.2 ± 10.4	24.2 ± 11.5	22.6 ± 11.9	21.0 ± 10.6	22.1 ± 13.7	23.1 ± 11.3	21.3 ± 10.3
TAD-S (mm)	1.6 ± 0.1	1.8 ± 0.2*	2.2 ± 0.3***	1.6 ± 0.1	1.8 ± 0.2 [†]	2.2 ± 0.3 ^{†,††}	1.6 ± 0.2	1.8 ± 0.3 [‡]	2.0 ± 0.3 ^{‡,‡‡}
TAA-S (mm)	4.4 ± 1.0	5.4 ± 1.1*	6.9 ± 1.7***	3.8 ± 0.5	5.3 ± 0.9 [†]	7.3 ± 1.6 ^{†,††}	3.9 ± 0.6	5.4 ± 1.1 [‡]	6.8 ± 1.7 ^{‡,‡‡}
TAP-S (mm)	8.2 ± 0.8	9.2 ± 1.0*	10.0 ± 1.1***	7.7 ± 0.7	9.0 ± 0.8 [†]	10.3 ± 1.1 ^{†,††}	7.9 ± 0.8	9.1 ± 0.9 [‡]	10.1 ± 1.1 ^{‡,‡‡}
TAD-D (mm)	2.0 ± 0.1	2.4 ± 0.1*	2.8 ± 0.2***	2.0 ± 0.2	2.3 ± 0.2 [†]	2.7 ± 0.3 ^{†,††}	2.1 ± 0.2	2.4 ± 0.3 [‡]	2.5 ± 0.4 ^{‡,‡‡}
TAA-D (mm)	6.0 ± 1.1	7.4 ± 1.2*	9.2 ± 1.4***	5.0 ± 0.5	7.2 ± 0.8 [†]	9.8 ± 1.1 ^{†,††}	5.3 ± 0.7	7.3 ± 1.0 [‡]	9.5 ± 1.4 ^{‡,‡‡}
TAP-D (mm)	9.8 ± 1.1	10.5 ± 1.0*	11.5 ± 1.0***	8.8 ± 0.6	10.4 ± 0.8 [†]	12.0 ± 0.6 ^{†,††}	8.8 ± 0.5	10.4 ± 0.7 [‡]	12.2 ± 0.4 ^{‡,‡‡}
TAFS (%)	18.0 ± 7.3	22.9 ± 9.4*	22.5 ± 7.6*	21.6 ± 7.1	21.8 ± 9.5	19.8 ± 7.1	22.8 ± 7.3	21.1 ± 9.4	21.3 ± 7.7
TAFAC (%)	26.9 ± 10.6	26.5 ± 10.7	25.5 ± 10.4	24.8 ± 9.8	26.9 ± 10.8	26.3 ± 10.5	26.5 ± 9.9	25.6 ± 10.8	29.5 ± 10.4

V_{max}, maximum end-systolic right atrial volume; V_{preA}, early diastolic pre-atrial contraction right atrial volume; V_{min}, minimum end-diastolic right atrial volume; TASV, total atrial stroke volume; TAEF, total (right) atrial emptying fraction; PASV, passive (right) atrial stroke volume; PAEF, passive (right) atrial emptying fraction; AASV, active (right) atrial stroke volume; AAEF, active (right) atrial emptying fraction; TAD, tricuspid annular diameter; TAA, tricuspid annular area; TAP, tricuspid annular perimeter; TAFS, tricuspid annular fractional shortening; TAFAC, tricuspid annular fractional area change; S, end-systolic; D, end-diastolic.

*p < 0.05 vs. TAD-D ≤ 2.1 cm.

**p < 0.05 vs. 2.1 cm < TAD-D < 2.7 cm.

†p < 0.05 vs. TAA-D ≤ 5.7 cm².

††p < 0.05 vs. 5.7 cm < TAA-D < 8.9 cm².

‡p < 0.05 vs. TAP-D ≤ 9.3 cm.

‡‡p < 0.05 vs. 9.3 cm < TAP-D < 11.7 cm.

systole, it closes to prevent backflow or regurgitation from the RV into the RA. The normal TA is a dynamic structure with a saddle-shape like MA, its dilation is accompanied with a more circular and planar shape (16, 17). Tricuspid regurgitation is organic only in 10–15% of cases (18), most of the cases show functional regurgitation (FTR) due to distorted RV, subvalvular apparatus, or TA, with structurally normal tricuspid leaflets (19, 20). FTR is mostly due to LV dysfunction, aortic or mitral valve disease or pulmonary vascular or interstitial disorders and is accompanied

with consequent pulmonary hypertension (PH). If FTR is secondary to TA dilation and leaflet tethering and associated to RV dilation and/or dysfunction, it has been called as “classical” or ventricular form of FTR for a long time. In case of absent PH or left heart disorders, FTR was called as idiopathic tricuspid regurgitation previously, which is related to age and atrial fibrillation (AF) (19, 20). Recently, a new distinct entity has been created called as atrial FTR, which can be found in AF patients, in which RA enlargement and dysfunction result in TA dilation,

TABLE 6 Intra- and interobserver variability for three-dimensional speckle-tracking echocardiography-derived tricuspid annular dimensions and right atrial volumes.

	Intraobserver agreement		Interobserver agreement	
	Mean ± 2SD difference in values obtained by 2 measurements of the same observer	ICC between measurements of the same observer	Mean ± 2SD difference in values obtained by 2 observers	ICC between independent measurements of 2 observers
End-diastolic TAD	0.02 ± 0.21 cm	0.96 (p < 0.0001)	0.03 ± 0.15 cm	0.96 (p < 0.0001)
End-diastolic TAA	−0.04 ± 1.14 cm ²	0.95 (p < 0.0001)	0.02 ± 0.56 cm ²	0.96 (p < 0.0001)
End-diastolic TAP	−0.03 ± 0.71 cm	0.95 (p < 0.0001)	−0.11 ± 0.58 cm	0.96 (p < 0.0001)
End-systolic TAD	−0.03 ± 0.32 cm	0.96 (p < 0.0001)	0.02 ± 0.44 cm	0.96 (p < 0.0001)
End-systolic TAA	−0.04 ± 0.31 cm ²	0.95 (p < 0.0001)	−0.05 ± 0.65 cm ²	0.97 (p < 0.0001)
End-systolic TAP	0.07 ± 0.55 cm	0.96 (p < 0.0001)	0.04 ± 0.59 cm	0.97 (p < 0.0001)
V _{max}	1.2 ± 6.3 ml	0.96 (p < 0.0001)	1.0 ± 5.2 ml	0.95 (p < 0.0001)
V _{preA}	−1.5 ± 8.6 ml	0.87 (p < 0.0001)	−1.5 ± 8.3 ml	0.90 (p < 0.0001)
V _{min}	0.8 ± 5.1 ml	0.94 (p < 0.0001)	0.9 ± 4.6 ml	0.94 (p < 0.0001)

ICC, interclass correlation coefficient; TAD, tricuspid annular diameter; TAA, tricuspid annular area; TAP, tricuspid annular perimeter; SD, standard deviation; V_{max}, maximum end-systolic right atrial volume; V_{preA}, early diastolic pre-atrial contraction right atrial volume; V_{min}, minimum end-diastolic right atrial volume.

leaflet malcoaptation and loss of TA sphincter-like function (21). Therefore, RA rather than RV dilation is more important to determine TA dilation and development of FTR in such cases (5). Similarly, following heart transplantation, overall RA diameter and native recipient RA diameter were found to be a risk factor for TA distension, which is reported to be a causative factor for the most common type of TV dysfunction (22).

Routine non-invasive TV assessment is based on 2D Doppler echocardiography, but results with 3D echocardiography are also available (23). 3DSTE has been demonstrated to be capable not only of performing RA chamber quantifications (14), but for determination of atrioventricular annular dimensions and its sphincter-like functional properties at the same time using the same 3D acquired datasets from the transthoracic window (15). Age- and gender-dependency and normal reference values for 3DSTE-derived RA and TA assessments were also determined with considerable intra- and interobserver agreements (14, 15). Therefore, 3DSTE seems to be an optimal option for simultaneous assessment of TA and RA for (patho)physiologic studies. According to present findings, although feasibility of simultaneous assessment of 3DSTE-derived RA volumes and TA dimensions proved to be limited, however, reproducibility was found to be acceptable in those cases where the measurements were feasible.

There can be a question whether associations between RA size and TA dimensions exist before FTR develops in healthy adults in sinus rhythm. It is known that with increasing left atrial volumes, mitral annulus dilated and became functionally impaired under healthy circumstances (24). The present study serves as an analogy for this by examining what happens in the right side of the heart under similar conditions. Results show similar findings demonstrating strong associations in case of dilation of TA in the presence of higher RA volumes. Moreover, dilation of TA and enlargement of RA predicted each other, as well. It is more important in the context of recent findings from the MAGYAR-Healthy Study, where strong associations between RA radial strains and end-diastolic TA area could also be detected in healthy subjects without FTR (9). However, further clinical studies are warranted to confirm our findings in a larger population or in different pathologic states and to demonstrate their possible clinical role in patient management. Moreover, long-term follow-up could confirm predictive role of TA/RA dilation on the development of AF and/or FTR.

Limitations

Several important limitations have arisen during assessments:

- 2D echocardiography still allows TA assessment with a better image quality as compared to 3DSTE.
- The results would have been much more convincing if the measurement results had been validated against those measured with the Tomtekt software. This topic could even be the subject of a subsequent study.
- Although TA has a special 3D saddle-shape, only its 2D-projected image was determined.
- The study did not aim to compare 2D echocardiography vs. 3DSTE in the assessment of TA.
- Speckle-tracking analysis of TA functionality was not purposed, as well.
- FTR was excluded by visual assessment, more advanced quantification method was not applied during evaluations.

Conclusions

3DSTE is suitable for non-invasive assessment of TA dimensions and RA volumes at the same time using the same 3D echocardiographic dataset. Significant associations between TA size and RA volumes exist in healthy circumstances. Strong associations in case of dilation of TA in the presence of higher RA volumes could partly explain FTR later developing in subjects in sinus rhythm.

Data availability statement

The datasets presented in this article are not readily available due to local restrictions. Requests to access the datasets should be directed to nemes.attila@med.u-szeged.hu.

Ethics statement

The study was conducted in accordance with the Declaration of Helsinki (as revised in 2013). The study was approved by the Institutional and Regional Human Biomedical Research Committee of University of Szeged, Hungary (No.: 71/2011 and updated versions) and informed consent was given by all subjects.

Author contributions

AN—original idea, writing manuscript. ÁK—data collection, measurements. GR—data collection, measurements. ZR—writing manuscript. AA—writing manuscript. NA—writing manuscript, control. CL—writing manuscript, control. All authors contributed to the article and approved the submitted version.

Conflict of interest

The authors declare that the research was conducted in the absence of any commercial or financial relationships that could be construed as a potential conflict of interest.

Publisher's note

All claims expressed in this article are solely those of the authors and do not necessarily represent those of their affiliated

organizations, or those of the publisher, the editors and the reviewers. Any product that may be evaluated in this article, or claim that may be made by its manufacturer, is not guaranteed or endorsed by the publisher.

References

- Lang RM, Badano LP, Mor-Avi V, Afkalo J, Armstrong A, Ernande L, et al. Recommendations for cardiac chamber quantification by echocardiography in adults: an update from the American society of echocardiography and the European association of cardiovascular imaging. *Eur Heart J Cardiovasc Imaging*. (2015) 16:233–70. doi: 10.1093/ehjci/jev014
- Rudski LG, Lai WW, Afkalo J, Hua L, Handschumacher MD, Chandresakaran K, et al. Guidelines for the echocardiographic assessment of the right heart in adults: a report from the American Society of Echocardiography endorsed by the European Association of Echocardiography, a registered branch of the European Society of Cardiology, and the Canadian Society of Echocardiography. *J Am Soc Echocardiogr*. (2010) 23:685–713. doi: 10.1016/j.echo.2010.05.010
- Muraru D, Hahn RT, Soliman OI, Faletta FF, Basso C, Badano LP. 3-Dimensional echocardiography in imaging the tricuspid valve. *JACC Cardiovasc Imaging*. (2019) 12:500–15. doi: 10.1016/j.jcmg.2018.10.035
- Tadic M. The right atrium, a forgotten cardiac chamber: an updated review of multimodality imaging. *J Clin Ultrasound*. (2015) 43:335–45. doi: 10.1002/jcu.22261
- Guta AC, Badano LP, Tomaselli M, Mihalcea D, Bartos D, Parati G, et al. The pathophysiological link between right atrial remodeling and functional tricuspid regurgitation in patients with atrial fibrillation: a three-dimensional echocardiography study. *J Am Soc Echocardiogr*. (2021) 34:585–594.e1. doi: 10.1016/j.echo.2021.01.004
- Muraru D, Addetia K, Guta AC, Ochoa-Jimenez R, Genovese D, Veronesi F, et al. Right atrial volume is a major determinant of tricuspid annulus area in functional tricuspid regurgitation: a three-dimensional echocardiography study. *Eur Heart J Cardiovasc Imaging*. (2021) 22:660–9. doi: 10.1093/ehjci/jeaa286
- Florescu DR, Muraru D, Florescu C, Volpato V, Caravita S, Perger E, et al. Right heart chambers geometry and function in patients with the atrial and the ventricular phenotypes of functional tricuspid regurgitation. *Eur Heart J Cardiovasc Imaging*. (2022) 23:930–40. doi: 10.1093/ehjci/jeab211
- Muraru D, Gavazzoni M, Heilbron F, Mihalcea DJ, Guta AC, Radu N, et al. Reference ranges of tricuspid annulus geometry in healthy adults using a dedicated three-dimensional echocardiography software package. *Front Cardiovasc Med*. (2022) 9:1011931. doi: 10.3389/fcvm.2022.1011931
- Nemes A, Kormányos Á, Ruzsa Z, Achim A, Ambrus N, Lengyel C. Three-dimensional speckle-tracking echocardiography-derived tricuspid annular dimensions and right atrial strains in healthy adults—is there a relationship? (insights from the MAGYAR-Healthy Study). *J Clin Med*. (2023) 12:4240. doi: 10.3390/jcm12134240
- Urbano-Moral JA, Patel AR, Maron MS, Arias-Godinez JA, Pandian NG. Three-dimensional speckle-tracking echocardiography: methodological aspects and clinical potential. *Echocardiography*. (2012) 29:997–1010. doi: 10.1111/j.1540-8175.2012.01773.x
- Ammar KA, Paterick TE, Khandheria BK, Jan MF, Kramer C, Umland MM, et al. Myocardial mechanics: understanding and applying three-dimensional speckle tracking echocardiography in clinical practice. *Echocardiography*. (2012) 29:861–72. doi: 10.1111/j.1540-8175.2012.01712.x
- Muraru D, Niero A, Rodriguez-Zanella H, Cherata D, Badano L. Three-dimensional speckle-tracking echocardiography: benefits and limitations of integrating myocardial mechanics with three-dimensional imaging. *Cardiovasc Diagn Ther*. (2018) 8:101–17. doi: 10.21037/cdt.2017.06.01
- Lancellotti P, Tribouilloy C, Hagendorff A, Popescu BA, Edvardsen T, Pierard LA, et al. Recommendations for the echocardiographic assessment of native valvular regurgitation: an executive summary from the European Association of Cardiovascular Imaging. *Eur Heart J Cardiovasc Imaging*. (2013) 14:611–44. doi: 10.1093/ehjci/jet105
- Nemes A, Kormányos Á, Domsik P, Kalapos A, Ambrus N, Lengyel C. Normal reference values of three-dimensional speckle-tracking echocardiography-derived right atrial volumes and volume-based functional properties in healthy adults (Insights from the MAGYAR-Healthy Study). *J Clin Ultrasound*. (2020) 48:263–8. doi: 10.1002/jcu.22795
- Nemes A, Kormányos Á, Rácz G, Ruzsa Z, Ambrus N, Lengyel C. Normal reference values of tricuspid annular dimensions and functional properties in healthy adults using three-dimensional speckle-tracking echocardiography (insights from the MAGYAR-Healthy Study). *Quant Imaging Med Surg*. (2023) 13:121–32. doi: 10.21037/qims-22-88
- Ton-Nu TT, Levine RA, Handschumacher MD, Dorer DJ, Yosef C, Fan D, et al. Geometric determinants of functional tricuspid regurgitation: insights from 3-dimensional echocardiography. *Circulation*. (2006) 114:143–9. doi: 10.1161/CIRCULATIONAHA.106.611889
- Addetia K, Muraru D, Veronesi F, Jenei C, Cavalli G, Besser SA, et al. 3-dimensional echocardiographic analysis of the tricuspid annulus provides new insights into tricuspid valve geometry and dynamics. *JACC Cardiovasc Imaging*. (2019) 12:401–12. doi: 10.1016/j.jcmg.2017.08.022
- Muraru D, Addetia K, Jarjour F, Lang RM, Badano LP. Organic tricuspid regurgitation. In: Badano LP, Lang RM, Muraru D, editors. *Textbook of three-dimensional echocardiography*. Cham, Switzerland: Springer (2019). p. 271–83
- Gual-Capllonch F, Cediel G, Ferrer E, Teis A, Juncà G, Vallejo N, et al. Sex-related differences in the mechanism of functional tricuspid regurgitation. *Heart Lung Circ*. (2021) 30:e16–22. doi: 10.1016/j.hlc.2020.06.018
- Badano LP, Muraru D, Enriquez-Sarano M. Assessment of functional tricuspid regurgitation. *Eur Heart J*. (2013) 34:1875–85. doi: 10.1093/eurheartj/ehs474
- Florescu DR, Muraru D, Volpato V, Gavazzoni M, Caravita S, Tomaselli M, et al. Atrial functional tricuspid regurgitation as a distinct pathophysiological and clinical entity: no idiopathic tricuspid regurgitation anymore. *J Clin Med*. (2022) 11:382. doi: 10.3390/jcm11020382
- Urbanowicz T, Michalak M, Kociemba A, Straburzyńska-Migaj E, Katarzyński S, Grajek S, et al. Predictors of tricuspid valve annulus dilation in a heart recipient population. *Transplant Proc*. (2016) 48:1742–5. doi: 10.1016/j.transproceed.2016.01.093
- Anwar AM, Geleijnse ML, Soliman OII, McGhie JS, Frowijn R, Nemes A, et al. Assessment of normal tricuspid valve anatomy in adults by real-time three-dimensional echocardiography. *Int J Cardiovasc Imaging*. (2007) 23:717–24. doi: 10.1007/s10554-007-9210-3
- Nemes A, Kormányos Á, Ambrus N, Lengyel C. Associations between mitral annular and left atrial volume changes in healthy adults—Detailed analysis from the three-dimensional speckle-tracking echocardiographic MAGYAR-Healthy Study. *Rev Cardiovasc Med*. (2022) 23:194. doi: 10.31083/j.rcm2306194



OPEN ACCESS

EDITED BY

Francesca Innocenti,
Careggi University Hospital, Italy

REVIEWED BY

Johannes Schwaiger,
District Hospital of St. Johann in Tirol, Austria
Kesavan Sankaramangalam,
East Carolina University, United States

*CORRESPONDENCE

Felix C. Tanner
✉ felix.tanner@usz.ch

[†]Present address

Kelly A. Reeve
NEXUS Personalized Health Technologies, ETH
Zurich, Zurich, Switzerland

RECEIVED 04 July 2023

ACCEPTED 24 August 2023

PUBLISHED 07 September 2023

CITATION

Winkler NE, Anwer S, Reeve KA, Michel JM,
Kasel AM and Tanner FC (2023) Right vs. left
ventricular longitudinal strain for mortality
prediction after transcatheter aortic valve
implantation.
Front. Cardiovasc. Med. 10:1252872.
doi: 10.3389/fcvm.2023.1252872

COPYRIGHT

© 2023 Winkler, Anwer, Reeve, Michel, Kasel
and Tanner. This is an open-access article
distributed under the terms of the [Creative
Commons Attribution License \(CC BY\)](#). The use,
distribution or reproduction in other forums is
permitted, provided the original author(s) and
the copyright owner(s) are credited and that the
original publication in this journal is cited, in
accordance with accepted academic practice.
No use, distribution or reproduction is
permitted which does not comply with these
terms.

Right vs. left ventricular longitudinal strain for mortality prediction after transcatheter aortic valve implantation

Neria E. Winkler¹, Shehab Anwer¹, Kelly A. Reeve^{1,2†},
Jonathan M. Michel¹, Albert M. Kasel¹ and
Felix C. Tanner^{1*}

¹Department of Cardiology, University Heart Center, University Hospital Zurich and University of Zurich, Zurich, Switzerland, ²Department of Biostatistics, Epidemiology, Biostatistics and Prevention Institute, University of Zurich, Zurich, Switzerland

Introduction: This study aims at exploring biventricular remodelling and its implications for outcome in a representative patient cohort with severe aortic stenosis (AS) undergoing transcatheter aortic valve implantation (TAVI).

Methods and results: Pre-interventional echocardiographic examinations of 100 patients with severe AS undergoing TAVI were assessed by speckle tracking echocardiography of both ventricles. Association with mortality was determined for right ventricular global longitudinal strain (RVGLS), RV free wall strain (RVFWS) and left ventricular global longitudinal strain (LVGLS). During a median follow-up of 1,367 [959–2,123] days, 33 patients (33%) died. RVGLS was lower in non-survivors [–13.9% (–16.4 to –12.9)] than survivors [–17.1% (–20.2 to –15.2); $P = 0.001$]. In contrast, LVGLS as well as the conventional parameters LV ejection fraction (LVEF) and RV fractional area change (RVFAC) did not differ ($P = ns$). Kaplan–Meier analyses indicated a reduced survival probability when RVGLS was below the –14.6% cutpoint ($P < 0.001$). Lower RVGLS was associated with higher mortality [HR 1.13 (95% CI 1.04–1.23); $P = 0.003$] independent of LVGLS, LVEF, RVFAC, and EuroSCORE II. Addition of RVGLS clearly improved the fitness of bivariable and multivariable models including LVGLS, LVEF, RVFAC, and EuroSCORE II with potential incremental value for mortality prediction. In contrast, LVGLS, LVEF, and RVFAC were not associated with mortality.

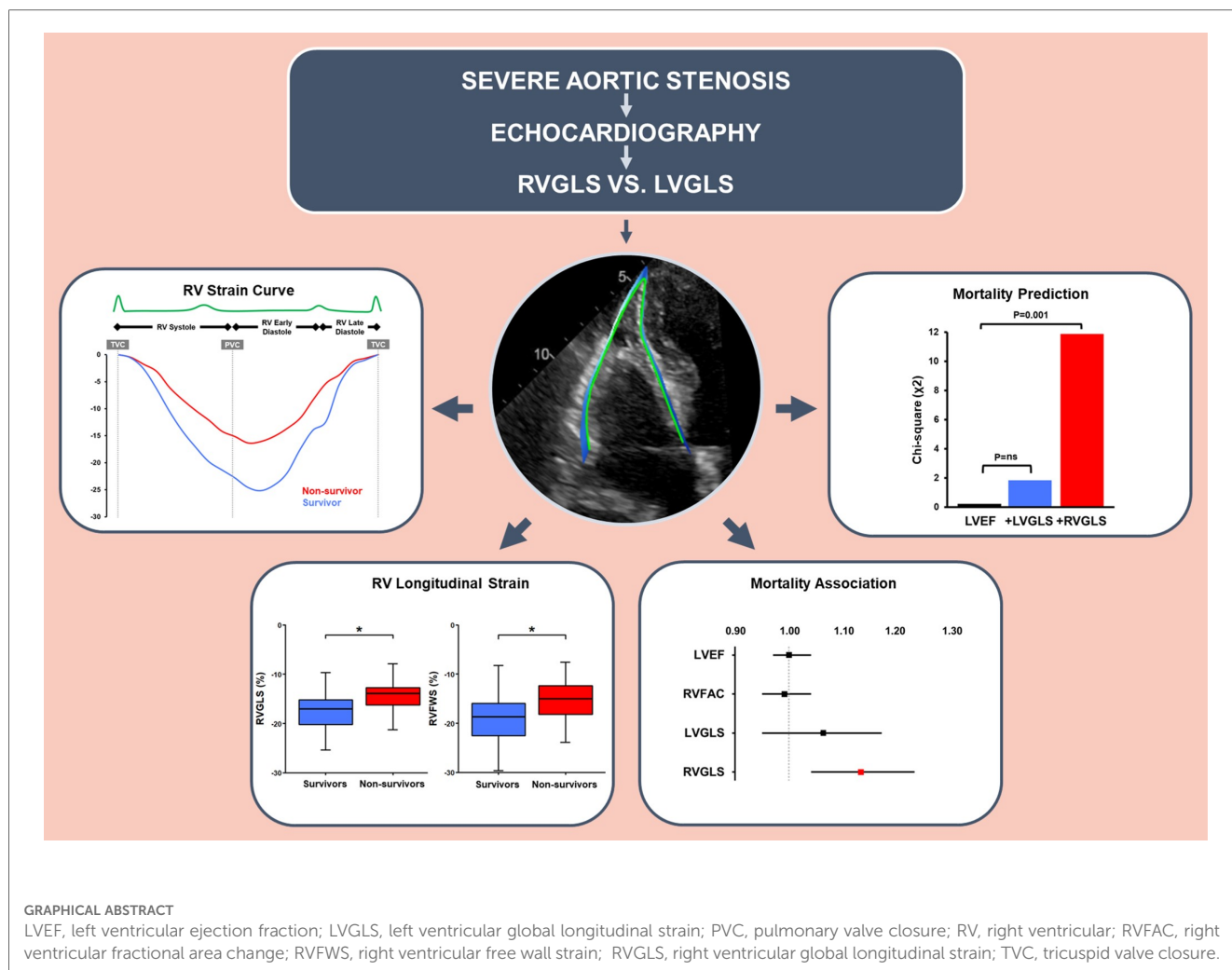
Discussion: In patients with severe AS undergoing TAVI, RVGLS but not LVGLS was reduced in non-survivors compared to survivors, differentiated non-survivors from survivors, was independently associated with mortality, and exhibited potential incremental value for outcome prediction. RVGLS appears to be more suitable than LVGLS for risk stratification in AS and timely valve replacement.

KEYWORDS

aortic stenosis, transcatheter aortic valve implantation, global longitudinal strain, speckle tracking echocardiography, mortality

Abbreviations

AS, aortic stenosis; LVEF, left ventricular ejection fraction; LVGLS, left ventricular global longitudinal strain; RVFAC, right ventricular fractional area change; RVFWS, right ventricular free wall strain; RVGLS, right ventricular global longitudinal strain; STE, speckle tracking echocardiography; TAVI, transcatheter aortic valve implantation.



1. Introduction

Degenerative aortic stenosis (AS) is the most common valvular heart disease in high-income countries (1, 2). Myocardial remodelling does not only occur in the left (LV) but also the right ventricle (RV) of affected patients (3, 4). Chronic pressure overload triggers an adaptive response of the LV (5–7) eventually leading to functional and structural changes of the RV and ultimately resulting in impaired biventricular function with poor prognosis (3, 8).

Current guidelines recommend aortic valve replacement in severe symptomatic AS or in severe asymptomatic AS with associated LV systolic dysfunction defined as impaired LV ejection fraction (LVEF <50%) (2). The prognostic value of LVEF in severe AS is controversial, as it often deteriorates late in the disease course when permanent myocardial damage has occurred already (6, 9, 10). Hence, LVEF is an insensitive marker for early detection of LV dysfunction with questionable benefit for patient management aiming at preserving ventricular function. Speckle tracking echocardiography (STE) has become a clinically feasible

method for assessing myocardial deformation (11–13). Global longitudinal strain may detect subclinical LV dysfunction (14–16) associated with reduced survival in AS incremental to other clinical (10, 15, 17) and echocardiographic parameters including LVEF (10, 13, 14, 15, 17, 18, 19).

Recent research highlights the importance of the RV for risk stratification in AS, but conventional echocardiographic parameters of RV function such as RV fractional area change (RVFAC), tricuspid annular plane systolic excursion (TAPSE), and RV lateral wall tissue velocity (S') have shown inconsistent results regarding outcome association in patients undergoing transcatheter aortic valve implantation (TAVI) (20–23). Analysis of longitudinal strain in both ventricles offers new perspectives for risk stratification of patients with severe AS. A recent cardiac magnetic resonance (CMR) study demonstrated that RV global longitudinal strain (RVGLS) but not LV global longitudinal strain (LVGLS) predicted one-year mortality in patients undergoing TAVI (24). Similarly, an echocardiographic study in patients with low-flow low-gradient AS suggested that RVGLS has incremental prognostic value compared to LVGLS (25).

This study aims at exploring the role of RVGLS vs. LVGLS assessed by STE for outcome prediction in a representative patient cohort with severe AS undergoing TAVI.

2. Materials and methods

2.1. Study population

One hundred patients with severe AS (aortic valve area $<1\text{ cm}^2$ or indexed AVA $<0.6\text{ cm}^2/\text{m}^2$) undergoing TAVI between 2008 and 2019 were retrospectively identified from the prospective AS registry of the University Heart Center Zurich. Patients were included when a comprehensive echocardiographic examination was available within three months prior to TAVI allowing complete strain analysis of both ventricles. A flow diagram ([Supplementary Figure S1](#)) illustrates how patients were enrolled for the study. Ethical committee approval and informed consent were obtained prior to patient inclusion.

2.2. Echocardiography and strain analysis

Transthoracic echocardiographic (TTE) examinations were performed using commercially available equipment (iE33 or Epiq 7, Philips Medical Systems, The Netherlands; E9 or E95, GE Healthcare, USA). Echocardiographic measurements were made by certified specialists according to current recommendations ([26–28](#)). Calculation of LVEF was based on Simpson's biplane method.

TomTec ImageArena Cardiac Performance Analysis (Version 4.6) was used for offline STE measurements of both ventricles according to current recommendations ([26, 27](#)). Endocardial tracing was performed manually excluding sigmoid septal hypertrophy, papillary muscles, and trabeculations. Heart cycle timing was identified from the M-mode.

Apical 2- (A2C), 3- (A3C) and 4-chamber (A4C) views were used for measuring LVGLS. End-diastole was set at the last frame before mitral valve closure and end-systole at the last frame before aortic valve closure. LVGLS is indicated as average peak systolic strain based on the 16-segment model. Focused RV views were used for measuring RV strain ([29](#)). End-diastole was defined as the last frame before tricuspid valve closure and end-systole as the smallest ventricular systolic dimension, respectively. RVGLS is indicated as average peak systolic strain based on the 6-segment model and RV free wall strain (RVFWS) on the 3 segments of the free wall, respectively.

2.3. Reproducibility of strain measurements

Reproducibility was tested on 15 echocardiographic examinations by two observers to investigate inter-observer agreement and repeated by the main observer with a difference of 3 months between the first and the second measurement to determine intra-observer agreement. Concordance correlation

coefficient was used for assessing reproducibility (inter-observer agreement) and repeatability (intra-observer agreement). These results are reported in [Supplementary Table S1](#). There is strong inter- and intra-observer agreement for LV and RV strain measurements.

2.4. Follow-up

The date of the echocardiography examination before TAVI (i.e., within 3 months prior to procedure) marks the date of study inclusion. The date of the TAVI procedure indicates the start of follow-up. All-cause mortality was defined as the primary endpoint. Patient survival status was evaluated through patient records and/or phone calls.

2.5. Statistics

The Shapiro–Wilk test was used to assess normal distribution, with most variables displaying a non-normal distribution. Continuous variables are given as median [interquartile range, IQR] and categorical variables as absolute number (percentage). Continuous variables were compared with the Mann–Whitney–Wilcoxon test, categorical variables with Fisher's exact test. Receiver operating characteristic (ROC) curve analysis was used to determine the optimal cutpoint value for distinguishing survivors from non-survivors, and model discrimination was summarised by area under the curve (AUC). The AUC from models was compared with the DeLong method using *pROC* (version 1.18.0) package. Kaplan–Meier survival curves and log-rank tests of time-to-event data were analysed with the *survminer* (version 0.4.9) package; variables were either dichotomised at their optimal cutpoint according to the ROC curve or according to the literature. For some analyses, variables were divided into tertiles or quartiles. Association with all-cause mortality was analysed in uni- and multivariable Cox regression models. Proportional hazard assumptions were assessed for all models using the scaled Schoenfeld residuals. Variables with clinical relevance such as age, sex, EuroSCORE II, STS score, AS severity, LVEF, RVFAC were included in multivariable models regardless of their significance level in univariable models and tested for sensitivity. A further sensitivity analysis was performed excluding periprocedural deaths from the total number of events. Cox regression analysis of variance (Cox-ANOVA) was used to test model fit. The chi-squared (χ^2) log-likelihood ratio and Harrell's C-statistic were used to examine the incremental value of predictors in the multivariable model compared to the nested univariable model. Collinearity between variables in the regression models was tested using Spearman's correlation and variance inflation factor tests. Standard mean difference (SMD) was used for determining the representativeness of the study cohort compared to the overall registry population. SMD values of 0.2, 0.5, and 0.8 are considered to represent small, medium, and large differences, respectively ([30, 31](#)). Statistical analyses were performed using MedCalc® version 19.6.4 and R version

4.1.3. Statistical significance was considered at a two-sided P value <0.05 .

3. Results

3.1. Baseline characteristics

Tables 1, 2 summarise the clinical and echocardiographic baseline characteristics, respectively. Almost all patients exhibited normal size and systolic function of both ventricles as determined by RV enddiastolic area index (RVEDAI), RVFAC, TAPSE, left ventricular enddiastolic volume index (LVEDVI), and LVEF. There was little difference between the baseline characteristics of the study cohort and those of the overall registry population ($N=1,467$; SMD 0.0–0.4; **Supplementary Table S2**). The study cohort was slightly younger and exhibited a lower EuroSCORE II, while mean transaortic pressure gradient (MTPG) was slightly higher, AVA was similar, and RVFAC, TAPSE, LVEF were marginally higher (**Supplementary Table S2**).

3.2. Ventricular systolic function

RVFAC [40.5% (37.8–44.0)] and LVEF [58.5% (53.0–64.3)] were preserved among the study population. In contrast, longitudinal deformation of both ventricles was impaired (RVGLS

[−16.5% (−19.8 to −13.8)]; RVFWS [−17.6% [−21.6 to −14.3]; LVGLS [−10.5% (−13.0 to −8.4); **Figure 1**].

The concordance correlation coefficient for assessing intra- and inter-observer variability was each 0.8 for LVGLS, each 0.9 for RVGLS, and 0.9 and 0.8 for RVFWS, respectively (**Supplementary Table S1**).

3.3. Survival

During a median follow-up time of 1,367 [959–2,123] days, 33 patients (33%) died, of which 23 (23%) due to a cardiovascular cause. There was no significant difference in survival between women and men (**Table 1**). Among the STE-derived parameters, RVGLS and RVFWS were significantly lower in non-survivors (−13.9% [−16.4 to −12.9]; $P=0.001$ and −15.7% [−18.3 to −12.8]; $P=0.002$, respectively) compared to survivors (−17.1% [−20.2 to −15.2]; $P=0.001$ and −18.7% [−22.6 to −15.9]; $P=0.002$, respectively), while LVGLS did not differ ($P=0.303$; **Table 2**). The cutpoint values for RVGLS ($\geq -14.6\%$; sensitivity 61%; specificity 79%; ROC AUC 70%; $P<0.001$) and RVFWS ($\geq -18.3\%$; sensitivity 79%; specificity 54%; ROC AUC 69%; $P=0.001$) differentiated survivors from non-survivors, while that for LVGLS did not ($P=0.243$). Kaplan–Meier analyses indicated a higher survival probability when the population was dichotomised according to the cutpoint value for RVGLS ($P<0.001$) and for RVFWS ($P=0.012$; **Figure 2**), but not for LVGLS ($P=0.580$).

TABLE 1 Clinical baseline characteristics.

Parameters	Overall ($N=100$)	Survivors ($N=67$)	Non-survivors ($N=33$)	P
Age, years	79.0 [75.8–84.0]	79.0 [74.5–83.0]	81.0 [77.0–84.0]	0.164
Women, N (%)	49 (49)	32 (48)	17 (52)	0.888
BMI, kg/m^2	26.6 [24.2–30.2]	26.3 [24.0–29.9]	27.3 [25.2–30.8]	0.221
BSA, m^2	1.8 [1.7–1.9]	1.8 [1.7–2.0]	1.9 [1.7–1.9]	0.716
Hypertension, N (%)	77 (77)	50 (75)	27 (82)	0.582
Diabetes, N (%)	36 (36)	23 (34)	13 (39)	0.784
Dyslipidaemia, N (%)	68 (68)	46 (69)	22 (67)	0.554
Clinically relevant CAD, N (%)	57 (57)	40 (60)	17 (52)	0.574
CABG, N (%)	16 (16)	10 (15)	6 (18)	0.923
PAD, N (%)	17 (17)	11 (16)	6 (18)	0.925
Cerebrovascular disease, N (%)	24 (24)	17 (25)	7 (21)	0.523
NYHA III or IV, N (%)	8 (8)	7 (11)	1 (3)	0.372
COPD, N (%)	13 (13)	8 (12)	5 (15)	0.560
eGFR, $\text{ml}/\text{min}/1.73 \text{ m}^2$	61.0 [48.0–73.5]	62.0 [50.0–75.5]	55.1 [39.0–69.0]	0.262
Atrioventricular block III, N (%)	1 (1)	1 (2)	0 (0)	0.210
Ventricular conduction abnormality, N (%)				0.005*
BFB	3 (3)	2 (3)	1 (3)	
LAHB	7 (7)	2 (3)	5 (15)	
LBBS	7 (7)	7 (11)	0 (0)	
RBSB	11 (11)	4 (6)	7 (21)	
EuroSCORE II, %	3.0 [1.7–4.9]	2.9 [1.5–4.2]	3.2 [1.8–5.7]	0.169
Periprocedural death, N (%)	3 (3)	0 (0)	3 (9)	0.055

BMI, body mass index; BSA, body surface area; CAD, coronary artery disease; CABG, coronary artery bypass graft; PAD, peripheral arterial disease; NYHA, New York Heart Association; COPD, chronic obstructive pulmonary disease; eGFR, estimated glomerular filtration rate; BFB, bifascicular block; LAHB, left anterior hemiblock; LBBS, left bundle branch block; RBSB, right bundle branch block.

Values are given as median (IQR, interquartile range) for continuous variables or number (percentage) for categorical variables.

*Significant values ($P<0.05$).

TABLE 2 Echocardiographic baseline characteristics.

Parameters	Overall (N = 100)	Survivors (N = 67)	Non-survivors (N = 33)	P
Aortic stenosis severity				
MTPG, mmHg	43.0 [35.0–52.0]	43.0 [34.5–50.5]	44.0 [38.0–56.0]	0.257
AVA, cm ²	0.8 [0.7–0.9]	0.8 [0.7–0.9]	0.8 [0.6–0.9]	0.304
AVAI, cm ² /m ²	0.4 [0.4–0.5]	0.4 [0.4–0.5]	0.4 [0.4–0.5]	0.126
Conventional				
RVEDAI, cm ² /m ²	9.2 [8.0–10.7]	9.1 [7.8–11.0]	9.4 [8.4–10.5]	0.913
RVFAC, %	40.5 [37.8–44.0]	41.0 [38.0–44.0]	40.0 [33.0–45.0]	0.537
TAPSE, mm	20.0 [18.0–22.5]	20.0 [18.0–22.0]	20.0 [17.0–23.0]	0.626
LVEF, %	58.5 [53.0–64.3]	58.0 [53.5–64.0]	60.0 [53.0–65.0]	0.657
LVEDVI, ml/m ²	53.0 [41.8–65.0]	54.0 [44.0–65.5]	51.0 [38.0–63.0]	0.328
LVSVI, ml/m ²	40.5 [32.3–48.0]	42.0 [35.0–48.0]	37.0 [27.0–48.0]	0.111
LVMMI, g/m ²	101.5 [86.8–122.3]	99.0 [88.5–116.5]	107.0 [76.0–151.0]	0.224
Speckle-tracking				
RVGLS, %	−16.5 [−19.8– −13.8]	−17.1 [−20.2– −15.2]	−13.9 [−16.4– −12.9]	0.001*
RVFWS, %	−17.6 [−21.6– −14.3]	−18.7 [−22.6– −15.9]	−15.7 [−18.3– −12.8]	0.002*
LVGLS, %	−10.5 [−13.0– −8.4]	−10.8 [−13.1– −8.7]	−10.3 [−12.5– −6.8]	0.303

MTPG, mean transaortic pressure gradient; AVA, aortic valve area; AVAI, aortic valve area index; RVEDAI, right ventricular end diastolic area index; RVFAC, right ventricular fractional area change; TAPSE, tricuspid annular plane systolic excursion; LVEF, left ventricular ejection fraction; LVEDVI, left ventricular end-diastolic volume index; LVSVI, left ventricular stroke volume index; LVMMI, left ventricular muscle mass index; RVGLS, right ventricular global longitudinal strain; RVFWS, right ventricular free wall strain; LVGLS, left ventricular global longitudinal strain.

Values are given as median (IQR, interquartile range).

*Significant values ($P < 0.05$).

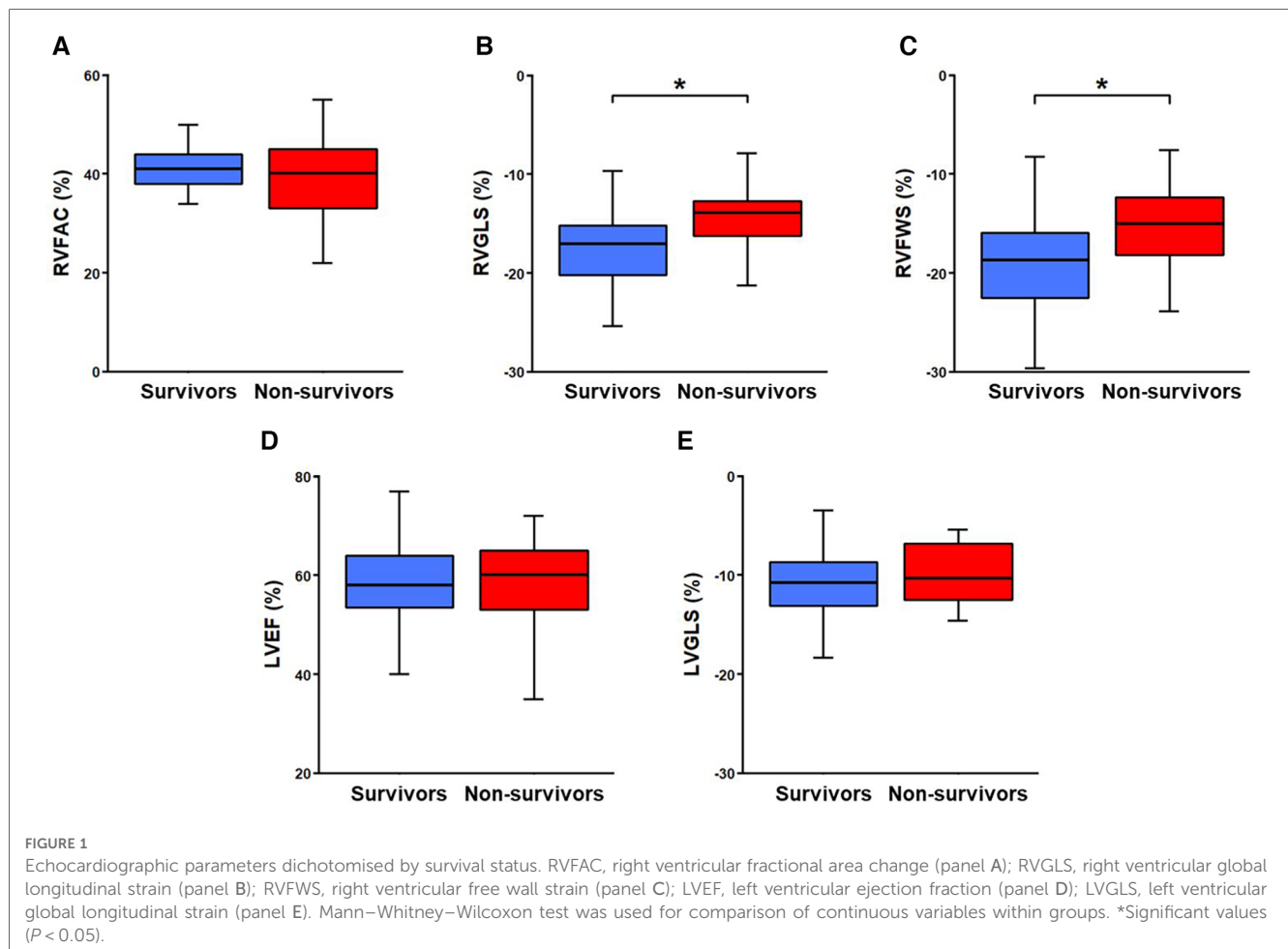
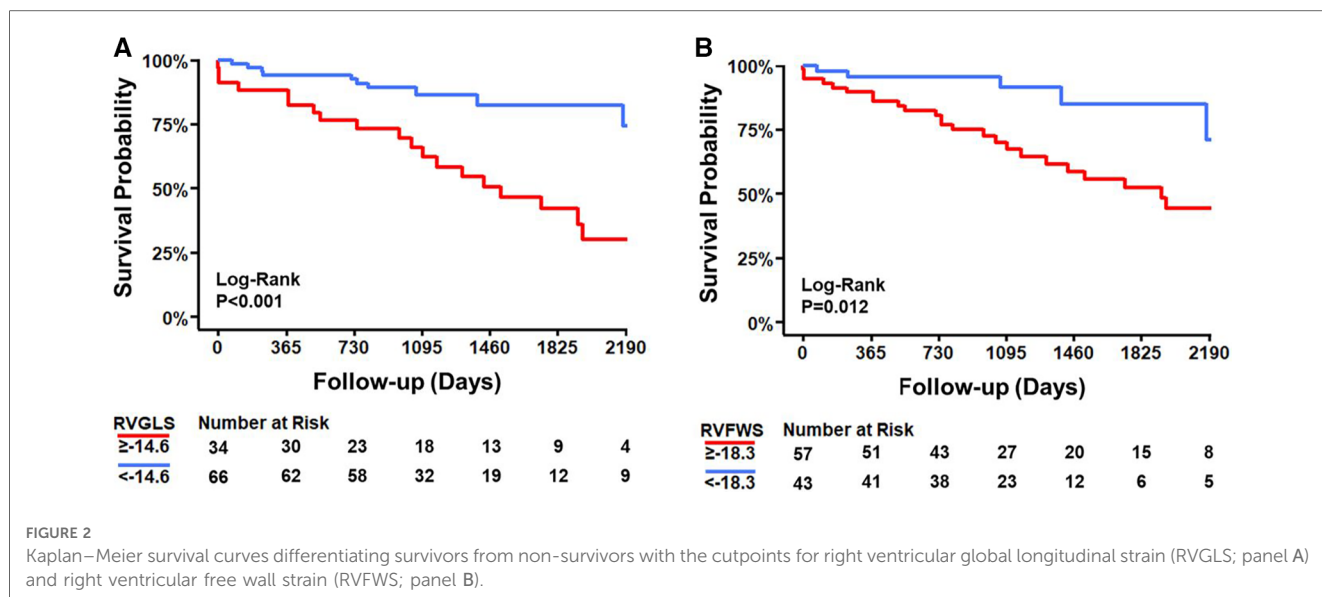


FIGURE 1

Echocardiographic parameters dichotomised by survival status. RVFAC, right ventricular fractional area change (panel A); RVGLS, right ventricular global longitudinal strain (panel B); RVFWS, right ventricular free wall strain (panel C); LVEF, left ventricular ejection fraction (panel D); LVGLS, left ventricular global longitudinal strain (panel E). Mann–Whitney–Wilcoxon test was used for comparison of continuous variables within groups. *Significant values ($P < 0.05$).



Univariable Cox regression analysis associated a lower RVGLS [HR 1.13 (95% CI 1.04–1.23); $P = 0.003$; ANOVA χ^2 9.27; $\chi^2 P = 0.002$] and RVFWS (data not shown) with an increased mortality risk, while this was not the case for LVGLS [HR 1.06 (0.95–1.17); $P = 0.300$; ANOVA χ^2 1.09; $\chi^2 P = 0.297$] or the

conventional echocardiographic parameters (Table 3). Bivariable Cox regression analysis demonstrated that the association of RVGLS and RVFWS with mortality remained independent of LVGLS or other clinically relevant covariables such as RVFAC, LVEF, and EuroSCORE II (Table 3; RVFWS data not shown).

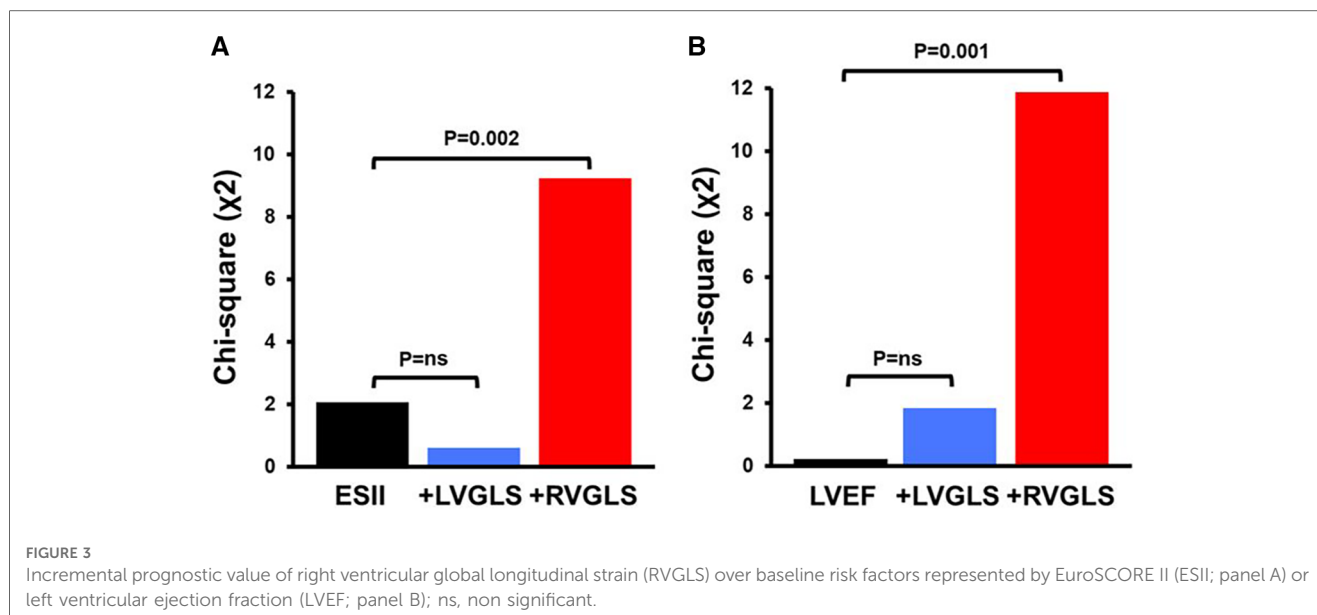
Table 3 Univariable and bivariable Cox regression models.

Nested Model	Cox Regression			Model Fit		Harrell's C-statistic	
Bivariable Model	HR	95% CI	P	χ^2	$\chi^2 P$	C-index	95% CI
RVGLS	1.13	1.04–1.23	0.003*	9.27	0.002*	0.69	0.58–0.80
RVGLS	1.14	1.04–1.25	0.007*	0.13	0.717	0.69	0.58–0.80
LVGLS	0.98	0.86–1.11	0.720				
RVGLS	1.06	0.95–1.17	0.300	1.09	0.297	0.58	0.47–0.70
LVGLS	0.98	0.86–1.11	0.720	8.31	0.004*	0.69	0.58–0.80
RVGLS	1.14	1.04–1.25	0.007*				
RVFAC	0.99	0.95–1.04	0.660	0.18	0.670	0.52	0.39–0.66
RVFAC	1.03	0.98–1.07	0.250	10.45	0.001*	0.68	0.57–0.79
RVGLS	1.17	1.06–1.29	0.002*				
RVFAC	1.00	0.95–1.05	0.970	0.91	0.341	0.58	0.47–0.70
LVGLS	1.06	0.94–1.18	0.340				
LVEF	1.00	0.97–1.04	0.850	0.03	0.853	0.46	0.34–0.57
LVEF	1.03	0.99–1.06	0.120	11.87	0.001*	0.67	0.55–0.78
RVGLS	1.18	1.06–1.30	0.001*				
LVEF	1.02	0.98–1.05	0.380	1.83	0.176	0.56	0.44–0.68
LVGLS	1.09	0.97–1.22	0.170				
LVEF	1.01	0.97–1.04	0.690	0.32	0.574	0.50	0.37–0.63
RVFAC	0.98	0.93–1.04	0.570				
EuroSCORE II	1.06	0.99–1.15	0.110	2.08	0.149	0.55	0.43–0.67
EuroSCORE II	1.06	0.98–1.15	0.120	9.22	0.002*	0.66	0.54–0.78
RVGLS	1.13	1.04–1.22	0.003*				
EuroSCORE II	1.06	0.98–1.14	0.170	0.61	0.435	0.56	0.44–0.68
LVGLS	1.04	0.94–1.16	0.430				
EuroSCORE II	1.06	0.98–1.15	0.120	0.13	0.719	0.52	0.39–0.65
RVFAC	0.99	0.95–1.04	0.710				

HR, hazard ratio; CI, confidence interval; χ^2 , chi-square. RVGLS, right ventricular global longitudinal strain; LVGLS, left ventricular global longitudinal strain; RVFAC, right ventricular fractional area change; LVEF, left ventricular ejection fraction.

Association with mortality in univariable (nested model) and bivariable Cox regression analysis. RVGLS showed incremental value over baseline LVGLS, conventional echocardiographic parameters, and clinical parameters as represented by EuroSCORE II.

*Significant values ($P < 0.05$).



Likelihood ratios showed that inclusion of RVGLS or RVFWS to these models significantly improved their fitness with potential incremental value for association with mortality, while LVGLS did not (Table 3; Figure 3; RVFWS data not shown). The greatest C-index was observed for the univariable RVGLS model and the bivariable model containing RVGLS and LVGLS [both 0.69 (0.58–0.80)].

A multivariable Cox regression analysis was performed to test for a possible interaction between LVGLS and RVGLS or RVFWS, respectively, with inclusion of EuroSCORE II to account for possible confounders (Table 4). RVGLS [1.15 (1.04–1.26); $P=0.005$] and RVFWS [1.14 (1.05–1.25); $P=0.003$] were associated with mortality independent of LVGLS and EuroSCORE II. There was a significant interaction

between RVGLS and LVGLS regarding the association with mortality [0.97 (0.95–1.00); $P=0.043$]. In contrast, RVFWS and LVGLS did not interact significantly in terms of association with mortality [0.98 (0.96–1.01); $P=0.210$]. The highest C-index [0.69 (0.58–0.80)] of the multivariable models was observed for the model containing RVFWS, LVGLS, their interaction, and the EuroSCORE II. However, this is no higher than the greatest univariable C-index and there were only small differences in C-index between the multivariable models. Finally, a sensitivity analysis was performed by replacing EuroSCORE II with either STS score, age and sex, or parameters defining AS severity (i.e., MTPG, AVA), revealing most compelling results for models including EuroSCORE II (data not shown).

Table 4 Multivariable Cox regression models.

Variables	Cox Regression			Model Fit		Harrell's c C-statistic	
	HR	95% CI	P	χ^2	$\chi^2 P$	C-index	95% CI
EuroSCORE II	1.07	1.00–1.16	0.055			0.66	0.54–0.79
RVGLS	1.15	1.04–1.26	0.005*				
LVGLS	0.95	0.83–1.09	0.470				
EuroSCORE II	1.08	1.00–1.17	0.059	4.85	0.028*	0.68	0.58–0.79
RVGLS	1.21	1.08–1.36	0.001*				
LVGLS	1.00	0.87–1.15	0.950				
RVGLS:LVGLS	0.97	0.95–1.00	0.043*				
EuroSCORE II	1.05	0.97–1.14	0.19			0.68	0.56–0.80
RVFWS	1.14	1.05–1.25	0.003*				
LVGLS	0.96	0.85–1.09	0.570				
EuroSCORE II	1.06	0.98–1.15	0.160	1.66	0.198	0.69	0.58–0.81
RVFWS	1.16	1.06–1.27	0.001*				
LVGLS	1.00	0.88–1.14	0.990				
RVFWS:LVGLS	0.98	0.96–1.01	0.210				

HR, hazard ratio; CI, confidence interval; χ^2 , chi-square. RVGLS, right ventricular global longitudinal strain; LVGLS, left ventricular global longitudinal strain; RVFWS, right ventricular free wall strain.

Association with mortality in multivariable Cox regression analysis including interaction between LVGLS and RVGLS or RVFWS, respectively. RV longitudinal strain showed incremental value over LVGLS and clinical parameters as represented by EuroSCORE II.

*Significant values ($P < 0.05$).

4. Discussion

This study demonstrates that in patients with severe AS undergoing TAVI (1) RV strain was lower in non-survivors than survivors; (2) RV strain was associated with mortality after TAVI; (3) RV strain was an independent predictor of mortality; and (4) RV strain improved the fitness of bivariable and multivariable models with potential incremental value for association with mortality. In contrast, none of the LV parameters was associated with mortality nor useful for predicting outcome in this cohort.

The present data indicate that RVGLS, but not LVGLS, is an independent predictor of mortality in patients with severe AS undergoing TAVI. Previous studies observed that pre-interventional RV strain plays a role in predicting outcomes in such patients (19, 23, 32). Those studies focused on RV strain without including LV deformation and exhibited a relatively short follow-up (23, 32) or small study population (19). To the best of our knowledge, the role of RVGLS vs. LVGLS has not been investigated by STE for predicting outcomes of patients with severe AS undergoing TAVI. A previous echocardiographic study reported an incremental prognostic value of RVFWS over LVGLS (25). In contrast to the present work, that study investigated patients with low-flow low-gradient AS undergoing surgical aortic valve replacement or conservative management and found a reduced survival associated with lower RVFWS in both groups (25). Similar to our study, appropriate RV views seemed to be a limiting factor (25). A recent CMR study showed that RVFWS, but not LVGLS, predicted 1-year all-cause mortality in patients with severe AS undergoing TAVI (24). The present findings are consistent with that observation, with STE having the advantages of lower cost, wider availability, and routine application in the pre-interventional assessment as compared to CMR. Finally, given the rather small but nevertheless representative cohort in the current study, neither definition criteria for severe AS nor parameters of ventricular function were compared for the representativeness analyses in that study (24). Similar findings were observed in patients with heart failure. RV strain measured by STE was independently associated with mortality (33), had a higher predictive value for mortality than LVGLS (34), was the main determinant of myocardial fibrosis (35) and showed good agreement with strain measurements by CMR in these patients (36).

LVGLS almost invariably exhibited clearly reduced values in the present cohort, regardless of survival status during follow-up, and did not even tend to be associated with mortality. This observation is consistent with some reports (24, 37, 38), but is contrary to other published literature (10, 11, 14, 16, 17, 25, 37, 38, 39, 40). In the present representative cohort with AS, all patients exhibited severe valvular heart disease and qualified for TAVI. The low median LVGLS with low variability in the population may indicate advanced cardiac disease due to long-standing increase in ventricular afterload. Adaptive cardiac remodelling seems to affect the LV in a rather uniform manner across the population while reaching the RV in part of the latter

only. In line with this interpretation, RV dysfunction may reflect more advanced cardiac remodelling, and its sustained outcome association after TAVI suggests that remodelling may have reached an irreversible stage. In addition to different stages of cardiac remodelling in response to AS, higher values for and/or larger variability of LVGLS may occur due to differences in study design or study population such as specific subsets of AS (17, 37, 39), different disease management (15, 16, 17, 37, 38, 41), different follow-up duration (14, 15), or different endpoint definition (17, 38).

RVFAC, TAPSE, and LVEF were not associated with outcome in the present cohort, which is consistent with previous observations and emphasises that longitudinal deformation as well as other strain-derived parameters such as ventricular twist are much more sensitive tools for detecting ventricular remodelling (14, 18, 42). The LV remodelling response indeed affects the myocardium gradually from the subendocardial to the subepicardial layer, with longitudinal, circumferential, and radial function being affected in corresponding order (12). As a result, LVEF may be preserved despite the progressive increase in ventricular afterload and the deranged longitudinal function (43). The RV exhibits a similar albeit simpler myocardial structure with fibres oriented longitudinally in the subendocardium and circumferentially in the subepicardium, respectively, provoking alterations in longitudinal strain vs. conventional parameters analogous to those occurring in the LV (44).

Timely assessment of RV longitudinal strain seems to be crucial for recognising the extent of myocardial remodelling in response to AS. Appropriate clinical decision-making early in the disease course may decrease the risk of irreversible myocardial damage and improve survival after aortic valve replacement.

4.1. Clinical implications

Assessment of RV systolic function is an integral part of every echocardiographic examination. RV strain is obtained from the RV focused apical view with little additional effort. However, care must be taken in the real-world setting to ensure that all methodological requirements are met in order to perform a reliable deformation analysis. Impaired RV longitudinal strain indicates increased mortality in patients with severe AS after valve replacement and emerges as an important parameter to improve the prognostic understanding of these patients. Hence, RV longitudinal strain should be measured in patients with severe AS and its reduced values should promote the decision to replace the aortic valve for avoiding persistent cardiac remodelling and reduced outcome after intervention.

4.2. Limitations

This study is limited by its retrospective single-center design; however, the cohort is representative of a typical TAVI population and the number of patients included, although

limited, is reasonable to address the research question. A selection bias cannot be excluded because inclusion criteria involved the quality of echocardiographic examinations as well as several additional parameters. Although multivariable models were generated, it cannot be excluded completely that unobserved confounding factors affected the results. The predictive performance, as measured by AUC, was greater for the parameters of interest than for EuroSCORE II, which contains several predictors important to understanding individual prognosis. Due to the limited amount of data, the EuroSCORE II was used as a single predictor and its individual components were not re-estimated with the data at hand, tipping the comparison in favor of the new parameters. More data on this population is needed to develop true clinical prediction models with limited risk of overfitting and performance overoptimism.

5. Conclusion

In patients with severe AS undergoing TAVI, RV longitudinal strain was lower in non-survivors than survivors and independently associated with mortality after TAVI. RV longitudinal strain improved the fitness of clinical and echocardiographic models with potential incremental value for mortality prediction. LVGLS was not associated with mortality in the current dataset. Hence, RV longitudinal strain may be incorporated in risk stratification of patients with severe AS and trigger timely aortic valve replacement.

Data availability statement

The raw data supporting the conclusions of this article will be made available by the authors, without undue reservation.

Ethics statement

The studies involving humans were approved by the Ethics Committee of Zurich, Switzerland. The studies were conducted

in accordance with the local legislation and institutional requirements. The participants provided their written informed consent to participate in this study.

Author contributions

All authors contributed substantially to this work and to the article, and approved the version presented.

Funding

This work was supported by the Swiss Heart Foundation.

Conflict of interest

The authors declare that the research was conducted in the absence of any commercial or financial relationships that could be construed as a potential conflict of interest.

Publisher's note

All claims expressed in this article are solely those of the authors and do not necessarily represent those of their affiliated organizations, or those of the publisher, the editors and the reviewers. Any product that may be evaluated in this article, or claim that may be made by its manufacturer, is not guaranteed or endorsed by the publisher.

Supplementary material

The Supplementary Material for this article can be found online at: <https://www.frontiersin.org/articles/10.3389/fcvm.2023.1252872/full#supplementary-material>

References

1. Ancona R PCS. Epidemiology of aortic valve stenosis (AS) and of aortic valve incompetence (AI): is the prevalence of AS/AI similar in different parts of the world? (2020); Volume 18. Available at: <https://www.escardio.org/Journals/E-Journal-of-Cardiology-Practice/Volume-18/epidemiology-of-aortic-valve-stenosis-as-and-of-aortic-valve-incompetence-ai>
2. Alec Vahanian FB, Praz F, Milojevic M, Baldus S, Bauersachs J, Capodanno D, et al. ESC/EACTS scientific document group. 2021 ESC/EACTS guidelines for the management of valvular heart disease: developed by the task force for the management of valvular heart disease of the European society of cardiology (ESC) and the European association for cardio-thoracic surgery (EACTS). *Eur Heart J*. (2022) 43(7):561–632. doi: 10.1093/eurheartj/ehab395
3. Génèreux P, Pibarot P, Redfors B, Mack MJ, Makkar RR, Jaber WA, et al. Staging classification of aortic stenosis based on the extent of cardiac damage. *Eur Heart J*. (2017) 38(45):3351–8. doi: 10.1093/eurheartj/ehx381
4. Calcuttea A, Holmgren A, Lindqvist P, Henein MY. Organised right ventricular remodelling in aortic stenosis even after valve replacement. *Int J Cardiol*. (2013) 168(2):1549–50. doi: 10.1016/j.ijcard.2012.12.029
5. Cohn JN, Ferrari R, Sharpe N. Cardiac remodeling—concepts and clinical implications: a consensus paper from an international forum on cardiac remodeling. *J Am Coll Cardiol*. (2000) 35(3):569–82. doi: 10.1016/S0735-1097(99)00630-0
6. Hein S, Arnon E, Kostin S, Schönborg M, Elsässer A, Polyakova V, et al. Progression from compensated hypertrophy to failure in the pressure-overloaded human heart: structural deterioration and compensatory mechanisms. *Circulation*. (2003) 107(7):984–91. doi: 10.1161/01.CIR.0000051865.66123.B7
7. Treibel TA, Badiani S, Lloyd G, Moon JC. Multimodality imaging markers of adverse myocardial remodeling in aortic stenosis. *Cardiovasc Imaging*. (2019) 12(8, Part 1):1532–48. doi: 10.1016/j.jcmg.2019.02.034

8. Galli E, Guirette Y, Feneon D, Daudin M, Fournet M, Leguerrier A, et al. Prevalence and prognostic value of right ventricular dysfunction in severe aortic stenosis. *Eur Heart J Cardiovasc Imaging*. (2015) 16(5):531–8. doi: 10.1093/ehjci/jeu290
9. Weidemann F, Herrmann S, Störk S, Niemann M, Frantz S, Lange V, et al. Impact of myocardial fibrosis in patients with symptomatic severe aortic stenosis. *Circulation*. (2009) 120(7):577–84. doi: 10.1161/CIRCULATIONAHA.108.847772
10. Fukui M, Thoma F, Sultan I, Mulukutla S, Elzomor H, Lee JS, et al. Baseline global longitudinal strain is associated with all-cause mortality after transcatheter aortic valve replacement. *JACC Cardiovasc Imaging*. (2020) 13(4):1092–4. doi: 10.1016/j.jcmg.2019.11.005
11. Zhu D, Ito S, Miranda WR, Nkomo VT, Pislaru SV, Villarraga HR, et al. Left ventricular global longitudinal strain is associated with long-term outcomes in moderate aortic stenosis. *Circ Cardiovasc Imaging*. (2020) 13(4):e009958. doi: 10.1161/CIRCIMAGING.119.009958
12. Ng AC, Delgado V, Bertini M, Antoni ML, van Bommel RJ, van Rijnsoever EP, et al. Alterations in multidirectional myocardial functions in patients with aortic stenosis and preserved ejection fraction: a two-dimensional speckle tracking analysis. *Eur Heart J*. (2011) 32(12):1542–50. doi: 10.1093/eurheartj/ehr084
13. Tadic M, Nita N, Schneider L, Kersten J, Buckert D, Gonska B, et al. The predictive value of right ventricular longitudinal strain in pulmonary hypertension, heart failure, and valvular diseases. *Front Cardiovasc Med*. (2021) 8:698158. doi: 10.3389/fcvm.2021.698158
14. Ng ACT, Prihadi EA, Antoni ML, Bertini M, Ewe SH, Ajmone Marsan N, et al. Left ventricular global longitudinal strain is predictive of all-cause mortality independent of aortic stenosis severity and ejection fraction. *Eur Heart J Cardiovasc Imaging*. (2018) 19(8):859–67. doi: 10.1093/ehjci/jex189
15. Kearney LG, Lu K, Ord M, Patel SK, Profitis K, Matalanis G, et al. Global longitudinal strain is a strong independent predictor of all-cause mortality in patients with aortic stenosis. *Eur Heart J Cardiovasc Imaging*. (2012) 13(10):827–33. doi: 10.1093/ehjci/jes115
16. Fries B, Liu D, Gaudron P, Hu K, Nordbeck P, Ertl G, et al. Role of global longitudinal strain in the prediction of outcome in patients with severe aortic valve stenosis. *Am J Cardiol*. (2017) 120(4):640–7. doi: 10.1016/j.amjcard.2017.05.032
17. Yingchongcharoen T, Gibby C, Rodriguez LL, Grimm RA, Marwick TH. Association of myocardial deformation with outcome in asymptomatic aortic stenosis with normal ejection fraction. *Circ Cardiovasc Imaging*. (2012) 5(6):719–25. doi: 10.1161/CIRCIMAGING.112.977348
18. Potter E, Marwick TH. Assessment of left ventricular function by echocardiography: the case for routinely adding global longitudinal strain to ejection fraction. *JACC Cardiovasc Imaging*. (2018) 11(2 Pt 1):260–74. doi: 10.1016/j.jcmg.2017.11.017
19. Vizzardi E, Gavazzoni M, Sciatti E, Dallapellegrina L, Bernardi N, Raddino R, et al. Right ventricular deformation and right ventricular-arterial coupling in patients with heart failure due to severe aortic stenosis undergoing TAVI: long-term results. *Am J Cardiovasc Dis*. (2020) 10(3):150–63. PMID: 32923096; PMCID: PMC7486529
20. Asami M, Stortecky S, Praz F, Lanz J, Räber L, Franzone A, et al. Prognostic value of right ventricular dysfunction on clinical outcomes after transcatheter aortic valve replacement. *JACC Cardiovasc Imaging*. (2019) 12(4):577–87. doi: 10.1016/j.jcmg.2017.12.015
21. Pardo Sanz A, Santoro C, Hinojar R, Salido L, Rajjoub EA, Monteagudo JM, et al. Right ventricle assessment in patients with severe aortic stenosis undergoing transcatheter aortic valve implantation. *Echocardiography*. (2020) 37(4):586–91. doi: 10.1111/echo.14633
22. Ren B, Spitzer E, Geleijnse ML, Zijlstra F, de Jaegere PPT, Van Mieghem NM, et al. Right ventricular systolic function in patients undergoing transcatheter aortic valve implantation: a systematic review and meta-analysis. *Int J Cardiol*. (2018) 257:40–5. doi: 10.1016/j.ijcard.2018.01.117
23. Medvedofsky D, Koifman E, Jarrett H, Miyoshi T, Rogers T, Ben-Dor I, et al. Association of right ventricular longitudinal strain with mortality in patients undergoing transcatheter aortic valve replacement. *J Am Soc Echocardiogr*. (2020) 33(4):452–60. doi: 10.1016/j.echo.2019.11.014
24. Schmid J, Kamml C, Zweiker D, Hatz D, Schmidt A, Reiter U, et al. Cardiac magnetic resonance imaging right ventricular longitudinal strain predicts mortality in patients undergoing TAVI. *Front Cardiovasc Med*. (2021) 8:644500. doi: 10.3389/fcvm.2021.644500
25. Dahou A, Clavel M-A, Capoulade R, Bartko PE, Magne J, Mundigler G, et al. Right ventricular longitudinal strain for risk stratification in low-flow, low-gradient aortic stenosis with low ejection fraction. *Heart*. (2016) 102(7):548–54. doi: 10.1136/heartjnl-2015-308309
26. Lang RM, Badano LP, Mor-Avi V, Afilalo J, Armstrong A, Ernande L, et al. Recommendations for cardiac chamber quantification by echocardiography in adults: an update from the American society of echocardiography and the European association of cardiovascular imaging. *J Am Soc Echocardiogr*. (2015) 28(1):1–39.e14. doi: 10.1016/j.echo.2014.10.003
27. Voigt J-U, Pedrizzetti G, Lysyansky P, Marwick TH, Houle H, Baumann R, et al. Definitions for a common standard for 2D speckle tracking echocardiography: consensus document of the EACVI/ASE/industry task force to standardize deformation imaging. *J Am Soc Echocardiogr*. (2015) 28(2):183–93. doi: 10.1016/j.echo.2014.11.003
28. Holy EW, Nguyen-Kim TDL, Hoffelner L, Stocker D, Stadler T, Stähli BE, et al. Multimodality imaging derived energy loss index and outcome after transcatheter aortic valve replacement. *Eur Heart J Cardiovasc Imaging*. (2020) 21(10):1092–102. doi: 10.1093/ehjci/jeaa100
29. Anwer S, Guastafierro F, Erhart L, Costa S, Akdis D, Schuermann M, et al. Right atrial strain and cardiovascular outcome in arrhythmogenic right ventricular cardiomyopathy. *Eur Heart J Cardiovasc Imaging*. (2022) 23(7):970–8. doi: 10.1093/ehjci/jeac070
30. Cohen J. *Statistical power analysis for the behavioral sciences*. 2nd edn. Hillsdale, NJ: Lawrence Erlbaum Associates Publishers (1988).
31. Austin PC. Balance diagnostics for comparing the distribution of baseline covariates between treatment groups in propensity-score matched samples. *Stat Med*. (2009) 28(25):3083–107. doi: 10.1002/sim.3697
32. Omran H, Polimeni A, Brandt V, Rudolph V, Rudolph TK, Bleiziffer S, et al. Pre-procedural right ventricular longitudinal strain and post-procedural tricuspid regurgitation predict mortality in patients undergoing transcatheter aortic valve implantation (TAVI). *J Clin Med*. (2021) 10(24):5877. doi: 10.3390/jcm10245877
33. Iacoviello M, Citarelli G, Antoncacci V, Romito R, Monitillo F, Leone M, et al. Right ventricular longitudinal strain measures independently predict chronic heart failure mortality. *Echocardiography*. (2016) 33(7):992–1000. doi: 10.1111/echo.13199
34. Cameli M, Righini FM, Lisi M, Bennati E, Navarri R, Lughetti S, et al. Comparison of right versus left ventricular strain analysis as a predictor of outcome in patients with systolic heart failure referred for heart transplantation. *Am J Cardiol*. (2013) 112(11):1778–84. doi: 10.1016/j.amjcard.2013.07.046
35. Lisi M, Cameli M, Righini FM, Malandrino A, Tacchini D, Focardi M, et al. RV longitudinal deformation correlates with myocardial fibrosis in patients with end-stage heart failure. *JACC Cardiovasc Imaging*. (2015) 8(5):514–22. doi: 10.1016/j.jcmg.2014.12.026
36. Tee M, Noble JA, Bluemke DA. Imaging techniques for cardiac strain and deformation: comparison of echocardiography, cardiac magnetic resonance and cardiac computed tomography. *Expert Rev Cardiovasc Ther*. (2013) 11(2):221–31. doi: 10.1586/erc.12.182
37. Kamperidis V, van Rosendaal PJ, Ng AC, Katsanos S, van der Kley F, Debonnaire P, et al. Impact of flow and left ventricular strain on outcome of patients with preserved left ventricular ejection fraction and low gradient severe aortic stenosis undergoing aortic valve replacement. *Am J Cardiol*. (2014) 114(12):1875–81. doi: 10.1016/j.amjcard.2014.09.030
38. Dahl JS, Videbæk L, Poulsen MK, Rudbæk TR, Pelikka PA, Møller JE. Global strain in severe aortic valve stenosis: relation to clinical outcome after aortic valve replacement. *Circ Cardiovasc Imaging*. (2012) 5(5):613–20. doi: 10.1161/CIRCIMAGING.112.973834
39. Dahou A, Bartko PE, Capoulade R, Clavel MA, Mundigler G, Grondin SL, et al. Usefulness of global left ventricular longitudinal strain for risk stratification in low ejection fraction, low-gradient aortic stenosis: results from the multicenter true or pseudo-severe aortic stenosis study. *Circ Cardiovasc Imaging*. (2015) 8(3):e002117. doi: 10.1161/CIRCIMAGING.114.002117
40. Stens NA, van Iersel O, Rooijackers MJP, van Wely MH, Nijveldt R, Bakker EA, et al. Prognostic value of preprocedural LV global longitudinal strain for post-TAVR-related morbidity and mortality: a meta-analysis. *JACC Cardiovasc Imaging*. (2023) 16(3):332–41. doi: 10.1016/j.jcmg.2023.01.005
41. Huded CP, Kusunose K, Shahid F, Goodman AL, Alashi A, Grimm RA, et al. Novel echocardiographic parameters in patients with aortic stenosis and preserved left ventricular systolic function undergoing surgical aortic valve replacement. *Am J Cardiol*. (2018) 122(2):284–93. doi: 10.1016/j.amjcard.2018.03.359
42. Erhart L, Donati T, Anwer S, Schindler M, Gremminger M, Renzulli M, et al. Left ventricular twist predicts mortality in severe aortic stenosis. *Heart*. (2022) 108(3):225–32. doi: 10.1136/heartjnl-2020-318800
43. Reant P, Metras A, Detaille D, Reynaud A, Diolet P, Jaspard-Vinassa B, et al. Impact of afterload increase on left ventricular myocardial deformation indices. *J Am Soc Echocardiogr*. (2016) 29(12):1217–28. doi: 10.1016/j.echo.2016.09.006
44. Greenbaum RA, Ho SY, Gibson DG, Becker AE, Anderson RH. Left ventricular fibre architecture in man. *Heart*. (1981) 45(3):248–63. doi: 10.1136/hrt.45.3.248



OPEN ACCESS

EDITED BY

Sanjeev Bhattacharyya,
Barts Heart Centre, United Kingdom

REVIEWED BY

Francesco Bianco,
Azienda Ospedaliero Universitaria Ospedali
Riuniti, Italy
Nicole Panhuyzen-Goedkoop,
Amsterdam University Medical Center,
Netherlands

*CORRESPONDENCE

J. Schellenberg
✉ jana.schellenberg@uniklinik-ulm.de

RECEIVED 14 June 2023

ACCEPTED 25 September 2023

PUBLISHED 09 October 2023

CITATION

Schellenberg J, Matits L, Bizjak DA, Kersten J,
Kirsten J, Vollrath S and Steinacker JM (2023)
Assessment of myocardial function and cardiac
performance using left ventricular global
longitudinal strain in athletes after COVID-19: a
follow-up study.
Front. Cardiovasc. Med. 10:1240278.
doi: 10.3389/fcvm.2023.1240278

COPYRIGHT

© 2023 Schellenberg, Matits, Bizjak, Kersten,
Kirsten, Vollrath and Steinacker. This is an open-
access article distributed under the terms of the
Creative Commons Attribution License (CC BY).
The use, distribution or reproduction in other
forums is permitted, provided the original
author(s) and the copyright owner(s) are
credited and that the original publication in this
journal is cited, in accordance with accepted
academic practice. No use, distribution or
reproduction is permitted which does not
comply with these terms.

Assessment of myocardial function and cardiac performance using left ventricular global longitudinal strain in athletes after COVID-19: a follow-up study

J. Schellenberg^{1*}, L. Matits^{1,2}, D. A. Bizjak¹, J. Kersten¹, J. Kirsten¹,
S. Vollrath¹ and J. M. Steinacker¹

¹Division of Sports and Rehabilitation Medicine, University Ulm Hospital, Ulm, Germany, ²Clinical & Biological Psychology, Institute of Psychology and Education, Ulm University, Ulm, Germany

Background: It has not yet been conclusively determined whether reduced left ventricular global longitudinal strain (LV GLS) after COVID-19 contributes to a reduction in exercise capacity. Our own studies showed a possible mild myocardial involvement in the form of reduced LV GLS in athletes after COVID-19 compared with healthy athletes. The aims of this prospective follow-up study were to investigate the development of LV GLS over a 3-month period in athletes after COVID-19 and the possible relationship between LV GLS and physical performance.

Methods: LV GLS was determined in four-, two-, and three-chamber views and assessed offline by a blinded investigator in 96 recreational athletes (mean age 33.15 ± 12.40 years, 53 male, peak VO_2 38.82 ± 11.14 ml/min/kg) at a median of two (t_0) and five months (t_1) after COVID-19. Cardiopulmonary exercise testing (CPET) was performed on a bicycle ergometer on both examination dates.

Results: LV GLS improved significantly between t_0 and t_1 (t_0 -18.82 ± 2.02 vs. t_1 -19.46 ± 2.05 , $p < 0.001$). Echocardiographic and spiroergometric parameters were within the normal clinical reference range. Maximum power increased significantly from t_0 to t_1 (t_0 283.17 ± 83.20 vs. t_1 286.24 ± 85.22 Watt, $p = 0.009$) and there was a trend toward increased peak oxygen uptake (t_0 36.82 ± 11.14 vs. t_1 38.68 ± 10.26 ml/min/kg, $p = 0.069$). We found no correlation between LV GLS and performance parameters, except for the respiratory exchange ratio (RER) [ρ -0.316 , (-0.501 ; -0.102), $p < 0.050$].

Conclusions: Significant improvement in LV GLS approximately five months after COVID-19 may be due to mild myocardial involvement during or shortly after COVID-19, which seems to recover. There was no correlation between LV GLS and performance parameters, except for an inverse correlation of LV GLS and RER, suggesting insufficient exercise intolerance at lower GLS values. Further studies on the development of GLS in athletes or in the general population with moderate and severe disease courses would be informative as well as the comparison of pre-COVID-19 with post-COVID-19 echocardiography to evaluate the effects of COVID-19 on cardiac function.

KEYWORDS

sport, COVID-19, speckle tracking echocardiography, performance, CPET

1. Introduction

Coronavirus Disease 2019 (COVID-19) is a systemic viral infection caused by Severe Acute Respiratory Syndrome-Coronavirus-2 (SARS-CoV-2) that primarily affects the respiratory system but can also cause myocardial damage (1–3). Studies in elite athletes have shown that the infection is often mild (46%–82%) or asymptomatic (16%–58%) (4–7), with myocarditis occurring only in rare cases (1%–3%) (8–9). Most athletes can return to competitive and amateur sports after a training break adapted to current symptoms (10–12). However, having passed through COVID-19 does not necessarily imply a complete recovery to former health or performance status and a return-to-sport examination with echocardiography should be performed especially in case of cardiac symptoms during and/or after infection (11).

Analysis of myocardial deformation by speckle-tracking echocardiography (STE) can provide additional information to the standard echocardiography examination (13). The global longitudinal strain of the left ventricle (LV GLS) is more sensitive than left ventricular ejection fraction (LV EF) alone in detecting subclinical LV dysfunction (14) and is a prognostic parameter for long-term risk of cardiovascular morbidity and mortality (15). Individual studies demonstrated reduced LV GLS with preserved ejection fraction (pEF) in the setting of acute SARS-CoV-2 infection in hospitalized patients regardless of infection severity (16–19) and in patients recovered from COVID-19 (20–23). No changes in LV GLS have been observed in athletes compared with healthy athletes 22 days (24) and 19 days (25) after COVID-19. Conversely, we demonstrated reduced LV GLS and diastolic function in a cohort of athletes at a median of two months after COVID-19 compared with non-infected healthy athletes (26).

Longitudinally, hospitalized patients showed no significant improvement in LV GLS at two months (27) or three months after acute infection (28), and 25% of patients still had abnormal LV GLS three months after acute infection (28). However, in the follow-up study by Karagodin et al., improvements in LV GLS were noted in patients with impaired baseline function (29). Further long-term observations in athletes are scarce.

The two main aims of this prospective follow-up study were, first, to investigate the development of LV GLS in athletes without history of LV dysfunction at an average of two months after SARS-CoV-2 infection to a follow-up of three months, and, second, to find if there may be a relationship between myocardial changes detected by LV GLS determination and physical performance.

2. Methods

2.1. Study population

Ninety-six recreational athletes presenting to the Ulm Clinic for Sports and Rehabilitation Medicine after COVID-19 were included in this prospective, single-center, longitudinal cohort study after being informed of the study procedures and providing written informed consent. The results presented in this study are

from baseline clinical assessment between June 2020 and July 2022, a median of two months (IQR: one to five months) after COVID-19, and follow-up three months later. Study participants were included consecutively. They engaged in endurance sports, strength sports, team sports, or technical sports with a training volume of at least three times per week, corresponding to more than 20 metabolic equivalents of task (MET) per week. The weekly training time among the recreational athletes was about five to eight hours. Additional inclusion criteria were: ≥ 18 years of age and a positive SARS-CoV-2 PCR test or antibody detection with additional typical symptoms. The exclusion criteria were: acute or chronic illness that precluded a planned physical examination, acute SARS-CoV-2 infection, refusal of peripheral venous blood sampling, inadequate German language skills, and withdrawal from study participation. Athletes provided written informed consent after being instructed of the study procedures (30). The study was conducted in accordance with the Declaration of Helsinki and approved by the local ethics committee of the University of Ulm (EK 408/20).

2.2. Clinical evaluation of the participants

All athletes underwent a clinical evaluation that included a medical history and physical examination, 12-lead electrocardiogram (ECG), transthoracic echocardiography (TTE) including determination of left ventricular global longitudinal strain (LV GLS), and cardiopulmonary exercise testing (CPET). To examine the long-term course of echocardiographic and CPET findings, participants were invited for a follow-up three months after the initial clinical evaluation.

2.3. Transthoracic echocardiography

Transthoracic examination was performed using an EPIQ 7 ultrasound system with a phased-array probe X5-1 (Philips GmbH, Hamburg, Germany). The following parameters were collected: left ventricular internal diameter end diastole (LVIDd) and end systole (LVIDs). LVIDd (LVIDd/BSA) and LVIDs (LVIDs/BSA) were indexed to body surface area (BSA), left ventricular ejection fraction (LV-EF by biplane LV planimetry by Simpson), fractional shortening (FS), left ventricular mass (LV mass), LV mass/BSA, stroke volume (SV), septal thickness [= interventricular septal end diastole (IVSd)] and posterior wall thickness [= left ventricular posterior wall end diastole (LVPWd)] and right ventricle longitudinal function by tricuspid annular plane systolic excursion (TAPSE). Diastolic function was characterized by E/A ratio, E/É lateral ratio, E/E' medial ratio and deceleration time (Dec Time) (31, 32).

2.4. Strain measurements

LV GLS was determined offline using TomTec postprocessing software (2D Cardiac Performance Analysis, TomTec Imaging Systems, Unterschleissheim, Germany) by an examiner who was

blinded to patient history. LV GLS was obtained in apical four-chamber, two-chamber and long-axis views in the apical, midline, and basal segments (33). The endocardial contour was manually adjusted. Regardless of provider or clinical covariates, a LV GLS $\geq -16\%$ (less negative) was considered abnormal (34). A selection of 20 images was reviewed a second time by the same blinded investigator and by a second blinded investigator to determine intrarater and interrater reliability.

2.5. Cardiopulmonary exercise testing (CPET)

CPET was performed on a cycle ergometer (Excalibur Sport, LODE B.V., Groningen, The Netherlands) using a breath-by-breath gas analysis system (Ergostik, Geratherm Respiratory, Bad Kissingen, Germany). All athletes performed an incremental exercise test. An individually adjusted ramp protocol was chosen according to age, gender, weight and estimated fitness level to exhaust subjects within 8–12 min (35). A 12 lead ECG recording system (Cardiopart 12 Blue/Blue-P, AMEDTEC Medizintechnik Aue GmbH, Aue, Germany) was used. All CPETs were evaluated by the same investigator according to Wasserman et al. (35) and Clinical Recommendations for Cardiopulmonary Exercise Testing Data Assessment in Specific Patient Populations (36). The following variables were measured or calculated: maximum power and predicted maximum power, respiratory oxygen uptake at first ventilatory threshold ($\text{VO}_2/\text{VT1/kg}$) and peak respiratory oxygen uptake (peak VO_2/kg), peak respiratory exchange rate (RER), heart rate (HR) at VT1 (HR@VT1), HR at peak respiratory oxygen uptake (HR@peak VO_2) and predicted HR at peak respiratory oxygen uptake (predicted HR@peak VO_2), peak oxygen pulse (peak O_2/HR) and predicted peak oxygen pulse and the ventilation/volume of CO_2 slope (VE/VCO_2 slope).

2.6. Statistical analysis

Statistical analyses were performed using R Project for Statistical Computing version 4.1.1 (RRID:SCR_001905) (37) and GraphPad Prism 9 (Version 9.4.1, GraphPad Software Inc., California, USA, RRID:SCR_002798). The descriptive data are presented as median and interquartile ranges (IQR). Assumptions for linear regression were visually verified using residual, QQ plots, and histograms. For distribution analysis, Shapiro-Wilk test was used. Correlations between LV GLS and age and BMI were analyzed using Spearman's ρ . The change of cardiac and performance parameters over the three month period was assessed using robust linear mixed effects regression models (38) separately controlling for possible confounding variables (BMI, age, sex, HR, systolic and diastolic blood pressure). A p -value of <0.05 was considered significant. We performed an additional exploratory analysis in a subsample of six athletes with a GLS $\geq -16\%$, defined as reduced GLS. Comparisons were made with a paired t -test if the distribution was normal, otherwise a Wilcoxon signed-rank test was used.

3. Results

3.1. Cohort characteristics

A total of 96 athletes (mean age 33.15 ± 12.40 years, 53 male) were included in the statistical analysis. The sports practiced were divided as follows: 61% endurance sports, 13% strength and combat sports, 21% team sports and 5% technical sports (Table 1). Symptoms reported during COVID-19 infection were standard clinical symptoms of viral infection: fever (39%), cough (46%), rhinorrhea (52%), sore throat (45%), resting dyspnea (21%) or exertional dyspnea (34%), and subjectively perceived reduction in performance (39%) compared with maximal performance before COVID-19. Cardiac symptoms were observed in the form of palpitations (21%), chest pain (21%), increased resting heart rate (26%) or exertional dyspnea after COVID-19 (30%) (Table 2).

3.2. Echocardiographic parameters

LV GLS improved significantly between t_0 and t_1 (t_0 -18.82 ± 2.02 vs. t_1 -19.46 ± 2.05 , $p < 0.001$). All echocardiographic

TABLE 1 Demographic characteristics.

Number	96	
Sex (male/female)	53/43 (55/45%)	
	Means \pm SD	Median (IQR)
Age (years)	33.15 ± 12.40	30 (22.75–40.50)
Weight (kg)	73.93 ± 14.86	71.50 (63.64–84.40)
Height (cm)	175.81 ± 9.05	175.25 (169–183.25)
BMI (kg/m ²)	23.68 ± 3.51	23.05 (21.20–25.38)
BSA (g/m ²)	1.89 ± 0.21	1.88 (1.72–2.06)
CK (U/l) [normal 20–180 U/l]	204.34 ± 419.69	109 (75.25–170.75)
Troponin T (ng/l) [normal <14 ng/l]	5.94 ± 4.00	4 (3–7.5)
CRP (mg/l) [normal < 0.6 mg/l]	1.10 ± 1.81	0.6 (0.6–0.9)
Ferritin ($\mu\text{g/l}$) [normal 22–112 ($\mu\text{g/l}$)]	127.97 ± 111.16	86.50 (52.25–174.75)
Hemoglobin (g/dl) [normal 12.3–15.3]	14.33 ± 1.35	14.20 (13.20–15.30)
Training volume	At least three times per week; > 20 MET/week; five to eight hours/week	
Endurance sports	59 (61%)	
Running	20 (21%)	
Triathlon	11 (12%)	
Cycling	8 (8%)	
Nordic Walking	7 (7%)	
Rowing	6 (6%)	
Others	7 (7%)	
Strength sports	12 (13%)	
Team sports	20 (21%)	
Soccer	13 (14%)	
Handball	4 (4%)	
Others	3 (3%)	
Technical sports	5 (5%)	

SD, standard deviation; IQR, interquartile range; BMI, body mass index; MET, metabolic equivalents of task. Sports are differentiated according to the predominant component. Based on the 2020 ESC Guidelines on sports cardiology and exercise in patients with cardiovascular disease (39).

parameters were within the normal range. There were no significant differences between the study time points (**Table 3**, **Supplementary Table S1**). Significant changes in LV GLS persisted over time even after adjustment for confounding variables (age, sex, heart rate, BMI, systolic or diastolic blood pressure) (**Supplementary Table S2**). Intrarater and interrater reliability with respect to the LV GLS measure showed high agreement (intrarater: 0.892 [95%CI, 0.593–0.973]; interrater: 0.794 [95%CI, 0.159–0.949]).

TABLE 2 Symptoms during COVID-19 presented as absolute values and relative frequencies.

Symptoms	Present	Not present	Missing
Fever	37 (39%)	45 (46%)	14 (15%)
Cough	45 (46%)	37 (39%)	14 (15%)
Rhinorrhea	50 (52%)	32 (33%)	14 (15%)
Sore throat	43 (45%)	39 (40%)	14 (15%)
Resting dyspnea	20 (21%)	62 (64%)	14 (15%)
Exertional dyspnea during covid-19	33 (34%)	49 (51%)	14 (15%)
Exertional dyspnea after covid-19	29 (30%)	61 (64%)	6 (6%)
Palpitations	20 (21%)	70 (73%)	6 (6%)
Chest pain	20 (21%)	70 (73%)	6 (6%)
Increased resting heart rate	25 (26%)	65 (68%)	6 (6%)
Subjective perceived performance limitation	37 (39%)	53 (55%)	6 (6%)
Dizziness	27 (28%)	63 (66%)	6 (6%)

TABLE 3 Echocardiographic parameters at study time t_0 and t_1 presented as means and standard deviation or median and IQR.

	Means \pm SD	t_0^a	Means \pm SD	t_1^b	p -value [#]
		Median (IQR)		Median (IQR)	
HR (bpm)	64.09 \pm 10.15	63.50 (57.5–69.25)	63.02 \pm 11.15	62.50 (54.75–70)	0.290
Systolic BP, mmHg	118.68 \pm 12.78	120 (110–125)	120.47 \pm 14.49	120 (110–125)	0.540
Diastolic BP, mmHg	77.14 \pm 8.92	80 (70–80)	77.47 \pm 9.59	80 (70–80)	0.885
LVIDd (mm)	50.24 \pm 4.64	49.50 (47.30–53.2)	49.63 \pm 5.13	49.60 (45.85–53.65)	0.147
LVIDd/BSA	26.71 \pm 2.36	26.65 (25.01–28.14)	26.43 \pm 2.40	26.44 (24.82–28.02)	0.220
LVIDs (mm)	31.95 \pm 4.76	31.85 (28.7–35.38)	31.85 \pm 5.20	30.90 (28.7–34.3)	0.492
LVIDs/BSA	16.97 \pm 2.35	16.99 (15.77–18.45)	16.95 \pm 2.35	16.82 (15.47–18.56)	0.667
LV EF (%)	70.62 \pm 7.73	71.35 (66.33–77.3)	69.66 \pm 10.87	71.10 (65.6–77.15)	0.864
FS (%)	36.61 \pm 6.24	35.75 (32.3–39.95)	35.47 \pm 7.32	36 (30.5–40.7)	0.487
LV mass (g)	155.21 \pm 47.99	146.50 (120.5–182.75)	154.54 \pm 46.33	149.50 (119.5–179)	0.554
LV mass/BSA (g/m ²)	81.25 \pm 18.52	79.86 (67.12–91.89)	81.32 \pm 17.93	81.65 (66.38–92.19)	0.717
IVSd (mm)	8.63 \pm 1.48	8.65 (7.7–9.38)	8.76 \pm 1.26	8.90 (8–9.6)	0.259
LVPWd (mm)	8.72 \pm 1.56	8.60 (7.4–9.8)	8.76 \pm 1.49	8.60 (7.85–9.7)	0.693
SV (ml)	92.99 \pm 25.89	89.10 (78.50–115)	89.82 \pm 27.43	87.35 (71.18–110.25)	0.241
LV GLS (%)	−18.82 \pm 2.02	−18.86 (−19.87 to −17.30)	−19.46 \pm 2.05	−19.52 (−20.67 to −18.28)	<.001***
TAPSE (mm)	25.64 \pm 4.84	24.55 (22.38–28.5)	26.12 \pm 4.18	25.60 (23.4–27.7)	0.247
E/A	1.45 \pm 0.43	1.40 (1.15–1.7)	1.46 \pm 0.36	1.40 (1.2–1.7)	0.717
E/Ēl	5.79 \pm 1.72	5.40 (4.8–6.7)	6.17 \pm 5.29	5.40 (4.5–6.7)	0.662
E/Ēm	7.87 \pm 2.43	7.25 (6.38–8.7)	7.94 \pm 2.58	7.40 (6.3–9.2)	0.839
DecTime (ms)	173.42 \pm 56.47	164 (129–209)	173.66 \pm 50.21	166 (137–202)	0.775

t_0 , first clinical evaluation; t_1 , second clinical evaluation; SD, standard deviation; IQR, interquartile range; HR, heart rate; Bpm, beats per minute; BP, blood pressure; LVIDd, left ventricular internal diameter end diastole; LVIDd/BSA, left ventricular internal diameter end diastole/body surface area; LVIDs, left ventricular internal diameter end systole; LVIDs/BSA, left ventricular internal diameter end systole/body surface area; LV EF, left ventricular ejection fraction by Simpson; FS, fractional shortening; LV mass, left ventricular mass; LV mass/BSA, left ventricular mass/body surface area; IVSd, interventricular septal end diastole; LVPWd, left ventricular posterior wall end diastole; SV, stroke volume; LV GLS, left ventricular longitudinal strain; TAPSE, tricuspid annular plane systolic excursion. E/A ratio. E/Ēl ratio. E/Ēm ratio. Dec Time, Deceleration Time. Significant results were presented as follows: *** < 0.001.

^a96 athletes.

^b96 athletes.

[#] P -values from robust linear mixed-effects regression analysis (see **Supplementary Table S1**).

3.3. Cardiopulmonary exercise testing (CPET)

Maximum power was significant higher at t_1 than at t_0 (t_0 283.17 \pm 83.20 Watt vs. t_1 286.24 \pm 85.22 Watt, p = 0.009). There were no significant differences between t_0 and t_1 in performance parameters such as peak oxygen pulse or VE/VCO₂ slope but there was a trend toward increased peak oxygen uptake (t_0 36.82 \pm 11.14 ml/min/kg vs. t_1 38.68 \pm 10.26 ml/min/kg, p = 0.069) (**Table 4**, **Supplementary Table S1**). Baseline heart rate was 64.09 \pm 10.15 bpm at t_0 and 63.02 \pm 11.15 bpm at t_1 and was not significantly different. Heart rate increased only slightly but not significantly (t_0 170.70 \pm 17.50 bpm vs. t_1 172.63 \pm 14.10 bpm, p = 0.480). Athletes achieved the same maximal effort at both time points (RER 1.22 vs. 1.22, p = 0.424) (**Table 4**).

3.4. Correlation of LV GLS with performance parameters

LV GLS correlates inversely with RER (−0.316 [−0.501; 0.102], S = 129,938.15, p = 0.027) (**Supplementary Table S3**). This means that athletes with inadequate exercise intolerance also have the worse (more positive) GLS values. LV GLS did not correlate with other performance parameters such as oxygen uptake, peak oxygen pulse or VE/VCO₂ slope (**Supplementary Table S3**).

TABLE 4 CPET parameters at study time t_0 and t_1 presented as means and standard deviation or median and IQR.

	t_0		t_1		p -value ^a
	Means \pm SD	Median (IQR)	Means \pm SD	Median (IQR)	
Maximum Power (Watt)	283.17 \pm 83.20	289 (216–350)	286.24 \pm 85.22	288.50 (224.5–250)	0.009**
Predicted maximum Power (%) ^b	160.65 \pm 38.04	158.50 (136.75–180.5)	163.04 \pm 37.56	161 (139.25–181.75)	0.099
VO ₂ @VT1/kg (ml/min/kg)	22.58 \pm 6.91	22.15 (17.68–26.68)	22.66 \pm 7.28	22 (18.05–27.82)	0.615
Peak VO ₂ /kg (ml/min/kg)	36.82 \pm 11.14	37.80 (29.80–44.2)	38.68 \pm 10.26	38.65 (30.95–45.88)	0.069
Peak RER	1.22 \pm 0.08	1.22 (1.18–1.28)	1.22 \pm 0.08	1.21 (1.17–1.26)	0.424
HR@VT1 (bpm)	125.40 \pm 16.88	124 (113–136)	125.65 \pm 17.13	125.50 (115.5–138.25)	0.678
HR@peak VO ₂ (bpm)	170.70 \pm 17.50	174 (165.5–180.5)	172.63 \pm 14.10	174.50 (166–182)	0.480
Predicted HR@peak VO ₂ (%) ^b	93.95 \pm 9.01	95 (88.5–99)	95.02 \pm 7.07	96 (90.25–99)	0.557
Peak Oxygen pulse (ml/beat)	16.27 \pm 5.06	16.15 (12.73–19.65)	16.29 \pm 4.79	16.80 (12.15–19.90)	0.327
Predicted peak Oxygen pulse (%) ^b	117.39 \pm 25.13	116 (103.5–129.5)	118.56 \pm 25.73	115 (102.25–130.75)	0.666
VE/VCO ₂ slope	25.20 \pm 4.11	24.95 (22.45–27.53)	24.70 \pm 3.35	24.70 (22.4–27.15)	0.203

t_0 , first clinical evaluation; t_1 , second clinical evaluation; SD, standard deviation; VO₂@VT1/kg, respiratory oxygen uptake at first ventilatory threshold; Peak VO₂/kg, peak respiratory oxygen uptake; Predicted VO₂, predicted peak respiratory oxygen uptake; Peak RER, Respiratory Exchange Rate; HR@VT1, heart rate at first ventilatory threshold; HR@peak VO₂, heart rate at peak respiratory oxygen uptake; Predicted HR@peak VO₂, predicted heart rate at peak respiratory oxygen uptake; VE/VCO₂ slope, ventilation/volume of CO₂ slope. Significant results were presented as follows: ** < 0.01.

^a P -values from robust linear mixed-effects regression analysis (see [Supplementary Table S1](#)).

^bCalculated.

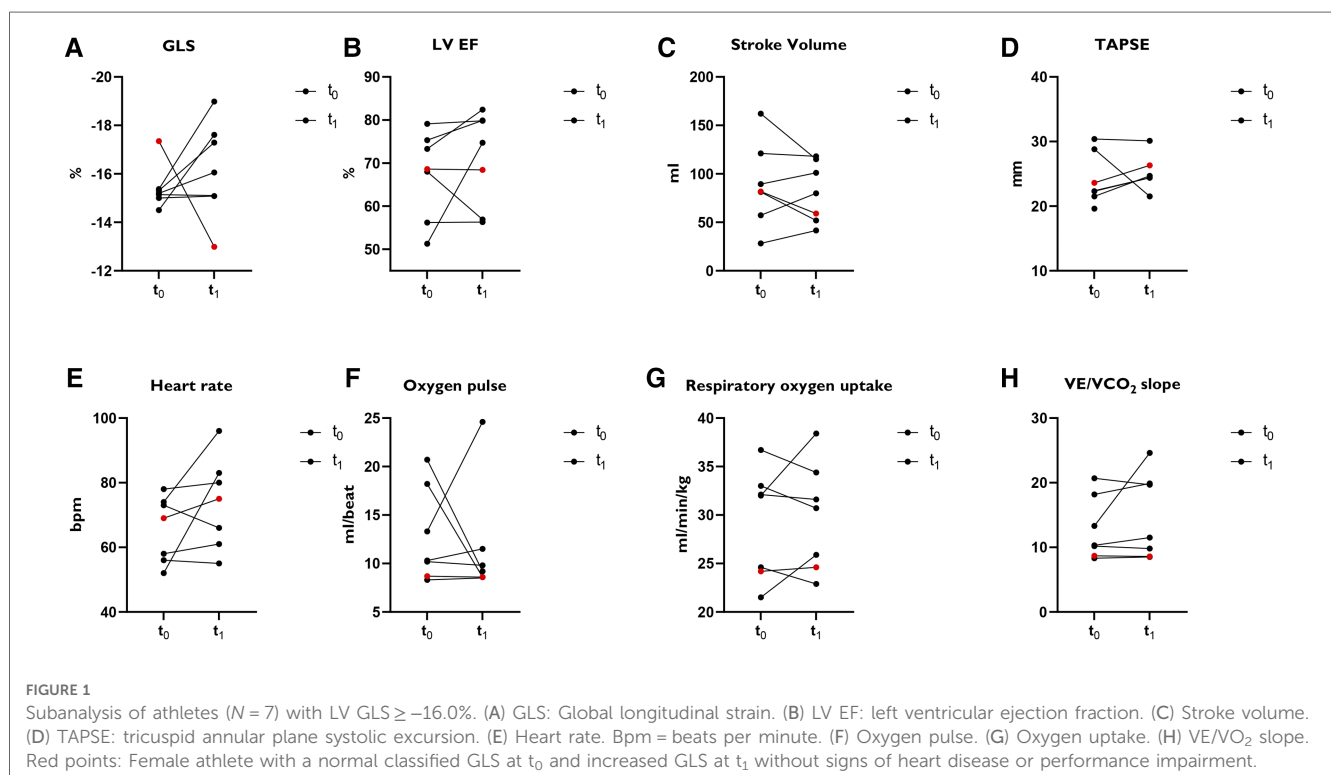
3.5. Subgroup analysis of athletes with reduced LV GLS

Six athletes (mean age 37 years, three male) had a reduced LV GLS of $\geq -16.0\%$ (less negative) ([Figure 1](#)). In four athletes the LV GLS normalized and in two athletes it remained constantly slightly reduced. Subacute myocarditis was detected by MRI in a female athlete with reduced LV GLS. LV EF improved here (51.3% vs. 74%), and performance was identical at both examination time points. An increase in peak VO₂ was seen in two cases. In three cases it remained the same and in one athlete there was a decrease

in peak VO₂. In one female athlete (red points in [Figure 1](#)) out of 96 studied, a LV GLS previously classified as normal, increased without evidence of heart disease or performance impairment. For all parameters shown in [Figure 1](#), there was no significant difference between the two study time points.

4. Discussion

Whether a reduction in LV GLS also leads to reduced performance in athletes after SARS-CoV-2 infection has been



insufficiently investigated. We observed significant improvement in LV GLS approximately five months after COVID-19 compared to baseline at a median of two months after COVID-19, while we did not find any correlation between LV GLS and performance parameters, with the exception of RER.

4.1. Development of LV GLS

To our knowledge, this is the first study to investigate the course of LV GLS and the impact on performance in athletes after COVID-19. Our preliminary study results indicate a mild myocardial involvement in the form of reduced LV GLS in athletes after COVID-19 compared with healthy athletes (26). However, to date, there are no clear results and evidence that cardiac involvement occurs in athletes after COVID-19, and long-term observations in athletes are scarce (24, 25). Hospitalized patients without athletic background did not show significant improvement in LV-GLS at two months (27) or three months (28) or after acute infection: In the study by Baruch et al., 80 hospitalized patients (mean age 57.7 ± 14.9 years, 54 male) showed no significant difference in LV GLS 88.2 ± 33 days after baseline assessment, but 20 patients (25%) still had abnormal LV GLS (28). Fifty-two patients had moderate disease (pneumonia with a grade of $\geq 94\%$ without oxygenation) and 28 patients had a severe disease course, so it is obvious that the included study population does not correspond to that of athletes in our work. In addition, the patients were significantly older and had previous cardiopulmonary diseases. Obesity, which may affect left ventricular function as measured by LV EF and LV GLS, was present in 19 patients (23.8%) (40–42).

Similar results were seen in the Danish prospective longitudinal cohort study ECHOVID-19 by Lassen et al. (27). Whereas right ventricular function improved after a median of 77 days, in contrast, LV GLS did not improve significantly. In addition, recovered COVID-19 patients had significantly lower LV GLS compared with age- and sex-matched controls from individuals participating in the Copenhagen City Heart Study (43). These 91 patients (mean age 63 ± 12 years, 54 male) were elderly and had heart failure or ischemic heart disease (11%) and hypertension (48%) and, most importantly, were also not athletes. LV GLS has been shown to be significantly reduced in patients with hypertension compared with normotensive control subjects (44) because blood pressure correlates with LV GLS (45, 46).

The findings of Baruch et al. and Lassen et al. lead in a different direction than our results, but this may be due to differences in the population studied (age, preexisting conditions, disease course). Patients who required hospitalization may have a higher prevalence of undetected subclinical heart disease than COVID-19 patients who were not hospitalized. Prolonged follow-up examinations may be needed here to show possible recovery. However, in the follow-up study by Karagodin et al., improvements in LV GLS were noted in patients with impaired baseline function (29). Overall, in this study, there was no significant change in LV GLS over time (230 ± 115 days) in 153 hospitalized patients (median age 57, 80 male). The improvement

in LV GLS in patients with impaired baseline function may reflect recovery from acute myocardial injury in severely ill patients (31% in intensive care unit, 16.3% with ventilation, 8.5% with hemodynamic support). Our non-hospitalized athletes described mild courses with standard clinical symptoms of viral infection such as fever, cough, rhinorrhea, sore throat, dyspnea at rest or on exertion, and subjectively perceived decrease in performance (4). Cardiac symptoms such as palpitations, chest pain, and increased resting heart rate occurred in only 21%–26%. Recovery appears to be faster in healthy subjects without pre-existing myocardial dysfunction, which may be reflected in improvement of LV GLS. In general, highly trained athletes are known to have normal, albeit slightly lower, LV GLS and strain rate parameters compared to untrained control subjects (47, 48). Thus, there seems not to be a difference in baseline LV GLS here with that in the long-term studies presented. It still remains unknown what are the origins of the decreased LV myocardial function. It may be a consequence of direct cardiac injury from SARS-CoV-2 infection or a secondary consequence of systemic inflammation, or a combination of both (1, 3). Of course, ischemic injury caused by cardiac microvascular dysfunction cannot be excluded (49).

4.2. LV GLS and performance parameters

To date, no study has examined the relationship between LV GLS and physical performance in athletes recovering from COVID-19. However, in patients with ischemic heart disease (IHD), LV GLS is associated with decreased maximal oxygen uptake, which is an independent risk factor for adverse cardiovascular events (50). In addition, LV GLS correlated independently with peak VO_2 in studies of patients with reduced (rEF) and pEF and was superior to LV EF in identifying patients with reduced exercise capacity (51–53).

In a study by Shimoni et al, patients were examined 57 (27–100) days after COVID-19. Subclinical impairment of LV function was shown to correlate with lower physical performance and duration, but no direct cause-effect relationship could be demonstrated (54). The correlation of LV GLS and physical performance could be due to persistent myocardial damage, and perhaps also to significant age differences (mean age 48 ± 12 years, 87 men) compared with our study group. In our study population of athletes, LV GLS was within the normal range at t_0 and t_1 , and we assume normal cardiac function with only mild myocardial involvement. Therefore, without the exception of RER, we could not demonstrate a correlation with performance parameters. The inverse correlation of GLS with RER indicates insufficient load intolerance at lower GLS values. There is no study to date that reflects this fact. However, in previous studies, submaximal exercise was observed in severe initial disease course (55) or as a sign of possible deconditioning (56) in Post-COVID patients. The number of athletes with reduced LV GLS ($\geq -16.0\%$) may be too small to demonstrate statistical significance. Whether LV GLS correlates independently of COVID-19 with performance parameters in athletes in general

has not been investigated to date. However, this could provide interesting additional information about cardiac adaptation processes in competitive as well as recreational athletes and could be integrated into diagnostics of the annual sports medical screening or return-to-sport examination in the future.

4.3. Development of spiroergometric parameters

Maximum power increased significantly from t_0 to t_1 and there is a trend toward increased peak oxygen uptake. It cannot be ruled out that a break in training in the context of SARS-CoV-2 infection is causing poorer performance, which subsequently improves during the course. Improvement in performance could also be explained by the athletes' increasing recovery and predominantly being symptom-free at t_1 . The oxygen pulse, reflecting the maximal aerobic capacity, does not change significantly and heart rate increases only slightly but not significantly. These results emphasize that cardiac function does not appear to be impaired. Athletes achieved the same maximal effort at both time points (RER 1.22 vs. 1.22, $p = 0.424$). Similarly, in subgroup analysis of six athletes with probable myocardial dysfunction ($GLS \geq -16.0\%$), heart rate, LV GLS, peak oxygen pulse, or maximal oxygen uptake did not differ significantly between study time points.

This is broadly consistent with results from Komici et al, who found no decreased physical performance or impairment in pulmonary and cardiovascular function during the early recovery period (10–30 days) after COVID-19 in 24 competitive soccer players (mean age 23.5 years, 24 male) compared to healthy control athletes. However, LV GLS was not examined here (57). Two previously published studies showed an improvement in symptoms after COVID with corresponding improvements in CPET parameters over a longer observation period (58, 59). The main difference between the study by Moulson et al. and ours was that it included athletes with persistent cardiopulmonary symptoms, thus presenting a highly selected subgroup of athletes after COVID-19. These athletes were significantly more likely to report symptoms of dyspnea (76% vs. 21%), exercise intolerance (76% vs. 39%), chest pain (71% vs. 21%), and palpitations (57% vs. 21%) than the athletes we studied (who had partially recovered and were symptom-free), which may explain initially worse performance and subsequent improvement (58). Due to the different study populations and designs, there are no consensus data available so far, which limits the comparability between current studies.

4.4. Strengths and limitations

This presented study is limited by the longitudinal design, as strain values and performance parameters of athletes from periods prior to COVID-19 are not available. Follow-up

examinations were performed after five months on the assumption that this period was sufficiently long to detect recovery of cardiac function. For possible variables influencing GLS, such as age, sex, heart rate, BMI, systolic or diastolic blood pressure, we performed multivariate linear regression. Significant changes in LV GLS persisted over the observation period. Although the LV GLS determination can be software and investigator experience dependent, our results show high intrarater and interrater reliability. On the one hand, the clearly defined population of study participants, consisting of athletes, limits the generalizability of the results to the general population. But, on the other hand, it allows an assessment of a specific group. It should also be emphasized that we achieved a meaningful case number of athletes for a single-centre study. Finally, although an association between COVID-19 and the occurrence of pathological examination findings up to myocarditis is suggested, direct evidence is still lacking.

4.5. Conclusion

We observed significant improvements in LV GLS approximately five months after COVID-19 compared with baseline at a median of two months after COVID-19. Therefore, we assume that the significant LV-GLS differences reflect possible mild myocardial involvement during or shortly after COVID-19. Except for RER, we did not find a correlation between LV GLS and performance parameters. This could indicate that mild cardiac dysfunction in athletes with mild disease course does not necessarily contribute to decreased performance after COVID-19. However, an inverse correlation between GLS and RER seems to indicate insufficient load intolerance at lower GLS values. Here, further studies on the development of GLS in athletes or in the general population with moderate and severe disease courses would be informative as well as the comparison of pre-COVID-19 with post-COVID-19 echocardiography to evaluate the effects of COVID-19 on cardiac function.

Data availability statement

The original contributions presented in the study are included in the article/**Supplementary Material**, further inquiries can be directed to the corresponding author.

Ethics statement

The studies involving humans were approved by Local Ethics Committee of the University of Ulm (EK 408/20). The studies were conducted in accordance with the local legislation and institutional requirements. The participants provided their written informed consent to participate in this study.

Author contributions

Conceptualization, JS and JMS; Data curation, JS and SV; Formal analysis, JS and LM; Funding acquisition, JMS; Investigation, JS and SV; Methodology, JS, LM, DAB, JKe, SV, and JMS; Project administration, JMS; Resources, JS; Software, JS and LM; Supervision, JMS; Validation, JS, LM, DAB, and JMS; Visualization, JS and LM; Writing—original draft, JS; Writing—review & editing, JS, DAB, LM, JKi, JKe, SV, and JMS All authors have read and agreed to the published version of the manuscript. All authors contributed to the article and approved the submitted version.

Funding

This work was supported primarily by the University Hospital Ulm and funds from the German Federal Institute for Sport Science, Cologne by resolution of the German Bundestag [ZMVI4-070106/20-23].

References

- Akhmerov A, Marban E. COVID-19 and the heart. *Circ Res.* (2020) 126(10):1443–55. doi: 10.1161/CIRCRESAHA.120.317055
- Huang C, Wang Y, Li X, Ren L, Zhao J, Hu Y, et al. Clinical features of patients infected with 2019 novel coronavirus in Wuhan, China. *Lancet.* (2020) 395(10223):497–506. doi: 10.1016/S0140-6736(20)30183-5
- Zheng YY, Ma YT, Zhang JY, Xie X. COVID-19 and the cardiovascular system. *Nat Rev Cardiol.* (2020) 17(5):259–60. doi: 10.1038/s41569-020-0360-5
- Krzywanski J, Mikulski T, Krysztofiak H, Pokrywka A, Mlynarczyk M, Malek LA, et al. Elite athletes with COVID-19—predictors of the course of disease. *J Sci Med Sport.* (2022) 25(1):9–14. doi: 10.1016/j.jsams.2021.07.003
- Rajpal S, Tong MS, Borchers J, Zareba KM, Obarski TP, Simonetti OP, et al. Cardiovascular magnetic resonance findings in competitive athletes recovering from COVID-19 infection. *JAMA Cardiol.* (2021) 6(1):116–8. doi: 10.1001/jamacardio.2020.4916. Erratum in: *JAMA Cardiol.* (2021) 6(1):123.
- Schumacher YO, Tabben M, Hassoun K, Al Marwani A, Al Hussein I, Coyle P, et al. Resuming professional football (soccer) during the COVID-19 pandemic in a country with high infection rates: a prospective cohort study. *Br J Sports Med.* (2021) 55(19):1092–8. doi: 10.1136/bjsports-2020-103724
- Clark DE, Parikh A, Dendy JM, Diamond AB, George-Durrett K, Fish FA, et al. COVID-19 Myocardial pathology evaluation in athletes with cardiac magnetic resonance (COMPETE CMR). *Circulation.* (2021) 143(6):609–12. doi: 10.1161/CIRCULATIONAHA.120.052573
- Moulson N, Petek BJ, Drezner JA, Harmon KG, Kliethermes SA, Patel MR, et al. SARS-CoV-2 cardiac involvement in young competitive athletes. *Circulation.* (2021) 144(4):256–66. doi: 10.1161/CIRCULATIONAHA.121.054824
- Martinez MW, Tucker AM, Bloom OJ, Green G, DiFiori JP, Solomon G, et al. Prevalence of inflammatory heart disease among professional athletes with prior COVID-19 infection who received systematic return-to-play cardiac screening. *JAMA Cardiol.* (2021) 6(7):745–52. doi: 10.1001/jamacardio.2021.0565
- Steinacker JM*, Schellenberg J*, Bloch W, Deibert P, Friedmann-Bette B, Grim C, et al. Recommendations for return-to-sport after COVID-19: expert consensus. *DZSM.* (2022) 73(4):127–36. doi: 10.5960/dzsm.2022.532
- Wilson MG, Hull JH, Rogers J, Pollock N, Dodd M, Haines J, et al. Cardiorespiratory considerations for return-to-play in elite athletes after COVID-19 infection: a practical guide for sport and exercise medicine physicians. *Br J Sports Med.* (2020) 54(19):1157–61. doi: 10.1136/bjsports-2020-102710
- Halle M, Bloch W, Niess AM, Predel HG, Reinsberger C, Scharhag J, et al. Exercise and sports after COVID-19—guidance from a clinical perspective. *Transl Sports Med.* (2021) 4(3):310–8. doi: 10.1002/tsm.2247
- Blessberger H, Binder T. Two dimensional speckle tracking echocardiography: clinical applications. *Heart.* (2010) 96(24):2032–40. doi: 10.1136/hrt.2010.199885
- Smiseth OA, Torp H, Opdahl A, Haugaa KH, Urheim S. Myocardial strain imaging: how useful is it in clinical decision making? *Eur Heart J.* (2016) 37(15):1196–207. doi: 10.1093/eurheartj/ehv529
- Biering-Sorensen T, Biering-Sorensen SR, Olsen FJ, Sengelov M, Jorgensen PG, Mogelvang R, et al. Global longitudinal strain by echocardiography predicts long-term risk of cardiovascular morbidity and mortality in a low-risk general population: the Copenhagen City Heart Study. *Circ Cardiovasc Imaging.* (2017) 10(3):e005521. doi: 10.1161/CIRCIMAGING.116.005521
- Croft LB, Krishnamoorthy P, Ro R, Anastasius M, Zhao W, Buckley S, et al. Abnormal left ventricular global longitudinal strain by speckle tracking echocardiography in COVID-19 patients. *Future Cardiol.* (2021) 17(4):655–61. doi: 10.2217/fca-2020-0121
- Stobe S, Richter S, Seige M, Stehr S, Laufs U, Hagendorff A. Echocardiographic characteristics of patients with SARS-CoV-2 infection. *Clin Res Cardiol.* (2020) 109(12):1549–66. doi: 10.1007/s00392-020-01727-5
- Li R, Wang H, Ma F, Cui GL, Peng LY, Li CZ, et al. Widespread myocardial dysfunction in COVID-19 patients detected by myocardial strain imaging using 2-D speckle-tracking echocardiography. *Acta Pharmacol Sin.* (2021) 42(10):1567–74. doi: 10.1038/s41401-020-00595-z
- Minhas AS, Gilotra NA, Goerlich E, Metkus T, Garibaldi BT, Sharma G, et al. Myocardial work efficiency, a novel measure of myocardial dysfunction, is reduced in COVID-19 patients and associated with in-hospital mortality. *Front Cardiovasc Med.* (2021) 8:667721. doi: 10.3389/fcvm.2021.667721
- Baum P, Do L, Deterding L, Lier J, Kunis I, Saur D, et al. Cardiac function in relation to functional status and fatigue in patients with post-COVID syndrome. *Sci Rep.* (2022) 12(1):19575. doi: 10.1038/s41598-022-24038-3
- Mahajan S, Kunal S, Shah B, Garg S, Palleda GM, Bansal A, et al. Left ventricular global longitudinal strain in COVID-19 recovered patients. *Echocardiography.* (2021) 38(10):1722–30. doi: 10.1111/echo.15199
- Kujur PP, Jhala M, Bhondve A, Lanjewar C, Matta R, Deshmukh H. Left ventricular global longitudinal strain imaging in identifying subclinical myocardial dysfunction among COVID-19 survivors. *Indian Heart J.* (2022) 74(1):51–5. doi: 10.1016/j.ihj.2021.12.007
- Oikonomou E, Lampsas S, Theofilis P, Souvaliotis N, Papamikroulis GA, Katsarou O, et al. Impaired left ventricular deformation and ventricular-arterial coupling in post-COVID-19: association with autonomic dysregulation. *Heart Vessels.* (2023) 38(3):381–93. doi: 10.1007/s00380-022-02180-2
- Lakatos BK, Tokodi M, Fabian A, Ladanyi Z, Vago H, Szabo L, et al. Frequent constriction-like echocardiographic findings in elite athletes following mild COVID-19: a propensity score-matched analysis. *Front Cardiovasc Med.* (2021) 8:760651. doi: 10.3389/fcvm.2021.760651

Conflict of interest

The authors declare that the research was conducted in the absence of any commercial or financial relationships that could be construed as a potential conflict of interest.

Publisher's note

All claims expressed in this article are solely those of the authors and do not necessarily represent those of their affiliated organizations, or those of the publisher, the editors and the reviewers. Any product that may be evaluated in this article, or claim that may be made by its manufacturer, is not guaranteed or endorsed by the publisher.

Supplementary material

The Supplementary Material for this article can be found online at: <https://www.frontiersin.org/articles/10.3389/fcvm.2023.1240278/full#supplementary-material>

25. Fikenzer S, Kogel A, Pietsch C, Lavall D, Stobe S, Rudolph U, et al. SARS-CoV2 infection: functional and morphological cardiopulmonary changes in elite handball players. *Sci Rep.* (2021) 11(1):17798. doi: 10.1038/s41598-021-97120-x
26. Schellenberg J, Ahathaller M, Matits L, Kirsten J, Kersten J, Steinacker JM. Left ventricular global longitudinal strain as a parameter of mild myocardial dysfunction in athletes after COVID-19. *J Cardiovasc Dev Dis.* (2023) 10(5):189. doi: 10.3390/jcdd10050189
27. Lassen MCH, Skaarup KG, Lind JN, Alhakak AS, Sengelov M, Nielsen AB, et al. Recovery of cardiac function following COVID-19—eCHOVID-19: a prospective longitudinal cohort study. *Eur J Heart Fail.* (2021) 23(11):1903–12. doi: 10.1002/ehf.2347
28. Baruch G, Rothschild E, Sadon S, Szekely Y, Lichter Y, Kaplan A, et al. Evolution of right and left ventricle routine and speckle-tracking echocardiography in patients recovering from coronavirus disease 2019: a longitudinal study. *Eur Heart J Cardiovasc Imaging.* (2022) 23(8):1055–65. doi: 10.1093/ehjci/jeab190
29. Karagodin I, Singulane CC, Descamps T, Woodward GM, Xie M, Tucay ES, et al. Ventricular changes in patients with acute COVID-19 infection: follow-up of the world alliance societies of echocardiography (WASE-COVID) study. *J Am Soc Echocardiogr.* (2022) 35(3):295–304. doi: 10.1016/j.echo.2021.10.015
30. Niess AM, Widmann M, Gaidai R, Golz C, Schubert I, Castillo K, et al. COVID-19 in German competitive sports: protocol for a prospective multicenter cohort study (CoSmo-S). *Int J Public Health.* (2022) 67:1604414. doi: 10.3389/ijph.2022.1604414
31. Lang RM, Badano LP, Mor-Avi V, Afilalo J, Armstrong A, Ernande L, et al. Recommendations for cardiac chamber quantification by echocardiography in adults: an update from the American Society of Echocardiography and the European Association of Cardiovascular Imaging. *Eur Heart J Cardiovasc Imaging.* (2015) 16(3):233–70. doi: 10.1093/ehjci/jev014
32. Quinones MA, Otto CM, Stoddard M, Waggoner A, Zoghbi WA, Doppler Quantification Task Force of the N, et al. Recommendations for quantification of doppler echocardiography: a report from the doppler quantification task force of the nomenclature and standards committee of the American Society of Echocardiography. *J Am Soc Echocardiogr.* 2002;15(2):167–84. doi: 10.1067/mje.2002.120202
33. Voigt JU, Pedrizzetti G, Lysyansky P, Marwick TH, Houle H, Baumann R, et al. Definitions for a common standard for 2D speckle tracking echocardiography: consensus document of the EACVI/ASE/industry task force to standardize deformation imaging. *J Am Soc Echocardiogr.* (2015) 28(2):183–93. doi: 10.1016/j.echo.2014.11.003
34. D'Elia N, Caselli S, Kosmala W, Lancellotti P, Morris D, Muraru D, et al. Normal global longitudinal strain: an individual patient meta-analysis. *JACC Cardiovasc Imaging.* (2020) 13(1 Pt 1):167–9. doi: 10.1016/j.jcmg.2019.07.020
35. Wassermann K, Pothoff G, Subbe C, Bahra J, Hilger HH. Air trapping and cardiopulmonary exercise testing in patients with mild to moderate bronchial obstruction: clinical role of trapped gas measurements. *Z Kardiol.* (1994) 83(Suppl 3):149–54.
36. Guazzi M, Arena R, Halle M, Piepoli MF, Myers J, Lavie CJ. 2016 Focused update: clinical recommendations for cardiopulmonary exercise testing data assessment in specific patient populations. *Circulation.* (2016) 133(24):e694–711. doi: 10.1161/CIR.0000000000000406
37. R-Core-Team. R: A language and environment for statistical computing. R Foundation for Statistical Computing; 2022.
38. Koller M. Robustlmm: an R package for robust estimation of linear mixed-effects models. *J Stat Softw.* (2016) 75(6):1–24. doi: 10.18637/jss.v075.i06
39. Pelliccia A, Sharma S, Gati S, Back M, Borjesson M, Caselli S, et al. 2020 ESC guidelines on sports cardiology and exercise in patients with cardiovascular disease. *Eur Heart J.* (2021) 42(1):17–96. doi: 10.1093/eurheartj/ehaa605. Erratum in: *Eur Heart J.* (2021) 42(5):548–49.
40. Blomstrand P, Sjöblom P, Nilsson M, Wijkman M, Engvall M, Lanne T, et al. Overweight and obesity impair left ventricular systolic function as measured by left ventricular ejection fraction and global longitudinal strain. *Cardiovasc Diabetol.* (2018) 17(1):113. doi: 10.1186/s12933-018-0756-2
41. Arenas IA, Podesta CA, Issa O, Lin J, Brenes JC. Myocardial longitudinal strain, fitness, and heart failure risk factors in young adults. *Echocardiography.* (2020) 37(3):404–11. doi: 10.1111/echo.14613
42. Siurana JM, Ventura PS, Yeste D, Riazia-Martin L, Arciniegas L, Clemente M, et al. Myocardial geometry and dysfunction in morbidly obese adolescents (BMI 35–40 kg/m²). *Am J Cardiol.* (2021) 157:128–34. doi: 10.1016/j.amjcard.2021.07.026
43. Skaarup KG, Lassen MCH, Johansen ND, Olsen FJ, Lind JN, Jorgensen PG, et al. Age- and sex-based normal values of layer-specific longitudinal and circumferential strain by speckle tracking echocardiography: the Copenhagen City Heart Study. *Eur Heart J Cardiovasc Imaging.* (2022) 23(5):629–40. doi: 10.1093/ehjci/jeab032
44. Tadic M, Majstorovic A, Pencic B, Ivanovic B, Neskovic A, Badano L, et al. The impact of high-normal blood pressure on left ventricular mechanics: a three-dimensional and speckle tracking echocardiography study. *Int J Cardiovasc Imaging.* (2014) 30(4):699–711. doi: 10.1007/s10554-014-0382-3
45. Galderisi M, Esposito R, Schiano-Lomoriello V, Santoro A, Ippolito R, Schiattarella P, et al. Correlates of global area strain in native hypertensive patients: a three-dimensional speckle-tracking echocardiography study. *Eur Heart J Cardiovasc Imaging.* (2012) 13(9):730–8. doi: 10.1093/ehjci/jeo026
46. Saghir M, Arecas M, Mekan M. Strain rate imaging differentiates hypertensive cardiac hypertrophy from physiologic cardiac hypertrophy (athlete's heart). *J Am Soc Echocardiogr.* (2007) 20(2):151–7. doi: 10.1016/j.echo.2006.08.006
47. Caselli S, Montesanti D, Autore C, Di Paolo FM, Pisicchio C, Squeo MR, et al. Patterns of left ventricular longitudinal strain and strain rate in Olympic athletes. *J Am Soc Echocardiogr.* (2015) 28(2):245–53. doi: 10.1016/j.echo.2014.10.010
48. D'Ascenzi F, Solari M, Mazzolai M, Cameli M, Lisi M, Andrei V, et al. Two-dimensional and three-dimensional left ventricular deformation analysis: a study in competitive athletes. *Int J Cardiovasc Imaging.* (2016) 32(12):1697–705. doi: 10.1007/s10554-016-0961-6
49. Fox SE, Lameira FS, Rinker EB, Vander Heide RS. Cardiac endothelitis and multisystem inflammatory syndrome after COVID-19. *Ann Intern Med.* (2020) 173(12):1025–7. doi: 10.7326/L20-0882
50. Zhang S, Liu Y, Jiang L, Wang Z, Liu W, Zuo H. Diagnostic accuracy of global longitudinal strain for detecting exercise intolerance in patients with ischemic heart disease. *J Cardiovasc Dev Dis.* (2023) 10(1):10. doi: 10.3390/jcdd10010010
51. Maia RJC, Brandao SCS, Leite J, Parente GB, Pinheiro F, Araújo BTS, et al. Global longitudinal strain predicts poor functional capacity in patients with systolic heart failure. *Arq Bras Cardiol.* (2019) 113(2):188–94. doi: 10.5935/abc.20190119
52. Hasselberg NE, Haugaa KH, Sarvari SI, Gullestad L, Andreassen AK, Smiseth OA, et al. Left ventricular global longitudinal strain is associated with exercise capacity in failing hearts with preserved and reduced ejection fraction. *Eur Heart J Cardiovasc Imaging.* (2015) 16(2):217–24. doi: 10.1093/ehjci/jeu277
53. Li M, Lu Y, Fang C, Zhang X. Correlation between myocardial deformation on three-dimensional speckle tracking echocardiography and cardiopulmonary exercise testing. *Echocardiography.* (2017) 34(11):1640–8. doi: 10.1111/echo.13675
54. Shimoni O, Korenfeld R, Goland S, Meledin V, Haberman D, George J, et al. Subclinical myocardial dysfunction in patients recovered from COVID-19 disease: correlation with exercise capacity. *Biology (Basel).* (2021) 10(11):1201. doi: 10.3390/biology10111201
55. Romero-Ortuno R, Jennings G, Xue F, Duggan E, Gormley J, Monaghan A. Predictors of submaximal exercise test attainment in adults reporting long COVID symptoms. *J Clin Med.* (2022) 11(9):2376. doi: 10.3390/jcm11092376
56. Rinaldo RF, Mondoni M, Parazzini EM, Pitari F, Brambilla E, Luraschi S, et al. Deconditioning as main mechanism of impaired exercise response in COVID-19 survivors. *Eur Respir J.* (2021) 58(2):2100870. doi: 10.1183/13993003.00870-2021
57. Komici K, Bianco A, Perrotta F, Dello Iacono A, Bencivenga L, D'Agnano V, et al. Clinical characteristics, exercise capacity and pulmonary function in post-COVID-19 competitive athletes. *J Clin Med.* (2021) 10(14):3053. doi: 10.3390/jcm10143053
58. Moulson N, Gustus SK, Scirica C, Petek BJ, Vanatta C, Churchill TW, et al. Diagnostic evaluation and cardiopulmonary exercise test findings in young athletes with persistent symptoms following COVID-19. *Br J Sports Med.* (2022) 56:927–32. doi: 10.1136/bjsports-2021-105157
59. Vollrath S, Bizjak DA, Zorn J, Matits L, Jerg A, Munk M, et al. Recovery of performance and persistent symptoms in athletes after COVID-19. *PLoS One.* (2022) 17(12):e0277984. doi: 10.1371/journal.pone.0277984



OPEN ACCESS

EDITED BY

Francesca Innocenti,
Careggi University Hospital, Italy

REVIEWED BY

Attila Oláh,
Semmelweis University, Hungary
Gaspar Del Rio Pertuz,
University of Minnesota, United States

*CORRESPONDENCE

Changqing Du
✉ ddcq82@126.com
Wenbin Zhang
✉ 3313011@zju.edu.cn

[†]These authors have contributed equally
to this work

RECEIVED 24 February 2023

ACCEPTED 09 October 2023

PUBLISHED 02 November 2023

CITATION

Chen Q, Li D, Jiang H, Hu T, Tao Y, Du C and
Zhang W (2023) Cardiac remodeling on
echocardiogram is related to contrast-
associated acute kidney injury after coronary
angiography: a cross-section study.
Front. Cardiovasc. Med. 10:1173586.
doi: 10.3389/fcvm.2023.1173586

COPYRIGHT

© 2023 Chen, Li, Jiang, Hu, Tao, Du and Zhang.
This is an open-access article distributed under
the terms of the [Creative Commons Attribution
License \(CC BY\)](#). The use, distribution or
reproduction in other forums is permitted,
provided the original author(s) and the
copyright owner(s) are credited and that the
original publication in this journal is cited, in
accordance with accepted academic practice.
No use, distribution or reproduction is
permitted which does not comply with these
terms.

Cardiac remodeling on echocardiogram is related to contrast-associated acute kidney injury after coronary angiography: a cross-section study

Qingqing Chen^{1†}, Duanbin Li^{2,3†}, Hangpan Jiang⁴, Tianli Hu⁴,
Yecheng Tao², Changqing Du^{1*} and Wenbin Zhang^{2,3*}

¹Department of Cardiology, Affiliated Zhejiang Hospital, College of Medicine, Zhejiang University, Hangzhou, China, ²Department of Cardiology, Sir Run Run Shaw Hospital, College of Medicine, Zhejiang University, Hangzhou, China, ³Key Laboratory of Cardiovascular Intervention and Regenerative Medicine of Zhejiang Province, Hangzhou, China, ⁴Department of Cardiology, The Fourth Affiliated Hospital, College of Medicine, Zhejiang University, Yiwu, China

Background: Cardiac dysfunction is a well-established risk factor for contrast-associated acute kidney injury (CA-AKI). Nevertheless, the relationship between cardiac remodeling, as assessed by echocardiography, and CA-AKI remains uncertain.

Method: A total of 3,241 patients undergoing coronary angiography (CAG) with/without percutaneous coronary intervention (PCI) were enrolled in this retrospective study. Collected echocardiographic parameters were normalized by body surface area (BSA) and divided according to quartile, including the left ventricular internal end-diastolic diameter index (LVDDI), left ventricular internal end-systolic diameter index (LVDSI), and left ventricular mass index (LVMI). Logistic regression analysis was conducted to ascertain the association between structural parameter changes and CA-AKI. Further investigation was performed in different subgroups.

Results: The mean age of the participants was 66.6 years, and 16.3% suffered from CA-AKI. LVDSI ≥ 22.9 mm/m²: OR = 1.953, 95%CI (1.459 to 2.615), $P < 0.001$, LVDDI ≥ 33.2 mm/m²: OR = 1.443, 95%CI (1.087 to 1.914), $P = 0.011$, and LVMI ≥ 141.0 g/m²: OR = 1.530, 95%CI (1.146 to 2.044), $P = 0.004$ in quartile were positively associated with CA-AKI risk in general (all P for trend < 0.05). These associations were consistent when stratified by age, left ventricular ejection fraction, estimated glomerular filtration rate, and N-terminal brain natriuretic peptide (all P for interaction > 0.05). The presence of eccentric hypertrophy [OR = 1.400, 95%CI (1.093 to 1.793), $P = 0.008$] and the coexistence of hypertrophy and dilation [OR = 1.397, 95%CI (1.091 to 1.789), $P = 0.008$] carried a higher CA-AKI risk.

Conclusion: The presence of cardiac remodeling, assessed by echocardiography, is associated with a higher risk of CA-AKI.

KEYWORDS

echocardiography, cardiac remodeling, contrast associated acute kidney injury, coronary angiography, percutaneous coronary intervention

1. Introduction

Contrast-associated acute kidney injury (CA-AKI) is a dreadful complication characterized by a rapid deterioration of renal function within 72 h after administering the iodine contrast medium (1). The incidence of CA-AKI has increased recently following the widespread application of coronary angiography (CAG) and percutaneous coronary intervention (PCI) to diagnose and treat coronary artery disease (CAD) (2).

CA-AKI has been ranked as the third most common cause of nosocomial acute kidney injury in the United States, with a 30% rate among patients undergoing CAG/PCI (1). Patients suffering from CA-AKI tend to confront longer hospitalization but worse long-term prognosis and even permanently damaged renal function (3). Therefore, as for patients receiving CAG/PCI, CA-AKI has been a growing health concern, and targeting patients with a high risk of CA-AKI is imperative for clinicians. Existing research has demonstrated the significant association of impaired organ function with CA-AKI risk, such as cardiac dysfunction (4, 5).

Cardiac dysfunction commonly accompanies cardiac remodeling, which involves both functional and structural changes. Cardiac remodeling occurs in both cardiovascular and non-cardiovascular diseases in compensatory response to the overload (6). More than a compensatory change, cardiac remodeling not only plays a formidable role in the progression of cardiac dysfunction to heart failure but also participates in the functional impairment of the kidney (7). Accumulating evidence demonstrates the remarkable correlation between cardiac remodeling and the development of chronic kidney disease (CKD); in turn, impaired renal function is more susceptible to developing into cardiac remodeling (8, 9). As for patients undergoing operation, hemodynamic perturbation caused by decreased cardiac function can be attributed to postoperative acute kidney injury (10, 11). Nevertheless, the association between the presence of cardiac remodeling and CA-AKI risk after CAG/PCI remains unknown.

Accordingly, the current retrospective research was conducted to figure out the association of cardiac remodeling with CA-AKI risk in a cohort of CAG patients undergoing CAG/PCI. With the help of an echocardiogram, certain structural parameters were measured to evaluate cardiac remodeling (6). Further investigation into the association between different patterns of cardiac remodeling and CA-AKI risk was also conducted.

2. Materials and methods

2.1. Study design

Conforming to the STROBE (Strengthening the Reporting of Observational Studies in Epidemiology) guidelines, this cross-section study was conducted to explore the association of structural and functional cardiac remodeling on an echocardiogram with the risk of CA-AKI (12). A large cohort of

CAD patients was consequently recruited at Sir Run Run Shaw Hospital from March 2018 to February 2022 (**Supplementary Figure S1**). The inclusion criteria for the enrolled patients were set as follows: (1) had undergone CAG/PCI operation; (2) had available Scr levels on admission and after CAG/PCI with 72 h; (3) had accessible echocardiographic parameters during the hospitalization. The patients with one of the following criteria were excluded: (1) the presence of end-stage chronic kidney disease; (2) had underwent more than one administration of iodine contrast agents (3); being exposed to the usage of nephrotoxic medication during the perioperative phase; (4) suffering from a shock, malignant tumor, and lactation condition; (5) expectant mothers.

This retrospective study has been authorized by the Ethics Committee of the Sir Run Run Shaw Hospital (No. 20201217-36) and performed following the Helsinki statement. Given the nature of a retrospective cross-section study, informed consent could be skipped.

2.2. Study endpoint

According to the ESUR (European Society of Urogenital Radiology) guidelines, CA-AKI was set as the primary endpoint, and diagnosing by the Scr level increased by $\geq 44 \mu\text{mol/L}$ (0.5 mg/dl), or the proportion increased by $\geq 25\%$ compared to the level on admission (13).

The secondary outcome was considered the percentage of the Scr elevation, which was evaluated by the difference of the Scr level after the CAG/PCI divided baseline Scr level [the percentage of Scr elevation = (postoperative Scr—baseline Scr)/baseline Scr].

2.3. Echocardiographic parameters and criteria

Certain echocardiographic parameters were measured to detect the presence of cardiac structural remodeling during the perioperative period (within 3 days before or after the CAG/PCI). All of the echocardiographic parameters were collected during the hospitalization by the clinical operators with long-term specialized training. The criteria of reference for analysis were from the 2015 American Society of Echocardiography (ASE)/European Association of Cardiovascular Imaging (EACVI) document for chamber quantification (14).

Left ventricular (LV) geometry and ejection fraction (EF) were assessed using two-dimensional (2D) echocardiography. All measurements were standardized to body surface area. LVM was calculated according to the Devereux formula: $0.8 \times 1.04 \times [(IVSD + LVIDD + LVPWD)^3 - LVIDD^3] + 0.6 \text{ g}$. Relative wall thickness (RWT) was calculated as $2 \times LVPWD$ divided by LVIDD to depict left ventricular (LV) geometry.

In the 2015 ASE/EACVI document, abnormal LVMI ($>95 \text{ g/m}^2$ in females and $>115 \text{ g/m}^2$ in males) was applied to assess the abnormal LV geometry, and elevated LVDDI ($>30 \text{ mm/m}^2$ in

males and $>31 \text{ mm/m}^2$ in females) and LVIDSI ($>21 \text{ mm/m}^2$) could reflect the enlarged size of the heart chambers to some extent. Therefore, in the present study, LVMI, LVDDI, and LVIDSI were measured to demonstrate the alterations in the shape and size of the heart, respectively.

According to guidelines in China, the ventricular internal end-diastolic diameter was commonly used to assess the ventricular size, and consequently, elevated LVDDI was applied to indicate the dilated left ventricle in this study. Abnormally increased LVMI indicates the presence of left ventricular hypertrophy (LVH). Then, with the help of RWT and LVMI, concentric remodeling was defined as $\text{RWT} > 0.42$ and $\text{LVMI} \leq 115 \text{ g/m}^2$ in males or $\leq 95 \text{ g/m}^2$ in females; moreover, concentric LVH was diagnosed by $\text{RWT} > 0.42$ and $\text{LVMI} > 55 \text{ mm}$ in males or $>50 \text{ mm}$ in females, while RWT was ≤ 0.42 for eccentric LVH.

2.4. Definitions and data collection

Data acquired on admission included demographic data, laboratory tests, previous usage of medications, and past history. Fasting blood samples for various clinical routine biochemistry tests and blood examinations at baseline were drawn from antecubital veins. Anemia was defined as hemoglobin $<120 \text{ g/L}$ in adult males and hemoglobin $<110 \text{ g/L}$ in adult females (non-pregnant) at sea level. Hypotension was defined as a systolic blood pressure $<90 \text{ mmHg}$ or a diastolic blood pressure $<60 \text{ mmHg}$ during the procedure. Abnormal N-terminal pro-brain natriuretic peptide (NT-proBNP) was defined as NT-proBNP exceeding the upper limit of the normal level. For patients <45 years old, the upper limit of normal was 300 pg/ml ; for patients between 45 and 70 years of age, the upper limit of normal was 900 pg/ml ; and for patients >70 years old, the upper limit of normal was $1,800 \text{ pg/ml}$ (15).

The procedures of CAG/PCI for all patients were performed by physicians with longstanding expertise in interventional therapy and acted in accordance with standard practice (16). Detailed procedural data of CAG/PCI were recorded. All patients received perioperative hydration (specific protocol: intravenous infusion of 0.9% saline at a rate of 1 ml/kg/h for 3–4 h preoperatively and 4–6 h postoperatively) (1).

2.5. Statistical analysis

Categorical variables were displayed as counts (%) and analyzed by chi-square or Fisher's exact test as appropriate. Continuous data were presented as means \pm standard deviations (SD) or median (interquartile range). Comparisons among continuous variables were conducted by the independent Student's *t*-test or non-parametric Mann–Whitney *U* test in variables with normal distribution or non-normal distribution, respectively.

Between the patients with normal and abnormal echocardiographic parameters (LVDDI, LVIDSI, and LVMI included), we compared the percentage of Scr elevation through

the Mann–Whitney *U* test and the proportion of CA-AKI utilizing the chi-square test. The results of the two analyses were plotted in a violin plot. The associations of echocardiographic structural alterations with the risk of CA-AKI were explored by logistic regression. All of the collected echocardiographic parameters were divided according to quartile. After adjusting for covariables, such as demographic data, laboratory tests, CAG/PCI data, and medication history, multivariable logistic regression was performed, and the restricted cubic spline (RCS) curves were drawn to exhibit the result from the multivariable logistic regression analysis.

The receiver operating characteristics (ROC) curve was drawn to visualize the predictive value of the echocardiographic structural parameters for CA-AKI utilizing the area under curve (AUC). Considering the echocardiographic standard discrepancy between the different sexes, the ROC curve would be plotted for male and female individuals. Given that different individuals had different features, subgroup analysis was performed in various subgroups. Then, we screened the patients with cardiac remodeling that was facilitating changes of the echocardiographic parameters. Further investigation was conducted to explore the association of abnormal LV geometry with CA-AKI development by utilizing multivariable logistic regression. To verify the conclusions drawn from the current study, several sensitivity analyses were performed: first, the status of NT-proBNP was additionally incorporated into multivariable regression models, owing to its relationship with both cardiac function and structure; then, considering that the development of cardiac remodeling has a longstanding progression, multivariable logistic regression was repeated after adjusting the situation of acute cardiac dysfunction, such as myocardial infarction.

A two-tailed *P* value below 0.05 was considered statistically significant. All of the statistical analyses were carried out by SPSS (version 23.0, SPSS Inc., USA) and the R software (version 4.2.0, R core Team 2022).

3. Results

3.1. Baseline characteristics of CAD patients undergoing CAG/PCI

A total of 3,241 CAD patients undergoing CAG/PCI were incorporated into the study with a mean age of 66.6 ± 11.4 years; their baseline characteristics are displayed in Table 1. Overall, 1,169 (36.0%) patients were female, and 531 (16.3%) patients suffered from CA-AKI following CAG/PCI. As for baseline echocardiographic data, the patients who developed CA-AKI showed higher measurements of echocardiographic structural parameters (LVMI: 120.0 ± 36.9 vs. $132.1 \pm 43.3 \text{ g/m}^2$, LVDDI: 30.5 ± 4.9 vs. $32.0 \pm 5.5 \text{ mm/m}^2$, LVIDSI: 20.5 ± 5.4 vs. $22.8 \pm 6.3 \text{ mm/m}^2$, all $P < 0.001$) but a lower level of the echocardiographic functional parameter (LVEF: $61.7\% \pm 11.9$ vs. $56.3\% \pm 13.8\%$, $P < 0.001$). The presence of LVH was more common in patients suffering from CA-AKI (58.1% vs. 71.1%, $P < 0.001$); meanwhile, the group with CA-AKI exhibited a higher proportion of LV dilation (46.1% vs. 56.6%, $P < 0.001$).

TABLE 1 Baseline characteristics of patients enrolled.

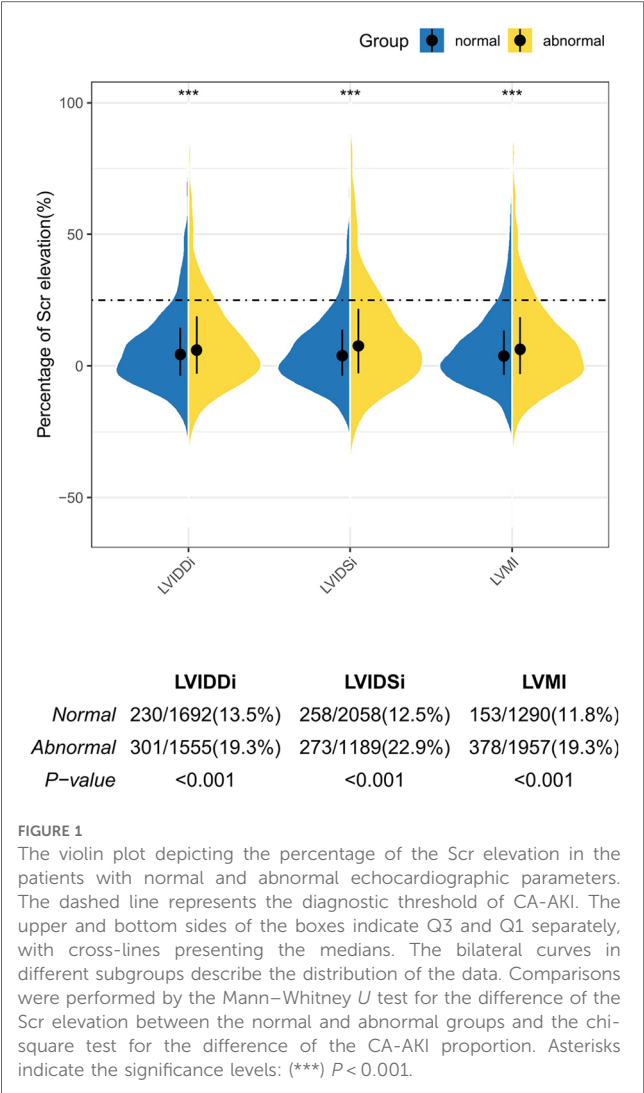
	Overall	Without CA-AKI	With CA-AKI	P value
	N = 3,247	N = 2,716	N = 531	
Demographic data				
Female, n (%)	1,169 (36.03)	965 (35.53)	205 (38.61)	0.19
Age, years	66.6 ± 11.4	66.4 ± 11.3	67.8 ± 11.7	0.01
BSA, m ²	1.7 ± 0.2	1.7 ± 0.2	1.6 ± 0.2	<0.01
Smoke (%)	524 (16.14)	448 (16.49)	76 (14.31)	0.24
Drink (%)	481 (14.81)	415 (15.28)	66 (12.43)	0.1
Diabetes (%)	772 (23.78)	621 (22.86)	151 (28.44)	0.01
Hypertension (%)	1,943 (59.84)	1,613 (59.39)	330 (62.15)	0.26
Anemia	582 (17.9)	463 (17.0)	119 (22.4)	0.004
Echocardiographic parameters				
EF, %	60.8 ± 12.4	61.7 ± 11.9	56.3 ± 13.8	<0.01
LVMI, g/m ²	122.0 ± 38.2	120.0 ± 36.9	132.1 ± 43.3	<0.01
LVDDI, mm/m ²	30.8 ± 5.1	30.5 ± 4.9	32.0 ± 5.5	<0.01
LVDSI, mm/m ²	20.9 ± 5.6	20.5 ± 5.4	22.8 ± 6.3	<0.01
RWT	0.4 ± 0.1	0.4 ± 0.1	0.4 ± 0.1	0.36
Hypertrophy, n (%)	1,957 (60.27)	1,579 (58.14)	378 (71.19)	<0.01
Dilation, n (%)	1,555 (47.89)	1,254 (46.17)	301 (56.69)	
Laboratory examination				
CRP, mg/L	1.9 [0.8,5.9]	1.7 [0.8,5.1]	3.5 [1.2,11.2]	<0.01
Proportion of Scr elevation, %	5.5 [−3.2, 17.4]	2.5 [−4.6, 10.6]	39.1 [30.5, 59.6]	<0.01
eGFR, ml/min/1.73 m ²	93.9 [75.1,113.2]	93.9 [76.2,112.1]	94.1 [69.2,120.1]	0.59
NTproBNP, µg/ml	452.0 [119.0,1427.5]	358.0 [102.0,1108.5]	1475.0 [401.5,3440.0]	<0.01
HbA1c, %	6.4 ± 1.3	6.4 ± 1.3	6.5 ± 1.4	0.03
PCI/CAG Data				
CTO (%)	244 (7.51)	189 (6.96)	55 (10.36)	0.01
Procedure, n (%)				0.01
Without PCI	1,935 (59.59)	1,639 (60.35)	296 (55.74)	
Single-vessel PCI	511 (15.74)	434 (15.98)	77 (14.50)	
Multiple-vessel PCI	801 (24.67)	643 (23.67)	158 (29.76)	
Hypotension	439 (13.5)	361 (13.3)	78 (14.7)	0.405
Type of contrast				0.15
Ioversol	544 (16.8)	462 (17.0)	82 (15.4)	
Iohexol	859 (26.5)	735 (27.1)	124 (23.4)	
Iodixanol	1,626 (50.1)	1,337 (49.2)	289 (54.4)	
Iopamidol	218 (6.7)	182 (6.7)	36 (6.8)	
Medication (%)				
Statin	2,693 (82.94)	2,274 (83.73)	419 (78.91)	0.01
ACEI or ARB	1,334 (41.08)	1,117 (41.13)	217 (40.87)	0.95
CCB	938 (28.89)	792 (29.16)	146 (27.50)	0.47

Data are presented as number (percentage) or median (Q1, Q3) for categorical variables and continuous variables. CA-AKI, contrast-associated acute kidney injury; BSA, body surface area; LVEF, left ventricular ejection fraction; LVMI, left ventricular mass index; LVDDI, left ventricular internal diameters at end-diastole index; LVDSI, left ventricular internal diameters at end-systole index; RWT, relative wall thickness; NT proBNP, N-terminal pro-brain natriuretic peptide; SCr, serum creatine; CRP, C-reactive protein; eGFR, estimated glomerular filtration rate; CAG, coronary angiography; PCI, percutaneous coronary intervention; CTO, chronic total occlusion; ACEI, angiotensin-converting enzyme inhibitor; ARB, angiotensin receptor blocker; CCB, calcium channel blocker.

Moreover, compared with the patients without CA-AKI, patients in the CA-AKI group had worse renal function (Scr increased proportion: 2.50% [−4.60 to 10.60] vs. 39.10% [30.50 to 59.60], $P < 0.001$), worse cardiac status (NT-proBNP: 358.0 [102.0 to 1108.5] vs. 1475.0 [401.5 to 3440.0] µg/ml, $P < 0.001$), higher inflammatory level (CRP: 1.70 mg/L [0.80 to 5.10] vs. 3.50 mg/L [1.20 to 11.20], $P < 0.001$), higher prevalence of diabetes (22.8% vs. 28.4%, $P = 0.01$), and less frequent usage of statin (83.7% vs. 78.9%, $P = 0.01$).

3.2. The associations of echocardiographic parameters with the percentage of Scr elevation and the proportion of CA-AKI

A violin plot was drawn to uncover the difference in Scr elevation percentage between the groups with abnormal and normal echocardiographic parameters (**Figure 1**). The abnormal higher structural parameters were not only correlated with a higher percentage of Scr elevation (LVMI: 3.8% vs. 6.5%, LVDDI:



4.75% vs. 6.40%, LVDSi: 4.20% vs. 8.00%, all *P* < 0.001) but also carried a greater proportion of CA-AKI (19.3%, 22.9%, and 19.3% for abnormal LVDDi, LVDSi, and LVMI, respectively; all *P* < 0.001).

3.3. The associations of CA-AKI with echocardiographic structural and functional alterations

To investigate the association of echocardiographic structural alterations with CA-AKI risk, logistic regression models were established. Echocardiographic structural parameters, including LVMI, LVDDi, and LVDSi, were divided into quartiles and then separately incorporated into a logistic regression analysis. In the univariable logistic regression analysis, the structural parameters were positively associated with CA-AKI risk (Supplementary Table S1). After adjustment for demographic data, laboratory tests, CAG/PCI data, and medication history, such an association between CA-AKI risk and echocardiographic

TABLE 2 Multivariable logistic regression analysis of different echocardiographic parameters on CA-AKI.

		OR	CI	P value	P for trend
LVMI	[Min, 95.0]	1	Ref.		<0.001
	[95.0,115.0]	0.963	(0.709, 1.308)	0.809	
	[115.0,141.0]	1.219	(0.906, 1.641)	0.191	
	[141.0, Max]	1.53	(1.146, 2.044)	0.004	
LVDDi	[Min, 27.50]	1	Ref.		<0.001
	[27.50,30.00]	0.988	(0.73, 1.339)	0.94	
	[30.00,33.20]	1.218	(0.913, 1.625)	0.179	
	[33.20, Max]	1.443	(1.087, 1.914)	0.011	
LVDSi	[Min, 17.2]	1	Ref.		<0.001
	[17.2,19.5]	1.245	(0.911, 1.7)	0.169	
	[19.5,22.9]	1.238	(0.914, 1.678)	0.167	
	[22.9,62.4]	1.953	(1.459, 2.615)	<0.001	

The covariates adjusted in multivariable logistic regression included female (yes or no), age (per 10 years), diabetes (yes or no), hypertension (yes or no), CRP (<6 and ≥6 mg/L), eGFR (<30, 30–59, 60–89, ≥90 ml/min × 1.73 m²), cTnI (<0.11 and ≥0.11 ng/ml), CAG/PCI procedure (CAG without/with single-vessel/with multiple-vessel PCI), CTO (yes or no), IVUS/OCT/FFR (yes or no), volume of contrast agent (<100 and ≥100 mg), medications (administration of statin) (yes or no), NTproBNP (abnormal or normal), hypotension (no or yes), and anemia (no or yes). LVMI, left ventricular mass index; LVDDi, left ventricular internal diameters at end-diastole index; LVDSi, left ventricular internal diameters at end-systole index.

structural parameters was still valid in multivariable logistic regression (Table 2). To be specific, a patient with higher levels of LVMI, LVDDi, and LVDSi carried a higher risk of CA-AKI, with a fully adjusted OR of 1.53 [1.146 to 2.044], 1.443 [1.087 to 1.914], and 1.953 [1.459 to 2.615] for the highest quartile compared with the lowest quartile (LVMI: *P* = 0.004; LVDDi: *P* = 0.011; LVDSi: *P* < 0.001). Significant linear trends of structural parameters were validated among the consecutive categories (all *P* for trend < 0.05), and similar relationship patterns were visualized by the RCS models (Figure 2). The change of CA-AKI risk in different levels appeared as a linear increment, as for LVDDi, LVDSi, and LVMI (all *P* for non-linearity > 0.05). Such associations between echocardiographic parameters and CA-AKI risk also remained stable in the sensitivity analysis (Supplementary Table S2).

Further investigation of the echocardiographic parameters' predictive value was plotted on the ROC curves and exhibited the AUC of the parameters (Figure 3). Considering the structural discrepancy between male and female individuals, the analysis was sex-stratified, and the AUC in different sexes did not exhibit significant differences (LVMI: male vs. female = 0.592 vs. 0.592; LVDDi: male vs. female = 0.581 vs. 0.577; LVDSi: male vs. female = 0.625 vs. 0.602, all *P* > 0.05), which hinted that the predictive value of echocardiographic parameters would not be affected by sex.

3.4. The echocardiographic predictor of CA-AKI in different subgroups

Considering the distribution of the data among different subgroups, the parameters were taken into subgroup analyses without division (Figure 4). The analysis verified that the

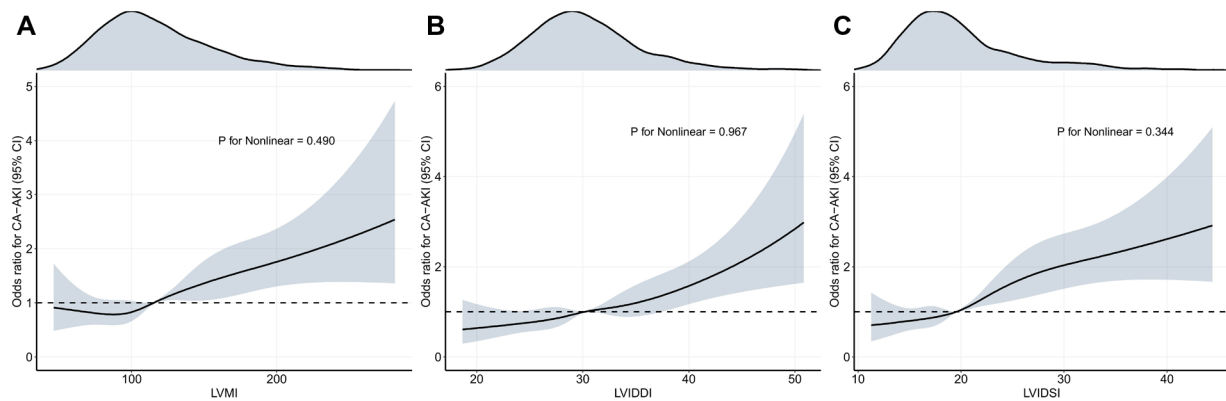


FIGURE 2

Restricted cubic spline (RCS) analyses for exploring the association of echocardiographic parameters with CA-AKI. The solid black lines show the adjusted odds ratios of different echocardiographic parameters (A for LVMI, B for LVDDI, C for LVDSI) for CA-AKI, and the gray ribbon around the line indicates a 95% confidence interval of the curves.

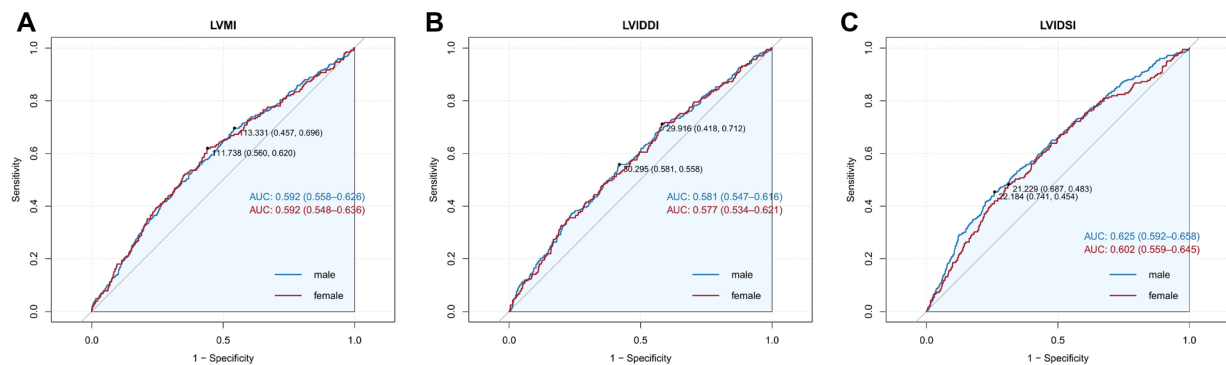


FIGURE 3

(A) The cutoff value of LVMI for predicting CA-AKI was analyzed by the ROC curve. (B) The cutoff value of LVDDI for predicting CA-AKI was analyzed by the ROC curve. (C) The cutoff value of LVDSI for predicting CA-AKI was analyzed by the ROC curve.

positive association between LVDDI, LVDSI, and CA-AKI risk was consistent (all P for interaction >0.05) when stratified by age (<70 or ≥ 70 years), left ventricular ejection fraction (<50 or $\geq 50\%$), estimated glomerular filtration rate (<60 or ≥ 60 ml/min/ 1.73 m^2), and N-terminal brain natriuretic peptide (normal or abnormal).

3.5. The associations between CA-AKI and abnormal left ventricular geometry

In the current study, abnormal LVMI and LVDDI signified LV hypertrophy and dilation. Compared with the patients without structural remodeling, the two abnormal LV geometries were found to possess a significant relationship with CA-AKI risk in the multivariable logistic analysis (hypertrophy: OR = 1.348, 95% CI [1.086 to 1.673], $P = 0.007$; dilation: OR = 1.234, 95% CI [1.012 to 1.506], $P = 0.038$, in **Table 3**). By means of RWT and LVMI, four types of LVH were classified. The association between LVH and CA-AKI risk was significant in patients with eccentric LVH

[OR = 1.400, 95%CI (1.093 to 1.793), $P = 0.008$]. Then, recruited patients were roughly categorized into three statuses: normal LV geometry, the existence of LVH or dilation, and the coexistence of LV hypertrophy and dilation. Multivariable logistic regression was performed to verify the correlation between abnormal LV geometry and CA-AKI risk, which demonstrated that the coexistence of LV hypertrophy and dilation carried the highest risk of CA-AKI [OR = 1.397, 95%CI (1.091 to 1.789), $P = 0.008$].

4. Discussion

Among this consequent cohort of CAD patients after CAG/PCI, echocardiographic data were available to indicate cardiac remodeling, and 531 (16.3%) patients suffered from CA-AKI. Patients with higher LVMI, LVDDI, and LVDSI carried a higher risk of CA-AKI and abnormal LVMI associated with the CA-AKI risk, especially in patients with preserved LVEF. In other words, the presence of cardiac remodeling, namely, left ventricular hypertrophy and dilation, was significantly associated

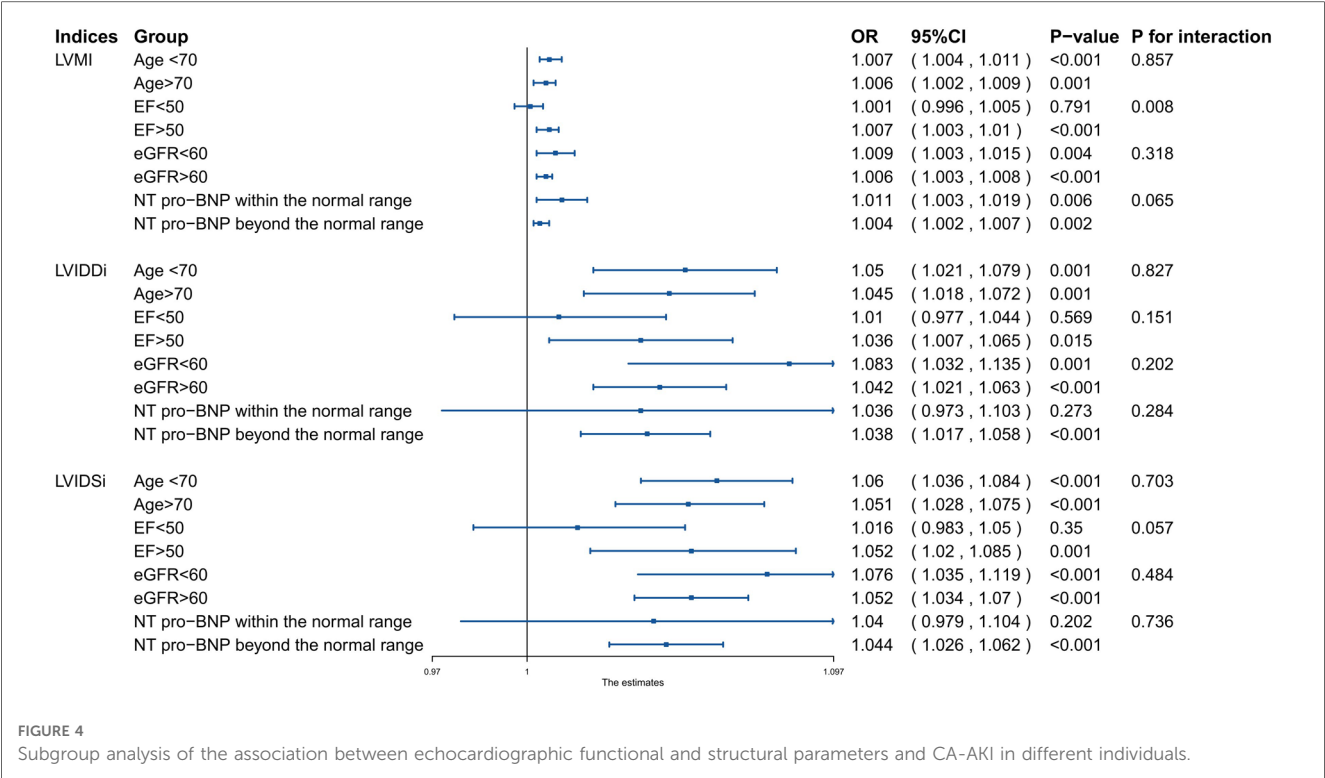


TABLE 3 Multivariable logistic regression analysis of echocardiographic abnormal ventricular geometry on CA-AKI.

	OR	95%CI	P value
Model 1			
Echocardiographic dilatation	1.234	(1.012, 1.506)	0.038
Model 2			
Echocardiographic hypertrophy	1.348	(1.086, 1.673)	0.007
Model 3			
Normal	1	Ref.	
Echocardiographic dilatation/hypertrophy	1.066	(0.812, 1.398)	0.647
Echocardiographic dilatation and hypertrophy	1.397	(1.091, 1.789)	0.008
Model 4			
Normal	1	Ref.	
Concentric remodeling	0.876	(0.569, 1.351)	0.55
Concentric LVH	1.141	(0.852, 1.53)	0.376
Eccentric LVH	1.4	(1.093, 1.793)	0.008

Echocardiographic LV dilation and hypertrophy were incorporated into Model 1 and Model 2, respectively, and various situations of echocardiographic ventricular geometry were incorporated into Model 3. Adjusted for female (yes or no), age (per 10 years), diabetes (yes or no), hypertension (yes or no), CRP (<6 and ≥6 mg/L), eGFR (<30, 30–59, 60–89, ≥90 ml/min × 1.73 m²), cTnI (<0.11 and ≥0.11 ng/ml), CAG/PCI procedure (CAG without/with single-vessel/with multiple-vessel PCI), CTO (yes or no), IVUS/OCT/FFR (yes or no), volume of contrast agent (<100 and ≥100 mg), medications (administration of statin) (yes or no), NTproBNP (abnormal or normal), hypotension (no or yes), and anemia (no or yes). Echocardiographic LV dilation was diagnosed by abnormal elevated LVDDI. Echocardiographic LVH was evaluated by LV mass index (LVMI), >115 g/m² in males or >95 g/m² in females. Concentric remodeling was set as relative wall thickness (RWT) > 0.42 and LV mass index (LVMI) ≤ 115 g/m² in males or ≤95 g/m² in females, and concentric LVH was diagnosed by RWT > 0.42 and LVMI > 55 mm in males or >50 mm in females, while RWT was ≤0.42 for eccentric LVH. LVMI, left ventricular mass index; LVDDI, left ventricular internal diameters at end-diastole index; LVDSI, left ventricular internal diameters at end-systole index; LVH, left ventricular hypertrophy.

with the CA-AKI risk. The coexistence of LV hypertrophy and dilation possessed the highest risk of CA-AKI among different remodeling patterns, and subjects with eccentric hypertrophy confronted a higher CA-AKI risk. The development of cardiac remodeling involves alterations in cardiac size, shape, and function (6). An abnormally increased LVMI could detect the occurrence of echocardiographic hypertrophy. LVDDI and LVDSI were recorded to evaluate the size of heart chambers. Both the physiological and pathological ways lead to changes in echocardiographic parameters, but it is well established that cardiac remodeling is associated with numerous pathological conditions, including various cardiovascular diseases and chronic kidney disease, among others (17, 18). One of the leading culprits for cardiac remodeling is hypertension (6). Under the circumstance of long-term hypertension, diffuse fibrosis has been shown to occur in the primary target organ, resulting in the development of remodeling and deteriorated function (7). LV hypertrophy is a common impairment of the target organ in hypertensive patients, considering a marker of uncontrolled hypertension, which exacerbates the progression of kidney disease (19). Patients with LV hypertrophy are susceptible to progressive deterioration in kidney function and increased requirement of dialysis (20). LV dilation not only occurs in the later period of hypertension but also develops due to cardiac myocyte damage, which leads to renal fibrosis and decreased blood flow (21). A cross-sectional study carried out by Kensuke et al. suggested that reduced eGFR is related to both cardiac hypertrophy and dilation (20). As for postoperative renal function, research performed by Lee et al. has

validated the predictive role played by LV remodeling during the occurrence of postoperative AKI within 7 days after non-cardiac surgery through RWT (22). LV dilation detected by LVIDD was found to be a predictive value for CA-AKI in CAD patients by Li et al. (23). In the current study, the relationship between left ventricular remodeling and CA-AKI risk was consistent with the previous results. Moreover, this relationship was consistent among different subgroups, while the predictive values of structural parameters were less affected by sex. However, compared with the study conducted by Kensuke et al., no significant difference in RWT between the patients with or without CA-AKI was detected in the present study, which might be explained by the higher baseline level of LVMI and different operation types among the patients enrolled in this study. Furthermore, probably due to a higher LVMI level, 16.3% of the subjects suffered from CA-AKI in the current study, in which the proportion of CA-AKI patients was higher than in the previous study.

Patients with cardiac remodeling often carry more potential risk factors than others, such as diabetes mellitus, anemia, and renal dysfunction. Similar patterns of relationships were also found in the current study for patients with structural remodeling, with a higher CA-AKI risk compared to patients without remodeling. It is conceived that cardiac structural remodeling often relates to decreased stroke volume and worse diastolic function, later showing more severe deterioration in the impaired kidney function than in the systolic function (24–26). The exact mechanisms underlying the association between cardiac remodeling and postoperative AKI have not yet been elucidated. However, the traditional association of LV remodeling with impaired renal function is suspected from the presence of hypertension, which results in glomerular sclerosis (27). The potential contribution of the undetectable alteration in the regional renal perfusion also cannot be ruled out. Haruyama et al. found a relationship between LVH and the percentage of nephrosclerosis, even in kidney donors with normal eGFR (28). The relationship between LV dilation and subclinical renal impairment in hypertensive patients was uncovered in the work conducted by Ratto et al. (29).

Of note is that not only does the presence of cardiac remodeling increase the CA-AKI risk but also the different patterns of cardiac remodeling show different risks. To be specific, patients with both LV hypertrophy and dilation confront the highest risk. Yamanaka et al. also argued that the combination of LV dilation and hypertrophy has the worst prognosis compared with other structural patterns among patients with heart failure with preserved ejection fraction (30). The CASCADE Study showed that patients with end-stage chronic kidney disease carry the highest incidence of both LV hypertrophy and dilation compared to chronic kidney disease patients at other stages, which implies that cardiac structural remodeling and its progression might be closely related to worse renal function at baseline (31).

There are also certain limitations in this retrospective research. First, the authority of the conclusions is inevitably limited by the nature of retrospective cross-section research. Therefore, large-scale prospective research is required in the future to further

confirm the association of cardiac remodeling with CA-AKI risks. Second, there was a shortage of the calculation for LVM. The linear method was likely to overestimate LVH, but as the most widespread echocardiographic method to evaluate LV geometry, its usefulness in a tremendous number of clinical trials has been verified (14). Therefore, the discrepancy caused by the different methods might have a few significant influences on the final result. Last, in the current study, we failed to record other detailed medication history, such as the diuretic, which inevitably caused a modest effect on the conclusion.

In conclusion, the present study established a significant association of cardiac remodeling, detected by echocardiogram, with the risk of CA-AKI among CAD patients receiving CAG/PCI. Abnormal structural echocardiographic parameters were correlated with CA-AKI, showing that patients with abnormal cardiac structure should take timely protective measures, even those with LV hypertrophy but preserved LVEF.

Data availability statement

The raw data supporting the conclusions of this article will be made available by the authors, without undue reservation.

Ethics statement

This research is a cross-section study, which has been authorized by the Ethics Committee of the Sir Run Run Shaw Hospital (No. 20201217-36) and performed following the Helsinki statement. Written informed consent for participation was not required from the participants or the participants' legal guardians/next of kin in accordance with the national legislation and institutional requirements.

Author contributions

QC and HJ: finished the manuscript writing and revision. DL and TH: did statistical analyses. All author contributed to the formation of idea. QC and DL: contributed equally to this work. WZ and CD: are the corresponding authors of this article. All authors contributed to the article and approved the submitted version.

Conflict of interest

The authors declare that the research was conducted in the absence of any commercial or financial relationships that could be construed as a potential conflict of interest.

Publisher's note

All claims expressed in this article are solely those of the authors and do not necessarily represent those of

their affiliated organizations, or those of the publisher, the editors and the reviewers. Any product that may be evaluated in this article, or claim that may be made by its manufacturer, is not guaranteed or endorsed by the publisher.

References

- Fahling M, Seeliger E, Patzak A, Persson PB. Understanding and preventing contrast-induced acute kidney injury. *Nat Rev Nephrol.* (2017) 13(3):169–80. doi: 10.1038/nrneph.2016.196
- Mehran R, Dargas GD, Weisbord SD. Contrast-associated acute kidney injury. *New Engl J Med.* (2019) 380(22):2146–55. doi: 10.1056/NEJMr1805256
- Mohebi R, Karimi Galougahi K, Garcia JJ, Horst J, Ben-Yehuda O, Radhakrishnan J, et al. Long-term clinical impact of contrast-associated acute kidney injury following PCI: an ADAPT-DES substudy. *JACC Cardiovasc Interv.* (2022) 15(7):753–66. doi: 10.1016/j.jcin.2021.11.026
- Mehran R, Aymong ED, Nikolsky E, Lasic Z, Iakovou I, Fahy M, et al. A simple risk score for prediction of contrast-induced nephropathy after percutaneous coronary intervention: development and initial validation. *J Am Coll Cardiol.* (2004) 44(7):1393–9.
- Nijssen EC, Wildberger JE. A novel risk score for contrast-associated acute kidney injury: the heart of the matter. *Lancet.* (2021) 398(10315):1941–3. doi: 10.1016/S0140-6736(21)02445-4
- Cohn JN, Ferrari R, Sharpe N. Cardiac remodeling—concepts and clinical implications: a consensus paper from an international forum on cardiac remodeling. Behalf of an international forum on cardiac remodeling. *J Am Coll Cardiol.* (2000) 35(3):569–82. doi: 10.1016/S0735-1097(99)00630-0
- Mavrogeni S, Piaditis G, Bacopoulou F, Chrousos GP. Cardiac remodeling in hypertension: clinical impact on brain, heart, and kidney function. *Horm Metab Res.* (2022) 54(5):273–9. doi: 10.1055/a-1793-6134
- Glasscock RJ, Pecoito-Filho R, Barberato SH. Left ventricular mass in chronic kidney disease and ESRD. *Clin J Am Soc Nephrol.* (2009) 4(Suppl 1):S79–91. doi: 10.2215/CJN.04860709
- Li Q, Chen W, Shi S, Huang H, Lai W, Liu L, et al. Acute kidney injury increase risk of left ventricular remodeling: a cohort of 1,573 patients. *Front Physiol.* (2021) 12:744735. doi: 10.3389/fphys.2021.744735
- Mathis MR, Naik BI, Freundlich RE, Shanks AM, Heung M, Kim M, et al. Preoperative risk and the association between hypotension and postoperative acute kidney injury. *Anesthesiology.* (2020) 132(3):461–75. doi: 10.1097/ALN.0000000000003063
- Sessler DI, Bloomstone JA, Aronson S, Berry C, Gan TJ, Kellum JA, et al. Perioperative quality initiative consensus statement on intraoperative blood pressure, risk and outcomes for elective surgery. *Br J Anaesth.* (2019) 122(5):563–74. doi: 10.1016/j.bja.2019.01.013
- Vandenbroucke JP, von Elm E, Altman DG, Gøtzsche PC, Mulrow CD, Pocock SJ, et al. Strengthening the reporting of observational studies in epidemiology (STROBE): explanation and elaboration. *PLoS Med.* (2007) 4(10):e297. doi: 10.1371/journal.pmed.0040297
- van der Molen AJ, Reimer P, Dekkers IA, Bongartz G, Bellin MF, Bertolotto M, et al. Post-contrast acute kidney injury—part 1: definition, clinical features, incidence, role of contrast medium and risk factors: recommendations for updated ESUR contrast medium safety committee guidelines. *Eur Radiol.* (2018) 28(7):2845–55. doi: 10.1007/s00330-017-5246-5
- Lang RM, Badano LP, Mor-Avi V, Afilalo J, Armstrong A, Ernande L, et al. Recommendations for cardiac chamber quantification by echocardiography in adults: an update from the American society of echocardiography and the European association of cardiovascular imaging. *Eur Heart J Cardiovasc Imaging.* (2015) 16(3):233–70. doi: 10.1093/ehjci/jev014
- Ibrahim I, Kuan WS, Frampton C, Troughton R, Liew OW, Chong JP, et al. Superior performance of N-terminal pro brain natriuretic peptide for diagnosis of acute decompensated heart failure in an Asian compared with a western setting. *Eur J Heart Fail.* (2017) 19(2):209–17. doi: 10.1002/ehf.1612
- Windecker S, Kolh P, Alfonso F, Collet JP, Cremer J, Falk V, et al. 2014 ESC/EACTS guidelines on myocardial revascularization: the task force on myocardial revascularization of the European society of cardiology (ESC) and the European association for cardio-thoracic surgery (EACTS) Developed with the special contribution of the European association of percutaneous cardiovascular interventions (EAPCI). *Eur Heart J.* (2014) 35(37):2541–619. doi: 10.1093/eurheartj/ehu278
- Nakamura M, Sadoshima J. Mechanisms of physiological and pathological cardiac hypertrophy. *Nat Rev Cardiol.* (2018) 15(7):387–407. doi: 10.1038/s41569-018-0007-y
- Frantz S, Hundertmark MJ, Schulz-Menger J, Bengel FM, Bauersachs J. Left ventricular remodelling post-myocardial infarction: pathophysiology, imaging, and novel therapies. *Eur Heart J.* (2022) 43(27):2549–61. doi: 10.1093/eurheartj/ehac223
- Fu X, Ren H, Xie J, Wang W, Li Y, Gao P, et al. Association of nighttime masked uncontrolled hypertension with left ventricular hypertrophy and kidney function among patients with chronic kidney disease not receiving dialysis. *JAMA Netw Open.* (2022) 5(5):e2214460. doi: 10.1001/jamanetworkopen.2022.14460
- Dahan M, Siohan P, Viron B, Michel C, Paillole C, Gourgon R, et al. Relationship between left ventricular hypertrophy, myocardial contractility, and load conditions in hemodialysis patients: an echocardiographic study. *Am J Kidney Dis.* (1997) 30(6):780–5. doi: 10.1016/S0272-6386(97)90082-2
- Burchfield JS, Xie M, Hill JA. Pathological ventricular remodeling: mechanisms: part 1 of 2. *Circulation.* (2013) 128(4):388–400. doi: 10.1161/CIRCULATIONAHA.113.001878
- Goeddel LA, Erlinger S, Murphy Z, Tang O, Bergmann J, Moeller S, et al. Association between left ventricular relative wall thickness and acute kidney injury after noncardiac surgery. *Anesth Analg.* (2022) 135(3):605–16. doi: 10.1213/ANE.0000000000006055
- Li Q, Chen S, Huang H, Chen W, Liu L, Wang B, et al. Dilated left ventricular end-diastolic diameter is a new risk factor of acute kidney injury following coronary angiography. *Front Cardiovasc Med.* (2022) 9:827524. doi: 10.3389/fcvm.2022.827524
- Shigematsu Y, Hamada M, Ohtsuka T, Hashida H, Ikeda S, Kuwahara T, et al. Left ventricular geometry as an independent predictor for extracardiac target organ damage in essential hypertension. *Am J Hypertens.* (1998) 11(10):1171–7. doi: 10.1016/S0895-7061(98)00140-X
- Cerasola G, Nardi E, Palermo A, Mulè G, Cottone S. Epidemiology and pathophysiology of left ventricular abnormalities in chronic kidney disease: a review. *J Nephrol.* (2011) 24(1):1–10. doi: 10.5301/JN.2010.2030
- Chen SC, Su HM, Hung CC, Chang JM, Liu WC, Tsai JC, et al. Echocardiographic parameters are independently associated with rate of renal function decline and progression to dialysis in patients with chronic kidney disease. *Clin J Am Soc Nephrol.* (2011) 6(12):2750–8. doi: 10.2215/CJN.04660511
- Taddei S, Nami R, Bruno RM, Quatrini I, Nuti R. Hypertension, left ventricular hypertrophy and chronic kidney disease. *Heart Fail Rev.* (2011) 16(6):615–20. doi: 10.1007/s10741-010-9197-z
- Haruyama N, Tsuchimoto A, Masutani K, Nagata M, Kitada H, Tanaka M, et al. Subclinical nephrosclerosis is linked to left ventricular hypertrophy independent of classical atherogenic factors. *Hypertens Res.* (2014) 37(5):472–7. doi: 10.1038/hr.2013.154
- Ratto E, Viazzzi F, Bonino B, Gonnella A, Garneri D, Parodi EL, et al. Left ventricular dilatation and subclinical renal damage in primary hypertension. *J Hypertens.* (2015) 33(3):605–11; discussion 11. doi: 10.1097/HJH.0000000000000430
- Yamanaka S, Sakata Y, Nochioka K, Miura M, Kasahara S, Sato M, et al. Prognostic impacts of dynamic cardiac structural changes in heart failure patients with preserved left ventricular ejection fraction. *Eur J Heart Fail.* (2020) 22(12):2258–68. doi: 10.1002/ehf.1945
- Cai QZ, Lu XZ, Lu Y, Wang AY. Longitudinal changes of cardiac structure and function in CKD (CASCADE study). *J Am Soc Nephrol.* (2014) 25(7):1599–608. doi: 10.1681/ASN.2013080899

Supplementary material

The Supplementary Material for this article can be found online at: <https://www.frontiersin.org/articles/10.3389/fcvm.2023.1173586/full#supplementary-material>



OPEN ACCESS

EDITED BY

Francesca Innocenti,
Careggi University Hospital, Italy

REVIEWED BY

Fabiana Isabella Gambarin,
Fondazione Salvatore Maugeri (IRCCS), Italy
Cristina Tudoran,
Victor Babes University of Medicine and
Pharmacy, Romania

*CORRESPONDENCE

Oleksii Honchar
✉ ov.honchar@knu.edu.ua

RECEIVED 30 June 2023

ACCEPTED 06 November 2023

PUBLISHED 22 November 2023

CITATION

Honchar O and Ashcheulova T (2023)
Short-term echocardiographic follow-up after
hospitalization for COVID-19: a focus on early
post-acute changes.
Front. Cardiovasc. Med. 10:1250656.
doi: 10.3389/fcvm.2023.1250656

COPYRIGHT

© 2023 Honchar and Ashcheulova. This is an
open-access article distributed under the terms
of the [Creative Commons Attribution License](#)
(CC BY). The use, distribution or reproduction in
other forums is permitted, provided the original
author(s) and the copyright owner(s) are
credited and that the original publication in this
journal is cited, in accordance with accepted
academic practice. No use, distribution or
reproduction is permitted which does not
comply with these terms.

Short-term echocardiographic follow-up after hospitalization for COVID-19: a focus on early post-acute changes

Oleksii Honchar* and Tetiana Ashcheulova

Department of Propedeutics of Internal Medicine, Nursing and Bioethics, Kharkiv National Medical University, Kharkiv, Ukraine

Background: Impaired physical functional status is one of the typical long-term sequelae of COVID-19 infection that significantly affects the quality of life and work capacity. Minor changes in cardiac structure and function that are unable to cause the manifestation of overt heart failure may remain undetected in COVID-19 convalescents, at the same time potentially contributing to the persistence of symptoms and development of long COVID syndrome.

Purpose: To study the typical features and short-term dynamics of cardiac remodeling and possible signs of cardiac dysfunction following hospitalization for COVID-19.

Methods: This is a combined cross-sectional and longitudinal cohort study in which 176 hospitalized patients (93 female and 83 male, mean age 53.4 ± 13.6 years) with COVID-19 infection underwent comprehensive transthoracic echocardiography pre-discharge (22.6 ± 7.1 days from the onset of symptoms) with repeated evaluation after 1 month. The control group included 88 age-, sex-, height- and weight-matched healthy individuals, with a subset of those ($n = 53$) matched to the subset of non-hypertensive study participants ($n = 106$).

Results: Concentric left ventricular geometry was revealed in 59% of participants, including 43% of non-hypertensive subjects; predominantly Grade I diastolic dysfunction was found in 35 and 25% of patients, respectively. Other findings were naturally following from described phenotype of the left ventricle and included a mild increase in the absolute and relative wall thickness (0.45 ± 0.07 vs. 0.39 ± 0.04 , $p < 0.001$), worsening of diastolic indices (e' velocity 9.2 ± 2.2 vs. 11.3 ± 2.6 cm/s, $p < 0.001$, E/e' ratio 7.5 ± 1.8 vs. 6.8 ± 1.7 , $p = 0.002$) and global longitudinal strain (17.5 ± 2.4 vs. 18.6 ± 2.2 , $p < 0.001$). No significant improvement was found on re-evaluation at 1 month.

Conclusions: Hospitalized patients recovering from COVID-19 were characterized by a high prevalence of left ventricular concentric remodeling, predominantly Grade I diastolic dysfunction, and a mild decrease in the longitudinal systolic function. These changes were less frequent but still prevalent in the non-hypertensive subgroup and largely persisted throughout the 1-month follow-up.

KEYWORDS

COVID-19, long COVID, echocardiography, cardiac remodeling, cardiac dysfunction, hospitalization, convalescence

Cardiac Remodeling in Early Post-Acute COVID-19

LV concentric geometry is common among convalescents, frequently accompanied by grade I diastolic dysfunction in both hypertensive and normotensive patients

Prerequisites

- Post-acute COVID-19 symptoms persist beyond 30d in >70-80% of hospitalized patients
- RV remodeling and dysfunction have been shown to resolve by the end of acute phase
- Minor cardiac alterations may remain undetected in COVID-19 convalescents, at the same time contributing to development of long COVID syndrome

Study Design

265 eligible patients:
• ≥ 18 years
• Hospitalized pneumonia
• SARS-CoV-2 PCR "+"

89 declined participation

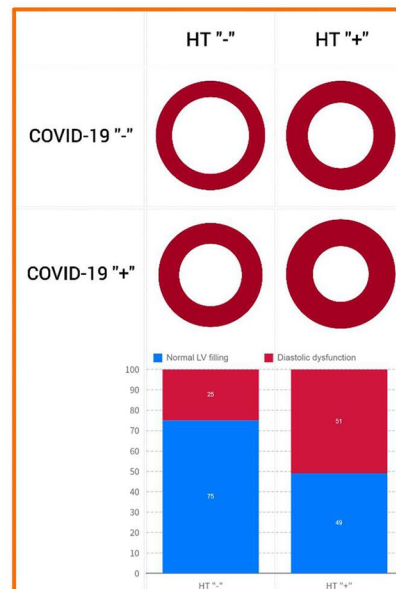
Visit 1, n = 176:
• 1-2 days pre-discharge
• Resting SpO₂ >93%
• Baseline characteristics
• Baseline TTE + 6MWT

50 unable/unwilling to come

Visit 2, n = 126:
• 1 month post-discharge
• Repeated TTE + 6MWT



Honchar O., Ashcheulova T.
KNMU, Kharkiv, Ukraine



GRAPHICAL ABSTRACT

1. Introduction

Cardiac impairment during the acute phase of COVID-19 includes a wide spectrum of possible presentations ranging from overt cardiovascular emergencies such as acute myocardial infarction or life-threatening arrhythmias, through clearly defined clinical entities such as pulmonary embolism (PE), myo- and pericarditis, Takotsubo cardiomyopathy (1, 2), to the systemic cytokine hyperactivation mediated effects such as endothelial dysfunction, hypercoagulability, and vasoconstriction that may contribute to development of non-PE-related pulmonary hypertension and right ventricular dysfunction, microvascular ischemia resulting in left ventricular dysfunction, and form the basis for persistence of the impaired cardiac morphophysiology (3–6).

Compared to the acute phase, post-acute and chronic COVID-related cardiovascular sequelae are less thoroughly studied, and the underlying mechanisms are still not completely understood (7–9). To date, few studies using echocardiography (which is the logical first-line tool to assess cardiac structure and function) in the long COVID setting have been reported (10–19). At the same time, part of these studies were characterized by the lack of control and/or non-comprehensive echocardiographic assessment, and the emerging general picture remains at times contradictory (7).

Some of the mentioned uncertainties could be potentially related to differences in enrolled populations. Geography, gender, age, ethnicity, locally prevailing SARS-CoV-2 variants, reserve capacity

of the health care system at the time the study was recruiting participants, and available logistics for the follow-up visits all inevitably affect characteristics of the observed populations in terms of disease severity and existing comorbidities, including those that have been associated with adverse prognosis both short-term in the acute COVID-19 setting (6, 20) and long-term in the general population. For instance, the prevalence of hypertension (which is the most frequent comorbidity in COVID-19 patients that is also characterized by a fairly typical phenotype of structural and functional alterations of left cardiac chambers) ranged from 15 to 57% according to different reports based on large datasets from China and the US, which, together with a similar variation in the prevalence of obesity (12–48%) and diabetes (8–34%), could at least partially account for the observed variability in echo findings (20–22).

The purpose of the current study was to identify possible echocardiographic patterns and markers of cardiac impairment in the short-term follow-up of post-acute COVID-19 patients with an additional focus on the role of hypertension as a potential confounding factor.

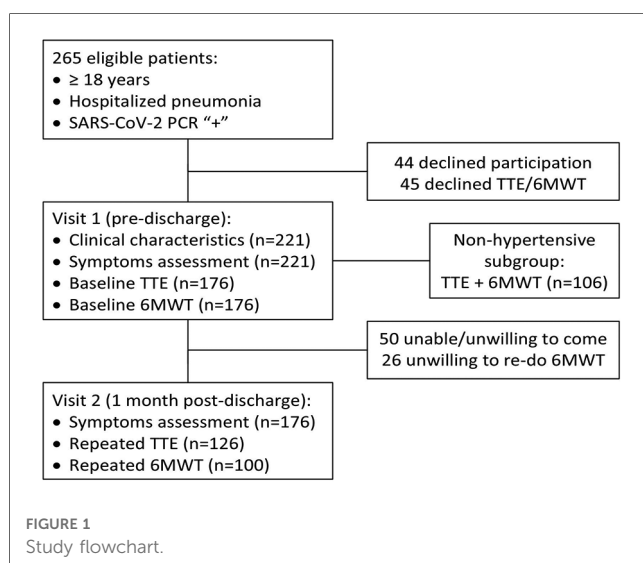
2. Material and methods

2.1. Study design and population

By design, this is a combined cross-sectional and longitudinal cohort study. Between January and November 2021, eligible

patients who were hospitalized at the pulmonological department of Kharkiv City Hospital #13 (which is a regional pulmonological center that has been reorganized to the specialized COVID-19 care center and was serving the area of about 2.4 million people at the period of recruiting) were invited to participate in the study. Eligibility criteria included the age of ≥ 18 years and the diagnosis of COVID-19 pneumonia that had been confirmed with a positive polymerase chain reaction test. Exclusion criteria included stage D chronic heart failure, acute heart failure, history of myocardial infarction, permanent atrial fibrillation, stroke within 6 months, severe uncontrolled hypertension (defined as systolic BP ≥ 180 mm Hg and/or diastolic BP ≥ 110 mm Hg), significant valvular heart disease (defined as at least moderate valvular stenosis and/or at least moderate-to-severe valvular regurgitation), active cancer or systemic autoimmune pathology, inability to provide informed consent, and persisting O₂ supplementation dependence by the time of discharge.

Out of a total of 265 consecutive eligible patients, 89 declined participation (mainly due to anticipated logistical difficulties in conducting the repeat visit or being reluctant to engage due to ongoing symptoms) and 176 were enrolled in the study, being a source of data for cross-sectional analysis. After the exclusion of 50 patients who were unable/unwilling to do a follow-up visit, the final cohort that was used for longitudinal comparisons included 126 participants—see **Figure 1** for the study flowchart.



The control group included 88 individuals (Control 1) selected from the internal database representative of the local population from the 2018–2019 (pre-COVID) period. These subjects were individually matched to the study group at a 1:2 ratio using a nearest-neighbor strategy to adjust for age, sex, height, weight, and prevalence of hypertension and diabetes mellitus (see **Table 1** for comparison on the available parameters). Considering the lack of reliable data available on the severity of hypertension and the quality of its control, a subset of self-reported non-hypertensive control subjects (Control 2, $n = 53$) was additionally compared to the cohort of non-hypertensive study participants to properly exclude the possible confounding effect of hypertension on the studied parameters.

2.2. Clinical data collection

The first visit was performed 1–2 days before discharge, after stabilization of patients' clinical condition (capillary blood oxygen saturation $>93\%$ on room air) and achievement of clinical criteria of epidemic safety (normal body temperature and absence of acute respiratory disease symptoms for ≥ 3 days starting from the 10th day after onset of symptoms) (23). During this visit, demographic characteristics (age, gender), data on laboratory parameters, computed tomography findings, and treatment were obtained from the medical records, data on symptoms, smoking status, and comorbidities were collected by interview, and anthropometry was performed, followed by comprehensive transthoracic echocardiography (TTE). 6 min walk distance (6MWD) was assessed using a 20 m track; respective log-linear models (24) were used to calculate the individual predicted values.

The follow-up visit for re-assessment of symptoms, changes in clinical parameters, structural and functional state of the cardiovascular system was carried out at 1 month.

2.3. Echocardiography

Transthoracic echocardiography was performed using the Radmir ULTIMA Expert ultrasound system (Radmir Co., Ukraine). Linear and volumetric measurements were performed in accordance with the current guidelines for chamber quantification by the American Society of Echocardiography

TABLE 1 Baseline characteristics of the study population and its non-hypertensive subgroup vs. control.

Parameters	COVID-19 general, $n = 176$	Control 1, $n = 88$	P -values	COVID-19 non-HT, $n = 106$	Control 2, $n = 53$	P -values
Age	53.4 \pm 13.6	52.3 \pm 13.3	0.51	50.7 \pm 13.9	53.0 \pm 14.5	0.32
Female sex	93 (52.8)	46 (52.3)	0.97	55 (51.9)	28 (52.3)	0.91
Height, cm	169.8 \pm 9.1	170.6 \pm 7.6	0.47	169.3 \pm 8.7	170.0 \pm 6.9	0.64
Weight, kg	84.5 \pm 18.5	85.6 \pm 16.7	0.64	78.9 \pm 15.8	79.0 \pm 11.9	0.98
BMI, kg/m ²	29.1 \pm 5.2	29.3 \pm 4.9	0.76	27.4 \pm 4.4	27.3 \pm 3.5	0.85
Hypertension	70 (39.8)	34 (38.6)	0.96	0 (0.0)	0 (0.0)	1.00
Obesity	67 (38.1)	35 (39.8)	0.89	25 (23.6)	13 (24.5)	0.90
Diabetes	17 (9.6)	8 (9.1)	0.94	2 (1.9)	1 (1.9)	1.00

BMI, body mass index. Matching quality was preserved for the cohort of patients who underwent repeated evaluation ($n = 126$) with P -values ≥ 0.83 for all used parameters.

(ASE) and the European Association of Cardiovascular Imaging (EACVI) (25). Linear left ventricular (LV) dimensions and walls' thickness were obtained using 2D measurements in the parasternal long-axis view, and LV end-diastolic length (LV L) in the apical 4-chamber view. Left ventricular end-diastolic (EDV) and end-systolic (ESV) volumes and ejection fraction (EF), as well as left atrial volume, were measured in the apical 4- and 2-chamber views using Simpson's biplane method. Tricuspid (TAPSE) and mitral (MAPSE) annular plane systolic excursion were measured using M-mode in the apical 4-chamber view, with MAPSE being calculated as a mean value of excursion of its lateral and medial portions.

Left ventricular global longitudinal strain was calculated as LV GLS = MAPSE/LVL* 100% using the recently proposed linear method (26–28). Similarly, right ventricular free wall longitudinal strain was calculated as RVLS = TAPSE/RVL* 100%. LV GLS and RVLS are reported as absolute values.

Mitral and tricuspid annular motion velocities, as well as parameters of transmitral and transtricuspid blood flow, were measured in pulsed-wave tissue Doppler mode according to the standard methods provided in the current guidelines (29, 30).

TABLE 2 Clinical characteristics of pre-discharge COVID-19 patients who participated in the study in comparison with matched control.

Active smoking status pre-disease, pack years	29 (16.5) 1 [1; 15]
Comorbidities	
Hypertension	70 (39.8)
Obesity	67 (38.1)
Diabetes mellitus, type 2	17 (9.6)
Chronic obstructive pulmonary disease	5 (2.8)
Bronchial asthma	4 (2.3)
Pulmonary emphysema	3 (1.7)
Angina pectoris	3 (1.7)
History of stroke/TIA	6 (3.4)
Chronic kidney disease	5 (2.8)
Chronic liver disease	2 (1.1)
History of peptic ulcer	13 (7.4)
History of cancer	10 (5.7)
Charlson comorbidity index	0.5 ± 0.8
Minimal SpO ₂ , %	89 [85; 94]
Pulmonary tissue involvement by CT*, %	32.5 ± 20.2
Laboratory parameters	
Peak IL-6, pg/ml	10.0 [3.1; 25.2]
Peak CRP, mg/L	24.0 [7.3; 55.0]
Peak ESR, mm/h	30 [20; 40]
Peak procalcitonin, ng/ml	0.06 [0.04; 0.12]
Peak D-dimer, ng/ml	278 [154; 508]
Oxygen supplementation	
Via nasal cannula	101 (57.4)
Noninvasive/invasive ventilation	9 (5.1)
Treatment	
Methylprednisolone pulse therapy	115 (65.3)
Dexamethasone	155 (88.1)
Remdesivir	82 (46.6)

*Assessment was performed using the methodology for the simplified RALE score as proposed by Wong et al. (44), mean value of the reported % range was taken for analysis; BMI, body mass index; TIA, transient ischemic attack; SpO₂, peripheral capillary oxygen saturation; IL-6, interleukin 6; CRP, C-reactive protein; ESR, erythrocyte sedimentation rate.

Diagnosis and grading of the left ventricular diastolic dysfunction (DD) were performed in accordance with the 2016 ASE/EACVI algorithm (29) with inclusion of the myocardial disease concept; in cases of lacking data on tricuspid regurgitation velocity, we only ruled patients as having DD when present structural abnormality was corroborated by tissue Doppler findings (i.e., isolated left atrial dilation or LV remodeling were not considered signs of DD).

2.4. Statistical analysis

The collected data was analyzed using StatSoft STATISTICA Version 12 statistical analysis software package. Data distribution was assessed using Shapiro-Wilk test. For all variables, descriptive statistics are reported as mean ± standard deviation (SD) or median [interquartile range] for normally distributed and skewed continuous variables, respectively. Categorical variables are reported as counts (percentages). Cross-sectional comparisons of continuous variables were performed using independent samples *t*-test for normally distributed parameters and Mann-Whitney *U*-test for skewed variables; Chi-Square test was used to compare binary and categorical variables. Longitudinal comparisons were made using paired samples *t*-test or Wilcoxon signed-rank test. *P* values reported were calculated using two-sided Fisher's exact test, the differences were considered significant if *P* < 0.05. Correlation analysis was performed using the linear Pearson method.

3. Results

3.1. Clinical characteristics

The mean age of the initial 176 participants who entered the study (including 53% female and 47% male patients) was 53.4 ± 13.6 years. The average time from symptoms onset was 22.6 ± 7.1 days for Visit 1 and 54.3 ± 8.2 days for Visit 2. The most frequent comorbidities were hypertension and obesity with the prevalence of both close to 40%; the complete report on comorbidities and further clinical characteristics are presented in **Table 2**.

3.2. Echocardiographic data at baseline

Echocardiographic assessment of cardiac structure in observed patients has revealed a mild increase in LA size and volume, interventricular septum (IVS) and posterior LV wall thickness, and myocardial mass parameters compared to matched control (see **Table 3**). The observed changes resulted in a high proportion of patients with concentric LV geometry, whereas the LV hypertrophy rate was insignificantly increased vs. control and remained generally in line with common knowledge of its prevalence in the European population (31).

Assessment of the LV systolic parameters in the study cohort has revealed a mild decrease in the B-mode derived indices of

TABLE 3 Echocardiographic characteristic of the study participants.

Parameters	COVID-19 general, <i>n</i> = 176	Control 1, <i>n</i> = 88	Difference (95% CI)	2-sided <i>p</i>
Left chambers morphometry				
LA size, mm	37.6 ± 4.0	36.4 ± 3.5	1.3 (0.3; 2.3)	0.010
LA volume index, ml/m ²	28.6 ± 6.6	25.1 ± 4.9	3.5 (1.9; 5.1)	<0.001
Interventricular septum, mm	10.3 ± 1.6	9.1 ± 1.0	1.3 (0.9; 1.6)	<0.001
LV posterior wall, mm	9.9 ± 1.3	9.0 ± 0.8	0.9 (0.6; 1.2)	<0.001
LV relative wall thickness	0.45 ± 0.07	0.39 ± 0.04	0.07 (0.05; 0.08)	<0.001
LV end-diastolic diameter, mm	45.2 ± 4.0	46.9 ± 3.3	−1.8 (−3.1; −0.4)	<0.001
LV end-systolic diameter, mm	28.9 ± 3.5	31.1 ± 2.5	−2.2 (−3.0; −1.4)	<0.001
LV length, mm	81.1 ± 7.2	81.7 ± 6.2	−0.6 (−2.2; 1.0)	0.505
LV mass index (BSA), g/m ²	81.4 ± 16.9	72.8 ± 10.2	8.6 (4.7; 12.4)	<0.001
LV mass index (height ^{2.7}), g/m ^{2.7}	38.1 ± 8.9	33.9 ± 5.8	4.1 (2.1; 6.2)	<0.001
LV concentric geometry	104 (59.1)	15 (17.0)		<0.001
LV hypertrophy	21 (11.9)	6 (6.8)		0.196
Left ventricular systolic function				
LV ejection fraction, %	65.3 ± 6.7	62.2 ± 4.6	3.2 (1.0; 5.4)	<0.001
MAPSE, mm	14.2 ± 2.3	15.1 ± 2.1	−1.0 (−1.5; −0.3)	0.002
LV global longitudinal strain, %	17.5 ± 2.4	18.6 ± 2.2	−1.0 (−1.6; −0.4)	<0.001
LV midwall shortening, %	15.7 ± 2.1	16.4 ± 1.9	−0.7 (−1.2; −0.2)	0.006
LV stroke volume index, ml/m ²	31.7 ± 6.4	32.3 ± 5.7	−0.6 (−2.1; −1.0)	0.495
LV s', cm/s	9.7 ± 1.7	10.0 ± 1.4	−0.3 (−0.7; 0.1)	0.199
Left ventricular diastolic function				
LV e', cm/s	9.2 ± 2.2	11.3 ± 2.6	−2.1 (−2.7; −1.5)	<0.001
LV E, cm/s	67.4 ± 17.2	74.3 ± 16.0	−6.9 (−11.3; −2.6)	0.002
LV E/A ratio	1.01 ± 0.26	1.09 ± 0.33	−0.07 (−0.15; 0.00)	0.055
LV E/e' ratio	7.5 ± 1.8	6.8 ± 1.7	0.7 (0.3; 1.2)	0.002
LV diastolic dysfunction	62 (35.2)	12 (13.6)		<0.001
Right chambers evaluation				
RA size, mm	35.8 ± 3.8	36.6 ± 4.1	−0.8 (−1.8; 0.2)	0.110
RV size (proximal outflow tract)	31.8 ± 3.3	32.4 ± 3.5	−0.6 (−1.6; 0.3)	0.164
TAPSE, mm	24.8 ± 4.3	25.6 ± 3.9	−0.8 (−1.9; 0.3)	0.143

CI, confidence interval; LA, left atrium; LV, left ventricle; BSA, body surface area; MAPSE, mitral annular plane systolic excursion; RA, right atrium; RV, right ventricle; TAPSE, tricuspid annular plane systolic excursion.

longitudinal function (MAPSE and GLS) and the midwall shortening vs. control. At the same time, a minimal increase in ejection fraction in the setting of a mildly decreased LV cavity resulted in the absence of changes in the cardiac output as assessed by the stroke volume index.

LV diastolic function was characterized by a 20% reduction of mean *e'* velocities, reaching subnormal values in 47% of participants. An *E/e'* increase that was observed, however, was of little magnitude, leaving the vast majority of study subjects well below the cut-off values suggestive of increased LV filling pressures. The lack of traceable tricuspid regurgitation in the majority of patients (together with no evidence of right chambers remodeling or dysfunction) suggested normal pulmonary artery pressures but complicated the grading of diastolic dysfunction. As a result, out of 62 patients with diastolic dysfunction, 47 (26.7%) were categorized as Grade I DD and 15 (8.5%) as having indeterminate filling pressures. In the absence of data on left atrial strain, re-classification of these patients using LV GLS values (29, 32) with a cut-off of 16% (33) has allowed us to identify 7 (4.0%) subjects with apparently increased filling pressures.

Considering the similarities of changes in cardiac morphology and function that we observed in the study group to the hypertensive phenotype, a sub-analysis focused on the cohort of non-hypertensive participants (*n* = 106) was additionally performed to completely eliminate the possible confounding effect of differences in hypertension severity and quality of its control.

In the proposed setting, we observed less pronounced changes that were still similar to the concentric phenotype described above (see Table 4). Despite the 0.5 mm lesser absolute LV wall thickness, their mean values were still higher vs. control, as was the relative wall thickness, resulting in a 43% prevalence of concentric LV geometry. Myocardial mass parameters were also mildly increased, showing intermediate values between hypertensive participants (85.6 ± 21.0 g/m² for BSA-indexed LV myocardial mass in the latter) and the control group.

A similar pattern was observed when assessing LV diastolic filling, with a statistically significant decrease in mitral *e'* velocity and an increase in *E/e'* ratio resulting in a 25% prevalence of Grade I diastolic dysfunction. MAPSE and GLS values were also mildly decreased in non-hypertensive COVID-19 patients on the background of a clinically insignificant increase in ejection fraction.

TABLE 4 Echocardiographic characteristic of non-hypertensive hospitalized COVID-19 patients.

Parameters	COVID-19 non-HT, <i>n</i> = 106	Control 2, <i>n</i> = 53	Difference (95% CI)	2-sided <i>p</i>
Left chambers morphometry				
LA size, mm	36.3 ± 3.7	35.2 ± 3.1	1.1 (0.1; 2.3)	0.064
LA volume index, ml/m ²	28.5 ± 6.8	25.4 ± 5.5	3.1 (1.0; 5.2)	0.004
Interventricular septum, mm	9.7 ± 1.2	8.8 ± 0.9	0.9 (0.5; 1.3)	<0.001
LV posterior wall, mm	9.4 ± 1.1	8.8 ± 0.8	0.6 (0.3; 1.0)	<0.001
LV relative wall thickness	0.42 ± 0.05	0.38 ± 0.04	0.04 (0.02; 0.06)	<0.001
LV end-diastolic diameter, mm	45.5 ± 3.5	46.3 ± 3.1	−0.8 (−1.9; 0.4)	0.178
LV end-systolic diameter, mm	29.4 ± 3.7	30.9 ± 2.6	−1.5 (−2.6; −0.4)	0.009
LV length, mm	80.3 ± 6.1	81.0 ± 5.5	−0.8 (−2.5; 9.7)	0.365
LV mass index (BSA), g/m ²	78.4 ± 14.0	71.5 ± 10.2	6.9 (2.6; 11.2)	0.002
LV mass index (height ^{2.7}), g/m ^{2.7}	35.6 ± 6.8	32.4 ± 4.9	3.4 (1.3; 5.4)	0.002
LV concentric geometry	46 (43.4)	7 (13.2)		<0.001
LV hypertrophy	4 (3.8)	0 (0)		0.371
Left ventricular systolic function				
LV ejection fraction, %	64.7 ± 7.1	61.9 ± 4.7	2.9 (0.8; 5.0)	0.008
MAPSE, mm	14.2 ± 2.1	15.0 ± 2.0	−0.8 (−1.4; −0.2)	0.023
LV global longitudinal strain, %	17.8 ± 2.3	18.5 ± 2.2	−0.7 (−1.4; −0.2)	0.068*
LV midwall shortening, %	16.2 ± 1.8	16.5 ± 1.8	−0.3 (−0.9; 0.3)	0.310
LV stroke volume index, ml/m ²	32.8 ± 5.9	32.4 ± 5.6	0.3 (−1.6; 2.2)	0.755
LV s', cm/s	9.7 ± 1.7	9.9 ± 1.4	−0.2 (−0.7; 0.3)	0.465
Left ventricular diastolic function				
LV e', cm/s	9.8 ± 2.2	11.5 ± 2.5	−1.8 (−2.5; −1.0)	<0.001
LV E, cm/s	68.6 ± 18.9	71.6 ± 14.4	−6.9 (−11.3; −2.6)	0.311
LV E/A ratio	1.09 ± 0.28	1.09 ± 0.32	−0.07 (−0.15; 0.00)	0.876
LV E/e' ratio	7.1 ± 1.6	6.4 ± 1.5	0.7 (0.2; 1.3)	0.006
LV diastolic dysfunction	27 (25.5)	5 (9.4)		0.017
Right chambers evaluation				
RA size, mm	35.9 ± 3.7	36.1 ± 4.4	−0.2 (−1.5; 1.1)	0.308
RV size (proximal outflow tract)	30.8 ± 2.9	31.9 ± 3.6	−1.1 (−2.3; 0.0)	0.048
TAPSE, mm	24.7 ± 4.1	25.4 ± 3.9	−0.8 (−1.9; 0.3)	0.304

*1-sided *p* = 0.034. CI, confidence interval; LA, left atrium; LV, left ventricle; BSA, body surface area; MAPSE, mitral annular plane systolic excursion; RA, right atrium; RV, right ventricle; TAPSE, tricuspid annular plane systolic excursion.

3.3. 1-Month follow-up

Another aspect of our study was focused on the assessment of short-term post-discharge dynamics of echocardiographic parameters in observed COVID-19 patients based on the results of repeated comprehensive transthoracic echocardiography after a median of 31 days from the first visit. **Table 5** summarizes the obtained results and presents data on the comparison of Visit 2 parameters vs. control.

Despite the natural post-hospitalization reconditioning resulting in a previously reported increase in the 6MWD among the study participants from 401 ± 71 to 463 ± 65 m (62.7 ± 10.6–74.0 ± 11.1% of the predicted values, *p* < 0.001 for both indices) during a one-month follow-up (34), we were only able to detect minimal dynamic changes in cardiac morphology. Those were limited to a 2% decrease in the interventricular septum thickness which resulted in a borderline decrease in myocardial mass parameters compared to Visit 1. Evaluation of cardiac function revealed a minimal decrease in the estimated minute volume of blood that was associated with unidirectional and proportional (circa −3 to −5%) change of most systolic parameters vs. baseline, including LV ejection fraction and midwall shortening, RV free wall longitudinal strain, TAPSE, and

both mitral and tricuspid annular s' velocities, accompanied with a minimal increase in LV end-systolic diameter. Assessment of the diastolic filling of both ventricles did not reveal any significant changes during a short-term follow-up.

Thus, the observed cohort of COVID-19 patients at the time point of 1 month after discharge has retained the features indicative of the shift towards concentric LV geometry (an increase in absolute and relative wall thickness and higher values of myocardial mass indices), with RWT reaching values >0.42 in 64% of participants, including 55% of non-hypertensive subjects. These changes were accompanied by a mild depression of ventricular longitudinal function, manifested as a persisting 5%–10% decrease in LV GLS, MAPSE, TAPSE, and mitral annular velocities vs. control. LV diastolic dysfunction remained highly prevalent and was detected in 36% of cases in the general cohort and 30%—among non-hypertensive participants.

Out of the parameters assessed in our study, it was the LV wall absolute and relative thickness and myocardial mass parameters at Visit 1 that had a weak-to-moderate, but significant correlation with the increase in the reached percent of predicted 6-minute walk distance during the follow-up period—the strongest links were detected for interventricular septum (*r* = 0.37) and LV MMI by height^{2.7} (*r* = 0.31). These findings implied that those were the

TABLE 5 Results of a 1-month echocardiographic follow-up of observed patients with COVID-19.

Parameters	COVID-19 general		Visit 2 vs. Visit 1		Visit 2 vs. Control 1	
	Visit 1	Visit 2	Difference (95% CI)	2-sided <i>p</i>	Difference (95% CI)	2-sided <i>p</i>
Left chambers morphometry						
LA size, mm	37.5 ± 4.0	37.5 ± 4.6	0.0 (−0.5; 0.5)	0.920	1.1 (0.0; 2.3)	0.053
LA volume index, ml/m ²	28.3 ± 5.8	27.5 ± 6.2	−0.8 (−1.9; 0.3)	0.154	2.3 (1.0; 3.7)	<0.001
Interventricular septum, mm	10.3 ± 1.5	10.1 ± 1.4	−0.2 (−0.3; 0.0)	0.031	1.0 (0.7; 1.4)	<0.001
LV posterior wall, mm	9.9 ± 1.3	9.9 ± 1.3	0.0 (−0.2; 0.1)	0.569	0.9 (0.5; 1.2)	<0.001
LV relative wall thickness	0.45 ± 0.08	0.45 ± 0.08	0.00 (−0.01; 0.01)	0.340	0.06 (0.05; 0.08)	<0.001
LV end-diastolic diameter, mm	44.8 ± 4.0	44.8 ± 4.2	0.0 (−0.4; 0.4)	0.965	−2.0 (−3.1; −1.0)	<0.001
LV end-systolic diameter, mm	28.6 ± 3.6	29.0 ± 4.0	0.4 (0.0; 0.8)	0.034	−2.2 (−3.1; −1.2)	<0.001
LV mass, g	155.6 ± 35.4	153.3 ± 34.2	−2.3 (−5.1; 0.5)	0.102	9.2 (0.4; 17.9)	0.040
LV mass index (BSA), g/m ²	79.5 ± 14.2	77.3 ± 12.2	−2.2 (−3.6; 0.8)	0.002	4.5 (1.3; 7.6)	0.005
LV mass index (H ^{2.7}), g/m ^{2.7}	36.8 ± 7.7	36.2 ± 7.1	−0.6 (−1.2; 0.1)	0.085	2.3 (0.5; 4.1)	0.013
LV concentric geometry	74 (58.7)	81 (64.3)		0.437		<0.001
LV hypertrophy	11 (8.7)	11 (8.7)		1.000		0.801
Left ventricular systolic function						
LV ejection fraction, %	65.7 ± 6.8	64.6 ± 6.8	−1.0 (1.0; 5.4)	<0.001	2.7 (1.0; 4.3)	0.002
MAPSE, mm	14.1 ± 2.1	14.1 ± 2.2	0.0 (−0.5; 0.4)	0.823	−1.1 (−1.6; −0.6)	<0.001
LV GLS, %	17.3 ± 2.4	17.3 ± 2.1	0.0 (−0.4; 0.4)	0.879	−1.3 (−1.9; −0.7)	<0.001
LV midwall shortening, %	15.7 ± 2.1	15.5 ± 2.0	−0.2 (−1.2; −0.2)	0.006	−0.9 (−1.4; −0.4)	0.001
LV SVI, ml/m ²	31.2 ± 6.3	30.1 ± 5.3	−1.0 (−2.1; 0.0)	0.060	−2.2 (−3.7; −0.6)	0.005
Minute volume of blood, L	5.15 ± 1.54	4.89 ± 1.21	−0.26 (−0.49; 0.02)	0.031		
LV s', cm/s	9.7 ± 1.9	9.3 ± 1.7	−0.4 (−0.7; 0.2)	0.001	−0.7 (−1.2; −0.3)	0.001
Left ventricular diastolic function						
LV e', cm/s	9.5 ± 2.3	9.8 ± 2.8	0.2 (−0.1; 0.6)	0.131	−1.5 (−2.3; −0.8)	<0.001
LV E, cm/s	69.6 ± 17.6	67.9 ± 15.7	−1.7 (−4.8; 1.4)	0.271	−6.5 (−10.8; −2.1)	0.004
LV E/A ratio	1.06 ± 0.26	1.03 ± 0.29	−0.02 (−0.07; 0.02)	0.328	−0.05 (−0.14; 0.03)	0.224
LV E/e' ratio	7.5 ± 1.7	7.3 ± 2.3	−0.1 (−0.4; 0.1)	0.300	0.6 (0.0; 1.1)	0.055
LV diastolic dysfunction	39 (31.0)	46 (36.5)		0.424		<0.001
Right chambers evaluation						
RA size, mm	36.1 ± 4.1	35.7 ± 4.1	−0.3 (−1.1; 0.4)	0.365	−0.9 (−2.0; 0.3)	0.130
RA area index, mm ² /m ²	8.3 ± 2.2	7.7 ± 1.4	−0.6 (−1.0; 0.1)	0.014		
RV size	31.8 ± 3.3	31.9 ± 3.3	0.1 (−0.4; 0.6)	0.751	−0.5 (−1.5; 0.6)	0.378
TAPSE, mm	24.8 ± 4.1	24.0 ± 3.5	−0.8 (−1.5; 0.1)	0.020	−1.4 (−2.5; −0.4)	0.006
RVLS, %	36.2 ± 6.4	34.8 ± 5.9	−1.4 (−2.5; 0.3)	0.010		
RV s', cm/s	14.6 ± 2.6	14.0 ± 2.6	−0.7 (−1.2; 0.1)	0.014		
RV e', cm/s	11.3 ± 2.3	10.9 ± 2.1	−0.4 (−0.9; 0.1)	0.086		
RV E/e' ratio	4.4 ± 1.3	4.5 ± 1.1	0.1 (−0.1; 0.4)	0.236		

CI, confidence interval; LA, left atrium; LV, left ventricle; BSA, body surface area; MAPSE, mitral annular plane systolic excursion; GLS, global longitudinal strain; SVI, stroke volume index; RA, right atrium; RV, right ventricle; TAPSE, tricuspid annular plane systolic excursion; RVLS, RV free wall longitudinal strain.

patients with initially thicker walls who could potentially gain higher 6MWD increment vs. those in whom LV walls had a closer to normal thickness by the moment of discharge. Correlation analysis of dynamic changes in LV morphology has confirmed these suggestions, showing that the only parameters related to the increase in the 6 min walk distance % were a decrease in the IVS thickness ($r = -0.31$) and LV myocardial mass / MMI by height^{2.7} ($r = -0.31$). (See **Supplementary Table S1** for the detailed report on revealed correlations).

4. Discussion

A lot of attention has been drawn recently to the problem of long COVID syndrome (35–38). Compared to the acute phase, underlying pathogenetic mechanisms are less profoundly known,

with limited and at times conflicting data available on the specific features of post-acute cardiovascular sequelae of COVID-19 (7–9).

This combined cross-sectional case-control and longitudinal cohort study reports the results of comprehensive transthoracic echocardiographic assessment in hospitalized COVID-19 patients that was performed 1–2 days pre-discharge at the baseline and repeated after a 1-month follow-up.

The main findings included a high prevalence of concentric LV geometry that was present in 59% of participants, including 43% prevalence in the non-hypertensive subgroup, and predominantly Grade I diastolic dysfunction that was found in 35% and 25% of patients, respectively, presenting a significant difference compared to the age-, sex-, height-, weight-, and comorbidities-matched control. The observed changes persisted throughout the follow-up period, showing no significant improvement at 1 month.

Other findings naturally followed from the described LV phenotype and included a mild relative increase in LV wall thickness and myocardial mass parameters vs. control and a mild decrease in the indices of both diastolic and longitudinal systolic ventricular function. The magnitude of these changes, however, was little, leaving the mean values (except wall thickness) within normal limits and therefore being hardly clinically significant when taken isolated.

In the assessment of the biventricular longitudinal systolic function, we applied a recently proposed linear method that was later validated on 1266 cardiovascular disease-free individuals in the HUNT study, showing a close to linear correlation and no significant differences to the 2D speckle tracking-obtained values (26–28). The advantages of the selected method include universal availability, vendor independence, and low dependence on the image quality, which allowed us to obtain valid results in 100% of participants.

Most of the echocardiographic studies that had been performed to date in COVID-19 patients were focused on the assessment of changes in cardiac structure and function during the acute phase of disease and on the evaluation of their prognostic significance, mostly using a hard endpoint of COVID-19-related death (14, 39–41). The main findings on focused TTE that was usually used in this setting included RV dilation and dysfunction in a significant proportion of the patients, followed by LV functional alterations that in case of being clinically significant were typically related to pre-existing cardiac pathology. RV dilation and strain values, TAPSE, and LV GLS were most frequently identified as independent predictors of mortality. At the same time, it is worth noting in the context of our study that the LV diastolic dimensions, when reported, were typically less compared to the usual values in the general population, with mean values reaching as low as 42–43 mm when performed early during the hospitalization period (39, 41) and coming closer to 45 mm when examining patients later (14, 40). Szekely et al. also report in detail on LV tissue Doppler parameters obtained during 24 h from hospitalization that included low mean values of mitral annular velocities (7.4 cm/s for both s' and e') and a high E/e' ratio (weighted mean 10.4 for all patients), most likely indicating a high prevalence of diastolic dysfunction (41).

The study by Moody et al. (14) is among the few that included a baseline in-hospital echocardiographic evaluation (at a median of 8 days after admission) with subsequent longitudinal follow-up; similar to most of the above, it also used a focused TTE protocol and therefore did not report on most of the parameters that were evaluated in our study. However, the results reported on the LV end-diastolic diameter were similar to those observed by us, and a high prevalence of RV overload and dysfunction (defined as TAPSE <17 mm) that was not detected in our study was mostly resolved by the moment of re-evaluation at 3 months.

Out of studies available on recovery after COVID-19, few have used comprehensive sonographic assessment of cardiac structure and function. In a study by Catena et al. (11), the authors report LV morphology features in patients who were troponin-negative at hospitalization that are virtually indistinguishable from those that we observed in the control group. Even more interesting is the fact that troponin-positive patients in that study displayed a clear tendency to an increase in the LV wall thickness and

myocardial mass index, despite the differences not reaching the significance levels (most likely due to the low number of patients, $n = 18$). Similar findings were observed for mitral annular e' velocity and E/e' ratio that were equal between troponin-negative patients and Control 1 subjects in our study but insignificantly deteriorated in ex-troponin-positive participants in (11). The values of LV ejection fraction, being somewhat higher compared to our study, were also characterized by a minor increase in a “worse” clinical group. At the same time, the authors report no difference in MAPSE and TAPSE, presenting values that are lower compared to both groups in our study.

In another development by the same team, Sechi et al. compare the same general cohort of 105 hospitalized COVID-19 patients to a set of 1:1 matched control subjects, providing to date the most detailed echocardiographic characterization of the latter that was obtained in the closest setting to that of our study (at a median of 41 days from the date of COVID-19 diagnosis) (12). An indirect comparison of our results to the presented data has both corroborated the findings in the main group and allowed us to externally validate the control group used in our study—it was characterized by a minimal uni-directed shift towards “more concentric” geometry vs. controls in (12), thus being unlikely to partially account for the observed differences vs. study group (see **Supplementary Table S2**). Similar to our results, the authors demonstrate (an insignificant) tendency to increase in the LV relative wall thickness due to a minimal decrease in end-diastolic diameter. Contrary to our findings, no significant changes have been reported regarding the longitudinal ventricular function despite the almost identical values of MAPSE both in the main and control groups to those in our study.

Another study by Ingul et al. (16) presents a comprehensive functional echocardiographic assessment of 204 COVID-19 survivors that was performed at 3 months follow-up using the comparison to the age-, sex-, BMI-, systolic blood pressure- and comorbidities-matched control. Similar to our findings, it reports a decrease in LV end-diastolic volume index, which should have been accompanied by increased relative wall thickness unless associated with proportionally lower myocardial mass. Other corroborating results include the evidence of a relatively poorer biventricular longitudinal function, manifested as a mild but statistically significant decrease in MAPSE, mitral e' velocity, TAPSE, and RV free wall strain; despite a minimal decrease in ejection fraction, LV GLS is reported to be paradoxically higher vs. control, being interpreted by authors as a clinically insignificant sign that could be operator dependent.

Tudoran et al. (19) report a high prevalence of LV diastolic dysfunction among patients with long COVID syndrome, reaching 63% in obese and 22% in non-obese subjects. Despite the important discrepancies in the study population (selected long COVID vs. general COVID-19 cohort; mainly outpatient management vs. hospitalized patients), participants were enrolled at 4–10 weeks from the onset of symptoms, which was approximating the timing of Visit 2 in our study, and adjustment of the mentioned rates to the prevalence of obesity in our cohort results in a weighted mean rate of diastolic dysfunction of 38%, coming very close to the factual prevalence that we observed.

We did not identify prior studies longitudinally assessing echocardiographic dynamics within the early post-acute period of COVID-19 that would not use the parameters obtained during the early acute phase as a baseline. The current study presents data on the 1-month follow-up in the period from a median of 23–54 days after manifestation of symptoms, demonstrating no significant changes in cardiac morphology during this phase. The minimal decrease in the systolic indices that we observed was not associated with clinical deterioration and most likely resulted from the gradual reversal of a somewhat higher output state due to SARS-CoV-2-induced pulmonary affection. The same process could have explained the tendency to a minimal decrease in myocardial mass parameters (the observed changes of BSA-indexed LV MMI were partially driven by the restoration of the weight loss during the acute phase—in the follow-up period the patients gained 2.6 ± 3.3 kg). At the same time, the observed minimal changes in myocardial mass were contrasted with the expected dynamics during the period of post-hospitalization reconditioning (42) and could also be hypothetically explained (along with an increase in myocardial mass vs. control) by mild myocardial edema persisting in some patients [as shown in series of cardiac magnetic resonance studies (43)]. In this scenario, its gradual resolution during the observation period could potentially explain the correlations found in our study between the decrease in IVS thickness/myocardial mass and the improvement in 6MWD.

In the report on a long-term echocardiographic follow-up at a later phase after hospitalization for COVID-19, Ovrebotten et al. (17) demonstrated no changes in both LV and RV parameters (including morphometry and longitudinal strain) during the period from 3 to 12 months. These findings, along with the results of our study, suggest that identification of patients with delayed/incomplete resolution of minor COVID-19-related cardiac alterations may be performed as early as during the late acute/early post-acute period of SARS-CoV-2 infection.

4.1. Strengths and limitations

To our knowledge, this is the first study focusing on the comprehensive assessment of echocardiographic changes in hospitalized COVID-19 patients during the early post-discharge period. Simultaneous cross-sectional comparison to the matched control allowed us to more clearly outline the existing minor changes in the cardiac structure and function that still appeared to be linked to the observed functional improvement during one month of follow-up. A sub-analysis that was performed in a cohort of non-hypertensive individuals has allowed us to more reliably mitigate the confounding effect of hypertension compared to the simple matching of its self-reported presence, given that the latter does not account for the possible differences in the severity and control of hypertension.

Being a single-center study, it could be susceptible to hospital-related confounding effects. The most notable difference between the used treatment and the commonly applied standards was the high proportion of patients who received pulse therapy with Methylprednisolone during the first days of hospitalization. However, one would expect its possible effects on cardiac geometry

and function to be transitory if existing at all, and to resolve by the moment of baseline evaluation, which was confirmed by the absence of any correlations between its use and the studied parameters. There was a source of selection bias in the design and protocol of the study—candidates with severe underlying cardiac pathology were specifically excluded for possible subtle changes in evaluated parameters not to get confounded by more severe manifestations of pre-existing disease that would be hard to adequately match to control. In addition, patients with a more severe course of COVID-19 could have been less likely to participate due to being still oxygen-dependent by the moment of discharge or reluctant to leave the floor and/or to engage in the 6 min walk test, and thus the study population might not truly reflect the characteristics of the general mass of consecutively hospitalized patients. Lastly, the prevailing SARS-CoV-2 variants at the time of enrollment were different compared to more recent time, and a higher proportion of patients were not vaccinated, mandating caution in generalizing the obtained results to the current setting of post-acute COVID-19 care.

5. Conclusions

Hospitalized patients recovering from COVID-19 were characterized by the high prevalence of LV concentric remodeling, predominantly Grade I diastolic dysfunction, and a mild decrease in the longitudinal systolic function compared to matched control. The changes in LV geometry and diastolic dysfunction were less frequent but still prevalent in the non-hypertensive subgroup. The observed changes largely persisted during a one-month follow-up showing no general tendency to improvement, with a minor decrease in the IVS thickness and LV mass index correlating with an increase in the 6MWD.

Data availability statement

The raw data supporting the conclusions of this article will be made available by the authors, without undue reservation.

Ethics statement

The studies involving humans were approved by Ethical Committee of Kharkiv National Medical University. The studies were conducted in accordance with the local legislation and institutional requirements. The participants provided their written informed consent to participate in this study.

Author contributions

OH: study design, literature search, data collection, data analysis, data interpretation, writing manuscript, and revision of manuscript. TA: study design, data interpretation, and revision of manuscript. All authors contributed to the article and approved the submitted version.

Acknowledgments

The authors would like to thank M. Yerzina for the technical support in data collection and to acknowledge the work of the hospital staff: A. Bobeiko, V. Byzov, V. Blazhko, E. Khodosh, N. Matiash, O. Morozova, L. Kolisnyk, I. Talalay, V. Kozlov, L. Avdeyeva, who have set conditions for the proper functioning of the clinic.

Conflict of interest

The authors declare that the research was conducted in the absence of any commercial or financial relationships that could be construed as a potential conflict of interest.

References

- Palmisano A, Gambardella M, D'Angelo T, Vignale D, Ascione R, Gatti M, et al. Advanced cardiac imaging in the spectrum of COVID-19 related cardiovascular involvement. *Clin Imaging*. (2022) 90:78–89. doi: 10.1016/j.clinimag.2022.07.009
- Pesce M, Agostoni P, Botker HE, Brundel B, Davidson SM, Caterina R, et al. COVID-19-related cardiac complications from clinical evidences to basic mechanisms: opinion paper of the ESC working group on cellular biology of the heart. *Cardiovasc Res*. (2021) 117(10):2148–60. doi: 10.1093/cvr/cvab201
- Tschope C, Ammirati E, Bozkurt B, Caforio ALP, Cooper LT, Felix SB, et al. Myocarditis and inflammatory cardiomyopathy: current evidence and future directions. *Nat Rev Cardiol*. (2021) 18(3):169–93. doi: 10.1038/s41569-020-00435-x
- Varga Z, Flammer AJ, Steiger P, Haberecker M, Andermatt R, Zinkernagel AS, et al. Endothelial cell infection and endotheliitis in COVID-19. *Lancet*. (2020) 395(10234):1417–8. doi: 10.1016/S0140-6736(20)30937-5
- Babapoor-Farrokhran S, Gill D, Walker J, Rasekhi RT, Bozorgnia B, Amanullah A. Myocardial injury and COVID-19: possible mechanisms. *Life Sci*. (2020) 253:117723. doi: 10.1016/j.lfs.2020.117723
- Azevedo RB, Botelho BG, Hollanda JVG, Ferreira LVL, Junqueira de Andrade LZ, Oei S, et al. COVID-19 and the cardiovascular system: a comprehensive review. *J Hum Hypertens*. (2021) 35(1):4–11. doi: 10.1038/s41371-020-0387-4
- Raman B, Bluemke DA, Luscher TF, Neubauer S. Long COVID: post-acute sequelae of COVID-19 with a cardiovascular focus. *Eur Heart J*. (2022) 43(11):1157–72. doi: 10.1093/eurheartj/ehac031
- Wang W, Wang CY, Wang SI, Wei JC. Long-term cardiovascular outcomes in COVID-19 survivors among non-vaccinated population: a retrospective cohort study from the TriNetX US collaborative networks. *EclinicalMedicine*. (2022) 53:101619. doi: 10.1016/j.eclinm.2022.101619
- Xie Y, Xu E, Bowe B, Al-Aly Z. Long-term cardiovascular outcomes of COVID-19. *Nat Med*. (2022) 28(3):583–90. doi: 10.1038/s41591-022-01689-3
- Hall J, Myall K, Lam JL, Mason T, Mukherjee B, West A, et al. Identifying patients at risk of post-discharge complications related to COVID-19 infection. *Thorax*. (2021) 76(4):408–11. doi: 10.1136/thoraxjnl-2020-215861
- Catena C, Colussi G, Bulfone L, Da Porto A, Tascini C, Sechi LA. Echocardiographic comparison of COVID-19 patients with or without prior biochemical evidence of cardiac injury after recovery. *J Am Soc Echocardiogr*. (2021) 34(2):193–5. doi: 10.1016/j.echo.2020.10.009
- Sechi LA, Colussi G, Bulfone L, Brosolo G, Da Porto A, Peghin M, et al. Short-term cardiac outcome in survivors of COVID-19: a systematic study after hospital discharge. *Clin Res Cardiol*. (2021) 110(7):1063–72. doi: 10.1007/s00392-020-01800-z
- de Graaf MA, Antoni ML, Ter Kuile MM, Arbous MS, Duiniveldt AJF, Feltkamp MCW, et al. Short-term outpatient follow-up of COVID-19 patients: a multidisciplinary approach. *EclinicalMedicine*. (2021) 32:100731. doi: 10.1016/j.eclinm.2021.100731
- Moody WE, Liu B, Mahmoud-Elsayed HM, Senior J, Lalla SS, Khan-Kheil AM, et al. Persisting adverse ventricular remodeling in COVID-19 survivors: a longitudinal echocardiographic study. *J Am Soc Echocardiogr*. (2021) 34(5):562–6. doi: 10.1016/j.echo.2021.01.020
- Sonnweber T, Sahanic S, Pizzini A, Luger A, Schwabl C, Sonnweber B, et al. Cardiopulmonary recovery after COVID-19: an observational prospective multicentre trial. *Eur Respir J*. (2021) 57(4). doi: 10.1183/13993003.03481-2020
- Ingul CB, Grimsø J, Mecinaj A, Trebinjac D, Berger Nossen M, Andrup S, et al. Cardiac dysfunction and arrhythmias 3 months after hospitalization for COVID-19. *J Am Heart Assoc*. (2022) 11(3):e023473. doi: 10.1161/JAHA.121.023473
- Ovrebotten T, Myhre P, Grimsø J, Mecinaj A, Trebinjac D, Nossen MB, et al. Changes in cardiac structure and function from 3 to 12 months after hospitalization for COVID-19. *Clin Cardiol*. (2022) 45(10):1044–52. doi: 10.1002/clc.23891
- Karagodin I, Singulane CC, Besser SA, Singh A, Addetia K, DeCara JM, et al. Comparison of clinical and echocardiographic features of first and second waves of COVID-19 at a large, tertiary medical center serving a predominantly African American patient population. *Int J Cardiovasc Imaging*. (2021) 37(11):3181–90. doi: 10.1007/s10554-021-02393-y
- Tudoran C, Tudoran M, Cut TG, Lazureanu VE, Bende F, Fofiu R, et al. The impact of metabolic syndrome and obesity on the evolution of diastolic dysfunction in apparently healthy patients suffering from post-COVID-19 syndrome. *Biomedicine*. (2022) 10(7). doi: 10.3390/biomedicine10071519
- Hu Y, Sun J, Dai Z, Deng H, Li X, Huang Q, et al. Prevalence and severity of corona virus disease 2019 (COVID-19): a systematic review and meta-analysis. *J Clin Virol*. (2020) 127:104371. doi: 10.1016/j.jcv.2020.104371
- Garg S, Kim L, Whitaker M, O'Halloran A, Cummings C, Holstein R, et al. Hospitalization rates and characteristics of patients hospitalized with laboratory-confirmed coronavirus disease 2019—COVID-NET, 14 states, march 1–30, 2020. *MMWR Morb Mortal Wkly Rep*. (2020) 69(15):458–64. doi: 10.15585/mmwr.mm6915e3
- Richardson S, Hirsch JS, Narasimhan M, Crawford JM, McGinn T, Davidson KW, et al. Presenting characteristics, comorbidities, and outcomes among 5700 patients hospitalized with COVID-19 in the New York city area. *JAMA*. (2020) 323(20):2052–9. doi: 10.1001/jama.2020.6775
- World Health Organization (WHO). *COVID-19 clinical management: living guidance*. (2021). Available at: <https://www.who.int/publications/i/item/WHO-2019-nCoV-clinical-2021-1>
- Duncan MJ, Mota J, Carvalho J, Nevill AM. An evaluation of prediction equations for the 6 Minute walk test in healthy European adults aged 50–85 years. *PLoS One*. (2015) 10(9):e0139629. doi: 10.1371/journal.pone.0139629
- Lang RM, Badano LP, Mor-Avi V, Afilafo J, Armstrong A, Ernande L, et al. Recommendations for cardiac chamber quantification by echocardiography in adults: an update from the American society of echocardiography and the European association of cardiovascular imaging. *Eur Heart J Cardiovasc Imaging*. (2015) 16(3):233–70. doi: 10.1093/ehjci/jev014
- Stoylen A, Molmen HE, Dalen H. Left ventricular global strains by linear measurements in three dimensions: interrelations and relations to age, gender and body size in the HUNT study. *Open Heart*. (2019) 6(2):e001050. doi: 10.1136/openhrt-2019-001050
- Stoylen A, Molmen HE, Dalen H. Relation between mitral annular plane systolic excursion and global longitudinal strain in normal subjects: the HUNT study. *Echocardiography*. (2018) 35(5):603–10. doi: 10.1111/echo.13825
- Aurich M, Fuchs P, Muller-Hennessen M, Uhlmann L, Niemers M, Greiner S, et al. Unidimensional longitudinal strain: a simple approach for the assessment of longitudinal myocardial deformation by echocardiography. *J Am Soc Echocardiogr*. (2018) 31(6):733–42. doi: 10.1016/j.echo.2017.12.010

Publisher's note

All claims expressed in this article are solely those of the authors and do not necessarily represent those of their affiliated organizations, or those of the publisher, the editors and the reviewers. Any product that may be evaluated in this article, or claim that may be made by its manufacturer, is not guaranteed or endorsed by the publisher.

Supplementary material

The Supplementary Material for this article can be found online at: <https://www.frontiersin.org/articles/10.3389/fcvm.2023.1250656/full#supplementary-material>

29. Nagueh SF, Smiseth OA, Appleton CP, Byrd BF 3rd, Dokainish H, Edvardsen T, et al. Recommendations for the evaluation of left ventricular diastolic function by echocardiography: an update from the American society of echocardiography and the European association of cardiovascular imaging. *J Am Soc Echocardiogr.* (2016) 29(4):277–314. doi: 10.1016/j.echo.2016.01.011
30. Rudski LG, Lai WW, Afilalo J, Hua L, Handschumacher MD, Chandrasekaran K, et al. Guidelines for the echocardiographic assessment of the right heart in adults: a report from the American society of echocardiography endorsed by the European association of echocardiography, a registered branch of the European society of cardiology, and the Canadian society of echocardiography. *J Am Soc Echocardiogr.* (2010) 23(7):685–713. quiz 86–8. doi: 10.1016/j.echo.2010.05.010
31. Schirmer H, Lunde P, Rasmussen K. Prevalence of left ventricular hypertrophy in a general population; the tromso study. *Eur Heart J.* (1999) 20(6):429–38. doi: 10.1053/eurhj.1998.1314
32. Del Castillo JM, de Albuquerque ES, da Mota Silveira CA, Lamprea DP, Medeiros Sena AD. Diastolic function assessment with Doppler echocardiography and two-dimensional strain. *ABC Imagem Cardiovascular.* (2017) 30:46. doi: 10.5935/2318-8219.20170012
33. Pieske B, Tschope C, de Boer RA, Fraser AG, Anker SD, Donal E, et al. How to diagnose heart failure with preserved ejection fraction: the HFA-PEFF diagnostic algorithm: a consensus recommendation from the heart failure association (HFA) of the European society of cardiology (ESC). *Eur Heart J.* (2019) 40(40):3297–317. doi: 10.1093/eurheartj/ehz641
34. Honchar O, Ashcheulova T. Spontaneous physical functional recovery after hospitalization for COVID-19: insights from a 1 month follow-up and a model to predict poor trajectory. *Front Med (Lausanne).* (2023) 10:1212678. doi: 10.3389/fmed.2023.1212678
35. Shah W, Hillman T, Playford ED, Hishmeh L. Managing the long term effects of COVID-19: summary of NICE, SIGN, and RCGP rapid guideline. *Br Med J.* (2021) 372:n136. doi: 10.1136/bmj.n136
36. Gyongyosi M, Alcaide P, Asselbergs FW, Brundel B, Camici GG, Martins PDC, et al. Long COVID and the cardiovascular system-elucidating causes and cellular mechanisms in order to develop targeted diagnostic and therapeutic strategies: a joint Scientific Statement of the ESC Working Groups on Cellular Biology of the Heart and Myocardial and Pericardial Diseases. *Cardiovasc Res.* (2023) 119(2):336–56. doi: 10.1093/cvr/cvac115
37. Soriano JB, Murthy S, Marshall JC, Relan P, Diaz JV, Condition WHOCCDWGoP-C-. A clinical case definition of post-COVID-19 condition by a delphi consensus. *Lancet Infect Dis.* (2022) 22(4):e102–e7. doi: 10.1016/S1473-3099(21)00703-9
38. Honchar O, Ashcheulova T, Chumachenko T, Chumachenko D, Bobeiko A, Blazhko V, et al. A prognostic model and pre-discharge predictors of post-COVID-19 syndrome after hospitalization for SARS-CoV-2 infection. *Front Public Health.* (2023) 11:1276211. doi: 10.3389/fpubh.2023.1276211
39. Mahmoud-Elsayed HM, Moody WE, Bradlow WM, Khan-Kheil AM, Senior J, Hudsmith LE, et al. Echocardiographic findings in patients with COVID-19 pneumonia. *Can J Cardiol.* (2020) 36(8):1203–7. doi: 10.1016/j.cjca.2020.05.030
40. Li Y, Li H, Zhu S, Xie Y, Wang B, He L, et al. Prognostic value of right ventricular longitudinal strain in patients with COVID-19. *JACC Cardiovasc Imaging.* (2020) 13(11):2287–99. doi: 10.1016/j.jcmg.2020.04.014
41. Szekely Y, Lichter Y, Taieb P, Banai A, Hochstadt A, Merdler I, et al. Spectrum of cardiac manifestations in COVID-19: a systematic echocardiographic study. *Circulation.* (2020) 142(4):342–53. doi: 10.1161/CIRCULATIONAHA.120.047971
42. Nash MS, Bilsker S, Marcillo AE, Isaac SM, Botelho LA, Klose KJ, et al. Reversal of adaptive left ventricular atrophy following electrically-stimulated exercise training in human tetraplegics. *Paraplegia.* (1991) 29(9):590–9.
43. Petersen SE, Friedrich MG, Leiner T, Elias MD, Ferreira VM, Fenski M, et al. Cardiovascular magnetic resonance for patients with COVID-19. *JACC Cardiovasc Imaging.* (2022) 15(4):685–99. doi: 10.1016/j.jcmg.2021.08.021
44. Wong HYF, Lam HYS, Fong AH, Leung ST, Chin TW, Lo CSY, et al. Frequency and distribution of chest radiographic findings in patients positive for COVID-19. *Radiology.* (2020) 296(2):E72–E8. doi: 10.1148/radiol.2020201160



OPEN ACCESS

EDITED BY

Francesca Innocenti,
Careggi University Hospital, Italy

REVIEWED BY

Alexandru Achim,
Cantonal Hospital Baselland (KSBL), Switzerland
Lei Zuo,
Air Force Medical University, China

*CORRESPONDENCE

Wei Zhu
✉ 15985064@qq.com
Huiming Guo
✉ guohuiming@gdph.org.cn
Jimei Chen
✉ jimei_1965@outlook.com

[†]These authors have contributed equally to this work and share first authorship

RECEIVED 11 September 2023

ACCEPTED 21 November 2023

PUBLISHED 06 December 2023

CITATION

Liu J, Tan T, Wei P, Ma J, Zhong L, Qiu H, Wang S, Zhuang J, Zhu W, Guo H and Chen J (2023) Anomalous papillary muscle insertion into the mitral valve leaflet in hypertrophic obstructive cardiomyopathy: a lip nevus sign in echocardiography.
Front. Cardiovasc. Med. 10:1292142.
doi: 10.3389/fcvm.2023.1292142

COPYRIGHT

© 2023 Liu, Tan, Wei, Ma, Zhong, Qiu, Wang, Zhuang, Zhu, Guo and Chen. This is an open-access article distributed under the terms of the [Creative Commons Attribution License \(CC BY\)](https://creativecommons.org/licenses/by/4.0/). The use, distribution or reproduction in other forums is permitted, provided the original author(s) and the copyright owner(s) are credited and that the original publication in this journal is cited, in accordance with accepted academic practice. No use, distribution or reproduction is permitted which does not comply with these terms.

Anomalous papillary muscle insertion into the mitral valve leaflet in hypertrophic obstructive cardiomyopathy: a lip nevus sign in echocardiography

Jian Liu^{1,2†}, Tong Tan^{1,2,3†}, Peijian Wei^{1,2†}, Jianrui Ma^{1,2}, Lishan Zhong⁴, Hailong Qiu^{1,2}, Shengwen Wang^{1,2}, Jian Zhuang^{1,2}, Wei Zhu^{4*}, Huiming Guo^{1,2*} and Jimei Chen^{1,2*}

¹Guangdong Cardiovascular Institute, Guangdong Provincial People's Hospital, Guangdong Academy of Medical Sciences, Guangzhou, Guangdong, China, ²Guangdong Provincial Key Laboratory of South China Structural Heart Disease, Guangzhou, Guangdong, China, ³Beijing Anzhen Hospital, Capital Medical University, Beijing Institute of Heart, Lung and Blood Vascular Diseases, Beijing, China, ⁴Division of Adult Echocardiography, Guangdong Provincial People's Hospital (Guangdong Academy of Medical Sciences), Guangzhou, China

Background: Anomalous papillary muscle (APM) insertion into the mitral valve leaflet is rare but clinically important in hypertrophic obstructive cardiomyopathy (HOCM). In this study, we report the detection rate of APM insertion into the mitral valve using preoperative imaging modalities and the surgical outcomes of the patients.

Methods: By retrospectively reviewing the clinical records of patients with HOCM who underwent surgical treatment by a single operation group at our center from January 2020 to June 2023, patients with APM insertion into the mitral valve leaflet were identified. Baseline data, image characteristics, and surgical outcomes were analyzed.

Results: The incidence of APM insertion into the mitral valve leaflet was 5.1% (8/157). The insertion site was located at A3 in six cases, which was more common than at A2 ($n = 2$). Preoperative echocardiography was used to identify two patients (25%) with APM insertion. We observed a particular echocardiographic feature for APM in HOCM patients, which was noted as a "lip nevus sign", with a higher detection rate (62.5%). All patients successfully underwent septal myectomy with concomitant APM excision or mitral valve replacement via the transaortic ($n = 5$) or transmitral ($n = 3$) approach. The mean age was 49.0 ± 17.4 years and seven patients (87.5%) were female. Interventricular septum thickness (17.0 mm vs. 13.3 mm, $P = 0.012$) and left ventricular outflow gradient (117.5 mmHg vs. 7.5 mmHg, $P = 0.012$) were significantly decreased after surgery. Residual outflow obstruction, systolic anterior motion, and $\geq 3+$ mitral regurgitation were negative. During the follow-up of 26.2 ± 12.2 months, there were no reported operations, adverse events, mitral regurgitation aggravations, recurrences of outflow obstruction, or instances of SAM.

Conclusions: Papillary muscles inserted into the mitral valve leaflet are a subtype of subvalvular malformation in HOCM that requires surgical correction. The lip nevus sign on echocardiography is a characteristic of APM insertion in HOCM and may improve the preoperative detection rate. Adequate myectomy with anomalous papillary muscle excision has achieved good results in reducing the outflow gradient and eliminating mitral regurgitation, with good outcomes at short-to-intermediate follow-up.

KEYWORDS

anomalous papillary muscles, subvalvular malformation, hypertrophic obstructive cardiomyopathy, echocardiography, surgical outcomes, imaging modalities

1. Introduction

In hypertrophic obstructive cardiomyopathy (HOCM), left ventricular outflow tract (LVOT) obstruction is well established with respect to defined anatomical landmarks such as the hypertrophic septum. The mitral valve apparatus and subvalvular abnormalities are associated with systolic anterior motion (SAM) and related LVOT obstruction (1–3). Invasive septal reduction treatments, such as percutaneous alcohol septal ablation and surgical extended myectomy, are necessary for some symptomatic HOCM patients. However, the decision regarding the specific treatment approach is not always a one-size-fits-all situation, with imaging findings like echocardiography playing a major role in determining the most suitable course of action (4). For instance, HOCM patients with intrinsic mitral valve diseases or valve apparatus abnormalities may derive greater benefit from surgical treatment. Several studies have mentioned that attention should be paid to anomalous papillary muscles (APM) during the extended myectomy procedure (5, 6). Likewise, in the case of HOCM with APM, invasive surgery was the preferred treatment strategy due to the need to manage APM; however, this was based on the premise that APM was detected by preoperative echocardiography, a widely performed and accessible examination in the context of HOCM management. The insertion of APM into the mitral valve leaflet is a rare occurrence, attributed not only to its low incidence but also to the challenges associated with its detection. Because imaging detection of APM insertion into the mitral valve and the associated surgical outcomes have been reported infrequently, the aim of the study was to examine these aspects and provide new insights into the characteristics of APM as observed through echocardiography.

2. Methods

2.1. Study design and patient selection

This study is a retrospective cross-sectional study of consecutive patients with a diagnosis of HOCM seen in the Guangdong Cardiovascular Institute, Guangdong Provincial People's Hospital. A total of 157 patients with HOCM who underwent surgical correction by a single operation group at our center from January 2020 to June 2023 were included. The medical history, auxiliary inspection data, and surgical outcomes were collected from our inpatient electronic medical record system. We reviewed their preoperative echocardiography, cardiac magnetic resonance imaging (MRI), and computed tomography (CT) records to assess the presence of APM insertion into the mitral valve. The echocardiography was reviewed by two experienced cardiac sonographers, and two radiologists in the laboratory of artificial intelligence and 3D technology for cardiovascular diseases department were responsible for the MRI and CT records. Patients with

low-quality imaging data were excluded. APM insertion into the mitral leaflet was confirmed by individual surgical records.

2.2. Surgical intervention

Symptomatic patients with HOCM who were tolerant to medication and had ≥ 50 mmHg of left ventricular outflow tract gradient (LVOTG) received surgical treatment as recommended by the management guideline for HOCM (7). Extended myectomy, via the transaortic or transmitral approach, was performed as described previously (8). Surgical strategies for mitral valves and APMs include mitral valve replacement, papillary muscle dissociation and excision, and other mitral repair techniques, as needed. When the subvalvular APM (Figure 1) is identified, its insertion site and surrounding chordae tendineae should be explored using a retractor. In case of valve injury, the APM insertion into the body of the leaflet was cut approximately 1 cm from the leaflet. The hypertrophic papillary muscles were partially sliced to palliate the narrow space within the left ventricle.

2.3. Surgical outcome assessment

The surgical outcome data included the success rate of surgery, major adverse cardiovascular events, and echocardiographic parameters of HOCM. Major adverse cardiovascular events include death, reoperation, severe arrhythmias (such as new-onset atrial fibrillation), myocardial infarction, stroke, progressive heart failure, and sudden death. Echocardiography before discharge and during the follow-up period was used to analyze the clinicopathological indices of HOCM, including interventricular septum (IVS) thickness, LVOTG, degree of mitral regurgitation (MR), SAM, and other abnormalities within the cardiac cavity.

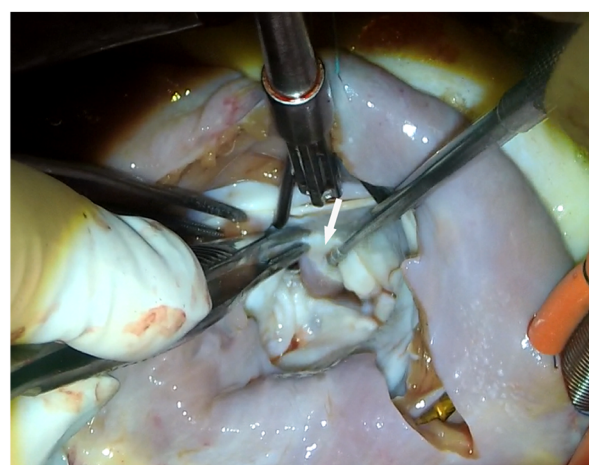


FIGURE 1
View of anomalous papillary muscles (arrow) directly inserted into the anterior mitral valve.

TABLE 1 Baseline characteristics of hypertrophic obstructive cardiomyopathy patients with anomalous papillary muscles inserting into the mitral valve.

Characteristic	N = 8
Female	7 (87.5%)
Age, years	49.0 ± 17.4
BMI, kg/m ²	22.0 ± 0.9
Hypertension	2 (25.0%)
History of PCI	1 (12.5%)
Stroke history	1 (12.5%)
Family history of cardiomyopathy	0
NYHA class ≥ III	7 (87.5%)
EuroSCORE II, %	1.7 ± 1.0

BMI, body mass index; PCI, percutaneous coronary intervention; NYHA, New York Heart Association.

2.4. Statistical analysis

Data are expressed as *N* (%), mean ± standard deviation, or median (interquartile range) where appropriate. Statistical analyses were conducted using SPSS software. Differences in continuous variables between the groups were analyzed using Student's *t*-test or a Mann–Whitney *U*-test. Fisher's exact test was performed to compare the counting data between groups.

3. Results

Of the 157 patients in our series, eight patients with HOCM (1 male and 7 females) that had APM insertion into the mitral valve leaflet were identified by surgical records. The baseline characteristics are summarized in **Table 1**. The mean age was 49.0 ± 17.4 years. The most common clinical symptom was chest distress (62.5%); one patient had a history of syncope, and one asymptomatic patient with HOCM was found during the annual physical examination. Six (75.0%) patients were on β-blocker therapy before hospitalization. All APMs were anterolateral papillary muscles. The insertion sites were located at A3 (75%) and A2 (25%). The median IVS was 17.0 (16.0, 23.3) mm. Compared with the IVS [20.0 (18.0, 24.0) mm] of patients with HOCM without APM in this cohort (**Table 2**), the IVS was thinner, but the difference was not statistically significant

TABLE 2 Echocardiographic parameters of HOCM patients with and without anomalous papillary muscles.

Variable	APM (<i>n</i> = 8)	Non-APM (<i>n</i> = 149)	<i>P</i> -value
IVS, mm	17.0 (16.0, 23.3)	20.0 (18.0, 24.0)	0.206
LVOTG, mmHg	117.5 (82.3, 136.8)	85.0 (67.5, 99.8)	0.034
SAM	7 (87.5%)	130 (87.2%)	1.000
MR ≥ 3+	5 (62.5%)	116 (77.9%)	0.385
EF, %	66.0 ± 2.9	67.8 ± 4.2	0.227
LAD, mm	41.1 ± 3.4	43.0 ± 7.3	0.462
LVDD, mm	42.6 ± 4.8	41.6 ± 5.0	0.589

IVS, interventricular septum; LVOTG, left ventricular outflow tract gradient; SAM, systolic anterior motion; MR, mitral regurgitation; EF, ejection fraction; LAD, left atrial diameter; LVDD, left ventricular diastolic diameter.

(*P* = 0.595). However, the median LVOTG was 117.5 (82.3, 136.8) mmHg, which showed a significant increase compared with the non-APM group [85.0 (67.5, 99.8) mmHg, *P* = 0.034]. Two patients (25.0%) had midventricular obstruction. Hypertrophic papillary muscles were found in two patients (25.0%) and chordal rupture was found in one patient (12.5%). Mild to severe SAM was observed in seven patients (87.5%), contributing to a ≥ 3+ degree of MR in five patients (62.5%).

Among these patients with HOCM, two cases of APM insertion were preoperatively detected using transthoracic echocardiography, with a sensitivity of 25%. CT was performed in seven patients, and MRI was available for six patients. However, only two and one cases of APM insertion were operatively detected, leading to sensitivities of 28.6% and 16.7% for CT and MRI, respectively. By reviewing the echocardiographic images, we observed a particular feature of APM insertion: the APM adhering to the leaflet looked like a lip nevus in the horizontal cross-section (**Figure 2** and **Supplementary Video S1**). By contrast, **Supplementary Video S2** shows the echocardiography findings for HOCM without APM insertion. The “lip nevus sign” was found in 62.5% (5/8) of patients.

The extended myectomy and APM resection procedures were successfully performed. In this series, the two eldest patients (a 62-year-old and 69-year-old) and one patient with midventricular obstruction underwent myectomy via a minimally invasive transmitral approach; they had concomitant mitral valve replacement. The other five patients underwent thoracotomy; one patient required coronary artery bypass grafting, one underwent ventricular aneurysmectomy, and one underwent posterior band annuloplasty with artificial chord implantation. The mean cardiopulmonary bypass time was 144.4 ± 31.9 min, and the aortic cross-clamp time was 82.9 ± 21.7 min. Postoperative ICU stay length was 2.6 (1.8, 4.5) days. Except for one case of persistent pleural effusion, there were no instances of death, reoperation, new-onset atrial fibrillation, permanent pacemaker implantation, or other adverse cardiovascular events before discharge. The postoperative echocardiography showed that IVS [17.0 (16.0, 23.3) mm vs. 13.3 (11.3, 14.0) mm, *P* = 0.012] and LVOTG [117.5 (82.3, 136.8) mmHg vs. 7.5 (5.0, 15.5) mmHg, *P* = 0.012] were significantly decreased. One patient had a residual mid-ventricular obstruction (55 mmHg) due to asymmetric mid-septal hypertrophy, which was difficult to resect via the transaortic approach. Postoperative ≥ 3+ MR and SAM were negative. Ejection fraction, left atrial diameter, and left ventricular diastolic diameter were 61.3% ± 7.9%, 35.9 ± 4.3 mm, and 38.9 ± 2.6 mm, respectively. The cutoff date for follow-up was 15 July 2023. All patients survived, without any reoperation or adverse events reported during the 26.2 ± 12.2 months follow-up period. Echocardiographic parameters remained consistent with the postoperative measurements—the LVOTG was 3.0 (1.0, 13.6) mmHg; three patients had no MR, while the other five patients remained 2+ MR; SAM disappeared in all cases. Left ventricular diastolic diameter exhibited a reduction due to the improvement in MR compared with the preoperative data (37.5 ± 3.2 mm vs. 42.6 ± 4.8 mm, *P* = 0.022).

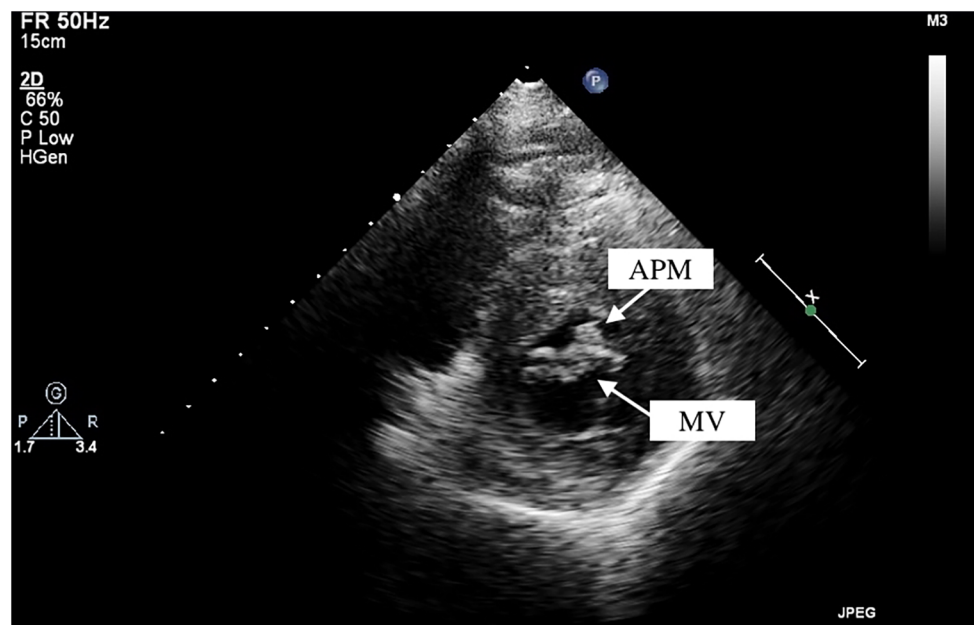


FIGURE 2
Anomalous papillary muscle (upper arrow) insertion into the mitral valve (lower arrow) visualized by transthoracic echocardiography. APM, anomalous papillary muscle; MV, mitral valve.

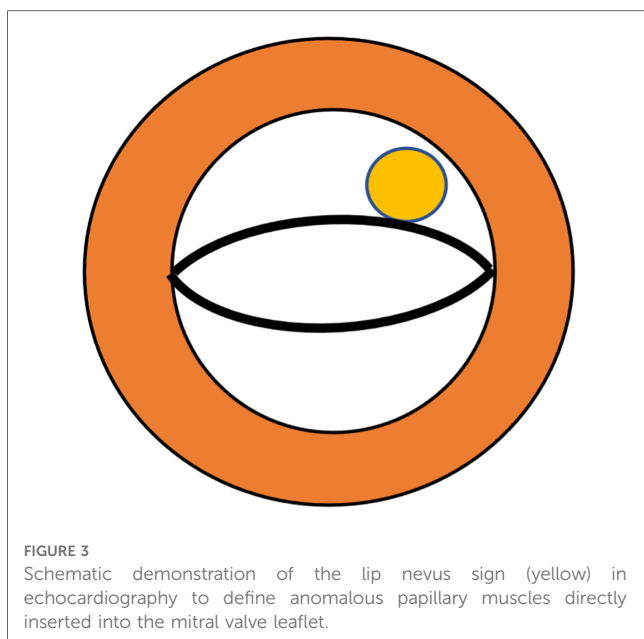
4. Discussion

HOCM with APM insertion is a rare phenotype that has mostly been described in case reports or series. The reported incidence of APM insertion ranges from 4% to 13% (9–11). Most studies on APM in HOCM have reported it to be a significant pathological component of dynamic obstruction (12–15). Although the papillary muscles and chordae tendineae have anatomical variations in origin sites, sizes, and number of bellies, the tendinous cords usually interconnect the mitral valve leaflet and papillary muscles; hence, such interposition affects the opening and closing of the mitral valve. Congenital failure of chordal development at 11–13 weeks of gestation leads to APM insertion into the mitral valve leaflets (16, 17). The APM (especially the anterolateral one) directly inserted into the mitral valve leaflet provides a rigid structure that occupies a cavity between the ventricular wall and the left ventricular outflow tract; therefore, it aggravates the gradient of the outflow tract or mid-ventricle during the systolic phase. In a severe case (18), a long and profoundly hypertrophied APM divides the ventricular cavity into two chambers. In addition to the space-occupying effect, abnormal fluid dynamics along the APM may cause shear stress and trigger fibrotic tissue growth in the septal wall, causing dynamic obstruction (19, 20). Carvalho et al. (11) reported the largest sample size ($N=73$) for APM insertion and categorized them into three types depending on the insertion site. Specifically, APM inserting directly into the body of the anterior leaflet, the free margin, or both, were classified as type I, III, and II, respectively. This classification system, along with the findings of the study, underscores the significance of type I and II APM in addition to myocardial hypertrophy, all of which collectively

influence treatment decisions (21, 22). Along with the APM insertion into the leaflet, the coexistence of other abnormalities, including accessory papillary muscles (most common), fusion to the ventricle wall/septum, hypertrophic papillary muscles, chordae slack, bifid papillary muscles, and APM anterior displacement, was found. These combinations also contribute to a dynamic obstruction, which requires concomitant surgical palliation.

SAM is a classical pathophysiological characteristic of HOCM, in which the anterior mitral valve leaflet is dragged into the outflow tract and comes into contact with the IVS. The factors contributing to SAM have been well studied and are divided into three categories: structural, geometric, and kinetic (23, 24). A bulging septum is the most common cause of SAM; however, APM, a subvalvular mitral valve apparatus anomaly, is another structural factor that independently promotes SAM. A fixed-length APM that is directly inserted into the anterior mitral valve leaflet tethers the leaflet itself; thus, the leaflet is anteriorly displaced toward the outflow tract, and the distance between the septum and the coaptation point is shortened. These anomalies finally result in SAM and MR, which even occurs in non-HOCM patients (25, 26).

Our primary finding is the “lip nevus sign” (Figure 3) in 2D-echocardiography, which has a high detection rate in our study, and could be used to identify the APM directly inserting into the mitral valve leaflet. Diagnosing APM demands a degree of expertise and knowledge about it. The diagnostic challenge is exacerbated by variations in the acoustic window, making it challenging to differentiate APM from a thickened free edge of the leaflet, hypertrophic chordae tendineae, or secondary papillary muscles. Consequently, there is a compelling need for a



distinctive visual feature in image examinations. In the short axis of the mitral valve, the anterior and posterior leaflets were similar to those of human lips. A circular muscular structure that tightly adheres to the leaflet constitutes the “lip nevus sign” as a characteristic ultrasound finding. In addition, in the apical four- or three-chamber view, a long muscular structure overriding the body of the mitral valve leaflet and the surrounding papillary muscles indicates APM insertion. Sonographers should regard APM detection as a regular step in the evaluation of HOCM. It is essential to observe the location, morphology, hypertrophy, and movement of the papillary muscles within the most lucid visual field attainable. The presence of restricted mitral leaflet mobility should prompt suspicion of APM as the aberrant attachment of the leaflet to a fixed structure (e.g., the ventricle wall) may be the underlying etiology. This will lead the examiner to perform detailed examination, even multimodality imaging (27). Furthermore, APM can be considered when the identified structural anomalies could not explain all the pathophysiological manifestations. For example, in the scenario of mild degree of septal hypertrophy but severe MR without mitral valve diseases, APM might be the factor exacerbating MR. Likewise, the dynamic obstruction mechanisms through APM insertion is most commonly and independently derived from its space-occupying effect instead of SAM (28). In our study cohort, HOCM patients with APM showed a significantly higher LVOT gradient than those without APM, suggesting that this could also serve as a diagnostic clue for APM. In a word, when cardiac ultrasound typically finds a mismatch between a large outflow gradient and a less serious SAM or septal hypertrophy, APM insertion should be considered. With these technical advantages, more APM insertions may be detected by echocardiography. In this study, we also found that APM insertion occurred frequently in the anterolateral group, with the insertion site at A2 or A3. Whether the precise insertion site has significant impacts on the dynamic change in HOCM remains an open question, necessitating further studies with a larger cohort.

In addition to echocardiography, MRI and CT are the main imaging modalities used for the diagnosis of APM insertion, which provide more details of the papillary muscles and mitral valve with higher resolution and multiplanar capabilities (13, 29, 30). A continuous muscular-like density structure between the mitral leaflet and ventricular free wall is a sign of APM insertion in three-dimensional images. However, this has usually been overlooked, as was found in our study. As previously described (31), the three-dimensional printing technique is an adjunct to common imaging examinations and helps surgeons achieve an intuitive visualization of APM insertion. It can not only identify the APM insertion preoperatively but also assist in surgical planning by providing more details such as the diameter of the APM and a simulated view of the surgical approach. Nevertheless, given the comparable sensitivity and popularity of echocardiography, these three-dimensional imaging modalities are not the principal examinations for all patients with HOCM (7).

APM insertion into the mitral valve leaflet usually requires excision to relieve the obstruction, unless it is inserted into the free edge of the mitral valve (32). In our experience, cutting off the APM does not affect valve movement. Both extended myectomy and APM dissociation from the mitral valve are necessary for the treatment of HOCM. Leaving any anomalies increases the risk of residual obstruction. Therefore, we performed the extended myectomy procedure as usual and sacrificed all the inserted APM. No secondary prolapse occurred, with normal papillary muscles and chordae tendineae preserved. Some studies have demonstrated feasible outcomes of APM insertion treated using mitral repair techniques (6, 33). Except in intrinsic mitral valve disease, the valve leaflet itself is less likely to cause obstruction or SAM. Our study provides additional clinical evidence supporting this finding. Further studies are recommended to determine the long-term effects of these two surgical tactics.

There are some limitations to this study that warrant consideration. First, the overall sample size of this cohort was small due to the low incidence rate of APM. Although the lip nevus sign is proven to be a practical and visualized feature in echocardiography, further studies with large sample sizes encompassing patients with and without HOCM are clearly needed to verify its prevalence, as well as the sensitivity and specificity. Second, the preoperative imaging examinations were performed and reported by doctors with different seniority; however, detection of APM lacks a standardized benchmark in imaging diagnostics instead of intraoperative exploration. Consequently, the reliability of such diagnoses relies on the experience of cardiac sonographers, which may introduce a bias in detection rates. Third, given that only eight patients were identified as having APM in this study, and the morphology and original sites displayed similarities, this helps us propose the concept of the lip nevus sign; however, it is hard to categorize them into subtypes. The surgical treatment for APM in this study involved a resection strategy only. Alternative treatments, such as shaving or mobilization APM, may be more appropriate depending on the subtypes; therefore, we are unable to conclude

what the optimal surgical strategy may be for each type of APM at this stage.

5. Conclusion

Papillary muscles inserted into the mitral valve leaflet are a subtype of subvalvular malformation in HOCM that requires surgical correction. The lip nevus sign on echocardiography is a characteristic of APM insertion and may improve the preoperative detection rate. Adequate myectomy with APM excision has achieved good results in reducing the outflow gradient and eliminating mitral regurgitation, with good outcomes at short-to-intermediate follow-up.

Data availability statement

The original contributions presented in the study are included in the article/**Supplementary Material**, further inquiries can be directed to the corresponding authors.

Ethics statement

The studies involving humans were approved by This study was granted by the Ethics Committee of Guangdong Provincial People's Hospital (KY-Q-2022-442-01). The studies were conducted in accordance with the local legislation and institutional requirements. Written informed consent for participation was not required from the participants or the participants' legal guardians/next of kin in accordance with the national legislation and institutional requirements.

Author contributions

JL: Conceptualization, Writing – original draft, Writing – review & editing. TT: Conceptualization, Writing – original draft, Writing – review & editing, Methodology. PW: Conceptualization, Methodology, Writing – original draft, Writing – review & editing. JM: Data curation, Formal Analysis, Writing – original draft. LZ: Data curation, Formal Analysis, Writing – original draft. HQ: Data curation, Formal Analysis, Writing – original draft. SW: Data

curation, Formal Analysis, Writing – original draft. JZ: Writing – review & editing. WZ: Writing – review & editing. HG: Supervision, Writing – review & editing. JC: Writing – review & editing.

Funding

The author(s) declare financial support was received for the research, authorship, and/or publication of this article.

This study was funded by the Science and Technology Planning Project of Guangdong Province (2020B1111170011), Science and Technology Program of Guangzhou (202201010768), Cardiovascular Special Project of Guangdong Provincial People's Hospital (2020XXG010), National Natural Science Foundation of Guangdong (2022A1515010157), Clinical High-Tech and Major Technologies of Guangzhou (2023P-ZD09), Guangdong Medical Science and Technology Research Fund Project (A2022269), and Guangdong special funds for Science and Technology Innovation Strategy, China (stability support for scientific research institutions affiliated to Guangdong Province-GDCI 2021).

Conflict of interest

The authors declare that the research was conducted in the absence of any commercial or financial relationships that could be construed as a potential conflict of interest.

Publisher's note

All claims expressed in this article are solely those of the authors and do not necessarily represent those of their affiliated organizations, or those of the publisher, the editors and the reviewers. Any product that may be evaluated in this article, or claim that may be made by its manufacturer, is not guaranteed or endorsed by the publisher.

Supplementary material

The Supplementary Material for this article can be found online at: <https://www.frontiersin.org/articles/10.3389/fcvm.2023.1292142/full#supplementary-material>

References

- Guigui SA, Torres C, Escolar E, Mihos CG. Systolic anterior motion of the mitral valve in hypertrophic cardiomyopathy: a narrative review. *J Thorac Dis.* (2022) 14 (6):2309–25. doi: 10.21037/jtd-22-182
- Sherrid MV, Balaram S, Kim B, Axel L, Swistel DG. The mitral valve in obstructive hypertrophic cardiomyopathy: a test in context. *J Am Coll Cardiol.* (2016) 67(15):1846–58. doi: 10.1016/j.jacc.2016.01.071
- Sherrid MV, Adams DH. The mitral valve in hypertrophic cardiomyopathy: other side of the outflow tract. *J Am Coll Cardiol.* (2020) 76(19):2248–51. doi: 10.1016/j.jacc.2020.09.580
- Achim A, Serban AM, Mot SDC, Leibundgut G, Marc M, Sigwart U. Alcohol septal ablation in hypertrophic cardiomyopathy: for which patients? *ESC Heart Fail.* (2023) 10(3):1570–9. doi: 10.1002/ehf2.14272
- Hodges K, Rivas CG, Aguilera J, Borden R, Alashi A, Blackstone EH, et al. Surgical management of left ventricular outflow tract obstruction in a specialized hypertrophic obstructive cardiomyopathy center. *J Thorac Cardiovasc Surg.* (2019) 157(6):2289–99. doi: 10.1016/j.jtcvs.2018.11.148
- Mutsuga M, Tokuda Y, Fujimoto K, Terazawa S, Ito H, Narita Y, et al. Surgery for anomalous papillary muscle directly into the anterior

- mitral leaflet. *Ann Thorac Surg.* (2021) 111(5):1512–8. doi: 10.1016/j.athoracsurg.2020.07.031
7. Ommen SR, Mital S, Burke MA, Day SM, Deswal A, Elliott P, et al. 2020 AHA/ACC guideline for the diagnosis and treatment of patients with hypertrophic cardiomyopathy: a report of the American college of cardiology/American heart association joint committee on clinical practice guidelines. *Circulation.* (2020) 142(25):e558–631. doi: 10.1161/CIR.0000000000000937
 8. Wei P, Ma J, Tan T, Zhu W, Yuan H, Zhuang J, et al. Thoracoscopic trans-mitral myectomy for hypertrophic obstructive cardiomyopathy: a retrospective single-centre study. *Eur J Cardiothorac Surg.* (2023) 63(4):ezac508. doi: 10.1093/ejcts/ezac508
 9. Klues HG, Maron BJ, Dollar AL, Roberts WC. Diversity of structural mitral valve alterations in hypertrophic cardiomyopathy. *Circulation.* (1992) 85(5):1651–60. doi: 10.1161/01.cir.85.5.1651
 10. Kadkhodayan A, Schaff HV, Eleid MF. Anomalous papillary muscle insertion in hypertrophic cardiomyopathy. *Eur Heart J Cardiovasc Imaging.* (2016) 17(5):588. doi: 10.1093/ehjci/jew007
 11. Carvalho JL, Schaff HV, Morris CS, Nishimura RA, Ommen SR, Maleszewski JJ, et al. Anomalous papillary muscles-implications in the surgical treatment of hypertrophic obstructive cardiomyopathy. *J Thorac Cardiovasc Surg.* (2022) 163(1):83–9 e1. doi: 10.1016/j.jtcvs.2020.04.007
 12. Klues HG, Roberts WC, Maron BJ. Anomalous insertion of papillary muscle directly into anterior mitral leaflet in hypertrophic cardiomyopathy. Significance in producing left ventricular outflow obstruction. *Circulation.* (1991) 84(3):1188–97. doi: 10.1161/01.cir.84.3.1188
 13. Yang HS, Lee KS, Chaliki HP, Tazelaar HD, Lusk JL, Chandrasekaran K, et al. Anomalous insertion of the papillary muscle causing left ventricular outflow obstruction: visualization by real-time three-dimensional echocardiography. *Eur J Echocardiogr.* (2008) 9(6):855–60. doi: 10.1093/ejehoccard/jen197
 14. Rowin EJ, Maron BJ, Lesser JR, Rastegar H, Maron MS. Papillary muscle insertion directly into the anterior mitral leaflet in hypertrophic cardiomyopathy, its identification and cause of outflow obstruction by cardiac magnetic resonance imaging, and its surgical management. *Am J Cardiol.* (2013) 111(11):1677–9. doi: 10.1016/j.amjcard.2013.01.340
 15. Minami Y, Kajimoto K, Terajima Y, Yashiro B, Okayama D, Haruki S, et al. Clinical implications of midventricular obstruction in patients with hypertrophic cardiomyopathy. *J Am Coll Cardiol.* (2011) 57(23):2346–55. doi: 10.1016/j.jacc.2011.02.033
 16. Wenink AC, Gittenberger-de Groot AC, Brom AG. Developmental considerations of mitral valve anomalies. *Int J Cardiol.* (1986) 11(1):85–101. doi: 10.1016/0167-5273(86)90202-0
 17. Lekovic A, Zivkovic V, Nikolic S. Anomalous papillary muscle insertion into mitral valve leaflet: autopsy study and implications. *J Forensic Sci.* (2023) 68(1):176–84. doi: 10.1111/1556-4029.15182
 18. Shah AS, Kukar A, Chaudhry FA, Sherrid MV. Unusual anomalous single papillary muscle causing symptomatic mid-left ventricular cavity obstruction: octopus papillary muscle. *J Am Soc Echocardiogr.* (2006) 19(7):939–9. doi: 10.1016/j.echo.2006.03.014
 19. Oliver JM, Gonzalez A, Gallego P, Sanchez-Recalde A, Benito F, Mesa JM. Discrete subaortic stenosis in adults: increased prevalence and slow rate of progression of the obstruction and aortic regurgitation. *J Am Coll Cardiol.* (2001) 38(3):835–42. doi: 10.1016/s0735-1097(01)01464-4
 20. Samura T, Toda K, Saito S, Miyagawa S, Yoshikawa Y, Fukushima S, et al. Midventricular obstruction caused by abnormal intra-left ventricular septum and papillary muscles. *Ann Thorac Surg.* (2017) 104(3):e247–9. doi: 10.1016/j.athoracsurg.2017.04.002
 21. Wei LM. Commentary: bringing conformity to anomaly. *J Thorac Cardiovasc Surg.* (2022) 163(1):92–3. doi: 10.1016/j.jtcvs.2020.05.027
 22. Blitzer D, Nguyen S, Takayama H. Commentary: going beyond the septum for complete repair of obstructive hypertrophic cardiomyopathy. *J Thorac Cardiovasc Surg.* (2022) 163(1):90–1. doi: 10.1016/j.jtcvs.2020.04.047
 23. Ibrahim M, Rao C, Ashrafian H, Chaudhry U, Darzi A, Athanasiou T. Modern management of systolic anterior motion of the mitral valve. *Eur J Cardiothorac Surg.* (2012) 41(6):1260–70. doi: 10.1093/ejcts/ezr232
 24. Manabe S, Kasegawa H, Arai H, Takanashi S. Management of systolic anterior motion of the mitral valve: a mechanism-based approach. *Gen Thorac Cardiovasc Surg.* (2018) 66(7):379–89. doi: 10.1007/s11748-018-0915-0
 25. Korabathina R, Chiu K, van Gelder HM, Labovitz A. Anomalous papillary muscle insertion causing dynamic left ventricular outflow tract obstruction without hypertrophic obstructive cardiomyopathy. *Case Rep Cardiol.* (2017) 2017:9878049. doi: 10.1155/2017/9878049
 26. Patel P, Dhillon A, Popovic ZB, Smedira NG, Rizzo J, Thamilarasan M, et al. Left ventricular outflow tract obstruction in hypertrophic cardiomyopathy patients without severe septal hypertrophy: implications of mitral valve and papillary muscle abnormalities assessed using cardiac magnetic resonance and echocardiography. *Circ Cardiovasc Imaging.* (2015) 8(7):e003132. doi: 10.1161/CIRCIMAGING.115.003132
 27. Nalawade D, Borikar N, Bawaskar P, Chaurasia A. Anomalous papillary muscle insertion as a cause of mitral regurgitation: multimodality imaging-based diagnosis. *Circ Cardiovasc Imaging.* (2020) 13(12):e010592. doi: 10.1161/CIRCIMAGING.120.010592
 28. Kwon DH, Setser RM, Thamilarasan M, Popovic ZV, Smedira NG, Schoenhagen P, et al. Abnormal papillary muscle morphology is independently associated with increased left ventricular outflow tract obstruction in hypertrophic cardiomyopathy. *Heart.* (2008) 94(10):1295–301. doi: 10.1136/hrt.2007.118018
 29. Kang E-J, Lee J, Lee K-N. Incidental finding on cardiac CT of anomalous anterior papillary muscle without left ventricular outflow obstruction: a case report. *J Korean Soc Radiol.* (2016) 74(3):195–8. doi: 10.3348/jksr.2016.74.3.195
 30. Rajiah P, Fulton NL, Bolen M. Magnetic resonance imaging of the papillary muscles of the left ventricle: normal anatomy, variants, and abnormalities. *Insights Imaging.* (2019) 10(1):83. doi: 10.1186/s13244-019-0761-3
 31. Wei P, Liu J, Zhuang W, Guo H. Identification of anomalous anterior papillary muscle insert directly into mitral leaflet in a patient with hypertrophic obstructive cardiomyopathy. *J Card Surg.* (2022) 37(1):236–7. doi: 10.1111/jocs.16115
 32. Nguyen A, Schaff HV. Surgical myectomy: subaortic, midventricular, and apical. *Cardiol Clin.* (2019) 37(1):95–104. doi: 10.1016/j.ccl.2018.08.006
 33. Minakata K, Dearani JA, Nishimura RA, Maron BJ, Danielson GK. Extended septal myectomy for hypertrophic obstructive cardiomyopathy with anomalous mitral papillary muscles or chordae. *J Thorac Cardiovasc Surg.* (2004) 127(2):481–9. doi: 10.1016/j.jtcvs.2003.09.040



OPEN ACCESS

EDITED BY

Sanjeev Bhattacharyya,
Barts Heart Centre, United Kingdom

REVIEWED BY

Yosef Manla,
Cleveland Clinic Abu Dhabi,
United Arab Emirates
Johannes Schwaiger,
District Hospital of St. Johann in Tirol, Austria
Antonio De Luca,
Azienda Sanitaria Universitaria Giuliano
Isontina, Italy

*CORRESPONDENCE

Vidhu Anand
✉ anand.vidhu@mayo.edu

RECEIVED 04 September 2023

ACCEPTED 11 December 2023

PUBLISHED 11 January 2024

CITATION

Anand V, Covington MK, Saraswati U,
Scott CG, Lee AT, Frantz RP, Anavekar NS,
Geske JB, Arruda-Olson AM and Klarich KW
(2024) Prevalence, sex differences, and
implications of pulmonary hypertension in
patients with apical hypertrophic
cardiomyopathy.
Front. Cardiovasc. Med. 10:1288747.
doi: 10.3389/fcvm.2023.1288747

COPYRIGHT

© 2024 Anand, Covington, Saraswati, Scott,
Lee, Frantz, Anavekar, Geske, Arruda-Olson
and Klarich. This is an open-access article
distributed under the terms of the [Creative
Commons Attribution License \(CC BY\)](#). The
use, distribution or reproduction in other
forums is permitted, provided the original
author(s) and the copyright owner(s) are
credited and that the original publication in
this journal is cited, in accordance with
accepted academic practice. No use,
distribution or reproduction is permitted
which does not comply with these terms.

Prevalence, sex differences, and implications of pulmonary hypertension in patients with apical hypertrophic cardiomyopathy

Vidhu Anand^{1*}, Megan K. Covington¹, Ushasi Saraswati¹,
Christopher G. Scott², Alexander T. Lee², Robert P. Frantz¹,
Nandan S. Anavekar¹, Jeffrey B. Geske¹,
Adelaide M. Arruda-Olson¹ and Kyle W. Klarich¹

¹Department of Cardiovascular Medicine, Mayo Clinic, Rochester, MN, United States, ²Department of Quantitative Health Sciences, Mayo Clinic, Rochester, MN, United States

Introduction: Apical hypertrophic cardiomyopathy (ApHCM) is a subtype of hypertrophic cardiomyopathy (HCM) that affects up to 25% of Asian patients and is not as well understood in non-Asian patients. Although ApHCM has been considered a more “benign” variant, it is associated with increased risk of atrial and ventricular arrhythmias, apical thrombi, stroke, and progressive heart failure. The occurrence of pulmonary hypertension (PH) in ApHCM, due to elevated pressures on the left side of the heart, has been documented. However, the exact prevalence of PH in ApHCM and sex differences remain uncertain.

Methods: We sought to evaluate the prevalence, risk associations, and sex differences in elevated pulmonary pressures in the largest cohort of patients with ApHCM at a single tertiary center. A total of 542 patients diagnosed with ApHCM were identified using ICD codes and clinical notes searches, confirmed by cross-referencing with cardiac MRI reports extracted through Natural Language Processing and through manual evaluation of patient charts and imaging records.

Results: In 414 patients, echocardiogram measurements of pulmonary artery systolic pressure (PASP) were obtained at the time of diagnosis. The mean age was 59.4 ± 16.6 years, with 181 (44%) being females. The mean PASP was 38 ± 12 mmHg in females vs. 33 ± 9 mmHg in males ($p < 0.0001$). PH as defined by a PASP value of > 36 mmHg was present in 140/414 (34%) patients, with a predominance in females [79/181 (44%)] vs. males [61/233 (26%), $p < 0.0001$]. Female sex, atrial fibrillation, diagnosis of congestive heart failure, and elevated filling pressures on echocardiogram remained significantly associated with PH (PASP > 36 mmHg) in multivariable modeling. PH, when present, was independently associated with mortality [hazard ratio 1.63, 95% CI (1.05–2.53), $p = 0.028$] and symptoms [odds ratio 2.28 (1.40, 3.71), $p < 0.001$].

Abbreviations

ApHCM, apical hypertrophic cardiomyopathy; PH, pulmonary hypertension; PASP, pulmonary artery systolic pressure; TTE, transthoracic echocardiogram.

Conclusion: PH was present in 34% of patients with ApHCM at diagnosis, with female sex predominance. PH in ApHCM was associated with symptoms and increased mortality.

KEYWORDS

apical hypertrophic cardiomyopathy, pulmonary hypertension, pulmonary artery systolic pressure, sex differences, all-cause mortality

Introduction

Apical hypertrophic cardiomyopathy (ApHCM) is a subtype of hypertrophic cardiomyopathy (HCM) with hypertrophy localized to the left ventricular (LV) apex. The estimated prevalence rate among patients with HCM varies from 25% in the Asian population to 1%–10% in the non-Asian population (1, 2). Patients with ApHCM have a widely variable clinical presentation, ranging from being asymptomatic with a normal lifespan to being symptomatic with dyspnea, reduced exercise capacity, chest pain, atrial fibrillation, heart failure, thromboembolic events, and ventricular arrhythmias, or experiencing sudden cardiac death (2–5). The development of an apical pouch and aneurysm is known to have negative prognostic effect, predisposing to both ventricular arrhythmias and intracardiac thrombus formation (4, 6, 7).

Pulmonary hypertension (PH) is prevalent in HCM, with an estimated prevalence rate of 38% by echocardiography (8). It has been shown that older age and systolic dysfunction are independent risk factors for developing PH in HCM (9). Another case–control study found female sex, moderate or greater mitral regurgitation, and atrial fibrillation as independent risk factors for PH beyond the effect of age (10). The prevalence of PH was similar in obstructive and non-obstructive HCM in one study (8), and it was higher in obstructive and end-stage HCM in another (9). Despite the slight differences in prevalence, PH was an independent predictor of mortality in patients with both obstructive and non-obstructive HCM (8, 9, 11). A high prevalence of PH by echocardiography in ApHCM with a female predominance has been described, but the study was not designed to evaluate the risk associations and implications of PH (7). Therefore, in this study, we sought to evaluate the prevalence, sex differences, and risk associations of PH in ApHCM and to assess the prognostic implications of PH in a large cohort of patients with isolated ApHCM at a single referral center in the United States.

Methods

Patient population

This study was approved by the institutional review board and deemed exempt. All patients provided consent to the use of their data for research. A total of 542 patients diagnosed with ApHCM were identified by using ICD-9/10 codes and a search of text contained within clinical notes. The diagnosis was further confirmed by cross-referencing with cardiac MRI reports extracted

through Natural Language Processing, as well as through manual review of patient charts, echocardiograms, and cardiac MRIs from January 1999 to May 2018. ApHCM was defined on imaging as the presence of apical wall thickness measuring ≥ 15 mm or ≥ 13 mm in individuals with a positive family history or positive genetic mutation. Patients with other patterns of LV hypertrophy without clear apical predominance (reverse curve, sigmoid, neutral septum), infiltrative cardiomyopathies including amyloidosis, Fabry disease, or secondary causes of LV hypertrophy including hypertensive heart disease were excluded. Patients with eosinophilic heart disease/eosinophilic myocarditis were also excluded after conducting a careful review of their cardiac MRI and pathology results when available. While patients with hypertensive heart disease were excluded, those with ApHCM and a concomitant diagnosis of hypertension were not excluded (12). All included patients underwent a comprehensive transthoracic echocardiography (TTE), and the initial study that diagnosed ApHCM was used for analysis. Baseline characteristics recorded at the time of index TTE, including demographic data, diagnosis of congestive heart failure and comorbidities determined from ICD codes, and Charlson comorbidity index, were extracted from the electronic medical records. The New York Heart Association (NYHA) functional class and the presence of symptoms (NYHA functional classes II–IV) were manually abstracted by review of charts. The vital status was retrieved using the Mayo Clinic records. Patients not known to be deceased were censored at the date of the last follow-up.

Echocardiography

Echocardiographic assessment was reported by Level 3 trained echocardiographer, and data included LV linear dimensions and ejection fraction, mitral inflow early/late diastolic velocity (E/A), mitral annular early tissue Doppler velocity (e'), medial E/ e' (surrogate of elevated filling pressures), left atrial volume index, pulmonary artery systolic pressure (PASP), estimated right atrial pressure, RV size, and RV systolic function. Pulmonary hypertension was defined as none (PASP < 36 mmHg), mild-to-moderate (PASP 36–59 mmHg), and severe (PASP ≥ 60 mmHg). The PASP was evaluated from the highest (or average of five cardiac cycles in patients with atrial fibrillation or significant respiratory variation) and most complete signal of tricuspid regurgitation from the RV inflow, parasternal short axis, and apical views using modified Bernoulli equation as $4v^2 +$ estimated right atrial pressure, where v is the velocity of the tricuspid regurgitation jet in m/s. The right atrial pressure was estimated

based on the size and collapse of the inferior vena cava as follows: 5 mmHg when it displayed both normal size and collapse, 10 mmHg when it was either enlarged or had reduced collapse, 15 mmHg when it was both enlarged and had reduced collapse, and 20 mmHg when it was enlarged with no collapse. The RV was considered enlarged if its size exceeded mild enlargement, and its function was categorized as reduced if it was more than mildly reduced. RV size and function assessments, as specified in the echocardiographic reports, primarily included qualitative evaluations and, when available, quantitative measures (available in less than 50% of the patients).

Outcomes

The primary outcome was the prevalence of PH in patients with ApHCM, sex differences in the same, and impact of PH on all-cause mortality. The secondary outcomes were the risk associations of PH and the impact of PH on symptoms.

Statistical analysis

Data are presented as frequencies and percentages for categorical variables, and as mean with standard deviation (SD) for approximately normally distributed continuous variables or median and quartiles for those that were not. Chi-square test was used to compare the categorical variables and *t*-test or Kruskal–Wallis for continuous variables, as appropriate. The survival curves were constructed using the Kaplan–Meier method, and the groups of PH patients were compared using the log-rank test. Cox proportional hazards regression was used to examine the association between PH and all-cause mortality after adjusting for other factors noted to be significant in the univariate analysis. These results are presented as hazard ratios (HR) with 95% confidence intervals (CI). Multivariable models were created using backward selection starting from those variables that were significant in the univariate analyses. Logistic regression was used to examine the factors associated with PH and to assess the association between PH and symptoms, and these results are presented in terms of odds ratios (OR) and 95% CI. The model assumptions were checked graphically to ensure that no violations were noted. The risk for mortality by PASP was illustrated graphically after fitting the PASP using penalized smoothing splines, and Youden's *J* index was used to identify the optimal cut point for this association. All analyses were performed using SAS version 9.4 (SAS Institute, Inc. Cary, NC, USA), and a *p*-value of <0.05 was considered statistically significant.

Results

The study cohort consisted of 414/542 (76%) patients who had a sufficient tricuspid regurgitation Doppler signal for estimating PASP. The mean age was 59.4 ± 16.6 years, with 181 (44%) being females. Among the patients, 184 (47%) had hypertension, 41

(10%) had diabetes, 39 (10%) had a diagnosis of coronary artery disease, and 21 (5%) had prior myocardial infarction (Table 1). In terms of history of ventricular arrhythmias, 34 (9%) patients had ventricular tachycardia, seven (2%) had ventricular fibrillation, and three (1%) had prior cardiac arrest. The baseline characteristics are presented in Table 1. Pulmonary hypertension was present in 140 (34%) patients, with a higher prevalence in females ($n = 79/181$, 44%) than males ($n = 61/233$, 26%), $p < 0.001$ (Figure 1). Severe PH was present in 10 (2%) patients with a higher prevalence in females than males [seven (4%) vs. three (1%), $p = 0.001$]. The baseline characteristics of males and females are presented separately in Supplementary Table S1. The univariate factors associated with PH were found to be age, female sex, moderate or greater MR, larger left atrial volume index, higher medial E/e' , atrial fibrillation, diagnosis of congestive heart failure, and Charlson comorbidity index. MR etiology included annular dilatation (atrial functional MR) in 11 patients, mitral valve prolapse in one patient, and annular dilatation along with significant mitral annulus calcification in one patient. In the multivariable model, female sex [OR 1.88 (1.17, 3.04), $p = 0.009$], medial $E/e' > 15$ [OR 2.06 (1.22, 3.49), $p = 0.007$], atrial fibrillation [OR 2.09 (1.09, 4.01), $p = 0.026$], and a diagnosis of congestive heart failure [OR 2.48 (1.28, 4.81), $p = 0.007$] remained independently associated with PH (Table 2). In another model, when left atrial volume index was substituted for medial E/e' , it was also observed to have a statistically significant correlation (Supplementary Table S2).

Mortality was assessed over a median of 4.4 years (IQR: 0.1–10.7). The spline curves analysis showed that the risk of death started to rise continuously after the PASP reached a level between 35 and 36 mmHg for the whole cohort (Figure 2), and in males and females separately (Supplementary Figures S1A and B). Therefore, PASP of 36 mmHg was used as a cutoff, and PH (PASP > 36 mmHg) was associated with higher all-cause mortality in the univariate and multivariable analysis [HR for PH 1.63, 95% CI (1.05–2.53), $p = 0.028$] (Table 3 and Figure 3). Other independent factors associated with mortality were female sex [HR 1.88, 95% CI (1.20, 2.96), $p = 0.006$] and Charlson comorbidity index [HR 1.10, 95% CI (1.03, 1.18), $p = 0.005$] (Table 3). The correlation between PH and higher mortality was observed in both males and females (Supplementary Figures S2A, B). However, after adjusting for other factors, this correlation became non-significant ($p = 0.08$) for females.

PH, when present, was also found to be independently associated with symptoms (NYHA functional Class II–IV) [OR 2.28, 95% CI (1.40, 3.71), $p < 0.001$] in addition to the diagnosis of congestive heart failure [OR 5.01, 95% CI (2.30, 10.89), $p < 0.001$] (Table 4). PH was also independently associated with the presence of significant symptoms (NYHA Class III and IV) [OR 2.73 (1.60, 4.64), $p < 0.001$].

Discussion

This study, which involved a large cohort of patients with ApHCM, has identified several significant findings: (1) PH as

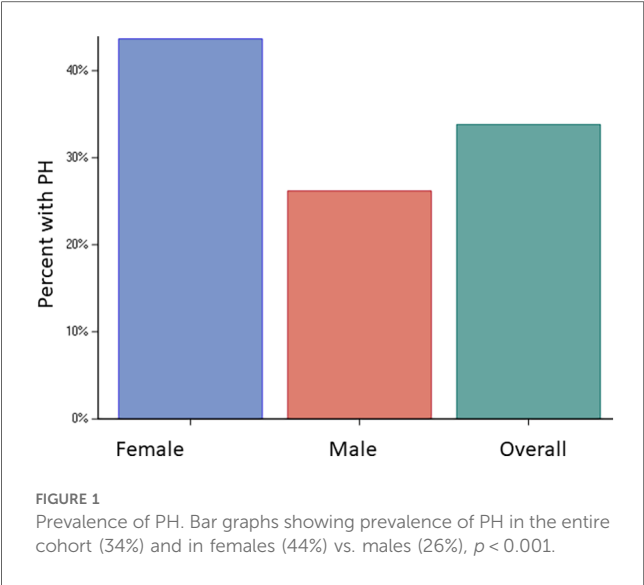
TABLE 1 Baseline characteristics.

Variables	Total (N = 414)	No PH (N = 274)	PH (N = 140)	p-value
Age	59.4 (16.63)	56.7 (16.62)	64.7 (15.39)	<0.001
Female sex, <i>n</i> (%)	181 (43.7%)	102 (37.2%)	79 (56.4%)	<0.001
Race, <i>n</i> (%)				0.708
White	341 (82.4%)	226 (82.5%)	115 (82.1%)	
Black	20 (4.8%)	13 (4.7%)	7 (5.0%)	
Asian	17 (4.1%)	12 (4.4%)	5 (3.6%)	
Choose not to disclose	4 (1.0%)	4 (1.5%)	0 (0.0%)	
Other	9 (2.2%)	5 (1.8%)	4 (2.9%)	
Unknown	23 (5.6%)	14 (5.1%)	9 (6.4%)	
Body mass index	28.3 (5.20)	28.4 (5.25)	28.1 (5.11)	0.655
Heart rate (<i>n</i> = 408)	63.9 (11.97)	63.5 (11.49)	64.8 (12.85)	0.299
Systolic blood pressure (<i>n</i> = 410)	124.2 (19.41)	122.6 (18.96)	127.5 (19.97)	0.017
Atrial fibrillation, <i>n</i> (%) (<i>n</i> = 396)	58 (14.6%)	25 (9.5%)	33 (25.0%)	<0.001
Prior myocardial infarction, <i>n</i> (%) (<i>n</i> = 395)	21 (5.3%)	9 (3.5%)	12 (8.9%)	0.023
Congestive heart failure, <i>n</i> (%) (<i>n</i> = 395)	57 (14.4%)	21 (8.1%)	36 (26.7%)	<0.001
Ventricular tachycardia, <i>n</i> (%) (<i>n</i> = 395)	34 (8.6%)	25 (9.6%)	9 (6.7%)	0.322
Ventricular fibrillation, <i>n</i> (%) (<i>n</i> = 395)	7 (1.8%)	5 (1.9%)	2 (1.5%)	0.752
Cardiac arrest, <i>n</i> (%) (<i>n</i> = 395)	3 (0.8%)	1 (0.4%)	2 (1.5%)	0.234
PVC, <i>n</i> (%) (<i>n</i> = 395)	29 (7.3%)	23 (8.8%)	6 (4.4%)	0.112
Transient ischemic attack, <i>n</i> (%) (<i>n</i> = 395)	22 (5.6%)	12 (4.6%)	10 (7.4%)	0.251
Ischemic stroke, <i>n</i> (%) (<i>n</i> = 395)	18 (4.6%)	14 (5.4%)	4 (3.0%)	0.274
Hypertension, <i>n</i> (%) (<i>n</i> = 395)	184 (46.6%)	113 (43.5%)	71 (52.6%)	0.084
Diabetes, <i>n</i> (%) (<i>n</i> = 395)	41 (10.4%)	25 (9.6%)	16 (11.9%)	0.489
Chronic kidney disease, <i>n</i> (%) (<i>n</i> = 395)	10 (2.5%)	7 (2.7%)	3 (2.2%)	0.778
Lung disease, <i>n</i> (%) (<i>n</i> = 395)	50 (12.7%)	27 (10.4%)	23 (17.0%)	0.059
Coronary artery disease, <i>n</i> (%) (<i>n</i> = 395)	39 (9.9%)	24 (9.2%)	15 (11.1%)	0.552
Charlson Index, median (Q1, Q3) (<i>n</i> = 395)	2 (0, 6)	1 (0, 4.5)	2 (1, 7)	0.002
LV ejection fraction	66.8 (6.40)	67.0 (5.51)	66.5 (7.86)	0.450
Diastolic dysfunction grade, <i>n</i> (%) (<i>n</i> = 126)				0.006
Normal	14 (11.1%)	12 (15.2%)	2 (4.3%)	
1 (normal filling pressures)	21 (16.7%)	17 (21.5%)	4 (8.5%)	
1a (mildly elevated filling pressures with A-predominant mitral inflow)	13 (10.3%)	11 (13.9%)	2 (4.3%)	
2 (mild-moderately elevated filling pressures)	32 (25.4%)	18 (22.8%)	14 (29.8%)	
3+ (severely elevated filling pressures)	7 (5.6%)	2 (2.5%)	5 (10.6%)	
Indeterminate	39 (31.0%)	19 (24.1%)	20 (42.6%)	
Medial <i>e'</i> (<i>n</i> = 366)	0.06 (0.07)	0.07 (0.09)	0.05 (0.02)	<0.001
Medial <i>E/e'</i> , median (Q1, Q3)	12 (10, 16)	12 (10, 15)	14 (12, 18)	<0.001
Medial <i>E/e'</i> >15, <i>n</i> (%)	108 (26.1%)	55 (20.1%)	53 (37.9%)	<0.001
<i>E/A</i> , median (Q1, Q3) (<i>n</i> = 340)	1.3 (0.9, 1.8)	1.2 (0.9, 1.8)	1.5 (1.0, 2.0)	0.009
RV <i>S'</i> (<i>n</i> = 200)	0.12 (0.03)	0.12 (0.02)	0.12 (0.04)	0.893
TAPSE (<i>n</i> = 59)	20.0 (5.38)	20.0 (3.50)	20.0 (7.17)	0.962
PASP	35.1 (10.56)	29.0 (4.24)	47.0 (8.89)	<0.001
PASP, <i>n</i> (%)				<0.001
≤36	274 (66.2%)	274 (100.0%)	0 (0.0%)	
37–60	130 (31.4%)	0 (0.0%)	130 (92.9%)	
>60	10 (2.4%)	0 (0.0%)	10 (7.1%)	
RV enlargement present, <i>n</i> (%) (<i>n</i> = 242)	14 (5.8%)	3 (2.0%)	11 (12.0%)	0.001
RV function reduced, <i>n</i> (%) (<i>n</i> = 73)	16 (21.9%)	3 (7.3%)	13 (40.6%)	<0.001
Right atrial pressure, median (Q1, Q3) (<i>n</i> = 407)	5 (5, 5)	5 (5, 5)	10 (5, 10)	<0.001
LA volume index (<i>n</i> = 349)	41.3 (16.21)	36.4 (11.07)	51.5 (20.06)	<0.001
Max. instantaneous intracavitary gradient (<i>n</i> = 102)	27.3 (16.75)	27.6 (18.24)	26.7 (13.13)	0.803
≥moderate mitral regurgitation, <i>n</i> (%) (<i>n</i> = 405)	13 (3.2%)	3 (1.1%)	10 (7.3%)	<0.001

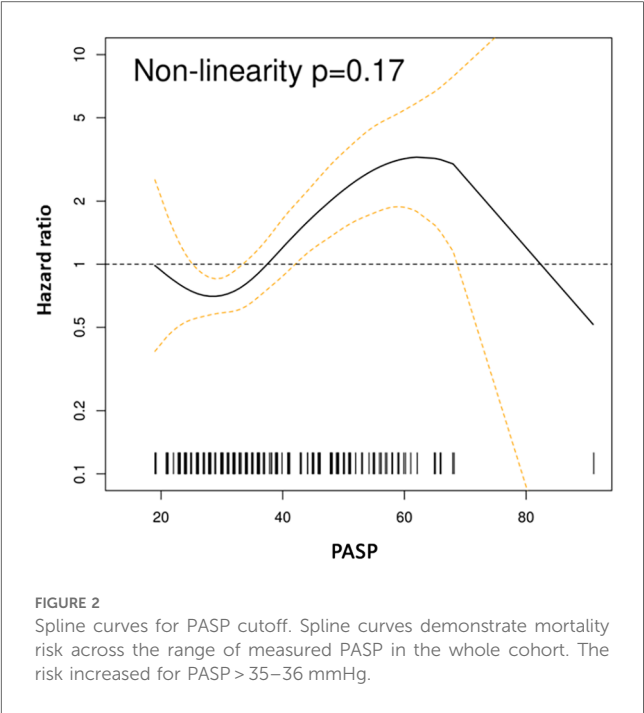
PVC, premature ventricular contraction; LV, left ventricle; *E/e'*, mitral early inflow diastolic/mitral annulus early tissue Doppler velocity; *E/A*, mitral inflow early/late diastolic velocity; PASP, pulmonary artery systolic pressure; RV, right ventricle; LA, left atrium.

defined by a PASP value of > 36 mmHg on TTE was present in one-third of the patients, (2) female sex, atrial fibrillation, diagnosis of congestive heart failure, and elevated filling pressures were

independently associated with PH in ApHCM patients, and (3) PH, when present, was associated with worse symptoms and higher all-cause mortality even after adjusting for known risk factors.



ApHCM is an understudied variant of HCM characterized by hypertrophy localized to the LV apex. It was previously considered “benign” due to the absence of obstruction, but studies have shown an increased risk of heart failure, arrhythmias, thromboembolic events, and death (4, 6, 7, 13). Although dynamic LV outflow tract obstruction is infrequent in ApHCM, elevated filling pressures due to diastolic dysfunction are frequently observed (7, 13–15) and serve as a mechanism for PH. In HCM, PH is thought to be post-capillary initially, and then over time, develop pre-capillary remodeling, leading to combined pre- and post-capillary PH (8, 9, 11). When present, PH is associated with worse outcomes in both patients with obstructive and non-obstructive HCM (8–11); however, there has



been no specific research of the prevalence, risk associations, and implications of PH in ApHCM.

This study found a high prevalence of PH in up to one-third of patients with ApHCM. The results are similar to the reported prevalence rate of 38% in patients with other subtypes of HCM (predominantly septal, reverse-curve, neutral) using similar echocardiographic criteria (8). The factors associated with PH in ApHCM patients were found to be female sex, atrial fibrillation, diagnosis of congestive heart failure, and elevated filling pressures

TABLE 2 Univariate and multivariable analyses of factors associated with PH.

Variable	Univariate logistic regression		Multivariable logistic regression (N missing = 45)	
	Odds ratio (95% CI)	p-value	Odds ratio (95% CI)	p-value
Age	1.03 (1.02, 1.05)	<0.001	1.02 (1.00, 1.03)	0.073
Female sex	2.18 (1.44, 3.30)	<0.001	1.88 (1.17, 3.04)	0.009
Coronary artery disease	1.23 (0.62, 2.43)	0.553		
Hypertension	1.44 (0.95, 2.19)	0.085		
Chronic kidney disease	0.82 (0.21, 3.23)	0.778		
Diabetes	1.26 (0.65, 2.46)	0.490		
Lung disease	1.77 (0.97, 3.23)	0.062		
≥Moderate MR	6.95 (1.88, 25.69)	0.004	3.40 (0.81, 14.23)	0.094
LV ejection fraction	0.99 (0.96, 1.02)	0.450		
Medial E/e' > 15	2.43 (1.54, 3.81)	<0.001	2.06 (1.22, 3.49)	0.007
LA volume index	1.08 (1.06, 1.10)	<0.001		
LVOT MIG	1.02 (0.99, 1.05)	0.212		
Intracavitary MIG	0.997 (0.97, 1.02)	0.801		
Atrial fibrillation	3.19 (1.80, 5.64)	<0.001	2.09 (1.09, 4.01)	0.026
Congestive heart failure	4.14 (2.30, 7.44)	<0.001	2.48 (1.28, 4.81)	0.007
Charlson comorbidity index	1.09 (1.02, 1.16)	0.008	1.06 (0.99, 1.14)	0.103

MR, mitral regurgitation; LV, left ventricle; E/e', mitral early inflow diastolic/mitral annulus early tissue Doppler velocity; LA, left atrial; LVOT, left ventricular outflow tract; MIG, maximal instantaneous gradient.

TABLE 3 Multivariable analysis of factors associated with mortality.

Multivariable cox regression (N missing = 19)		
Variable	Hazard ratio (95% CI)	p-value
Pulmonary hypertension	1.63 (1.05, 2.53)	0.028
Age	1.01 (0.998, 1.03)	0.083
Female sex	1.88 (1.20, 2.96)	0.006
Charlson comorbidity index	1.10 (1.03, 1.18)	0.005
Medial E/e' > 15	1.43 (0.88, 2.32)	0.148

E/e', mitral early inflow diastolic/mitral annulus early tissue Doppler velocity.

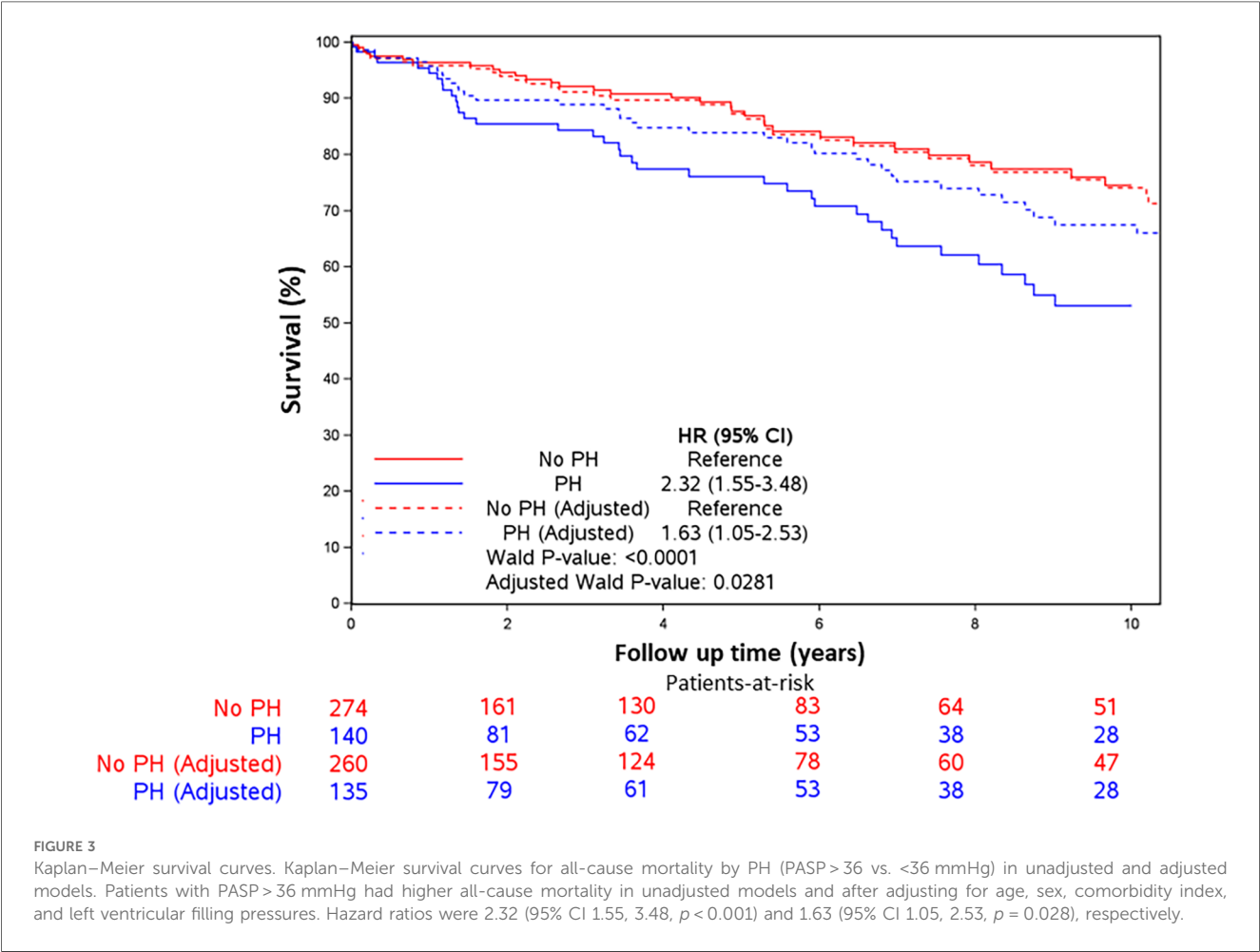
on echocardiogram, similar to what has been previously reported in non-selected HCM cohorts (8–10). The association between elevated filling pressures on echocardiogram (medial E/e') and a larger left atrial volume index, which reflects long-standing elevated left-sided filling pressures, suggests a group 2 mechanism of PH. Although a systematic approach to defining PH etiology was not performed in this retrospective assessment, a thorough chart review did not reveal alternative etiologies of PH. There are data showing worse outcomes in females with HCM (16, 17), and data herein clarify that this relationship persists in patients with ApHCM (7).

PH, when present, was independently associated with all-cause mortality, with other significant factors being female sex and

TABLE 4 Multivariable analysis of factors associated with symptoms (NYHA Class II–IV).

Multivariable logistic regression (N missing = 48)		
Variable	Odds ratio (95% CI)	p-value
Pulmonary hypertension	2.28 (1.40, 3.71)	<0.001
Age	0.99 (0.98, 1.01)	0.394
Female sex	1.21 (0.77, 1.90)	0.406
Congestive heart failure	5.01 (2.30, 10.89)	<0.001
Charlson comorbidity index	0.99 (0.92, 1.06)	0.708

Charlson comorbidity index. In the spline curve analysis, there was a continuous increase in the risk of mortality above a cutoff of PASP > 35–36 mmHg. This cutoff corresponds to a mean PA pressure of 25 mmHg, is recommended by the society guidelines for detecting PH with high sensitivity, and is previously shown to be associated with an increased risk of death in non-obstructive and obstructive HCMs without prior septal reduction treatment (8, 18, 19). PH has been shown to be associated with worse outcomes in left-sided heart disease including heart failure with a reduced and preserved ejection fraction and left-sided valve diseases (20). There are a few studies including one large study with over 1,500 patients showing worse outcomes



associated with PH in patients with HCM (8–11), and to our knowledge, the current study is the first to systematically evaluate the prognostic significance of PH in patients with an apical subtype of HCM.

The novel myosin inhibitor, Mavacamten, was recently evaluated in a phase 2 trial (MAVERICK-HCM), which included a small group of patients with non-obstructive HCM (21). The study found that the treatment was well tolerated by the majority of patients and was associated with a reduction in cardiac biomarkers, indicating a decrease in wall stress. Mavacamten is currently under further investigation to assess improvements in clinical parameters (22). In addition, there is a need to explore its effects in patients with ApHCM.

Limitations

Our study has several limitations—retrospective study design, single-center experience, and unavailability of TR jet to estimate PASP in approximately 25% of the patients from the original cohort which may change the true prevalence of PH in this population. The retrospective design limits the assessment of predictors, and only risk associations can be determined. The interobserver agreement of echocardiographic measurements is unavailable, but it is unlikely to affect the study results. Hemodynamic right heart catheterization, labs (autoimmune antibodies, NT-pro brain natriuretic peptide), pulmonary function tests, and ventilation perfusion scan were unavailable in most patients, which limits the exact characterization of the type (pre-capillary, post-capillary, or combined pre- and post-capillary) and etiology of PH (13). However, a systematic chart review of this large cohort did not reveal an obvious alternate etiology of PH in these patients. Some comorbidities, such as coronary artery disease and lung disease, could also potentially be associated with PH. However, the proportion of patients with these comorbidities was small, and their association with PH was not significant in the univariate analyses. Genetic testing for sarcomere mutations was not routinely available due to the retrospective nature of the study; therefore, genetic associations could not be tested.

Conclusions

The present study shows a high prevalence rate of PH of 34% as determined by echocardiography in patients with ApHCM, with significantly higher prevalence in females vs. males (44% vs. 26%). The factors associated with PH were found to be female sex, atrial fibrillation, diagnosis of congestive heart failure, and elevated filling pressures on echocardiogram. PH when present was associated with both worse symptoms and higher all-cause mortality. There is a need for larger prospective studies to further evaluate the sex differences in PH, as well as the role of PH in categorizing risk and deciding the most suitable timing for intervention in these patients.

Data availability statement

The datasets presented in this article are not readily available until they receive approval from the institution and the IRB. Requests to access the datasets should be directed to the corresponding author.

Ethics statement

The studies involving humans were approved by Mayo Clinic IRB number 20-008555. The studies were conducted in accordance with the local legislation and institutional requirements. Written informed consent for participation was not required from the participants or the participants' legal guardians/next of kin in accordance with the national legislation and institutional requirements.

Author contributions

VA: Conceptualization, Data curation, Funding acquisition, Investigation, Methodology, Supervision, Writing – original draft, Writing – review & editing. MC: Data curation, Writing – review & editing. US: Data curation, Writing – review & editing. CS: Formal Analysis, Methodology, Validation, Writing – review & editing. AL: Writing – review & editing. RF: Writing – review & editing. NA: Writing – review & editing. JG: Writing – review & editing. AA-O: Data curation, Writing – review & editing. KK: Methodology, Supervision, Writing – review & editing.

Funding

The author(s) declare financial support was received for the research, authorship, and/or publication of this article.

This research was funded by a grant from Mayo Clinic CV Prospective Award.

Conflict of interest

The authors declare that the research was conducted in the absence of any commercial or financial relationships that could be construed as a potential conflict of interest.

The author(s) declared that they were an editorial board member of Frontiers, at the time of submission. This had no impact on the peer review process and the final decision.

Publisher's note

All claims expressed in this article are solely those of the authors and do not necessarily represent those of their affiliated organizations, or those of the publisher, the editors and the reviewers. Any product that may be evaluated in this article, or claim that may be made by its manufacturer, is not guaranteed or endorsed by the publisher.

Supplementary material

The Supplementary Material for this article can be found online at: <https://www.frontiersin.org/articles/10.3389/fcvm.2023.1288747/full#supplementary-material>

SUPPLEMENTARY FIGURE 1

Spline curves for PASP cutoff for males and females. Spline curves demonstrate mortality risk across the range of measured PASP in A. Males

B. Females. The risk increased for PASP > 35–36 mmHg in both males and females.

SUPPLEMENTARY FIGURE 2

Kaplan–Meier survival curves for males and females. Kaplan–Meier survival curves for all-cause mortality by PH (PASP > 36 vs. < 36 mmHg) in unadjusted and adjusted models. Patients with PASP > 36 mmHg had higher all-cause mortality in unadjusted models and after adjusting for age, comorbidity index, and left ventricular filling pressures. Unadjusted and adjusted hazard ratios were 2.26 (95% CI 1.18, 4.31, $p = 0.013$) and 2.03 (95% CI 1.03, 4.01, $p = 0.040$), respectively, for males and 1.91 (95% CI 1.10–3.32, $p = 0.021$) and 1.71 (95% CI 0.94, 3.11), $p = 0.078$), respectively, for females.

References

- Kitaoka H, Doi Y, Casey SA, Hitomi N, Furuno T, Maron BJ. Comparison of prevalence of apical hypertrophic cardiomyopathy in Japan and the United States. *Am J Cardiol.* (2003) 92:1183–6. doi: 10.1016/j.amjcard.2003.07.027
- Hughes RK, Knott KD, Malcolmson J, Augusto JB, Mohiddin SA, Kellman P, et al. Apical hypertrophic cardiomyopathy: the variant less known. *J Am Heart Assoc.* (2020) 9:e015294. doi: 10.1161/JAHA.119.015294
- Jan MF, Todaro MC, Oretto L, Tajik AJ. Apical hypertrophic cardiomyopathy: present status. *Int J Cardiol.* (2016) 222:745–59. doi: 10.1016/j.ijcard.2016.07.154
- Sakamoto T. Apical hypertrophic cardiomyopathy (apical hypertrophy): an overview. *J Cardiol.* (2001) 37(Suppl 1):161–78.
- Hebl VB, Miranda WR, Ong KC, Hodge DO, Bos JM, Gentile F, et al. The natural history of nonobstructive hypertrophic cardiomyopathy. *Mayo Clin Proc.* (2016) 91:279–87. doi: 10.1016/j.mayocp.2016.01.002
- Webb JG, Sasson Z, Rakowski H, Liu P, Wigle ED. Apical hypertrophic cardiomyopathy: clinical follow-up and diagnostic correlates. *J Am Coll Cardiol.* (1990) 15:83–90. doi: 10.1016/0735-1097(90)90180-W
- Klarich KW, Attenhofer Jost CH, Binder J, Connolly HM, Scott CG, Freeman WK, et al. Risk of death in long-term follow-up of patients with apical hypertrophic cardiomyopathy. *Am J Cardiol.* (2013) 111:1784–91. doi: 10.1016/j.amjcard.2013.02.040
- Ong KC, Geske JB, Hebl VB, Nishimura RA, Schaff HV, Ackerman MJ, et al. Pulmonary hypertension is associated with worse survival in hypertrophic cardiomyopathy. *Eur Heart J Cardiovasc Imaging.* (2016) 17:604–10. doi: 10.1093/ehjci/jew024
- Musumeci MB, Mastromarino V, Casenghi M, Tini G, Francia P, Maruotti A, et al. Pulmonary hypertension and clinical correlates in hypertrophic cardiomyopathy. *Int J Cardiol.* (2017) 248:326–32. doi: 10.1016/j.ijcard.2017.07.010
- Wu X, Cui H, Xiao MH, Lu J, Zhu CS, Wang SY, et al. Prevalence of pulmonary hypertension in patients with hypertrophic obstructive cardiomyopathy: a case-control study. *Zhonghua Xin Xue Guan Bing Za Zhi.* (2016) 44:1010–4. doi: 10.3760/cma.j.issn.0253-3758.2016.12.004
- Mitra A, Ghosh RK, Bandyopadhyay D, Ghosh GC, Kalra A, Lavie CJ. Significance of pulmonary hypertension in hypertrophic cardiomyopathy. *Curr Probl Cardiol.* (2020) 45:100398. doi: 10.1016/j.cpcardiol.2018.10.002
- Geske JB, Ong KC, Siontis KC, Hebl VB, Ackerman MJ, Hodge DO, et al. Women with hypertrophic cardiomyopathy have worse survival. *Eur Heart J.* (2017) 38:3434–40. doi: 10.1093/eurheartj/ehx527
- Moon J, Shim CY, Ha JW, Cho IJ, Kang MK, Yang WI, et al. Clinical and echocardiographic predictors of outcomes in patients with apical hypertrophic cardiomyopathy. *Am J Cardiol.* (2011) 108:1614–9. doi: 10.1016/j.amjcard.2011.07.024
- Aslannif R, Suraya K, Koh HB, Tey YS, Tan KL, Tham CH, et al. Diastolic dysfunction grading, echocardiographic and electrocardiogram findings in 50 patients with apical hypertrophic cardiomyopathy. *Med J Malaysia.* (2019) 74:521–6.
- Finocchiaro G, Haddad F, Pavlovic A, Magavern E, Sinagra G, Knowles JW, et al. How does morphology impact on diastolic function in hypertrophic cardiomyopathy? A single centre experience. *BMJ Open.* (2014) 4:e004814. doi: 10.1136/bmjopen-2014-004814
- Siontis KC, Ommen SR, Geske JB. Sex, survival, and cardiomyopathy: differences between men and women with hypertrophic cardiomyopathy. *J Am Heart Assoc.* (2019) 8:e014448. doi: 10.1161/JAHA.119.014448
- Trongtorsak A, Polpichai N, Thangui S, Kewcharoen J, Yodsuan R, Devkota A, et al. Gender-Related differences in hypertrophic cardiomyopathy: a systematic review and meta-analysis. *Pulse (Basel).* (2021) 9:38–46. doi: 10.1159/000517618
- Galiè N, Hoeper MM, Humbert M, Torbicki A, Vachiery JL, Barbera JA, et al. Guidelines for the diagnosis and treatment of pulmonary hypertension: the Task Force for the Diagnosis and Treatment of Pulmonary Hypertension of the European Society of Cardiology (ESC) and the European Respiratory Society (ERS), endorsed by the International Society of Heart and Lung Transplantation (ISHLT). *Eur Heart J.* (2009) 30:2493–537. doi: 10.1093/eurheartj/ehp297
- Bossone E, D'Andrea A, D'Alto M, Citro R, Argiento P, Ferrara F, et al. Echocardiography in pulmonary arterial hypertension: from diagnosis to prognosis. *J Am Soc Echocardiogr.* (2013) 26:1–14. doi: 10.1016/j.echo.2012.10.009
- Vachiery JL, Tedford RJ, Rosenkranz S, Palazzini M, Lang I, Guazzi M, et al. Pulmonary hypertension due to left heart disease. *Eur Respir J.* (2019) 53:1801897. doi: 10.1183/13993003.01897-2018
- Ho CY, Mealiffe ME, Bach RG, Bhattacharya M, Choudhury L, Edelberg JM, et al. Evaluation of mavacamten in symptomatic patients with nonobstructive hypertrophic cardiomyopathy. *J Am Coll Cardiol.* (2020) 75:2649–60. doi: 10.1016/j.jacc.2020.03.064
- Rosenzweig A, Garg N, Rao SJ, Kanwal AK, Kanwal A, Aronow WS, et al. Current and emerging pharmacotherapy for the management of hypertrophic cardiomyopathy. *Expert Opin Pharmacother.* (2023) 24:1349–60. doi: 10.1080/14656566.2023.2219840



OPEN ACCESS

EDITED BY

Francesca Innocenti,
Careggi University Hospital, Italy

REVIEWED BY

Diana Mihalcea,
Carol Davila University of Medicine and
Pharmacy, Romania
Martino Deidda,
University of Cagliari, Italy

*CORRESPONDENCE

Nguyen H. Hai

✉ bsnguyenhoanghai@gmail.com

[†]These authors have contributed equally to
this work and share first authorship

RECEIVED 08 September 2023

ACCEPTED 08 January 2024

PUBLISHED 19 January 2024

CITATION

Nhat GM, Hai NH, Duc VT, Tri HHQ and
Hoa CN (2024) Features of trastuzumab-
related cardiac dysfunction: deformation
analysis outside left ventricular global
longitudinal strain.
Front. Cardiovasc. Med. 11:1291180.
doi: 10.3389/fcvm.2024.1291180

COPYRIGHT

© 2024 Nhat, Hai, Duc, Tri and Hoa. This is an
open-access article distributed under the
terms of the [Creative Commons Attribution
License \(CC BY\)](#). The use, distribution or
reproduction in other forums is permitted,
provided the original author(s) and the
copyright owner(s) are credited and that the
original publication in this journal is cited, in
accordance with accepted academic practice.
No use, distribution or reproduction is
permitted which does not comply with
these terms.

Features of trastuzumab-related cardiac dysfunction: deformation analysis outside left ventricular global longitudinal strain

Giang M. Nhat^{1,2†}, Nguyen H. Hai^{1*†}, Vo T. Duc^{3†}, Ho H. Q. Tri^{4†}
and Chau N. Hoa^{5†}

¹Department of Cardiac Intensive Care and Cardiomyopathy, Nhan dan Gia Dinh Hospital, Ho Chi Minh City, Vietnam, ²University of Medicine and Pharmacy at Ho Chi Minh City, Ho Chi Minh City, Vietnam, ³Diagnostic Imaging Department, University Medical Center of Ho Chi Minh City, Ho Chi Minh City, Vietnam, ⁴Heart Institute, Ho Chi Minh City, Vietnam, ⁵Faculty of Medicine, University of Medicine and Pharmacy at Ho Chi Minh City, Ho Chi Minh City, Vietnam

Background: Cancer therapy-related cardiac dysfunction due to trastuzumab has been well-known for many years, and echocardiographic surveillance is recommended every 3 months in patients undergoing trastuzumab treatment, irrespective of the baseline cardiotoxicity risk. However, the potential harm and cost of overscreening in low- and moderate-risk patients have become great concerns.

Objectives: This study aimed to identify the incidence of early cancer therapy-related cardiac dysfunction (CTRCD) and the behaviours of left and right heart deformations during trastuzumab chemotherapy in low- and moderate-risk patients.

Methods: We prospectively enrolled 110 anthracycline-naïve women with breast cancer and cardiovascular risk factors who were scheduled to receive trastuzumab. The left ventricular ejection fraction (LVEF), left ventricular global longitudinal strain (LV-GLS), and right ventricular and left atrial longitudinal strains were evaluated using echocardiography at baseline, before every subsequent cycle and 3 weeks after the final dose of trastuzumab. The baseline risk of CTRCD was graded according to the risk score proposed by the Heart Failure Association (HFA) Cardio-Oncology Working Group and the International Cardio-Oncology Society (ICOS). CTRCD and its severity were defined according to the current European Society of Cardiology (ESC) guidelines.

Results: Twelve (10.9%) patients had asymptomatic CTRCD. All CTRCD occurred sporadically during the first 9 months of the active trastuzumab regimen in both low- and moderate-risk patients. While CTRCD was graded as moderate severity in 41.7% of patients and heart failure therapy was initiated promptly, no irreversible cardiotoxicity or trastuzumab interruption was recorded at the end of follow-up. Among the left and right heart deformation indices, only LV-GLS decreased significantly in the CTRCD group during the trastuzumab regimen.

Conclusions: CTRCD is prevalent in patients with non-high-risk breast cancer undergoing trastuzumab chemotherapy. Low- and moderate-risk patients show distinct responses to trastuzumab. The LV-GLS is the only deformation index sensitive to early trastuzumab-related cardiac dysfunction.

KEYWORDS

early cancer therapy-related cardiotoxicity, trastuzumab, left ventricular global longitudinal strain, left ventricular ejection fraction, left atrial longitudinal strain, right ventricular longitudinal strain

Introduction

Although the introduction of HER-2 inhibitors, including trastuzumab, pertuzumab and lapatinib in the chemotherapy regimen of HER-2 positive invasive breast cancer, has dramatically improved the remission and mortality rate in both early and metastatic settings, cancer-related cardiac dysfunction (CTRCD) due to this targeted therapy has been a concern, especially in combined anthracycline and trastuzumab therapy (1). The subsequent protocol of trastuzumab following anthracycline can lower the risk of cardiotoxicity compared to the conjunctive regimen; however, CTRCD remains prevalent from 3% to 19% (2). When anthracycline is safely removed from the chemotherapy protocol for HER2-positive breast cancer in recent clinical trials, the risk of CTRCD has been reduced from 0.4% to 3.2% (3, 4). Although anthracycline is no longer preferred for most trastuzumab-containing regimens, echocardiography surveillance every 3 months is recommended to detect subclinical or asymptomatic CTRCD during chemotherapy for all patients according to the current European Society of Cardiology (ESC) guidelines, irrespective of baseline cardiotoxicity risk (5). This recommendation is suggested according to the echocardiography protocol of trastuzumab clinical trials with limited validation in low and high-baseline risk categories (6). Since echocardiography surveillance is performed in a manner of one-size-fits-all, the potential harmfulness and cost regarding overscreening in low- and moderate-risk patients has become a great concern. Identifying the incidence of CTRCD in low- and moderate-risk patients receiving trastuzumab without anthracycline may indicate the need for guideline-directed echocardiography in these non-high-risk groups.

Compared to serial LVEF monitoring, frequent assessment of left ventricular global longitudinal strain (LV-GLS) is recommended to detect CTRCD earlier during trastuzumab chemotherapy and promptly initiate medical treatment for heart failure; however, the role of LV-GLS in this clinical scenario is mainly extrapolated from anthracycline-based treatment data (5). The incidence of asymptomatic CTRCD defined by LV-GLS reduction has not been identified in most contemporary pivotal trials of trastuzumab regimen (7). Furthermore, the involvement of the right ventricular and left atrial longitudinal strain in CTRCD has recently become an active area of research. Although some studies have shown that right ventricular global longitudinal strain (RV-GLS) (8), right ventricular free-wall longitudinal strain (RV-FWLS) (9) or left atrial reservoir strain (LASr) (10) decreased significantly with the trastuzumab regimen, most patients were pre-exposed to anthracycline. In contrast to anthracycline, primary myocyte injury does not occur and dose-dependent cardiotoxicity has not been clearly elucidated in patients receiving trastuzumab monotherapy. Neuregulin ERBB pathway, which was found to be connected to the stress response of the heart, is proposed to play a principal role in this type II chemotherapy-related cardiac dysfunction (11). While the main features of trastuzumab-induced cardiotoxicity include the lack ultrastructural damage and

reversibility (2), it remains unclear whether the right ventricle and left atrium are affected concurrently with the left ventricle and which cardiac chamber is more sensitive to trastuzumab-induced cardiotoxicity. Therefore, this study aimed to identify the incidence of early CTRCD and the behaviours of left and right heart deformations during trastuzumab chemotherapy in low- and moderate-risk patients by incorporating all echocardiographic deformation indices measured at baseline and before every subsequent trastuzumab cycle in an anthracycline-naive breast cancer cohort with cardiovascular risk factors.

Methods

Design

This multicentre prospective cohort study enrolled 110 consecutive female patients who received trastuzumab as adjuvant or neoadjuvant chemotherapy for newly diagnosed breast cancer (stages I–IV) at the Nhan Dan Gia Dinh Hospital and Oncology Hospital, Ho Chi Minh City, Vietnam between 01 September 2020 and 31 December 2022. All patients received an 18-cycle trastuzumab regimen with a 21-day inter-cycle interval. Patients were eligible for inclusion in this study if they presented at least one of the following cardiovascular risk factors: ≥ 60 years of age, hypertension, diabetes mellitus, dyslipidaemia, atrial fibrillation, obesity (BMI > 30 kg/m²), or chronic kidney disease. The exclusion criteria included severe valvular heart disease and poor image quality on echocardiogram, defined as ≥ 2 inadequate visualised myocardial segments (in an 18-segment model) or previous exposure to anthracycline. Patients were evaluated for standard demographic and clinical data, HFA-ICOS risk scores for CTRCD (6), echocardiography findings, and medical therapy at baseline. All patients underwent clinical examination and standard echocardiography before every trastuzumab cycle and 3 weeks after the final dose, irrespective of their HFA-ICOS risk categories. The primary end point was CTRCD occurrence during trastuzumab therapy. The severity of CTRCD was stratified according to the recent ESC guidelines, in which mild CTRCD was defined as a new relative decline in GLS by $>15\%$ from the baseline value with LVEF $\geq 50\%$, and moderate CTRCD as a new LVEF reduction by ≥ 10 percentage points to an LVEF 40%–49% with or without a new relative decline in GLS by $>15\%$ from the baseline value (5). When LVEF reduction was confirmed by two consecutive echocardiography to $<50\%$, moderate and severe CTRCD was recorded. If CTRCD was detected, trastuzumab was interrupted only in the severe presentation, whereas heart failure medications with ACE-i/ARB, beta-blockers and MRA were initiated promptly in moderate and severe settings. Regarding CTRCD reversibility after trastuzumab treatment, LVEF recovery was categorised as follows: fully reversible (to within 5 percentage points of the baseline) or partially reversible (improved by ≥ 10 percentage points but remained >5 percentage points below baseline) (12). This study was conducted in accordance with the

principles of the Declaration of Helsinki and was approved by the ethical committee of the University of Medicine and Pharmacy at Ho Chi Minh City (approval number: NCT04547465), and all patients provided informed consent. Patients or the public were not involved in the design, or conduct, or reporting, or dissemination plans of our research.

Two-dimensional echocardiography

Echocardiography was performed at a resting condition using a Philips Affiniti ultrasound system (Philips Healthcare, Andover, MA, USA) by a single examiner, according to the current guidelines of the American Society of Echocardiography and the European Association of Cardiovascular Imaging (12, 13). Data from four-, three-, and two-chamber and right ventricular-focused apical views acquired in three consecutive cardiac cycles at a frame rate of >50 fps were stored in raw DICOM format for offline analysis. Images were obtained at baseline (before the first trastuzumab cycle), before every subsequent cycle, and 3 weeks after the completion of chemotherapy. Nineteen echocardiographic examinations were performed on each patient during the study period. All images were transferred to a core laboratory and computed by two cardiologists (H. H. N. and D. T. V.) who were blinded to the patients' clinical data. Right ventricular strains (RV-FWLS and RV-GLS) and R-R gating left atrial strains (LASr, LAScd and LASct) were assessed using right ventricular-focused and apical four-chamber views, respectively. Strain analyses by speckle-tracking (LV-GLS, RV-FWLS, RV-GLS, LASr, LAScd and LASct) and semiautomatic LVEF calculations were performed using a Philips aCMQ (QLAB 15.0, Philips Healthcare, Andover, MA, USA). The LA border was automatically defined in the LASr, LAScd, and LASct procedures, and zero strain reference was set at left ventricular end-diastole. LASr, LAScd and LASct were measured as the difference of the strain value at mitral valve opening minus ventricular end-diastole, the difference of the strain value at the onset of atrial contraction minus mitral valve opening, and the difference of the strain value at ventricular end-diastole minus onset of atrial contraction, respectively (13). The strain indices at each trastuzumab cycle were compared with the corresponding values at baseline, and the difference was defined as the relative change [relative change at each cycle = (current strain value – baseline strain value)/baseline strain value]. The baseline strain index was identical to the strain value before cycle 1.

Statistical analysis

Data were provided as means \pm standard deviation when normally distributed, medians and interquartile ranges for skewed distributions and frequencies and percentages for categorical variables. A Chi-squared or unpaired *t*-test was used to compare the demographic data, cardiovascular risk factors, HFA-ICOS risk levels and medical therapy between the mild CTRCD, moderate CTRCD and no-CTRCD groups. A paired

t-test was used to demonstrate significant changes in Δ LV-GLS, Δ RV-FWLS, Δ RV-GLS, Δ LASr, Δ LAScd and Δ LASct between independent groups at each anthracycline cycle. Statistical analyses were performed using IBM SPSS Statistics version 27 (IBM Corp., Armonk, NY, USA) and R version 4.0.3 (R Foundation for Statistical Computing, Vienna, Austria). Two-sided *P*-values were used, and statistical significance was set at *P* < 0.05.

Results

Patient characteristics and CTRCD incidence

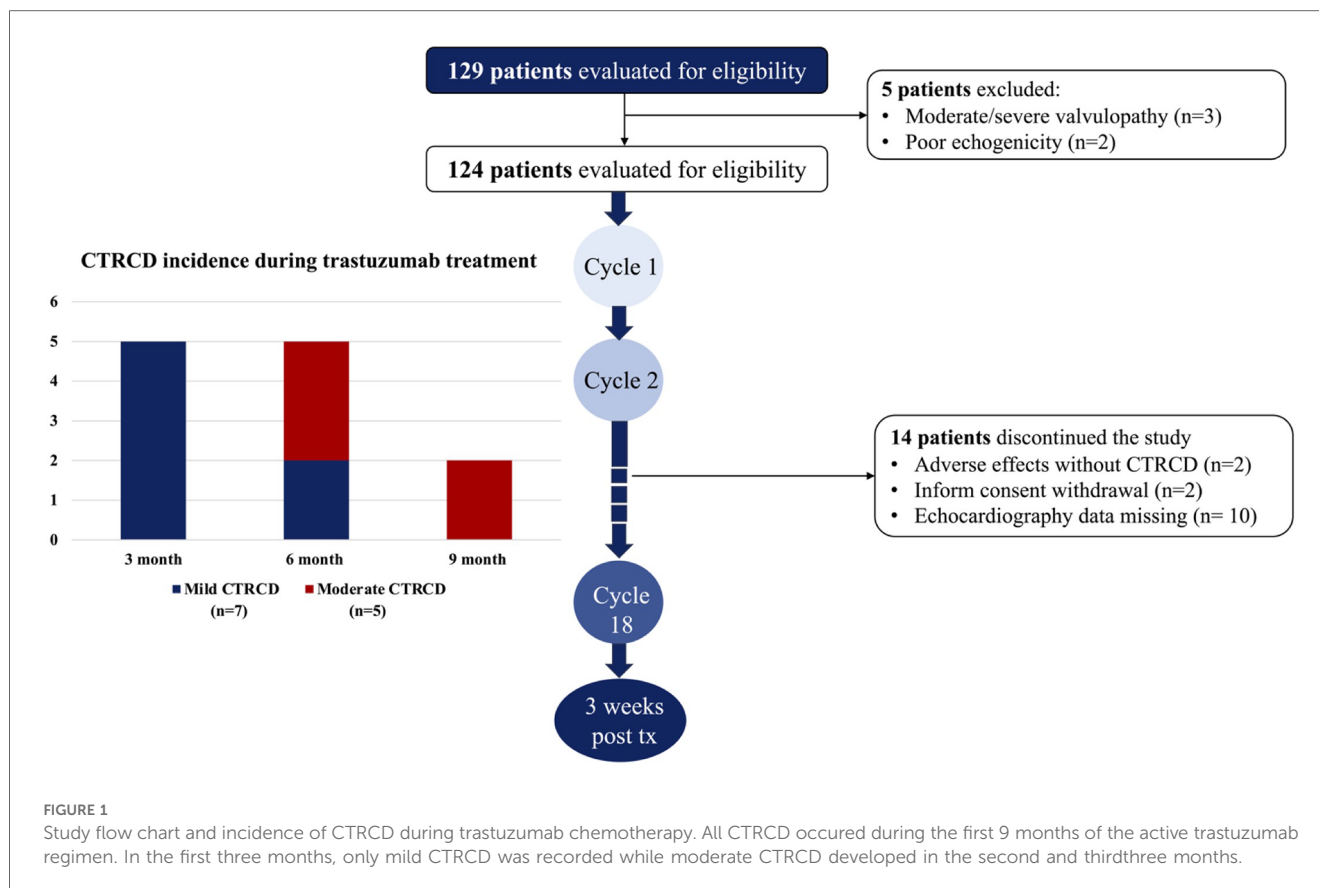
Of the 110 patients with breast cancer and cardiovascular risk factors, 12 (10.9%) developed CTRCD during trastuzumab chemotherapy and were asymptomatic at the time of detection. All CTRCD events were defined as mild or moderate severity with LVEF \geq 40%, and no CTRCD event was recorded after 9 months of trastuzumab chemotherapy. Moderate CTRCD developed later than mild CTRCD, only after the first 3 months (Figure 1).

At baseline, patients' average age was 60.2 ± 8.3 years (33–78 years). No patient presented with LVEF <50%, prior CTRCD, heart failure, cardiomyopathy or a history of myocardial infarction with or without coronary revascularization. Hypertension was the predominant cardiovascular risk factor in 69 (62.7%) patients, followed by dyslipidaemia in 43 (39.1%), diabetes mellitus in 25 (22.7%), chronic kidney disease in 10 (9.1%) and obesity in five (4.5%). All cardiovascular risk factors at baseline were similar between the CTRCD and non-CTRCD groups. Given that all the patients had cardiovascular risk factors, 28 (25.4%) received cardioprotective therapy with ACE-i/ARB (23.9%) and beta-blockers (11.8%) before trastuzumab treatment. Baseline left ventricular function (LVEF and LV-GLS), right ventricular strain (RV-GLS and RV-FWLS) and left atrial mechanics (LASr, LAScd, and LASct) assessed using echocardiography did not differ between the no-CTRCD and CTRCD groups. Moderate CTRCD did not have a lower LV-GLS value or other strain parameters at baseline than mild CTRCD or no CTRCD. The baseline characteristics of the patients in the CTRCD and non-CTRCD groups are summarised in Table 1.

According to the HFA-ICOS risk categories, 52 (47.3%) patients were classified as moderate-risk, and moderate CTRCD occurred only in patients with moderate risk at baseline.

Left and right heart deformation evolution during trastuzumab chemotherapy

In the CTRCD group, when significant LV-GLS reduction always preceded LVEF reduction, the left atrial longitudinal strain (LASr, LAScd and LASct) and right ventricular longitudinal strain (RV-FWLS and RV-GLS) values did not differ



between the CTRCD and no-CTRCD groups or between the mild and moderate CTRCD groups (Figure 2).

According to the baseline HFA-ICOS risk, moderate-risk patients had a persistent negative relative change in LV-GLS during subsequent trastuzumab cycles, in contrast to the stable trend observed in low-risk patients. Although mean LV-GLS values were similar between the low-risk and moderate-risk patients at baseline, after completing trastuzumab chemotherapy, mean LV-GLS in moderate-risk patients was significantly lower ($-18.5 \pm 1\%$ vs. $-18.9 \pm 0.9\%$; $P = 0.032$) (Figure 3).

At the end of treatment, although LVEF fully improved in all patients with mild and moderate CTRCD, the LV-GLS did not return to the baseline value. In moderate CTRCD patients, the mean LV-GLS at 3 weeks after trastuzumab completion was lower ($-17.7 \pm 0.5\%$ vs. $-19.1 \pm 1.2\%$ at baseline; $P = 0.043$). At the time of moderate CTRCD occurrence, the mean LV-GLS and relative reduction of LV-GLS were $-15.4 \pm 0.7\%$ and $19.0 \pm 3.6\%$, respectively. The lowest LVEF in moderate CTRCD patients was $47.4 \pm 1.1\%$.

Discussion

When left and right heart myocardial mechanics were concurrently monitored using echocardiography, the most important finding of this prospective study was that CTRCD developed in 10.9% of anthracycline-naïve breast cancer patients undergoing trastuzumab treatment, and half of these CTRCD

were mild. However, low- and moderate-risk patients showed different responses to trastuzumab exposure, with more severe CTRCD occurring later and only in non-low-risk patients. In contrast to LV-GLS, right ventricle and left atrial deformation imaging were not sensitive enough to detect the cardiotoxicity induced by trastuzumab when medical therapy for heart failure was implemented in a timely manner.

Although the first signal of CTRCD due to trastuzumab has been recognised for more than 20 years, most of this adverse event was described in the conjunctive chemotherapy protocol with anthracycline (2). In addition, the incidence of trastuzumab-related cardiac dysfunction is inconsistent between clinical trials and observational studies when stringent criteria for patient enrolment and strict protocols of cardiac function monitoring lowered the risk of cardiotoxicity. In trials with non-anthracycline adjuvant (BCIRG-006) (3) or neoadjuvant (TRYPHAENA) (14) regimens, trastuzumab was associated with 0.4% and 1.3% symptomatic heart failure, respectively, but this number could be increased to 14%–27% based on retrospective data that included older patients with cardiovascular diseases treated with trastuzumab (15, 16). Acknowledging the cumulative effect of cardiovascular risk factors on the expression of cardiotoxicity, baseline risk assessment using the HFA-ICOS score was recommended before initiating cancer therapy to individualise cardiac function. However, in contrast to anthracycline, a single algorithm was suggested irrespective of the baseline risk category owing to the lack of validated data in low- or high-risk patients. Although more frequent echocardiography

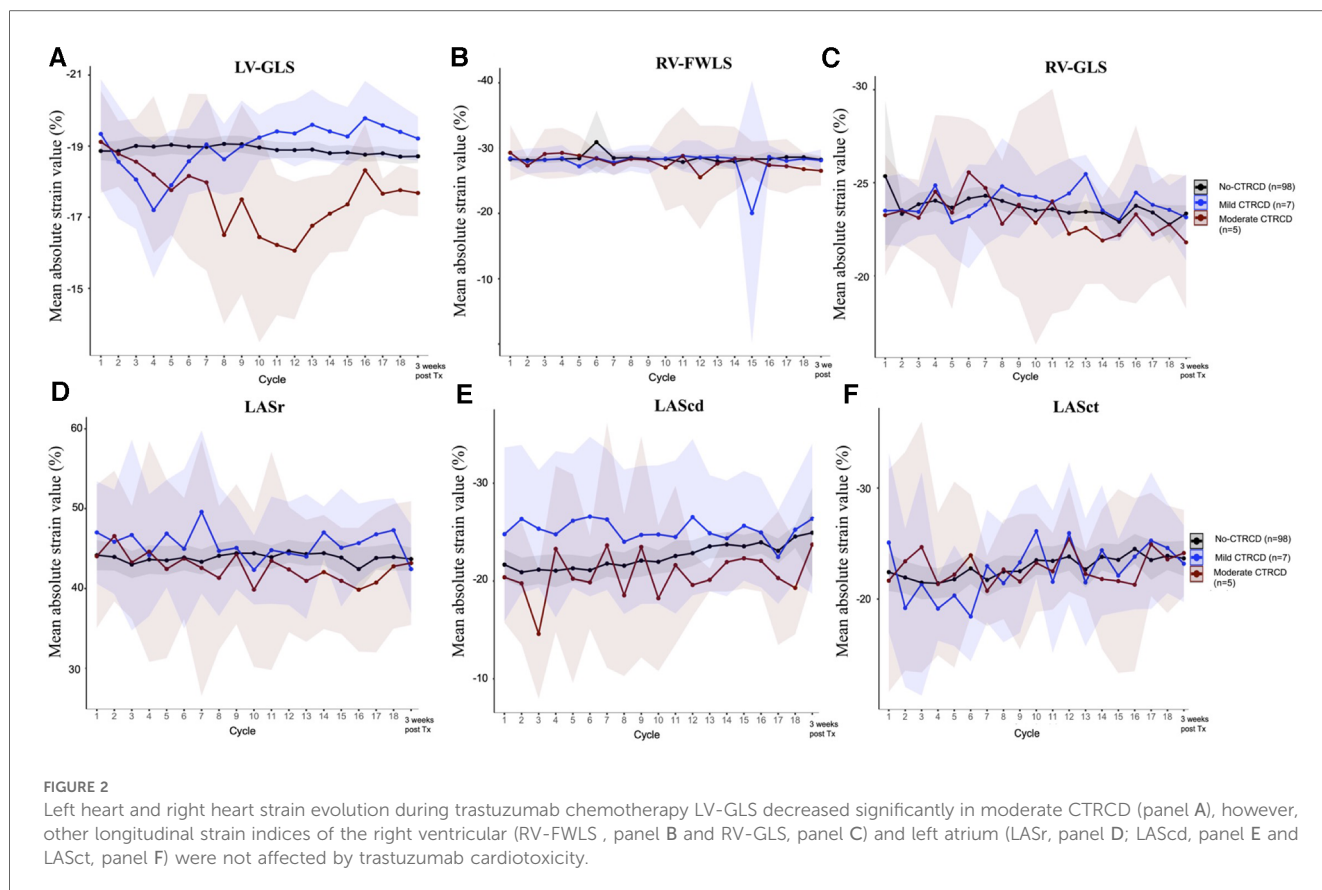
TABLE 1 Patient characteristics.

	Total (<i>n</i> = 110)	No-CTRCD (<i>n</i> = 98)	CTRCD (<i>n</i> = 12)			<i>P</i> ₁	<i>P</i> ₂	<i>P</i> ₃
			All CTRCD (<i>n</i> = 12)	Mild CTRCD (<i>n</i> = 7)	Moderate CTRCD (<i>n</i> = 5)			
Age	60.2 (8.3)	60.5 (7.9)	57.9 (11.4)	54.4 (10.8)	62.8 (11.4)	0.316	0.268	0.677
BMI	24.2 (2.8)	24.2 (2.9)	24.1 (2.3)	24.7 (2)	23.2 (2.6)	0.894	0.231	0.435
Breast cancer stage								
Stage 0–1	9 (8.2)	7 (7.1)	2 (16.7)	1 (14.3)	1 (20)	0.327	0.531	0.704
Stage 2	57 (51.8)	50 (51)	7 (58.3)	4 (57.1)	3 (60)			
Stage 3	35 (31.8)	32 (32.7)	2 (25)	2 (28.6)	1 (20)			
Stage 4	9 (8.2)	9 (9.2)	0 (0)	0 (0)	0 (0)			
Cardiovascular risk factor								
Hypertension	69 (62.7)	62 (63.3)	7 (58.3)	4 (57.1)	3 (60)	0.738	0.921	0.883
Diabetes mellitus	25 (22.7)	21 (21.4)	4 (33.3)	2 (28.6)	2 (40)	0.543	0.679	0.331
Atrial fibrillation	1 (0.9)	1 (1)	0 (0)	0 (0)	0 (0)	0.725	NA	0.82
Dyslipidemia	43 (39.1)	39 (39.8)	4 (33.3)	2 (28.6)	2 (40)	0.665	0.679	0.943
Obesity (BMI > 30 kg/m ²)	5 (4.5)	4 (4.1)	1 (8.3)	1 (10)	0 (0)	0.213	0.377	0.665
Chronic kidney disease	10 (9.1)	10 (10.2)	0 (0)	0 (0)	0 (0)	0.246	N.A	0.452
HFA-ICOS category								
Low risk	58 (52.7)	51 (52)	7 (58.3)	7 (100)	0 (0)	0.678	0.001	0.023
Moderate risk	52 (47.3)	47 (48)	5 (41.7)	0 (0)	5 (100)			
Baseline medical therapy								
ACE-i	12 (10.9)	12 (12.2)	0 (0)	0 (0)	4 (80)	0.199	0.004	0.162
ARB	16 (14.5)	12 (12.2)	4 (33.3)	0 (0)	1 (20)	0.05	0.217	0.489
Beta blocker	13 (11.8)	12 (12.2)	1 (8.3)	1 (14.3)	0 (0)	0.692	0.377	0.344
Baseline echocardiography								
LVEF (%)	63.6 (5.3)	63.8 (5.31)	61.5 (5.4)	61.1 (5.5)	62 (5.7)	0.175	0.801	0.517
LV-GLS (%)	−18.9 (1.3)	−18.9 (1.3)	−19.3 (1.4)	−19.3 (1.7)	−19.1 (1.2)	0.385	0.790	0.653
>18%	83 (75.5)	73 (74.5)	10 (83.3)	6 (85.7)	4 (80)	0.456	0.743	0.567
16%–18%	26 (23.6)	24 (24.5)	2 (16.7)	1 (14.3)	1 (20)	0.982	0.878	0.978
<16%	1 (0.9)	1 (1)	0 (0)	0 (0)	0 (0)	N.A	N.A	N.A
RV-FWLS (%)	−28.3 (2)	−28.3 (2)	−28.8 (2.3)	−28.4 (1.1)	−29.3 (3.4)	0.487	0.617	0.557
RV-GLS (%)	−25.1 (19.1)	−25.4 (20.2)	−23.4 (2.2)	−23.5 (2)	−23.3 (2.6)	0.362	0.868	0.378
LASr (%)	44.3 (9.1)	44.2 (9.4)	45.8 (6.9)	47 (6.9)	44 (7.2)	0.477	0.494	0.970
LAScd (%)	−21.8 (7.7)	−21.7 (7.7)	−23 (7.8)	−24.8 (9.6)	−20.4 (3.7)	0.599	0.301	0.510
LASct (%)	−22.6 (8.4)	−22.4 (8.5)	−23.7 (8.3)	−25.1 (8.7)	−21.7 (8.1)	0.635	0.501	0.845

Value are mean ± SD or *n* (%).
*P*₁, *P* value between CTRCD vs. no-CTRCD; *P*₂, *P* value between mild CTRCD vs. moderate-CTRCD; *P*₃, *P* value between no-CTRCD vs. moderate-CTRCD.
ACE-i, angiotensin-converting enzyme inhibitor; ARB, angiotensin receptor blocker; BMI, body mass index; LAScd, left atrial conduit strain; LASct, left atrial contractile strain; LASr, left atrial resevoir strain; LVEF, left ventricular ejection fraction; LV-GLS, left ventricular global longitudinal strain; RV-FWLS, right ventricular free-wall longitudinal strain; RV-GLS, right ventricular global longitudinal strain.
The bold values mean significant different.

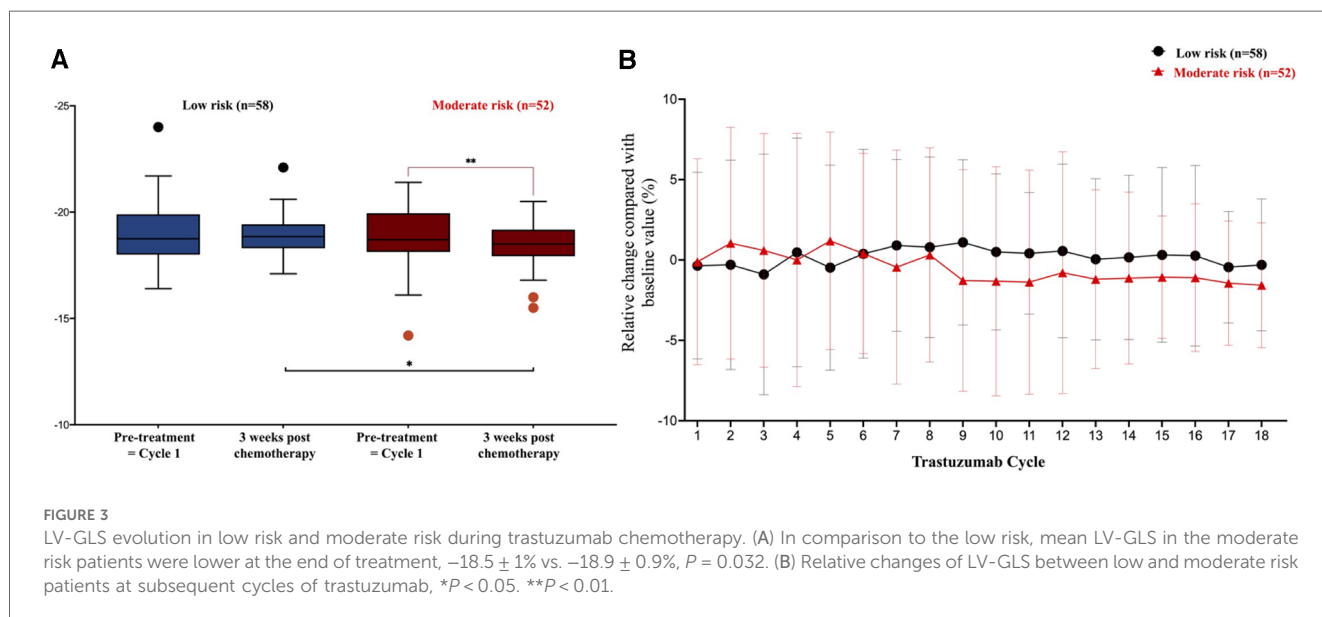
surveillance is performed, a higher likelihood of CTRCD is detected (17), the cost associated with overscreening in the low-risk category is of great concern. Battisti et al. (18) demonstrated that the HFA-ICOS score had a good correlation with increasing rate of cardiac dysfunction, in which the rate of LVEF decline below 50% was 4.5% in low-risk patients and 6.4% in moderate-risk patients; however, most of the patients in this study (65%) were treated concurrently with anthracycline, and cardiotoxicity was defined by LVEF reduction only. In this study, we showed that CTRCD in the low and moderate HFA-ICOS risk categories had different features. The relative decrease in LV-GLS in moderate-risk patients was higher than that in low-risk patients throughout the 18 cycles of trastuzumab treatment. Consequently, at the end of chemotherapy, the mean LV-GLS of moderate-risk patients was significantly lower. In addition, while the incidence of CTRCD was 12.1% and 9.6% in low-risk and moderate- to high-risk patients, respectively, all

CTRCD associated with low baseline risk were mild and all CTRCDs occurring in the moderate- to high-risk category had LVEF decline to below 50%. Relative reduction of LV-GLS > 15% in the mild CTRCD in our study did not lead to significant LVEF and LV-GLS reduction after completing trastuzumab treatment, and no heart failure medical treatment was implemented. Since patients treated with trastuzumab are less likely to be associated with guideline-adherent cardiac monitoring compared to other chemotherapy regimens, such as taxane or anthracycline (19), our study suggests that one-size-fits-all echocardiography surveillance every 3 months during the trastuzumab regimen may not be necessary for low-risk patients at baseline. Because all these CTRCD cases developed within the first 6 months, frequent echocardiography can only be considered during this period.
Findings from our study were consistent with data from Battisti (18), Keramida (9), Negishi (20) or Banke (21) in which CTRCD



was detected by LV-GLS and/or LVEF reduction in a median time from 5 to 9 months after initiating trastuzumab. While breast cancer patients with a moderate baseline risk were more likely to develop more severe CTRCD, our study suggests that frequent echocardiography surveillance is crucial during the first 9 months of trastuzumab treatment at baseline. In CTRCD of moderate severity, all patients in this study had full recovery at the end of

chemotherapy, defined by reversible LVEF with an insignificant reduction of LV-GLS in comparison with the baseline value when medical treatment for heart failure was promptly initiated and trastuzumab chemotherapy was maintained. Although data from previous studies showed that LVEF decline following trastuzumab administration can be persistent (3, 22), this finding from our study confirms the recent ESC guidelines'



recommendation regarding safe continuation of anti-HER2 under cardiovascular monitoring if CTRCD can be detected and managed in a timely manner, at least in a moderate setting (5).

To the best of our knowledge, this is the first prospective study to evaluate the role of left atrial and right ventricular deformations in anthracycline-naïve cancer patients undergoing trastuzumab treatment concurrently with LV-GLS. Given the fact that interventricular septum is a major part of left ventricular, RV-GLS evolution is more prone to be affected by left ventricular deformation than RV-FWLS (13). Mazzuti et al. showed that RV-GLS decreased during the trastuzumab regimen; however, this was not associated with the CTRCD events (8). After initiating trastuzumab, deterioration of the both right ventricular longitudinal strain parameters (RV-GLS and RV-FWLS) occurred several months following the significant decline of LV-GLS; however, no specific heart failure medical treatment was implemented in the study of Keramida et al. (9). These findings support the result of our study in that when CTRCD was detected and treated early by a significant relative reduction of LV-GLS and mildly reduced LVEF, the chance to recognize any deterioration of isolated right ventricular deformation (RV-FWLS) due to trastuzumab cardiotoxicity is extremely low. Although RV-GLS evolution in moderate CTRCD patients had the similar trend of LV-GLS, mean RV-GLS values at the end of chemotherapy were not different between moderate and no-/mild CTRCD.

For left atrial strain analysis, Park et al. demonstrated that LASr at baseline had a better predictive value for CTRCD than LVGLS after initiating trastuzumab; however, most patients had previously been exposed to anthracycline (10). Similar to right ventricular longitudinal strain, our study showed that no atrial deformation indices (LASr, LAScd or CASct) were sensitive enough to detect trastuzumab-related cardiac dysfunction.

Study limitations

This study has some limitations. First, no patient was classified into the high-risk HFA-ICOS category. Therefore, our findings may not represent the behaviour of the left and right heart deformations in this group. Second, in the echocardiography protocol, although we assessed LVEF using a well-known semi-automatic software to improve the reproducibility of this measurement, 3D LVEF is the preferred method in recent guidelines owing to its superior accuracy in detecting LV dysfunction. Finally, the incidence of CTRCD was low in our study, which limited the multivariate analysis and the power of Chi-squared test in comparing baseline characteristics among the study groups. Other studies with a considerable proportion of high-risk patients are needed to validate the HFA-ICOS risk category and to identify independent risk factors for early CTRCD development during trastuzumab treatment.

Conclusions

CTRCD is prevalent in anthracycline-naïve breast cancer patients undergoing trastuzumab chemotherapy, even in non-high-risk categories. However, moderate CTRCD, defined as a reduction in LVEF of <50%, is not encountered frequently. The one-size-fits-all echocardiography surveillance suggested by the recent guidelines is not necessary for low-risk patients.

Data availability statement

The raw data supporting the conclusions of this article will be made available by the authors, without undue reservation.

Ethics statement

The studies involving human participants were reviewed and approved by The University of Medicine and Pharmacy at Ho Chi Minh City. The patients/participants provided their written informed consent to participate in this study.

Author contributions

GN: Writing – original draft, Writing – review & editing. NH: Methodology, Writing – original draft. DVVD: Formal Analysis, Writing – review & editing. HT: Supervision, Writing – review & editing. CH: Supervision, Writing – review & editing.

Funding

The author(s) declare that no financial support was received for the research, authorship, and/or publication of this article.

Conflict of interest

The authors declare that the research was conducted in the absence of any commercial or financial relationships that could be construed as a potential conflict of interest.

Publisher's note

All claims expressed in this article are solely those of the authors and do not necessarily represent those of their affiliated organizations, or those of the publisher, the editors and the reviewers. Any product that may be evaluated in this article, or claim that may be made by its manufacturer, is not guaranteed or endorsed by the publisher.

References

- Seidman A, Hudis C, Pierri MK, Shak S, Paton V, Ashby M, et al. Cardiac dysfunction in the trastuzumab clinical trials experience. *J Clin Oncol.* (2002) 20:1215–21. doi: 10.1200/JCO.2002.20.5.1215
- Florio R, Smith KL, Cuomo KK, Russell SD. Cardiotoxicity from human epidermal growth factor receptor-2 (HER2) targeted therapies. *J Am Heart Assoc.* (2017) 6. doi: 10.1161/JAHA.117.006915
- Slamon D, Eiermann W, Robert N, Pienkowski T, Martin M, Press M, et al. Cancer international research, adjuvant trastuzumab in HER2-positive breast cancer. *N Engl J Med.* (2011) 365:1273–83. doi: 10.1056/NEJMoa0910383
- van der Voort A, van Ramshorst MS, van Werkhoven ED, Mandjes IA, Kemper I, Vulink AJ, et al. Three-year follow-up of neoadjuvant chemotherapy with or without anthracyclines in the presence of dual ERBB2 blockade in patients with ERBB2-positive breast cancer: a secondary analysis of the TRAIN-2 randomized, phase 3 trial. *JAMA Oncol.* (2021) 7:978–84. doi: 10.1001/jamaoncol.2021.1371
- Lyon AR, Lopez-Fernandez T, Couch LS, Asteggiano R, Aznar MC, Bergler-Klein J, et al. 2022 ESC guidelines on cardio-oncology developed in collaboration with the European hematology association (EHA), the European society for therapeutic radiology and oncology (ESTRO) and the international cardio-oncology society (IC-OS). *Eur Heart J.* (2022) 43:4229–361. doi: 10.1093/eurheartj/ehac244
- Celutkienė J, Pudil R, Lopez-Fernandez T, Grapsa J, Nihoyannopoulos P, Bergler-Klein J, et al. Role of cardiovascular imaging in cancer patients receiving cardiotoxic therapies: a position statement on behalf of the heart failure association (HFA), the European association of cardiovascular imaging (EACVI) and the cardio-oncology council of the European society of cardiology (ESC). *Eur J Heart Fail.* (2020) 22:1504–24. doi: 10.1002/ehf.1957
- Oikonomou EK, Kokkinidis DG, Kampaktsis PN, Amir EA, Marwick TH, Gupta D, et al. Assessment of prognostic value of left ventricular global longitudinal strain for early prediction of chemotherapy-induced cardiotoxicity: a systematic review and meta-analysis. *JAMA Cardiol.* (2019) 4:1007–18. doi: 10.1001/jamacardio.2019.2952
- Mazzutti G, Pivatto Junior F, Costa GOM, Foppa M, Biolo A, Santos ABS. Right ventricular function during trastuzumab therapy for breast cancer. *Int J Cardiovasc Imaging.* (2021) 38:779–87. doi: 10.1007/s10554-021-02470-2
- Keramida K, Farmakis D, Bingcan J, Sulemane S, Sutherland S, Bingcan RA, et al. Longitudinal changes of right ventricular deformation mechanics during trastuzumab therapy in breast cancer patients. *Eur J Heart Fail.* (2019) 21:529–35. doi: 10.1002/ehf.1385
- Park H, Kim KH, Kim HY, Cho JY, Yoon HJ, Hong YJ, et al. Left atrial longitudinal strain as a predictor of cancer therapeutics-related cardiac dysfunction in patients with breast cancer. *Cardiovasc Ultrasound.* (2020) 18:28. doi: 10.1186/s12947-020-00210-5
- Suter TM, Ewer MS. Cancer drugs and the heart: importance and management. *Eur Heart J.* (2013) 34:1102–11. doi: 10.1093/eurheartj/ehs181
- Plana JC, Galderisi M, Barac A, Ewer MS, Ky B, Scherrer-Crosbie M, et al. Expert consensus for multimodality imaging evaluation of adult patients during and after cancer therapy: a report from the American society of echocardiography and the European association of cardiovascular imaging. *Eur Heart J Cardiovasc Imaging.* (2014) 15:1063–93. doi: 10.1093/ehjci/jeu192
- Badano LP, Kolia TJ, Muraru D, Abraham TP, Aurigemma G, Edvardsen T, et al. Reviewers: this document was reviewed by members of the, standardization of left atrial, right ventricular, and right atrial deformation imaging using two-dimensional speckle tracking echocardiography: a consensus document of the EACVI/ASE/industry task force to standardize deformation imaging. *Eur Heart J Cardiovasc Imaging.* (2018) 19:591–600. doi: 10.1093/ehjci/jeu042
- Schneeweiss A, Chia S, Hickish T, Harvey V, Eniu A, Waldron-Lynch M, et al. Long-term efficacy analysis of the randomised, phase II TRYPHAENA cardiac safety study: evaluating pertuzumab and trastuzumab plus standard neoadjuvant anthracycline-containing and anthracycline-free chemotherapy regimens in patients with HER2-positive early breast cancer. *Eur J Cancer.* (2018) 89:27–35. doi: 10.1016/j.ejca.2017.10.021
- Chen J, Long JB, Hurria A, Owusu C, Steingart RM, Gross CP. Incidence of heart failure or cardiomyopathy after adjuvant trastuzumab therapy for breast cancer. *J Am Coll Cardiol.* (2012) 60:2504–12. doi: 10.1016/j.jacc.2012.07.068
- Guarneri V, Lenihan DJ, Valero V, Durand JB, Broglio K, Hess KR, et al. Long-term cardiac tolerability of trastuzumab in metastatic breast cancer: the M.D. Anderson cancer center experience. *J Clin Oncol.* (2006) 24:4107–15. doi: 10.1200/JCO.2005.04.9551
- Dang CT, Blaes A, Lynce F, Swain SM, Dent S. Left ventricular ejection fraction monitoring adherence rates: why so low? *JACC Cardiovasc Imaging.* (2018) 11:1094–7. doi: 10.1016/j.jcmg.2018.02.027
- Battisti NML, Andres MS, Lee KA, Ramalingam S, Nash T, Mappouridou S, et al. Incidence of cardiotoxicity and validation of the heart failure association-international cardio-oncology society risk stratification tool in patients treated with trastuzumab for HER2-positive early breast cancer. *Breast Cancer Res Treat.* (2021) 188:149–63. doi: 10.1007/s10549-021-06192-w
- Henry ML, Niu J, Zhang N, Giordano SH, Chavez-MacGregor M. Cardiotoxicity and cardiac monitoring among chemotherapy-treated breast cancer patients. *JACC Cardiovasc Imaging.* (2018) 11:1084–93. doi: 10.1016/j.jcmg.2018.06.005
- Negishi K, Negishi T, Hare JL, Haluska BA, Plana JC, Marwick TH. Independent and incremental value of deformation indices for prediction of trastuzumab-induced cardiotoxicity. *J Am Soc Echocardiogr.* (2013) 26:493–8. doi: 10.1016/j.echo.2013.02.008
- Banke A, Schou M, Ewertz M, Dahl J, Frederiksen PH, Videbaek L, et al. Immediate evaluation of global longitudinal strain at initiation of trastuzumab treatment in breast cancer patients. *Echocardiography.* (2021) 38:1702–10. doi: 10.1111/echo.15190
- Dang C, Guo H, Najita J, Yardley D, Marcom K, Albain K, et al. Cardiac outcomes of patients receiving adjuvant weekly paclitaxel and trastuzumab for node-negative, ERBB2-positive breast cancer. *JAMA Oncol.* (2016) 2:29–36. doi: 10.1001/jamaoncol.2015.3709



OPEN ACCESS

EDITED BY

Francesca Innocenti,
Careggi University Hospital, Italy

REVIEWED BY

Francisco Calvo Iglesias,
Alvaro Cunqueiro Hospital, Spain
Sebastiano Cicco,
University of Bari Aldo Moro, Italy

*CORRESPONDENCE

Sebastian Szmit
✉ s.szmit@gmail.com

[†]These authors share senior authorship

RECEIVED 27 August 2023

ACCEPTED 10 January 2024

PUBLISHED 24 January 2024

CITATION

Kępski J, Szmit S and Lech-Marañda E (2024)

Characteristics of patients with newly
diagnosed hematological malignancies
referred for echocardiography.

Front. Oncol. 14:1283831.

doi: 10.3389/fonc.2024.1283831

COPYRIGHT

© 2024 Kępski, Szmit and Lech-Marañda. This is an open-access article distributed under the terms of the [Creative Commons Attribution License \(CC BY\)](https://creativecommons.org/licenses/by/4.0/). The use, distribution or reproduction in other forums is permitted, provided the original author(s) and the copyright owner(s) are credited and that the original publication in this journal is cited, in accordance with accepted academic practice. No use, distribution or reproduction is permitted which does not comply with these terms.

Characteristics of patients with newly diagnosed hematological malignancies referred for echocardiography

Jarosław Kępski¹, Sebastian Szmit^{1*†} and Ewa Lech-Marañda^{2†}

¹Department of Cardio-Oncology, Centre of Postgraduate Medical Education, Warsaw, Poland,

²Department of Hematology, Institute of Hematology and Transfusion Medicine, Warsaw, Poland

Objective: The importance of cardio-hemato-oncology programs is increasing. The main aim of the study was to identify all coexisting cardiovascular disorders in patients with new hematological malignancies referred for echocardiography during baseline evaluation before anticancer therapy.

Material and methods: The study was based on 900 echocardiographic examinations performed within 12 months at the Institute of Hematology and Transfusion Medicine in Poland: 669 tests (74.3%) were dedicated to hemato-oncology patients at the different stages of cancer therapy, however almost a third of the tests (277, 30.8%) were part of a baseline evaluation before starting first line anticancer therapy due to newly diagnosed hematological malignancies.

Results: The group of 277 patients with new hematological malignancies (138 women, 49.82%) with a median age of 66 years (interquartile range: 53–72 years) was included in the main analyses. The three most frequent new histopathological diagnoses were: non-Hodgkin lymphoma (63 cases; 22.74%), acute myeloid leukaemia (47 cases; 16.97%), and multiple myeloma (45 cases; 16.25%). The three most common clinical cardiology disorders were arterial hypertension (in 133 patients, 48.01%), arrhythmias (48 patients, 17.33%), and heart failure (39 patients, 14.08%). Among 48 patients with arrhythmias there were 22 cases with atrial fibrillation. The most frequently detected echocardiographic abnormality was Left Atrial Volume Index >34 ml/m² which was present in 108 of 277 patients (38.99%) and associated with a significantly greater chance of concomitant diagnosis of arrhythmias (OR=1.98; p=0.048) especially atrial fibrillation (OR=3.39; p=0.025). The second most common echocardiographic finding was diastolic dysfunction 2nd or 3rd degree revealed in 43 patients (15.52%) and associated with a greater chance of simultaneous diagnosis of heart failure (OR=8.32; p<0.0001) or arrhythmias (OR=4.44; p<0.0001) including atrial fibrillation (OR=5.40; p=0.0003).

Conclusions: In patients with newly diagnosed hematological malignancies left ventricular diastolic dysfunction is a common abnormality in echocardiography and may determine diagnoses of heart failure or arrhythmias.

KEYWORDS

cardiooncology, echocardiography, hematology malignance, diastolic dysfunction, heart failure

Introduction

Cardio-oncology is a dynamically developing scientific field. Its primary task is to provide appropriate quality of cardiological care for patients undergoing or after cancer therapy (1). The overriding goal is to ensure optimal anticancer treatment for patients with coexisting cardiovascular diseases diagnosed before or during cancer treatment. In many countries, scientific institutions create clinical programs dedicated to cardio-oncology (2). The emergence of cardio-oncology clinics is becoming a reality (3–5).

The development of modern therapies used in onco-hematology results in improved prognoses for patients. However, this favorable trend is limited by the increasing number of early and late cardiovascular complications mainly due to using novel anticancer drugs (6). They may reduce the overall survival rate and affect patients' quality of life. For these reasons, programs dedicated to cardio-hemato-oncology have also been created (7, 8).

Cardiovascular risk stratification should be an integral element of each cancer patient assessment before initiating potentially cardiotoxic oncological therapy (9). Echocardiography seems to be necessary during such evaluation especially in hemato-oncology (10). Patients with a history of cardiovascular disease appear to be at greater risk of an unfavorable prognosis (11). The direct impact of cancer itself on the cardiovascular system is constantly underestimated (12).

The study aimed to summarize the first year of experience from the work of a new team of cardiologists at the Institute of Hematology and Transfusion Medicine in Warsaw, i.e. the Polish reference center for hematology. The main goal was to draw special attention to the importance of baseline cardiology evaluation of patients with a new diagnosis of hematological malignancies.

Materials and methods

Indications for echocardiographic examinations of the heart performed from April 2021 to March 2022 were retrospectively analyzed. This period constituted the first 12 months of work of the new team of cardiologists at the Institute of Hematology and Transfusion Medicine in Warsaw, who are also members of the International Cardio-Oncology Society and certified cardio-oncologists.

There were 900 echocardiographic examinations performed for different clinical indications (Figure 1). Nearly one fourth of the examinations was performed in patients treated for reasons other than hematological malignancies: non hematology therapy (13.3%) or coagulopathies (12.3%). Most of the tests (669; 74.3%) were

dedicated directly to hemato-oncology. The distribution of echocardiographic imaging in hemato-oncology was as follows:

- 277 (30.8%) patients at baseline evaluation
- 327 (36.3%) patients during active anticancer therapy
 - 103 (11.4%) patients with new symptomatic events
 - 224 (24.9%) patients under monitoring at different stages of hematological malignancy treatment:
 - 93 before hematopoietic stem cell transplantation (HSCT),
 - 51 with malignancy progression,
 - 80 as asymptomatic patients under surveillance.
- 22 (2.4%) patients during long-term follow-up after anticancer therapy
- 43 (4.78%) patients in clinical trials on an experimental therapy.

The final step was to identify coexisting cardiovascular diseases before anticancer therapy among patients starting treatment (baseline evaluation) and analyzing their echocardiographic diagnoses.

Echocardiographic studies were conducted on the patients in the left lateral decubitus position using a medical ultrasound device (EPIQ 5, Philips Medical System, USA). Left and right ventricular systolic function, left ventricular diastolic function, and exponents of pulmonary hypertension were assessed.

Echocardiograms were performed following the American Society of Echocardiography guidelines, using imaging in the following projections: subcostal, parasternal in the long and short axis, apical four-, two- and three-chamber projections and suprasternal projection (13, 14). Ejection fraction was assessed using the Simpson method in the four- and two-chamber views. Diastolic function was assessed according to the American Society of Echocardiography and the European Association of Cardiovascular Imaging Guidelines (15). Not all tests were performed with simultaneous electrocardiogram monitoring. When assessing the diastolic function of the left ventricle, the average value of e' from the septal and lateral values of the left ventricle was used. In our daily practice, we use TDI imaging of the right ventricle. Patients have their S' value, i.e. systolic excursion velocity, assessed.

All cardiovascular disorders were diagnosed according to the thematically relevant recommendations of the European Society of Cardiology in force in Poland (16–18).

All clinical and echocardiographic diagnoses as nominal variables were expressed as percentages. Values of odds ratios (ORs) and respective 95% confidence intervals (CIs) were calculated by the logistic regression model to find relationships between echocardiographic findings and classical risk factors like

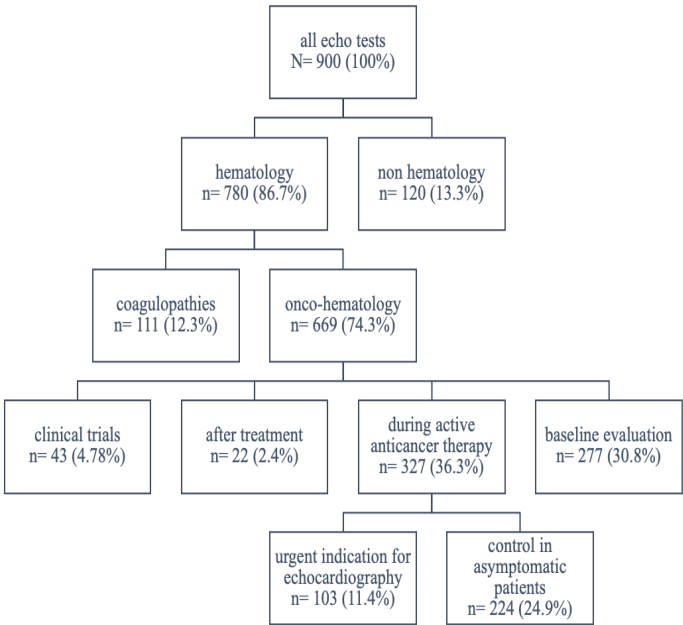


FIGURE 1
The flowchart of patients undergoing echocardiography.

arterial hypertension and coronary artery disease. The second purpose was to evaluate the chance of diagnosing heart failure or arrhythmias depending on different echocardiographic abnormalities, not only decreased ejection fraction (EF). All analyses were performed by STATISTICA software. The value of the test's probability level $p < 0.05$ was understood as significant.

The study was approved by the Bioethical Committee of the Centre of Postgraduate Medical Education: opinion number: 74/2022, Warsaw 08.JUNE.2022.

Results

The main analysis of the study was focused on 277 patients (138 women, 49.82%) with a median age of 66 years (interquartile range: 53-72 years) who had newly recognized hematological malignancies and had undergone echocardiography as an element of risk stratification before anticancer therapy. The frequency distribution of new blood cancers diagnoses is presented in Table 1.

Among 277 patients with new hematological malignancies, three concomitant clinical cardiology diagnoses were the most common (Table 2): arterial hypertension (133 patients, 48.01%), arrhythmias (48 patients, 17.33%), heart failure (39 patients, 14.08%). The most common five new echocardiographic findings included (Table 3): LAVI >34 ml/m² (108 cases, 38.99%), diastolic dysfunction 2nd or 3rd degree (43 cases, 15.52%), TRV >2.8 m/sec (40 cases, 14.44%), E/e' >14 (18 cases, 6.55), left ventricular systolic dysfunction with ejection fraction EF $<50\%$ (10 cases, 3.61%).

Patients with arterial hypertension or coronary artery disease had significantly greater chance of diagnosis of diastolic dysfunction grade 2nd or 3rd (OR=4.23 or OR=3.46 respectively, $p < 0.05$ for both). Diagnosis of EF $<50\%$ was significantly associated with

coronary artery disease (OR=9.19; $p = 0.001$) and borderline related to arterial hypertension (Table 4).

Diastolic dysfunction 2nd or 3rd degree on echocardiography was strongly related to a greater chance of diagnosis of heart failure (OR=8.32; $p < 0.0001$) or arrhythmias (OR=4.44; $p < 0.0001$) including atrial fibrillation (OR=5.40; $p = 0.0003$) (Table 5).

TABLE 1 Eight most frequent histopatological diagnoses of new hematological malignancies among 277 patients referred to echocardiography.

	Diagnosis	Number of patients
1	Non-Hodgkin lymphoma	63 (22.74%)
2	Acute myeloid leukaemia (AML)	47 (16.97%)
3	Multiple myeloma (MM)	45 (16.25%)
4	B-cell chronic lymphocytic leukaemia (CLL)	33 (11.91%)
5	Myeloproliferative neoplasms BCR/ABL negative	25 (9.03%)
6	Acute lymphoblastic leukaemia (ALL)	13 (4.69%)
7	Hodgkin lymphoma	13 (4.69%)
8	Myelodysplastic syndromes	9 (3.25%)
	Total	248 (89.53%)

TABLE 2 Clinical cardiovascular diseases identified in 277 patients with new hematological malignancies.

	Diagnosis	Number of patients (%)
1	Arterial hypertension	133 (48.01%)
2	Arrhythmias	48 (17.33%)
3	Atrial fibrillation (AF)	22 (7.94%)
4	Heart failure (HF)	39 (14.08%)
5	Coronary artery disease (CAD)	22 (7.94%)
6	Venous thromboembolic event (VTE)	10 (3.61%)

There were other interesting relationships between echocardiographic findings and clinical cardiology diagnoses (Table 5):

- Left Atrial Volume Index LAVI >34 ml/m² was found significantly more often together with a diagnosis of arrhythmias (OR=1.98; p=0.048) especially with atrial fibrillation (OR=3.39; p=0.025). LAVI >34 ml/m² was not significantly associated with a chance of diagnosis of heart failure.
- Tricuspid regurgitation velocity TRV >2.8 m/sec could indicate a higher chance of a diagnosis of heart failure (OR=2.85; p=0.01) but not arrhythmias.
- E/e' >14 was strongly associated with a greater chance of concomitant diagnosis of heart failure (OR=7.83; p<0.0001) or arrhythmias (OR=7.4; p<0.0001) including arterial fibrillation (OR=7.5; p=0.0003).

TABLE 3 Echocardiographic diagnoses in 277 patients with new hematological malignancies.

	Diagnosis	Number of patients (%)
1	Left ventricular systolic dysfunction with ejection fraction EF<50%	10 (3.61%)
2	Diastolic dysfunction 2nd or 3rd degree	43 (15.52%)
3	Left Atrial Volume Index: LAVI >34 ml/m ²	108 (38.99%)
4	E/e' >14	18 (6.50%)
5	Tricuspid regurgitation velocity: TRV >2.8 m/s	40 (14.44%)
6	Tricuspid annular plane systolic excursion: TAPSE <17 mm	6 (2.17%)
7.	Peak S wave velocity of the lateral tricuspid annulus by tissue Doppler imaging: RVS'<9.5 cm/s	8 (2.89%)

All 10 patients with recognized EF < 50% had concomitant diagnoses of heart failure.

Among 43 patients with new diagnoses of hematological malignancies and recognized diastolic dysfunction 2nd or 3rd degree: 10 had coexisting atrial fibrillation (p<0.0001) and 8 had concomitant LVEF<50% (p<0.0001). It should be highlighted that only 2 patients had simultaneously atrial fibrillation, LVEF <50% and diastolic dysfunction 2nd or 3rd degree.

Discussion

The new ESC guidelines dedicated to cardio-oncology recommend cardiological and echocardiographic assessment of cancer patients at various stages of anticancer treatment, i.e. as in our study (19). Echocardiography should be part of the baseline cardiovascular risk stratification before anticancer treatment. The coexistence of cardiac diseases may be associated with a worse prognosis in patients treated for cancer (20). Cancer and its treatment favor the development of new and progression of existing cardiac diseases. Therefore, risk stratification before anticancer therapy seems extremely important (21). To a large extent, in terms of many anticancer drugs, this stratification is based on the result of echocardiography, although clinical diagnoses are also of integral importance (9). It should be emphasized that the initial risk stratification has its prognostic justification (11, 22).

Our analysis confirms a high frequency of diagnoses of cardiac diseases among patients with new hematological malignancies. Our data show that 14.08% of patients with echocardiographic examinations at baseline had a diagnosis of heart failure, and 17.33% had arrhythmias. Echocardiographic findings were even more critical: 3.61% had left ventricular systolic dysfunction with EF <50%, 15.52% had grade 2 or 3 diastolic dysfunction, and 14.44% of patients had TRV >2.8 m/2. Notably, as many as 38.99% of patients had LAVI >34 ml/m² and that was the most frequent echocardiographic abnormality in this population. In our opinion, both LAVI and diastolic function should be evaluated not only at baseline but also during active anticancer treatment, which seems necessary to monitor them. Such modern monitoring may explain some reasons for the diagnosis of new episodes of heart failure or arrhythmias related to anticancer drugs activity.

The ESC guidelines emphasize the need to perform planned examinations serially, even in asymptomatic patients, during their anticancer treatment. This course of treatment makes it possible to recognize echocardiographic signs of heart damage very early. As a result, it is possible to start secondary cardio protection effectively. Echocardiographic assessment of patients after completion of anticancer treatment is of critical importance as part of long-term follow-up including reassessment of the patient at the time of cancer recurrence. In hemato-oncology, this becomes particularly important at the moment of qualification for bone marrow transplantation (23).

Cardiovascular risk stratification in cardio-oncology is a dynamic process. A cancer patient with low or moderate risk may become a high- or very-high-risk patient during or after oncological treatment if new echocardiographic abnormalities occur. In this

TABLE 4 The odds ratio of recognition of five main echocardiographic abnormalities in relation to arterial hypertension and coronary artery disease.

	LAVI >34 ml/m2	2nd or 3rd degree diastolic dysfunction	TRV >2.8 m/s	E/e' >14	EF <50%
Arterial hypertension	OR=3.52 95%CI:2.05-6.05 p<0.0001	OR=4.23 95%CI:1.98-9.04 p=0.0002	OR=2.39 95%CI:1.17-4.9 p=0.02	OR=9.66 95%CI:2.16-43.14 p=0.003	OR=4.51 95%CI:0.93-21.8 p=0.06
Coronary artery disease	OR=4.31 95%CI: 1.52-12.27 p=0.006	OR=3.46 95%CI:1.35-8.89 p=0.01	OR=2.8 95%CI:1.07-7.42 p=0.04	OR=1.56 95%CI:0.33-7.34 p=0.57	OR=9.19 95%CI:2.36-35.74 p=0.001

dynamic process of risk re-stratification, the basis is, of course, performing echocardiography before anticancer treatment.

Our analysis concerns the period before the announcement of the latest guidelines of the European Society of Cardiology, created in cooperation with the European Hematology Association. The aim was to illustrate the situation before the publication of the guidelines, which for the first time, defined the principles of cardiovascular risk stratification and formal echocardiographic assessment in oncology and hematology.

Echocardiography plays a vital role in cardio-oncology (24). The number of important echocardiographic diagnoses during routine scheduled echocardiographic examinations supports the necessity of performing these examinations regularly and frequently in everyday practice, as recommended by experts (10). This is the optimal way to plan early prevention (25). Our data show

how important it is to assess cancer patients optimally at baseline and have additional echocardiographic parameters associated with the diastolic function of the left ventricle or function of the left atrium to compare them during active cancer therapy.

Optimal baseline evaluation of cancer patients may predict symptomatic and sometimes acute cardiac events as an element of cardio-oncology care (26). At baseline the most common diagnoses can be clinical problems related to arterial hypertension, heart failure and arrhythmias as in our study. Hematological patients with such baseline diagnoses are most vulnerable to further severe complications during active cancer therapy. These events have recently been discussed in a consensus published by the experts from the Acute CardioVascular Care Association (ACVC) and the ESC Council of Cardio-Oncology (27).

In onco-hematology, drug toxicity can affect any structure of the cardiovascular system. Therefore, cardio-hemato-oncology includes not only the diagnosis and treatment of heart failure but also of many vascular complications (28). Moreover, it has been confirmed that arterial hypertension together with coronary artery disease presents one of the most important risk factors in cardio-hemato-oncology (29). Arterial hypertension was the most common coexisting vascular problem in patients with newly diagnosed hematological malignancies in our study. Preexisting coronary artery disease was also recognized in some patients. Both arterial hypertension and coronary artery disease are well-known and important risk factors for the development of heart failure in general cardiology. Our h emato-oncology study highlights how both provoke greater chance of finding different echocardiographic abnormalities (Table 4).

In our observations, arrhythmias were the second most common clinical problem with atrial fibrillation comprising 7.94% of cases. This type of arrhythmia will undoubtedly focus the attention of cardio-oncologists on both the implementation of rhythm control strategies and antithrombotic prophylaxis (30). In the world of cardio-oncology growing attention is being paid to cardiac arrhythmias, mainly atrial fibrillation (31, 32). Cardiac arrhythmias, especially atrial fibrillation and other tachyarrhythmias, may indicate subclinical left ventricle dysfunction in hemato-oncology (33). The complex proarrhythmic mechanism in this group of patients results from water and electrolyte disorders, advanced age, coexisting cardiovascular diseases, and the direct effect of anticancer drugs (34).

Atrial fibrillation is becoming the special focus of arrhythmias in cardio-hematology (35, 36). Patients with previously diagnosed

TABLE 5 The odds ratio of diagnosing heart failure or arrhythmias (including atrial fibrillation) in relation to echocardiographic abnormalities.

	Heart failure	Arrhythmias	Atrial fibrillation
LAVI >34 ml/m2	OR=1.53 95%CI: 0.72-3.29 p=0.27	OR=1.98 95%CI: 1.00-3.92 p=0.048	OR=3.39 95%CI: 1.16-9.90 p=0.025
2 nd or 3 rd degree diastolic dysfunction	OR=8.32 95%CI: 3.82-18.1 p<0.0001	OR=4.44 95%CI: 2.14-9.20 p<0.0001	OR=5.40 95%CI: 2.15-13.56 p=0.0003
TRV >2.8 m/sec	OR=2.85 95%CI: 1.26-6.44 p=0.01	OR=1.93 95%CI: 0.88-4.24 p=0.1	OR=1.65 95%CI: 0.57-4.78 p=0.36
E/e' >14	OR=7.83 95%CI: 2.86-21.41 p<0.0001	OR=7.4 95%CI: 2.73-20.06 p<0.0001	OR=7.5 95%CI: 2.48-22.71 p=0.0003
EF <50%	#	OR=5.19 95%CI: 1.43-18.79 p=0.01	OR=3.08 95%CI: 0.61-15.57 p=0.17

#all patients with EF<50% had heart failure diagnosis.

atrial fibrillation are at higher risk of death and cardiovascular complications in connection with stem cell transplantation (37). In patients receiving anthracyclines, a significant relationship has been revealed between heart failure development and atrial fibrillation recognized before or during chemotherapy (38). It seems extremely important that our study shows that even baseline echocardiographic parameters related to diastolic dysfunction may help predict a greater chance of the development of arrhythmias including arterial fibrillation.

In our analysis, diastolic dysfunction (2nd or 3rd degree) was the second most common abnormality recognized by echocardiography. This was a determining factor in many cases of diagnosed heart failure before anticancer therapy. Moreover, a diagnosis of diastolic dysfunction (2nd or 3rd degree) was more common than left ventricular systolic dysfunction with $EF < 50\%$. Other exponents of diastolic dysfunction like $E/e' > 14$ or $TRV > 2.8$ m/s were more frequent as well (Table 5). The importance of diastolic dysfunction is underestimated in cardio-oncology. Our study confirms that the assessment of diastolic function before oncological treatment is crucial and echocardiography should not be limited only to parameters of systolic cardiac function. This may help diagnose heart failure with preserved left ventricular ejection fraction and identify very high-risk patients in cardio-oncology.

Evaluation of left ventricular diastolic function is one of the elements of echocardiography. To identify it, we used: peak flow velocities through the mitral valve - waves E and A, the velocity of the tissue mitral annulus e' in the Doppler examination, mean E/e' , the indexed volume of the left atrium and maximum velocity of the regurgitant wave through the tricuspid valve (15). The latest ESC guidelines do not recommend additional specific parameters for cancer patients. Meanwhile, diastolic dysfunction may precede the appearance of systolic dysfunction and full-blown heart failure at significantly lower doses of anthracyclines (39, 40). Such early diagnosis is possible only if all cancer patients are evaluated by means of echocardiography before cancer therapy. It should be highlighted that in patients with active cancer, deterioration of diastolic function may be a risk factor for all-cause mortality (41).

Our publication shows the validity of diastolic function assessment before anticancer treatment. Further careful observation will be required as to what drugs used in hemato-oncology affect the development of diastolic dysfunction of the left ventricle; hence it is important to assess the parameters of diastolic function in the initial examination. Another remaining issue is determining the prognostic role of diastolic dysfunction in hemato-oncology.

The limitations of the study

The study is purely epidemiological in nature to reflect the scale of cardiac problems in hemato-oncology. The authors tried to prove that the permanent employment of cardiologists in a leading hematology center in the country has a deep justification. The study analyses the experience of cardiologists gained by them in the

period of 12 months before the publication of the first European guidelines on cardio-oncology. At that time there was no uniform echocardiographic monitoring algorithm developed and the indications for testing asymptomatic patients depended on the hematologist's decision taking place at important moments in the treatment of blood cancer, i.e. when the next line of treatment was planned. This situation changed after the publication of the ESC guidelines. The experience regarding monitoring of patients during active cancer therapy with a comparison period before and after the publication of ESC guidelines will be the topic of our subsequent study showing how much the diagnosis of cardiac events increases. Meanwhile, we have proven how important it is to perform echocardiography in all patients with new hematological cancers. The percentage of abnormalities in echocardiography is significant.

The next significant limitation is the lack of global longitudinal strain (GLS) value measurements. The reason is very simple, the evaluation of GLS became standard in our hematology center after the publication of ESC guidelines.

The last limitation is the fact that fluid overload and sinus tachycardia make measurements difficult in hemato-oncology. As confirmed by our study, common arrhythmias including atrial fibrillation will significantly complicate the assessment of left ventricular diastolic dysfunction. The diagnostic accuracy may be questionable. Moreover, it is still unknown in cardio-oncology if the occurrence of abnormal diastolic function parameters may reflect subclinical LV dysfunction. Such an understanding of modern cardio-oncology requires an evaluation of diastolic function in each patient before anticancer therapy.

Conclusion

The new clinical diagnoses in hemato-oncology coexist mainly with arterial hypertension, heart failure and arrhythmias including atrial fibrillation.

Abnormalities in left ventricular diastolic function are clearly more frequent than systolic dysfunction in patients with newly diagnosed hematological malignancies and are associated significantly with concomitant diagnoses of heart failure or cardiac arrhythmias.

Data availability statement

The raw data supporting the conclusions of this article will be made available by the authors, without undue reservation.

Ethics statement

The studies involving humans were approved by Bioethical Committee at the Medical Center for Postgraduate Education in Warsaw. The studies were conducted in accordance with the local

legislation and institutional requirements. The participants provided their written informed consent to participate in this study.

Author contributions

JK: Conceptualization, Investigation, Writing – original draft, Writing – review & editing. SS: Conceptualization, Writing – original draft, Writing – review & editing. EL-M: Writing – review & editing.

Funding

The author(s) declare that no financial support was received for the research, authorship, and/or publication of this article.

References

- Lee GA, Aktaa S, Baker E, Gale CP, Yaseen IF, Gulati G, et al. European Society of Cardiology quality indicators for the prevention and management of cancer therapy-related cardiovascular toxicity in cancer treatment. *Eur Heart J - Qual Care Clin Outcomes* (2022) 9:1–7. doi: 10.1093/ehjqcco/qcac070
- Sadler D, Arnold A, Herrmann J, Daniele A, Silva CMPDC, Ghosh AK, et al. Reaching across the aisle: cardio-oncology advocacy and program building. *Curr Oncol Rep* (2021) 23:64. doi: 10.1007/s11912-021-01059-1
- Snipelisky D, Park JY, Lerman A, Mulvagh S, Lin G, Pereira N, et al. How to develop a cardio-oncology clinic. *Heart Failure Clinics* (2017) 13:347–59. doi: 10.1016/j.hfc.2016.12.011
- Mitroi C, Martín-García A, Mazón Ramos P, Virizuela Echaburu JA, Arenas-Prat M, García-Sanz R, et al. Current functioning of cardio-oncology units in Spain. *Clin Transl Oncol* (2020) 22:1418–22. doi: 10.1007/s12094-019-02250-4
- Lehmann LH, Stein F, Jäger D, Frey N. The Heidelberg cardio-oncology unit (COUNT)-a possible blueprint for improved care of cardio-oncological patients. *Clin Res Cardiol* (2022) 111:227–9. doi: 10.1007/s00392-021-01894-z
- Breccia M, Carver JR, Szmit S, Jurczak W, Salvatorelli E, Minotti G. Mechanisms and clinical course of cardiovascular toxicity of cancer treatment II. *Hematology☆. Semin Oncol* (2019) 46:403–7. doi: 10.1053/j.seminoncol.2019.10.005
- Herrmann J, Loprinzi C, Ruddy K. Building a cardio-onco-hematology program. *Curr Oncol Rep* (2018) 20:81. doi: 10.1007/s11912-018-0725-7
- López-Fernández T, Martín García A, Santaballa Beltrán A, Montero Luis Á, García Sanz R, Mazón Ramos P, et al. Cardio-onco-hematology in clinical practice. Position paper and recommendations. *Rev Española Cardiología (English Edition)* (2017) 70:474–86. doi: 10.1016/j.rec.2016.12.041
- Lyon AR, Dent S, Stanway S, Earl H, Brezden-Masley C, Cohen-Solal A, et al. Baseline cardiovascular risk assessment in cancer patients scheduled to receive cardiotoxic cancer therapies: a position statement and new risk assessment tools from the Cardio-Oncology Study Group of the Heart Failure Association of the European Society of Cardiology in collaboration with the International Cardio-Oncology Society. *Eur J Heart Fail* (2020) 22:1945–60. doi: 10.1002/ehf.1920
- Čelutkienė J, Pudil R, López-Fernández T, Grapsa J, Nihoyannopoulos P, Bergler-Klein J, et al. Role of cardiovascular imaging in cancer patients receiving cardiotoxic therapies: a position statement on behalf of the Heart Failure Association (HFA), the European Association of Cardiovascular Imaging (EACVI) and the Cardio-Oncology Council of the European Society of Cardiology (ESC). *Eur J Heart Fail* (2020) 22:1504–24. doi: 10.1002/ehf.1957
- Caro-Codón J, López-Fernández T, Álvarez-Ortega C, Zamora Auñón P, Rodríguez IR, Gómez Prieto P, et al. Cardiovascular risk factors during cancer treatment. Prevalence and prognostic relevance: insights from the CARDIOTOX registry. *Eur J Prev Cardiol* (2022) 29:859–68. doi: 10.1093/eurjpc/zwaa034
- Anker MS, Sanz AP, Zamorano JL, Mehra MR, Butler J, Riess H, et al. Advanced cancer is also a heart failure syndrome: a hypothesis. *Eur J Heart Fail* (2021) 23:140–4. doi: 10.1002/ehf.2071
- Lang RM, Badano LP, Mor-Avi V, Afkalo J, Armstrong A, Ernande L, et al. Recommendations for cardiac chamber quantification by echocardiography in adults: an update from the American society of echocardiography and the European association of cardiovascular imaging. *J Am Soc Echocardiography* (2015) 28:1–39.e14. doi: 10.1016/j.echo.2014.10.003
- Mitchell C, Rahko PS, Blauwet LA, Canaday B, Finstuen JA, Foster MC, et al. Guidelines for performing a comprehensive transthoracic echocardiographic examination in adults: recommendations from the American society of echocardiography. *J Am Soc Echocardiography* (2019) 32:1–64. doi: 10.1016/j.echo.2018.06.004
- Nagueh SF, Smiseth OA, Appleton CP, Byrd BF, Dokainish H, Edvardsen T, et al. Recommendations for the evaluation of left ventricular diastolic function by echocardiography: an update from the American society of echocardiography and the European association of cardiovascular imaging. *J Am Soc Echocardiography* (2016) 29:277–314. doi: 10.1016/j.echo.2016.01.011
- Williams B, Mancia G, Spiering W, Agabiti Rosei E, Azizi M, Burnier M, et al. 2018 ESC/ESH Guidelines for the management of arterial hypertension. *Eur Heart J* (2018) 39:3021–104. doi: 10.1093/eurheartj/ehy339
- Knuuti J, Wijns W, Saraste A, Capodanno D, Barbato E, Funck-Brentano C, et al. 2019 ESC Guidelines for the diagnosis and management of chronic coronary syndromes. *Eur Heart J* (2020) 41:407–77. doi: 10.1093/eurheartj/ehz425
- McDonagh TA, Metra M, Adamo M, Gardner RS, Baumbach A, Böhm M, et al. 2021 ESC Guidelines for the diagnosis and treatment of acute and chronic heart failure. *Eur Heart J* (2021) 42:3599–726. doi: 10.1093/eurheartj/ehab368
- Lyon AR, López-Fernández T, Couch LS, Asteggiano R, Aznar MC, Bergler-Klein J, et al. 2022 ESC Guidelines on cardio-oncology developed in collaboration with the European Hematology Association (EHA), the European Society for Therapeutic Radiology and Oncology (ESTRO) and the International Cardio-Oncology Society (IC-OS). *Eur Heart J* (2022):ehac244. doi: 10.1093/eurheartj/ehac244
- Mędrek S, Szmit S. Are cardiovascular comorbidities always associated with a worse prognosis in patients with lung cancer? *Front Cardiovasc Med* (2022) 9:984951. doi: 10.3389/fcvm.2022.984951
- Martín García A, Mitroi C, Mazón Ramos P, García Sanz R, Virizuela JA, Arenas M, et al. Stratification and management of cardiovascular risk in cancer patients. A consensus document of the SEC, FEC, SEOM, SEOR, SEHH, SEMG, AEEMT, AECC, and AECC. *Rev Española Cardiología (English Edition)* (2021) 74:438–48. doi: 10.1016/j.rec.2020.11.020
- Mędrek S, Szmit S. Baseline electrocardiographic and echocardiographic assessment may help predict survival in lung cancer patients—A prospective cardio-oncology study. *Cancers* (2022) 14:2010. doi: 10.3390/cancers14082010
- López-Fernández T, Vadillo IS, de la Guía AL, Barbier KH. Cardiovascular issues in hematopoietic stem cell transplantation (HSCT). *Curr Treat Options Oncol* (2021) 22:51. doi: 10.1007/s11864-021-00850-3
- Keramida K, Farmakis D, López Fernández T, Lancellotti P. Focused echocardiography in cardio-oncology. *Echocardiography* (2020) 37:1149–58. doi: 10.1111/echo.14800
- López-Fernández T. Cardiac imaging in oncology patients in Europe: a model for advancement of CV safety and development of comprehensive CV care. *J Cardiovasc Trans Res* (2020) 13:490–4. doi: 10.1007/s12265-020-10028-1
- López-Fernández T, de Castro Carpeño J. Cancer and acute cardiovascular diseases: team work to transform the clinical practice. *Eur Heart J Acute Cardiovasc Care* (2021) 10:840–2. doi: 10.1093/ehjacc/zuab079
- Gevaert SA, Halvorsen S, Sinnaeve PR, Sambola A, Gulati G, Lancellotti P, et al. Evaluation and management of cancer patients presenting with acute cardiovascular

Conflict of interest

The authors declare that the research was conducted in the absence of any commercial or financial relationships that could be construed as a potential conflict of interest.

Publisher's note

All claims expressed in this article are solely those of the authors and do not necessarily represent those of their affiliated organizations, or those of the publisher, the editors and the reviewers. Any product that may be evaluated in this article, or claim that may be made by its manufacturer, is not guaranteed or endorsed by the publisher.

disease: a Clinical Consensus Statement of the Acute CardioVascular Care Association (ACVC) and the ESC council of Cardio-Oncology-part 2: acute heart failure, acute myocardial diseases, acute venous thromboembolic diseases, and acute arrhythmias. *Eur Heart J Acute Cardiovasc Care* (2022) 11:865–74. doi: 10.1093/ehjacc/zuac107

28. Campia U, Moslehi JJ, Amiri-Kordestani L, Barac A, Beckman JA, Chism DD, et al. Cardio-oncology: vascular and metabolic perspectives: A scientific statement from the American heart association. *Circulation* (2019) 139(15):e579–602. doi: 10.1161/CIR.0000000000000641

29. Szmít S, Jurczak W, Zaucha JM, Drozd-Sokołowska J, Spychałowicz W, Joks M, et al. Pre-existing arterial hypertension as a risk factor for early left ventricular systolic dysfunction following (R)-CHOP chemotherapy in patients with lymphoma. *J Am Soc Hypertension* (2014) 8:791–9. doi: 10.1016/j.jash.2014.08.009

30. Szmít S, Kępski J, Wilk M. Management of anticoagulation in cancer patients with atrial fibrillation. *Isr Med Assoc J* (2022) 24:183–5.

31. López-Fernández T, Martín-García A, Roldán Rabadán I, Mitroi C, Mazón Ramos P, Díez-Villanueva P, et al. Atrial fibrillation in active cancer patients: expert position paper and recommendations. *Rev Española Cardiología (English Edition)* (2019) 72:749–59. doi: 10.1016/j.rec.2019.03.019

32. Gawlik M, Zimodro JM, Gasecka A, Filipiak KJ, Szmít S. Cardiac arrhythmias in oncological patients—Epidemiology, risk factors, and management within the context of the new ESC 2022 guidelines. *Curr Oncol Rep* (2023) 25(10):1107–15. doi: 10.1007/s11912-023-01445-x

33. Heemelaar JC, Krol ADG, Louwerens M, Beeres SLMA, Holman ER, Schalijs MJ, et al. Elevated resting heart rate is a marker of subclinical left ventricular dysfunction in Hodgkin lymphoma survivors. *IJC Heart Vasculture* (2021) 35:100830. doi: 10.1016/j.ijcha.2021.100830

34. Essa H, Dobson R, Lip GYH. Chemotherapy induced arrhythmias. *J Cardiovasc Pharmacol* (2021) 80(4):531–9. doi: 10.1097/FJC.0000000000001216

35. Alexandre J, Salem J-E, Moslehi J, Sassier M, Ropert C, Cautela J, et al. Identification of anticancer drugs associated with atrial fibrillation: analysis of the WHO pharmacovigilance database. *Eur Heart J - Cardiovasc Pharmacotherapy* (2021) 7:312–20. doi: 10.1093/ehjcvp/pvaa037

36. Alexandre J, Boismoreau L, Morice P-M, Sassier M, Da-Silva A, Plane A-F, et al. Atrial fibrillation incidence associated with exposure to anticancer drugs used as monotherapy in clinical trials. *JACC: CardioOncology* (2023) 5:216–26. doi: 10.1016/j.jacc.2022.11.019

37. Ammad Ud Din M, Chowdhury M, Shahzad M, Zahid S, Liaqat H, Osama M, et al. Trends and in-hospital cardiac complications in patients with atrial fibrillation undergoing allogeneic stem cell transplant: A National Inpatient Sample analysis (2002–2019). *Eur J Haematology* (2023) 110:754–61. doi: 10.1111/ejh.13960

38. Onoue T, Kang Y, Lefebvre B, Smith AM, Denduluri S, Fradley MG, et al. Impact of atrial fibrillation on heart failure in patients treated with anthracycline chemotherapy. *Am J Cardiol* (2024) 211:268–74. doi: 10.1016/j.amjcard.2023.11.038

39. Minotti G, Reggiardo G, Camilli M, Salvatorelli E, Menna P. From cardiac anthracycline accumulation to real-life risk for early diastolic dysfunction. *JACC: CardioOncology* (2022) 4:139–40. doi: 10.1016/j.jacc.2021.12.002

40. Serrano JM, González I, Del Castillo S, Muñoz J, Morales LJ, Moreno F, et al. Diastolic dysfunction following anthracycline-based chemotherapy in breast cancer patients: incidence and predictors. *Oncologist* (2015) 20:864–72. doi: 10.1634/theoncologist.2014-0500

41. Arnold JH, Rozenbaum Z, Hochstadt A, Rosen R, Sherez C, Sivan A, et al. Diastolic function as an early marker for systolic dysfunction and all-cause mortality among cancer patients. *Echocardiography* (2021) 38:540–8. doi: 10.1111/echo.15012

Frontiers in Cardiovascular Medicine

Innovations and improvements in cardiovascular treatment and practice

Focuses on research that challenges the status quo of cardiovascular care, or facilitates the translation of advances into new therapies and diagnostic tools.

Discover the latest Research Topics

[See more →](#)

Frontiers

Avenue du Tribunal-Fédéral 34
1005 Lausanne, Switzerland
frontiersin.org

Contact us

+41 (0)21 510 17 00
frontiersin.org/about/contact



Frontiers in Cardiovascular Medicine

